Dissertation zur Erlangung des Doktorgrades
der Fakultät für Chemie und Pharmazie
der Ludwig-Maximilians-Universität München

Lewis Base Organocatalysis by Pyridines and Phosphanes – Experimental and Computational Studies

Julian Helberg

aus

Dachau, Deutschland

2020

Erklärung

Diese Dissertation wurde im Sinne von § 7 der Promotionsordnung vom 28. November 2011 von Herrn Prof. Dr. Hendrik Zipse betreut.

Eidesstattliche Versicherung

Diese Dissertation wurde eigenständig und ohne unerlaubte Hilfe erarbeitet.

München, 15.6.2020

Julian Helberg

Dissertation eingereicht am:	24.02.2020
1. Gutachter:	Prof. Dr. Hendrik Zipse
2. Gutachter:	Prof. Dr. Konstantin Karaghiosoff
Mündliche Prüfung am:	23.04.2020

Acknowledgement

I want to start by thanking Prof. Hendrik Zipse for giving me the opportunity to work in this fascinating line of research and giving me a lot of freedom in finding and developing my own projects. I am grateful for him always being available and helping me a great deal not only in my development as a scientist, but also as a person over the course of the last years.

Next, I would like to extend my thanks to Prof. Konstantin Karaghiosoff for kindly agreeing to be the "Zweitgutachter" for this thesis. I am also thankful to all the members of the review committee for committing their time and efforts.

Also, I want to convey my gratitude to my colleagues. To Prof. Yohei OE, with whom I worked on the oligomerization project and to Prof. Marta Marin-Luna, who initiated the chemoselectivity project and who showed me how one can streamline such an endeavor. Her amazing organizational skill and synthetic capabilities were an inspiration.

I also want to convey my gratitude to the students who worked on my projects and often did the hard job of finding out what does not work with great enthusiasm: Alexander Wagner, Petr Tatarskiy, Christoph Gross and Nikolas Schneider. Special thanks in this group goes to Torsten Ampßler, who worked on the ion pair catalyst project early on and helped me to see its potential.

Davor Sakic showed me that coding is not incomprehensible magic and therefore enabled me to deal with the demands of my computational projects in a semi-automated way. I am deeply grateful for this and the spirited conversations in the evenings.

Then, there are the former colleagues, Florian Achrainer, Florian Barth and Pascal Patschinski who made me feel welcome and taught me the specifics of the experimental Zipse lab. Prof. Sandhiya Lakshmanan did not only impress me with her dedication to research but also was excellent company. I fondly remember our lunchtime-conversations. Jutta Tumpach, Ieva Teikmane and Heena Ugale were good company and supportive in times when things ran less smoothly.

Also, I want to thank my current colleagues not only for proof-reading this thesis. Harish Jangra also welcomed me to the group, but fortunately is still an always helpful and friendly presence in the computational lab, ready to deal with the multitude of issues that arise when experimental chemists do computational chemistry. Benjamin Pölloth excelled for long years in the role of bench-neighbor and our discussions helped me innumerable times. Stefanie Mayr was the other member of the organocatalyst taskforce and aside from an impressive attitude of meeting problems head-on, provided non-scientific counsel in the later stages of my PhD. Both of them were very helpful in the writing of this thesis. Salavat Ashirbaev does not only know "all about chemistry", but is also good company for a couple of beers and a fascinating repository of obscure internet facts. The same is true for Fabian Zott, with whom I rarely agreed in political discussions, but who was a very helpful colleague. I also want to thank Veronika Burger and Vasily Korotenko for helping me out on several occasions.

Outside of science, the Raw-Crew, primarily Stefan, Vinz, Sebi, Jonas, Basti, Achim and Max, helped to retain a personal life with the “regular” meetings and concert visits. The same goes for Basti, Ben, Julia and Julia, who despite the fact that our last festival is years back, are still an entertaining – although more serious – crowd.

I also want to convey my thanks to the members of my gaming groups and beg their forgiveness for not being able to join as often as I liked: Andy, Elina, Alex and Christian in the “temporary” one and of course Sand´s Finest: Sascha, Joni, Jonas and Domi.

Sincere thanks also go out to the friends I acquired during my undergrad studies (and also did their PhD at LMU), most noticeably Andreas Bellan and Christian Petermayer who were always there to talk science and even more non-science and have been helping me in numerous ways since I had the privilege of knowing them.

Last, but not least, I want to thank the people that have made all of this possible from an early stage on. My parents Angelika and Rainer and my grandparents Irmgard and Hans, who have been nothing but supportive ever since. I also thank my brother Jonas, my sister Joana, both their partners, and my aunt Irm.

Undoubtedly, the most credit and gratitude belongs to my amazing wife Domi, who has accompanied, encouraged and supported me for so many years.

Thank you all. This would not have been possible without you.

List of Publications

Parts of this thesis have been published as studies 1 – 3:

1. **Pyridinyl Amide Ion Pairs as Lewis Base Organocatalysts**
   J. Helberg, T. Ampßler, H. Zipse, *J. Org. Chem.* **2020**, *85*, 5390 – 5402.

2. **Chemoselectivity in Esterification Reactions – Size Matters after All**
   J. Helberg, Y. OE, H. Zipse, *Chem. Eur. J.* **2018**, *24*, 14387 – 14391.

3. **Mechanistic Analysis and Characterization of Intermediates in the Phosphane-Catalyzed Oligomerization of Isocyanates**
   J. Helberg, M. Marin-Luna, H. Zipse, *Synthesis* **2017**, *49*, 3460 – 3470.

4. **Highly Diastereoselective Preparation of Aldol Products Using New Functionalized Allylic Aluminum Reagents**
   Z.-L. Shen, Z. Peng, C.-M. Yang, J. Helberg, P. Mayer, I. Marek, P. Knochel, *Org. Lett.* **2014**, *16*, 956 – 959.

Table of Content

Summary 1

Chapter 1. Introduction 3

1.1 Lewis Base Organocatalysis 3

1.1.1 Phosphane Lewis Base Organocatalysts 4

1.1.2 Pyridine Lewis Base Organocatalysts 5

1.2 Investigation of Lewis Base Organocatalysis 7

1.2.1 Computational Investigation of Lewis Base Organocatalysts Using Affinity Values 7

1.2.2 Experimental Investigation of Organocatalyst-Mediated Reactions 9

References 11

Chapter 2. Mechanistic Analysis and Characterization of Intermediates in the Phosphane-Catalyzed Oligomerization of Isocyanates 12

2.1 Supporting Information 18

2.1.1 General Experimental Information 18

2.1.2 Synthesis of ^{15}N-Labeled Compounds 18

2.1.3 Synthesis of Oligomers and Reference Compounds 23

2.1.4 Oligomerization Experiments 27

2.1.5 Low Temperature NMR Measurements 33

2.1.6 Details of ^{1}H NMR Kinetic Measurements 36

2.1.7 NMR Spectra of Synthesized Compounds 51

2.1.9 Investigation of Temperature- and Concentration-Dependence of ^{31}P NMR Measurements 81

2.1.10 Computational Chemistry Procedures 82

2.1.11 Calculation of ^{13}C, ^{15}N, and ^{31}P NMR Signals 83

References 92

Thermochemical Data 93

Isotropic Shielding Data 101

Chapter 3. Chemoselectivity in Esterification Reactions – Size Matters After All 107

Chemoselectivity in Esterification Reactions – Size matters after all 108

3.1. Supporting Information 117

3.1.1 Investigation of the Formation of TCAP-Acid Chloride Adducts. 117

3.1.2 Competition Experiments 122

3.1.3 Selectivity Curves: Simulation and Plotting 124

3.1.4 Chemoselectivity and Conversion Factors 125

3.1.5 Selectivity Curves of Competition Experiments 131

3.1.6 Stacked ^{1}H NMR Spectra of all Competition Experiments 138

3.1.7 Solvent Influence on the Chemoselectivity 155

3.1.8 Temperature Effect on the Chemoselectivity 156

3.1.9. ^{1}H NMR and ^{13}C NMR Spectra of Synthesized Compounds 157

3.1.10. X-Ray Crystal Structure Data 176

References 178

Chapter 4. Pyridinyl Amide Ion Pairs as Lewis Base Organocatalysts 179

4.1. Supporting Information 193

4.1.1 Benchmark Reaction 1 – Urethane Synthesis 193
4.1.2 Benchmark Reaction 2 – *Aza*-Morita-Baylis-Hillman Reaction 237
4.1.3 Esterification Reactions Mediated by Ion Pair Catalysts 248
4.1.4 Deprotonation of More Acidic Cations in Ion Pair Catalysis 257
4.1.5 Crystallographic Data 262
4.1.6 Assigned NMR Spectra of Synthesized Compounds 300
4.1.7 General Computational Methods 344
4.1.8 Calculated Phenyl Isocyanate Affinities (ΔPIAs) and Methyl Cation Affinities (ΔMCAs) 351
4.1.9 Effect of Exclusion of Cations for Computed Affinity Values 352
4.1.10 Affinity Values of Pyridine-N vs. Amide-N 354
References 356
Thermochemical Data 356

Summary

This thesis consists of an introduction and three main chapters, each focusing on different aspects of Lewis base organocatalysis. The introduction gives a brief overview of selected topics in organocatalysis that are relevant for the studies presented within this thesis. In the second chapter, we investigated the mechanism of a commercially important oligomerization reaction, the oligomerization of isocyanates. Since conflicting reports have been made regarding the mechanism when this reaction is catalyzed by phosphanes as Lewis base organocatalyts, we studied an example of one such reaction both experimentally and computationally in:

Mechanistic Analysis and Characterization of Intermediates in the Phosphane-Catalyzed Oligomerization of Isocyanates[a]

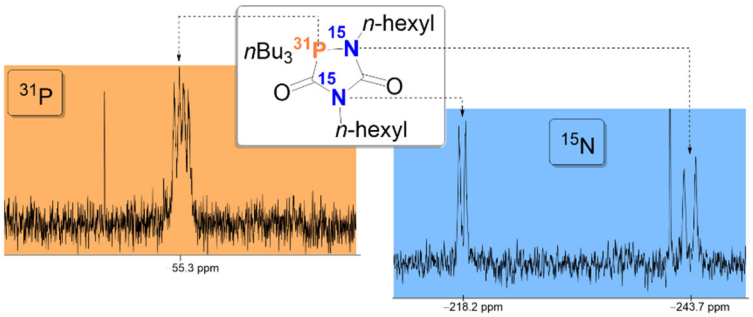

The mechanism of the oligomerization of aliphatic isocyanates catalyzed by trialkylphosphanes has been studied through low temperature ^{31}P and ^{15}N NMR spectroscopy combined with computational chemistry. A revised mechanism is proposed that contains several (spiro)cyclic pentacoordinate phosphorous intermediates. Previously reported spectroscopic data of a transient intermediate has been reevaluated and assigned to a cyclic intermediate containing a P-N bond by experiments with ^{15}N-labeled isocyanate. ^{13}C, ^{15}N, and ^{31}P NMR shifts that support this assignment have been calculated using quantum chemical methods.

Unlike this mechanistic study, the one representing the third chapter focuses on a different aspect of organocatalysis – selectivity. We set out to investigate substrate size effects on the chemoselectivity in esterification reactions of alcohols and the effect of the addition of a pyridine-derived organocatalyst in:

Chemoselectivity in Esterification Reactions – Size matters after all[b]

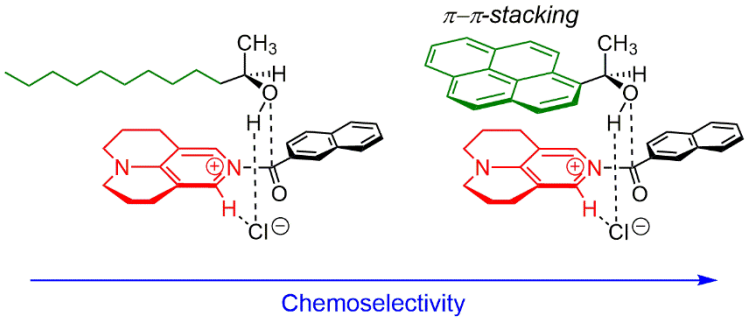

The reaction of carboxylic acid chlorides with secondary alcohols carrying either flexible alkyl or rigid aryl substituents was studied through a series of competition experiments. Aliphatic acid chlorides react preferentially with the aryl-substituted alcohols, while acid chlorides derived from aromatic carboxylic acids react with very low selectivity. Catalysis by 9-azajulolidine (TCAP) increases the selectivity strongly, while solvent and temperature effects are only moderate. The size of the alcohol substituents

[a] Reprinted with permission from *Chem. Eur. J.* **2018**, *24,* 14387 – 14391 © 2018 Wiley-VCH Verlag GmbH & Co. KGaA, Weinheim.
[b] Reprinted with permission from *Synthesis* **2017**, *49*, 3460 – 3470 © Georg Thieme Verlag KG.

seems to impact selectivities only for rigid aryl substituents, and highest selectivities have been found for 1-(1-pyrenyl)ethanol.

In the fourth chapter, we again switched focus to another feature of Lewis base organocatalysts, the catalytic activity. Therefore, we investigated a largely overlooked but promising class of anionic pyridine organocatalysts mainly focusing on their activity for activation of two selected electrophiles, but also regarding their stability and structural features in the solid state. Additionally, we intended to find a computational modeling strategy for such conformationally demanding ion pairs to quantify their Lewis basicity *in silico* and investigate the catalytically active center of such pyridinyl anions in:

Pyridinyl Amide Ion Pair Organocatalysts – A Class of Accessible, Inexpensive High Performance Lewis Bases[c]

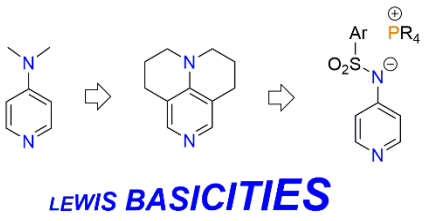

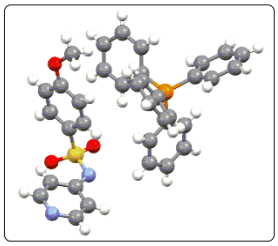

Pyridinyl amide ion pairs carrying various electron withdrawing substituents were synthesized with selected ammonium or phosphonium counter ions. Compared to neutral pyridine-based organocatalysts these new ion pair Lewis bases display superior catalytic reactivity in the reaction of isocyanates with alcohols and the *aza*-Morita-Baylis-Hillman reaction of hindered electrophiles. The high catalytic activity of ion pair catalysts appears to be due to their high Lewis basicities towards neutral electrophiles as quantified through quantum chemically calculated affinity data.

[c] Reproduced with permission from *J. Org. Chem.* **2020**, *85*, 5390 – 5402 © 2020 American Chemical Society.

Chapter 1. Introduction

Since the field of Lewis base organocatalysis is by now a mature and continuously expanding area of research, the following sections will give a brief overview of selected topics of significance to the studies presented within this thesis.

1.1 Lewis Base Organocatalysis

The term “Organocatalysis” was coined by MacMillan in 2000, although the cyanide-catalyzed benzoin addition first described by Liebig and Wöhler is widely considered the first published organocatalyzed reaction.[1] In general, organocatalysis is defined as, “… the acceleration of chemical reactions with a substoichiometric amount of an organic compound which does not contain a metal atom”.[2] The before mentioned catalysis by cyanide is also an example of a Lewis base catalyzed reaction, although it can only truly be considered as an example of organocatalysis if the presence of the potassium cation is ignored. Extending the definition by Gilbert N. Lewis to accommodate the catalysis part, Denmark defined Lewis base catalysis as “... the process by which an electron-pair donor increases the rate of a given chemical reaction by interacting with an acceptor atom in one of the reagents or substrates. The binding event may enhance either the electrophilic or nucleophilic character of the bound species. Furthermore, the Lewis base should not be consumed or altered during the course of the reaction — a hallmark of any catalytic process”.[3]

Depending on whether the Lewis base is a neutral or anionic molecule and whether the electrophilic substrate contains a leaving group or not, the reactions described in this thesis are presumed to follow one of the four simplified primary mechanisms given in Scheme 1.

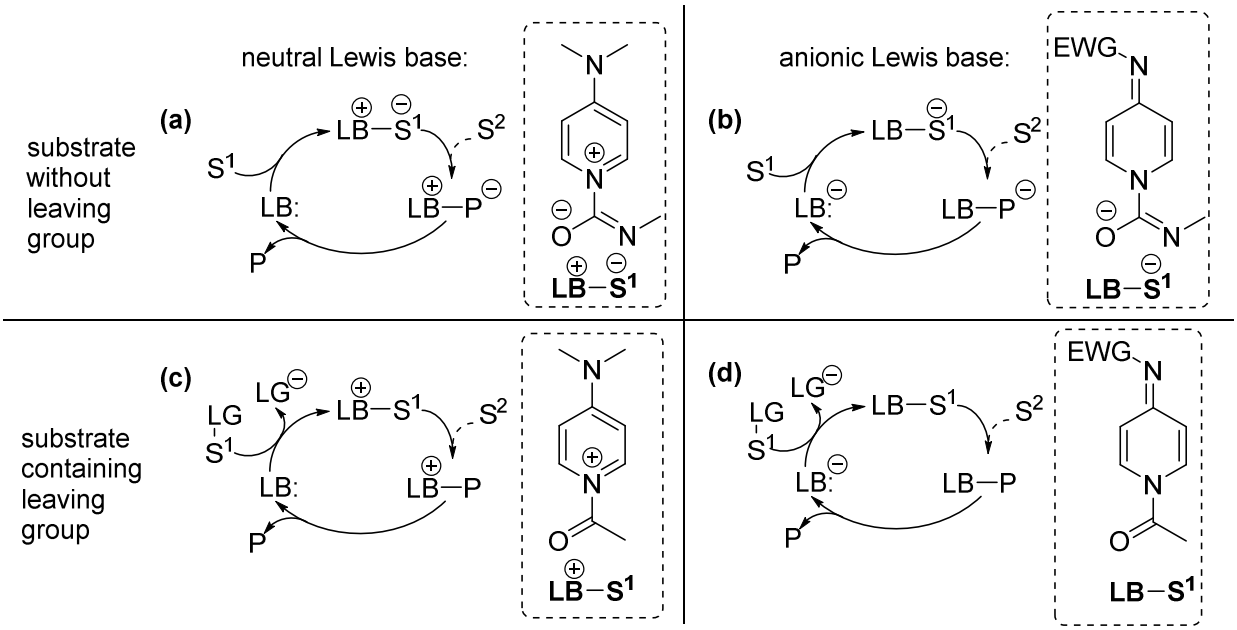

Scheme 1. *Simplified mechanisms of Lewis base (LB) catalysis for neutral and anionic Lewis bases upon reaction with substrates (S) devoid of a leaving group (LG) or containing one to form the product (P). In the boxes, an example of the Lewis base-adduct is given. EWG stands for electron-withdrawing group.*

In these cases, the catalyst acts in a similar way. First, there is a nucleophilic attack on the substrate, that generates a catalyst-substrate adduct, selected examples for those are given in the boxes. In the intermolecular reactions investigated in this study, this adduct then reacts with a second substrate and a catalyst-product complex is formed. Finally, the catalyst is regenerated and the product is released.

These simplified mechanistic schemes mainly differ in the charge of the Lewis base-substrate adduct. Scheme 1(a) represents the reaction of a neutral Lewis base with a substrate without a leaving group, while Scheme 1(b) shows the catalytic cycle for the same kind of substrate when the Lewis base is an anion. The initially formed adduct is a zwitterionic species in Scheme 1(a) or an anion in Scheme 1(b), respectively. In the two cases representing reactions of a substrate containing a leaving group, the adduct formed is cationic in Scheme 1(c) after elimination of the leaving group following an attack by a neutral Lewis base. Reaction with an anionic Lewis base, on the other hand gives a neutral “adduct” as shown in Scheme 1(d).

The oligomerization of isocyanates investigated in chapter two is best represented by Scheme 1(a),[4] while the esterification reactions described in chapter three are considered to proceed according to a mechanism similar to Scheme 1(c).[5] The fourth chapter deals primarily with the activation of isocyanates and (separately) Michael acceptors by pyridinyl anions and neutral pyridine catalysts, mechanistically represented by Scheme 1(b) and Scheme 1(a).[6] However, a few exploratory experiments regarding the activation of carboxylic anhydrides by the same catalyst system, which presumably proceeds through a mechanisms similar to Scheme 1(d) and Scheme 1(c), respectively can be found in the attached supporting information.[6]

In the case of weakly acidic substrates, such as alcohols, there is also the possibility of activation through formation of a hydrogen bond between the hydrogen atom and the base, then acting as classic Brønsted base.[7] Whether this is applicable strongly depends on the investigated system, which is why the following discussion focusses on Lewis basic behavior.

1.1.1 Phosphane Lewis Base Organocatalysts

Most applications of phosphanes as Lewis base organocatalysts are based on the tendency of such compounds to add to activated carbon-carbon multiple bonds and other electrophiles.[8] This was first described by Horner in 1955, who isolated zwitterionic adducts after reaction of triethylphosphane and triphenylphosphane with 1,1-dicyanoethene (Scheme 2(a)) and further utilized phosphanes as initiators in the polymerization of acrylonitrile and other vinyl compounds.[9] Shortly after, Rauhut and Currier patented the phosphane-catalyzed addition reaction of two molecules of the same electron-deficient olefin (Scheme 2(b)), which has been named after the inventors.[10] The Rauhut-Currier (RC) reaction has by now evolved to accompany desirable features like enantioselectivity and intramolecular reaction, often accomplished by specifically engineered phosphanes.[8, 11] Closely related is the “reaction of acrylonitrile or methyl acrylate with various aldehydes in the presence of tricyclohexylphosphine …”, reported by Morita in 1968.[12] After extension by Baylis and Hillman, who replaced the phosphane with sterically unhindered, cyclic tertiary amines like diazabicyclo-[2,2,2]-octane (DABCO), this kind of reaction became known as the Morita-Baylis-Hillman (MBH) reaction (Scheme 2(c)).[13] Just as the RC reaction, the MBH reaction has been further developed to enable enantioselectivity while accommodating a huge array of substrates as the electron deficient Michael acceptor and both aldehydes/ketones and imines as electrophiles.[11b, 14] The latter case is referred to as an *aza*-MBH reaction, whose mechanism and scope has been investigated in the Zipse group recently.[15] Chapter 4 of this thesis includes (attempted) phosphane catalysis for both an *aza*-MBH reaction and urethane formation from isocyanate and alcohol for comparison with the other catalyst system featured

there.[6] The activation of isocyanates by phosphanes is known for more than 150 years now, initially dealing with the oligomerization of isocyanates by such Lewis bases (Scheme 2(d)).[16] Since the mechanism of this commercially relevant reaction was still subject to contradictory publications a few years ago,[17] we performed an experimental and computational study elucidating the key intermediate, which is presented as the second chapter of this thesis.[4]

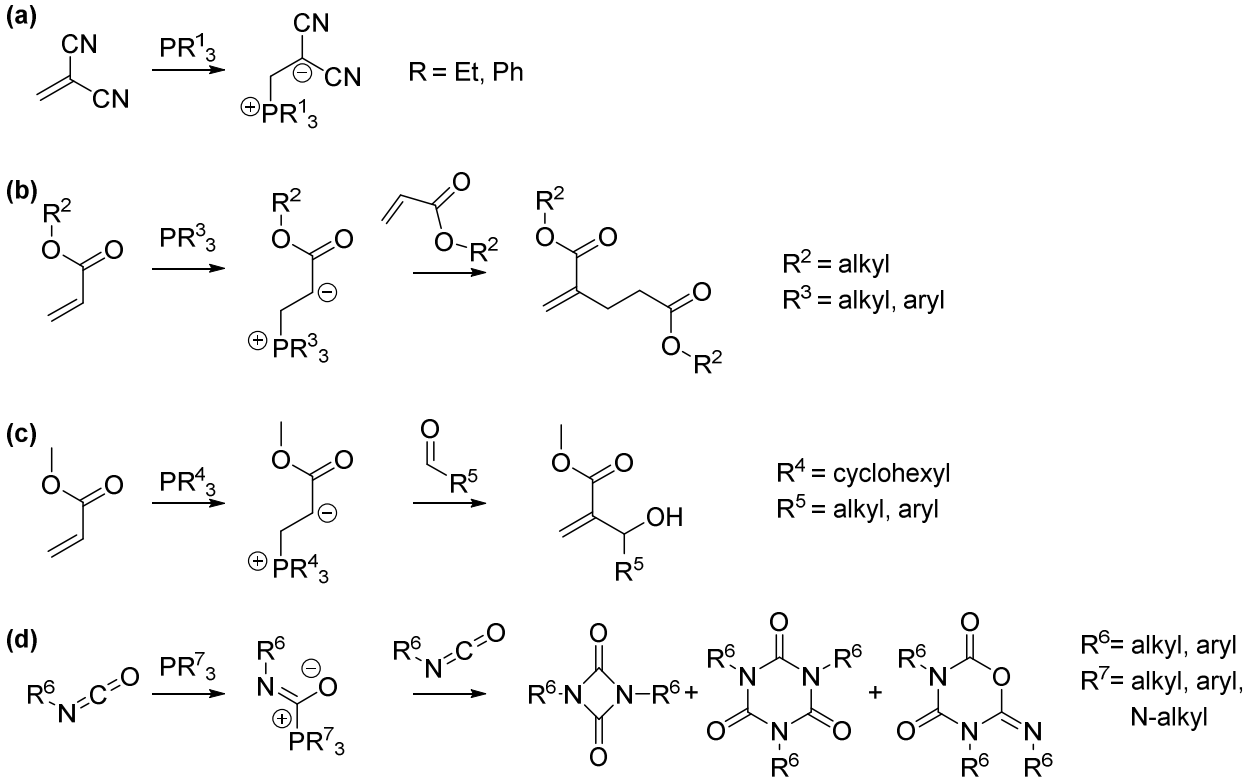

Scheme 2. *(a) Horner zwitterion, and phosphane Lewis base catalyzed (b) RC reaction, (c) MBH reaction, and (d) isocyanate oligomerization.*

1.1.2 Pyridine Lewis Base Organocatalysts

As early as 1898, Einhorn and Hollandt discovered that pyridine promoted acetylation reactions,[18] but it took several decades until the catalytic potential of 4-dimethylaminopyridine (**DMAP**), the archetypical pyridine-derived Lewis base was reported by Litvinenko and Kirichenko in 1967,[19] independently followed shortly after by Steglich and Höfle in 1969 (Scheme 3).[20] Steglich and coworkers continued to push the boundaries of catalytic activity with 4-pyrrolidinopyridine (**PPY**)[21] in 1970 and 9-azajulolidine (**TCAP**) in 2003 by increasing positive inductive effects towards the pyridine ring and further planarizing the 4-amino moiety (Scheme 3).[22] Since then, TCAP has set the standard as a highly Lewis basic, commercially available organocatalyst, that we also used in the investigation of size effects in acylation reactions contained in the third chapter of this thesis.[5] So far, no other pyridine-based organocatalyst scaffold managed to significantly exceed the reactivity provided by TCAP, although a range of different structural motives have been investigated to increase electron density at the pyridine nitrogen atom to generate more active catalysts (Scheme 3). The concept of 4-guanidinyl pyridine catalysts was first studied by Hassner, but the most active example investigated then, tetramethylated compound **A** (Scheme 3) showed inferior reactivity compared to PPY.[23] Later computational modeling led to improved catalytic activity of derivates of

this class of Lewis base catalysts in acylation experiments done in the Zipse lab.[24] However, the same study also used 3,4-diaminopyridine catalyst **B** (Scheme 3), which performed better than all tested 4-guadinyl pyridine catalysts, only to be surpassed in turn by TCAP. Bicyclic 3,4-diaminopyridine Lewis base organocatalysts with 3,4-diaminopyridine **C** (Scheme 3) as their simplest example were originally developed by Han[25] and –independently– Zipse[26] in 2007. Contrary to a computational study indicating they should be more active acylation catalysts than TCAP, this was not found experimentally.[26]

Mimicking TCAP, further planarization of the 3,4-diaminopyridine motif by incorporation into a tricyclic system was accomplished a few years ago by Tandon and Zipse.[27] The tricyclic 3,4-diaminopyridine catalyst **D** (Scheme 3), was reported to be most active for this class of catalysts. Depending on the investigated reaction, this class of tricyclic 3,4-diaminopyridines performed either slightly better or slightly poorer than TCAP.[6, 27]

Han et al. developed 3,4,5-triaminopyridines, the next logical step in the attempt to induce higher electron density and therefore catalytic activity towards the pyridine-N.[25] Scheme 3 shows tricyclic 3,4,5-triaminopyridine compound **E**, that was reported to be a slightly more active catalyst for acylation reactions by Han but noticeably less active for the same reaction in a different solvent by Zipse et al.[27] Similar results for these highly Lewis basic catalyst systems are also reported for MBH and *aza*-MBH reactions. The activity is very similar to the one of TCAP, sometimes exceeding it and sometimes falling short of it, depending on the studied reaction.[15a, 28] As one can see in Scheme 3, the pyridine ring system has been systematically substituted to increase organocatalytic activity, however, substitution at the 2,6-positions is detrimental to this goal due to increased steric hindrance.[29] Substitutions in C-2 position were undertaken in investigations focusing on other key aspects of pyridine Lewis bases like enantioselective organocatalysis or ligand design.[30]

A previously largely overlooked approach that utilizes stabilized 4-pyridinyl amide anions is presented as the fourth chapter of this thesis.[6, 17a, 31] We found those ion pair catalysts to facilitate the turnover of the investigated reactions several times faster than TCAP. 4-Pyridinyl amide ion pair catalyst **F** (Scheme 3), was found to be most active, while remaining remarkably stable in this study.

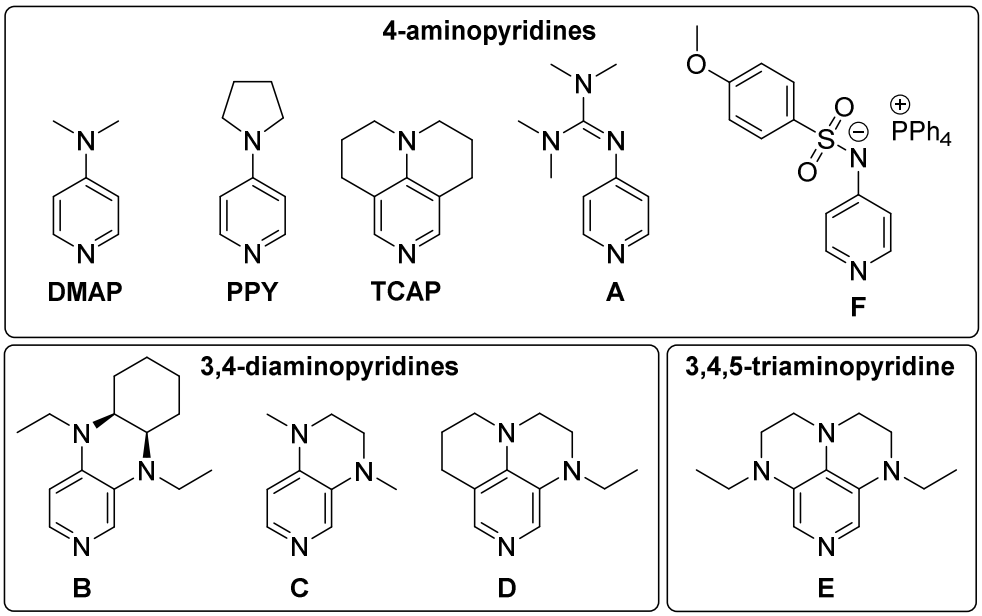

Scheme 3. *Selected pyridine Lewis base organocatalysts.*

Although pyridine-based Lewis base organocatalysts were initially developed for acylation reactions, they are by far not limited to these reactions. Silylation reactions, sulfonylations and the previously discussed RC and MBH reactions are also successfully facilitated by pyridine bases, as well as the activation of isocyanates, with the latter two being used as benchmark reactions in the fourth chapter of this thesis.[6, 11b, 27, 32]

In these cases, the generally accepted mode of activation of the substrate is by attack of the electrophile by the pyridine-nitrogen atom lone pair. The pyridine species thus forms a stabilized pyridinium adduct as shown in Scheme 4 for both DMAP and a simplified anionic Lewis base.[32a]

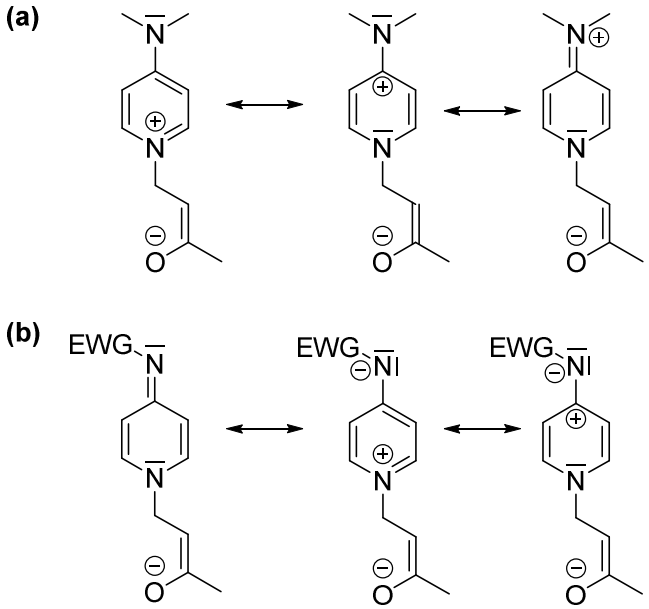

Scheme 4. *Mesomeric forms of the pyridine ring system for Lewis base adducts with example substrate methyl vinyl ketone: (a) shows DMAP-pyridinium ion and (b) represents pyridinyl-amide adduct.*

1.2 Investigation of Lewis Base Organocatalysis

As discussed before in the context of the simplified mechanisms shown in Scheme 1, organocatalyst-mediated reactions are usually multi-step reactions involving complex mechanisms. Several of them are continuously investigated which leads to refined understanding of the process in many cases.[4, 7, 33] Due to this complexity, quantitative evaluation of Lewis Base organocatalysis remains challenging. The following part aims to give a brief overview of the computational and experimental methods used in the studies presented in this thesis.

1.2.1 Computational Investigation of Lewis Base Organocatalysts Using Affinity Values

Computational chemistry offers the possibility to gain deeper insights in reactions and the underlying principles. However, a mechanistic study usually focusses on a narrowly defined system, which enables extensive computational modeling providing a thorough understanding of the separate steps of the catalytic cycle as shown in the second chapter of this thesis.[4] Applied Lewis base organocatalysis on the other hand, usually means having to choose from a variety of catalysts, substrates and solvents at hand. Even considering the continuously increasing computational resources, the number of potential combinations is still prohibitive in terms of computational costs. Especially for catalyst systems with a large conformational

space like the ion pair organocatalysts investigated in the fourth chapter of this thesis, computed catalyst affinity data can be a valuable guideline in both understanding the reactivity and further catalyst development.[6]

The generation of affinity values by computational methods has become a widely applied, fast and reasonably accurate method that has been used on a variety of different systems.[34] In principle, the enthalpy of an isodesmic group transfer reaction of the investigated catalyst against a reference is calculated as shown in Scheme 5. In the given example, a methyl cation is transferred between a substituted pyridine and pyridine as reference Lewis base. The difference in methyl cation affinities (ΔMCA) is obtained.

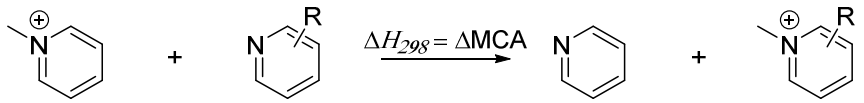

Scheme 5. *Isodesmic group transfer reactions calculated to obtain differences in methyl cation affinities (ΔMCA).*

These affinity values represent the stability of the catalyst-methyl cation adduct and can be used as a measure of carbon Lewis basicity of the organocatalyst towards this smallest possible carbon electrophile. Several comprehensive studies list both a sizable number of MCA values for Lewis base catalysts and assessed computational methods to obtain them,[34, 35] making computation of MCA values a frequently used tool to study carbon Lewis basicities for organocatalysts and ligands.[27, 30c, 30d, 36]

However, the methyl cation is not a frequently encountered species in Lewis base-mediated reactions and does not accurately reflect the substrate-adducts that are expected to be formed in– for example – base-catalyzed acylation- or silylation reactions, regarding both steric and electronic effects. Aided by the increase in available computational resources, acetyl cation affinities (ACAs),[37] silyl cation affinities (SCAs),[33] and recently, in the study forming the fourth chapter of this thesis, phenyl isocyanate affinities (PIAs)[6] have been calculated in the same manner as the previously described MCA values. Scheme 6 shows the isodesmic group transfer reactions for a substituted pyridine and pyridine as Lewis base reference leading to the corresponding ΔACA, ΔSCA, and ΔPIA values.

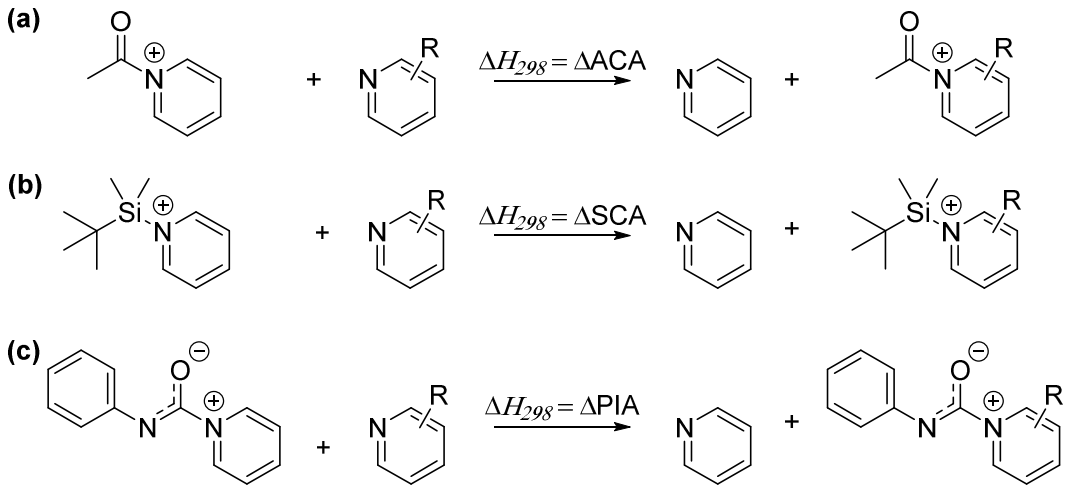

Scheme 6. *Isodesmic group transfer reactions calculated to obtain differences in (a) acetyl cation affinity (ΔACA), (b) silyl cation affinities (ΔSCA), and (c) phenyl isocyanate affinities (ΔPIA).*

Experimentally determined reaction rates have been plotted against computed affinity values and have shown linear correlation in several studies.[6, 15a, 33, 37b, 37d] This procedure can be used to estimate the effect of the Lewis basicity of the catalyst on its activity.[33] Comparison of Scheme 6 with Scheme 1 and Scheme 4 shows why (thermodynamic) affinity values may correlate with experimentally obtained (kinetic) reaction rates. The adducts used to compute the affinity data are models for the intermediates that are expected to be formed in the catalytic cycles of the corresponding reactions by the attack of the Lewis base on the electrophile. These intermediates are frequently considered to be key intermediates of the corresponding catalytic cycle. As the affinity value is a measure of the Lewis basicity of the catalyst towards the electrophile, it influences the concentration by shifting the chemical equilibrium towards the formed intermediate in the case of higher affinity values.[38] Therefore, the affinity values may correlate with the catalyst activity, if the rate determining step is strongly influenced by the concentration of the intermediate adduct.[33]
However, as already stated, reactions mediated by Lewis base organocatalysts usually tend to be more complex processes governed by a series of influencing factors. By measuring effective rates of reactions (k_{eff}), as described in the following, those factors can be accumulated into a condition-specific, quantitative measure of catalyst performance.

1.2.2 Experimental Investigation of Organocatalyst-Mediated Reactions

In the studies that are part of this thesis, we monitored selected benchmark reactions to investigate the effect of catalyst addition under these specific conditions. For measuring selectivities in the study included as the third chapter, competition experiments as shown for an example in Scheme 7 were run until equilibrium was reached. Subsequently, the product mixture was analyzed to calculate the chemoselectivity from the distribution of products and starting materials in an approach originally developed for kinetic resolution in stereochemistry.[5, 39]

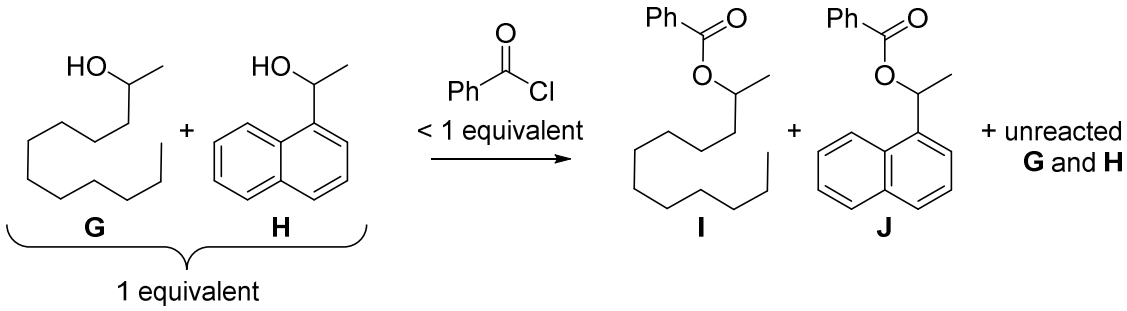

Scheme 7. *Competition experiment performed to measure chemoselectivity.*

With the data of a series of such competition experiments, the selectivity factor *S* is either obtained using equations developed by Kagan,[7, 32c, 39] or by fitting the concentration-dependent chemoselectivity to simulated selectivity curves as it was done in the third chapter of this thesis and earlier studies of the Zipse group.[5, 33b] The selectivity factor *S* is the ratio of the two effective rates for esterification of the corresponding alcohols.

Effective rates of reactions can also be obtained by direct rate kinetic measurements, as performed in chapters two and four by observing the time-dependent reaction progress of selected benchmark reactions.[4, 6] Reaction progress can be measured by NMR spectroscopy, gas chromatography, IR spectroscopy or other analytical methods. The obtained turnover values are then evaluated based on a

proposed mechanism by numerical simulation or fitting of an effective rate-law equation to give an effective rate k_{eff}.[40] Figure 1 (taken from the fourth chapter of this thesis, see Chapter 4, p. 185) shows an example of one of the employed benchmark reactions along with the measured turnover values and curves fitted based on the results of simulations.[6]

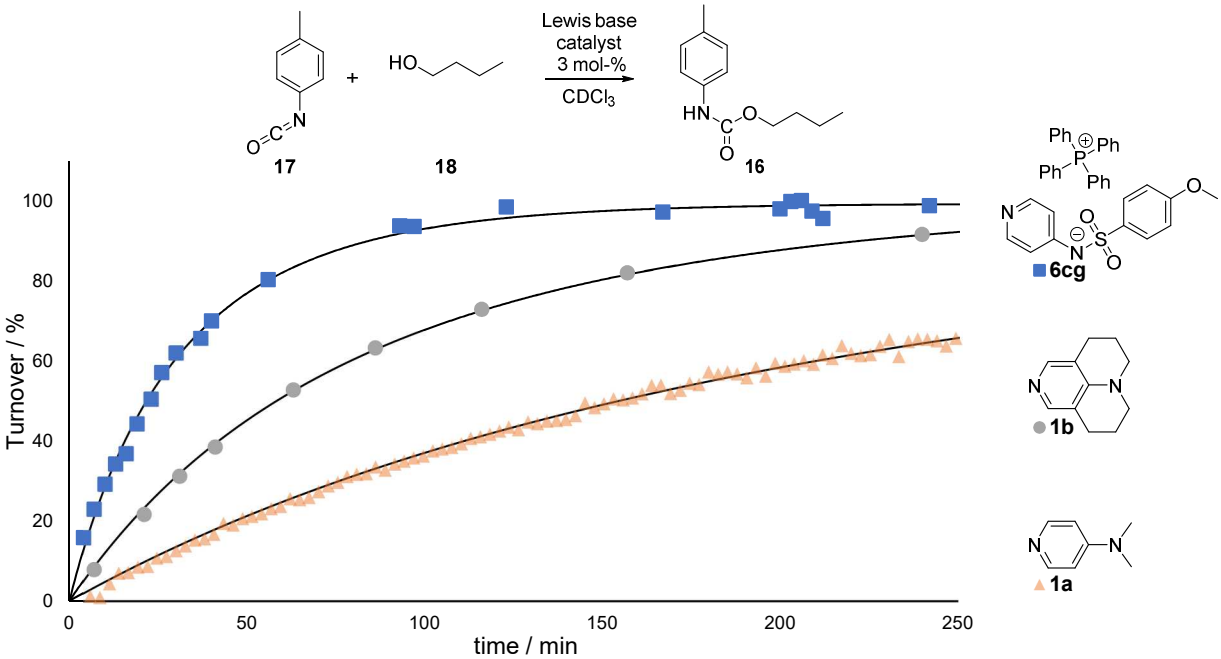

Figure 1. *Measured turnover values and fitted curves obtained for the Lewis base catalyzed reaction of p-tolyl isocyanate with n-butanol. The figure was copied from chapter 4 (labeled there as Figure 3a).*[d]

This system-specific mode of investigation of the effect of addition of Lewis base organocatalyst gives very reliable data for the chosen benchmark reaction. However, generalization of this data for different reactions or conditions is difficult as all factors present are represented. For the purpose of comparing the activity of a range of Lewis base organocatalysts however, it is a trusted tool, that has been used in several studies and aided in answering queries into mechanistic processes.[15, 27, 37d]

It should also be noted, that less elaborate approaches like stopping all reactions after the time it took the most active catalyst to convert all substrate and then comparing the turnover have also been used successfully to compare Lewis base organocatalyst activity.[25] However, as with most methods that rely on a single point of observation, the possibility of getting insight beyond the observable is potentially limited.

[d] Reproduced with permission from *J. Org. Chem.* **2020**, *85*, 5390 – 5402 © 2020 American Chemical Society.

References

[1] a) K. A. Ahrendt, C. J. Borths, D. W. C. MacMillan, *J. Am. Chem. Soc.* **2000,** *122,* 4243-4244; b) F. Wöhler, J. Liebig*, Ann. Pharm.* **1832**, *3*, 249 – 282.

[2] P. I. Dalko, L. Moisan, *Angew. Chem. Int. Ed.* **2004**, *43*, 5138 – 5175.

[3] a) S. E. Denmark, G. L. Beutner, *Angew. Chem. Int. Ed.* **2008**, *47*, 1560 – 1638; b) G. N. Lewis, Valence and The Structure of Atoms and Molecules, Chemical Catalog, New York, **1923**.

[4] J. Helberg, Y. OE, H. Zipse, *Chem. Eur. J.* **2018**, *24*, 14387 – 14391.

[5] J. Helberg, M. Marin-Luna, H. Zipse, *Synthesis* **2017**, *49*, 3460 – 3470.

[6] J. Helberg, T. Ampßler, H. Zipse, *J. Org. Chem.* **2020**, *85*, 5390 – 5402.

[7] M. Marin-Luna, P. Patschinski, H. Zipse, *Chem. Eur. J.* **2018**, *24,* 15052 – 15058.

[8] H. Guo, Y. C. Fan, Z. Sun, Y. Wu, O. Kwon, *Chem. Rev*. **2018**, *118*, 10049 − 10293.

[9] a) L. Horner, K. Klupfel, *Liebigs Ann. Chem.* **1955**, *591*, 69 – 98; b) L. Horner, W. Jurgeleit, K. Klupfel, *Liebigs Ann. Chem.* **1955**, *591*, 108 − 117.

[10] M. M. Rauhut, H. Currier (American Cyanamid Company), US3074999, **1963**.

[11] a) C. E. Aroyan, A. Dermenci, S. J. Miller, *Tetrahedron*, **2009**, *65*, 4069 –4084; b) A. M. Wensley, N. T. McDougal, S. E. Schaus, in Lewis Base Catalysis in Organic Synthesis (Eds.: E. Vedejs, S. E. Denmark), Wiley-VCH, Weinheim, **2016**, p. 655 – 714.

[12] K. Morita, Z. Suzuki, H. Hirose, *Bull. Chem. Soc. Jpn.* **1968**, *41*, 2815 − 2816.

[13] A. B. Baylis, M. E. D. Hillman, (Cleanese Corporation), DE2155113A1, **1971**; A. B. Baylis, M. E. D. Hillman, (Cleanese Corporation), US3743669, **1973**.

[14] a) Y. Wei, M. Shi, *Chem. Rev.* **2013**, *113*, 6659 – 6690; b) H. Pellissier, *Tetrahedron*, **2017**, *73*, 2831 – 2861.

[15] a) C. Lindner, R. Tandon, Y. Liu, B. Maryasin, H. Zipse, *Org. Biomol. Chem.* **2012**, *10*, 3210 – 3218; b) C. Lindner, Y. Liu, K. Karaghiosoff, B. Maryasin, H. Zipse, *Chem. Eur. J.* **2013**, *19*, 6429 – 6434.

[16] a) A. W. v. Hofmann, *Ber. Dtsch. Chem. Ges.* **1870**, *3*, 761 – 772; b) K. H. Slotta, R. Tschesche, *Ber. Dtsch. Chem. Ges.* **1927**,*60*, 295 – 301.

[17] a) J. Köcher (Bayer MaterialScience AG), DE102006023262A1, **2007**; J. Köcher (Bayer MaterialScience AG), US20070270565A1, **2007**; b) J. S. Tang, J. G. Verkade, *Angew. Chem. Int. Ed.* **1993**, *32*, 896 – 898; c) J. N. Gibb, J. M. Goodman, *Org. Biomol. Chem.* **2013**, *11*, 90 – 97; d) Z. Pusztai, G. Vlad, A. Bodor, I. T. Horvath, H. J. Laas, R. Halpaap, F. U. Richter, *Angew. Chem. Int. Ed.* **2006**, *45*, 107 – 110; e) U. Tracht, F. U. Richter*, Macromol. Symp.* **2013**, *324*, 33 – 40.

[18] A. Einhorn, F. Hollandt, *Liebigs Ann. Chem*. **1898**, *301*, 95 – 115.

[19] L. M. Litvinenko, A. I. Kirichenko, *Dokl. Akad. Nauk SSSR, Ser. Khim.* **1967**, *176*, 97 – 100.

[20] a) W. Steglich, G. Höfle, *Angew. Chem. Int. Ed. Engl.* **1969**, *8*, 981; b) A. Hassner, A. P. Hart, J. A. Pigza in Encyclopedia of Reagents for Organic Synthesis, Vol. 8 (Ed.: P. L. Fuchs), Wiley, New York, **2016**, p.1 – 6.

[21] a) W. Steglich, G. Höfle, *Tetrahedron Lett.* **1970**, *11,* 4727 – 4730; b) G. Höfle, W. Steglich, H. Vorbrüggen, *Angew. Chem.* **1978**, *90*, 602 – 615.

[22] M. R. Heinrich, H. S. Klisa, H. Mayr, W. Steglich, H. Zipse, *Angew. Chem. Int. Ed.* **2003**, *42*, 4826 –4828.

[23] A. Hassner, L. R. Krepski, V. Alexanian, *Tetrahedron* **1978**, *34*, 2069 – 2076.

[24] I. Held, E. Larionov, C. Bozler, F. Wagner, H. Zipse, *Synthesis* **2009**, *13*, 2267 - 2277.

[25] S. Singh, G. Das, O. V. Singh, H. Han, *Org. Lett.* **2007**, *9*, 401 – 404.

[26] a) I. Held, S. Xu, H. Zipse, *Synthesis* **2007**, *8*, 1185 – 1196; b) H. Zipse, I. Held, (Ludwig-Maximilians-Universität München), DE102006057580B3, **2008**.

[27] R. Tandon, T. Unzner, T. A. Nigst, N. De Rycke, P. Mayer, B. Wendt, O. R. P. David, H. Zipse. *Chem. Eur. J.* **2013**, *19*, 6435 – 6442.

[28] V. Barbier, F. Couty, O. R. P. David, *Eur. J. Org. Chem.* **2015**, *17*, 3679 – 3688.

[29] E. Follet, H. Zipse, S. Lakhdar, A. R. Ofial, G. Berionni, *Synthesis* **2017**, *49*, 3495 - 3504.

[30] a) E. Vedejs, X. *Chen, J. Am. Chem. Soc.* **1996**, *118*, 1809 – 1810; b) C. Spivey, A. Maddaford, A. Redgrave, *Org. Prep. Proced*. **2000**, *32*, 331 – 365; c) P. Hommes, C. Fischer, C. Lindner, H. Zipse, H.-U. Reissig, *Angew. Chem. Int. Ed.* **2014**, *53*, 7647 – 7651; d) M. Kleoff, S. Suhr, B. Sarkar, R. Zimmer, H.-U. Reissig, M. Marin-Luna, H. Zipse, *Chem. Eur. J.* **2019**, *25,* 7526 – 7533.

[31] J. Köcher, H. J. Laas (Bayer MaterialScience AG), DE10336184A1, **2005**; J. Köcher, H. J. Laas (Bayer MaterialScience AG), US20050033006A1, **2005**; J. Köcher, H. J. Laas (Bayer MaterialScience AG), WO2005016984A1, **2005**.

[32] a) N. De Rycke, F. Couty, O. R. P. David*, Chem. Eur. J.* **2011**, *17*, 12852 – 12871; b) P. Patschinski, H. Zipse, *Org. Lett.* **2015**, *17*, 3318 – 3321; c) M. Marin-Luna, B. Poelloth, F. Zott, H. Zipse, *Chem. Sci.* **2018**, *9,* 6509 – 6515; d) E. Guibe-Jampel, M. Wakselman, D. Raulais, *Chem. Commun.* **1980**, 993 – 994; e) J. N. Naoum, K. Chandra, D. Shemesh, R. B. Gerber, C. Gilon, M, Hurevich, *Beilstein J. Org. Chem*. **2017**,*13*, 806 – 816.

[33] a) P. Patschinski, C. Zhang, H. Zipse, *J. Org. Chem.* **2014**, *79*, 8348 – 8357; b) P. Patschinski, Dissertation, Ludwig-Maximilians-Universität München (München), **2015**.

[34] a) C. Lindner, R. Tandon, B. Maryasin, E. Larionov, H. Zipse, *Beilstein J. Org. Chem.* **2012**, *8*, 1406 – 1442; b) C. Lindner, B. Maryasin, F. Richter, H. Zipse, *J. Phys. Org. Chem.* **2010**, *23*, 1036 – 1042; c) Y. Wei, G. N. Sastry, H. Zipse, *J. Am. Chem. Soc.* **2008**, *130*, 3473 – 3477.

[35] Y. Wei, T. Singer, H. Mayr, G. N. Sastry, H. Zipse, *J. Comp. Chem.* **2008**, *29*, 291 – 297.

[36] A. Levens, F. An, M. Breugst, H. Mayr, D. W. Lupton, *Org.Lett.* **2016**, *18*, 3566 − 3569.

[37] a) A. Tamaki, S. Kojima, Y. Yamamoto, *J. Org. Chem.* **2016**, *81*, 8710 – 8721; b) R. Tandon, H. Zipse in Lewis Base Catalysis in Organic Synthesis (Eds.: E. Vedejs, S. E. Denmark), Wiley-VCH, Weinheim, **2016**, p. 121 – 144; c) R. Tandon, Dissertation, Ludwig-Maximilians-Universität München (München), **2013**; d) E. Larionov, F. Achrainer, J. Humin, H. Zipse, *ChemCatChem.* **2012**, *4*, 559 – 566.

[38] S. Lakhdar in Lewis Base Catalysis in Organic Synthesis (Eds.: E. Vedejs, S. E. Denmark), Wiley-VCH, Weinheim, **2016**, p. 85 – 118.

[39] H. B. Kagan, J. C. Fiaud, *Top. Stereochem.* **1988**, *18*, 249 – 330.

[40] E. Larionov, Dissertation, Ludwig-Maximilians-Universität München (München), **2011**; C. Lindner, Dissertation, Ludwig-Maximilians-Universität München (München), **2012**.

Chapter 2. Mechanistic Analysis and Characterization of Intermediates in the Phosphane-Catalyzed Oligomerization of Isocyanates

Julian Helberg, Yohei Oe, and Hendrik Zipse

Chem. Eur. J. **2018**, *24,* 14387 – 14391.

Authors contributions

H.Z. conceived the project. The experimental study was designed jointly by J.H. and H.Z. and executed by J.H. The computational strategy was designed by H.Z. and Y.O. Computational benchmarking was done by Y.O., who also started the computational investigation. The computational results presented in the study were obtained by J.H. The manuscript was jointly written by J.H., Y.O. and H.Z. The supporting information was prepared by J.H. and H.Z.

Copyright

(Link to article: https://onlinelibrary.wiley.com/doi/full/10.1002/chem.201804016)

The full supporting information can be found following the link below:
https://onlinelibrary.wiley.com/action/downloadSupplement?doi=10.1002%2Fchem.201804016&file=chem201804016-sup-0001-misc_information.pdf

Additional information

The supporting information presented in this thesis is a shortened and altered version of the originally published supporting information and has been optimized for printing purposes. The published files of the manuscript and the supporting information can be found on the electronic attachment to this thesis. For comparison of this thesis and the original SI file, the numbering includes the original caption as shown below:

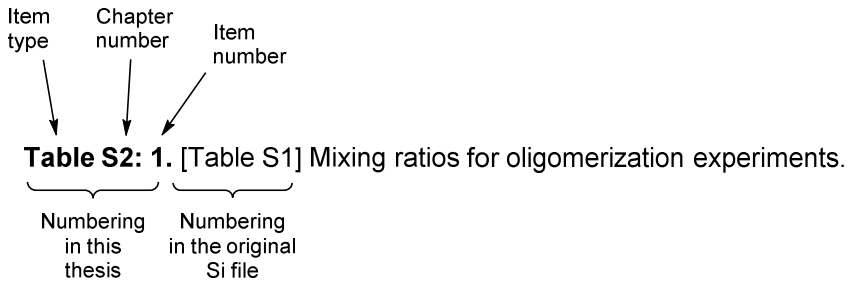

ChemPubSoc Europe
DOI: 10.1002/chem.201804016
CHEMISTRY A European Journal
Communication

Organocatalysis

Mechanistic Analysis and Characterization of Intermediates in the Phosphane-Catalyzed Oligomerization of Isocyanates

Julian Helberg,[a] Yohei Oe,[b] and Hendrik Zipse*[a]

Abstract: The mechanism of the oligomerization of aliphatic isocyanates catalyzed by trialkylphosphanes has been studied through low temperature ^{31}P and ^{15}N NMR spectroscopy combined with computational chemistry. A revised mechanism is proposed that contains several (spiro)cyclic pentacoordinate phosphorous intermediates. Previously reported spectroscopic data of a transient intermediate has been reevaluated and assigned to a cyclic intermediate containing a P–N bond by experiments with ^{15}N-labeled isocyanate. ^{13}C, ^{15}N, and ^{31}P NMR shifts that support this assignment have been calculated using quantum chemical methods.

The oligomerization of aliphatic isocyanates **1** using Lewis base catalysts is an important industrial process for the synthesis of building blocks for highly durable polyurethane (PU) coatings.[1] The use of oligomers provides a higher degree of safety during the polymerization process due to significantly lower vapor pressures and provides the basis for tuning polymer properties.[2] Addition of (aliphatic) isocyanurates **3** often enhances the physical properties of polymers, for example in the production of flame-retardant materials used for the lamination of electrical devices.[3] Depending on the Lewis base catalyst and the reaction conditions, the oligomerization of isocyanates generates variable amounts of uretdiones **2**, isocyanurates **3**, iminooxadiazinediones **4**, and higher oligomers (Scheme 1 A). In the case of trialkylphosphane-catalyzed oligomerizations of aliphatic isocyanates, the reaction is believed to be initiated through attack of phosphane **5** at the central carbon atom of isocyanate **1** and formation of zwitterion **6** as a first transient intermediate. Subsequent reaction of **6** with a second equivalent of isocyanate then generates acyclic, tetracoordinated phosphane intermediate **7L**, whose detection by low temperature ^{31}P and ^{13}C NMR spectroscopy was reported by Horvath et al. for the oligomerization of aliphatic isocyanate **1** catalyzed by trialkylphosphane **5**.[2a,4] The reaction then either proceeds through elimination of catalyst **5** and (reversible) formation of uretdione **2**, or addition of a third isocyanate monomer and elimination of catalyst **5** to form isocyanurate **3** or iminooxadiazinedione **4**. Based on a computational study on the azaphosphatrane **14**-catalyzed oligomerization of isocyanates, Goodman et al. proposed another pathway to the trimers **3** and **4** by reaction of monoadduct **6** with uretdione **2**. They also suggested stabilization of intermediate **7** as a five-membered ring in which O coordinates to P (labeled **7O** in this study).[5]

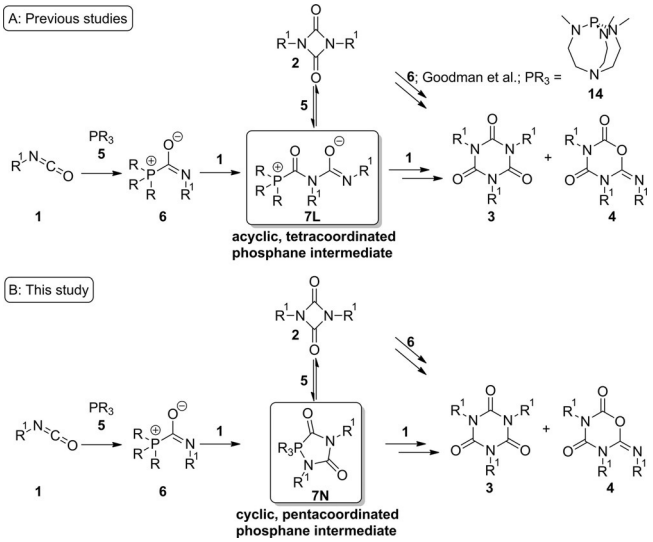

Scheme 1. Simplified mechanism showing key intermediates in the phosphane-catalyzed oligomerization of aliphatic isocyanates **1** in previous studies (A) and in the current study (B).

The ^{31}P NMR signal at −54.0 ppm assigned by Horvath et al. to the acyclic, tetracoordinated phosphane intermediate **7L** neither fits the chemical shift (>0 ppm) usually associated with tetracoordinated phosphorus,[2a,6] nor the one published for monoadduct **6** of azaphosphatrane **14** and phenyl isocyanate (+29.46 ppm) by Verkade.[7] This prompted us to reinvestigate the mechanism proposed for the phosphane-catalyzed oligomerization of alkyl isocyanates **1**, using a combination of computational NMR shift predictions and experimental NMR measurements employing ^{15}N-labeled isocyanate. Herein, we show a quantitative assignment for the signals reported previously and in consequence, propose a new mechanism includ-

[a] J. Helberg, Prof. Dr. H. Zipse
Department of Chemistry, LMU München
Butenandtstrasse 5–13, 81377 München (Germany)
E-mail: zipse@cup.uni-muenchen.de
Homepage: http://www.cup.lmu.de/oc/zipse/
[b] Prof. Y. Oe
Graduate School of Life and Medical Sciences
Department of Biomedical Information
Faculty of Life and Medical Sciences, Doshisha University
1-3 Tatara Miyakodani, Kyotanabe, Kyoto 610-0394 (Japan)
Supporting information and the ORCID identification number(s) for the author(s) of this article can be found under: https://doi.org/10.1002/chem.201804016.

ing key intermediate **7N** for the phosphane-catalyzed oligomerization of aliphatic isocyanates (Scheme 1 B).

Initially, we reproduced the kinetic measurements and low-temperature NMR experiments published by Horvath et al. and were able to confirm these results while using a different analytical method for the kinetics.[2a] Figure 1 shows the time-resolved oligomerization of *n*-hexyl isocyanate **1a** measured by ^{1}H NMR, which indicates that the initial formation of dimer **2a** and subsequent formation of trimers **3a** and **4a** proceeds in a tightly coupled fashion.

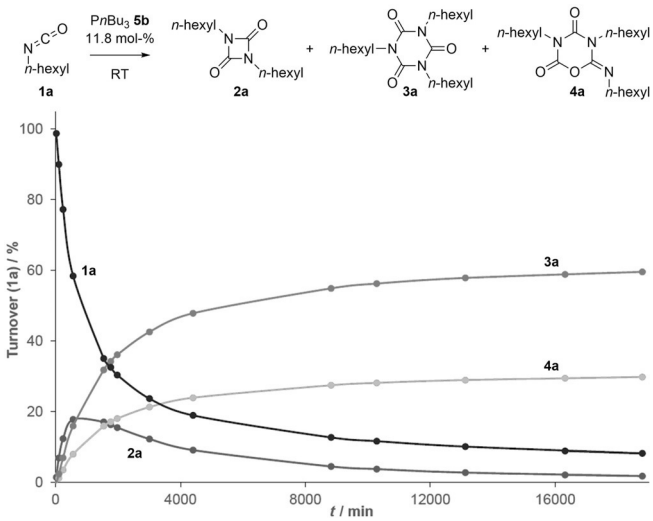

Figure 1. Time-resolved oligomerization of **1a** observed by ^{1}H NMR spectroscopy.

Low-temperature NMR measurements were performed under neat conditions on oligomerization reactions of isocyanate **1a** catalyzed by 50 mol% **5b**. Figure 2 (top) shows the proton decoupled ^{31}P NMR spectrum at −20 °C with integrals for two species: catalyst **5b** and intermediate **7ab**. Bis-adduct **7ab** appears as a temperature-dependent signal at −55.7 ± 0.4 ppm with an integral of approximately 0.5% of free phosphane **5b** that broadens and shifts with increasing temperature (bottom). Because we suspected the signal of intermediate **7ab** to represent one of the cyclic, pentacoordinate intermediates **7Nab** or **7Oab** rather than acyclic, tetracoordinated **7Lab** (Scheme 2), the low temperature NMR measurements were repeated with ^{15}N-labeled *n*-hexyl isocyanate **1a^{15}**.

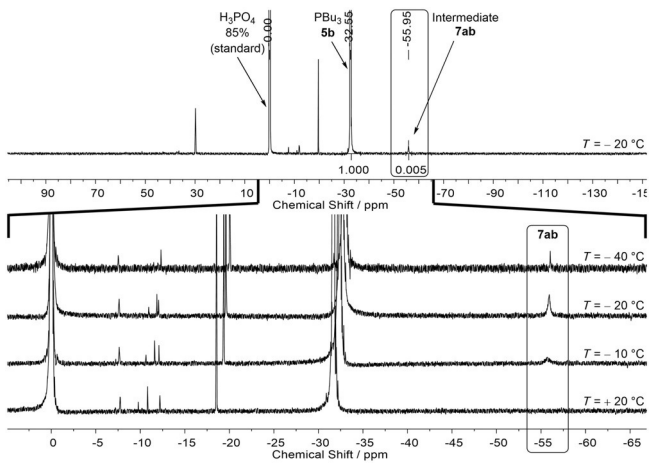

Figure 2. ^{31}P{^{1}H} NMR spectra of the reaction of **1a** and **5b** (50 mol%). Top: at −20 °C; bottom: spectra at different temperatures.

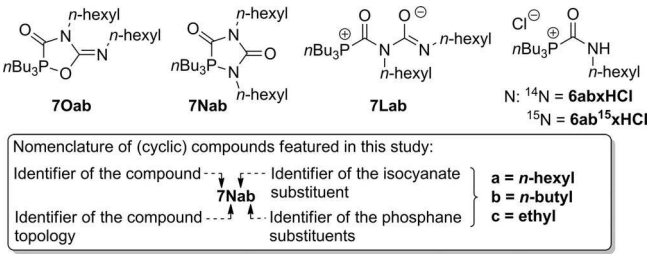

Scheme 2. Conceivable structures for intermediate **7ab** and H^{+}-trapped model compound **6abxHCl**.

This allowed for the differentiation of the possible intermediates shown in Scheme 2, based on their ^{31}P/^{15}N couplings and ^{15}N chemical shifts. **1a^{15}** was obtained in three steps starting from heptanoic anhydride and $^{15}NH_4Cl$ (see the Supporting Information). In order to obtain a stable reference compound structurally related to the potential intermediate, the H^{+}-trapped phosphonium **6ab×HCl** and its ^{15}N-labeled analogue **6ab^{15}×HCl** were synthesized in situ by mixing of equimolar amounts of isocyanate **1a** and tri-*n*-butylphosphonium chloride **16b** (see the Supporting Information). This resulted in next-to-quantitative formation of **6ab×HCl**, as verified by ^{1}H, ^{31}P, ^{13}C NMR spectroscopy and high resolution mass spectrometry. The ^{31}P NMR spectrum of compound **6ab×HCl** shows a singlet at a typical "phosphonium" chemical shift of +29.6 ppm that turns into a doublet (J = 28.4 Hz) in the case of the ^{15}N-labled **6ab^{15}×HCl**. The ^{15}N NMR spectrum of this compound shows a doublet of doublets at −236.54 ppm, formed by ^{1}H/^{15}N coupling (J = 90.7 Hz) and ^{31}P/^{15}N coupling (J = 28.4 Hz).

Repeating the earlier NMR measurements at −40 °C using **1a^{15}** and 50 mol% **5b** yields a proton decoupled ^{31}P spectrum where the intermediate signal appears as a well-defined doublet of doublets with coupling constants of J = 50.6 Hz and J = 27.7 Hz (Figure 3). ^{15}N NMR shows the corresponding doublets at −218.2 ppm (J = 31.5 Hz) and −243.7 ppm (J = 53.6 Hz).

The minor deviation in the coupling constants results most likely from the ^{15}N NMR being measured in a proton-coupled fashion. This is required because the doublet at −243.7 ppm does not appear in proton decoupled ^{15}N NMR, presumably due to nuclear Overhauser effects. The doublet at −218.2 ppm gives a coupling constant of J = 27.5 Hz in the proton decoupled measurements in complete agreement with the ^{31}P NMR results (see the Supporting Information).

Since the ^{15}N atoms show coupling only to the ^{31}P atom, assignment of both signals is possible based on the spectroscopic data for **6ab^{15}×HCl**. Comparison of the coupling constants in ^{15}N NMR spectroscopy clearly shows that the doublet gener-

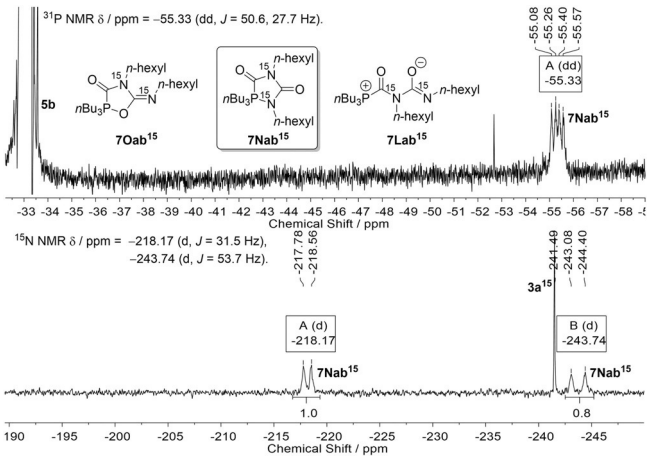

Figure 3. NMR spectra of the reaction of **1a**[15] and **5b** (50 mol%) at −40 °C: $^{31}P\{^1H\}$ spectrum showing intermediate **7Nab**[15] to form a doublet of doublets (top) and ^{15}N spectrum with the corresponding doublets (bottom).

ated by intermediate **7Nab** at −218.17 ppm (J = 27.5–31.5 Hz) represents the nitrogen atom next to the P-bound carbonyl group. Because the other ^{15}N doublet at −243.74 ppm (J = 53.6 Hz) shows a much larger coupling constant and therefore stronger coupling, we see this as evidence of the second ^{15}N atom being closer to the phosphorous atom in the detected intermediate. This strongly supports assignment of cyclic, pentacoordinate phosphane **7Nab**[15] as the observed intermediate, as highlighted in Figure 3. The preference of phosphorous atoms to form cycles by bonding to isocyanate nitrogen atoms rather than the oxygen atoms is not unprecedented. Neutral cyclic monoalkyl phosphanes structurally similar to **7Nab** were generated by condensation of phospholenes and isocyanates, and more recently Grützmacher et al. reported several cyclic, anionic P–N bond containing species found in the cyclo-oligomerization of isocyanates by "P^-" anions.[8]

Having obtained experimental evidence that the observed intermediate is cyclic, pentacoordinate phosphane **7Nab**, we decided to use computational chemistry to further elucidate the reaction mechanism. We found that consistent results were obtained at the B2PLYP/cc-pVTZ//B3LYP/6–31+G(d,p) level of theory and used a SMD($CHCl_3$) solvation model to simulate the rather polar conditions in the oligomerization mixture.[9] Figure 4 shows the potential energy surface (gas phase ΔH_{298} and solution phase ΔG_{298}) for the triethylphosphane-(**5c**)-catalyzed oligomerization of ethyl isocyanate **1c**. In the following, the discussion focusses on the gas-phase enthalpy values (ΔH_{298}). It is noteworthy that acyclic intermediate **7Lcc** is much less stable than the corresponding cyclic isomers **7Occ** and **7Ncc**, which are both located significantly lower in energy. Of these two cyclic bis-adducts, **7Ncc** is slightly preferred.

While initial formation of the cyclic intermediates **7Occ** and **7Ncc** is possible through reaction of monoadduct **6cc** with another monomer **1c**, interconversion is also possible via transition state **TSRcc** located +58.8 kJ mol^{-1} above **7Ncc**. Uretdione **2c** is exclusively formed from cyclic intermediate **7Ncc** through transition state **TSD0cc**. Dimer **2c** is then able to react with monoadduct **6cc** forming previously unreported *spiro*-intermediate **9cc**, which is conceptually similar to the *spiro*-tetramers formed by reductive oligomerization in the presence of silanes reported by Süss-Fink.[10] Acyclic, trimeric intermediate **8cc** is either formed by interconversion of **9cc** through transition state **TSD2cc** or by addition of one molecule of **1c** to cyclic adduct **7Occ** through transition state **TS3cc**. Trimers **3c** and **4c** are finally obtained from **8cc** via the low-lying transition states **TS5cc** and **TS4cc**. Based on both the experimental and computational results, we propose the revised reaction mechanism shown in Scheme 3.

For all intermediates found in the revised mechanism, ^{13}C, ^{15}N, and ^{31}P NMR chemical shifts (see Figure 5) were predicted at the B3LYP/IGLO-III//B3LYP/6–31+G(d,p) level of theory (see the Supporting Information). The methodology used combines

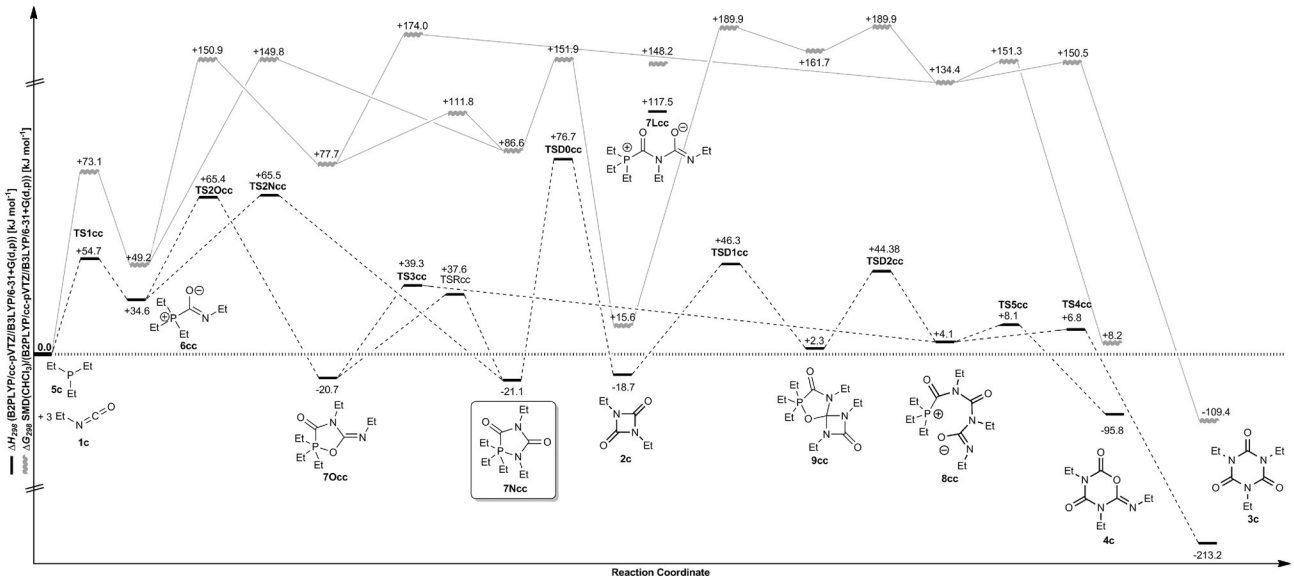

Figure 4. Potential energy surface of the oligomerization of ethyl isocyanate **1c** catalyzed by triethylphosphane **5c** [in kJ mol^{-1}].

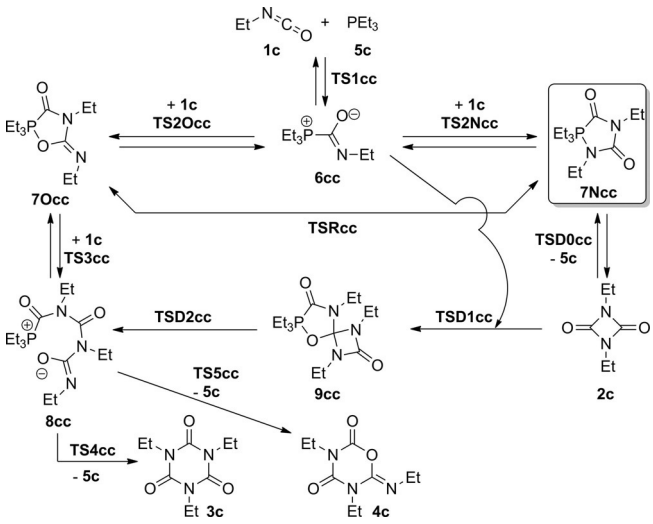

Scheme 3. Proposed reaction mechanism of the (alkyl) phosphane-catalyzed oligomerization of alkyl isocyanates formulated for all-ethyl substituents in analogy to the computational study.

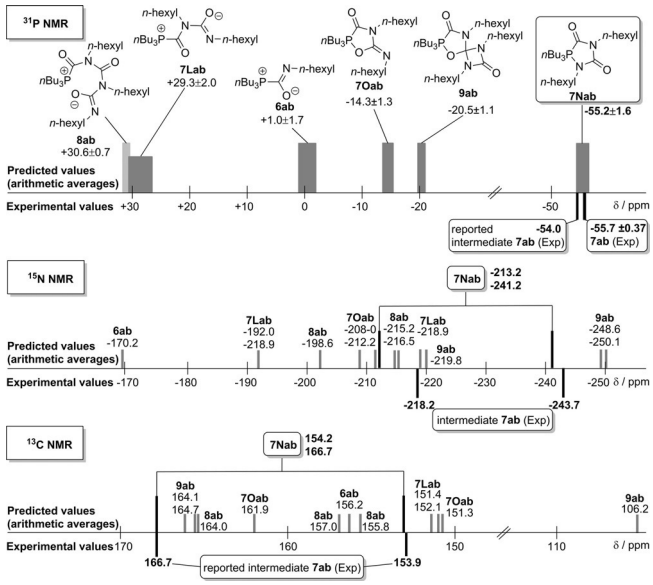

Figure 5. Comparison of predicted and experimentally obtained ^{31}P, ^{15}N, and ^{13}C NMR shifts.

theoretically calculated shieldings for the ethyl-substituted systems shown in Figure 4 with a system of increments for the influence of longer alkyl chain substituents. The predicted ^{31}P chemical shifts perfectly fit our assignment of cyclic, pentacoordinate intermediate **7Nab** to the signals reported by Horvath and Richter (theoretically predicted: −55.2 ppm; experimentally found: −55.6 ppm here and −55.0 ppm in ref. [2]).[2a] In addition, the predicted ^{31}P chemical shift for acyclic intermediate **7Lab** of +29.3 ppm is that of a "typical" phosphonium species. In case of ^{15}N NMR spectroscopy, the predicted signals vary more from the measured ones, probably because of the partially anionic character of the nitrogen atoms in the intermediates that was not reflected in our set of reference compounds. Still, **7Nab** is the only intermediate whose predicted NMR shifts fit for all three measured nuclei in complete agreement with all other results.

In conclusion, we provide here a comprehensive study on the phosphane-catalyzed oligomerization of aliphatic isocyanates, which includes the validation of earlier ^{31}P NMR and kinetic measurements,[2a] and the combined experimental/theoretical analysis of ^{15}N and ^{31}P NMR spectral data in reactions of ^{15}N-labeled isocyanates. Calculation of the potential energy surface leads us to a revised reaction mechanism featuring previously unknown spiro intermediate **9** formed from uretdione **2**. Cyclic intermediate **7N** is responsible for the signals visible at low temperature NMR measurements as shown by the prediction of ^{31}P, ^{15}N, and ^{13}C chemical shifts. Further evidence was obtained from the ^{31}P–^{15}N couplings and the multiplicities found for signals in low temperature NMR measurements. The new mechanism provides the basis for a better understanding of an important industrial process and its possible improvement through the development of new catalyst systems. This study also shows the potential of the employed methodology to solve further unanswered questions of isocyanate activation by organocatalysts.[11]

Acknowledgements

The authors wish to thank Dr. D. Stephenson (LMU München) for recording the low-temperature NMR spectra, Dr. F. Richter (Covestro AG) for fruitful discussions and the Leibnitz Supercomputer Centre (www.lrz.de) for generous allocation of computational resources.

Conflict of interest

The authors declare no conflict of interest.

Keywords: computational chemistry · isotopic labeling · Lewis base organocatalysis · NMR spectroscopy · reaction mechanisms

[1] a) C. Six, F. Richter in *Isocyanates, Organic, Ullman's Encyclopedia of Industrial Chemistry*, Wiley-VCH, **2003**; b) F. Richter, *Nachr. Chem.* **2007**, *55*, 380–384.
[2] a) Z. Pusztai, G. Vlad, A. Bodor, I. T. Horvath, H. J. Laas, R. Halpaap, F. U. Richter, *Angew. Chem. Int. Ed.* **2006**, *45*, 107–110; *Angew. Chem.* **2006**, *118*, 113–116; b) H. J. Laas, R. Halpaap, J. Pedain, *J. Prakt. Chem.* **1994**, *336*, 185–200.
[3] a) S. M. Raders, J. G. Verkade, *J. Org. Chem.* **2010**, *75*, 5308–5311; b) H. A. Duong, M. J. Cross, J. Louie, *Org. Lett.* **2004**, *6*, 4679–4681.
[4] U. Tracht, F. U. Richter, *Macromol. Symp.* **2013**, *324*, 33–40.
[5] J. N. Gibb, J. M. Goodman, *Org. Biomol. Chem.* **2013**, *11*, 90–97.
[6] a) B. E. Mann, *J. Chem. Soc. Perkin Trans. 2* **1972**, 30–34; b) B. Maryasin, H. Zipse, *Phys. Chem. Chem. Phys.* **2011**, *13*, 5150–5158; c) M. M. Kayser, K. L. Hatt, D. L. Hooper, *Can. J. Chem.* **1991**, *69*, 1929–1939.
[7] J. S. Tang, J. G. Verkade, *Angew. Chem. Int. Ed. Engl.* **1993**, *32*, 896–898; *Angew. Chem.* **1993**, *105*, 934–936.
[8] a) F. U. Richter, *Chem. Eur. J.* **2009**, *15*, 5200–5202; b) D. Heift, Z. Benko, H. Grützmacher, A. R. Jupp, J. M. Goicoechea, *Chem. Sci.* **2015**, *6*, 4017–4024.
[9] a) A. D. Becke, *J. Chem. Phys.* **1993**, *98*, 5648–5652; b) S. Grimme, *J. Chem. Phys.* **2006**, *124*, 034108–034101; c) A. V. Marenich, C. J. Cramer, D. G. Trular, *J. Phys. Chem. B* **2009**, *113*, 6378–6396.

[10] a) G. Süss-Fink, G. Herrmann, G. F. Schmidt, *Polyhedron* **1988**, *7*, 2341 – 2344; b) G. Herrmann, G. Süss-Fink, *Chem. Ber.* **1985**, *118*, 3959 – 3965; c) G. Süss-Fink, G. Herrmann, U. Thewalt, *Angew. Chem. Int. Ed. Engl.* **1983**, *22*, 880 – 881; *Angew. Chem.* **1983**, *95*, 899 – 900.

[11] a) H. Sardon, A. Pascual, D. Mecerreyes, D. Taton, H. Cramail, J. L. Hedrick, *Macromolecules* **2015**, *48*, 3153 – 3165; b) J. Alsarraf, Y. A. Ammar, F. Robert, E. Cloutet, H. Cramail, Y. Landais, *Macromolecules* **2012**, *45*, 2249 – 2256.

Manuscript received: August 6, 2018
Accepted manuscript online: August 7, 2018
Version of record online: September 3, 2018

2.1 Supporting Information

For: *Mechanistic Analysis and Characterization of Intermediates in the Phosphane-Catalyzed Oligomerization of Isocyanates*

2.1.1 General Experimental Information

All air and water sensitive manipulations were carried out under N_2-atmosphere using standard Schlenk techniques. Highly sensitive compounds were brought into the glovebox immediately after synthesis and/or purification and handled there under argon atmosphere. All commercial chemicals were of reagent grade and used as received unless noted otherwise. $CDCl_3$ was refluxed for at least one hour over CaH_2 and subsequently distilled. ^{1}H, ^{13}C, ^{31}P and ^{15}N NMR spectra were recorded on Varian INOVA 400 or Bruker Avance III HD 400 machines, on a Bruker Ascend 400 machine or on a Varian Mercury 200 MHz spectrometer. All ^{1}H chemical shifts are reported in ppm (δ) relative to TMS (0.00, internal standard); ^{13}C chemical shifts are reported in ppm (δ) relative to $CDCl_3$ (77.16, internal standard), ^{31}P chemical shifts are reported in ppm (δ) relative to 85% H_3PO_4 in water (0.00, external standard) and ^{15}N chemical shifts are reported in ppm δ) relative to $MeNO_2$ (0.00, internal standard).

2.1.2 Synthesis of ^{15}N-Labeled Compounds

^{15}N-labeled *n*-hexyl isocyanate **1a^{15}** was synthesized in three steps starting from $^{15}NH_4Cl$ as shown in **Scheme S2: 1**. The first step gave ^{15}N-heptanamide **10a^{15}** which was transformed into ^{15}N-methyl hexylcarbamate **11a^{15}** by Hofmann rearrangement in methanol.[1] Carbamate **11a^{15}** was then reacted with boron trichloride to give ^{15}N-hexyl isocyanate **1a^{15}**.[2] By protecting the isocyanate as carbamate, we were able to recycle 36% of **11a^{15}** from impure fractions obtained during the purification of **1a^{15}**. ^{15}N-labeled urea **12a^{15}** and acetamide **13a^{15}** were obtained as secondary products and characterized for benchmarking purposes.

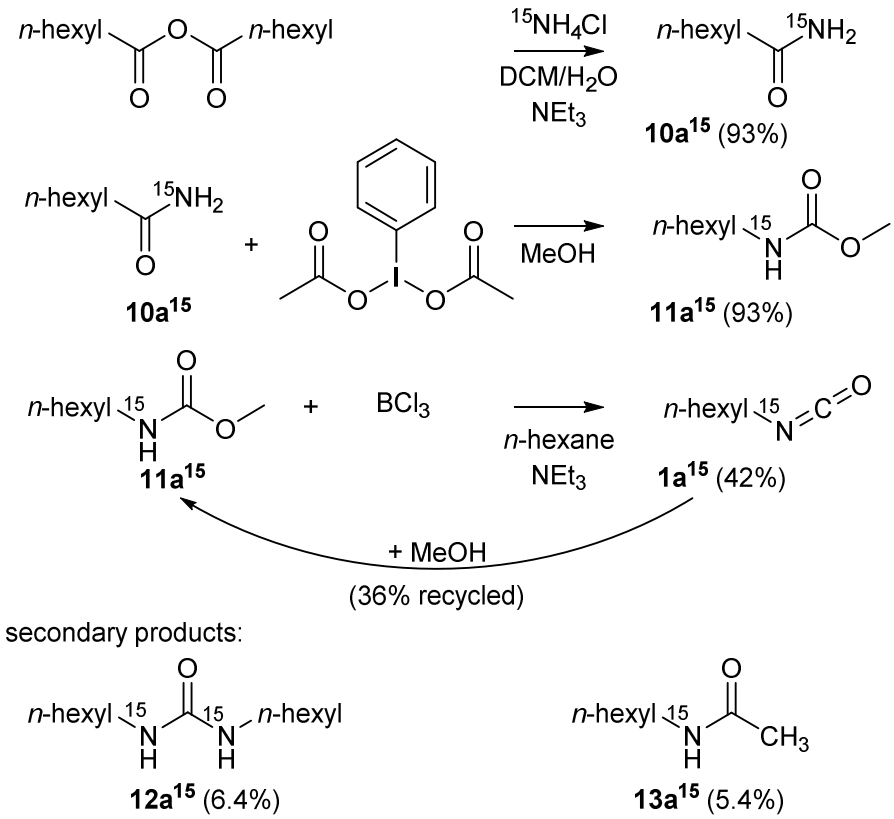

Scheme S2: 1. *[Scheme S1] Synthesis of ^{15}N-labeled n-hexyl isocyanate* ***1a^{15}*** *and secondary products isolated during purification.*

^{15}N-Heptanamide ***10a^{15}***

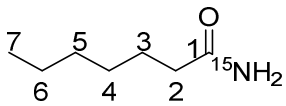

10.2 mL (73.4 mmol, 4 eq.) Triethylamine were dissolved in 50 mL of dry DCM under N_2 and cooled to 0 °C. 8.92 g (36.8 mmol, 2 eq.) Heptanoic anhydride were added and the solution was stirred at 0 °C for 20 min. 1.0 g (18.4 mmol, 98% ^{15}N) Ammonium chloride were dissolved in 10 mL of H_2O separately and the solution was added in one portion to the vigorously stirred organic phase. After 15 min, another 1.11 g (0.25 eq.) of heptanoic anhydride were added, the ice bath removed and the reaction stirred overnight at RT. Solvents were removed *in vacuo* and the crude reaction mixture was taken up in 60 mL of K_2CO_3 (1/2 conc. in H_2O). This aqueous mixture was extracted with ethyl acetate (3 × 50 mL) and DCM (2 × 50 mL). Subsequent removal of solvents gave the crude product, which was further purified by column chromatography (SiO_2, gradient *iso*hexane/EtOAc = 3/2 → 0/1) to yield 2.22 g, (17.1 mmol, 93%) ^{15}N amide **10a^{15}** in the form of a colorless solid.

Rf: 0.27 (*iso*hexane/EtOAc = 1/3).

^{1}H NMR (400 MHz, $CDCl_3$) δ [ppm] = 5.92 (dd, J = 179.8, 89.3 Hz, 2H, H-N), 2.18 (t, J = 8.0 Hz, 2H, H-2), 1.59 (p, J = 7.9 Hz, 2H, H-3), 1.36 – 1.19 (m, 6H, H-4, H-5, H-6), 0.85 (t, J = 7.1 Hz, 3H, H-7).

^{13}C NMR (101 MHz, $CDCl_3$) δ [ppm] = 176.29 (d, J = 13.8 Hz, C-1), 36.08 (d, J = 7.9 Hz, C-2), 31.60 (C-3), 28.98 (C-4), 25.60 (C-5), 22.56 (C-6), 14.08 (C-7).

^{15}N NMR (41 MHz, $CDCl_3$) δ [ppm] = -277.11 (t, J = 88.4 Hz).

Elemental analysis: $C_7H_{15}{}^{15}NO$ (130.20 g/mol); Calc. (%): C, 64.58; H, 11.61; N, 11.52; Found (%): C, 64.73; H, 11.51; N, 11.44.

HRMS (EI): *m/z* calculated for: $C_7H_{15}{}^{15}NO^+$ $[M]^+$, 130.1119, found: 130.1125.

*^{15}N-Methyl hexylcarbamate **11a^{15}***

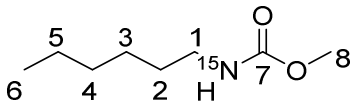

2.13 g (16.4 mmol) Amide **10a^{15}** and 6.34 g (19.7 mmol, 1.2 eq.) (diacetoxyiodo)benzene were dissolved in 44 mL (1090 mmol) dry MeOH under N_2. This reaction mixture was stirred at RT for 15 h before all solvents were removed *in vacuo*. The resulting residue was taken up in 150 ml of 1/3 saturated K_2CO_3 and extracted with ethyl acetate (2 × 50mL) and DCM (2 × 50mL). After drying over Na_2SO_4 and removal of solvents, column chromatography (SiO_2, gradient *iso*hexane/ethyl acetate 1/0→0/1) yielded 2.43 g (15.2 mmol, 93%) carbamate **11a^{15}** in the form of a colorless liquid.

Rf: 0.30 (*iso*hexane/EtOAc = 85/15)

^{1}H NMR (400 MHz, $CDCl_3$) δ [ppm] = 4.70 (dt, *J* = 90.3, 5.6 Hz, 1H, H-N), 3.67 (s, 3H, H-8), 3.17 (q, *J* = 6.4 Hz, 2H, H-1), 1.57 – 1.42 (m, 2H, H-2), 1.40 – 1.22 (m, 6H, H-3, H-4, H-5), 0.89 (d, *J* = 7.1 Hz, 3H, H-6).

^{13}C NMR (101 MHz, $CDCl_3$) δ [ppm] = 157.04 (d, *J* = 25.9 Hz, C-7), 51.93 (C-8), 41.08 (d, *J* = 11.6 Hz, C-1), 31.46 (C-3), 29.97 (C-2), 26.38 (C-4), 22.54 (C-5), 13.98 (C-6).

^{15}N NMR (41 MHz, $CDCl_3$) δ [ppm] = -298.40 (d, *J* = 91.8 Hz).

Elemental analysis: $C_8H_{17}{}^{15}NO_2$ (160.22 g/mol); Calc. (%): C, 59.97; H, 10.70; N, 9.36; Found (%): C, 59.41; H, 11.53; N, 8.83.

HRMS (EI): *m/z* calculated for: $C_8H_{18}{}^{15}NO_2^+$ $[M+H]^+$, 161.1302, found: 161.1303; calculated for: $C_8H_{17}{}^{15}NO_2^+$ $[M]^+$, 160.1224, found: 160.1224 (traces).

*^{15}N-Hexyl isocyanate **1a^{15}***

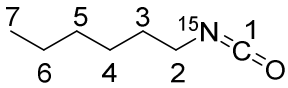

2.85 g (17.8 mmol) Carbamate **11a^{15}** were dissolved in 40 mL of dry *n*-hexane under N_2 atmosphere. After addition of 8.9 mL BCl_3 (1 M in hexane, 8.9 mmol, 0.5 eq.) and stirring for 20 min at RT, 2.97 mL NEt_3 (21.3 mmol, 1.2 eq.) were added and the resulting suspension was stirred at RT for 40 min. Subsequently, solids were filtered of and solvents were removed *in vacuo*. Bulb-to-bulb distillation (20 mbar, 140 °C) was performed twice to yield 0.94 g (7.3 mmol, 42%) of ^{15}*N*-hexyl isocyanate **1a^{15}**.

^{1}H NMR (400 MHz, $CDCl_3$) δ [ppm] = 3.28 (td, *J* = 6.7, 1.0 Hz, 2H, H-2), 1.66 – 1.55 (m, 2H, H-3), 1.42 – 1.20 (m, 6H, H-4, H-5, H-6), 0.90 (t, *J* = 7.0 Hz, 3H, H-7).

^{13}C NMR (101 MHz, $CDCl_3$) δ [ppm] = 122.08 (d, *J* = 46.0 Hz, C-1), 43.11 (d, *J* = 8.6 Hz, C-2), 31.42 (C-3), 31.27 (C-5/C-6), 26.34 (d, *J* = 1.6 Hz, C-4), 26.35 (C-5/C-6), 22.64, 14.07 (C-7).

^{15}N NMR (41 MHz, $CDCl_3$) δ [ppm] = -349.99 (tt, *J* = 3.5, 1.0 Hz).

Elemental analysis: $C_7H_{13}{}^{15}NO$ (128.18 g/mol): Calc. (%): C, 65.59; H, 10.22; N, 11.70; Found (%): C, 65.63; H, 10.43; N, 11.23.

HRMS (EI): calculated for: $C_7H_{12}{}^{15}NO^+$ $[M-H]^+$, 127.0884, found: 127.0882.

All impure fractions from workup and distillation were combined in 200 mL of dry MeOH and left do quench overnight. Workup by column chromatography as described above yielded 1.02 g, 6.37 mmol, 36% recycled carbamate **11a**[15].

*[15]N-Hexylacetamide **13a**[15] and ^{15}N-dihexylurea **12a**[15]*

After eluting amide **10a**[15] and carbamate **11a**[15] (both initial and recycled) minor amounts of [15]*N*-containing compounds were washed of the columns with EtOAc/MeOH = 8/2. Further column chromatography (SiO_2, *iso*hexane/EtOAc = 85/15 → 0/1) yielded 0.15 g (1.0 mmol, 5.4%) acetamide **13a**[15] in the form of a yellow oil. Continued elution (MeOH/$CHCl_3$ = 2/8) gave 0.27 g (1.2 mmol, 6.4%) of urea **12a**[15] as colorless solid.

13a[15]:

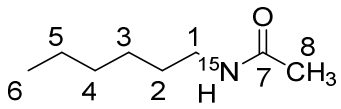

Rf: 0.47 (*iso*hexane/EtOAc = 65/35)

^{1}H NMR (400 MHz, $CDCl_3$) *δ* [ppm] = 5.93 (dt, *J* = 90.0, 5.7 Hz, 1H, H-N), 3.17 (q, *J* = 6.1 Hz, 2H, H-1), 1.92 (d, *J* = 1.4 Hz, 3H, H-8), 1.52 – 1.36 (m, 2H, H-2), 1.32 – 1.17 (m, 6H, H-3, H-4, H-5), 0.84 (t, *J* = 7.0 Hz, 3H, H-6).

^{13}C NMR (101 MHz, $CDCl_3$) *δ* [ppm] = 170.27 (d, *J* = 14.4 Hz, C-7), 39.73 (d, *J* = 10.0 Hz, C-1), 31.55 (C-3/C-4/C5), 29.57 (C-2), 26.67 (d, *J* = 1.5 Hz, C-3/C-4/C5), 23.32 (d, *J* = 8.5 Hz, C-8), 22.61 (C-3/C-4/C5), 14.08 (C-6).

^{15}N NMR (41 MHz, $CDCl_3$) *δ* [ppm] = -260.98 (dddd, *J* = 90.0, 3.3, 2.3, 1.2 Hz).

Elemental analysis: $C_8H_{17}{}^{15}NO$ (144.22 g/mol); Calc. (%): C, 66.62; H, 11.88; N, 10.40; Found (%): C, 65.46; H, 11.57; N, 11.50.

HRMS (EI): *m/z* calculated for: $C_8H_{17}{}^{15}NO^+$ $[M]^+$, 144.1275, found: 144.1271; calculated for: $C_8H_{18}{}^{15}NO^+$ $[M+H]^+$, 145.1353, found: 145.1349.

12a[15]:

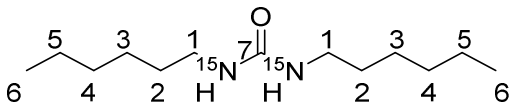

Rf: 0.61 (MeOH/$CHCl_3$ = 2/8)

^{1}H NMR (400 MHz, $CDCl_3$) *δ* [ppm] = 5.04 (dt, *J* = 88.5, 5.3 Hz, 2H, H-N), 3.11 (q, *J* = 6.9 Hz, 4H, H-1), 1.45 (p, *J* = 6.6 Hz, 4H, H-2), 1.37 – 1.19 (m, 12H, H-3, H-4, H-5), 0.86 (t, *J* = 7.0 Hz, 6H, H-6).

^{13}C NMR (101 MHz, $CDCl_3$) *δ* [ppm] = *δ* 159.01 (t, *J* = 20.3 Hz, C-7), 40.54 (d, *J* = 11.5 Hz, C-1), 31.73 (C-3/C-4/C-5), 30.46 (C-2), 26.78 (C-3/C-4/C-5), 22.73 (C-3/C-4/C-5), 14.16 (C-6).

^{15}N NMR (41 MHz, $CDCl_3$) *δ* [ppm] = -297.41 (d, *J* = 87.6 Hz).

Elemental analysis: $C_{13}H_{28}{}^{15}N_2O$ (230.37 g/mol); Calc. (%): C, 67.78; H, 12.25; N, 13.02; Found (%): C, 67.62; H, 11.90; N, 12.11.

HRMS (EI): *m/z* calculated for: $C_{13}H_{28}{}^{15}N_2O^+$ $[M]^+$, 230.2137, found: 230.2131.

*^{15}N-Hexyl uretdione **2a^{15}** and ^{15}N-hexyl isocyanurate **3a^{15}***

Two of the oligomerization reactions containing 50 mol-% **5b** (**1a^{15}**: 0.185 g, 1.44 mmol; **5b**: 0.147 g, 0.727 mmol) were quenched by addition of 0.13 mL (2.16 mmol, 1.3 eq) Iodomethane. After 4 h, the resulting mixture was taken up in DCM, solvents and unreacted isocyanate was distilled of. The residue containing phosphonium, **2a^{15}** and **3a^{15}** was separated by column chromatography (SiO_2; *iso*hexane / $CHCl_3$ = 1/0 → 1/1). 0.026 g (0.10 mmol, 6.9%) uretdione **2a^{15}** and 0.163 g (0.42 mmol, 44 %) isocyanurate **3a^{15}** were obtained in the form of colorless oils.

2a^{15}:

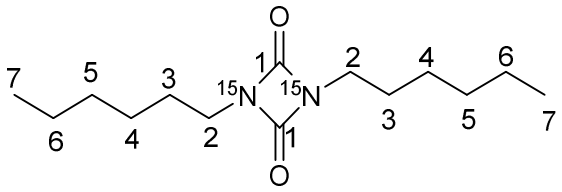

Rf: 0.54 (*iso*hexane / $CHCl_3$ = 3/2)

^{1}H NMR (400 MHz, $CDCl_3$) δ [ppm] = 3.18 (t, *J* = 7.1 Hz, 4H, H-2), 1.60 (p, *J* = 7.4, 6.6 Hz, 4H, H-3), 1.41 – 1.21 (m, 12H, H-4, H-5, H-6), 0.88 (t, *J* = 7.0 Hz, 6H, H-7).

^{13}C NMR (101 MHz, $CDCl_3$) δ [ppm] = 158.15 (t, *J* = 13.3 Hz, C-1), 40.63 (t, *J* = 4.0 Hz, C-2), 31.32 (C-4/C-5/C-6), 28.71 (C-3, 26.53 (C-4/C-5/C-6), 22.62 (C-4/C-5/C-6), 14.12.

^{15}N NMR (41 MHz, $CDCl_3$) δ [ppm] = −250.73 (t, *J* = 1.4 Hz).

3a^{15}:

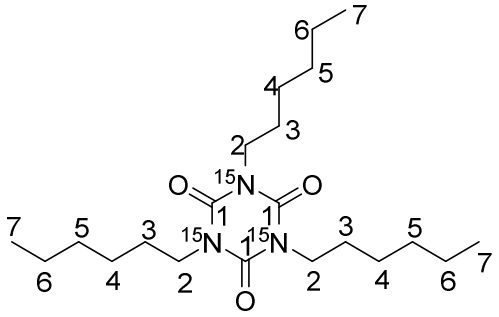

Rf: 0.07 (*iso*hexane / $CHCl_3$ = 5/1)

^{1}H NMR (400 MHz, $CDCl_3$) δ [ppm] = 3.85 (t, *J* = 7.5 Hz, 6H, H-2), 1.62 (p, *J* = 7.1 Hz, 6H, H-3), 1.43 – 1.20 (m, 18H, H-3, H-4, H-5, H-6), 0.87 (t, *J* = 6.8 Hz, 9H, H-7).

^{13}C NMR (101 MHz, $CDCl_3$) δ [ppm] = 149.13 (ddd, *J* = 19.2, 18.4, 2.0 Hz, C-1), 43.31 – 42.98 (m, C-2), 31.51 (C-4/C-5/C-6), 27.91 (C-3), 26.51 (C-4/C-5/C-6), 22.65(C-4/C-5/C-6), 14.12 (C-7).

^{15}N NMR (41 MHz, $CDCl_3$) δ [ppm] = −239.37.

Elemental analysis: $C_{21}H_{39}\,^{5}N_3O_3$ (384.54 g/mol); Calc. (%): C, 65.59; H, 10.22; N, 11.70; Found (%): C, 65.85; H, 10.16; N, 11.38.

HRMS (EI): *m/z* calculated for: $C_{21}H_{39}{}^{15}N_3O_3^+$ $[M]^+$, 384.2897, found: 384.2896.

2.1.3 Synthesis of Oligomers and Reference Compounds

*n-Hexyl uretdione **2a** and n-hexyl isocyanurate **3a***

5.19 g (40.8 mmol) Isocyanate **1a** were placed in a flame-dried, N_2-filled Schlenk flask fitted with a still. 0.51 mL (2.04 mmol, 5 mol-%) **5b** were added and the mixture was stirred for 4 h at 60 °C and subsequently at room temperature for another 17 h. Monitoring by ^{1}H NMR spectroscopy showed 53 % conversion. The reaction was quenched by addition of 0.39 mL (4.08 mmol) dimethyl sulfate and heating to 80 °C for 5 min. Unreacted monomer was removed at 35 °C and 1 mbar. A fraction containing **2a** was removed at 190 °C and 0.09 mbar (Fraction 2a) and the remaining fraction consisted mostly of quenched catalyst and **3a** (fraction 3a). Fraction 2a was further purified by column chromatography (SiO_2, IH/EtOAc = 5/1) and bulb-to-bulb distillation to yield 0.315 g (1.24 mmol, 6.1%) of uretdione **2a** as colorless oil.
Fraction 3a was purified by column chromatography (SiO_2, IH/EtOAc = 5/1) and bulb-to-bulb distillation to yield 0.498 g (1.31 mmol, 9.6%) of isocyanurate **3a** as colorless oil.

2a:

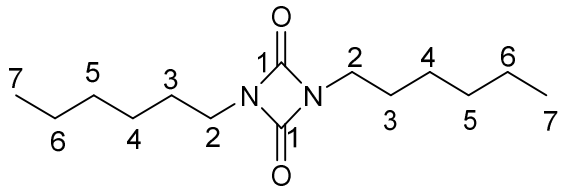

Rf: 0.76 (IH/EA = 5/1).
^{1}H NMR (400 MHz, Chloroform-*d*) *δ* [ppm] = 3.17 (t, *J* = 7.1 Hz, 4H, H-2), 1.60 (p, *J* = 7.2 Hz, 4H, H-3), 1.38 – 1.19 (m, 12H, H-4,H-5,H-6), 0.87 (t, *J* = 7.1 Hz, 6H, H-7).
^{13}C NMR (101 MHz, $CDCl_3$) *δ* [ppm] = 158.13 (C-1), 40.62 (C-2), 31.31 (C-4/C-5/C-6), 28.69 (C-3), 26.51 (C-4/C-5/C-6), 22.60 (C-4/C-5/C-6), 14.09 (C-7).
Elemental analysis: $C_{14}H_{26}N_2O_2$ (254.37 g/mol); Calc. (%): C, 66.11; H, 10.30; N, 11.01; Found (%): C, 65.89; H, 1023; N, 12.84.

3a:

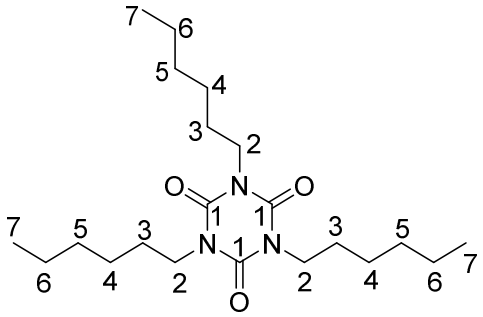

Rf: 0.83 (IH/EA = 5/1).
^{1}H NMR (400 MHz, Chloroform-*d*) *δ* [ppm] = 3.85 (t, *J* = 7.7 Hz, 6H, H-2), 1.71 – 1.52 (m, 6H, H-3), 1.39 – 1.21 (m, 18H, H-4,H-5,H-6), 0.88 (t, *J* = 7.3 Hz, 9H, H-7).
^{13}C NMR (101 MHz, $CDCl_3$) *δ* [ppm] = 149.14 (C-1), 43.17 (C-2), 31.51 (C-4/C-5/C-6), 27.90 (C-3), 26.51 (C-4/C-5/C-6), 22.66 (C-4/C-5/C-6), 14.15 (C-7).

IR (ATR) $\tilde{\nu}$ [cm^{-1}]: 2957 (m), 2929 (m), 2859 (w), 1682 (vs), 1510 (vw), 1455 (vs), 1425 (s), 1378 (m), 1335 (m), 1101 (vw), 764 (s), 726 (w).

Elemental analysis: $C_{21}H_{39}N_3O_3$ (381.56 g/mol); Calc. (%): C, 66.11; H, 10.30; N, 11.01; Found (%): C, 65.62; H, 10.10; N, 12.22.

HRMS (EI): *m/z* calculated for: $C_{21}H_{39}N_3O_3^+$ $[M]^+$, 381.2986, found: 381.2996.

NMR data of this compound is in line with reported data.[3]

*n-Butyl isocyanurate **3b***

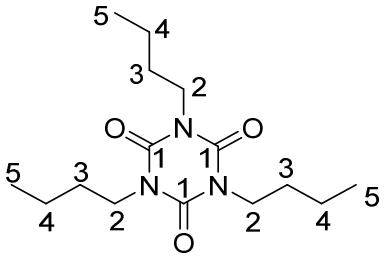

1.30 mL (11.5 mmol) Butyl isocyanate **1b** were placed in a flame-dried, N_2-filled Schlenk flask fitted with a still. 0.13 mL (1.15 mmol, 8.5 mol-%) **5b** were added and the mixture was stirred at room temperature overnight. Unreacted isocyanate was removed *in vacuo* and recovered while the crude product was further purified by distillation and subsequent column chromatography (SiO_2, IH/EtOAc = 8/1 → 5/1) to yield 0.268 g (0.90 mmol, 23.5 %) isocyanurate **3b** as colorless oil.

Rf: 0.69 (IH/EA = 5/1).

^{1}H NMR (400 MHz, Chloroform-*d*) δ [ppm] = 3.87 (t, *J* = 9.0, 7.4 Hz, 6H, H-2), 1.61 (td, *J* = 13.4, 11.7, 5.4 Hz, 6H, H-3), 1.36 (h, *J* = 7.4 Hz, 6H, H-4), 0.95 (t, *J* = 7.3 Hz, 9H, H-5).

^{13}C NMR (101 MHz, $CDCl_3$) δ [ppm] = 149.13 (C-1), 42.93(C-2), 30.00 (C-3), 20.11 (C-4), 13.82 (C-5).

IR (ATR) $\tilde{\nu}$ [cm^{-1}]: 2960 (m), 2935 (w), 2874 (w), 1680 (vs), 1511 (vw), 1454 (vs), 1425 (s), 1377 (m), 1332 (m), 1278 (vw), 1116 (vw), 1095 (vw), 1056 (vw), 1020 (vw), 951 (vw), 919 (vw), 764 (s), 739 (w).

Elemental analysis: $C_{15}H_{27}N_3O_3$ (297.40 g/mol); Calc. (%): C, 60.58; H, 9.15; N, 14.13; Found (%): C, 60.59; H, 9.27; N, 13.92

HRMS (EI): *m/z* calculated for: $C_{15}H_{27}N_3O_3^+$ $[M]^+$, 297.2045, found: 297.2048.

*Tri-n-butyl(methyl)phosphonium iodide **15b***

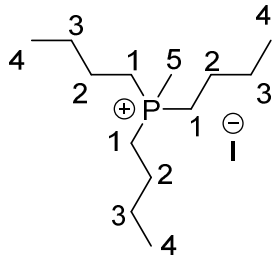

0.5 mL (2.0 mmol) Freshly distilled tri-*n*-butylphosphine were dissolved in 3 mL of hexane in a flame-dried Schlenk flask under N_2-atmosphere. 0.25 mL (4.0 mmol) of methyl iodide were added dropwise and the mixture was stirred at room temperature overnight. The colorless precipitate was filtered of and washed with THF to yield 0.672 g (1.95 mmol, 97.5%) tri-*n*-butyl(methyl)phosphonium iodide as colorless solid.

^{31}P {^{1}H} NMR (162 MHz, $CDCl_3$) δ [ppm] = 32.09.

^{1}H NMR (400 MHz, Chloroform-*d*) *δ* [ppm] = 2.49 – 2.30 (m, 6H, H-1), 2.03 (d, *J* = 13.3 Hz, 3H, H-5), 1.47 (m, 12H, H-2, H-3), 0.91 (t, *J* = 6.8 Hz, 9H, H-4).

^{13}C NMR (101 MHz, $CDCl_3$) *δ* [ppm] = 23.81 (d, *J* = 15.6 Hz, C-2), 23.66 (d, *J* = 4.7 Hz, C-3), 20.56 (d, *J* = 48.9 Hz, C-1), 13.57 (C-4), 5.65 (d, *J* = 52.2 Hz, C-5).

IR (ATR) $\tilde{\nu}$ [cm^{-1}]: 2959 (vs), 2934 (s), 2874 (s), 1660 (vw), 1463 (s), 1444 (m), 1384 (m), 1360 (w), 1345 (w), 1307 (m), 1279 (w), 1202 (m), 1191 (w), 1099 (m), 1078 (m), 972 (s), 955 (vs), 928 (s), 819 (s), 767 (m), 717 (m).

Elemental analysis: $C_{13}H_{30}IP$ (344.11 g/mol); Calc. (%): C, 45.36; H, 8.78; N, 0.00; Found (%): C, 45.12; H, 8.69; N, 0.00.

HRMS (ESI): *m/z* calculated for: $C_{13}H_{30}P^+$ $[M]^+$, 217.20796, found: 217.20791.

Tri-n-butylphosphonium chloride ***16b***

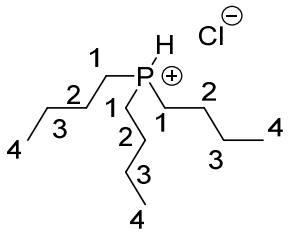

0.5 mL (2.0 mmol) Freshly distilled tri-*n*-butylphosphine were dissolved in 0.12 mL (3.0 mmol, 1.5 eq.) dry methanol in a flame dried, N_2-filled Schlenk flask. The mixture was cooled by means of an ice bath and 0.38 mL (3.0 mmol, 1.5 eq.) TMSCl were added dropwise. After stirring at room temperature for 2 h, ^{31}P NMR confirmed full conversion of the phosphine and the silyl ether and remaining reagents were removed under reduced pressure. The crude product was purified by bulb to bulb distillation (5.5 × 10^{-2} bar, 130 °C) to give tri-*n*-butylphosphonium chloride **16b** as colorless solid (0.426 g, 1.78 mmol, 89.0 %). The product is highly hygroscopic and was therefore stored and handled under argon.

^{31}P {^{1}H} NMR (162 MHz, $CDCl_3$) *δ* [ppm] = 11.65.

^{31}P NMR (162 MHz, $CDCl_3$) *δ* [ppm] = 11.64 (dtt, *J* = 492.9, 24.5, 12.0 Hz).

^{1}H NMR (400 MHz, $CDCl_3$) *δ* [ppm] = 7.13 (dhept, *J* = 492.8 Hz, 5.5 1H, H-P), 2.32 (td, *J* = 14.0, 5.4 Hz, 6H, H-1), 1.52 (h, *J* = 9.1, 8.3 Hz, 6H, H-2), 1.37 (q, *J* = 7.3 Hz, 6H, H-3), 0.82 (t, *J* = 7.3 Hz, 9H, H-4).

^{13}C NMR (101 MHz, $CDCl_3$) *δ* [ppm] = 24.73 (d, *J* = 4.7 Hz, C-3), 23.62 (d, *J* = 15.2 Hz, C-2), 17.04 (d, *J* = 46.9 Hz, C-1), 13.29 (s, C-4).

Elemental analysis: $C_{12}H_{28}ClP$ (238.78 g/mol); Calc. (%): C, 60.36; H, 11.82; N, 0.00; Found (%): C, 60.16; H, 11.75; N, 0.00.

***In Situ* Synthesis and Elucidation of Trapped Monoadduct 6ab×HCl and 6ab^{15}×HCl**

In order to have a stable compound structurally close to the investigated transient intermediates, we synthesized H^+-trapped monoadduct **6ab×HCl** from isocyanate **1a** and phosphonium chloride **16b** *in situ* in $CDCl_3$.

Tributyl(hexylcarbamoyl)phosphonium chloride ***6ab×HCl***

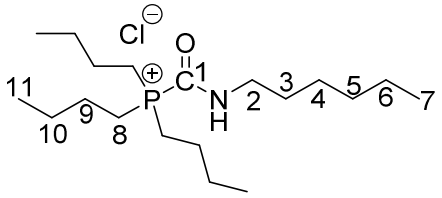

0.062 g (0.260 mmol) **16b** and 0.033 g (0.259 mmol) **1a** were dissolved in 0.6 mL $CDCl_3$ in the glovebox. The sample was stored at room temperature. Conversion was monitored by ^{1}H and ^{31}P NMR measurements until no more changes were observed after 14 d. Removal of the solvent gave a colorless oil in > 98% yield (^{1}H and ^{31}P NMR).

^{31}P {^{1}H} NMR (162 MHz, $CDCl_3$) *δ* [ppm] = 29.62.

^{1}H NMR (400 MHz, $CDCl_3$) *δ* [ppm] = 11.51 (t, 5.6 Hz, 1H, N-H), 3.39 (q, *J* = 6.5 Hz, 2H, H-2), 2.80 – 2.55 (m, 6H, H-8), 1.77 – 1.60 (m, 2H, H-3), 1.60 – 1.43 (m, 12H, H-9, H-10), 1.41 – 1.20 (m, 6H, H-4,), 0.98 (t, *J* = 7.2 Hz, 9H, H-11), 0.86 (t, *J* = 7.0 Hz, 3H, H-7).

^{13}C NMR (101 MHz, $CDCl_3$) *δ* [ppm] = 158.87 (d, *J* = 88.4 Hz, C-1), 40.73 (C-2), 30.93 (C-6/C-5/C-4), 28.32 (C-3), 26.29 (C-6/C-5/C-4), 23.54 (d, *J* = 3.4 Hz, C-10), 23.41 (d, *J* = 15.6 Hz, C-9), 22.15 (C-6/C-5/C-4), 17.88 (d, *J* = 41.1 Hz, H-8), 13.65 (C-7), 13.09 (C-11).

HRMS (ESI): *m/z* calculated for: $C_{19}H_{41}NOP^+$ [M$^+$], 330.29203, found: 330.29185.

^{15}N-Tributyl(hexylcarbamoyl)phosphonium chloride ***6ab^{15}×HCl***

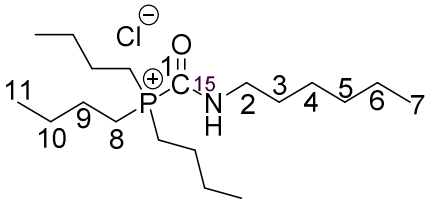

0.061 g (0.257 mmol) **16b** and 0.032 g (0.250 mmol) **1a^{15}** were dissolved in 0.45 mL $CDCl_3$ in the glovebox. The sample was stored at room temperature. Conversion was monitored by ^{1}H and ^{31}P NMR measurements until no more changes were observed. The reported spectra were recorded after 37 d at room temperature. As evidenced in the spectra in the next section, residuals of both starting materials are visible as well as protonated isocyanate **1a^{15}**, which was identified by proton-coupled ^{15}N NMR.

^{31}P {^{1}H} NMR (162 MHz, $CDCl_3$) *δ* [ppm] = 29.46 (d, *J* = 28.4 Hz).

^{31}P NMR (162 MHz, $CDCl_3$) *δ* [ppm] = 29.46.

^{1}H NMR (400 MHz, $CDCl_3$) *δ* [ppm] = 11.07 (dt, *J* = 90.8, 5.6 Hz, 1H, N-H), 3.20 (q, *J* = 6.8 Hz, 2H, H-2), 2.63 – 2.48 (m, 6H, H-8), 1.59 – 1.43 (m, 2H, H-3), 1.45 – 1.26 (m, 12H, H-9, H-10), 1.23 – 1.04 (m, 6H, H-4,), 0.79 (t, *J* = 7.1 Hz, 9H, H-11), 0.68 (t, *J* = 6.8 Hz, 3H, H-7).

^{13}C NMR (101 MHz, $CDCl_3$) *δ* [ppm] = 158.93 (dd, *J* = 88.5, 15.5 Hz, C-1), 40.89 (dd, *J* = 7.2, 5.3 Hz, C-2), 31.05 (C-6/C-5/C-4), 28.44 (C-3), 26.41 (d, *J* = 1.2 Hz, C-6/C-5/C-4), 23.68 (d, *J* = 4.4 Hz, C-10), 23.52 (d, *J* = 15.1 Hz, C-9), 22.25 (C-6/C-5/C-4), 18.10 (d, *J* = 41.1 Hz, C-8), 13.73 (C-7), 13.17 (C-11).

^{15}N {^{1}H} NMR (41 MHz, $CDCl_3$) *δ* [ppm] = -236.54 (d, *J* = 28.4 Hz).

^{15}N NMR (41 MHz, $CDCl_3$) *δ* [ppm] = -236.54 (dd, *J* = 90.8, 28.4 Hz).

HRMS (ESI): *m/z* calculated for: $C_{19}H_{41}{}^{15}NOP^+$ [M$^+$], 331.28906, found: 331.28886.

2.1.4 Oligomerization Experiments

Sample Preparation

P*n*-Bu_3 **5b** (99%) and *n*-hexyl isocyanate (97%) **1a** were purchased from Sigma Aldrich, distilled under reduced pressure and stored in a glovebox. ^{15}*N*-hexyl isocyanate **1a^{15}** was synthesized as detailed above and stored in a glovebox as well. Samples were prepared by mixing different ratios (as detailed in **Table S2: 1**) of **5b** with **1a** or **1a^{15}** in a NMR tube containing a capillary filled of aceton-d_6 (for locking of the NMR machine) and a capillary filled with H_3PO_4 conc. (external standard for ^{31}P measurements). The NMR tube was capped, sealed with Parafilm, exported from the glovebox and flame-sealed under N_2 atmosphere.

Table S2: 1. [Table S1] Mixing ratios for oligomerization experiments.

Experiment	m (**1a**) / g	n (**1a**) / mmol	m (**5b**) / g	n (**5b**) / mmol	**5b** / mol-%
o1[a]	0.1935	1.521	0.1575	0.778	51.17
o2[a]	0.2235	1.757	0.1225	0.605	34.46
o3[a]	0.2312	1.818	0.1222	0.604	33.23
o4[a]	0.3051	2.399	0.0573	0.283	11.81
o5[a]	0.3042	2.392	0.0568	0.281	11.74
o6[a]	0.3596	2.827	0.0069	0.034	1.21
o7[a]	0.3562	2.801	0.0072	0.035	1.26
o8[a]	0.1936	1.522	0.1528	0.755	49.62
o9[b]	0.1848	1.442	0.1471	0.727	50.43

[a] Experiment performed with 14*N* hexyl isocyanate **1a**. [b] Experiment performed with 15*N* hexyl isocyanate **1a^{15}**.

Kinetic Measurements

After flame-sealing, ^{1}H NMR spectra were obtained repeatedly from a 400 MHz NMR machine. Between measurements, the samples were stored at 23 °C by means of a thermostat. **Figure S2: 1** shows the area of interest in ^{1}H NMR spectra with assignment of the signals to the protons of the α-CH_2 groups of the respective compounds. For better resolution, samples taken from neat reaction mixtures were diluted with $CDCl_3$ and measured in a 600 MHz machine.

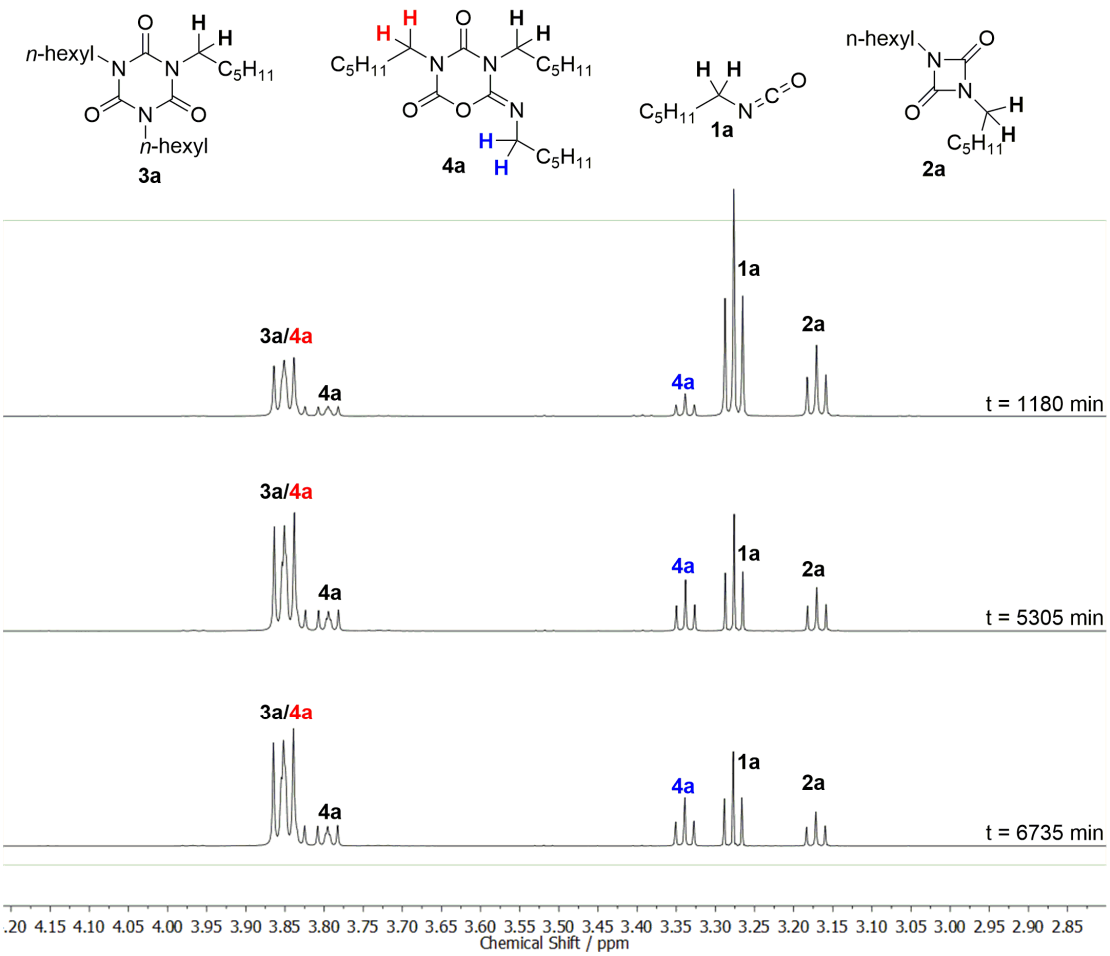

Figure S2: 1. *[Figure S1] ^{1}H NMR spectra of the oligomerization of* ***1a*** *catalyzed by 11.8 mol-%* ***5b****. Spectra were obtained by dissolving 30 mg of reaction mixture in 0.5 mL $CDCl_3$ after different reaction times and immediately measuring on a 600 MHz NMR machine.*

Except for the signals generated by trimers **3a** and **4a** from ca. 3.88 - 3.83 ppm all signals are well separated. However, due to increasing viscosity in the course of the reaction and concentration dependent shifts, quantitative interpretation of the spectra obtained from measuring the neat reaction mixtures is more challenging as shown in **Figure S2: 2**:

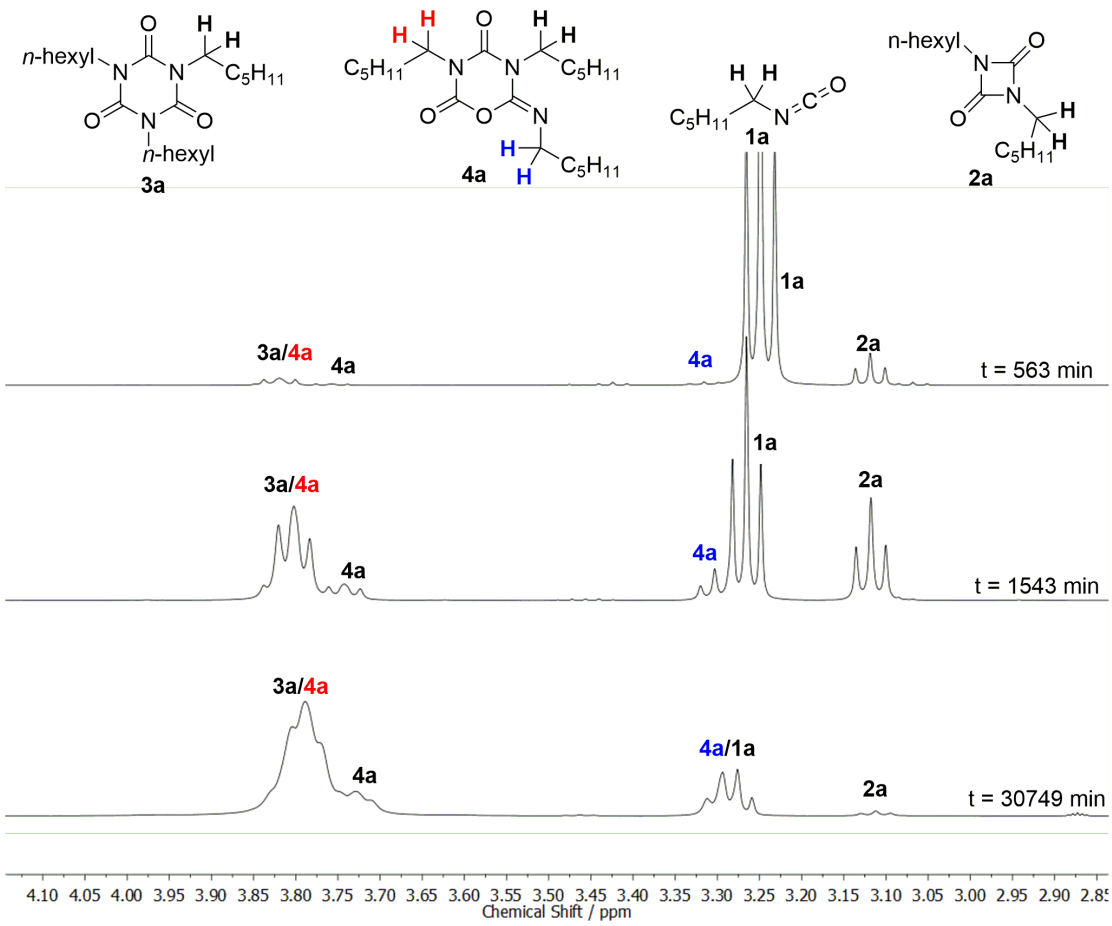

Figure S2: 2. *[Figure S2] ^{1}H NMR spectra of the oligomerization of **1a** catalyzed by 11.8 mol-% **5b** (o4). Spectra were obtained by directly measuring the neat reaction mixture in a 400 MHz machine.*

Due to the fact of overlapping signals for **1a**/**4a** and **3a**/**4a**, only the content of **2a** could be discerned directly by integration. All other compounds had to be calculated from mixed integrals. The following areas were integrated:

- 4.000 – 3.000 ppm (Integral 1, containing all compounds)
- 3.900 – 3.600 ppm (Integral 2, containing isocyanurate **3a** and 4 out of 6 protons of **4a**)
- 3.350 – 3.175 ppm (Integral 3, containing **1a** + 2 out of 6 protons of **4a**)
- 3.175 – 3.025 ppm (Integral 4, containing uretdione **2a**)

These integral areas were used to calculate the amount of the compounds of interest (in % of monomer **1a**) as follows:

1) The content of dimer **2a** is determined by dividing integral 4 by integral 1 and multiplying with 100.
2) The ratio of integral 2 and the reference integral 1 multiplied with 18/16 and then with 100 gives the total percentage of trimers **3a** and **4a**.
3) Integrals 2, 3 and 4 are combined and divided by integral 1. This value is multiplied by 100. The total percentage of of trimers **3a** and **4a** and the amount of dimer **2a** is subtracted from this value, thus giving the share of monomer **1a**.
4) The percentage of trimer **4a** is calculated by subtracting the share of monomer **1a** from integral 3 and multiplication by factor 3.

5) Finally, the content of trimer **3a** is determined by subtracting the amount of trimer **4a** from the total percentage of trimers **3a** and **4a**.

This method reproduces very well the ratio of 2/1 for **3a**/**4a** that was reported previously.[4]

Consideration of ^{13}C NMR

Since all oligomerization experiments were performed neat without any solvent, ^{13}C NMR measurements that gave well-resolved spectra could be done with 64 cycles in less than 5 min. **Figure S2: 3** shows the stacked ^{13}C NMR spectra of oligomerization reaction o4 whose reaction times are given in **Table S2: 2**. Assignment of signals was done in accordance to Horvath and Richter, which we found to be accurate after consulting 2D NMR spectroscopy.[4]

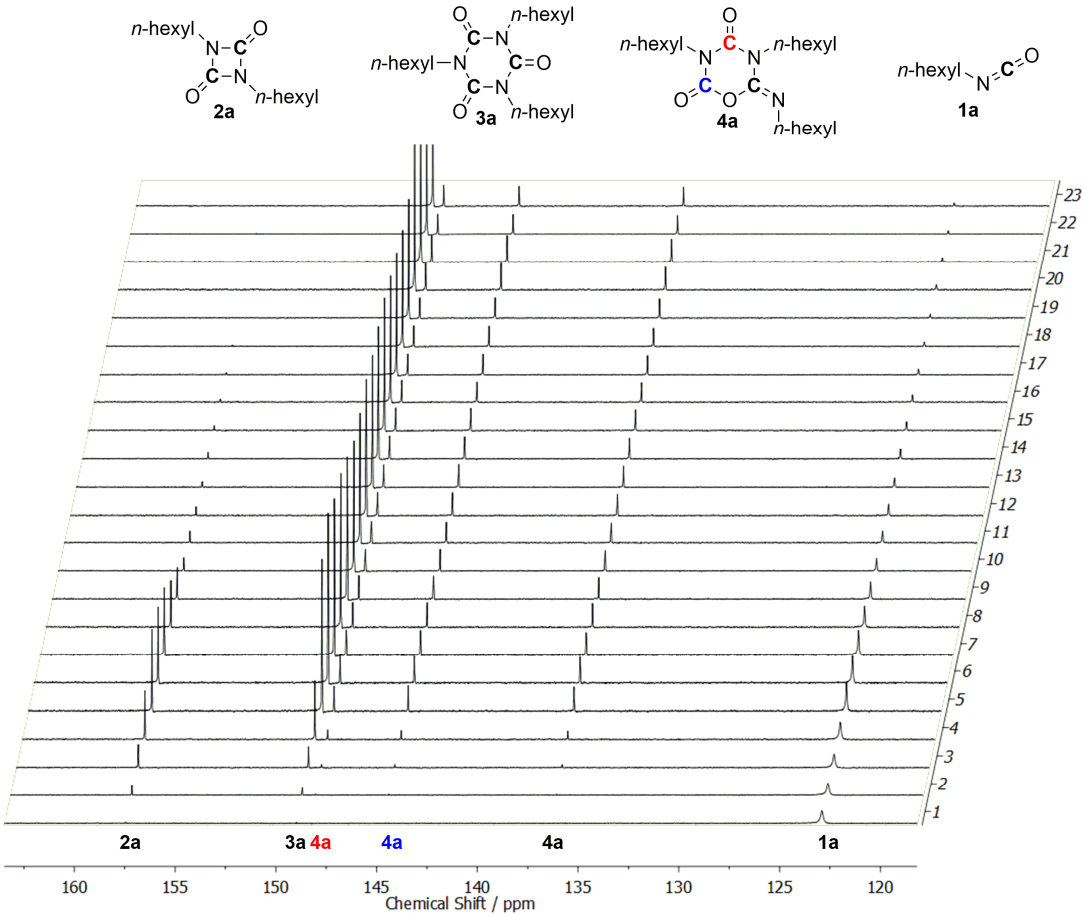

Figure S2: 3. *[Figure S3] ^{13}C NMR spectra of the carbonyl region of the oligomerization of **1a** catalyzed by 11.8 mol-% **5b** (o4).*

Table S2: 2. [Table S2] Number of ^{13}C NMR spectra and reaction times of o4.

Nr.	1	2	3	4	5	6	7	8	9	10	11	12
t / min	25	107	244	566	1555	1767	1978	3009	4404	8826	10287	13128
Nr.	13	14	15	16	17	18	19	20	21	22	23	
t / min	16318	21649	21673	30752	39001	60956	69567	93642	99731	111801	139841	

We were however not able to extract values from the ^{13}C NMR spectra that matched the ones obtained from ^{1}H and therefore concluded that ^{13}C might be used to visualize reaction progress as shown above but not for quantitative determination of turnover.

Identification of Key NMR Signals for Asymmetric Trimer 4a From Oligomerization Mixtures

Since our attempts to isolate asymmetric trimer **4a** were not successful, presumably due to the thermodynamically favored isomerization to isocyanurate **3a**, we extracted key ^{13}C and ^{15}N NMR signals from oligomerization reactions of **1a** and **1a^{15}** catalyzed by **5b**. This was done by assigning the signals already known from isolated compounds and literature and subsequent assigning of unknown signals based on 2D NMR spectra and splitting of signals. **Figure S2: 4** shows the carbonyl region of a ^{13}C NMR spectrum of the oligomerization of **1a^{15}** catalyzed by 50 mol-% **5b** after 1333 min at 23 °C (top) and spectrum 4 from **Table S2: 2** giving the signals for the ^{14}N oligomers for comparison (below).

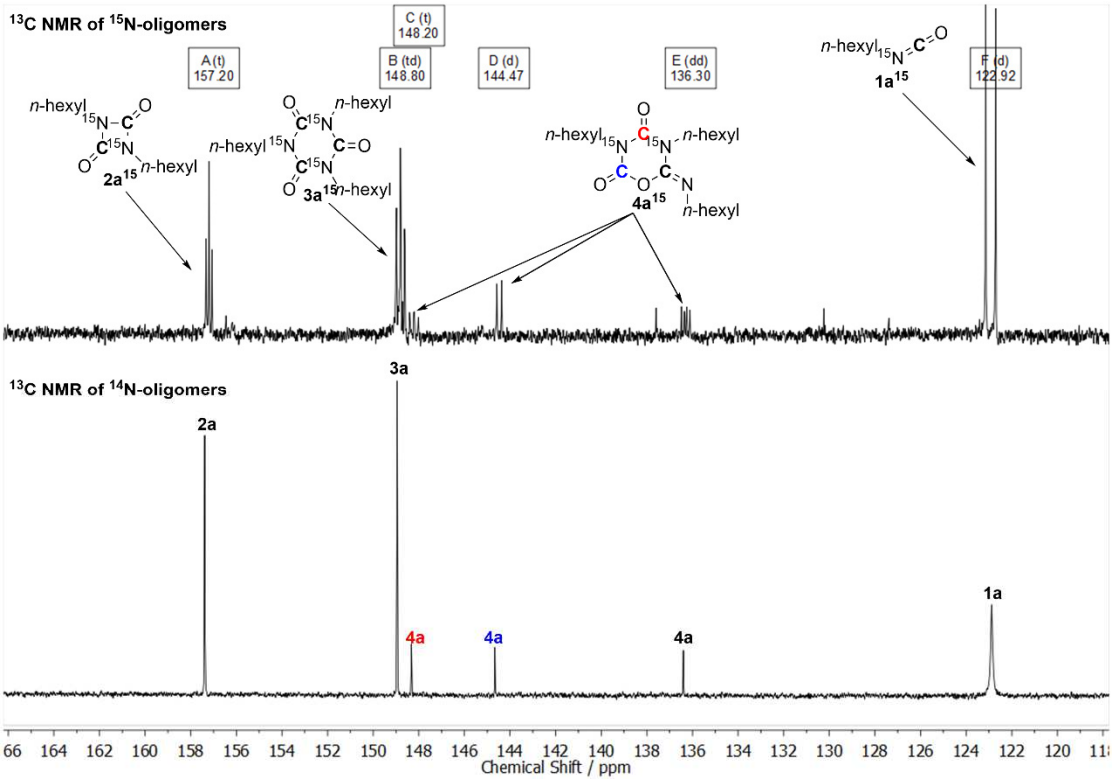

Figure S2: 4. *[Figure S4] ^{13}C NMR spectra of the carbonyl region of the oligomerization of **1a^{15}/1a** catalyzed by **5b**.*

For identification of the ^{15}N signals of asymmetric trimer **4a^{15}** we followed the same strategy. **Figure S2: 5** shows a $^{15}N\{^{1}H\}$ NMR spectrum of the range of ^{15}N oligomer signals for the oligomerization of **1a^{15}** catalyzed by 50 mol-% **5b**, while the full spectrum is shown in **Figure S2: 6**. Since this spectrum was measured under neat conditions, the signals observed here differ slightly from the ones measured for the purified compounds in $CDCl_3$. For both **2a^{15}** and **3a^{15}**, the signals shift to higher fields: 1.28 ppm and 2.08 ppm respectively. Asymmetric trimer **4a^{15}** is the only non-ionic oligomer to show signal splitting in proton-decoupled ^{15}N NMR. The imine-type ^{15}N-atom displays a doublet at −185.17 ppm (d, J = 5.2 Hz), the imide- type ^{15}N-atom, being structurally closest to the ones of **3a** forms a doublet at −250.29 ppm (d, J = 2.9 Hz) and the amide type ^{15}N-atom couples with both of the other ones to show a doublet of doublets at −259.14 ppm (dd, J = 5.2, 3.0 Hz).

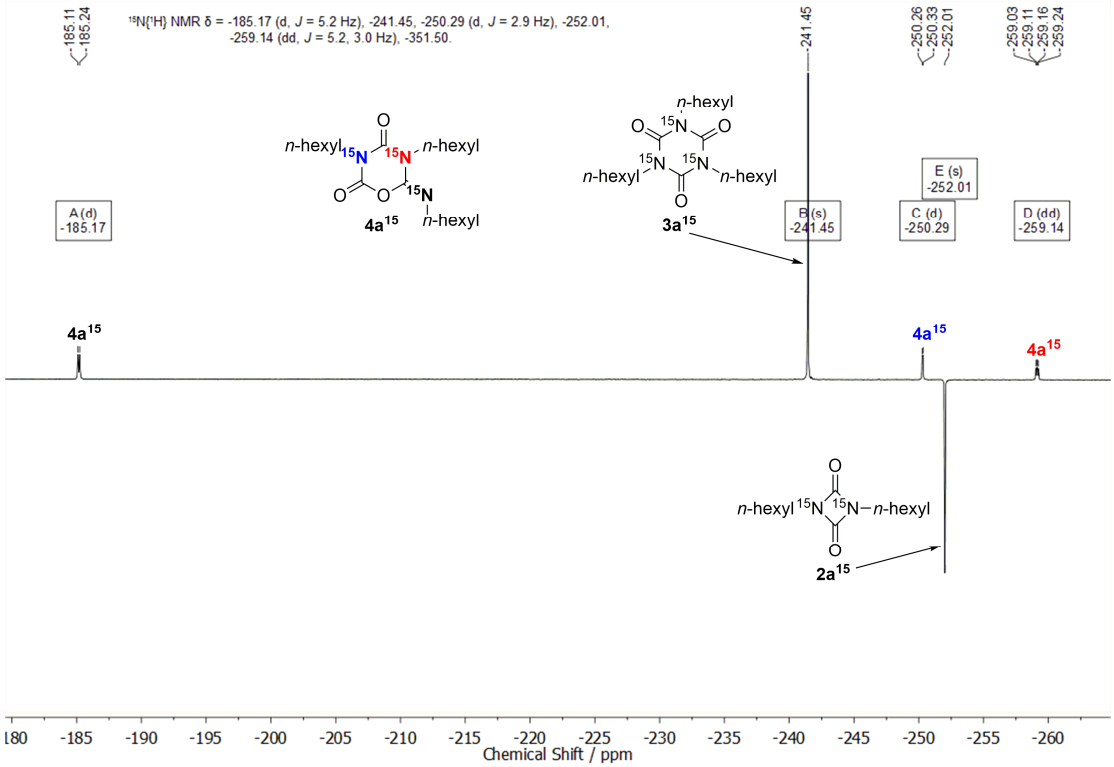

Figure S2: 5. *[Figure S5] $^{15}N\{^1H\}$ NMR spectrum of the reaction of* ***1a^{15}*** *catalyzed by 50 mol-%* ***5b*** *showing the range of the oligomer signals.*

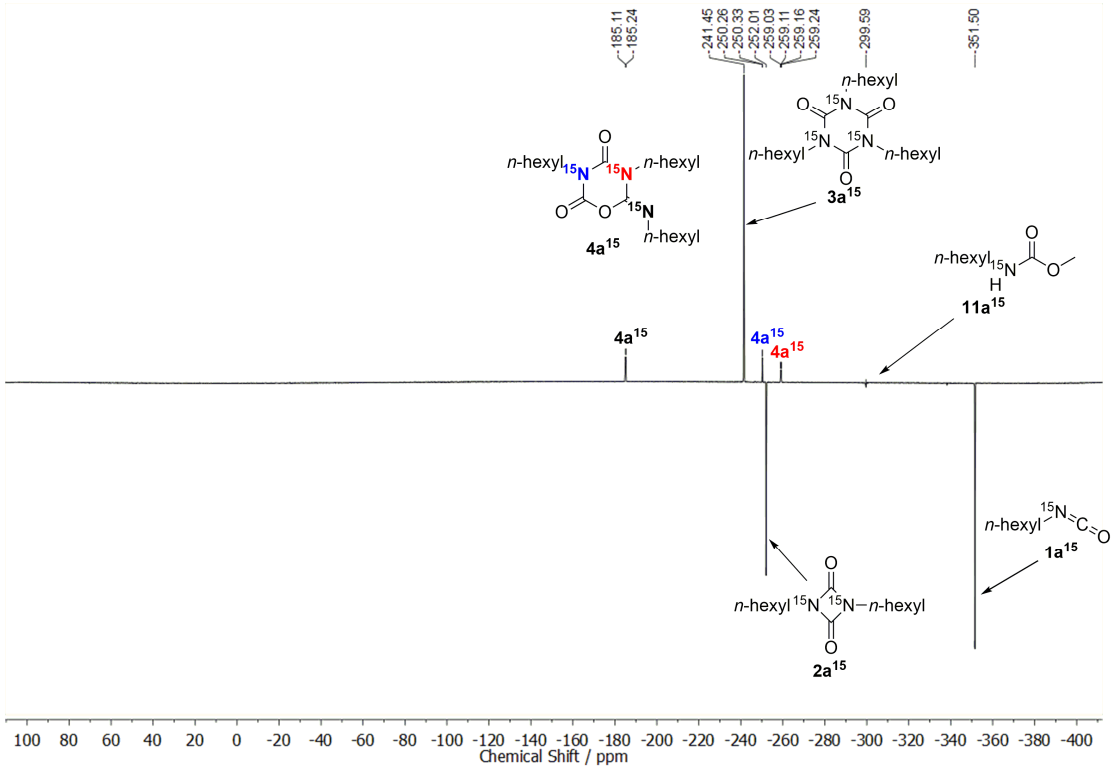

Figure S2: 6. *[Figure S6] Full $^{15}N\{^1H\}$ NMR spectrum of the reaction of* ***1a^{15}*** *catalyzed by 50 mol-%* ***5b****.*

2.1.5 Low Temperature NMR Measurements

After flame-sealing, the NMR samples were stored at −78 °C until measuring. Low temperature NMR measurements of oligomerization reactions were performed with 50 mol-% of PBu_3 (**Table S2: 1**, o8, o9). Reproducing of the results published by Horvath and Richter was done as described by measuring freshly prepared oligomerization mixtures.[4] The signal at −55.9 ±0.15 ppm was the only one found to appear in a temperature dependent manner, indicating a transient intermediate. **Figure S2: 7** shows the full $^{31}P\{^1H\}$ spectra of experiment o8 measured over the course of 3 h at different temperatures in the order they were obtained from top to bottom. The duration of the experiment was caused by the time it took to bring the NMR machine to the new temperature in between measurements and extended duration of the measurements (^{31}P: ca. 10 min). The first two spectra were recorded with 32 scans while the lower three were measured with 128 scans giving a satisfactory signal-to-noise ratio. Therefore, all further low temperature ^{31}P NMR spectra were recorded with 128 scans.

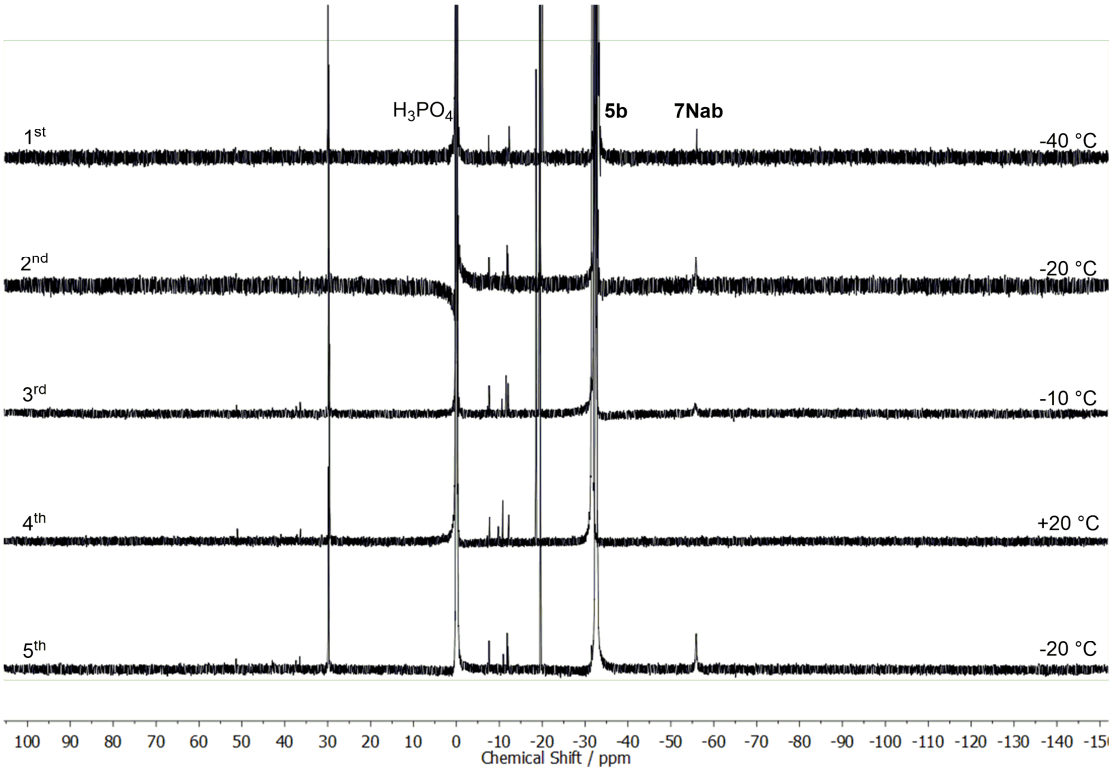

Figure S2: 7. *[Figure S7] $^{31}P\{^1H\}$ NMR spectra of experiment o8 measured at different temperatures. The spectra were recorded in the order indicated on the left.*

During these 3 h, the reaction progressed to a minor extent as indicated by **Figure S2: 8**, which shows the ^1H NMR spectra of the same reaction taken directly after each respective ^{31}P spectrum.

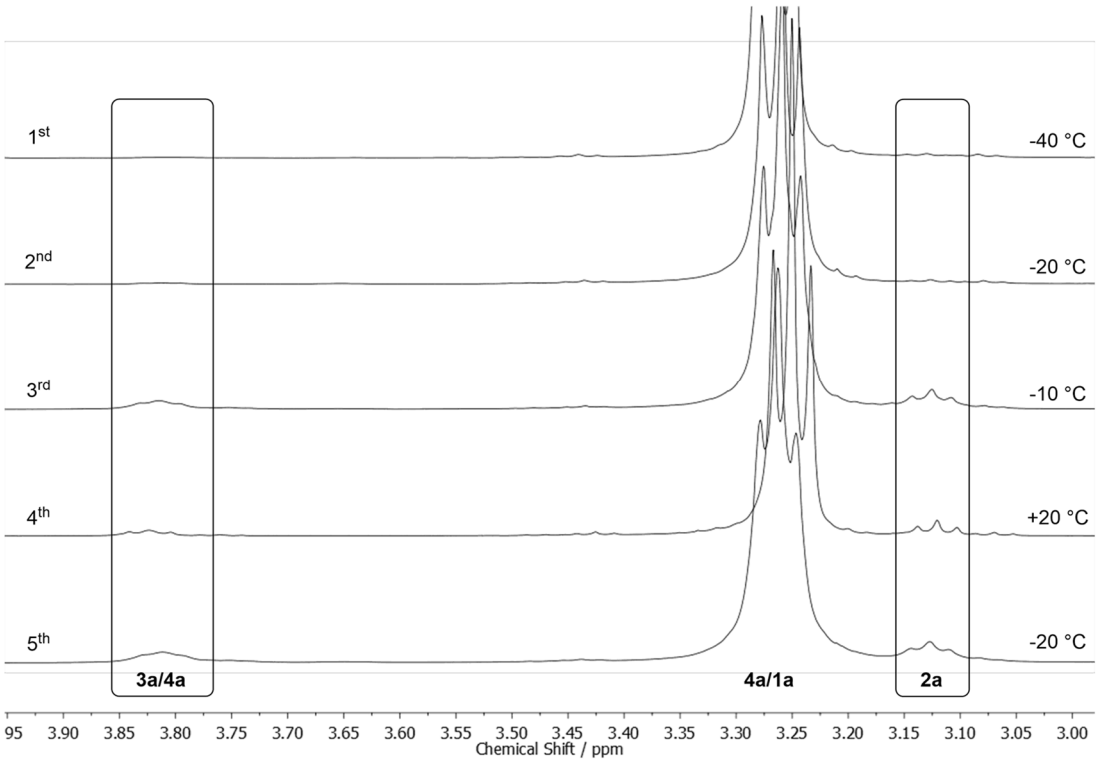

Figure S2: 8. *[Figure S8] ^{1}H NMR spectra of experiment o8 measured at different temperatures directly after the respective ^{31}P NMR spectra. The spectra were recorded in the order indicated on the left.*

Low temperature NMR measurements of the oligomerization of ^{15}*N*-hexyl isocyanate **1a**[15] were done in the same manner with 50 mol-% of **5b** (experiment o9). The ^{31}P{^{1}H}, ^{15}N{^{1}H}, ^{15}N spectra obtained at −40 °C are shown in **Figure S2: 9** – **Figure S2: 11** below and key regions showing cyclic intermediate **7Nab**[15] are magnified.

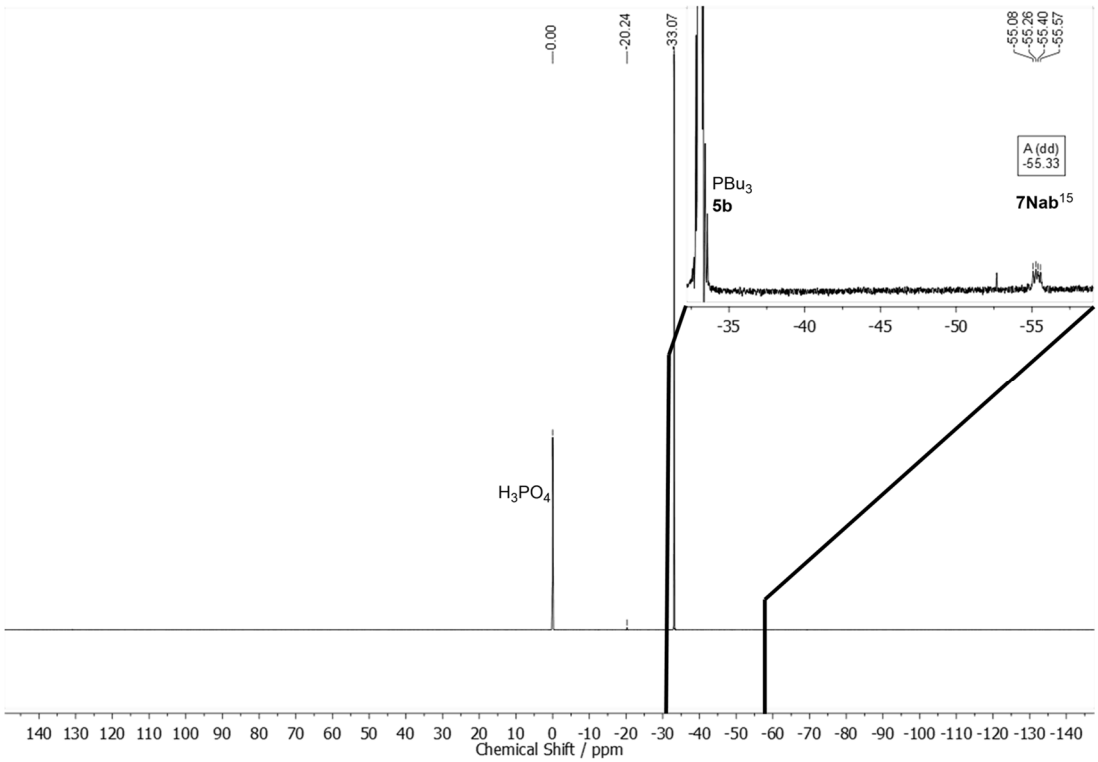

Figure S2: 9. *[Figure S9] ^{31}P{^{1}H} NMR spectrum of experiment o9 measured at −40 °C.*

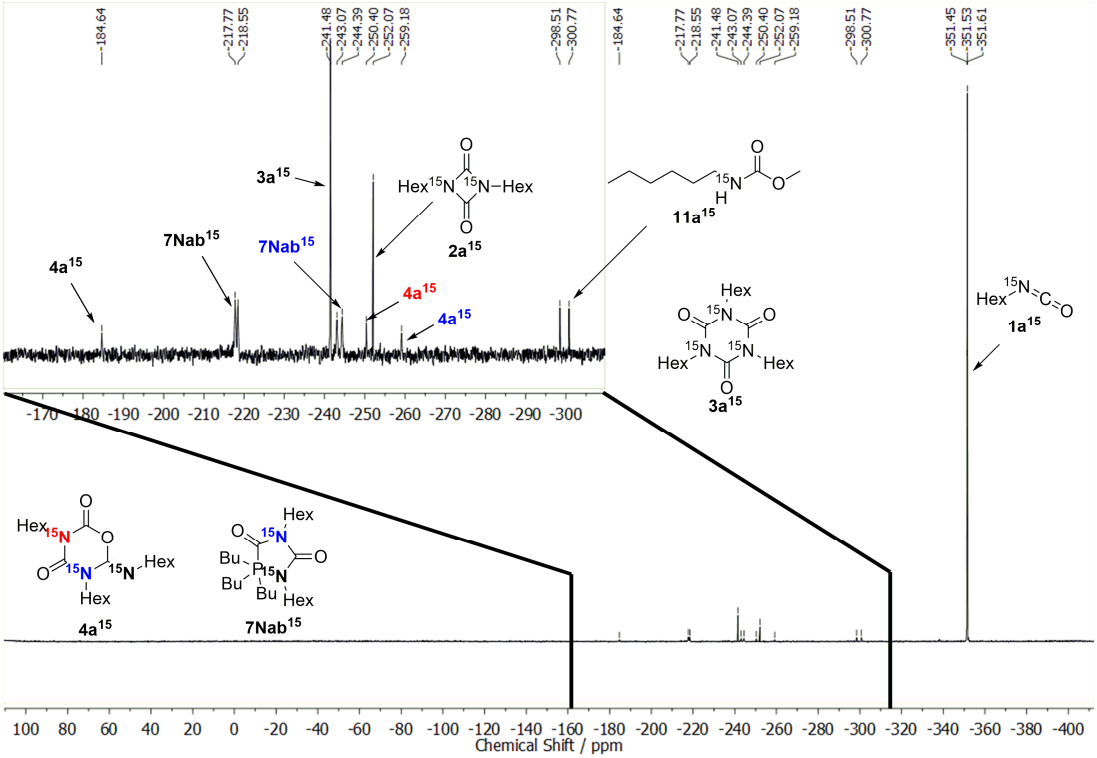

Figure S2: 10. *[Figure S10] ^{15}N NMR spectrum of experiment o9 measured at −40 °C.*

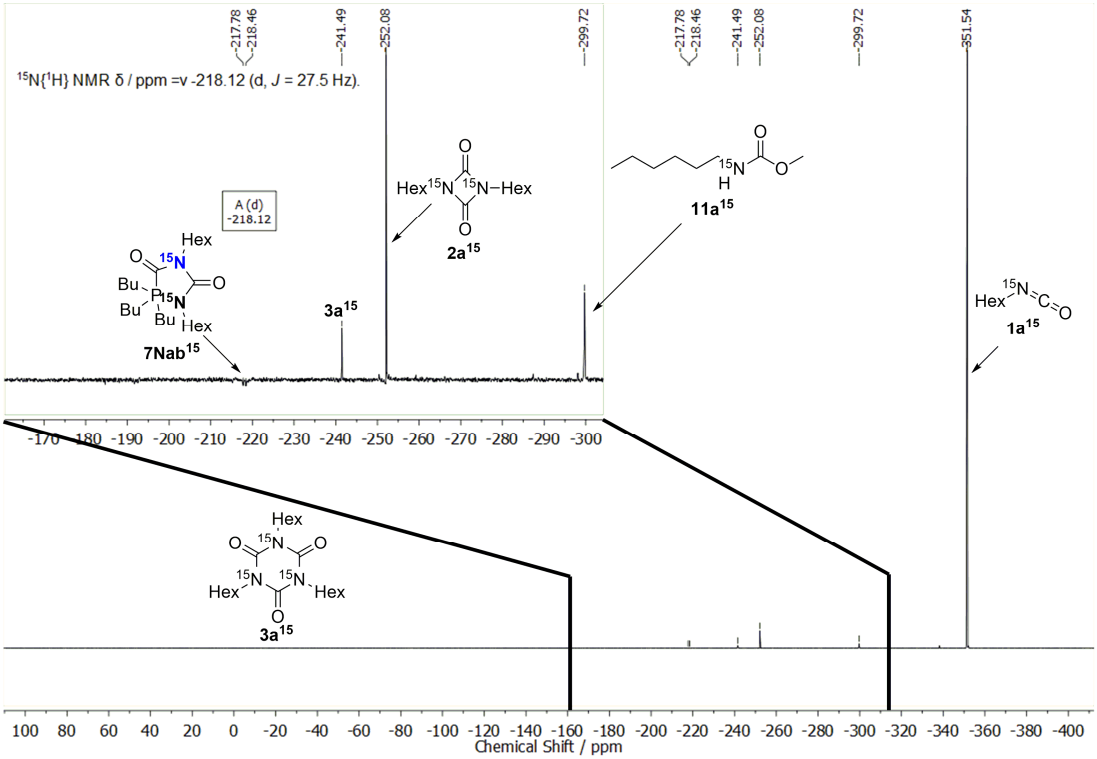

Figure S2: 11. *[Figure S11] ^{15}N{^{1}H} NMR spectrum of experiment o9 measured at −40 °C.*

2.1.6 Details of ^{1}H NMR Kinetic Measurements

Experiment o1 (1.521 mmol **1a** catalyzed by 0.778 mmol **5b**)

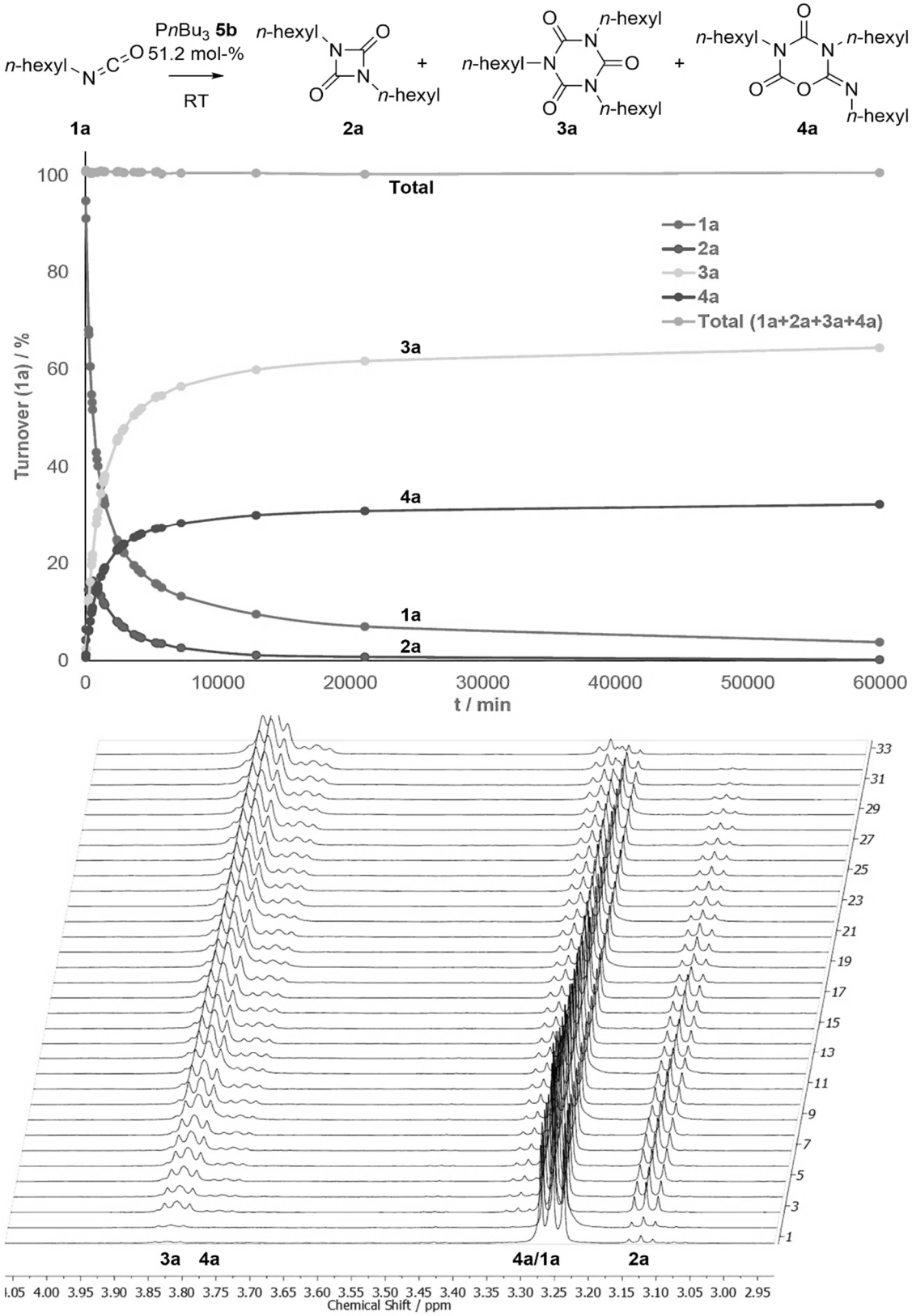

Figure S2: 12. *[Figure S12] Top: Visualization of the turnover values obtained for experiment o1; Turnover values are given as a mass-fraction of isocyanate* ***1a*** *Bottom: Stacked ^{1}H NMR spectra of experiment o1 (oligomerization of* ***1a*** *catalyzed by 51.2 mol-%* ***5b****) region of CH_2-groups adjacent to NCO-moiety.*

Experiment o2 (1.757 mmol **1a** catalyzed by 0.605 mmol **5b**)

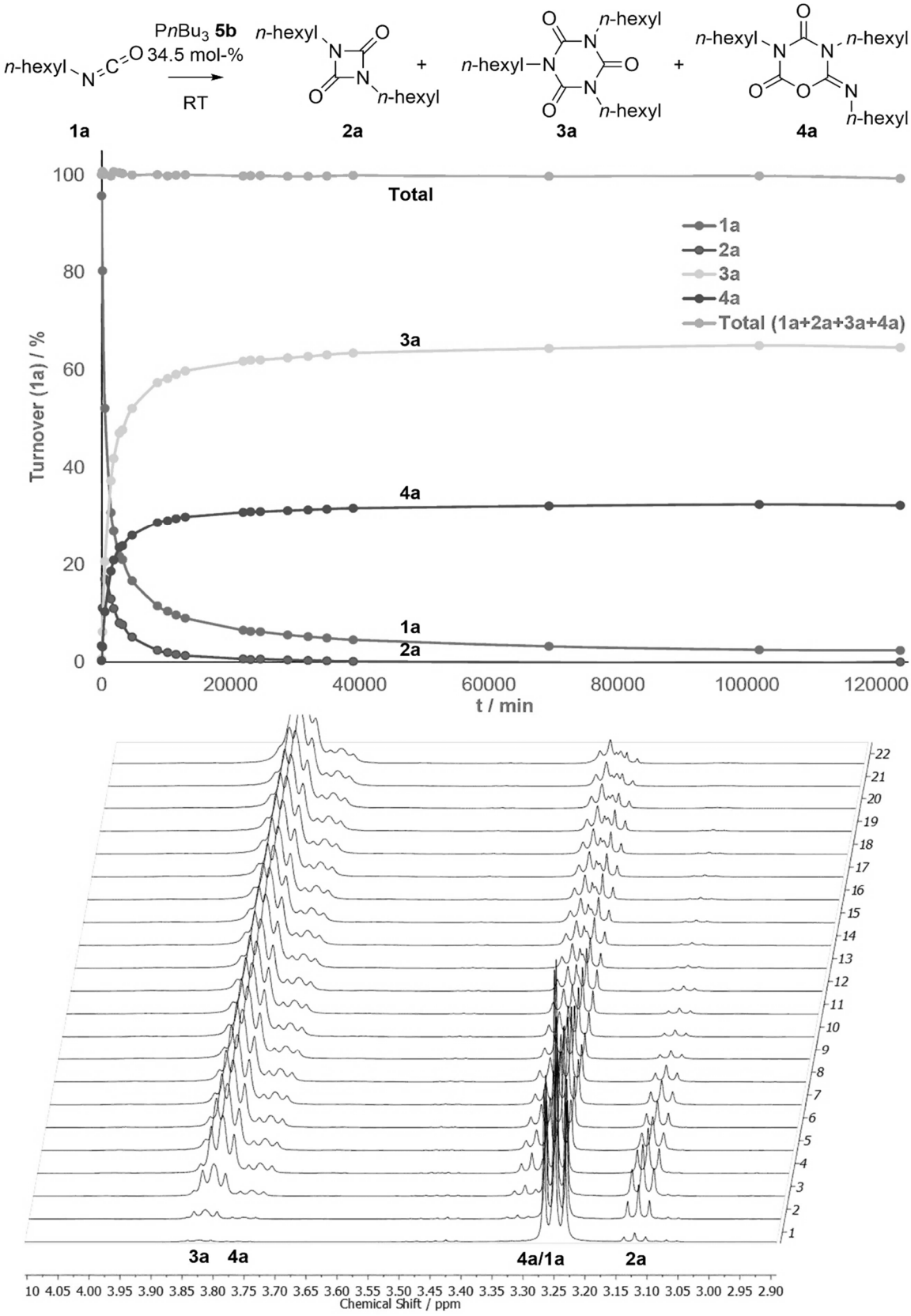

Figure S2: 13. *[Figure S13] Top: Visualization of the turnover values obtained for experiment o2. Turnover values are given as a mass-fraction of isocyanate* ***1a****; Bottom: Stacked* ^{1}*H NMR spectra of experiment o2 (oligomerization of* ***1a*** *catalyzed by 34.5 mol-%* ***5b****) region of* CH_2*-groups adjacent to NCO-moiety.*

Experiment o3 (1.818 mmol **1a** catalyzed by 0.604 mmol **5b**)

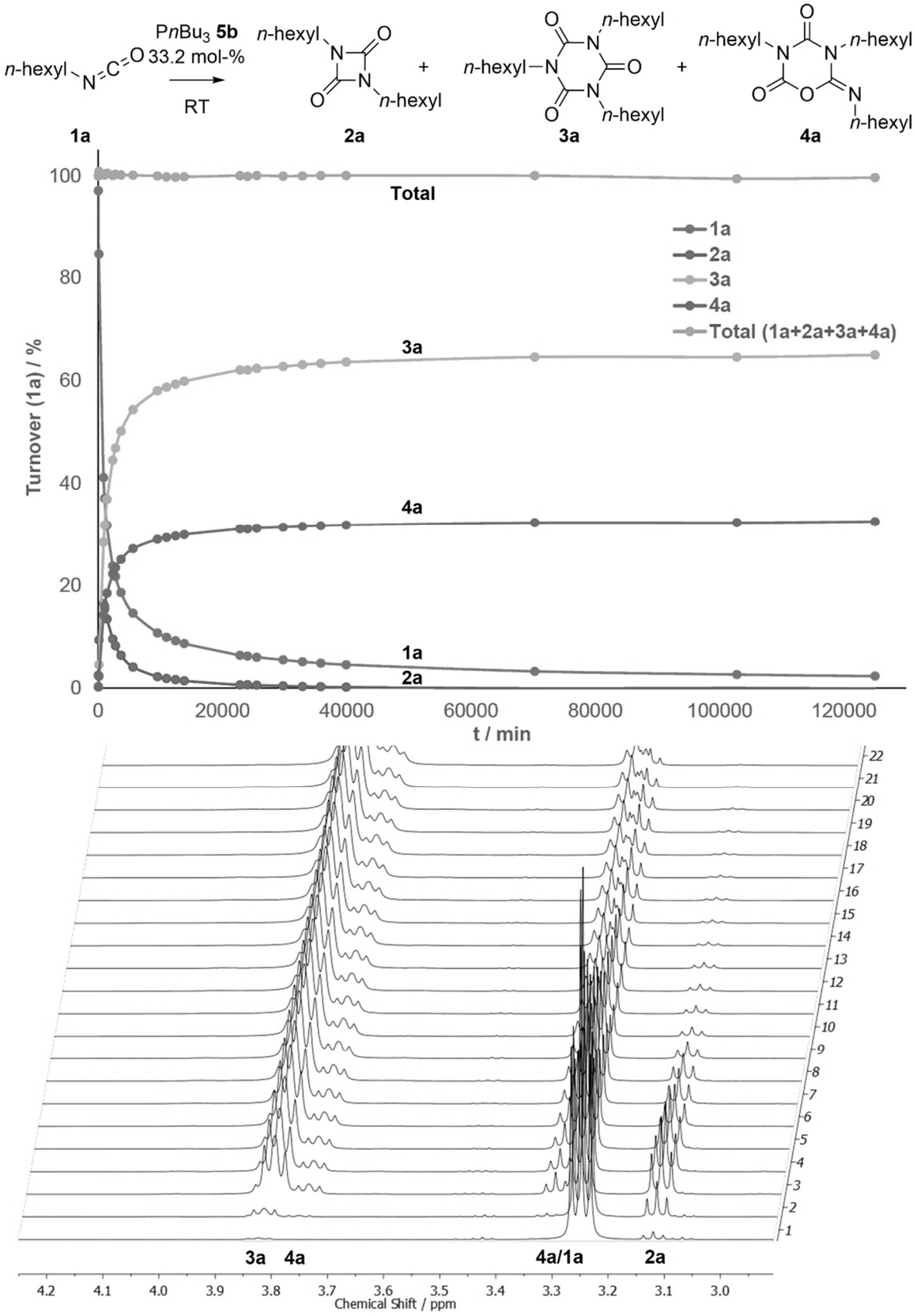

Figure S2: 14. *[Figure S14] Top: Visualization of the turnover values obtained for experiment o3. Turnover numbers are given as a mass-fraction of isocyanate* ***1a****; Bottom: Stacked* ^{1}*H NMR spectra of experiment o3 (oligomerization of* ***1a*** *catalyzed by 33.2 mol-%* ***5b****) region of* CH_2*-groups adjacent to NCO-moiety.*

Experiment o4 (2.399 mmol **1a** catalyzed by 0.283 mmol **5b**)

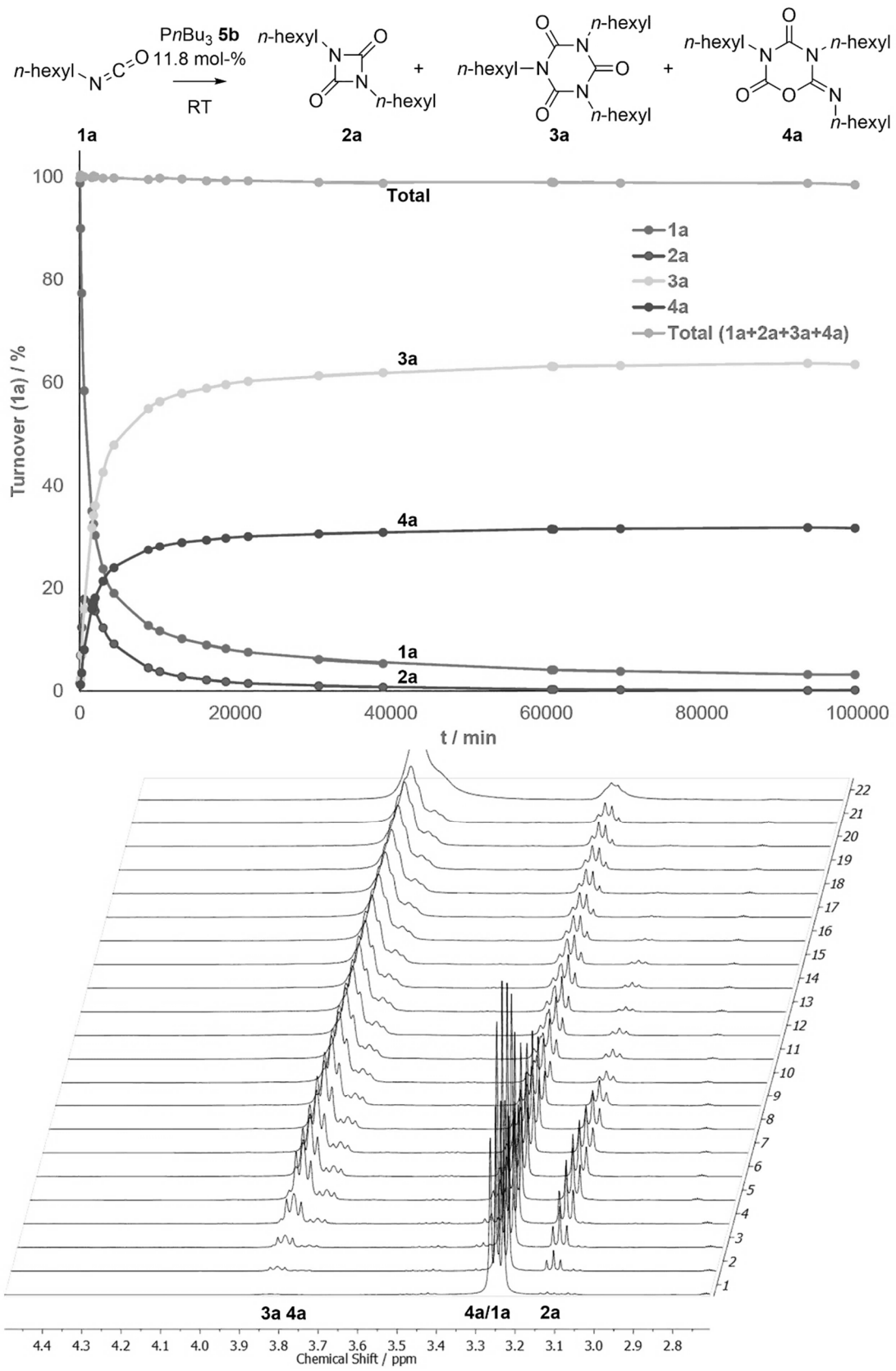

Figure S2: 15. *[Figure S15] Top: Visualization of the turnover values obtained for experiment o4. Turnover numbers are given as a mass-fraction of isocyanate* ***1a****; Bottom: Stacked* ^{1}*H NMR spectra of experiment o4 (oligomerization of* ***1a*** *catalyzed by 11.8 mol-%* ***5b****) region of* CH_2*-groups adjacent to NCO-moiety.*

Experiment o5 (2.392 mmol **1a** catalyzed by 0.281 mmol **5b**)

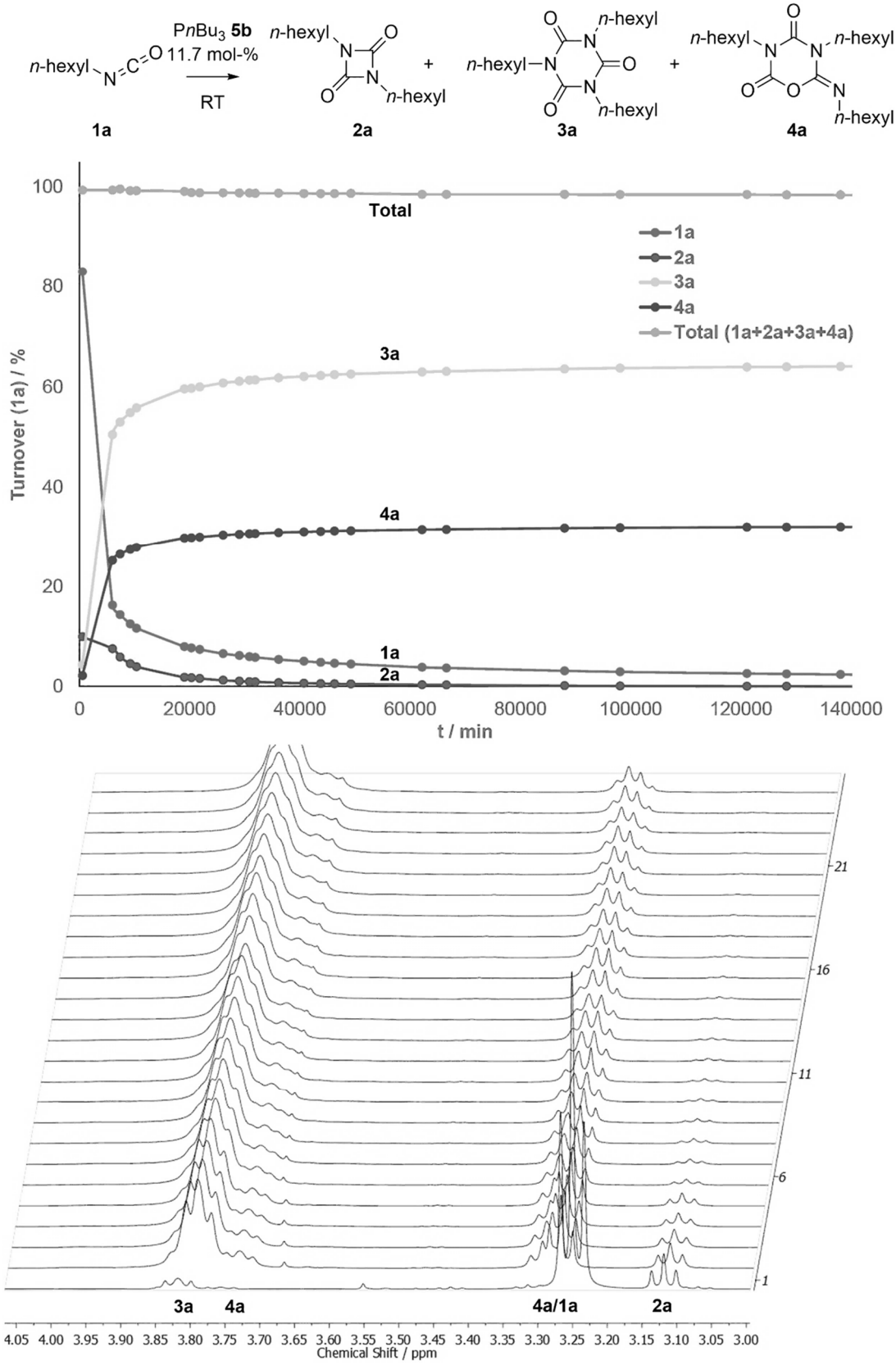

Figure S2: 16. *[Figure S16] Top: Visualization of the turnover values obtained for experiment o5. Turnover numbers are given as a mass-fraction of isocyanate* ***1a****; Bottom: Stacked* ^{1}*H NMR spectra of experiment o5 (oligomerization of* ***1a*** *catalyzed by 11.7 mol-%* ***5b****) region of* CH_2*-groups adjacent to NCO-moiety.*

Experiment o6 (2.827 mmol **1a** catalyzed by 0.034 mmol **5b**)

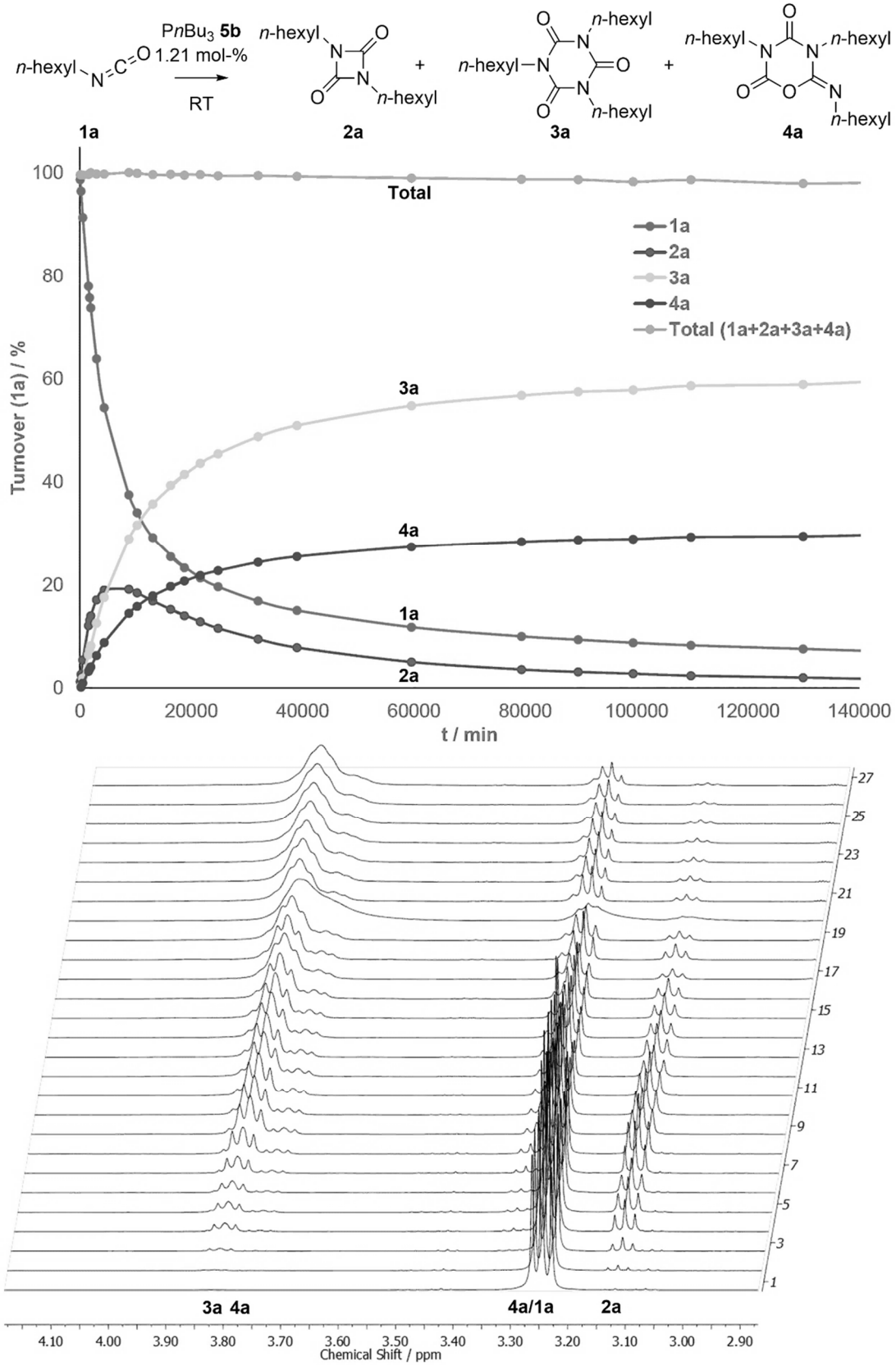

Figure S2: 17. *[Figure S17] Top: Visualization of the turnover values obtained for experiment o6. Turnover numbers are given as a mass-fraction of isocyanate* ***1a****; Bottom: Stacked* ^{1}*H NMR spectra of experiment o6 (oligomerization of* ***1a*** *catalyzed by 1.21 mol-%* ***5b****) region of* CH_2*-groups adjacent to NCO-moiety.*

Experiment o7 (2.801 mmol **1a** catalyzed by 0.035 mmol **5b**)

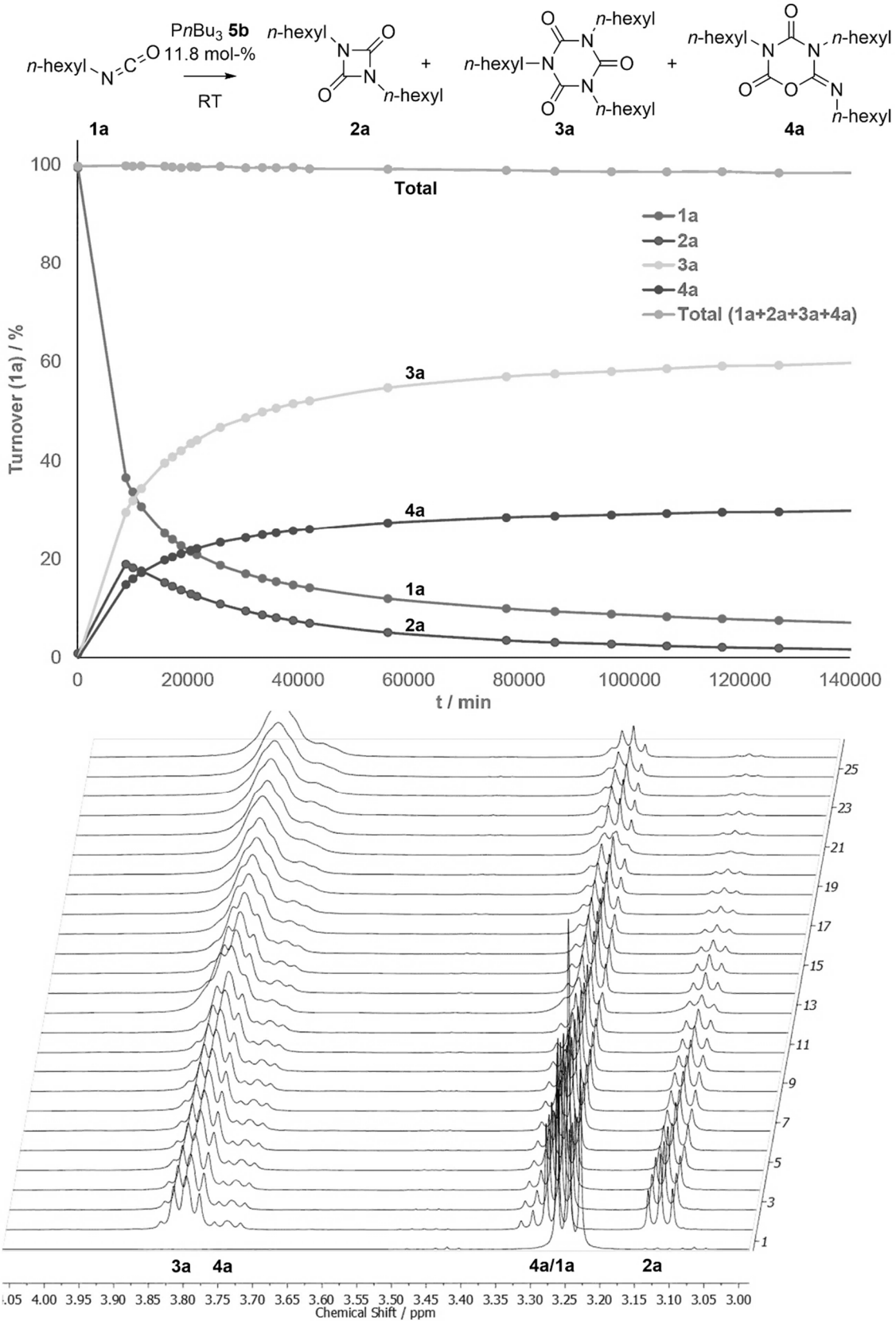

Figure S2: 18. *[Figure S18] Top: Visualization of the turnover values obtained for experiment o7. Turnover numbers are given as a mass-fraction of isocyanate* ***1a****; Bottom: Stacked* ^{1}*H NMR spectra of experiment o7 (oligomerization of* ***1a*** *catalyzed by 1.26 mol-%* ***5b****) region of* CH_2*-groups adjacent to NCO-moiety.*

Simulations of Kinetic Parameters Using COPASI[5]

Using the turnover values for the different observable compounds as detailed in the previous section, we simulated kinetic parameters of interest. Since the mechanism proposed in this study contains several species that are not quantitatively observable, we used two heavily simplified models for the parameter estimation option (default settings) of COPASI.

Model 1:

Model 1 concentrates the whole reaction into just one reversible step completely ignoring the amounts of catalyst added and combining the stable final products in one named Trimer as shown in **Scheme S2: 2**.

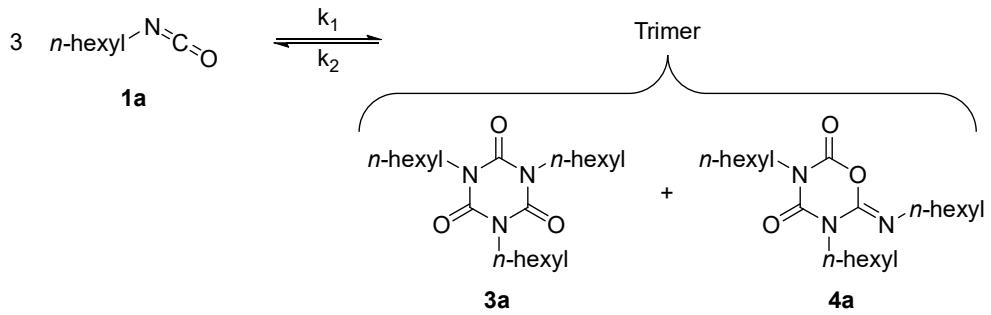

Scheme S2: 2. *[Scheme S2] Model 1 used in COPASI simulations.*

This very basic model allowed generating one overall rate constant for the formation of trimers **3a** and **4a** whose amounts are combined into one value for overall final product. The value obtained this way was then plotted vs. the concentration of catalyst **5b** present in the oligomerization mixture. A linear correlation is found which shows a very good fit for the measurements using up to 34 mol-% of catalyst (o2 – o7) (**Figure S2: 19a**, **Table S2: 3**, Entries 2 – 7). The measurement containing 51 mol-% of phosphane **5b** (o1) does decrease the quality of the linear fit to some degree, although some deviation from the expected values is explainable by the very simplified model not taking into account the amount of catalyst (**Figure S2: 19b**, **Table S2: 3**, Entry 1).

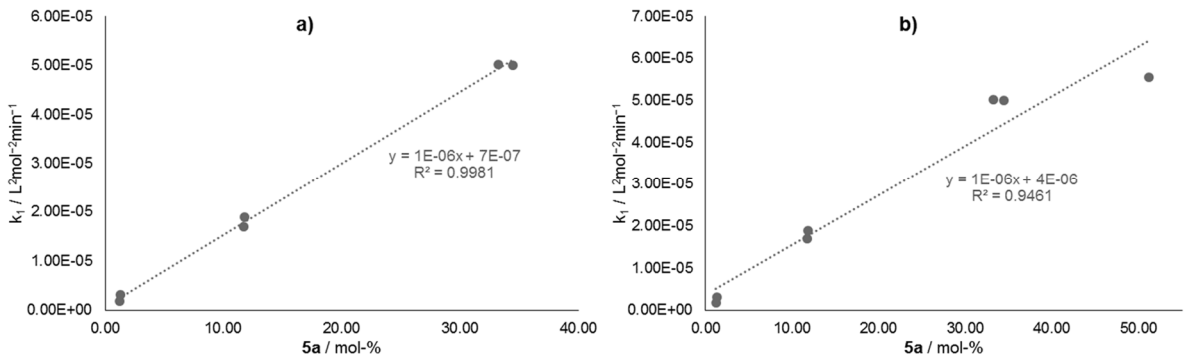

Figure S2: 19. *[Figure S19] Reaction rates k_1 plotted against catalyst concentration c(**5b**). a) shows oligomerization experiments o2 – o7 with concentrations ranging from 1.2 mol-% to 34 mol-% while b) also includes o1 containing 51 mol-% of phosphine **5b**.*

Table S2: 3. [Table S10] Rate constants k_1 and k_2 obtained by Model1.

Entry	Reaction	k_1 / $L^2mol^{-2}min$	k_2 / $1min^{-1}$	Catalyst **5b** / mol-%
1	o1	5.56E-05	1.24E-20	51.17
2	o2	5.01E-05	3.69E-22	34.46
3	o3	5.03E-05	1.89E-21	33.23
4	o4	1.88E-05	5.51E-22	11.81
5	o5	1.69E-05	5.73E-22	11.74
6	o6	1.76E-06	5.78E-22	1.21
7	o7	3.14E-06	1.00E-30	1.26

The estimation of the rate of the uncatalyzed background reaction ($k_1 = 7\times10^{-7}\ L^2\,mol^{-2}\,min^{-1}$) resulting from the linear correlation for truly "catalytic amounts" is in full agreement with the stability and storability of pure isocyanates.

Model 2:

Model 2 simplifies the mechanism into two reversible steps and four that we model to be irreversible due to the stability of the final products (**Scheme S2: 3**). This requires eight rate constants which are fitted with COPASI to the experimental kinetic data (time-dependent concentrations of compounds **1a**, **2a**, **3a** and **4a**).

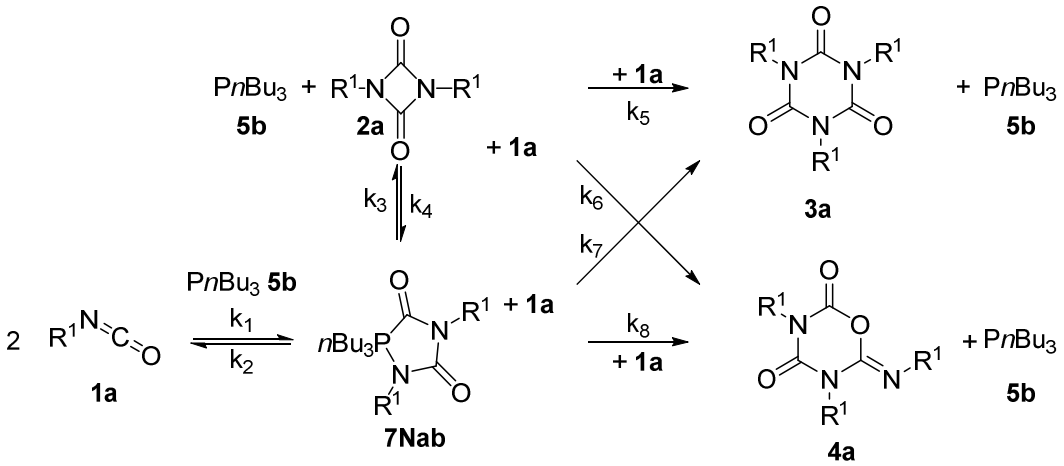

Scheme S2: 3. *[Scheme S3] Model 2 used in COPASI simulations.*

Fitting the rate constants to the mechanism shown in **Scheme S2: 3** was done in an iterative fashion, starting from the individual rate constants determined for each of the measurements (**Table S2: 4**, Entries 1 – 7). Reducing the number of "variable rate constants" in an iterative fashion, we finally arrived at the single set of rate constants shown in **Table S2: 5** for all kinetic measurements.

Table S2: 4. [Table S11] Rate constants k_1 to k_8 obtained by Model2. Individual rate constants determined for each of the independent measurements.

Entry	Reaction	Catalyst **5b** / mol-%	k_1 / L^2 mol^{l-2} min^{-1}	k_2 / 1 min^{-1}	k_3 / 1 min^{-1}	k_4 / L mol^{-1} min^{-1}	k_5 / L mol^{-2} min^{-2}	k_6 / L mol^{-2} min^{-2}	k_7 / L mol^{-1} min^{-1}	k_8 / L mol^{-1} min^{-1}
1	o1	51.17	5.413E-04	3.182E+01	6.305E+00	4.276E-04	2.503E-04	1.248E-04	4.340E-01	2.210E-01
2	o2	34.46	8.637E-03	1.192E+01	1.275E-01	3.361E-04	2.502E-04	1.247E-04	7.984E-03	4.021E-03
3	o3	33.23	1.269E-03	3.434E+00	2.763E-01	3.609E-04	2.640E-04	1.312E-04	1.455E-02	7.422E-03
4	o4	11.81	1.361E-03	3.386E+00	2.964E-01	3.941E-04	2.808E-04	1.378E-04	1.262E-02	6.567E-03
5	o5	11.74	2.872E-04	7.209E-01	3.674E-01	4.018E-04	2.672E-04	1.279E-04	1.937E-02	1.065E-02
6	o6	1.21	1.204E-04	1.267E-01	4.328E+00	6.575E-03	3.706E-04	1.823E-04	1.160E-10	1.000E-10
7	o7	1.26	1.308E-04	1.637E-01	3.670E+00	7.048E-03	3.507E-04	1.732E-04	4.857E-10	2.665E-10
8		Average (without Entry 2)	6.183E-04	7.367E+00	2.196E+00	2.221E-03	2.905E-04	1.431E-04	6.979E-02	3.566E-02
9		Standard deviation (without Entry 2)	5.125E-04	1.136E+01	2.364E+00	3.027E-03	4.603E-05	2.282E-05	1.584E-01	8.060E-02

Table S2: 5. [Table S12] Full set of rate constants k_1 to k_8.

k_1 / L^2 mol^{l-2} min^{-1}	k_2 / 1 min^{-1}	k_3 / 1 min^{-1}	k_4 / L mol^{-1} min^{-1}	k_5 / L mol^{-2} min^{-2}	k_6 / L mol^{-2} min^{-2}	k_7 / L mol^{-1} min^{-1}	k_8 / L mol^{-1} min^{-1}
6.183E-04	1.625E+01	2.857E+00	3.206E-04	3.050E-04	1.509E-04	8.621E-02	4.357E-02

Throughout the fitting process, the fit of the mechanistic model towards the experimental values remains quite good. Nevertheless, in order to test the validity of the single set of rate constants, we use the “Time-Course” function of COPASI generating a simulated set of time-dependent concentration curves for comparison with the experimental data (**Figure S2: 20** – **Figure S2: 26**).

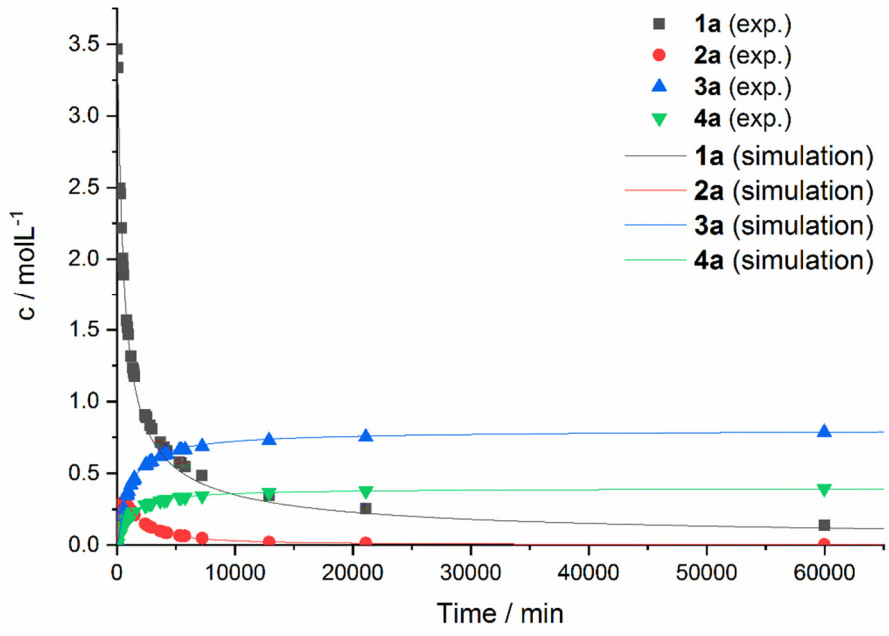

Figure S2: 20. *[Figure S20] Comparison of experimentally determined and simulated concentrations for oligomerization reaction o1.*

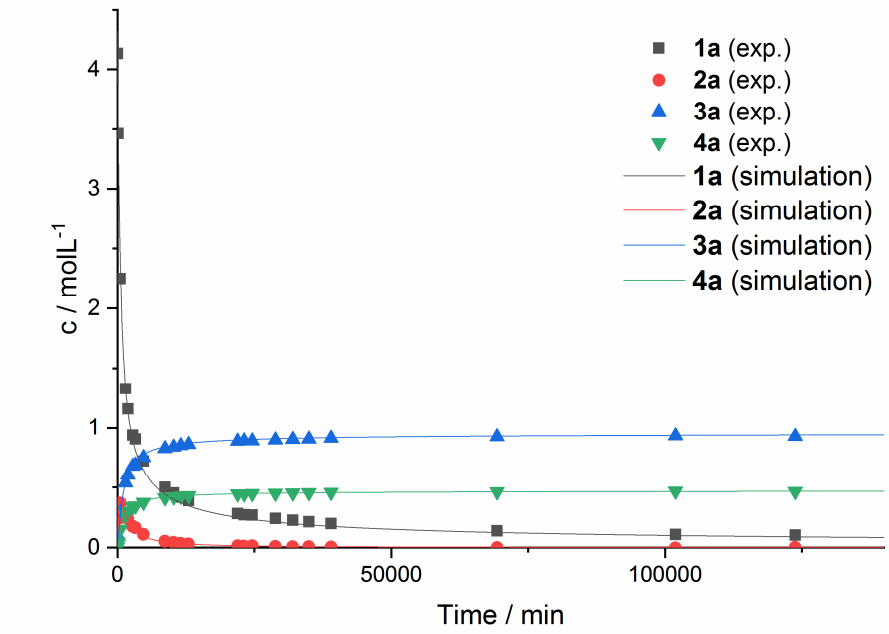

Figure S2: 21. *[Figure S21] Comparison of experimentally determined and simulated concentrations for oligomerization reaction o2.*

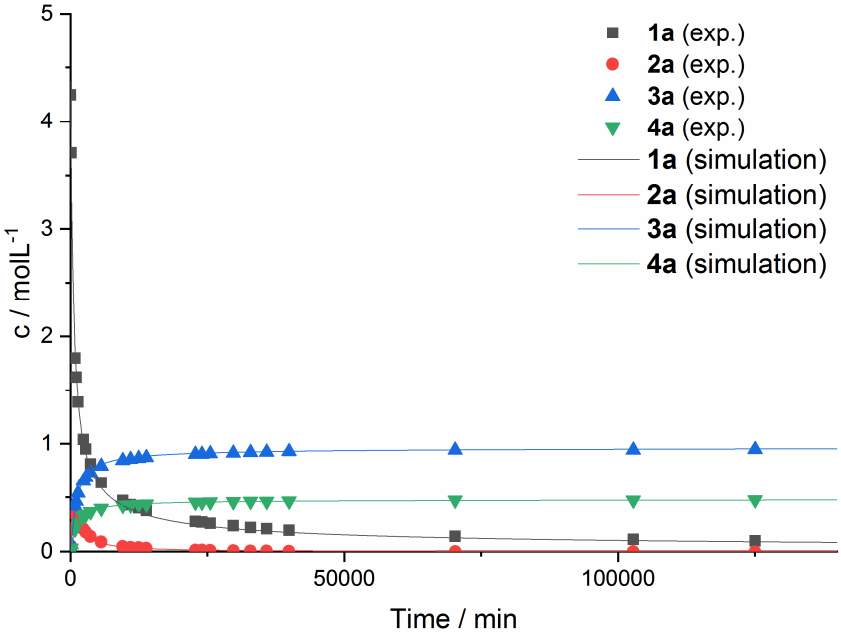

Figure S2: 22. *[Figure S22] Comparison of experimentally determined and simulated concentrations for oligomerization reaction o3.*

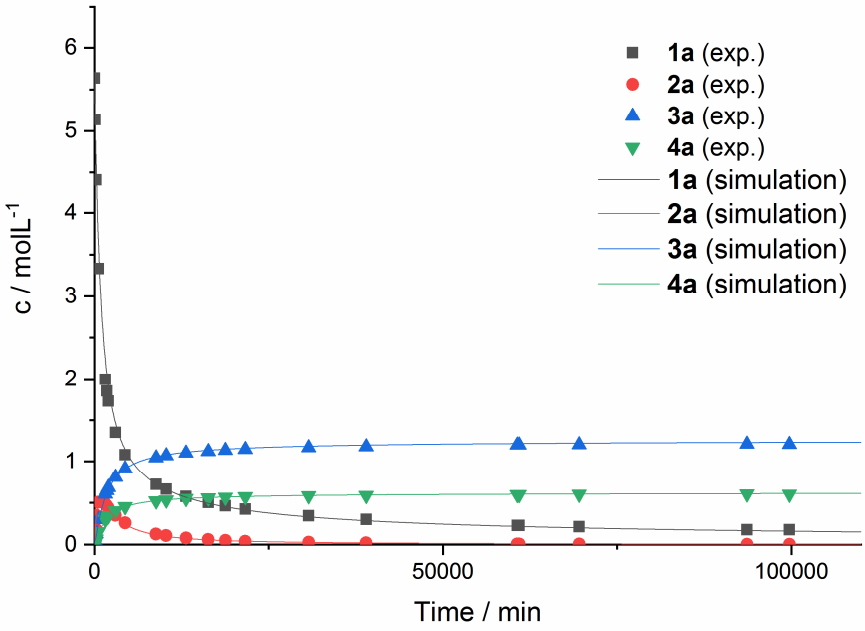

Figure S2: 23. *[Figure S23] Comparison of experimentally determined and simulated concentrations for oligomerization reaction o4.*

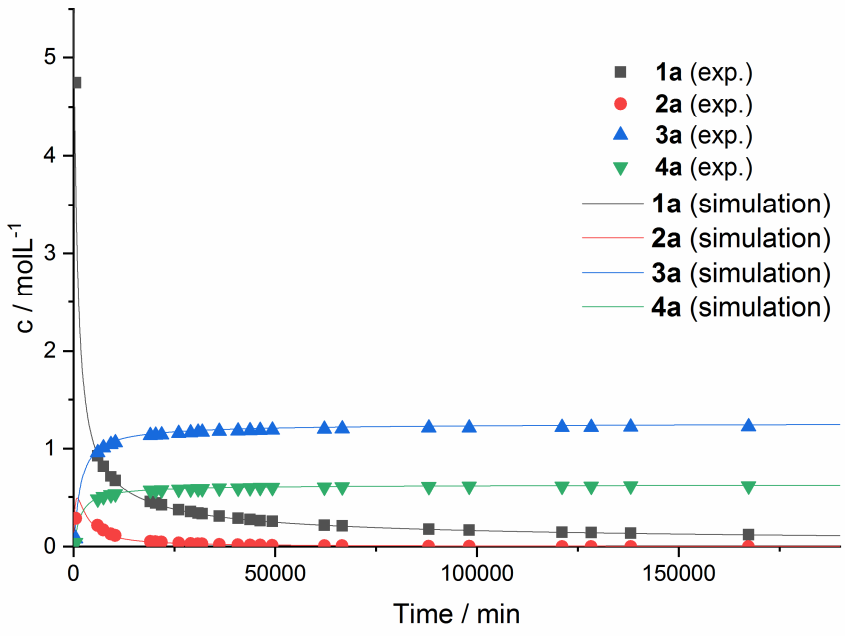

Figure S2: 24. *[Figure S24] Comparison of experimentally determined and simulated concentrations for oligomerization reaction o5.*

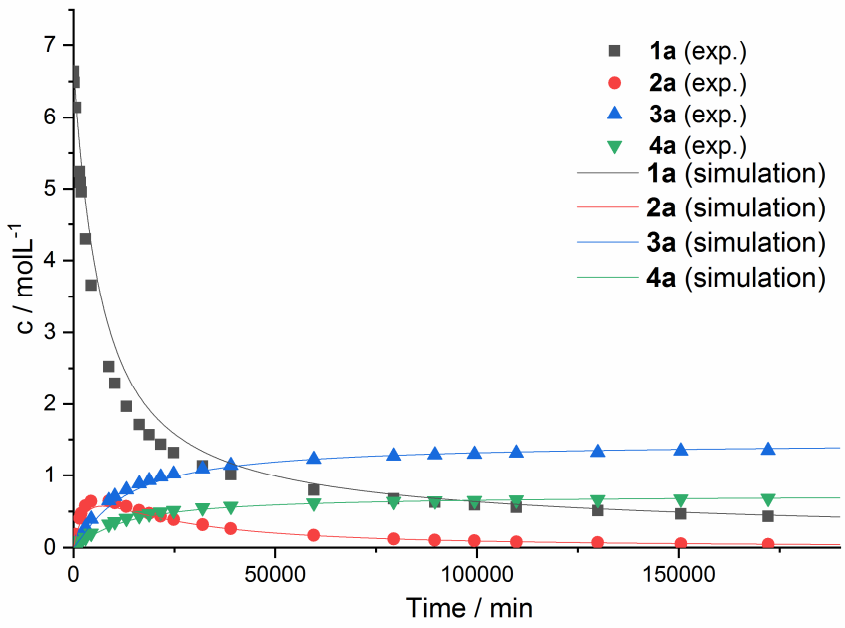

Figure S2: 25. *[Figure S25] Comparison of experimentally determined and simulated concentrations for oligomerization reaction o6.*

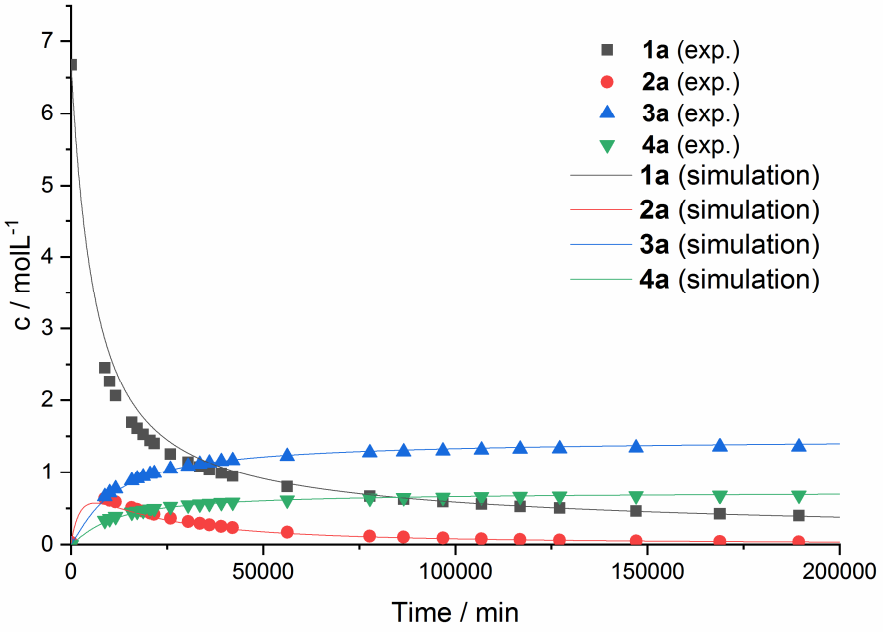

Figure S2: 26. *[Figure S26] Comparison of experimentally determined and simulated concentrations for oligomerization reaction o7.*

We also used the "Time-Course" function of COPASI to calculate the time dependent concentrations of intermediate **7Nab** first for the initially generated, widely varying set of individual rate constants (**Table S2: 4**, Entries 1 – 7), displayed in **Figure S2: 27**, and then for the single set of constants (**Table S2: 5**), shown in **Figure S2: 28**.

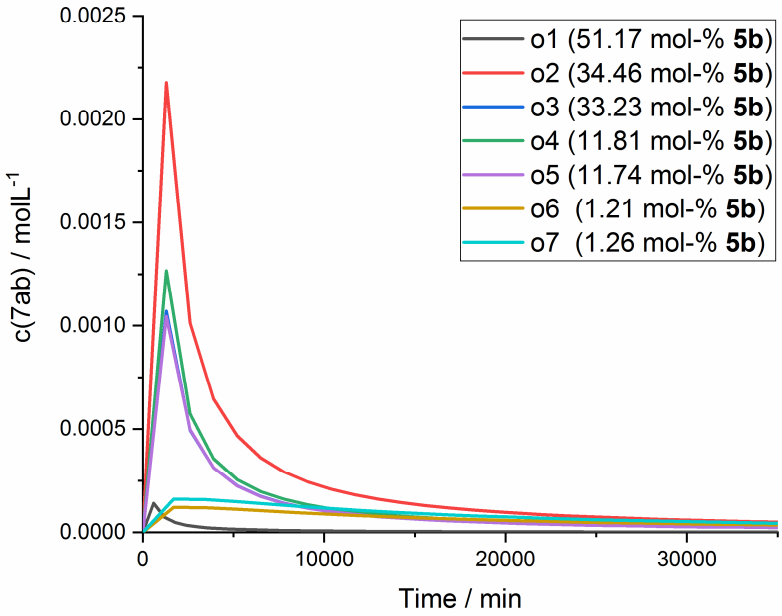

Figure S2: 27. *[Figure S27] Time dependent concentrations for intermediate **7Nab** simulated using COPASI according to Model2 (initially generated set of individual rate constants).*

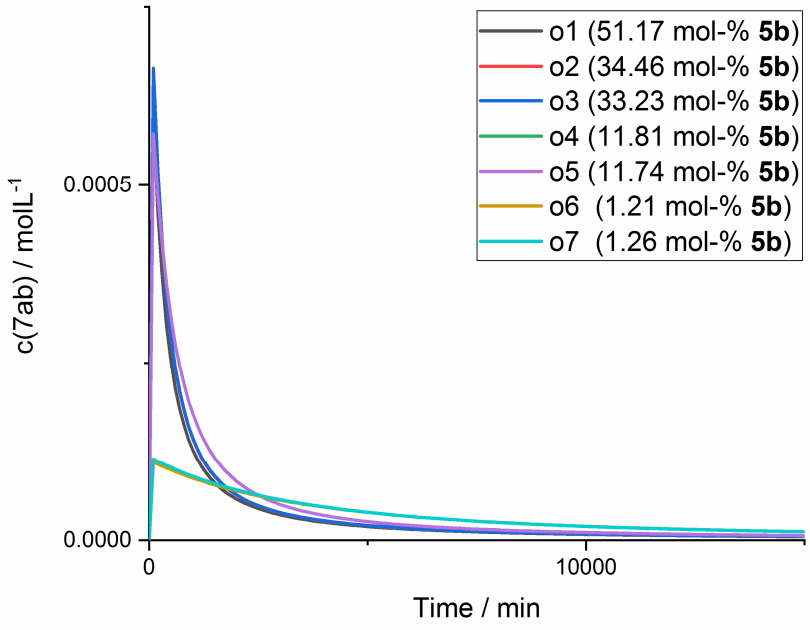

Figure S2: 28. *[Figure S28] Time dependent concentrations for intermediate* ***7Nab*** *simulated using COPASI according to Model 2 (single set of rate constants).*

It must be stressed that these simulated concentrations for intermediate **7Nab** are generated from values derived from measurements at +23 °C where no intermediate was detectable in NMR measurements. Nonetheless, it is obvious that the concentration of the intermediate is much lower than the one of catalyst **5b** ranging from 0.081 mol L^{-1} (o6) – 1.871 mol L^{-1} (o1). This is in complete agreement with the observation that signals for intermediate **7Nab** are only visible in NMR at low temperatures and then still account for just a fraction of the integrals of the other compounds present in the oligomerization mixture.

More importantly, the concentrations obtained from the single set of rate constants are much smaller and the intermediate´s peak in concentration is much shorter and more shifted to the beginning of the reaction. This is in agreement with our experiences detecting the intermediate.

2.1.7 NMR Spectra of Synthesized Compounds

^{15}N-Heptanamide ***10a***[15]

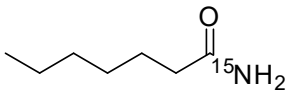

a)

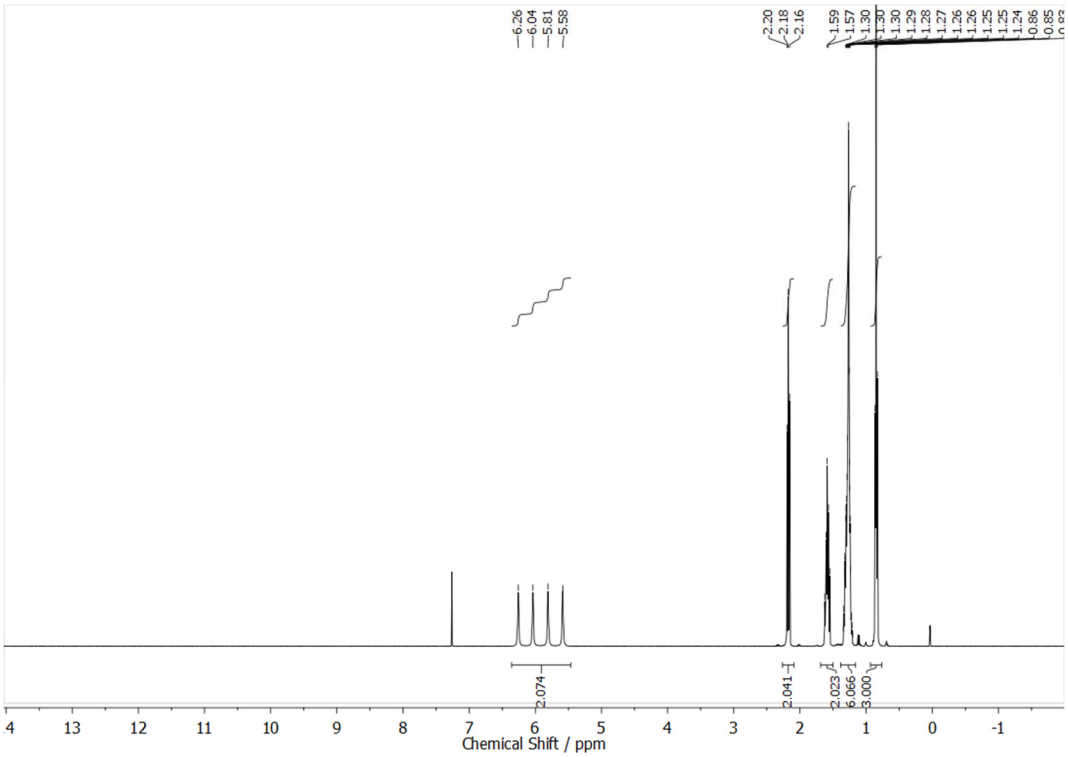

b)

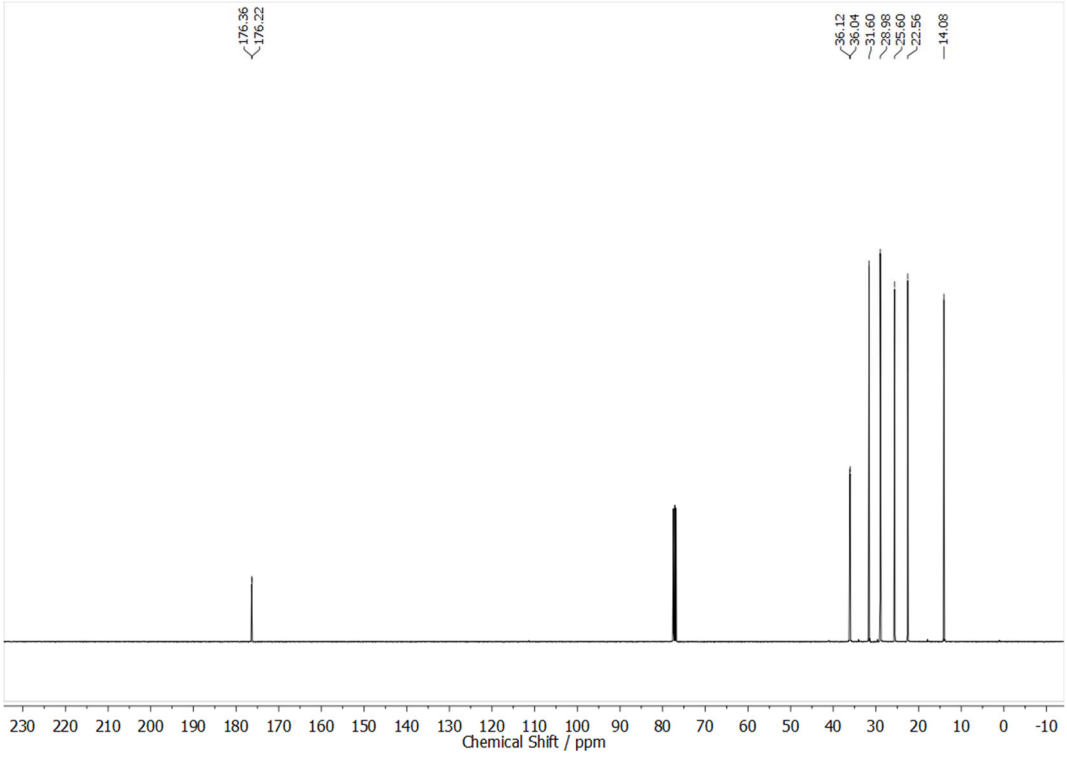

c)

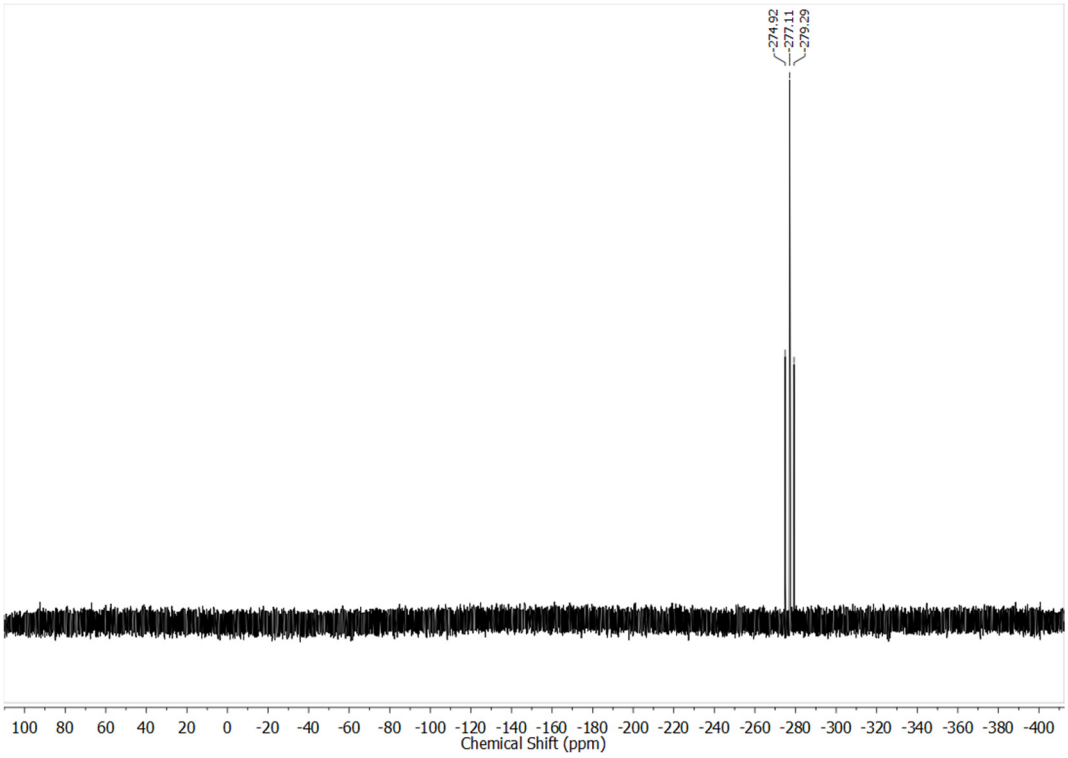

d)

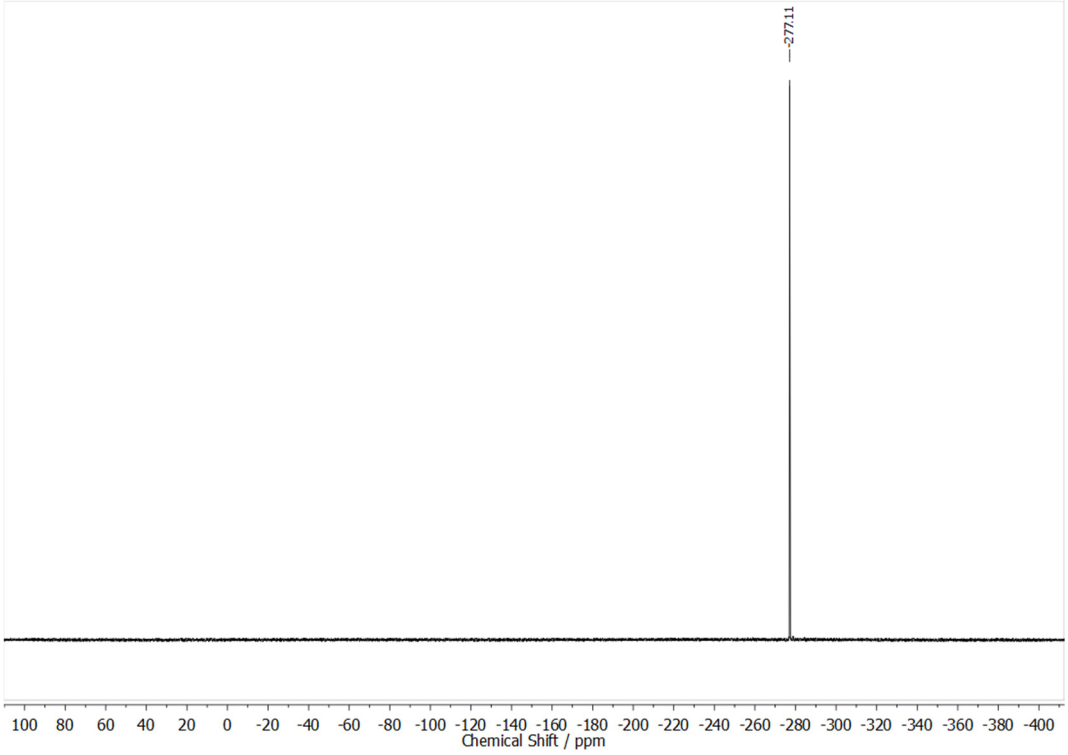

***Figure S2: 29**. [Figure S29] NMR spectra of amide **10a**[15] ($CDCl_3$, 400 MHz): a) ^1H NMR spectrum, b) ^{13}C NMR spectrum, c) ^{15}N NMR spectrum, d) $^{15}N\{^1H\}$ NMR spectrum.*

^{15}N-Methyl hexylcarbamate ***11a***[15]

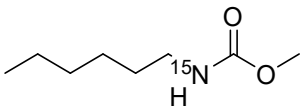

a)

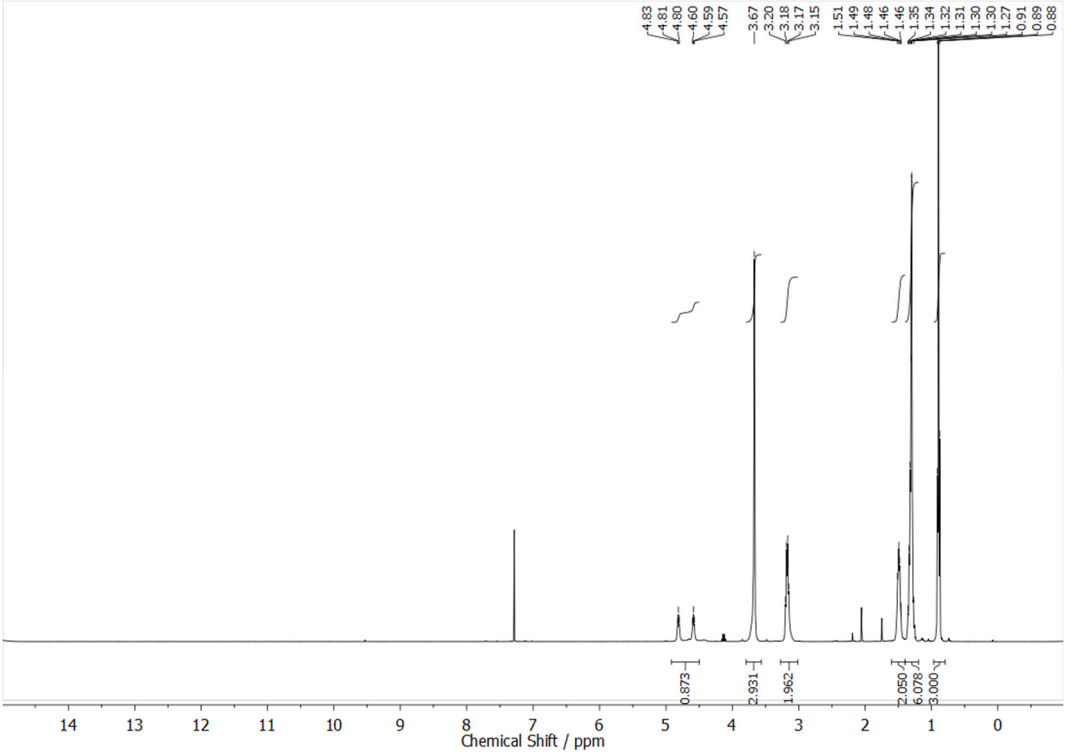

b)

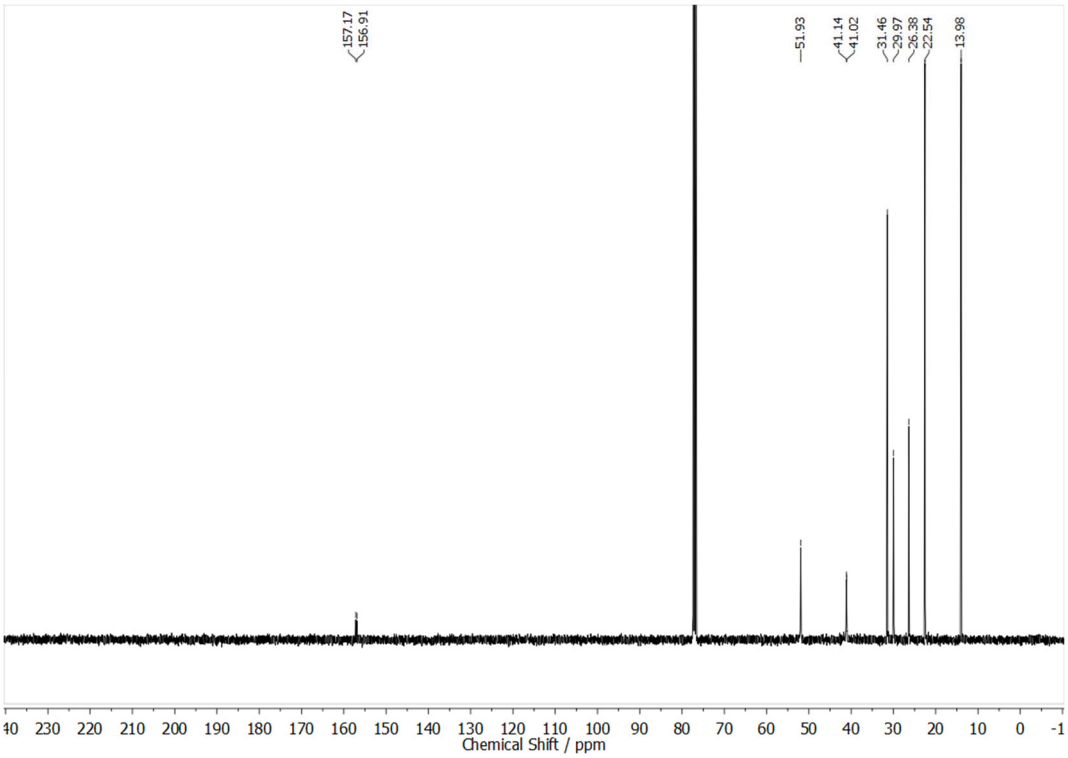

c)

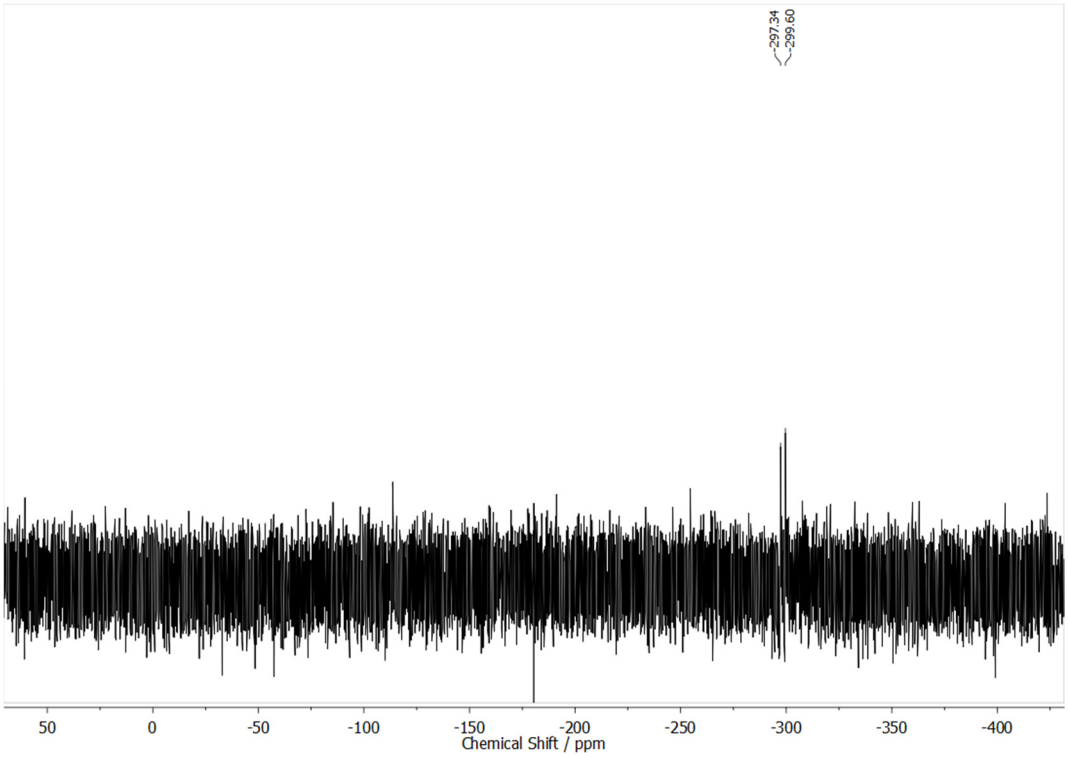

d)

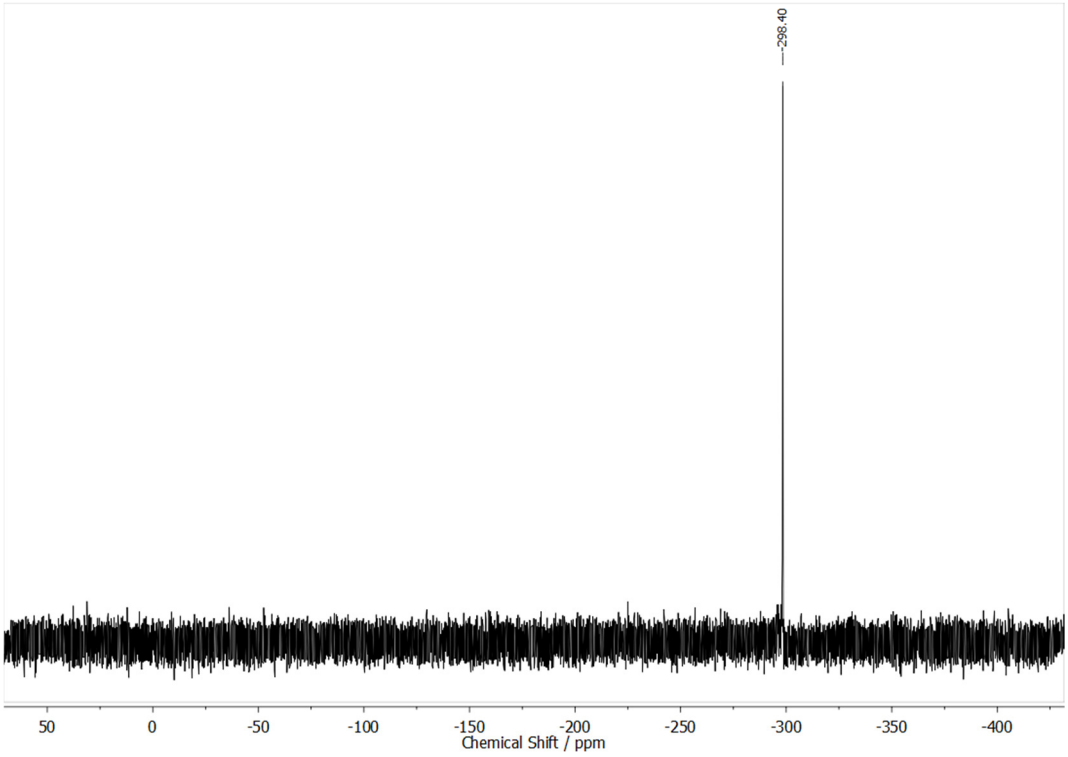

Figure S2: 30. *[Figure S30] NMR spectra of carbamate* ***11a***[15] *($CDCl_3$, 400 MHz): a) ^1H NMR spectrum, b) ^{13}C NMR spectrum, c) ^{15}N NMR spectrum, d) $^{15}N\{^1H\}$ NMR spectrum.*

^{15}N-Hexyl isocyanate ***1a***[15]

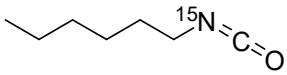

a)

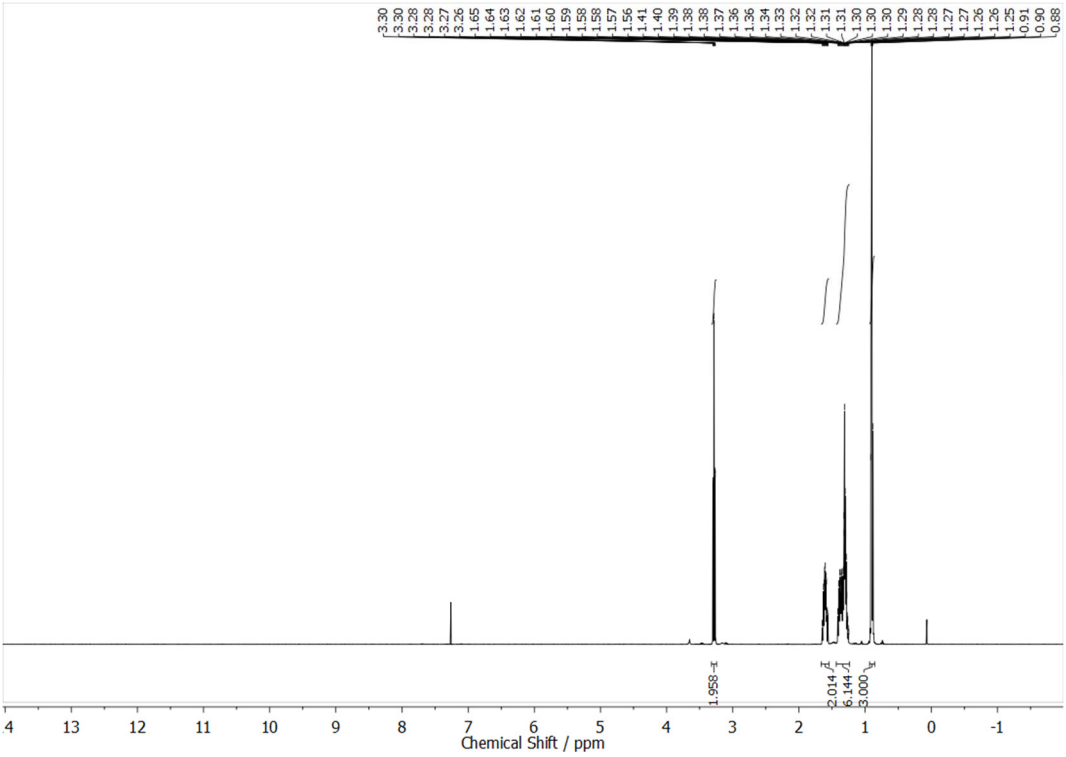

b)

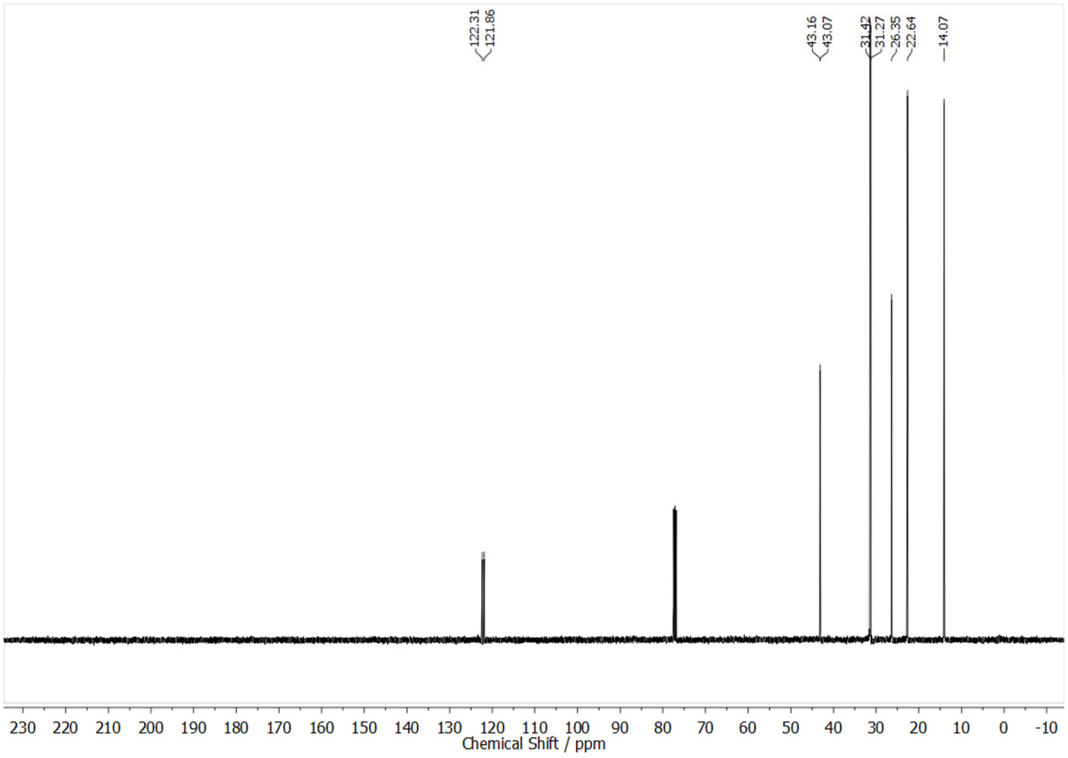

c)

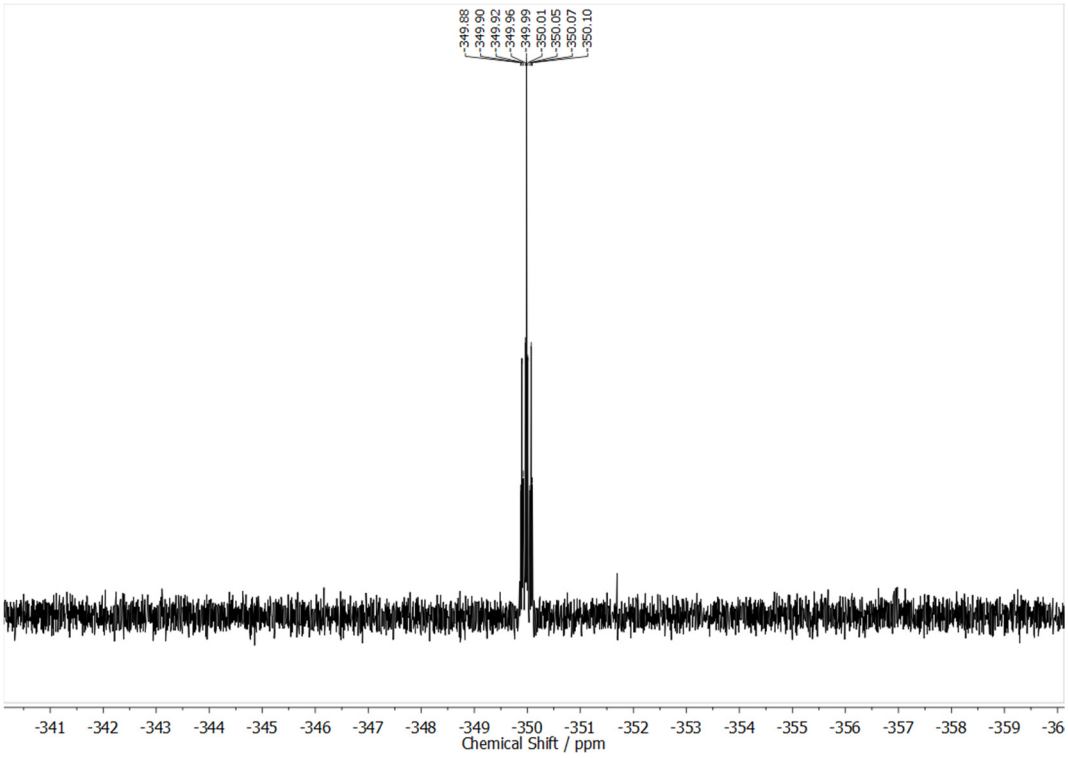

d)

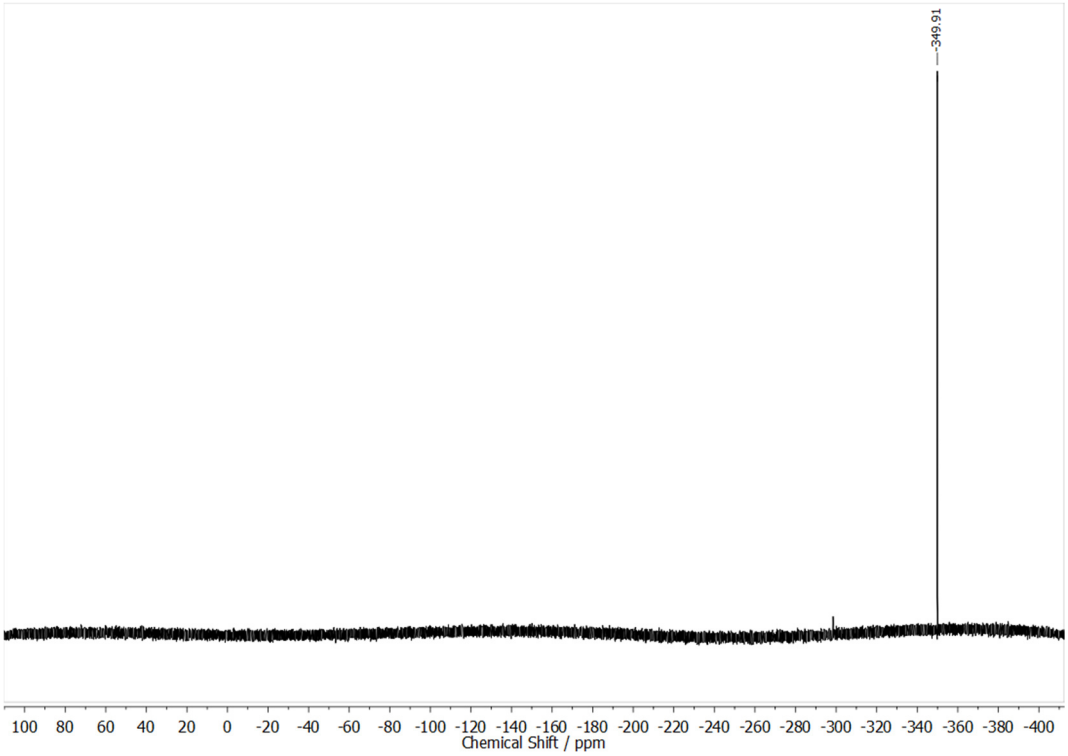

Figure S2: 31. *[Figure S31] NMR spectra of isocyanate* ***1a***[15] *($CDCl_3$, 400 MHz): a) ^1H NMR spectrum, b) ^{13}C NMR spectrum, c) ^{15}N NMR spectrum, d) $^{15}N\{^1H\}$ NMR spectrum.*

^{15}N-Hexylacetamide ***13a***[15]

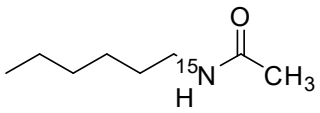

a)

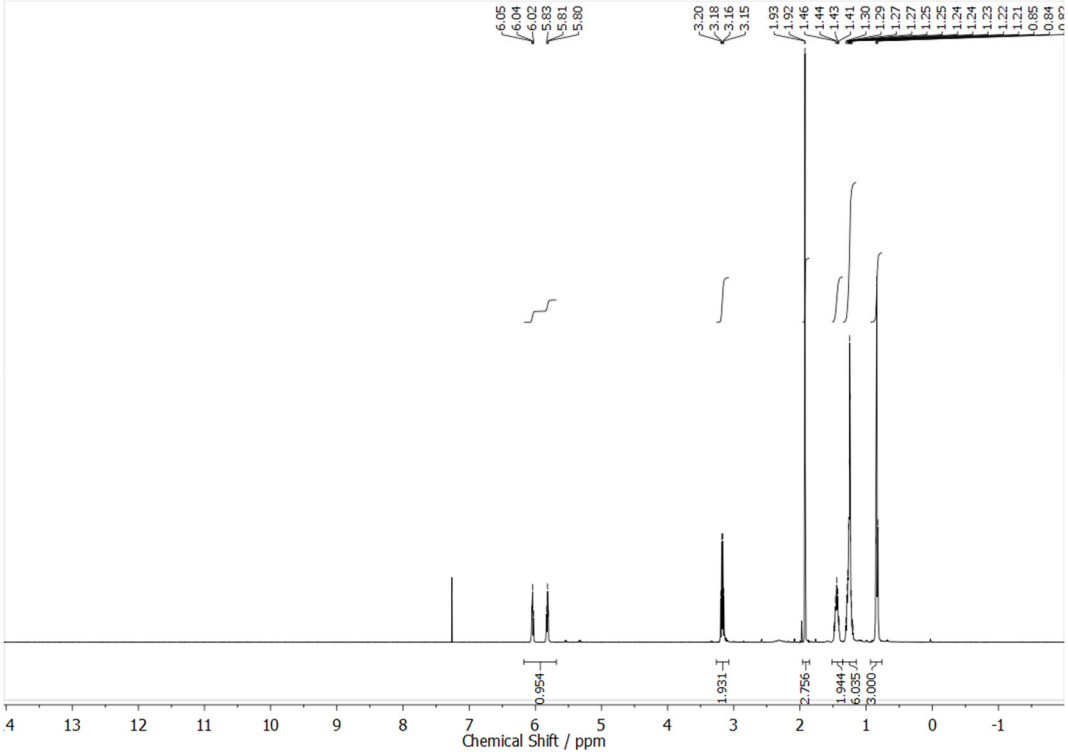

b)

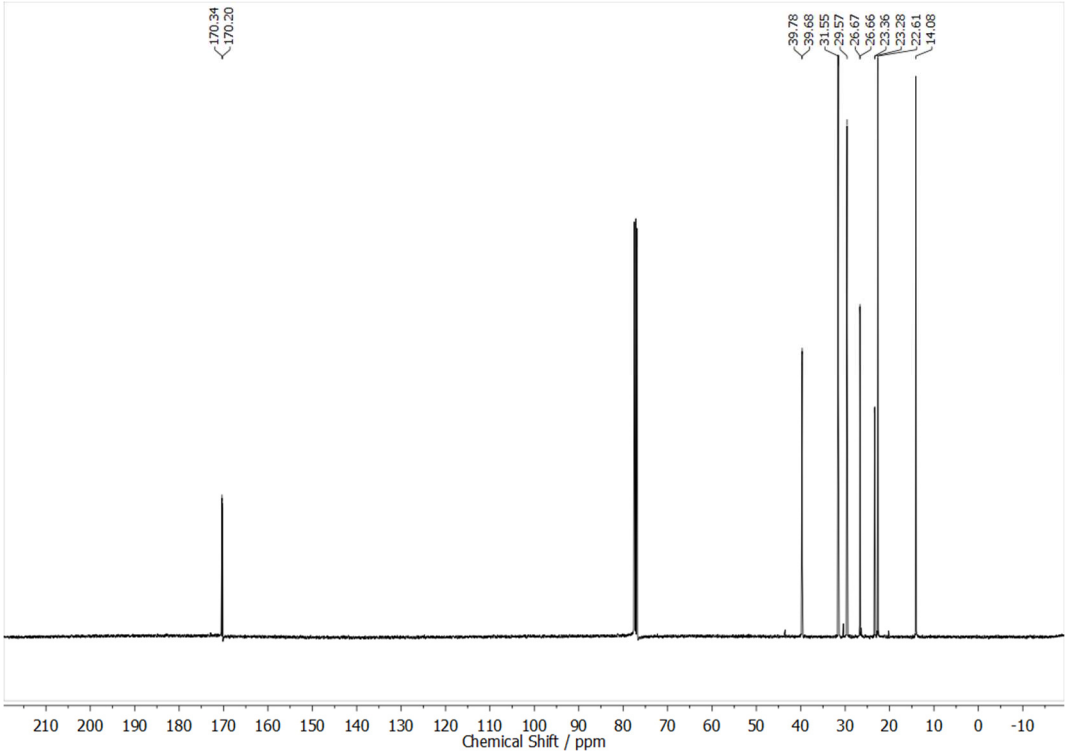

c)

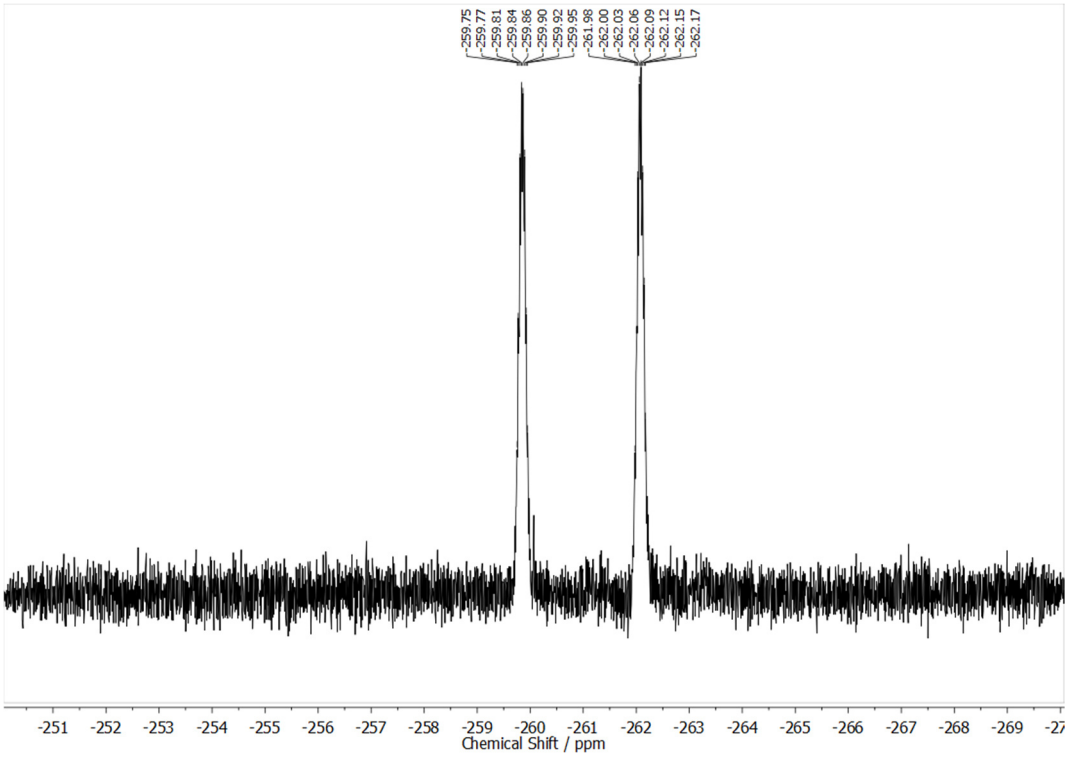

d)

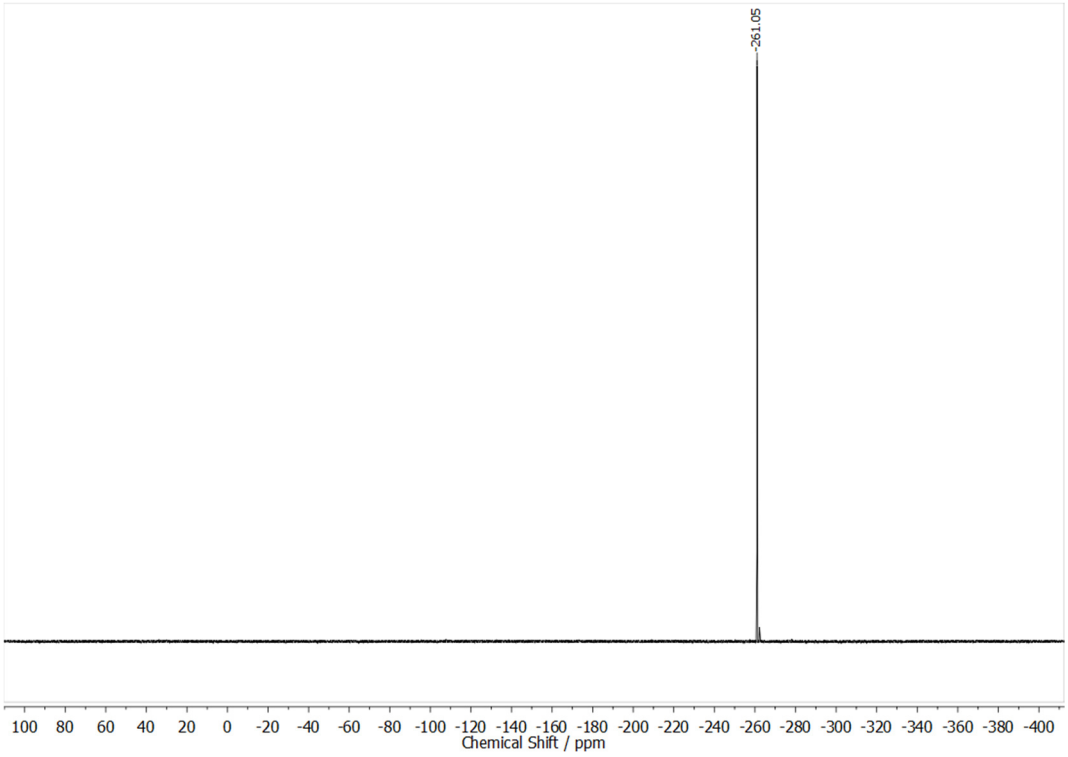

Figure S2: 32. *[Figure S32] NMR spectra of acetamide* ***13a***[15] *($CDCl_3$, 400 MHz): a) ^1H NMR spectrum, b) ^{13}C NMR spectrum, c) ^{15}N NMR spectrum, d) $^{15}N\{^1H\}$ NMR spectrum.*

*^{15}N-Dihexylurea **12a**^{15}*

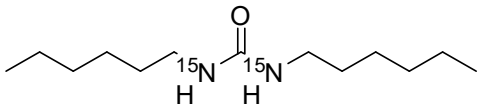

a)

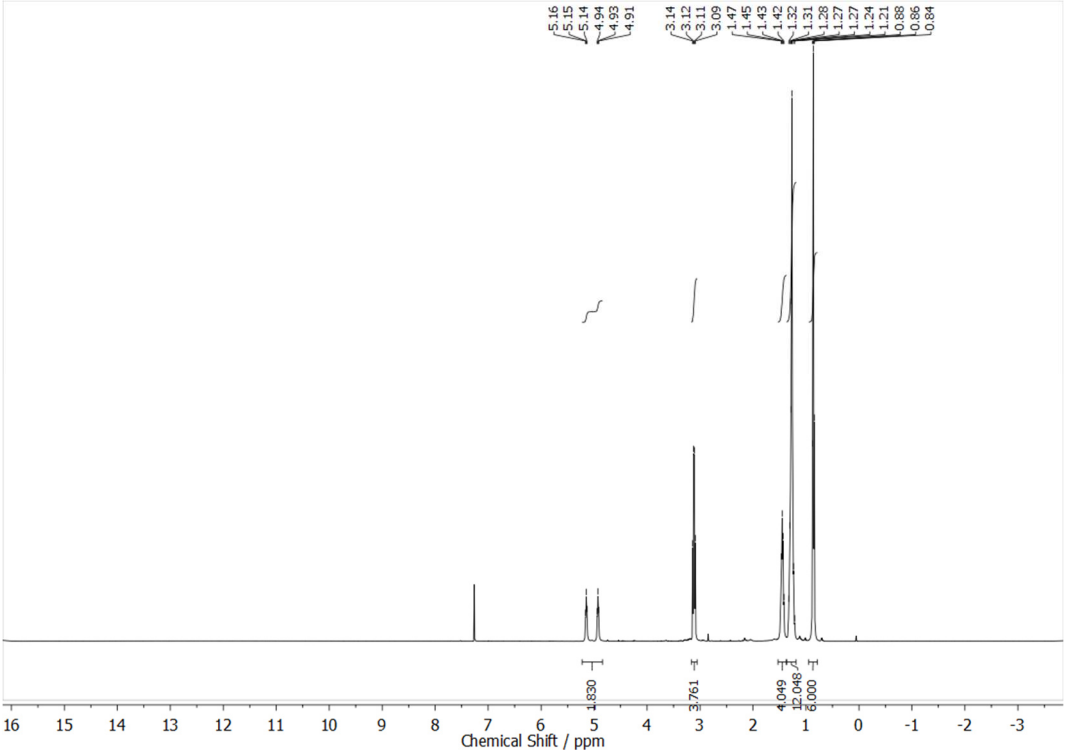

b)

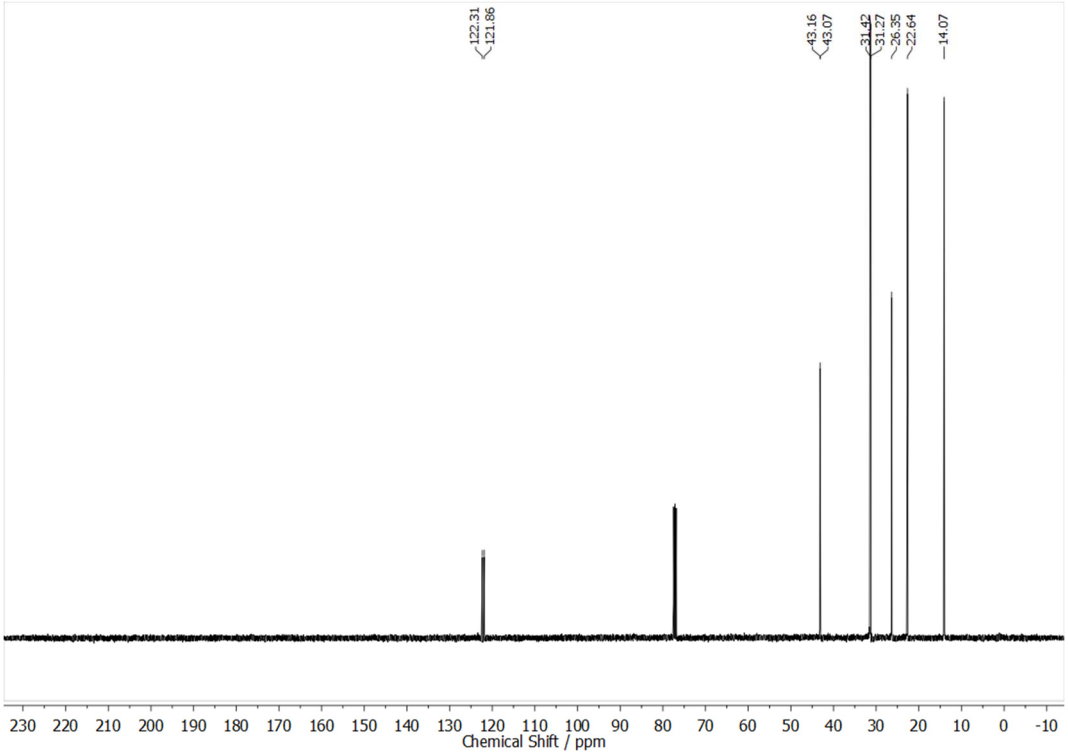

c)

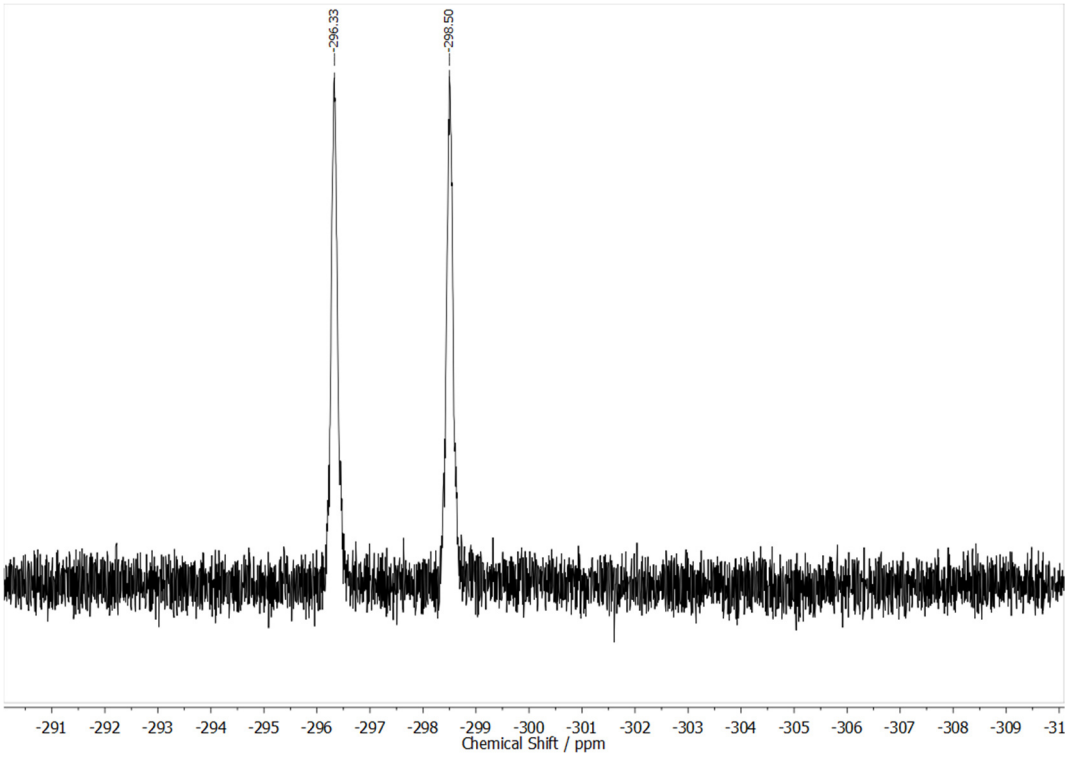

d)

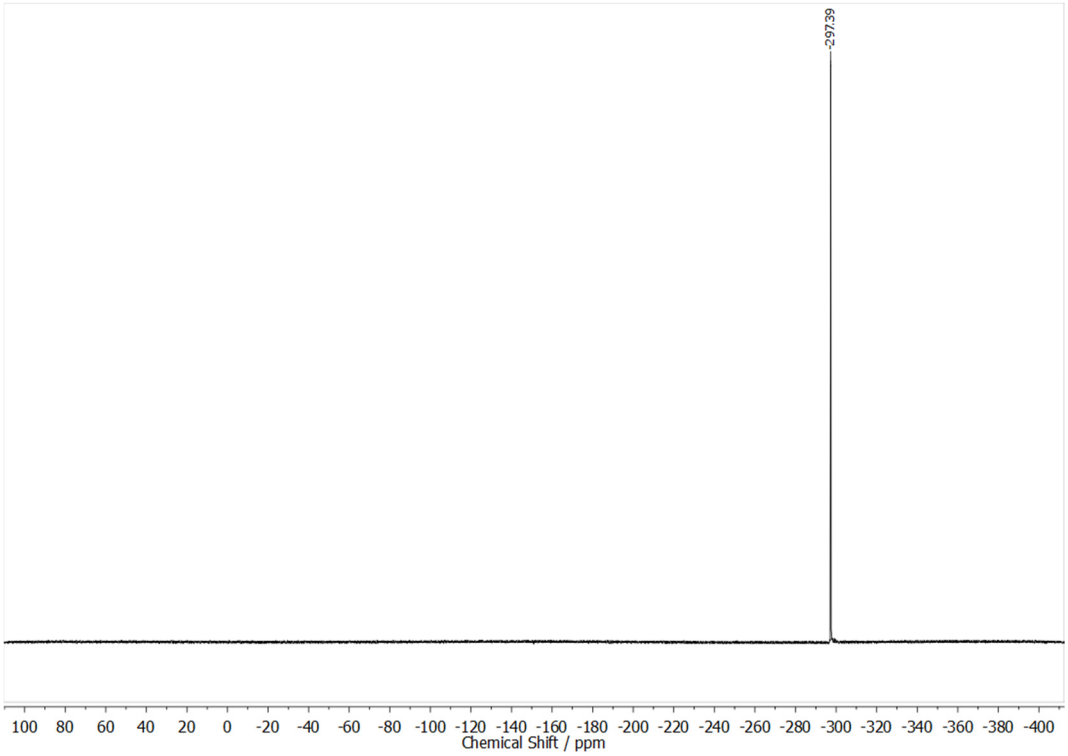

***Figure S2: 33**. [Figure S33] NMR spectra of urea **12a**[15] ($CDCl_3$, 400 MHz): a) ^1H NMR spectrum, b) ^{13}C NMR spectrum, c) ^{15}N NMR spectrum, d) $^{15}N\{^1H\}$ NMR spectrum.*

^{15}N-Hexyl uretdione ***2a^{15}***

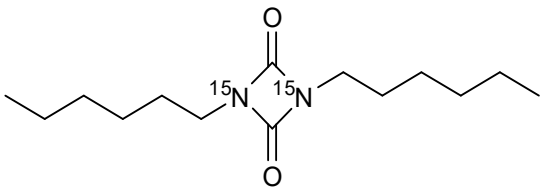

a)

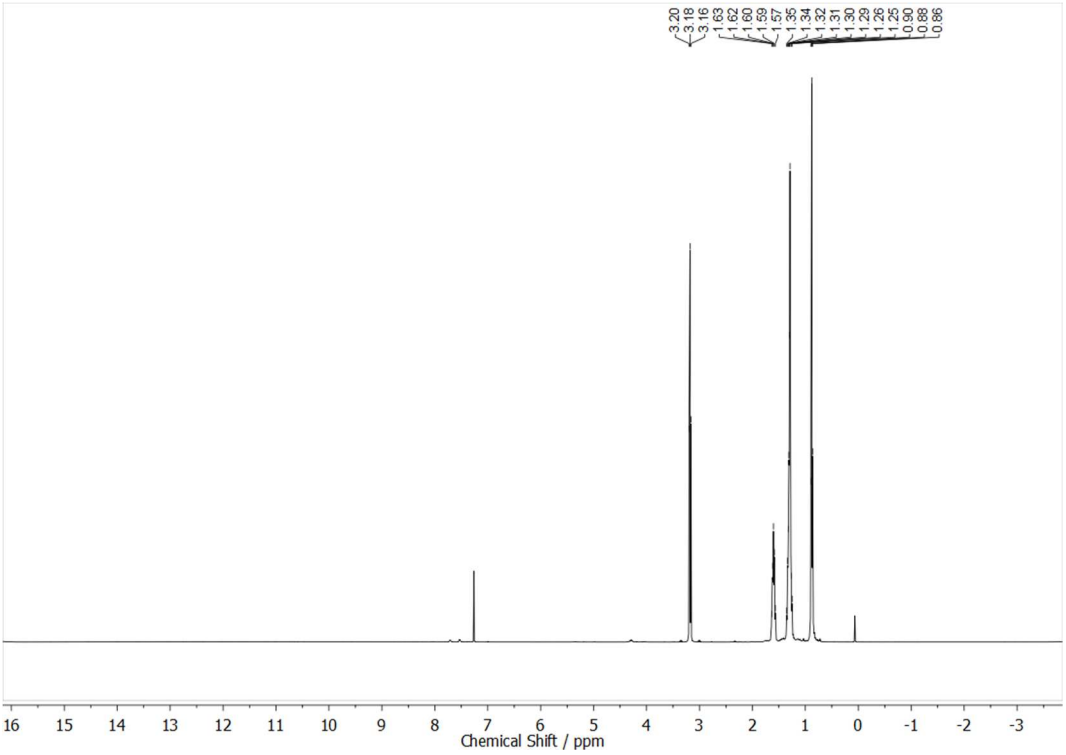

b)

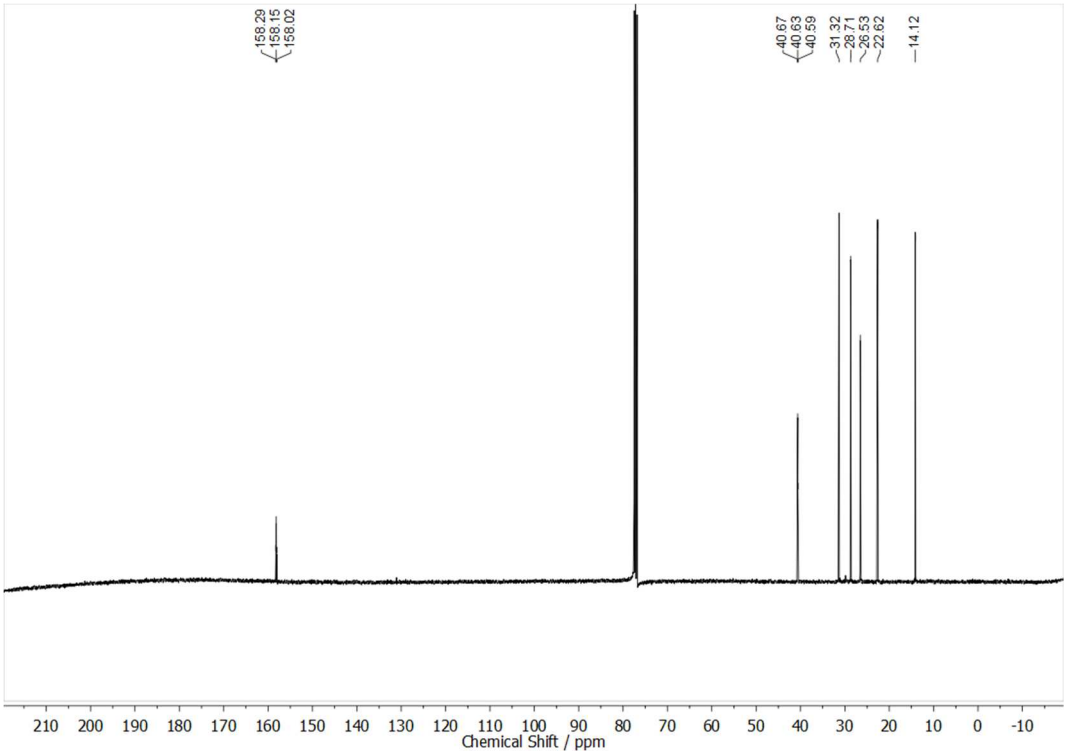

c)

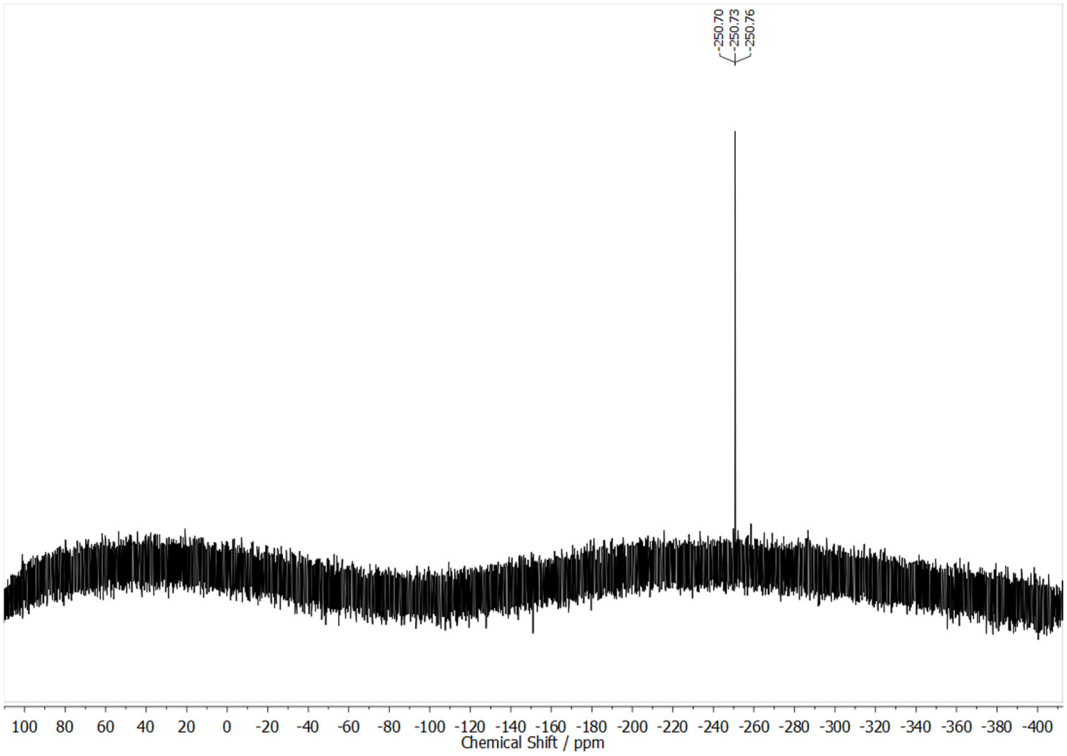

d)

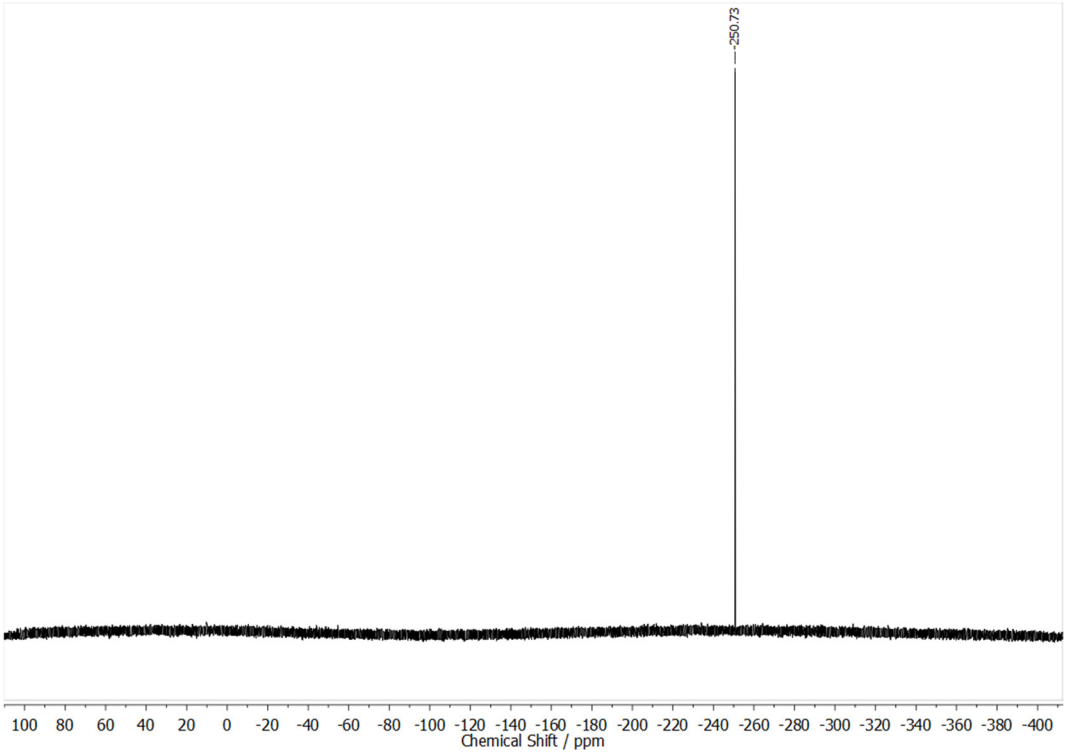

Figure S2: 34. *[Figure S34] NMR spectra of uretdione* ***2a***[15] *($CDCl_3$, 400 MHz): a) ^1H NMR spectrum, b) ^{13}C NMR spectrum, c) ^{15}N NMR spectrum, d) $^{15}N\{^1H\}$ NMR spectrum.*

*^{15}N-Hexyl isocyanurate **3a**^{15}*

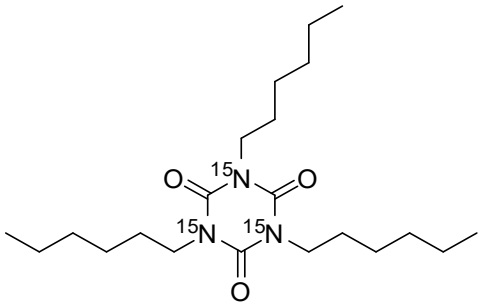

a)

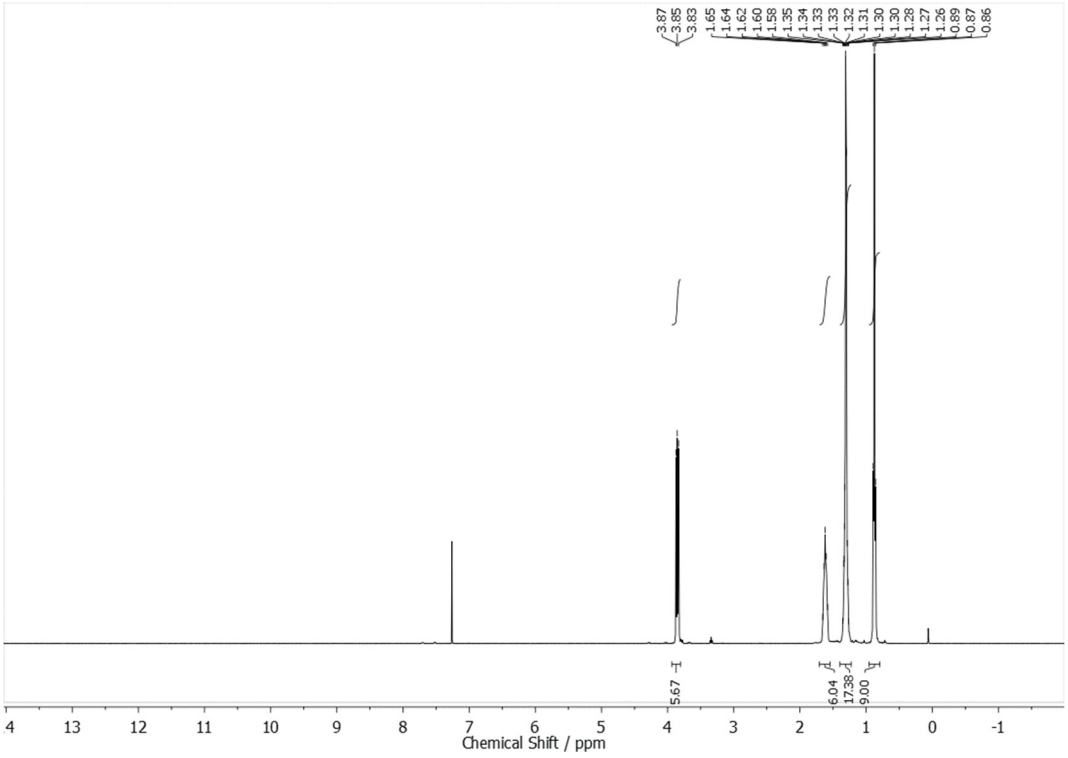

b)

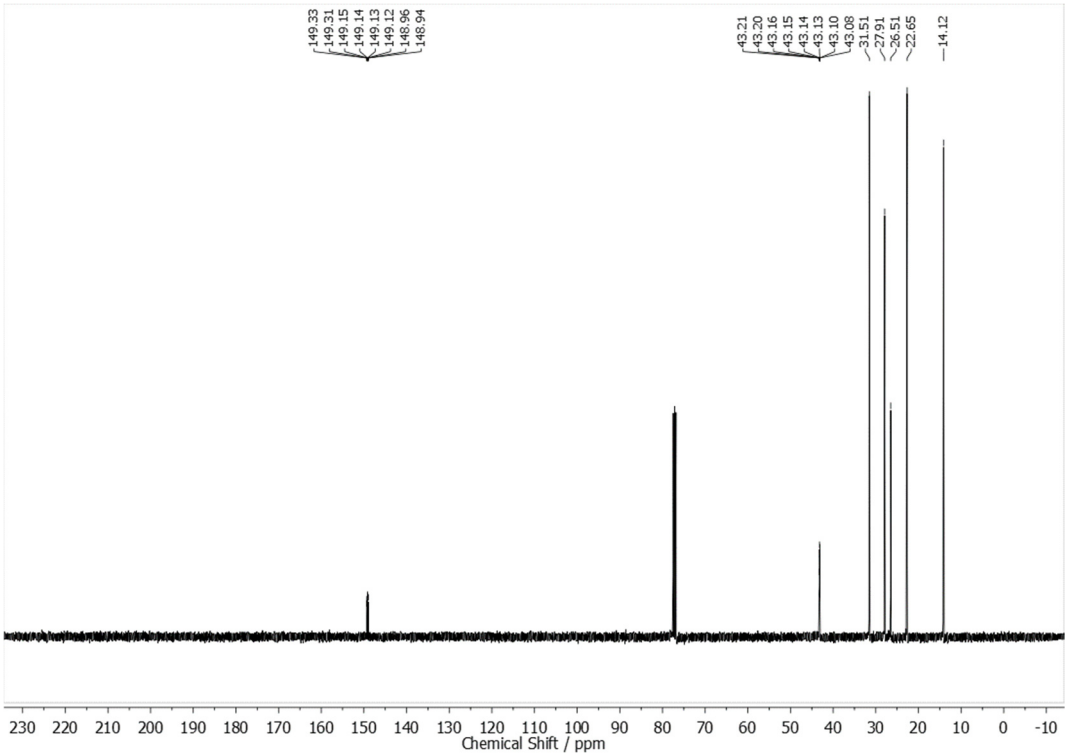
149.33
149.31
149.15
149.14
149.13
149.12
148.96
148.94
43.21
43.20
43.16
43.15
43.14
43.13
43.10
43.08
31.51
27.91
26.51
22.65
14.12
230 220 210 200 190 180 170 160 150 140 130 120 110 100 90 80 70 60 50 40 30 20 10 0 -10
Chemical Shift / ppm

c)

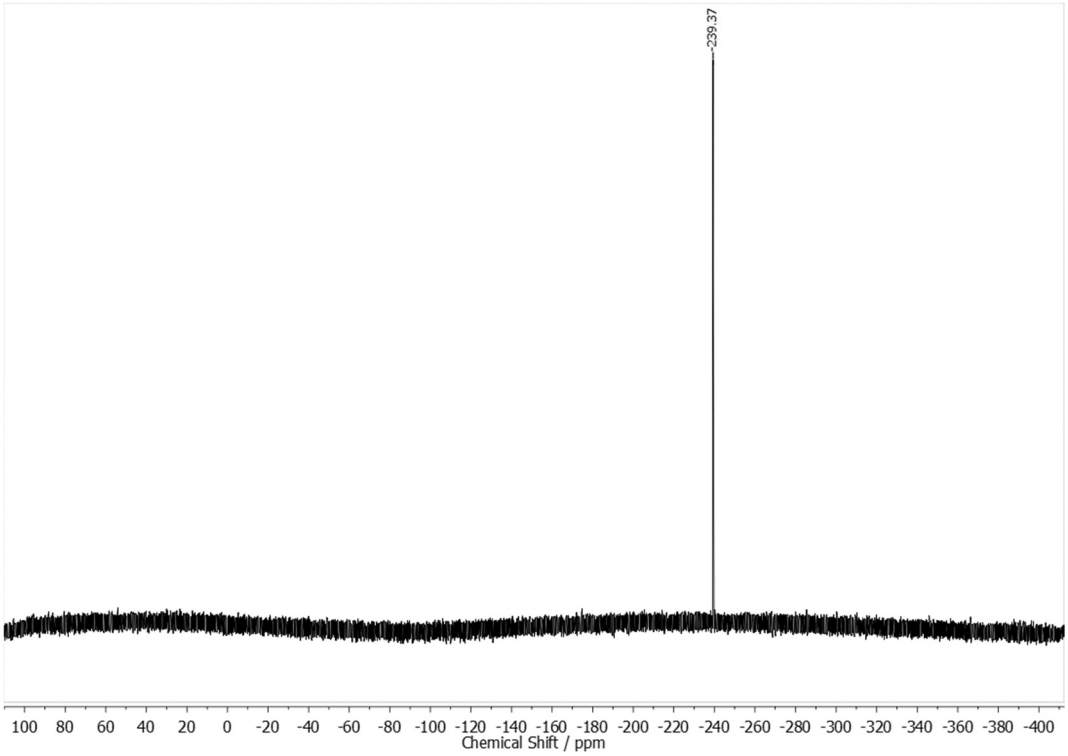
-239.37
100 80 60 40 20 0 -20 -40 -60 -80 -100 -120 -140 -160 -180 -200 -220 -240 -260 -280 -300 -320 -340 -360 -380 -400
Chemical Shift / ppm

d)

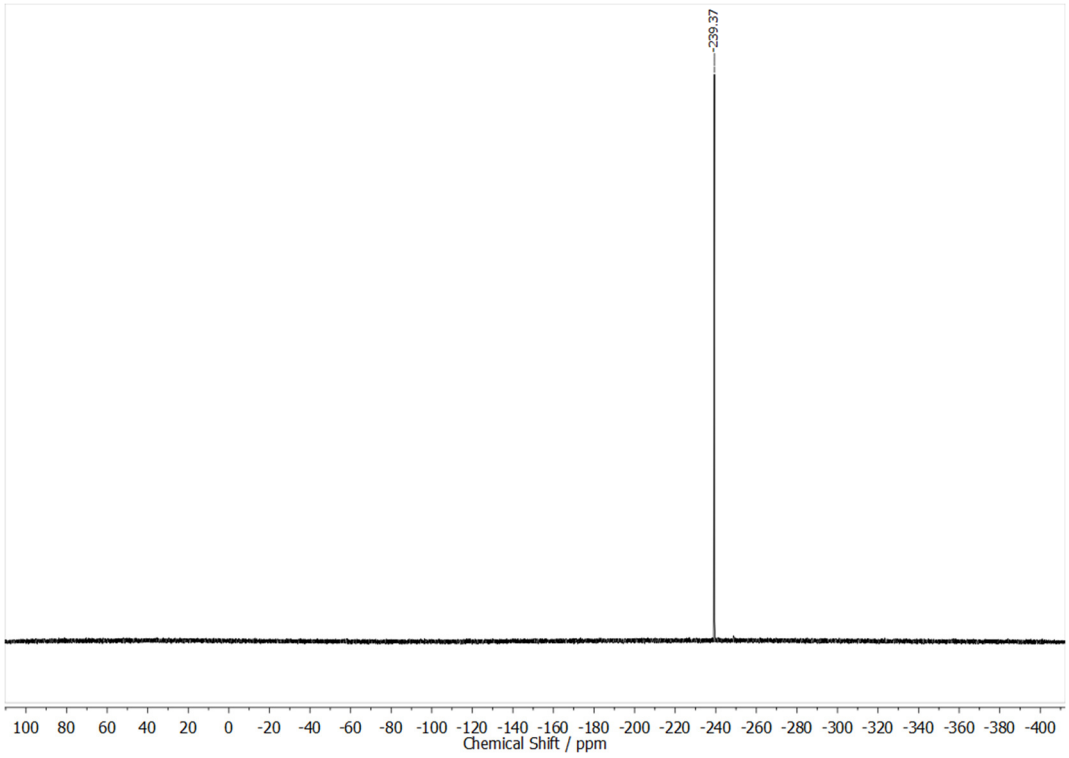

Figure S2: 35. *[Figure S35] NMR spectra of isocyanurate* ***3a***[15] *($CDCl_3$, 400 MHz): a) ^1H NMR spectrum, b) ^{13}C NMR spectrum, c) ^{15}N NMR spectrum, d) $^{15}N\{^1H\}$ NMR spectrum.*

n-Hexyl uretdione ***2a***

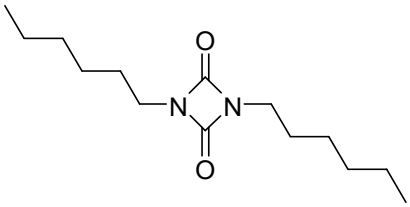

a)

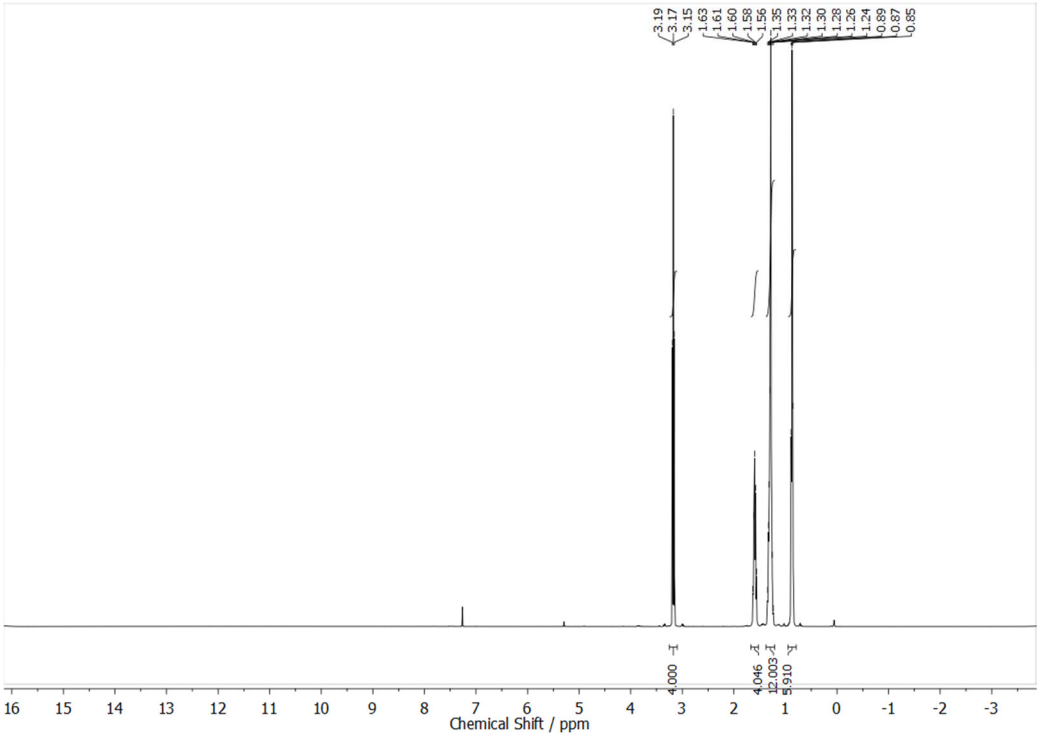

b)

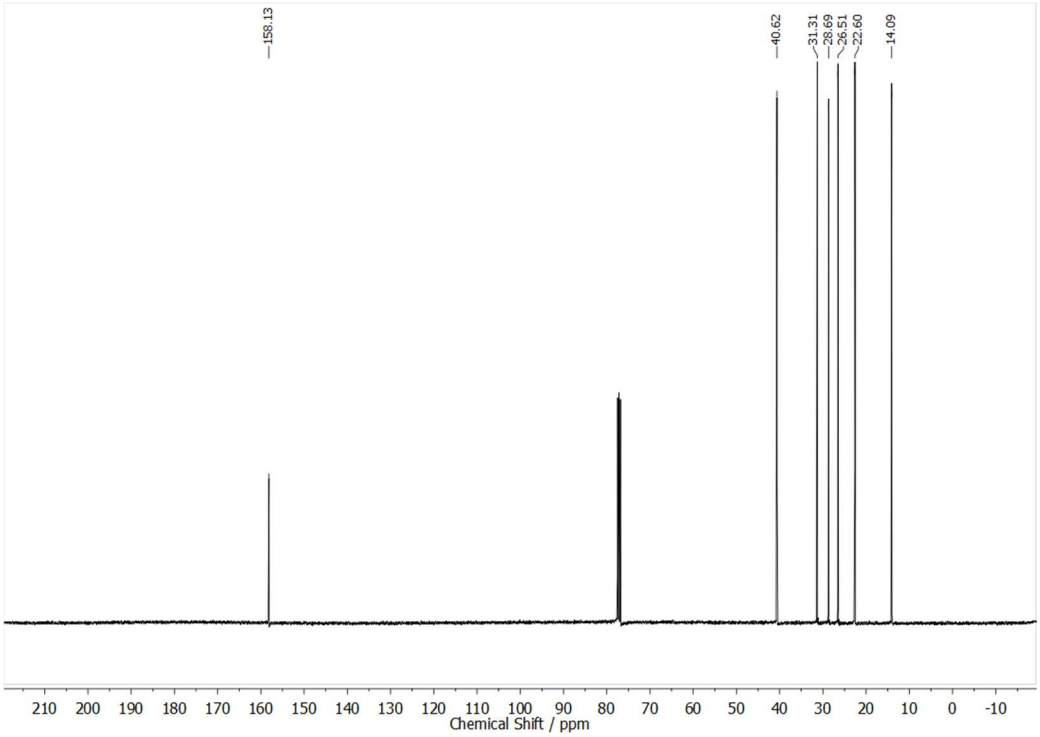

Figure S2: 36. *[Figure S36] NMR spectra of uretdione* ***2a*** *($CDCl_3$, 400 MHz): a) ^1H NMR spectrum, b) ^{13}C NMR spectrum.*

n-Hexyl isocyanurate ***3a***

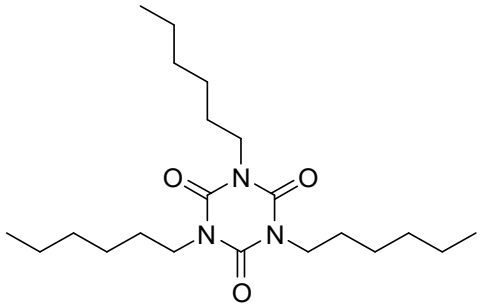

a)

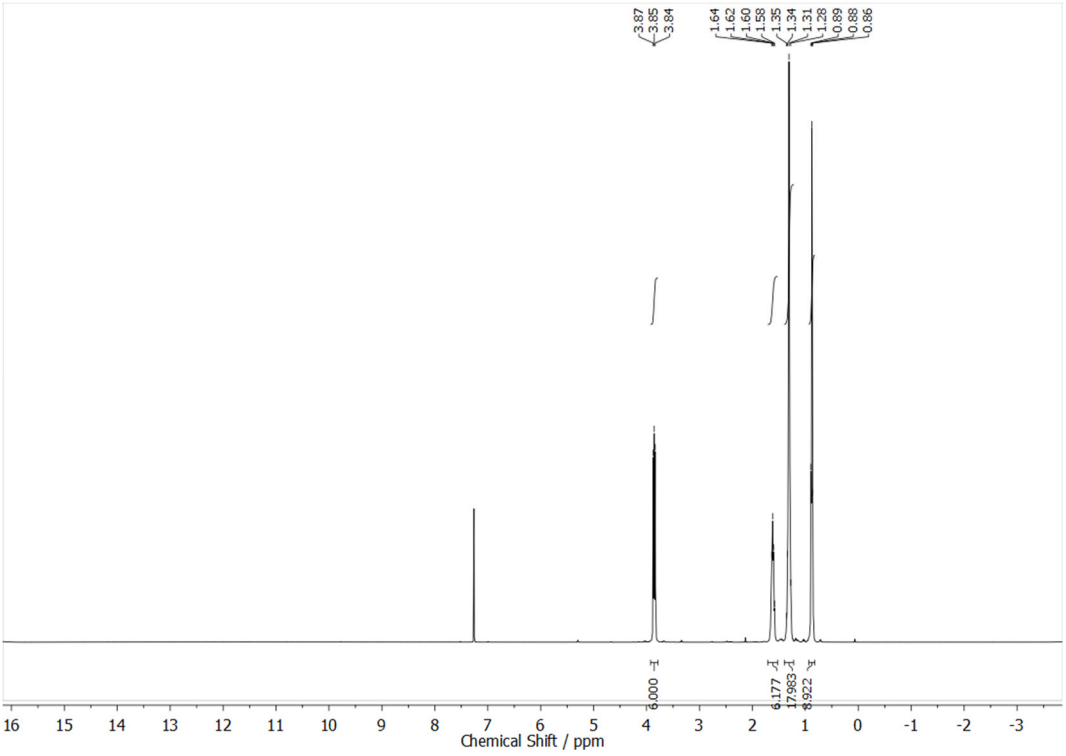

b)

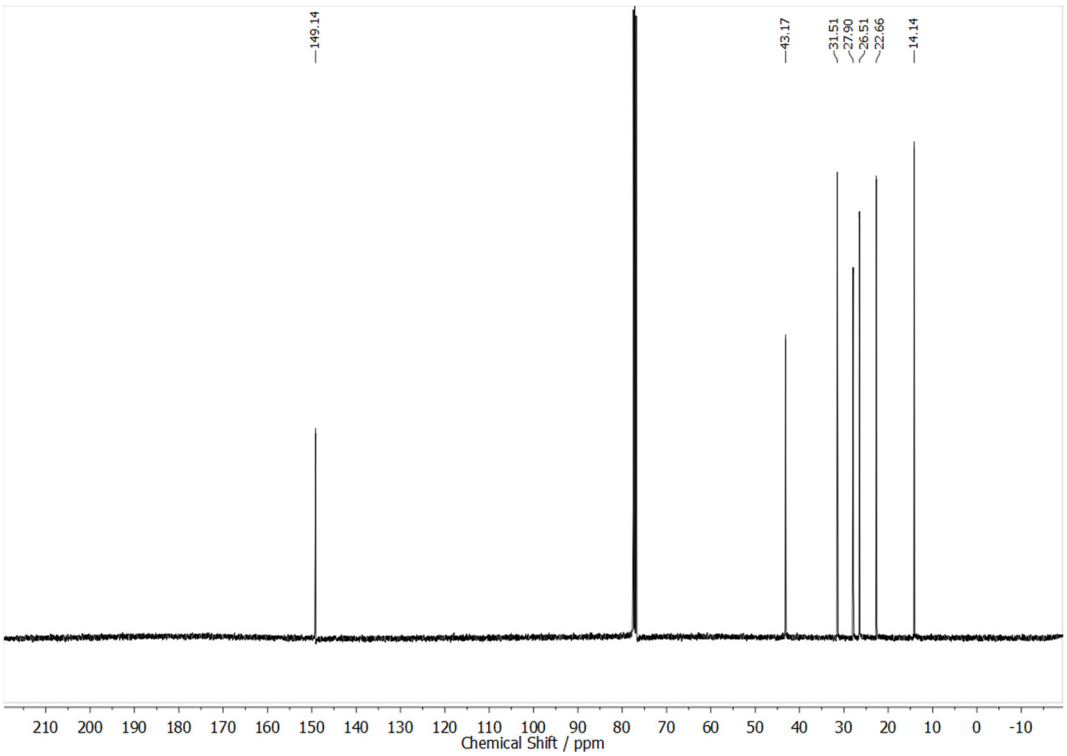

Figure S2: 37. *[Figure S37] NMR spectra of isocyanurate* ***3a*** *($CDCl_3$, 400 MHz): a) ^1H NMR spectrum, b) ^{13}C NMR spectrum.*

n-Butyl isocyanurate ***3b***

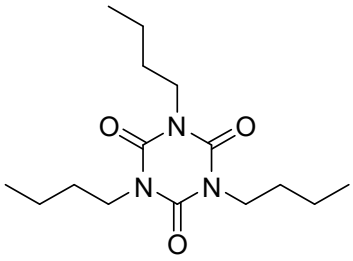

a)

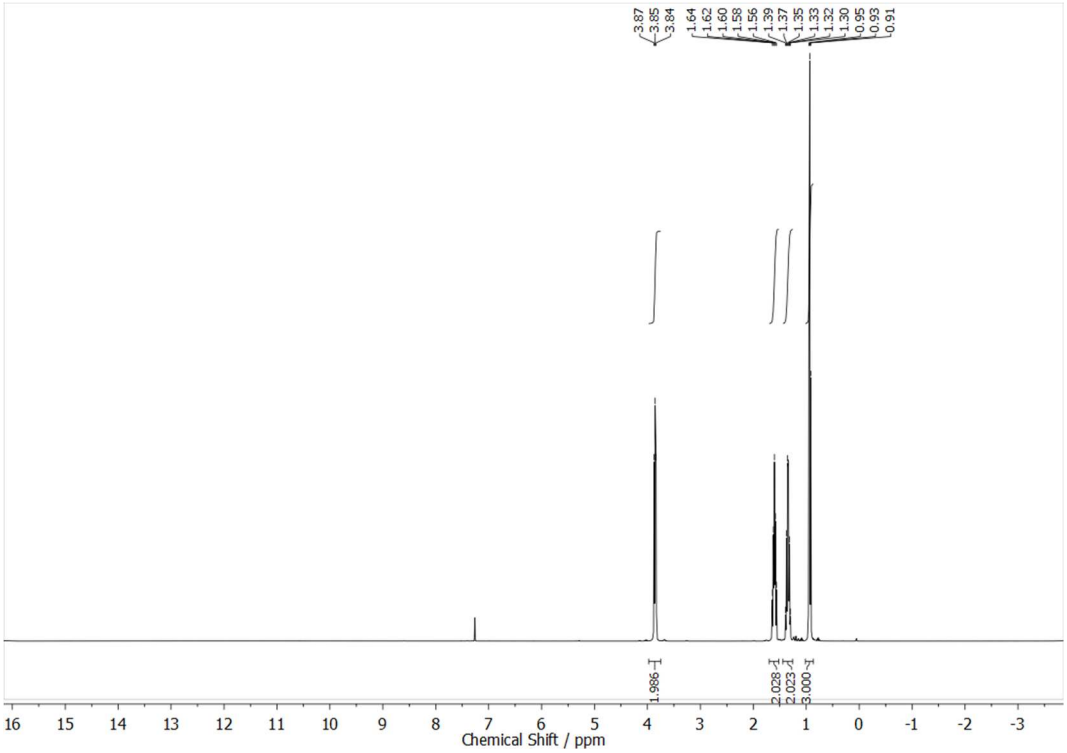

b)

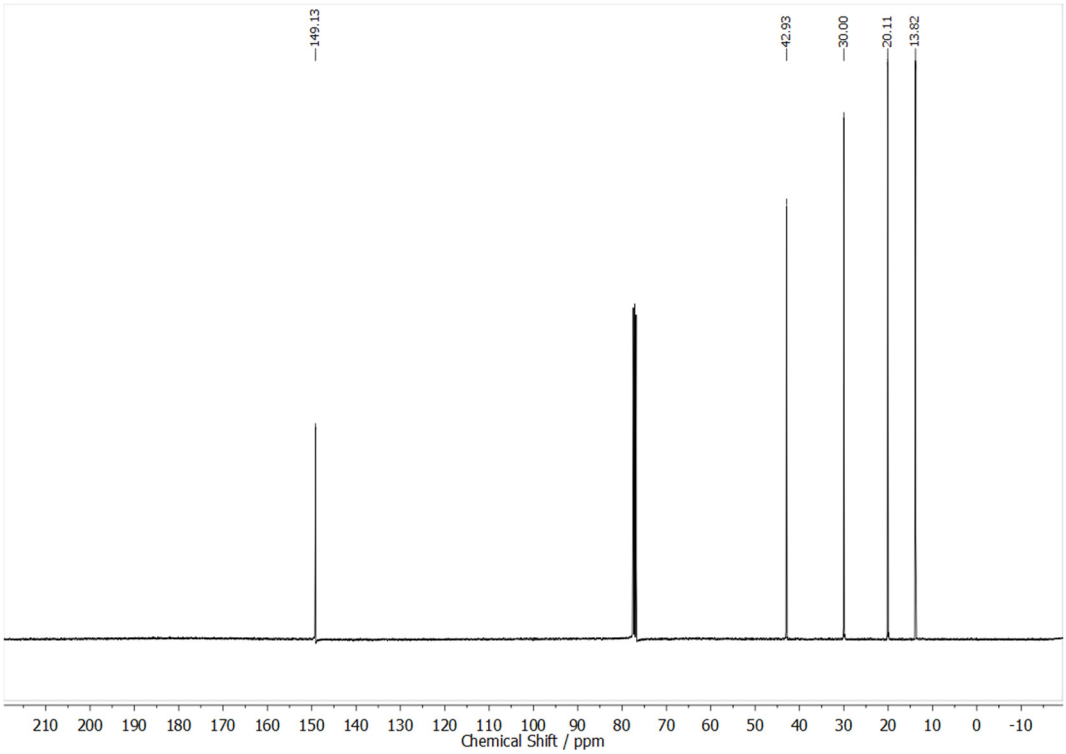

Figure S2: 38. *[Figure S38] NMR spectra of isocyanurate* ***3b*** *($CDCl_3$, 400 MHz): a) ^1H NMR spectrum, b) ^{13}C NMR spectrum.*

Tri-n-butyl(methyl)phosphonium iodide ***15b***

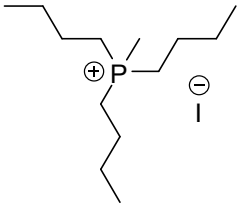

a)

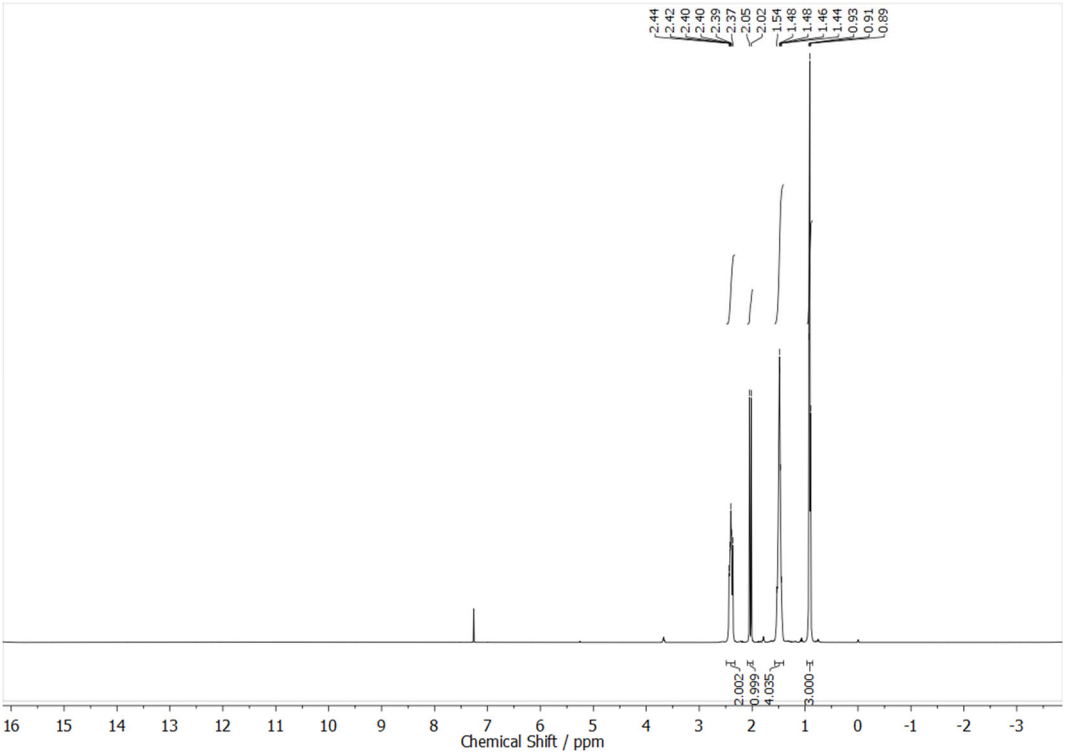

b)

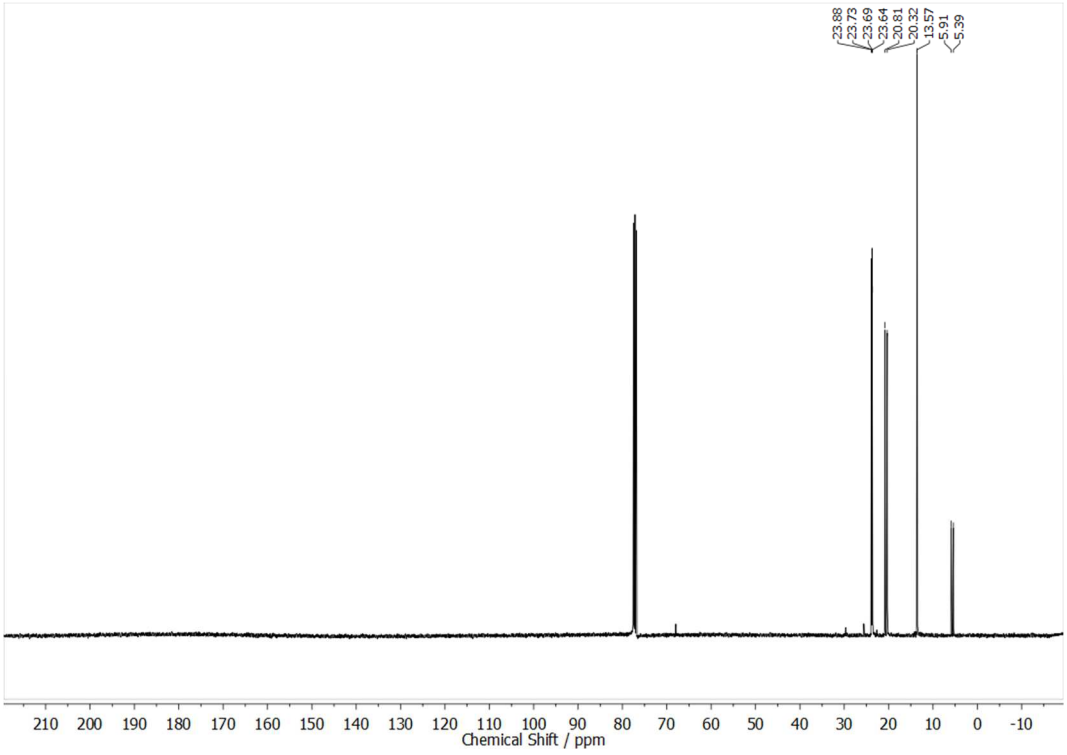

c)

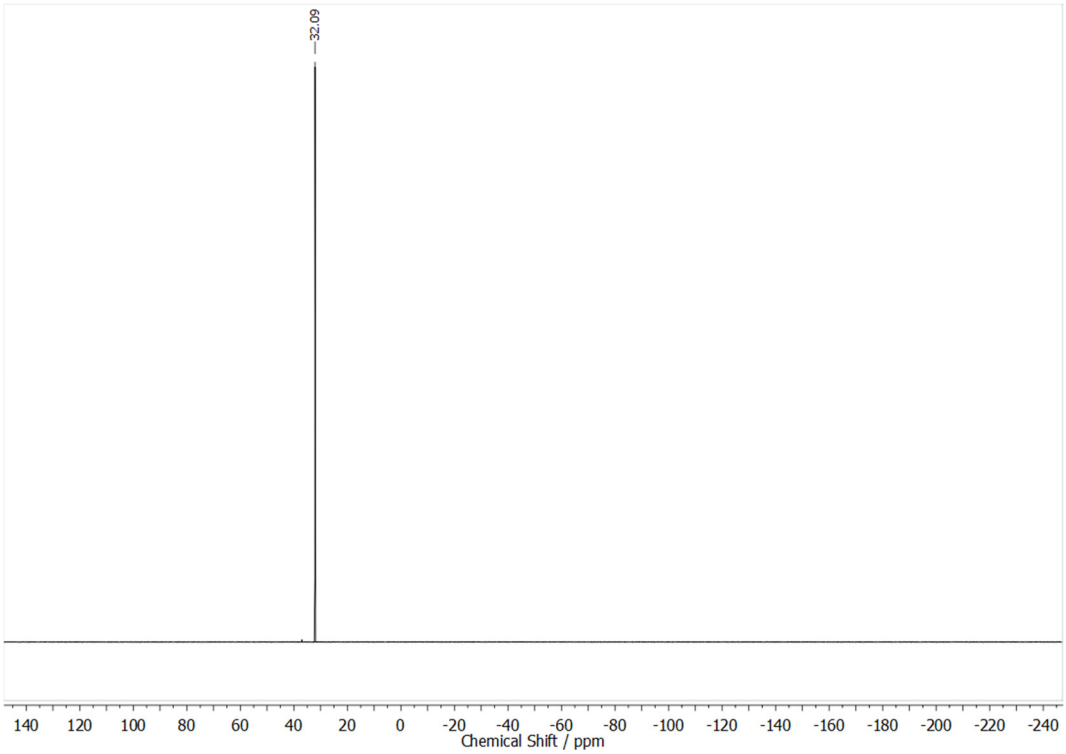

Figure S2: 39. *[Figure S39] NMR spectra of methyl phosphonium iodide* ***15b*** *($CDCl_3$, 400 MHz): a) ^1H NMR spectrum, b) ^{13}C NMR spectrum, c) $^{31}P\{^1H\}$ NMR spectrum.*

Tri-n-butylphosphonium chloride ***16b***

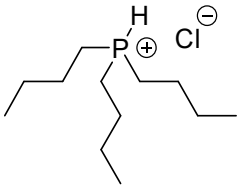

a)

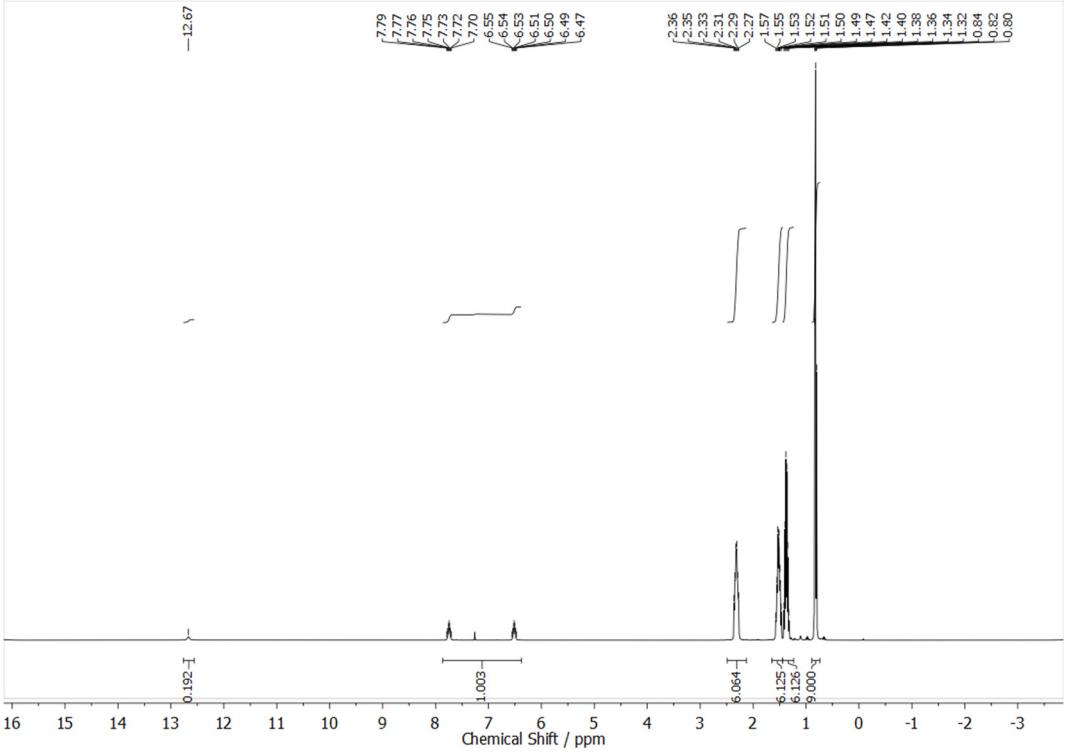

b)

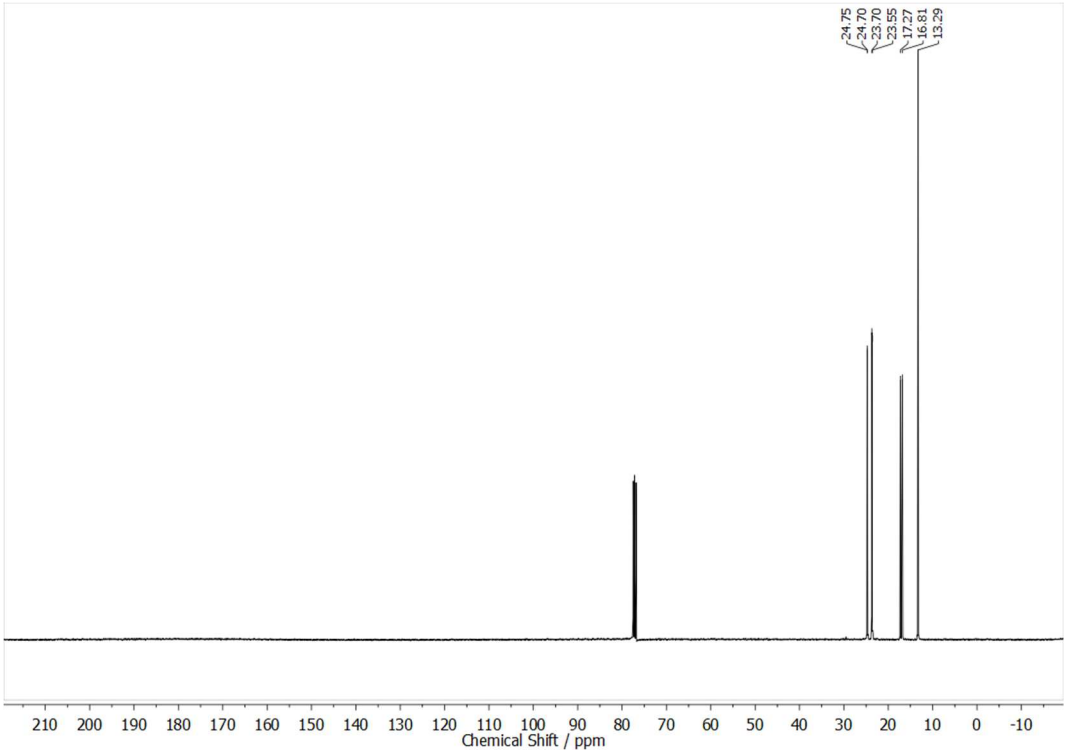

c)

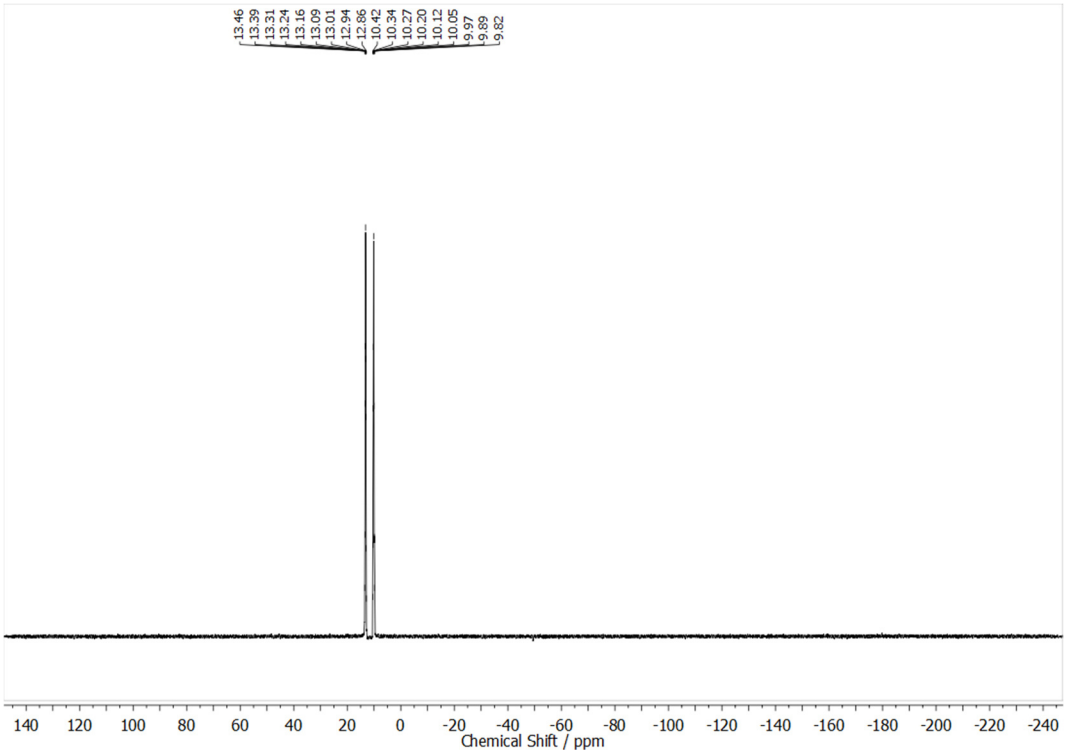

d)

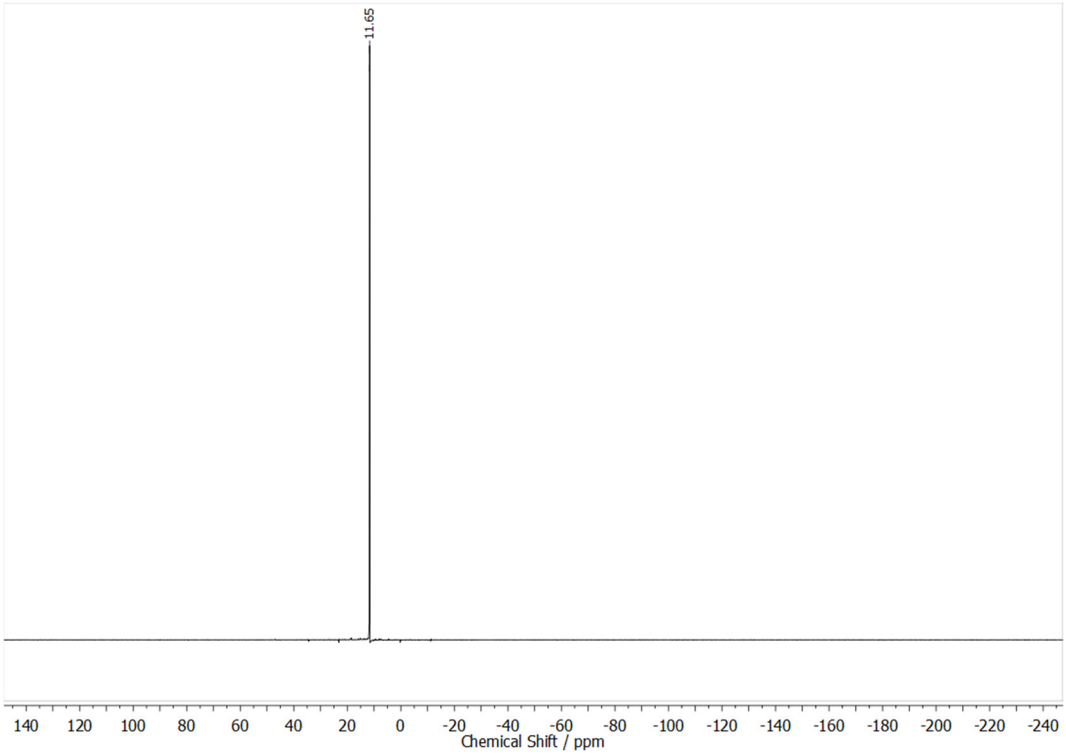

Figure S2: 40. *[Figure S40] NMR spectra of phosphonium chloride* ***16b*** *($CDCl_3$, 400 MHz): a) ^1H NMR spectrum, b) ^{13}C NMR spectrum, c) ^{31}P NMR spectrum, d) $^{31}P\{^1H\}$ NMR spectrum.*

Tributyl(hexylcarbamoyl)phosphonium chloride ***6ab×HCl*** *(in Situ)*

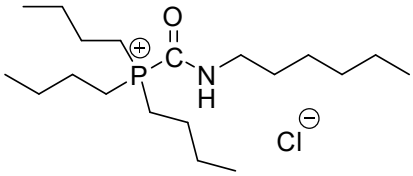

a)

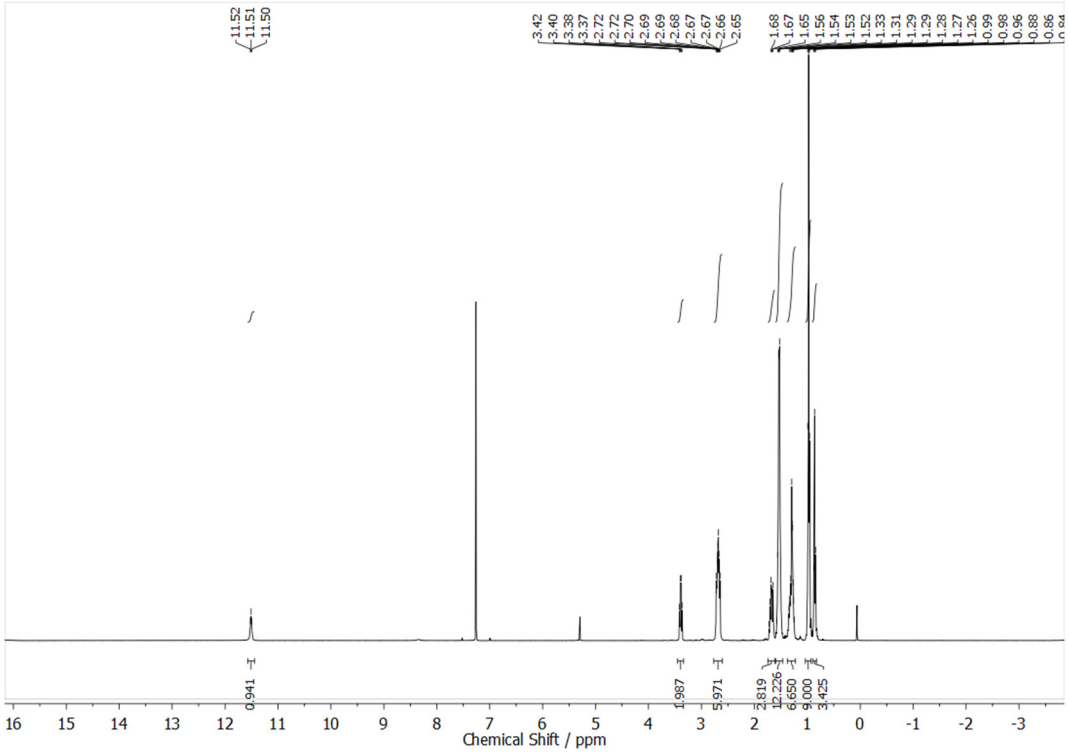

b)

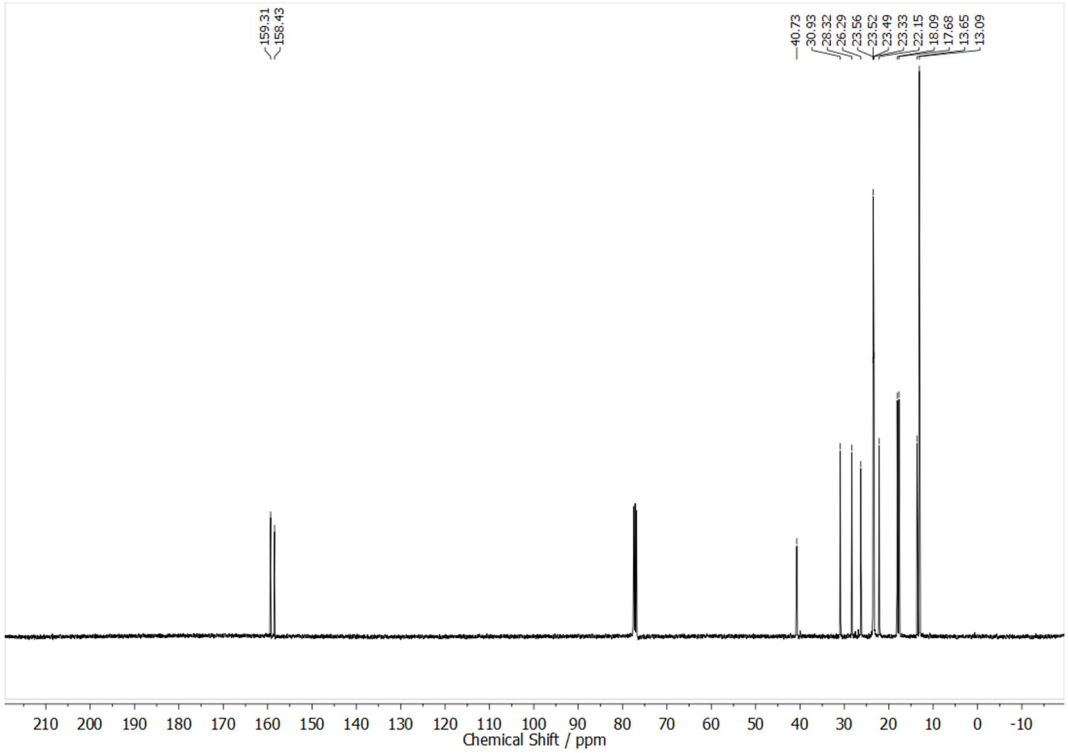

c)

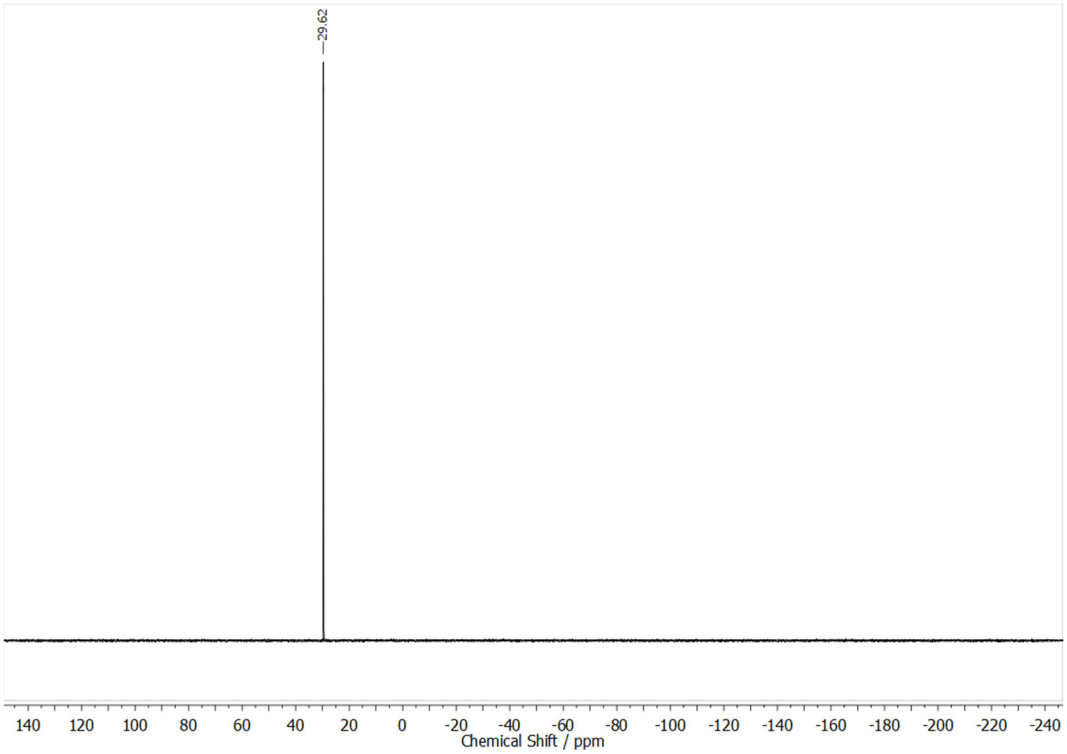

d)

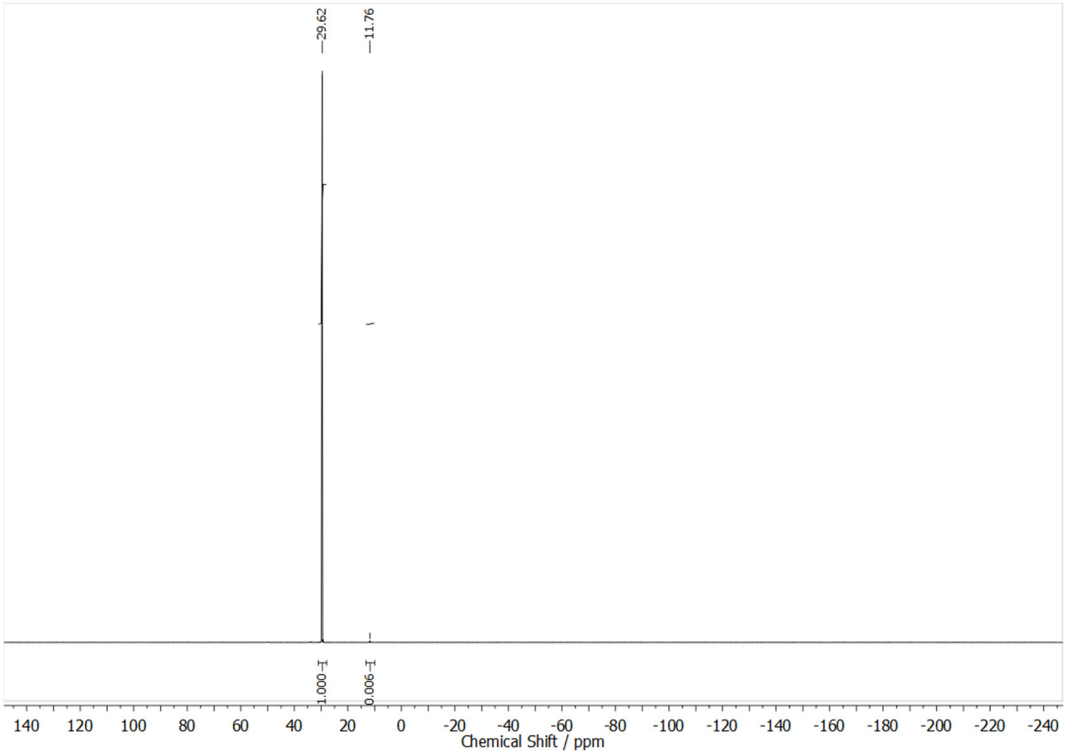

Figure S2: 41. *[Figure S41] NMR spectra of phosphonium chloride* ***6ab×HCl*** *($CDCl_3$, 400 MHz): a) ^1H NMR spectrum, b) ^{13}C NMR spectrum, c) ^{31}P NMR spectrum, d) $^{31}P\{^1H\}$ NMR spectrum.*

^{15}N-Tributyl(hexylcarbamoyl)phosphonium chloride ***6ab^{15}×HCl*** *(in Situ)*

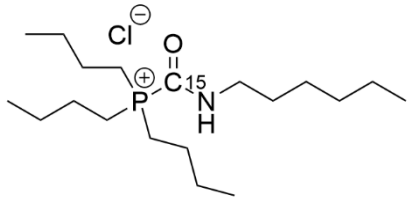

a)

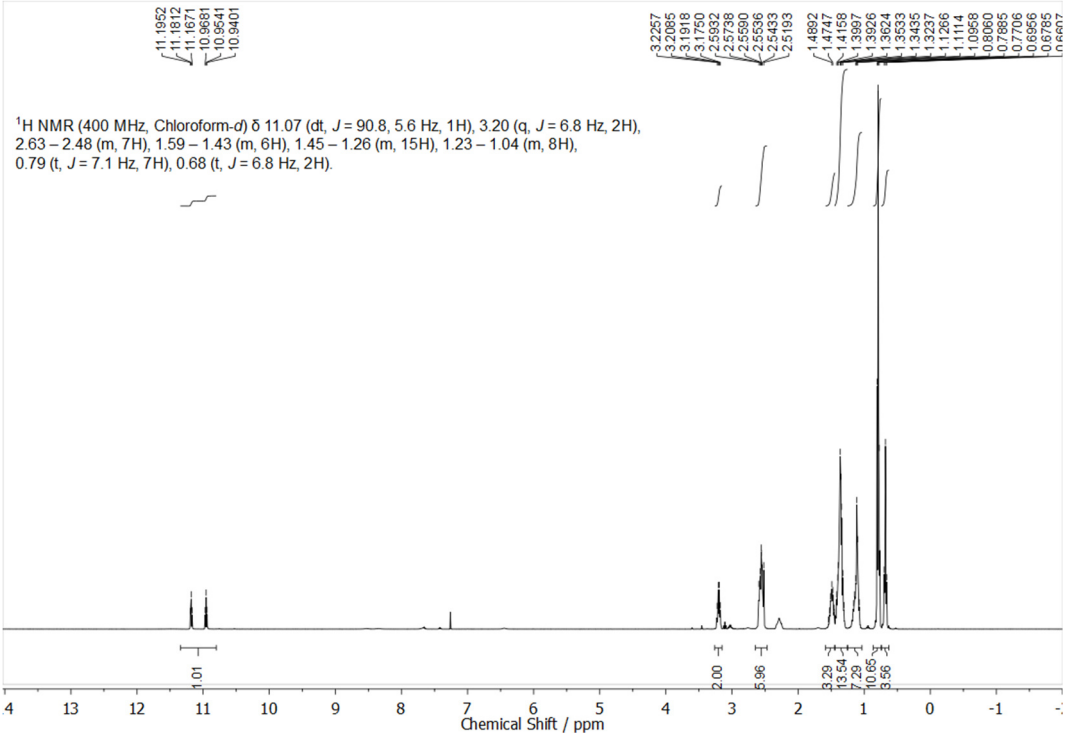

b)

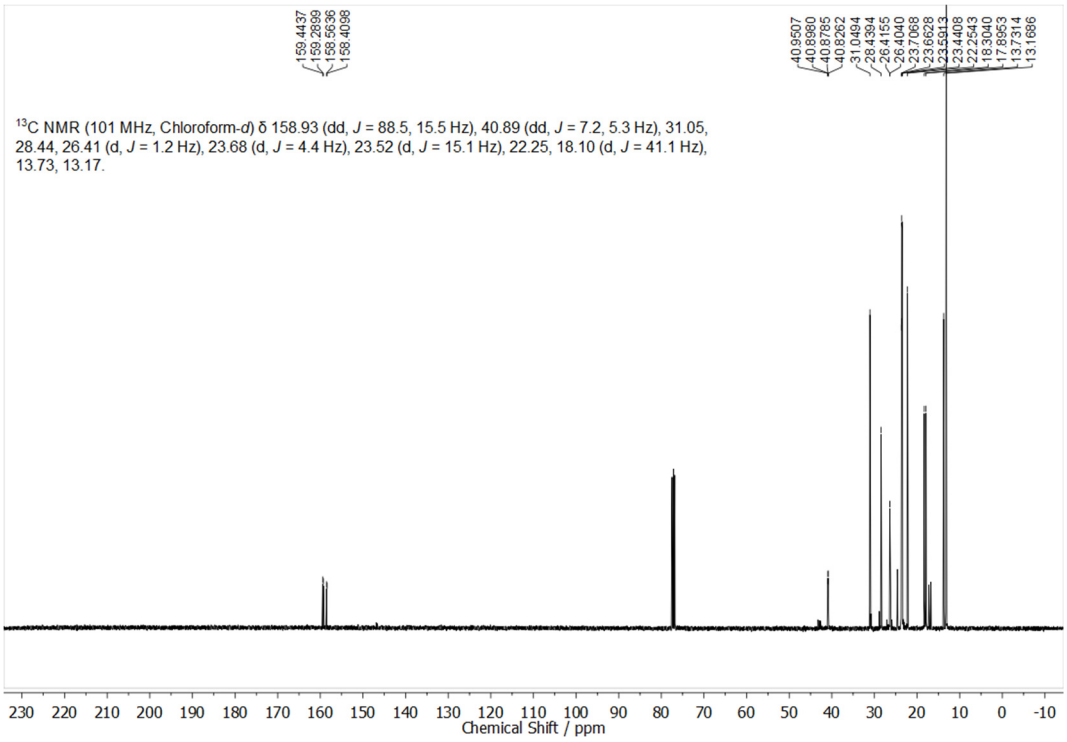

c)

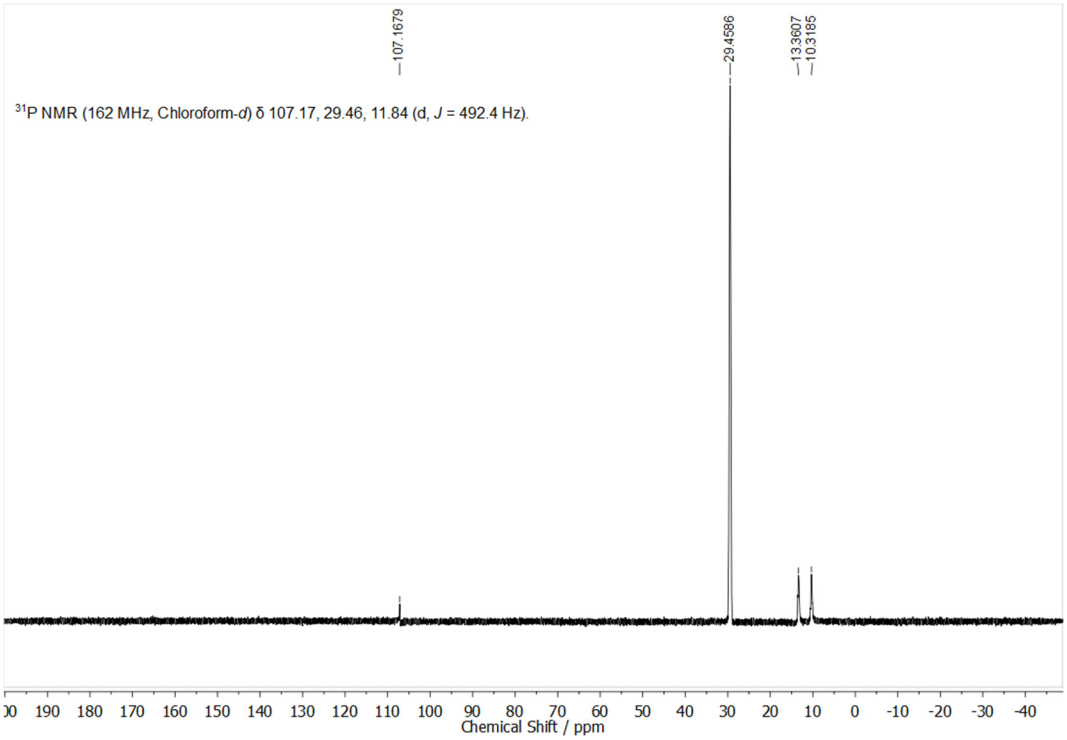
107.1679
29.4586
13.3607
10.3185
31P NMR (162 MHz, Chloroform-d) δ 107.17, 29.46, 11.84 (d, J = 492.4 Hz).
190 180 170 160 150 140 130 120 110 100 90 80 70 60 50 40 30 20 10 0 -10 -20 -30 -40
Chemical Shift / ppm

d)

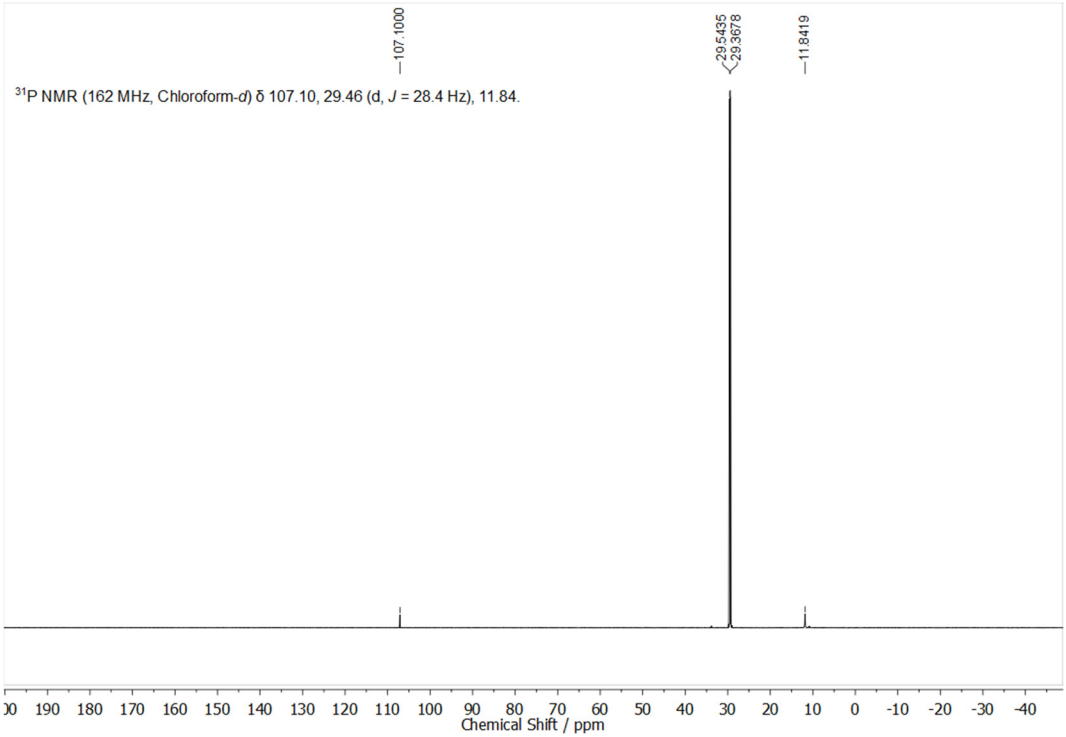
107.1000
29.5435
29.3678
11.8419
31P NMR (162 MHz, Chloroform-d) δ 107.10, 29.46 (d, J = 28.4 Hz), 11.84.
190 180 170 160 150 140 130 120 110 100 90 80 70 60 50 40 30 20 10 0 -10 -20 -30 -40
Chemical Shift / ppm

e)

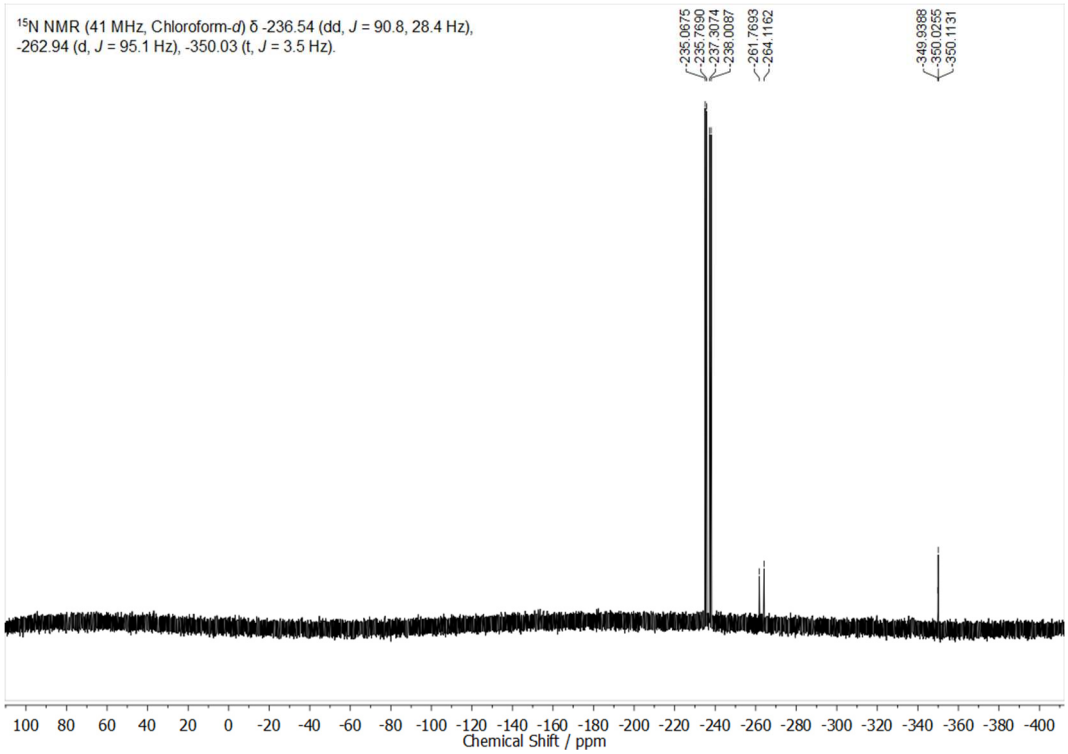

f)

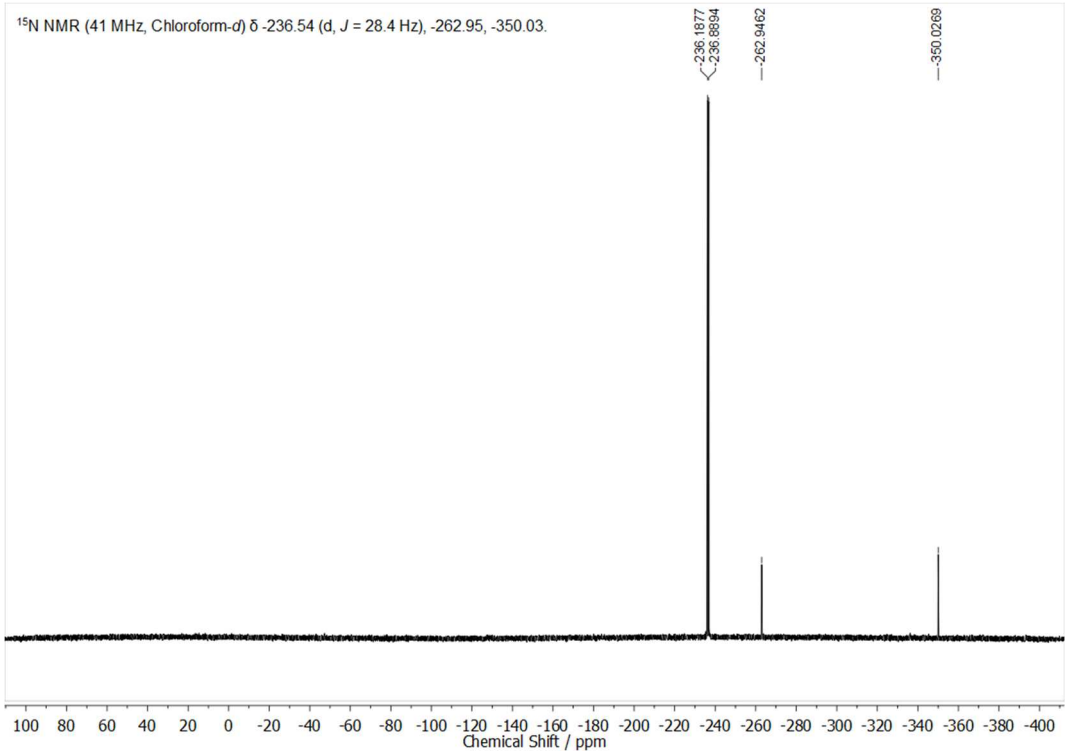

Figure S2: 42. *[Figure S42] NMR spectra of phosphonium chloride* ***6ab^{15}×HCl*** *($CDCl_3$, 400 MHz): a) ^{1}H NMR spectrum, b) ^{13}C NMR spectrum, c) ^{31}P NMR spectrum, d) $^{31}P\{^{1}H\}$ NMR spectrum, e) ^{15}N NMR spectrum, f) $^{15}N\{^{1}H\}$ NMR spectrum (all spectra contain traces of starting material and/or protonated isocyanate* ***1a^{15}*** *as detailed in the synthesis section.*

Aside from starting material **1a**^{15} (hexy isocyanate: signal at −350.03 ppm in ^{15}N NMR and minor signals in ^{1}H NMR and ^{13}C NMR), starting material **16b** (tributyl phosphonium chloride: signal at +11.8 ppm in ^{31}P NMR and minor signals in ^{1}H NMR and ^{13}C NMR), evidence for protonated isocyanate **1a**^{15} was found. This hints at a stepwise formation of **6ab**^{15}**×HCl** consisting of initial protonation of isocyanate and subsequent formation of the phosphonium adduct. Furthermore, this is in line with extensive record of activation of isocyanates by acids.[6] We believe this to be the case because of the signal at −262.9 ppm in ^{15}N {^{1}H} NMR (**Figure S2: 42f**). Once proton coupling is enabled, this signal splits into a doublet with a coupling of 95.1 Hz which is consistent with the couplings of other ^{15}N-bound protons. **Figure S2: 43** shows a ^{1}H-^{15}N HSQC spectrum which connects this signal to a doublet-of-triplets signal at 7.53 ppm (J = 95.0, 5.9 Hz) in the ^{1}H NMR spectrum:

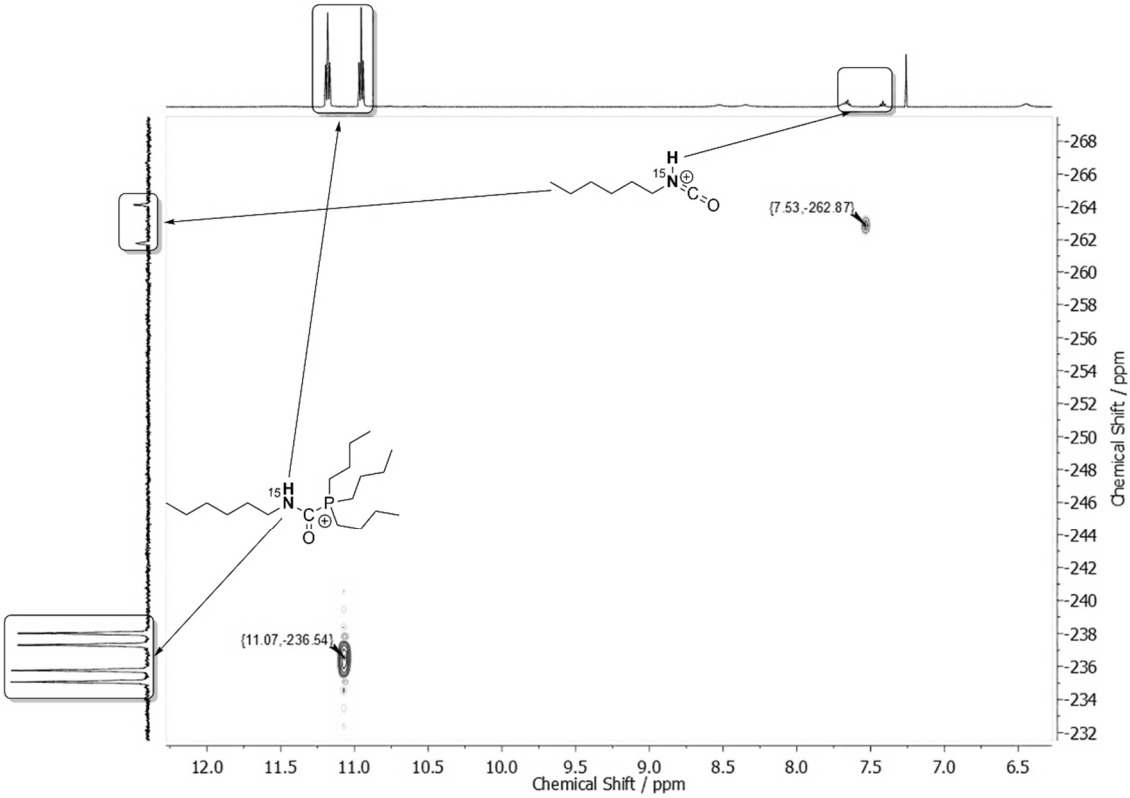

Figure S2: 43. *[Figure S43] ^{1}H-^{15}N HSQC spectrum the proton signal at 7.53 shows a coupling of* J *= 95.0 Hz, 5.9 Hz in close agreement with the N-H of compound* ***6ab***^{15}***×HCl****. The lack of coupling of ^{15}N to ^{31}P causes us to believe this signal represents protonated isocyanate as shown above.*

2.1.9 Investigation of Temperature- and Concentration-Dependence of ^{31}P NMR Measurements

Since we observed a temperature dependence of the ^{31}P NMR signals in the low-temperature measurements of oligomerization reactions, we performed a few experiments to quantify the extent of temperature- and concentration dependence for benchmarking our calculations of NMR shifts. To ensure accurate ^{31}P{^{1}H} NMR shifts, a sealed capillary containing 85% H_3PO_4 was added as external standard.

Table S2: 6 as well as **Figure S2: 44** show the data obtained for **5b**, **17b**, **17c** and **19b** for different concentrations and temperatures in $CDCl_3$ or under neat conditions.

Table S2: 6. [Table S13] Concentration- and temperature dependent ^{31}P{^{1}H} NMR signals of **5a, 18a**, **18c** and **19a**.

Compound	c / gL^{-1} ($CDCl_3$)	Chemical Shift / ppm (20°C)	Chemical Shift / ppm (23°C)	Chemical Shift / ppm (27°C)
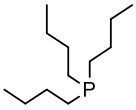 **5b**	19.8	-30.081	-30.007	-29.964
	43.2	-30.096	-30.041	-29.973
	96.2	-30.13	-30.065	-30.011
	263.25	-30.23	-30.167	-30.109
	neat		-31.851	-31.732
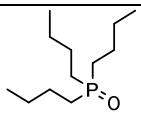 **17b**	25.2	49.133		48.991
	10.2	49.124		48.98
	90.6	49.159		49.012
 **17c**	5.6	52.98		
	15.2	53.007		
	29.2	53.034		
	41.6	53.035		
	79.8	53.069		
	134.2	53.081		
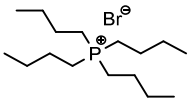 **19b**	25.26	32.78		
	36.5	32.77		
	75.69	32.74		
	168.4	32.59		
	243.1	32.44		

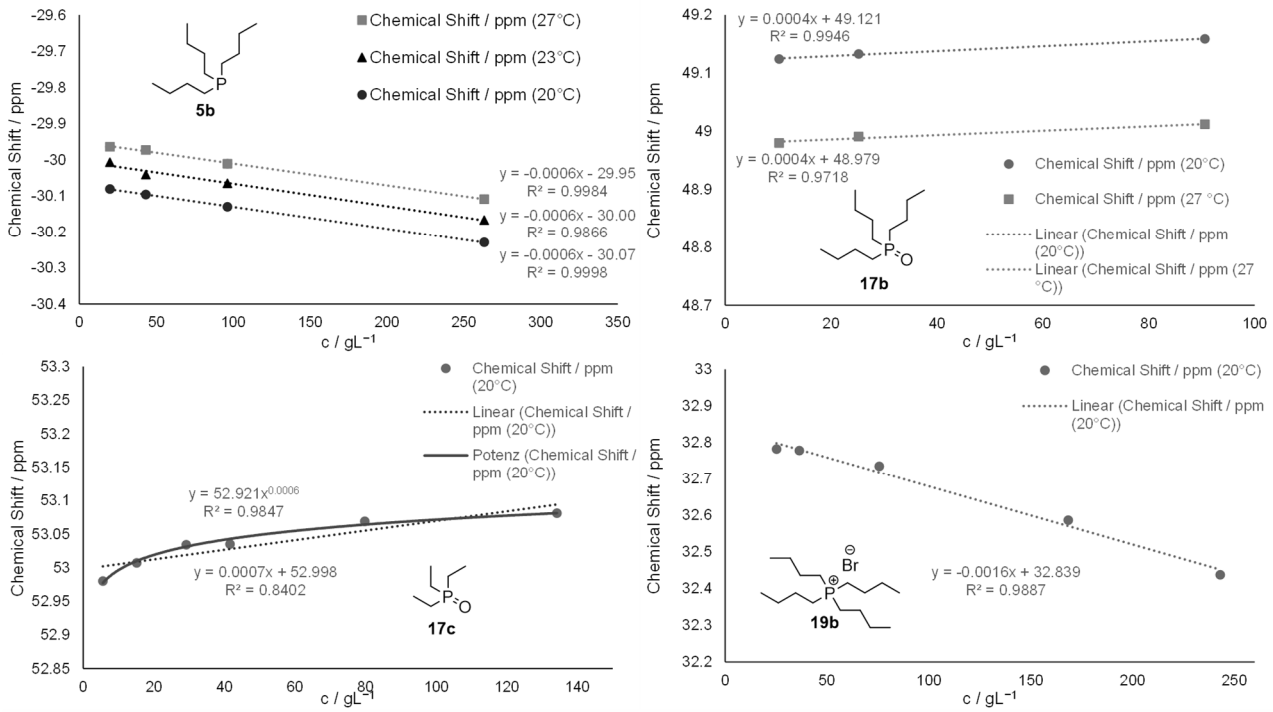

***Figure S2: 44**. [Figure S49] $^{31}P\{^{1}H\}$ NMR signals shifting at different temperatures and concentrations in $CDCl_3$.*

In the case of higher concentrations, we observed linear correlations between concentration and chemical shift, while this behavior seems not to be the case for low concentrations as shown for the example of $OPEt_3$ **17c**, which fits a potential equation much better. Changes in temperature however do shift the signals of all concentrations in a constant manner. For the limited change of temperature employed here, higher temperatures lead to a high-field shift of the signals in both **5b** and **17b** in $CDCl_3$. Since all effects described here cause only minor effects when compared to the broad range of ^{31}P NMR signals of more than 200 ppm, the influence of temperature and concentration was not taken into account for validating calculated NMR shifts in this study.

2.1.10 Computational Chemistry Procedures

Selection of Methodology

In order to identify suitable theoretical methods for all species involved in the proposed reaction mechanism, preliminary calculations have been performed for the dimerization of methyl isocyanate (**1d**) to *N*,*N*-dimethyluretdione (**2d**) and for the reaction of methyl isocyanate (**1d**) with trimethyl-phospane (**5d**) to zwitterionic intermediate **6dd**. This includes geometry optimizations with the B3LYP[8] and MPW1K[9] hybrid DFT methods, and single point calculations with the MP2(FC)[12] and B2PLYP[10] calculations in combination with medium-sized basis sets, and with the G3B3[11] compound method. All subsequent geometry optimizations have been performed at the B3LYP/6-31+G(d,p) level of theory. Thermal corrections at 298.15 K were calculated without scaling using the rigid rotor/harmonic oscillator model at the same level. Improved energies were obtained from B2PLYP/cc-pVTZ//B3LYP/6-31+G(d,p) calculations. Initial

coordinates were generated by applying the MM3* force field implemented in MacroModel (Schrödinger program package). [13]. NMR shielding calculations were performed at the B3LYP/IGLO-III level of theory. Except for initial force field conformational search, all calculations have been done with Gaussian 09 Rev C.01.[14]

2.1.11 Calculation of ^{13}C, ^{15}N, and ^{31}P NMR Signals

All NMR shieldings were calculated using the B3LYP/IGLO-III//B3LYP/6-31+G(d,p) level of theory. Additionally to gas-phase values, we also applied implicit solvation in $CHCl_3$ by both the PCM[15] and the SMD[16] method. Only conformers that contributed more than 1% towards the Boltzmann averaged Enthalpy $<H_{298K}>$ were selected for calculation of shieldings. These shieldings were then themselves Boltzmann averaged according to the weighting factors for H_{298K}. The averaged shieldings were transformed into NMR shifts by applying scaling terms obtained by correlating experimental NMR shifts of characterized or well-known compounds to their respective short-chain analogues as detailed in the section for the specific elements below. While the experimentally used compounds incorporated either *n*-butyl or *n*-hexyl substituents, we limited these substituents to ethyl groups for our theoretical study. This was done due to the massive increase in conformers and computational cost that comes with using longer aliphatic groups.

^{13}C NMR Signals:

In order to generate a training set for the prediction of NMR chemical shifts, ^{13}C NMR spectra of *n*-hexyl isocyanate **1a**, *n*-hexyl uretdione **2a**, *n*-hexyl isocyanurate **3a**, ^{15}*N*-methyl hexylcarbamate **11a**[15], ^{15}*N*-dihexylurea **12a**[15], ^{15}*N*-Hexylacetamide **13a**[15] and tributyl(hexylcarbamoyl)phosphonium chloride **6ab×HCl** were measured. Only the carbonyl ^{13}C signals have been taken into account since these are well separated from the rest and, more importantly, part of the reactive regions. As specified above, the experimental NMR shifts were correlated to the calculated averaged ^{13}C carbonyl shieldings of the corresponding ethyl-compounds as shown in **Table S2: 7** and **Figure S2: 45**.

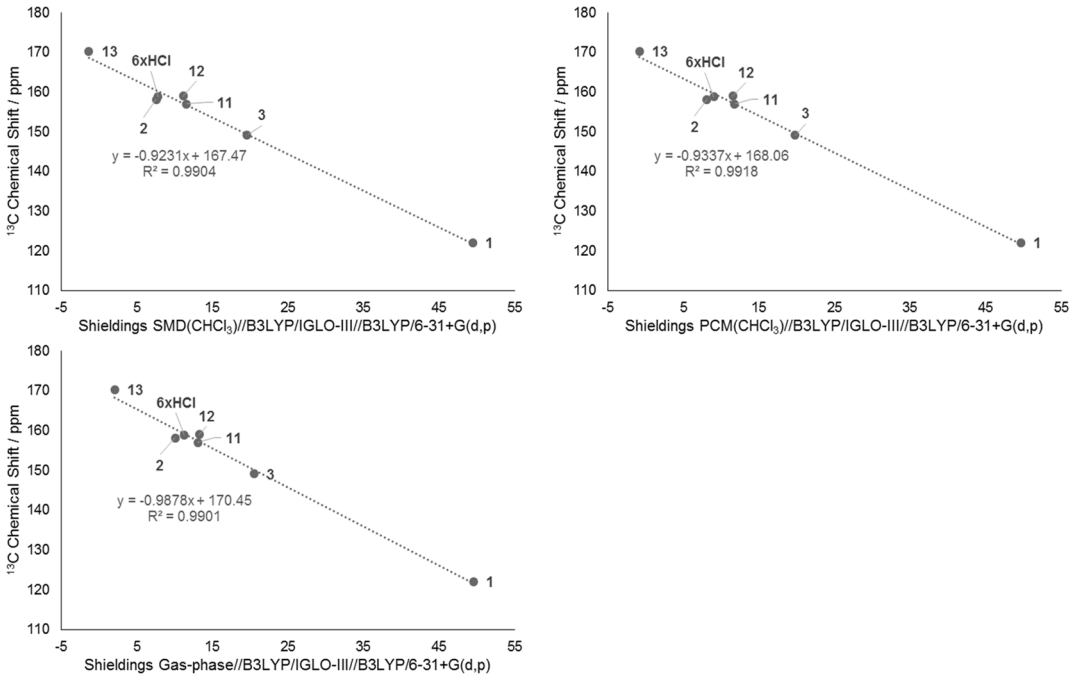

Figure S2: 45. *[Figure S52] Correlation of experimentally determined ^{13}CNMR (carbonyl) signals in $CHCl_3$ and shieldings calculated in different phases at the B3LYP/IGLO-III//B3LYP/6-31+G(d,p) level of theory.*

Table S2: 7. [Table S14] Experimentally determined ^{13}CNMR (carbonyl) signals in $CHCl_3$ and shieldings calculated in different phases at the B3LYP/IGLO-III//B3LYP/6-31+G(d,p) level of theory.

Compound	Shielding: B3LYP/IGLO-III//B3LYP/6-31+G(d,p)			Experimental shift / ppm
	$R^1 = R^2 = Et$			$R^1 = Bu$, $R^2 = Hex$
	SMD($CHCl_3$)	PCM($CHCl_3$)	Gas phase	$CHCl_3$
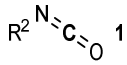 **1**	49.4871	49.6424	49.5969	122.02
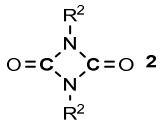 **2**	7.59176196 [a]	8.1313734 [a]	10.126762 [a]	158.13
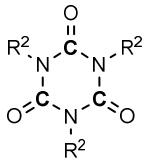 **3**	19.5829161 [a]	19.7941533 [a]	20.5493501 [a]	149.13
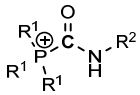 **6xHCl**	7.85356469	9.05305885	11.3359575	158.87[b]
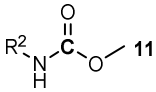 **11**	11.5834903	11.8153094	13.0836346	157.04
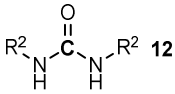 **12**	11.165331	11.5340669	13.3140125	159.01
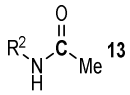 **13**	-1.326	-0.8023	2.1091	170.27

[a] Arithmetic average of the values obtained for the highlighted carbon atoms. [b] Counter ion = Cl^-.

Since the phase model did not influence the obtained shielding values strongly and we found good fits for all three methods, SMD($CHCl_3$) and PCM($CHCl_3$) solvation models as well as gas-phase calculations were used for the purpose of simulating the shifts of compounds identified as important for the mechanism. The correlations found in **Figure S2: 45** were used in the form of Equations S2: 1 – S2: 3.

$$^{13}\text{C NMR shift (SMD(CHCl}_3\text{))} / \text{ppm} = -0.9231 \times {}^{13}\text{C Shielding (SMD(CHCl}_3\text{))} + 167.47 \qquad \text{Eq. S2: 1}$$

$$^{13}\text{C NMR shift (PCM(CHCl}_3\text{))} / \text{ppm} = -0.9337 \times {}^{13}\text{C Shielding (PCM(CHCl}_3\text{))} + 168.06 \qquad \text{Eq. S2: 2}$$

$$^{13}\text{C NMR shift (Gas-phase)} / \text{ppm} = -0.9878 \times {}^{13}\text{C Shielding (Gas-phase)} + 170.45 \qquad \text{Eq. S2: 3}$$

Table S2: 8 and **Figure S2: 46** show the shieldings obtained for and the shifts calculated for carbonyl atoms in intermediates that were either proposed previously[4] or in the case of this study for the mechanism of the phosphane catalysed oligomerization of isocyanates:

Table S2: 8. [Table S15] ^{13}C carbonyl shieldings of intermediates and derived corresponding ^{13}C NMR shifts obtained in different phases at the B3LYP/IGLO-III//B3LYP/6-31+G(d,p) level of theory.

Compound	# of C	B3LYP/IGLO-III//B3LYP/6-31+G(d,p)						Arithmetic average±standard deviation / ppm
		SMD($CHCl_3$)		PCM($CHCl_3$)		Gas-phase		
		R^1=R^2=Et	R^1=*n*Bu, R^2=*n*Hex	R^1=R^2=Et	R^1=*n*Bu, R^2=*n*Hex	R^1 = R^2 = Et	R^1=*n*Bu, R^2=*n*Hex	
		^{13}C Shielding	^{13}C NMR shift (calc.) / ppm	^{13}C Shielding	^{13}C NMR shift (calc.) / ppm	^{13}C Shielding	^{13}C NMR shift (calc.) / ppm	
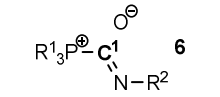 **6**	C^1	11.9026	156.48	12.7500	156.16	14.7496	155.88	156.17±0.25
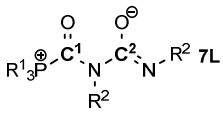 **7L**	C^1	16.0601	152.64	17.1283	152.07	21.3402	149.37	151.36±1.43
	C^2	16.7816	151.98	17.0912	152.10	18.5000	152.18	152.09±0.08
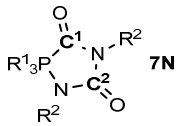 **7N**	C^1	1.0533	166.50	1.6351	166.53	3.4608	167.03	166.69±0.24
	C^2	14.7293	153.87	14.9415	154.11	15.9121	154.73	154.24±0.36
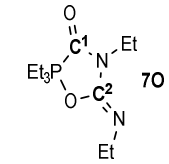 **7O**	C^1	5.8381	162.08	6.6249	161.87	8.7498	161.81	161.92±0.12
	C^2	17.4650	151.35	18.0603	151.20	19.2964	151.39	151.31±0.08
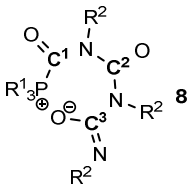 **8**	C^1	3.8534	163.91	4.4757	163.88	6.2020	164.32	164.04±0.20
	C^2	13.1903	155.29	13.4694	155.48	14.0653	156.56	155.78±0.56
	C^3	11.5328	156.82	12.0519	156.81	13.3370	157.28	156.97±0.22
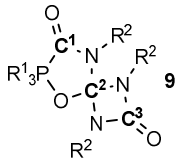 **9**	C^1	3.8261	163.94	4.3875	163.96	6.1424	164.38	164.09±0.20
	C^2	65.8384	106.69	65.8576	106.57	65.9010	105.35	106.21±0.60
	C^3	3.1188	164.59	3.4265	164.86	5.9254	164.60	164.68±0.13

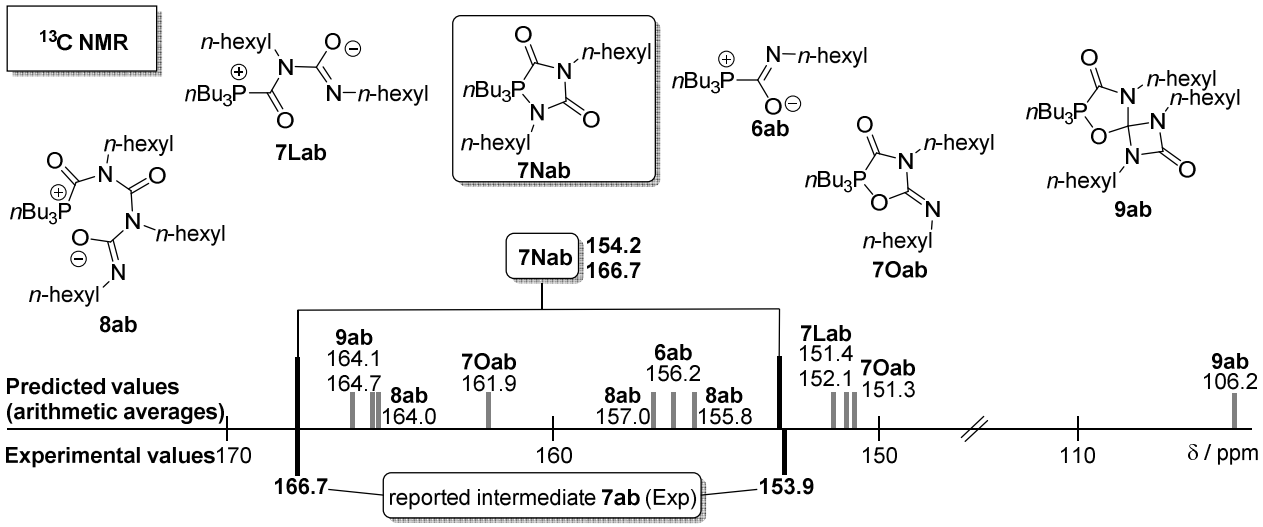

Figure S2: 46. *[Figure S53] Comparison of predicted (arithmetic averaged) and previously reported experimental ^{13}C NMR shifts for the carbonyl atoms of intermediates and selected reference compounds.*

^{15}N NMR Signals:

For benchmarking purposes, ^{15}N{^{1}H} NMR spectra of the ^{15}N enriched compounds ^{15}*N*-hexyl isocyanate **1a^{15}**, ^{15}*N*-hexyl uretdione **2a^{15}**, ^{15}*N*-hexyl isocyanurate **3a^{15}**, ^{15}*N*-tributyl(hexylcarbamoyl)phosphonium chloride **6ab^{15}×HCl**, ^{15}*N*-methyl hexylcarbamate **11a^{15}**, ^{15}*N*-dihexylurea **12a^{15}** and ^{15}*N*-hexylacetamide **13a^{15}** in $CDCl_3$ were recorded. As specified above, these experimental shifts were then correlated to the calculated averaged ^{15}N shieldings of the corresponding ethyl-compounds as shown in **Table S2: 9** and **Figure S2: 47**:

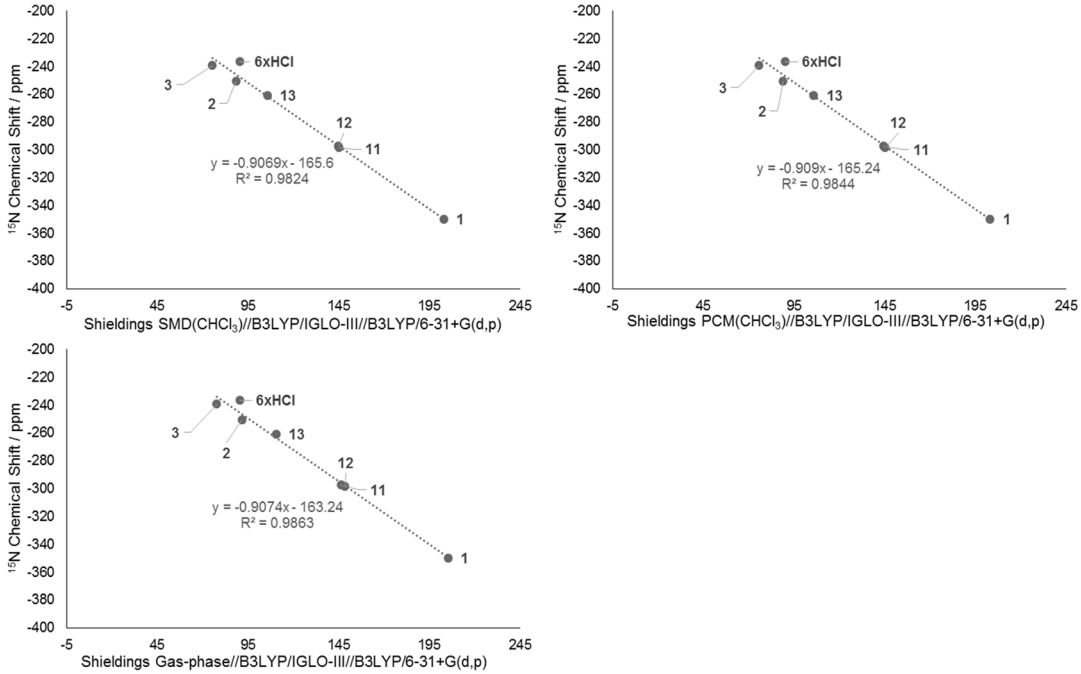

Figure S2: 47. *[Figure S54] Correlation of experimentally determined ^{15}NNMR signals in $CHCl_3$ and shieldings calculated in different phases at the B3LYP/IGLO-III//B3LYP/6-31+G(d,p) level of theory.*

Table S2: 9. [Table S16] Experimentally determined ^{15}NNMR signals in $CHCl_3$ and shieldings calculated in different phases at the B3LYP/IGLO-III//B3LYP/6-31+G(d,p) level of theory.

Compound	Shielding: B3LYP/IGLO-III//B3LYP/6-31+G(d,p) $R^1 = R^2 = Et$ SMD($CHCl_3$)	PCM($CHCl_3$)	Gas phase	Experimental shift / ppm $R^1 = Bu$, $R^2 = Hex$ $CHCl_3$
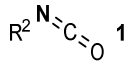 **1**	203.0571	203.3317	205.5902	-349.99
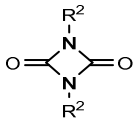 **2**	88.4545[a]	89.2028[a]	91.7156[a]	-250.73
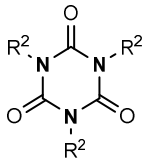 **3**	75.4733[a]	75.9340[a]	77.8129[a]	-239.37
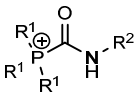 **6xHCl**	90.5825	90.0659	90.7805	-236.54[b]
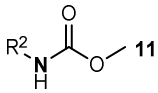 **11**	145.3601	145.4179	148.5415	-298.40
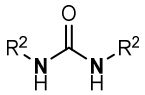 **12**	144.9362[a]	144.6026[a]	146.3606[a]	-297.41
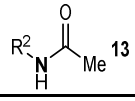 **13**	105.8542	105.9370	110.6411	-260.98

[a] Arithmetic average of the values obtained for the highlighted carbon atoms. [b] Counter ion = Cl^-.

Since the phase model did not influence the obtained shielding values strongly and we found good fits for all three methods, SMD($CHCl_3$) and PCM($CHCl_3$) solvation models as well as gas-phase calculations for the purpose of simulating the shifts of compounds identified as important for the mechanism. The correlations found in **Figure S2: 47** were used in the form of Equations S2: 4 – S2: 6.

$$^{15}\text{N NMR shift (SMD(CHCl}_3\text{))} / \text{ppm} = -0.9069 \times {}^{15}\text{N Shielding (SMD(CHCl}_3\text{))} - 165.6 \qquad \text{Eq. S2: 4}$$

$$^{15}\text{N NMR shift (PCM(CHCl}_3\text{))} / \text{ppm} = -0.909 \times {}^{15}\text{N Shielding (PCM(CHCl}_3\text{))} - 165.24 \qquad \text{Eq. S2: 5}$$

$$^{15}\text{N NMR shift (Gas-phase)} / \text{ppm} = -0.9074 \times {}^{15}\text{N Shielding (Gas-phase)} - 163.24 \qquad \text{Eq. S2: 6}$$

Table S2: 10 and **Figure S2: 48** show the shieldings obtained for and the shifts calculated for ^{15}N atoms in intermediates that were either proposed previously[4] or in the case of our study for the mechanism of the phosphane catalysed oligomerization of isocyanates:

Table S2: 10. [Table S17] ^{15}N shieldings of intermediates and derived corresponding ^{15}N NMR shifts obtained in different phases at the B3LYP/IGLO-III//B3LYP/6-31+G(d,p) level of theory.

Compound	# of N	B3LYP/IGLO-III//B3LYP/6-31+G(d,p) SMD($CHCl_3$) R^1=R^2=Et ^{15}N Shielding	SMD($CHCl_3$) R^1=*n*Bu, R^2=*n*Hex ^{15}N NMR shift (calc.) / ppm	PCM($CHCl_3$) R^1=R^2=Et ^{15}N Shielding	PCM($CHCl_3$) R^1=*n*Bu, R^2=*n*Hex ^{15}N NMR shift (calc.) / ppm	Gas-phase R^1 = R^2 = Et ^{15}N Shielding	Gas-phase R^1=*n*Bu, R^2=*n*Hex ^{15}N NMR shift (calc.) / ppm	Arithmetic average±standard deviation / ppm
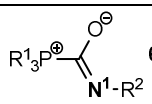 **6**	N^1	10.5401	-175.16	6.2046	-170.88	1.2850	-164.41	-170.15±4.42
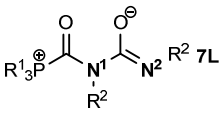 **7L**	N^1	31.6341	-194.29	30.8189	-193.25	27.7228	-188.40	-191.98±2.57
	N^2	62.7941	-222.55	59.8076	-219.61	56.5607	-214.56	-218.91±3.30
 **7N**	N^1	53.3473	-213.98	53.2321	-213.63	53.5702	-211.85	-213.15±0.93
	N^2	83.0699	-240.94	83.5416	-241.18	86.2371	-241.49	-241.20±0.23
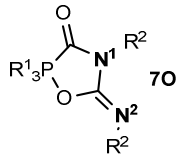 **7O**	N^1	52.5269	-213.24	52.2115	-212.70	52.3453	-210.74	-212.22±1.07
	N^2	52.4261	-213.15	48.8516	-209.65	41.9312	-201.29	-208.03±4.97
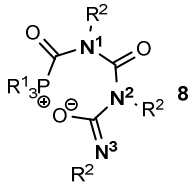 **8**	N^1	55.6892	-216.10	55.8429	-216.00	55.4386	-213.54	-215.22±1.18
	N^2	57.5247	-217.77	57.1929	-217.23	56.5462	-214.55	-216.52±1.41
	N^3	42.2511	-203.92	38.4516	-200.19	31.2281	-191.58	-198.56±5.17
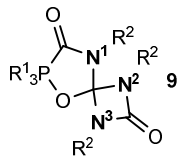 **9**	N^1	60.8535	-220.79	60.6395	-220.36	60.5524	-218.19	-219.78±1.14
	N^2	93.2245	-250.15	93.4801	-250.21	95.5915	-249.98	-250.11±0.10
	N^3	91.6304	-248.70	91.8672	-248.75	93.9411	-248.48	-248.64±0.12

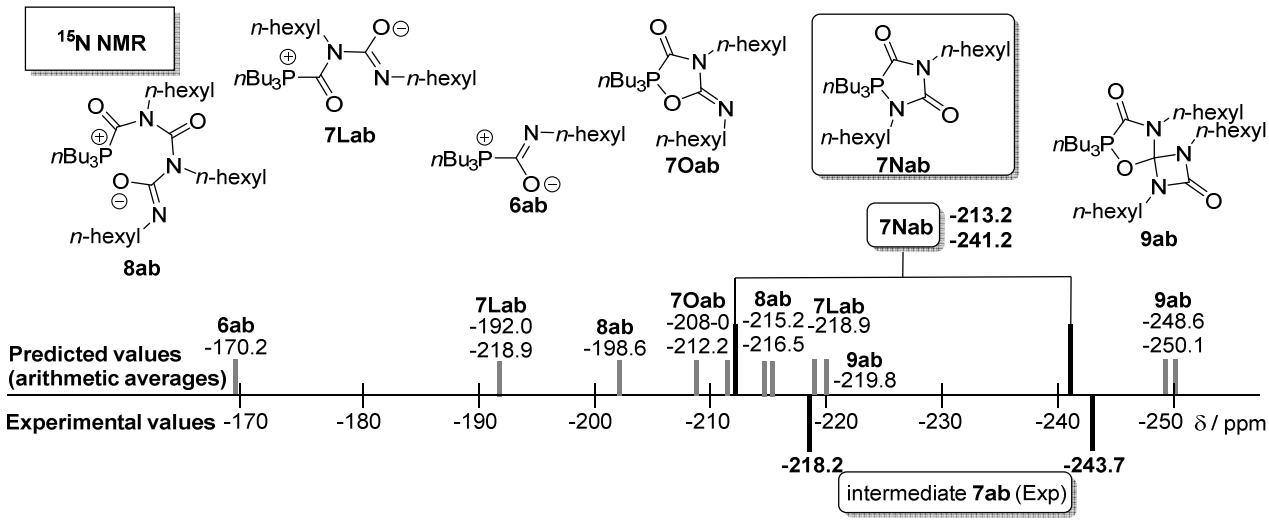

Figure S2: 48. *[Figure S55] Comparison of predicted (arithmetic averages) and experimentally determined ^{15}NNMR signals for intermediates and selected reference compounds.*

^{31}P NMR Signals:

For correlating purposes, ^{31}P{^{1}H} NMR spectra of tri-*n*-butyl phosphane **5b**, tri-*n*-butylphosphonium chloride **16b** ,tri-*n*-butyl(methyl)phosphonium iodide **15b**, tetrabutyl phosphonium bromide **19b**, tri-*n*-butylphosphine oxide **17b**, tri-*n*-butyl phosphate **18b** and tributyl(hexylcarbamoyl)phosphonium chloride **6ab×HCl** were recorded. As specified above, the experimental NMR shifts were correlated to the calculated averaged ^{31}P shieldings of the corresponding ethyl-compounds as shown in **Table S2: 11** and **Figure S2: 49**:

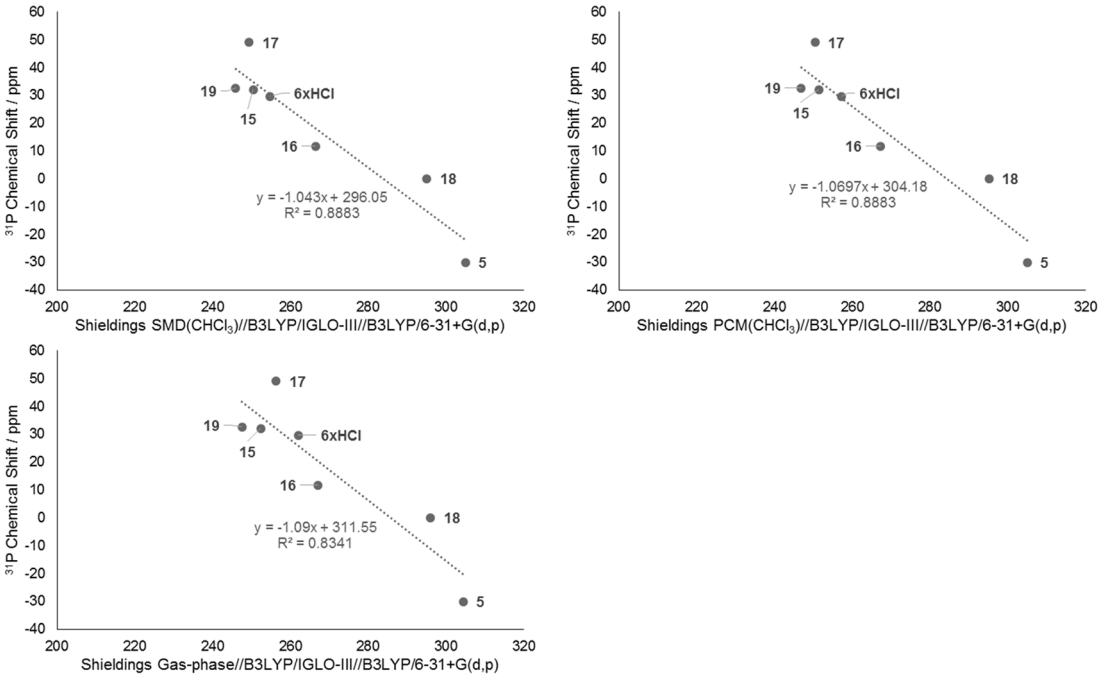

Figure S2: 49. *[Figure S56] Correlation of experimentally determined ^{31}PNMR signals in $CHCl_3$ and shieldings calculated in different phases at the B3LYP/IGLO-III//B3LYP/6-31+G(d,p) level of theory.*

Table S2: 11. [Table S18] Experimentally determined ^{31}PNMR signals in $CHCl_3$ and shieldings calculated in different phases at the B3LYP/IGLO-III//B3LYP/6-31+G(d,p) level of theory.

Compound	Shielding: B3LYP/IGLO-III//B3LYP/6-31+G(d,p) $R^1 = R^2 = Et$ SMD($CHCl_3$)	PCM($CHCl_3$)	Gas phase	Experimental shift / ppm $R^1 = Bu$, $R^2 = Hex$ $CHCl_3$
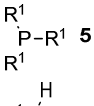 **5**	305.1325	305.0275	304.5160	-30.12[a]
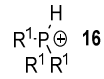 **16**	266.4493	267.3313	267.1838	11.65[b]
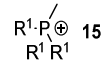 **15**	250.4360	251.4571	252.3983	32.09[d]
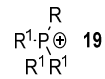 **19**	245.9389	246.9228	247.5830	32.66[a, b]
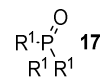 **17**	249.3981	250.4589	256.3861	48.99[a]
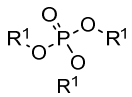 **18**	295.1240	295.2296	296.1391	-0.04
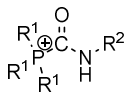 **6xHCl**	254.8066	257.2945	262.0464	29.62[b]

[a] Arithmetic average of the values listed in **Table S2: 6**. [b] Counter ion = Cl^-. [c] Counter ion = Br^-. [d] Counter ion = I^-.

Because of the apparent influence of the phase model on the quality of the fit, we decided to use SMD($CHCl_3$) and PCM($CHCl_3$) solvation models for calculation of the shifts of compounds identified as important for the mechanism. The correlations found in **Figure S2: 49** were used in the form of Equation S2: 7 and Equation S2: 8.

$$^{31}\text{P NMR shift (SMD(CHCl}_3\text{))} / \text{ppm} = -1.043 \times {}^{31}\text{P Shielding (SMD(CHCl}_3\text{))} + 296.05 \qquad \text{Eq. S2: 7}$$

$$^{31}\text{P NMR shift (PCM(CHCl}_3\text{))} / \text{ppm} = -1.0697 \times {}^{31}\text{P Shielding (PCM(CHCl}_3\text{))} + 304.18 \qquad \text{Eq. S2: 8}$$

Table S2: 12 and **Figure S2: 50** show the shieldings obtained for and the shifts calculated for phosphorous containing species that were either proposed previously[4] or in the case of our study for the mechanism of the phosphane catalysed oligomerization of isocyanates:

Table S2: 12. [Table S19] ^{31}P shieldings of intermediates and derived corresponding ^{31}P NMR shifts obtained for different solvation models at the B3LYP/IGLO-III//B3LYP/6-31+G(d,p) level of theory.

Compound	B3LYP/IGLO-III//B3LYP/6-31+G(d,p)				
	SMD($CHCl_3$)		PCM($CHCl_3$)		Arithmetic average±standard deviation / ppm
	R^1=R^2=Et	R^1=*n*Bu, R^2=*n*Hex	R^1=R^2=Et	R^1=*n*Bu, R^2=*n*Hex	
	^{31}P Shielding	^{31}P NMR shift (calc.) / ppm	^{31}P Shielding	^{31}P NMR shift (calc.) / ppm	
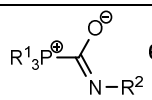 **6**	281.6763	2.26	284.5443	-0.20	1.03±1.74
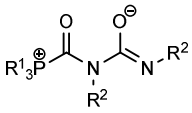 **7L**	254.4432	30.67	258.2824	27.90	29.28±1.96
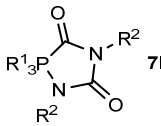 **7N**	335.6536	-54.04	336.9593	-56.27	-55.15±1.58
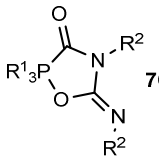 **7O**	296.6261	-13.33	298.5837	-15.21	-14.27±1.33
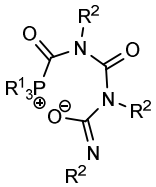 **8**	254.0579	31.07	256.1695	30.16	30.61±0.65
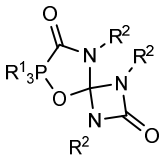 **9**	302.7538	-19.72	304.2439	-21.27	-20.50±1.09

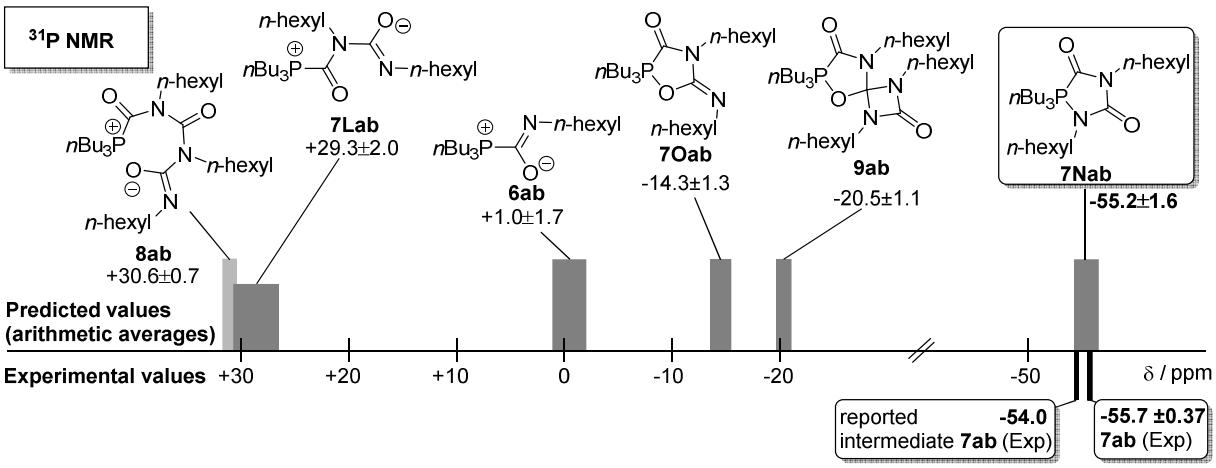

Figure S2: 50. *[Figure S57] Comparison of predicted (arithmetic averages) and experimentally determined ^{31}PNMR signals for intermediates and selected reference compounds.*

References

[1] a) G. M. Loudon, A. S. Radhakrishna, M. R. Almond, J. K. Blodgett, R. H. Boutin, *J. Org. Chem.* **1984**, *49*, 4272 – 4276, b) A. Yoshimura, M. W. Luedtke, V. V. Zhdankin, *J. Org. Chem.* **2012**, *77*, 2087 – 2091.

[2] D. C. D. Butler, H. Alper, *Chem. Commun.* **1998**, 2575 – 2576.

[3] M. Ozaki, Y. Obora, Y. Tada, Y. Ishii, *Journal of Organometallic Chemistry* **2013**, *741-742*, 109 – 113.

[4] Z. Pusztai, G. Vlad, A. Bodor, I. T. Horvath, H. J. Laas, R. Halpaap, F. U. Richter, *Angew. Chem. Int. Ed.* **2006**, *45*, 107 – 110.

[5] S. Hoops, S. Sahle, R. Gauges, C. Lee, J. Pahle, N. Simus, M. Singhal, L. Xu, P. Mendes, U. Kummer, *Bioinformatics*, **2006**, *22*, 3067 – 3074.

[6] a) H. Sardon, A. Pascual, D. Mecerreyes, D. Taton, H. Cramail, J. L. Hedrick, *Macromolecules*, **2015**, *48*, 3153 – 3165; b) A. Benalil, P. Roby, B. Carboni, M. Vaultier, *Synthesis*, **1991**, *9*, 787 – 788.

[7] J. Keller, Dissertation, Ludwig-Maximilians-Universität München (München), **2007**.

[8] A. D. Becke, *J. Chem. Phys.* **1993**, *98*, 5648 – 5652.

[9] B. J. Lynch, P. I. Fast, M. Harris, D. G. Truhlar, *Phys. Chem. A*, **2000**, *104*, 4811 – 4815.

[10] S. Grimme, *J. Chem. Phys.* **2006**, *124*, 034108-1 – 034108-16.

[11] A. G. Baboul, L. A. Curtiss, P. C. Redfern, K. Raghavachari, *J. Chem. Phys.* **1999**, *110*, 7650 – 7657.

[12] a) M. Head-Gordon, J. A. Pople, M. J. Frisch, *Chem. Phys. Lett.* **1988**, *153*, 503 - 506; b) S. Saebø and J. Almlöf, *Chem. Phys. Lett.* **1989**, *154*, 83-89; c) M. J. Frisch, M. Head-Gordon, J. A. Pople, *Chem. Phys. Lett.* **1990**, *166*, 275-280.

[13] MacroModel, Schrödinger, LLC, New York, NY, **2018**.

[14] Gaussian 09, Revision C.01, M. J. Frisch, G. W. Trucks, H. B. Schlegel, G. E. Scuseria, M. A. Robb, J. R. Cheeseman, G. Scalmani, V. Barone, G. A. Petersson, H. Nakatsuji, X. Li, M. Caricato, A. Marenich, J. Bloino, B. G. Janesko, R. Gomperts, B. Mennucci, H. P. Hratchian, J. V. Ortiz, A. F. Izmaylov, J. L. Sonnenberg, D. Williams-Young, F. Ding, F. Lipparini, F. Egidi, J. Goings, B. Peng, A. Petrone, T. Henderson, D. Ranasinghe, V. G. Zakrzewski, J. Gao, N. Rega, G. Zheng, W. Liang, M. Hada, M. Ehara, K. Toyota, R. Fukuda, J. Hasegawa, M. Ishida, T. Nakajima, Y. Honda, O. Kitao, H. Nakai, T. Vreven, K. Throssell, J. A. Montgomery, Jr., J. E. Peralta, F. Ogliaro, M. Bearpark, J. J. Heyd, E. Brothers, K. N. Kudin, V. N. Staroverov, T. Keith, R. Kobayashi, J. Normand, K. Raghavachari, A. Rendell, J. C. Burant, S. S. Iyengar, J. Tomasi, M. Cossi, J. M. Millam, M. Klene, C. Adamo, R. Cammi, J. W. Ochterski, R. L. Martin, K. Morokuma, O. Farkas, J. B. Foresman, and D. J. Fox, Gaussian, Inc., Wallingford CT, **2016**.

[15] G. Scalmani, M. J. Frisch, *J. Chem. Phys.* **2010**,*132*, 114110.

[16] A. V. Marenich, C. J. Cramer, D. G. Trular, *J. Phys. Chem. B*, **2009**, *113*, 6378 – 6396.

Thermochemical Data

Table S2: 13. [Table S20] Thermochemical data in Hartree (Boltzmann averaged values and Δ <*H*>/Δ <*G*> in kJ mol^{-1} are given in bold font).

Nr.	B3LYP/6-31+G(d,p)				B2PLYP/cc-pVTZ//B3LYP/6-31+G(d,p)			
	E_{tot}	H_{298K}	G_{298K}	G_{298K}, SMD($CHCl_3$)	E_{tot}	H_{298K}	G_{298K}	G_{298K}, SMD($CHCl_3$)
	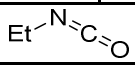 **1c**							
1c-001	-247.322571	-247.236554	-247.273036	-247.278470	-247.202901	-247.116884	-247.153366	-247.158800

Nr.	B3LYP/6-31+G(d,p)				B2PLYP/cc-pVTZ//B3LYP/6-31+G(d,p)			
	E_{tot}	H_{298K}	G_{298K}	G_{298K}, SMD($CHCl_3$)	E_{tot}	H_{298K}	G_{298K}	G_{298K}, SMD($CHCl_3$)
	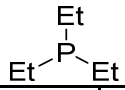 **5c**							
5c-005	-579.060822	-578.850400	-578.898405	-578.906548	-578.764049	-578.553627	-578.601632	-578.609776
5c-004	-579.061076	-578.850571	-578.898286	-578.906398	-578.764416	-578.553911	-578.601626	-578.609737
5c-003	-579.061146	-578.850799	-578.898726	-578.906837	-578.764051	-578.553704	-578.601631	-578.609743
5c-002	-579.062443	-578.852103	-578.900156	-578.908187	-578.765407	-578.555067	-578.603120	-578.611152
5c-001	-579.062473	-578.852156	-578.900190	-578.908190	-578.765420	-578.555103	-578.603137	-578.611137
<H> / <G>		**-578.851779**	**-578.899836**	**-578.907843**		**-578.554726**	**-578.602774**	**-578.610786**

Nr.	B3LYP/6-31+G(d,p)				B2PLYP/cc-pVTZ//B3LYP/6-31+G(d,p)			
	E_{tot}	H_{298K}	G_{298K}	G_{298K}, SMD($CHCl_3$)	E_{tot}	H_{298K}	G_{298K}	G_{298K}, SMD($CHCl_3$)
	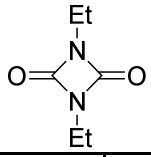 **2c**							
2c-003	-494.659633	-494.484393	-494.534974	-494.551929	-494.415880	-494.240640	-494.291221	-494.308177
2c-002	-494.659846	-494.484632	-494.535919	-494.552811	-494.416067	-494.240853	-494.292140	-494.309032
2c-001	-494.660011	-494.484784	-494.534901	-494.551729	-494.416285	-494.241058	-494.291175	-494.308003
<H> / <G>		**-494.484629**	**-494.535512**	**-494.552407**		**-494.240880**	**-494.291740**	**-494.308634**
Δ<H>/Δ<G> / kJmol^{-1}		**-30.249501**	**+27.724138**	**+3.972647**		**-18.674736**	**+39.360570**	**+15.610146**

Nr.	B3LYP/6-31+G(d,p)				B2PLYP/cc-pVTZ//B3LYP/6-31+G(d,p)			
	E_{tot}	H_{298K}	G_{298K}	G_{298K}, SMD($CHCl_3$)	E_{tot}	H_{298K}	G_{298K}	G_{298K}, SMD($CHCl_3$)
	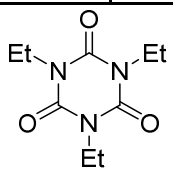 **3c**							
3c-002	-742.057749	-741.791374	-741.851824	-741.871552	-741.698225	-741.431850	-741.492300	-741.512029
3c-001	-742.057822	-741.791398	-741.851701	-741.871605	-741.698260	-741.431836	-741.492139	-741.512043
<H> / <G>		**-741.791386**	**-741.851766**	**-741.871579**		**-741.431843**	**-741.492226**	**-741.512036**
Δ<H>/Δ<G> / kJmol^{-1}		**-214.566287**	**-85.744439**	**-110.819697**		**-213.168492**	**-84.354474**	**-109.420390**

Table S2: 13 (continuation). [Table S20] Thermochemical data in Hartree (Boltzmann averaged values and Δ <H>/Δ <G> in kJ mol^{-1} are given in bold font)

Nr.	B3LYP/6-31+G(d,p)				B2PLYP/cc-pVTZ//B3LYP/6-31+G(d,p)			
	E_{tot}	H_{298K}	G_{298K}	G_{298K}, SMD($CHCl_3$)	E_{tot}	H_{298K}	G_{298K}	G_{298K}, SMD($CHCl_3$)
	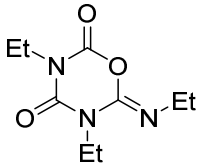 **4c**							
4c-004	-742.012439	-741.747050	-741.808808	-741.826258	-741.652135	-741.386746	-741.448504	-741.465954
4c-003	-742.012728	-741.747625	-741.809699	-741.827325	-741.652402	-741.387299	-741.449373	-741.466998
4c-002	-742.012750	-741.747725	-741.810274	-741.828074	-741.652163	-741.387138	-741.449687	-741.467487
4c-001	-742.012808	-741.747782	-741.810191	-741.827991	-741.652226	-741.387200	-741.449609	-741.467410
<H> / <G>		**-741.747621**	**-741.810012**	**-741.827804**		**-741.387138**	**-741.449470**	**-741.467242**
Δ<H>/Δ<G> / kJmol^{-1}		**-99.660790**	**+23.880883**	**+4.113404**		**-95.794300**	**+27.902947**	**+8.185675**

Nr.	B3LYP/6-31+G(d,p)				B2PLYP/cc-pVTZ//B3LYP/6-31+G(d,p)			
	E_{tot}	H_{298K}	G_{298K}	G_{298K}, SMD($CHCl_3$)	E_{tot}	H_{298K}	G_{298K}	G_{298K}, SMD($CHCl_3$)
	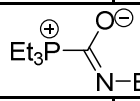 **6cc**							
6cc-021	-826.371481	-826.073058	-826.137902	-826.162635	-825.954966	-825.656543	-825.721387	-825.746120
6cc-020	-826.371727	-826.073029	-826.137128	-826.160363	-825.956547	-825.657849	-825.721948	-825.745183
6cc-019	-826.371793	-826.073018	-826.137055	-826.160210	-825.956620	-825.657845	-825.721882	-825.745037
6cc-018	-826.371888	-826.073547	-826.138826	-826.161790	-825.956397	-825.658056	-825.723335	-825.746299
6cc-017	-826.371914	-826.073395	-826.136817	-826.160546	-825.956037	-825.657518	-825.720940	-825.744669
6cc-016	-826.371944	-826.073280	-826.138778	-826.162411	-825.956484	-825.657820	-825.723318	-825.746951
6cc-015	-826.371961	-826.073380	-826.138246	-826.161848	-825.956513	-825.657932	-825.722798	-825.746400
6cc-014	-826.372006	-826.073356	-826.140088	-826.163785	-825.956563	-825.657913	-825.724645	-825.748342
6cc-013	-826.372021	-826.073357	-826.140591	-826.164304	-825.956521	-825.657857	-825.725091	-825.748804
6cc-012	-826.372035	-826.073324	-826.137451	-826.159953	-825.957027	-825.658316	-825.722443	-825.744944
6cc-011	-826.372085	-826.073272	-826.136689	-826.159206	-825.957005	-825.658192	-825.721609	-825.744127
6cc-010	-826.372140	-826.073546	-826.138025	-826.161308	-825.957014	-825.658420	-825.722899	-825.746181
6cc-009	-826.372453	-826.073740	-826.137927	-826.161306	-825.957066	-825.658353	-825.722540	-825.745918
6cc-008	-826.372475	-826.073816	-826.137788	-826.161310	-825.957064	-825.658405	-825.722377	-825.745899
6cc-007	-826.372740	-826.074269	-826.137932	-826.161486	-825.956977	-825.658506	-825.722169	-825.745722
6cc-006	-826.372851	-826.074527	-826.139776	-826.163759	-825.956881	-825.658557	-825.723806	-825.747790
6cc-005	-826.372919	-826.074309	-826.138669	-826.163035	-825.957176	-825.658566	-825.722926	-825.747292
6cc-004	-826.372975	-826.074586	-826.138698	-826.161614	-825.957320	-825.658931	-825.723043	-825.745959

Table S2: 13 (continuation). [Table S20] Thermochemical data in Hartree (Boltzmann averaged values and Δ <H>/Δ <G> in kJ mol^{-1} are given in bold font).

6cc-003	-826.373140	-826.074729	-826.138688	-826.162369	-825.957489	-825.659078	-825.723037	-825.746718
6cc-002	-826.373487	-826.074978	-826.138488	-826.162312	-825.957485	-825.658976	-825.722486	-825.746310
6cc-001	-826.373913	-826.075613	-826.140095	-826.164844	-825.957567	-825.659267	-825.723749	-825.748497
<H> / <G>		**-826.074366**	**-826.139500**	**-826.163779**		**-825.658429**	**-825.723850**	**-825.747820**
Δ<H>/Δ<G> / kJmol^{-1}		**+36.670319**	**+87.616840**	**+51.234050**		**+34.607103**	**+84.776749**	**+49.216524**
Nr.	B3LYP/6-31+G(d,p)				B2PLYP/cc-pVTZ//B3LYP/6-31+G(d,p)			
	E_{tot}	H_{298K}	G_{298K}	G_{298K}, SMD($CHCl_3$)	E_{tot}	H_{298K}	G_{298K}	G_{298K}, SMD($CHCl_3$)
	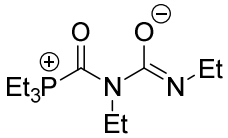 **7Lcc**							
7Lcc-003	-1073.663512	-1073.276685	-1073.354809	-1073.400721	-1073.129068	-1072.742241	-1072.820365	-1072.866276
7Lcc-002	-1073.663857	-1073.277062	-1073.355273	-1073.399926	-1073.129339	-1072.742544	-1072.820755	-1072.865408
7Lcc-001	-1073.664709	-1073.278067	-1073.356451	-1073.399350	-1073.130799	-1072.744157	-1072.822541	-1072.865440
<H> / <G>		**-1073.277644**	**-1073.356022**	**-1073.400322**		**-1072.743742**	**-1072.822152**	**-1072.865895**
Δ<H>/Δ<G> / kJmol^{-1}		**+124.037968**	**+235.994619**	**+153.384929**		**+117.494907**	**+229.347979**	**+148.210830**
Nr.	B3LYP/6-31+G(d,p)				B2PLYP/cc-pVTZ//B3LYP/6-31+G(d,p)			
	E_{tot}	H_{298K}	G_{298K}	G_{298K}, SMD($CHCl_3$)	E_{tot}	H_{298K}	G_{298K}	G_{298K}, SMD($CHCl_3$)
	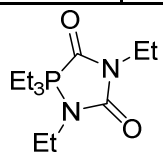 **7Ncc**							
7Ncc-012	-1073.710146	-1073.321127	-1073.394294	-1073.415091	-1073.182741	-1072.793722	-1072.866889	-1072.887685
7Ncc-011	-1073.710436	-1073.321336	-1073.393601	-1073.414302	-1073.183181	-1072.794081	-1072.866346	-1072.887047
7Ncc-010	-1073.710547	-1073.321368	-1073.393870	-1073.414444	-1073.183108	-1072.793929	-1072.866431	-1072.887004
7Ncc-009	-1073.710581	-1073.321420	-1073.393338	-1073.413959	-1073.183394	-1072.794233	-1072.866151	-1072.886772
7Ncc-008	-1073.710918	-1073.321684	-1073.394018	-1073.415085	-1073.183677	-1072.794443	-1072.866777	-1072.887845
7Ncc-007	-1073.711071	-1073.321903	-1073.394569	-1073.415525	-1073.183918	-1072.794750	-1072.867416	-1072.888372
7Ncc-006	-1073.711391	-1073.322396	-1073.396366	-1073.417163	-1073.184271	-1072.795276	-1072.869246	-1072.890043
7Ncc-005	-1073.711705	-1073.322582	-1073.396220	-1073.417017	-1073.184478	-1072.795355	-1072.868993	-1072.889790
7Ncc-004	-1073.712313	-1073.323276	-1073.395739	-1073.415962	-1073.185778	-1072.796741	-1072.869204	-1072.889426
7Ncc-003	-1073.712336	-1073.323203	-1073.395469	-1073.415691	-1073.185570	-1072.796437	-1072.868703	-1072.888925
7Ncc-002	-1073.712669	-1073.323695	-1073.396241	-1073.416495	-1073.185937	-1072.796963	-1072.869509	-1072.889763
7Ncc-001	-1073.713023	-1073.323880	-1073.395867	-1073.416090	-1073.186376	-1072.797233	-1072.869220	-1072.889442
<H> / <G>		**-1073.323100**	**-1073.395757**	**-1073.416281**		**-1072.796542**	**-1072.868969**	**-1072.889376**
Δ<H>/Δ<G> / kJmol^{-1}		**+4.693015**	**+131.671149**	**+111.485065**		**-21.129824**	**+106.429586**	**+86.561781**

Table S2: 13 (continuation). [Table S20] Thermochemical data in Hartree (Boltzmann averaged values and Δ <H>/Δ <G> in kJ mol^{-1} are given in bold font).

Nr.	B3LYP/6-31+G(d,p)				B2PLYP/cc-pVTZ//B3LYP/6-31+G(d,p)			
	E_{tot}	H_{298K}	G_{298K}	G_{298K}, SMD($CHCl_3$)	E_{tot}	H_{298K}	G_{298K}	G_{298K}, SMD($CHCl_3$)
	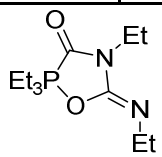 **7Occ**							
7Occ-010	-1073.713255	-1073.324776	-1073.399922	-1073.422025	-1073.182831	-1072.794352	-1072.869498	-1072.891601
7Occ-009	-1073.713379	-1073.324917	-1073.400110	-1073.422213	-1073.183054	-1072.794592	-1072.869785	-1072.891888
7Occ-008	-1073.713656	-1073.325133	-1073.400347	-1073.422195	-1073.183619	-1072.795096	-1072.870310	-1072.892158
7Occ-007	-1073.713686	-1073.325092	-1073.399433	-1073.421330	-1073.183661	-1072.795067	-1072.869408	-1072.891304
7Occ-006	-1073.713853	-1073.325376	-1073.399751	-1073.421089	-1073.184140	-1072.795663	-1072.870038	-1072.891376
7Occ-005	-1073.714138	-1073.325549	-1073.399927	-1073.421074	-1073.184487	-1072.795898	-1072.870276	-1072.891423
7Occ-004	-1073.714216	-1073.325736	-1073.401709	-1073.423542	-1073.184038	-1072.795558	-1072.871531	-1072.893364
7Occ-003	-1073.714240	-1073.325740	-1073.401516	-1073.423412	-1073.184073	-1072.795573	-1072.871349	-1072.893245
7Occ-002	-1073.715010	-1073.326455	-1073.400946	-1073.422014	-1073.185468	-1072.796913	-1072.871404	-1072.892472
7Occ-001	-1073.715137	-1073.326586	-1073.401157	-1073.422384	-1073.185680	-1072.797129	-1072.871700	-1072.892927
<H> / <G>		**-1073.325902**	**-1073.401049**	**-1073.422825**		**-1072.796383**	**-1072.871167**	**-1072.892743**
Δ<H>/Δ<G> / kJmol^{-1}		**-2.662981**	**+117.775953**	**+94.304261**		**-20.713163**	**+100.659170**	**+77.721257**

Nr.	B3LYP/6-31+G(d,p)				B2PLYP/cc-pVTZ//B3LYP/6-31+G(d,p)			
	E_{tot}	H_{298K}	G_{298K}	G_{298K}, SMD($CHCl_3$)	E_{tot}	H_{298K}	G_{298K}	G_{298K}, SMD($CHCl_3$)
	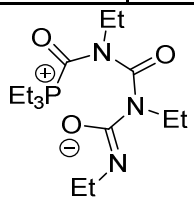 **8cc**							
8cc-016	-1321.028984	-1320.551856	-1320.641529	-1320.676509	-1320.378960	-1319.901832	-1319.991505	-1320.026484
8cc-015	-1321.029088	-1320.551717	-1320.642126	-1320.676293	-1320.378902	-1319.901531	-1319.991940	-1320.026107
8cc-014	-1321.029137	-1320.551640	-1320.640045	-1320.669033	-1320.381091	-1319.903594	-1319.991999	-1320.020987
8cc-013	-1321.029299	-1320.552195	-1320.641243	-1320.675218	-1320.380113	-1319.903009	-1319.992057	-1320.026033
8cc-012	-1321.029557	-1320.552435	-1320.641379	-1320.672821	-1320.379399	-1319.902277	-1319.991221	-1320.022662
8cc-011	-1321.029698	-1320.552521	-1320.641739	-1320.672639	-1320.380164	-1319.902987	-1319.992205	-1320.023105
8cc-010	-1321.029718	-1320.552295	-1320.640401	-1320.669723	-1320.381542	-1319.904119	-1319.992225	-1320.021547
8cc-009	-1321.029743	-1320.552538	-1320.641718	-1320.675790	-1320.380282	-1319.903077	-1319.992257	-1320.026328
8cc-008	-1321.030088	-1320.553020	-1320.643183	-1320.677955	-1320.379275	-1319.902207	-1319.992370	-1320.027142
8cc-007	-1321.030563	-1320.552856	-1320.641844	-1320.673302	-1320.381668	-1319.903961	-1319.992949	-1320.024407
8cc-006	-1321.030698	-1320.552918	-1320.642444	-1320.673439	-1320.382061	-1319.904281	-1319.993807	-1320.024802
8cc-005	-1321.030847	-1320.553216	-1320.643059	-1320.674373	-1320.381637	-1319.904006	-1319.993849	-1320.025163
8cc-004	-1321.031033	-1320.553991	-1320.644256	-1320.679172	-1320.380162	-1319.903120	-1319.993385	-1320.028301
8cc-003	-1321.031416	-1320.554176	-1320.644659	-1320.676754	-1320.381451	-1319.904211	-1319.994694	-1320.026789
8cc-002	-1321.031710	-1320.554573	-1320.644884	-1320.676724	-1320.381879	-1319.904742	-1319.995053	-1320.026893

Table S2: 13 (continuation). [Table S20] Thermochemical data in Hartree (Boltzmann averaged values and Δ <H>/Δ <G> in kJ mol^{-1} are given in bold font).

8cc-001	-1321.032146	-1320.554832	-1320.644018	-1320.675843	-1320.381912	-1319.904598	-1319.993784	-1320.025608
<H> / <G>		**-1320.553763**	**-1320.644013**	**-1320.678231**		**-1319.903828**	**-1319.993737**	**-1320.026932**
Δ<H>/Δ<G> / kJmol^{-1}		**+20.158468**	**+196.730614**	**+146.929912**		**+4.067990**	**+181.511430**	**+134.407919**
	B3LYP/6-31+G(d,p)				B2PLYP/cc-pVTZ//B3LYP/6-31+G(d,p)			
	E_{tot}	H_{298K}	G_{298K}	G_{298K}, SMD($CHCl_3$)	E_{tot}	H_{298K}	G_{298K}	G_{298K}, SMD($CHCl_3$)
Nr.	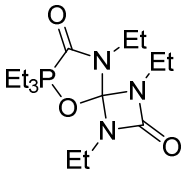 **9cc**							
9cc-040	-1321.028711	-1320.551431	-1320.637891	-1320.663787	-1320.381071	-1319.903791	-1319.990251	-1320.016147
9cc-039	-1321.028715	-1320.551418	-1320.637449	-1320.663345	-1320.381596	-1319.904299	-1319.990330	-1320.016226
9cc-038	-1321.028725	-1320.551363	-1320.638137	-1320.662982	-1320.381759	-1319.904397	-1319.991171	-1320.016015
9cc-037	-1321.028753	-1320.551142	-1320.635957	-1320.661263	-1320.381958	-1319.904347	-1319.989162	-1320.014468
9cc-036	-1321.028759	-1320.551162	-1320.636116	-1320.662139	-1320.381329	-1319.903732	-1319.988686	-1320.014709
9cc-035	-1321.028759	-1320.551405	-1320.638306	-1320.663341	-1320.381593	-1319.904239	-1319.991140	-1320.016175
9cc-034	-1321.028759	-1320.551162	-1320.636125	-1320.662149	-1320.381327	-1319.903730	-1319.988693	-1320.014717
9cc-033	-1321.028786	-1320.551277	-1320.636094	-1320.661767	-1320.381172	-1319.903663	-1319.988480	-1320.014153
9cc-032	-1321.028833	-1320.551353	-1320.636761	-1320.662546	-1320.381145	-1319.903665	-1319.989073	-1320.014857
9cc-031	-1321.028851	-1320.551442	-1320.637353	-1320.663074	-1320.381452	-1319.904043	-1319.989954	-1320.015675
9cc-030	-1321.028905	-1320.551608	-1320.638118	-1320.665289	-1320.381215	-1319.903918	-1319.990428	-1320.017599
9cc-029	-1321.028923	-1320.551506	-1320.637643	-1320.664607	-1320.381510	-1319.904093	-1319.990230	-1320.017194
9cc-028	-1321.028929	-1320.551480	-1320.638747	-1320.665106	-1320.380663	-1319.903214	-1319.990481	-1320.016839
9cc-027	-1321.028973	-1320.551615	-1320.637586	-1320.663657	-1320.381970	-1319.904612	-1319.990583	-1320.016655
9cc-026	-1321.029019	-1320.551599	-1320.637586	-1320.664055	-1320.381097	-1319.903677	-1319.989664	-1320.016134
9cc-025	-1321.029032	-1320.551634	-1320.636684	-1320.661783	-1320.382373	-1319.904975	-1319.990025	-1320.015124
9cc-024	-1321.029058	-1320.551579	-1320.636604	-1320.662293	-1320.381351	-1319.903872	-1319.988897	-1320.014586
9cc-023	-1321.029082	-1320.551511	-1320.636928	-1320.662936	-1320.381797	-1319.904226	-1319.989643	-1320.015651
9cc-022	-1321.029098	-1320.551580	-1320.636492	-1320.662882	-1320.382182	-1319.904664	-1319.989576	-1320.015966
9cc-021	-1321.029107	-1320.551637	-1320.637453	-1320.663572	-1320.381420	-1319.903950	-1319.989766	-1320.015885
9cc-020	-1321.029127	-1320.551692	-1320.637066	-1320.662022	-1320.382275	-1319.904840	-1319.990214	-1320.015169
9cc-019	-1321.029130	-1320.551520	-1320.636544	-1320.661882	-1320.382273	-1319.904663	-1319.989687	-1320.015025
9cc-018	-1321.029154	-1320.551518	-1320.636152	-1320.661283	-1320.382360	-1319.904724	-1319.989358	-1320.014489
9cc-017	-1321.029176	-1320.551674	-1320.637357	-1320.663126	-1320.381463	-1319.903961	-1319.989644	-1320.015413
9cc-016	-1321.029406	-1320.552004	-1320.637333	-1320.663563	-1320.382388	-1319.904986	-1319.990315	-1320.016546
9cc-015	-1321.029510	-1320.552120	-1320.638245	-1320.664157	-1320.382092	-1319.904702	-1319.990827	-1320.016739
9cc-014	-1321.029541	-1320.552099	-1320.637003	-1320.663521	-1320.382170	-1319.904728	-1319.989632	-1320.016149
9cc-013	-1321.029565	-1320.552206	-1320.638259	-1320.664729	-1320.381669	-1319.904310	-1319.990363	-1320.016832
9cc-012	-1321.029594	-1320.552199	-1320.638711	-1320.664798	-1320.381790	-1319.904395	-1319.990907	-1320.016995
9cc-011	-1321.029650	-1320.552249	-1320.636462	-1320.662071	-1320.382847	-1319.905446	-1319.989659	-1320.015268
9cc-010	-1321.029723	-1320.552384	-1320.638810	-1320.664785	-1320.382239	-1319.904900	-1319.991326	-1320.017302
9cc-009	-1321.029754	-1320.552304	-1320.638139	-1320.663971	-1320.381984	-1319.904534	-1319.990369	-1320.016201
9cc-008	-1321.029867	-1320.552512	-1320.638758	-1320.665037	-1320.382096	-1319.904741	-1319.990987	-1320.017265
9cc-007	-1321.029946	-1320.552360	-1320.636366	-1320.662023	-1320.383192	-1319.905606	-1319.989612	-1320.015269

Table S2: 13 (continuation). [Table S20] Thermochemical data in Hartree (Boltzmann averaged values and Δ <H>/Δ <G> in kJ mol^{-1} are given in bold font).

9cc-006	-1321.029953	-1320.552586	-1320.638273	-1320.663468	-1320.383044	-1319.905677	-1319.991364	-1320.016558
9cc-005	-1321.029993	-1320.552660	-1320.638738	-1320.663853	-1320.382871	-1319.905538	-1319.991616	-1320.016731
9cc-004	-1321.030129	-1320.552625	-1320.637836	-1320.664274	-1320.382163	-1319.904659	-1319.989870	-1320.016308
9cc-003	-1321.030131	-1320.552694	-1320.637695	-1320.663751	-1320.382737	-1319.905300	-1319.990301	-1320.016356
9cc-002	-1321.030245	-1320.552719	-1320.637702	-1320.663885	-1320.382803	-1319.905277	-1319.990260	-1320.016443
9cc-001	-1321.030568	-1320.553182	-1320.638032	-1320.663482	-1320.383517	-1319.906131	-1319.990981	-1320.016431
<H> / <G>		**-1320.551717**	**-1320.637762**	**-1320.664208**		**-1319.904518**	**-1319.990284**	**-1320.016521**
Δ<H>/Δ<G> / kJmol^{-1}		**+25.531617**	**+213.143480**	**+183.746299**		**+2.255261**	**+190.579044**	**+161.741453**

Nr.	B3LYP/6-31+G(d,p)				B2PLYP/cc-pVTZ//B3LYP/6-31+G(d,p)			
	E_{tot}	H_{298K}	G_{298K}	G_{298K}, SMD($CHCl_3$)	E_{tot}	H_{298K}	G_{298K}	G_{298K}, SMD($CHCl_3$)
TS1cc-015	-826.360587	-826.063736	-826.130134	-826.144987	-825.944399	-825.647548	-825.713946	-825.728799
TS1cc-014	-826.360676	-826.063810	-826.130624	-826.145795	-825.944150	-825.647284	-825.714098	-825.729269
TS1cc-013	-826.362471	-826.065675	-826.132444	-826.147217	-825.946317	-825.649521	-825.716290	-825.731063
TS1cc-012	-826.362882	-826.066292	-826.134648	-826.149644	-825.946649	-825.650059	-825.718415	-825.733410
TS1cc-011	-826.362895	-826.066257	-826.134132	-826.149144	-825.946533	-825.649895	-825.717770	-825.732782
TS1cc-010	-826.363388	-826.067556	-826.130919	-826.145915	-825.946955	-825.651123	-825.714486	-825.729482
TS1cc-009	-826.363443	-826.066710	-826.133665	-826.148852	-825.947071	-825.650338	-825.717293	-825.732480
TS1cc-008	-826.363475	-826.066676	-826.132769	-826.147908	-825.947119	-825.650320	-825.716413	-825.731552
TS1cc-007	-826.363602	-826.066974	-826.134078	-826.149041	-825.947441	-825.650813	-825.717917	-825.732881
TS1cc-006	-826.363612	-826.066931	-826.133428	-826.148424	-825.947472	-825.650791	-825.717288	-825.732284
TS1cc-005	-826.363625	-826.067001	-826.133416	-826.148412	-825.947374	-825.650750	-825.717165	-825.732161
TS1cc-004	-826.363810	-826.066987	-826.132928	-826.147557	-825.947451	-825.650628	-825.716569	-825.731198
TS1cc-003	-826.363971	-826.067202	-826.134352	-826.149093	-825.947875	-825.651106	-825.718256	-825.732997
TS1cc-002	-826.363977	-826.067236	-826.133951	-826.148692	-825.947865	-825.651124	-825.717839	-825.732580
TS1cc-001	-826.364057	-826.067267	-826.133184	-826.148132	-825.947879	-825.651089	-825.717006	-825.731954
<H> / <G>		**-826.067013**	**-826.133951**	**-826.148896**		**-825.650780**	**-825.717759**	**-825.732683**
Δ<H>/Δ<G> / kJmol^{-1}		**+55.977621**	**+102.185339**	**+74.450817**		**+54.688847**	**+100.769585**	**+73.099183**

Nr.	B3LYP/6-31+G(d,p)				B2PLYP/cc-pVTZ//B3LYP/6-31+G(d,p)			
	E_{tot}	H_{298K}	G_{298K}	G_{298K}, SMD($CHCl_3$)	E_{tot}	H_{298K}	G_{298K}	G_{298K}, SMD($CHCl_3$)
TS2Occ-010	-1073.676209	-1073.290353	-1073.367847	-1073.391161	-1073.144075	-1072.758219	-1072.835713	-1072.859027
TS2Occ-009	-1073.678782	-1073.293247	-1073.372326	-1073.395449	-1073.147170	-1072.761635	-1072.840714	-1072.863837
TS2Occ-008	-1073.679214	-1073.293605	-1073.373063	-1073.395612	-1073.147789	-1072.762180	-1072.841638	-1072.864188
TS2Occ-007	-1073.679327	-1073.293730	-1073.372559	-1073.395204	-1073.147383	-1072.761786	-1072.840615	-1072.863260
TS2Occ-006	-1073.680375	-1073.294339	-1073.370368	-1073.396343	-1073.149042	-1072.763006	-1072.839035	-1072.865011
TS2Occ-005	-1073.680376	-1073.294336	-1073.370407	-1073.396415	-1073.149037	-1072.762997	-1072.839068	-1072.865075
TS2Occ-004	-1073.680883	-1073.294860	-1073.370927	-1073.395819	-1073.149749	-1072.763726	-1072.839793	-1072.864685
TS2Occ-003	-1073.680975	-1073.294760	-1073.369627	-1073.395507	-1073.149594	-1072.763379	-1072.838246	-1072.864126
TS2Occ-002	-1073.681255	-1073.295105	-1073.369713	-1073.395976	-1073.149503	-1072.763353	-1072.837961	-1072.864224
TS2Occ-001	-1073.681551	-1073.295876	-1073.374735	-1073.397109	-1073.150002	-1072.764327	-1072.843186	-1072.865560
<H> / <G>		**-1073.295059**	**-1073.374092**	**-1073.396323**		**-1072.763579**	**-1072.842543**	**-1072.864877**
Δ<H>/Δ<G> / kJmol^{-1}		**+78.313649**	**+188.550806**	**+163.883335**		**+65.412327**	**+175.810652**	**+150.882721**

Table S2: 13 (continuation). [Table S20] Thermochemical data in Hartree (Boltzmann averaged values and Δ <H>/Δ <G> in kJ mol^{-1} are given in bold font).

Nr.	B3LYP/6-31+G(d,p)				B2PLYP/cc-pVTZ//B3LYP/6-31+G(d,p)			
	E_{tot}	H_{298K}	G_{298K}	G_{298K}, SMD($CHCl_3$)	E_{tot}	H_{298K}	G_{298K}	G_{298K}, SMD($CHCl_3$)
TS2Ncc-012	-1073.674164	-1073.288387	-1073.366070	-1073.389289	-1073.143411	-1072.757634	-1072.835317	-1072.858536
TS2Ncc-011	-1073.677494	-1073.291766	-1073.370094	-1073.392739	-1073.146840	-1072.761112	-1072.839440	-1072.862085
TS2Ncc-010	-1073.677854	-1073.292115	-1073.370923	-1073.393871	-1073.146780	-1072.761041	-1072.839849	-1072.862797
TS2Ncc-009	-1073.677968	-1073.292241	-1073.371051	-1073.393871	-1073.147173	-1072.761446	-1072.840256	-1072.863077
TS2Ncc-008	-1073.678061	-1073.292422	-1073.371285	-1073.394106	-1073.147078	-1072.761439	-1072.840302	-1072.863123
TS2Ncc-007	-1073.678068	-1073.292427	-1073.371512	-1073.394667	-1073.147512	-1072.761871	-1072.840956	-1072.864111
TS2Ncc-006	-1073.678481	-1073.292890	-1073.372354	-1073.395764	-1073.147485	-1072.761894	-1072.841358	-1072.864768
TS2Ncc-005	-1073.678552	-1073.293001	-1073.372246	-1073.395496	-1073.147738	-1072.762187	-1072.841432	-1072.864682
TS2Ncc-004	-1073.678712	-1073.293121	-1073.371930	-1073.395006	-1073.147691	-1072.762100	-1072.840909	-1072.863985
TS2Ncc-003	-1073.679163	-1073.293603	-1073.372376	-1073.395818	-1073.148261	-1072.762701	-1072.841474	-1072.864915
TS2Ncc-002	-1073.680208	-1073.294634	-1073.374262	-1073.396828	-1073.149439	-1072.763865	-1072.843493	-1072.866059
TS2Ncc-001	-1073.680418	-1073.294819	-1073.373867	-1073.396113	-1073.149940	-1072.764341	-1072.843389	-1072.865636
<H> / <G>		**-1073.294080**	**-1073.373507**	**-1073.396001**		**-1072.763530**	**-1072.842895**	**-1072.865286**
Δ<H>/Δ<G> / kJmol^{-1}		**+80.884064**	**+190.087333**	**+164.730245**		**+65.542330**	**+174.885552**	**+149.809689**

Nr.	B3LYP/6-31+G(d,p)				B2PLYP/cc-pVTZ//B3LYP/6-31+G(d,p)			
	E_{tot}	H_{298K}	G_{298K}	G_{298K}, SMD($CHCl_3$)	E_{tot}	H_{298K}	G_{298K}	G_{298K}, SMD($CHCl_3$)
TS3cc-006	-1321.005880	-1320.530485	-1320.620205	-1320.658866	-1320.356566	-1319.881171	-1319.970891	-1320.009552
TS3cc-005	-1321.006329	-1320.530885	-1320.619979	-1320.658863	-1320.357447	-1319.882003	-1319.971097	-1320.009980
TS3cc-004	-1321.007201	-1320.531968	-1320.621821	-1320.649151	-1320.360139	-1319.884906	-1319.974759	-1320.002089
TS3cc-003	-1321.007711	-1320.532312	-1320.621950	-1320.661439	-1320.358515	-1319.883116	-1319.972754	-1320.012244
TS3cc-002	-1321.012950	-1320.537811	-1320.628783	-1320.655078	-1320.365684	-1319.890545	-1319.981517	-1320.007812
TS3cc-001	-1321.013789	-1320.538638	-1320.629658	-1320.656749	-1320.365383	-1319.890232	-1319.981252	-1320.008343
<H> / <G>		**-1320.538383**	**-1320.629406**	**-1320.661108**		**-1319.890404**	**-1319.981399**	**-1320.011848**
Δ<H>/Δ<G> / kJmol^{-1}		**+60.539306**	**+235.080194**	**+191.885402**		**+39.313997**	**+213.904988**	**+174.012481**

Nr.	B3LYP/6-31+G(d,p)				B2PLYP/cc-pVTZ//B3LYP/6-31+G(d,p)			
	E_{tot}	H_{298K}	G_{298K}	G_{298K}, SMD($CHCl_3$)	E_{tot}	H_{298K}	G_{298K}	G_{298K}, SMD($CHCl_3$)
TS4cc-003	-1320.969800	-1320.495182	-1320.581923	-1320.616425	-1320.322651	-1319.848033	-1319.934774	-1319.969275
TS4cc-002	-1321.025617	-1320.549223	-1320.634772	-1320.666963	-1320.378589	-1319.902195	-1319.987744	-1320.019934
TS4cc-001	-1321.026913	-1320.550402	-1320.636209	-1320.668431	-1320.379542	-1319.903031	-1319.988838	-1320.021061
<H> / <G>		**-1320.550139**	**-1320.635951**	**-1320.668175**		**-1319.902787**	**-1319.988577**	**-1320.020799**
Δ<H>/Δ<G> / kJmol^{-1}		**+29.674792**	**+217.896762**	**+173.330838**		**+6.801584**	**+195.060824**	**+150.511568**

Table S2: 13 (continuation). [Table S20] Thermochemical data in Hartree (Boltzmann averaged values and Δ <H>/Δ <G> in kJ mol^{-1} are given in bold font).

Nr.	B3LYP/6-31+G(d,p)				B2PLYP/cc-pVTZ//B3LYP/6-31+G(d,p)			
	E_{tot}	H_{298K}	G_{298K}	G_{298K}, SMD($CHCl_3$)	E_{tot}	H_{298K}	G_{298K}	G_{298K}, SMD($CHCl_3$)
TS5cc-007	-1320.981095	-1320.507162	-1320.601285	-1320.643547	-1320.331294	-1319.857361	-1319.951484	-1319.993746
TS5cc-006	-1321.024032	-1320.548287	-1320.634846	-1320.666495	-1320.375061	-1319.899316	-1319.985875	-1320.017523
TS5cc-005	-1321.025536	-1320.549510	-1320.635979	-1320.668377	-1320.376203	-1319.900177	-1319.986646	-1320.019044
TS5cc-004	-1321.025787	-1320.549775	-1320.636076	-1320.668315	-1320.376588	-1319.900576	-1319.986877	-1320.019116
TS5cc-003	-1321.026760	-1320.550505	-1320.636690	-1320.668896	-1320.378477	-1319.902222	-1319.988407	-1320.020614
TS5cc-002	-1321.026962	-1320.550701	-1320.636160	-1320.668303	-1320.378554	-1319.902293	-1319.987752	-1320.019895
TS5cc-001	-1321.027715	-1320.551693	-1320.637579	-1320.669993	-1320.378742	-1319.902720	-1319.988606	-1320.021020
<H> / <G>		**-1320.551035**	**-1320.636891**	**-1320.669299**		**-1319.902286**	**-1319.988144**	**-1320.020488**
Δ<H>/Δ<G> / kJmol^{-1}		**+27.322374**	**+215.428931**	**+170.381381**		**+8.115936**	**+196.196977**	**+151.327229**

Nr.	B3LYP/6-31+G(d,p)				B2PLYP/cc-pVTZ//B3LYP/6-31+G(d,p)			
	E_{tot}	H_{298K}	G_{298K}	G_{298K}, SMD($CHCl_3$)	E_{tot}	H_{298K}	G_{298K}	G_{298K}, SMD($CHCl_3$)
TSD0cc-003	-1073.675786	-1073.289890	-1073.364493	-1073.392811	-1073.143896	-1072.758000	-1072.832603	-1072.860921
TSD0cc-002	-1073.677092	-1073.291158	-1073.367376	-1073.396794	-1073.145110	-1072.759176	-1072.835394	-1072.864812
TSD0cc-001	-1073.677245	-1073.291347	-1073.365878	-1073.395312	-1073.145481	-1072.759583	-1072.834114	-1072.863548
<H> / <G>		**-1073.291118**	**-1073.367022**	**-1073.396494**		**-1072.759278**	**-1072.835032**	**-1072.864504**
Δ<H>/Δ<G> / kJmol^{-1}		**+88.661801**	**+207.113392**	**+163.436689**		**+76.706233**	**+195.531798**	**+151.863812**

Nr.	B3LYP/6-31+G(d,p)				B2PLYP/cc-pVTZ//B3LYP/6-31+G(d,p)			
	E_{tot}	H_{298K}	G_{298K}	G_{298K}, SMD($CHCl_3$)	E_{tot}	H_{298K}	G_{298K}	G_{298K}, SMD($CHCl_3$)
TSD1cc-003	-1321.002103	-1320.527106	-1320.614095	-1320.642700	-1320.350954	-1319.875957	-1319.962946	-1319.991551
TSD1cc-002	-1321.009291	-1320.534090	-1320.622561	-1320.651182	-1320.358083	-1319.882882	-1319.971353	-1319.999974
TSD1cc-001	-1321.013354	-1320.538195	-1320.627931	-1320.656521	-1320.362915	-1319.887756	-1319.977492	-1320.006081
<H> / <G>		**-1320.538143**	**-1320.627913**	**-1320.656502**		**-1319.887728**	**-1319.977482**	**-1320.006071**
Δ<H>/Δ<G> / kJmol^{-1}		**+61.170131**	**+239.000301**	**+203.979163**		**+46.339239**	**+224.188946**	**+189.177900**

Nr.	B3LYP/6-31+G(d,p)				B2PLYP/cc-pVTZ//B3LYP/6-31+G(d,p)			
	E_{tot}	H_{298K}	G_{298K}	G_{298K}, SMD($CHCl_3$)	E_{tot}	H_{298K}	G_{298K}	G_{298K}, SMD($CHCl_3$)
TSD2cc-002	-1320.983000	-1320.508026	-1320.596249	-1320.629396	-1320.333045	-1319.858071	-1319.946294	-1319.979441
TSD2cc-001	-1321.012501	-1320.536772	-1320.622986	-1320.654109	-1320.364204	-1319.888475	-1319.974689	-1320.005812
<H> / <G>		**-1320.536772**	**-1320.622986**	**-1320.654109**		**-1319.888474**	**-1319.974688**	**-1320.005812**
Δ<H>/Δ<G> / kJmol^{-1}		**+64.769954**	**+251.937353**	**+210.262340**		**+44.378719**	**+231.524309**	**+189.860026**

Table S2: 13 (continuation). [Table S20] Thermochemical data in Hartree (Boltzmann averaged values and Δ <H>/Δ <G> in kJ mol^{-1} are given in bold font).

Nr.	B3LYP/6-31+G(d,p)				B2PLYP/cc-pVTZ//B3LYP/6-31+G(d,p)			
	E_{tot}	H_{298K}	G_{298K}	G_{298K}, SMD($CHCl_3$)	E_{tot}	H_{298K}	G_{298K}	G_{298K}, SMD($CHCl_3$)
TSRcc-014	-1073.689412	-1073.302869	-1073.378069	-1073.408953	-1073.155914	-1072.769371	-1072.844571	-1072.875455
TSRcc-013	-1073.689412	-1073.302869	-1073.378069	-1073.408953	-1073.155914	-1072.769371	-1072.844571	-1072.875455
TSRcc-012	-1073.689412	-1073.302869	-1073.378069	-1073.408953	-1073.155914	-1072.769371	-1072.844571	-1072.875455
TSRcc-011	-1073.689412	-1073.302869	-1073.378069	-1073.408953	-1073.155914	-1072.769371	-1072.844571	-1072.875455
TSRcc-010	-1073.689412	-1073.302869	-1073.378069	-1073.408953	-1073.155914	-1072.769371	-1072.844571	-1072.875455
TSRcc-009	-1073.689412	-1073.302869	-1073.378069	-1073.408953	-1073.155914	-1072.769371	-1072.844571	-1072.875455
TSRcc-008	-1073.689412	-1073.302869	-1073.378069	-1073.408953	-1073.155914	-1072.769371	-1072.844571	-1072.875455
TSRcc-007	-1073.689412	-1073.302869	-1073.378069	-1073.408953	-1073.155914	-1072.769371	-1072.844571	-1072.875455
TSRcc-006	-1073.689412	-1073.302869	-1073.378069	-1073.408953	-1073.155914	-1072.769371	-1072.844571	-1072.875455
TSRcc-005	-1073.689412	-1073.302869	-1073.378069	-1073.408953	-1073.155914	-1072.769371	-1072.844571	-1072.875455
TSRcc-004	-1073.689412	-1073.302869	-1073.378069	-1073.408953	-1073.155914	-1072.769371	-1072.844571	-1072.875455
TSRcc-003	-1073.689412	-1073.302869	-1073.378069	-1073.408953	-1073.155914	-1072.769371	-1072.844571	-1072.875455
TSRcc-002	-1073.689412	-1073.302869	-1073.378069	-1073.408953	-1073.155914	-1072.769371	-1072.844571	-1072.875455
TSRcc-001	-1073.689412	-1073.302869	-1073.378069	-1073.408953	-1073.155914	-1072.769371	-1072.844571	-1072.875455
<H> / <G>		**-1073.306511**	**-1073.382048**	**-1073.412265**		**-1072.774178**	**-1072.849644**	**-1072.879783**
Δ<H>/Δ<G> / kJmol^{-1}		**+48.247323**	**+167.663884**	**+122.030097**		**+37.586590**	**+157.167693**	**+111.747908**

Isotropic Shielding Data

Table S2: 14. [Table S21] (Carbonyl) ^{13}C, ^{15}N, ^{31}P Shieldings calculated for reference compounds **1c**, **2c**, **3c**, **6ccxHCl**, **11c**, **12c** and **13c** at the B3LYP/IGLO-III//B3LYP/6-31+G(d,p) level of theory with SMD ($CHCl_3$) solvation model.

B3LYP/6-31+G(d,p)				SMD($CHCl_3$)/B3LYP/IGLO-III//B3LYP/6-31+G(d,p)						
Structure	Nr	E_{tot}	H_{298K}	C^1	C^2	C^3	N^1	N^2	N^3	P
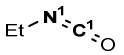 **1c**	1c-001	-247.322571	-247.236554	**49.4871**			**203.0571**			
Structure	Nr	E_{tot}	H_{298K}	C^1	C^2	C^3	N^1	N^2	N^3	P
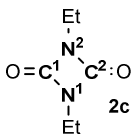 **2c**	2c-003	-494.659633	-494.484393	8.4262	6.3253		89.5421	89.5380		
	2c-002	-494.659846	-494.484632	7.7487	7.7651		86.8443	90.1172		
	2c-001	-494.660011	-494.484784	8.1183	7.0774		88.4155	87.0147		
	< Shielding >[a]			**8.0741**	**7.1126**		**88.1795**	**88.7295**		
	average of < Shielding >[b]			**7.5918**			**88.4545**			
Structure	Nr	E_{tot}	H_{298K}	C^1	C^2	C^3	N^1	N^2	N^3	P
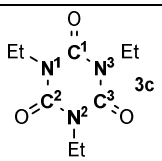 **3c**	3c-002	-742.057749	-741.791374	19.5909	19.5888	19.6065	75.5228	75.5038	75.4598	
	3c-001	-742.057822	-741.791398	19.5700	19.5741	19.5700	75.4953	75.4951	75.3647	
	< Shielding >[a]			**19.5803**	**19.5814**	**19.5880**	**75.5089**	**75.4994**	**75.4116**	
	average of < Shielding >[b]			**19.5829**			**75.4733**			

Table S2: 14 (continuation). [Table S21] (Carbonyl) ^{13}C, ^{15}N, ^{31}P Shieldings calculated for reference compounds **1c**, **2c**, **3c**, **6ccxHCl**, **11c**, **12c** and **13c** at the B3LYP/IGLO-III//B3LYP/6-31+G(d,p) level of theory with SMD ($CHCl_3$) solvation model.

B3LYP/6-31+G(d,p)				SMD($CHCl_3$)/B3LYP/IGLO-III//B3LYP/6-31+G(d,p)						
Structure	Nr	E_{tot}	H_{298K}	C^1	C^2	C^3	N^1	N^2	N^3	P
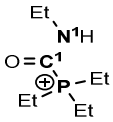 **6ccxHCl**	6ccxHCl-022	-826.788932	-826.475918	8.5617			87.2515			254.2246
	6ccxHCl-021	-826.788992	-826.476114	8.7898			87.4646			254.8510
	6ccxHCl-020	-826.788979	-826.476231	8.4358			87.9592			254.8123
	6ccxHCl-019	-826.789299	-826.476245	6.4871			90.8567			256.6291
	6ccxHCl-018	-826.789372	-826.476283	7.5283			90.4344			260.7141
	6ccxHCl-017	-826.789380	-826.476313	6.3654			91.0482			256.8737
	6ccxHCl-016	-826.789403	-826.476458	6.5737			90.8977			256.0617
	6ccxHCl-015	-826.789397	-826.476466	6.5726			90.8985			256.0550
	6ccxHCl-014	-826.789453	-826.476531	6.6224			90.9384			256.6246
	6ccxHCl-013	-826.789418	-826.476561	6.4138			91.5353			256.5965
	6ccxHCl-012	-826.789399	-826.476566	7.7800			90.6332			260.5027
	6ccxHCl-011	-826.789662	-826.476878	8.9637			94.5676			255.6236
	6ccxHCl-010	-826.789829	-826.477086	9.1730			94.3163			256.3003
	6ccxHCl-009	-826.790172	-826.477230	8.4659			92.3059			256.8790
	6ccxHCl-008	-826.789345	-826.477240	7.7195			90.1264			260.6343
	6ccxHCl-007	-826.790218	-826.477279	8.6206			92.3537			256.2126
	6ccxHCl-006	-826.790216	-826.477287	7.6534			90.4595			253.3395
	6ccxHCl-005	-826.790326	-826.477415	7.9110			90.3836			254.1277
	6ccxHCl-004	-826.790353	-826.477481	8.6098			92.3922			256.7270
	6ccxHCl-003	-826.790268	-826.477495	8.6033			92.5871			257.3334
	6ccxHCl-002	-826.791462	-826.478467	7.4944			89.0128			251.9038
	6ccxHCl-001	-826.791587	-826.478649	7.6932			89.1656			251.8846
	< Shielding >[a]			**7.8536**			**90.5825**			**254.8066**
Structure	Nr	E_{tot}	H_{298K}	C^1	C^2	C^3	N^1	N^2	N^3	P
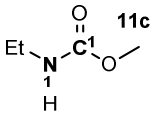 **11c**	11c-002	-363.093795	-362.948219	11.7046			143.2875			
	11c-001	-363.095903	-362.950419	11.5705			145.5618			
	< Shielding >[a]			**11.5824**			**145.3601**			
Structure	Nr	E_{tot}	H_{298K}	C^1	C^2	C^3	N^1	N^2	N^3	P
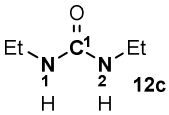 **12c**	12c-007	-382.547882	-382.360212	11.0748			142.3887	144.3744		
	12c-006	-382.547863	-382.360256	12.1381			144.1237	148.8502		
	12c-005	-382.548306	-382.360632	11.4655			142.3433	146.4700		
	12c-004	-382.548945	-382.361314	11.3623			142.4176	145.0298		
	12c-003	-382.549701	-382.362298	13.3034			147.3959	147.3968		
	12c-002	-382.550168	-382.362571	10.3508			144.9545	142.5501		
	12c-001	-382.550472	-382.362901	10.6857			144.7415	144.7417		
	< Shielding >[a]			**11.2387**			**145.0186**	**144.8539**		
	average of < Shielding >[b]						**144.9362**			
Structure	Nr	E_{tot}	H_{298K}	C^1	C^2	C^3	N^1	N^2	N^3	P
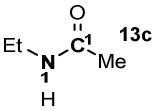 **13c**	13c-001	-287.868952	-287.729779	**-1.3260**			**105.8542**			

[a] Boltzman averaged by H_{298K} weighting factors. [b] Arithmetic average of the Boltzmann weighted factors in case of chemical equivalent atoms.

Table S2: 15. [Table S23] ^{31}P Shieldings calculated for reference compounds **5c**, **15c**, **16c**, **17c**, **18c** and **19c** at the B3LYP/IGLO-III//B3LYP/6-31+G(d,p) level of theory in different media.

B3LYP/6-31+G(d,p)				B3LYP/IGLO-III//B3LYP/6-31+G(d,p)		
				SMD($CHCl_3$)	PCM($CHCl_3$)	Gas phase
Structure	Nr	E_{tot}	H_{298K}	P	P	P
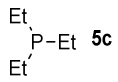 **5c**	5c-005	-579.060822	-578.8504	307.5492	307.4689	306.9341
	5c-004	-579.061076	-578.850571	309.3981	309.3044	308.6957
	5c-003	-579.061146	-578.850799	303.5472	303.4286	302.9816
	5c-002	-579.062443	-578.852103	304.7235	304.6127	304.1096
	5c-001	-579.062473	-578.852156	304.7232	304.6210	304.1079
	< Shielding >[a]			**305.1325**	**305.0275**	**304.5160**
Structure	Nr	E_{tot}	H_{298K}	P	P	P
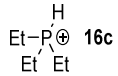 **16c**	16c-006	-579.440213	-579.218026	275.2401	276.1672	276.7689
	16c-005	-579.44036	-579.218322	268.1958	269.0202	269.2406
	16c-004	-579.440815	-579.218758	263.8631	264.7349	264.4160
	16c-003	-579.442099	-579.220102	268.1539	268.9732	269.0421
	16c-002	-579.442277	-579.220234	268.5160	269.4447	269.4759
	16c-001	-579.442481	-579.220447	263.1860	264.0785	263.5700
	< Shielding >[a]			**266.4493**	**267.3313**	**267.1838**
Structure	Nr	E_{tot}	H_{298K}	P	P	P
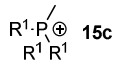 **15c**	15c-007	-618.777723	-618.525125	254.0014	255.0661	256.1948
	15c-006	-618.777806	-618.525196	253.5194	254.6038	255.7681
	15c-005	-618.777646	-618.525218	252.7550	253.8314	254.9150
	15c-004	-618.77934	-618.526866	250.4884	251.4837	252.3655
	15c-003	-618.779358	-618.526902	250.2837	251.2969	252.1803
	15c-002	-618.779557	-618.527044	250.0575	251.0664	252.0543
	15c-001	-618.779773	-618.527347	249.8760	250.9100	251.8335
	< Shielding >[a]			**250.4360**	**251.4571**	**252.3983**
Structure	Nr	E_{tot}	H_{298K}	P	P	P
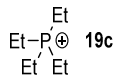 **19c**	19c-005	-658.093998	-657.811283	250.1105	251.0366	251.9118
	19c-004	-658.09414	-657.811387	249.6031	250.6305	251.5061
	19c-003	-658.095845	-657.813512	246.7306	247.7168	248.3690
	19c-002	-658.096399	-657.813596	245.1370	246.1193	246.7658
	19c-001	-658.096419	-657.813617	245.3175	246.3016	246.9441
	< Shielding >[a]			**245.9389**	**246.9228**	**247.5830**
Structure	Nr	E_{tot}	H_{298K}	P	P	P
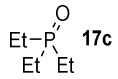 **17c**	17c-007	-654.320788	-654.104633	252.1455	253.1961	259.2937
	17c-006	-654.321658	-654.105523	252.6985	253.6940	255.0148
	17c-005	-654.32212	-654.10604	247.3122	248.4035	255.0148
	17c-004	-654.322384	-654.106299	246.6401	247.7779	254.5016
	17c-003	-654.322922	-654.106819	249.7979	250.8583	256.5660
	17c-002	-654.322941	-654.106874	250.1112	251.1670	256.8584
	17c-001	-654.322982	-654.106883	249.6224	250.6510	256.3512
	< Shielding >[a]			**249.3981**	**250.4589**	**256.3861**

Table S2: 15 (continuation). [Table S23] ^{31}P Shieldings calculated for reference compounds **5c**, **15c**, **16c**, **17c**, **18c** and **19c** at the B3LYP/IGLO-III//B3LYP/6-31+G(d,p) level of theory in different media.

Structure	Nr	E_{tot}	H_{298K}	P	P	P
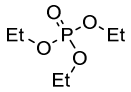 **18c**	18c-014	-880.048784	-879.814123	298.4739	298.6470	300.4038
	18c-013	-880.049005	-879.814376	299.1895	299.3770	301.2157
	18c-012	-880.049219	-879.814493	290.8595	291.0130	291.7906
	18c-011	-880.049228	-879.814518	291.1611	291.3133	292.0855
	18c-010	-880.049277	-879.814555	290.4487	290.6066	291.4418
	18c-009	-880.049574	-879.814958	300.4967	300.6623	302.5361
	18c-008	-880.050239	-879.815584	293.0915	293.2193	294.0734
	18c-007	-880.050239	-879.815585	293.0922	293.2200	294.0746
	18c-006	-880.051116	-879.816455	295.3438	295.4415	296.2954
	18c-005	-880.051089	-879.816456	295.3138	295.4095	296.2633
	18c-004	-880.05112	-879.816458	295.3696	295.4655	296.3297
	18c-003	-880.051118	-879.816461	295.3656	295.4623	296.3312
	18c-002	-880.05112	-879.816468	295.3355	295.4281	296.2898
	18c-001	-880.051115	-879.816469	295.4552	295.5470	296.4192
	< Shielding >[a]			**295.1240**	**295.2296**	**296.1391**

[a] Boltzman averaged by H_{298K} weighting factors.

Table S2: 16. [Table S24] (Carbonyl) ^{13}C, ^{15}N, ^{31}P Shieldings calculated for identified intermediates **6cc**, **7Lcc**, **7Ncc**, **7Occ**, **8cc**, and **9cc** at the B3LYP/IGLO-III//B3LYP/6-31+G(d,p) level of theory with SMD ($CHCl_3$) solvation model.

B3LYP/6-31+G(d,p)				SMD($CHCl_3$)/B3LYP/IGLO-III//B3LYP/6-31+G(d,p)						
Structure	Nr	E_{tot}	H_{298K}	C^1	C^2	C^3	N^1	N^2	N^3	P
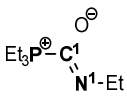 **6cc**	6cc-019	-826.371793	-826.073018	12.2135			5.3599			283.1700
	6cc-020	-826.371727	-826.073029	12.2204			6.3085			282.6398
	6cc-021	-826.371481	-826.073058	10.9145			9.7221			282.1899
	6cc-011	-826.372085	-826.073272	9.4518			10.6220			288.9605
	6cc-016	-826.371944	-826.073280	11.0677			17.3079			280.3554
	6cc-012	-826.372035	-826.073324	9.2734			10.9439			288.0693
	6cc-014	-826.372006	-826.073356	11.1016			18.8185			279.8607
	6cc-013	-826.372021	-826.073357	11.3146			19.4827			279.8461
	6cc-015	-826.371961	-826.073380	11.1778			17.8440			279.9072
	6cc-017	-826.371914	-826.073395	11.6541			8.1554			283.3828
	6cc-010	-826.372140	-826.073546	11.3465			19.2440			281.2802
	6cc-018	-826.371888	-826.073547	13.2577			10.9460			284.6280
	6cc-009	-826.372453	-826.073740	10.7982			10.3966			281.0780
	6cc-008	-826.372475	-826.073816	11.1060			10.8944			280.7804
	6cc-007	-826.372740	-826.074269	13.4468			3.9386			283.0320
	6cc-005	-826.372919	-826.074309	11.5560			9.0300			278.5914
	6cc-006	-826.372851	-826.074527	12.1752			14.7417			280.1290
	6cc-004	-826.372975	-826.074586	10.6848			8.5616			288.5751
	6cc-003	-826.373140	-826.074729	12.4553			17.1883			282.0115
	6cc-002	-826.373487	-826.074978	11.9135			8.7183			282.0822
	6cc-001	-826.373913	-826.075613	12.6538			7.1249			278.9609
	< Shielding >[a]			**11.9026**			**10.5401**			**281.6763**
Structure	Nr	E_{tot}	H_{298K}	C^1	C^2	C^3	N^1	N^2	N^3	P
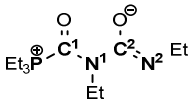 **7Lcc**	7Lcc-003	-1073.663512	-1073.276685	18.8416	17.1096		31.9046	64.4306		250.4206
	7Lcc-002	-1073.663857	-1073.277062	15.8840	17.5687		28.4656	67.0793		258.8914
	7Lcc-001	-1073.664709	-1073.278067	15.4770	16.4341		32.6649	60.9364		253.8392
	< Shielding >[a]			**16.0601**	**16.7816**		**31.6341**	**62.7941**		**254.4432**

Table S2: 16 (continuation). [Table S24**]** (Carbonyl) ^{13}C, ^{15}N, ^{31}P Shieldings calculated for identified intermediates **6cc**, **7Lcc**, **7Ncc**, **7Occ**, **8cc**, and **9cc** at the B3LYP/IGLO-III//B3LYP/6-31+G(d,p) level of theory with SMD ($CHCl_3$) solvation model.

B3LYP/6-31+G(d,p)				SMD($CHCl_3$)/B3LYP/IGLO-III//B3LYP/6-31+G(d,p)						
Structure	Nr	E_{tot}	H_{298K}	C^1	C^2	C^3	N^1	N^2	N^3	P
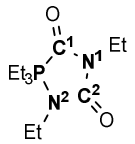 **7Ncc**	7Ncc-012	-1073.710146	-1073.321127	1.4739	15.8122		53.1347	74.7993		340.1914
	7Ncc-011	-1073.710436	-1073.321336	0.1113	16.1660		54.4554	76.9184		345.6160
	7Ncc-010	-1073.710547	-1073.321368	1.5749	16.0363		53.4860	73.3028		340.0057
	7Ncc-009	-1073.710581	-1073.321420	0.0439	15.9684		54.9978	77.2414		344.8234
	7Ncc-008	-1073.710918	-1073.321684	0.4028	15.3860		54.7363	76.1115		338.1253
	7Ncc-007	-1073.711071	-1073.321903	0.6964	15.7913		55.4563	74.3411		337.5433
	7Ncc-006	-1073.711391	-1073.322396	-0.1727	14.6285		53.0430	84.6282		335.4811
	7Ncc-005	-1073.711705	-1073.322582	0.0449	14.8747		52.9993	83.7285		335.5571
	7Ncc-003	-1073.712336	-1073.323203	0.8833	14.8852		52.9342	86.1530		336.4233
	7Ncc-004	-1073.712313	-1073.323276	0.9476	14.7906		53.8813	86.1191		335.8452
	7Ncc-002	-1073.712669	-1073.323695	1.3633	14.1756		52.8107	83.9168		333.9454
	7Ncc-001	-1073.713023	-1073.323880	1.6334	14.5261		53.2690	82.5038		334.2655
	< Shielding >[a]			**1.0533**	**14.7293**		**53.3473**	**83.0699**		**335.6536**
Structure	Nr	E_{tot}	H_{298K}	C^1	C^2	C^3	N^1	N^2	N^3	P
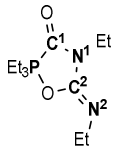 **7Occ**	7Occ-010	-1073.713255	-1073.324776	6.5486	17.7981		53.4092	53.1961		288.5737
	7Occ-009	-1073.713379	-1073.324917	6.5542	18.2242		53.7223	52.2627		288.0889
	7Occ-007	-1073.713686	-1073.325092	3.7714	17.8743		54.0497	52.3217		301.8478
	7Occ-008	-1073.713656	-1073.325133	3.8859	17.7029		53.7738	53.0655		301.6948
	7Occ-006	-1073.713853	-1073.325376	5.2700	18.2748		54.1522	51.1514		299.0989
	7Occ-005	-1073.714138	-1073.325549	4.5988	18.0371		54.1185	52.4527		304.6202
	7Occ-004	-1073.714216	-1073.325736	5.6869	17.0724		52.0557	52.8834		293.3182
	7Occ-003	-1073.714240	-1073.325740	5.6291	17.0494		51.9707	53.0022		293.5955
	7Occ-002	-1073.715010	-1073.326455	6.4431	17.1033		51.5320	52.5831		296.7146
	7Occ-001	-1073.715137	-1073.326586	6.6457	17.3803		51.9162	52.0122		296.2603
	< Shielding >[a]			**5.8381**	**17.4650**		**52.5269**	**52.4261**		**296.6261**
Structure	Nr	E_{tot}	H_{298K}	C^1	C^2	C^3	N^1	N^2	N^3	P
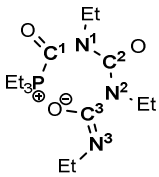 **8cc**	8cc-016	-1321.028984	-1320.551856	4.8869	11.8257	8.9362	40.7444	65.5021	42.2148	243.4485
	8cc-013	-1321.029299	-1320.552195	4.9117	10.6679	11.0490	39.3772	64.7067	44.0712	243.9119
	8cc-010	-1321.029718	-1320.552295	2.7604	14.2322	11.8209	70.0277	61.3597	38.3978	271.5891
	8cc-012	-1321.029557	-1320.552435	4.8540	13.7303	13.6121	63.4790	57.8394	40.3783	259.0890
	8cc-011	-1321.029698	-1320.552521	3.8664	15.0617	10.3789	65.0866	58.7848	42.2015	260.2509
	8cc-009	-1321.029743	-1320.552538	4.7651	10.6893	10.5764	38.5948	64.6462	42.1368	243.9670
	8cc-007	-1321.030563	-1320.552856	3.3620	14.5695	8.8650	66.1034	55.3523	43.7127	257.9930
	8cc-006	-1321.030698	-1320.552918	5.7228	15.1752	8.9941	63.0806	56.4669	42.6335	260.5089
	8cc-008	-1321.030088	-1320.553020	5.5093	11.1402	8.8834	41.9894	61.5279	49.0275	243.9202
	8cc-005	-1321.030847	-1320.553216	3.7979	14.7872	8.3536	61.0021	55.1753	43.1814	258.5458
	8cc-004	-1321.031033	-1320.553991	4.9370	9.9467	13.1347	39.7617	62.8277	46.9397	243.6525
	8cc-003	-1321.031416	-1320.554176	2.9540	13.2883	13.3595	60.5017	55.7537	39.5157	254.6997
	8cc-002	-1321.031710	-1320.554573	3.7212	14.7556	9.6803	60.8700	56.1578	42.1641	257.3045
	8cc-001	-1321.032146	-1320.554832	3.3451	13.0215	13.1378	55.4175	55.7129	40.6813	254.7192
	< Shielding >[a]			**3.8534**	**13.1903**	**11.5328**	**55.6892**	**57.5247**	**42.2511**	**254.0579**

Table S2: 16 (continuation). [Table S24**]** (Carbonyl) ^{13}C, ^{15}N, ^{31}P Shieldings calculated for identified intermediates **6cc**, **7Lcc**, **7Ncc**, **7Occ**, **8cc**, and **9cc** at the B3LYP/IGLO-III//B3LYP/6-31+G(d,p) level of theory with SMD ($CHCl_3$) solvation model.

B3LYP/6-31+G(d,p)				SMD($CHCl_3$)/B3LYP/IGLO-III//B3LYP/6-31+G(d,p)						
Structure	Nr	E_{tot}	H_{298K}	C^1	C^2	C^3	N^1	N^2	N^3	P
	9cc-039	-1321.028715	-1320.551418	2.7756	65.0547	5.2363	60.7746	95.4730	91.1532	306.5550
	9cc-040	-1321.028711	-1320.551431	4.8833	65.2671	5.2191	60.8452	95.4047	92.1568	294.2095
	9cc-031	-1321.028851	-1320.551442	2.2224	66.3932	1.7571	61.9909	95.6221	90.1389	306.6663
	9cc-028	-1321.028929	-1320.551480	4.8127	66.3137	1.6174	60.6614	94.3808	91.5277	293.8605
	9cc-029	-1321.028923	-1320.551506	0.6589	63.6256	6.8678	65.0770	91.9267	89.6036	312.1701
	9cc-023	-1321.029082	-1320.551511	5.6414	66.2186	1.9428	58.2775	92.2529	93.7079	298.5600
	9cc-018	-1321.029154	-1320.551518	3.0016	66.4910	2.5119	62.4082	92.4463	94.8233	309.6748
	9cc-019	-1321.029130	-1320.551520	3.6706	66.0782	2.6704	60.1506	95.4305	90.9039	308.2673
	9cc-024	-1321.029058	-1320.551579	2.4797	66.5870	3.4503	63.0360	91.9581	92.4592	307.5368
	9cc-022	-1321.029098	-1320.551580	1.3737	63.7829	6.6792	64.4449	92.3921	89.0500	314.8972
	9cc-026	-1321.029019	-1320.551599	4.4946	66.1147	1.1248	58.1374	94.9692	89.5834	294.8017
	9cc-030	-1321.028905	-1320.551608	3.0895	63.8168	6.9654	64.6456	91.9422	89.5083	300.3338
	9cc-027	-1321.028973	-1320.551615	2.0353	64.0420	5.1992	65.7968	94.4437	88.3242	313.1853
	9cc-025	-1321.029032	-1320.551634	4.0658	65.3783	5.3470	61.0152	95.6644	91.9327	305.7189
	9cc-021	-1321.029107	-1320.551637	2.6758	66.2790	1.5315	61.5110	94.6868	89.8607	305.4824
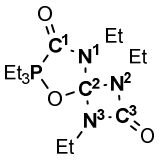	9cc-017	-1321.029176	-1320.551674	4.4258	66.8713	1.4782	61.9008	96.4242	89.7510	296.1018
	9cc-020	-1321.029127	-1320.551692	3.4061	67.0524	1.8659	63.0833	97.1206	89.8609	308.1869
	9cc-016	-1321.029406	-1320.552004	2.2135	63.9310	6.7273	65.1822	91.6940	89.9351	311.3823
	9cc-014	-1321.029541	-1320.552099	6.3509	64.9475	3.0667	55.5181	91.5010	91.7966	294.3840
9cc	9cc-015	-1321.029510	-1320.552120	2.2751	66.4607	2.2595	63.1454	91.3291	95.2377	306.0848
	9cc-012	-1321.029594	-1320.552199	4.9420	66.6734	2.0733	61.4286	94.8173	92.5104	295.3695
	9cc-013	-1321.029565	-1320.552206	4.7088	66.0143	1.8201	58.3151	91.3571	94.4226	294.7958
	9cc-011	-1321.029650	-1320.552249	3.7317	65.4373	3.3481	59.6173	92.8728	90.3734	306.7668
	9cc-009	-1321.029754	-1320.552304	4.5683	66.7560	2.0322	62.0405	91.6084	95.5819	295.8304
	9cc-007	-1321.029946	-1320.552360	3.9607	65.4821	3.2030	58.3972	91.7809	90.8663	306.6839
	9cc-010	-1321.029723	-1320.552384	2.8367	66.4627	2.0303	61.3206	94.4362	91.5698	307.1592
	9cc-008	-1321.029867	-1320.552512	5.3454	65.9787	2.9685	59.5611	93.7699	90.5208	292.9576
	9cc-006	-1321.029953	-1320.552586	4.1639	66.7688	2.3035	61.5628	94.6571	92.6079	306.4270
	9cc-004	-1321.030129	-1320.552625	5.2767	65.6724	3.2105	59.0396	92.0166	92.1959	291.3585
	9cc-005	-1321.029993	-1320.552660	3.8002	66.7918	2.3260	62.6571	96.0140	91.4469	306.0819
	9cc-003	-1321.030131	-1320.552694	2.9967	65.6811	3.0824	59.8566	92.6908	90.3487	305.0195
	9cc-002	-1321.030245	-1320.552719	3.0488	65.3864	3.2263	59.9512	91.6817	91.1341	303.7319
	9cc-001	-1321.030568	-1320.553182	4.3246	65.7852	3.4113	59.8593	91.8193	92.3064	304.8645
	< Shielding >[a]			**3.8261**	**65.8384**	**3.1188**	**60.8535**	**93.2245**	**91.6304**	**302.7538**

[a] Boltzman averaged by H_{298K} weighting factors.

Chapter 3. Chemoselectivity in Esterification Reactions – Size Matters After All

Julian Helberg, Marta Marin-Luna, Hendrik Zipse

Synthesis ***2017****, 49,* 3460 – 3470.

Authors contributions

H.Z. conceived the project. The study was designed jointly by J.H., M.M.-L. and H.Z. and executed by J.H. and M.M.-L. The manuscript was jointly written by J.H., M.M.-L. and H.Z and the supporting information was prepared by M.M.-L., J.H. and H.Z.

J.H and M.M.-L. contributed equally to this work.

Copyright

For full supporting information, please follow the link below:

https://www.thieme-connect.de/media/synthesis/201715/supmat/sup_ss-2017-z0305-op_10-1055_s-0036-1588854.pdf

Additional information

Since the synthetic and analytical information for synthesized compounds is duplicated both in the manuscript and the supporting information, it was omitted in the given supporting information in chapter 3.1. Furthermore, the following chapter is a shortened and altered version of the originally published supporting information and has been optimized for printing purposes. The original files for the manuscript and the supporting information can be found on the electronic attachment to this thesis. For comparison of this thesis and the original SI file, the numbering includes the original caption as shown below:

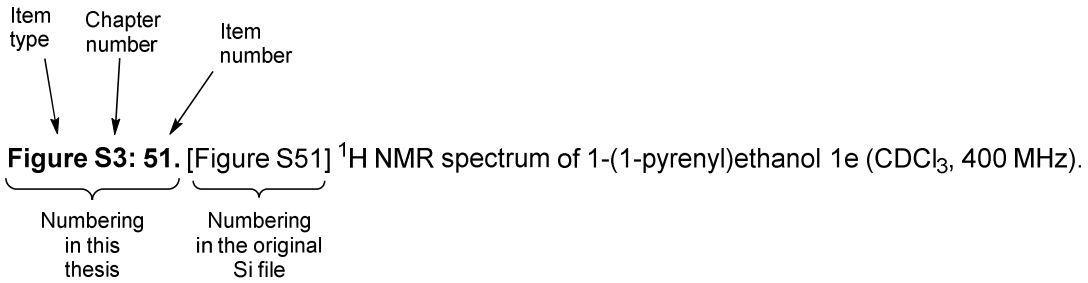

Chemoselectivity in Esterification Reactions – Size matters after all

Julian Helberg
Marta Marin-Luna
Hendrik Zipse*

Department of Chemistry
LMU München
Butenandtstrasse 5-13
D-81377 München
Germany

zipse@cup.uni-muenchen.de

Dedicated to Herbert Mayr on occasion of his 70th birthday

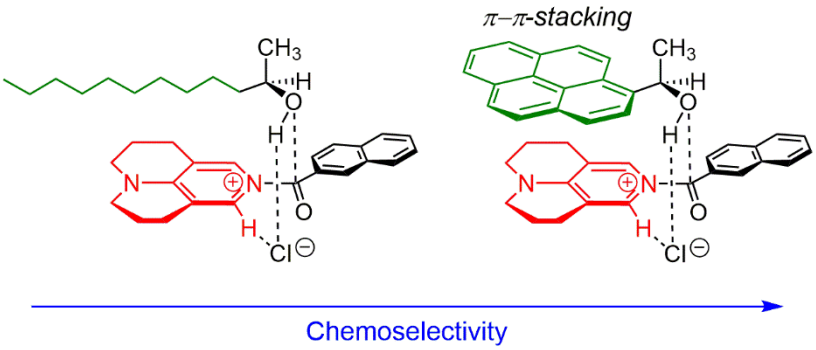

Abstract The reaction of carboxylic acid chlorides with secondary alcohols carrying either flexible alkyl or rigid aryl substituents was studied through a series of competition experiments. Aliphatic acid chlorides react preferentially with the aryl-substituted alcohols, while acid chlorides derived from aromatic carboxylic acids react with very low selectivity. Catalysis by 9-azajulolidine (TCAP) increases the selectivity strongly, while solvent and temperature effects are only moderate. The size of the alcohol substituents seems to impact selectivities only for rigid aryl substituents, and highest selectivities have been found for 1-(1-pyrenyl)ethanol.

Key words chemoselective esterification, acyl chlorides, organocatalysis, competition experiments, dispersion energy donor

The concept of dispersion energy donor (DED) guided chemistry has recently emerged as a new paradigm in fields as diverse as stereoselective catalysis and main group organic chemistry.[1] The basic tenet of this concept is that attractive London forces between properly placed large molecular structures can guide reactions to be more reactive, more selective, or provide larger driving force as compared to the same reactions involving smaller substituents. In addition, notable effects can only be expected when using fairly rigid DED groups, as otherwise the entropic price for 'properly placing' becomes prohibitive. Since experimental validation of this concept has been sparse so far, we explored here its applicability in the context of acylation reactions of alcohols, a reaction of fundamental importance in the synthesis of complex molecular targets.[2] Depending on the reaction conditions and the mode of catalysis these reactions involve either carboxylic acids or their activated derivatives such as acid anhydrides or halides.[3,4] Due to their superior intrisic reactivity we selected here carboxylic acid chlorides as reagents, as these allow reactions to proceed in a catalyzed as well as uncatalyzed fashion. The challenge of chemoselectivity arises when molecules contain two sterically and electronically similar alcohol functions. Therefore, we have designed intermolecular competition experiments between two secondary alcohol substrates containing different structural organization levels each, that is. a flexible alcohol **1a** (smaller effective surface R_1) and a *pre*-organized (larger effective surface R_2) alcohol **1b** (Scheme 1). This was also applied to differently sized preorganized secondary alcohols. As indicated in Scheme 1, differentiation between these alcohols is facilitated by (activated) carboxylic chloride reagents, for which the effect of the size of the substituent (R_3) was investigated. For activation, we decided to employ 9–azajulodine (TCAP) due to its well-documented high reactivity in acylation reactions.[5]

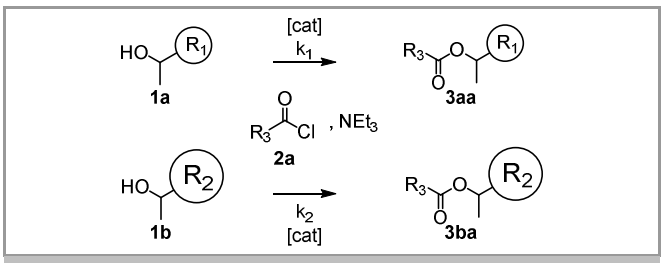

Scheme 1 Competition experiment between secondary alcohols carrying alkyl and aryl substituents R_1 and R_2 of different effective surface

Carboxylic acid derivatives carrying large aromatic or aliphatic substituents such as 1-adamantyl carboxylic acid[6] or the substituted benzoic anhydrides in the Yamaguchi[7] and Shiina[8] esterification reactions, respectively, are known to be capable of selective transformations. We therefore initiated our studies with reagents from this latter class and use acetyl chloride as the smallest possible reference.

Kinetic data from these types of 1:1 competition experiments can be extracted following an approach developed for kinetic resolution experiments.[9] While the intrinsic selectivity of this process S is reflected in the ratio of the two effective rate constants $S = k_2/k_1$ (Figure 1, eq. 1), the experimentally determined chemoselectivity C is apparent from the product distribution (Figure 1, eq. 2) and depends on the actual conversion of the reaction which is defined in Figure 1, eq. 3. Selectivity factors S were therefore derived from a series of experiments involving the determination of chemoselectivity C at different conversions.

$$Selectivity\ (S) = \frac{k_2}{k_1} \quad (1)$$

$$Chemoselectivity\ (C) = \frac{[\mathbf{3ba}] - [\mathbf{3aa}]}{[\mathbf{3ba}] + [\mathbf{3aa}]} \quad (2)$$

$$Conversion[\%] = \left\{\frac{[\mathbf{3aa}] + [\mathbf{3ba}]}{[\mathbf{3aa}] + [\mathbf{3ba}] + [\mathbf{1a}] + [\mathbf{1b}]}\right\} \times 100 \quad (3)$$

Figure 1 Selectivity eq. 1, chemoselectivity eq. 2 and conversion eq. 3 of benchmark alcohols **1a** and **1b** with varying carbonyl chlorides **2a**

How this procedure is put into practice is shown in Scheme 2 for the competition between dodecan-2-ol (**1a**) and 1-(1-naphthyl)ethanol (**1b**). These two alcohols contain substituents of identical carbon count, but different degrees of preorganization: while the n-decyl side chain in **1a** enjoys a large degree of conformational freedom, all side chain carbon atoms are confined to the plane of the naphthyl ring system in **1b**. Equal amounts of these two alcohols **1** (0.1 mol/L each) were reacted with different concentrations of benzoyl chloride (**2a**; 20, 35, 50, 65 and 80% with respect to the total amount of both alcohols **1**) in $CDCl_3$ in the presence of NEt_3 (1.16 eq. relative to **2a**) and TCAP (**4**; 0%, 2.5%, 5% or 7.5% with respect to the total amount of both alcohols **1**).

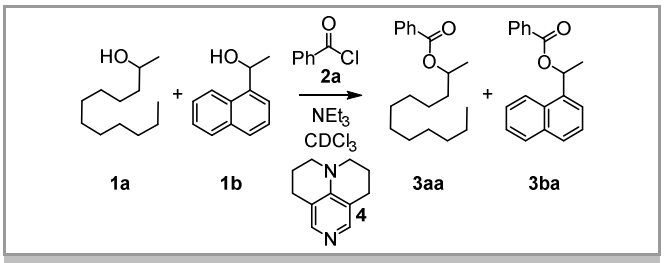

Scheme 2 Representative competition experiment between alcohols **1a** and **1b** with benzoyl chloride **2a**

The reactions were stirred under nitrogen at constant temperature of +23 °C until full turnover of acid chloride was observed by ^{1}H NMR measurements. The chemoselectivity *C* was then determined through integration of the reactant and product signals (Figure 2, top) and plotted vs. the actual conversion (Figure 2, bottom) as detailed in the SI. Turnover curves corresponding to constant selectivity factors *S* were then fitted to the data points such that deviations were minimized. For the example shown in Scheme 2 the resulting chemoselectivity *versus* conversion plot fits best to the selectivity curve with $S = 9.5$.

In a first set of experiments, the selectivity between alcohols **1a** and **1b** was tested with a variety of aliphatic chlorides without addition of catalyst **4** (Table 1, Entries 1-4). For the smallest reagent acetyl chloride (**2b**) used here, reaction of naphthyl-substituted alcohol **1b** is preferred with $S = 7$. A slightly lower selectivity is determined for the much larger diphenylacetyl chloride **2e** ($S = 6$), while even lower values are found for the acid chlorides **2c** and **2d** (both, $S = 3$-4). However, in all of these experiments, traces of secondary products such as β-keto ester **7** are formed, which might cause the low selectivities observed in these cases. These β-keto esters are most likely formed via diketene intermediates **6** or from enol ester tautomers **3taut** as shown in Scheme 3 for acetyl chloride **2b**.[10] The formation of these secondary products can be reduced to some extent through slow addition of the acid chlorides, but only through the use of aromatic carbonyl chlorides lacking a deprotonable α-position can the formation of these side reactions be avoided completely (entries 5 - 18).

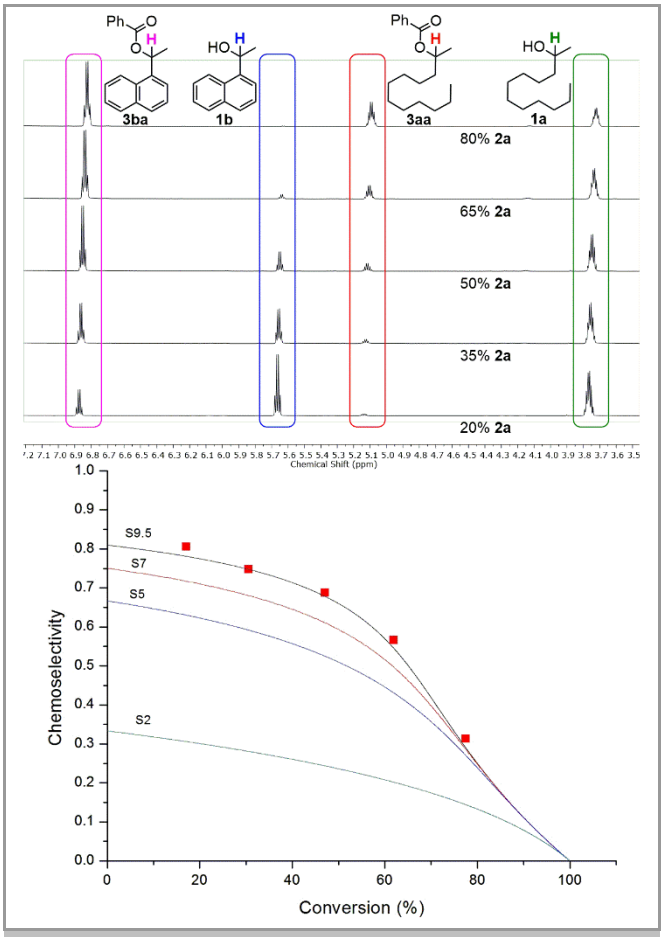

Figure 2 Example of ^{1}H NMR signals used for *in situ* determination of conversion and chemoselectivity (top) and corresponding chemoselectivity vs conversion plot underlain by simulated selectivity curves (bottom)

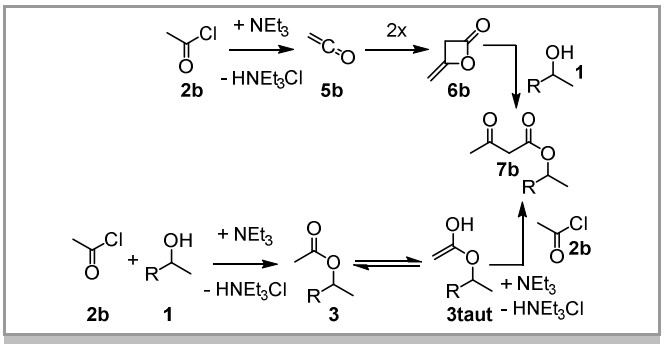

Scheme 3 Proposed pathways for formation of β-keto ester **7b**

The selectivities determined for uncatalyzed esterifications of alcohols **1b**/**1a** with aromatic carboxylic acid chlorides show larger variations and range from $S = 0.7$ in the case of 1-naphthoyl chloride (**2f**) to $S = 6$ when anthracenylcarboxylic acid chloride (**2h**) is employed (Table 1, entries 5, 9, 13, 17). In fact, the reaction with 1-naphthoyl chloride (**2f**) is the only one found to prefer dodecan-2-ol (**1a**) over any other alcohol in the

1:1 competition experiments. The broad range of selectivities found for aromatic carboxylic acid chlorides may, in part, be due to changes in the substitution mechanism. Scheme 4 summarizes three of the more likely mechanisms for the reaction of acid chlorides with alcohols. For sterically demanding acid chlorides such as 9-anthracenylcarboxylic acid chloride (**2h**) earlier studies[11] have established that the reaction proceeds through an S_N1-type mechanism with rate-limiting formation of the respective acylium ion **S1** and subsequent reaction with the alcohol substrates. This mechanism also appears to persist in the presence of Lewis base catalysts as the observed selectivity factor of $S = 6$ remains unchanged upon addition of 5% of TCAP (entries 17 and 18).

Table 1 Competition Experiments for Alcohols **1a** and **1b** with Variations in Acyl Chlorides **2x** and Amounts of Catalyst **4**

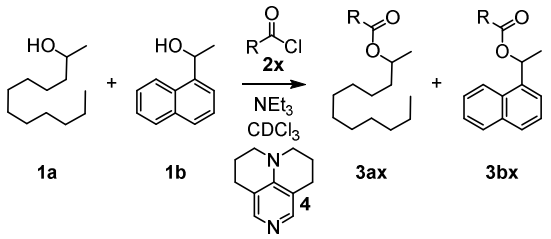

Entry	Chloride **2x**	% of **4**	*S*
1	 **2b**	0	7[a]
2	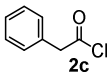 **2c**	0	3-4[a]
3	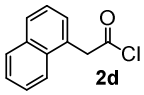 **2d**	0	3-4[a]
4	 **2e**	0	6[a]
5	 **2a**	0	2[a]
6		2.5	7[a]
7		5	9.5[a]
8		7.5	9.5[a]
9	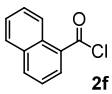 **2f**	0	0.7[a]
10		2.5	3-4[b]
11		5	4-5[b]
12		7.5	10[b]
13	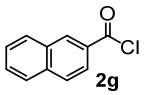 **2g**	0	2[a]
14		2.5	6[a]
15		5	8.5[a]
16		7.5	8.5[a]
17	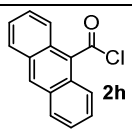 **2h**	0	6[a]
18		5	5-6[a]

[a] Selectivity values *S* derived from chemoselectivites at five different turnover values (see SI for details).
[b] Selectivity values *S* derived from chemoselecivity *C* at 20% turnover.

Uncatalyzed reactions of all other (sterically less biased) acyl chlorides appear to follow an S_N2-type pathway involving direct encounter of acid chlorides and alcohols in the rate-limiting steps. The selectivity factors observed for these reactions are quite low and range between 0.7 (for **2f**) to 2.0 (**2a** and **2g**). In these cases, addition of pyridine catalyst **4** leads to a change in selectivity factor *S* and therefore to a change in the ratio of the effective rate constants (k_2/k_1). The selectivity in this third pathway is thus due to the interaction of substrate alcohols with acylpyridinium ions **S3** (Scheme 4), whose formation through direct reaction of acid chlorides with the structurally related 4-dimethylaminopyridine (DMAP) have been described before.[12] The large, planar structure of acylpridinium ion **S3** may, in part, be responsible for the preferred reaction of alcohol **1b** over **1a** under these conditions. The selectivity factors *S* shows no simple dependence on the catalyst concentration, but a saturation effect between 5% and 7.5% in the case of **2a** and **2g**. This is presumably caused by the conversion being dominated by the catalyzed reaction pathway. In the case of acyl chloride **2f**, product transesterification processes appear to be involved which become more notable at higher (absolute) reagent concentrations and longer reaction times are causeing atypical chemoselectivites (see SI). Therefore selectivity factors could only be determined with some confidence at conversion levels below 20% (Table 1, entries 10 - 12). Despite these complications, all selectivity data collected in Table 1 clearly document that acylpyridinium **S3** appears to be the most competent 'selector' in differentiating the two alcohols **1a** and **1b**.

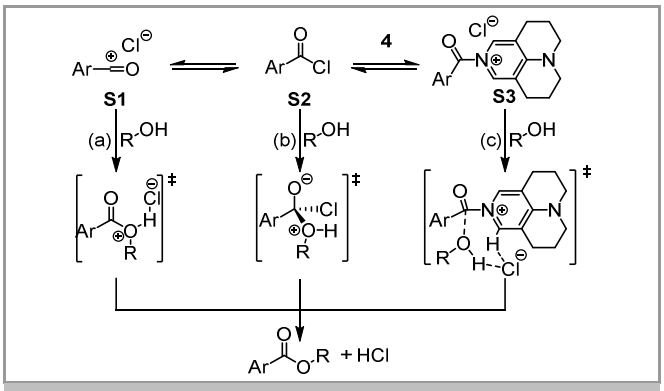

Scheme 4 Limiting mechanisms for reaction of alcohols with acyl chlorides: (a) S_N1 pathway with acylium ion **S1**, (b) S_N2 pathway; and (c) TCAP-catalyzed pathway involving acylpyridinium ion **S3**

In order to gain insight into the TCAP-catalyzed esterification of aromatic chlorides, a series of in situ ^{1}H NMR experiments in $CDCl_3$ was conducted. TCAP (**4**) was mixed with equimolar amounts of the aromatic acyl chlorides **2a**, **2f**, and **2g**. Figure 3 shows the spectra obtained with benzoyl chloride (**2a**) (spectrum IV) in comparison to those for pure TCAP (**4**) (spectrum III), TCAP·HCl (spectrum II), and the corresponding pyridinium carboxylate (spectrum I). Analysis of these spectra allows for the following conclusions: 1) TCAP and benzoyl chloride react quantitatively under formation of two adducts in a ratio of 70:30 (spectrum IV); 2) The signals for the major component correspond to acylpyridinium ion **S3** due to the large shifts downfield compared to pure TCAP (spectra III, IV);[13] 3) These large shifts of the aromatic proton peak (7.8 ppm -> 8.1 ppm) and the aliphatic ones (especially the one from 3.2 ppm to 3.8 ppm) are presumably caused by the rehybridization of the nitrogen atoms in the TCAP/acid chloride adduct (spectra III, IV); 4). The minor component in spectrum IV most likely corresponds to a rapidly interchanging mixture of TCAP·HCl (spectrum II) and the pyridinium carboxylate product (spectrum I) (see SI for further details). The assignments for

TCAP·HCl are further supported through an X-ray crystal structure obtained after recrystallization from hexane (Figure 4). The chloride anion is coordinated to the C2-H bond of the pyridine ring with a Cl–H distance of 263.1 pm. A similar arrangement may also be envisioned for the aromatic chloride adducts **S3** shown in Scheme 4.

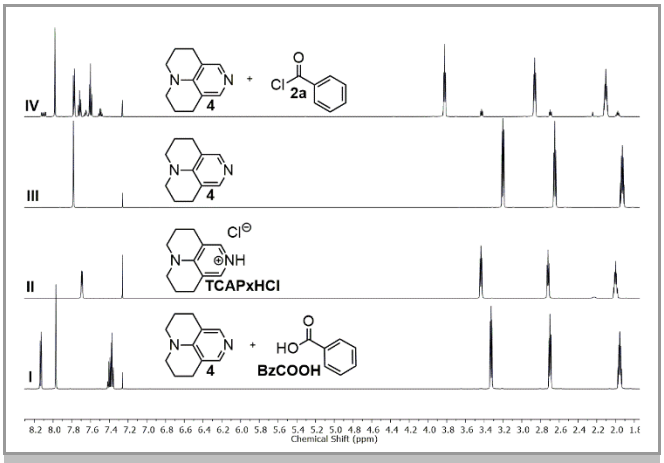

Figure 3 ^{1}H NMR investigation of TCAP-activation of benzoyl chloride **2a**.

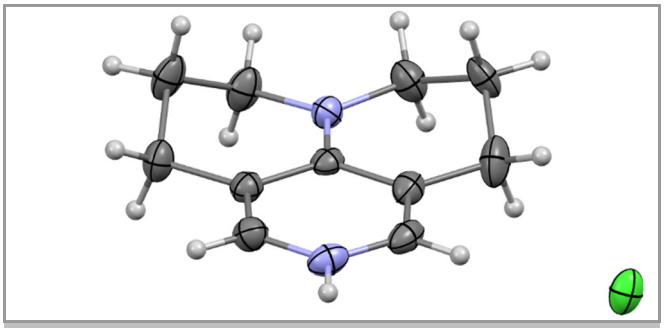

Figure 4 X-ray crystal structure of the TCAP·HCl adduct; the compound crystallizes with one molecule of H_2O (removed for clarity)

Having obtained satisfactory selectivites, we turned towards the influence of the reaction conditions on the chemoselectivity (Table 2). Since the total amount of NEt_3 changes with the amount of chloride in all experiments described in Table 1, we performed the standard experiment while keeping the concentration of NEt_3 constant at the highest level used previously for all concentrations of **2g** (Table 2, **A**). Only a small change in selectivity is observed at these (on average) higher base concentrations, in line with the effects of auxiliary bases in other acylation reactions.[14] Since a decrease in temperature is commonly expected to increase selectivity,[15] the standard experiment with acyl chloride **2g** was conducted at +10 °C instead of +23 °C (Table 2, **B**). Again, only a moderate increase in selectivity (S = 8.5 → S = 10) is observed which translates into a difference in activation enthalpies of 8.7 kJmol^{-1} and of activation entropies of 11.6 JK^{-1}mol^{-1} by use of the Eyring Equation (see SI).[15] In contrast, much larger variations can be observed on rerunning the 1:1 competition experiment between alcohols **1a** and **1b** in different solvents in the presence of 5% catalyst **4** (Table 2, **C**). Selectivity is highest with $S = 11$ in trifluoromethylbenzene, closely followed by $CDCl_3$ with $S = 9.5$. Still lower values are found for the polar solvent acetonitrile and aromatic solvents such as toluene or benzene. The reaction is least selective in THF with $S = 2$-3, and it is not immediately obvious from this series what solvent property governs the S-value variations.

Table 2 Competition Experiments for Alcohols **1a** and **1b** with Variations in the Reaction Conditions

Method	[NEt_3] (mol/L)	Solvent	T [°C]	S
Bench-mark	0.05, 0.08, 0.12, 0.15, 0.19	$CDCl_3$	23	8.5[a]
A	0.19 for all experiments	$CDCl_3$	23	9.5[a]
B	0.05, 0.08, 0.12, 0.15, 0.19	$CDCl_3$	10	10[a]
C	0.05 for all	$CF_3C_6H_5$	23 for all	11[b]
		$CDCl_3$		9.5[b]
		Acetonitrile		7.5[b]
		Toluene		6[b]
		Benzene		5.5[b]
		THF		2-3[b]

[a] Selectivity values S derived from chemoselectivities at five different turnover values (see SI for details).
[b] Selectivity values S derived from chemoselecivity C at 10% turnover.

Since the results described so far gave little indication to change the experimental setup, an investigation into the role of the size and shape of the competing alcohols was launched. Therefore, we used standard conditions with 2.5% and 7.5% of catalyst **4** and 2-naphthoyl chloride (**2g**) while changing the pair of alcohols (Table 3). In order to study whether steric hindrance imposed through the aliphatic chain in dodecan-2-ol (**1a**) causes the preference for the pre-organized 1-(1-naphthyl)ethanol (**1b**) in reactions of all examined activated aromatic chlorides, a number of experiments with the smaller pentan-2-ol (**1c**) were conducted. The comparison of entry 1 with 3 and 2 with 4 respectively, clearly shows that steric hindrance by the chain of **1a** plays no substantial role in determining selectivity for the reactions of interest in this study.[16]

Due to these results, we focussed on competition experiments comparing differently sized aromatic alcohols. Beginning with the pair of 1-(1-naphthyl)ethanol (**1b**) and 1-phenylethanol (**1d**) we found a small preference ($S = 1.5$) towards the larger aromatic system (Table 3, Entries 5, 6). Selectivity is inverted for the pair of **1b** and the larger 1-(1-pyrenyl)ethanol (**1e**) ($S = 0.4$-0.5), again clearly favouring the larger aromatic system (entries 7, 8). Since the competition between aromatic and aliphatic alcohols always showed the best selectivity, three differently sized aromatic alcohols **1b**, **1d**, and **1e** were tested against dodecan-2-ol (**1a**) (Figure 5).

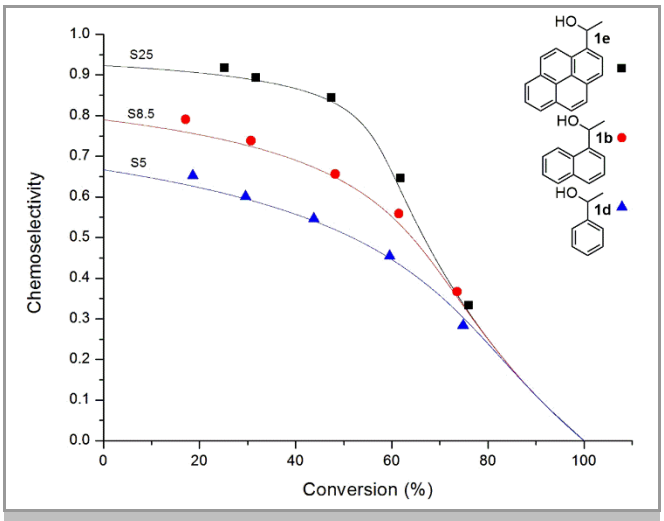

Figure 5 Visualization of the competition experiment of different aromatic alcohols with **1a** catalyzed by 7.5% of TCAP (Table3, entries 4, 10, 12)

Table 3 Competitive Acylations of Selected Secondary Alcohol Pairs with 2-Naphthoyl Chloride (**2g**)

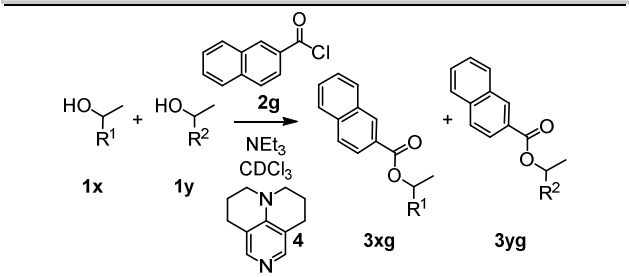

Entry	Alcohols **1**		% of **4**	S^a
1	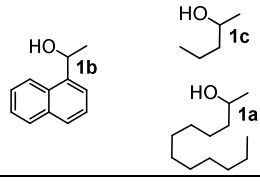		2.5	8
2			7.5	10
3[b]			2.5	6
4[b]			7.5	8.5
5	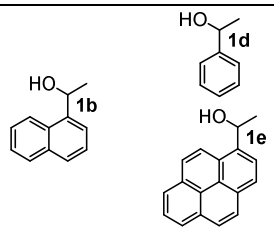		2.5	1.5
6			7.5	1.5
7			2.5	0.4-0.5
8			7.5	0.4-0.5
9[c]	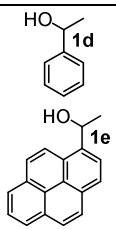		2.5	4-5
10[c]			7.5	5
11[c]			2.5	25
12[c]			7.5	25

[a] Selectivity values *S* derived from chemoselectivities at five different turnover values (see SI for details).
[b] These results are also included in Table 1.

Screening catalyst concentrations of 2.5% and 7.5%, excellent selectivities ($S = 25$) are obtained for reactions of 1-(1-pyrenyl)ethanol (**1e**) as compared to alcohol **1a** (Table 1, entries 11, 12). All of the measurements with a catalyst concentration of 7.5% clearly show an increase in selectivity if the size of the aromatic competitor is increased: $S = 5$ for **1d** to $S = 8.5$ for **1b** up to $S = 25$ for **1e** (Figure 5, Table 3, entries 4, 10, 12). Similar, but less distinct, observations can be made for a concentration of 2.5% of TCAP (**4**). The overall trend observed for competition experiments between differently sized aromatic alcohols as well as one aliphatic alcohol with several differently sized aromatic alcohols shows a correlation between the size of the aromatic system and the selectivity: *Increase of the aromatic system increases selectivity towards that aromatic system.*

These experimental observations may be rationalized with the transition state cartoon shown in Figure 6, where π-π stacking interactions between the TCAP-derived acylpyridinium ion and the aromatic moiety of the attacking alcohol interact favourably through electrostatic as well as dispersion forces. This type of orientation may also provide an argument for the comparatively small dependence of selectivity factors *S* on the size of the acyl chloride reagent documented in Table 1.[17]

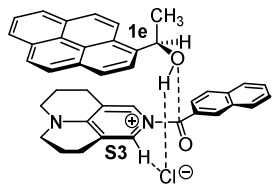

Figure 6 Proposed transition state structure causing high selectivity for alcohols carrying extended aromatic side chains

In conclusion, we have devised a system of aromatic carbonyl chlorides and TCAP (**4**), which react with high selectivity with an equimolar solution of two secondary alcohols favouring the one that contains the larger effective surface. For that purpose, we designed intermolecular competition experiments between pre-organized (aromatic) and unorganized (aliphatic) secondary alcohols with different acid chlorides. Catalytic amounts of TCAP (**4**) have a considerable impact on selectivity. The reaction conditions were examined, leading us to believe that temperature, concentration of auxiliary base NEt_3, and selection of solvent influence the selectivity to a minor degree. While the influence of the chain length of the aliphatic alcohol is neglibile, the size of the pre-organized alcohol towards the selectivity of the esterification reaction is significant. In situ ^1H NMR experiments of TCAP-activated acid chlorides in combination with X-ray structure analysis of TCAP·HCl are used to propose both a pyridinium acid chloride as selectivity selector and specific transition state interactions to explain the observed preferences. A combination of electronic effects on the aromatic alcohols with π-π stacking and dispersive interactions between the aromatic surface of the alcohols and the pyridinium moiety of the TCAP-acid chloride adducts are proposed to explain the different selectivities achieved in favor of the more sizable (pre-organized) alcohols. According to this, a combination of new, larger pyridine-derived catalysts and more sizable alcohols is expected to react with even higher selectivity. Further investigations, both experimental and theoretical aiming at full elucidation of the results described here are currently ongoing.

^{1}H NMR spectra were recorded in $CDCl_3$ 400 MHz or 600 MHz. ^{13}C NMR spectra were recorded in $CDCl_3$ at 101 MHz or 151 MHz. The chemical shifts are expressed in ppm, relative to $CHCl_3$ at δ = 7.26 for ^{1}H, while the chemical shifts for ^{13}C are reported relative to the resonance of $CDCl_3$ at δ = 77.1. Spectra were imported and processed in the MestreNova 10.0.2 program. Melting points are uncorrected.

Dodecan-2-ol (**1a**), 1-(1-napthyl)ethanol (**1b**), pentan-2-ol (**1c**), 1phenylethanol (**1d**), acetyl chloride (**2b**), phenylacetyl chloride (**2c**), diphenylacetyl chloride (**2e**), benzoyl chloride (**2a**), 1-naphthoyl chloride (**2f**), 2-naphthoyl chloride (**2g**), and 9-azajulolidine (**4**) were purchased from Sigma Aldrich or TCI and used without further purification.

The ester compounds 1-(naphthalen-1-yl)ethyl acetate (**3bb**),[18] 1-(naphthalen-1-yl)ethyl 2-phenylacetate (**3bc**),[19] 1-(naphthalen-1yl)ethyl 2,2-diphenylacetate (**3be**),[20] 1-(naphthalen-1-yl)ethyl benzoate (**3ba**),[21] 1-(naphthalen-1-yl)ethyl 2-naphthoate (**3bg**),[22] and 1(phenalen-1-yl)ethyl 2-napthoate (**3dg**)[23] are already known. Published analytical data match with the compounds observed by us.

1-(1-Pyrenyl)ethanol (1e)

To a solution of 1-pyrenaldehyde (2.46 g, 10.7 mmol) in anhyd THF (30 mL) was added a 3 M solution of MeMgBr in THF (8 mL, 14 mmol) under N_2. The reaction mixture was stirred at r.t. for 2 h. Then sat. aq NH_4Cl (10 mL) was added and the resulting mixture was extracted with CH_2Cl_2 (2 × 30 mL). The combined organic layers were washed with brine (2 × 20 mL) and dried (anhyd $MgSO_4$). After removal of the solvents at reduced pressure, the resulting solid was recrystallized from *n*-hexane to give **1e** as white prisms in 85% yield (2.27 g, 9.15 mmol).

^{1}H NMR ($CDCl_3$, 400 MHz): δ = 8.32 (d, *J* = 9.3 Hz, 1 H, ArH), 8.22 (d, *J* = 8.0 Hz, 1 H, ArH), 8.18 (d, *J* = 7.2 Hz, 3 H, ArH), 8.09 (d, *J* = 9.3 Hz, 1 H, ArH), 8.04 (s, 2 H, ArH), 8.0 (t, *J* = 7.6 Hz, 3 H, ArH), 5.96 (q, *J* = 6.4 Hz, 1 H, OC*H*CH_3), 2.15 (s, 1 H, OH), 1.77 (d, *J* = 6.4 Hz, 1 H, CH_3).

^{13}C NMR ($CDCl_3$, 101 MHz): δ = 139.07 (s), 131.37 (s), 130.64 (s), 130.62 (s) , 127.62 (CH), 127.48 (CH), 127.23 (s), 127.19 (CH), 125.94 (CH), 125.24 (CH), 125.12 (CH),125.03 (CH), 124.91 (s), 124.83 (s), 122.547 (CH), 122.40 (CH), 67.34 (CH), 25.08 (CH_3).

HRMS (EI): *m/z* calcd for $C_{18}H_{14}O$: 246.1045; found: 246.1040.

2-(Naphthalen-1-yl)acetyl Chloride (2d)

2-(Naphthalen-1-yl)acetic acid (5 g, 26.8 mmol) was suspended in methyl *tert*-butyl ether (10 mL) under N_2 atmosphere. To this suspension was added $SOCl_2$ (5.9 mL, 80.6 mmol) and the resulting clear solution was stirred at r.t. for 3 h. The excess of $SOCl_2$ was removed in vacuo and the crude product was purified by bulb-to-bulb distillation (160 °C, 3.8 × 10^{-1} mbar) to afford the acid chloride **2d** in 60% yield (3.674 g, 19.3 mmol) as a yellow oil.

^{1}H NMR ($CDCl_3$, 400 MHz): δ = 7.96–7.85 (m, 3 H, ArH), 7.58 (m, 2 H, ArH), 7.52–7.41 (m, 2 H, ArH), 4.59 (s, 2 H, CH_2).

^{13}C NMR ($CDCl_3$, 101 MHz): δ = 172.00 (s, C=O), 133.96 (s), 131.77 (s), 129.41 (CH), 129.12 (CH), 128.97 (CH), 128.01 (s), 127.11 (CH), 126.30 (CH), 125.58 (CH), 123.29 (CH), 50.98 (CH_2).

HRMS (EI): *m/z* calcd for $C_{12}H_9ClO$ 204.0342; found: 204.0331.

Anal. Calcd for $C_{12}H_9ClO$ (204.65): C, 70.43; H, 4.43; Cl, 17.32. Found: C, 70.20; H, 4.41; Cl, 17.34.

9-Anthracenoyl Chloride (2h)

Anthracene-9-carboxylic acid (4 g, 18 mmol) was suspended in $SOCl_2$ (12 mL, 165 mmol) and DMF (0.5 mL) under N_2. The reaction mixture turned into a clear solution after stirring for 5 min at r.t., which was continued for a total of 20 min followed by removal of all liquids in vacuo. The resulting crude product was recrystallized from boiling isohexane to give the chloride **2h** in 66% yield (2.86 g, 11.9 mmol) in the form of yellow needles; mp 98–101 °C. For X-ray crystal structure, see SI.

^{1}H NMR ($CDCl_3$, 400 MHz): δ = 8.51 (s, 1 H), 8.13 (dd, *J* = 8.8, 0.8 Hz, 2 H), 7.99 (d, *J* = 8.5 Hz, 2 H), 7.65–7.57 (m, 2 H), 7.51 (ddd, *J* = 7.7, 6.6, 0.9 Hz, 2 H).

^{13}C NMR ($CDCl_3$, 101 MHz): δ = 170.66 (s, C=O), 131.70 (s), 130.78 (s), 130.73 (s), 128.86 (CH), 128.04 (CH), 126.25 (s), 125.96 (CH), 123.99 (CH).

HRMS (EI): *m/z* calcd for $C_{15}H_9ClO$: 240.0342; found: 240.0336.

Anal. Calcd for $C_{15}H_9ClO$ (240.69): C, 74.85; H, 3.77. Found: C, 75.09; H, 3.90.

Dodecan-2-yl Acetate (3ab) and Dodecan-2-yl 3-Oxobutanoate (7b)

Dodecan-2-ol (**1a**; 0.70 g 3.76 mmol) and Et_3N (0.61 mL, 4.37 mmol) were dissolved in $CHCl_3$ (10 mL) under N_2. Then, AcCl (0.295 mL, 3.76 mmol) was added and the mixture was stirred at r.t. for 3 d. Salts were precipitated by addition of THF (50 mL) and filtered off. The crude product mixture was purified by repeated column chromatography on silica gel by using a mixture of CH_2Cl_2/isohexane (0:1 → 2:1 v/v) as eluent.

3ab

Yield: 0.182 g (0.80 mmol, 21%); colorless oil.

^{1}H NMR ($CDCl_3$, 400 MHz): δ = 4.84–4.78 (m, 1 H, OC*H*CH_3), 1.96 (s, 3 H, $COCH_3$), 1.53–1.46 (m, 1 H, CHC*H*HCH_2), 1.42–1.36 (m, 1 H, CHCH*H*CH_2), 1.23–1.19 (m, 16 H, 8 × CH_2), 1.13 (d, *J* = 8.4 Hz, 3 H, OCHC*H*$_3$), 0.81 (t, *J* = 8.4 Hz, 3 H, CH_2C*H*$_3$).

^{13}C NMR ($CDCl_3$, 101 MHz): δ = 170.83 (s, C=O), 71.10 (CH), 35.93 (CH_2), 31.92 (CH_2), 29.62 (CH_2), 29.59 (CH_2), 29.55 (CH_2), 29.47 (CH_2), 29.35 (CH_2), 29.34 (CH_2), 25.43 (CH_2), 22.70 (CH_2), 21.43 (CH_3), 19.98 (CH_3), 14.14 (CH_3).

HRMS (EI): *m/z* calcd for $C_{14}H_{27}O$ (M – OH): 211.2062; found: 211.2054; *m/z* calcd for $C_{12}H_{25}O$ (M – $COCH_3$): 185.1905; found: 185.1899.

Anal. Calcd for $C_{14}H_{28}O_2$ (228): C, 73.63; H, 12.36. Found: C, 73.49; H, 12.24.

7b

Yield: 0.235 g (0.87 mmol, 23%); colorless oil

^{1}H NMR ($CDCl_3$, 400 MHz): δ = 2.19 [s, 1 H, OH (t)], 4.99–4.94 (m, 1 H, OC*H*CH_3), 3.42 (s, 2 H, COC*H*$_2$CO), 2.26 (s, 3 H, $COCH_3$), 1.94 [s, 1 H, CH_3 (t)] 1.62–1.56 (m, 1 H, CHC*H*HCH_2), 1.51–1.44 (m, 1 H, CHCH*H*CH_2), 1.25–1.22 (m, 19 H, 8 × CH_2 and OCHC*H*$_3$), 0.88 (t, *J* = 8.4 Hz, 3 H, CH_2C*H*$_3$).

This compound presents keto-enol tautomerism and 't' means: signals associated to the enol tautomer of **7b**.

^{13}C NMR ($CDCl_3$, 101 MHz): δ = 200.75 (s, C=O), 166.79 (s, C=O), 72.50 (CH), 50.54 (CH_2), 35.79 (CH_2), 31.91 (CH_2), 30.12 (CH_2), 29.60 (CH_2), 29.58 (CH_2), 29.53 (CH_2), 29.42 (CH_2), 29.34 (CH_2), 25.35 (CH_2), 22.70 (CH_3), 19.86 (CH_3), 14.14 (CH_3).

MS (EI): *m/z* calcd for $C_{16}H_{30}O_3$: 270.22; found: 270.30 (M^+), 185.22 (M – $COCH_2COCH_3$).

Anal. Calcd for $C_{16}H_{30}O_3$ (270): C, 71.07; H, 11.18. Found: C, 71.17; H, 11.57.

1-(Naphthalen-1-yl)ethyl Anthracene-9-carboxylate (3bh)

1-(1-Naphthyl)ethanol (**1b**; 0.3 g 1.74 mmol) and 9-anthracenoyl chloride (**2h**; 0.419 g 1.74 mmol) were suspended in Et_3N (0.36 mL, 2.6 mmol) and toluene (1 mL) under N_2 and stirred at r.t. for 22 h. After the addition of acetone (4 mL), the resulting yellow suspension was filtered and the residue was washed with an additional amount of acetone (6 mL). All solvents contained in the filtrate were evaporated and the crude product was recrystallized from acetone/$CHCl_3$ (3 mL, 2:1, v/v) to provide the ester **3bh** in 39% yield (0.253 g, 0.67 mmol) in the form of pale yellow crystals; mp 104–106 °C.

^{1}H NMR ($CDCl_3$, 400 MHz): δ = 8.53 (s, 1 H, ArH), 8.33 (d, *J* = 8.4 Hz, 1 H, ArH), 8.03–8.00 (m, 4 H, ArH), 7.94 (d, *J* = 8 Hz, 1 H, ArH), 7.86 (d, *J* = 8.4 Hz, 1 H, ArH), 7.71 (d, *J* = 7.2 Hz, 1 H, ArH), 7.63 (t, *J* = 7.2 Hz, 1 H, ArH), 7.56 (t, *J* = 7.6 Hz, 1 H, ArH), 7.49–7.44 (m, 5 H), 7.32 (q, *J* = 6.8 Hz, 1 H, OC*H*CH_3), 2.01 (d, *J* = 6.4 Hz, 1 H, CH_3).

^{13}C NMR ($CDCl_3$, 101 MHz): δ = 169.17 (s, C=O), 137.16 (s, CH), 134.00 (s, CH), 131.10 (s, CH), 130.35 (s, CH), 129.37 (s, CH), 129.14 (s, CH), 128.81 (s, CH), 128.71 (s, CH), 128.48 (s, CH), 128.10 (s, CH), 127.00 (s, CH), 126.61 (s, CH), 125.95 (s, CH), 125.57 (s, CH), 125.13 (s, CH), 123.83 (s, CH), 123.34 (s, CH), 71.05 (O*C*HCH_3), 22.37 (CH_3).

HRMS (EI): *m/z* calcd for $C_{27}H_{20}O_2$: 376.1463; found: 376.1456.

Esters 3; General Procedures

General Procedure A

To a solution of selected alcohol **1** (1.6 mmol) in anhyd toluene (5 mL) was added Et_3N (0.3 mL, 2 mmol) under N_2. The corresponding acid chloride **2** (1.7 mmol) was added to the reaction mixture and stirred at 60 °C for 24–30 h. Then, the crude reaction mixture was filtered through a thin pad of silica gel (1 cm^3) and washed with acetone (6 mL). All solvents were removed under reduced pressure and the crude product was purified by column chromatography on silica gel with a mixture of isohexane/EtOAc (9:1 v/v) as eluent.

General Procedure B

To a solution of selected alcohol **1** (1.6 mmol) in anhyd toluene (5 mL) was added Et_3N (0.3 mL, 2 mmol) under N_2. The corresponding acid chloride **2** (1.7 mmol) was added to the reaction mixture and stirred at r.t. overnight. Then, the crude reaction mixture was filtered through a thin pad of silica gel (1 cm^3) washing with acetone (6 mL). All solvents were removed under reduced pressure and the crude product was purified by column chromatography on silica gel with a mixture of isohexane/EtOAc (9.5:0.5 v/v) as eluent.

General Procedure C

Selected alcohol **1** (2 mmol) and 1-naphthoyl chloride (**2f**) or 2-naphthoyl chloride (**2g**) (0.381 g, 2 mmol) were dissolved in a mixture of Et_3N (0.42 mL, 3 mmol) and anhyd toluene (1 mL) under N_2, and stirred at r.t. for 43 h. The solution was passed through a 1 cm plug of silica gel and washed with acetone (4 mL). The resulting crude product was purified by column chromatography on silica gel by using a mixture of CH_2Cl_2/isohexane (1:2 → 2:1 v/v) as eluent.

Ester 3ac

Prepared following GP B; yield: 0.365 g (1.2 mmol, 75%); colorless oil.

^{1}H NMR ($CDCl_3$, 400 MHz): δ = 7.27–7.18 (m, 5 H, ArH), 4.87–4.79 (m, 1 H, OC*H*CH_3), 3.52 (s, 2 H, C*H*$_2$Ar), 1.51–1.46 (m, 1 H, CHC*H*HCH_2), 1.40–1.35 (m, 1 H, CHCH*H*CH_2), 1.25–1.06 (m, 19 H, 8 × CH_2 and OCHC*H*$_3$), 0.81 (t, *J* = 8.0 Hz, 3 H, CH_2C*H*$_3$).

^{13}C NMR ($CDCl_3$, 101 MHz): δ = 171.29 (s, C=O), 134.39 (s), 129.20 (CH), 128.49 (CH), 126.95 (CH), 71.57 (CH), 41.83 (CH_2), 35.89 (CH_2), 31.93 (CH_2), 29.63 (CH_2), 29.57 (CH_2), 29.54 (CH_2), 29.41 (CH_2), 29.35 (CH_2), 25.31 (CH_2), 22.72 (CH_2), 19.95 (CH_3), 14.16 (CH_3).

HRMS (EI): *m/z* calcd for $C_{20}H_{32}O_2$: 304.2402; found: 304.2399

Anal. Calcd for $C_{20}H_{32}O_2$ (304.48): C, 78.9; H, 10.6. Found: C, 78.65; H, 10.57.

Ester 3bd

Prepared following GP B; yield: 0.470 g (1.3 mmol, 86%); yellow oil.

^{1}H NMR ($CDCl_3$, 400 MHz): δ = 7.97 (m, 2 H, ArH), 7.88–7.75 (m, 4 H, ArH), 7.50–7.33 (m, 8 H, ArH), 6.66 (q, *J* = 6.8 Hz, 1 H, OC*H*CH_3), 4.15 (s, 2 H, CH_2), 1.65 (d, *J* = 6.8 Hz, 1 H, CH_3).

^{13}C NMR NMR ($CDCl_3$, 151 MHz): δ = 170.87 (s, C=O), 137.10 (s), 133.76 (s), 133.75 (s), 132.12 (s), 130.58 (s), 130.17 (s), 128.83 (CH), 128.68 (CH), 128.42 (CH), 128.06 (CH), 128.04 (CH), 126.297 (CH), 126.21 (CH), 125.77 (CH), 125.61 (CH), 125.48 (CH), 125.25 (CH), 123.88 (CH), 123.28 (CH), 123.19 (CH), 70.28 (CH), 39.58 (CH_2), 21.59 (CH_3).

HRMS (EI): *m/z* calcd for $C_{24}H_{20}O_2$: 340.1463; found: 340.1457.

Anal. Calcd for $C_{24}H_{20}O_2$ (340.42): C, 84.7; H, 5.92. Found: C, 83.96; H, 6.01.

Ester 3ad

Prepared following GP B; yield: 0.540 g (1.54 mmol, 95%); colorless oil.

^{1}H NMR ($CDCl_3$, 600 MHz): δ = 8.04 (d, *J* = 9.6 Hz, 1 H, ArH), 7.87 (d, *J* = 8.4 Hz, 1 H, ArH), 7.80 (dd, *J* = 7.0, 2.5 Hz, 1 H, ArH), 7.54 (t, *J* = 8.4 Hz, 1 H, ArH), 7.50 (t, *J* = 8.1 Hz, 1 H, ArH), 7.46–7.42 (m, 2 H, ArH), 4.96– 4.89 (m, 1 H, OC*H*CH_3), 4.05 (s, 2 H, C*H*$_2$Ar), 1.57–1.49 (m, 1 H, CHC*H*HCH_2), 1.46–1.40 (m, 1 H, CHCH*H*CH_2), 1.36–1.12 (m, 19 H, 8 × CH_2 and OCHC*H*$_3$), 0.92 (t, *J* = 6.6 Hz, 3 H, CH_2C*H*$_3$).

^{13}C NMR ($CDCl_3$, 151 MHz): δ = 171.26 (s, C=O), 133.83 (s), 133.82 (s), 132.14 (s), 132.14 (s), 130.96 (s), 128.67 (s), 127.91 (CH), 127.90 (CH), 126.17 (CH), 125.69 (CH), 125.44 (CH), 123.90 (CH), 71.68 (CH), 39.67 (CH_2), 35.85 (CH_2), 31.95 (CH_2), 29.63 (CH_2), 29.55 (CH_2), 29.50 (CH_2), 29.37 (CH_2), 29.37 (CH_2), 29.35 (CH_2), 25.23 (CH_2), 22.72 (CH_2), 19.93 (CH_3), 14.15 (CH_3).

HRMS (EI): *m/z* calcd for $C_{24}H_{34}O_2$: 354.2559; found: 354.2553.

Anal. Calcd for $C_{24}H_{34}O_2$ (354.54): C, 81.3; H, 9.67. Found: C, 81.80; H, 9.74.

Ester 3ae

Prepared following GP B; yield: 0.550 g (1.45 mmol, 91%); colorless oil.

^{1}H H NMR ($CDCl_3$, 400 MHz): δ = 7.24–7.15 (m, 10 H, ArH), 4.92–4.87 (m, 1 H, OC*H*CH_3), 4.90 (s, 1 H, C*H*Ar), 1.51–1.45 (m, 1 H, CHC*H*HCH_2), 1.41–1.33 (m, 1 H, CHCH*H*CH_2), 1.25–1.05 (m, 19 H, 8 × CH_2 and OCHC*H*$_3$), 0.81 (t, *J* = 6.0 Hz, 3 H, CH_2C*H*$_3$).

^{13}C C NMR ($CDCl_3$, 101 MHz): δ = 172.12 (s, C=O), 138.90 (s), 138.88 (s), 128.64 (CH), 128.62 (CH), 128.52 (CH), 128.49 (CH), 127.14 (CH), 127.12 (CH), 71.97 (CH), 57.43 (CH), 35.83 (CH_2), 31.94 (CH_2), 29.64 (CH_2), 29.55 (CH_2), 29.52 (CH_2), 29.37 (CH_2), 29.36 (CH_2), 25.26 (CH_2), 22.73 (CH_2), 19.90 (CH_3), 14.16 (CH_3).

HRMS (EI): *m/z* calcd for $C_{26}H_{36}O_2$: 380.2715; found: 380.2704.

Anal. Calcd for $C_{26}H_{36}O_2$ (380.55): C, 82.06; H, 9.54. Found: C, 81.52; H, 9.54.

Ester 3aa

Prepared following GP A; yield: 0.319 g (1.10 mmol, 69%); colorless oil.

^{1}H NMR ($CDCl_3$, 600 MHz): δ = 8.05 (d, *J* = 6.4 Hz, 2 H, ArH), 7.54 (t, *J* = 6.4 Hz, 1 H, ArH), 7.43 (d, *J* = 6.4 Hz, 2 H, ArH), 5.18–5.13 (m, 1 H, OC*H*CH_3), 1.77–1.71 (m, 1 H, CHC*H*HCH_2), 1.64–1.58 (m, 1 H, CHCH*H*CH_2), 1.41–1.23 (m, 19 H, 8 × CH_2 and OCHC*H*$_3$), 0.88 (t, *J* = 6.0 Hz, 3 H, CH_2C*H*$_3$).

^{13}C NMR ($CDCl_3$, 151 MHz): δ = 166.19 (s, C=O), 132.63 (CH), 130.93 (s) , 129.48 (CH), 128.23 (CH), 71.73 (CH), 36.05 (CH_2), 31.88 (CH_2), 29.58 (CH_2), 29.56 (CH_2), 29.52 (CH_2), 29.48 (CH_2), 29.31 (CH_2), 25.42 (CH_2), 22.66 (CH_2), 20.07 (CH_3), 14.10 (CH_3).

HRMS (EI): *m/z* calcd for $C_{19}H_{30}O_2$: 290.2246; found: 290.2234.

Anal. Calcd for $C_{19}H_{30}O_2$ (290.45): C, 78.6; H, 10.41. Found: C, 77.51; H, 10.41.

Ester 3bf

Prepared following GP C; yield: 0.256 g (0.78 mmol, 45%); colorless oil.

^{1}H NMR ($CDCl_3$, 600 MHz): δ = 8.94 (d, *J* = 8.4 Hz, 1 H, ArH), 8.26 (t, *J* = 6.8 Hz, 1 H, ArH), 8.03 (d, *J* = 8.0 Hz, 1 H, ArH), 7.90 (t, *J* = 8.0 Hz, 1 H, ArH), 7.84 (t, *J* = 8.0 Hz, 1 H, ArH), 7.76 (d, *J* = 7.2 Hz, 1 H, ArH), 7.61– 7.48 (m, 6 H, ArH), 7.02 (q, *J* = 6.4 Hz, 1 H, OC*H*CH_3), 1.92 (d, *J* = 6.4 Hz, 1 H, CH_3).

^{13}C NMR ($CDCl_3$, 151 MHz): δ = 166.87 (s, C=O), 137.66 (s), 133.97 (s), 133.48 (CH), 131.52 (s), 130.41 (s), 130.31 (s), 129.06 (CH), 128.62 (CH), 128.60 (CH), 127.85 (CH), 127.42 (s), 126.52, 126.32 (CH), 125.92 (CH), 125.83 (CH), 125.55 (CH), 124.62 (CH), 123.39 (CH), 123.32 (CH), 70.31 (CH), 22.07 (CH_3).

HRMS (EI): *m/z* calcd for $C_{23}H_{18}O_2$: 326.1307; found: 326.1300.

Anal. Calcd for $C_{23}H_{18}O_2$ (326.40): C, 84.64; H, 5.56. Found: C, 84.54; H, 5.75.

Ester 3af

Prepared following GP A; yield: 0.424 g (1.24 mmol, 78%); colorless oil.

^{1}H NMR ($CDCl_3$, 600 MHz): δ = 8.92 (d, *J* = 6.4 Hz, 1 H, ArH), 8.17 (d, *J* = 6.4 Hz, 1 H, ArH), 8.01 (d, *J* = 6.4 Hz, 1 H, ArH), 7.88 (d, *J* = 6.4 Hz, 1 H, ArH), 7.62 (t, *J* = 6.4 Hz, 1 H, ArH), 7.54 (t, *J* = 6.4 Hz, 1 H, ArH), 7.50 (t, *J* = 12.0 Hz, 1 H, ArH), 5.34–5.27 (m, 1 H, OC*H*CH_3), 1.86–1.80 (m, 1 H, CHC*H*HCH_2), 1.70–1.64 (m, 1 H, CHCH*H*CH_2), 1.53–1.23 (m, 19 H, 8 × CH_2 and OCHC*H*$_3$), 0.89 (t, *J* = 6.0 Hz, 3 H, CH_2C*H*$_3$).

^{13}C NMR ($CDCl_3$, 151 MHz): δ = 167.28 (s, C=O), 133.84 (s), 132.96 (s), 131.33 (s), 129.76 (CH), 128.48 (CH), 128.06 (CH), 127.57 (CH), 126.11 (CH), 125.84 (CH), 124.48 (CH), 71.85 (CH), 36.14 (CH_2), 31.90 (CH_2), 29.61 (CH_2), 29.59 (CH_2), 29.56 (CH_2), 29.52 (CH_2), 29.34 (CH_2), 29.33 (CH_2), 25.56 (CH_2), 22.69 (CH_2), 20.15 (CH_3), 14.12 (CH_3).

HRMS (EI): *m/z* calcd for $C_{23}H_{32}O_2$: 340.2402; found: 340.2396.

Anal. Calcd for $C_{23}H_{32}O_2$ (340.51): C, 81.1; H, 9.47. Found: C, 80.53; H, 9.42.

Ester 3ag

Prepared following GP A; yield: 0.380 g (1.12 mmol, 70%); colorless oil.

^{1}H NMR ($CDCl_3$, 600 MHz): δ = 8.60 (s, 1 H, ArH), 8.17 (d, *J* = 6 Hz, 1 H, ArH), 8.06 (d, *J* = 7.2 Hz, 1 H, ArH), 7.96 (d, *J* = 8.0 Hz, 1 H, ArH), 7.88 (d, *J* = 8 Hz, 2 H, ArH), 7.58 (t, *J* = 7.2 Hz, 1 H, ArH), 7.54 (t, *J* = 5.6 Hz, 1 H, ArH), 5.24–5.19 (m, 1 H, OC*H*CH_3), 1.85–1.75 (m, 1 H, CHC*H*HCH_2), 1.70–1.64 (m, 1 H, CHCH*H*CH_2), 1.47–1.24 (m, 19 H, 8 × CH_2 and OCHC*H*$_3$), 0.87 (t, *J* = 6.4 Hz, 3 H, CH_2C*H*$_3$).

^{13}C NMR ($CDCl_3$, 151 MHz): δ = 166.47 (s), 135.50 (s), 132.57 (s), 130.91 (CH), 129.40 (CH), 128.24 (s), 128.16 (CH), 128.10 (CH), 127.82 (CH), 126.62 (CH), 125.39 (CH), 72.01 (CH), 36.19 (CH_2), 31.99 (CH_2), 29.69 (CH_2), 29.67 (CH_2), 29.63 (CH_2), 29.60 (CH_2), 29.42 (CH_2), 25.58 (CH_2), 22.77 (CH_2), 20.25 (CH_3), 14.22 (CH_3).

HRMS (EI): *m/z* calcd for $C_{23}H_{32}O_2$: 340.2402; found: 340.2390.

Ester 3ah

Prepared following GP B; yield: 0.330 g (0.84 mmol, 53%); colorless prisms; mp 75–77 °C.

^{1}H NMR ($CDCl_3$, 400 MHz): δ = 8.51 (s, 1 H, ArH), 8.03 (t, *J* = 8.8 Hz, 1 H, ArH), 7.56–7.47 (m, 4 H, ArH), 5.57–5.49 (m, 1 H, OC*H*CH_3), 1.88– 1.80 (m, 1 H, CHC*H*HCH_2), 1.74–1.65 (m, 1 H, CHCH*H*CH_2), 1.56 (d, *J* = 6 Hz, 1 H, ArH), 1.53–1.23 (m, 16 H, 8 × CH_2), 0.89 (t, *J* = 6.4 Hz, 3 H, CH_2C*H*$_3$).

^{13}C NMR ($CDCl_3$, 101 MHz): δ = 169.48 (s, C=O), 131.03 (s), 128.91 (s), 128.68 (s), 128.62 (CH), 128.14 (s), 126.82 (CH), 125.44 (CH), 124.91 (CH), 73.08 (CH), 36.09 (CH_2), 31.94 (CH_2), 29.66 (CH_2), 29.64 (CH_2), 29.62 (CH_2), 29.48 (CH_2), 29.48 (CH_2), 29.38 (CH_2), 25.68 (CH_2), 22.73 (CH_2), 20.37 (CH_3), 14.17 (CH_3).

HRMS (EI): *m/z* calcd for $C_{27}H_{34}O_2$: 390.2559; found: 390.2556.

Anal. Calcd for $C_{27}H_{34}O_2$ (390.57): C, 83.03; H, 8.77. Found: C, 82.66; H, 8.84.

Ester 3cf

Prepared following GP C; yield: 0.358 g (1.4 mmol, 70%); colorless oil.

^{1}H NMR ($CDCl_3$, 600 MHz): δ = 8.92 (d, *J* = 8.6 Hz, 1 H, ArH), 8.17 (d, *J* = 7.2 Hz, 1 H, ArH), 8.01 (d, *J* = 8.2 Hz, 1 H, ArH), 7.89 (d, *J* = 8.2 Hz, 2 H, ArH), 7.62 (t, *J* = 8.5 Hz, 1 H, ArH), 7.54 (t, *J* = 8.1 Hz, 1 H, ArH), 7.50 (t, *J* = 8.2 Hz, 1 H, ArH), 5.34–5.29 (m, 1 H, OC*H*CH_3), 1.83–1.79 (m, 1 H, CHC*H*HCH_2), 1.69–1.63 (m, 1 H, CHCH*H*CH_2), 1.55–1.45 (m, 4 H, 2 × CH_2), 1.40 (d, *J* = 6.4 Hz, 3 H, OCHC*H*$_3$), 0.98 (t, *J* = 7.4 Hz, 3 H, CH_2C*H*$_3$).

^{13}C NMR ($CDCl_3$, 151 MHz): δ = 167.28 (s, C=O), 133.84 (s), 132.99 (CH), 131.34 (s), 129.77 (CH), 128.49 (CH), 128.03 (s), 127.59 (CH), 126.12 (CH), 125.83 (CH), 124.49 (CH), 71.58 (CH), 38.29 (CH_2), 20.16 (CH_2), 18.83 (CH_3), 14.01 (CH_3).

HRMS (EI): *m/z* calcd for $C_{16}H_{18}O_2$: 242.1307; found: 242.1300.

Anal. Calcd for $C_{16}H_{18}O_2$ (242.32): C, 79.31; H, 7.49. Found: C, 79.18; H, 7.38.

Ester 3cg

Prepared following GP C; yield: 0.349 g (1.36 mmol, 68%); colorless oil.

^{1}H NMR ($CDCl_3$, 600 MHz): δ = 8.61 (s, 1 H, ArH), 8.09 (dd, *J* = 8.6, 1.7 Hz, 1 H, ArH), 7.96 (d, *J* = 8.06, 1.7 Hz, 1 H, ArH), 7.88 (d, *J* = 8.06, 1.7 Hz, 2 H, ArH), 7.58 (td, *J* = 8.2, 6.8 Hz, 1 H, ArH), 7.54 (td, *J* = 8.2, 6.8 Hz, 1 H, ArH), 5.28–5.24 (m, 1 H, OC*H*CH_3), 1.84–1.77 (m, 1 H, CHC*H*HCH_2), 1.67–1.62 (m, 1 H, CHCH*H*CH_2), 1.47–1.24 (m, 4 H, 2 × CH_2), 1.40 (d, *J* = 6.3 Hz, 3 H, OCHC*H*$_3$), 0.98 (t, *J* = 7.4 Hz, 3 H, CH_2C*H*$_3$).

^{13}C NMR ($CDCl_3$, 151 MHz): δ = 166.37 (s, C=O), 135.44 (s), 132.51 (s), 130.81 (CH), 129.31 (CH), 128.17 (s), 128.06 (CH), 128.02 (CH), 127.73 (CH), 126.53 (CH), 125.30 (CH), 71.63 (CH), 38.28 (CH_2), 20.16 (CH_2), 18.76 (CH_3), 14.00 (CH_3).

HRMS (EI): *m/z* calcd for $C_{16}H_{18}O_2$: 242.1307; found: 242.1300.

Anal. Calcd for $C_{16}H_{18}O_2$ (242.32): C, 79.31; H, 7.49. Found: C, 79.07; H, 7.46.

Ester 3eg

Prepared following GP B; yield: 0.353 g (0.88 mmol, 55%); colorless prisms; mp 154–156 °C.

^{1}H NMR ($CDCl_3$, 400 MHz): δ = 8.72 (s, 1 H, ArH), 8.52 (d, *J* = 9.2 Hz, 1 H, ArH), 8.31 (d, *J* = 7.6 Hz, 1 H, ArH), 8.25–8.16 (m, 5 H, ArH), 8.01– 7.90 (m, 4 H, ArH), 7.89 (t, *J* = 6 Hz, 1 H, ArH), 7.61–7.53 (m, 2 H, ArH), 7.27 (d, *J* = 6.4 Hz, 1 H, OC*H*CH_3), 2.02 (td *J* = 6.4 Hz, 3 H, CH_3).

^{13}C NMR ($CDCl_3$, 101 MHz): δ = 166.25 (s, C=O), 135.67 (s), 135.28 (s), 132.59 (s), 131.42 (s), 131.31 (CH), 131.14 (s), 130.76 (s), 129.49 (CH), 128.37 (CH), 128.30 (CH), 128.17 (CH), 127.87 (CH), 127.79 (s), 127.78 (s) 127.63 (CH), 127.49 (CH), 126.75 (CH), 126.13(CH), 125.51 (CH), 125.45 (CH), 125.34 (CH), 125.19 (CH), 125.04 (s), 124.97 (s), 123.55 (CH), 122.64 (CH), 70.75 (CH), 22.73 (CH_3).

HRMS (EI): *m/z* calcd for $C_{29}H_{22}O_2$: 402.1620; found: [M – $C_{11}H_7O_2$] 229.18; [M + H – $C_{18}H_{13}$] 172.10.

9-Azajulolidine Hydrochloride (TCAP·HCl)

9-Azajulolidine (**4**; 0.130 g 0.74 mmol) was dissolved in aq 2 M HCl (3 mL). The reaction mixture was stirred for 20 min and then, the solvent was removed under vacuum. The crude product was recrystallized from hexane to give 9-azajulolidine hydrochloride in 96% yield (0.15 g, 0.71 mmol) as colorless prisms; mp >230 °C.

^{1}H NMR ($CDCl_3$, 400 MHz): δ = 14.74 (br s, 1 H, NH), 7.68 (d, *J* = 5.2 Hz, 2 H, ArH), 3.43 (t, *J* = 6.4 Hz, 4 H, NCH_2), 2.72 (t, *J* = 6.4 Hz, 4 H, 2 × C*H*$_2$Ar), 2.00 (q, *J* = 6.4 Hz, 4 H, NCH_2C*H*).

^{13}C NMR ($CDCl_3$, 101 MHz): δ = 152.21 (s), 135.08 (s), 115.99 (CH), 49.92 (CH_2), 24.06 (CH_2), 19.56 (CH_2).

Anal. Calcd for $C_{11}H_{15}ClN_2$ (210.69): C, 62.70; H, 7.18; N, 13.3. Found: C, 60.68; H, 7.31; N, 12.88.

Funding Information

This work was financially supported by the Deutsche Forschungsgemeinschaft (DFG) through the Priority Program 'Control of London Dispersion Interactions in Molecular Chemistry' (SPP 1087). Marta Marin-Luna thanks the 'Xunta de Galicia' for her contract (ED481B 2016/166-0).

Supporting Information

Supporting information for this article is available online at https://doi.org/10.1055/s-0036-1588854.

References

(1) (a) Grimme, S.; Huenerbein, R.; Ehrlich, S. *ChemPhysChem* **2011**, *12*, 158. (b) Grimme, S.; Schreiner, P. R. *Angew. Chem. Int. Ed.* **2011**, *50*, 12639. (c) Rösel, S.; Balestrieri, C.; Schreiner, P. R. *Chem. Sci.*, **2017**, *8*, 405.

(2) (a) Zong, G.; Barber, E.; Aljewari, H.; Zhou, J.; Hu, Z.; Du, Y.; Shi, W. Q. *J. Org. Chem.* **2015**, *80*, 9279. (b) Baran, P. S.; Maimone, T. J.; Richter, J. M. *Nature* **2007**, *446*, 404. (c) Koshimizu, M.; Nagatomo, M.; Inoue, M. *Angew. Chem., Int. Ed.* **2016**, *55*, 2493.

(3) (a) Haines, A. H.; *Adv. Carbohydr. Chem. Biochem.* **1976**, *33,* 11. (b) Nahmany, M.; Melman, A. *Org. Biomol Chem.* **2004**, *2*, 1563. (c) Afagh, N. A.; Yudin, A. K. *Angew. Chem., Int. Ed.* **2010**, *49*, 262.

(4) (a) Green, T. W.; Wuts, P. G. M., *Protective Groups in Organic Synthesis*; Wiley, **1999**. (b) Araki, S.; Kambe, S.; Kameda, K.; Hirashita, T. *Synthesis*, **2003**, *5*, 751.

(5) Tandon, R.; Unzner, T.; Nigst, T. A.; de Rycke, N.; Mayer, P.; Wendt, B.; David, O. R. P.; Zipse, H. *Chem. Eur. J.* **2013**, *19*, 6435.

(6) Ishishara, K.; Nakayama, M.; Ohara, S; Yamamoto, H. *Tetrahedron*, **2002**, *58*, 8179.
(7) (a) Inanaga, J.; Hirata, K.; Saeki, H.; Katsuki, T., Yamaguchi, M. *Bull. Chem. Soc. Jpn.*, **1979**, *52*, 1989. (b) Kawanami, Y.; Dainobu, Y.; Inanaga, J.; Katsuki, T.; Yamaguchi, M. *Bull. Chem. Soc. Jpn.* **1981**, *54*, 943.
(8) Shiina, I.; Kubota, M.; Oshiumi, H.;Hashizume, M. *J. Org. Chem.,* **2004**, *69*, 1822.
(9) Kagan, H. B.; Fiaud, J. C., *Top. Stereochem.* **1988**, *18*, 249.
(10) (a) Larsen, R. D.; Corley, E. G.; Davis, P.; Reider, P.J.; Grabowski, E. J. J. *J. Am. Chem. Soc*, **1989**, *111*, 7650. (b) Calter, M. A., Orr, R. K., Song, W. *Org. Lett.* **2003**, *5*, 4745.
(11) (a) Bayliss, M. A.; Homer, R. B.; Shepherd, M. J. *J.Chem. Soc., Chem. Commun*, **1990**, 305. (b) Ruff, F.; Farkas, Ö. *J. Phys. Org. Chem*, **2011**, *24*, 480.
(12) Lutz, V.; Glatthaar, J.; Würtele, C.; Serafin, M.; Hausmann, H.; Schreiner, P. R. *Chem. Eur. J*, **2009**, *15*, 8548.
(13) Vellalath, S.; Van K., N.; Romo, D. *Tetrahedron Lett*, **2015**, *56*, 3647.
(14) (a) Patschinski, P.; Zhang, C.; Zipse, H. *J. Org. Chem.* **2014**, *79*, 8348. (b) Patschinski, P.; Zipse, H. *Org. Lett.* **2015**, *17*, 1010.
(15) (a) Giese, B. *Angew. Chem. Int. Ed. Engl.* **1977** *16*, 125. (b) Eyring, H. *J. Chem. Phys.* **1935**, *3*, 107.
(16) These results are further confirmed by competition esterifications of **1b**, **1c** and **2f**, which give values identical to those of **1a**, **1b** and **2f** (see SI).
(17) A complementary explanation is brought up by the ^{1}H NMR shifts of the methine proton O*CH*CH_3 of the aromatic ethanols **1g**, **1h**, and **1k**. These shift more downfield the larger the aromatic system becomes (ca. 4.85 ppm, 5.65 ppm and 5.9 ppm under reaction conditions). Since the adjacent molecular environment is identical, this might hint at different electronic environments that could be caused by deshielding from magnetic anisotropy effects or inductive effects. This would imply selectivity driven by the reactivity difference in the employed alcohols.

Savile, C. K.; Kazlauskas, R. J. *J. Am. Chem. Soc.* **2005**, *127*, 12228.
Kim, J. M.; Pincock, J. A. *Can. J. Chem.* **1995**, *73*, 885.
Kano, T.; Sasaki, K.; Maruoka, K. *Org. Lett.* **2005**, *7*, 1347.
Iwata, T.; Miyake, Y.; Nishibayashi, Y.; Uemura, S. *J. Chem. Soc., Perkin Trans. 1* **2002**, *13*, 1548.
De Sarkar, S.; Biswas, A.; Song, C. H.; Studer, A. *Synthesis* **2011**, 1974.
Simeonov, S. P.; Simeonov, A. P.; Todorov, A. R.; Kurteva, V. B. *Am. J. Analyt. Chem.* **2010**, *1*, 1.

3.1. Supporting Information

For: *Chemoselectivity in Esterification Reactions – Size Matters After All*

3.1.1 Investigation of the Formation of TCAP-Acid Chloride Adducts.

Scheme S3: 1 shows the preparation of the TCAP-Acid chloride adduct **4x2a**,**f-g** from TCAP **4** and the acid chlorides **2a**,**f-g**.

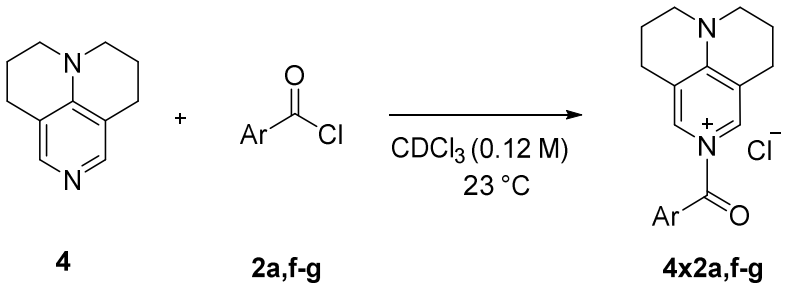

Scheme S3: 1. *[Scheme S1] General reaction scheme for the preparation of the TCAP-acid adducts* ***4x2a,f-g*** *from TCAP* ***4*** *and the acid chlorides* ***2a,f-g****.*

Four $CDCl_3$ stock solutions (ca 0.12 mol/L) containing TCAP **4**, benzoyl chloride **2a**, 1-napthoyl chloride **2f** and 2-napthoyl chloride **2g** were prepared in 2 mL calibrated flasks, which were dried in the oven at 110 °C for 12 h. 0.3 mL of both the TCAP stock solution and the selected acid chloride stock solution were transferred to a NMR-tube, which was previously dried under vacuum and flushed with nitrogen to remove the moisture. The NMR-tube was capped and turned upside down 3 – 5 times. Then, the ^{1}H NMR spectra of the three NMR-samples were measured at a 600 MHz NMR instrument. The resulting ^{1}H NMR spectra are shown in **Figure S3: 1 – Figure S3: 1**. Only the example involving benzoyl chloride **2i** will be discussed here since the results are similar for all investigated adducts.

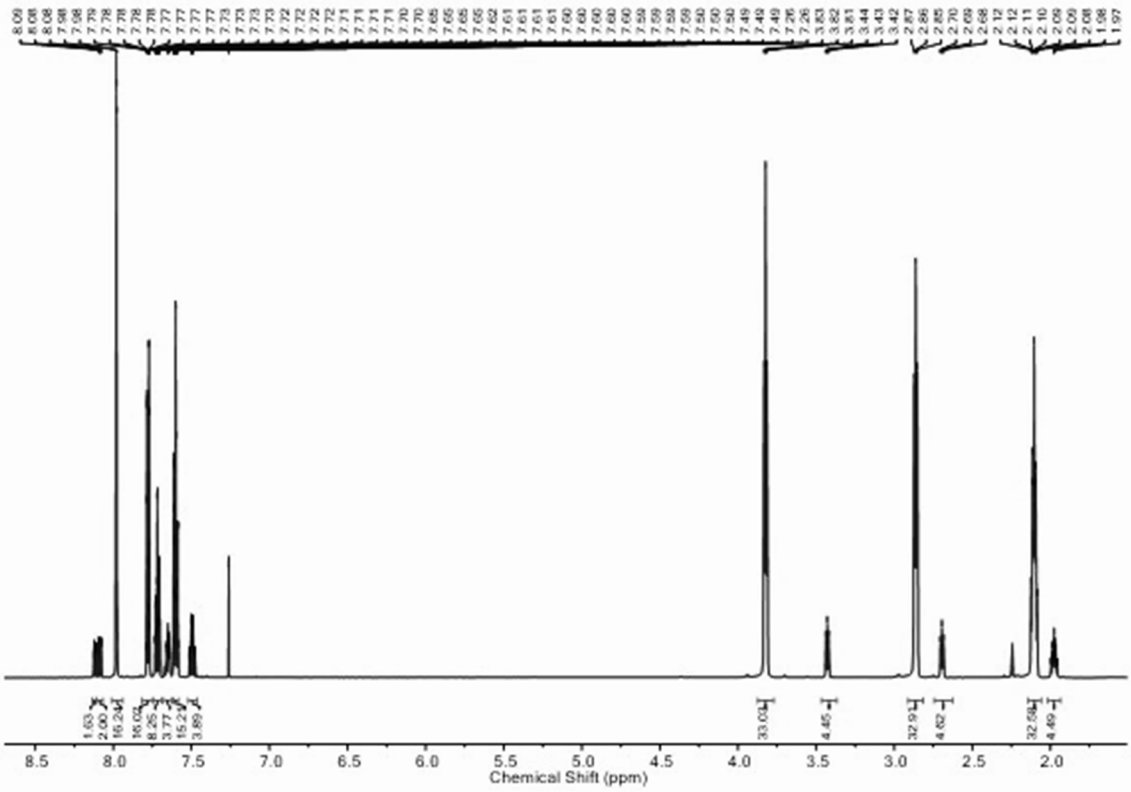

Figure S3: 1. *[Figure S1] ^{1}H NMR spectrum of the reaction of TCAP **4** with benzoyl chloride **2a** (600 MHz, $CDCl_3$).*

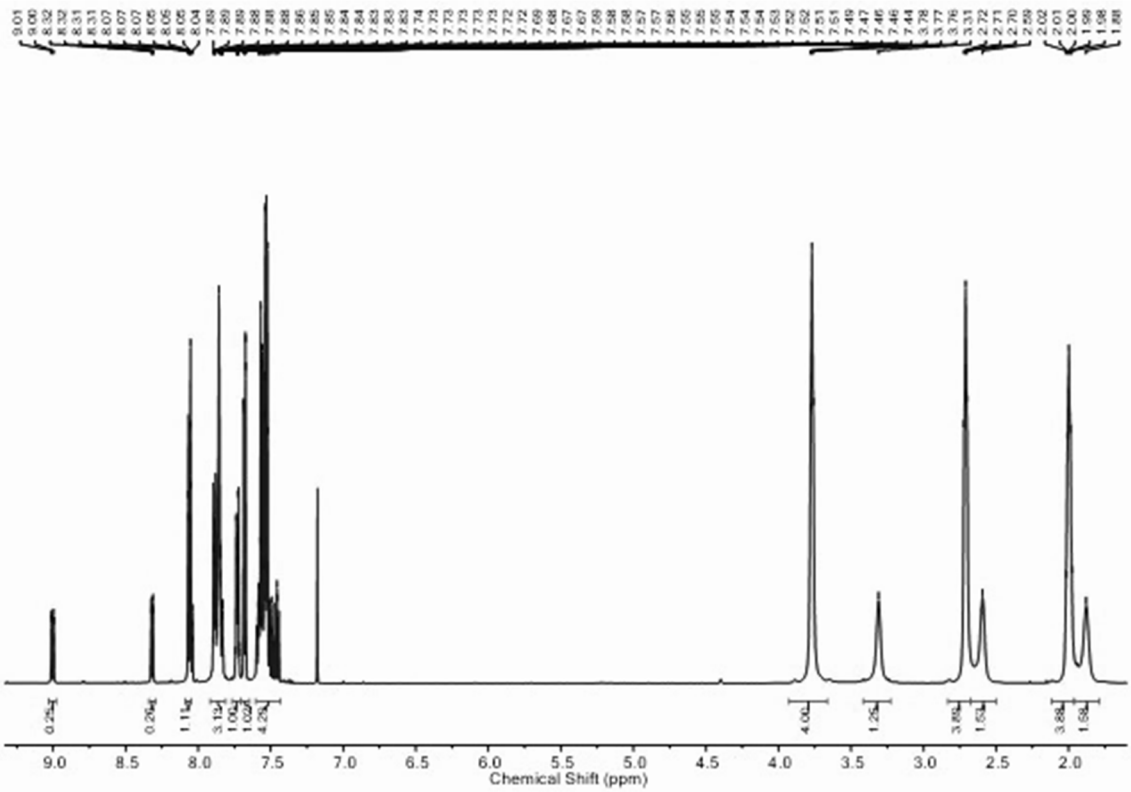

Figure S3: 2. *[Figure S2] ^{1}H NMR spectrum of the reaction of TCAP **4** with 1-napthoyl chloride **2f** (600 MHz, $CDCl_3$).*

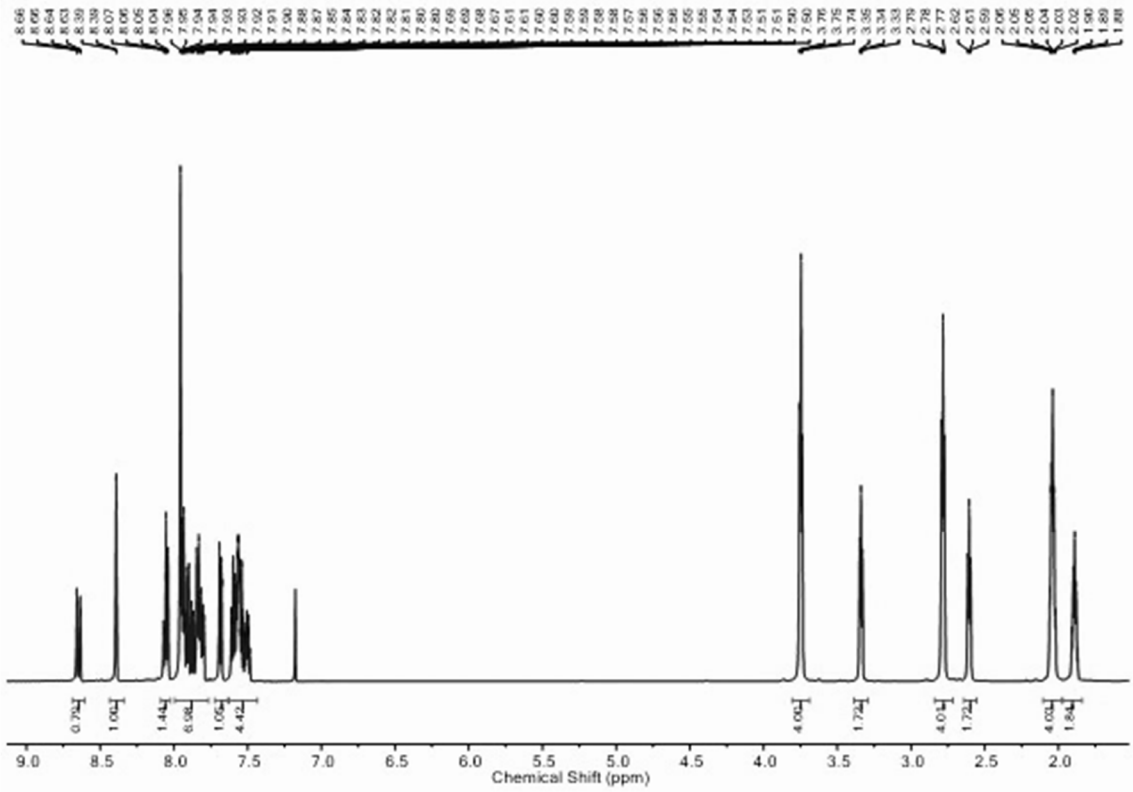

Figure S3: 3. *[Figure S3] ^{1}H NMR spectrum of the reaction of TCAP **4** with 2-napthoyl chloride **2g** (600 MHz, $CDCl_3$).*

As the ^{1}H NMR spectrum shows (**Figure S3: 1**), the reaction of TCAP **4** with benzoyl chloride **2a** in $CDCl_3$, at room temperature, lead to a mixture of two products in a ratio 70:30. We assumed that major intensity signals are associated to the expected TCAP-Acid chloride adduct **4x2a**. When this ^{1}H NMR spectrum and that of TCAP **4** are compared, it is clear that aromatic, as well as aliphatic proton signals of TCAP appear at higher chemical shift than those of the isolated TCAP **4** (see **Figure S3: 4**). For instance, the aromatic hydrogen atom H_A exhibits at chemical shift of 7.78 ppm in the TCAP ^{1}H NMR spectrum while that same proton resonance at 8.00 ppm in ^{1}H NMR spectrum of the adduct. The hydrogen atom H_B shows the largest chemical shift difference from 3.2 ppm at the TCAP ^{1}H NMR spectrum to 3.83 ppm in the TCAP adduct **4x2a**, mostly due to the influence of the amine-imine resonance forms present in the adduct. The hydrogen atoms H_C and H_D shift for about 0.5 ppm. Related to the benzoyl chloride moiety, the hydrogen atoms of the phenyl ring resonance at different chemical shift in the TCAP-adduct **4x2a** than in the benzoyl chloride **2a** (see **Figure S3: 5**). Of interest is also the chemical shift of the *ortho* hydrogen atoms from 8.10 ppm in the free benzoyl chloride **2a** to 7.77 ppm in the TCAP-adduct. These ^{1}H NMR spectra compilations indicate that free TCAP **4** and benzoyl chloride **2a** are complete gone and the resulting products are a combination of products of both.

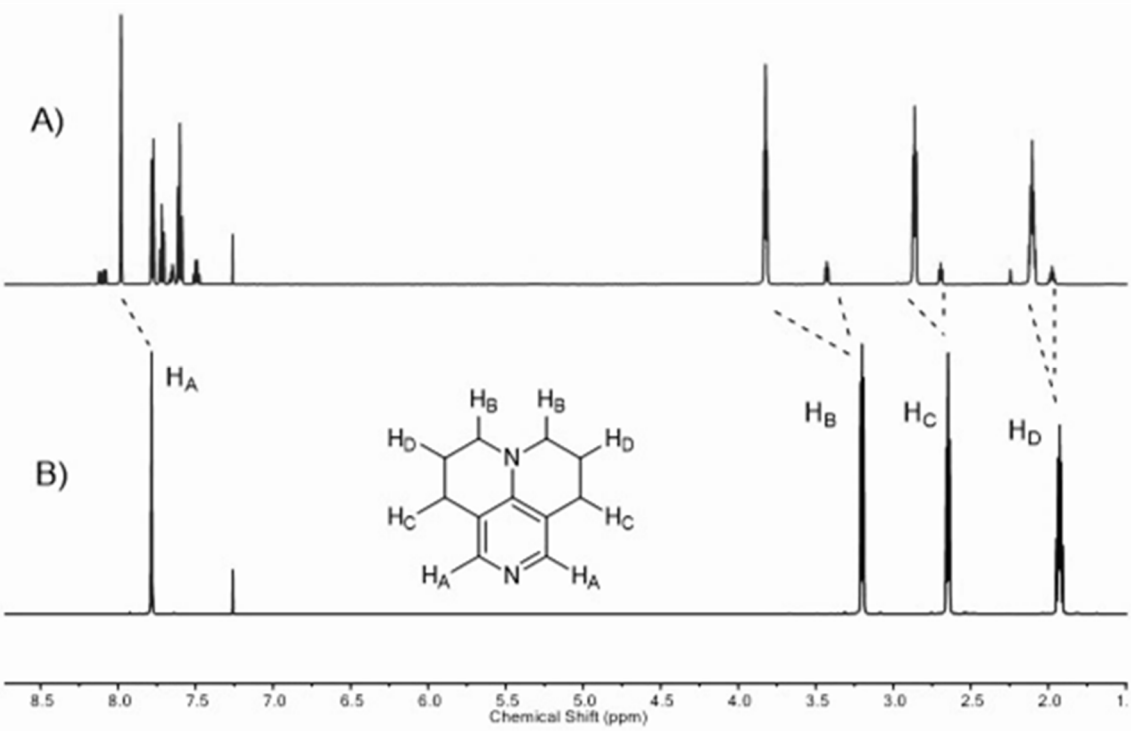

***Figure S3: 4**. [Figure S4] Compilation of ^{1}H NMR spectra of TCAP **4** (B) and TCAP-Benzoyl chloride adduct **4x2a** (A) (600 MHz, $CDCl_3$). The assignment of TCAP protons is shown.*

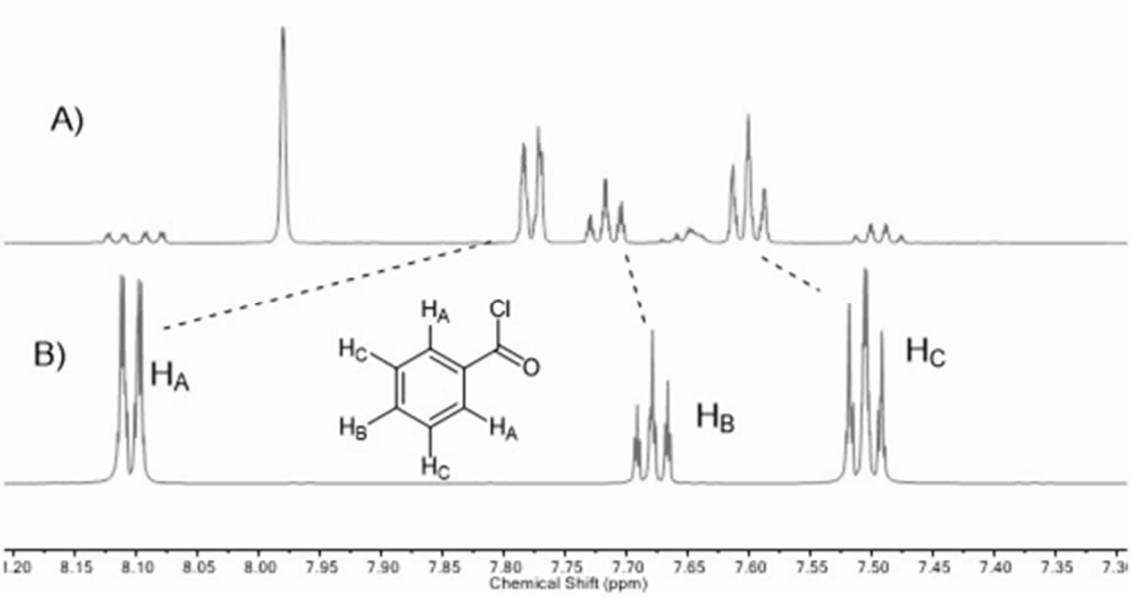

***Figure S3: 5.** [Figure S5] Comparation of ^{1}H NMR spectra of benzoyl chloride **2a** (B) and TCAP-benzoylchloride adduct **4x2a** (A) (600 MHz, $CDCl_3$). The assignment of the hydrogen atoms of the benzoyl chloride **2a** is shown.*

In order to figure out which compound is forming along with the TCAP-adduct **4x2a**, some further investigations were carried out. The TCAP compound is easily protonated and because of that we reasoned that **TCAPxHCl** could be formed during the reaction. Thus, **TCAPxHCl** was synthesized and its ^{1}H NMR spectrum recorded (**Figure S3: 6**). We were able to grow crystals of **TCAPxHCl** and they were measured by Ray-X diffraction (see Crystal Structure Data section). Interestingly, in the **TCAPxHCl** X-ray structure the

chlorine is interacting with one *ortho* aromatic proton (see **Figure S3: 90**). In addition, the complex **TCAPxBzCO$_2$H** was prepared by following the protocol described for the formation of the TCAP-adducts **4x2** (For ^{1}H NMR see **Figure S3: 7**).

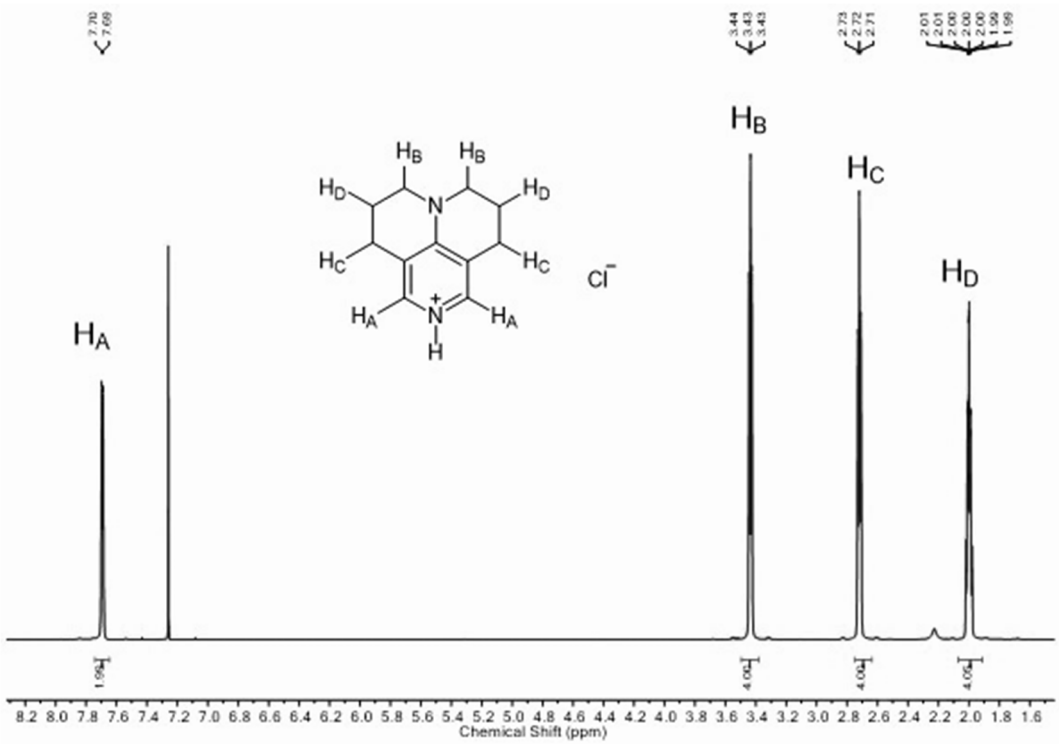

Figure S3: 6. *[Figure S6] ^{1}H NMR spectrum of* ***TCAPxHCl*** *(600 MHz, $CDCl_3$). The assignment of the* ***TCAPxHCl*** *protons is shown.*

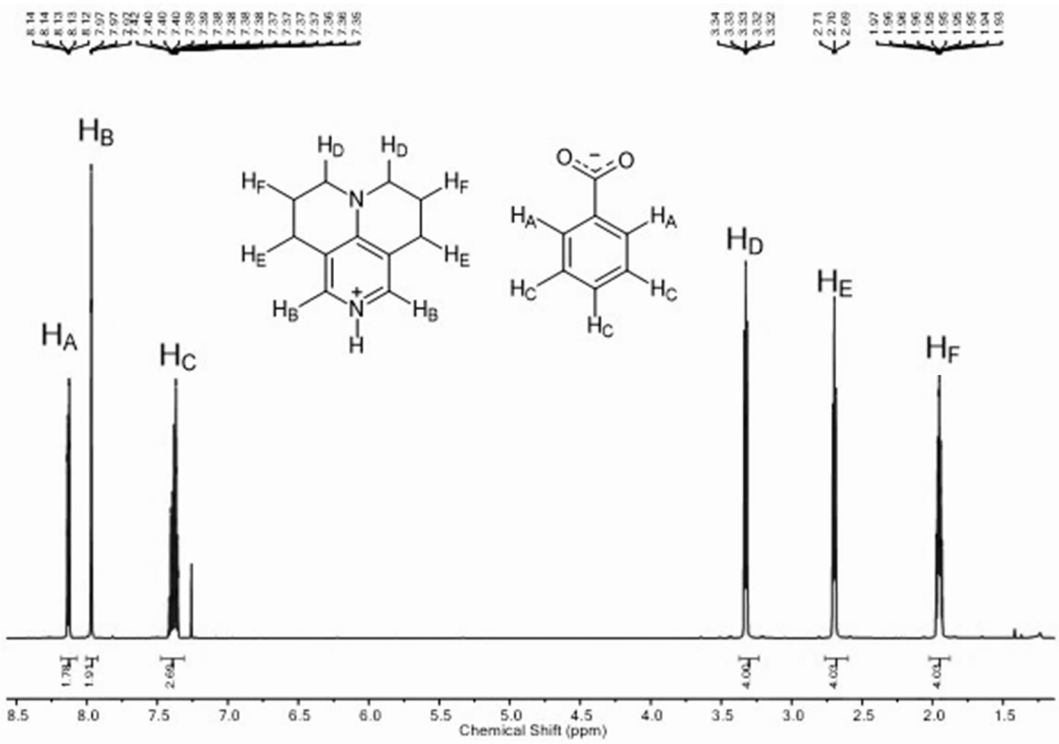

Figure S3: 7. *[Figure S7] ^{1}H NMR spectrum of* ***TCAPxBzCOOH*** *(600 MHz, $CDCl_3$). The assignment of the* ***TCAPxBzCOOH*** *protons is shown.*

By stacking of the TCAP-acid adduct **4x2a**, **TCAPxHCl** and **TCAPxBzCOOH** (**Figure S3: 8**), the signal sets of minor intensity could be assigned to a compound in equilibrium with the latter two. The minor proton signals in the aliphatic region well match with the average of those signals associated to the aliphatic hydrogen atoms of the protonated TCAP.

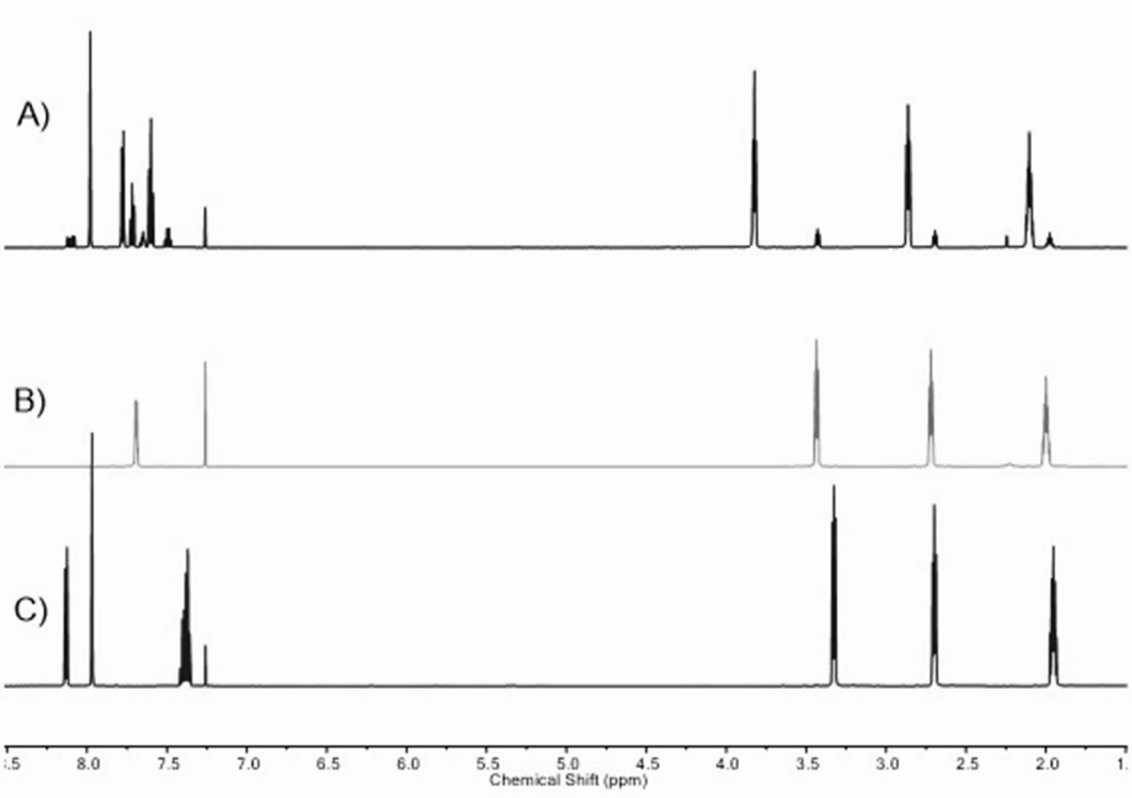

***Figure S3: 8**. [Figure S8] Comparison of ^{1}H NMR spectra of TCAP-Benzoyl chloride **4x2a** adduct (A) **TCAPxHCl** (B) and **TCAPxBzCOOH** (C) (600 MHz, $CDCl_3$).*

3.1.2 Competition Experiments

Technical details: All the experimental equipment, including calibrated flasks, magnetic stirring bars, gas chromatography vials (GC-vials) and NMR-tubes, was dried on the oven for at least 12h. $CDCl_3$ and Et_3N were freshly distilled under N_2 from CaH_2 before use. Hamilton syringes were cleaned with acetone, dried under vacuum, and flushed with nitrogen prior to every use. A GC-vial holder (Shimadzu 221-44998-91), which was placed on a magnetic stirrer was connected to the coolant circuit of a cryostat maintaining 23 °C constantly. The speed of stirring was fixed at 750 rpm for all the experiments described in this study.

Stock solutions preparation: A guideline to follow the preparation of the Stock solutions of a representative competition experiment is provided here.

Representative Example:

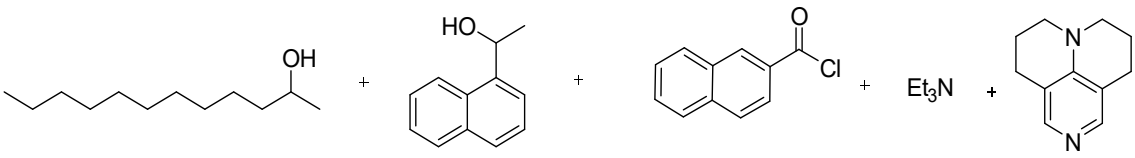

1a **1b** **2g** **4**

Temperature Control: 23 °C.

Four stock solutions in $CDCl_3$ are prepared under nitrogen. Stock A contains the secondary alcohols **1a** and **1b** having a concentration of 0.3 M each, and hexamethyldisilane **HMDS** which acts as internal standard (ca 0.1 M). Stock B gathers 2-napthoyl chloride **2g** (ca 0.6 M) while Stock C consists of a 0.7 M Et_3N. The last stock solution, Stock D, contains the catalyst TCAP **4** in a concentration of 0.6 M.

Table S3: 1. [Table S1] Preparation of initial $CDCl_3$ stock solutions.

Stock	Compound	Molarity (mol/L)	Volume (mL)	n (mol)	M.W (g/mol)	Mass (g)
Stock A	**1a**	0.3	20	$6 \cdot 10^{-3}$	186.34	1.118
	1b	0.3	20	$6 \cdot 10^{-3}$	172.23	1.033
	HMDS	0.1	20	$2 \cdot 10^{-3}$	146.38	0.293
Stock B	**2g**	0.6	20	$12 \cdot 10^{-3}$	190.7	2.288
Stock C	**Et_3N**	0.7	20	$14 \cdot 10^{-3}$	101.19	1.4166
Stock D	**4**	0.6	2	$1.2 \cdot 10^{-3}$	174.2	0.209

[a] Hexamethyldisilane

Following these initial preparations, five diluted stock solutions of Stock B and of Stock C are prepared at selected concentrations as shown in **Table S3: 2**. The concentrations of these solutions have been fixed at 20, 35, 50, 65 and 80% of the initial Stock B and C. Portions of Stock D, in this case 0.15 mL, are added to every diluted stock solution of Et_3N

Thus, every single reaction is catalyzed by the same amount of TCAP **4** (7.5%) with regard to the sum of both alcohol substrates. Please note that the amount of TCAP used is changed depending on the settings of each experiment.

Table S3: 2. [Table S2] Preparation of diluted $CDCl_3$ Stocks of Stock B and C.

	Molarity (mol/L)	Vol[b] B/C (mL)	Volume (mL)
Stock B1 (20%) [a]	0.12	1	5
Stock B2 (35%) [a]	0.21	1.75	5
Stock B3 (50%) [a]	0.3	2.5	5
Stock B4 (65%) [a]	0.39	3.2	5
Stock B5 (80%) [a]	0.48	4	5
Stock C1 + Stock D (0.15 mL)	0.14	0.4	2
Stock C2 + Stock D (0.15 mL)	0.245	0.7	2
Stock C3 + Stock D (0.15 mL)	0.35	1	2
Stock C4 + Stock D (0.15 mL)	0.45	1.3	2
Stock C5 + Stock D (0.15 mL)	0.56	1.6	2

[a] Relative to Stock B; [b] Solution volume got from initial Stock B or C.

Methodology: Under nitrogen, 0.5 mL of Stock A, 0.5 mL of diluted Stock C1 and 0.5 mL of diluted Stock B1 are transferred to a GC-vial by use of a Hamilton syringe. Then, the GC-vial is capped under nitrogen and placed in the GC-vial holder with stirring.

Composition of each prepared GC-vial for one competition experiment:

Related to the Stock solution volume:

GC-vial 1: 0.5 mL Stock A; 0.5 mL Stock C1; 0.5 mL Stock B1; **GC-vial 2**: 0.5 mL Stock A; 0.5 mL Stock C2; 0.5 mL Stock B2; **GC-vial 3**: 0.5 mL Stock A; 0.5 mL Stock C3; 0.5 mL Stock B3; **GC-vial 4**: 0.5 mL Stock A; 0.5 mL Stock C4; 0.5 mL Stock B4; **GC-vial 5**: 0.5 mL Stock A; 0.5 mL Stock C5; 0.5 mL Stock B5.

Related to the molar concentration (mol/L) of each compound:

GC-vial 1: **1a** and **1b**: 0.1 , **HMDS**: 0.33 , **2i**: 0.04 , **Et_3N**: 0.05 , **4**: 0.015 ; **GC-vial 2**: **1a** and **1b**: 0.1 , **HMDS**: 0.33 , **2i**: 0.07 , **Et_3N**: 0.09 , **4**: 0.015 ; **GC-vial 3**: **1a** and **1b**: 0.1 , **HMDS**: 0.33 , **2i**: 0.1 , **Et_3N**: 0.12 , **4**: 0.015 ; **GC-vial 4: 1a** and **1b**: 0.1 , **HMDS**: 0.33 , **2i**: 0.13 , **Et_3N**: 0.15 , **4**: 0.015 ; **GC-vial 5: 1a** and **1b**: 0.1 , **HMDS**: 0.33 , **2i**: 0.16 , **Et_3N**: 0.19 , **4**: 0.015.

Preparation of NMR-samples: The competition experiment is considered finished when the reaction of **GC-vial 5** is over, since it is the reaction with the highest concentration of acid chloride. The reaction is monitored by ^{1}H NMR.

NMR tubes are dried under vacuum using a Schlenk-type apparatus and flushed with nitrogen three times to eliminate moisture. The GC-vials are placed in a Schlenk-flask and purged with nitrogen three times as well. Then, 0.6 mL of the solution contained in the GC-vial is transferred to the NMR-tube under nitrogen. The NMR-tube is then capped and sealed with parafilm.

3.1.3 Selectivity Curves: Simulation and Plotting

Using the COPASI[1] and Origin Pro 8[2] programs, the *S*-values for the competition experiments have been simulated. **Scheme S3: 2** shows the simplified mechanistic scheme used in Copasi, in which the *k* values have been modified in order to achieve the *S*-values. The values k_1, k_{-1} and k_3 have been used as constants: k_1 = 0.1 L·mol^{-1}·s^{-1}; k_{-1} = 0.001 L·mol^{-1} s^{-1}, k_3 = 0.1 L·mol^{-1} ·s^{-1} while k_{ester1} and k_{ester2} have been simulated. Please note that the selectivity curves could also be obtained by using a general scheme with an uncatalyzed reaction.

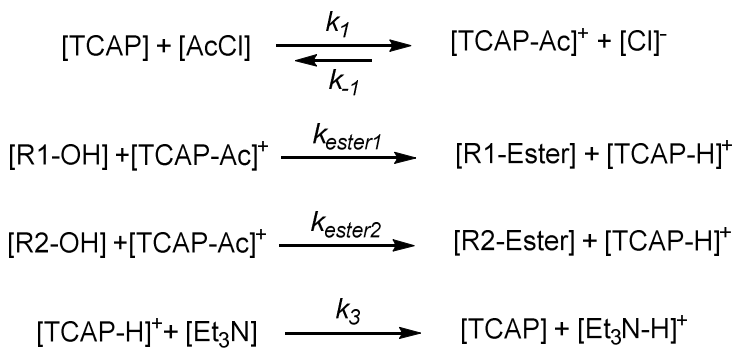

Scheme S3: 2. *[Scheme S2] Simplified mechanism used for simulating selectivity curves.*

The Selectivity factor *S* is given by Equation S3: 1:

$$Selectivity\ (S) = \frac{k_{ester1}}{k_{ester2}} \qquad \text{Eq. S3: 1}$$

Thus, with the data provided regarding concentrations of alcohols and esters during the course of the reaction, chemoselectivity and conversion terms are obtained by following Equations Eq. S3: 2 and Eq. S3: 3.

$$Chemoselectivity\ (C) = \frac{[R1\text{-}Ester]\text{-}[R2\text{-}Ester]}{[R1\text{-}Ester]+[R2\text{-}Ester]} \qquad \text{Eq. S3: 2}$$

$$Conversion\ [\%] = \left\{ \frac{[R1\text{-}Ester]\text{-}[R2\text{-}Ester]}{[R1\text{-}Ester]+[R2\text{-}Ester] + [R1\text{-}OH]+[R2\text{-}OH]} \right\} \times 100 \qquad \text{Eq. S3: 3}$$

The conversion is directly related to the amount of acid chloride, AcCl, used in the experiment. Therefore, 100% conversion means complete esterification of both alcohols.

Finally, the chemoselectivity vs conversion relationship is plotted by using the Origin Pro 8 software, obtaining curves that correspond to the simulated S-values (**Figure S3: 9**).

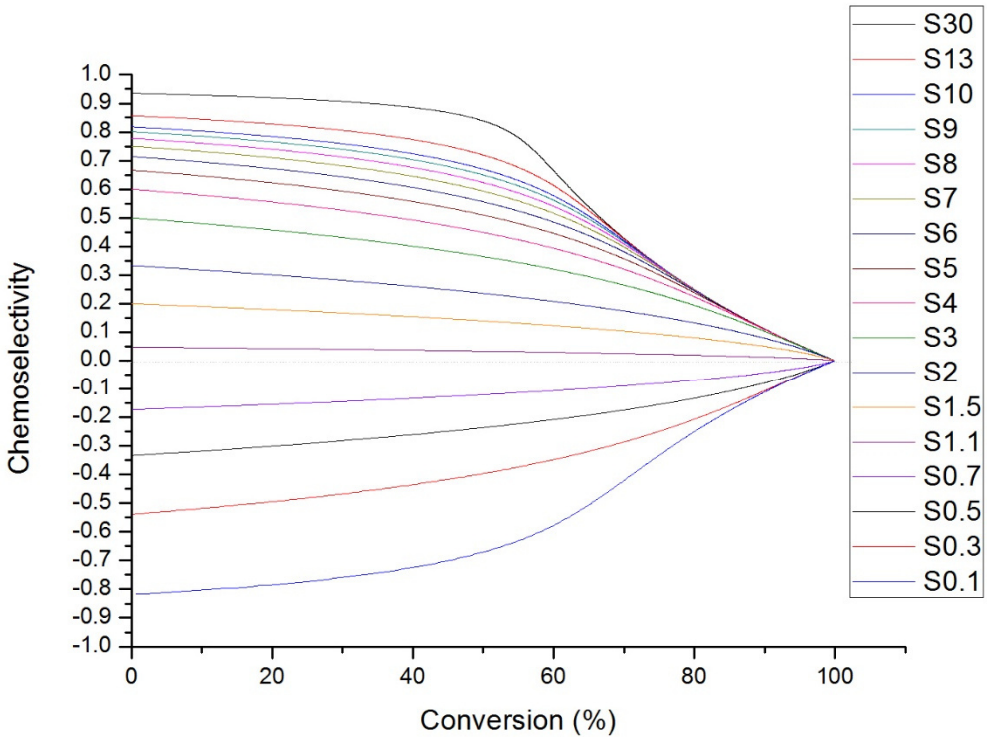

Figure S3: 9. *[Figure S9] Chemoselectivity vs Conversion relationship. Selectivity curves for competition experiments are shown.*

3.1.4 Chemoselectivity and Conversion Factors

As shown in the manuscript, the general equations for obtaining selectivity, chemoselectivity and conversion factors turn into Eq. S3: 4, Eq. S3: 5 and Eq. S3: 6, respectively, when they are applied directly to the alcohols and ester products involved in this work.

$$Selectivity\ (S) = \frac{k_2}{k_1} \qquad \text{Eq. S3: 4}$$

$$Chemoselectivity\ (C) = \frac{[3ba]-[3aa]}{[3ba]+[3aa]} \qquad \text{Eq. S3: 5}$$

$$Conversion\ [\%] = \left\{ \frac{[3ba]-[3aa]}{[3ba]+[3aa] + [1a]+[1b]} \right\} \times 100 \qquad \text{Eq. S3: 6}$$

These equations describe the particular case of the reaction involving both alcohols **1a** and **1b.** When other alcohols than **1a** and **1b** are involved in the experiment, the other alcohols replace **1a** and **1b** in the equations. For instance, in the competition experiment between alcohol substrates **1c** and **1b**, the selectivity is given by $S = k_2(1\mathbf{b})/k_1(\mathbf{1c})$, while if the experiment is performed with the alcohols **1a** and **1e**, $S = k_2(\mathbf{1e})/k_1(\mathbf{1a})$. These variations are extended to all the chemoselectivity and conversion equations.
In order to calculate chemoselectivity and conversion from integrals, Equations Eq. S3: 7 and Eq. S3: 8 are used. Integral values have been obtained from the chiral carbon proton signal of the alcohol substrates and the ester products (for detailed examples, see **Figure S3: 18** – **Figure S3: 49**).

$$Chemoselectivity\ (C) = \frac{I_{3ba} - I_{3aa}}{I_{3ba} + I_{3aa}} \qquad \text{Eq. S3: 7}$$

$$Conversion\ [\%] = \left\{ \frac{I_{3ba} + I_{3aa}}{I_{3ba} + I_{3aa} + I_{1a} + I_{1b}} \right\} \times 100 \qquad \text{Eq. S3: 8}$$

Table S3: 3 – **Table S3: 6** collect the chemoselectivity and conversion values of competition experiments described in this study, which are shown in Scheme **Scheme S3: 3** – **Scheme S3: 6**.

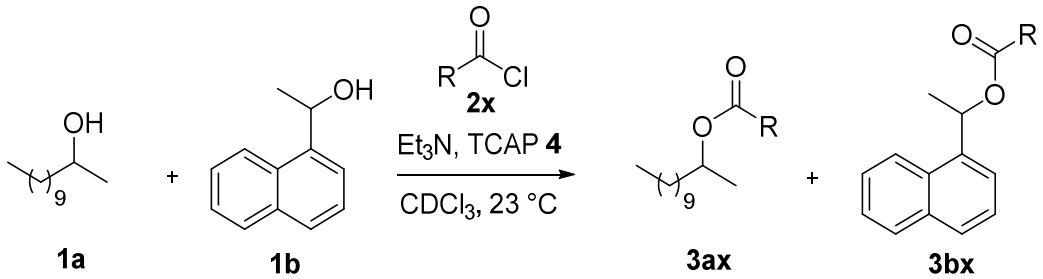

Scheme S3: 3. *[Scheme S3] Competition experiment between **1a** and **1b** with the acid chloride **2x** and TCAP **4** to give the ester compounds **3ax** and **3bx.***

Table S3: 3. [Table S3] Chemoselectivity and Conversion values of competition experiments shown in **Scheme S3: 3**. Selectivity values are shown.

		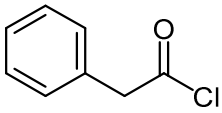		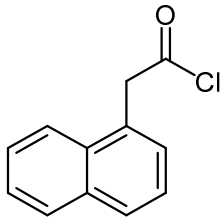		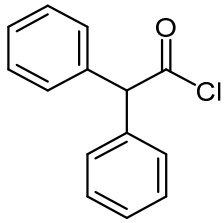	
S = 7		*S* = 3-4		*S* = 3-4		*S* = 6	
Chemosel	Conv. (%)	Chemosel.	Conv. (%)	Chemosel.	Conv. (%)	Chemosel.	Conv. (%)
0.702	18.15	0.542	20.24	0.571	14.17	0.667	18.64
0.665	29.85	0.482	31.39	0.498	33.92	0.645	32.11
0.587	45.58	0.430	42.27	0.423	47.26	0.589	46.41
0.504	60.08	0.366	53.87	0.359	59.25	0.487	61.12
0.491	61.37	0.323	60.66	0.284	68.69	0.332	76.08
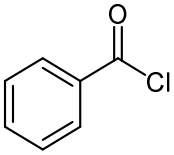		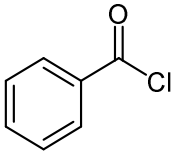 TCAP (2.5%)		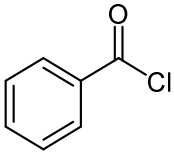 TCAP (5%)		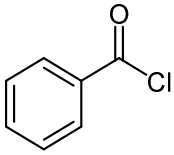 TCAP (7.5%)	
S = 2		*S* = 7		*S* = 9.5		*S* = 9.5	
Chemosel.	Conv. (%)	Chemosel.	Conv. (%)	Chemosel.	Conv. (%)	Chemosel.	Conv. (%)
0.229	11.22	0.736	17.32	0.791	17.09	0.804	17.07
0.277	24.51	0.681	31.26	0.741	30.26	0.746	30.53
0.257	36.90	0.613	46.84	0.677	46.77	0.686	47.05
0.199	60.45	0.540	60.97	0.557	62.58	0.566	61.96
--	--	0.350	74.36	0.365	75.13	0.313	77.54
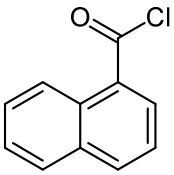		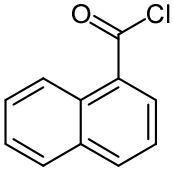 TCAP (2.5%)		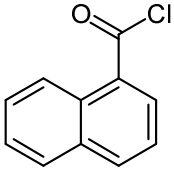 TCAP (5%)		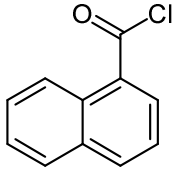 TCAP (7.5%)	
S = 0.7		*S* = Not computable[a]		*S* = Not computable[a]		*S* = Not computable[a]	
Chemosel.	Conv. (%)	Chemosel.	Conv. (%)	Chemosel.	Conv. (%)	Chemosel.	Conv. (%)
-0.120	17.04	0.519	16.53	0.596	17.22	0.782	17.41
-0.140	27.48	0.207	30.82	0.402	31.045	0.552	31.08
-0.150	36.88	0.179	46.33	0.302	46.039	0.426	46.56
-0.121	54.44	0.140	60.86	[b]		0.335	60.53
-0.121	66.23	0.037	70.00	[b]		0.256	75.88

[a] Points do not fit to a *S*-curve [b] Overlapped signals.

Table S3: 3 (continuation). [Table S3] Chemoselectivity and Conversion values of competition experiments shown in **Scheme S3: 3**. Selectivity values are shown.

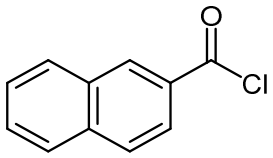		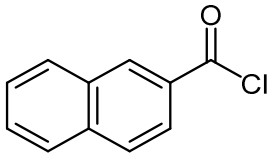 TCAP (2.5%)		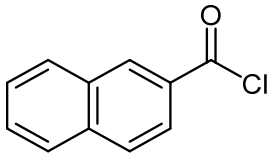 TCAP (5%)		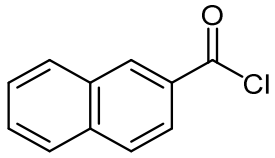 TCAP (7.5%)	
S = 2		*S* = 6		*S* = 8.5		*S* = 8.5	
Chemosel.	Conv. (%)	Chemosel.	Conv. (%)	Chemosel.	Conv. (%)	Chemosel.	Conv. (%)
0.189	11.01	0.692	16.87	0.748	17.84	0.790	17.09
0.255	23.54	0.651	29.77	0.715	30.64	0.737	30.70
0.253	36.88	0.589	45.32	0.652	46.16	0.656	48.21
0.248	52.01	0.517	59.68	0.498	67.27	0.558	61.46
0.204	61.61	0.395	71.98	0.388	72.88	0.366	73.59

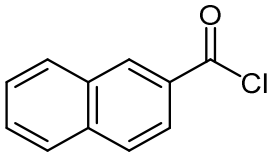 TCAP (5%) By using Stock C5 in all reactions		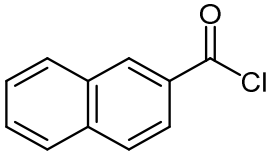 TCAP (5%) Temperature: + 10 °C		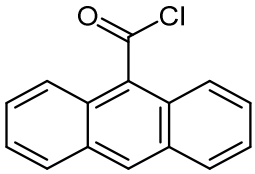		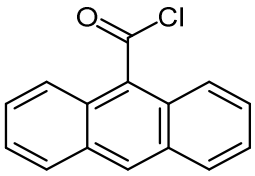 TCAP (5%)	
S = 9.5		*S* = 10		*S* = 6		*S* = 5-6	
Chemosel.	Conv. (%)	Chemosel.	Conv. (%)	Chemosel.	Conv. (%)	Chemosel.	Conv. (%)
0.758	15.80	0.808	13.82	0.682	20.37	0.665	14.32
0.755	29.63	0.786	30.11	0.625	34.47	0.637	32.50
0.678	44.56	0.694	45.30	0.560	49.08	0.580	39.34
0.487	65.25	0.59	62.50	0.474	62.02	0.499	48.78
0.464	68.90	-	-	0.340	75.29	0.388	61.65

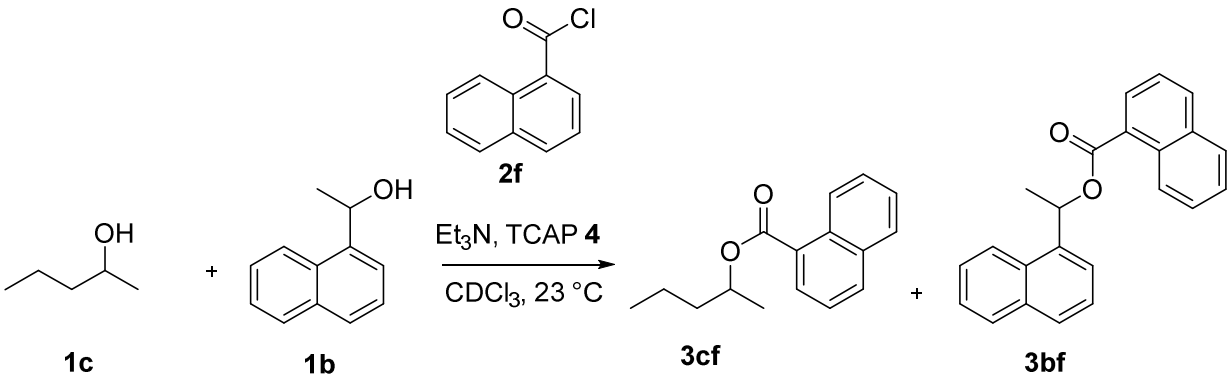

Scheme S3: 4. *[Scheme S4] Competition experiment between* ***1c*** *and* ***1b*** *with 1-napthoyl chloride* ***2f*** *and TCAP* ***4*** *to give the ester compounds* ***3cf*** *and* ***3bf.***

Table S3: 4. [Table S4] Chemoselectivity and Conversion values of competition experiments shown in **Scheme S3: 4**. Selectivity values are shown.

TCAP (2.5%)		TCAP (7.5%)	
S = Not computable[a]		*S* = Not computable[a]	
Chemosel.	Conv. (%)	Chemosel.	Conv. (%)
0.334	19.70	0.673	20.11
0.187	35.51	0.455	36.30
0.173	51.45	0.386	52.06
0.174	66.25	-[b]	-

[a] Points do not fit to a S-curve [b] Overlapped signals

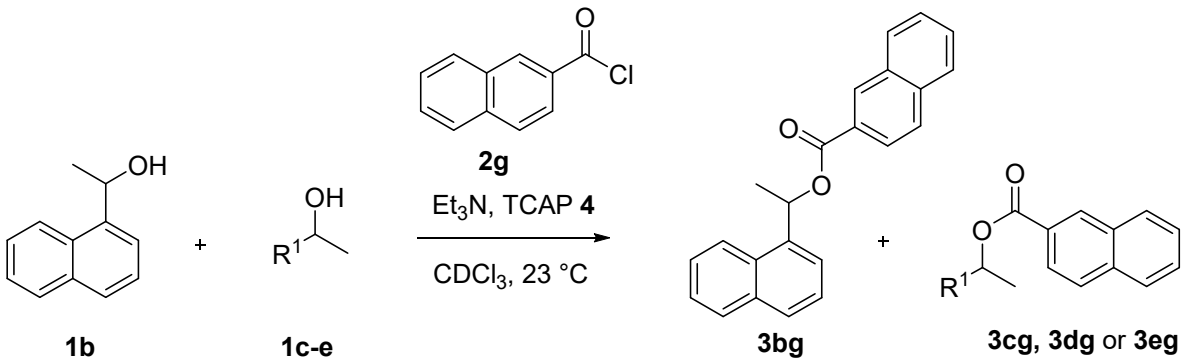

Scheme S3: 5. *[Scheme S5] Competition experiment between **1b** and **1c, 1d** or **1e** with the acid chloride **2g** and TCAP **4** to give the ester compounds **3bg** and **3cg, 3dg** or **3eg.***

Table S3: 5. [Table S5] Chemoselectivity and Conversion values of competition experiments shown in **Scheme S3: 5**. Selectivity values are shown.

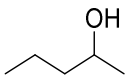 TCAP (2.5%)		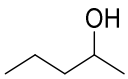 TCAP (7.5%)		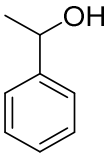 TCAP (2.5%)		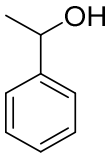 TCAP (7.5%)	
S = 8		*S* = 10		*S* = 1.5		*S* = 1.5	
Chemosel.	Conv. (%)	Chemosel.	Conv. (%)	Chemosel.	Conv. (%)	Chemosel.	Conv. (%)
0.722	19.62	0.808	19.21	0.158	17.23	0.240	18.56
0.669	35.80	0.741	35.5	0.150	34.02	0.192	29.74
0.618	52.50	0.675	51.80	0.128	49.61	0.160	44.01
0.511	66.26	[a]		0.076	62.85	0.137	62.51
0.312	81.01	0.406	76.23	0.073	78.09	0.100	76.87

[a]Not measurable

Table S3: 5 (continuation). [Table S5] Chemoselectivity and Conversion values of competition experiments shown in **Scheme S3: 5**. Selectivity values are shown.

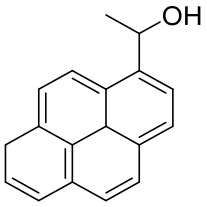 TCAP (2.5%)		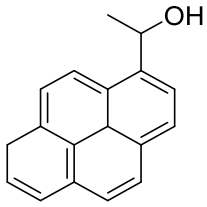 TCAP (7.5%)	
S = 0.4 – 0.5		*S* = 0.4 – 0.5	
Chemosel.	Conv. (%)	Chemosel.	Conv. (%)
-0.459	18.73	-0.477	15.68
-0.336	31.39	-0.355	30.26
-0.270	48.25	-0.291	47.29
-0.218	61.37	-0.235	61.39
-0.187	75.94	-0.178	76.23

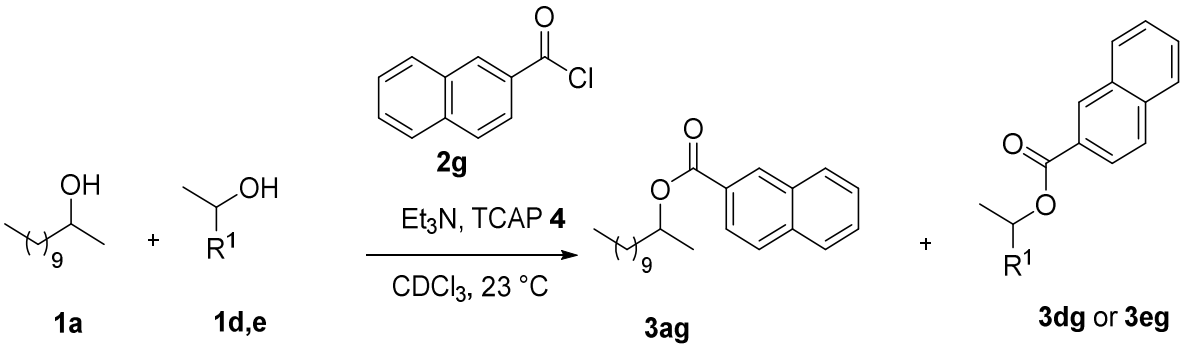

Scheme S3: 6. *[Scheme S6] Competition experiment between **1a** and **1d,e** with the acid chloride **2g** and TCAP **4** to give the ester compounds **3ag** and **3dg** or **3eg**.*

Table S3: 6 [Table S6] Chemoselectivity and Conversion values of competition experiments shown in **Scheme S3: 6**. Selectivity values are shown.

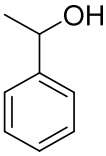 TCAP (2.5%)		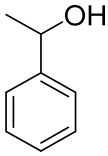 TCAP (7.5%)		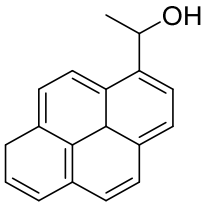 TCAP (2.5%)		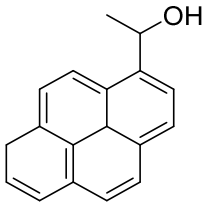 TCAP (7.5%)	
S = 4.5-5		*S* = 5		*S* = 25		*S* = 25	
Chemosel.	Conv. (%)	Chemosel.	Conv. (%)	Chemosel.	Conv. (%)	Chemosel.	Conv. (%)
0.565	17.14	0.651	18.59	0.909	26.45	0.917	25.25
0.551	32.24	0.601	29.57	0.895	31.18	0.893	31.74
0.514	46.71	0.546	43.79	0.842	46.20	0.843	47.44
0.462	59.3	0.454	59.55	0.638	61.12	0.646	61.84
0.268	75.36	0.283	74.80	0.329	74.4	0.333	76.05

3.1.5 Selectivity Curves of Competition Experiments

The chemoselectivity vs conversion relationship of each competition experiment has been compiled and plotted along the selectivity curves. Only the relevant *S*-curves are presented. Several chemoselectivity vs conversion relationship have been plotted together to present a comprehensive summary of the results.

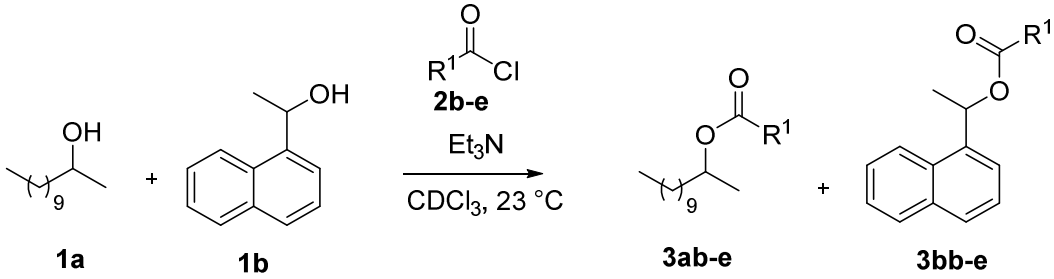

Scheme S3: 7. *[Scheme S7] Competition experiment between* ***1a*** *and* ***1b*** *with the acid chloride* ***2b-e*** *to give the ester compounds* ***3ab-e*** *and* ***3bb-e****.*

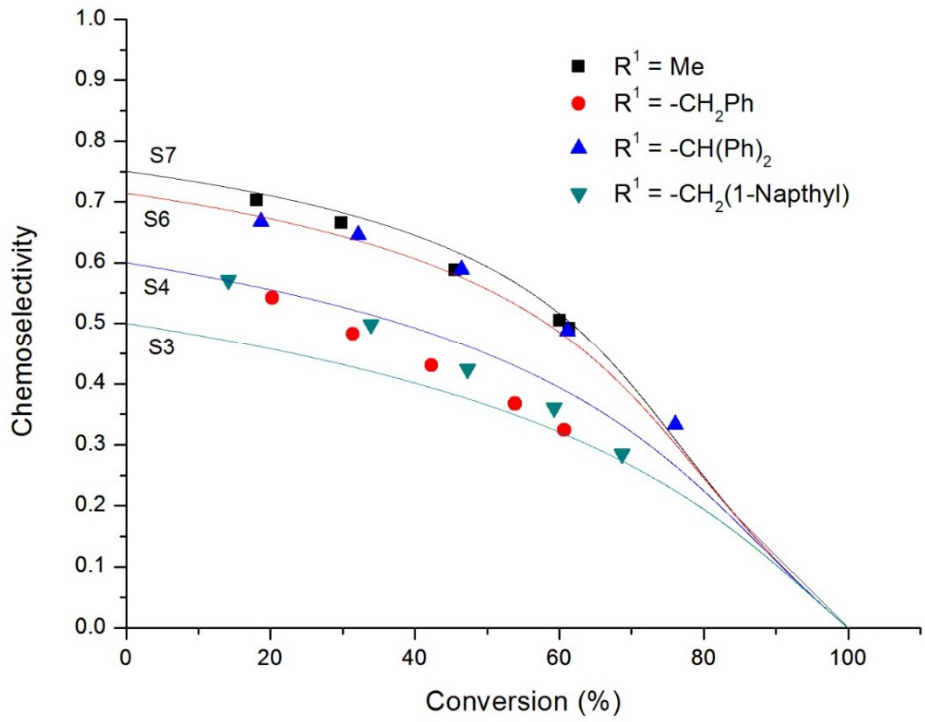

Figure S3: 10. *[Figure S10] Chemoselectivity vs Conversion of competition experiment shown in* ***Scheme S3: 7****.*

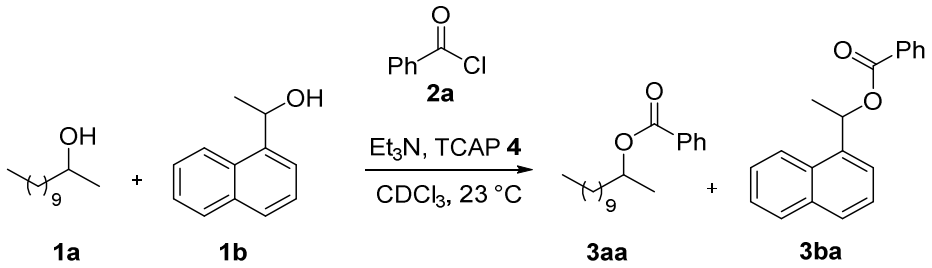

Scheme S3: 8. *[Scheme S8] Competition experiment between **1a** and **1b** with benzoyl chloride **2a** and TCAP **4** to give the ester compounds **3aa** and **3ba**.*

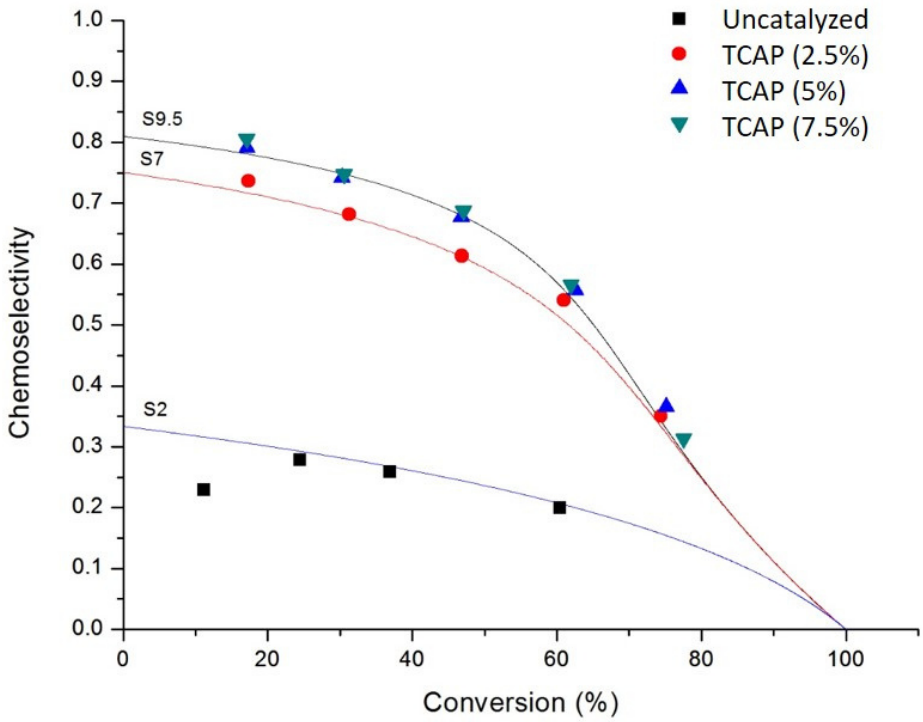

Figure S3: 11. *[Figure S11] Chemoselectivity vs Conversion of competition experiment shown in **Scheme S3: 8**.*

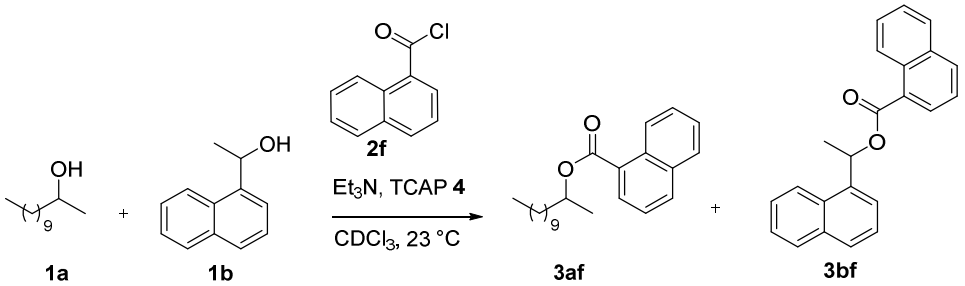

Scheme S3: 9. *[Scheme S9] Competition experiment between* ***1a*** *and* ***1b*** *with 1-napthoyl chloride* ***2f*** *and TCAP* ***4*** *to give the ester compounds* ***3af*** *and* ***3bf****.*

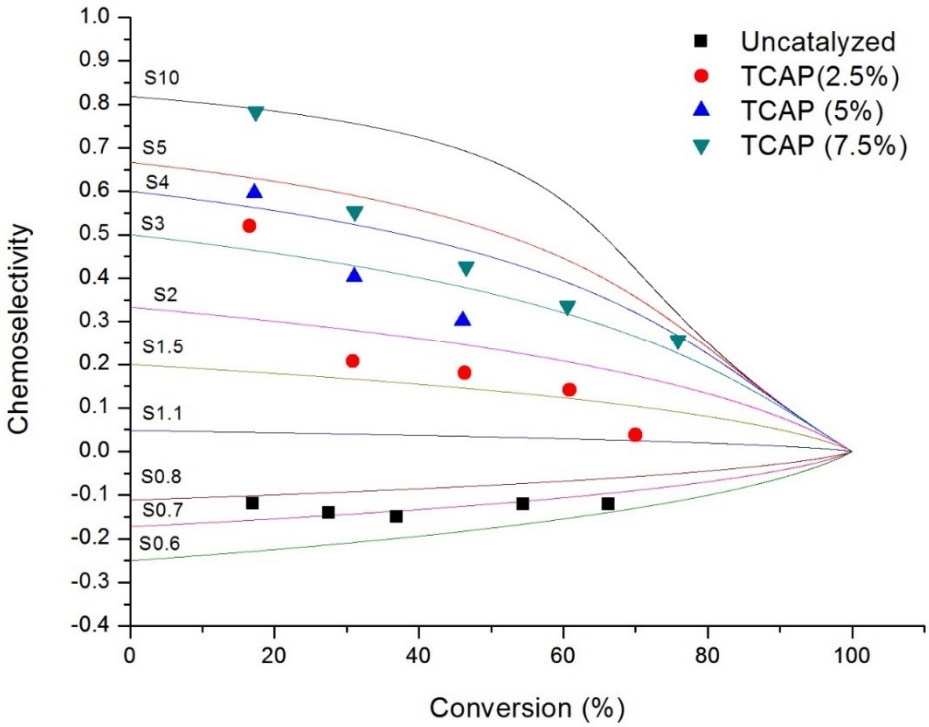

Figure S3: 12. *[Figure S12] Chemoselectivity vs Conversion of competition experiment shown in* ***Scheme S3: 9****.*

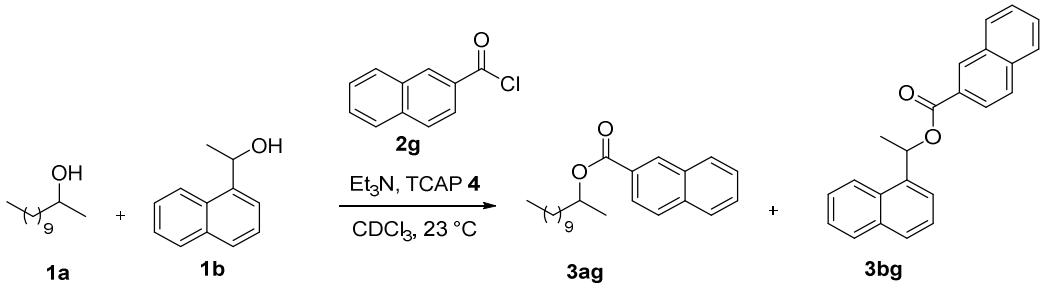

Scheme S3: 10. *[Scheme S10] Competition experiment between* ***1a*** *and* ***1b*** *with 1-napthoyl chloride* ***2g*** *and TCAP* ***4*** *to give the ester compounds* ***3ag*** *and* ***3bg****.*

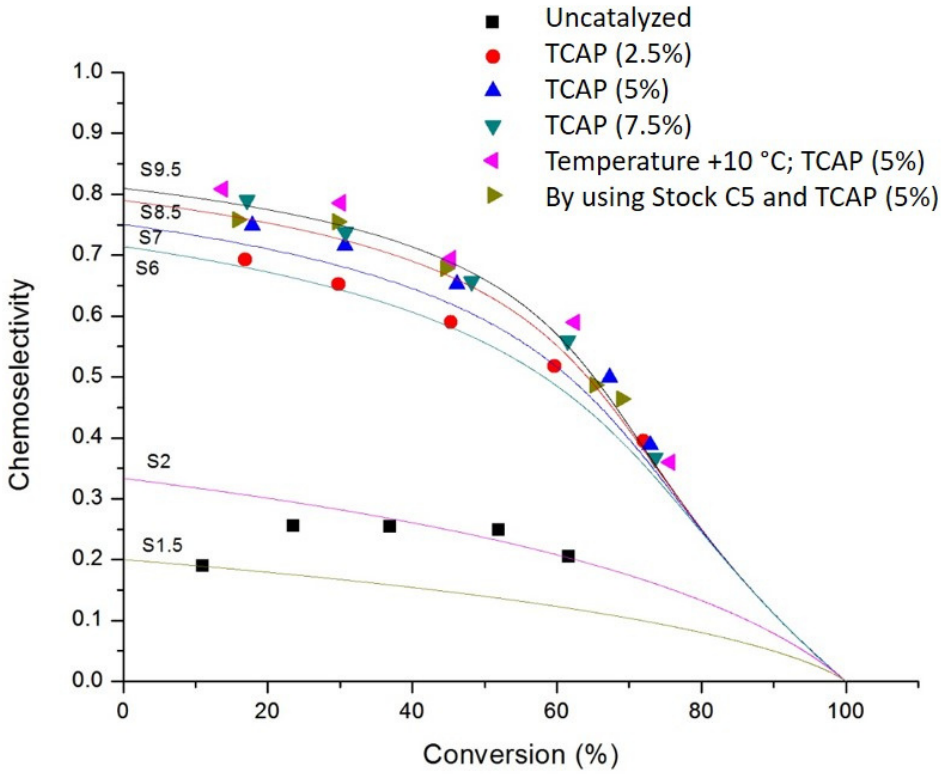

Figure S3: 13. *[Figure S13] Chemoselectivity vs Conversion of competition experiment shown in* ***Scheme S3: 10****.*

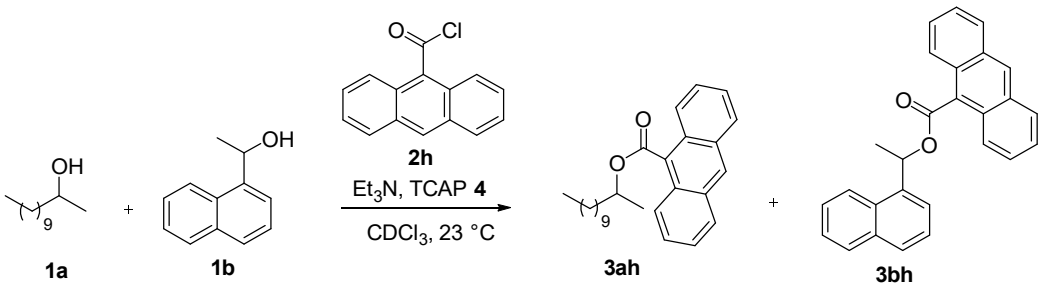

Scheme S3: 11. *[Scheme S11] Competition experiment between* ***1a*** *and* ***1b*** *with 1-napthoyl chloride* ***2h*** *and TCAP* ***4*** *to give the ester compounds* ***3ah*** *and* ***3bh****.*

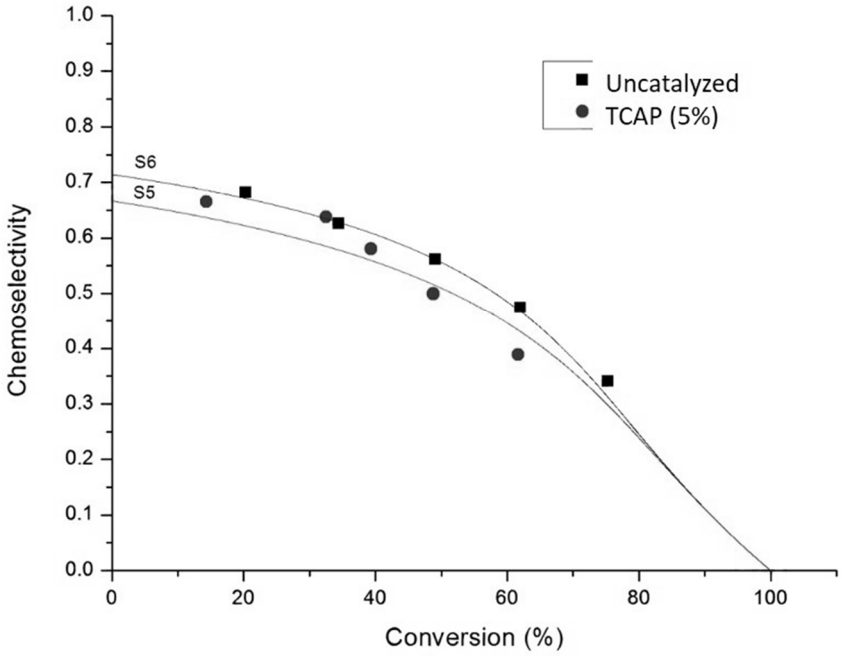

Figure S3: 14. *[Figure S14] Chemoselectivity vs Conversion of competition experiment shown in* ***Scheme S3: 11****.*

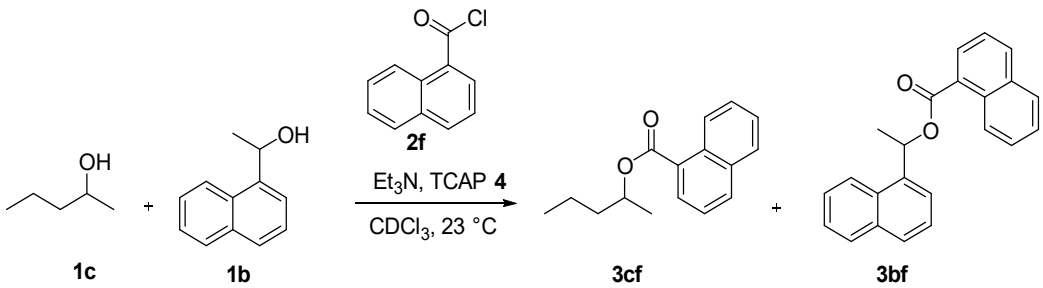

Scheme S3: 12. *[Scheme S12] Competition experiment between* ***1c*** *and* ***1b*** *with 9-anthracenoyl chloride* ***2f*** *and TCAP* ***4*** *to give the ester compounds* ***3cf*** *and* ***3bf****.*

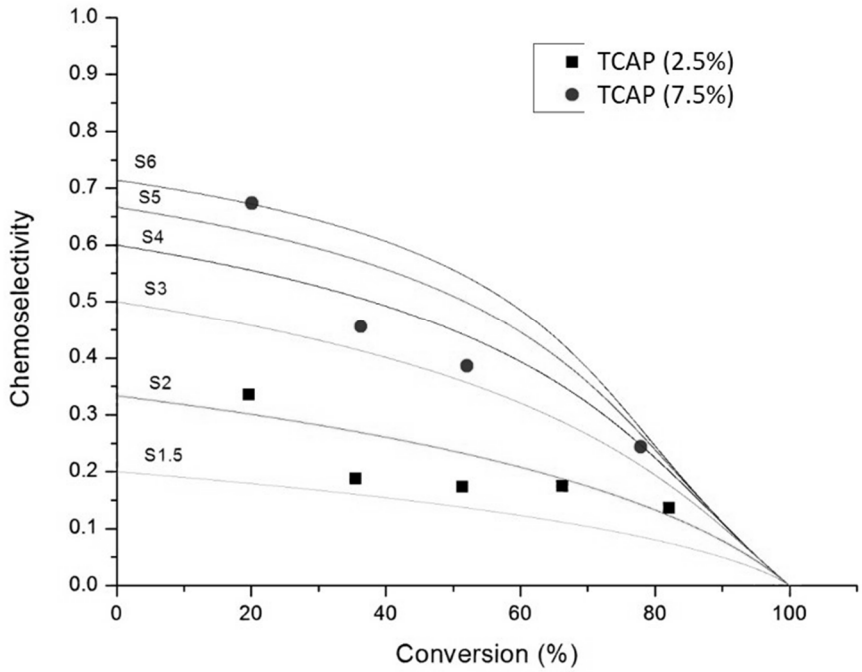

Figure S3: 15. *[Figure S15] Chemoselectivity vs Conversion of competition experiment shown in* ***Scheme S3: 12****.*

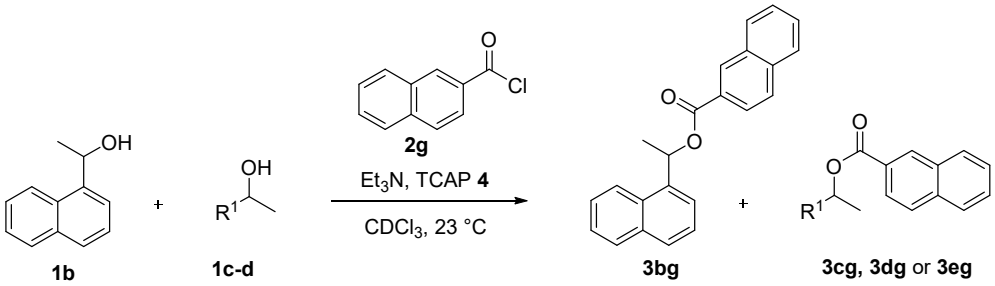

Scheme S3: 13. *[Scheme S13] Competition experiment between* ***1b*** *and* ***1c-d*** *with 2-napthoyl chloride* ***2i*** *and TCAP* ***4*** *to give the ester compounds* ***3bg*** *and* ***3cg****,* ***3dg*** *or* ***3eg****.*

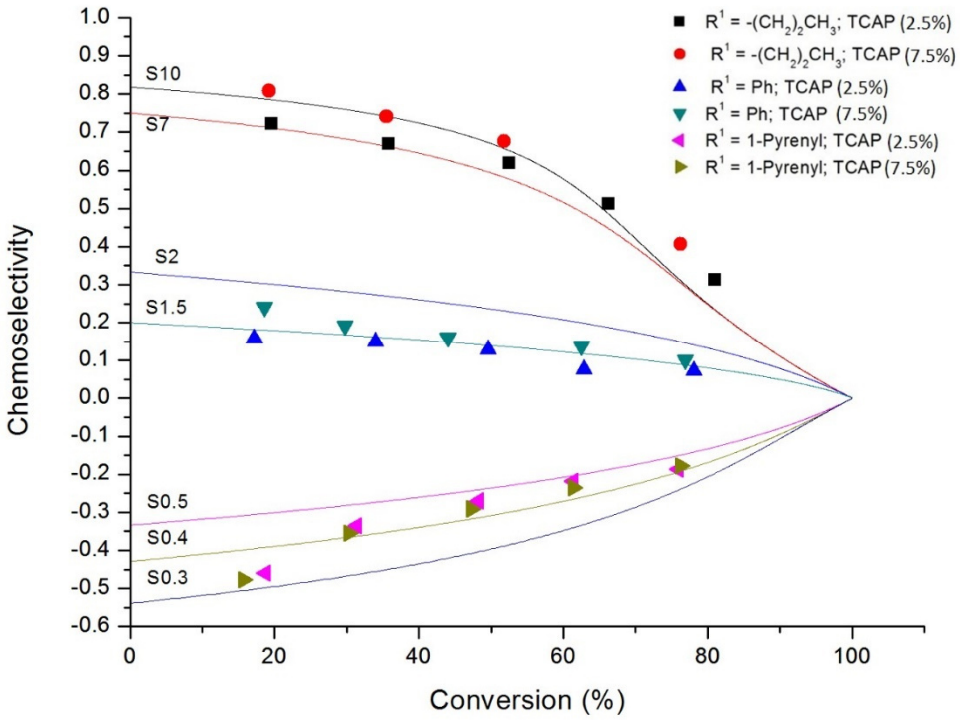

Figure S3: 16. *[Figure S16] Chemoselectivity vs Conversion of competition experiment shown in* ***Scheme S3: 13****.*

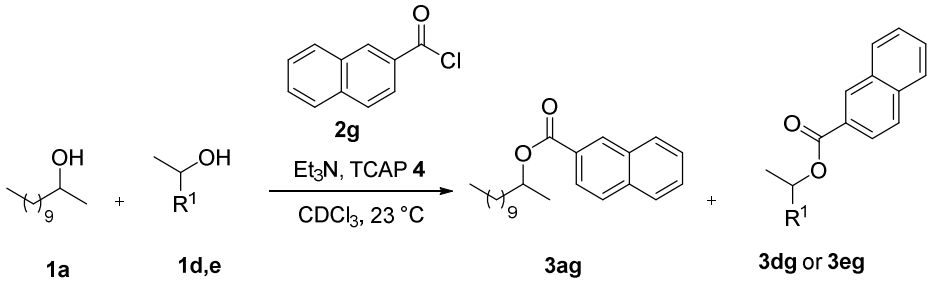

Scheme S3: 14. *[Scheme S14] Competition experiment between* ***1a*** *and* ***1d,e*** *with 2-napthoyl chloride* ***2g*** *and TCAP* ***4*** *to give the ester compounds* ***3ag*** *and* ***3dg*** *or* ***3eg****.*

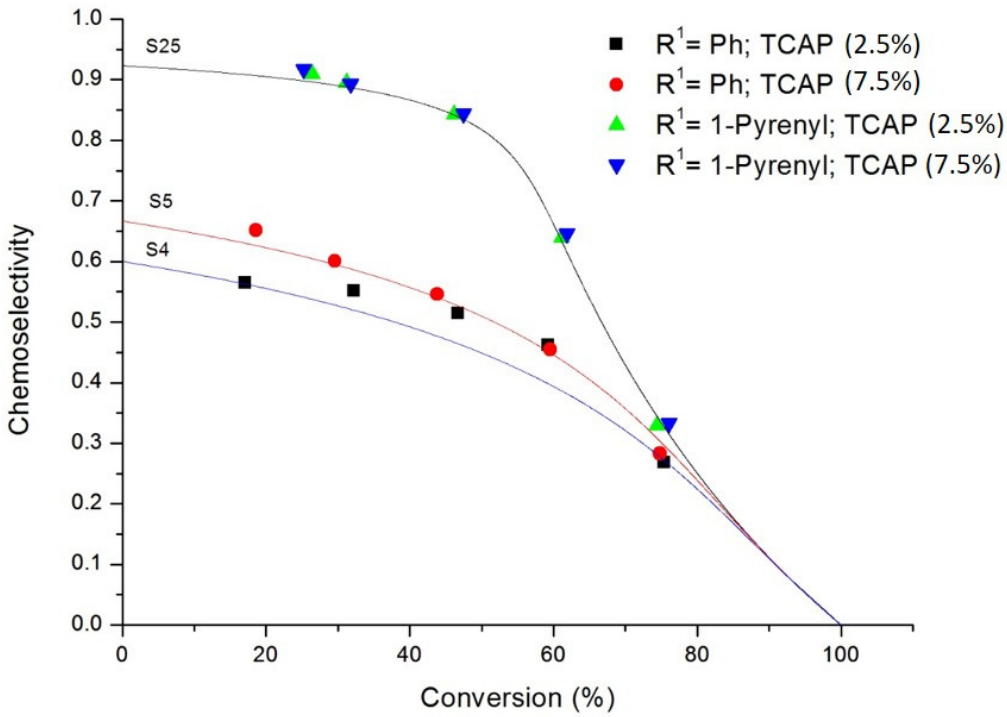

Figure S3: 17. *[Figure S17] Chemoselectivity vs Conversion of competition experiment shown in* ***Scheme S3: 14****.*

3.1.6 Stacked ^{1}H NMR Spectra of all Competition Experiments

^{1}H NMR spectra were recorded at 600 MHz at room temperature. All spectra were imported in Mestrenova 10.0.2 program and treated with the same settings: Apodization, exponential 0.1; Baseline Correction, Bernstein polynominal fit; Phase correction, Auto (Global Method). Just the relevant area of the ^{1}H NMR spectra is shown. The hydrogen atom associated to each signal is explicitly written in the structures (attached to chiral carbon atom).

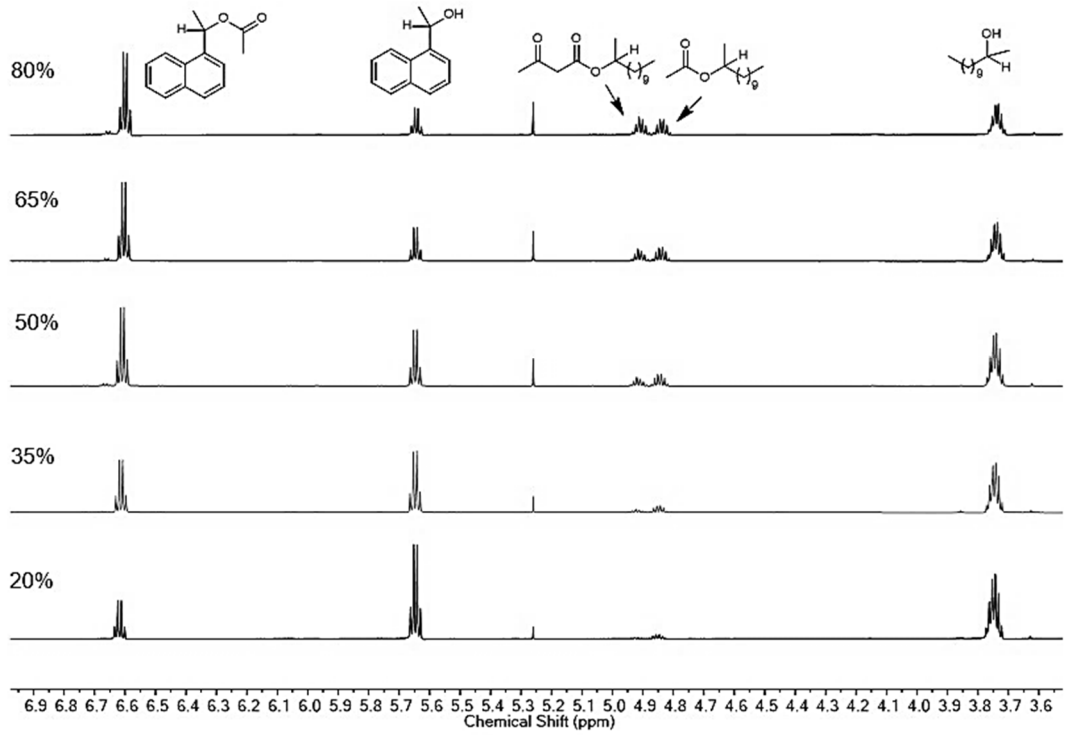

Figure S3: 18. *[Figure S18] Stacked spectra of the competition experiment involving alcohol substrates* ***1a*** *and* ***1b*** *and acetyl chloride* ***2b****.*

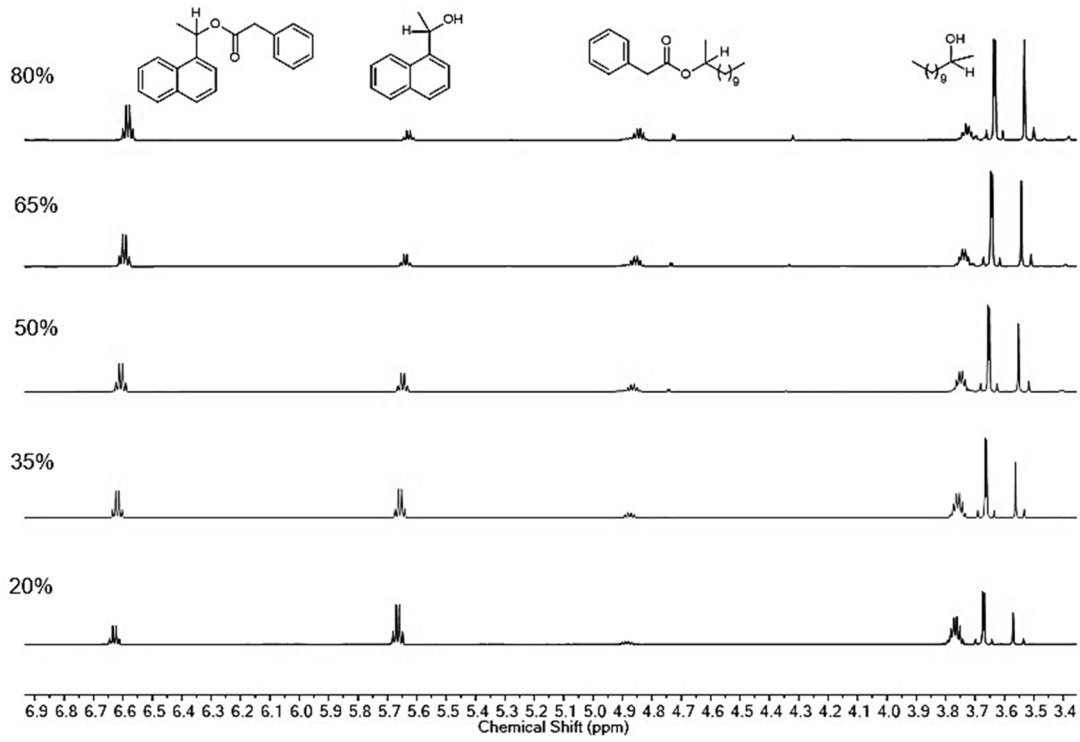

Figure S3: 19. *[Figure S19] Stacked spectra of the competition experiment involving alcohol substrates* ***1a*** *and* ***1b*** *and phenylacetyl chloride* ***2c****.*

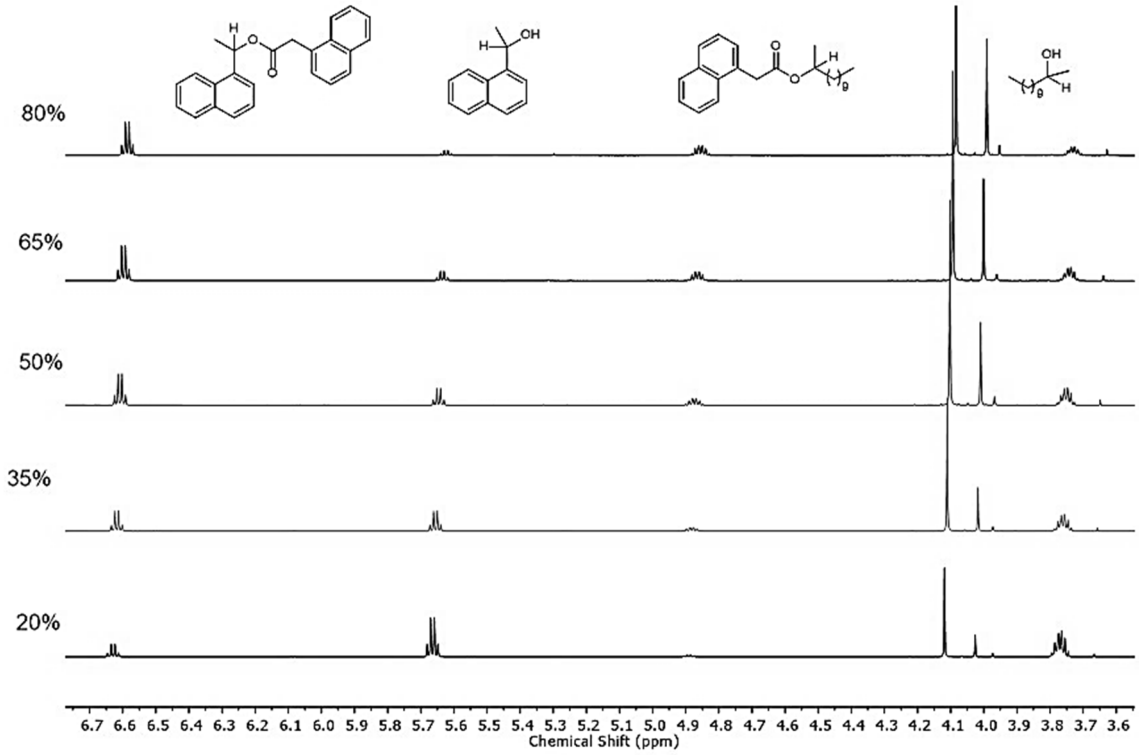

Figure S3: 20. *[Figure S20] Stacked spectra of the competition experiment involving alcohol substrates* ***1a*** *and* ***1b*** *and 2-(naphthalen-1-yl)acetyl chloride* ***2d****.*

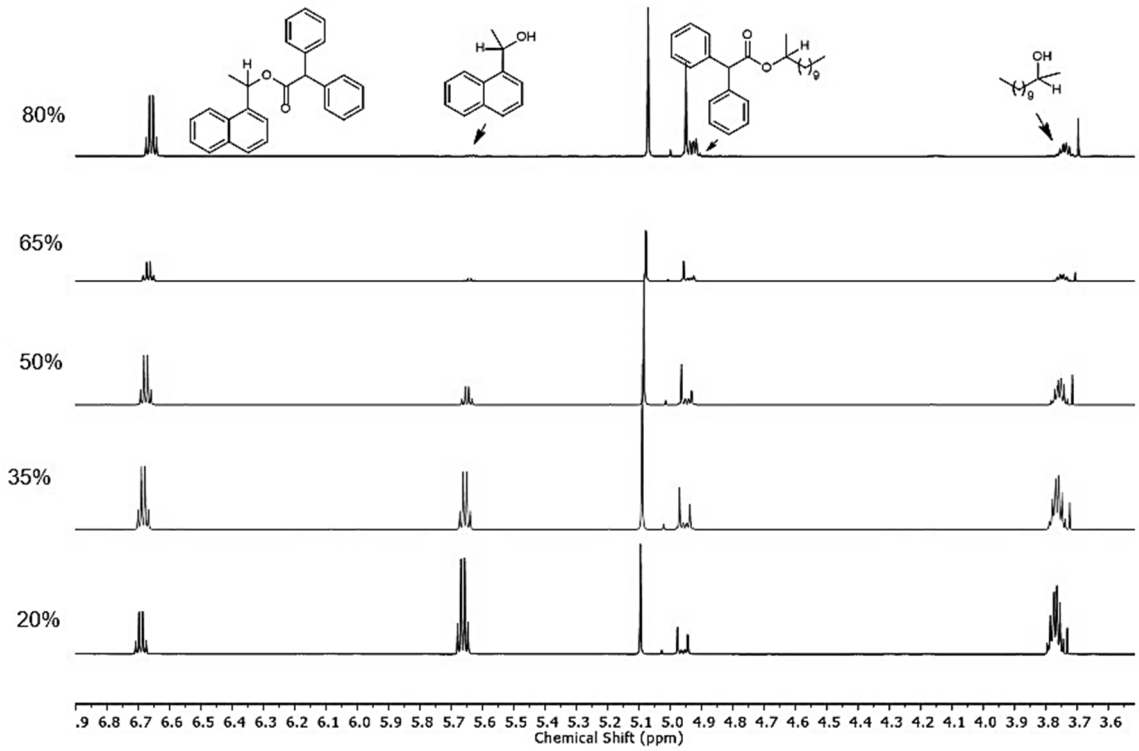

Figure S3: 21. *[Figure S21] Stacked spectra of the competition experiment involving alcohol substrates* ***1a*** *and* ***1b*** *and diphenylacetyl chloride* ***2e****.*

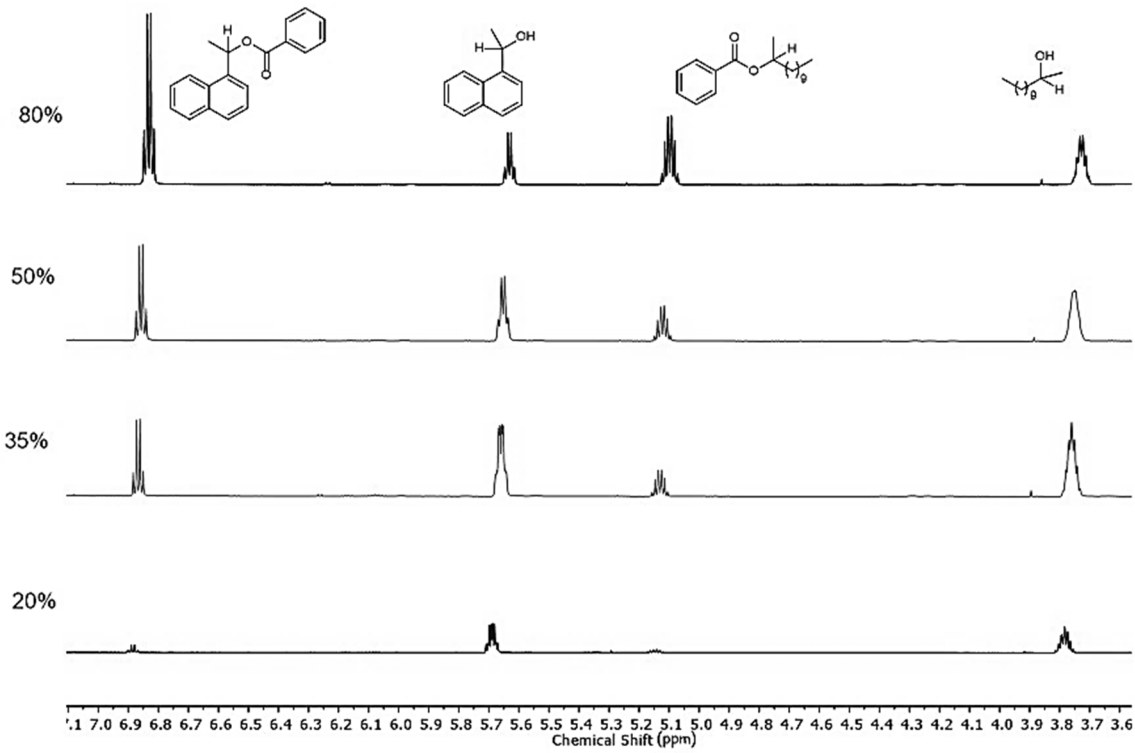

Figure S3: 22. *[Figure S22] Stacked spectra of the competition experiment involving alcohol substrates* ***1a*** *and* ***1b*** *and benzoyl chloride* ***2a****.*

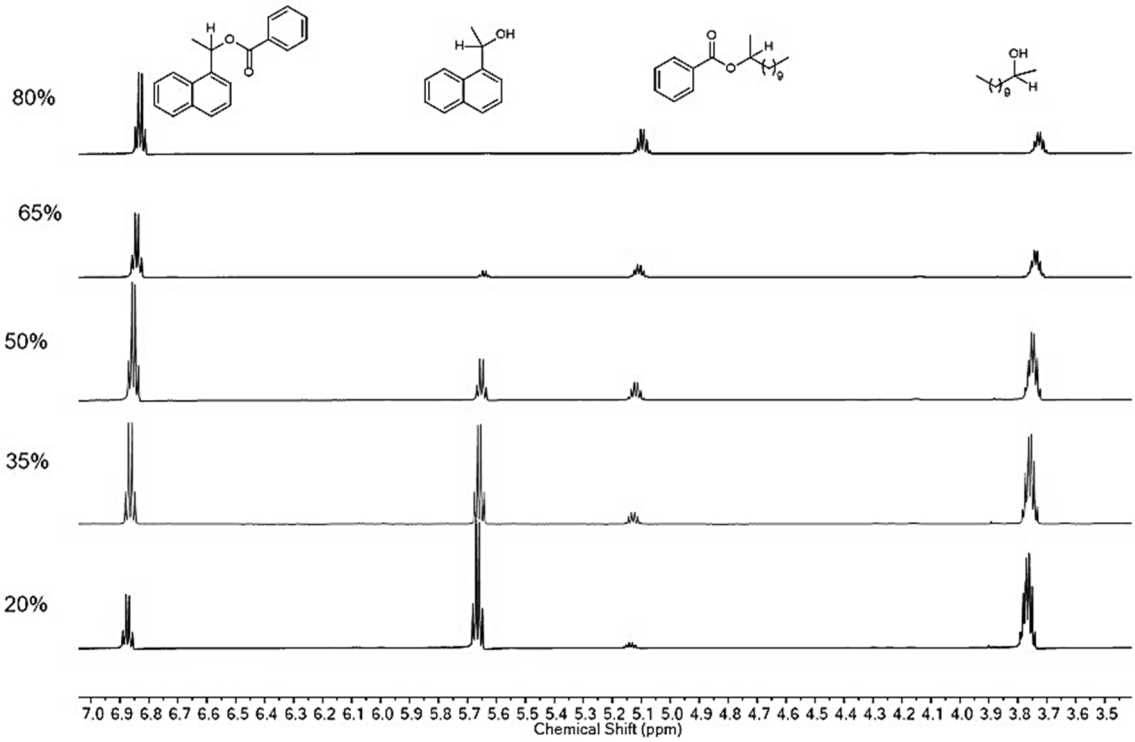

Figure S3: 23. [*Figure S23] Stacked spectra of the competition experiment involving alcohol substrates* ***1a*** *and* ***1b*** *and benzoyl chloride* ***2a****, and TCAP* ***4*** *(2.5%).*

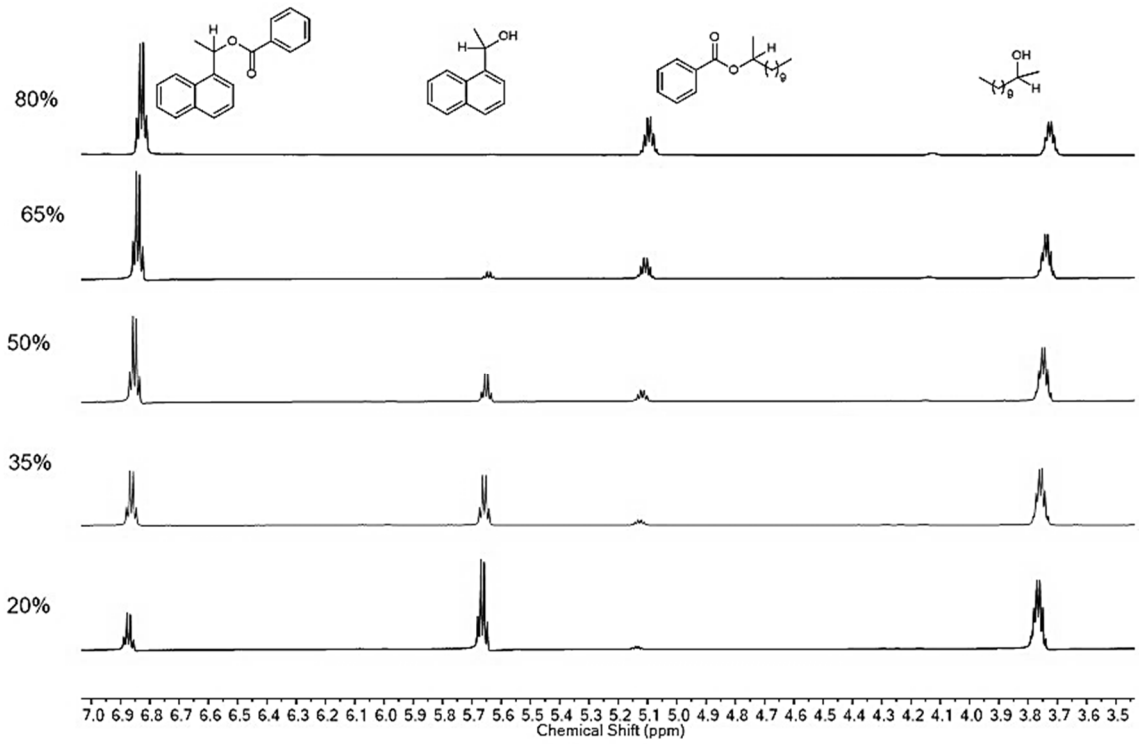

***Figure S3: 24**. [Figure S24] Stacked spectra of the competition experiment involving alcohol substrates **1a** and **1b** and benzoyl chloride **2a**, and TCAP **4** (5%).*

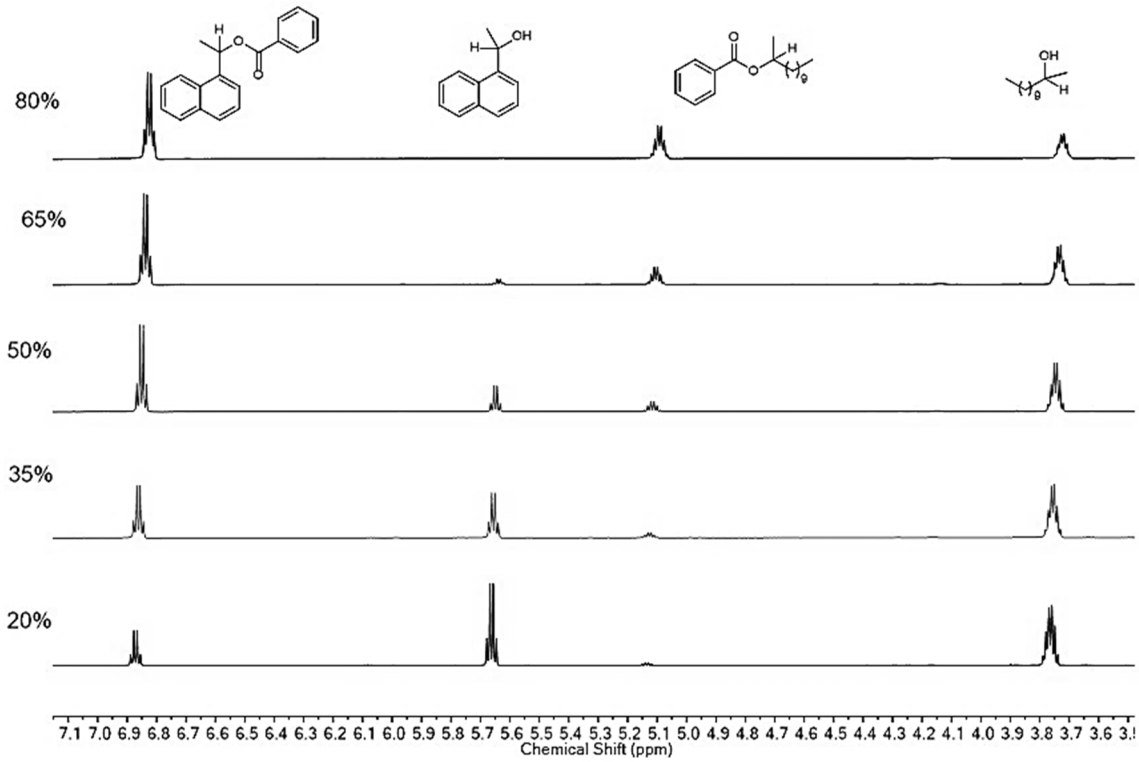

***Figure S3: 25.** [Figure S25] Stacked spectra of the competition experiment involving alcohol substrates **1a** and **1b** and benzoyl chloride **2a**, and TCAP **4** (7.5%).*

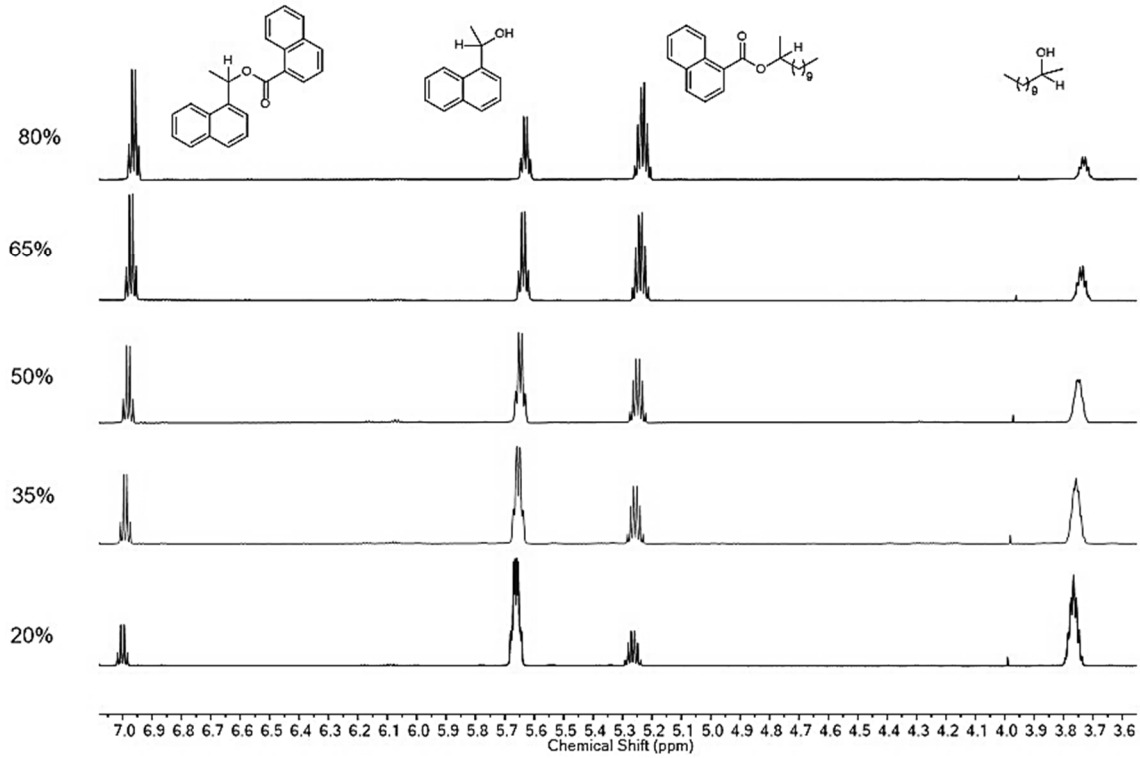

Figure S3: 26. *[Figure S26] Stacked spectra of the competition experiment involving alcohol substrates* ***1a*** *and* ***1b*** *and 1-napthoyl chloride* ***2f****.*

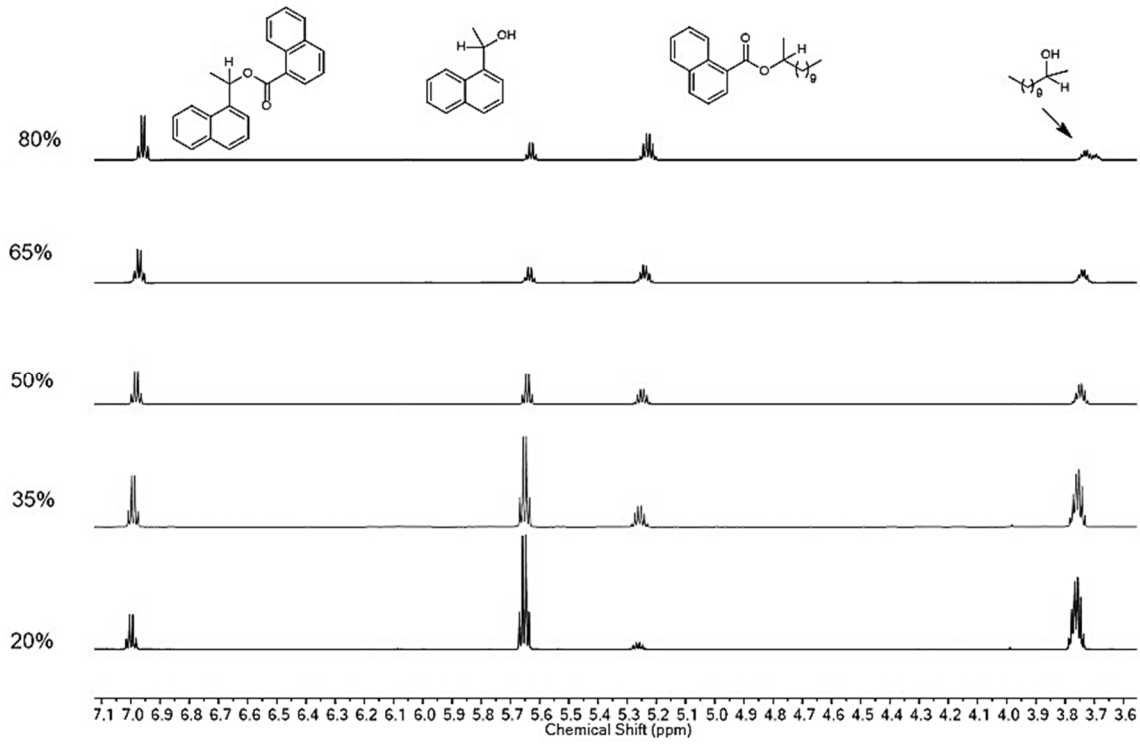

Figure S3: 27. *[Figure S27] Stacked spectra of the competition experiment involving alcohol substrates* ***1a*** *and* ***1b*** *and 1-napthoyl chloride* ***2f****, and TCAP* ***4*** *(2.5%).*

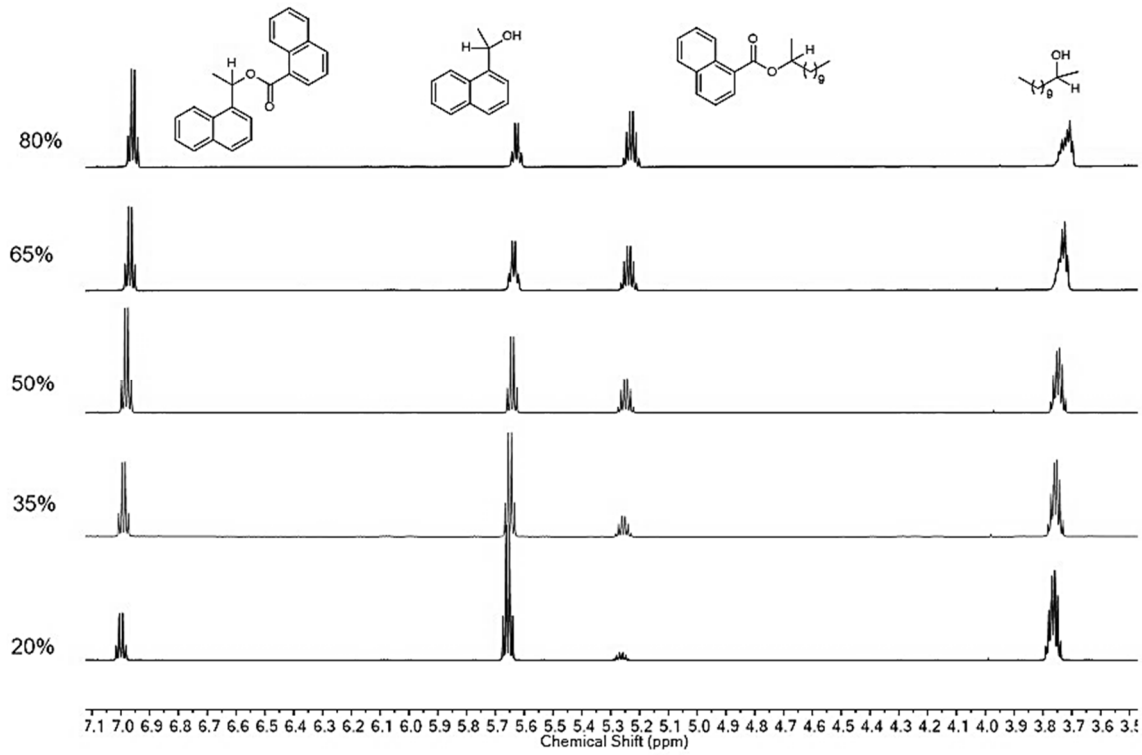

Figure S3: 28. *[Figure S28] Stacked spectra of the competition experiment involving alcohol substrates* ***1a*** *and* ***1b*** *and 1-napthoyl chloride* ***2f****, and TCAP* ***4*** *(5%).*

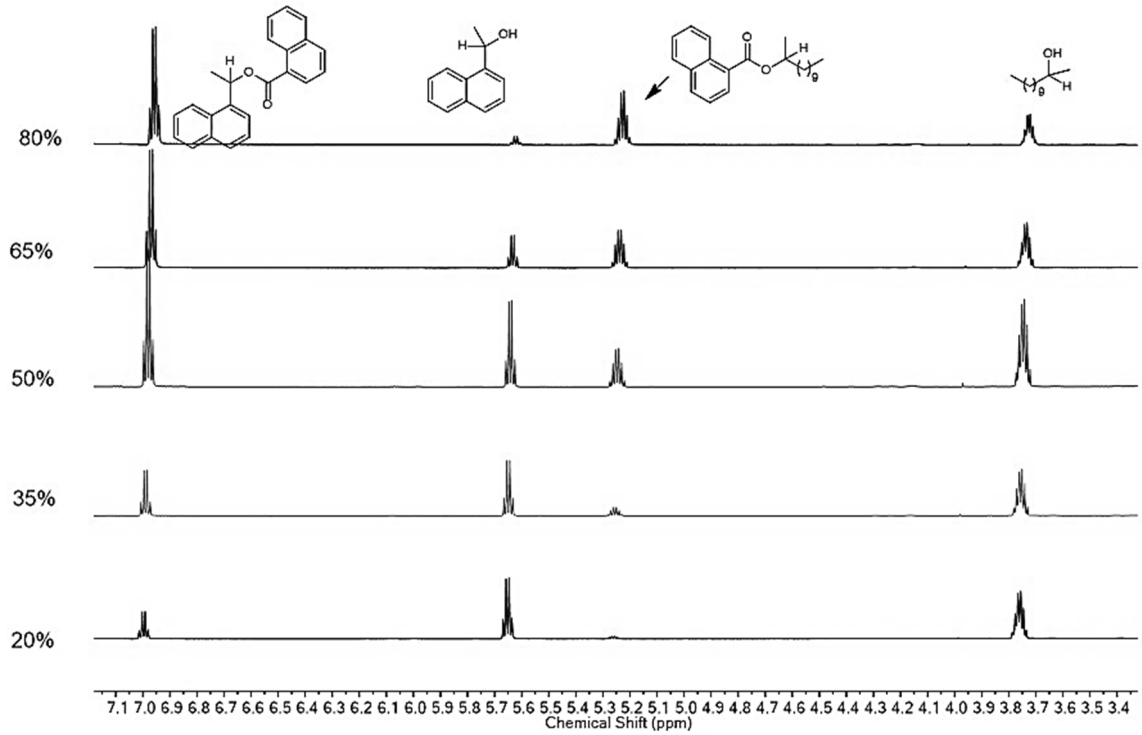

Figure S3: 29. *[Figure S29] Stacked spectra of the competition experiment involving alcohol substrates* ***1a*** *and* ***1b*** *and 1-napthoyl chloride* ***2f****, and TCAP* ***4*** *(7.5%).*

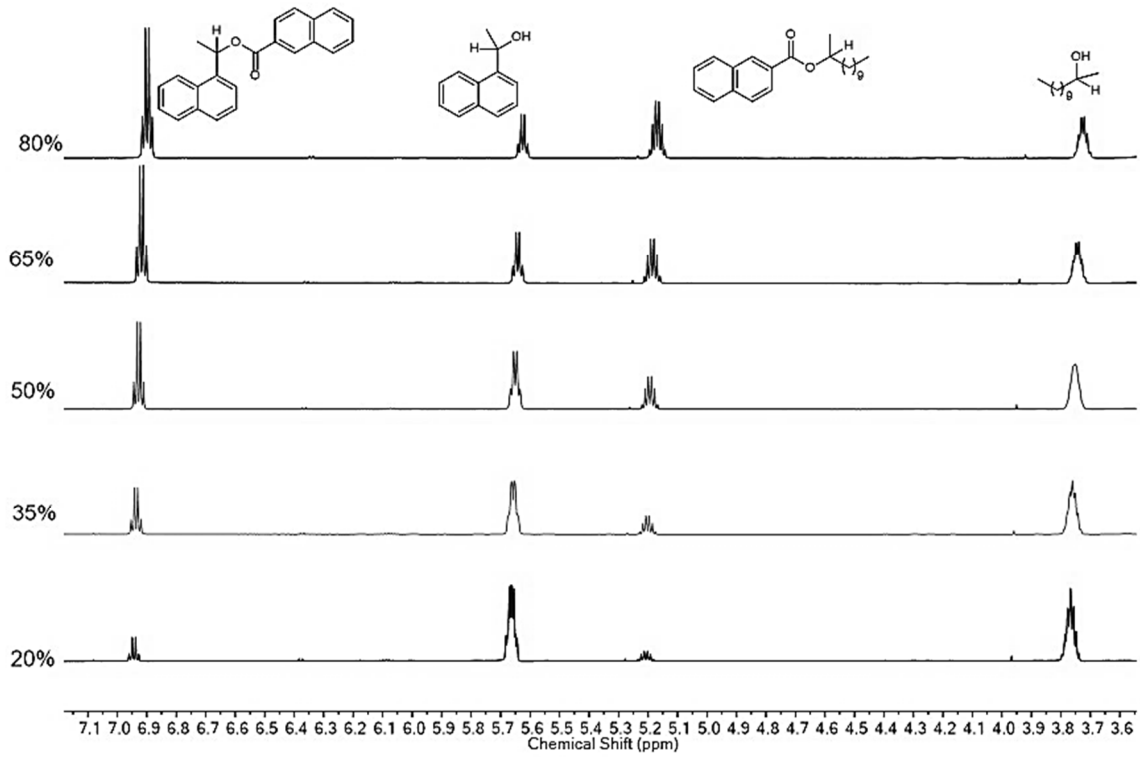

Figure S3: 30. *[Figure S30] Stacked spectra of the competition experiment involving alcohol substrates* ***1a*** *and* ***1b*** *and 2-napthoyl chloride* ***2g****.*

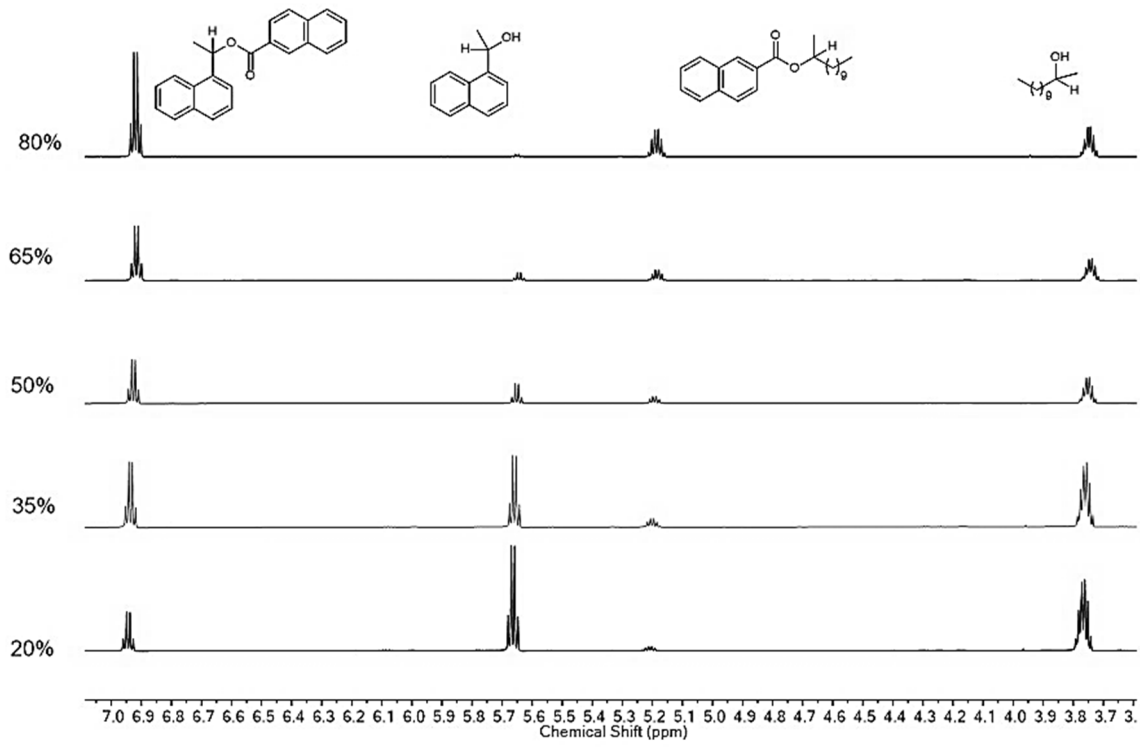

Figure S3: 31. *[Figure S31] Stacked spectra of the competition experiment involving alcohol substrates* ***1a*** *and* ***1b*** *and 2-napthoyl chloride* ***2g****, and TCAP* ***4*** *(2.5%).*

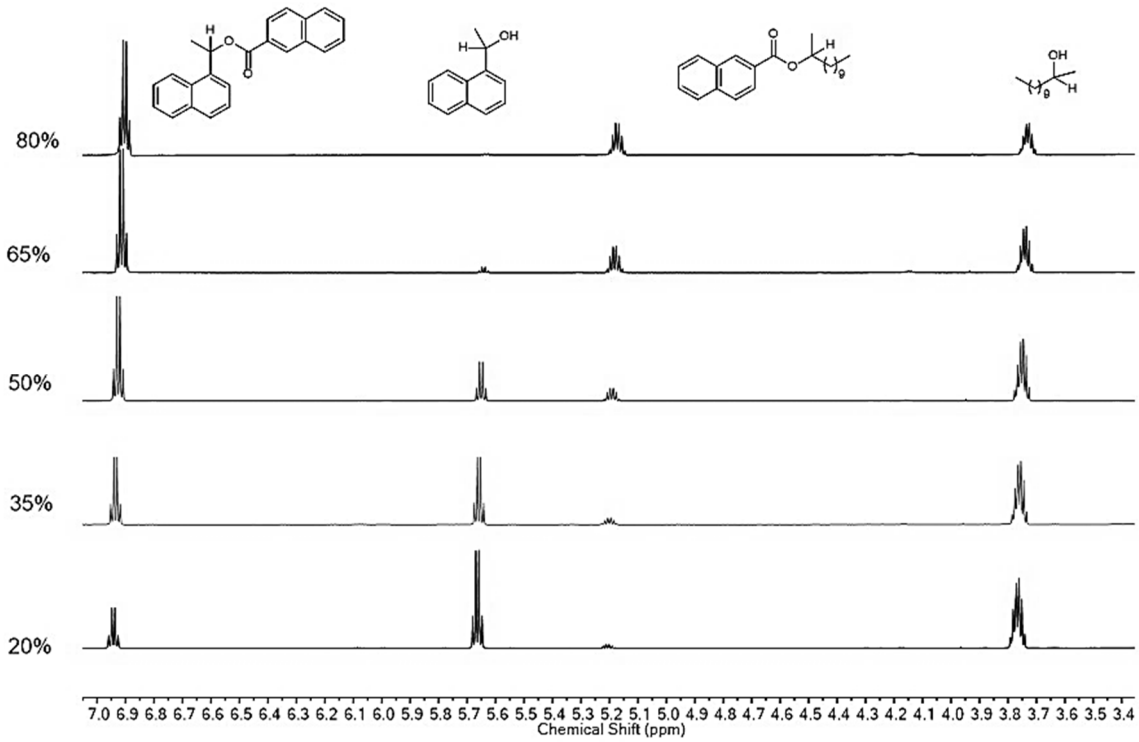

Figure S3: 32. *[Figure S32] Stacked spectra of the competition experiment involving alcohol substrates* ***1a*** *and* ***1b*** *and 2-napthoyl chloride* ***2g****, and TCAP* ***4*** *(5%).*

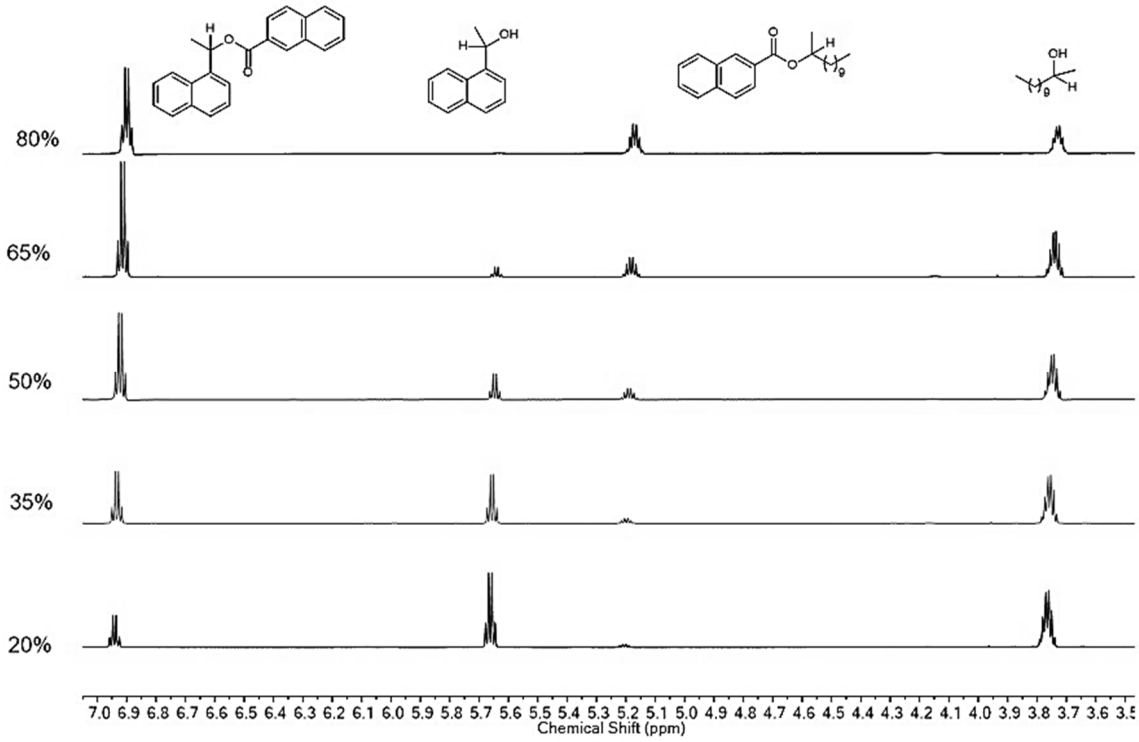

Figure S3: 33. *[Figure S33] Stacked spectra of the competition experiment involving alcohol substrates* ***1a*** *and* ***1b*** *and 2-napthoyl chloride* ***2g****, and TCAP* ***4*** *(7.5%).*

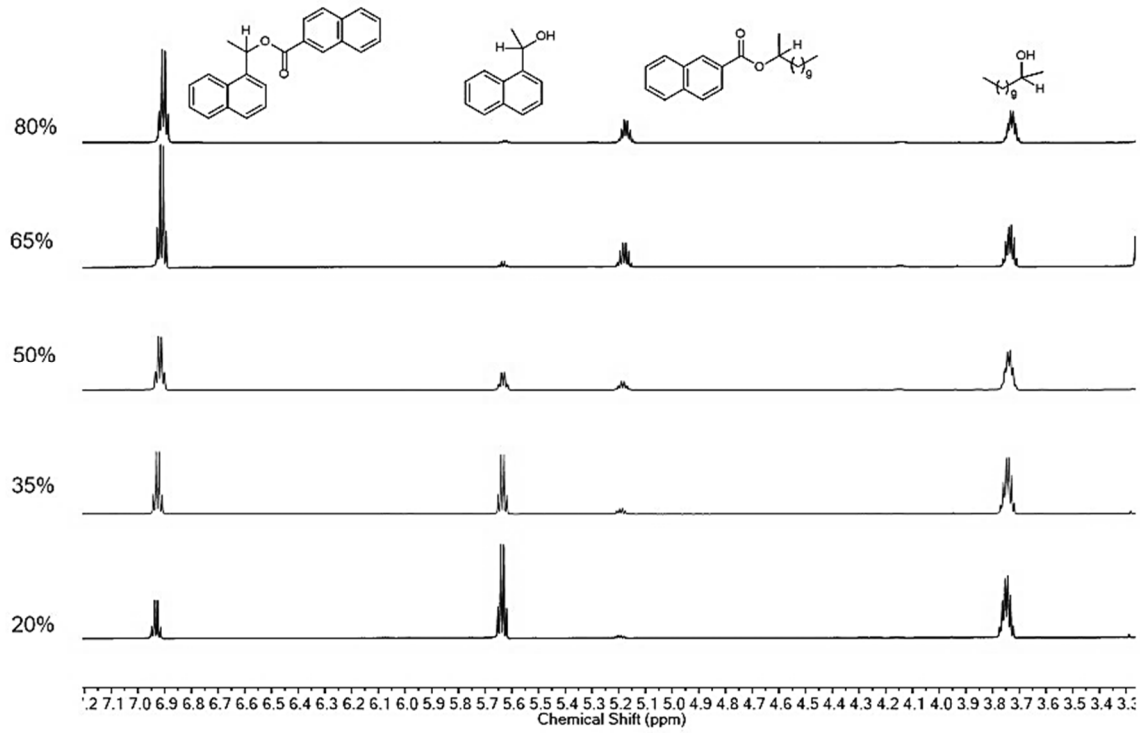

Figure S3: 34. *[Figure S34] Stacked spectra of the competition experiment involving alcohol substrates* ***1a*** *and* ***1b*** *and 2-napthoyl chloride* ***2g****, and TCAP* ***4*** *(5%). In this case, all the individual have been performed with the same amount of triethylamine (Stock C5).*

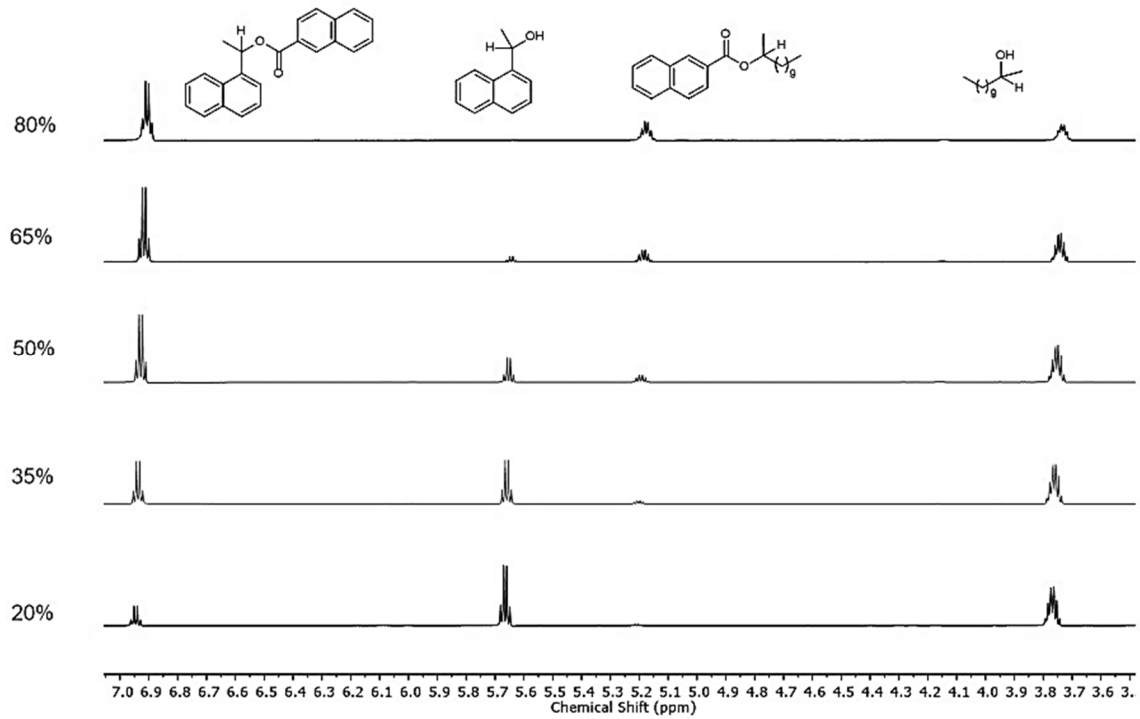

Figure S3: 35. *[Figure S35] Stacked spectra of the competition experiment involving alcohol substrates* ***1a*** *and* ***1b*** *and 2-napthoyl chloride* ***2g****, and TCAP* ***4*** *(5%). In this competition experiment the temperature has been maintained at +10 °C.*

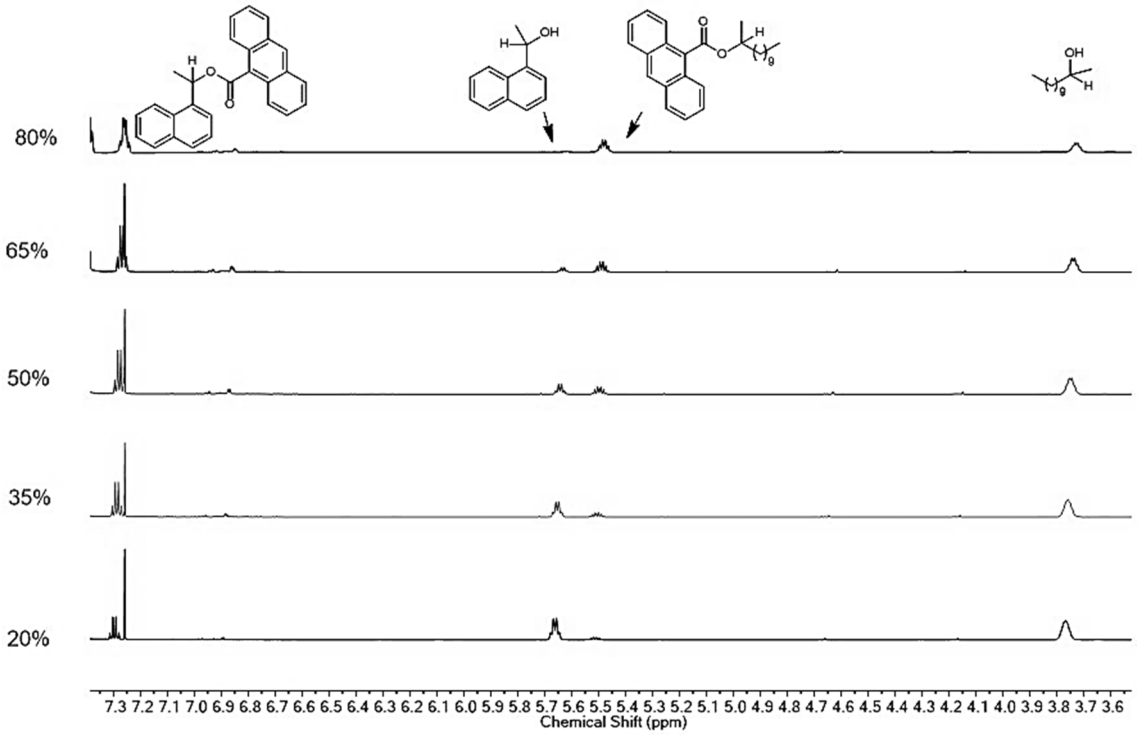

Figure S3: 36. *[Figure S36] Stacked spectra of the competition experiment involving alcohol substrates* ***1a*** *and* ***1b*** *and 9-anthracenoyl chloride* ***2h****.*

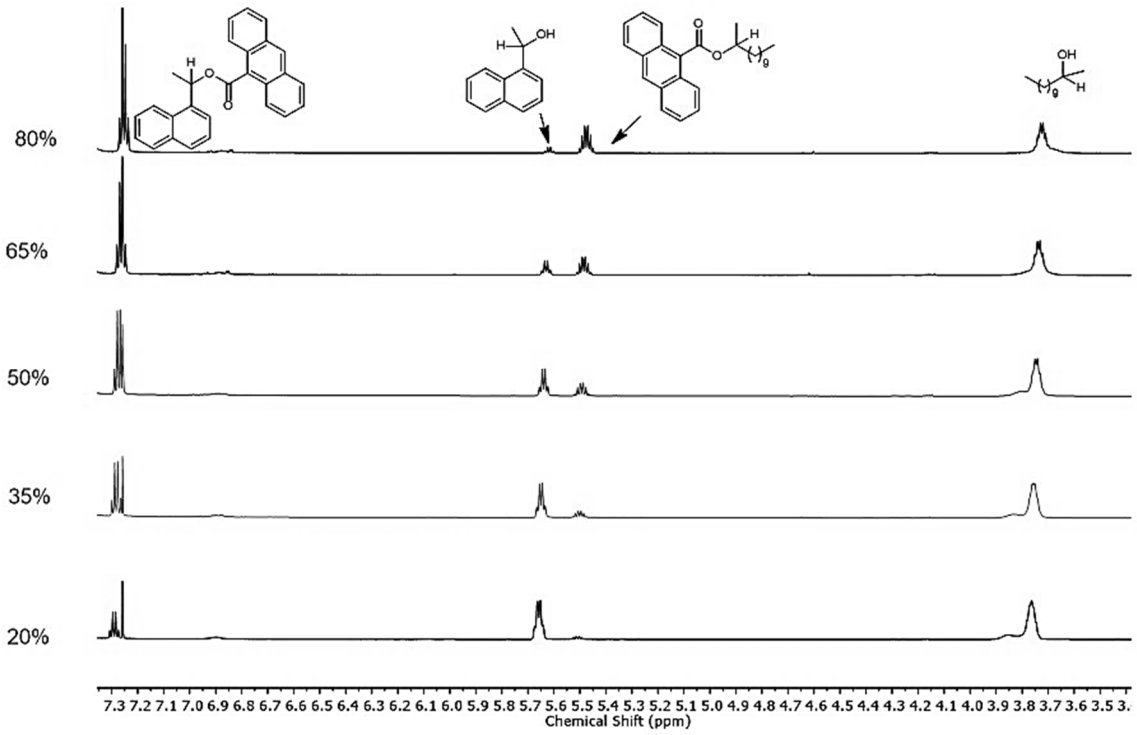

Figure S3: 37. *[Figure S37] Stacked spectra of the competition experiment involving alcohol substrates* ***1a*** *and* ***1b*** *and 9-anthracenoyl chloride* ***2h*** *and TCAP* ***4*** *(5%).*

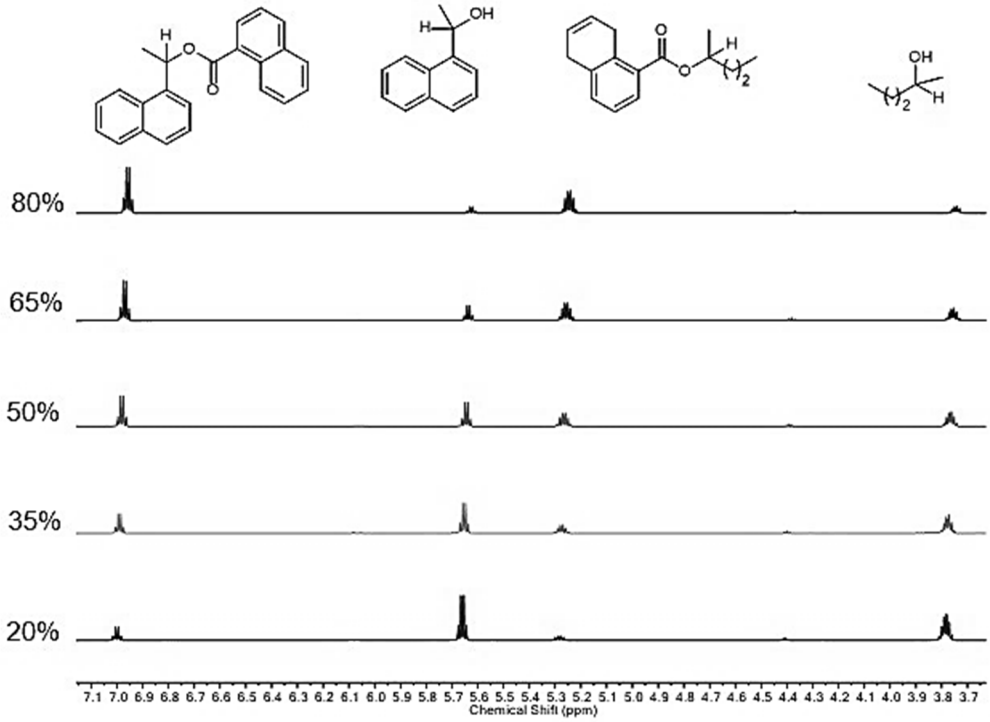

Figure S3: 38. *[Figure S38] Stacked spectra of the competition experiment involving alcohol substrates* ***1c*** *and* ***1b*** *and 1-napthoyl chloride* ***2f****, and TCAP* ***4*** *(2.5%).*

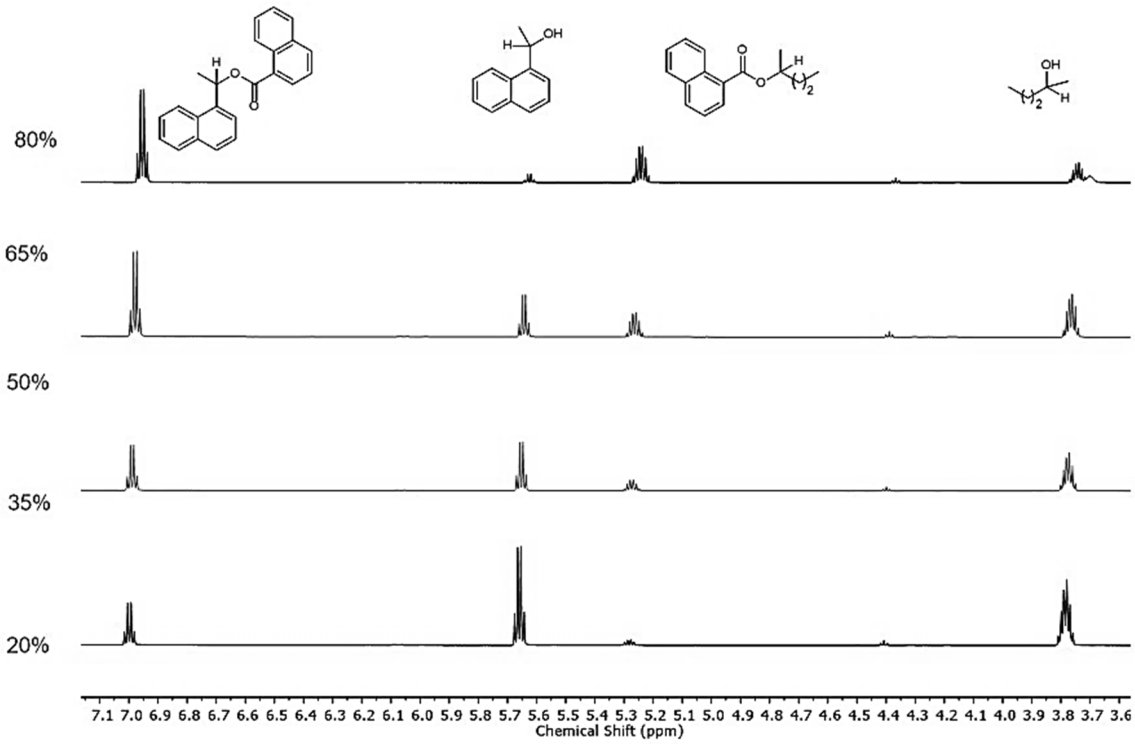

Figure S3: 39. *[Figure S39] Stacked spectra of the competition experiment involving alcohol substrates* ***1c*** *and* ***1b*** *and 1-napthoyl chloride* ***2f****, and TCAP* ***4*** *(7.5%).*

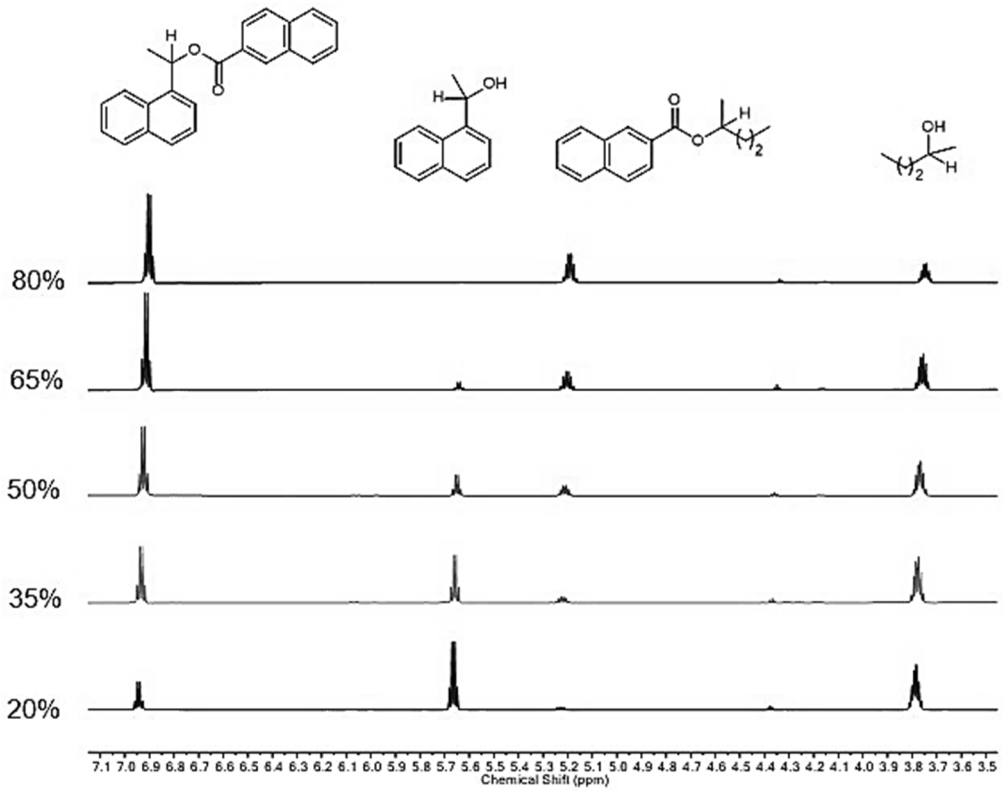

Figure S3: 40. *[Figure S40] Stacked spectra of the competition experiment involving alcohol substrates* ***1c*** *and* ***1b*** *and 2-napthoyl chloride* ***2g****, and TCAP* ***4*** *(2.5%).*

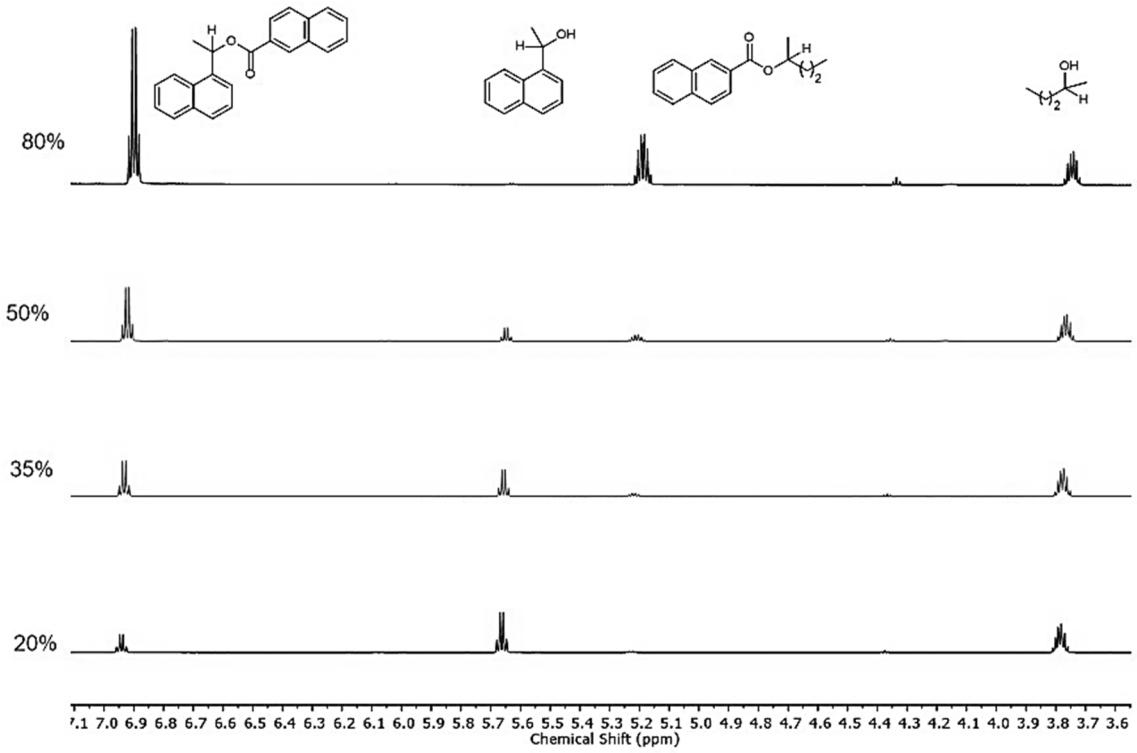

Figure S3: 41. *[Figure S41] Stacked spectra of the competition experiment involving alcohol substrates* ***1c*** *and* ***1b*** *and 2-napthoyl chloride* ***2g****, and TCAP* ***4*** *(7.5%).*

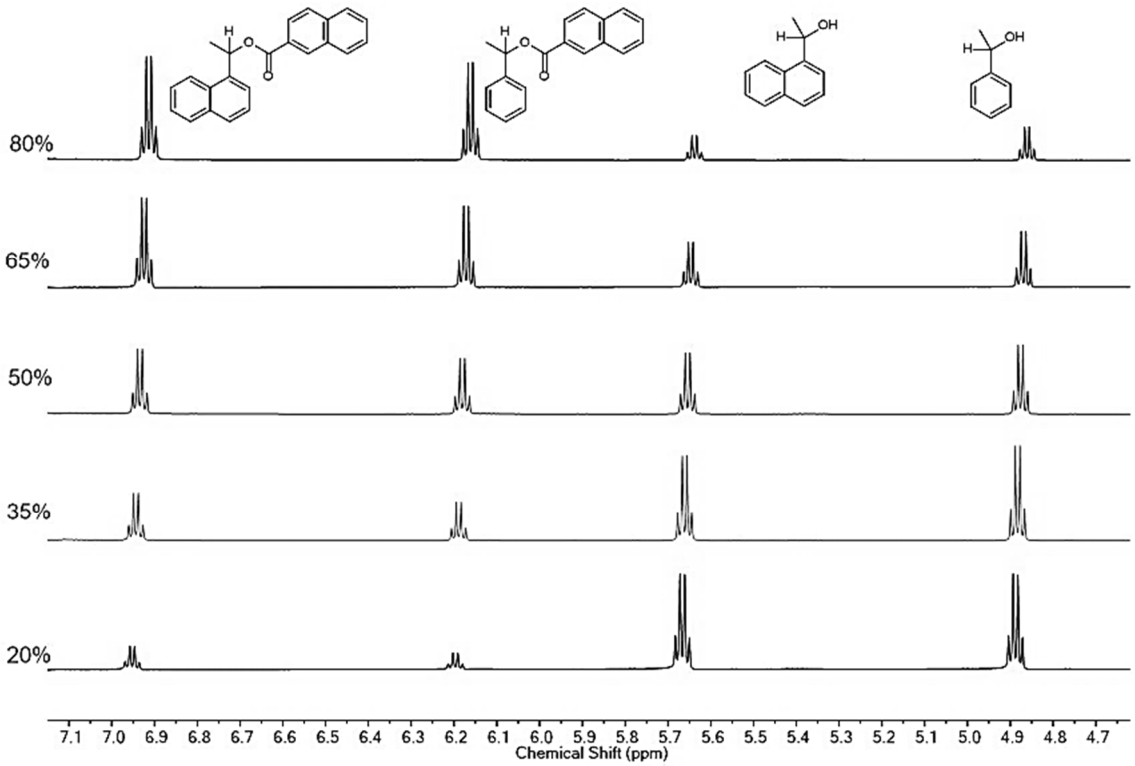

Figure S3: 42. *[Figure S42] Stacked spectra of the competition experiment involving alcohol substrates* ***1b*** *and* ***1d*** *and 2-napthoyl chloride* ***2g****, and TCAP* ***4*** *(2.5%).*

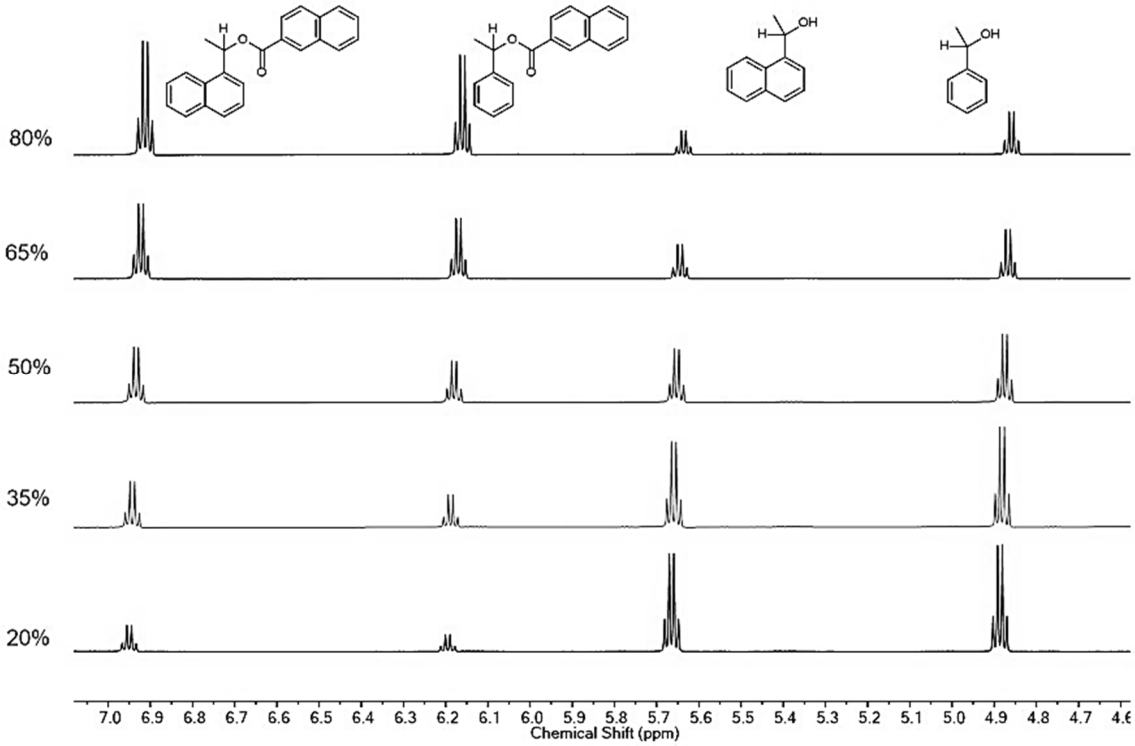

Figure S3: 43. *[Figure S43] Stacked spectra of the competition experiment involving alcohol substrates* ***1b*** *and* ***1d*** *and 2-napthoyl chloride* ***2g****, and TCAP* ***4*** *(7.5%).*

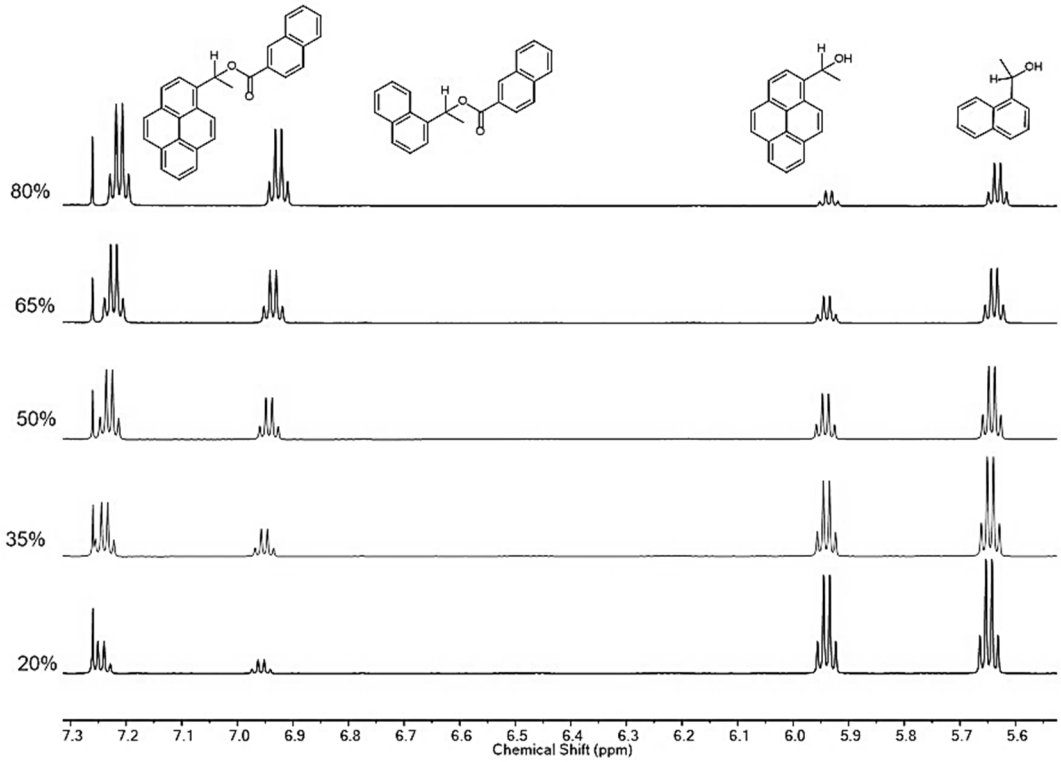

Figure S3: 44. *[Figure S44] Stacked spectra of the competition experiment involving alcohol substrates* ***1b*** *and* ***1e*** *and 2-napthoyl chloride* ***2g****, and TCAP* ***4*** *(2.5%).*

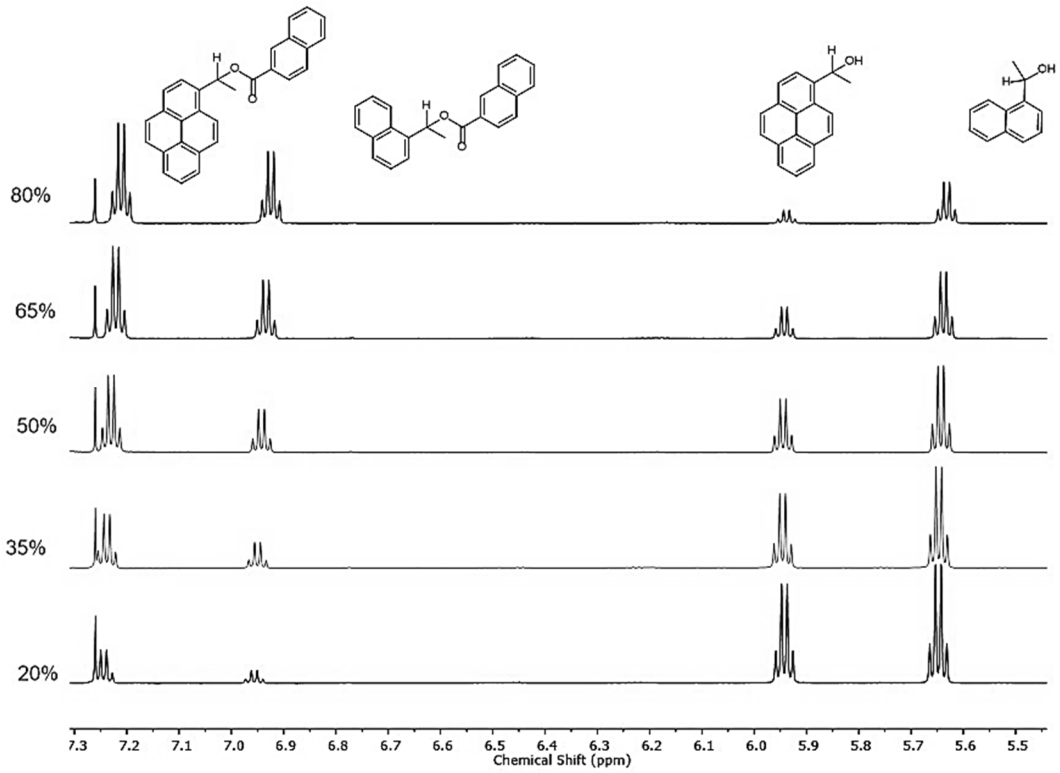

Figure S3: 45. *[Figure S45] Stacked spectra of the competition experiment involving alcohol substrates* ***1b*** *and* ***1e*** *and 2-napthoyl chloride* ***2g****, and TCAP* ***4*** *(7.5%).*

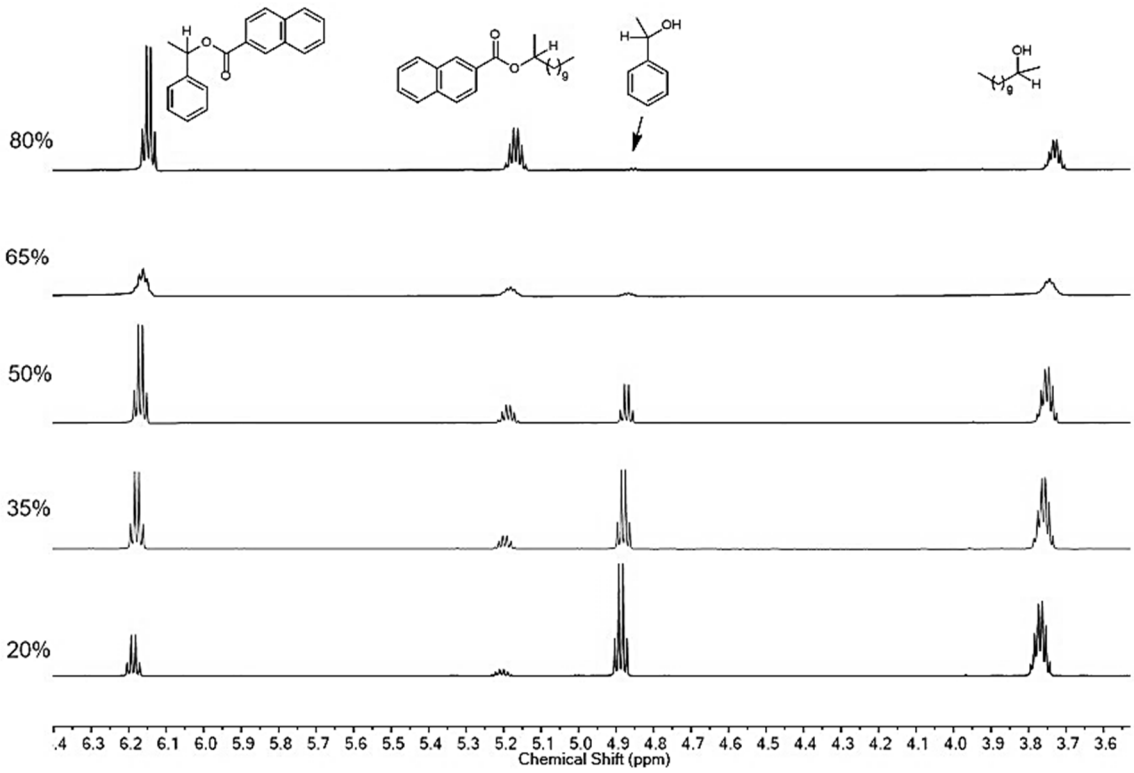

Figure S3: 46. *[Figure S46] Stacked spectra of the competition experiment involving alcohol substrates* ***1a*** *and* ***1d*** *and 2-napthoyl chloride* ***2g****, and TCAP* ***4*** *(2.5%).*

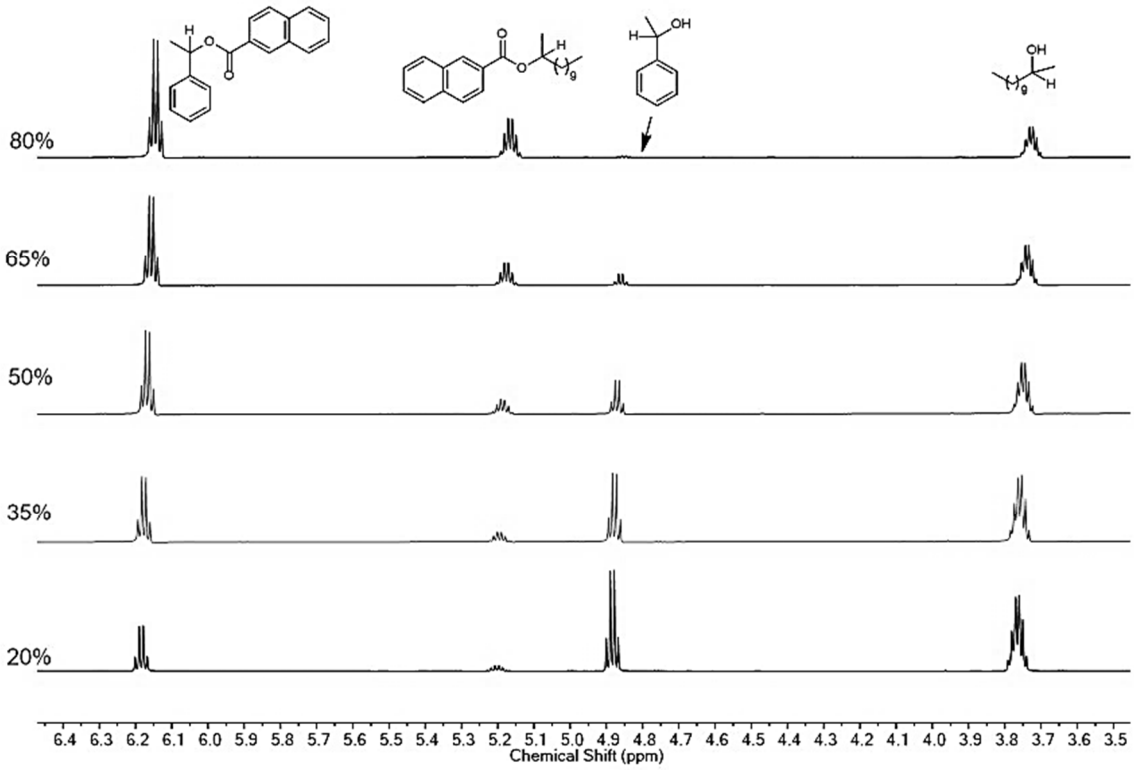

Figure S3: 47. *[Figure S47] Stacked spectra of the competition experiment involving alcohol substrates* ***1a*** *and* ***1d*** *and 2-napthoyl chloride* ***2g****, and TCAP* ***4*** *(7.5%).*

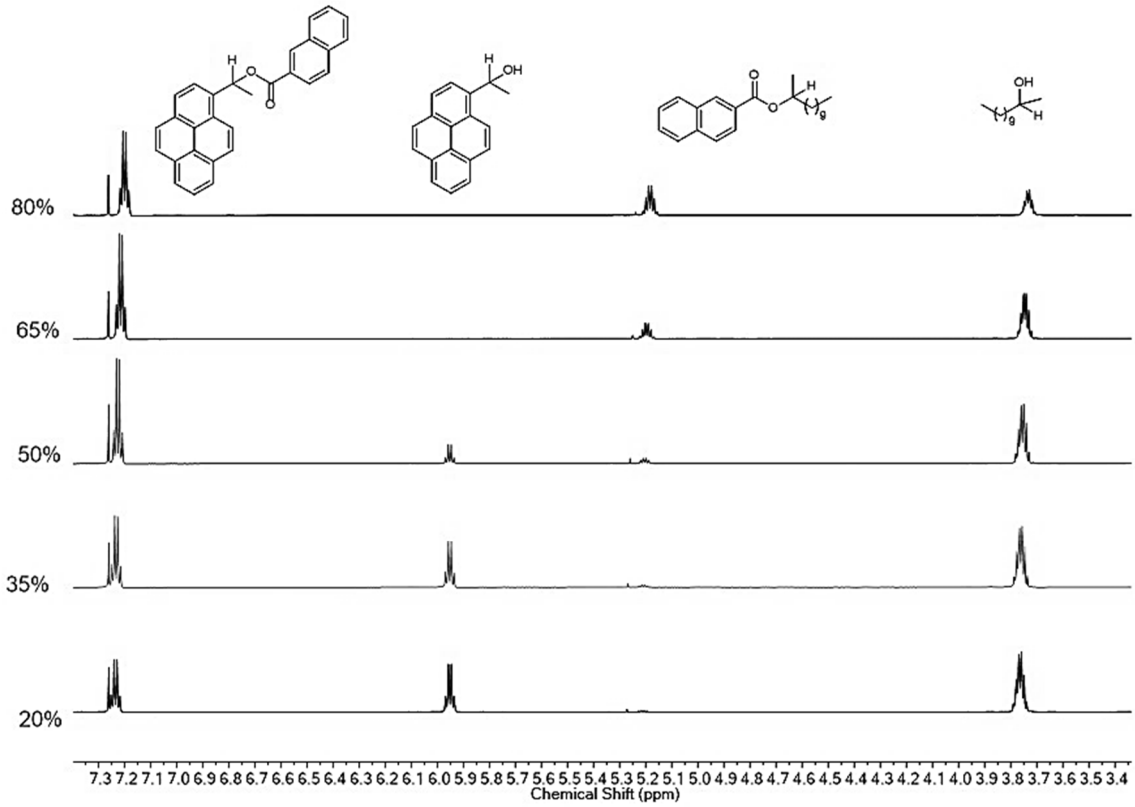

Figure S3: 48. *[Figure S48] Stacked spectra of the competition experiment involving alcohol substrates* ***1a*** *and* ***1e*** *and 2-napthoyl chloride* ***2g****, and TCAP* ***4*** *(2.5%).*

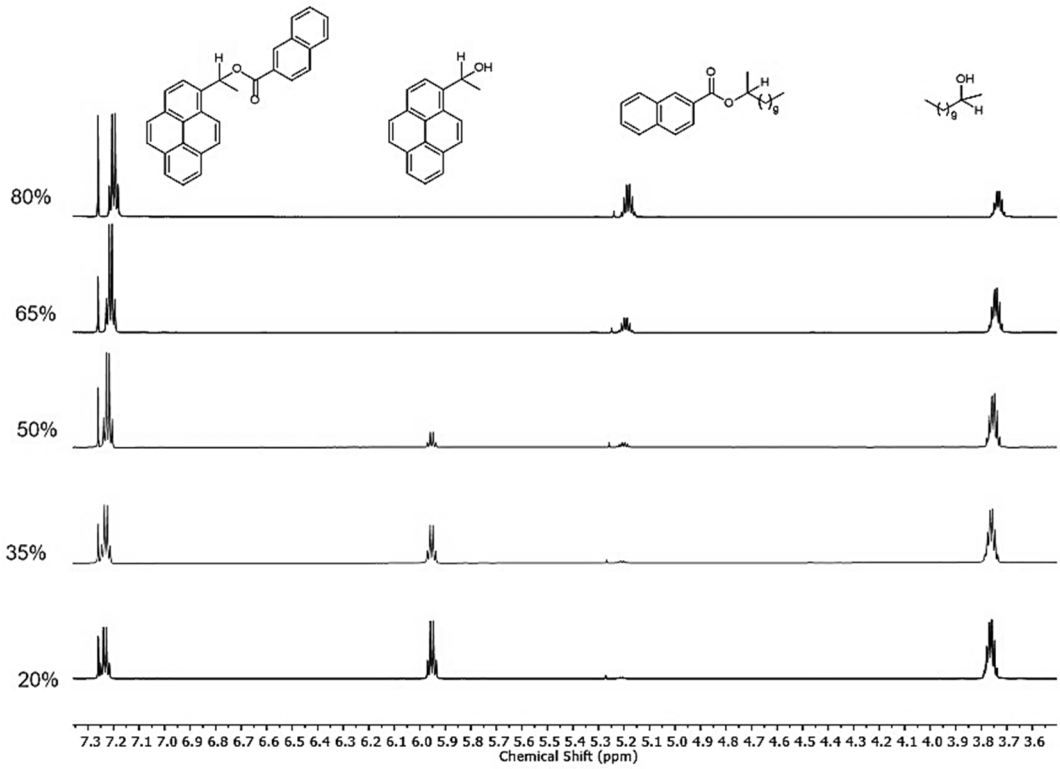

Figure S3: 49. *[Figure S49] Stacked spectra of the competition experiment involving alcohol substrates* ***1a*** *and* ***1e*** *and 2-napthoyl chloride* ***2g****, and TCAP* ***4*** *(7.5%).*

3.1.7 Solvent Influence on the Chemoselectivity

In order to quantify the influence of the solvent on the chemoselectivity, the competition experiment between the alcohol substrates **1a** and **1b** with 2-napthoyl chloride **2g** and in presence of 5% TCAP was carried out in different anhydrous solvents: trifluorotoluene, acetonitrile, toluene, benzene and tetrahydrofuran. With the aim of getting high chemoselectivities and, thus, a better appreciation of the results, only the competition experiment involving 10% of acid chloride with respect to both alcohols were performed. The concentrations of the starting materials were (in mol/L): **1a** 0.1, **1b** 0.1, **2i** 0.02, Et_3N 0.0049 and **TCAP** 0.01. This experiment was also performed in chloroform-*d1* as control reaction.

All of the reactions were carried out at the same time in 10 mL calibrated flasks, which were gathered into a desiccator flushed with a constant nitrogen current. The reaction mixtures were stirred at room temperature, without cryostat control, for ten days to be sure that all the reactions were complete and equilibrium was reached.

Table S3: 1 7 shows the chemoselectivity and conversion values obtained for each solvent while a stack of the ^{1}H NMR spectra is shown in **Figure S3: 50**.

Table S3: 7 [Table S7] Conversion and Chemoselectivity values of competition experiment between **1a**, **1b** and **2g** with different solvents.

Solvent	Conversion (%)	Chemoselectivity	Selectivity
Trifluorotoluene	7.93	0.831	11
Chloroform-d_1	8.48	0.802	9.5
Acetonitrile	6.96	0.750	7.5
Toluene	7.90	0.700	6
Benzene	8.22	0.671	5.5
Tetrahydrofuran	8.26	0.441	2-3

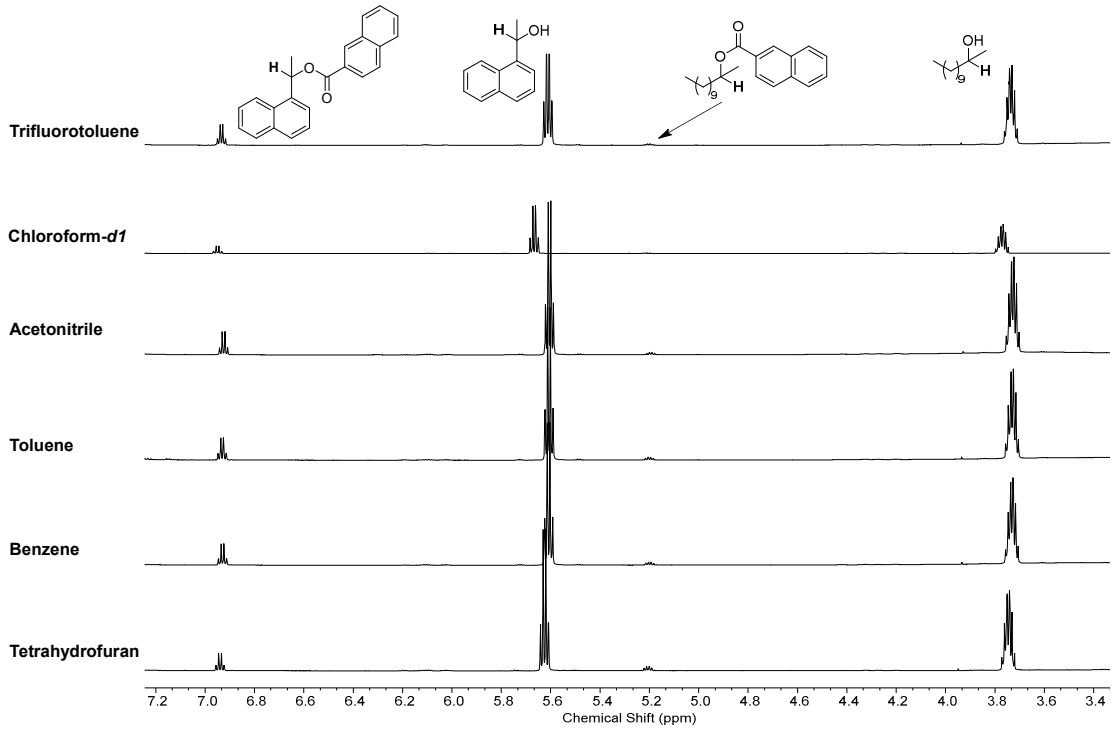

Figure S3: 50. *[Figure S50] Stacked ^{1}H NMR spectra of competition experiment between **1a** and **1b** and 2-napthoyl chloride **2g** and TCAP **4** (5%). The solvent used in the reaction is shown.*

3.1.8 Temperature Effect on the Chemoselectivity

As shown in the manuscript, a decrease in temperature is commonly expected to increase selectivity.[3] In the competition experiment that was carried out here, the variation from 23 °C to 10 °C in the temperature of the competition experiment provides a change in the selectivity from 8.5 to 10. This translates to a change in the entropy barrier of 11.64 J $L^{-1}\cdot mol^{-1}$. In order to clarify this entropy variation, the use of the well-known Eyring equation Eq. S3: 9 is presented here in detail.

$$\log\frac{k_1}{k_2} = \frac{\Delta\Delta H^{\neq}}{2.303\cdot R\cdot T} - \frac{\Delta\Delta S^{\neq}}{2.303\cdot R} \qquad \text{Eq. S3: 9}$$

Experimental selectivity at provided temperature, enthalpy (H) and entropy (S) barriers and the R constant are given by:

$$S = 8.5 \quad T = 23\ ℃ = 296.15\ K$$
$$S = 10 \quad T = 10\ ℃ = 283.15\ K$$
$$\Delta\Delta H^{\neq} = \Delta\Delta H_2^{\neq} - \Delta\Delta H_1^{\neq}$$
$$\Delta\Delta S^{\neq} = \Delta\Delta S_2^{\neq} - \Delta\Delta S_1^{\neq}$$
$$R = 8.31451\ J/K\cdot mol$$

When these values are incorporated to the Eq. S3: 9, Eq. S3: 10 and Eq. S3: 11 are obtained:

$$\log(8.5) = \frac{\Delta\Delta H^{\neq}}{2.303\cdot R\cdot 296.15} - \frac{\Delta\Delta S^{\neq}}{2.303\cdot R} = 0.9294 \qquad \text{Eq. S3: 10}$$

$$\log(10) = \frac{\Delta\Delta H^{\neq}}{2.303\cdot R\cdot 283.15} - \frac{\Delta\Delta S^{\neq}}{2.303\cdot R} = 1.0000 \qquad \text{Eq. S3: 11}$$

Eq. S3: 12 and Eq. S3: 13 results when Eq. S3: 10 and Eq. S3: 11 are multiplied by the constant factor 2.303·R.

$$\frac{\Delta\Delta H^{\neq}}{296.15} - \Delta\Delta S^{\neq} = 17.79683 \qquad \text{Eq. S3: 12}$$

$$\frac{\Delta\Delta H^{\neq}}{283.15} - \Delta\Delta S^{\neq} = 19.148317 \qquad \text{Eq. S3: 13}$$

These last equations translate immediately into Eq. S3: 14 by eliminating $\Delta\Delta S^{\neq}$

$$\frac{\Delta\Delta H^{\neq}}{296.15} - \frac{\Delta\Delta H^{\neq}}{283.15} = -1.351489 \qquad \text{Eq. S3: 14}$$

$$\Delta\Delta H^{\neq}\cdot\left(\frac{1}{296.15} - \frac{1}{283.15}\right) = -1.351489 \qquad \text{Eq. S3: 15}$$

Then, the enthalpy and entropy barriers are obtained by applying Eq. S3: 16 and Eq. S3: 17.

$$\Delta\Delta H^{\neq} = \Delta\Delta H_2^{\neq} - \Delta\Delta H_1^{\neq} = 8717.6\ J/mol = 8.72\ kJ/mol \qquad \text{Eq. S3: 16}$$

$$\Delta\Delta S^{\neq} = \Delta\Delta S_2^{\neq} - \Delta\Delta S_1^{\neq} = 11.64\ J/K\cdot mol \qquad \text{Eq. S3: 17}$$

3.1.9. ^{1}H NMR and ^{13}C NMR Spectra of Synthesized Compounds

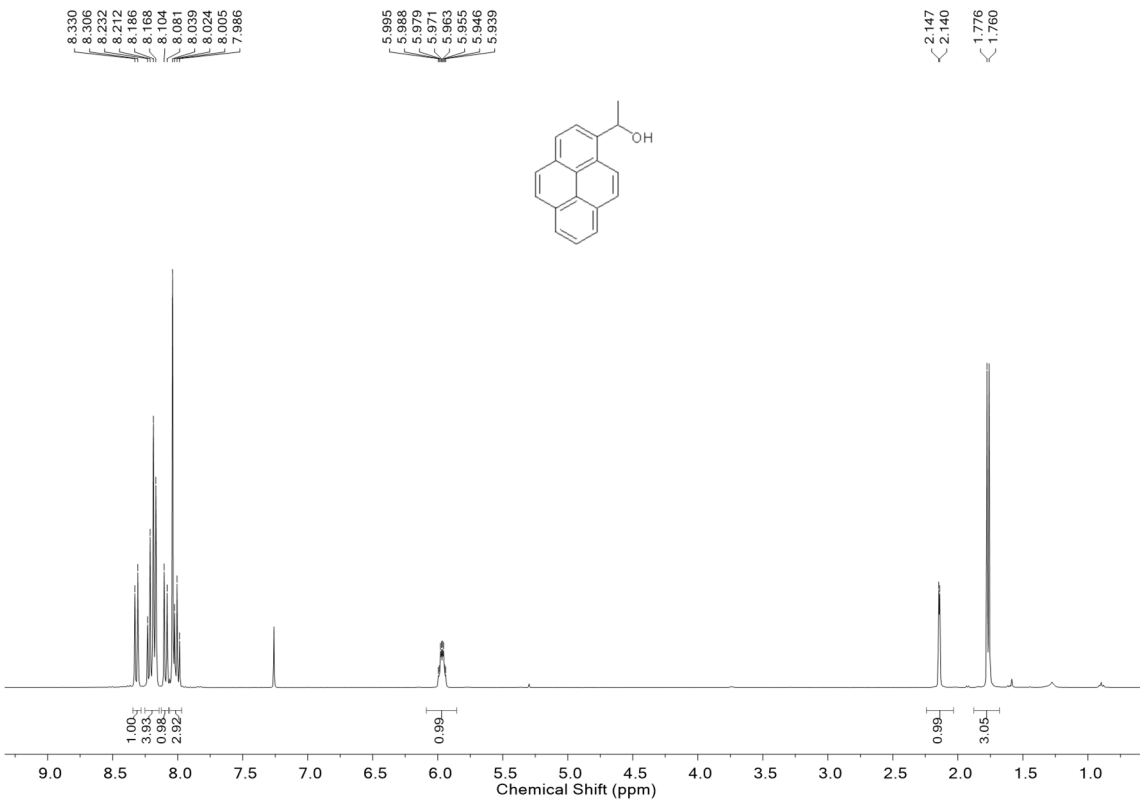

Figure S3: 51. *[Figure S51] ^{1}H NMR spectrum of 1-(1-pyrenyl)ethanol* ***1e*** *($CDCl_3$, 400 MHz).*

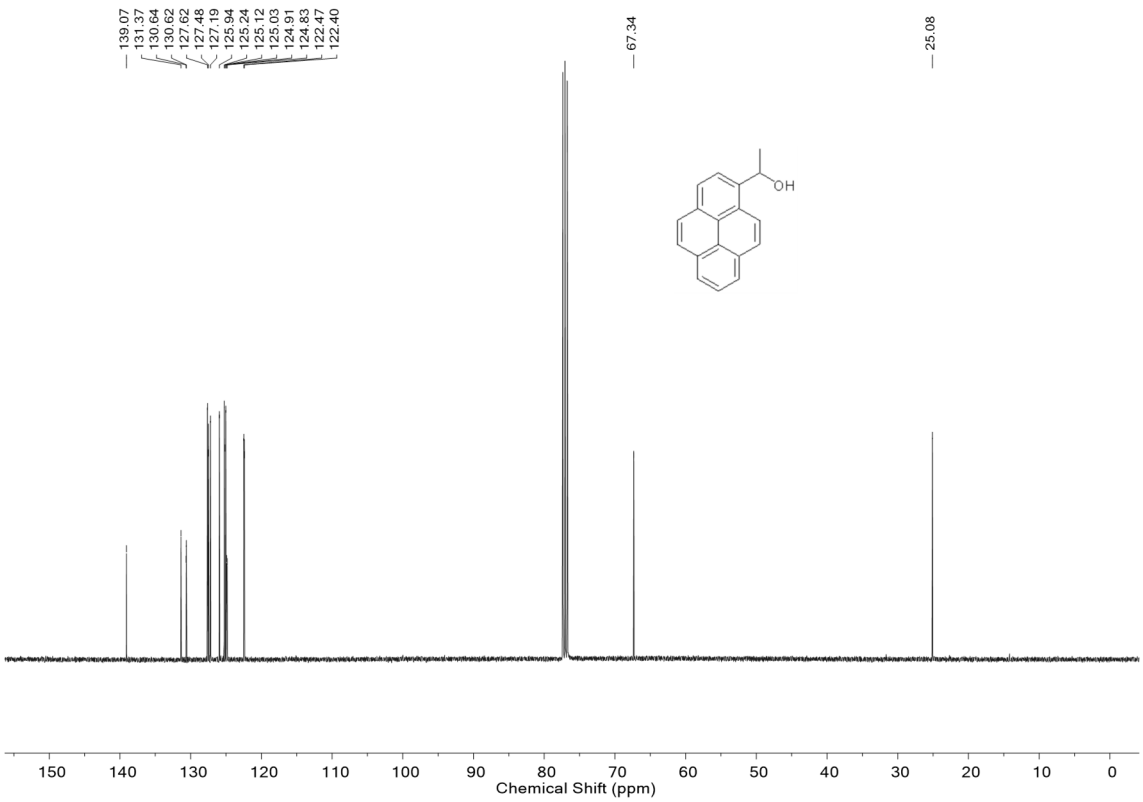

Figure S3: 52. *[Figure S52] ^{13}C NMR spectrum of 1-(1-pyrenyl)ethanol* ***1e*** *($CDCl_3$, 101 MHz).*

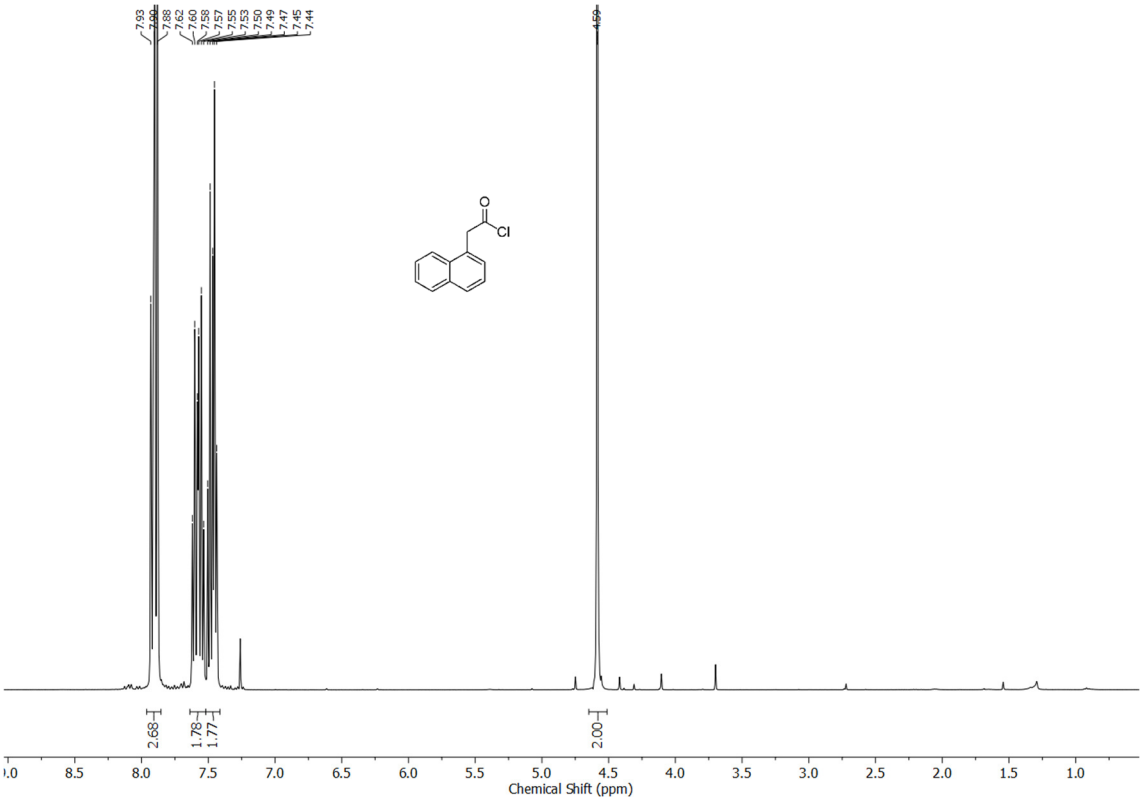

Figure S3: 53. *[Figure S53] ^{1}H NMR spectrum of 2-(1-napthalen-1-yl)acetyl chloride* ***2d*** *($CDCl_3$, 400 MHz).*

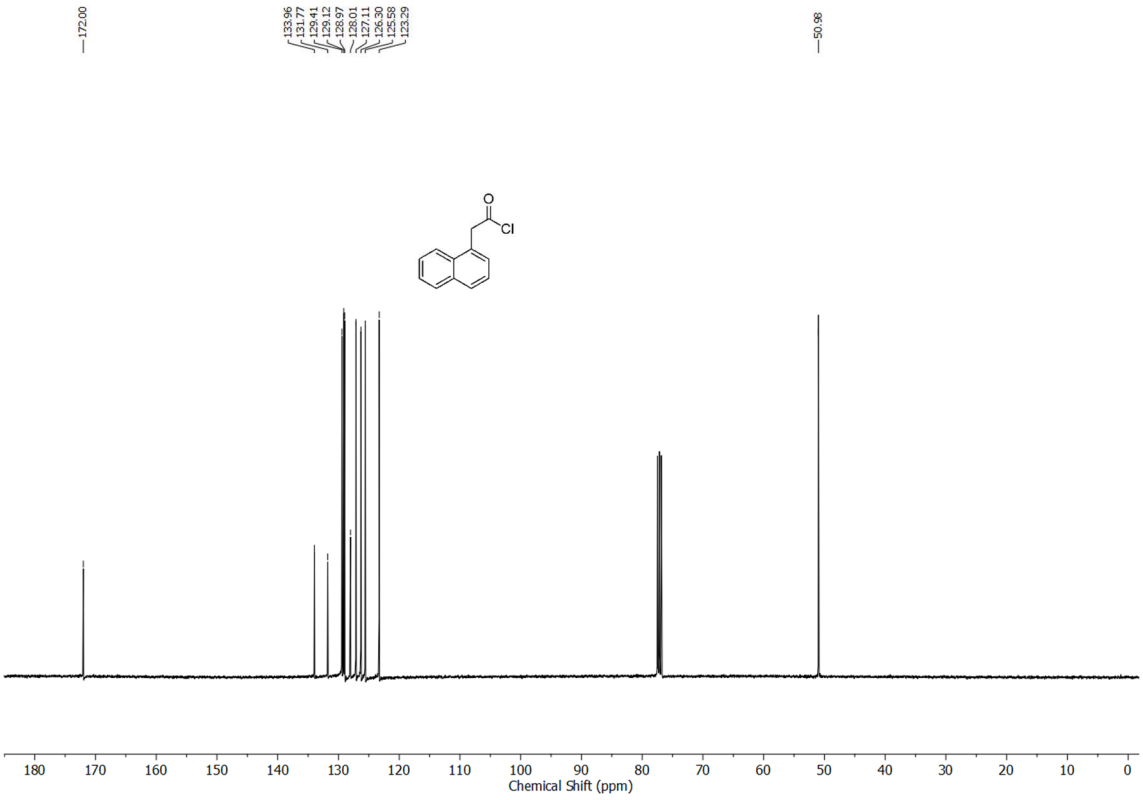

Figure S3: 54. *[Figure S54] ^{13}C NMR spectrum of 2-(1-napthalen-1-yl)acetyl chloride* ***2d*** *($CDCl_3$, 101 MHz).*

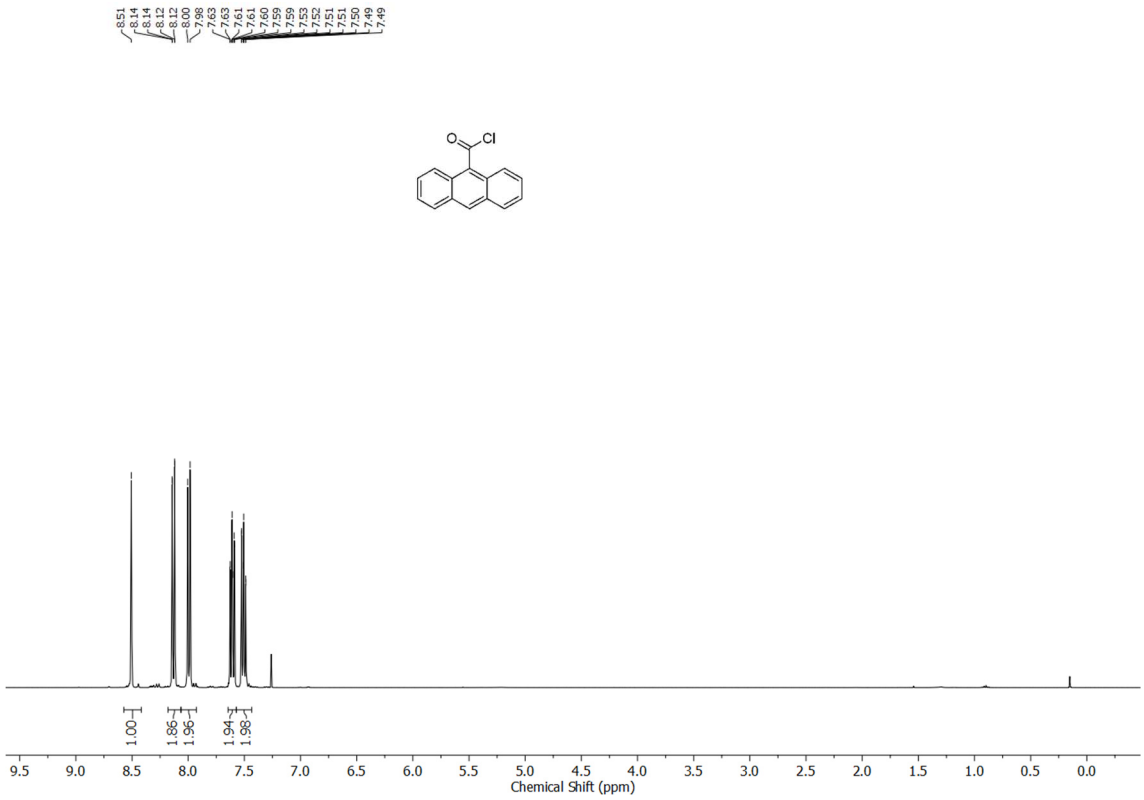

Figure S3: 55. *[Figure S55] ^{1}H NMR spectrum of 9-anthracenoyl chloride* ***2h*** *($CDCl_3$, 400 MHz).*

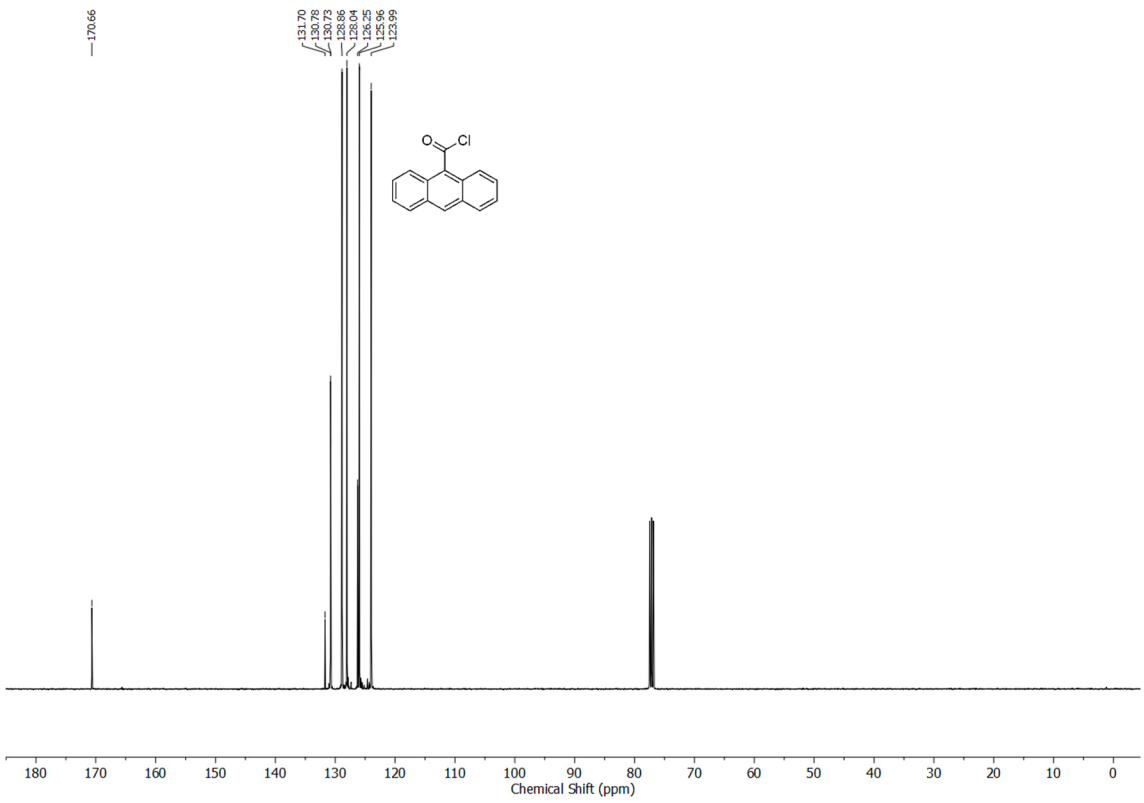

Figure S3: 56. *[Figure S56] ^{13}C NMR spectrum of of 9-anthracenoyl chloride* ***2h*** *($CDCl_3$, 101 MHz).*

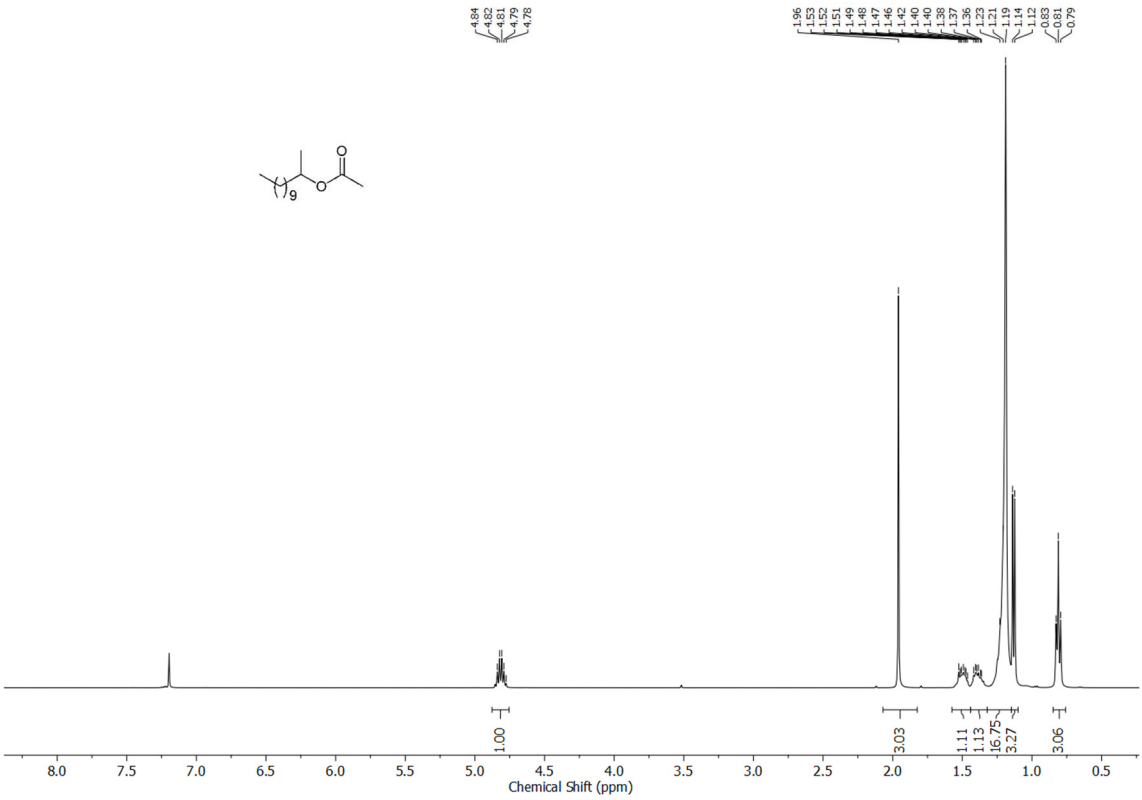

Figure S3: 57. *[Figure S57] ^{1}H NMR spectrum of the ester* ***3ab*** *($CDCl_3$, 400 MHz).*

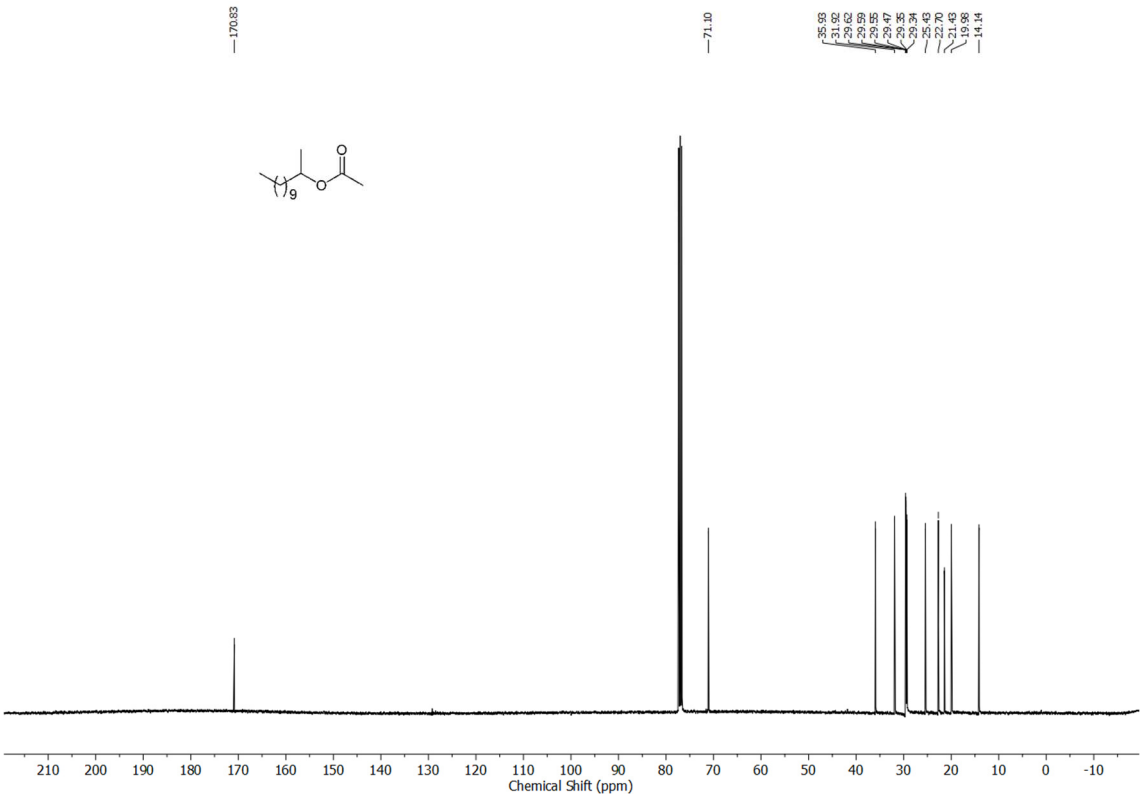

Figure S3: 58. *[Figure S58] ^{13}C NMR spectrum of the ester* ***3ab*** *($CDCl_3$, 101 MHz).*

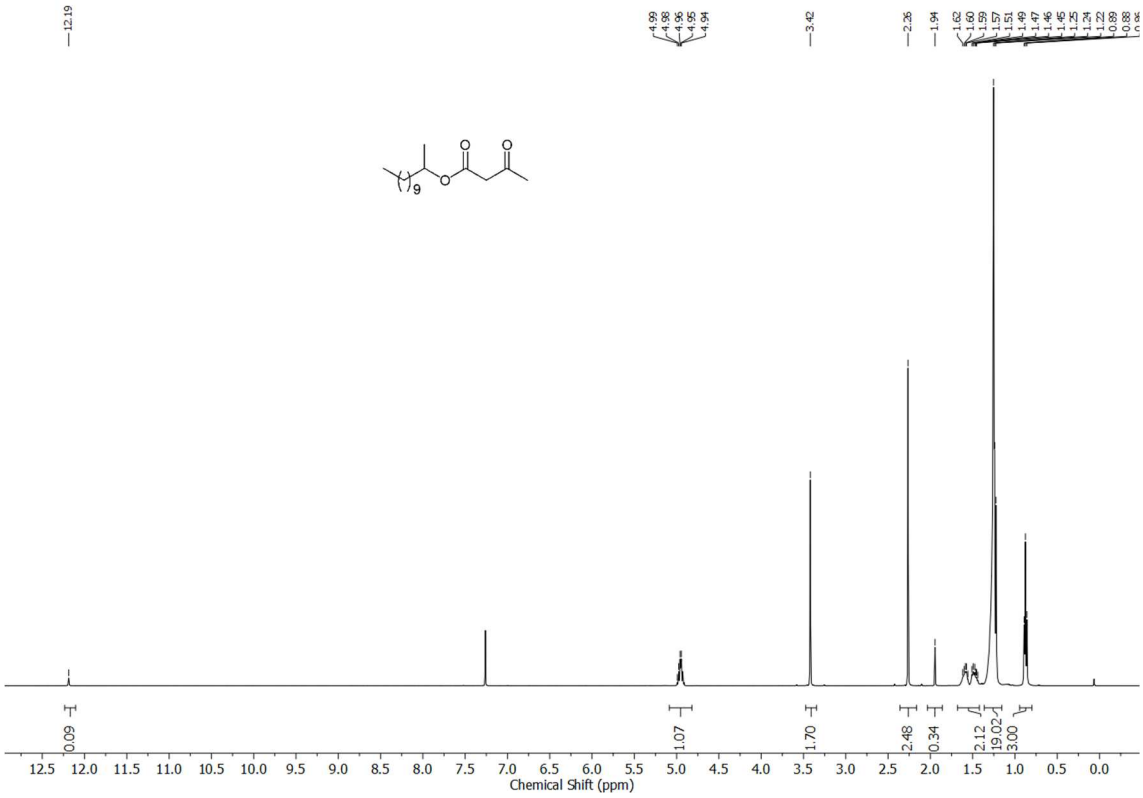

Figure S3: 59. *[Figure S59] ^{1}H NMR spectrum of the ester **7b** ($CDCl_3$, 400 MHz).*

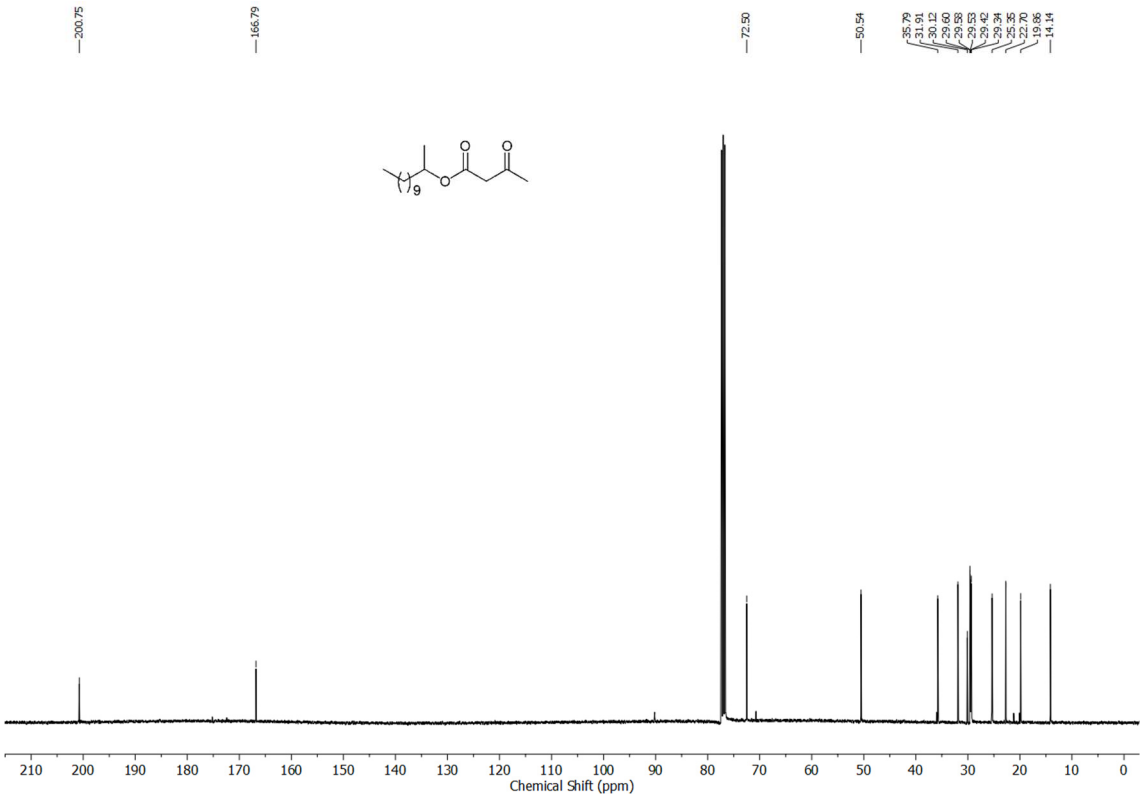

Figure S3: 60. *[Figure S60] ^{13}C NMR spectrum of the ester **7b** ($CDCl_3$, 101 MHz).*

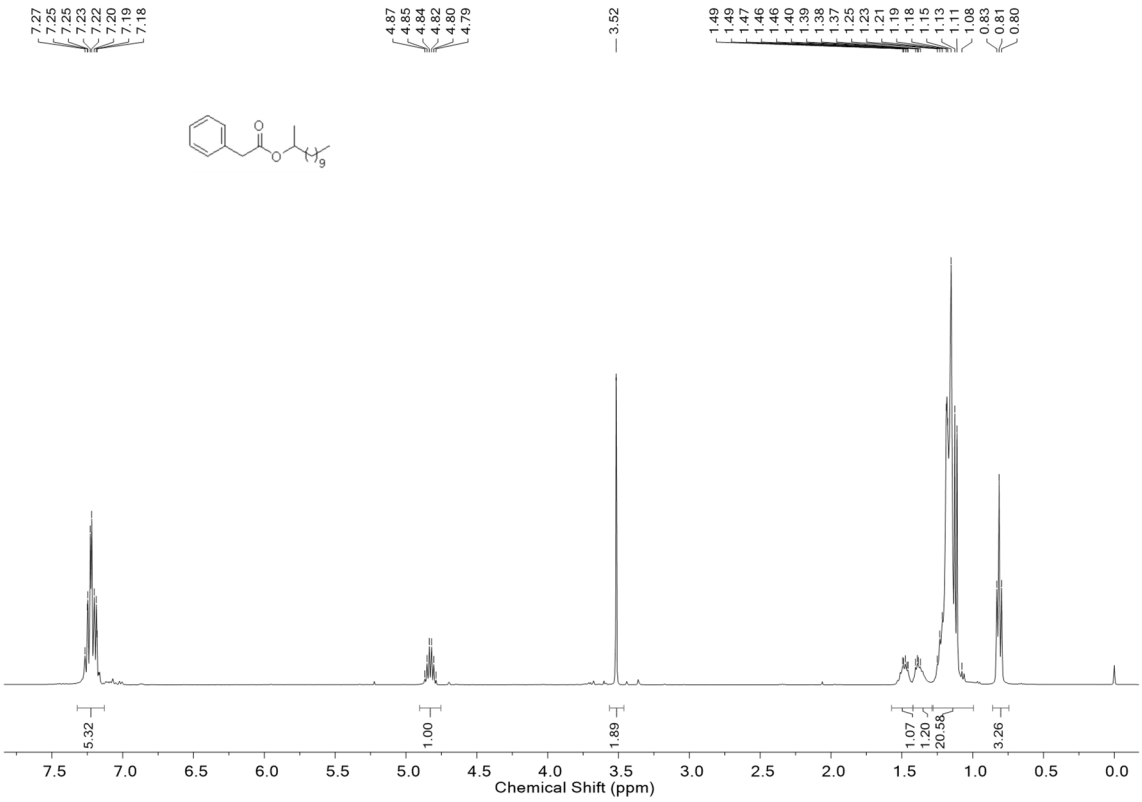

Figure S3: 61. *[Figure S61] ^{1}H NMR spectrum of the ester* ***3ac*** *($CDCl_3$, 400 MHz).*

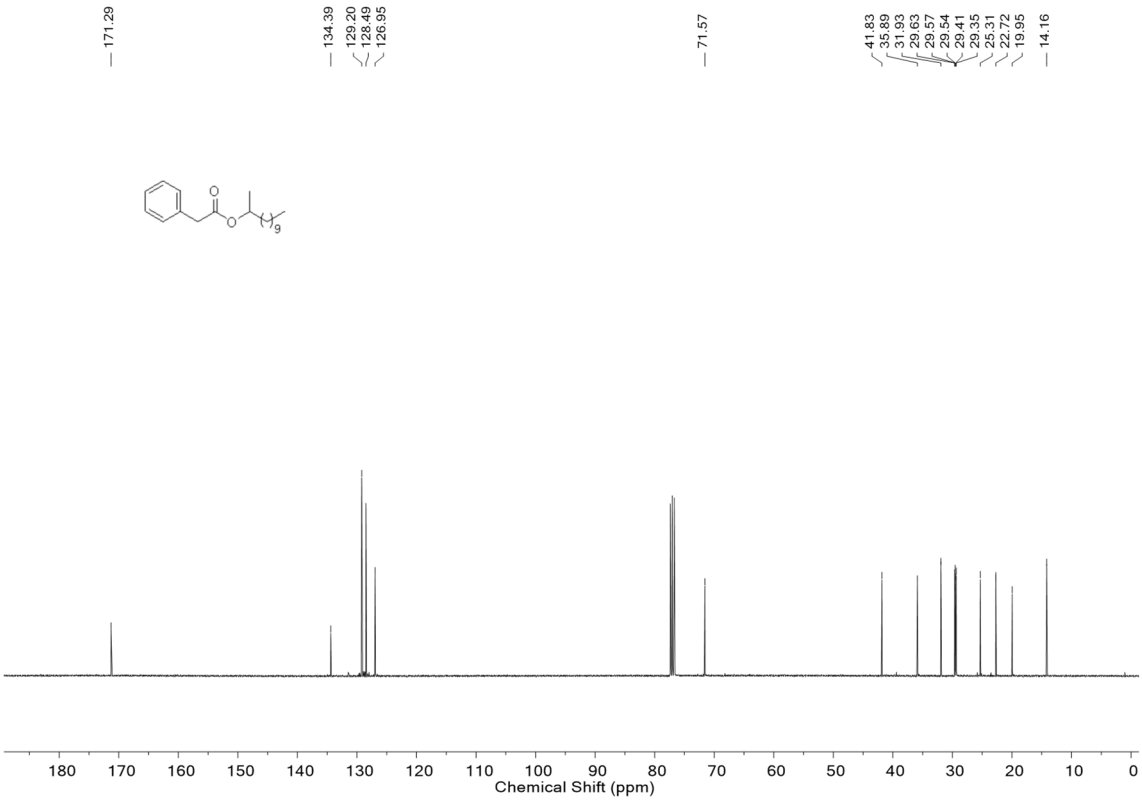

Figure S3: 62. *[Figure S62] ^{13}C NMR spectrum of the ester* ***3ac*** *($CDCl_3$, 101 MHz).*

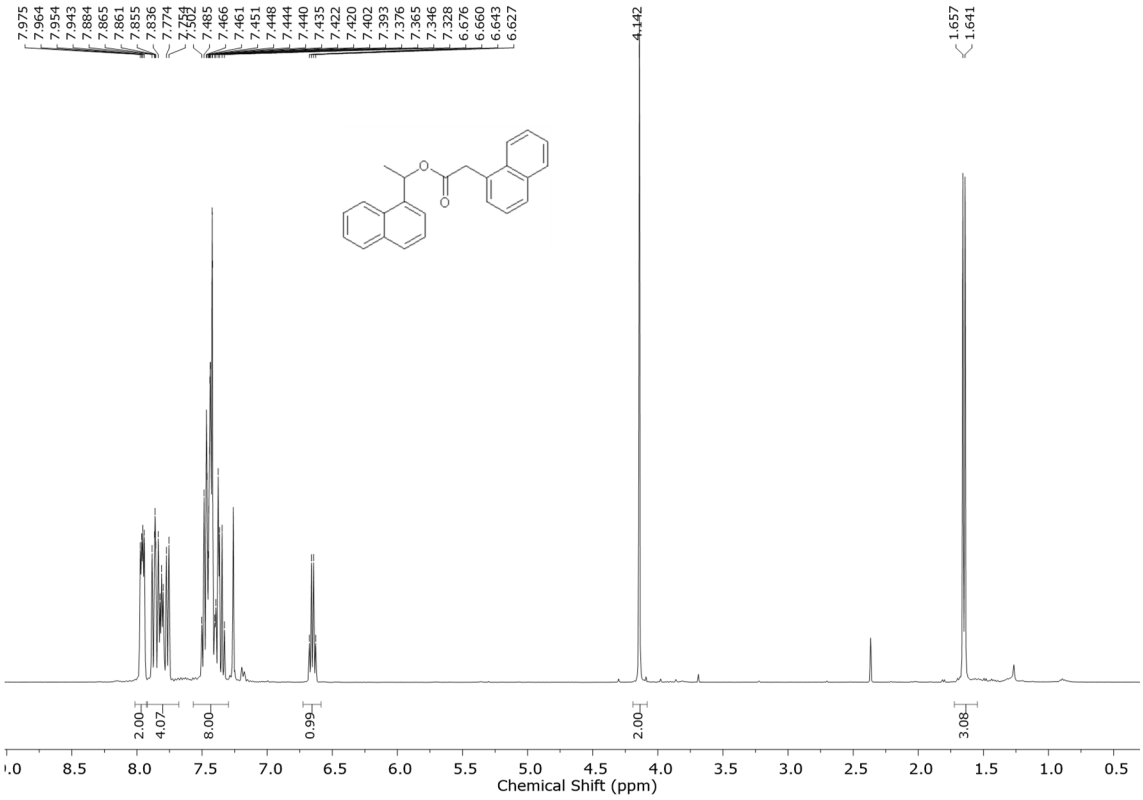

Figure S3: 63. *[Figure S63] ^{1}H NMR spectrum of the ester* ***3bd*** *($CDCl_3$, 400 MHz).*

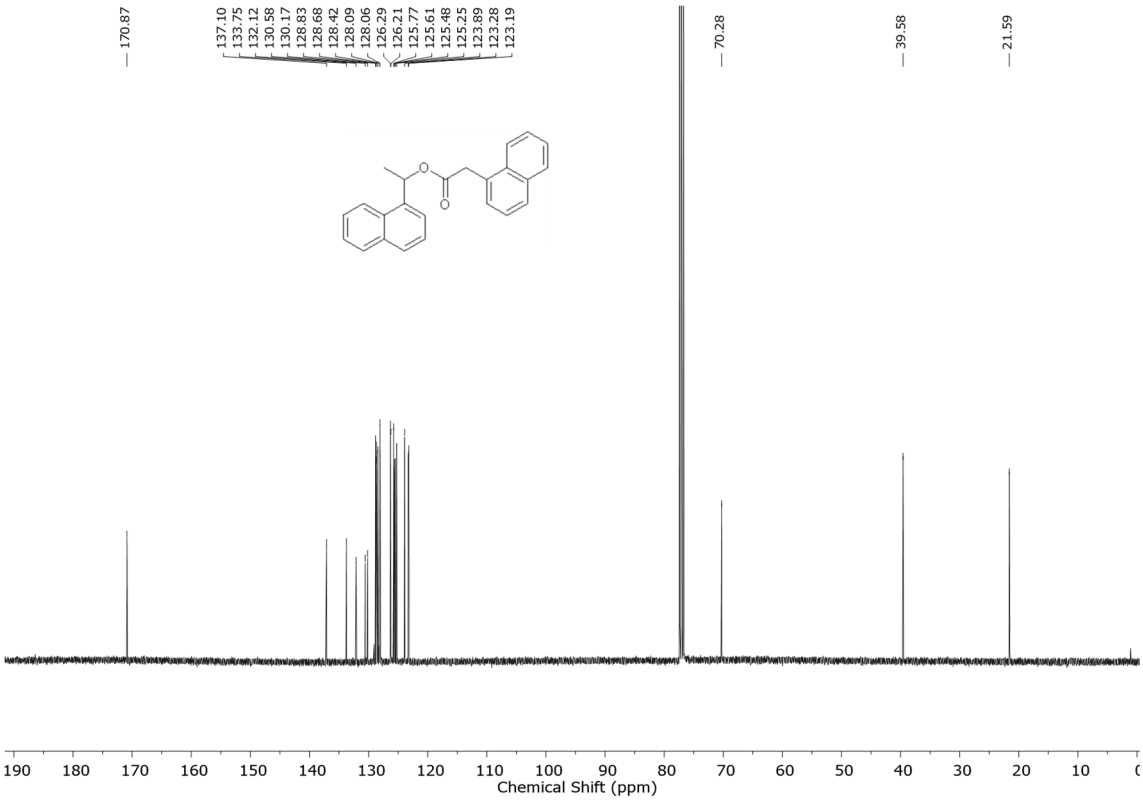

Figure S3: 64. *[Figure S64] ^{13}C NMR spectrum of the ester* ***3bd*** *($CDCl_3$, 101 MHz).*

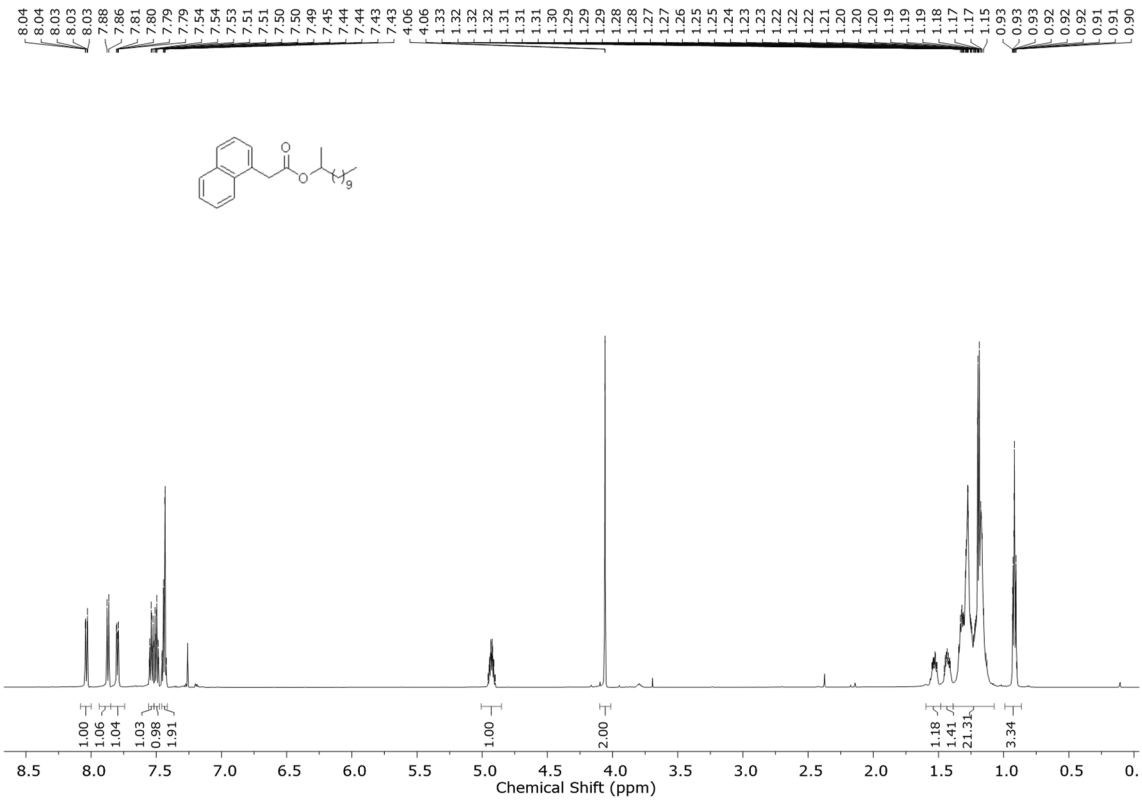

Figure S3: 65. *[Figure S65] ^{1}H NMR spectrum of the ester* ***3ad*** *($CDCl_3$, 600 MHz).*

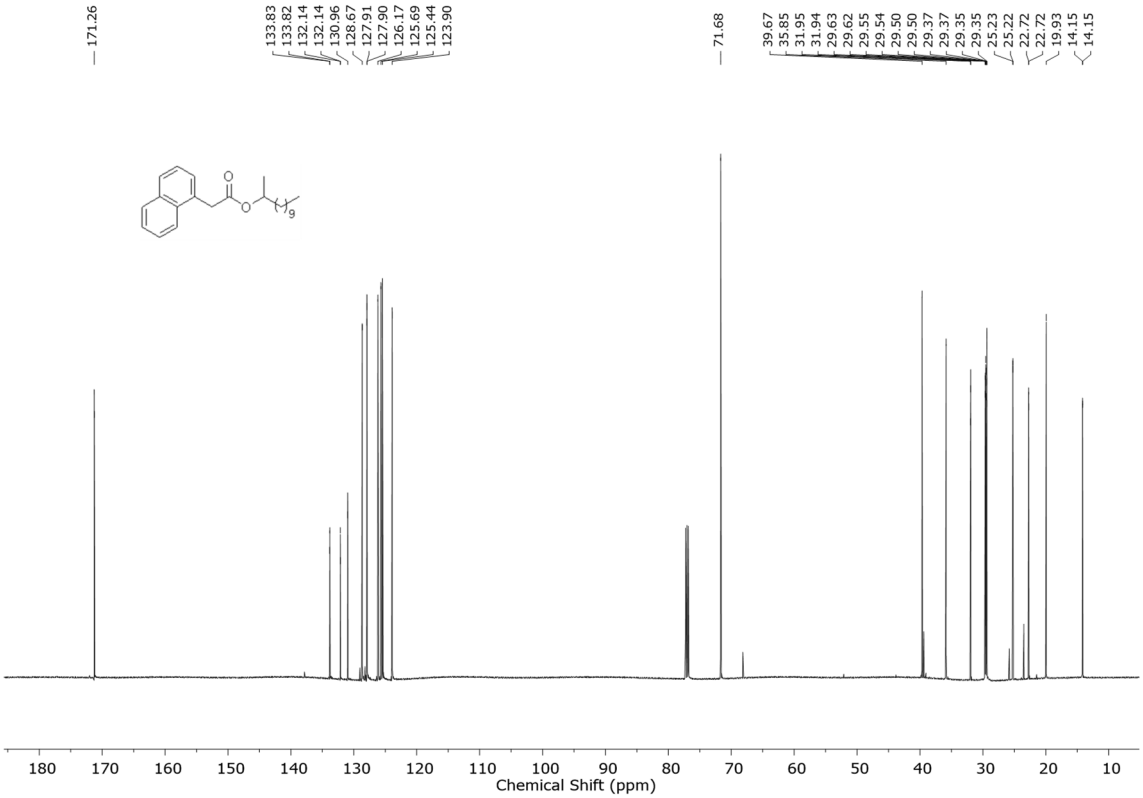

Figure S3: 66. *[Figure S66] ^{13}C NMR spectrum of the ester* ***3ad*** *($CDCl_3$, 151 MHz).*

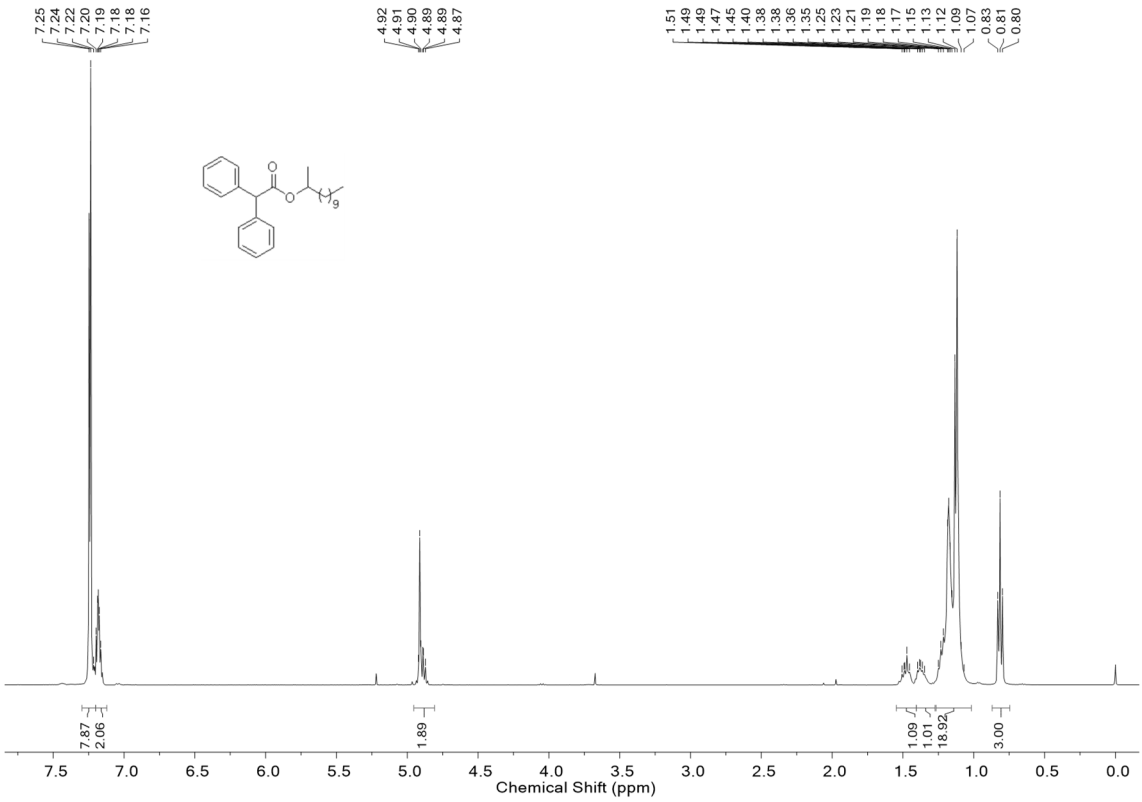

Figure S3: 67. *[Figure S67] ^{1}H NMR spectrum of the ester* ***3ae*** *($CDCl_3$, 400 MHz).*

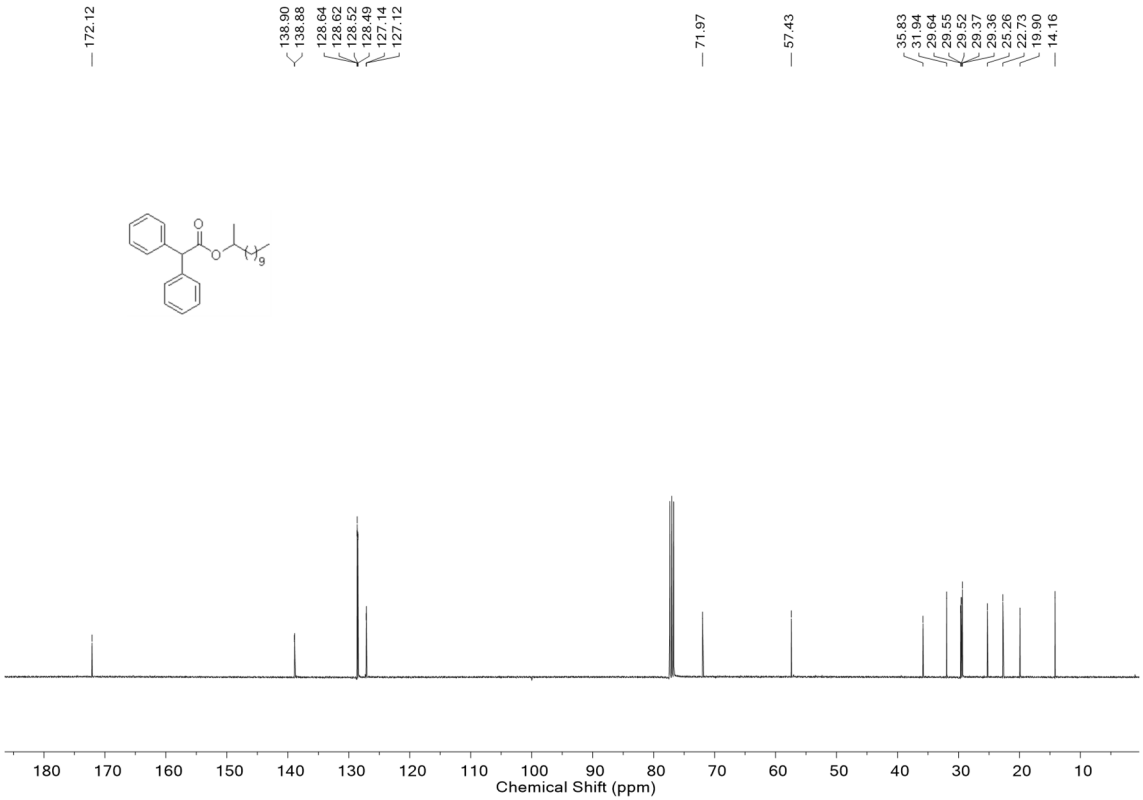

Figure S3: 68. *[Figure S68] ^{13}C NMR spectrum of the ester* ***3ae*** *($CDCl_3$, 101 MHz).*

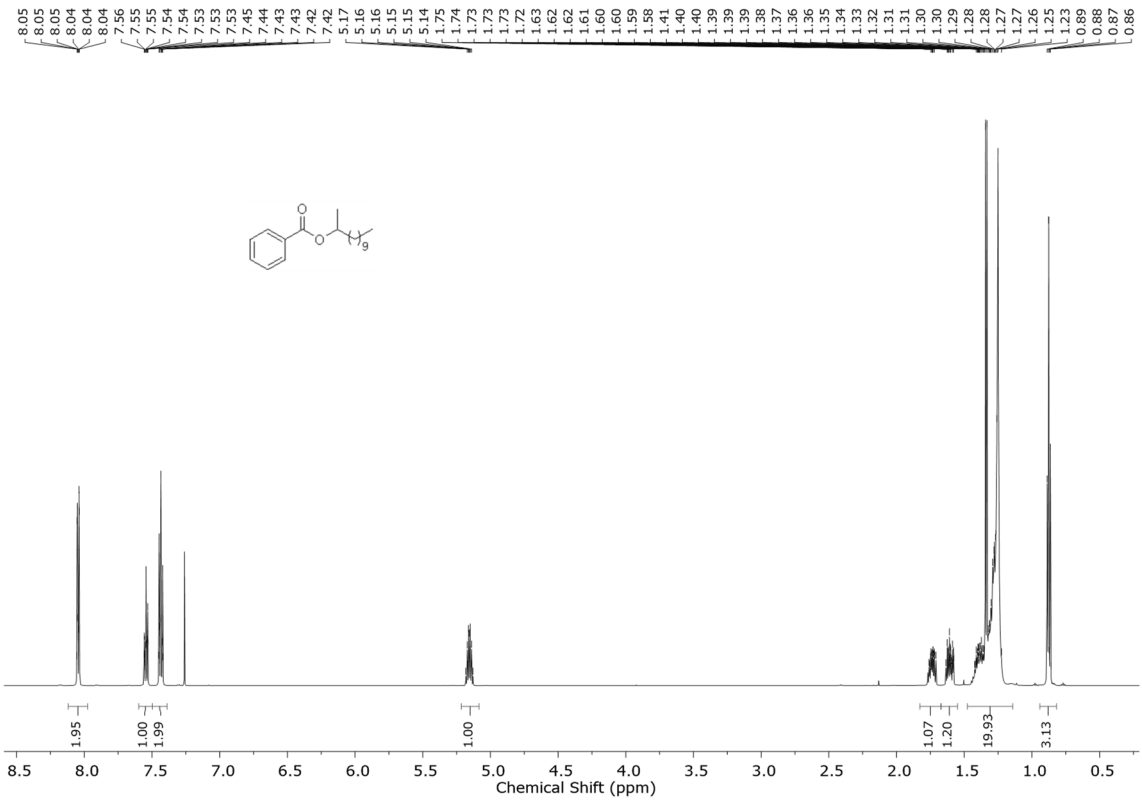

Figure S3: 69. *[Figure S69] ^{1}H NMR spectrum of the ester **3aa** ($CDCl_3$, 600 MHz).*

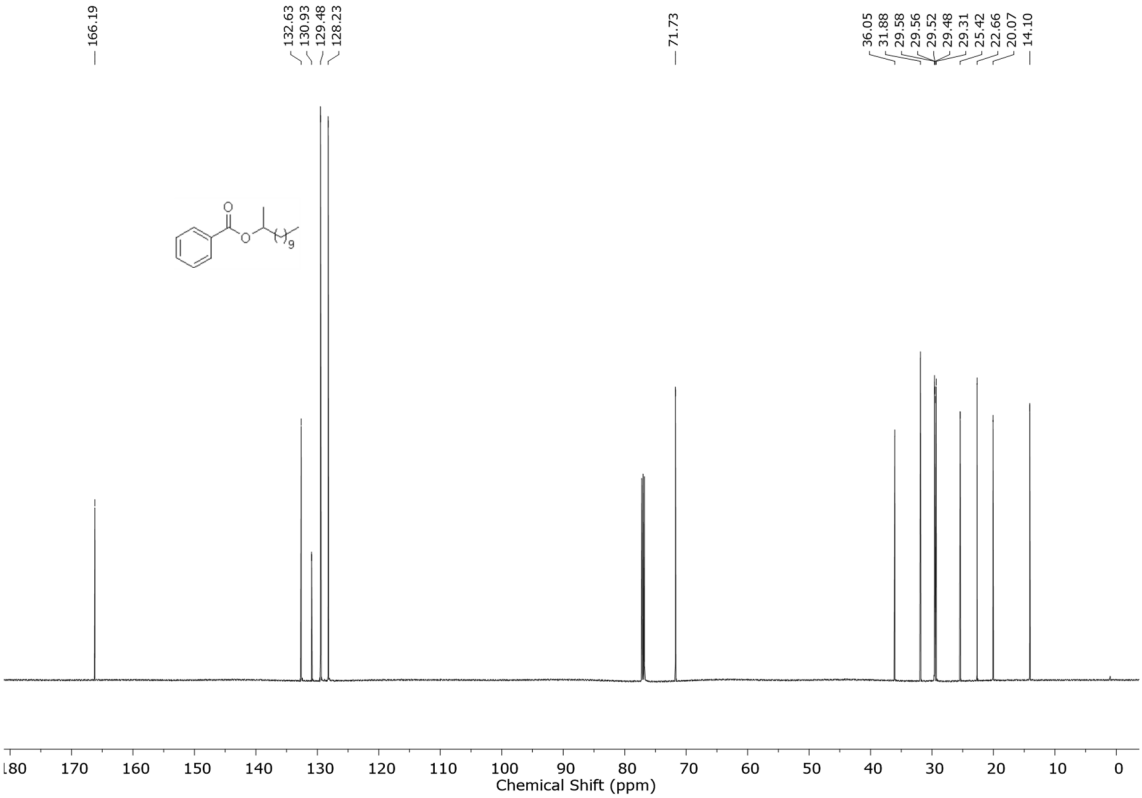

Figure S3: 70. *[Figure S70] ^{13}C NMR spectrum of the ester **3aa** ($CDCl_3$, 151 MHz).*

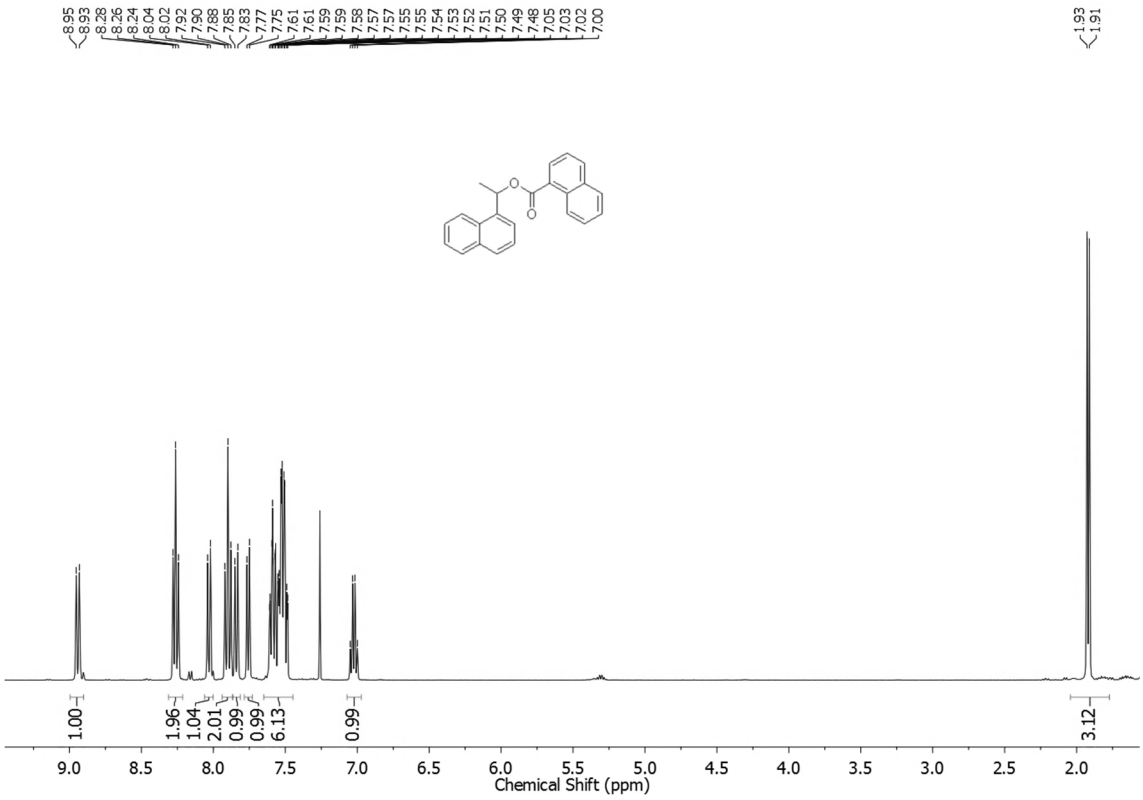

Figure S3: 71. *[Figure S71] ^{1}H NMR spectrum of the ester* ***3bf*** *($CDCl_3$, 400 MHz).*

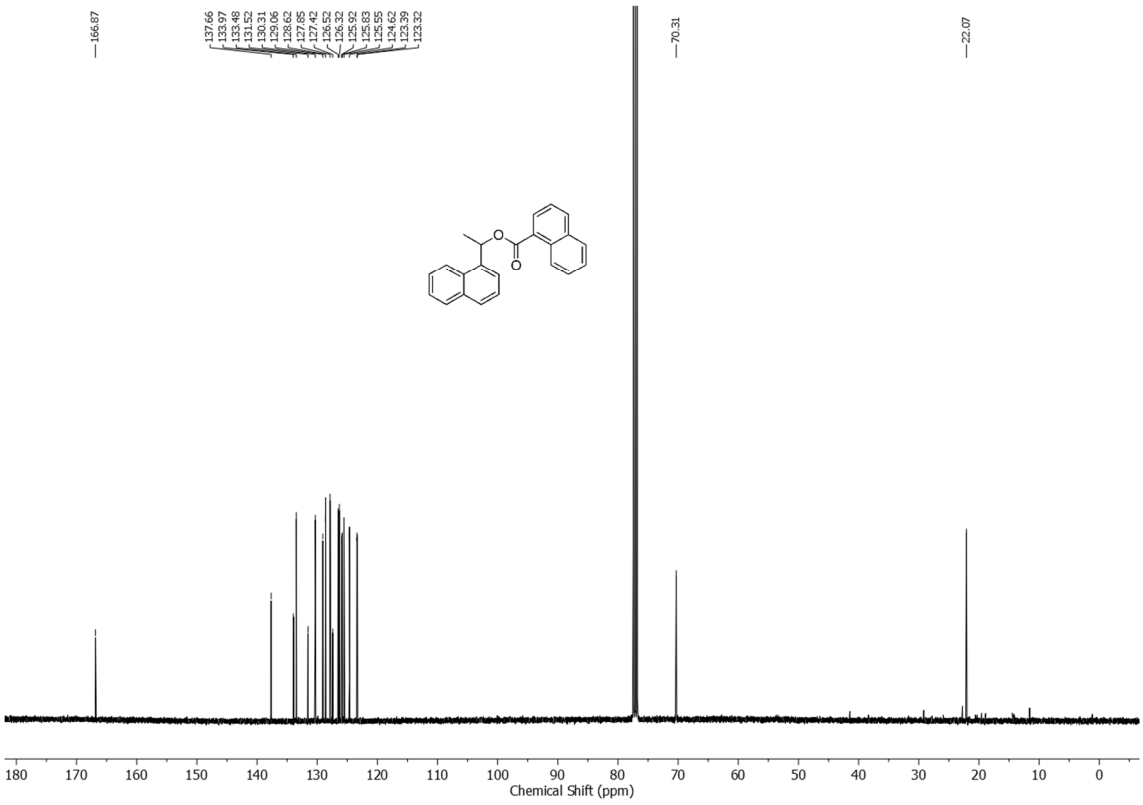

Figure S3: 72. *[Figure S72] ^{13}C NMR spectrum of the ester* ***3bf*** *($CDCl_3$, 101 MHz).*

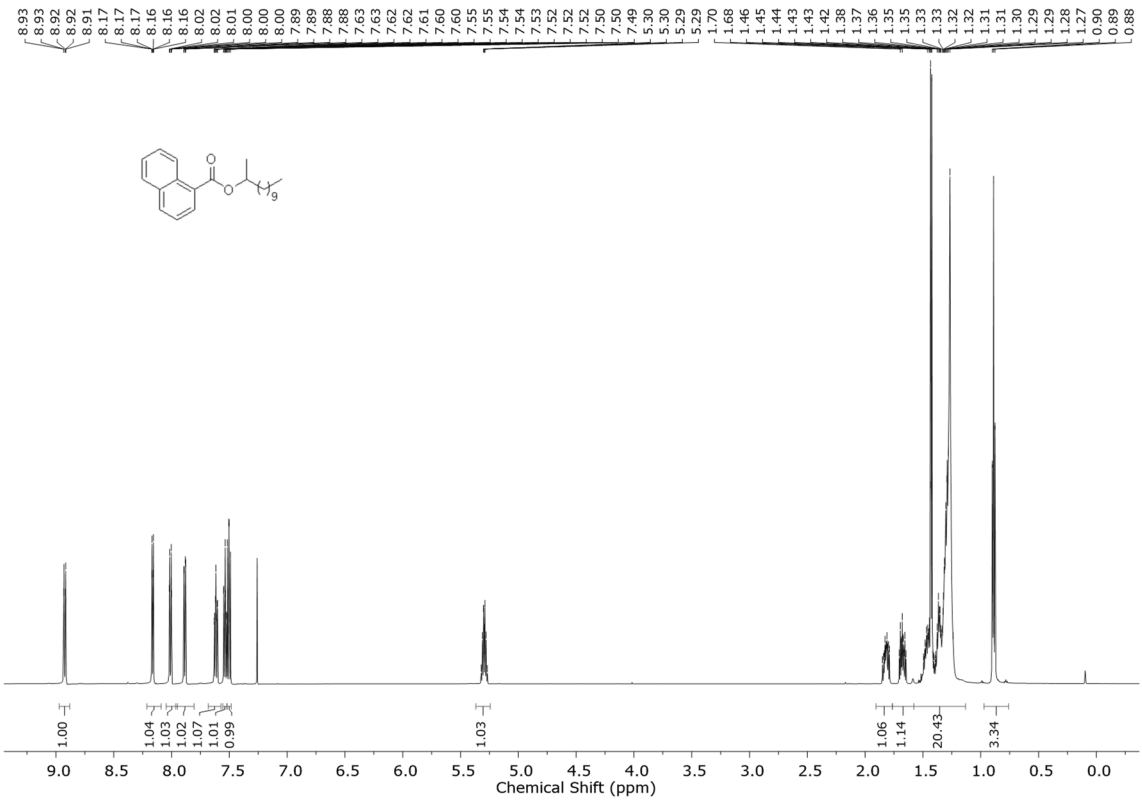

Figure S3: 73. *[Figure S73] ^{1}H NMR spectrum of the ester **3af** ($CDCl_3$, 600 MHz).*

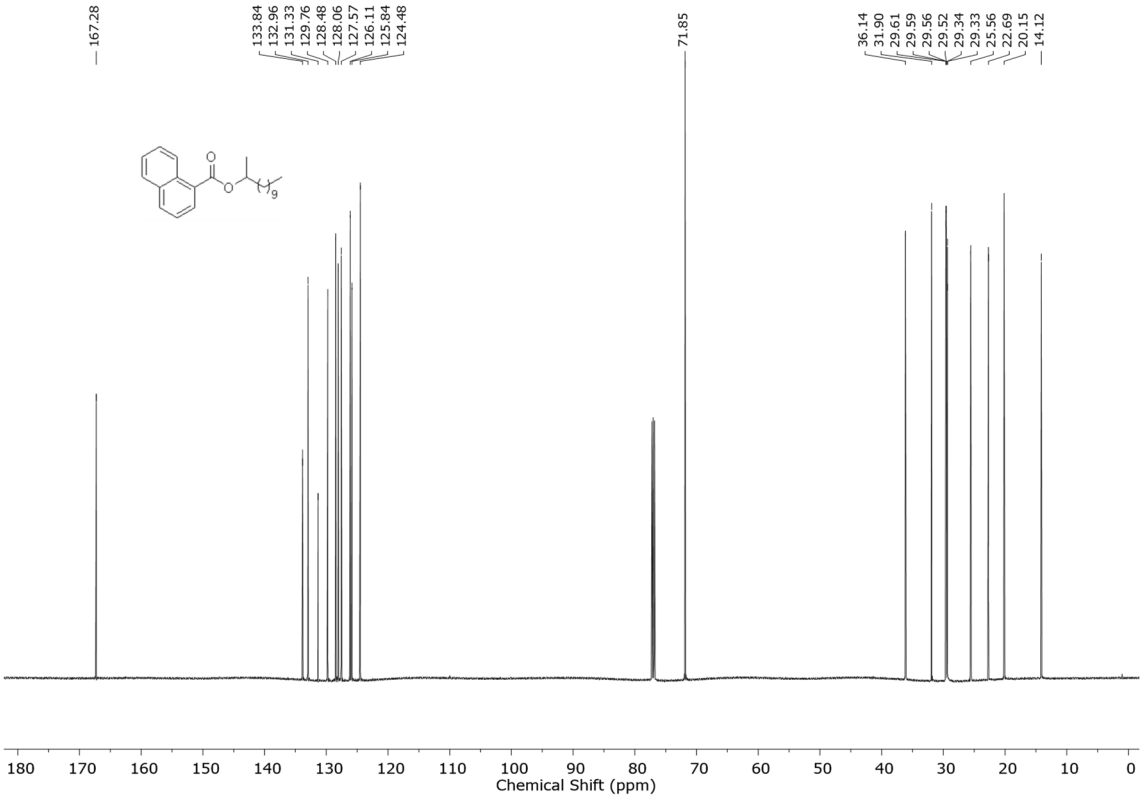

Figure S3: 74. *[Figure S74] ^{13}C NMR spectrum of the ester **3af** ($CDCl_3$, 151 MHz).*

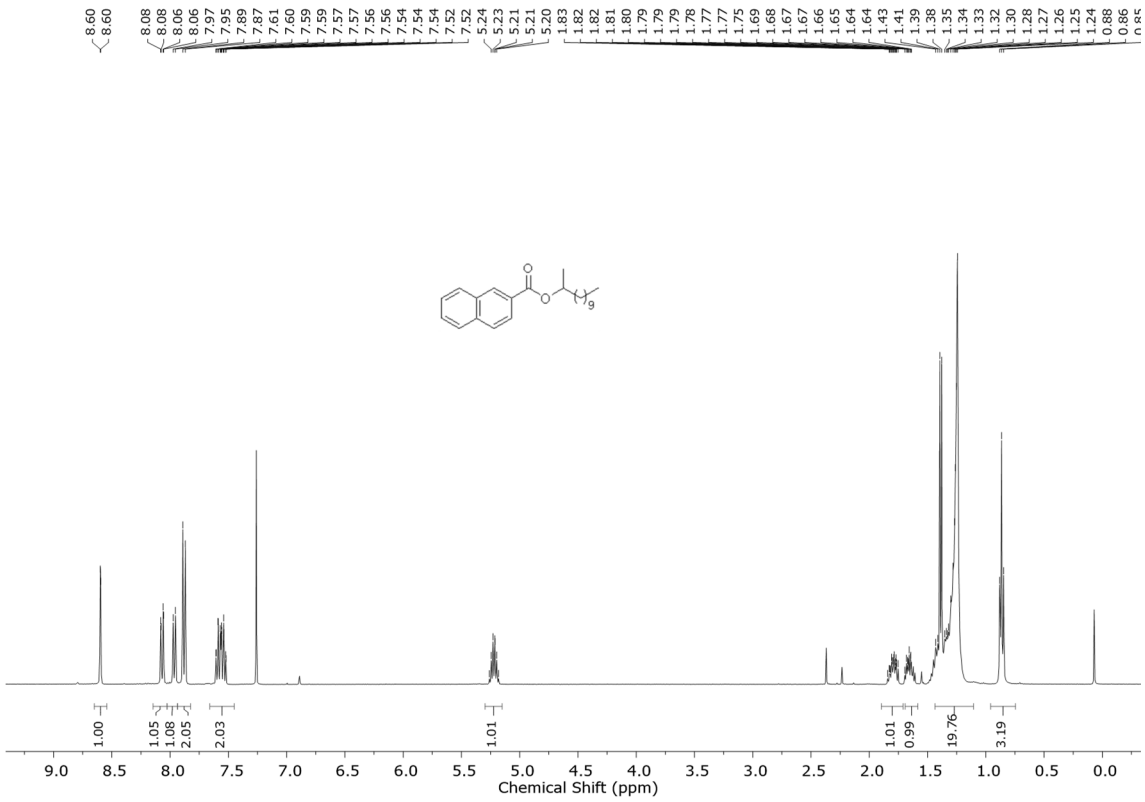

Figure S3: 75. *[Figure S75] ^{1}H NMR spectrum of the ester **3ag** ($CDCl_3$, 400 MHz).*

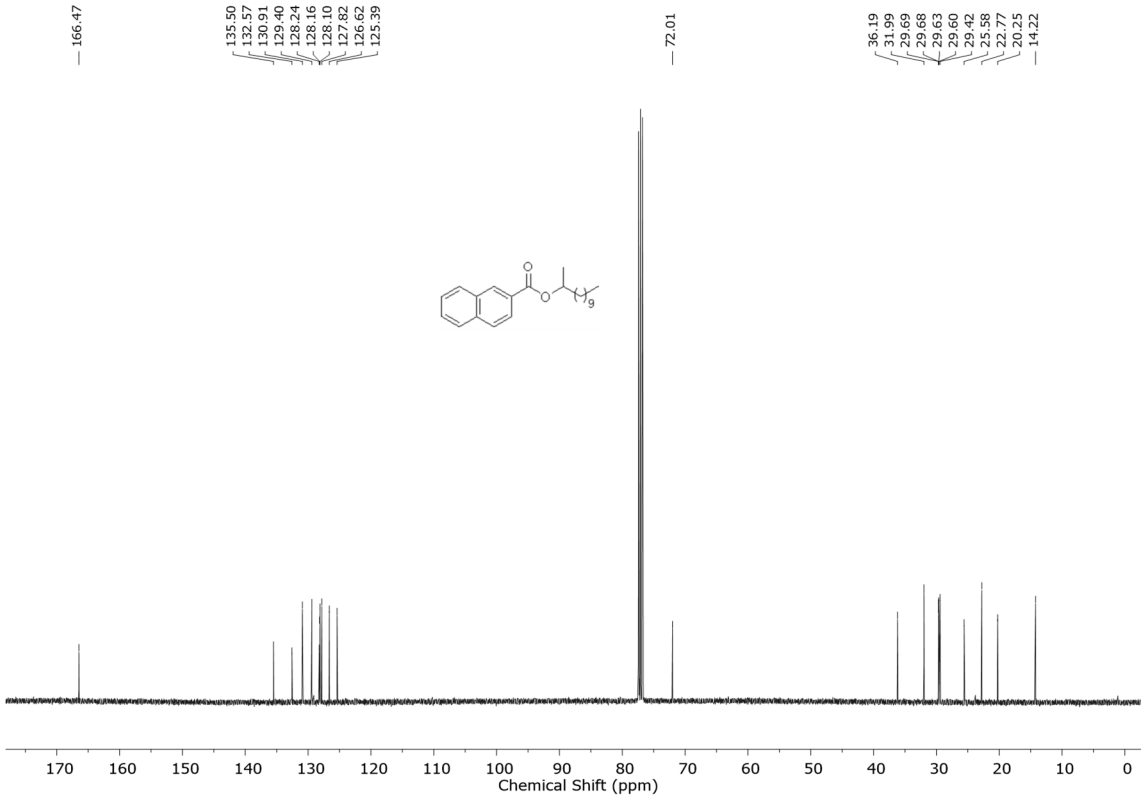

Figure S3: 76. *[Figure S76] ^{13}C NMR spectrum of the ester **3ag** ($CDCl_3$, 101 MHz).*

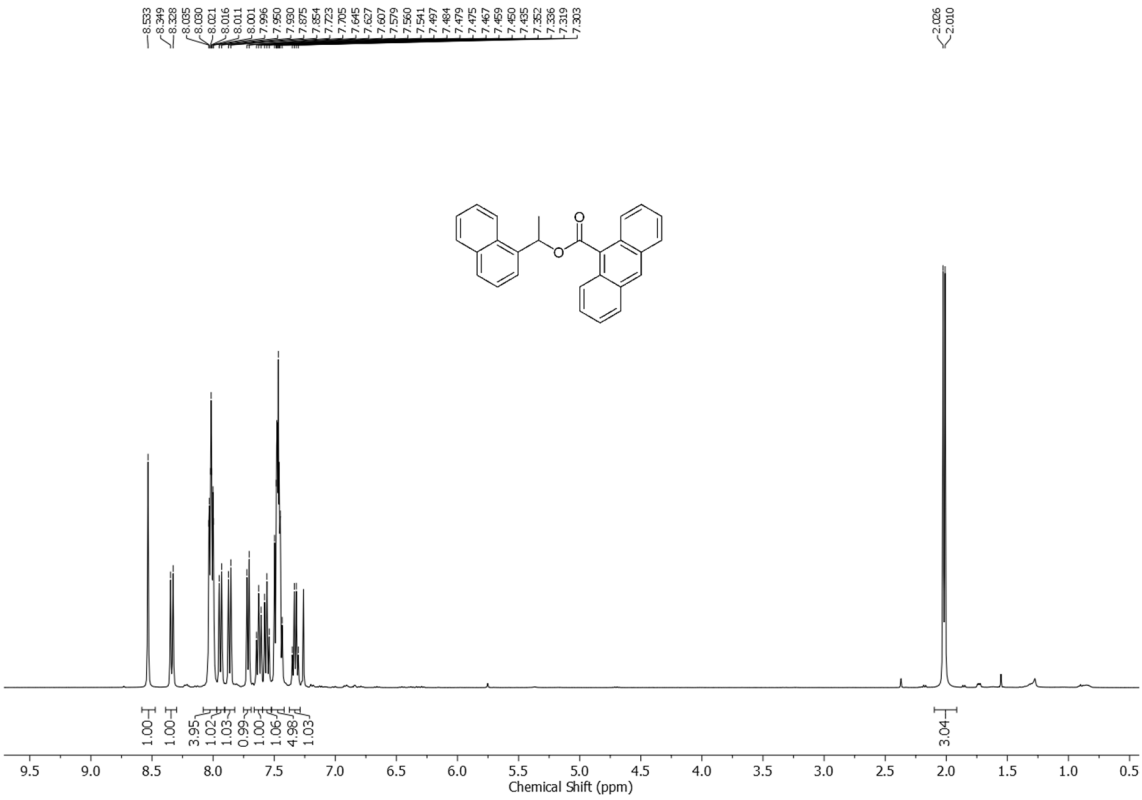

Figure S3: 77. *[Figure S77] ^{1}H NMR spectrum of the ester* ***3bh*** *($CDCl_3$, 400 MHz).*

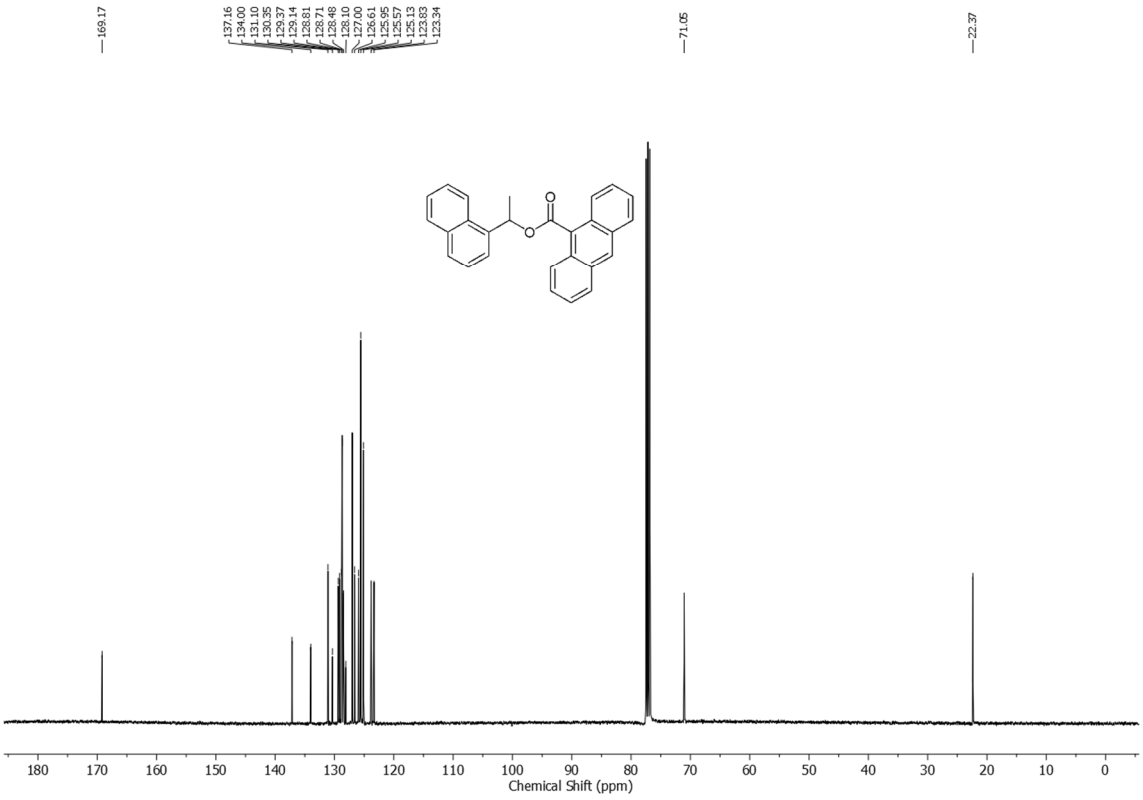

Figure S3: 78. *[Figure S78] ^{13}C NMR spectrum of the ester* ***3bh*** *($CDCl_3$, 101 MHz).*

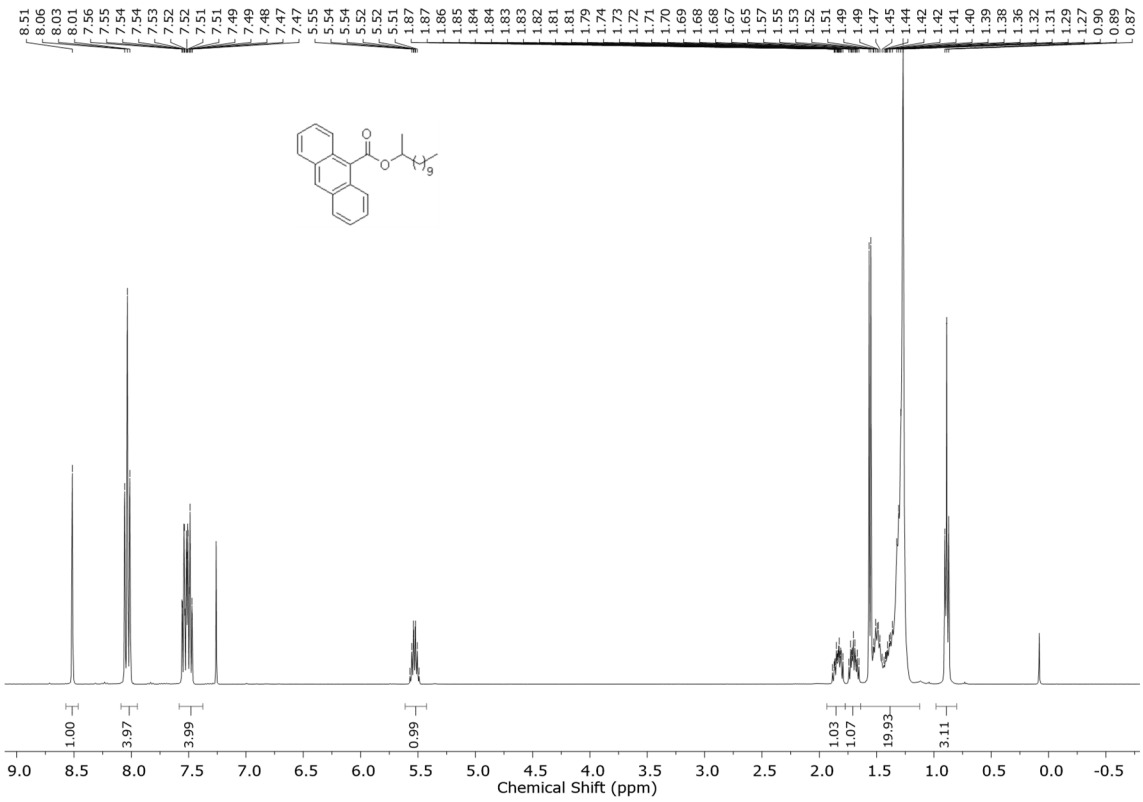

Figure S3: 79. *[Figure S79] ^{1}H NMR spectrum of the ester **3ah** ($CDCl_3$, 400 MHz).*

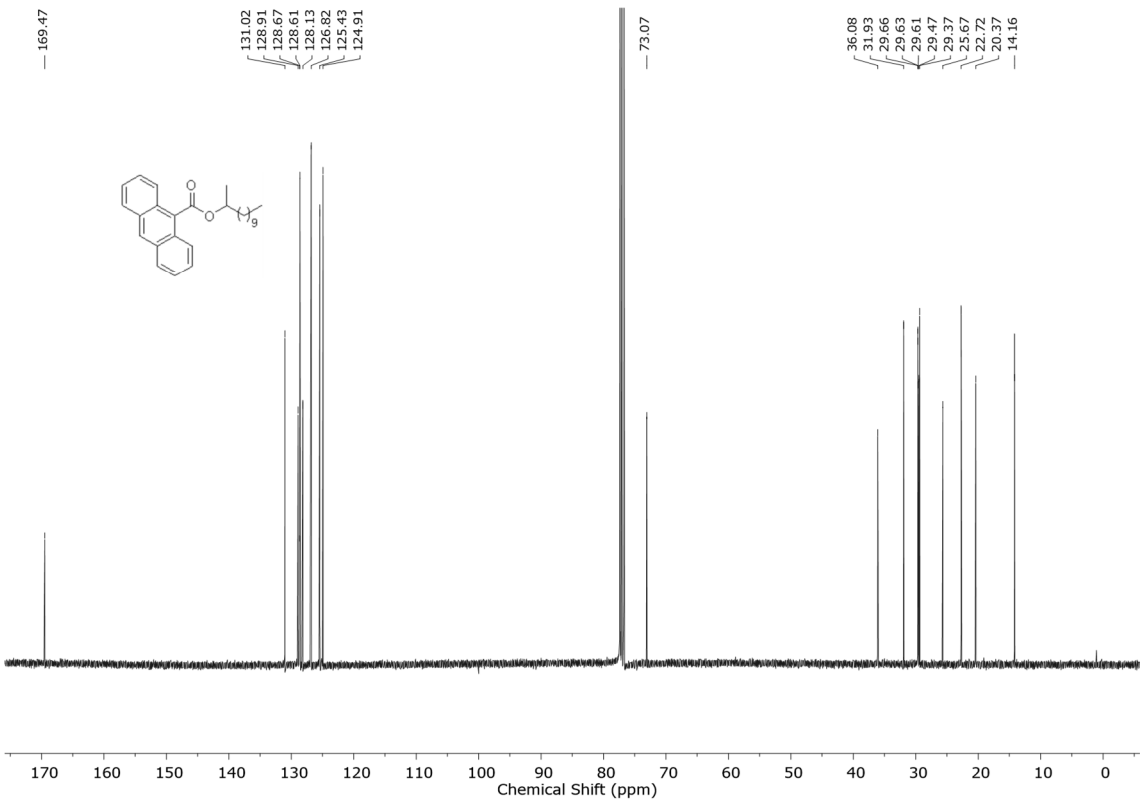

Figure S3: 80. *[Figure S80] ^{13}C NMR spectrum of the ester **3ah** ($CDCl_3$, 101 MHz).*

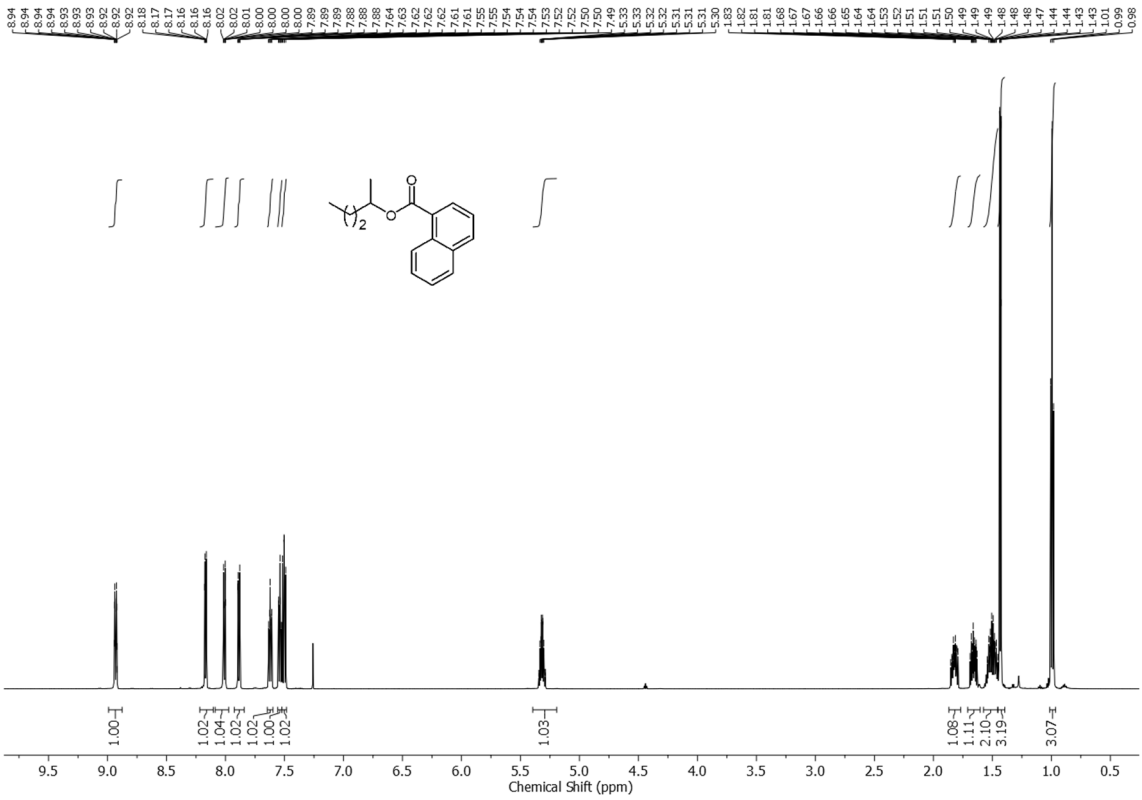

Figure S3: 81. *[Figure S81] ^{1}H NMR spectrum of the ester* ***3cf*** *($CDCl_3$, 600 MHz).*

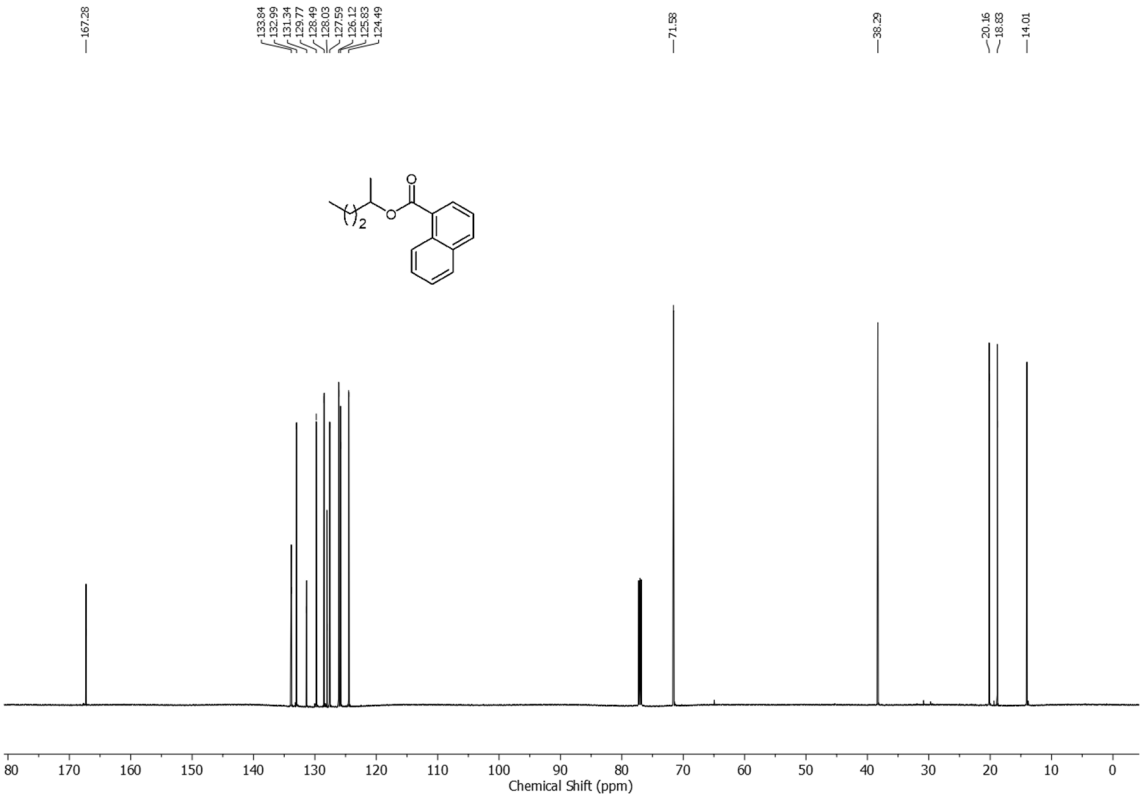

Figure S3: 82. *[Figure S82] ^{13}C NMR spectrum of the ester* ***3cf*** *($CDCl_3$, 151 MHz).*

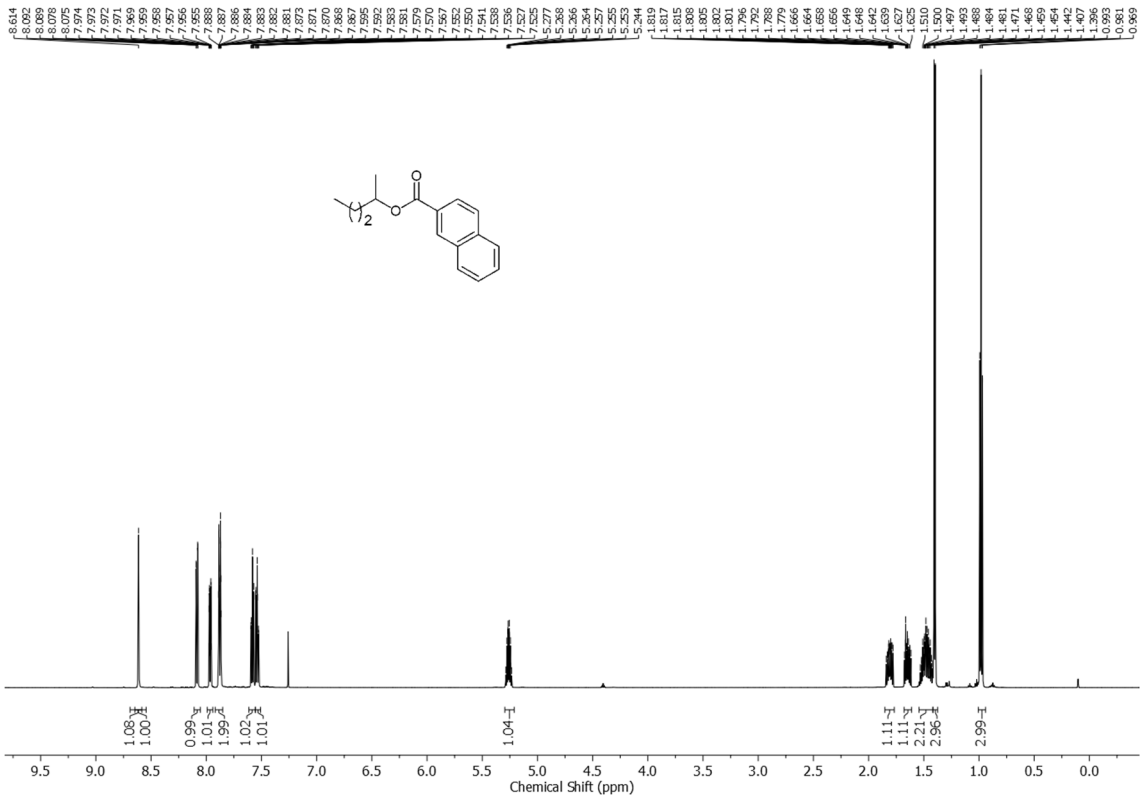

Figure S3: 83. *[Figure S83] ^{1}H NMR spectrum of the ester **3cg** ($CDCl_3$, 600 MHz).*

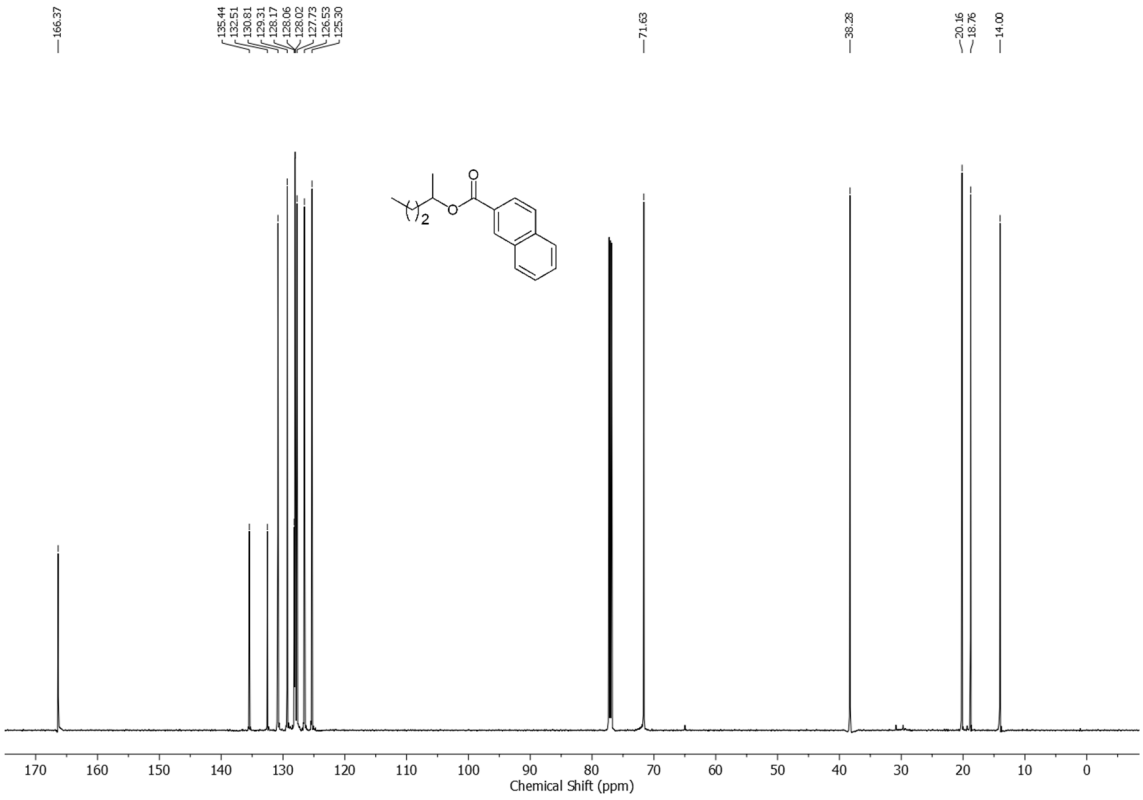

Figure S3: 84. *[Figure S84] ^{13}C NMR spectrum of the ester **3cg** ($CDCl_3$, 151 MHz).*

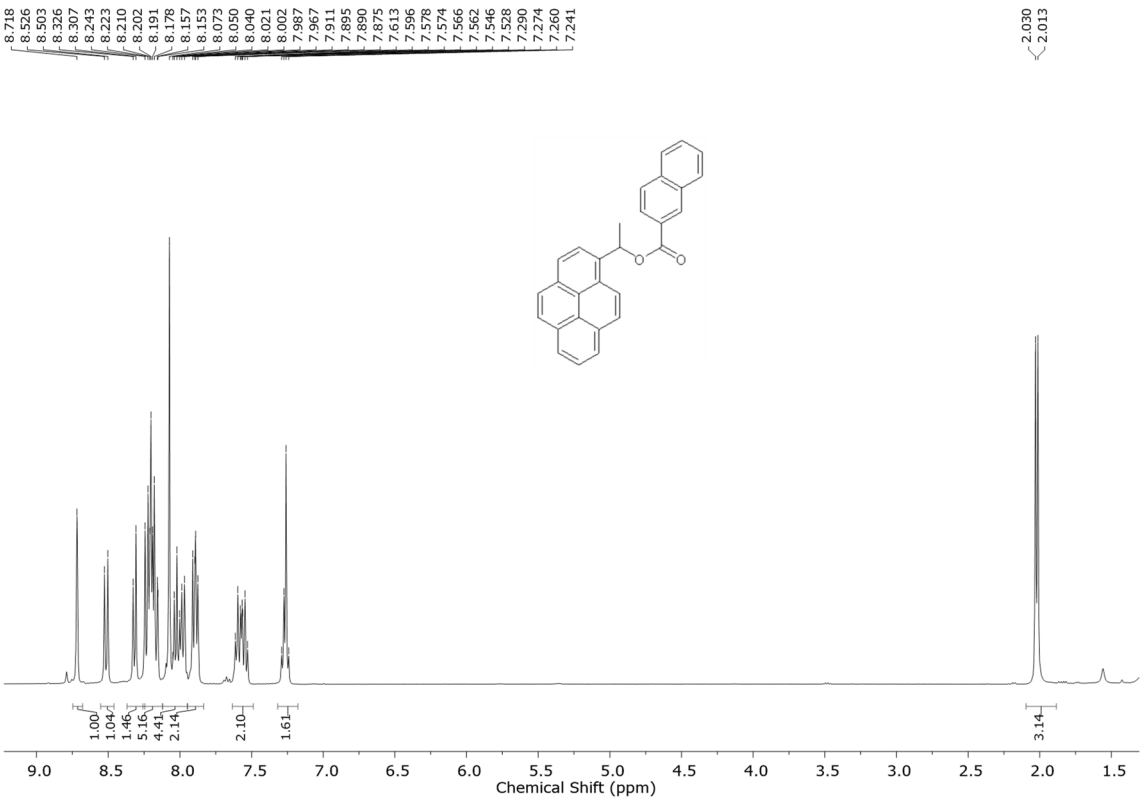

Figure S3: 85. *[Figure S85] ^{1}H NMR spectrum of the ester* ***3eg*** *($CDCl_3$, 400 MHz).*

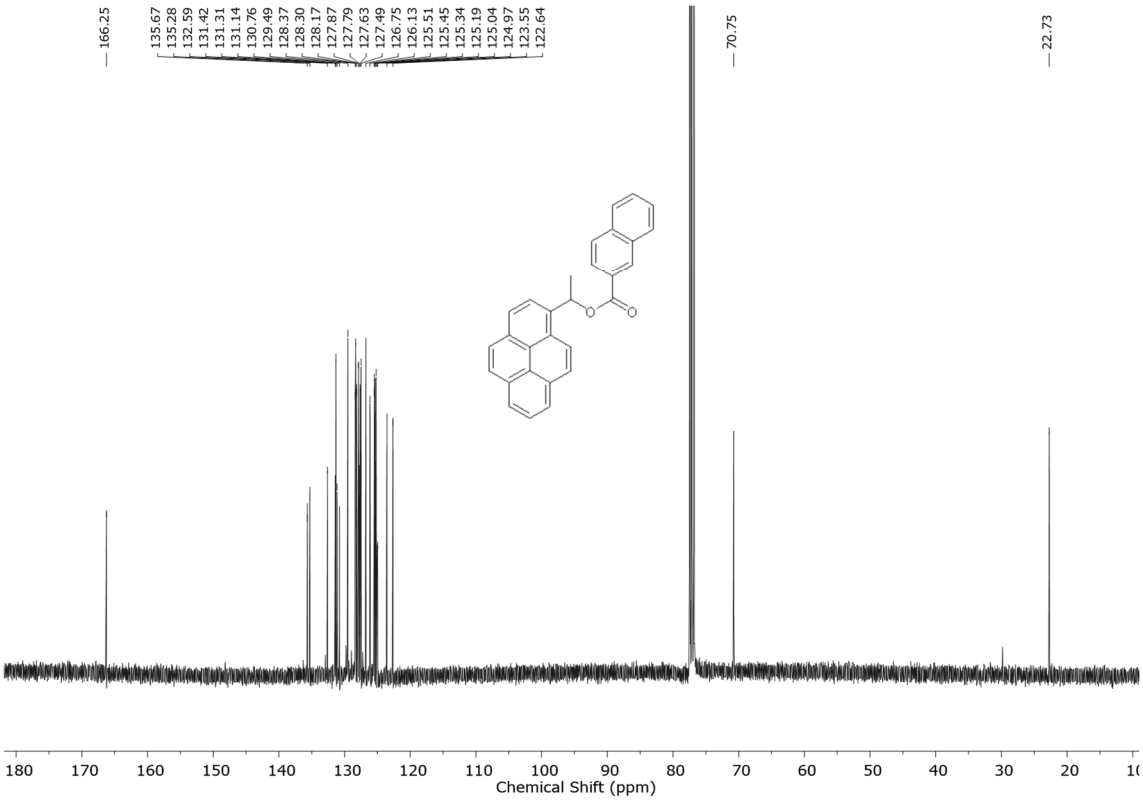

Figure S3: 86. *[Figure S86] ^{13}C NMR spectrum of the ester* ***3eg*** *($CDCl_3$, 101 MHz).*

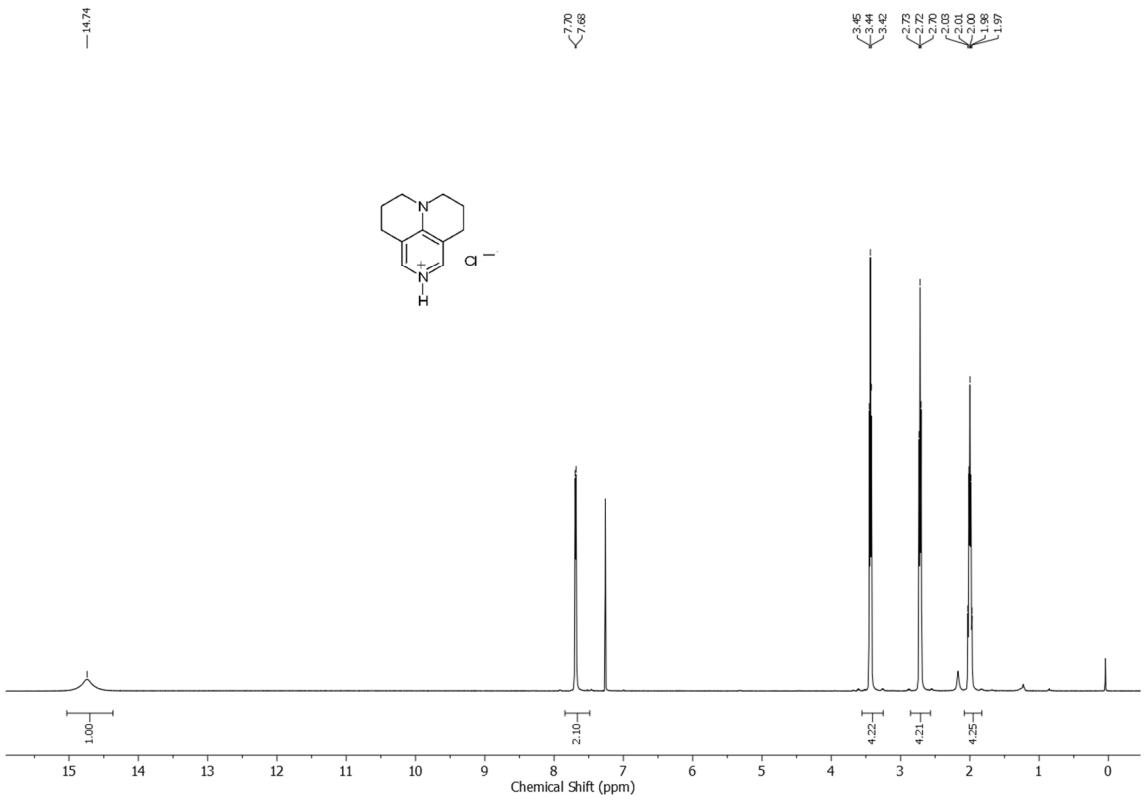

Figure S3: 87. *[Figure S87] ^{1}H NMR spectrum of TCAP hydrochloride* ***TCAPxHCl*** *($CDCl_3$, 400 MHz).*

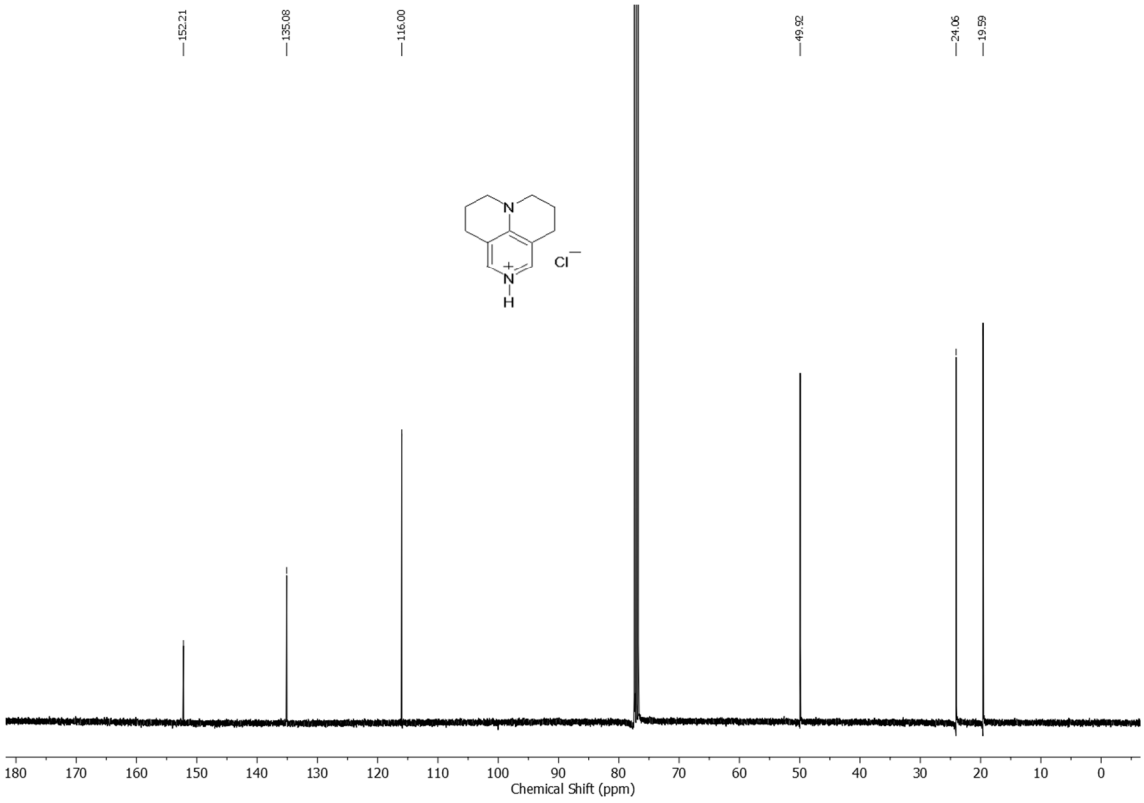

Figure S3: 88. *[Figure S88] ^{13}C NMR spectrum of TCAP hydrochloride* ***TCAPxHCl*** *($CDCl_3$, 101 MHz).*

3.1.10. X-Ray Crystal Structure Data

Table S3: 8. [Table S8] Crystallographic data of 9-anthacenoyl chloride **2h**.

net formula	C15H9ClO
Mr/g mol−1	240.67
crystal size/mm	0.100 × 0.080 × 0.040
T/K	100.(2)
Radiation	MoKα
Diffractometer	'Bruker D8 Venture TXS'
crystal system	Monoclinic
space group	'C 1 2/c 1'
a/Å	10.3077(5)
b/Å	15.2697(7)
c/Å	7.3286(4)
α/°	90
β/°	98.034(2)
γ/°	90
V/Å3	1142.17(10)
Z	4
calc. density/g cm−3	1.400
μ/mm−1	0.311
absorption correction	Multi-Scan
transmission factor range	0.9176–0.9705
refls. measured	6040
Rint	0.0339
mean σ(I)/I	0.0286
θ range	3.476–27.466
observed refls.	978
x, y (weighting scheme)	0.0387, 1.1873
hydrogen refinement	Constr
refls in refinement	1306
parameters	88
restraints	0
R(Fobs)	0.0477
Rw(F2)	0.1196
S	1.083
shift/errormax	0.001
max electron density/e Å−3	0.195
min electron density/e Å−3	−0.214

Cl1 and O1 disordered, sof fixed to 0.5 due to symmetry.

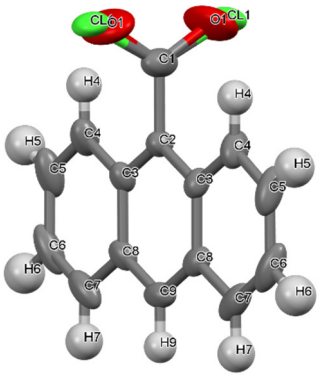

Figure S3: 89. *[Figure S89] Partial view of X-Ray structure of 9-anthracenoyl chloride* ***2h.*** *Probability level of ellipsoids (50%).*

Table S3: 9. [Table S9] Crystallographic data. of 9-azajulolidine hydrochloride **TCAPx HCl**.

net formula	$C_{11}H_{15.68}ClN_2O_{0.34}$
M_r/g mol^{-1}	216.85
crystal size/mm	0.090 × 0.030 × 0.020
T/K	100.(2)
Radiation	MoKα
Diffractometer	'Bruker D8 Venture TXS'
crystal system	monoclinic
space group	'P 1 21/n 1'
a/Å	8.7621(3)
b/Å	15.2289(6)
c/Å	8.7818(4)
α/°	90
β/°	111.7660(10)
γ/°	90
V/Å^3	1088.27(8)
Z	4
calc. density/g cm^{-3}	1.324
μ/mm^{-1}	0.318
absorption correction	Multi-Scan
transmission factor range	0.8995–0.9705
refls. measured	9457
R_{int}	0.0489
mean σ(*I*)/*I*	0.0388
θ range	3.661–26.371
observed refls.	1793
x, y (weighting scheme)	0.0399, 0.7692
hydrogen refinement	mixed
refls in refinement	2187
parameters	150
restraints	1
$R(F_{obs})$	0.0414
$R_w(F^2)$	0.1067
S	1.046
shift/error$_{max}$	0.001
max electron density/e Å^{-3}	0.260
min electron density/e Å^{-3}	−0.376

H(C) constr, H(N) refall, H(O) located from difference map, coordinates not refined, U(H)=1.5U(O).

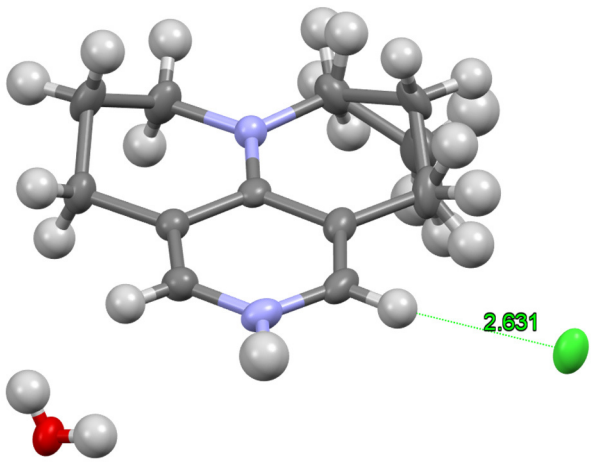

Figure S3: 90. *[Figure S90] Partial view of X-Ray structure of TCAP hydrochloride* ***TCAPxHCl.*** *It co-crystallized with a molecule of water. Probability level of ellipsoids (50%). Distances are shown in Angstrom. Disorder handled by a split model, sof ratio 0.66/0.34. Figure shows main part.*

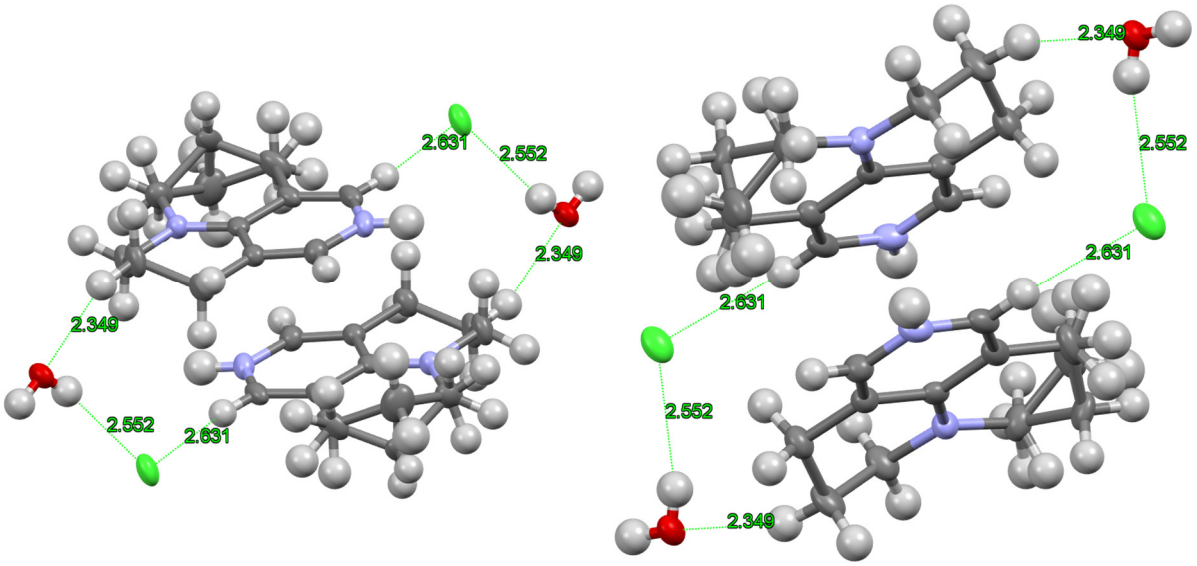

Figure S3: 91. *[Figure S91] Partial view of X-Ray structure of TCAP hydrochloride* ***TCAPxHCl*** *extended to two molecules. Distances are shown in Angstrom.*

References

[1] Hoops, S.; Sahle, S.; Gauges, R.; Lee, C.; Pahle, J.; Simus, N.; Singhal, M.; Xu, L.; Mendes, P; Kummer, U. *Bioinformatics* **2006**, *22*, 3067.
[2] 8 Origin (OriginLAb, Northampton, MA).
[3] Giese, B. *Angew. Chem. Int. Ed. Engl.* **1977**,*16*, 125.

Chapter 4. Pyridinyl Amide Ion Pairs as Lewis Base Organocatalysts

Julian Helberg, Torsten Ampßler, and Hendrik Zipse

J. Org. Chem. **2020**, *85,* 5390 – 5402 © 2020 American Chemical Society.

Authors contributions

J.H. conceived the project. The experimental study was designed by J.H. and H.Z. and executed by J.H and T.A., who worked under the guidance of J.H. as an intern. The computational strategy was designed by J.H. and H.Z in accordance with the cited studies. The computational study was done by J.H. The manuscript was jointly written by J.H. and H.Z and the supporting information was prepared by J.H. and H.Z.

Copyright

(Link to article: https://pubs.acs.org/doi/abs/10.1021/acs.joc.0c00114)

The full supporting information can be found following the link below:
https://pubs.acs.org/doi/suppl/10.1021/acs.joc.0c00114/suppl_file/jo0c00114_si_001.pdf

Additional information

The supporting information printed in this thesis is a shortened and altered version of the originally published supporting information and has been optimized for printing purposes. The supporting information file can be found on the electronic attachment to this thesis. For comparison of this thesis and the original SI file, the numbering includes the original caption as shown below:

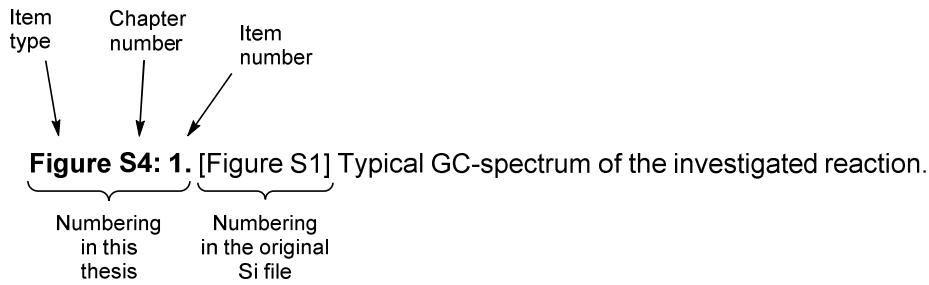

JOC The Journal of Organic Chemistry

pubs.acs.org/joc Article

Pyridinyl Amide Ion Pairs as Lewis Base Organocatalysts

Julian Helberg, Torsten Ampßler, and Hendrik Zipse*

Cite This: J. Org. Chem. 2020, 85, 5390−5402 Read Online

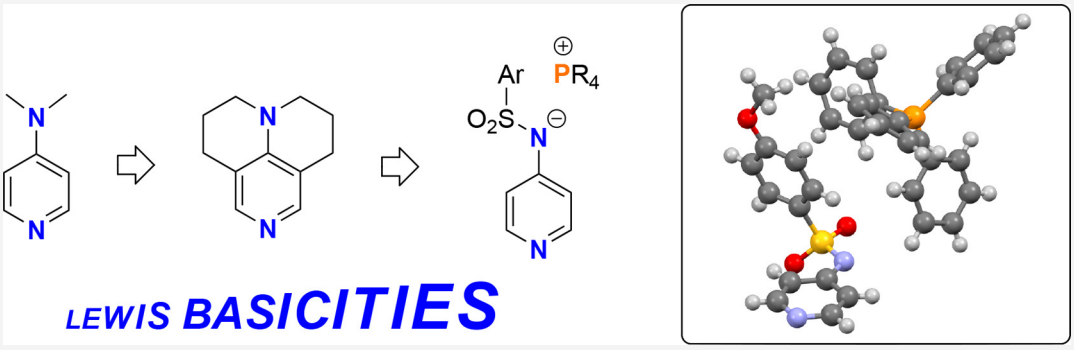

ABSTRACT: Pyridinyl amide ion pairs carrying various electron-withdrawing substituents were synthesized with selected ammonium or phosphonium counterions. Compared to neutral pyridine-based organocatalysts, these new ion pair Lewis bases display superior catalytic reactivity in the reaction of isocyanates with alcohols and the *aza*-Morita−Baylis−Hillman reaction of hindered electrophiles. The high catalytic activity of ion pair catalysts appears to be due to their high Lewis basicities toward neutral electrophiles as quantified through quantum chemically calculated affinity data.

■ INTRODUCTION

The vast increase in catalytic potential caused by electron-donating substituents attached to pyridine derivatives has been known and exploited for decades, 4-dimethylaminopyridine (DMAP, **1a**) being the most widely known example (Figure 1).[1]

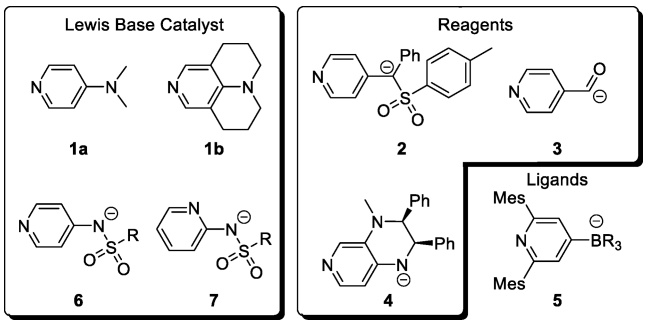

Figure 1. Neutral and anionic pyridine compounds used as Lewis base organocatalysts, reagents, or ligands.

Efforts to improve the catalytic performance of **1a** have eventually led to 9-azajulolidine (TCAP, **1b**), which still represents the standard for a commercially available, high-performance Lewis basic organocatalyst, and has not been significantly surpassed by other pyridine derivatives since.[2] Further increases in catalytic activity may be expected from pyridines carrying anionic substituents. Anders et al. found that sufficiently stabilized anions of 4-methylpyridine **2** underwent N-substitution instead of the expected reaction on the alkyl carbon and also isolated a stable adduct of pyridinyl anions and activated sulfonic acids that yielded sulfonic esters when reacted with alcohols.[3] This adduct matches what is believed to be the first intermediate in the corresponding catalytic cycle of Lewis base-catalyzed reactions. Also, Sheldrake reported that, depending on reaction conditions, *in situ* generated 4-pyridinyl carbonyl anions **3** were acylated exclusively at the N-position, while a mixture of constitutionally isomeric products was obtained in alkylation reactions.[4] When developing a synthetic route to alkyl-substituted 3,4-diaminopyridines, we had earlier observed that 4-pyridinylamide anions **4** react with alkylation reagents preferentially at the pyridine nitrogen atom.[5] Very recently, Böttcher et al. described the synthesis and characterization of 4-borate pyridine anion **5** intended for use as a strong ligand.[6]

The catalytic activity of anionic sulfonamide pyridines **6** and **7** has only been described for the oligomerization of isocyanates in the patent literature.[7] Unfortunately, no comparison has been made to commonly used (neutral) organocatalysts, and characterization was omitted. In contrast to most other

Received: January 15, 2020
Published: March 30, 2020

https://dx.doi.org/10.1021/acs.joc.0c00114
J. Org. Chem. 2020, 85, 5390−5402

reactions in organocatalysis, the oligomerization of isocyanates commonly proceeds under neat conditions and includes no proton transfer steps. We, therefore, analyze here whether the catalytic potential of ion pair catalysts based on the 4-pyridinylamide motif also present in anion **6** survives in reactions of unreactive electrophiles involving proton transfer steps. For the sake of comparison, we select here (a) the formation of urethane from alcohols and isocyanates as a common reaction type for this class of electrophile and (b) the *aza*-Morita−Baylis−Hillman reaction of terminally substituted Michael acceptors.[8] In addition, we also quantify the Lewis basicity of all catalysts through quantum chemical calculations.

■ RESULTS

Neutral sulfonamides **8** as the direct precursors for the anionic pyridine catalysts were synthesized by condensation of 4-aminopyridine **9** with the corresponding sulfonyl chlorides. X-ray crystallographic analysis indicates that **8** is mainly present as the sulfonimide tautomer as indicated in Scheme 1 (see

Scheme 1. Synthesis of Ion Pair Catalysts

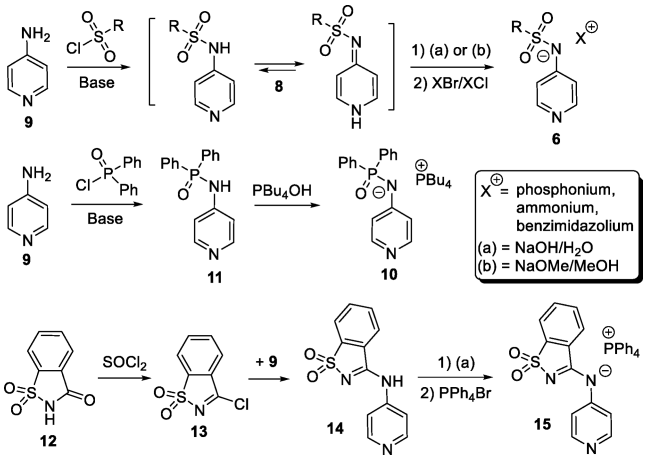

Supporting Information). The phosphonic amide salt **10** was synthesized in a similar manner using diphenylphosphinic chloride as the reagent. In the case of the "extended" sulfonamide **14**, saccharine **12** was first transformed into the corresponding imidoyl chloride **13**, which was then reacted with **9**. Deprotonation of neutral amides was carried out using aqueous sodium hydroxide or sodium methoxide solutions, followed by salt metathesis with the appropriate cation and extraction with CH_2Cl_2. Subsequent crystallization from CH_2Cl_2/toluene/heptane mixtures gave the ion pair catalysts **6**, **10**, and **15**.

X-ray crystallographic data for all synthesized ion pair catalysts shown in Figure 2 could be obtained except for **6ab**, which is a room-temperature ionic liquid (IL) (see Supporting Information). Table 1 collects the closest contacts between selected atoms of the cation and the pyridine anion that were derived from X-ray crystallographic data. Based on the values for those selected examples, some general observations can be made. In all cases, the shortest distance between the cation center atom (P or N) to the anion heteroatoms originates from an oxygen atom (distance D1). This is also true for the shortest interaction between an anion heteroatom and any cation atom (distance D4), except for the special case of **7e**, featuring a very strong intermolecular hydrogen bond (entry 4). Both

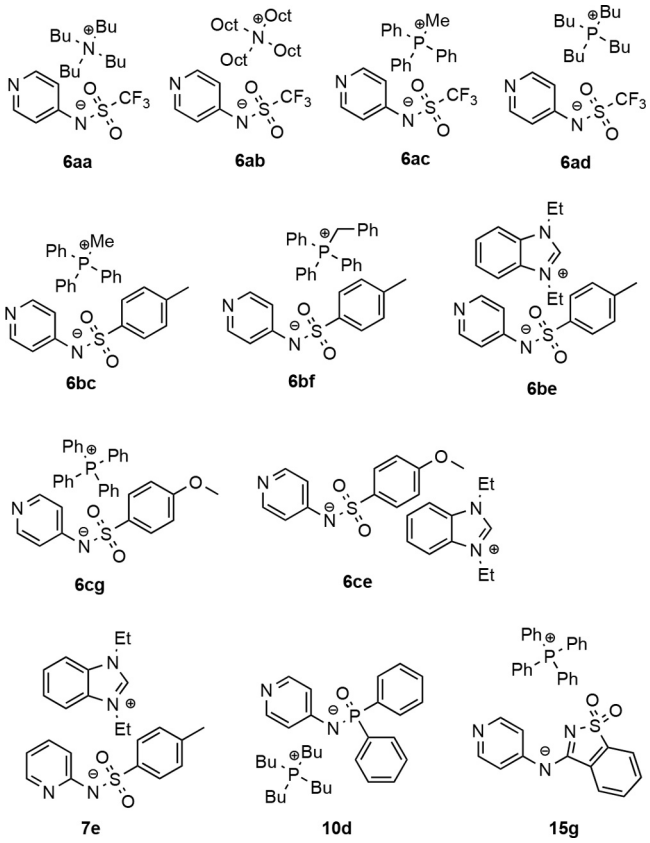

Figure 2. Pyridine ion pair catalysts synthesized and characterized in this study.

observations indicate that the cation is located closer to the formally charge-bearing amide groups than to the pyridine ring. This is actually not obvious when comparing the amide-N to cation distances (D3) with the pyridine-N to cation distances (D2), both of which are typically longer as compared to the shortest oxygen (anion) to cation distance D4 (see the full table for the 11 crystallized ion pair catalysts in the Supporting Information).

Due to the significance of catalytic activation of isocyanates for the nucleophilic attack, we chose the synthesis of urethane **16** from *p*-tolyl isocyanate (**17**) and butan-1-ol (**18**) as the primary benchmark reaction (Scheme 2).[9] The more reactive catalysts were then tested in the *aza*-MBH reaction of tosyl imine **19** and cyclohexenone **20** as an intrinsically unreactive substrate system.[8a,10] Also, an exploratory study of esterification reactions was conducted. After initial screening, this was not investigated further because reactions employing ion pair catalysts such as **6cg** (Figure 2) did not follow the same rate laws observed for the neutral organocatalysts **1a** and **1b** (see Supporting Information). Scheme 2 also shows the proposed Lewis base adducts occurring as intermediates after the first step of the catalytic cycle for the chosen benchmark reactions.

Reaction progress was quantified by ^{1}H NMR spectroscopy via integration of the well-separated signals of the hydrogen atoms highlighted in Scheme 2. For the synthesis of urethane **16**, the obtained turnover curves were validated by GC-FID measurements of reactions catalyzed by several of the neutral organocatalyts (see Supporting Information). Turnover values were fed into a numerical simulation based on the effective second-order mechanism represented by eq 1 to obtain the effective rate constant of the reaction k_{eff}, which can be used to

https://dx.doi.org/10.1021/acs.joc.0c00114
J. Org. Chem. 2020, 85, 5390−5402

Table 1. Selected Anion−Cation Distances Observed in the Solid State

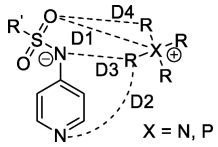

entry	catalyst	D1 heteroatom (anion)→P/N (cation)[a]	D2 pyridine-N→cation[a]	D3 amide-N→cation[a]	D4 heteroatom (anion)→cation[a]
1	**6aa**	395.0(O→N)	257.3(α-H)	246.3(α-H)	244.9(O→β-H)
2	**6bc**	399.5(O→P)	254.2(α-H)	254.2(α-H)	234.1(O→α-H)
3	**6cg**	467.9(Me-O→P)	285.7(α-H)	267.6(β-H)	241.4(Me-O→α-H)
4	**7e**	388.4(O→N)	243.6(α-H)	217.6(α-H)	217.6(amide-N→α-H)
5	**10d**	368.9(O→P)	247.9(α-H)	286.2(δ-H)	219.5(O→α-H)
6	**15g**	506.6(O→P)	251.8(γ-H)	280.1(β-H)	238.3(O→γ-H)

[a]In pm.

Scheme 2. Reference Reactions Used in This Study and the Proposed Lewis Base Adducts[a]

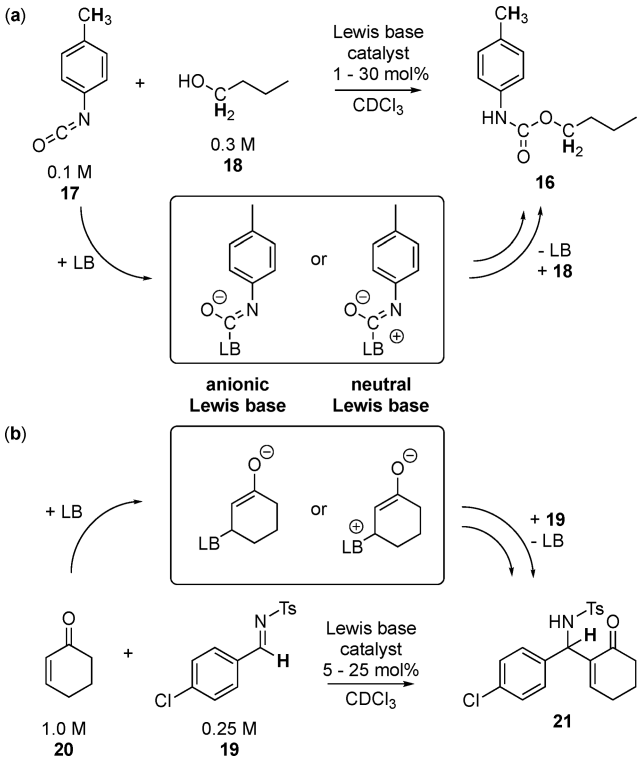

[a](a) Urethane synthesis and (b) *aza*-MBH reaction. Protons printed in bold are used to determine turnover by ^{1}H NMR spectroscopy.

$$\mathbf{17} + \mathbf{18} \overset{k_{eff}}{\rightleftharpoons} \mathbf{16} \quad (1)$$

obtain the concentration-independent rate constant of each catalyst according to eq 2. The kinetic data obtained for the

$$k_{eff} = k_{cat} \times [\text{catalyst}] \quad (2)$$

urethane synthesis reaction shown in Scheme 2a in the presence of various catalysts have been collected in Table 2. Figure 3a shows examples of the respective turnover curves in $CDCl_3$ catalyzed by 3 mol % each of **1a**, **1b**, and **6cg** together with the fitted curves. Effective rate constants obtained at 3 mol % catalyst loading ($k_{eff}(3)$) are shown graphically in Figure 3b. The reaction benefits notably from the addition of catalysts

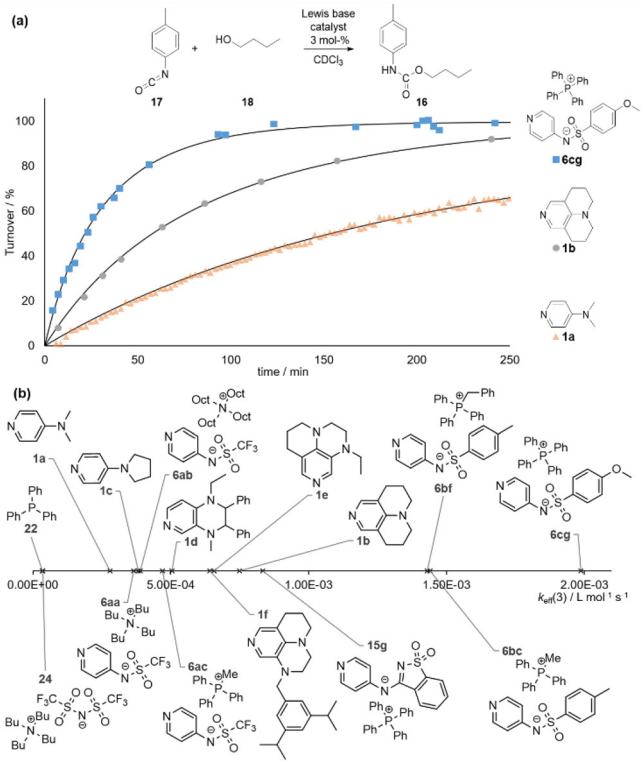

Figure 3. (a) Turnover curves obtained for the synthesis of urethane B, and (b) $k_{eff}(3)$ values obtained for this reaction.

since 3 mol % of **1a** accelerates it by more than a factor of 6 compared to the uncatalyzed background reaction (Table 2; entries 1 and 5).

TCAP (**1b**) performs the best of all investigated neutral catalyst systems, while the diaminosubstituted pyridines **1e** and **1f** show slightly lower activity (Table 2, entries 11−13). Triphenylphosphine (**22**) does not act as a catalyst under the chosen reaction conditions, which is also true for tetrabutylammonium bis-sulfonamide salt **24** included here to test the general catalytic activity of sulfonamide anions (Table 2, entries 2 and 3). The only catalyst systems more active than **1b** were four anionic pyridine catalysts. The novel, imine-bridged sulfonamide **15g** catalyzes the reaction three times faster than DMAP (Table 2, entry 14), while tosyl amides **6bc** and **6bf**, which only differ in the nature of the cation, are both approximately five times faster than DMAP (Table 2, entries 15 and 16). The highest catalytic activity was found for donor-

https://dx.doi.org/10.1021/acs.joc.0c00114
J. Org. Chem. 2020, 85, 5390−5402

Table 2. Effective Rate Constants k_{eff}(X) (Catalyzed by X mol % Catalyst Relative to 17) Obtained for the Synthesis of Urethane 16 (Ordered by k_{eff}(3))

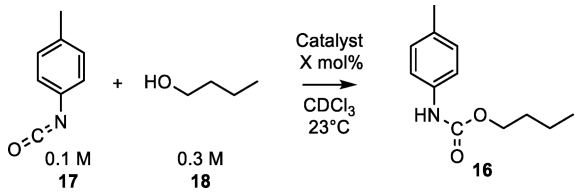

entry	catalyst	$k_{eff}(3)^{a,c}$	k_{eff}(3) (catalyst)/k_{eff}(3) (**1a**)	$k_{cat}{}^{a,b}$	$k_{eff}(X)^{a,c}$
1	none		0.16		4.54×10^{-05} (X = 0)
2	**22**	3.55×10^{-05}	0.13	0.006	3.50×10^{-05} (X = 30)
3	**24**	3.63×10^{-05}	0.13		
4	**23**	6.26×10^{-05}[d]	0.22[d]	0.006	1.14×10^{-04} (X = 15)
					1.72×10^{-04} (X = 30)
5	**1a**	2.80×10^{-04}	1	0.086	1.27×10^{-03} (X = 15)
					2.35×10^{-03} (X = 30)
6	**6aa**	3.65×10^{-04}	1.3	0.115	6.07×10^{-04} (X = 5)
					2.02×10^{-03} (X = 20)
7	**1c**	3.83×10^{-04}	1.37	0.18	5.02×10^{-05} (X = 0.1)
					1.44×10^{-04} (X = 1)
					2.50×10^{-04} (X = 2)
					6.54×10^{-04} (X = 5)
					1.25×10^{-03} (X = 10)
					2.64×10^{-03} (X = 20)
8	**6ab**	3.89×10^{-04}	1.39	0.13	
9	**6ac**	4.71×10^{-04}	1.68	0.379	
10	**1d**	5.05×10^{-04}	1.96	0.167	1.72×10^{-04} (X = 1)
					8.25×10^{-04} (X = 5)
11	**1e**	6.57×10^{-04}	2.35	0.234	2.43×10^{-04} (X = 1)
					1.16×10^{-03} (X = 5)
12	**1f**	6.61×10^{-04}	2.36	0.226	2.41×10^{-04} (X = 1)
					1.09×10^{-03} (X = 5)
13	**1b**	7.50×10^{-04}	2.68	0.364	6.32×10^{-05} (X = 0.1)
					2.78×10^{-04} (X = 1)
					1.37×10^{-03} (X = 5)
					6.63×10^{-03} (X = 30)
14	**15g**	8.34×10^{-04}	2.98	0.273	1.61×10^{-03} (X = 6)
					3.22×10^{-03} (X = 12)
15	**6bf**	1.43×10^{-03}	5.13	0.476	
16	**6bc**	1.44×10^{-03}			6.94×10^{-03} (X = 15)
17	**6cg**	1.99×10^{-03}	7.1	0.661	8.04×10^{-04} (X = 1.2)
					3.96×10^{-03} (X = 6)
					7.78×10^{-03}(X = 12)

[a]Averaged values (see Supporting Information). [b]In L^2 mol^{-2} s^{-1}. [c]In L mol^{-1} s^{-1}. [d]Extrapolated value.

substituted sulfonamide **6cg**, which exceeds the performance of **1a** by a factor of 7 (Table 2, entry 17). On the lower end of activities for ion pair catalysts, we find the highly stabilized triflic amides **6aa** (IL), **6ab** (a room temperature IL), and **6ac**, whose structures differ in the choice of the counterion, but whose catalytic activities are all rather similar and close to that of 4-pyrrolidinopyridine (PPY, **1c**). This implies that the influence of the counterion on the addition reaction studied here is rather moderate.

From the mode of activation shown in Scheme 2, it is expected that the catalyst concentration enters in first order in the respective rate equation. In order to test this hypothesis, concentration-dependent reaction rates were measured for all catalysts except for **6ab**, **6ac** (because of similar activity to **6aa**), and **24**. As an example of an unreactive pyridine compound, this also includes isoquinoline **23** (Table 2, entry 4). Figure 4 shows clear linear correlations between the catalyst concentrations and reaction rates for all of the investigated systems. For reasons of readability, we excluded labels for the less active or less established catalyst systems in Figure 4. The relative catalytic performance reflected in the concentration-independent rate constant k_{cat} (the slopes of the correlation lines in Figure 4) is almost identical to that seen already in the catalytic rate constant k_{eff}(3) at 3 mol % catalyst loading. It should be noted that, for the combinations of more (Brønsted) acidic cations and strongly basic anions, the final conversion is noticeably lower than expected. We find this having some effect when methyltriphenylphosphonium and benzyltriphenylphosphonium ions were used as cations (as in catalysts **6bc** and **6bf**), although this effect is negligible in experiments using 3 mol % catalyst loadings. When using diethyl benzimidazolium as a cation (as in ion pairs **6be**, **6ce**, and **7e**), we observe the

https://dx.doi.org/10.1021/acs.joc.0c00114
J. Org. Chem. 2020, 85, 5390−5402

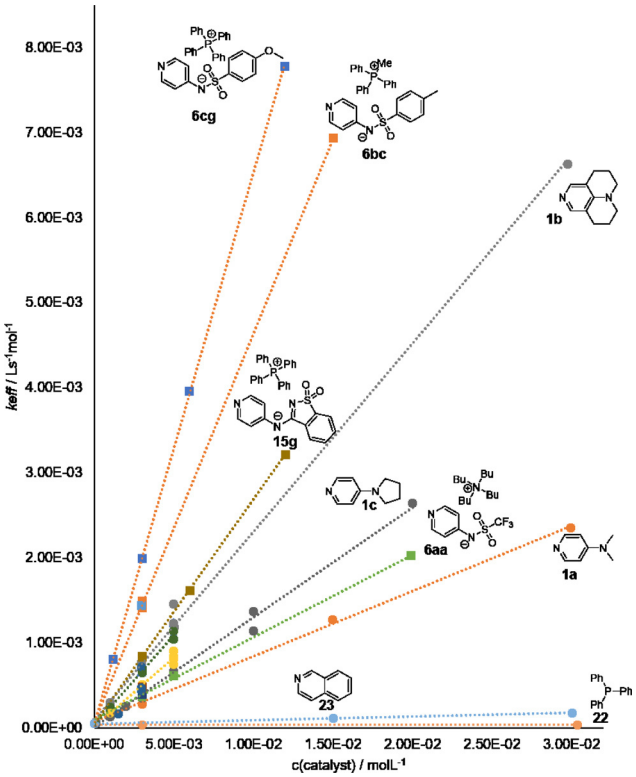

Figure 4. Catalytic activity at different catalyst loadings for the urethane synthesis.

formation of the formal adduct of this cation to isocyanate **17**, most likely through transient C2-deprotonation of diethyl benzimidazolium cation and formation of the respective N-heterocyclic carbene (see Supporting Information). For tetraphenylphosphonium as the counterion (present in **15g** and in the most active catalyst **6cg**), we found no such issues under the reaction conditions employed here. Finally, phosphonamide ion pair **10d** was not included in the catalysis studies due to its instability in $CDCl_3$ as well as CH_2Cl_2. Already when attempting to characterize this compound in these solvents by NMR spectroscopy, the compound degrades rapidly.

Having found that the catalytic performance of the investigated catalyst systems surpasses those of the most reactive commercially available pyridine organocatalysts, we turned to the *aza*-MBH reaction of **19** with **20** as the second benchmark reaction. This is an intrinsically slow addition reaction due to the steric hindrance present in the Michael acceptor **20**, and results for selected Lewis base catalysts are collected in Table 3 and graphically shown in Figure 5. The progress of the reaction was monitored by ^{1}H NMR signals of the protons highlighted in Scheme 2b. Since no conversion is observed without the addition of a catalyst, all plots are fitted through 0.0, and the slope of the fit is used to compare catalyst performance (k_{cat}).

Similar trends as for the urethane synthesis are found here. Again, the anionic pyridine catalysts are much more efficient as compared to their neutral counterparts. While DMAP (**1a**) shows quite low catalytic activity, TCAP (**1b**) is roughly 25 times more active. Reaction rates are significantly higher for the ion pair catalysts: **6bc** is more reactive than DMAP by a factor of 285 and **6cg** by a factor of 385. These results again show the

Table 3. *Aza*-MBH Reaction of 19 with 20 Catalyzed by Selected Lewis Base Catalysts (Entries Ordered by k_{cat})

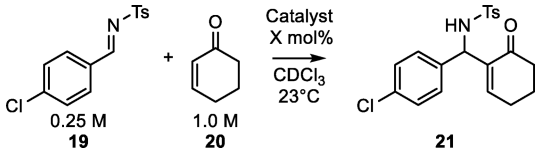

entry	catalyst	k_{cat} [a,b,c]	k_{cat} (catalyst)/ k_{cat} (**1a**)	k_{eff}(X) [a,d]
1	none	*e*		*e*
2	**22**	*e*		[e](X = 25)
3	**1a**	2.00×10^{-05}	1	1.46×10^{-06} (X = 25)
4	**1b**	5.00×10^{-04}	25	1.73×10^{-05} (X = 12.5)
				3.24×10^{-05} (X = 25)
5	**6bc**	5.70×10^{-03}	285	6.73×10^{-05} (X = 5.7)
				1.60×10^{-04} (X = 11.5)
				1.82×10^{-04} (X = 12.5)
				3.55×10^{-04} (X = 25)
6	**6cg**	7.70×10^{-03}	385	8.53×10^{-05} (X = 5)
				2.49×10^{-04} (X = 12.5)
				4.81×10^{-04} (X = 25)

[a]Averaged values (see Supporting Information). [b]k_{cat} is obtained as the slope of the correlations shown in Figure 5. [c]In L^2 mol^{-2} s^{-1}. [d]In L mol^{-1} s^{-1}. [e]No turnover after >18500 min.

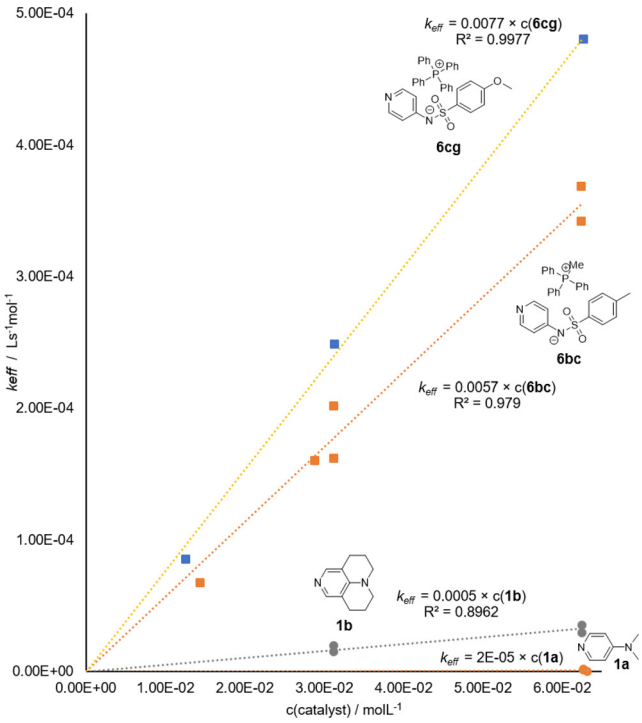

Figure 5. Benchmarking of catalyst activity at different catalyst loadings for selected catalysts in the *aza*-MBH reaction.

superiority of the anionic systems investigated in this study. As before, **22** is not active as a catalyst in this reaction.

In order to test whether the observed catalytic activities correlate with calculated Lewis basicity parameters, methyl cation affinities (MCA) and phenyl isocyanate affinities (PIA)

https://dx.doi.org/10.1021/acs.joc.0c00114
J. Org. Chem. 2020, 85, 5390−5402

have been calculated. Such relative affinity values have been shown to correlate well with experimentally determined rate constants in previous investigations.[11] In line with those studies, we calculated these affinities relative to pyridine as the reference base. Relative Lewis basicities toward Me^+ (ΔMCA) and phenyl isocyanate (ΔPIA) have been calculated as the reaction enthalpies at 298.15 K for the isodesmic group transfer reactions shown in eqs 3 and 4.

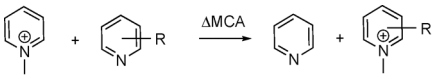

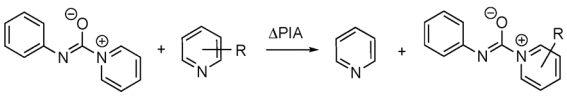

Recent studies showed that reliable results taking dispersive interactions into account are obtained at the DLPNO–CCSD(T)/def2-TZVPP//SMD($CHCl_3$)/B3LYP-D3/6-31+G(d) level of theory (in the following referred to as "CC"). The SMD($CHCl_3$)/B3LYP-D3/6-31+G(d) level used for geometry optimizations is referred to as "DFT".[12] ΔMCA and ΔPIA values calculated with these two approaches have been summarized in Table 4. For ion pair catalysts based on the 4-pyridinylamide core structure, the addition to the pyridine-N and amide-N positions may both be competitive. We have, therefore, listed reaction energies for both positions in Table 4. In order to cope with the enormous conformational space accessible to ion pair structures in a systematic manner, initial starting geometries for ion pair catalysts were generated using a randomization approach as detailed in the Supporting Information.[13] The results in Table 4 are based on the energetically most favorable conformations identified in these extensive search procedures.

Table 4. Calculated ΔMCA and ΔPIA Values Ordered by ΔPIA (DFT)

			ΔH_{298K} SMD($CHCl_3$)/B3LYP-D3/6-31+G(d)		ΔH_{298K}DLPNO–CCSD(T)/def2-TZVPP//SMD($CHCl_3$)/B3LYP-D3/6-31+G(d)	
entry	catalyst	lewis basic atom[a]	ΔMCA[b]	ΔPIA[b]	ΔMCA[b]	ΔPIA[b]
1	**6cg**	N1	−65.6	−61.2	−62.7	−61.7
2	**6bc**	N1	−64.8	−56.7	−63.0	−58.1
3	**10h**[c]	N1	−72.2	−53.1	−68.0	−53.3
4	**15g**	N1	−47.0	−45.7	−43.0	−42.1
5	**1f**	N1	−54.7	−39.3	−47.8	−37.2
6	**6ac**	N1	−43.2	−38.1	−38.4	−38.3
7	**1e**	N1	−52.2	−34.2	−46.3	−32.2
8	**1b**	N1	−48.8	−32.5	−43.9	−29.9
9	**6ah**[c]	N1	−40.5	−30.9	−37.9	−31.8
10	**1d**	N1	−45.7	−30.6	−39.0	−27.7
11	**6bc**	N2	−57.9	−28.5	−64.0	−34.7
12	**1c**	N1	−40.9	−27.2	−38.4	−26.3
13	**1a**	N1	−37.0	−25.7	−35.2	−24.8
14	**6cg**	N2	−61.2	−24.4	−67.8	−31.4
15	**15g**	N2	−32.0	−11.9	−42.8	−27.9
16	**23**	N1	−7.1	−1.7	−2.3	−0.5
17	**22**	P	−45.2	+8.2	−53.7	+8.8
18	**6ah**[c]	N2	−0.8	+10.7	−12.2	+3.9

[a]N1 = pyridine-N; N2 = amide-N. [b]In kJ mol^{-1}. [c]**h** = PEt_4^+.

Figure 6 shows a correlation of the calculated ΔMCA and ΔPIA values for the pyridine-N position with the logarithmic effective rate constant measured for 3 mol % catalyst loading ($\ln(k_{eff}(3))$) for the urethane formation reaction. Although calculated ΔMCA values correlated well with experimentally determined catalytic activities in earlier studies,[8] we find here that computational modeling closer to the experiment ultimately pays off for the broader selection of catalysts studied here. Already at the DFT level of theory, the correlation between experimental rate data and ΔPIA values is much better as compared to the ΔMCA values. On closer analysis of the two correlations shown in Figure 6, this is, at least in part, due to the affinity values calculated for triphenylphosphine (**22**). According to the ΔMCA values, **22** is expected to be a moderately active Lewis base that is much more active than the pyridine reference (Table 4, entry 17). However, the experimental observations as well as the ΔPIA values show that **22** is much less active than isoquinoline (**23**), whose basicity is close to that of pyridine. From all of the systems studied here, the ion pair catalysts such as **6cg** carrying electron-donating groups have the highest affinities toward phenyl isocyanate. This effect is less pronounced in the ΔMCA than the ΔPIA values. These findings are in complete agreement with the results from our two benchmark reactions, where catalyst **6cg** performs best. We believe the large difference in the catalytic activity between ion pair and neutral Lewis base catalysts originates from the already existing charge separation in the ion pair systems. This difference is most easily appreciated from the initial addition step of Lewis base catalysts to isocyanate **17** shown in Scheme 2a. For DMAP (**1a**), this addition step transforms the two neutral reactants into a zwitterionic adduct and thus requires the formal separation of unit charges. No such charge separation is required in the reaction of ion pair catalysts such as **6cg**, where the addition step simply transforms the reactant ion pair into a new (intermediate) ion pair structure.

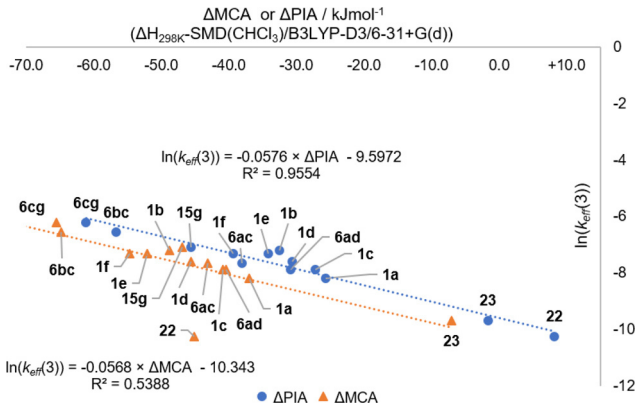

Figure 6. Correlation of reaction rates $k_{eff}(3)$ measured for urethane formation with Lewis basicity parameters ΔMCA and ΔPIA calculated for pyridine-N (DFT).

On a methodological note, it should be added that the affinity data calculated at the DFT or CC level are quite similar. However, whether the calculation of affinities is based on full ion pairs or only on the anionic fragment acting as the Lewis base leads to substantially different results. This is illustrated in Scheme 3 for the addition of phenylisocyanate (**PhNCO**) to ion pair catalyst **6cg**, which is exothermic by 61.2 kJ mol^{-1} at the

https://dx.doi.org/10.1021/acs.joc.0c00114
J. Org. Chem. 2020, 85, 5390−5402

Scheme 3. ΔPIA Values for the Pyridinyl Adduct 6c-PhNCO and for Ion Pair Adduct 6cg-PhNCO

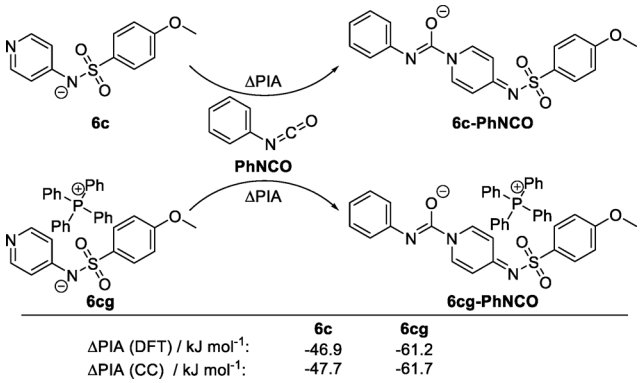

DFT level. The addition of the same electrophile to the corresponding 4-pyridinylamide anion **6c** is exothermic by only 46.9 kJ mol^{-1}, which represents a difference of 14.3 kJ mol^{-1}. Calculations on the anionic components of ion pair catalysts will thus not display the full Lewis base capacities of these systems! A final result from the calculated affinity data in Table 4 concerns the relative Lewis basicity of the pyridine-N vs the amide-N center. For neutral catalysts such as DMAP (**1a**), it is well established that the pyridine nitrogen atom is the more Lewis basic center. Therefore, the good correlation of calculated pyridine-N affinity values with experimental findings for both neutral and ionic catalysts supports the assumption that, in both cases, the pyridine nitrogen atom is the Lewis basic center involved in catalysis. The same insight is gained when comparing the ΔPIA values of the competing nitrogen atoms. In all cases listed in Table 4 (entries 1 and 14, 2 and 11, 4 and 15, as well as 9 and 18), the pyridine-N-isocyanate adduct is approximately 30−40 kJ mol^{-1} more stable as compared to the amide-N adduct. This leads us to believe that, in the investigated reactions, the pyridine-nitrogen atom is more Lewis basic and, therefore, the catalytically active center (see Supporting Information for more details).

■ CONCLUSION

We find that stabilized 4-amide pyridinyl anions, which so far have only been used for oligomerization reactions of isocyanides, show high catalytic activity in urethane synthesis and in *aza*-MBH reactions. Furthermore, the characterization of several such previously undescribed ion pairs could be achieved, including crystal structures. We also report and characterize ion pairs based on the imine-bridged pyridinyl anion **15** and the 4-pyridinyl phosphonamide **10**. Our results indicate that catalyst performance is primarily dictated by the anion substitution pattern, while only moderate effects appear to be due to the choice of cation (both in the experiments and the calculated affinity values). Extensive ion pair modeling involving randomized starting geometries allowed us to calculate phenyl isocyanate affinities (ΔPIA) that correlate very well with the experimental results. This finding documents the added benefit of computational modeling close to the experimental conditions, since the more established methyl cation affinities (ΔMCA) gave much poorer correlations. These quantum chemical results also confirm that the pyridine nitrogen atom is the Lewis basic center responsible for catalytic activity. In more general terms, we find the investigated pyridinyl salts to be a class of easily accessible, inexpensive, and modular catalyst systems that show very good performance for the investigated reactions. After beginning to understand the reactivity of such ion pair catalysts, we look forward to future modifications imparting selectivity. We expect this to be quite promising due to the exchangeability of the cations and high Lewis basicity of the pyridinyl "warheads".

■ EXPERIMENTAL SECTION

General Information. All air- and water-sensitive processes were performed under a N_2 atmosphere using standard Schlenk techniques. Commercial catalysts (purchased from Sigma-Aldrich, except for TCAP **1b**, which was bought from TCI) and Si_2Me_6 were of reagent grade and used as received unless stated otherwise. *p*-Tolyl isocyanate (**17**) was of reagent grade and distilled prior to use. Butan-1-ol (**18**) was of reagent grade and distilled and stored over molecular sieves under N_2. Catalysts **1d**, **1e**, and **1f** were prepared as described in our previous studies.[2,5,14] NMR spectra were recorded on a Bruker Avance III HD 400, a Bruker Ascend 400, or a Varian Mercury 200 MHz spectrometer. All ^{1}H chemical shifts are reported in ppm (δ) relative to TMS (0.00, internal standard). ^{13}C chemical shifts are reported in ppm (δ) relative to $CDCl_3$ (77.16, internal standard), and ^{31}P chemical shifts are reported in ppm (δ) relative to 85% H_3PO_4 in water (0.00). $CDCl_3$ was refluxed for at least 1 h over CaH_2 and subsequently distilled. GC measurements were done on a Shimadzu GC-2010 Plus Gas Chromatograph with an AOC-20i autosampler (with temperature-controlled sample holder) and an Optima 1701−0.26 μm (25 m × 0.25 mm) column.

Urethane Benchmark Reaction Experiments. Three different stock solutions were prepared under a N_2 atmosphere. (1) SSA: 0.30 mol L^{-1} isocyanate **17** in $CDCl_3$. (2) SSB: 0.90 mol L^{-1} butanol **18** and ca. 0.15 mol L^{-1} Si_2Me_6 in $CDCl_3$. (3) SSC: 0.0003−0.09 mol L^{-1} catalyst in $CDCl_3$. NMR kinetics: Samples were prepared by transferring 0.2 mL of SSB, the appropriate amount of SSC and $CDCl_3$, and 0.2 mL of SSA (total of 0.6 mL sample volume) into a dried, N_2-purged NMR tube. The sample was capped and sealed by Parafilm unless stated otherwise. It was then stored in the bath of a thermostat set at 23 °C or in an NMR machine temperature-controlled to remain at 23 °C. Once a sample was not kept in the NMR machine for continuous measuring anymore, it was stored in the bath of a thermostat until the reaction was complete. The samples were only taken out of the thermostat for measuring ^{1}H NMR spectra. The protons highlighted in Scheme 2 were used to calculate the conversion. GC kinetics: Samples were prepared by transferring 0.2 mL of SSB, the appropriate amount of SSC and $CDCl_3$, and 0.2 mL of SSA (total of 0.6 mL sample volume) into a dried, N_2-purged GC vial. The sample was capped under a N_2 atmosphere and stored in the temperature-controlled autosampler of the GC machine at 23 °C. Multiple identical samples were prepared and then measured repeatedly (up to 4 times each). This enabled us to measure at several points the reaction progress as well as to keep the sample protected from moisture. In between the individual measurements, cleaning runs were done. 55(0)-5−150(0)-20−280(5) was used as a heating regime of the column, meaning, start at 55 °C, remain at this temperature for 0 min, heating to 150 °C with a rate of 5 °C/min, hold at 150 °C for 0 min, and heating with a rate of 20 °C/min up to 280 °C, which remains constant for 5 min. The injector was heated to 200 °C. The conversion was calculated from the ratio of integrals with the internal standard Si_2Me_6. See Supporting Information for details on data processing.

***Aza*-MBH Benchmark Reaction Experiments.** Two different stock solutions were prepared under a N_2 atmosphere. (1) SSD: 0.30 mol L^{-1} tosyl imine **19**, 1.2 mol L^{-1} cyclohex-2-en-1-one **20**, and ca. 0.08 mol L^{-1} 1,3,5-trimethoxybenzene in $CDCl_3$. (2) SSE: 0.075−0.375 mol L^{-1} catalyst in $CDCl_3$. Samples were prepared by transferring 0.5 mL of SSD, the appropriate amount of SSE, and $CDCl_3$ (total of 0.6 mL sample volume) into a dried, N_2-purged NMR tube. The sample was flame-sealed unless stated otherwise. It was then stored in the bath of a thermostat set at 23 °C or in an NMR machine temperature-controlled to remain at 23 °C. Once a sample was not kept in the NMR machine for continuous measuring anymore, it was stored

https://dx.doi.org/10.1021/acs.joc.0c00114
J. Org. Chem. 2020, 85, 5390−5402

in the bath of a thermostat until the reaction was completed. The samples were only taken out of the thermostat for measuring ^{1}H NMR spectra. The protons highlighted in Scheme 2 were used to calculate the conversion. See Supporting Information for details on data processing.

Synthesis of Pyridinyl Amide Ion Pair Catalysts. All synthesized catalysts were bench stable and stored under ambient laboratory conditions unless stated otherwise. Despite the different syntheses given for the catalyst systems in the following section, the approach described for **6cg** may be the most practical in general terms.

*Tetrabutylammonium Pyridin-4-yl((trifluoromethyl)sulfonyl)-amide (**6aa**).* Sulfonamide **8a** (0.489 g, 2.26 mmol, 1.0 equiv) was suspended in 20 mL of dry methanol under N_2, and a solution of 0.052 g of sodium (2.26 mmol, 1.0 equiv) in 10 mL of dry methanol was added. After stirring the resulting, clear solution for 1 h at room temperature, 0.729 g (2.26 mmol, 1.0 equiv) of tetrabutylammonium bromide was added, and the mixture was stirred for another hour. The solvent was removed *in vacuo*, giving the crude product. Repeated recrystallization from a mixture of hexane/toluene (6:1) and CH_2Cl_2 (by evaporation of CH_2Cl_2 by means of a N_2 flux) gave 0.707 g of catalyst **6aa** (1.51 mmol, 67%) as colorless crystals with a mp of 83−85 °C. ^{1}H NMR (400 MHz, $CDCl_3$): δ [ppm] = 8.14 (d, J = 6.3 Hz, 2H), 7.03 (d, J = 6.3 Hz, 2H), 3.20−3.04 (m, 8H), 1.54 (p, J = 8.1, 7.7 Hz, 8H), 1.35 (h, J = 7.3 Hz, 8H), 0.93 (t, J = 7.3 Hz, 12H). ^{13}C{^{1}H} NMR (101 MHz, $CDCl_3$): δ [ppm] = 156.0, 149.4, 121.3 (q, J = 328.2 Hz), 118.1, 58.8, 23.9, 19.7, 13.6. ^{19}F NMR (377 MHz, $CDCl_3$): δ [ppm] = −76.8. IR (ATR): ν (cm^{-1}) = 3392 (vw), 2960 (m), 2935 (w), 2874 (w), 1633 (vw), 1585 (w), 1534 (vw), 1494 (w), 1476 (w), 1465 (w), 1418 (vw), 1379 (vw), 1346 (vw), 1321 (s), 1285 (s), 1194 (vs), 1164 (vs), 1130 (s), 1066 (vw), 1031 (vw), 999 (s), 984 (m), 965 (w), 927 (vw), 899 (vw), 885 (w), 832 (m), 782 (w), 764 (vw), 736 (w), 666 (w), 626 (m), 601 (vs), 567 (vs). Elemental analysis (%) calcd for $C_{22}H_{40}F_3N_3O_2S$ (467.64 g mol^{-1}): C, 56.51; H, 8.62; N, 8.99; S, 6.86. Found (%): C, 56.01; H, 8.54; N, 8.88; S, 6.73. HRMS (ESI) m/z: [M]$^+$ calcd for $C_{16}H_{36}N^+$, 242.2842; found, 242.2846. HRMS (ESI) m/z: [M]$^-$ calcd for $C_6H_4F_3N_2O_2S^-$, 224.9951; found, 224.9949.

*Tetraoctylammonium Pyridin-4-yl((trifluoromethyl)sulfonyl)-amide (**6ab**).* Sulfonamide **8a** (0.517 g, 2.39 mmol, 1.0 equiv) was suspended in 20 mL of dry methanol under N_2, and a solution of 0.055 g of sodium (2.39 mmol, 1.0 equiv) in 10 mL of dry methanol was added. After stirring the resulting, clear solution for 1 h at room temperature, 1.307 g of tetraoctylammonium bromide (2.39 mmol, 1.0 equiv) was added, and the mixture was stirred for 14 h. The solvent was removed *in vacuo*, and 16 mL of CH_2Cl_2 was added. Remaining solids were filtered off, and the solvent was removed. The process was repeated with decreasing amounts of CH_2Cl_2 several times, yielding 1.57 g of catalyst **6ab** (2.27 mmol, 95%) as a colorless oil. ^{1}H NMR (400 MHz, $CDCl_3$): δ [ppm] = 8.15 (d, J = 6.2 Hz, 2H), 7.05 (d, J = 6.3 Hz, 2H), 3.33−2.97 (m, 8H), 1.72−1.50 (m, 8H), 1.50−1.10 (m, 40H), 0.85 (t, J = 6.8 Hz, 12H). ^{13}C{^{1}H} NMR (101 MHz, $CDCl_3$): δ [ppm] = 155.8, 149.6, 122.3 (q, J = 328.2 Hz), 118.1, 59.0, 31.7, 29.1, 29.1, 26.3, 22.7, 22.1, 14.2. ^{19}F NMR (377 MHz, $CDCl_3$): δ [ppm] = −76.8. IR (ATR): ν (cm^{-1}) = 2954 (w), 2925 (m), 2856 (w), 1589 (m), 1534 (vw), 1495 (w), 1468 (w), 1378 (vw), 1314 (s), 1282 (s), 1195 (vs), 1156 (vs), 1132 (s), 1085 (vw), 1000 (s), 984 (w), 830 (w), 782 (w), 723 (w), 666 (vw), 628 (w), 602 (vs), 568 (s). Elemental analysis (%) calcd for $C_{38}H_{72}F_3N_3O_2S$ (692.07 g mol^{-1}): C, 65.95; H, 10.49; N, 6.07; S, 4.63. Found (%): C, 65.76; H, 10.49; N, 5.94; S, 4.76. HRMS (ESI) m/z: [M]$^+$ calcd for $C_{32}H_{68}N^+$, 466.5346; found, 466.5341. HRMS (ESI) m/z: [M]$^-$ calcd for $C_6H_4F_3N_2O_2S^-$, 224.9951; found, 224.9949.

*Methyltriphenylphosphonium Pyridin-4-yl((trifluoromethyl)-sulfonyl)amide (**6ac**).* Sulfonamide **8a** (0.532 g, 2.46 mmol, 1.0 equiv) was suspended in 20 mL of dry methanol under N_2, and a solution of 0.057 g of sodium (2.46 mmol, 1.0 equiv) in 10 mL of dry methanol was added. After stirring the resulting, clear solution for 1 h at room temperature, 0.879 g of methyltriphenylphosphonium bromide (2.46 mmol, 1.0 equiv) was added, and the mixture was stirred for 14 h. The solvent was removed *in vacuo*, and 5 mL of CH_2Cl_2 was added. The remaining solids were filtered off, and the solvent was removed *in vacuo*, giving the crude product, which was recrystallized from a mixture of hexane/toluene (6:1) and CH_2Cl_2 (by evaporation of CH_2Cl_2 by means of a N_2 flux) to give 0.484 g of catalyst **6ac** (0.96 mmol, 39%) as colorless crystals with a mp of 101−104 °C. ^{1}H NMR (400 MHz, $CDCl_3$): δ [ppm] = 8.05 (dd, J = 4.8, 1.5 Hz, 2H), 7.77 (tq, J = 7.0, 1.3 Hz, 3H), 7.63 (td, J = 7.9, 3.6 Hz, 6H), 7.60−7.52 (m, 6H), 6.94 (dd, J = 4.8, 1.5 Hz, 2H), 2.83 (d, J = 13.3 Hz, 3H). ^{13}C{^{1}H} NMR (101 MHz, $CDCl_3$): δ [ppm] = 155.8, 149.5, 135.5 (d, J = 3.0 Hz), 133.0 (d, J = 10.7 Hz), 130.7 (d, J = 12.9 Hz), 122.1 (q, J = 328.2 Hz), 118.8 (d, J = 88.8 Hz), 118.0, 9.7 (d, J = 58.4 Hz,). ^{19}F NMR (377 MHz, $CDCl_3$): δ [ppm] = −76.8. ^{31}P NMR (162 MHz, $CDCl_3$): δ [ppm] = +21.2. IR (ATR): ν (cm^{-1}) = 3056 (vw), 2973 (vw), 2901 (vw), 1586 (w), 1535 (vw), 1495 (w), 1482 (w), 1438 (m), 1323 (s), 1300 (m), 1288 (vw), 1195 (vs), 1156 (vs), 1146 (vs), 1116 (vs), 1004 (s), 998 (s), 986 (m), 911 (m), 904 (s), 856 (vw), 833 (m), 781 (w), 755 (m), 743 (s), 717 (s), 691 (s), 682 (s), 666 (m), 630 (m), 601 (vs), 566 (vs). Elemental analysis (%) calcd for $C_{25}H_{22}F_3N_2O_2PS$ (502.49 g mol^{-1}): C, 59.76; H, 4.41; N, 5.58; S, 6.38. Found (%): C, 59.57; H, 4.48; N, 5.57; S, 6.58. HRMS (ESI) m/z: [M]$^+$ calcd for $C_{19}H_{18}P^+$, 277.1146; found, 277.1136. HRMS (ESI) m/z: [M]$^-$ calcd for $C_6H_4F_3N_2O_2S^-$, 224.9951; found, 224.9949.

*Tetrabutylphosphonium Pyridin-4-yl((trifluoromethyl)sulfonyl)-amide (**6ad**).* Sulfonamide **8a** (0.40 g, 1.77 mmol, 1.0 equiv) was suspended in 1.24 mL of tetrabutylphosphonium hydroxide (40% in H_2O, 1.77 mmol, 1.0 equiv) and 2 mL of H_2O. The mixture was stirred at room temperature for 0.5 h, and the clear, separated phases were extracted with CH_2Cl_2. The organic phases were dried over Na_2SO_4 and the solvents removed to give the colorless crude product, which was recrystallized from toluene/CH_2Cl_2 to yield 0.682 g of catalyst **6ad** (1.41 mmol, 79%) in the form of colorless crystals with a mp of 56−60 °C. ^{1}H NMR (400 MHz, $CDCl_3$): δ [ppm] = 8.16 (dd, J = 6.4, 3.2 Hz, 2H), 7.03 (dd, J = 6.3, 3.2 Hz, 2H), 2.27−2.02 (m, 8H), 1.57−1.34 (m, 16H), 0.92 (t, J = 6.9 Hz, 12H). ^{13}C{^{1}H} NMR (101 MHz, $CDCl_3$): δ [ppm] = 155.7, 149.7, 122.1 (q, J = 328.3 Hz), 118.1, 23.9 (d, J = 15.2 Hz), 23.7 (d, J = 4.8 Hz), 18.7 (d, J = 47.5 Hz), 13.4. ^{19}F NMR (377 MHz, $CDCl_3$): δ [ppm] = −76.8. ^{31}P NMR (162 MHz, $CDCl_3$): δ [ppm] = +33.2. IR (ATR): ν (cm^{-1}) = 2959 (m), 2933 (w), 2873 (w), 2106 (vw), 1585 (m), 1534 (vw), 1493 (m), 1479 (w), 1465 (w), 1406 (vw), 1380 (vw), 1320 (s), 1279 (s), 1232 (w), 1192 (s), 1163 (vs), 1130 (s), 1101 (m), 1054 (vw), 998 (s), 984 (s), 907 (m), 830 (s), 782 (m), 747 (w), 730 (w), 702 (w), 666 (w), 626 (m), 599 (vs), 567 (vs). Elemental analysis (%) calcd for $C_{22}H_{40}F_3N_2O_2PS$ (484.60 g mol^{-1}): C, 54.53; H, 8.32; N, 5.78; S, 6.62. Found (%): C, 54.40; H, 8.41; N, 5.74; S, 6.23. HRMS (ESI) m/z: [M]$^+$ calcd for $C_{16}H_{36}P^+$, 259.2549; found, 259.2545. [M]$^-$ calcd for $C_6H_4F_3N_2O_2S^-$, 224.9951; found, 224.9949.

*Methyltriphenylphosphonium Pyridin-4-yl(tosyl)amide (**6bc**).* Sodium hydroxide (0.124 g, 3.1 mmol, 1.1 equiv) was dissolved in 5 mL of H_2O, and this solution was added to 0.70 g of sulfonamide **8b** (3 mmol, 1.0 equiv). After 10 min of stirring at room temperature, 1.00 g of methyltriphenylphosphonium bromide (3 mmol, 1.0 equiv) was added with an additional 3 mL of H_2O, and the resulting viscous suspension was stirred for 45 min. Extraction with CH_2Cl_2 (3 × 30 mL), drying of the organic phase over Na_2SO_4, and the removal of the solvent gave the crude product. It was recrystallized from 18 mL of CH_2Cl_2 by layering of 8 mL of toluene on top to yield 0.873 g of catalyst **6bc** (1.66 mmol, 54%) in the form of colorless needles with a mp of 195−199 °C. ^{1}H NMR (400 MHz, $CDCl_3$): δ [ppm] = 7.87 (d, J = 6.1 Hz, 2H), 7.83−7.66 (m, 5H), 7.66−7.49 (m, 12H), 7.05 (d, J = 7.9 Hz), 6.71 (d, J = 6.2 Hz, 2H), 2.93 (d, J = 13.2 Hz, 3H), 2.26 (s, 3H). ^{13}C{^{1}H} NMR (101 MHz, $CDCl_3$): δ [ppm] = 157.5, 149.2, 143.1, 139.7, 135.2 (d, J = 3.0 Hz), 133.1 (d, J = 10.7 Hz), 130.5 (d, J = 12.9 Hz), 128.8, 126.8, 119.1 (d, J = 88.6 Hz), 116.2, 21.4, 9.7 (d, J = 57.7 Hz). ^{31}P NMR (162 MHz, $CDCl_3$): δ [ppm] = +21.4. IR (ATR): ν (cm^{-1}) = 2965 (w), 2895 (w), 1640 (w), 1587 (m), 1515 (w), 1482 (m), 1438 (m), 1314 (s), 1240 (s), 1215 (m), 1165 (w), 1118 (vs), 1082 (vs), 1055 (m), 1022 (w), 990 (m-s), 968 (m), 931 (m), 914 (m), 860 (w), 830 (w), 815 (w), 798 (w), 778 (w), 763 (w), 745 (w), 719 (m), 696 (w), 690 (w), 665 (w). Elemental analysis (%) calcd for $C_{31}H_{29}N_2O_2PS$ (524.62 g mol^{-1}): C, 70.97; H, 5.57; N, 5.34; S, 6.11.

https://dx.doi.org/10.1021/acs.joc.0c00114
J. Org. Chem. 2020, 85, 5390−5402

Found (%): C, 71.04; H, 5.61; N, 5.31; S, 6.23. HRMS (ESI) *m/z*: $[M]^+$ calcd for $C_{19}H_{18}P^+$, 277.1146; found, 277.1138. HRMS (ESI) *m/z*: $[M]^-$ calcd for $C_{12}H_{11}N_2O_2S^-$, 247.0547; found, 247.0547.

*1,3-Diethyl-benzimidazolium Pyridin-4-yl(tosyl)amide (**6be**).* Sodium hydroxide (0.110 g, 2.75 mmol, 1.1 equiv) was dissolved in 5 mL of H_2O, and this solution was added to 0.621 g of sulfonamide **8b** (2.50 mmol, 1.0 equiv) with an additional 5 mL of H_2O. After 15 min of stirring at room temperature, a solution of 0.638 g of 1,3-diethyl-benzimidazolium bromide **26** (2.5 mmol, 1.0 equiv) in 5 mL of CH_2Cl_2 was added with an additional 5 mL of CH_2Cl_2, and the resulting mixture was stirred for 15 min. Extraction with CH_2Cl_2 (3 × 30 mL), drying of the organic phase over Na_2SO_4 (with the addition of 4 pellets of activated charcoal), and removal of the solvent gave the crude product. It was recrystallized from toluene/CH_2Cl_2 by layering of hexane on top to yield 0.607 g of catalyst **6be** (1.44 mmol, 58%) in the form of colorless crystals with a mp of 148−150 °C. ^{1}H NMR (400 MHz, $CDCl_3$): δ [ppm] = 10.49 (s, 1H), 7.95 (d, *J* = 6.3 Hz, 2H), 7.77 (d, *J* = 8.1 Hz, 2H), 7.69−7.51 (m, 4H, H-13), 7.10 (d, *J* = 8.0 Hz, 2H), 6.73 (d, *J* = 6.4 Hz, 2H), 4.49 (q, *J* = 7.3 Hz, 4H), 2.27 (s, 3H), 1.56 (t, *J* = 7.3 Hz, 6H). $^{13}C\{^1H\}$ NMR (101 MHz, $CDCl_3$): δ [ppm] = 156.9, 149.4, 142.3, 140.3, 131.2, 129.0, 127.1, 126.6, 115.9, 113.0, 42.9, 21.4, 14.8. Elemental analysis (%) calcd for $C_{23}H_{26}N_4O_2S$ (422.55 g mol^{-1}): C, 65.38; H, 6.20; N, 13.26; S, 7.59. Found (%): C, 65.29; H, 6.18; N, 13.18; S, 7.71. HRMS (ESI) *m/z*: $[M]^+$ calcd for $C_{11}H_{15}N_2^+$, 175.1230; found, 175.1230. HRMS (ESI) *m/z*: $[M]^-$ calcd for $C_{12}H_{11}N_2O_2S^-$, 247.0547; found, 247.0545.

*Benzyltriphenylphosphonium Pyridin-4-yl(tosyl)amide (**6bf**).* Sulfonamide **8b** (0.80 g, 3.2 mmol, 1.0 equiv) was added to a solution of 0.141 g of sodium hydroxide (3.52 mmol, 1.2 equiv) in 5 mL of H_2O. Benzyltriphenylphosphonium bromide (1.39 g) was added with 12 mL of CH_2Cl_2, and the mixture was stirred at room temperature for 30 min. Extraction with CH_2Cl_2, drying of the organic phase over Na_2SO_4, and removal of the solvent gave the crude product. It was dissolved in 10 mL of CH_2Cl_2, upon which were layered 10 mL of toluene and 3 mL of hexane to grow crystals overnight. This yielded 1.228 g of catalyst **6bf** (2.04 mmol, 64%) in the form of colorless crystals with mp 197−200 °C. ^{1}H NMR (400 MHz, $CDCl_3$): δ [ppm] = 7.84 (d, *J* = 6.4 Hz, 2H), 7.77−7.65 (m, 5H), 7.58−7.43 (m, 12H), 7.22−7.13 (m, 1H), 7.05 (t, *J* = 7.6 Hz, 2H), 7.01 (d, *J* = 8.0 Hz, 2H), 6.84 (d, *J* = 7.6 Hz, 2H), 6.73 (d, *J* = 6.4 Hz, 2H), 4.78 (d, *J* = 14.2 Hz, 2H), 2.23 (s, 3H). $^{13}C\{^1H\}$ NMR (101 MHz, $CDCl_3$): δ [ppm] = 157.7, 148.7, 143.1, 139.6, 135.2 (d, *J* = 3.0 Hz), 134.1 (d, *J* = 9.7 Hz), 131.3 (d, *J* = 5.5 Hz), 130.3 (d, *J* = 12.6 Hz), 129.0 (d, *J* = 3.3 Hz), 128.7, 128.6 (d, *J* = 3.8 Hz), 126.8 (d, *J* = 8.7 Hz), 126.8, 117.4 (d, *J* = 85.8 Hz), 116.2, 30.5 (d, *J* = 47.7 Hz), 21.4. $^{31}P\{^1H\}$ NMR (162 MHz, $CDCl_3$): δ [ppm] = +22.7. IR (ATR): ν (cm^{-1}) = 2938 (vw), 1980 (vw), 1586 (s), 1493 (m), 1478 (m), 1436 (m), 1308 (vs), 1219 (s) 1208 (m), 1121 (vs), 1090 (vs), 991 (s), 947 (m), 836 (m), 815 (w), 782 (w), 750 (vs), 719 (m), 691 (s), 666 (m), 656 (m). Elemental analysis (%) calcd for $C_{37}H_{33}N_2O_2PS$ (600.72 g mol^{-1}): C, 73.98; H, 5.54; N, 4.66; S, 5.34. Found (%): C, 71.82; H, 5.34; N, 4.48; S, 5.29. HRMS (ESI) *m/z*: $[M]^+$ calcd for $C_{25}H_{22}P^+$, 353.1454; found, 653.1451. HRMS (ESI) *m/z*: $[M]^-$ calcd for $C_{12}H_{11}N_2O_2S^-$, 247.0547; found, 247.0546.

*1,3-Diethyl-benzimidazolium ((4-Methoxyphenyl)sulfonyl)-(pyridin-4-yl)amide (**6ce**).* Sodium hydroxide (0.088 g, 2.2 mmol, 1.1 equiv) was dissolved in 5 mL of H_2O, and this solution was added to 0.529 g of sulfonamide **8c** (2.0 mmol, 1.0 equiv) with an additional 5 mL of H_2O. After 15 min of stirring at room temperature, a solution of 0.510 g of 1,3-diethyl-benzimidazolium bromide **26** (2.0 mmol, 1.0 equiv) in 5 mL of CH_2Cl_2 was added with an additional 5 mL of CH_2Cl_2, and the resulting mixture was stirred for 15 min. Extraction with 40 mL of CH_2Cl_2, drying of the organic phase over Na_2SO_4 (with the addition of 4 pellets of activated charcoal), and reduction of the solvent gave a concentrated, yellow solution. The product was crystallized by layering toluene/hexane (10:1) on top to yield 0.363 g of catalyst **6ce** (0.83 mmol, 41%) in the form of light-yellow crystals with a mp of 144−146 °C. ^{1}H NMR (400 MHz, $CDCl_3$): δ [ppm] = 10.53 (s, 1H), 7.97 (dd, *J* = 5.0, 1.4 Hz, 2H), 7.83 (dd, *J* = 8.8, 4.8 Hz, 2H), 7.70−7.55 (m, 4H, H-13), 6.81 (dd, *J* = 8.8, 4.9 Hz, 2H), 6.75 (dd, *J* = 4.9, 1.5 Hz, 2H), 4.51 (q, *J* = 7.3 Hz, 4H), 3.75 (s, 3H), 1.58 (t, *J* = 7.3 Hz, 6H). $^{13}C\{^1H\}$ NMR (101 MHz, $CDCl_3$): δ [ppm] = 161.0, 157.0, 149.5, 142.4, 137.4, 131.2, 128.5, 127.2, 115.9, 113.6, 113.1, 55.4, 43.0, 14.9. IR (ATR): ν (cm^{-1}) = 3057 (vw), 1556 (s), 1568 (m), 1520 (w), 1484 (s), 1432 (m), 1350 (vw), 1300 (s), 1252 (s), 1225 (s), 1120 (vs), 1081 (vs), 1030 (m), 1011 (w) 990 (s), 971 (s), 851 (vw), 822 (s), 805 (s), 780 (m), 756 (s), 667 (w). Elemental analysis (%) calcd for $C_{23}H_{26}N_4O_3S$ (438.55 g mol^{-1}): C, 62.99; H, 5.98; N, 12.78; S, 7.31. Found (%): C, 62.70; H, 5.81; N, 12.71; S, 7.35. HRMS (ESI) *m/z*: $[M]^+$ calcd for $C_{11}H_{15}N_2^+$, 175.1230; found, 175.1231. HRMS (ESI) *m/z*: $[M]^-$ calcd for $C_{12}H_{11}N_2O_3S^-$, 263.0496; found, 263.0500.

*Tetraphenylphosphonium ((4-Methoxyphenyl)sulfonyl)(pyridin-4-yl)amide (**6cg**).* NaOH (0.132 g, 2.0 mmol 1.1 equiv) was dissolved in 10 mL of H_2O, and the solution was added to 0.793 g of sulfonamide **8c** (3.0 mmol, 1.0 equiv). The mixture was stirred at room temperature for 15 min, forming a milky suspension. Tetraphenylphosphonium bromide (1.26 g, 3 mmol 1.0 equiv) was added with 10 mL of H_2O and stirring was continued for 10 min. The addition of 2 mL of toluene and 7 mL of CH_2Cl_2 caused separation of two clear phases, which were extracted with 40 mL of CH_2Cl_2. The organic phases were dried over $MgSO_4$ (under the addition of 10 pellets of activated charcoal), and removal of the solvents gave the crude product as a sticky, colorless foam. Crystallization from a mixture of 10 mL of toluene and 8 mL of CH_2Cl_2 by layering of 10 mL of toluene on top yielded 1.037 g (1.72 mmol, 57%) of catalyst **6cg** in the form of colorless crystals with a mp of 153−156 °C. ^{1}H NMR (400 MHz, $CDCl_3$): δ [ppm] = 7.88−7.75 (m, 8H), 7.70 (td, *J* = 7.8, 3.6 Hz, 8H), 7.53 (dd, *J* = 13.0, 7.5 Hz, 8H), 6.75 (d, *J* = 6.4 Hz, 2H), 6.72 (d, *J* = 8.8 Hz, 2H), 3.70 (s, 3H). $^{13}C\{^1H\}$ NMR (101 MHz, $CDCl_3$): δ [ppm] = 160.4, 157.8, 148.9, 138.8, 135.9 (d, *J* = 3.0 Hz), 134.4 (d, *J* = 10.3 Hz), 130.8 (d, *J* = 12.9 Hz), 128.6, 117.4 (d, *J* = 89.5 Hz), 116.2, 113.1, 55.3. ^{31}P NMR (162 MHz, $CDCl_3$): δ [ppm] = +23.06. IR (ATR): ν (cm^{-1}) = 3056 (vw), 1590 (m), 1484 (m), 1434 (m), 1317 (s), 1241 (s), 1238 (s), 1168 (w), 1123 (s) 1105 (s), 1084 (s), 1026 (w), 986 (s), 957 (s), 829 (m), 808 (m), 748 (w), 721 (vs), 692 (m), 661 (w). Elemental analysis (%) calcd for $C_{36}H_{31}N_2O_3PS$ (602.69 g mol^{-1}): C, 71.74; H, 5.18; N, 4.65; S, 5.32. Found (%): C, 71.00; H, 5.01; N, 4.55; S, 5.57. HRMS (ESI) *m/z*: $[M]^+$ calcd for $C_{24}H_{20}P^+$, 339.1297; found, 339.1293. HRMS (ESI) *m/z*: $[M]^-$ calcd for $C_{12}H_{11}N_2O_3S^-$, 263.0496; found, 263.0496.

*1,3-Diethyl-benzimidazolium Pyridin-2-yl(tosyl)amide (**7e**).* Sodium hydroxide (0.110 g, 2.75 mmol, 1.1 equiv) was dissolved in 5 mL of H_2O, and this solution was added to 0.621 g of sulfonamide **25** (2.5 mmol, 1.0 equiv) with an additional 5 mL of H_2O. After 15 min of stirring at room temperature, a solution of 0.638 g of 1,3-diethyl-benzimidazolium bromide **26** (2.5 mmol, 1.0 equiv) in 5 mL of CH_2Cl_2 was added with an additional 5 mL of CH_2Cl_2, and the resulting mixture was stirred for 15 min. Extraction with 40 mL of CH_2Cl_2, drying of the organic phase over Na_2SO_4 (with the addition of 4 pellets of activated charcoal), and reduction of the solvent gave a concentrated, yellow solution. The product was crystallized by layering toluene/hexane (10:1) on top to yield 0.596 g of catalyst **7e** (1.41 mmol, 56%) in the form of colorless, fine needles with a mp of 118−120 °C. ^{1}H NMR (400 MHz, $CDCl_3$): δ [ppm] = 11.85 (s, 1H), 8.02 (dd, *J* = 6.2, 1.3 Hz, 1H), 7.87 (d, *J* = 8.1 Hz, 2H), 7.74−7.50 (m, 4H), 7.22 (td, *J* = 8.7, 2.0 Hz, 1H), 7.10 (d, *J* = 8.0 Hz, 2H), 6.92 (d, *J* = 8.4 Hz, 1H), 6.44 (t, *J* = 6.0 Hz, 1H), 4.71 (q, *J* = 7.3 Hz, 4H), 2.28 (s, 3H), 1.59 (t, *J* = 7.3 Hz, 6H). $^{13}C\{^1H\}$ NMR (101 MHz, $CDCl_3$): δ [ppm] = 161.8, 148.0, 144.7, 143.3, 139.8, 136.7, 131.3, 128.8, 126.8, 126.7, 114.3, 112.97, 112.9, 42.8, 21.4, 15.0. IR (ATR): ν (cm^{-1}) = 2894 (w), 1585 (m), 1552 (m), 1462 (s), 1422 (s), 1351 (w), 1306 (s), 1294 (s), 1232 (s), 1142 (m), 1124 (s) 1097 (s), 1084 (vs), 1034 (m), 996 (s), 972 (m), 804 (m), 776 (vs), 756 (vs), 710 (m), 658 (s). Elemental analysis (%) calcd for $C_{23}H_{26}N_4O_2S$ (422.55 g mol^{-1}): C, 65.38; H, 6.20; N, 13.26; S, 7.59. Found (%): C, 64.63; H, 6.37; N, 13.21; S, 7.97. HRMS (ESI) *m/z*: $[M]^+$ calcd for $C_{11}H_{15}N_2^+$, 175.1230; found, 175.1230. HRMS (ESI) *m/z*: $[M]^-$ calcd for $C_{12}H_{11}N_2O_2S^-$, 247.0547; found, 247.0547.

*Tetrabutylphosphonium (Diphenylphosphoryl)(pyridin-4-yl)-amide (**10d**).* Phosphinic amide **11** (0.147 g, 0.5 mmol, 1.0 equiv) was dissolved in 0.5 mL of MeOH, and 0.35 mL of tetrabutylphosphonium hydroxide (40% in H_2O, 0.5 mmol, 1.0 equiv) was added.

https://dx.doi.org/10.1021/acs.joc.0c00114
J. Org. Chem. 2020, 85, 5390−5402

The solution was stirred for 10 min before all solvents were removed. The remaining solids were extracted with 4 mL of toluene, and the product was crystallized by layering hexane on top. Catalyst **10d** (0.134 g, 0.24 mmol, 48%) was obtained in the form of colorless crystals with a mp of 110−112 °C that were stored under N_2. Ion pair catalyst **10d** decomposes quickly when in contact with $CHCl_3$ or CH_2Cl_2 and appears to be highly hygroscopic. ^{1}H NMR (400 MHz, toluene-d_8): δ [ppm] = 8.42−8.22 (m, 4H), 8.12 (d, J = 5.3 Hz, 2H), 7.20 (td, J = 7.5, 2.2 Hz, 4H), 7.15−7.09 (m, 2H), 7.07 (d, J = 5.8 Hz, 2H), 2.22−1.92 (m, 8H), 1.30 (h, J = 7.2 Hz, 8H), 1.11 (dq, J = 15.6, 7.6 Hz, 8H), 0.88 (t, J = 7.3 Hz, 12H). ^{13}C{^{1}H} NMR (101 MHz, toluene-d_8): δ [ppm] = 163.2, 149.7 (d, J = 1.9 Hz), 142.7 (d, J = 122.0 Hz), 133.1 (d, J = 8.2 Hz), 129.4 (d, J = 2.4 Hz), 128.1 (d, J = 11.0 Hz), 119.4 (d, J = 21.1 Hz), 24.6 (d, J = 15.6 Hz), 24.4 (d, J = 4.7 Hz), 18.9 (d, J = 47.3 Hz), 14.2. ^{31}P{^{1}H} NMR (162 MHz, toluene-d_8): δ [ppm] = +32.16 (P$^+$), +10.86 (P = O). IR (ATR): ν (cm^{-1}) = 3053 (vw), 2957 (m), 2928 (m), 2870 (m), 1583 (vs), 1493 (vs), 1464 (m), 1434 (w), 1355 (vs), 1320 (m), 1226 (vw), 1206 (m), 1150 (vs), 1117 (s), 1103 (s), 1063 (w), 1000 (w), 986 (vs), 969 (s), 908 (w), 826 (s), 772 (w), 758 (w), 748 (m), 718 (s), 698 (vs), 658 (w). Elemental analysis (%) calcd for $C_{33}H_{50}N_2OP_2$ (552.72 g mol^{-1}): C, 71.71; H, 9.12; N, 5.07. Found (%): C, 69.63; H, 9.16; N, 4.77. HRMS (ESI) m/z: [M]$^+$ calcd for $C_{16}H_{36}P^+$, 259.2549; found, 259.2547. HRMS (ESI) m/z: [M]$^-$ calcd for $C_{17}H_{14}N_2OP^-$, 293.0849; found, 293.0850.

*Tetraphenylphosphonium (1,1-Dioxidobenzo[d]isothiazol-3-yl)-(pyridin-4-yl)amide (**15g**).* Sodium hydroxide (0.088 g, 2.2 mmol, 1.1 equiv) was dissolved in 5 mL of H_2O, and this solution was added to 0.519 g of sulfonamide **14** (2.0 mmol, 1.0 equiv) with an additional 5 mL of H_2O. After 15 min of stirring at room temperature, a solution of tetraphenylphosphonium bromide (0.839 g, 2.0 mmol, 1.0 equiv) in 5 mL of CH_2Cl_2 was added with an additional 5 mL of CH_2Cl_2, and the resulting mixture was stirred for 15 min. Extraction with 40 mL of CH_2Cl_2, drying of the organic phase over Na_2SO_4 (with the addition of 4 pellets of activated charcoal), and removal of the solvent gave the crude product. The product was crystallized from a mixture of 10 mL of toluene and 12 mL of CH_2Cl_2 by layering toluene/hexane (10:1) on top, yielding 0.872 g of catalyst **15g** (0.971 mmol, 49%) in the form of yellow needles with a mp of 189−192 °C. ^{1}H NMR (400.22 MHz, $CDCl_3$): δ [ppm] = 8.17 (d, J = 5.9 Hz, 2H), 7.93 (dd, J = 6.0, 1.5 Hz, 1H), 7.85−7.76 (m, 4H), 7.74−7.61 (m, 9H), 7.51 (ddd, J = 13.0, 8.3, 1.1 Hz, 8H), 7.42 (ddd, J = 7.2, 5.3, 1.4 Hz, 2H), 7.38 (dd, J = 4.7, 1.5 Hz, 2H). ^{13}C{^{1}H} NMR (101 MHz, $CDCl_3$): δ [ppm] = 158.9, 158.1, 149.4, 142.6, 137.6, 135.9 (d, J = 3.0 Hz), 134.4 (d, J = 10.3 Hz), 131.0, 130.8 (d, J = 12.9 Hz), 130.0, 123.1, 120.4, 119.8, 117.4 (d, J = 89.5 Hz). ^{31}P{^{1}H} NMR (162 MHz, $CDCl_3$): δ [ppm] = +22.06. IR (ATR): ν (cm^{-1}) = 2356 (vw), 1587 (w), 1552 (s), 1481 (w), 1436 (m), 1293 (m), 1248 (s), 1213 (w), 1165 (m), 1138 (s), 1107 (vs), 1055 (m), 994 (m), 777 (m), 754 (s), 722 (vs), 691 (s), 673 (s). Elemental analysis (%) calcd for $C_{36}H_{28}N_3O_2PS$ (597,67 g mol^{-1}): C, 72.35; H, 4.72; N, 7.03; S, 5.36. Found: C, 72.36; H, 4.48; N, 6.93; S, 5.39. HRMS (ESI) m/z: [M]$^+$ calcd for $C_{24}H_{20}P^+$, 339.1297; found, 339.1293. HRMS (ESI) m/z: [M]$^-$ calcd for $C_{12}H_8N_3O_2S^-$, 258.0343; found, 258.0341.

*Tetrabutylammonium Bis((trifluoromethyl)sulfonyl)amide (**24**).* Lithium bis((trifluoromethyl)sulfonyl)amide (0.500 g, 1.74 mmol, 1.0 equiv) was dissolved in 5 mL of *i*PrOH and added to a solution of 0.561 g of tetrabutylammonium bromide (1.74 mmol, 1.0 equiv) in 3 mL of *i*PrOH. The mixture was left stirring at room temperature overnight, after which the solvents were removed *in vacuo*. The solid residue was extracted with toluene and repeatedly recrystallized from toluene/hexane/CH_2Cl_2 to give 0.301 g of amide salt **24** (0.58 mmol, 33%) in the form of colorless needles with a mp of 88−90 °C. ^{1}H NMR (400 MHz, $CDCl_3$): δ [ppm] = 3.27−3.04 (m, 8H), 1.58 (p, J = 8.1, 7.7 Hz, 8H), 1.39 (h, J = 7.3 Hz, 8H), 0.97 (t, J = 7.3 Hz, 12H). ^{13}C{^{1}H} NMR (101 MHz, $CDCl_3$): δ [ppm] = 120.0 (q, J = 321.6 Hz), 58.7, 23.9, 19.6, 13.5. ^{19}F NMR (377 MHz, $CDCl_3$): δ [ppm] = −78.82. IR (ATR): ν (cm^{-1}) = 2968 (m), 2881 (w), 1463 (vw), 1381 (vw), 1348 (s), 1332 (m), 1224 (m), 1178 (vs), 1136 (s), 1110 (w), 1050 (vs), 884 (m), 791 (w), 762 (vw), 740 (m). Elemental analysis (%) calcd for $C_{18}H_{36}N_2O_4F_6S_2$ (522.61 g mol^{-1}): C, 41.37; H, 6.94; N, 5.36; S, 12.27. Found (%): C, 42.21; H, 7.07; N, 5.39; S, 11.90. HRMS (ESI) m/z: [M]$^+$ calcd for $C_{16}H_{36}N^+$, 242.2842; found, 242.2847. HRMS (ESI) m/z: [M]$^-$ calcd for $C_2F_6NOS_2^-$, 279.9178; found, 279.9177.

Synthesis of Neutral Amides. Despite the different syntheses given for the neutral amides in the following section, the approach described for **8c** may represent the most practical procedure for all amides.

*1,1,1-Trifluoro-N-(pyridin-4(1H)-ylidene)methanesulfonamide (**8a**).* 4-Dimethylaminopyridine **1a** (0.023 g, 0.191 mmol, 0.01 equiv) and 1.40 g of 4-aminopyridine **9a** (14.8 mmol, 1.0 equiv) were dissolved in 26 mL of CH_2Cl_2, 2.07 mL of NEt_3 (14.8 mmol, 1.0 equiv), and 1 mL of acetonitrile under a N_2 atmosphere. Trifluormethanesulfonyl chloride (1.58 mL, 14.8 mmol, 1.0 equiv) was added dropwise, and the reaction mixture was stirred at rt for 5 days before the solvents were removed *in vacuo*. The remaining solid was taken up in 30 mL of chloroform, heated to reflux, filtered off hot, and washed with chloroform, yielding 2.29 g (10.1 mmol, 68%) of compound **8a** as an off-white powder with a mp of 300−304 °C. ^{1}H NMR (400.22 MHz, DMSO-d_6): δ [ppm] = 13.63 (s, 1H), 8.28 (d, J = 7.4 Hz, 2H), 7.28 (d, J = 7.4 Hz, 2H). ^{13}C{^{1}H} NMR (100.65 MHz, DMSO-d_6): δ [ppm] = 163.8, 140.2, 120.8 (q, J = 325.5 Hz), 117.0. ^{19}F NMR (376.55 MHz, DMSO-d_6): δ [ppm] = −77.8. IR (ATR): ν (cm^{-1}) = 3237 (vw), 3052 (vw), 2934 (vw), 2891 (vw), 2848 (vw), 2794 (vw), 2663 (vw), 1911 (vw), 1820 (vw), 1635 (m), 1615 (w), 1514 (vw), 1483 (s), 1330 (s), 1312 (s), 1256 (w), 1209 (m), 1184 (vs), 1165 (vs), 1123 (vs), 1098 (s), 1009 (w), 970 (vs), 916 (vw), 825 (s), 782 (s), 749 (w), 654 (w). Elemental analysis (%) calcd for $C_6H_5F_3N_2O_2S$ (226.17 g mol^{-1}): C, 31.86; H, 2.23; N, 12.39; S, 14.17. Found (%): C, 31.93; H, 2.43; N, 12.36; S, 14.17. HRMS (EI) m/z: [M]$^+$ calcd for $C_6H_5F_3N_2O_2S^+$, 226.0018; found, 226.0019.

*4-Methyl-N-(pyridin-4(1H)-ylidene)benzenesulfonamide (**8b**).* 4-Aminopyridine **9a** (4.71 g, 21.2 mmol, 1.0 equiv) was dissolved in 50 mL of pyridine under a N_2 atmosphere. 4-Methylbenzenesulfonyl chloride (11.13 g, 58.4 mmol, 1.17 equiv) and 15 mL of NEt_3 were added, and the mixture was refluxed for 2 h before being allowed to cool to room temperature. The solvent phase was decanted off the precipitated solids, and the remaining solids were washed with 200 mL of hot H_2O. The solids were collected, and the filtrate was brought to pH = 5, which caused further precipitation. All precipitates were combined and washed with boiling H_2O, boiling MeCN, boiling acetone, and boiling chloroform repeatedly to give 11.22 g (45.1 mmol, 90%) of sulfonamide **8b** in the form of a colorless powder with a mp of 304−308 °C. Due to the very low solubility of sulfonamide **8b**, not all expected ^{13}C signals were found. ^{1}H NMR (400.22 MHz, DMSO-d_6): δ [ppm] = 12.25 (s, 1H), 8.01 (d, J = 5.9 Hz, 2H), 7.68 (d, J = 8.1 Hz, 2H), 7.30 (d, J = 7.9 Hz, 2H), 6.90 (d, J = 6.7 Hz, 2H), 2.33 (s, 3H). ^{13}C{^{1}H} NMR (100.65 MHz, DMSO-d_6): δ [ppm] = 141.6, 140.2, 129.3, 126.2, 114.3, 20.9. IR (ATR): ν (cm^{-1}) = 3054 (w), 2647 (w), 1928 (w), 1636 (m), 1620 (m), 1477 (s), 1382, (w), 1334 (s), 1296 (m), 1280 (m), 1250 (m), 1195 (m), 1135 (vs), 1102 (w), 1081, (vs), 1018 (w), 983 (w), 942 (vs), 838 (s), 812 (m), 801 (m), 773 (s), 707 (m), 660 (m). Elemental analysis (%) calcd for $C_{12}H_{12}N_2O_3S$ (248.30 g mol^{-1}): C, 58.05; H, 4.87; N, 11.28; S, 12.91; Found (%): C, 57.87; H, 4.87; N, 11.21; S, 13.18. HRMS (EI) m/z: [M]$^+$ calcd for $C_{12}H_{12}N_2O_3S^+$, 248.0614; found, 248.0612.

*N-(1,4-Dihydropyridin-4-yl)-4-methoxybenzenesulfonamide (**8c**).* To a solution of 0.941 g of 4-aminopyridine **9a** (10 mmol, 1.0 equiv) in 10 mL of pyridine under a N_2 atmosphere was added 2.07 g of 4-methoxybenzenesulfonyl chloride (10 mmol, 1.0 equiv). The mixture was stirred for 10 min at RT; 3 mL of NEt_3 was added and refluxed for 2 h. The solvents were then removed *in vacuo*, and the resulting dark brown solid was washed with boiling H_2O, boiling acetone, and boiling MTBE. After drying, 2.05 g (7.76 mmol, 78%) of sulfonamide **8c** was obtained in the form of a colorless solid with a mp of 279−280 °C. ^{1}H NMR (400 MHz, DMSO-d_6): δ [ppm] = 12.12 (s, 1H), 8.04 (d, J = 6.2 Hz, 2H), 7.75 (d, J = 8.8 Hz, 2H), 7.02 (d, J = 8.8 Hz, 2H), 6.93 (d, J = 6.8 Hz, 2H), 3.78 (s, 3H). ^{13}C{^{1}H} NMR (101 MHz, DMSO-d_6): δ [ppm] = 161.7, 157.3, 141.9, 134.4, 128.4, 114.1, 113.9, 55.5. Elemental analysis (%) calcd for $C_{12}H_{12}N_2O_3S$ (264.30 g mol^{-1}): C, 54.53; H, 4.58; N, 10.60; S, 12.13. Found (%): C, 53.86; H, 4.53; N,

https://dx.doi.org/10.1021/acs.joc.0c00114
J. Org. Chem. 2020, 85, 5390−5402

10.98; S, 13.74. HRMS (EI) m/z: $[M]^+$ calcd for $C_{12}H_{12}N_2O_3S^+$, 264.0563, found: 264.0567.

*P,P-Diphenyl-N-(pyridine-4-yl)phosphinic Amide (**11**).* 4-Aminopyridine **9a** (1.98 g, 21 mmol) was dissolved in acetonitrile (20.0 mL), CH_2Cl_2 (10.0 mL), and 2.9 mL of NEt_3 (21 mmol, 1.0 equiv) under N_2. This solution was added dropwise to a flask containing 5.0 g of diphenylphosphonic chloride (21 mmol, 1.0 equiv) under N_2, and the mixture was stirred for 24 h. The solvents were removed *in vacuo*, and the remaining solids were taken up in saturated Na_2CO_3 solution (20.0 mL) and filtered. The filtrate was brought to ca. pH 7, and the precipitate was filtered off. After drying, **11** was obtained as a white powder (1.76 g, 5.96 mmol, 28%), whose spectroscopic data is in agreement with the literature data.[15] ^{1}H NMR (400 MHz, $CDCl_3$): δ [ppm] = 8.15 (d, J = 6.0 Hz, 2H), 7.81 (dd, J = 12.6, 7.1 Hz, 4H), 7.54 (td, J = 7.5, 1.3 Hz, 2H), 7.44 (td, J = 7.5, 3.4 Hz, 4H), 6.85 (d, J = 6.2 Hz, 2H), 6.62 (s, 1H). $^{13}C\{^1H\}$ NMR (101 MHz, $CDCl_3$): δ [ppm] = 150.3, 148.4, 132.8 (d, J = 2.8 Hz), 131.9 (d, J = 10.3 Hz), 131.0 (d, J = 128.9 Hz), 129.1 (d, J = 13.2 Hz), 113.1 (d, J = 6.8 Hz).

*3-Chlorobenzo[d]isothiazole 1,1-Dioxide (**13**).* Saccharine (5.49 g, 30 mmol) and 0.4 mL of DMF were dissolved in 25 mL of 1,4-dioxane, and 9 mL (45 mmol, 1.5 equiv) of thionyl chloride was added. The mixture was refluxed for 46 h, and all liquids were removed under reduced pressure to give a yellow, gum-like substance. It was extracted with a boiling mixture of toluene and *n*-heptane (1:1) from which imidoyl chloride **13** crystallized in the form of light-yellow needles (5.32 g, 26.4 mmol, 88%), whose ^{1}H NMR spectrum is in agreement with the literature data.[16] ^{1}H NMR (400.22 MHz, $CDCl_3$): δ [ppm] = 7.96−7.90 (m, 1H), 7.90−7.80 (m, 3H). $^{13}C\{^1H\}$ NMR (100.65 MHz, $CDCl_3$): δ [ppm] = 166.3, 140.5, 135.2, 134.7, 129.9, 125.3, 122.6.

*3-(Pyridin-4-ylamino)benzo[d]isothiazole 1,1-Dioxide (**14**).* 4-Aminopyridine **9a** (1.05 g, 11.2 mmol, 2.0 equiv) was dissolved in 10 mL of dry dioxane under N_2. Imidoyl chloride **13** (1.13 g, 5.6 mmol) was added, and the mixture was stirred overnight at room temperature. The solvents were removed *in vacuo* and the solids taken up in 80 mL of H_2O and 4 mL of aqueous NaOH (40%). The remaining solids were filtered off, and the filtrate was brought to ca. pH = 7. The precipitate was filtered off, washed with H_2O, and dried to give 1.20 g (4.6 mmol, 83%) of compound **14** in the form of a colorless solid with a mp > 300 °C. ^{1}H NMR (400.22 MHz, DMSO-d_6): δ [ppm] = 11.14 (s, 1H), 8.62 (d, J = 5.7 Hz, 2H), 8.51 (d, J = 7.2 Hz, 1H), 8.12 (d, J = 6.7 Hz, 1H), 8.03−7.80 (m, 4H). $^{13}C\{^1H\}$ NMR (101 MHz, DMSO-d_6): δ [ppm] = 157.6, 150.5, 145.0, 140.4, 134.1, 133.6, 128.2, 124.1, 121.8, 115.7. IR (ATR): ν (cm^{-1}) = 3601 (vw), 2891 (b, w), 1634 (m), 1593 (m), 1546 (s), 1496 (m), 1465 (w), 1423 (m), 1366 (m), 1312 (vs), 1281 (w), 1214 (vw), 1158 (vs), 1127 (s), 1067 (vw), 1051 (vw), 1005 (w), 954 (s), 866 (w), 832 (m), 778 (vs), 749 (s), 707 (m), 664 (m), 650 (s). Elemental analysis (%) calcd for $C_{12}H_9N_3O_2S$ (259.28 g mol^{-1}): C, 55.59; H, 3.50; N, 16.21; O, 12.34; S, 12.36. Found (%): C, 52.65; H, 3.93; N, 15.23; S, 11.84. HRMS (EI) m/z: $[M]^+$ calcd for $C_{12}H_9N_3O_2S^+$, 259.0410; found, 259.0414.

*4-Methyl-N-(pyridin-2-yl)benzenesulfonamide (**25**).* 2-Aminopyridine **9b** (0.941 g, 10.0 mmol, 1.0 equiv) was dissolved in 10 mL of pyridine under a N_2 atmosphere. 4-Methyl-benzenesulfonyl chloride (2.287 g, 12 mmol, 1.2 equiv) and 4 mL of NEt_3 were added, and the mixture was refluxed for 2 h before being allowed to cool to room temperature. Cold H_2O was added, and the precipitate was filtered off. It was washed with toluene, and a boiling mixture of 3:1 EtOAc/acetone before drying yielded 0.855 g (3.36 mmol, 33%) of sulfonamide **25** in the form of a colorless solid. NMR spectroscopy is in agreement with the literature data.[17] ^{1}H NMR (400.22 MHz, DMSO-d_6): δ [ppm] = δ 11.90 (s, 1H), 8.01 (d, J = 4.6 Hz, 1H), 7.76 (d, J = 8.2 Hz, 2H), 7.73−7.64 (m, 1H), 7.33 (d, J = 8.1 Hz, 2H), 7.13 (d, J = 8.6 Hz, 1H), 6.92−6.77 (m, 1H), 2.33 (s, 3H). $^{13}C\{^1H\}$ NMR (101 MHz, DMSO-d_6): δ [ppm] = 153.1, 143.7, 142.5, 140.2, 129.0, 129.4, 126.7, 115.8, 113.6, 21.0.

Synthesis of Benchmark Reaction Precursors and Products. *N-(4-Chlorobenzylidene)-4-methylbenzenesulfonamide (**19**).* 4-Chlorobenzaldehyde (5.0 g, 35.55 mmol) and 4-methylbenzenesulfonamide (6.09 g, 35.55 mmol) were dissolved in 100 mL of toluene. The mixture was refluxed under a N_2 atmosphere for 24 h using a Dean−Stark trap. The solvents were removed under reduced pressure, and the resulting crude product was recrystallized twice from toluene and finally from $CHCl_3$ to give 6.74 g (22.9 mmol, 64%) of tosyl imine **19** in the form of colorless needles that were stored under N_2. The spectral data is in accordance with the one published in the literature.[18] ^{1}H NMR (400 MHz, $CDCl_3$): δ [ppm] = 8.98 (s, 1H), 7.97−7.78 (m, 4H, H-3), 7.45 (d, J = 8.5 Hz, 2H), 7.34 (d, J = 8.1 Hz, 2H), 2.43 (s, 3H). $^{13}C\{^1H\}$ NMR (101 MHz, $CDCl_3$): δ [ppm] = 168.8, 144.9, 141.5, 134.9, 132.5, 130.9, 130.0, 129.7, 128.2, 21.8.

*N-((4-Chlorophenyl)(6-oxocyclohex-1-en-1-yl)methyl)-4-methylbenzenesulfonamide (**21**).* After completion of the reaction, four MBH kinetic experiments catalyzed by TCAP (2 × 12.5 mol %, 2 × 25.0 mol %), initially containing a total of 0.176 g (0.60 mmol) of tosyl imine **19**, 0.232 g (2.4 mmol, 4.0 equiv) of cyclohexenone **20**, and 19.6 mg (0.113 mmol) of TCAP (**1b**) in 2.4 mL of $CDCl_3$, were combined, and the solvents were removed *in vacuo*. The crude mixture was purified by column chromatography (SiO_2, IH/EtOAc = 9:1 → EtOAc) and then recrystallization from IH/acetone to yield 0.196 g (0.50 mmol, 83%) of tosyl amine **21** in the form of colorless crystals. The analytical data is in accordance with the already published one.[10] ^{1}H NMR (400 MHz, $CDCl_3$): δ [ppm] = 7.61 (d, J = 8.3 Hz, 2H), 7.23 (d, J = 8.1 Hz, 2H), 7.18 (d, J = 8.6 Hz, 2H), 7.12 (d, J = 8.6 Hz, 2H), 6.79 (t, J = 4.1 Hz, 1H), 6.00 (d, J = 9.6 Hz, 1H), 5.05 (d, J = 9.6 Hz, 1H), 2.41 (s, 3H), 2.38−2.01 (m, 4H), 1.94−1.58 (m, 2H). $^{13}C\{^1H\}$ NMR (101 MHz, $CDCl_3$): δ [ppm] = 199.1, 149.5, 143.5, 138.0, 137.9, 136.6, 133.4, 129.6, 128.6, 127.8, 127.4, 59.2, 38.5, 25.9, 22.1, 21.6.

*Butyl p-Tolylcarbamate (**16**).* Butan-1-ol **18** (8.25 mL, 90.3 mmol, 3.0 equiv) and DMAP **1a** (0.367 g, 3.00 mmol, 0.1 equiv) were dissolved in 10 mL of $CHCl_3$ in a dried, nitrogen-filled Schlenk flask. To this solution was added 3.79 mL of *p*-tolyl isocyanate **17** (30.1 mmol, 1.0 equiv), and the mixture was stirred for 110 min at room temperature. The solvent was removed *in vacuo*, and the crude product was purified by column chromatography (SiO_2, hexane/EtOAc, 4:1) and recrystallized twice from hexane to give 2.51 g of urethane **16** (12.22 mmol, 40%) as colorless needles with a mp of 63−66 °C. The spectral data matched the one published in the literature.[19] R_f: 0.72 (hexane/EtOAc, 4:1). ^{1}H NMR (600 MHz, $CDCl_3$): δ [ppm] = 7.33−7.21 (m, 2H), 7.10 (d, J = 8.4 Hz, 2H), 6.56 (s, 1H), 4.16 (t, J = 6.7 Hz, 2H), 2.30 (s, 3H), 1.65 (p, J = 6.7 Hz, 2H), 1.42 (h, J = 7.4 Hz, 2H), 0.95 (t, J = 7.4 Hz, 3H). $^{13}C\{^1H\}$ NMR (151 MHz, $CDCl_3$): δ [ppm] = 154.0, 135.5, 133.0, 129.7, 118.9, 65.2, 31.1, 20.9, 19.2, 13.9. IR (ATR): ν (cm^{-1}) = 3318 (w), 3290 (vw), 3196 (vw), 3132 (vw), 3030 (vw), 2963 (w), 2930 (vw), 2870 (vw), 2301 (vw), 1892 (vw), 1786 (vw), 1719 (w), 1696 (m), 1599 (m), 1537 (s), 1515 (s), 1477 (w), 1463 (w), 1409 (m), 1390 (w), 1377 (vw), 1355 (vw), 1344 (vw), 1315 (s), 1297 (m), 1269 (w), 1233 (vs), 1211 (vs), 1131 (w), 1122 (w), 1064 (vs), 1017 (m), 979 (w), 937 (vw), 902 (vw), 854 (w), 814 (vs), 769 (m), 739 (m), 708 (m), 692 (m). Elemental analysis (%) calcd for $C_{12}H_{17}NO_2$ (207.27 g mol^{-1}): C, 69.54; H, 8.27; N, 6.76. Found (%): C, 69.75; H, 8.35; N, 6.74. HRMS (EI) m/z: $[M]^+$ calcd for $C_{12}H_{17}NO_2$, 207.1254; found, 207.1254.

■ ASSOCIATED CONTENT

Supporting Information

The Supporting Information is available free of charge at https://pubs.acs.org/doi/10.1021/acs.joc.0c00114.

Details regarding kinetic measurements, crystallographic data, NMR spectroscopic data, computational details, thermochemical data, and structural data for the quantum chemical study (PDF)

Crystallographic information file (CIF)

Crystal data (CIF)

■ AUTHOR INFORMATION

Corresponding Author

Hendrik Zipse − *Department of Chemistry, Ludwig-Maximilians-Universität, 81377 München, Germany;*

orcid.org/0000-0002-0534-3585; Email: zipse@cup.lmu.de

Authors

Julian Helberg − *Department of Chemistry, Ludwig-Maximilians-Universität, 81377 München, Germany;* orcid.org/0000-0001-9520-2913

Torsten Ampßler − *Department of Chemistry, Ludwig-Maximilians-Universität, 81377 München, Germany*

Complete contact information is available at: https://pubs.acs.org/10.1021/acs.joc.0c00114

Notes

The authors declare no competing financial interest.

■ ACKNOWLEDGMENTS

The authors wish to thank Dr. Peter Mayer for providing X-ray measurements and analysis and the Leibniz Supercomputer Center (www.lrz.de) for computational resources.

■ REFERENCES

(1) (a) Litvinenko, L. M.; Kirichenko, A. I. Basicity and stereospecificity in nucleophilic catalysis by tertiary amines. *Dokl. Akad. Nauk SSSR Ser. Khim.* **1967**, *176*, 97−100. (b) Steglich, W.; Höfle, G. N, N-Dimethyl-4-pyridinamine, a very effective acylation catalyst. *Angew. Chem., Int. Ed. Engl.* **1969**, *8*, 981.

(2) (a) Heinrich, M. R.; Klisa, H. S.; Mayr, H.; Steglich, W.; Zipse, H. Enhancing the catalytic activity of 4-(dialkylamino)pyridines by conformational fixation. *Angew. Chem., Int. Ed.* **2003**, *42*, 4826−4828. (b) Tandon, R.; Unzner, T.; Nigst, T. A.; De Rycke, N.; Mayer, P.; Wendt, B.; David, O. R. P.; Zipse, H. Annelated Pyridines as Highly Nucleophilic and Lewis Basic Catalysts for Acylation Reactions. *Chem. - Eur. J.* **2013**, *19*, 6435−6442. (c) Tamaki, A.; Kojima, S.; Yamamoto, Y. Examination of Pyridazine as a Possible Scaffold for Nucleophilic Catalysis. *J. Org. Chem.* **2016**, *81*, 8710−8721.

(3) (a) Anders, E.; Korn, U.; Stankowiak, A. Ferngesteuerte" nucleophile Eigenschaften der Anionen einiger 4-Alkylpyridine: AM1- und MNDO-Berechnungen sowie experimentelle Untersuchungen. *Chem. Ber.* **1989**, *122*, 105−111. (b) Anders, E.; Stankowiak, A. Übertragung der Trifluoromethansulfonyl- und p-Toluensulfonyl-Gruppe unter neutralen Bedingungen auf hydroxygruppenhaltige Verbindungen. *Synthesis* **1984**, *12*, 1039−1041.

(4) Sheldrake, P. W. The Anion of 4-Dimethoxymethylpyridine. *Synth. Commun.* **1993**, *23*, 1967−1971.

(5) Held, I.; Xu, S.; Zipse, H. Modular Design of Pyridine-Based Acyl-Transfer Catalysts. *Synthesis* **2007**, *8*, 1185−1196.

(6) Schmidlin, N. M. C.; Lokov, M.; Leito, I.; Böttcher, T. [4-(Ph_3B)-2,6-Mes_2Py]: A Sterically Demanding Anionic Pyridine. *Chem. - Eur. J.* **2018**, *24*, 16851−16856.

(7) (a) Köcher, J.; Laas, H. J. (Bayer MaterialScience AG), Neue Katalysatoren für die Selektive Isocyanatdimerisierung. DE DE10336184A1, Feb 02, 2005. (b) Kocher, J.; Laas, H. J. (Bayer MaterialScience AG), New Catalysts for Selective Isocyanate Dimerization. US US20050033006A1, 2005. (c) Köcher, J.; Laas, H. J. (Bayer Material Science AG), Neue Katalysatoren für die Selektive Isocyanatdimerisierung. WO WO2005016984A1, 2005. (d) Köcher, J. (Bayer Material Science AG), Neue Katalysatoren für die Selektive Isocyanatdimerisierung. DE DE102006023262A1, 2007. (e) Kocher, J. (Bayer MaterialScience AG), New Catalysts for Selective Isocyanate Dimerization. US US20070270565A1, 2007.

(8) (a) Lindner, C.; Tandon, R.; Liu, Y.; Maryasin, B.; Zipse, H. The *aza*-Morita-Baylis-Hillman Reaction of Electronically and Sterically Deactivated Substrates. *Org. Biomol. Chem.* **2012**, *10*, 3210−3218. For reactions of the same catalyst class with other electrophiles, see: (b) Larionov, E.; Achrainer, F.; Humin, J.; Zipse, H. The Catalytic Potential of Substituted Pyridines in Acylation Reactions: Theoretical Prediction and Experimental Validation. *ChemCatChem* **2012**, *4*, 559−566. (c) Helberg, J.; Marin-Luna, M.; Zipse, H. Chemoselectivity in Esterification Reactions-Size Matters After All. *Synthesis* **2017**, *49*, 3460−3470. (d) Patschinski, P.; Zipse, H. Leaving Group Effects on the Selectivity of the Silylation of Alcohols: The Reactivity-Selectivity Principle Revisited. *Org. Lett.* **2015**, *17*, 3318−3321.

(9) (a) Six, C.; Richter, F. Isocyanates, Organic, *Ullman's Encyclopedia of Industrial Chemistry*; Wiley-VCH, 2003, *20*, 63−82. (b) Richter, F. Iminooxadiazindione: vom Nebenprodukt zur Leitstruktur. *Nachr. Chem.* **2007**, *55*, 380−384. (c) Helberg, J.; Oe, Y.; Zipse, H. Mechanistic Analysis and Characterization of Intermediates in the Phosphane-Catalyzed Oligomerization of Isocyanates. *Chem. - Eur. J.* **2018**, *24*, 14387−14391.

(10) (a) Shi, M.; Xu, Y.-M.; Zhao, G.-L.; Wu, X.-F. Lewis Base Effects in the Baylis Hillman Reaction of Arenecarbaldehydes and N-Arylidene-4-methylbenzenesulfonamides with α,β-Unsaturated Cyclic Ketones. *Eur. J. Org. Chem.* **2002**, *2002*, 3666−3679. (b) He, L.; Jian, T.-Y.; Ye, S. N-Heterocyclic Carbene Catalyzed *aza*-Morita-Baylis-Hillman Reaction of Cyclic Enones with N-Tosylarylimines. *J. Org. Chem.* **2007**, *72*, 7466−7468. (c) Lindner, C.; Liu, Y.; Karaghiosoff, K.; Maryasin, B.; Zipse, H. The Aza-Morita-Baylis-Hillman Reaction: A Mechanistic and Kinetic Study. *Chem. - Eur. J.* **2013**, *19*, 6429−6434.

(11) (a) Wei, Y.; Sastry, G. N.; Zipse, H. Methyl Cation Affinities of Commonly Used Organocatalysts. *J. Am. Chem. Soc.* **2008**, *130*, 3473−3477. (b) Kleoff, M.; Suhr, S.; Sarkar, B.; Zimmer, R.; Reissig, H.-U.; Marin-Luna, M.; Zipse, H. Efficient Syntheses of New Super Lewis Basic Tris(dialkylamino)-Substituted Terpyridines and Comparison of Their Methyl Cation Affinities. *Chem. - Eur. J.* **2019**, *25*, 7526−7533. (c) Held, I.; Larionov, E.; Bozler, C.; Wagner, F.; Zipse, H. The Catalytic Potential of 4-Guanidinylpyridines in Acylation Reactions. *Synthesis* **2009**, *13*, 2267−2277. (d) Patschinski, P.; Zhang, C.; Zipse, H. The Lewis Base-Catalyzed Silylation of Alcohols — A Mechanistic Analysis. *J. Org. Chem.* **2014**, *79*, 8348−8357.

(12) (a) Marin-Luna, M.; Patschinski, P.; Zipse, H. Substituent Effects in the Silylation of Secondary Alcohols: A Mechanistic Study. *Chem. - Eur. J.* **2018**, *24*, 15052−15058. (b) Marin-Luna, M.; Pölloth, B.; Zott, F.; Zipse, H. Size-Dependent Rate Acceleration in the Silylation of Secondary Alcohols: the Bigger the Faster. *Chem. Sci.* **2018**, *9*, 6509−6515. (c) Becke, A. D. Density-functional thermochemistry. III. The role of exact exchange. *J. Chem. Phys.* **1993**, *98*, 5648−5652. (d) Marenich, A. V.; Cramer, C. J.; Truhlar, D. G. Universal Solvation Model Based on Solute Electron Density and on a Continuum Model of the Solvent Defined by the Bulk Dielectric Constant and Atomic Surface Tensions. *J. Phys. Chem. B* **2009**, *113*, 6378−6396. (e) Grimme, S.; Antony, J.; Ehrlich, S.; Krieg, H. A consistent and accurate ab initio parametrization of density functional dispersion correction (DFT-D) for the 94 elements H-Pu. *J. Chem. Phys.* **2010**, *132*, 154104−154119. (f) Riplinger, C.; Neese, F. An efficient and near linear scaling pair natural orbital based local coupled cluster method. *J. Chem. Phys.* **2013**, *138*, 034106. (g) Riplinger, C.; Sandhoefer, B.; Hansen, A.; Neese, F. Natural triple excitations in local coupled cluster calculations with pair natural orbitals. *J. Chem. Phys.* **2013**, *139*, 134101. (h) Weigend, F.; Ahlrichs, R. Balanced basis sets of split valence, triple zeta valence and quadruple zeta valence quality for H to Rn: Design and assessment of accuracy. *Phys. Chem. Chem. Phys.* **2005**, *7*, 3297−3305.

(13) (a) Saunders, M. Stochastic search for isomers on a quantum mechanical surface. *J. Comput. Chem.* **2004**, *25*, 621−626. (b) Vrček, V.; Kronja, O.; Saunders, M. Stochastic Search for Isomers of the *sec*-Butyl Cation. *J. Chem. Theory Comput.* **2007**, *3*, 1223−1230. (c) Sakic, D.; Hanzevacki, M.; Smith, D. M.; Vrcek, V. A computational study of the chlorination and hydroxylation of amines by hypochlorous acid. *Org. Biomol. Chem.* **2015**, *13*, 11740−11752.

(14) (a) Zipse, H.; Held, I. (Ludwig-Maximilians-Universität München), 3,4-Diaminopyridin-Derivate. DE DE102006057580B3, 2008. (b) Zipse, H.; Held, I. (Bayer Material Science AG), 3,4-Diaminopyridin Derivatives. US US2008176747A1, 2008.

(15) Gholivand, K.; Gholami, A.; Tizhoush, S. K.; Schenk, K. J.; Fadaei, F.; Bahrami, A. Steric and electronic control over the structural diversity of N-(n-pyridinyl) diphenylphosphinic amides (n = 2 and 4)

as difunctional ligands in triphenyltin(IV) adducts. *RSC Adv.* **2014**, *4*, 44509−44516.

(16) Ismael, A.; Borba, A.; Henriques, M. S. C.; Paixão, J. A.; Fausto, R.; Cristiano, M. L. S. Structure and photochemistry of a saccharyl thiotetrazole. *J. Org. Chem.* **2015**, *80*, 392−400.

(17) Lu, L.; Chen, C.; Jiang, H.; Yin, B. Three-Component Ring-Opening Reactions of Cyclic Ethers, α-Diazo Esters, and Weak Nucleophiles under Metal-Free Conditions. *J. Org. Chem.* **2018**, *83*, 14385−14395.

(18) Nishimura, T.; Yasuhara, Y.; Hayashi, T. Asymmetric Addition of Dimethylzinc to N-Tosylarylimines Catalyzed by a Rhodium-Diene Complex toward the Synthesis of Chiral 1-Arylethylamines. *Org. Lett.* **2006**, *8*, 979−981.

(19) Kumar, S. V.; Ma, D. Synthesis of N-(Hetero)aryl Carbamates via CuI/MNAO Catalyzed Cross-Coupling of (Hetero)aryl Halides with Potassium Cyanate in Alcohols. *J. Org. Chem.* **2018**, *83*, 2706−2713.

https://dx.doi.org/10.1021/acs.joc.0c00114
J. Org. Chem. 2020, 85, 5390−5402

4.1. Supporting Information

For: Pyridinyl Amide Ion Pairs as Lewis Base Organocatalysts.

4.1.1 Benchmark Reaction 1 – Urethane Synthesis

Due to the significance of catalytic activation of isocyanates for nucleophilic attack and our recent experience on the subject, we chose the synthesis of urethane **16** from *p*-methyl isoyanate **17** and 1-butanol **18** as the primary benchmark reaction (**Scheme S4: 1**).[1] Moreover, this reaction being a classic addition does not generate acids as it is the case with acetylation or silylation reactions, which also have been employed by our group to benchmark catalyst activity.[2] Since the $CDCl_3$ solvent signal is not clearly distinguishable in most of our aromatic moieties containing reactions, we chose to include hexamethyldisilane as inert internal standard. In order to minimize the oligomerization of isocyanate **17** as a potential side reaction, 3 equivalents of alcohol **18** were used.[1]

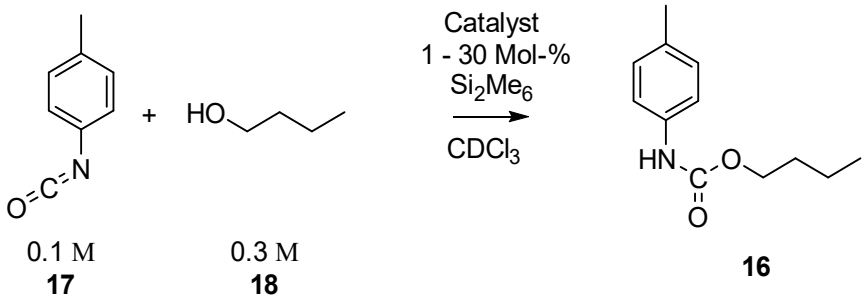

Scheme S4: 1. *[Scheme S1] Synthesis of urethane **16** used as benchmark reaction for investigated catalyst systems.*

Benchmark reactions were done as described in the main part of this publication.

Figure S4: 1 shows a typical GC-spectrum including the signals for starting materials, the product, solvent and internal standard.

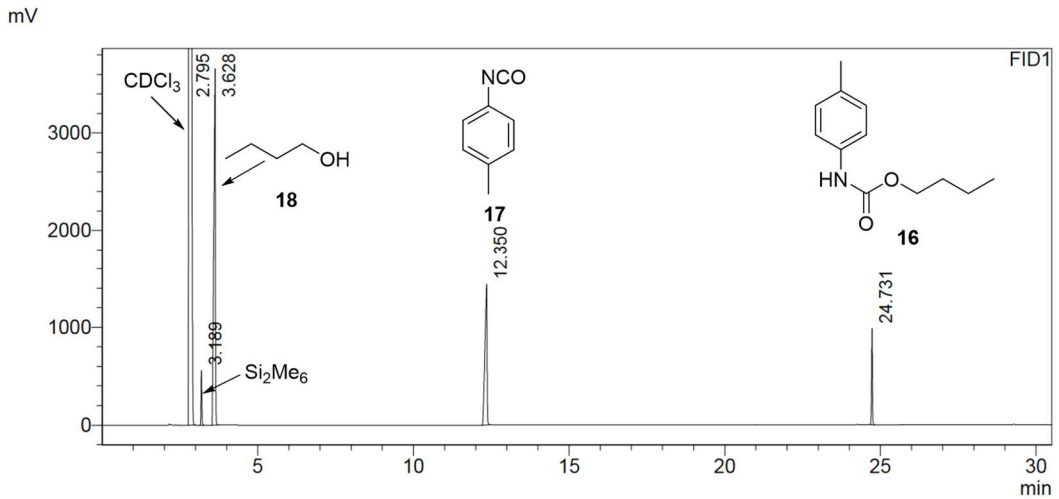

Figure S4: 1. *[Figure S1] Typical GC-spectrum of the investigated reaction.*

Data Processing

NMR:

Measured spectra were imported into MestReNova (Version 12.0.3) and superimposed. The following steps were applied to the superimposed spectra in this order:

- Reference set (Si_2Me_6 set to 0.02 ppm)
- Automatic phase correction
- Automatic baseline correction (Whittaker Smoother)

Three areas containing the signals highlighted in **Figure S4: 2** were integrated:

- **Integral U1**: 4.25 ppm → 4.0 ppm = urethane signal **16B** (CH_2) at 4.15 ppm
- **Integral U2**: 3.75 ppm → 3.5 ppm = butanol signal **18B** at 3.63 ppm (CH_2)
- **Integral U3**: 2.4 ppm → 2.3 ppm = combined methyl signals of isocyanate (**17A**) at 2.30 ppm and urethane (**16A**) at 2.28 ppm

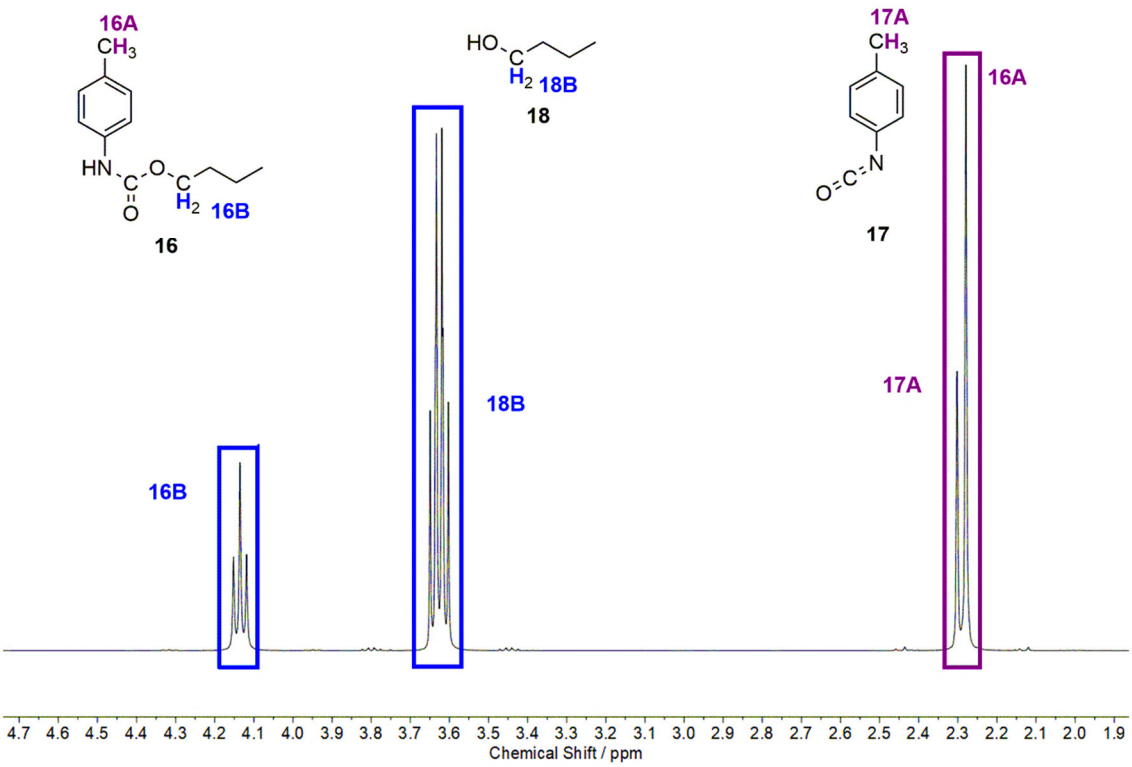

Figure S4: 2. *[Figure S2] Integrals of interest for the synthesis of urethane **16** from isocyanate **17** and butanol **18**.*

The values of these integrals were used to calculate turnover according to Equation S4: 1:

$$T_{Uret}\ /\ \% = \frac{3 \times \boldsymbol{Integral\ U1}}{2 * \boldsymbol{Integral\ U3}} \times\ 100 = \frac{3 \times \mathbf{16B}}{2 * (\mathbf{16}\boldsymbol{A} + \mathbf{17}\boldsymbol{A})} \times\ 100 \qquad \text{Eq. S4: 1}$$

The values obtained for turnover $\mathbf{T_{Uret}}$ were used for calculating concentrations of **16** at the time *t* based on initial concentrations c_0 as shown by Equation S4: 2:

$$c_t\ [\mathbf{16}]\ /\ \mathrm{mol\ L^{-1}} = \frac{c_0[\mathbf{16}] \times (100 - \boldsymbol{T}_{Uret(t)})}{100} \qquad \text{Eq. S4: 2}$$

Simulation of kinetic parameters was done using COPASI[3]. The obtained values for *t* and c_t[**16**] were imported into the program and the *Parameter Estimation* (default settings) option was used for the simplified model shown in **Scheme S4: 2**.

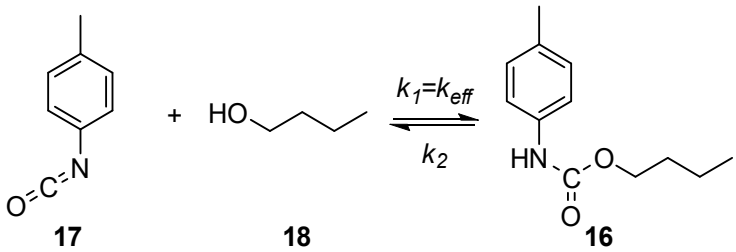

Scheme S4: 2. *[Scheme S2] Simplified model used for fitting of the experimental data obtained for the urethane synthesis in COPASI.*

The values obtained for k_{eff} were then used to compare the activity of different catalysts to each other as detailed in the next section.

GC:

We noticed, that under the chosen conditions, some decomposition of urethane **16** happened in the GC machine, especially after several injections of reaction mixture as visible from the spectrum of purified (as specified in the synthetic section) urethane in $CDCl_3$ shown in **Figure S4: 3**.

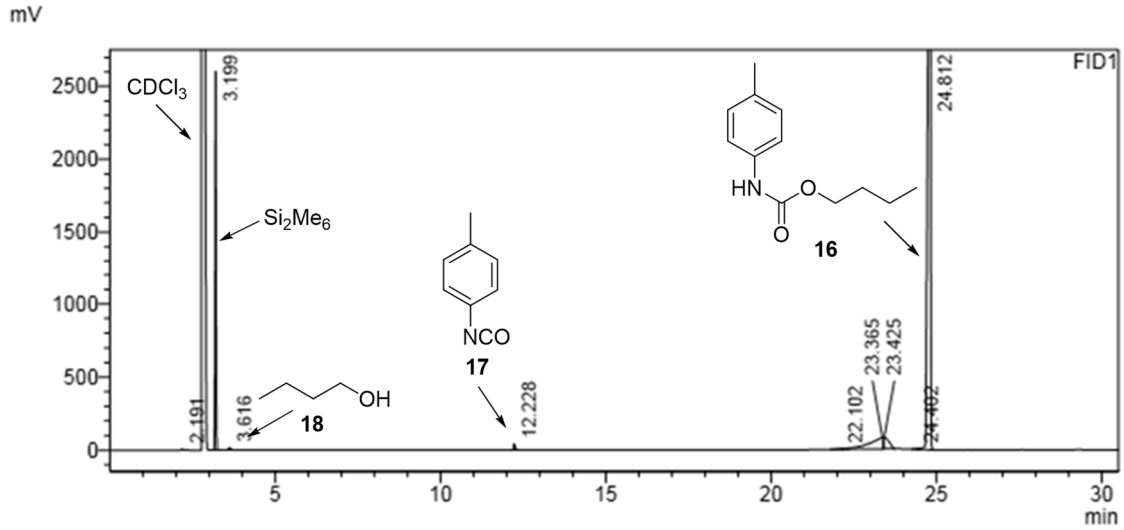

Figure S4: 3. *[Figure S3] GC-spectrum of urethane **16** showing decomposition in the injector leading to distinct peaks for butanol **18** and isocyanate **17**. The broad signal at ca. 22 – 24 min is attributed to gradual decomposition on the column at higher temperatures.*

Unfortunately, the short cleaning runs performed in between the measurements did not help solving the issue. We assume that the very small amounts of butanol **18** and isocyanate **17** indicate initial decomposition in the injector at 200 °C. In the reaction mixture, there would be no way of quantifying this, but we decided the amount was negligible. However, the broad signal at ca. 22 – 24 min accounts for up to 5 % of the integral of the peak of urethane **16** and we attributed it to gradual decomposition on the column at higher temperatures. This is in agreement with the known pyrolysis of urethanes at elevated temperatures, and so we decided to add the integral of this signal to the integral of the distinct urethane peak.

To be able to transform the integrals obtained for the product, urethane **16**, we measured different ratios of compound **16** and the internal standard Si_2Me_6 in $CDCl_3$. We then plotted the ratio of the concentrations of urethane and internal standard to the ratio of the Integrals of the same compounds generating the straight calibration lines shown in **Figure S4: 4**.

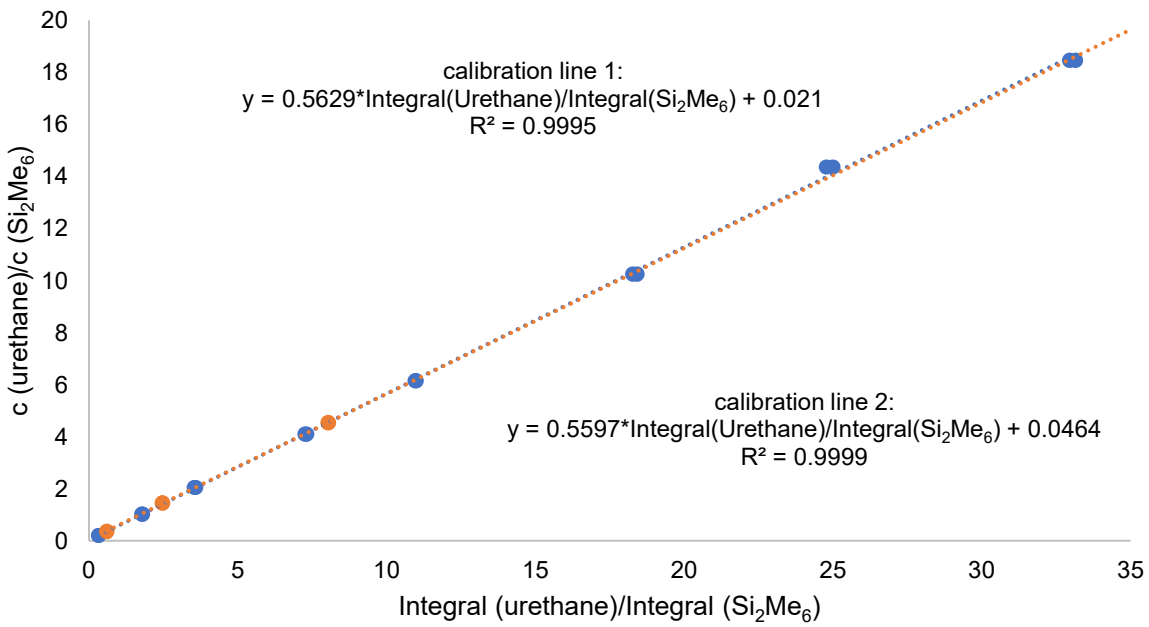

Figure S4: 4. *[Figure S4] Straight calibration lines for c(urethane)/c(Si_2Me_6) to Integral(urethane)/ Integral(Si_2Me_6).*

From the fits of the straight calibration lines, Equations Eq. S4: 3 and Eq. S4: 4 were derived, that give the concentration of urethane **16** at the time t: c_t[**16**].

$$c_{t1}\,[\mathbf{16}]\,/\,\mathrm{mol\,L^{-1}} = \left(0.5629 \times \frac{Int(\mathbf{16})}{Int(Si_2Me_6)} + 0.021\right) \times c(Si_2Me_6) \qquad \text{Eq. S4: 3}$$

$$c_{t2}\,[\mathbf{16}]\,/\,\mathrm{mol\,L^{-1}} = \left(0.5597 \times \frac{Int(\mathbf{16})}{Int(Si_2Me_6)} + 0.0464\right) \times c(Si_2Me_6) \qquad \text{Eq. S4: 4}$$

The obtained values for c_{t1}[**16**] and c_{t2}[**16**] were averaged obtaining c_t[**16**] and Simulation of kinetic parameters was done using COPASI[3]. The values for *t* and c_t[**16**] were imported into the program and the *Parameter Estimation* (default settings) option was used for the simplified model shown in **Scheme S4: 2**. The values obtained for k_{eff} were then used to compare the activity of different catalysts to each other as detailed in the next section.

Kinetic Data for the Urethane Synthesis Benchmark Reaction

Table S4: 1 gives details for the urethane synthesis benchmark reactions that were done in the course of this study while **Figure S4: 5** – **Figure S4: 81** shows the fitted turnover curves that are obtained as graphical output by COPASI:

Table S4: 1. [Table S1] Details for the urethane synthesis benchmark reactions.

Experiment	Method	Catalyst	mol-% catalyst (compared to isocyanate **17**)	c(Catalyst) / mol L^{-1}	k_{eff} / L mol^{-1} s^{-1}
urethane_01	NMR	none	0.0	0.00E+00	4.54E-05
urethane_02	NMR	1a	3.0	3.00E-03	2.80E-04
urethane_03	NMR	1a	15.1	1.50E-02	1.27E-03
urethane_04	NMR	1a	30.2	3.00E-02	2.35E-03
urethane_05	NMR	1b	0.1	9.98E-05	6.02E-05
urethane_06	NMR	1b	0.1	1.00E-04	5.91E-05
urethane_07	NMR	1b	1.0	9.98E-04	2.61E-04
urethane_08	NMR	1b	1.0	1.00E-03	2.72E-04
urethane_09	NMR	1b	3.0	2.97E-03	7.69E-04
urethane_10	NMR	1b	3.0	2.97E-03	7.31E-04
urethane_11	NMR	1b	5.0	4.99E-03	1.22E-03
urethane_12	NMR	1b	5.0	5.01E-03	1.19E-03
urethane_13	NMR	1b	29.7	2.97E-02	6.63E-03
urethane_14	NMR	1c	0.1	1.00E-04	4.95E-05
urethane_15	NMR	1c	1.0	9.99E-04	1.45E-04
urethane_16	NMR	1c	1.0	9.99E-04	1.42E-04
urethane_17	NMR	1c	2.0	2.00E-03	2.50E-04
urethane_18	NMR	1c	1.0	2.00E-03	1.59E-04
urethane_19	NMR	1c	3.0	3.00E-03	4.49E-04
urethane_20	NMR	1c	3.0	3.00E-03	3.47E-04
urethane_21	NMR	1c	3.0	3.00E-03	3.51E-04
urethane_22	NMR	1c	5.0	5.00E-03	6.45E-04
urethane_23	NMR	1c	10.0	1.00E-02	1.14E-03
urethane_24	NMR	1c	20.0	2.00E-02	2.64E-03
urethane_25	NMR	1d	1.0	9.99E-04	1.72E-04
urethane_26	NMR	1d	3.0	3.00E-03	5.05E-04
urethane_27	NMR	1d	5.0	5.00E-03	8.43E-04
urethane_28	NMR	1d	5.0	5.00E-03	7.44E-04
urethane_29	NMR	1e	1.0	9.95E-04	2.43E-04
urethane_30	NMR	1e	3.0	2.99E-03	6.57E-04
urethane_31	NMR	1e	5.0	4.98E-03	1.09E-03
urethane_32	NMR	1f	1.0	9.99E-04	2.38E-04
urethane_33	NMR	1f	3.0	3.00E-03	6.42E-04
urethane_34	NMR	1f	5.0	5.00E-03	1.04E-03
urethane_35	NMR	6aa	3.0	3.02E-03	3.65E-04
urethane_36	NMR	6aa	5.0	4.98E-03	6.07E-04
urethane_37	NMR	6aa	19.9	1.99E-02	2.02E-03
urethane_38	NMR	6ab	3.0	3.00E-03	3.89E-04

Table S4: 1 (continuation). [Table S1] Details for the urethane synthesis benchmark reactions.

urethane_39	NMR	6ac	3.0	3.00E-03	4.66E-04
urethane_40	NMR	6ac	3.0	3.00E-03	4.76E-04
urethane_41	NMR	6bc	3.0	3.00E-03	1.49E-03
urethane_42	NMR	6bc	3.0	3.00E-03	1.43E-03
urethane_43	NMR	6bc	3.0	3.01E-03	1.41E-03
urethane_44	NMR	6bc	15.0	1.50E-02	6.94E-03
urethane_45	NMR	6bf	3.0	3.00E-03	1.43E-03
urethane_46	NMR	6cg	1.2	1.20E-03	8.04E-04
urethane_47	NMR	6cg	3.0	3.01E-03	1.99E-03
urethane_48	NMR	6cg	6.0	5.98E-03	3.96E-03
urethane_49	NMR	6cg	11.9	1.20E-02	7.78E-03
urethane_50	NMR	15g	3.0	3.00E-03	8.32E-04
urethane_51	NMR	15g	3.0	3.00E-03	8.36E-04
urethane_52	NMR	15g	6.0	6.00E-03	1.61E-03
urethane_53	NMR	15g	12.0	1.20E-02	3.22E-03
urethane_54	NMR	22	3.0	3.04E-03	3.55E-05
urethane_55	NMR	22	30.3	3.04E-02	3.50E-05
urethane_56	NMR	23	15.0	1.50E-02	1.14E-04
urethane_57	NMR	23	30.1	3.01E-02	1.74E-04
urethane_58	NMR	23	30.1	3.01E-02	1.70E-04
urethane_59	NMR	24	3.0	3.00E-03	3.63E-05
urethane_60	GC	1b	0.1	9.98E-05	6.77E-05
urethane_61	GC	1b	0.1	1.00E-04	6.57E-05
urethane_62	GC	1b	1.0	9.98E-04	2.84E-04
urethane_63	GC	1b	1.0	1.00E-03	2.94E-04
urethane_64	GC	1b	5.0	4.99E-03	1.46E-03
urethane_65	GC	1b	5.0	5.01E-03	1.62E-03
urethane_66	GC	1c	0.1	1.00E-04	5.09E-05
urethane_67	GC	1c	1.0	9.99E-04	1.27E-04
urethane_68	GC	1c	1.0	9.99E-04	1.47E-04
urethane_69	GC	1c	5.0	5.00E-03	6.64E-04
urethane_70	GC	1c	10.0	1.00E-02	1.37E-03
urethane_71	GC	1d	5.0	5.00E-03	8.07E-04
urethane_72	GC	1d	5.0	5.00E-03	9.04E-04
urethane_73	GC	1e	3.0	2.99E-03	7.21E-04
urethane_74	GC	1e	5.0	4.98E-03	1.23E-03
urethane_75	GC	1f	1.0	9.99E-04	2.43E-04
urethane_76	GC	1f	3.0	3.00E-03	6.80E-04
urethane_77	GC	1f	5.0	5.00E-03	1.14E-03

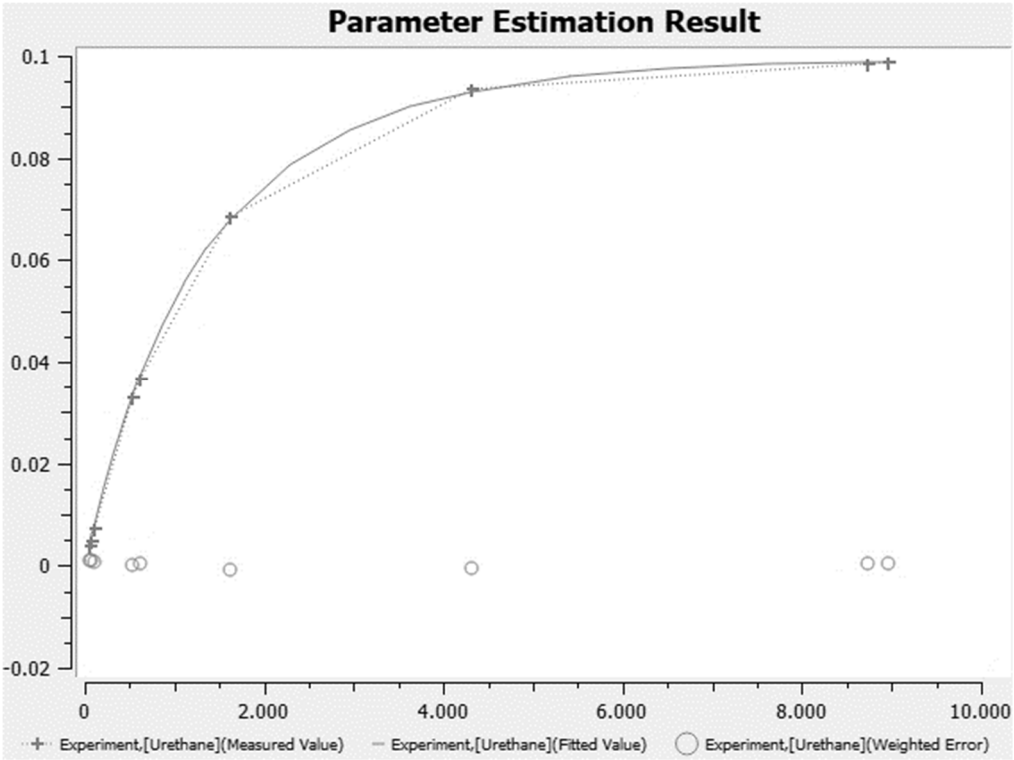

Figure S4: 5. *[Figure S5] Fitted turnover curve obtained as graphical output by COPASI for experiment urethane_01. Vertical axis gives the concentration of urethane* ***16*** *in mol L⁻¹, horizontal axis gives the time from 0 min to 10000 min.*

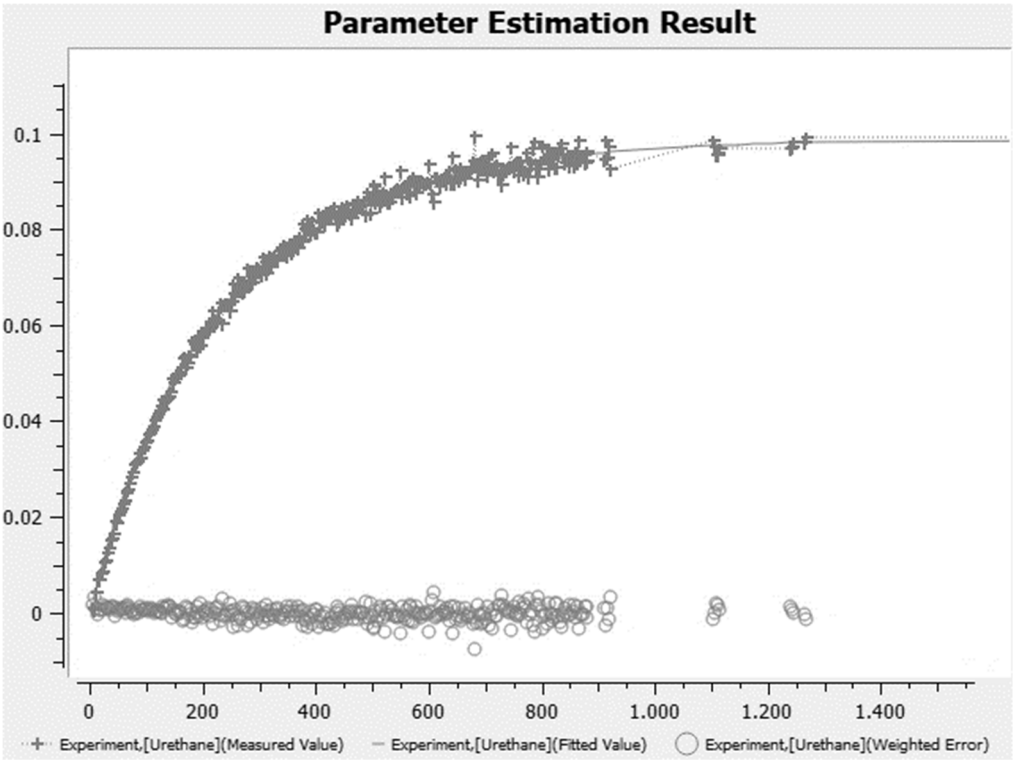

Figure S4: 6. *[Figure S6] Fitted turnover curve obtained as graphical output by COPASI for experiment urethane_02. Vertical axis gives the concentration of urethane* ***16*** *in mol L⁻¹, horizontal axis gives the time from 0 min to 1400 min.*

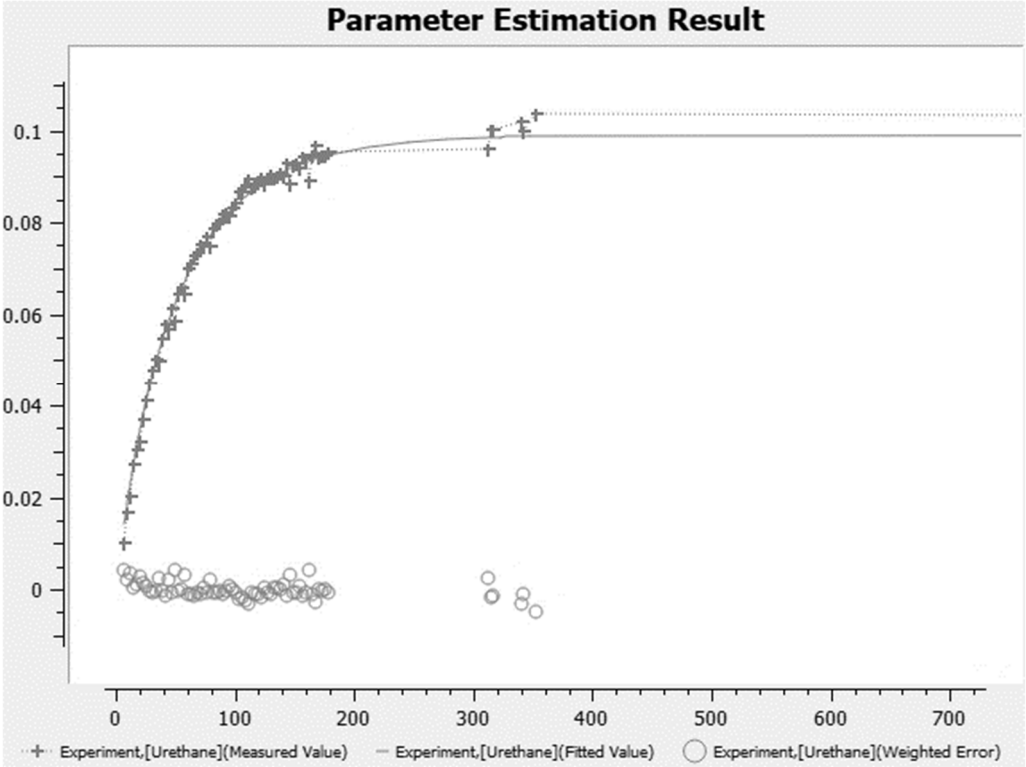

Figure S4: 7. *[Figure S7] Fitted turnover curve obtained as graphical output by COPASI for experiment urethane_03. Vertical axis gives the concentration of urethane* ***16*** *in mol L^{-1}, horizontal axis gives the time from 0 min to 700 min.*

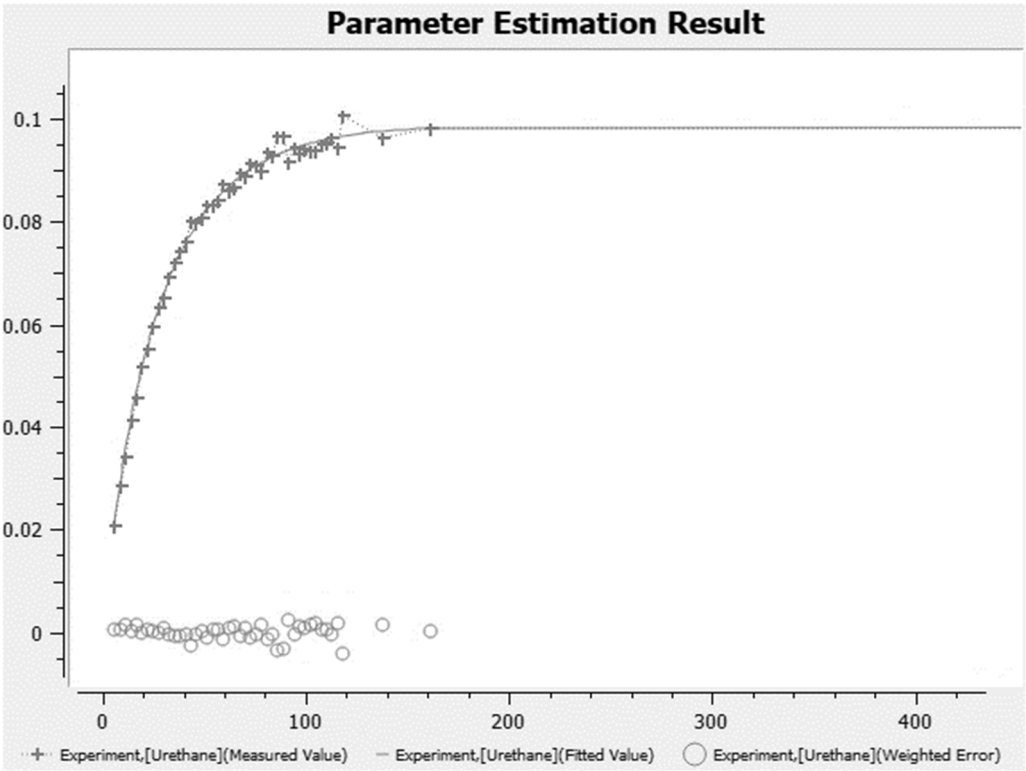

Figure S4: 8. *[Figure S8] Fitted turnover curve obtained as graphical output by COPASI for experiment urethane_04. Vertical axis gives the concentration of urethane* ***16*** *in mol L^{-1}, horizontal axis gives the time from 0 min to 400 min.*

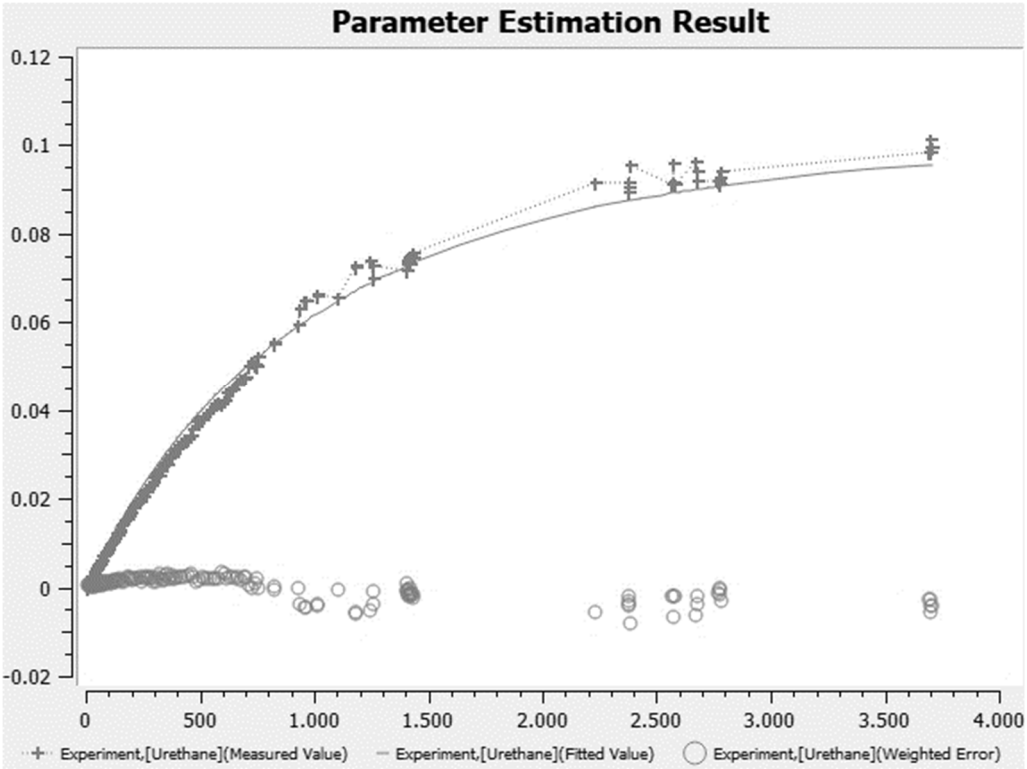

Figure S4: 9. *[Figure S9] Fitted turnover curve obtained as graphical output by COPASI for experiment urethane_05. Vertical axis gives the concentration of urethane* ***16*** *in mol L⁻¹, horizontal axis gives the time from 0 min to 4000 min.*

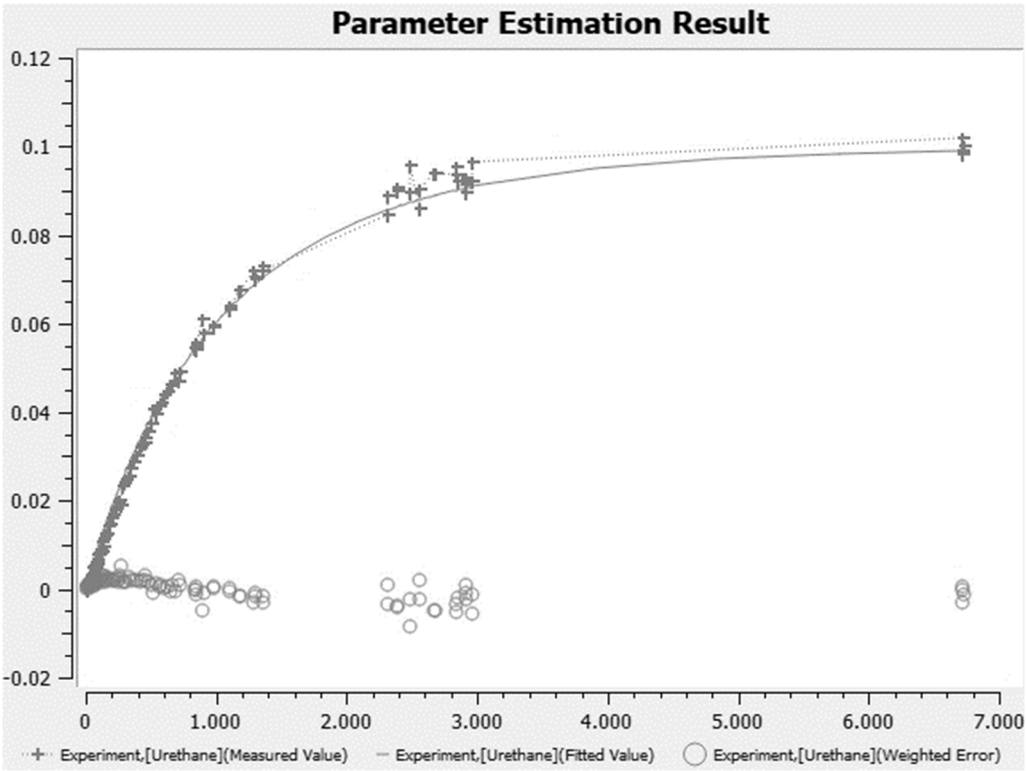

Figure S4: 10. *[Figure S10] Fitted turnover curve obtained as graphical output by COPASI for experiment urethane_06. Vertical axis gives the concentration of urethane* ***16*** *in mol L⁻¹, horizontal axis gives the time from 0 min to 7000 min.*

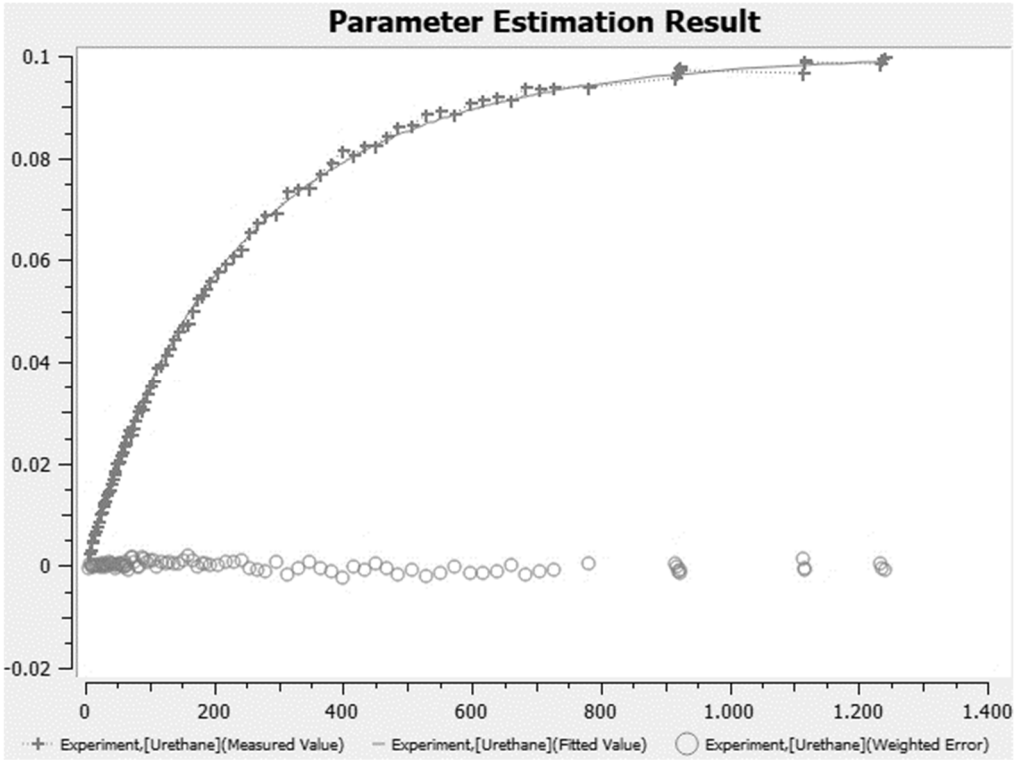

Figure S4: 11. *[Figure S11] Fitted turnover curve obtained as graphical output by COPASI for experiment urethane_07. Vertical axis gives the concentration of urethane* ***16*** *in mol L⁻¹, horizontal axis gives the time from 0 min to 1400 min.*

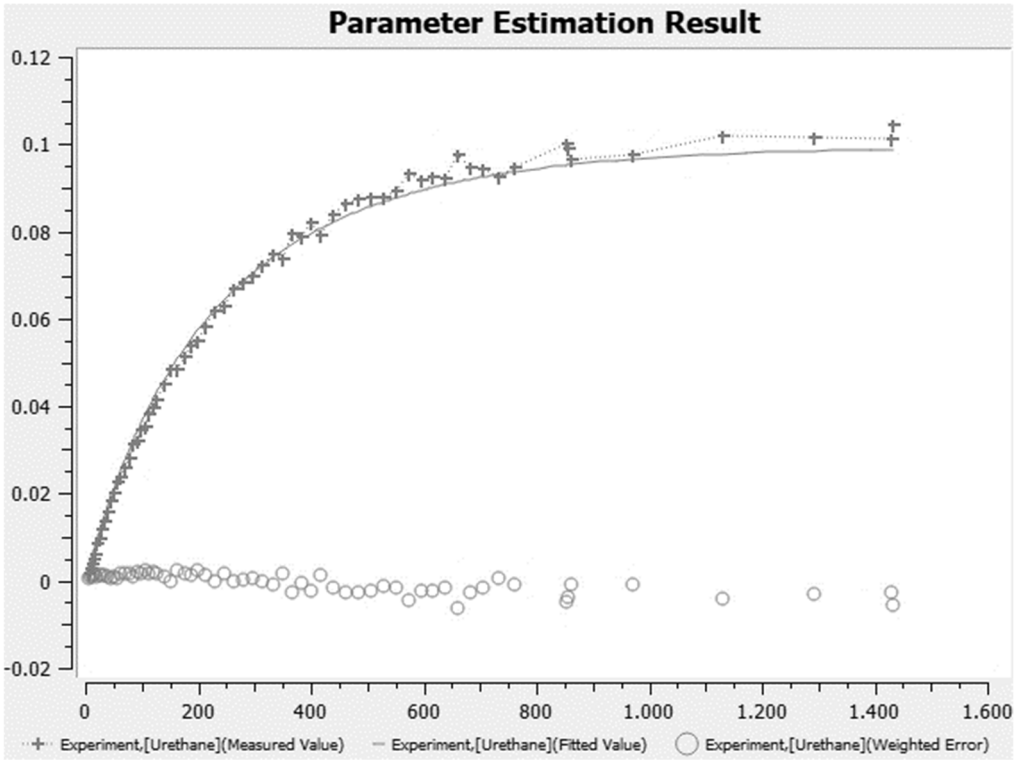

Figure S4: 12. *[Figure S12] Fitted turnover curve obtained as graphical output by COPASI for experiment urethane_08. Vertical axis gives the concentration of urethane* ***16*** *in mol L⁻¹, horizontal axis gives the time from 0 min to 1600 min.*

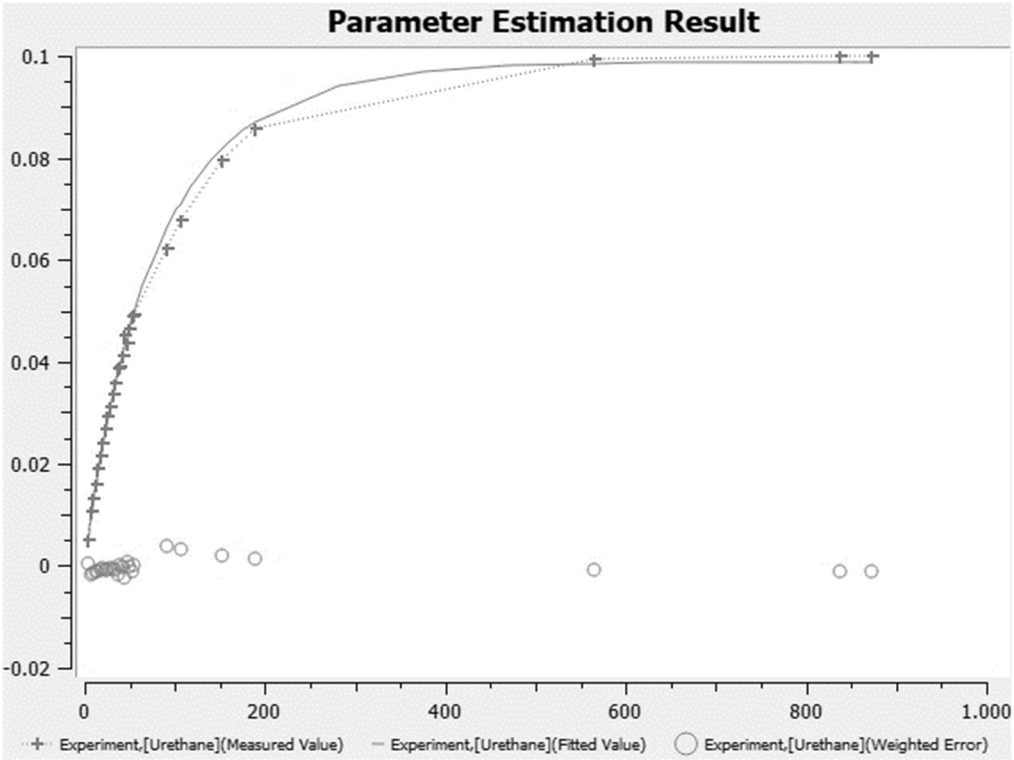

Figure S4: 13. *[Figure S13] Fitted turnover curve obtained as graphical output by COPASI for experiment urethane_09. Vertical axis gives the concentration of urethane* ***16*** *in mol L⁻¹, horizontal axis gives the time from 0 min to 1000 min.*

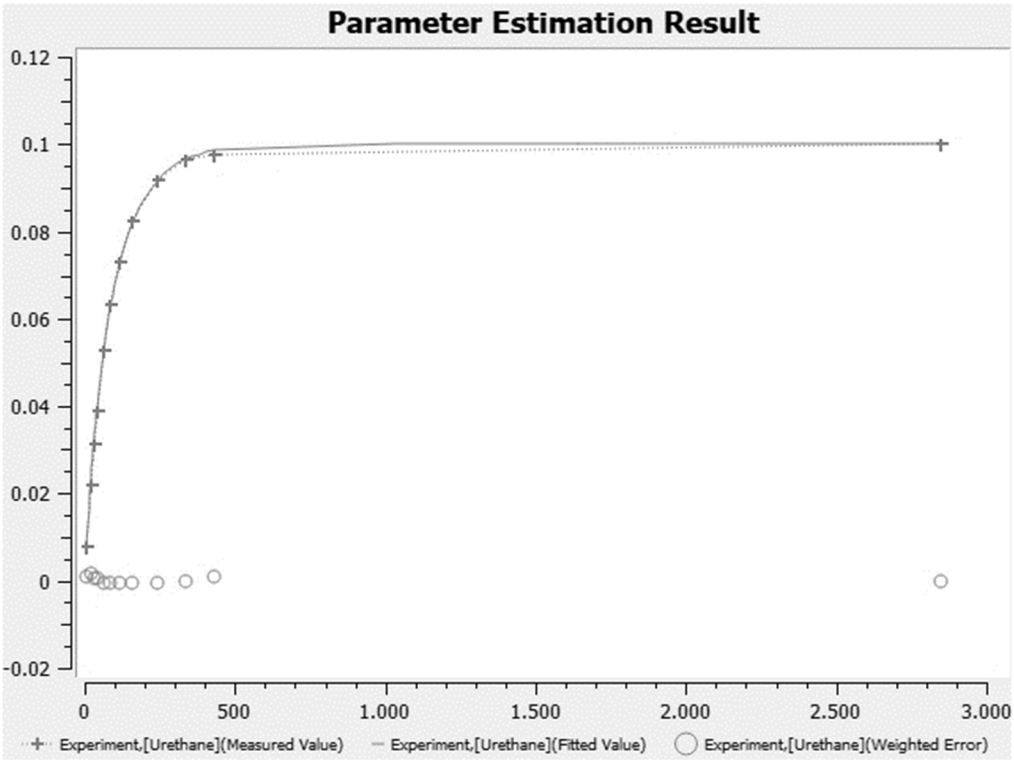

Figure S4: 14. *[Figure S14] Fitted turnover curve obtained as graphical output by COPASI for experiment urethane_10. Vertical axis gives the concentration of urethane* ***16*** *in mol L⁻¹, horizontal axis gives the time from 0 min to 3000 min.*

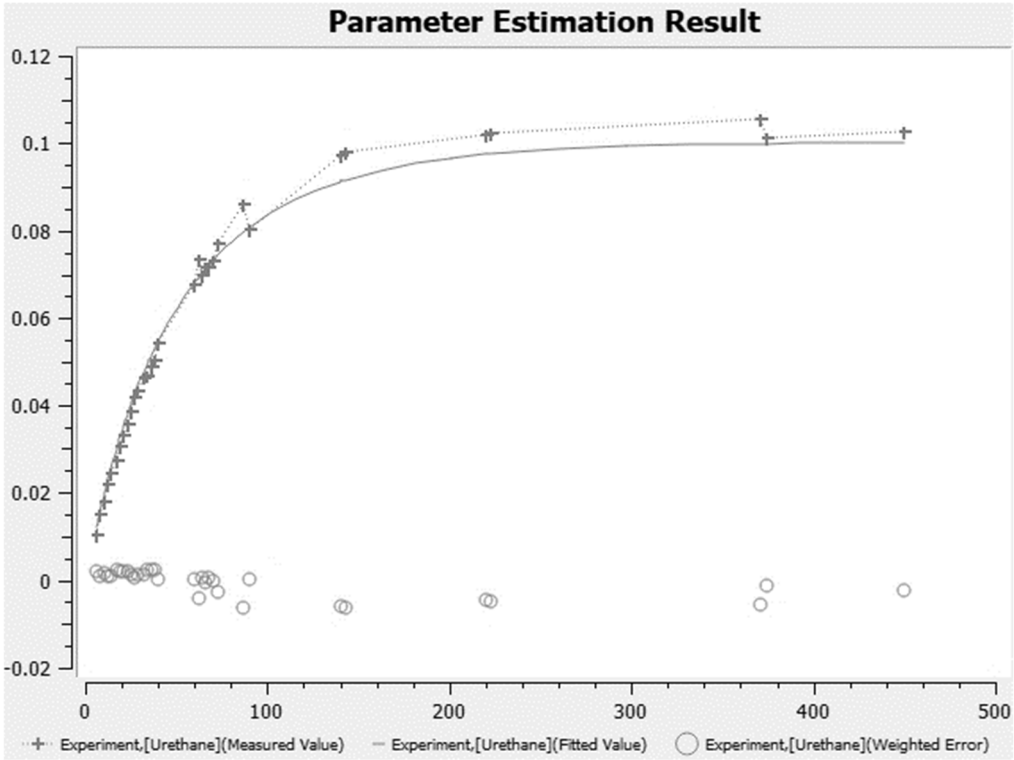

Figure S4: 15. *[Figure S15] Fitted turnover curve obtained as graphical output by COPASI for experiment urethane_11. Vertical axis gives the concentration of urethane* ***16*** *in mol L⁻¹, horizontal axis gives the time from 0 min to 500 min.*

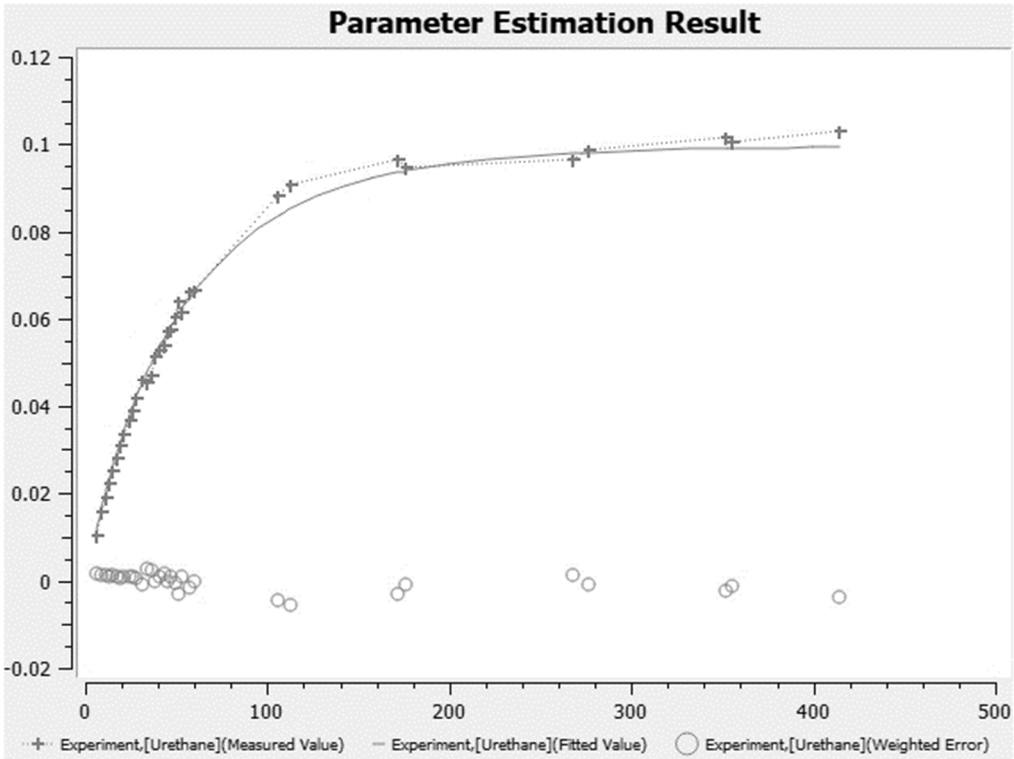

Figure S4: 16. *[Figure S16] Fitted turnover curve obtained as graphical output by COPASI for experiment urethane_12. Vertical axis gives the concentration of urethane* ***16*** *in mol L⁻¹, horizontal axis gives the time from 0 min to 500 min.*

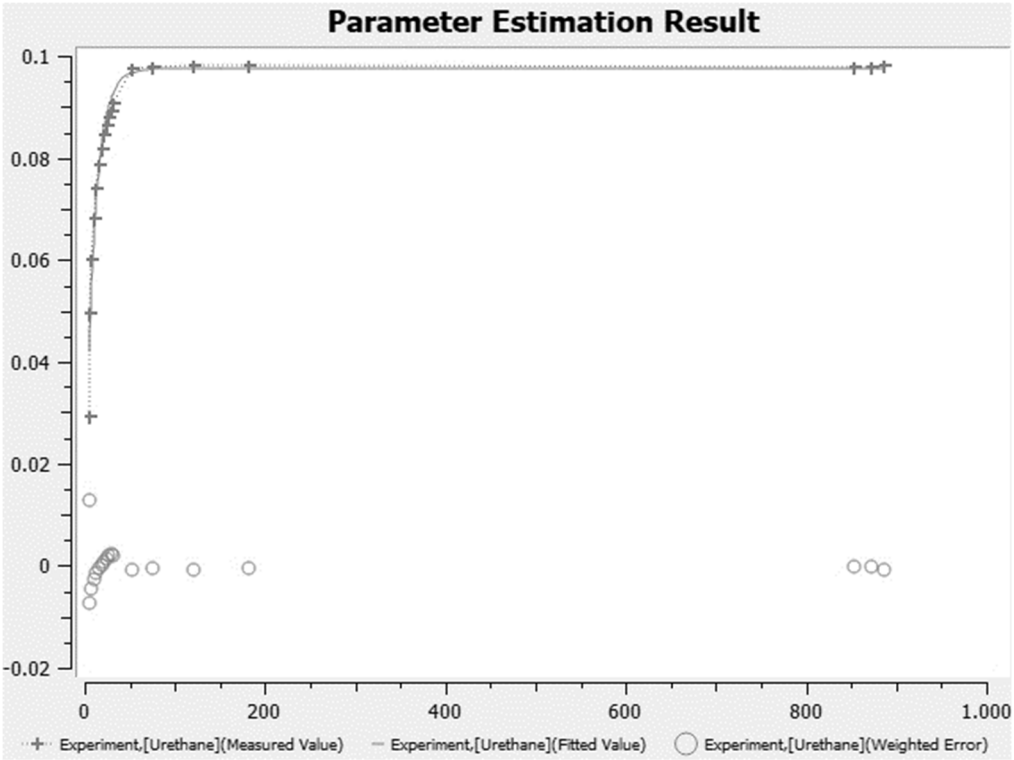

Figure S4: 17. *[Figure S17] Fitted turnover curve obtained as graphical output by COPASI for experiment urethane_13. Vertical axis gives the concentration of urethane* ***16*** *in mol L⁻¹, horizontal axis gives the time from 0 min to 1000 min.*

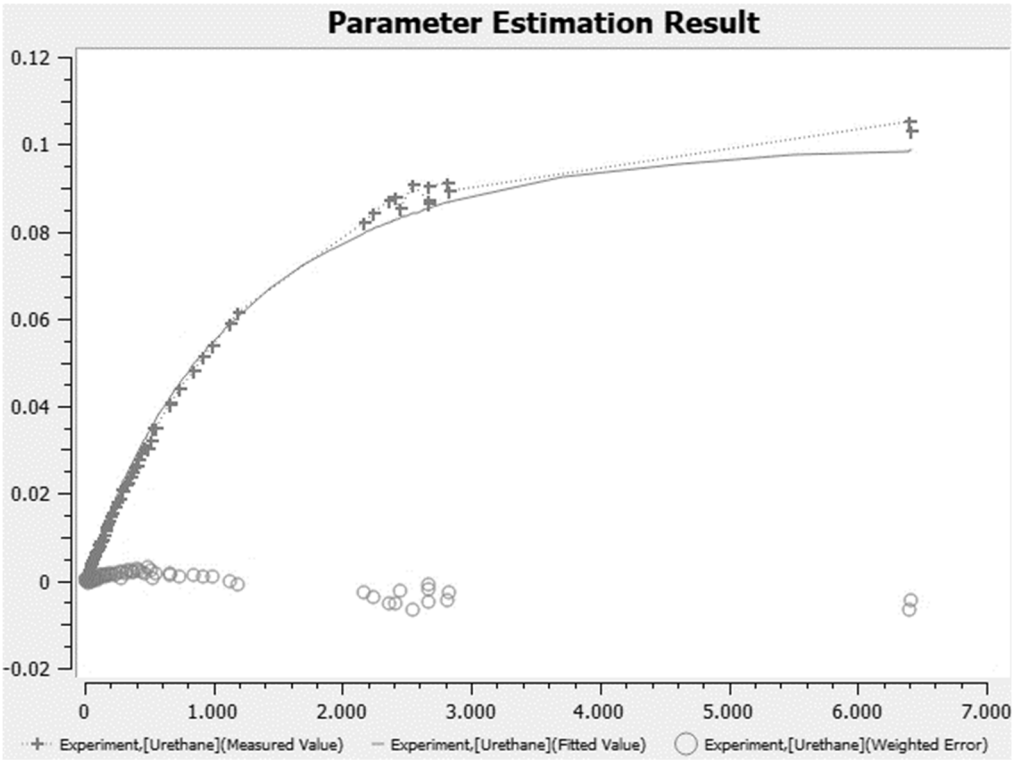

Figure S4: 18. *[Figure S18] Fitted turnover curve obtained as graphical output by COPASI for experiment urethane_14. Vertical axis gives the concentration of urethane* ***16*** *in mol L⁻¹, horizontal axis gives the time from 0 min to 7000 min.*

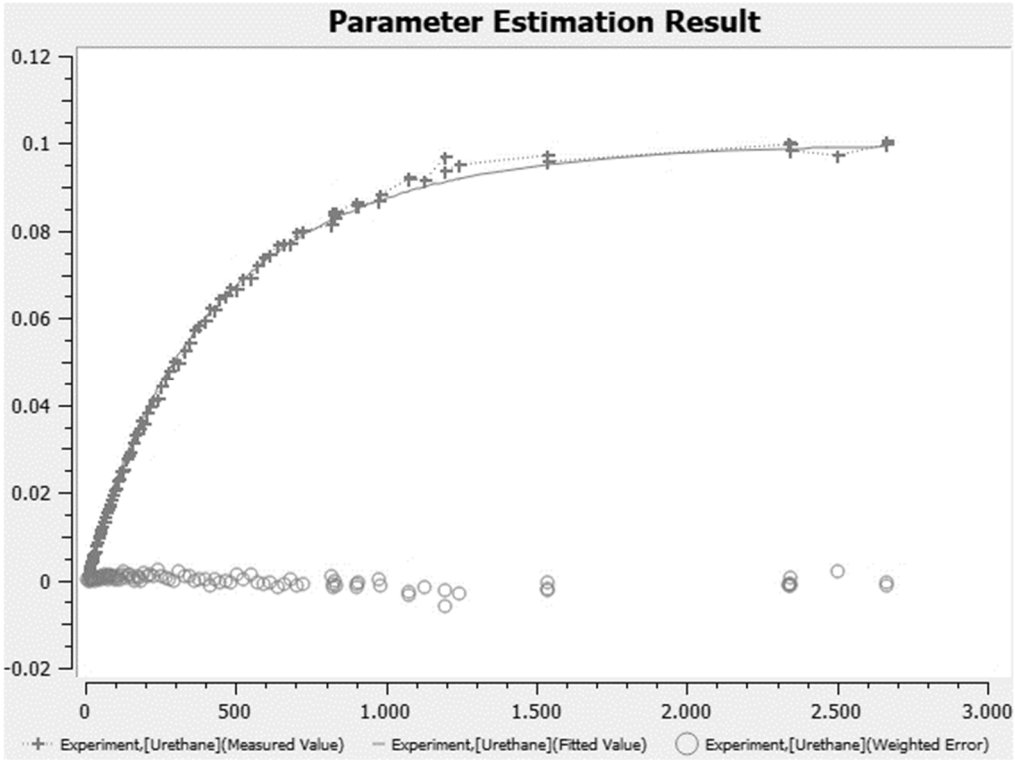

Figure S4: 19. *[Figure S19] Fitted turnover curve obtained as graphical output by COPASI for experiment urethane_15. Vertical axis gives the concentration of urethane* ***16*** *in mol L⁻¹, horizontal axis gives the time from 0 min to 3000 min.*

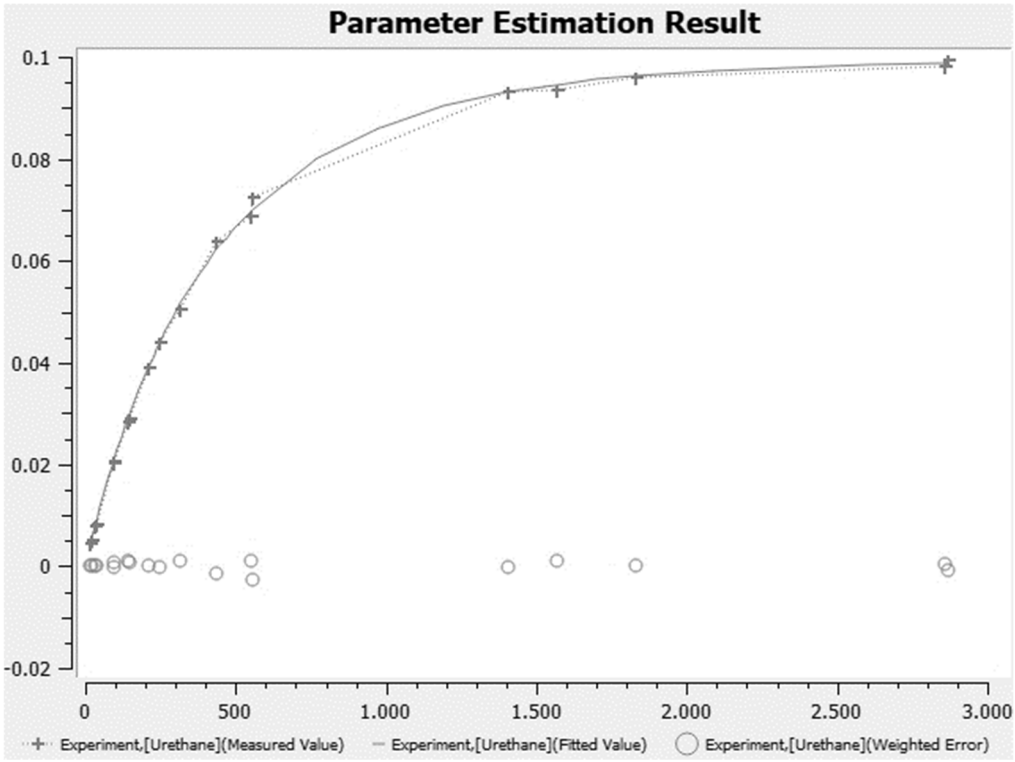

Figure S4: 20. *[Figure S20] Fitted turnover curve obtained as graphical output by COPASI for experiment urethane_16. Vertical axis gives the concentration of urethane* ***16*** *in mol L⁻¹, horizontal axis gives the time from 0 min to 3000 min.*

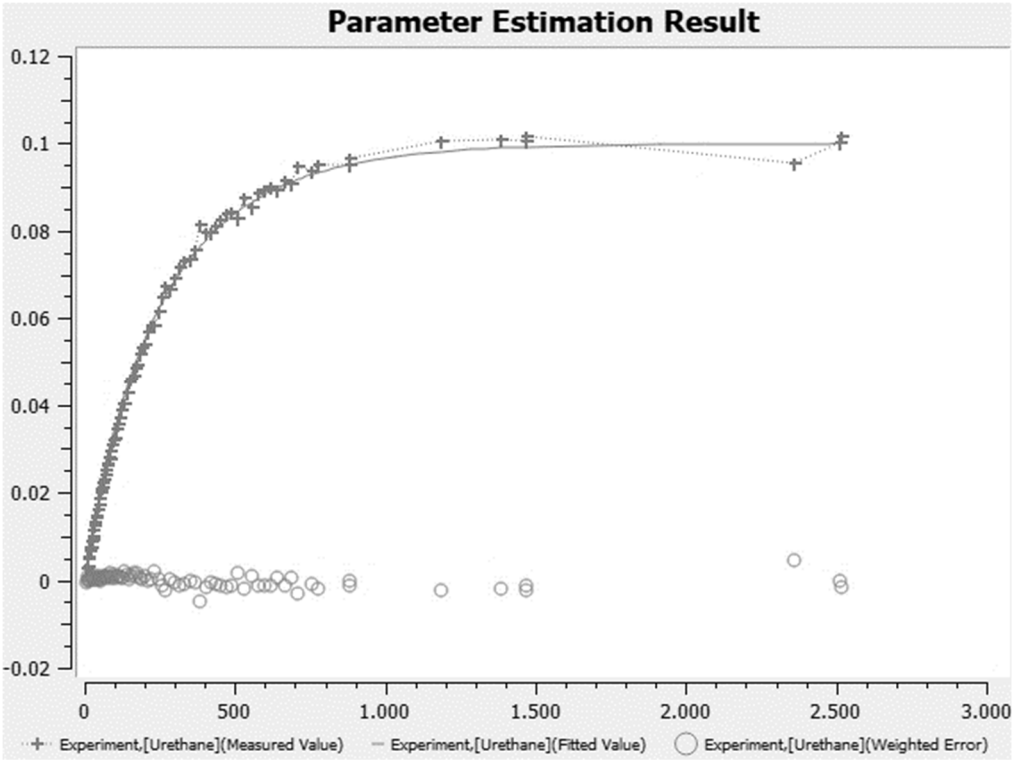

Figure S4: 21. *[Figure S21] Fitted turnover curve obtained as graphical output by COPASI for experiment urethane_17. Vertical axis gives the concentration of urethane* ***16*** *in mol* L^{-1}*, horizontal axis gives the time from 0 min to 3000 min.*

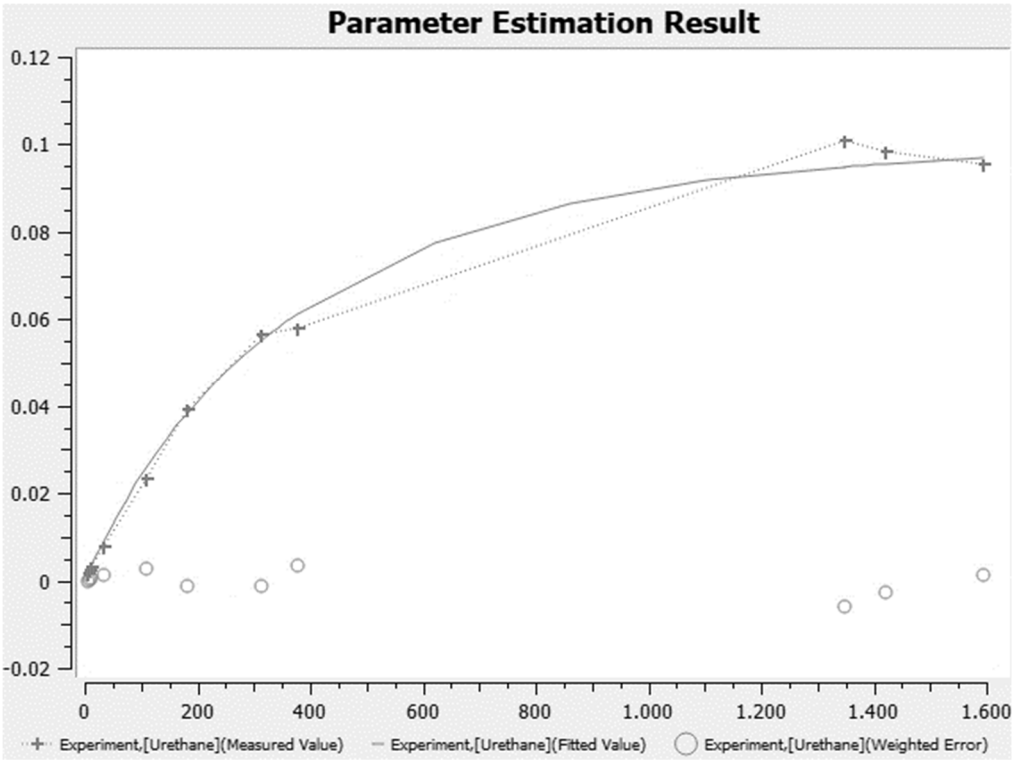

Figure S4: 22. *[Figure S22] Fitted turnover curve obtained as graphical output by COPASI for experiment urethane_18. Vertical axis gives the concentration of urethane* ***16*** *in mol* L^{-1}*, horizontal axis gives the time from 0 min to 1600 min.*

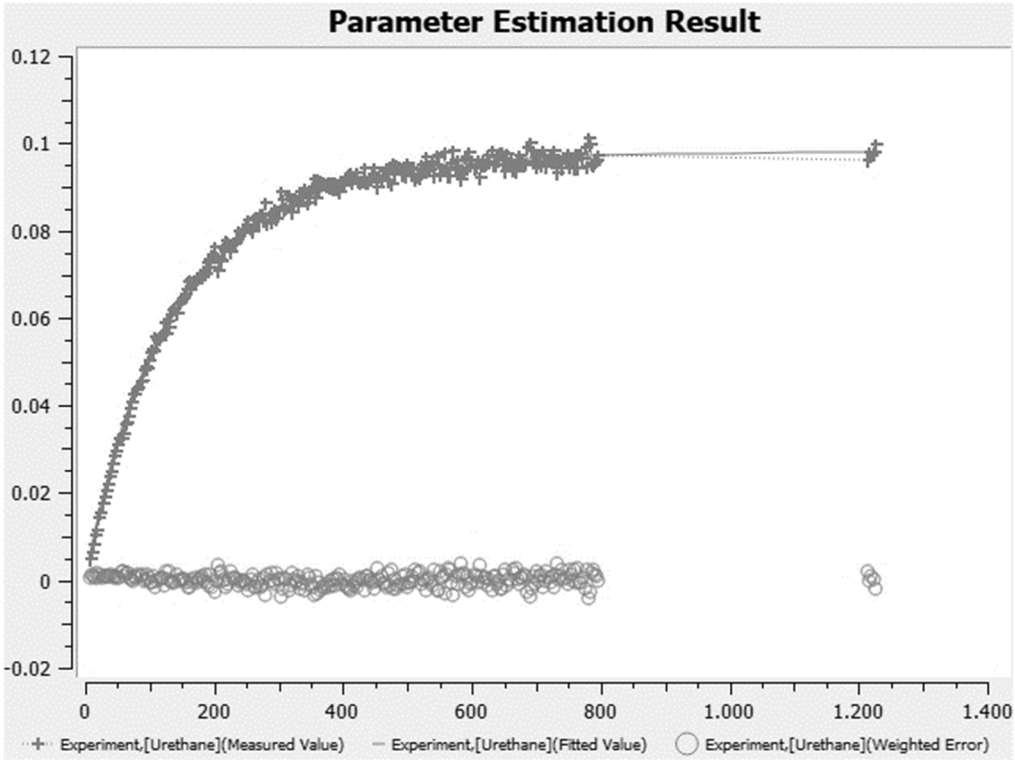

Figure S4: 23. *[Figure S23] Fitted turnover curve obtained as graphical output by COPASI for experiment urethane_19. Vertical axis gives the concentration of urethane* ***16*** *in mol L⁻¹, horizontal axis gives the time from 0 min to 1400 min.*

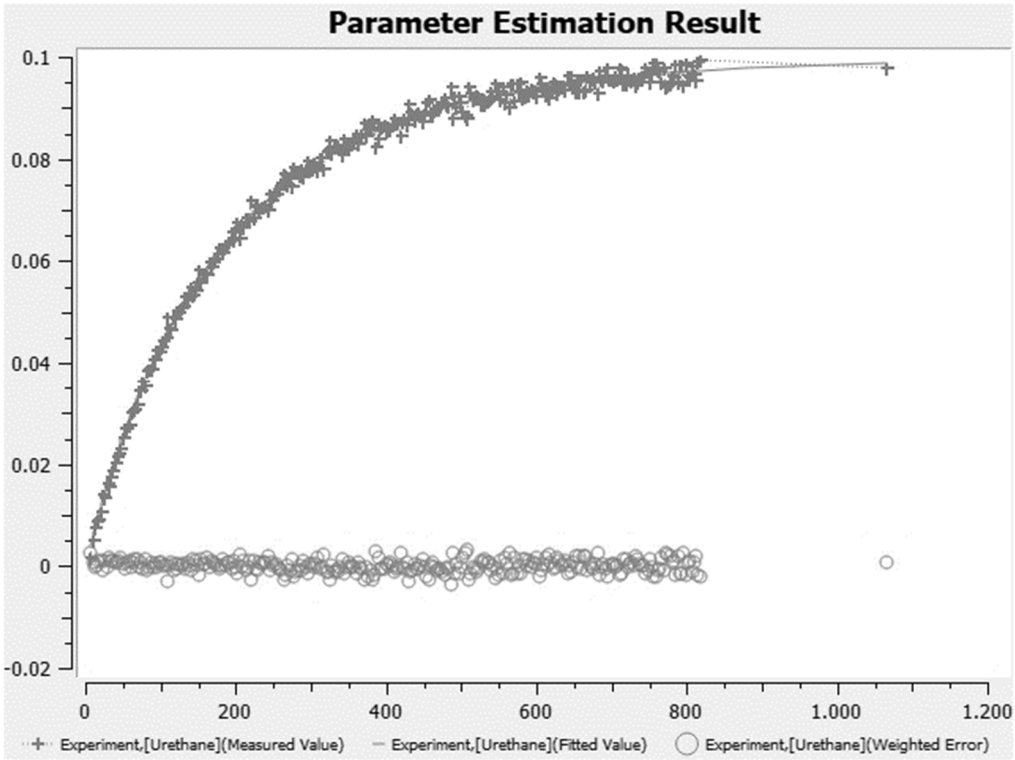

Figure S4: 24. *[Figure S24] Fitted turnover curve obtained as graphical output by COPASI for experiment urethane_20. Vertical axis gives the concentration of urethane* ***16*** *in mol L⁻¹, horizontal axis gives the time from 0 min to 1200 min.*

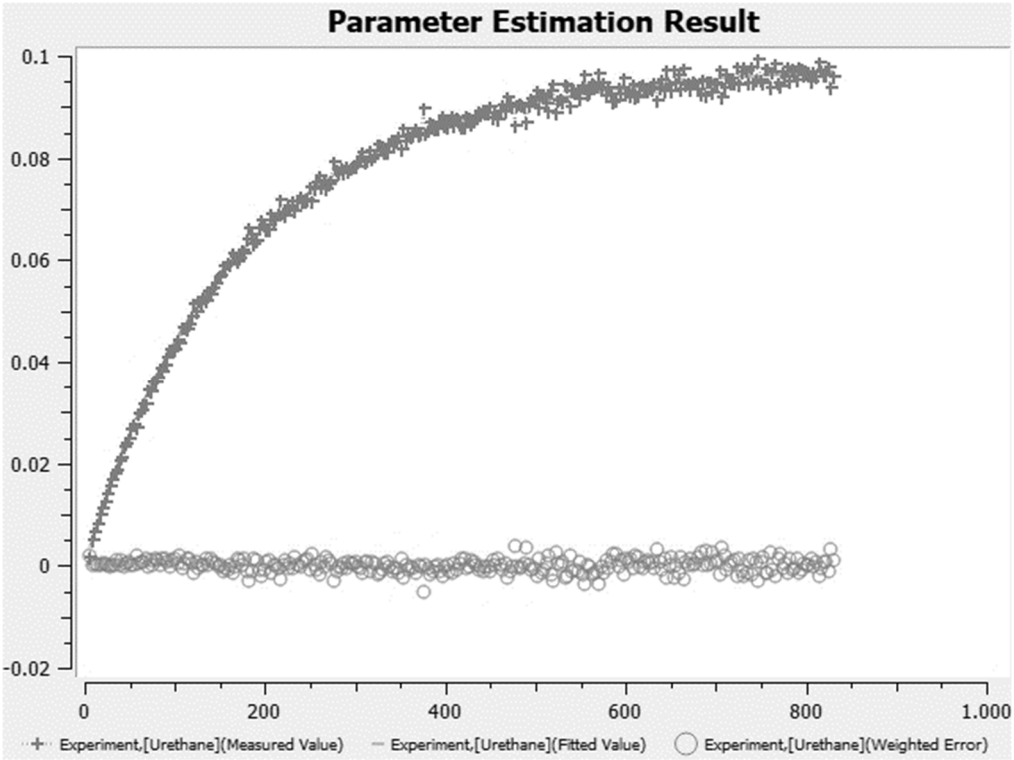

Figure S4: 25. *[Figure S25] Fitted turnover curve obtained as graphical output by COPASI for experiment urethane_21. Vertical axis gives the concentration of urethane* ***16*** *in mol L⁻¹, horizontal axis gives the time from 0 min to 1000 min.*

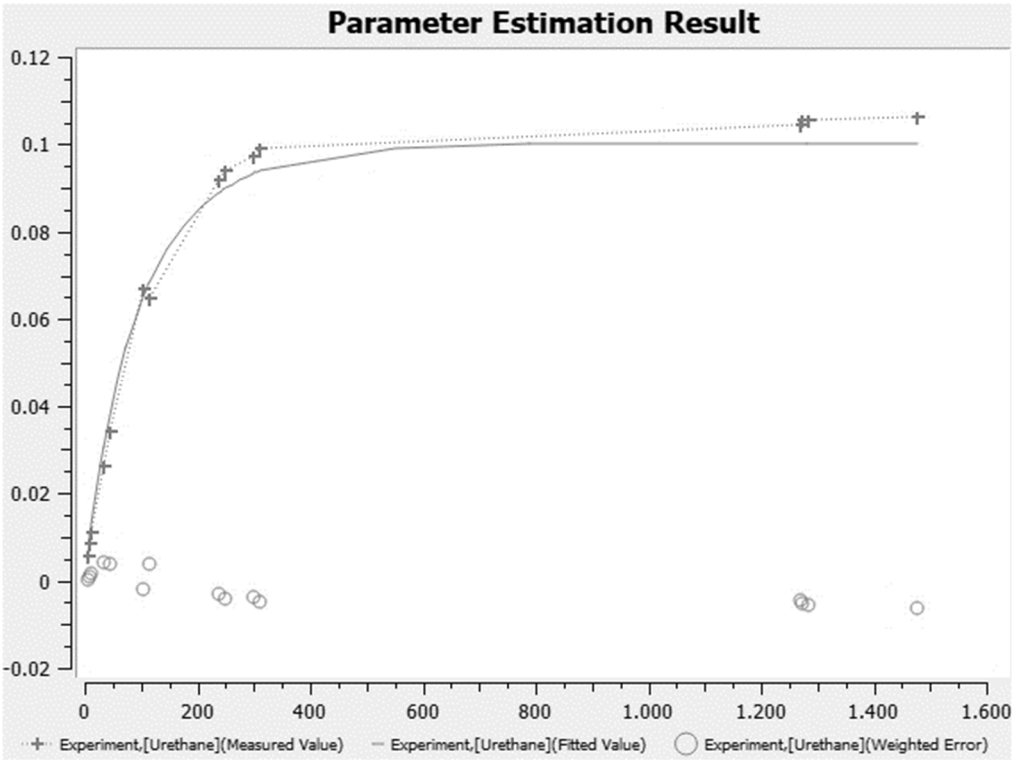

Figure S4: 26. *[Figure S26] Fitted turnover curve obtained as graphical output by COPASI for experiment urethane_22. Vertical axis gives the concentration of urethane* ***16*** *in mol L⁻¹, horizontal axis gives the time from 0 min to 1600 min.*

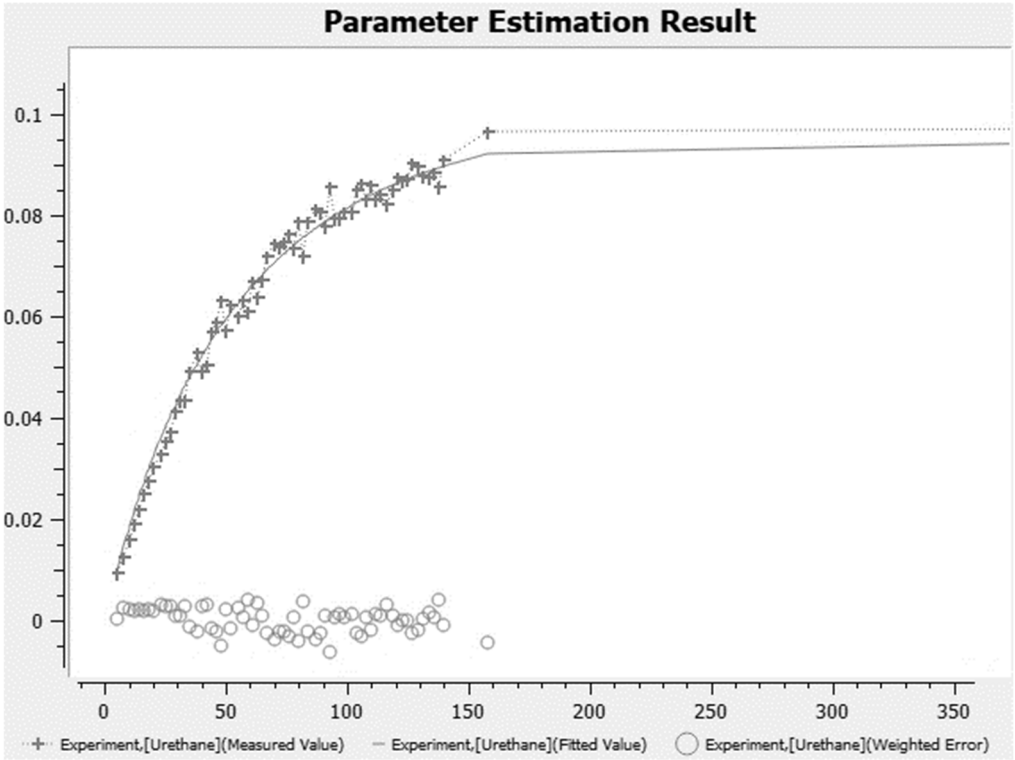

Figure S4: 27. *[Figure S27] Fitted turnover curve obtained as graphical output by COPASI for experiment urethane_23. Vertical axis gives the concentration of urethane* ***16*** *in mol L⁻¹, horizontal axis gives the time from 0 min to 350 min.*

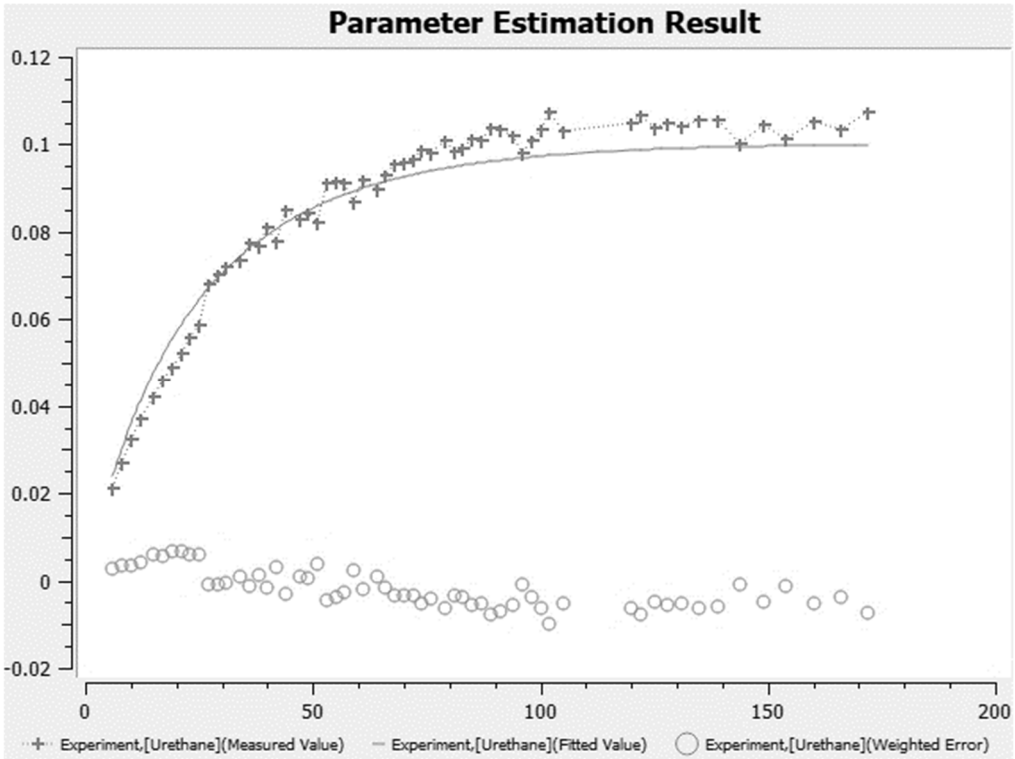

Figure S4: 28. *[Figure S28] Fitted turnover curve obtained as graphical output by COPASI for experiment urethane_24. Vertical axis gives the concentration of urethane* ***16*** *in mol L⁻¹, horizontal axis gives the time from 0 min to 200 min.*

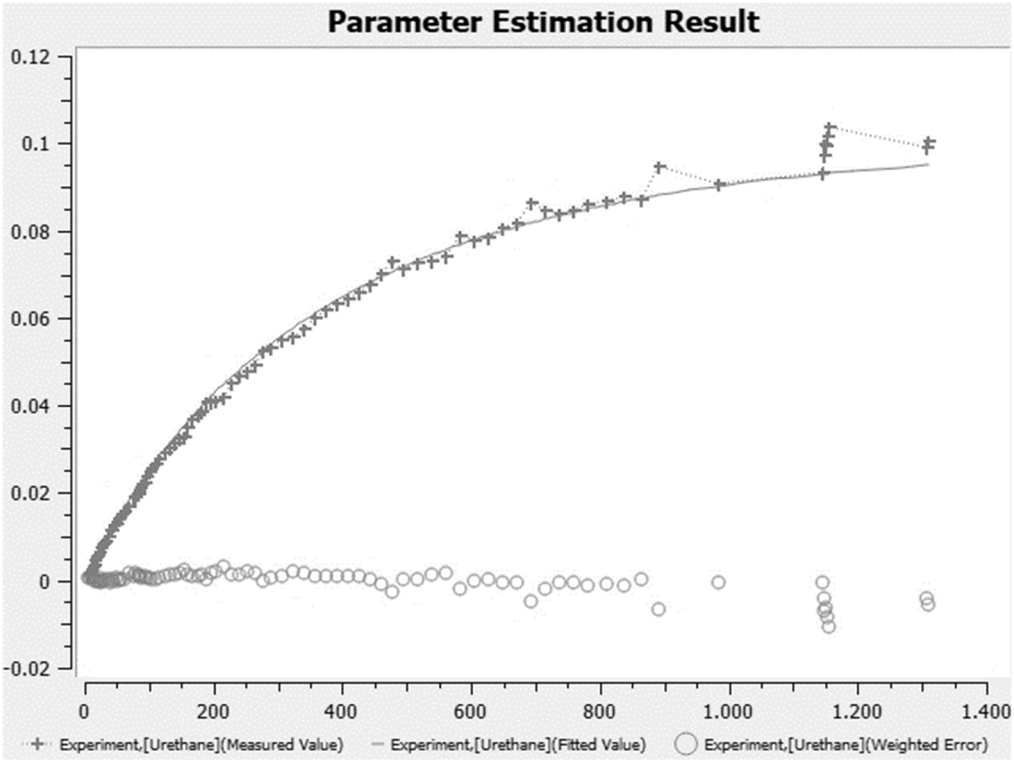

Figure S4: 29. *[Figure S29] Fitted turnover curve obtained as graphical output by COPASI for experiment urethane_25. Vertical axis gives the concentration of urethane* ***16*** *in mol L⁻¹, horizontal axis gives the time from 0 min to 1400 min.*

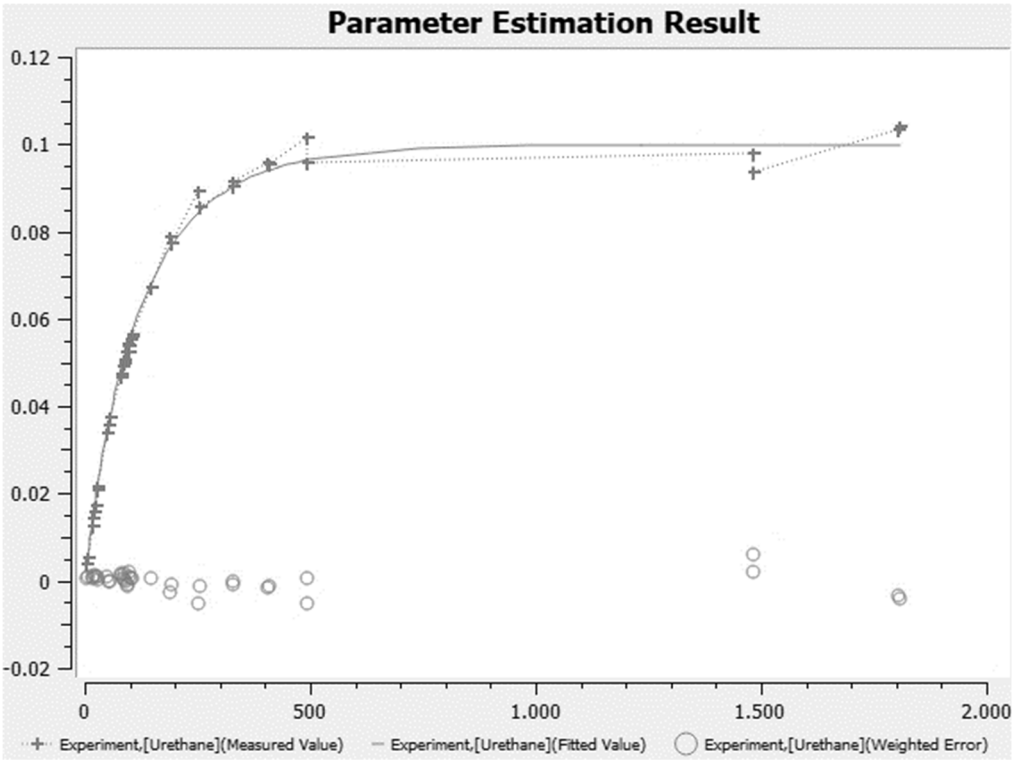

Figure S4: 30. *[Figure S30] Fitted turnover curve obtained as graphical output by COPASI for experiment urethane_26. Vertical axis gives the concentration of urethane* ***16*** *in mol L⁻¹, horizontal axis gives the time from 0 min to 2000 min.*

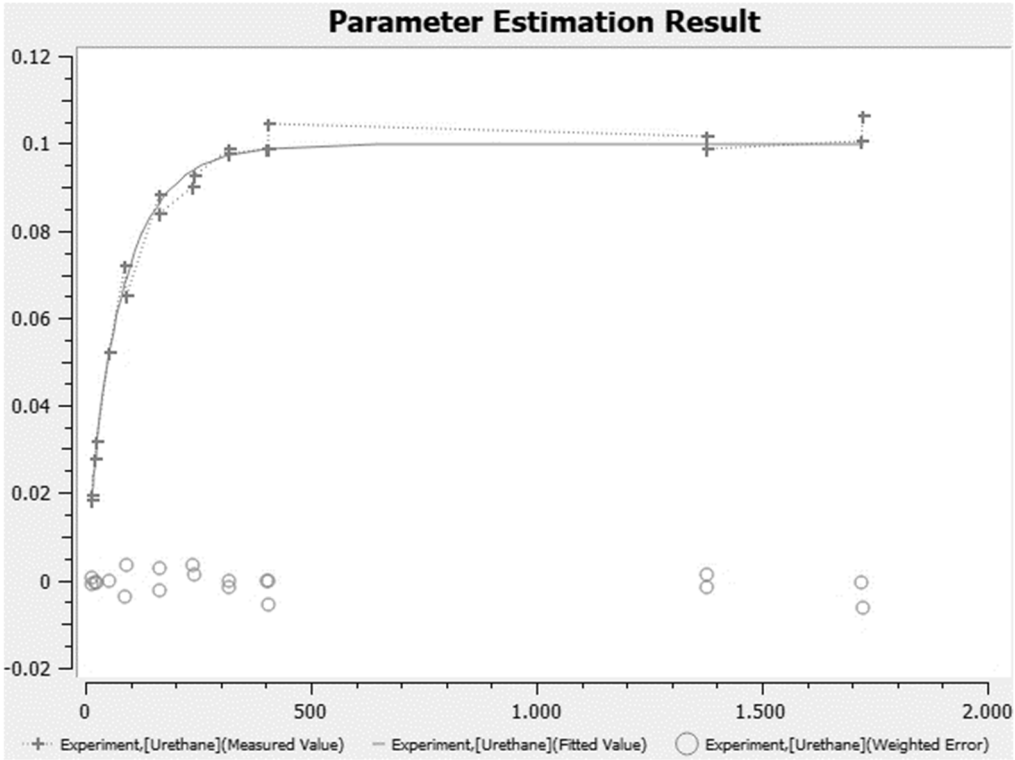

***Figure S4: 31**. [Figure S31] Fitted turnover curve obtained as graphical output by COPASI for experiment urethane_27. Vertical axis gives the concentration of urethane **16** in mol L^{-1}, horizontal axis gives the time from 0 min to 2000 min.*

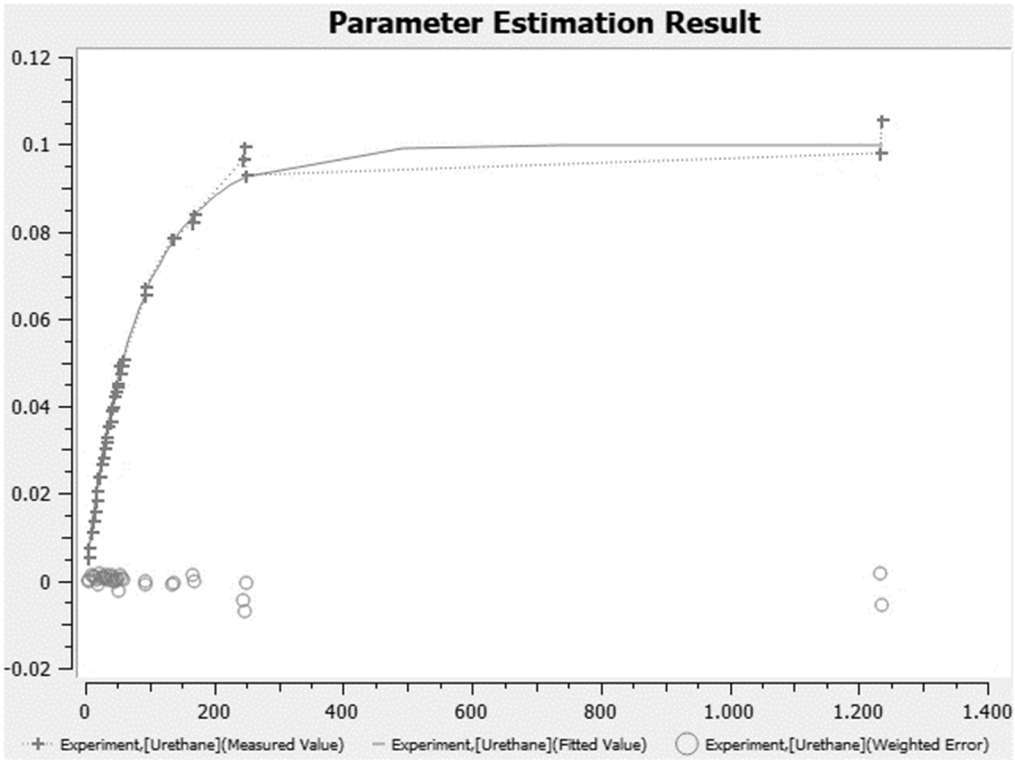

***Figure S4: 32.** [Figure S32] Fitted turnover curve obtained as graphical output by COPASI for experiment urethane_28. Vertical axis gives the concentration of urethane **16** in mol L^{-1}, horizontal axis gives the time from 0 min to 1400 min.*

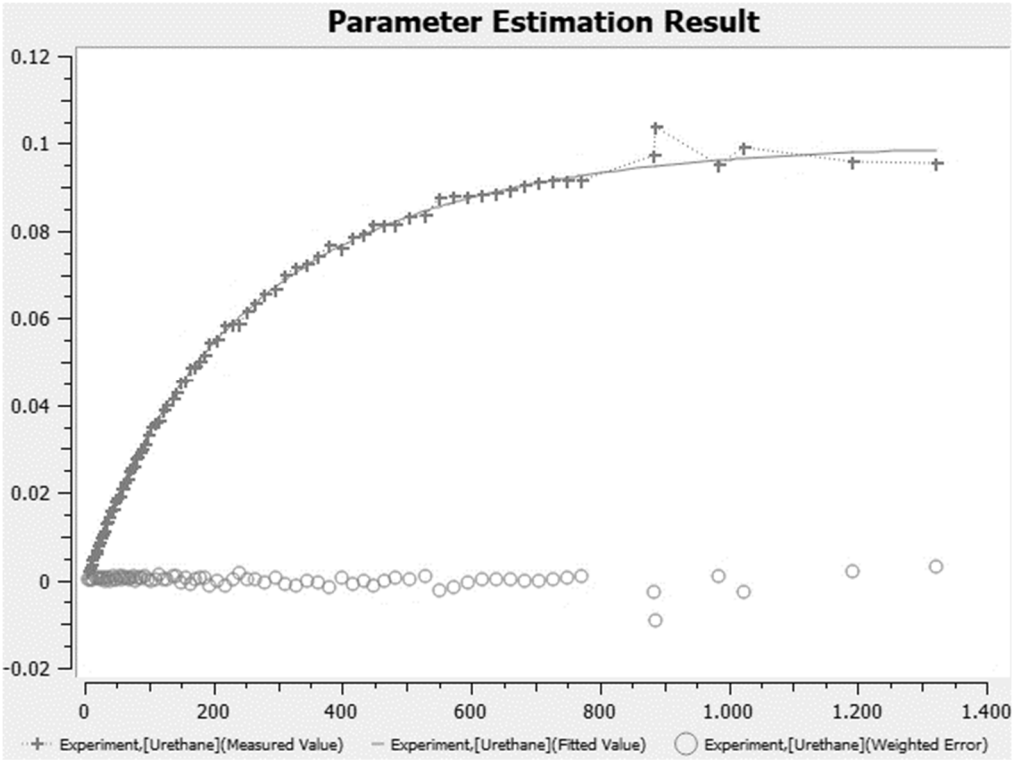

Figure S4: 33. *[Figure S33] Fitted turnover curve obtained as graphical output by COPASI for experiment urethane_29. Vertical axis gives the concentration of urethane* ***16*** *in mol L⁻¹, horizontal axis gives the time from 0 min to 1400 min.*

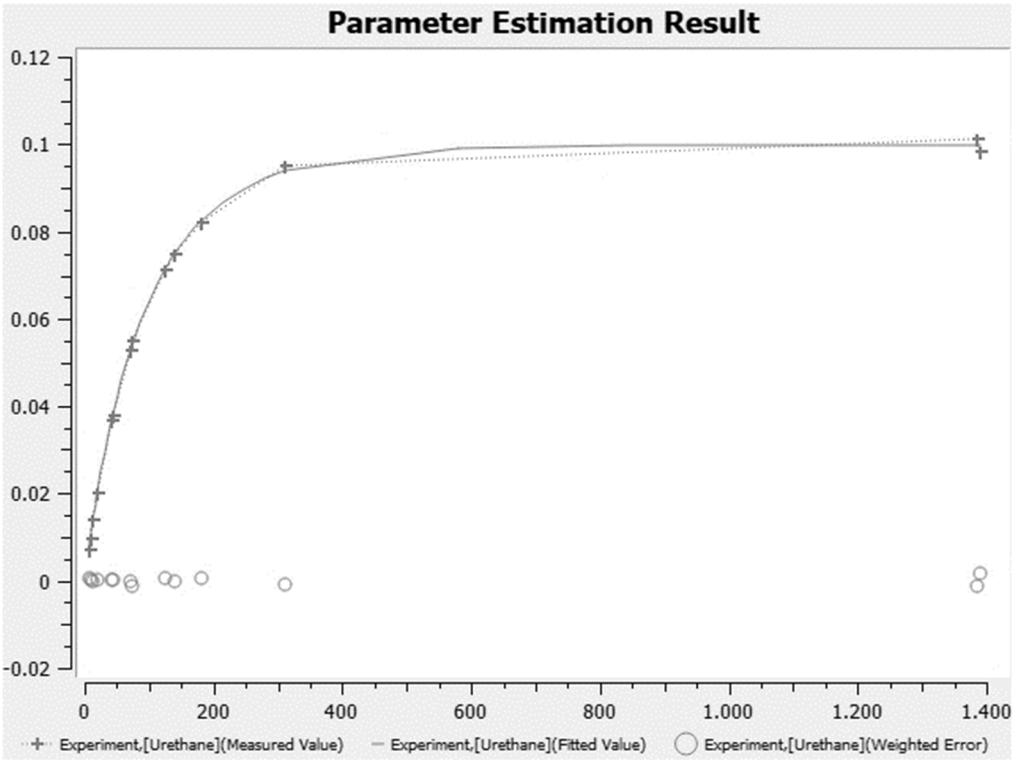

Figure S4: 34. *[Figure S34] Fitted turnover curve obtained as graphical output by COPASI for experiment urethane_30. Vertical axis gives the concentration of urethane* ***16*** *in mol L⁻¹, horizontal axis gives the time from 0 min to 1400 min.*

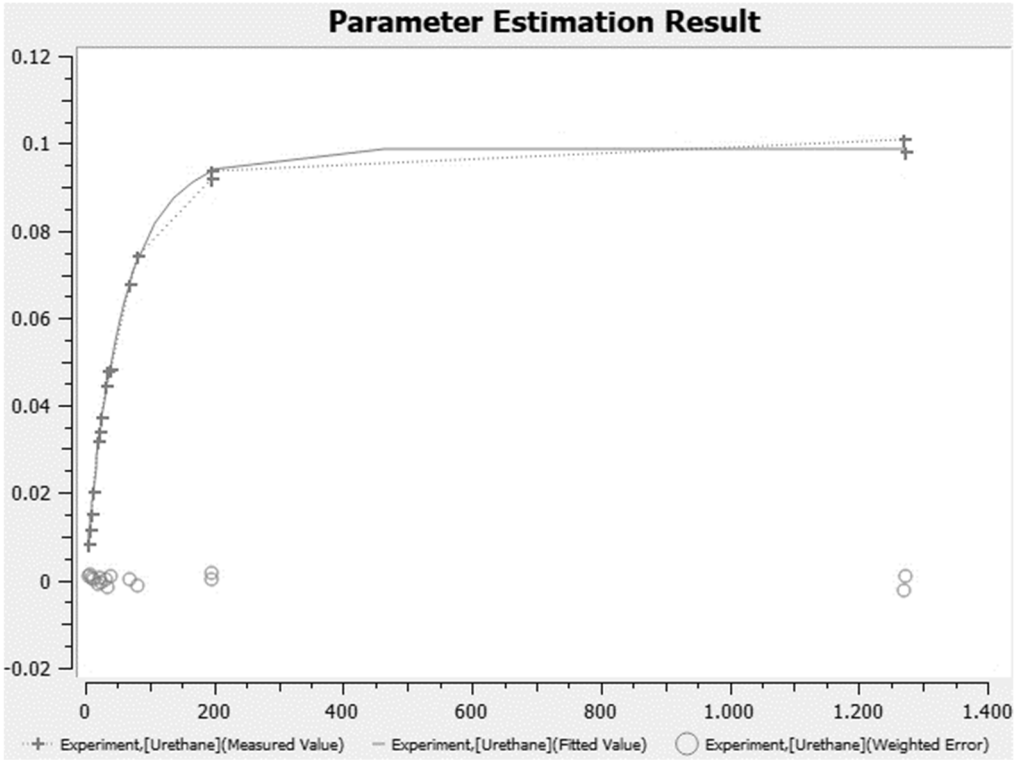

Figure S4: 35. *[Figure S35] Fitted turnover curve obtained as graphical output by COPASI for experiment urethane_31. Vertical axis gives the concentration of urethane* ***16*** *in mol L⁻¹, horizontal axis gives the time from 0 min to 1400 min.*

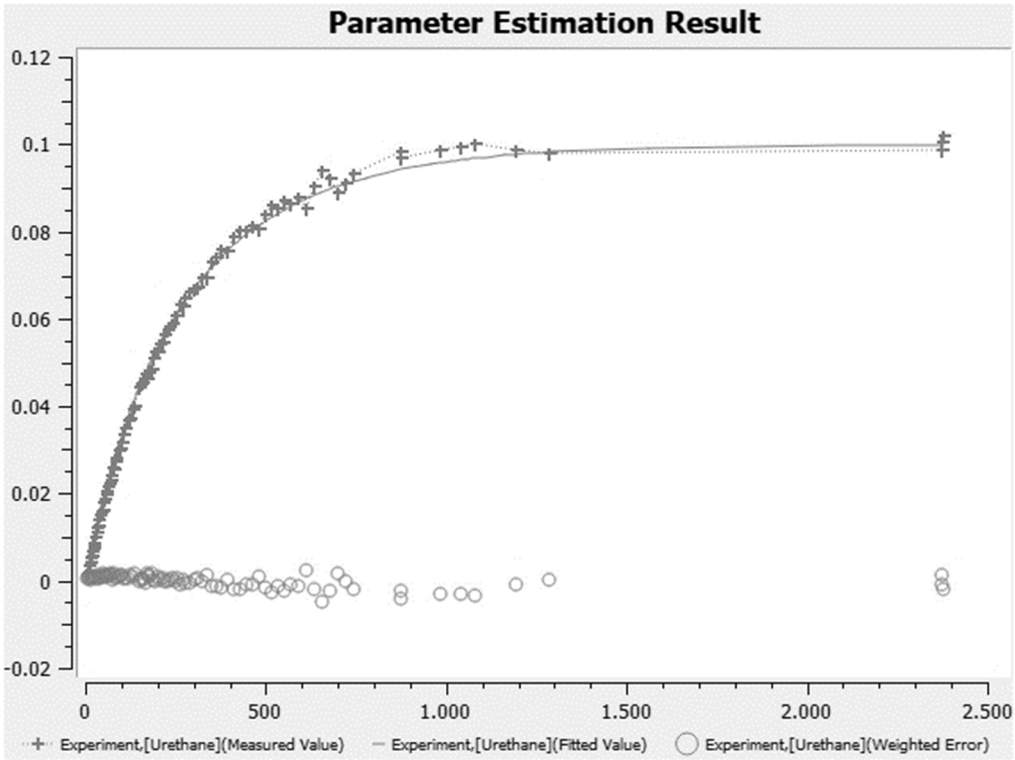

Figure S4: 36. *[Figure S36] Fitted turnover curve obtained as graphical output by COPASI for experiment urethane_32. Vertical axis gives the concentration of urethane* ***16*** *in mol L⁻¹, horizontal axis gives the time from 0 min to 2500 min.*

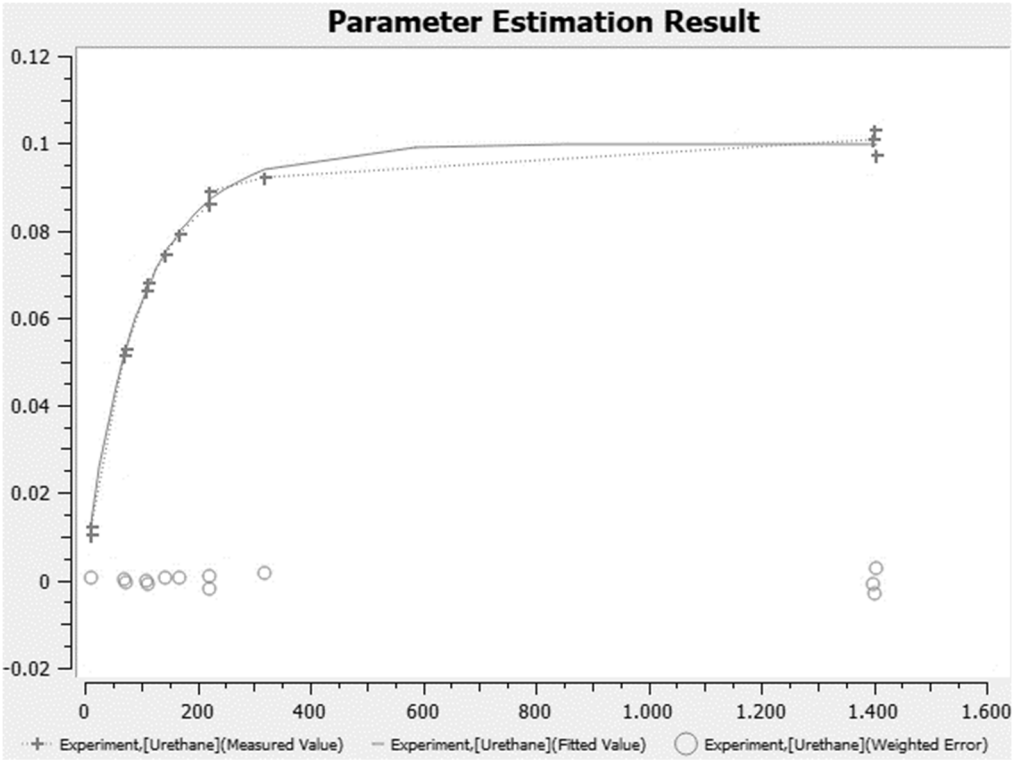

Figure S4: 37. *[Figure S37] Fitted turnover curve obtained as graphical output by COPASI for experiment urethane_33. Vertical axis gives the concentration of urethane* ***16*** *in mol L⁻¹, horizontal axis gives the time from 0 min to 1600 min.*

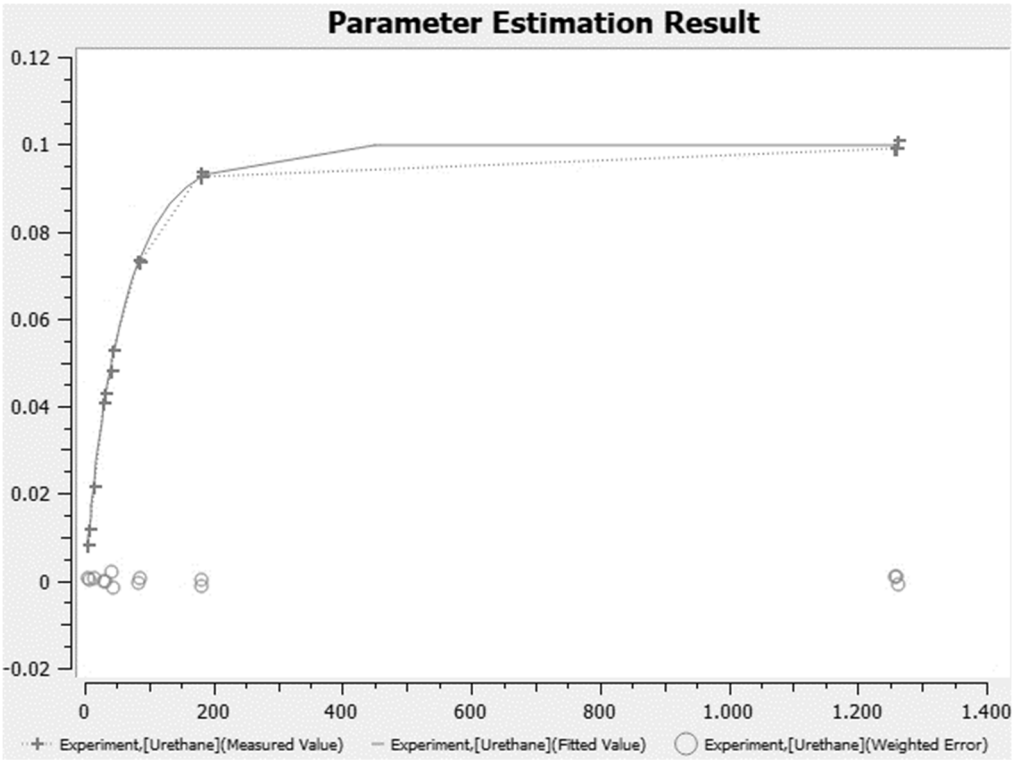

Figure S4: 38. *[Figure S38] Fitted turnover curve obtained as graphical output by COPASI for experiment urethane_34. Vertical axis gives the concentration of urethane* ***16*** *in mol L⁻¹, horizontal axis gives the time from 0 min to 1400 min.*

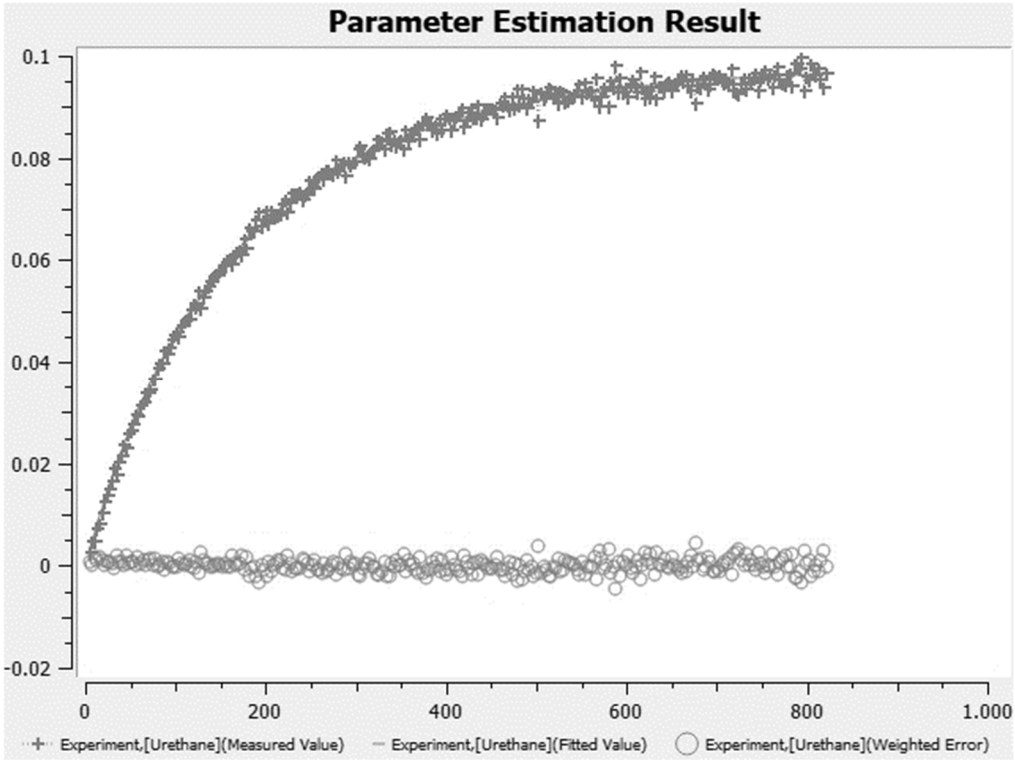

Figure S4: 39. *[Figure S39] Fitted turnover curve obtained as graphical output by COPASI for experiment urethane_35. Vertical axis gives the concentration of urethane* ***16*** *in mol L⁻¹, horizontal axis gives the time from 0 min to 1000 min.*

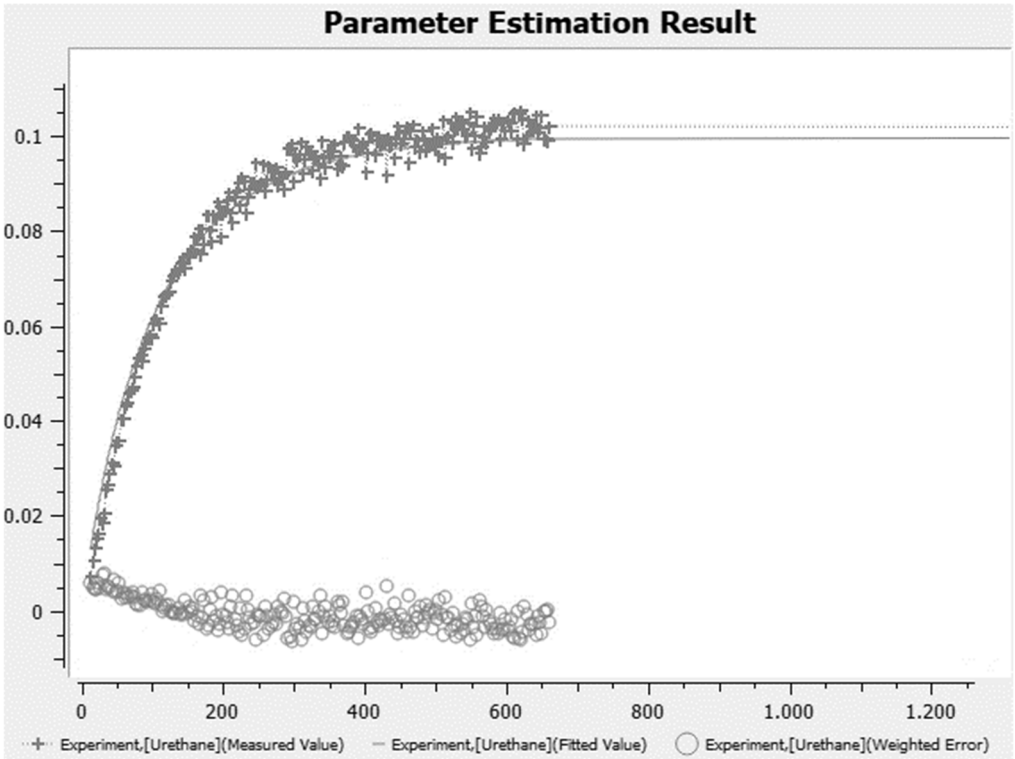

Figure S4: 40. *[Figure S40] Fitted turnover curve obtained as graphical output by COPASI for experiment urethane_36. Vertical axis gives the concentration of urethane* ***16*** *in mol L⁻¹, horizontal axis gives the time from 0 min to 1200 min.*

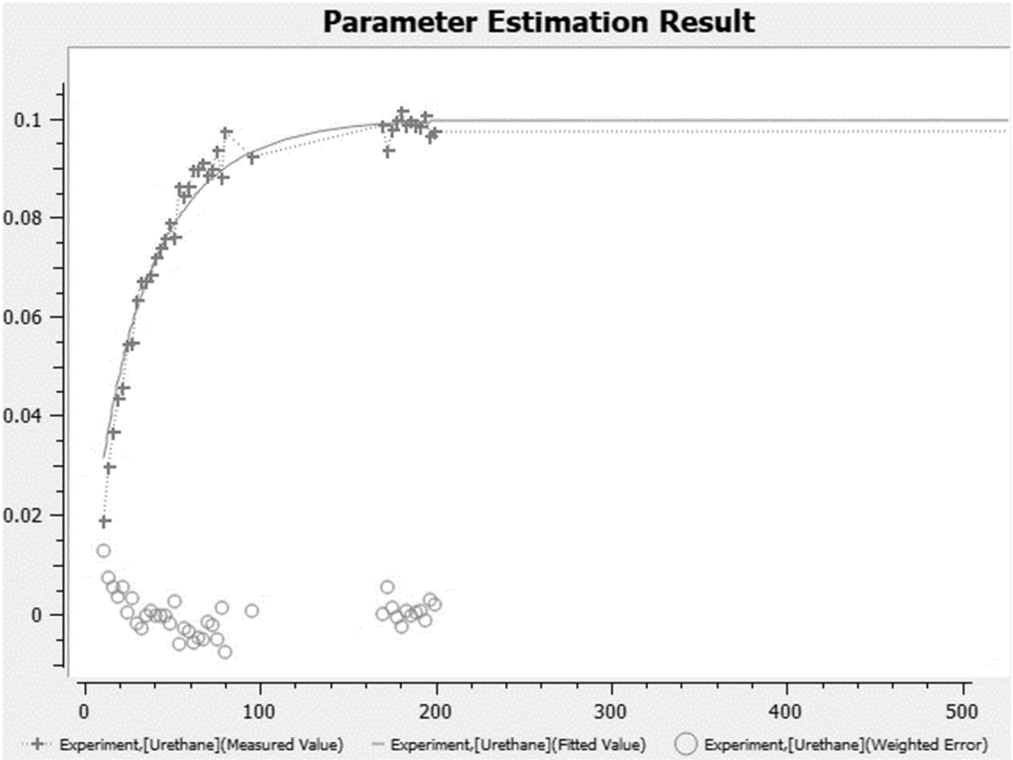

Figure S4: 41. *[Figure S41] Fitted turnover curve obtained as graphical output by COPASI for experiment urethane_37. Vertical axis gives the concentration of urethane* ***16*** *in mol L⁻¹, horizontal axis gives the time from 0 min to 500 min.*

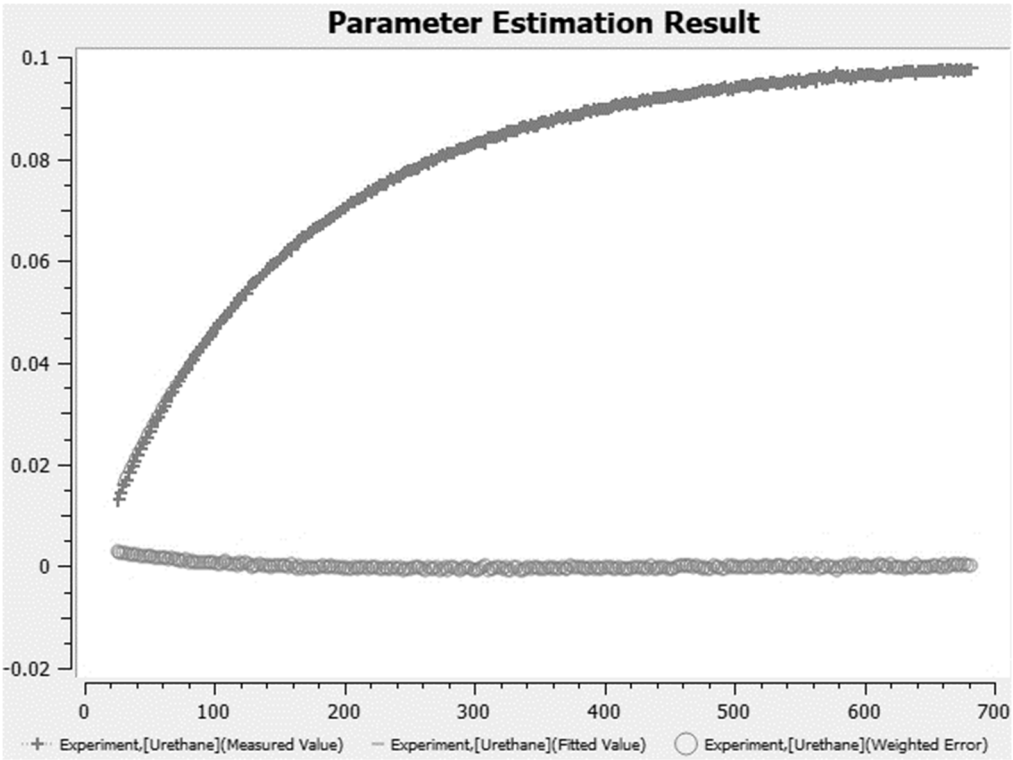

Figure S4: 42. *[Figure S42] Fitted turnover curve obtained as graphical output by COPASI for experiment urethane_38. Vertical axis gives the concentration of urethane* ***16*** *in mol L⁻¹, horizontal axis gives the time from 0 min to 700 min.*

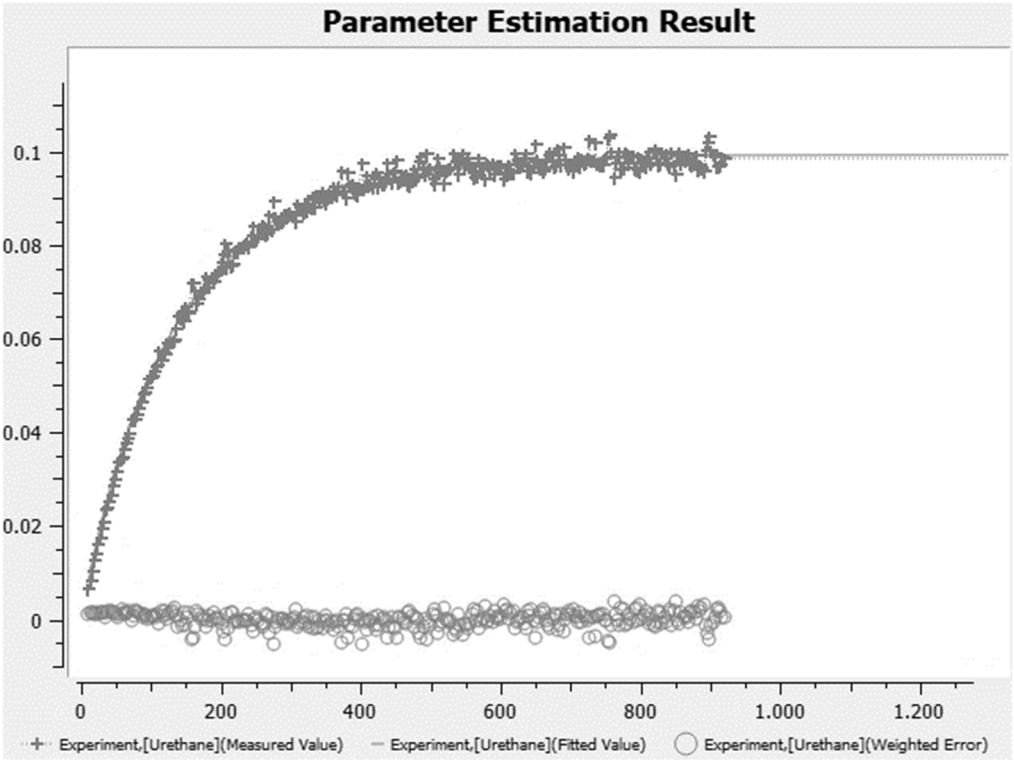

Figure S4: 43. *[Figure S43] Fitted turnover curve obtained as graphical output by COPASI for experiment urethane_39. Vertical axis gives the concentration of urethane* ***16*** *in mol L⁻¹, horizontal axis gives the time from 0 min to 1200 min.*

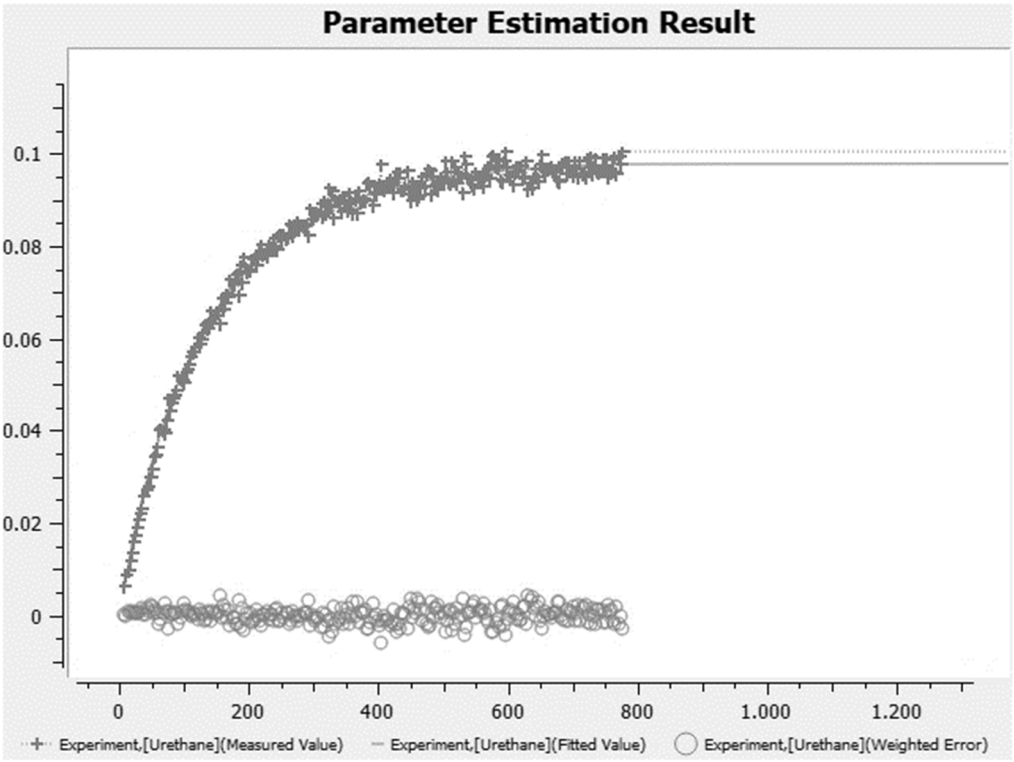

Figure S4: 44. *[Figure S44] Fitted turnover curve obtained as graphical output by COPASI for experiment urethane_40. Vertical axis gives the concentration of urethane* ***16*** *in mol L⁻¹, horizontal axis gives the time from 0 min to 1200 min.*

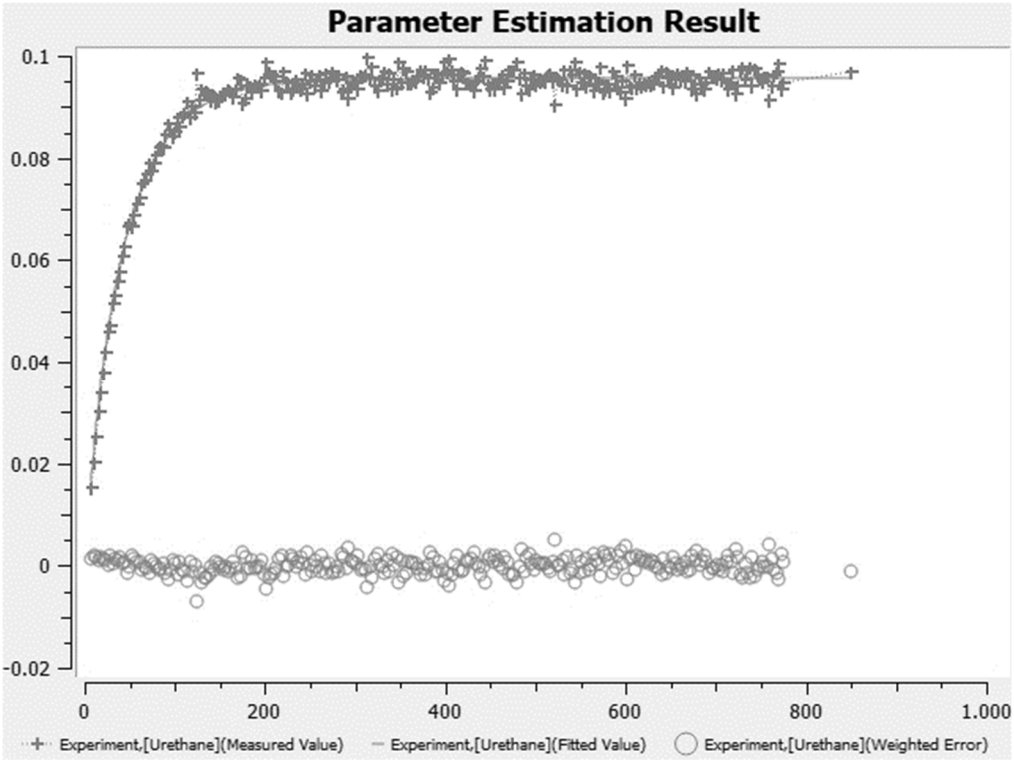

Figure S4: 45. *[Figure S45] Fitted turnover curve obtained as graphical output by COPASI for experiment urethane_41. Vertical axis gives the concentration of urethane* ***16*** *in mol* L^{-1}*, horizontal axis gives the time from 0 min to 1100 min.*

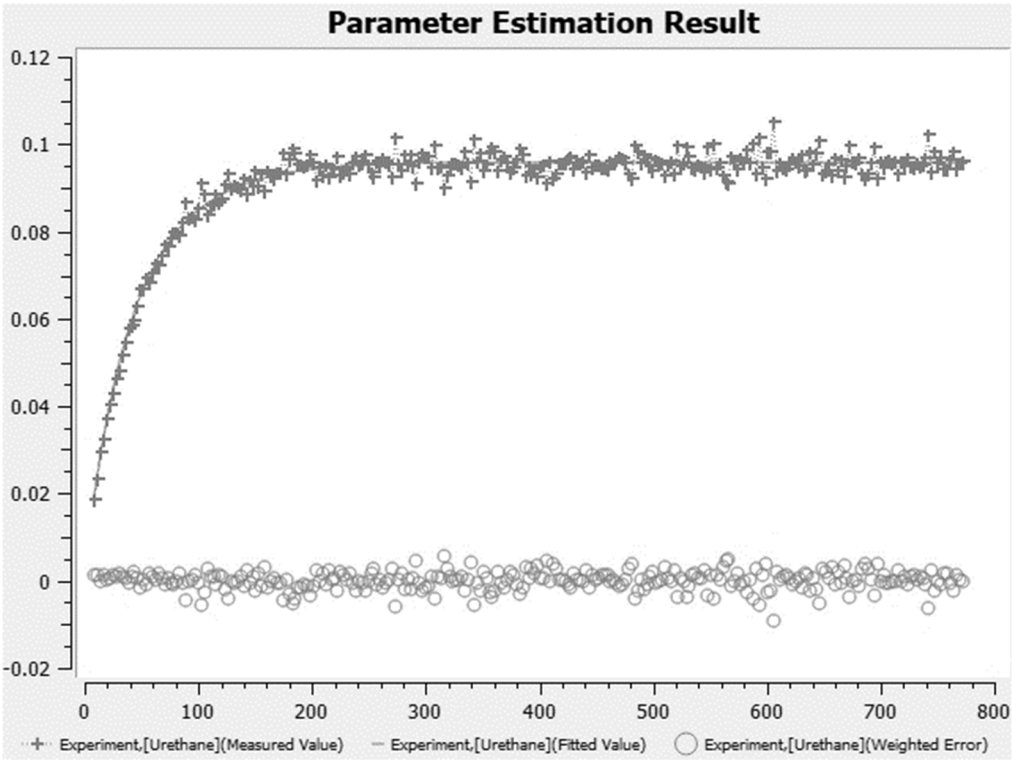

Figure S4: 46. *[Figure S46] Fitted turnover curve obtained as graphical output by COPASI for experiment urethane_42. Vertical axis gives the concentration of urethane* ***16*** *in mol* L^{-1}*, horizontal axis gives the time from 0 min to 800 min.*

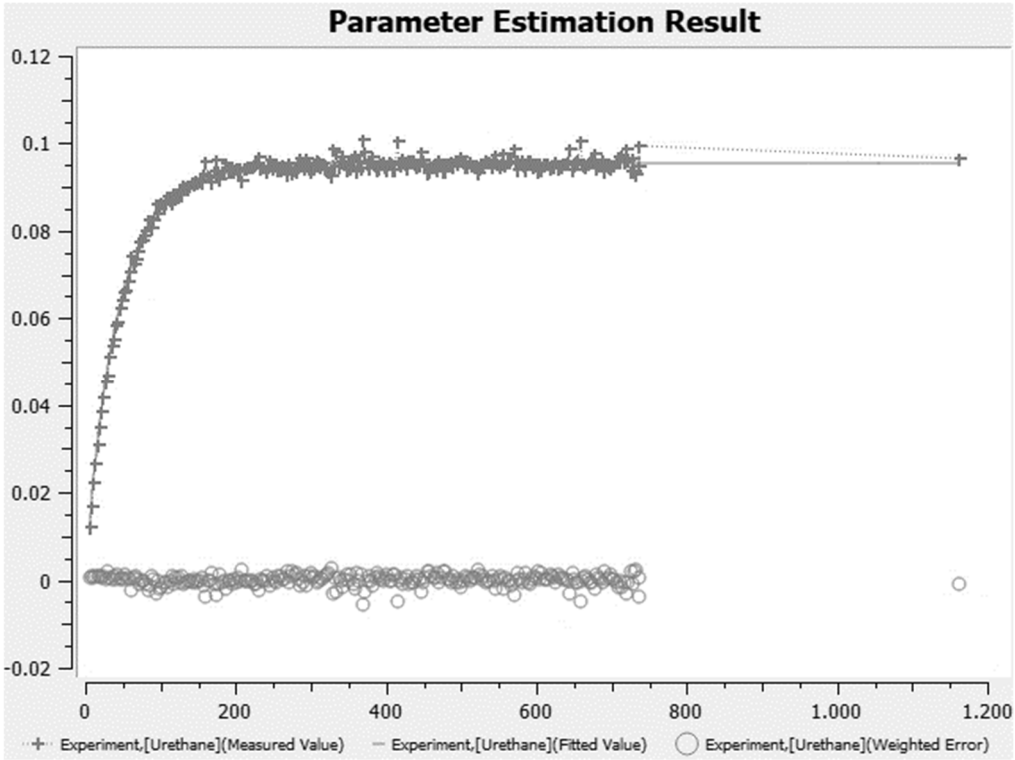

Figure S4: 47. *[Figure S47] Fitted turnover curve obtained as graphical output by COPASI for experiment urethane_43. Vertical axis gives the concentration of urethane* ***16*** *in mol L⁻¹, horizontal axis gives the time from 0 min to 1200 min.*

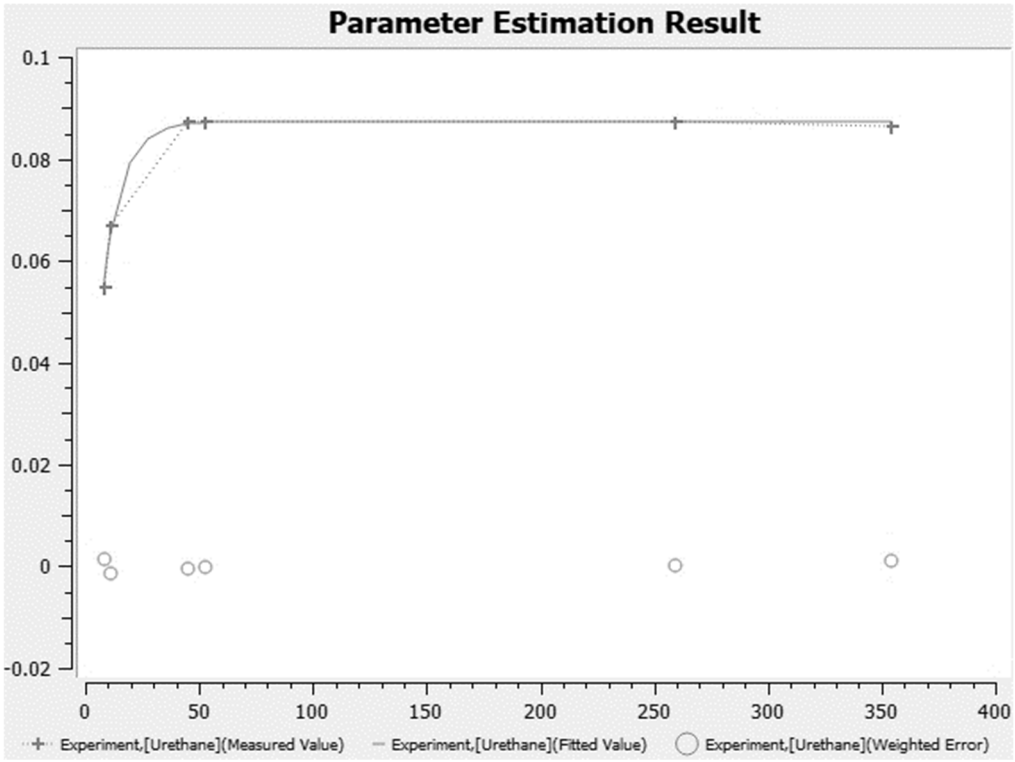

Figure S4: 48. *[Figure S48] Fitted turnover curve obtained as graphical output by COPASI for experiment urethane_44. Vertical axis gives the concentration of urethane* ***16*** *in mol L⁻¹, horizontal axis gives the time from 0 min to 400 min.*

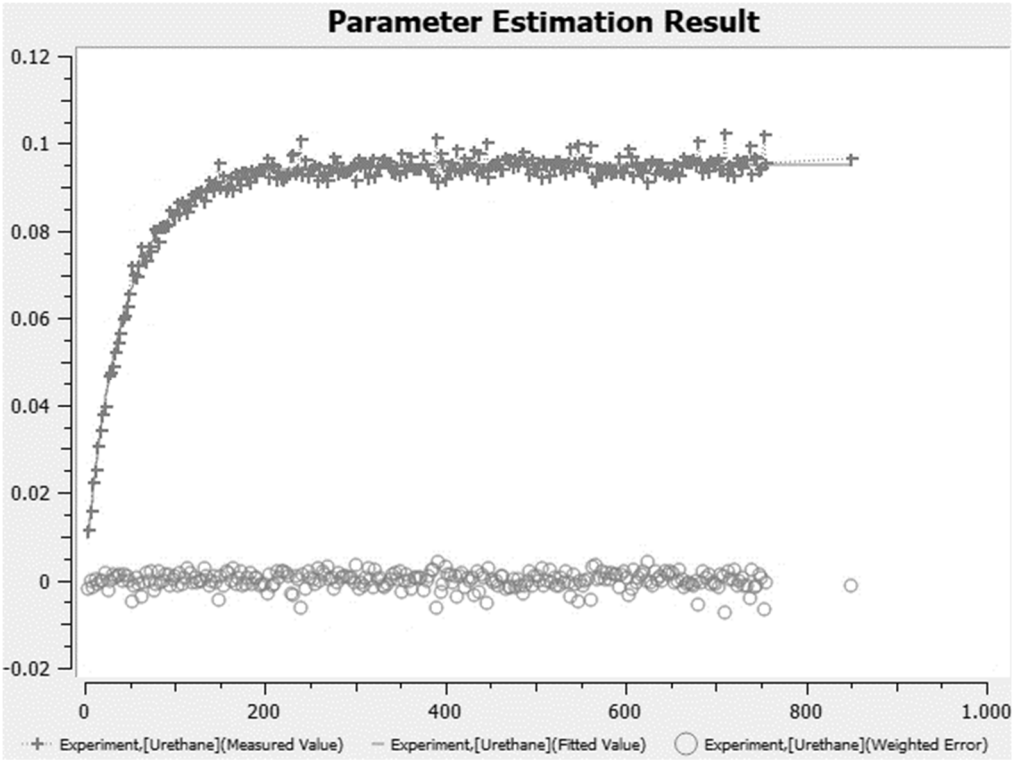

Figure S4: 49. *[Figure S49] Fitted turnover curve obtained as graphical output by COPASI for experiment urethane_45. Vertical axis gives the concentration of urethane* ***16*** *in mol L⁻¹, horizontal axis gives the time from 0 min to 1000 min.*

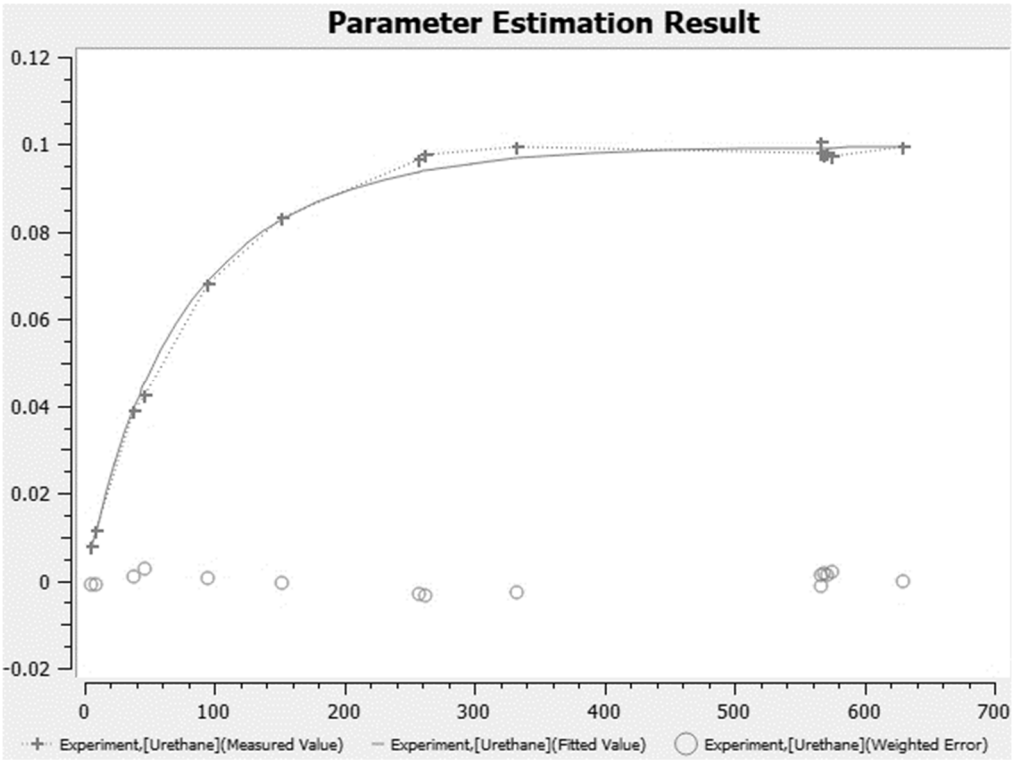

Figure S4: 50. *[Figure S50] Fitted turnover curve obtained as graphical output by COPASI for experiment urethane_46. Vertical axis gives the concentration of urethane* ***16*** *in mol L⁻¹, horizontal axis gives the time from 0 min to 700 min.*

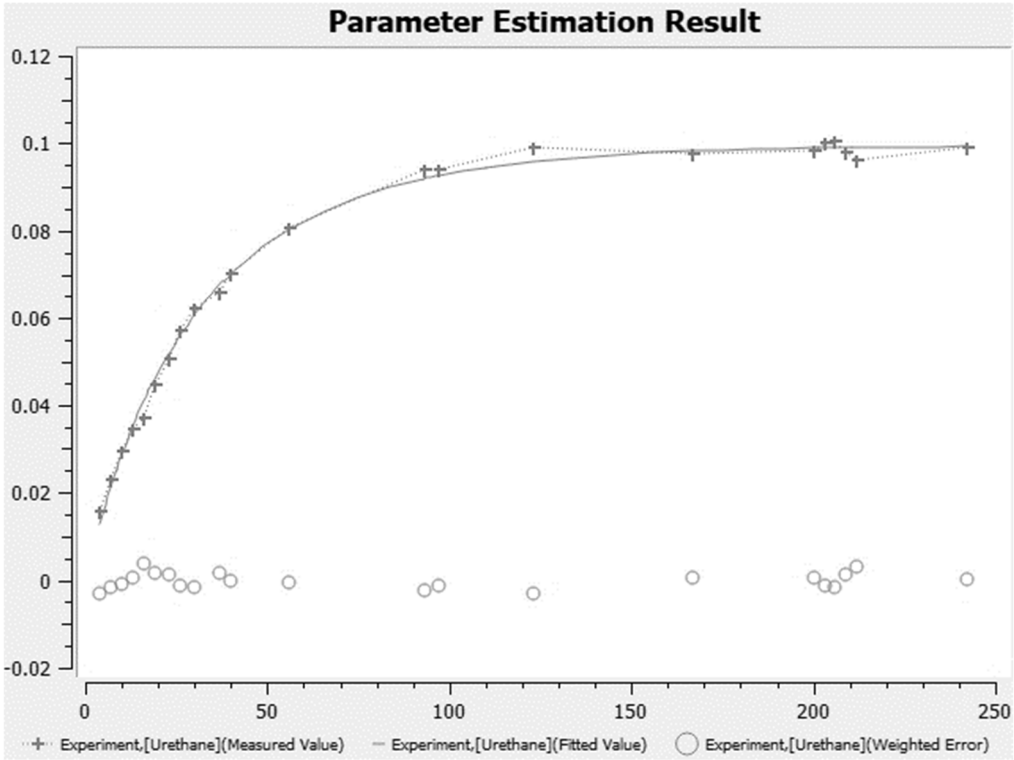

Figure S4: 51. *[Figure S51] Fitted turnover curve obtained as graphical output by COPASI for experiment urethane_47. Vertical axis gives the concentration of urethane* ***16*** *in mol L⁻¹, horizontal axis gives the time from 0 min to 250 min.*

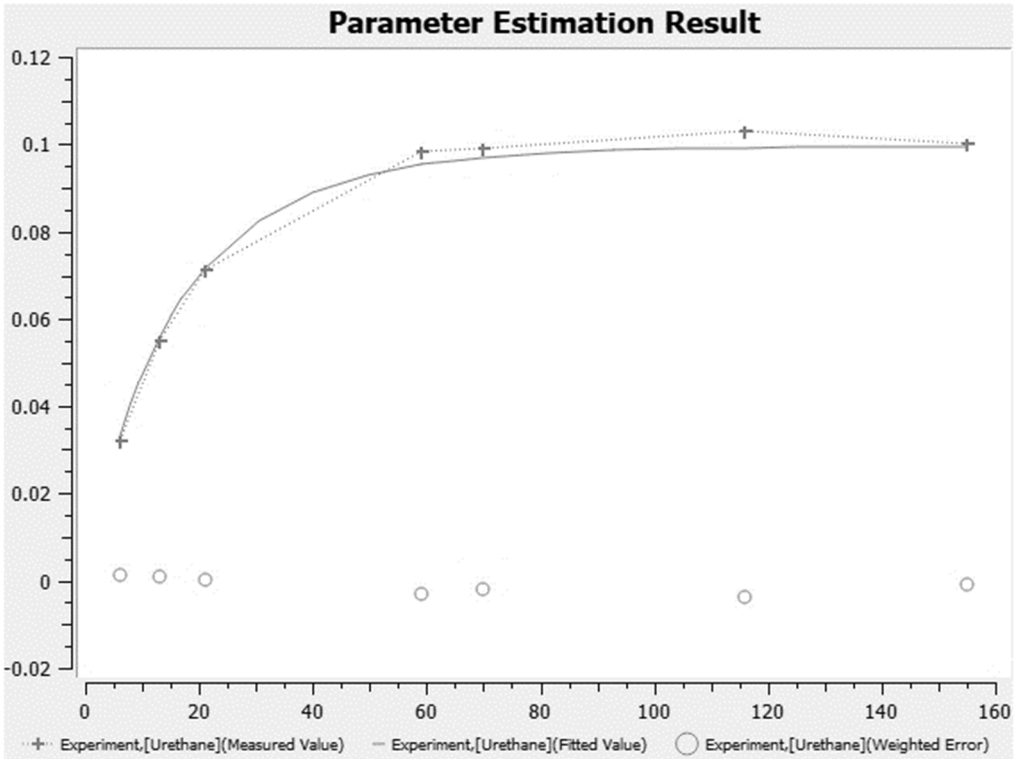

Figure S4: 52. *[Figure S52] Fitted turnover curve obtained as graphical output by COPASI for experiment urethane_48. Vertical axis gives the concentration of urethane* ***16*** *in mol L⁻¹, horizontal axis gives the time from 0 min to 160 min.*

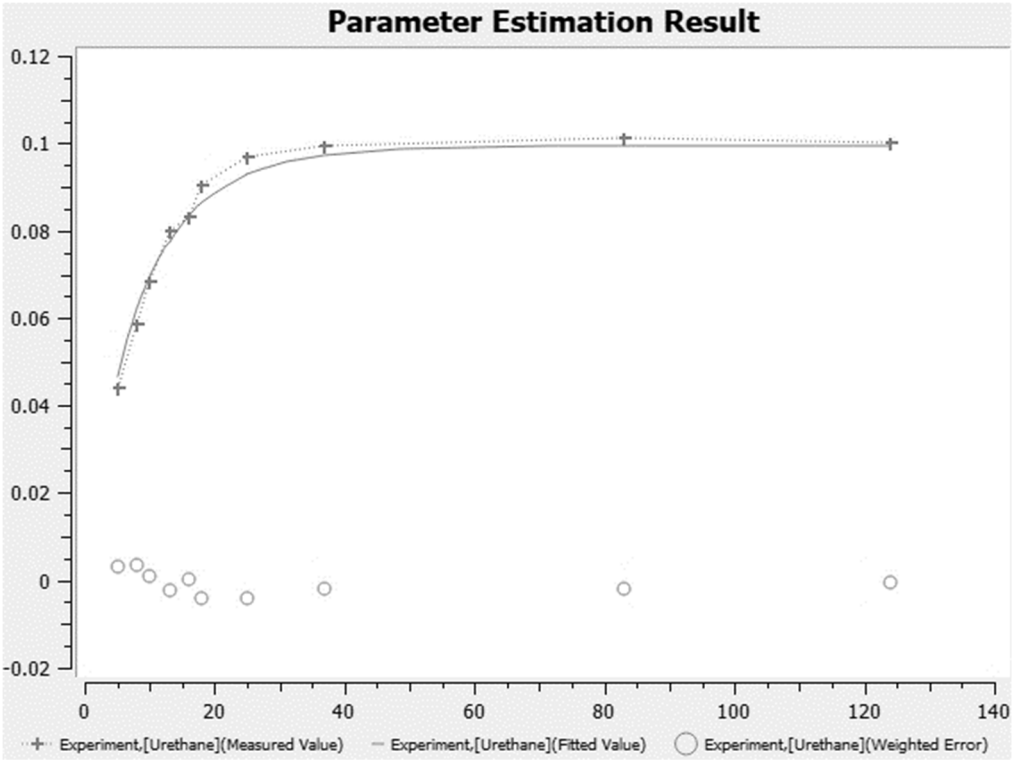

Figure S4: 53. *[Figure S53] Fitted turnover curve obtained as graphical output by COPASI for experiment urethane_49. Vertical axis gives the concentration of urethane* ***16*** *in mol L⁻¹, horizontal axis gives the time from 0 min to 140 min.*

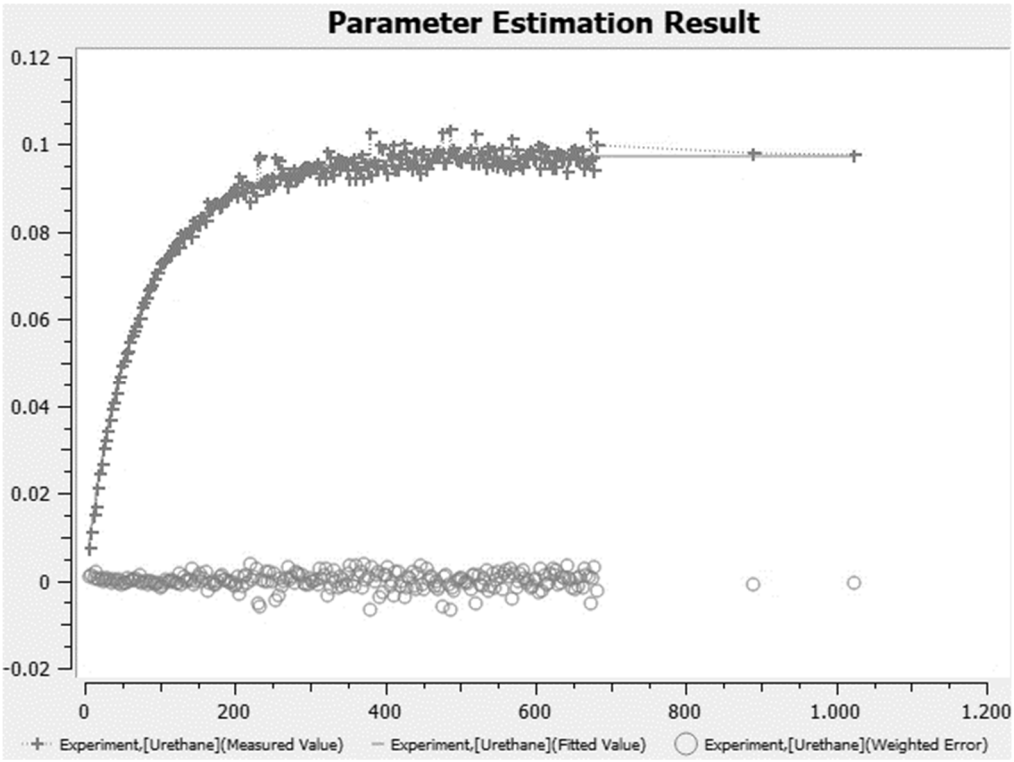

Figure S4: 54. *[Figure S54] Fitted turnover curve obtained as graphical output by COPASI for experiment urethane_50. Vertical axis gives the concentration of urethane* ***16*** *in mol L⁻¹, horizontal axis gives the time from 0 min to 1200 min.*

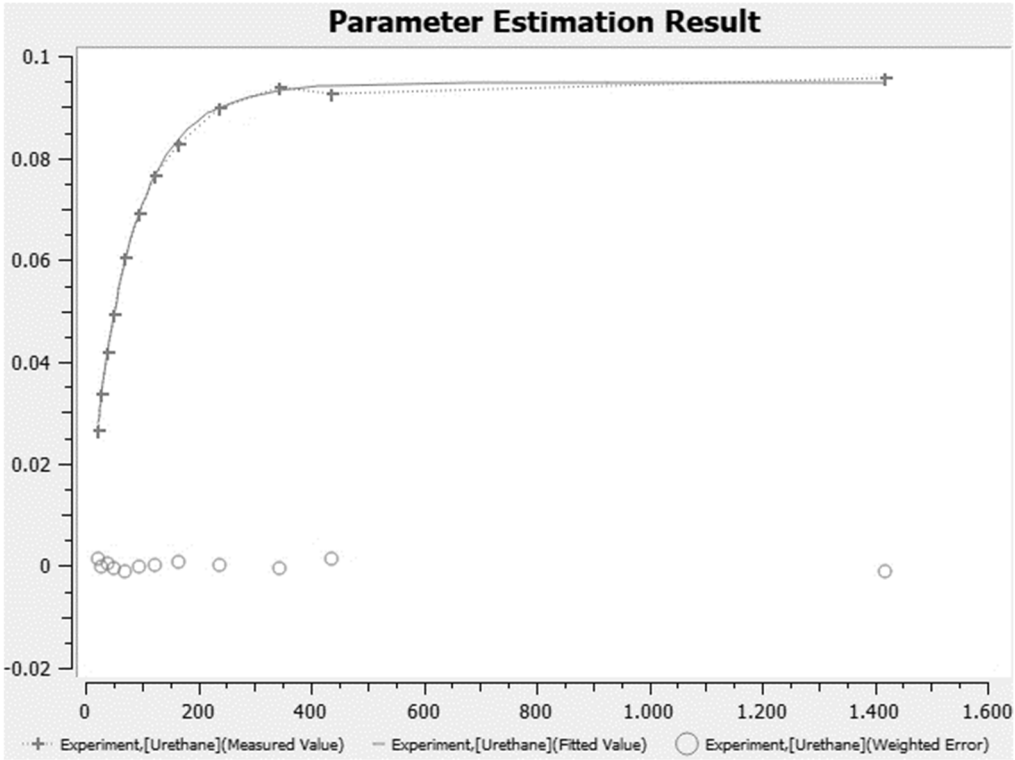

Figure S4: 55. *[Figure S55] Fitted turnover curve obtained as graphical output by COPASI for experiment urethane_51. Vertical axis gives the concentration of urethane* ***16*** *in mol L⁻¹, horizontal axis gives the time from 0 min to 1600 min.*

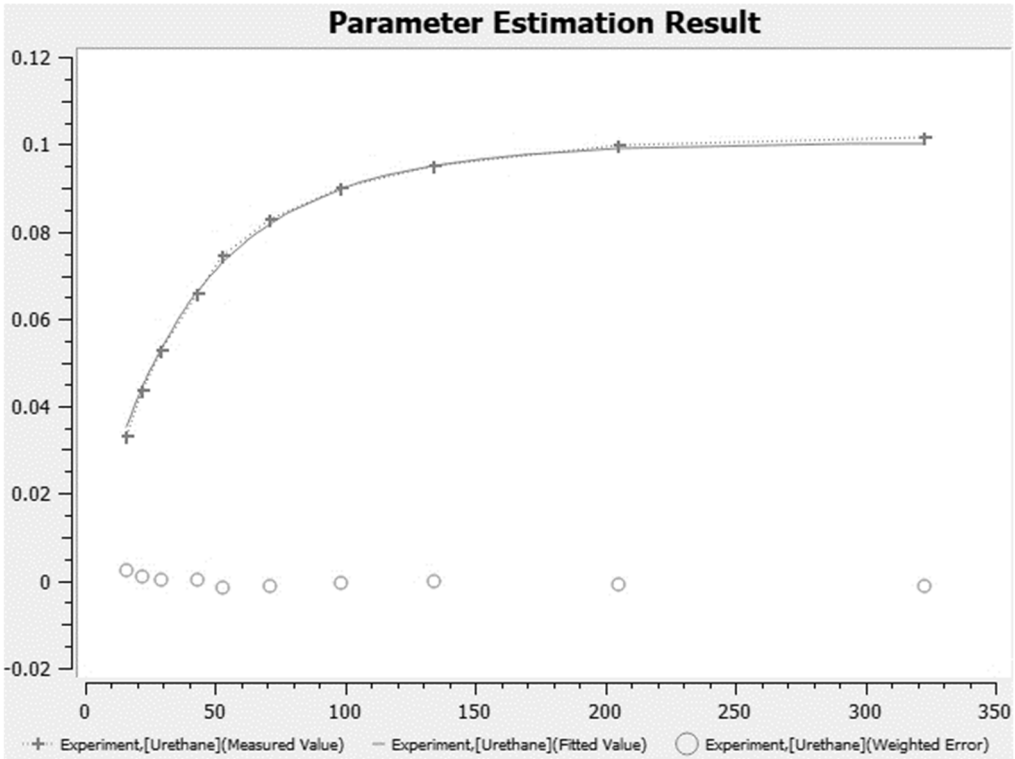

Figure S4: 56. *[Figure S56] Fitted turnover curve obtained as graphical output by COPASI for experiment urethane_52. Vertical axis gives the concentration of urethane* ***16*** *in mol L⁻¹, horizontal axis gives the time from 0 min to 350 min.*

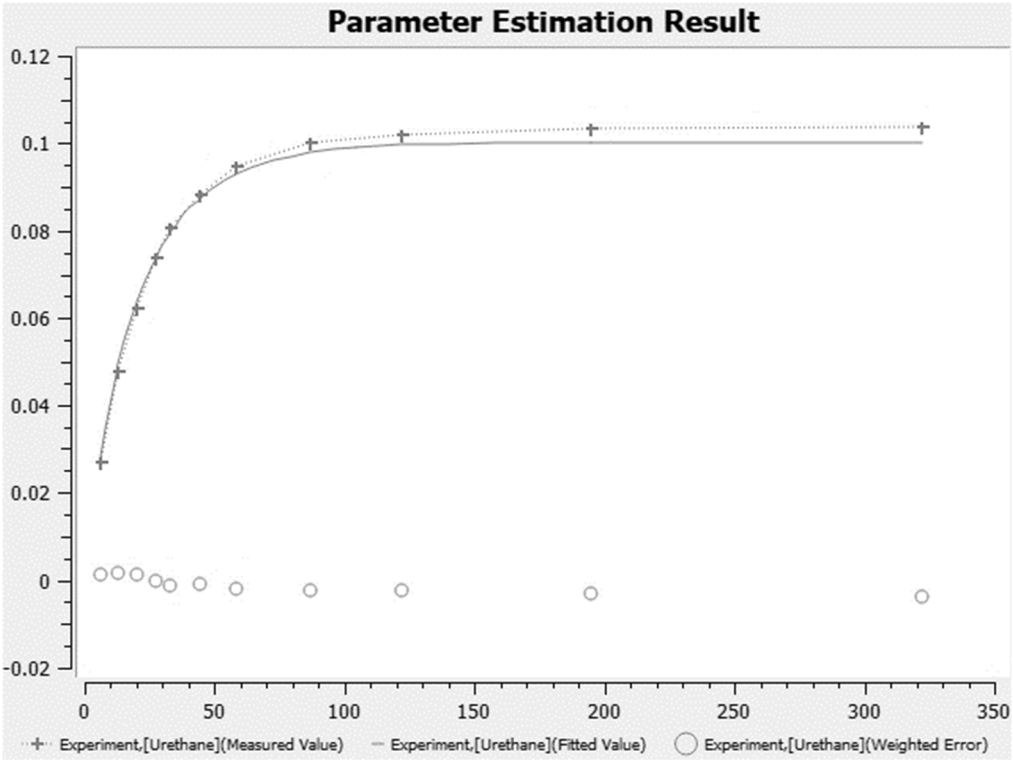

Figure S4: 57. *[Figure S57] Fitted turnover curve obtained as graphical output by COPASI for experiment urethane_53. Vertical axis gives the concentration of urethane* ***16*** *in mol L⁻¹, horizontal axis gives the time from 0 min to 350 min.*

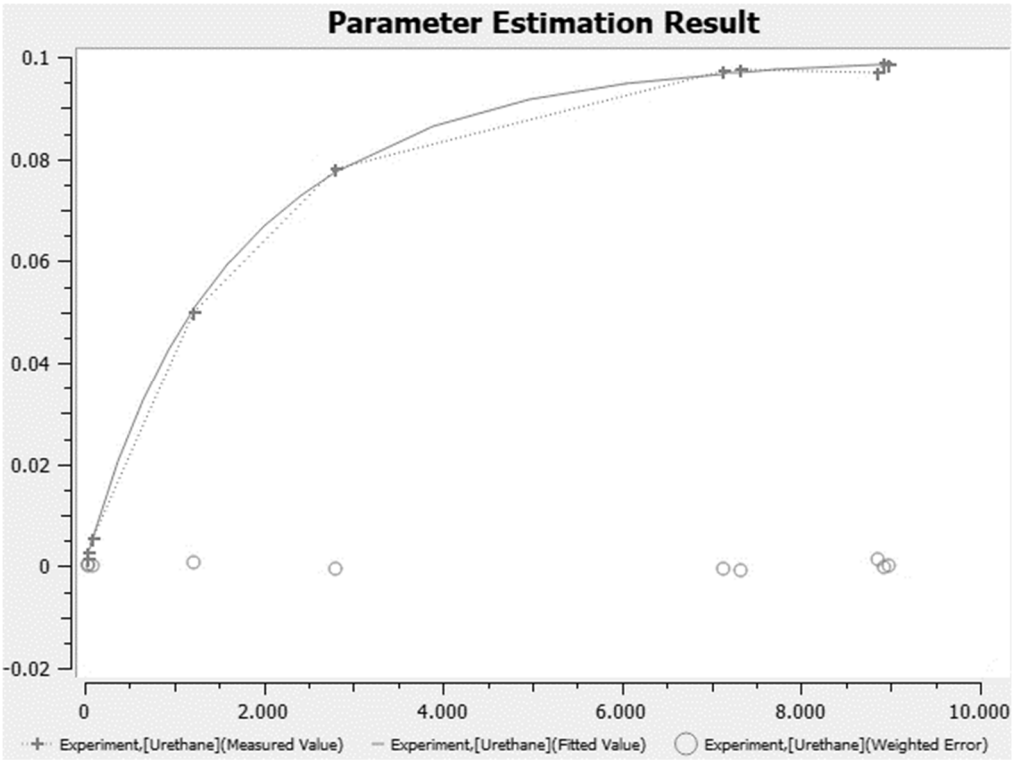

Figure S4: 58. *[Figure S58] Fitted turnover curve obtained as graphical output by COPASI for experiment urethane_54. Vertical axis gives the concentration of urethane* ***16*** *in mol L⁻¹, horizontal axis gives the time from 0 min to 10000 min.*

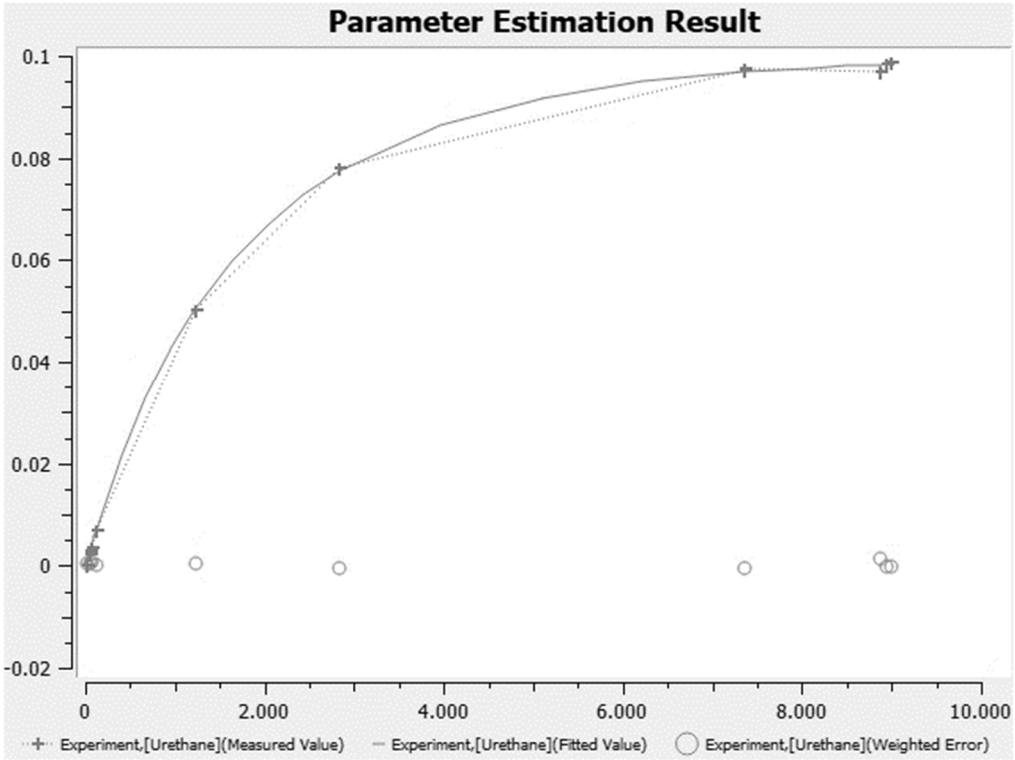

Figure S4: 59. *[Figure S59] Fitted turnover curve obtained as graphical output by COPASI for experiment urethane_55. Vertical axis gives the concentration of urethane* ***16*** *in mol L⁻¹, horizontal axis gives the time from 0 min to 10000 min.*

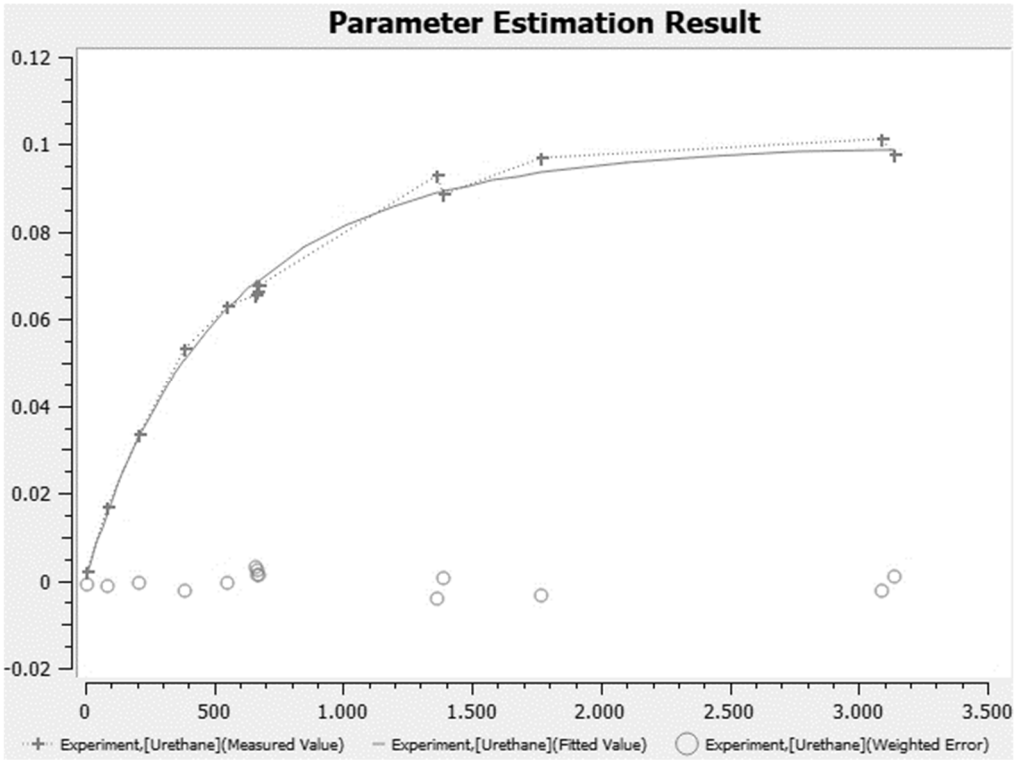

Figure S4: 60. *[Figure S60] Fitted turnover curve obtained as graphical output by COPASI for experiment urethane_56. Vertical axis gives the concentration of urethane* ***16*** *in mol L⁻¹, horizontal axis gives the time from 0 min to 3500 min.*

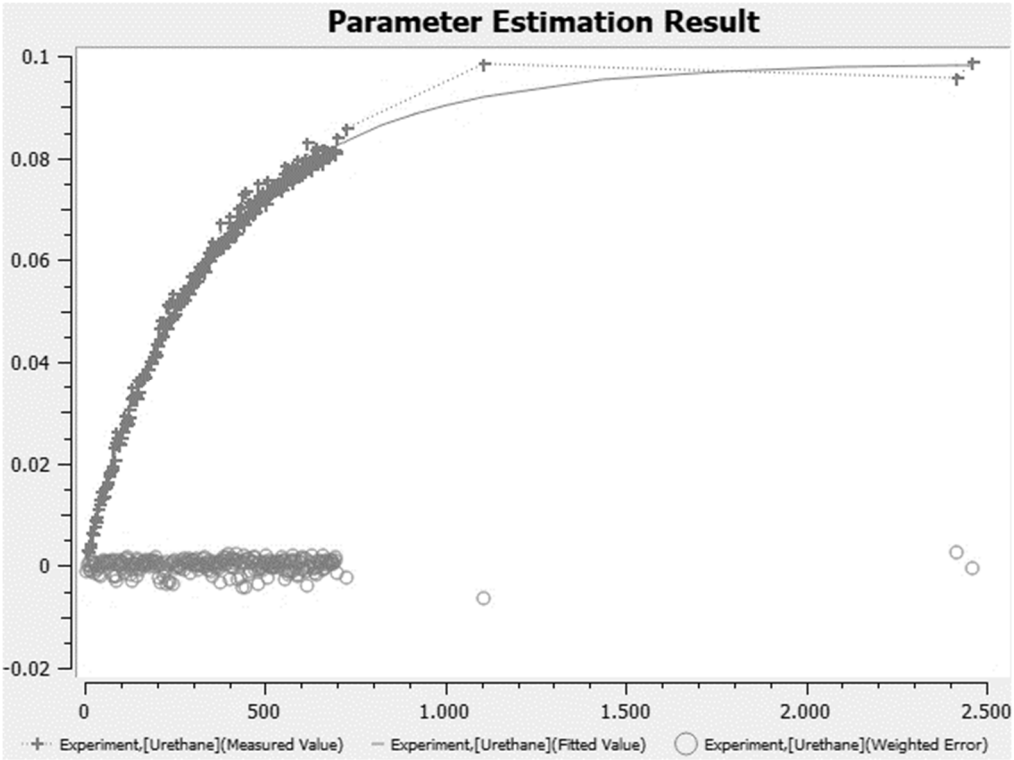

Figure S4: 61. *[Figure S61] Fitted turnover curve obtained as graphical output by COPASI for experiment urethane_57. Vertical axis gives the concentration of urethane* ***16*** *in mol L⁻¹, horizontal axis gives the time from 0 min to 2500 min.*

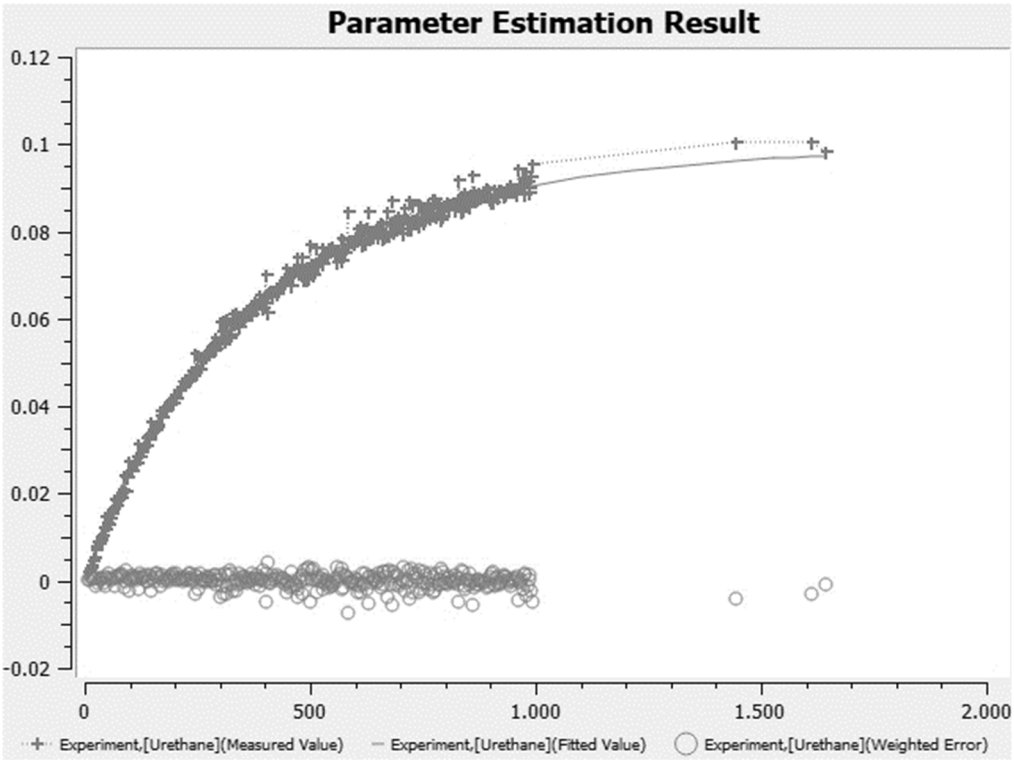

Figure S4: 62. *[Figure S62] Fitted turnover curve obtained as graphical output by COPASI for experiment urethane_58. Vertical axis gives the concentration of urethane* ***16*** *in mol L⁻¹, horizontal axis gives the time from 0 min to 2000 min.*

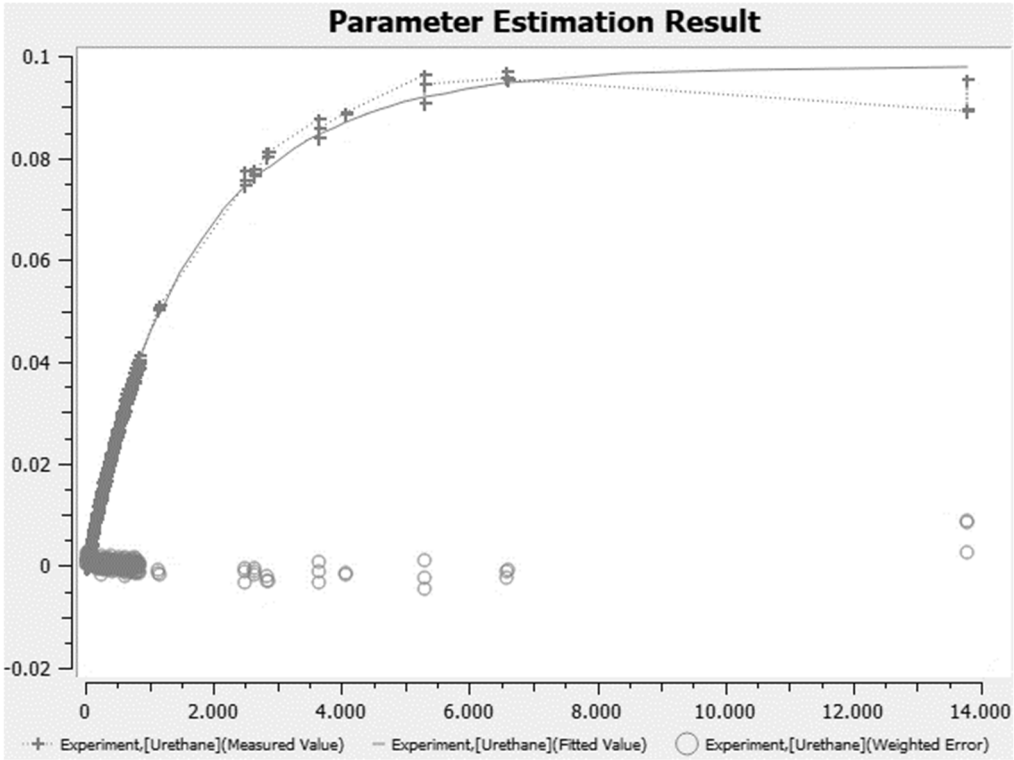

Figure S4: 63. *[Figure S63] Fitted turnover curve obtained as graphical output by COPASI for experiment urethane_59. Vertical axis gives the concentration of urethane* ***16*** *in mol L^{-1}, horizontal axis gives the time from 0 min to 14000 min.*

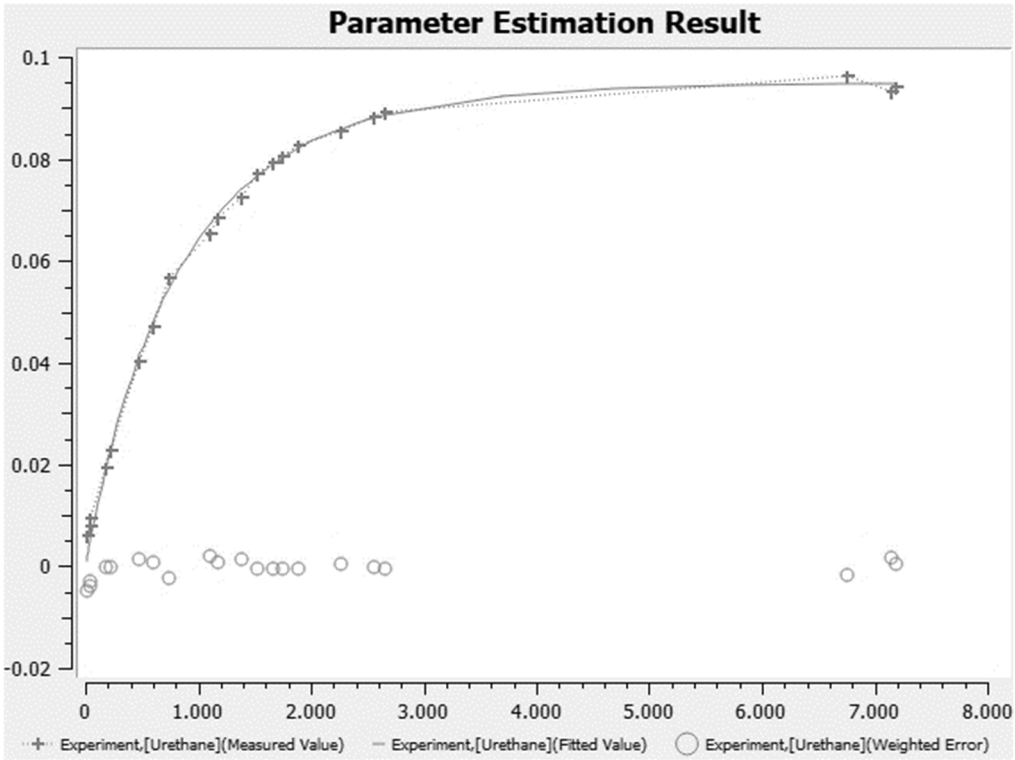

Figure S4: 64. *[Figure S64] Fitted turnover curve obtained as graphical output by COPASI for experiment urethane_60. Vertical axis gives the concentration of urethane* ***16*** *in mol L^{-1}, horizontal axis gives the time from 0 min to 8000 min.*

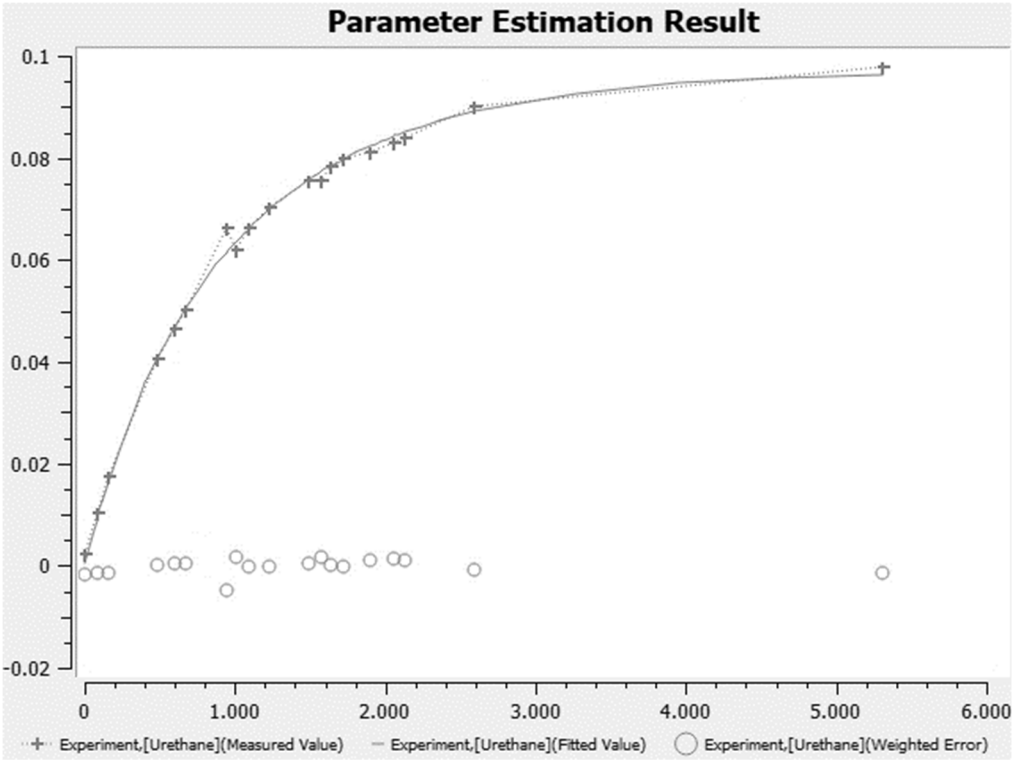

Figure S4: 65. *[Figure S65] Fitted turnover curve obtained as graphical output by COPASI for experiment urethane_61. Vertical axis gives the concentration of urethane* ***16*** *in mol L⁻¹, horizontal axis gives the time from 0 min to 6000 min.*

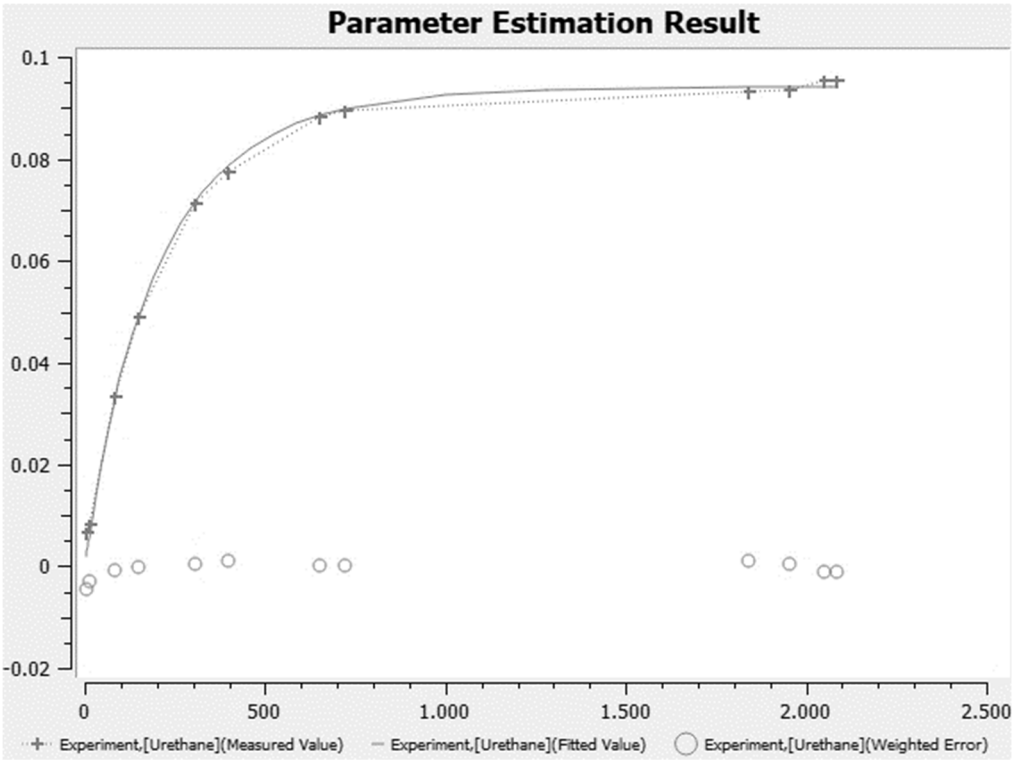

Figure S4: 66. *[Figure S66] Fitted turnover curve obtained as graphical output by COPASI for experiment urethane_62. Vertical axis gives the concentration of urethane* ***16*** *in mol L⁻¹, horizontal axis gives the time from 0 min to 2500 min.*

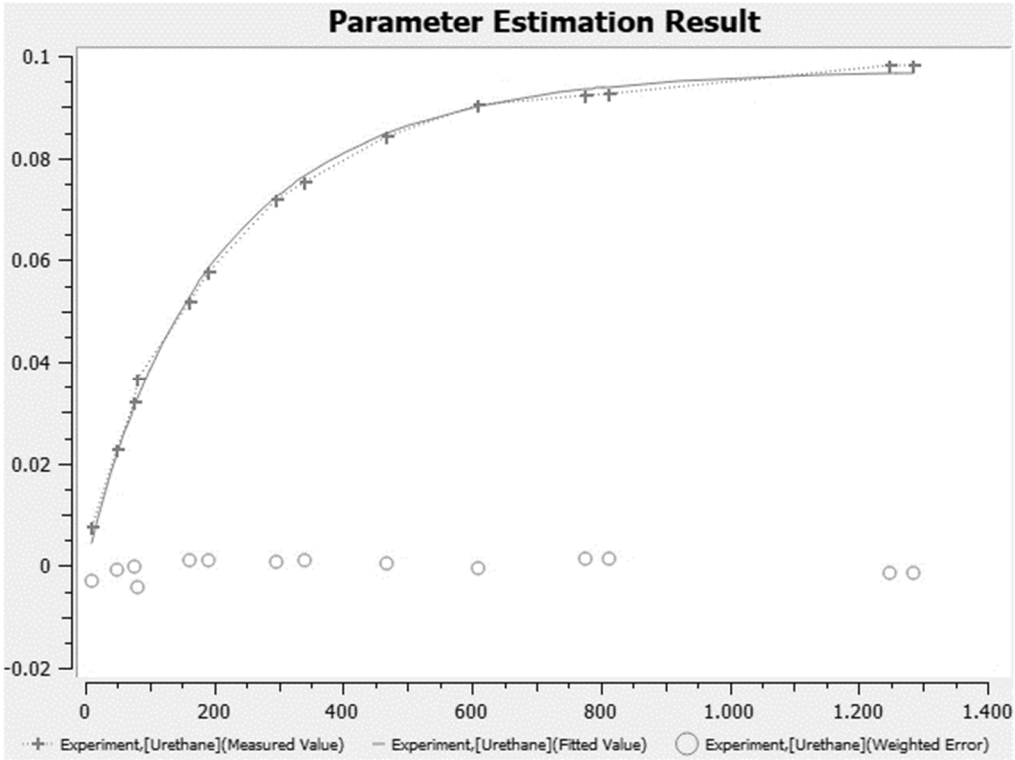

Figure S4: 67. *[Figure S67] Fitted turnover curve obtained as graphical output by COPASI for experiment urethane_63. Vertical axis gives the concentration of urethane* ***16*** *in mol L⁻¹, horizontal axis gives the time from 0 min to 1400 min.*

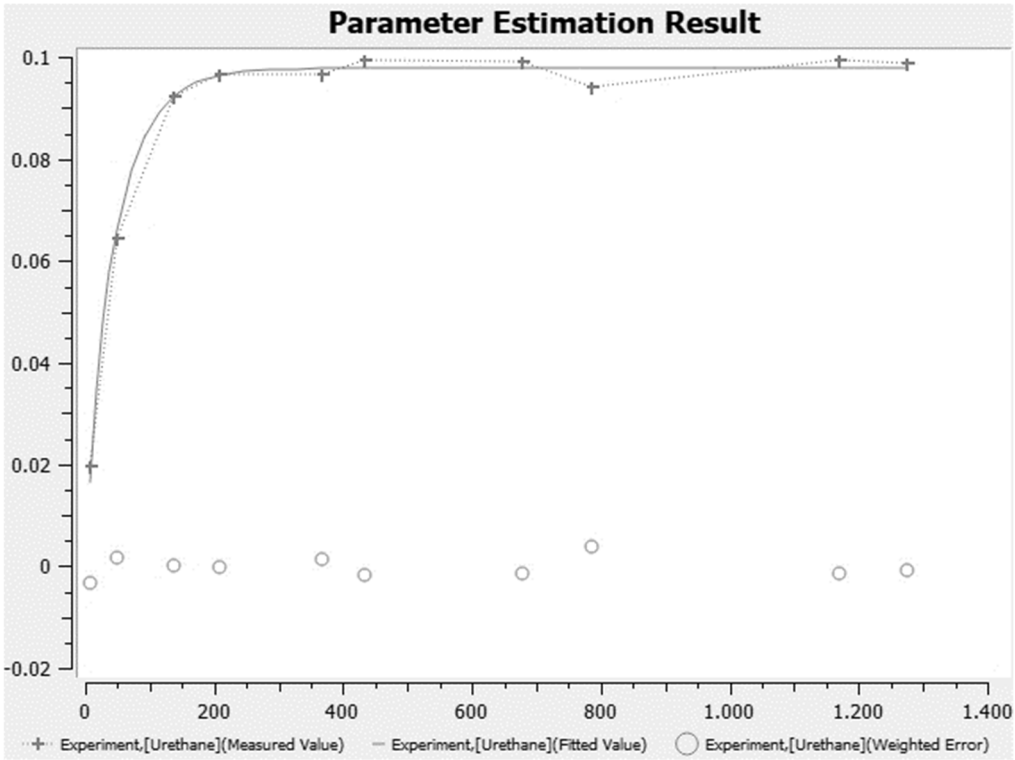

Figure S4: 68. *[Figure S68] Fitted turnover curve obtained as graphical output by COPASI for experiment urethane_64. Vertical axis gives the concentration of urethane* ***16*** *in mol L⁻¹, horizontal axis gives the time from 0 min to 1400 min.*

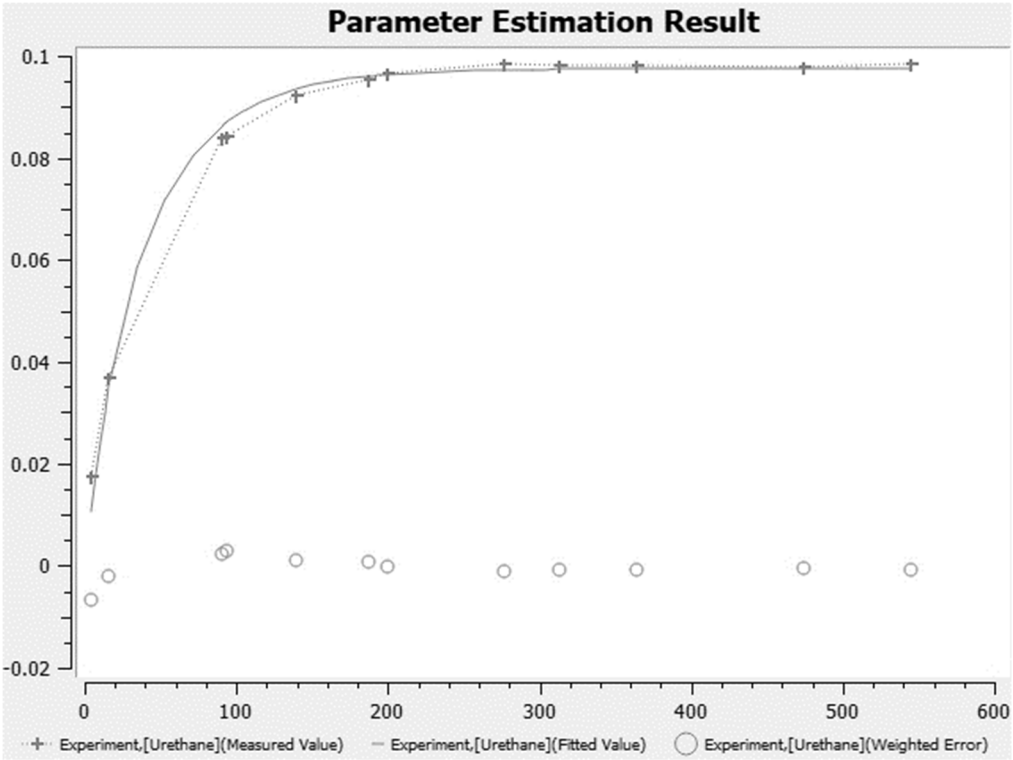

Figure S4: 69. *[Figure S69] Fitted turnover curve obtained as graphical output by COPASI for experiment urethane_65. Vertical axis gives the concentration of urethane* ***16*** *in mol L⁻¹, horizontal axis gives the time from 0 min to 600 min.*

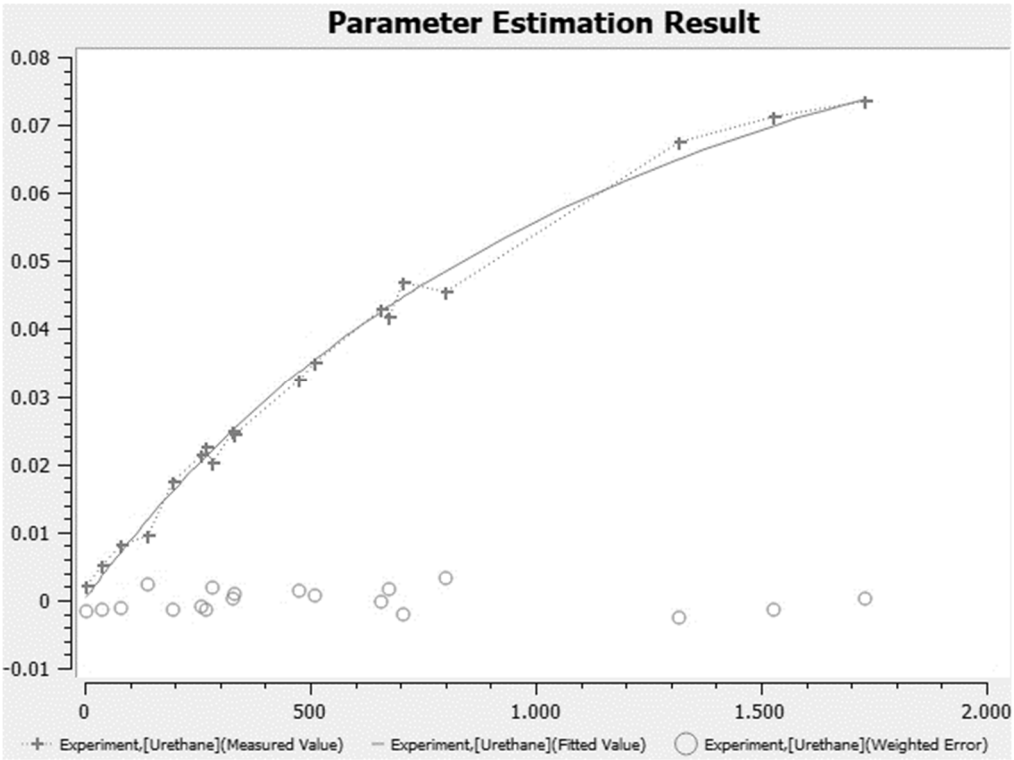

Figure S4: 70. *[Figure S70] Fitted turnover curve obtained as graphical output by COPASI for experiment urethane_66. Vertical axis gives the concentration of urethane* ***16*** *in mol L⁻¹, horizontal axis gives the time from 0 min to 2000 min.*

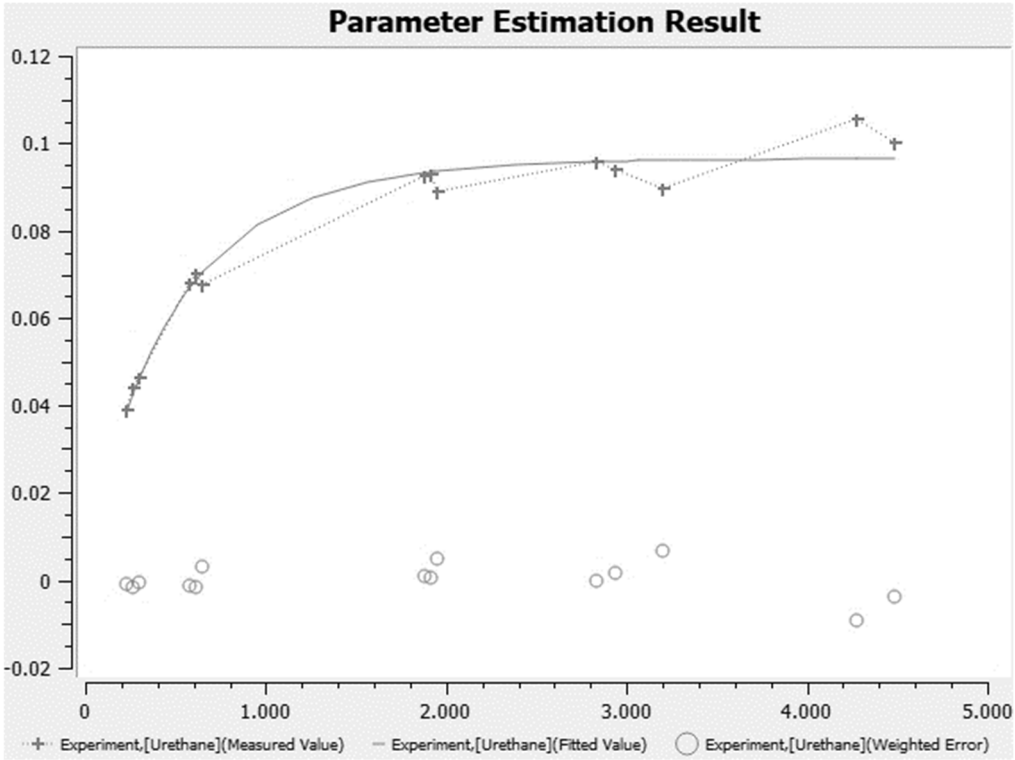

Figure S4: 71. *[Figure S71] Fitted turnover curve obtained as graphical output by COPASI for experiment urethane_67. Vertical axis gives the concentration of urethane* ***16*** *in mol L⁻¹, horizontal axis gives the time from 0 min to 5000 min.*

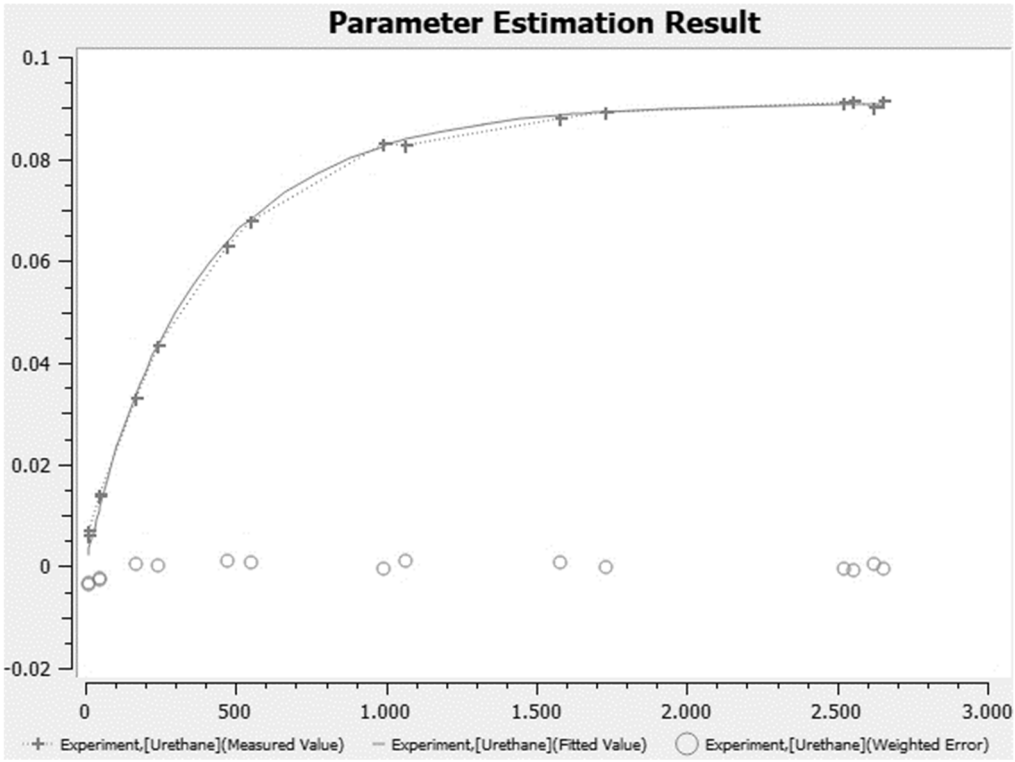

Figure S4: 72. *[Figure S72] Fitted turnover curve obtained as graphical output by COPASI for experiment urethane_68. Vertical axis gives the concentration of urethane* ***16*** *in mol L⁻¹, horizontal axis gives the time from 0 min to 3000 min.*

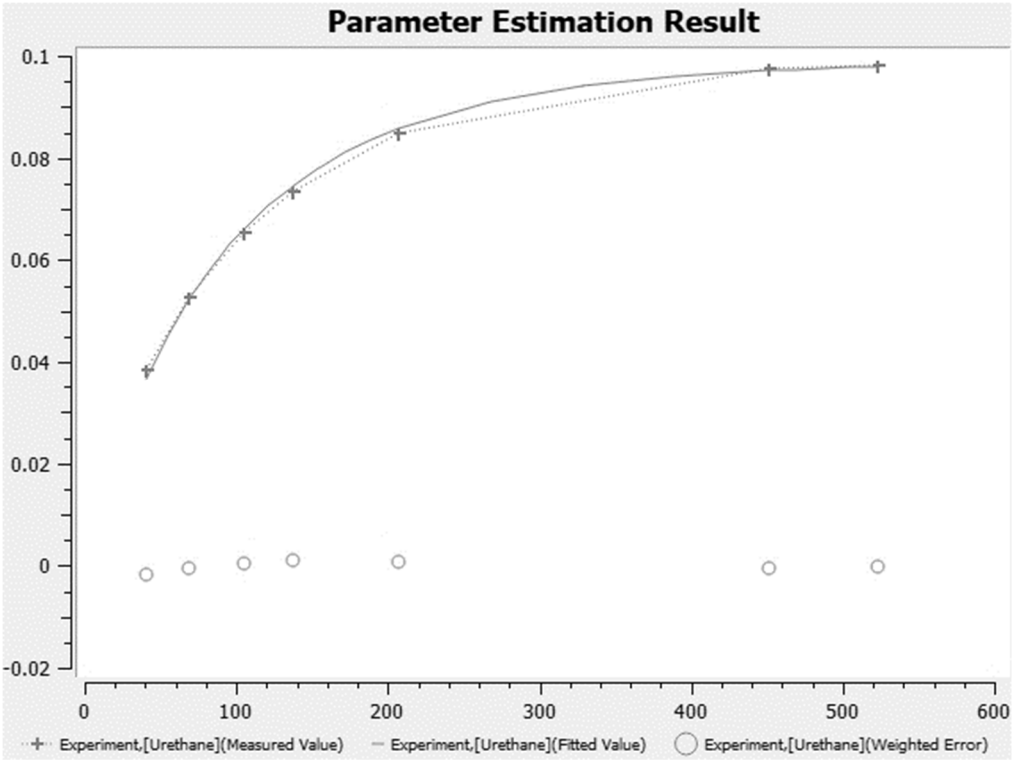

Figure S4: 73. *[Figure S73] Fitted turnover curve obtained as graphical output by COPASI for experiment urethane_69. Vertical axis gives the concentration of urethane* ***16*** *in mol L⁻¹, horizontal axis gives the time from 0 min to 600 min.*

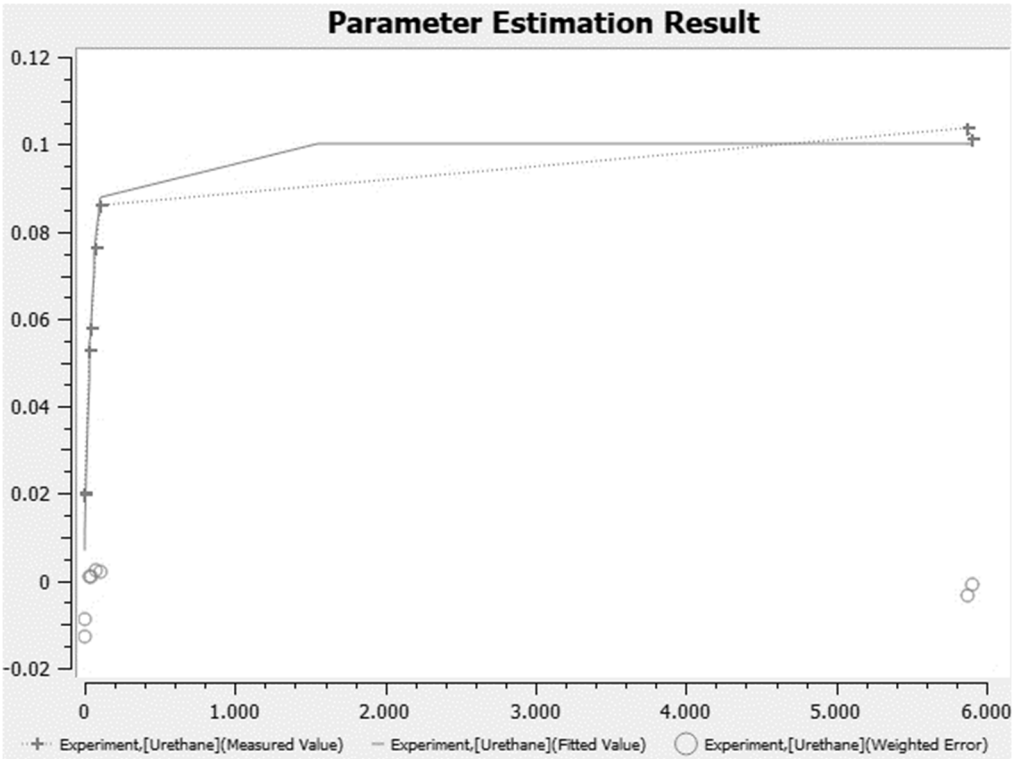

Figure S4: 74. [*Figure S74] Fitted turnover curve obtained as graphical output by COPASI for experiment urethane_70. Vertical axis gives the concentration of urethane* ***16*** *in mol L⁻¹, horizontal axis gives the time from 0 min to 6000 min.*

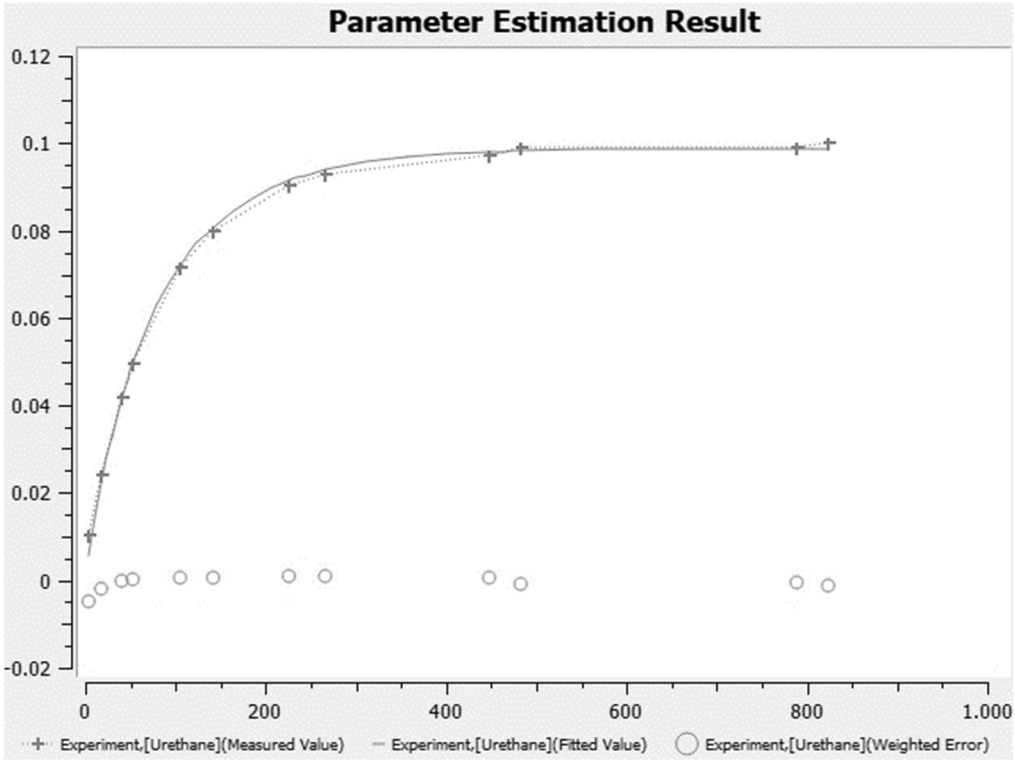

Figure S4: 75. *[Figure S75] Fitted turnover curve obtained as graphical output by COPASI for experiment urethane_71. Vertical axis gives the concentration of urethane* ***16*** *in mol L⁻¹, horizontal axis gives the time from 0 min to 1000 min.*

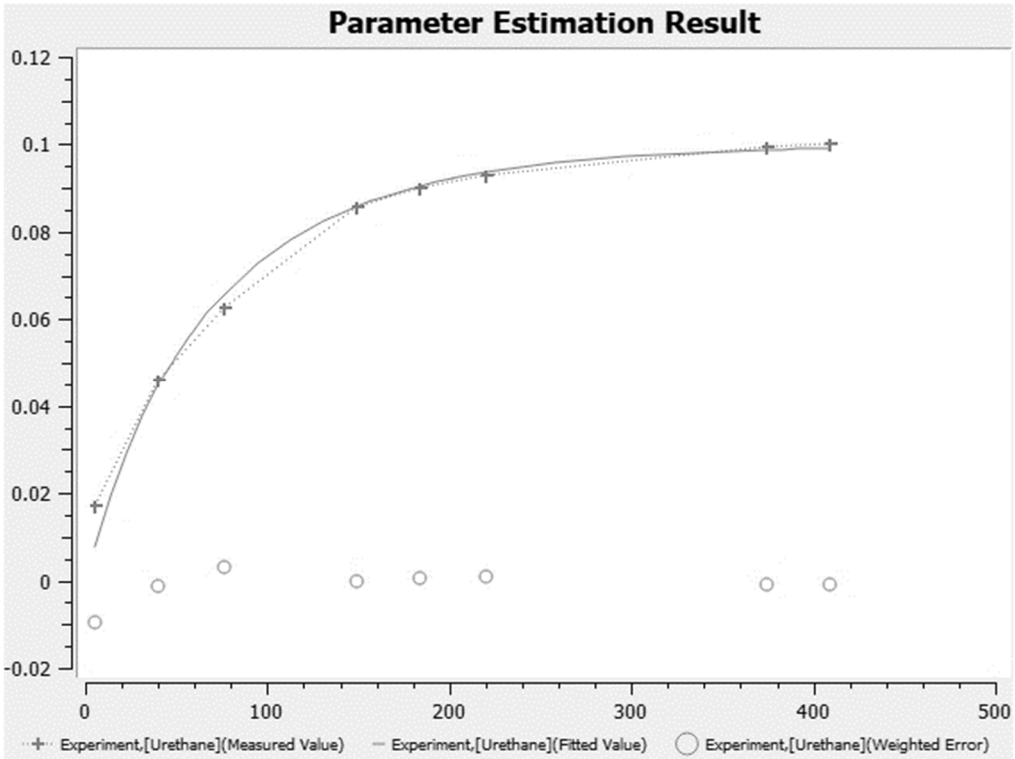

Figure S4: 76. *[Figure S76] Fitted turnover curve obtained as graphical output by COPASI for experiment urethane_72. Vertical axis gives the concentration of urethane* ***16*** *in mol L⁻¹, horizontal axis gives the time from 0 min to 500 min.*

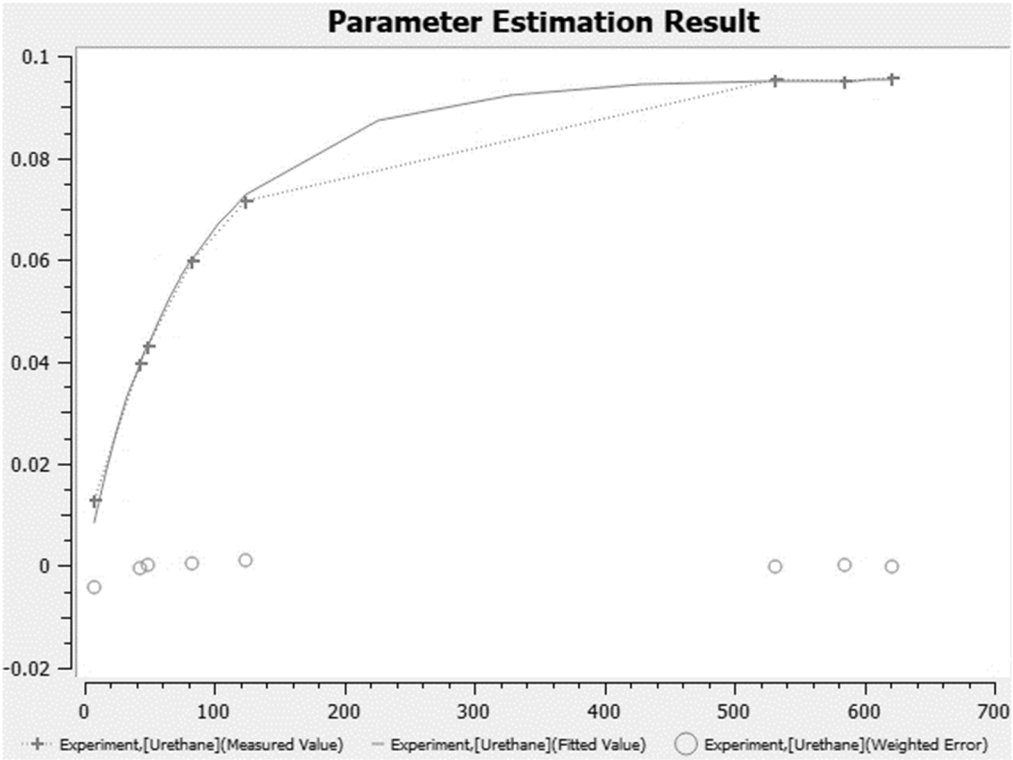

Figure S4: 77. *[Figure S77] Fitted turnover curve obtained as graphical output by COPASI for experiment urethane_73. Vertical axis gives the concentration of urethane* ***16*** *in mol L⁻¹, horizontal axis gives the time from 0 min to 700 min.*

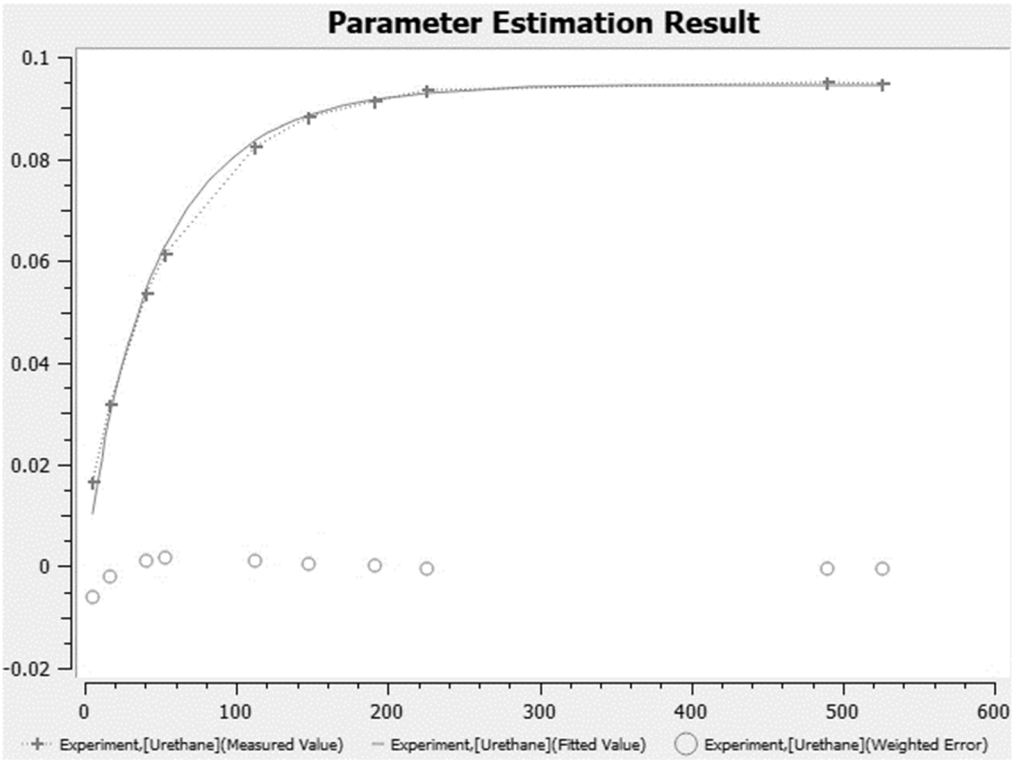

Figure S4: 78. *[Figure S78] Fitted turnover curve obtained as graphical output by COPASI for experiment urethane_74. Vertical axis gives the concentration of urethane* ***16*** *in mol L⁻¹, horizontal axis gives the time from 0 min to 600 min.*

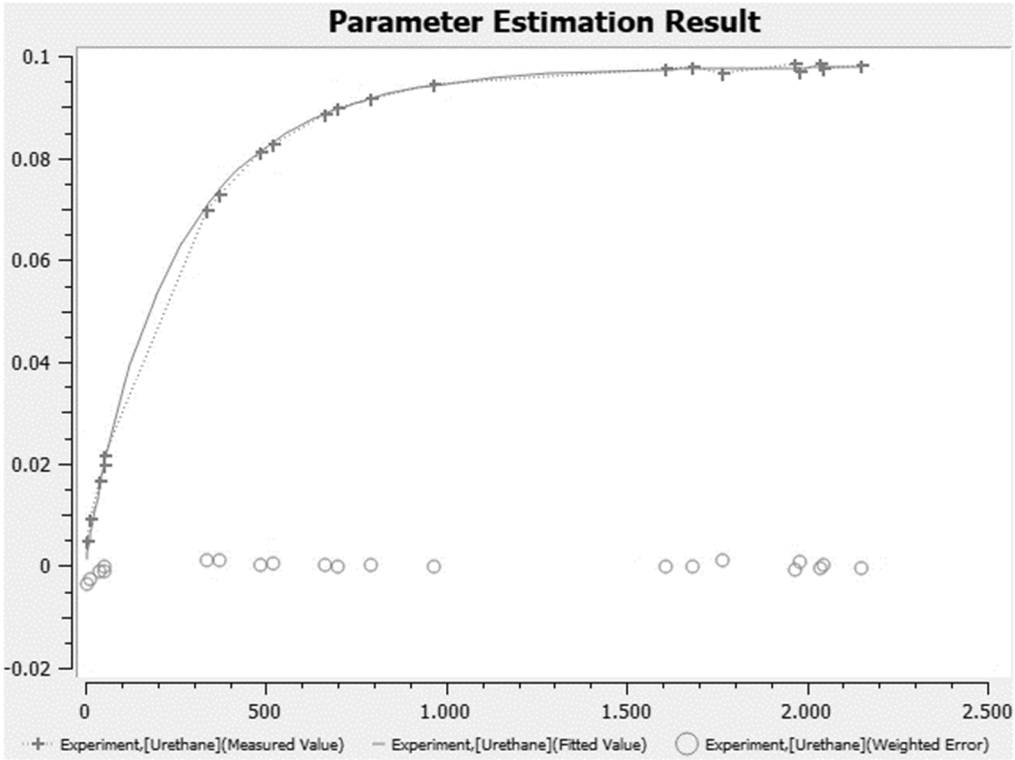

Figure S4: 79. *[Figure S79] Fitted turnover curve obtained as graphical output by COPASI for experiment urethane_75. Vertical axis gives the concentration of urethane* ***16*** *in mol L⁻¹, horizontal axis gives the time from 0 min to 2500 min.*

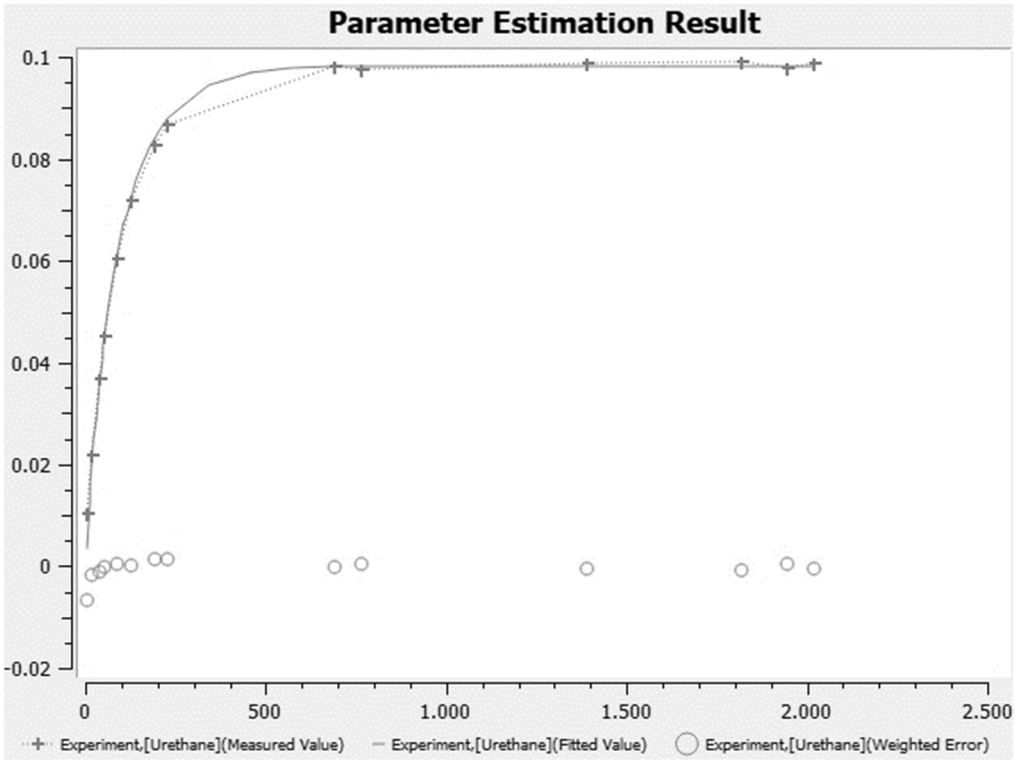

Figure S4: 80. *[Figure S80] Fitted turnover curve obtained as graphical output by COPASI for experiment urethane_76. Vertical axis gives the concentration of urethane* ***16*** *in mol L⁻¹, horizontal axis gives the time from 0 min to 2500 min.*

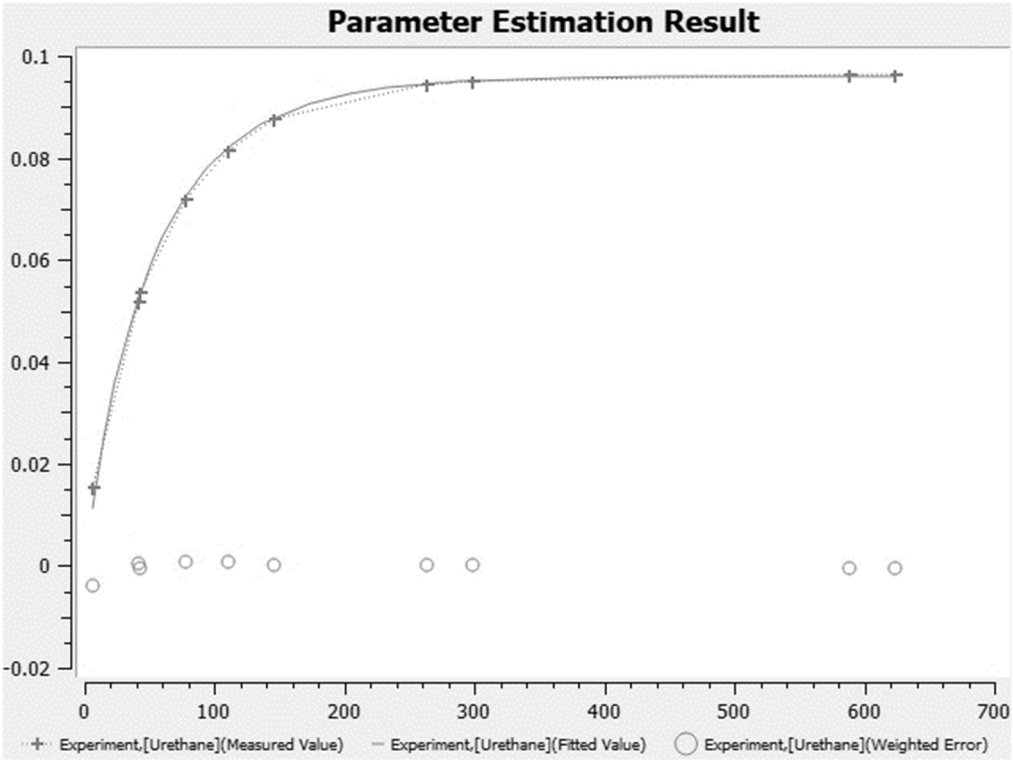

Figure S4: 81 *[Figure S81] Fitted turnover curve obtained as graphical output by COPASI for experiment urethane_77. Vertical axis gives the concentration of urethane* ***16*** *in mol L⁻¹, horizontal axis gives the time from 0 min to 700 min.*

4.1.2 Benchmark Reaction 2 – *Aza*-Morita-Baylis-Hillman Reaction

To show the efficiency of the investigated anionic pyridine catalysts, we decided to further test the ones that had performed best in the urethane synthesis. Therefore, we selected an electrophile that is considered very hard to activate, cyclohex-2-en-1-one **20** and decided to observe the corresponding *aza*-Morita-Baylis-Hillman (MBH) reaction with an activated imine. As reported by Shi (classical N- and P-bases), Ye (N-heterocyclic carbenes) and Zipse (bi- and tricyclic aminopyridines), this reaction is sluggish at best, taking at least 24 h to finish and shows no conversion at all without addition of an appropriate catalyst.[4] Since the $CDCl_3$ solvent signal is not clearly distinguishable in most of our reactions that are containing aromatic moieties, we chose to include 1,3,5-trimethoxybenzene as inert internal standard for the benchmark reaction shown in **Scheme S4: 3**. Benchmark reactions were done as described in the main part of this publication.

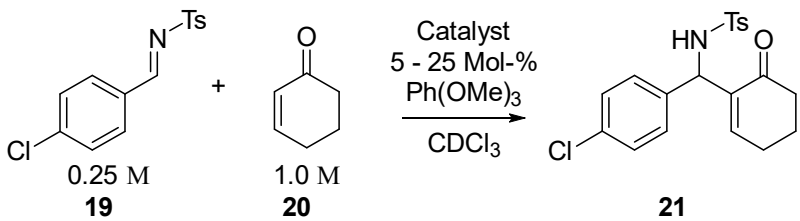

Scheme S4: 3. *[Scheme S3] aza-MBH reaction of tosyl imine* ***19*** *and cyclohex-2-en-1-one* ***20****.*

Data Processing

Since no other products than amine **21** were identified, we decided to measure conversion solely by the integrals of starting material **19** and product **21**.

Measured spectra were imported into MestReNova (Version 12.0.3) and superimposed. The following was done for the superimposed spectra in this order:

- Reference set ($Ph(OMe)_3$ set to 3.70 ppm)
- Automatic phase correction
- Automatic baseline correction (Whittaker Smoother)

Three areas containing the signals highlighted in **Figure S4: 82** were integrated:

- **Integral MBH1**: 9.05 ppm → 8.8 ppm = signal of tosyl imine **19** (CH) at 8.9 ppm
- **Integral MBH2**: 5.2 ppm → 4.95 ppm = signal of tosyl amine **21** at 5.1 ppm (CH)

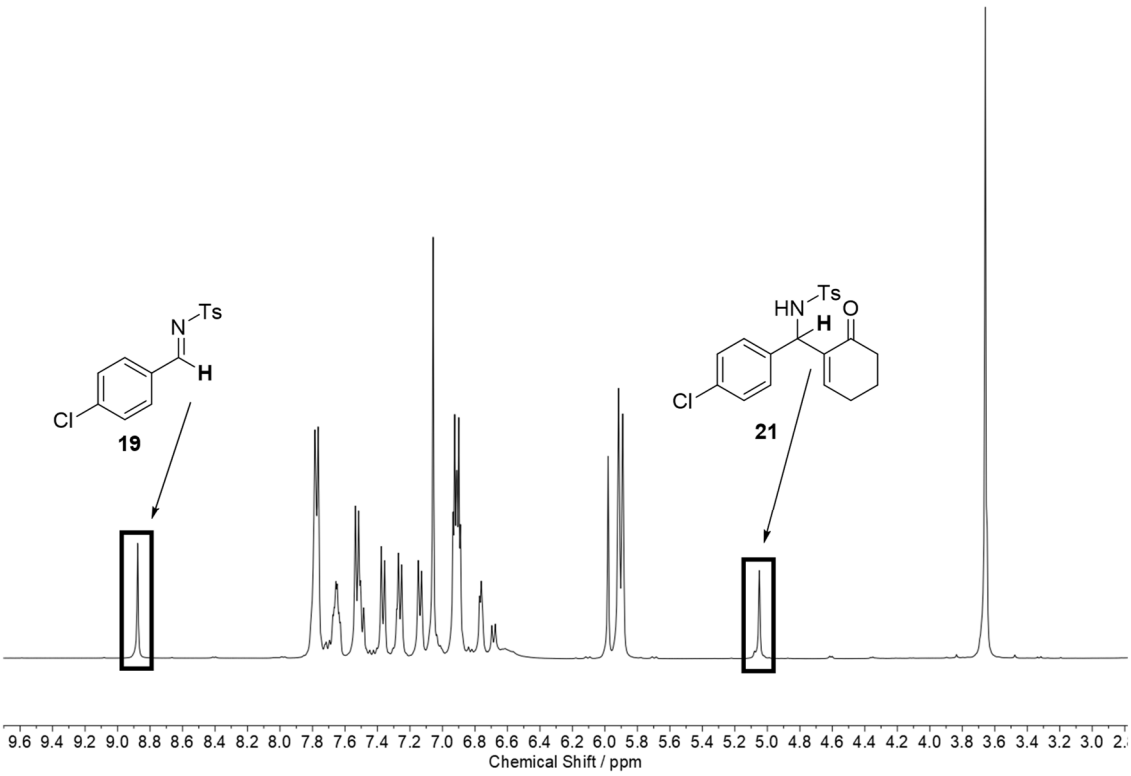

Figure S4: 82. *[Figure S82] Integrals of interest for the synthesis of tosyl amine **21** from tosyl imine **19** in a typical spectrum of the aza-MBH benchmark reaction.*

The values of these integrals were used to calculate turnovers according to Equation S4: 5:

$$T_{MBH}\ /\ \% = \frac{\boldsymbol{Integral\ MBH2}}{(\boldsymbol{Integral\ MBH2} + \boldsymbol{Integral\ MBH1})} \times 100 = \frac{\mathbf{21}}{(\mathbf{19} + \mathbf{21})} \times 100 \qquad \text{Eq. S4: 5}$$

The values obtained for turnover $\mathbf{T_{MBH}}$ were used for calculating concentrations of **21** at the time *t* based on initial concentrations c_0 as shown by Equation S4: 6:

$$c_t\ [\mathbf{21}]\ /\ \mathrm{mol\ L^{-1}} = \frac{c_0[\mathbf{19}] \times (100 - \boldsymbol{T}_{MBH(t)})}{100} \qquad \text{Eq. S4: 6}$$

Simulation of kinetic parameters was done using COPASI[3]. The obtained values for *t* and c_t[**21**] were imported into the program and the *Parameter Estimation* (default settings) option was used for the simplified model shown in **Scheme S4: 4**.

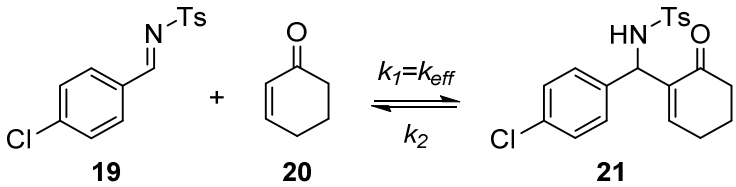

Scheme S4: 4. *[Scheme S4] Simplified model used for fitting the experimental data obtained for aza-MBH benchmark reactions in COPASI.*

The values obtained for k_{eff} were then used to compare the activity of different catalysts to each other as detailed in the next section.

Kinetic Data for the aza-MBH Benchmark Reaction

Table S4: 2 gives details for the aza-MBH benchmark reactions that were done in the course of this study while **Figure S4: 83** – **Figure S4: 99** show the fitted turnover curves that are obtained as graphical output by COPASI:

Table S4: 2. [Table S2] Details for the aza-MBH benchmark reactions.

Experiment	Catalyst	mol-% catalyst (compared to sulfonimine **19)**	c(Catalyst) / mol L^{-1}	k_{eff} / L mol^{-1} s^{-1}
mbh_1	**none**	0.0	---	---
mbh_2	**1a**	25.0	6.26E-02	1.51E-06
mbh_3	**1a**	25.0	6.27E-02	1.41E-06
mbh_4	**1c**	12.5	3.12E-02	1.51E-05
mbh_5	**1c**	12.5	3.12E-02	1.95E-05
mbh_6	**1c**	24.9	6.25E-02	2.97E-05
mbh_7	**1c**	24.9	6.25E-02	3.51E-05
mbh_8	**22**	25.0	6.25E-02	---
mbh_9	**6bc**	5.7	1.44E-02	6.73E-05
mbh_10	**6bc**	11.5	2.88E-02	1.60E-04
mbh_11	**6bc**	12.4	3.12E-02	1.62E-04
mbh_12	**6bc**	12.4	3.12E-02	2.02E-04
mbh_13	**6bc**	24.9	6.24E-02	3.42E-04
mbh_14	**6bc**	24.9	6.24E-02	3.69E-04
mbh_15	**6cg**	5.0	1.25E-02	8.53E-05
mbh_16	**6cg**	12.5	3.13E-02	2.49E-04
mbh_17	**6cg**	25.1	6.27E-02	4.81E-04

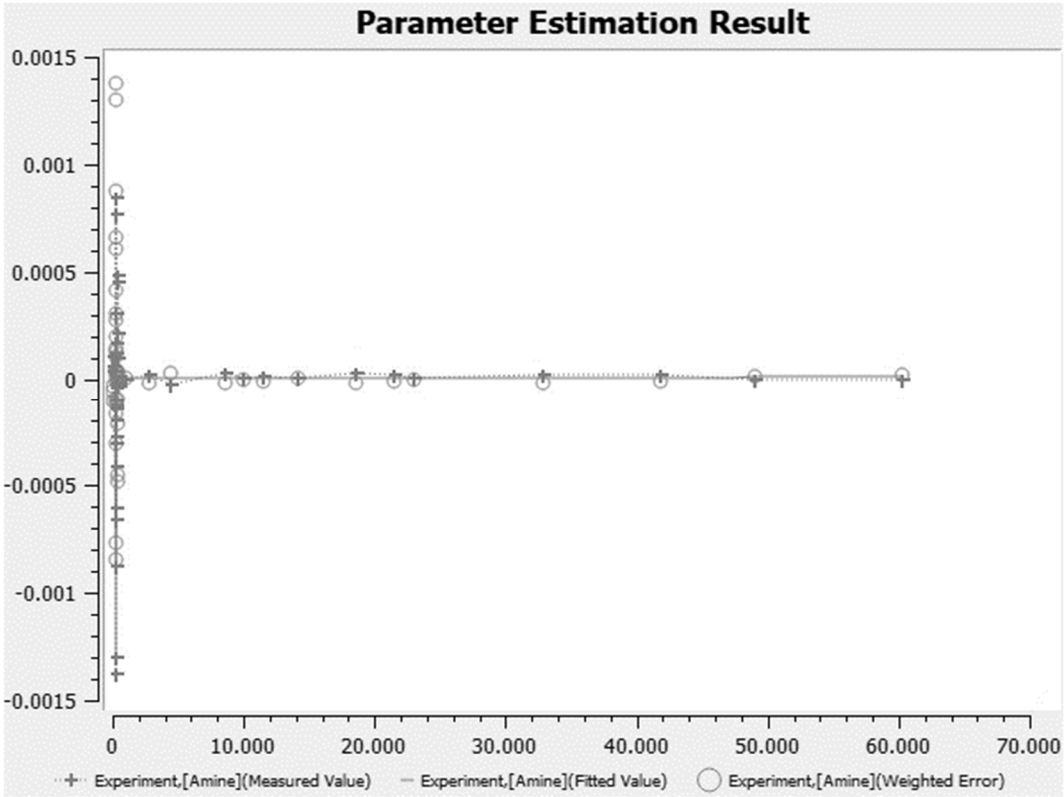

Figure S4: 83. *[Figure S83] Fitted turnover curve obtained as graphical output by COPASI for experiment mbh_01. Vertical axis gives the concentration of amine* ***21*** *in mol L⁻¹, horizontal axis gives the time from 0 min to 70000 min.*

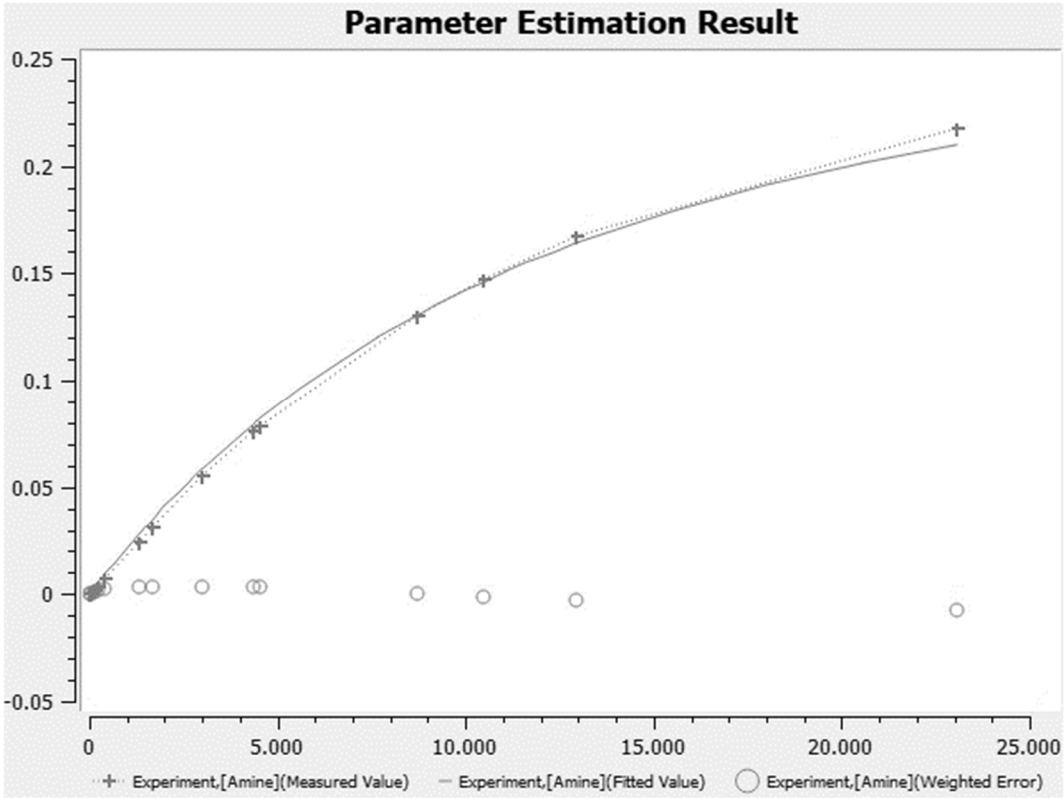

Figure S4: 84. *[Figure S84] Fitted turnover curve obtained as graphical output by COPASI for experiment mbh_02. Vertical axis gives the concentration of amine* ***21*** *in mol L⁻¹, horizontal axis gives the time from 0 min to 25000 min.*

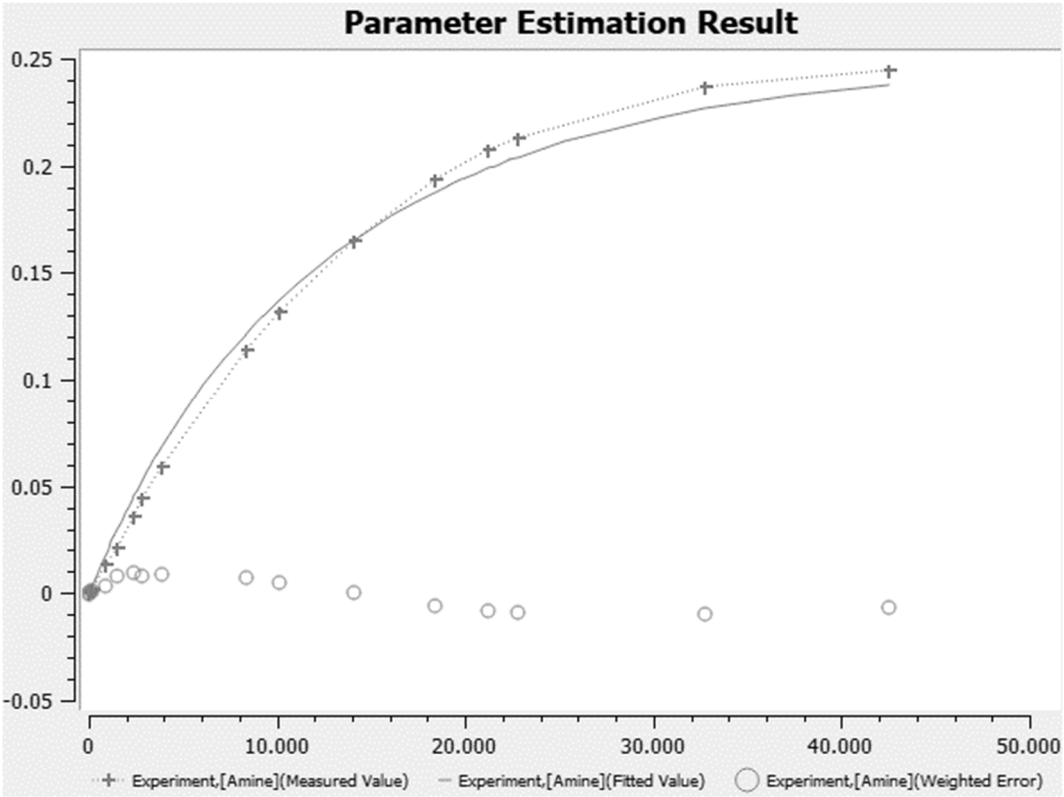

Figure S4: 85. *[Figure S85] Fitted turnover curve obtained as graphical output by COPASI for experiment mbh_03. Vertical axis gives the concentration of amine* ***21*** *in mol L^{-1}, horizontal axis gives the time from 0 min to 50000 min.*

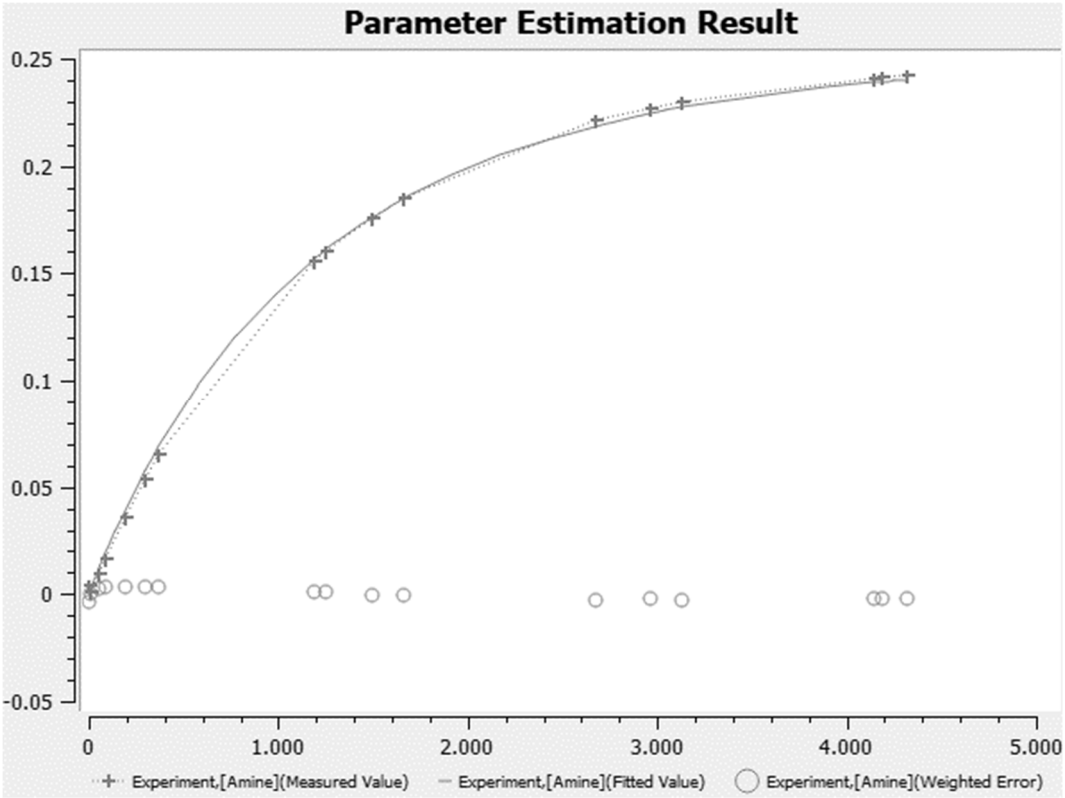

Figure S4: 86. *[Figure S86] Fitted turnover curve obtained as graphical output by COPASI for experiment mbh_04. Vertical axis gives the concentration of amine* ***21*** *in mol L^{-1}, horizontal axis gives the time from 0 min to 5000 min.*

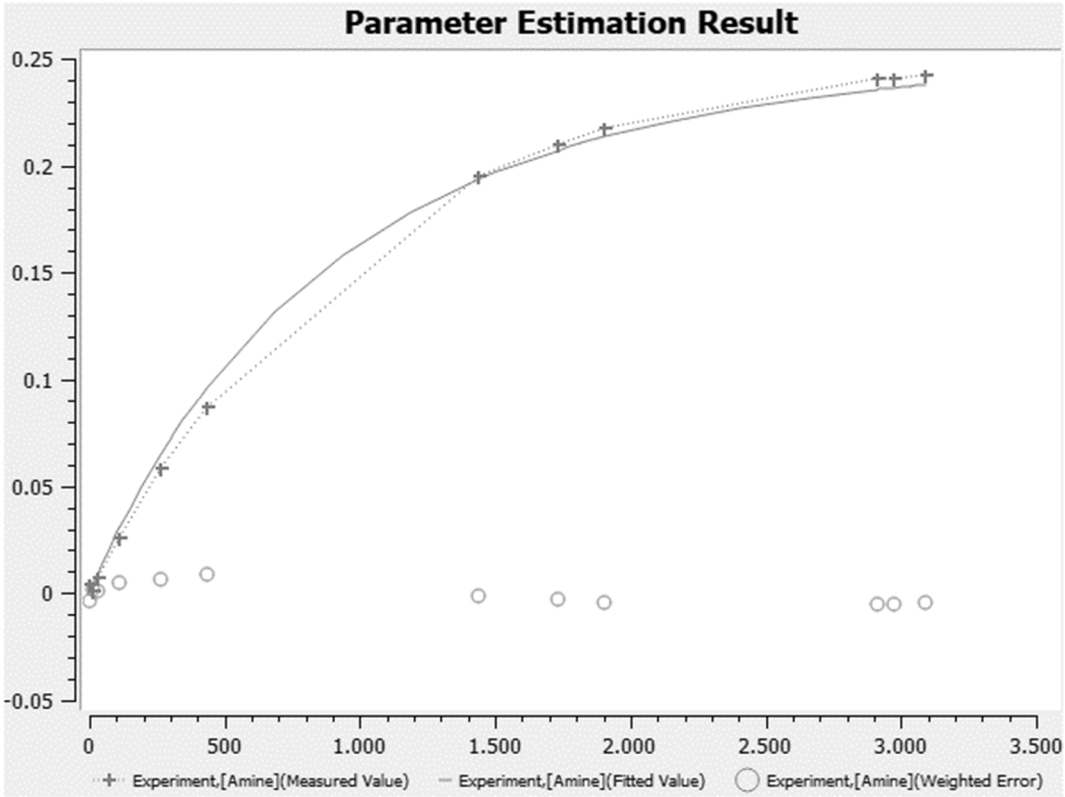

Figure S4: 87. *[Figure S87] Fitted turnover curve obtained as graphical output by COPASI for experiment mbh_05. Vertical axis gives the concentration of amine* ***21*** *in mol L⁻¹, horizontal axis gives the time from 0 min to 3500 min.*

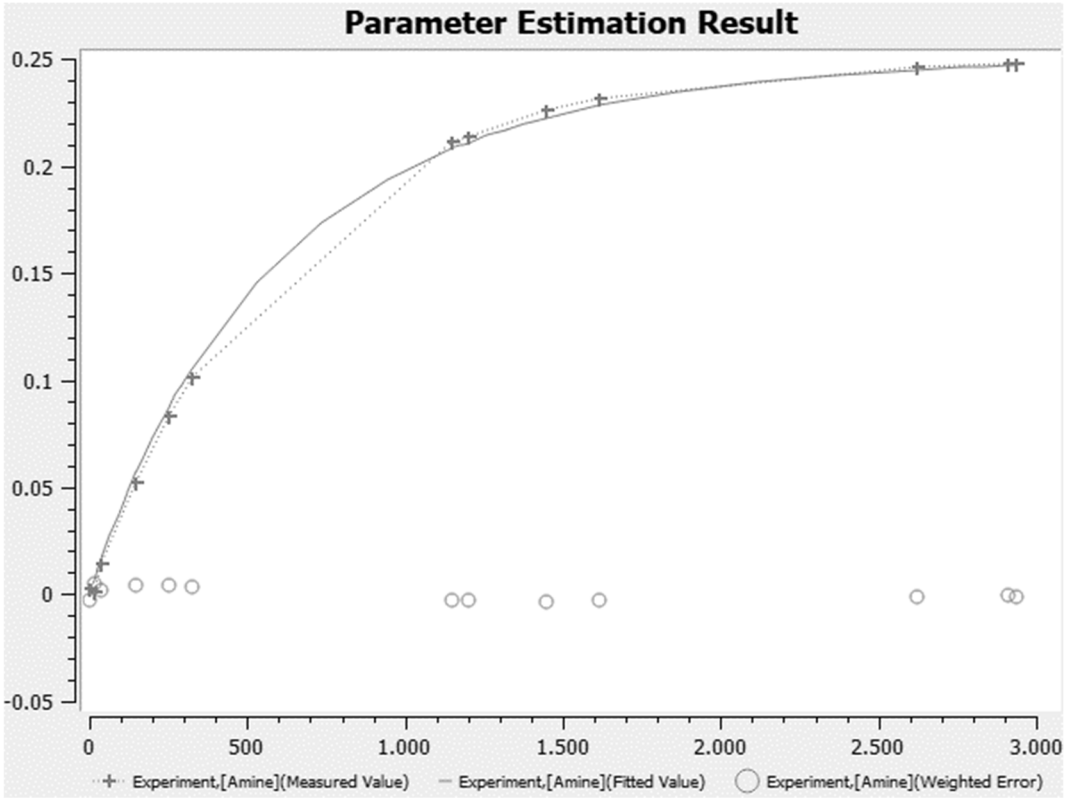

Figure S4: 88. *[Figure S88] Fitted turnover curve obtained as graphical output by COPASI for experiment mbh_06. Vertical axis gives the concentration of amine* ***21*** *in mol L⁻¹, horizontal axis gives the time from 0 min to 3000 min.*

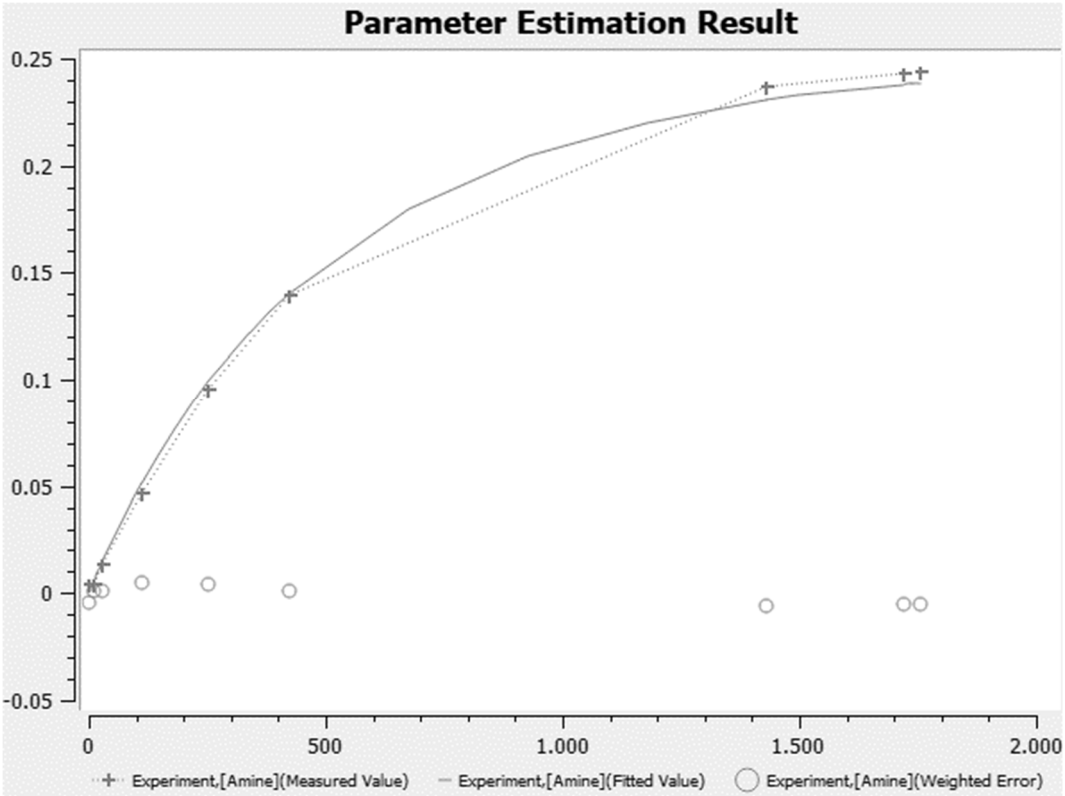

Figure S4: 89. *[Figure S89] Fitted turnover curve obtained as graphical output by COPASI for experiment mbh_07. Vertical axis gives the concentration of amine* ***21*** *in mol L⁻¹, horizontal axis gives the time from 0 min to 2000 min.*

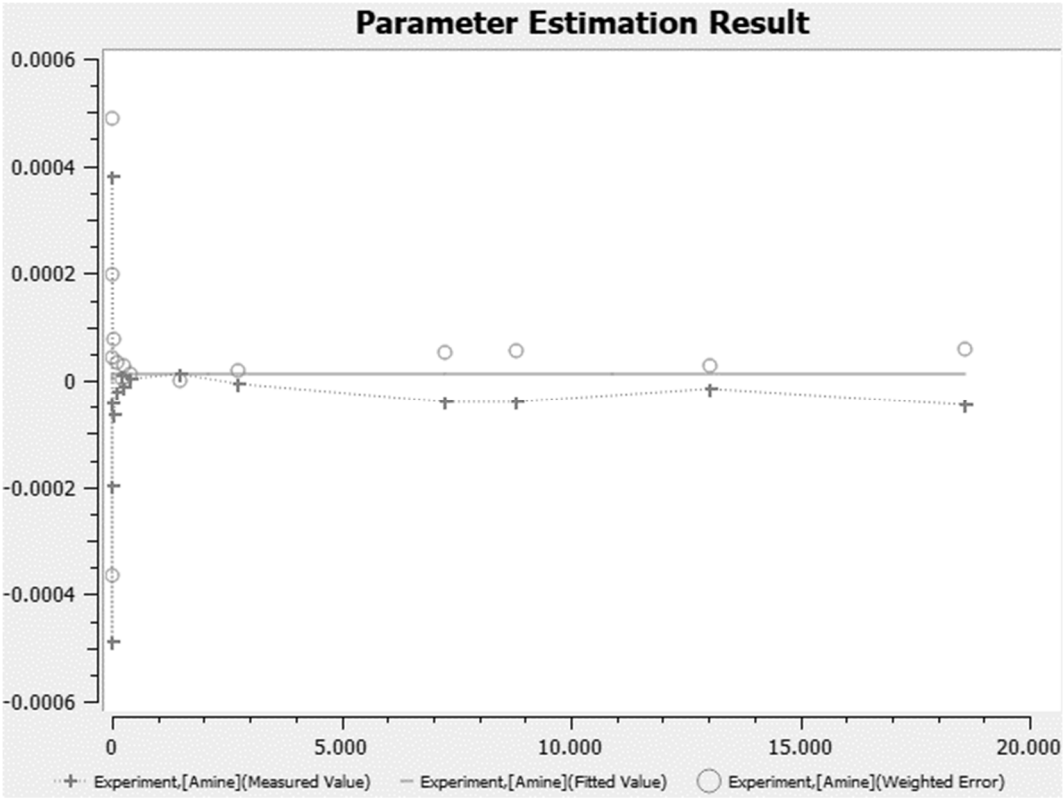

Figure S4: 90. *[Figure S90] Fitted turnover curve obtained as graphical output by COPASI for experiment mbh_08. Vertical axis gives the concentration of amine* ***21*** *in mol L⁻¹, horizontal axis gives the time from 0 min to 20000 min.*

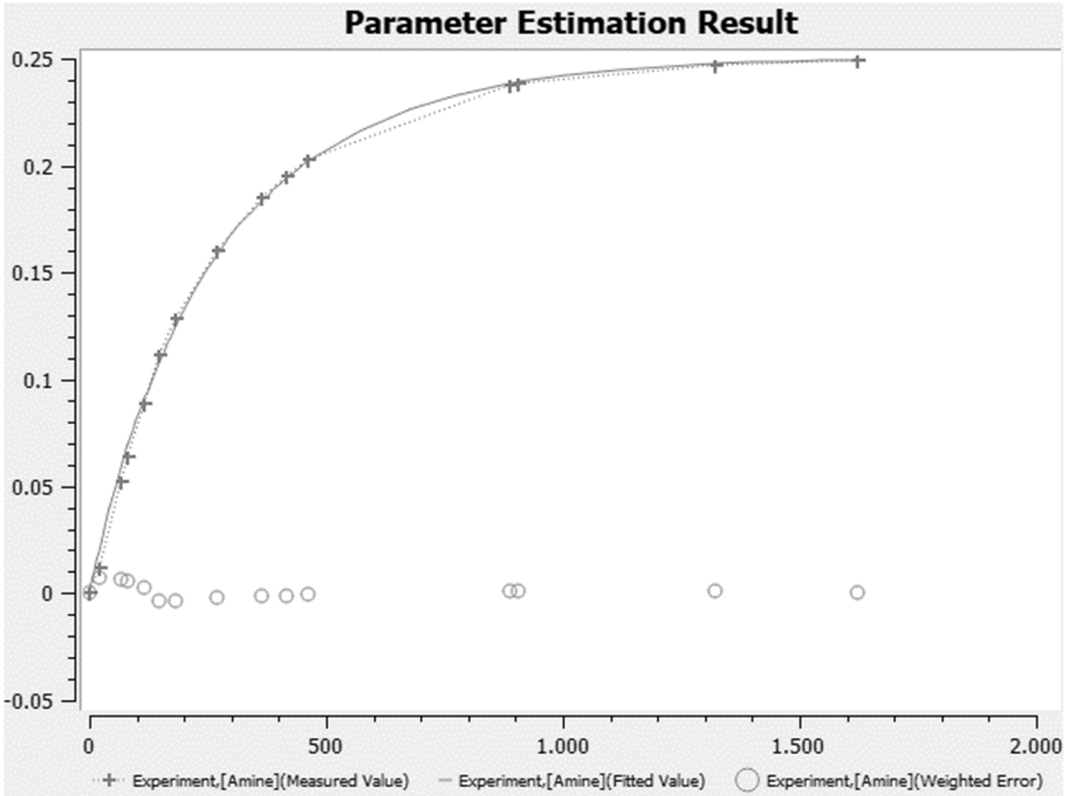

Figure S4: 91. *[Figure S91] Fitted turnover curve obtained as graphical output by COPASI for experiment mbh_09. Vertical axis gives the concentration of amine* ***21*** *in mol L⁻¹, horizontal axis gives the time from 0 min to 2000 min.*

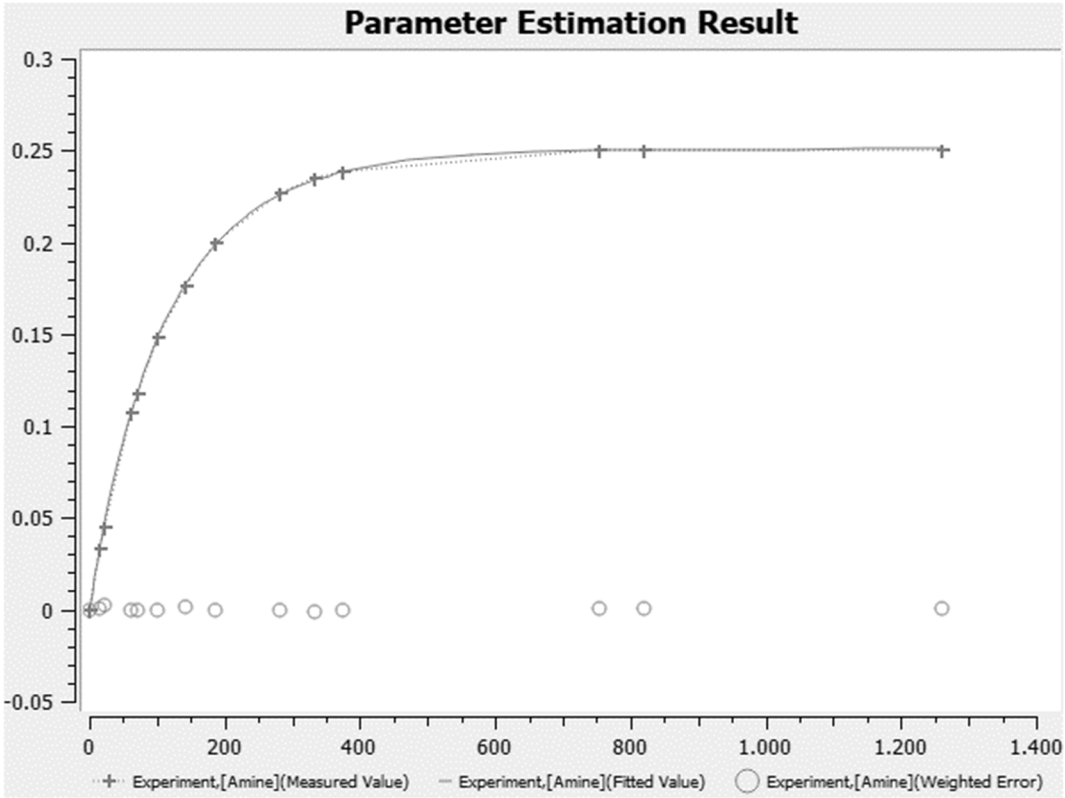

Figure S4: 92. *[Figure S92] Fitted turnover curve obtained as graphical output by COPASI for experiment mbh_10. Vertical axis gives the concentration of amine* ***21*** *in mol L⁻¹, horizontal axis gives the time from 0 min to 1400 min.*

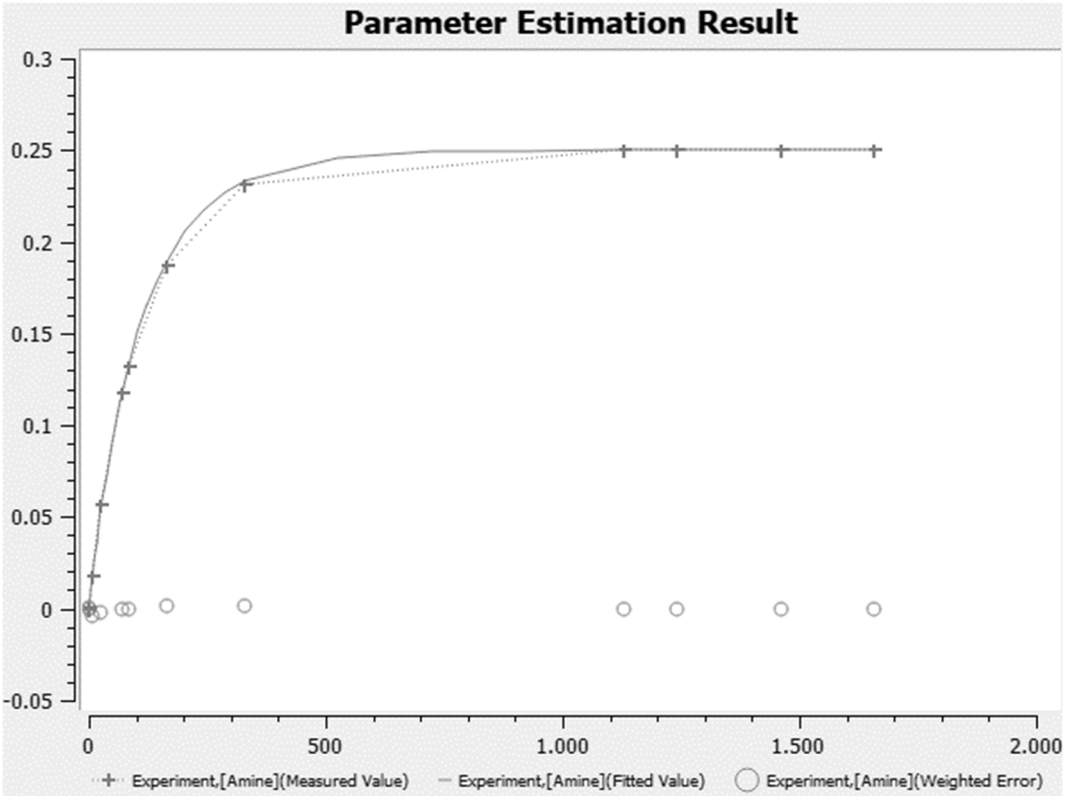

Figure S4: 93. *[Figure S93] Fitted turnover curve obtained as graphical output by COPASI for experiment mbh_11. Vertical axis gives the concentration of amine* ***21*** *in mol L⁻¹, horizontal axis gives the time from 0 min to 2000 min.*

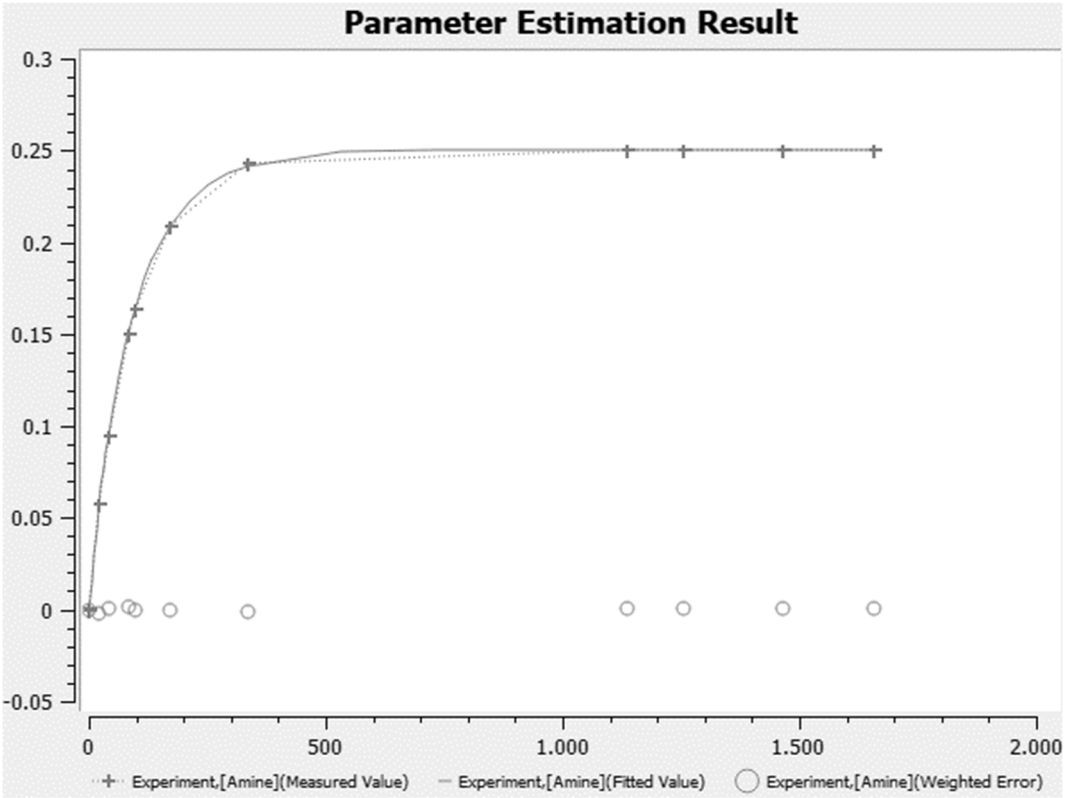

Figure S4: 94. *[Figure S94] Fitted turnover curve obtained as graphical output by COPASI for experiment mbh_12. Vertical axis gives the concentration of amine* ***21*** *in mol L⁻¹, horizontal axis gives the time from 0 min to 2000 min.*

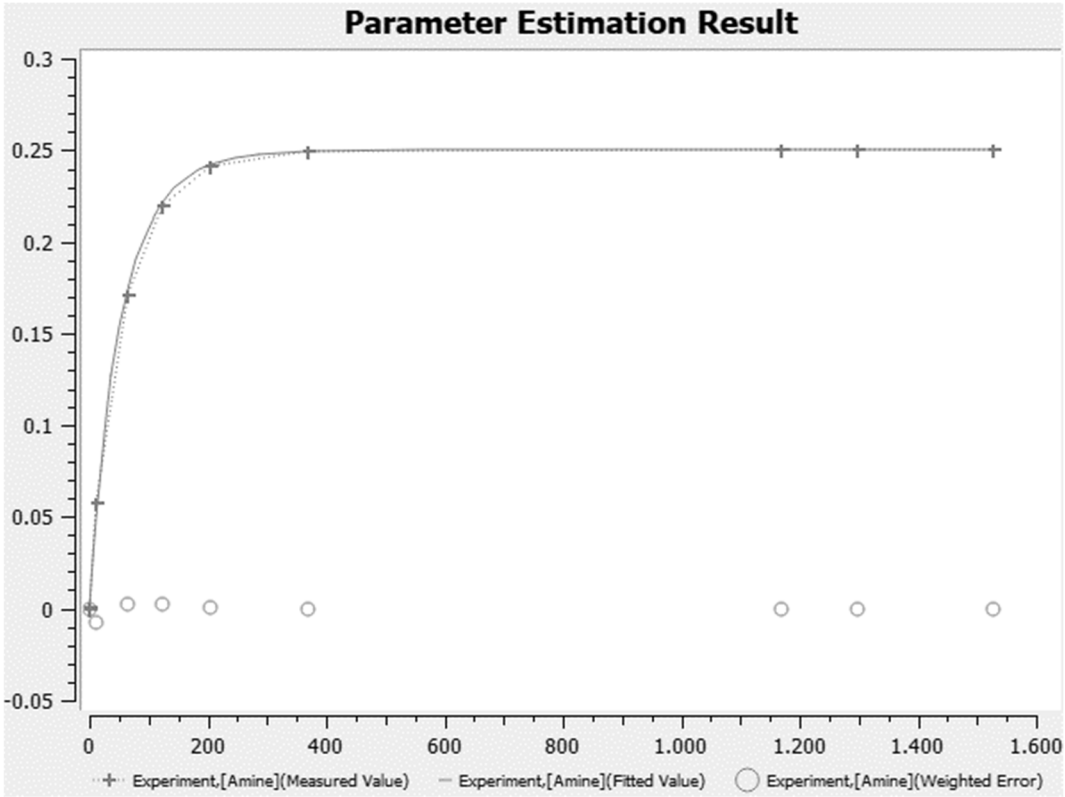

Figure S4: 95. *[Figure S95] Fitted turnover curve obtained as graphical output by COPASI for experiment mbh_13. Vertical axis gives the concentration of amine* ***21*** *in mol L⁻¹, horizontal axis gives the time from 0 min to 1600 min.*

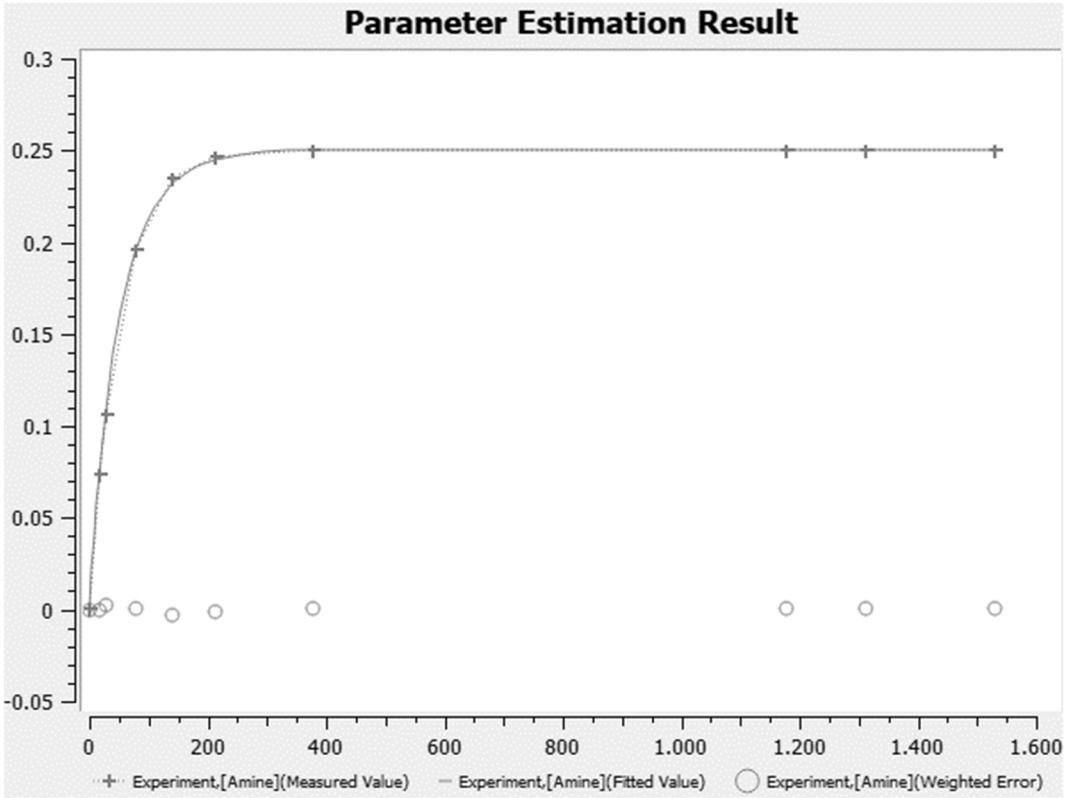

Figure S4: 96. *[Figure S96] Fitted turnover curve obtained as graphical output by COPASI for experiment mbh_14. Vertical axis gives the concentration of amine* ***21*** *in mol L⁻¹, horizontal axis gives the time from 0 min to 1600 min.*

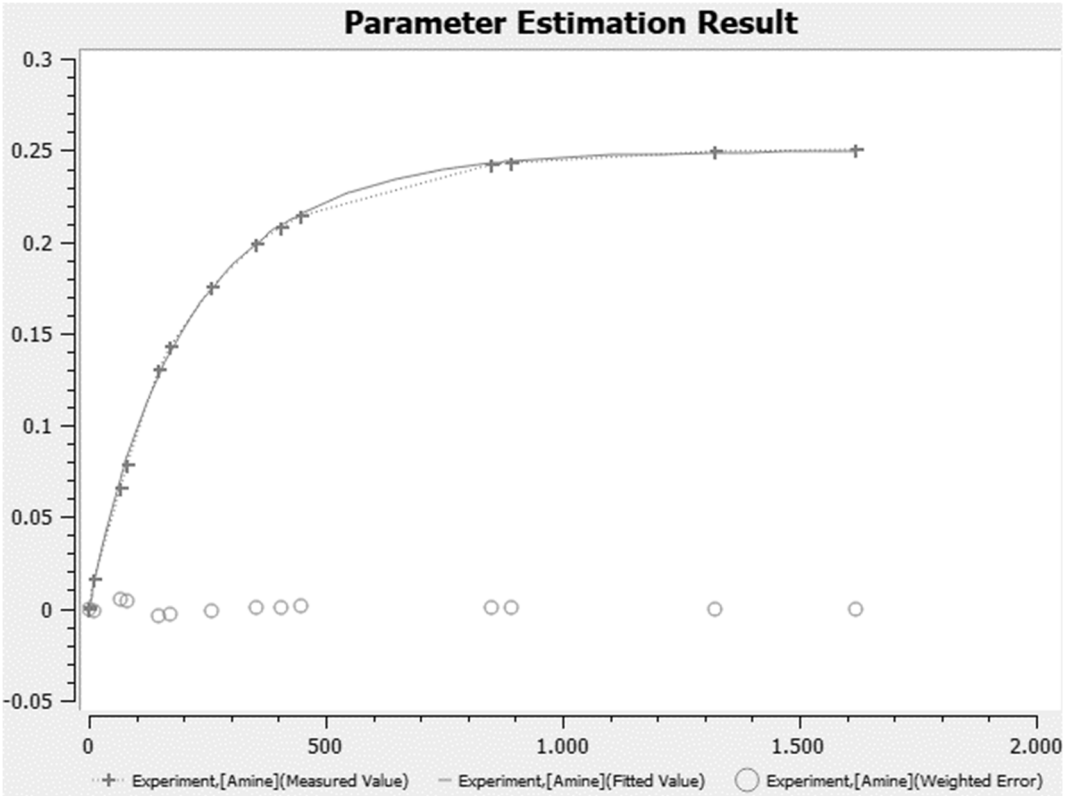

Figure S4: 97. *[Figure S97] Fitted turnover curve obtained as graphical output by COPASI for experiment mbh_15. Vertical axis gives the concentration of amine* ***21*** *in mol L⁻¹, horizontal axis gives the time from 0 min to 2000 min.*

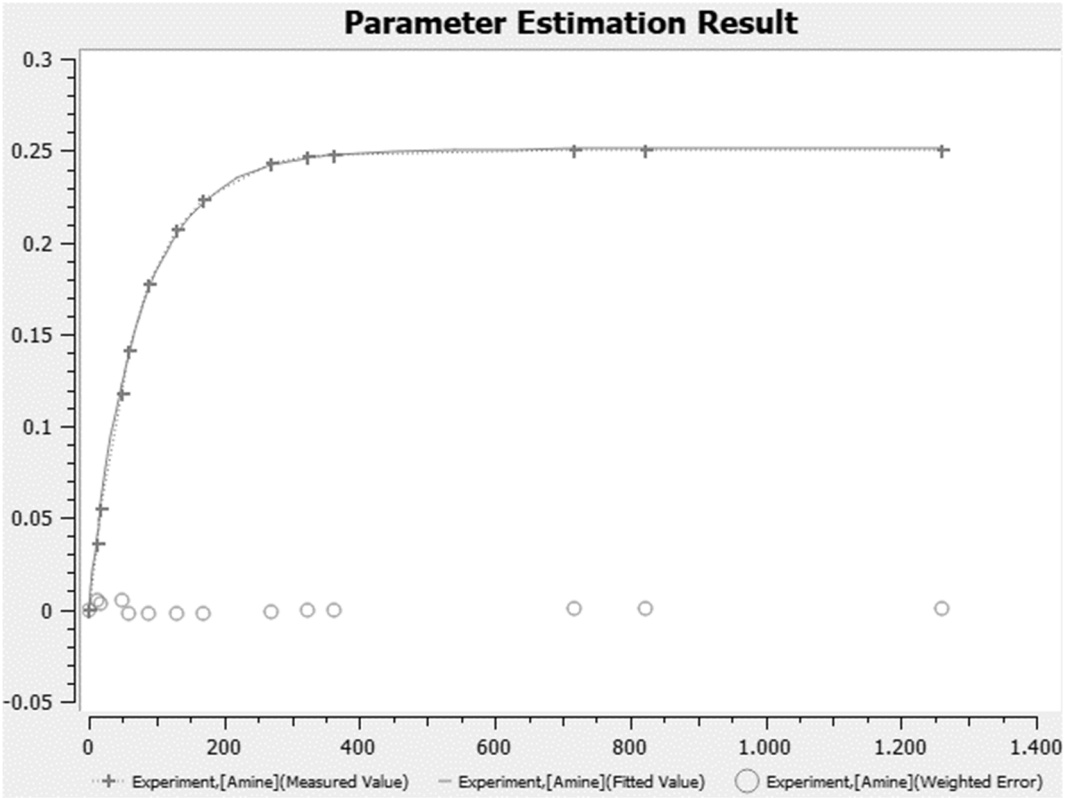

Figure S4: 98. *[Figure S98] Fitted turnover curve obtained as graphical output by COPASI for experiment mbh_16. Vertical axis gives the concentration of amine* ***21*** *in mol L⁻¹, horizontal axis gives the time from 0 min to 1400 min.*

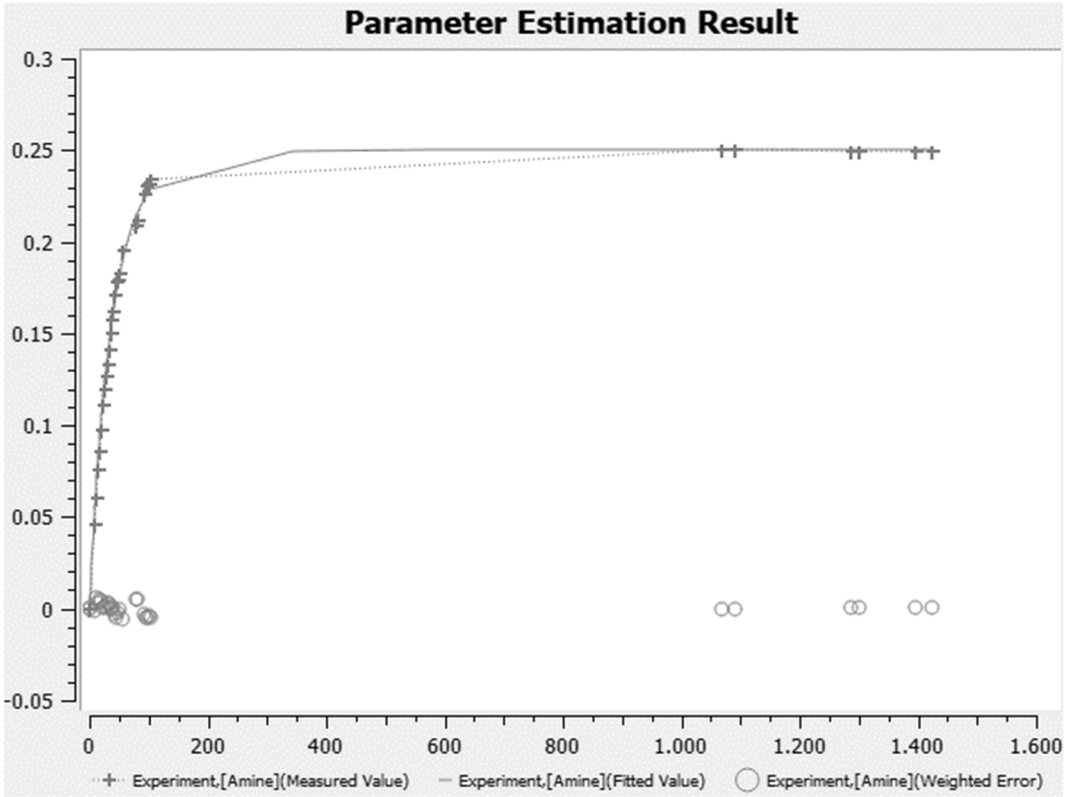

Figure S4: 99. *[Figure S99] Fitted turnover curve obtained as graphical output by COPASI for experiment mbh_17. Vertical axis gives the concentration of amine* ***21*** *in mol L^{-1}, horizontal axis gives the time from 0 min to 1600 min.*

4.1.3 Esterification Reactions Mediated by Ion Pair Catalysts

We were interested whether the ion pair catalysts employed in this study would be able to withstand the conditions present in esterification reactions. In classical, Lewis-base catalyzed esterification reactions, HCl or organic acids are generated as byproducts and need to be neutralized by auxiliary bases (such as NEt_3) to prevent protonation and therefore deactivation of the catalyst. The investigated catalyst systems are anionic bases, and able to act as Brønsted bases which would cause them to get deactivated. To test this, we performed a single set of experiments as shown in **Figure S4: 100**, mimicking the conditions of a previous study investigating acylation reactions catalyzed by DMAP (**1a**).[5]

Turnover was determined by comparison of the integrals of the ^{1}H-NMR signals of the CH_2-groups of both the ester and the benzyl alcohol as described in the next section and in the same manner as in our previous study of esterification reactions.[2]

We decided to use only 1 mol-% (with respect to benzyl alcohol) of catalyst **6aa** to be able to easily detect catalyst deactivation. However, judging from the turnover-curves in **Figure S4: 100**, there seems to be no deactivation of the ion pair catalyst. On the contrary, the reaction is sped up by a factor of more than 25 by the addition of 1 mol-% **6aa** compared to the uncatalyzed acylation.

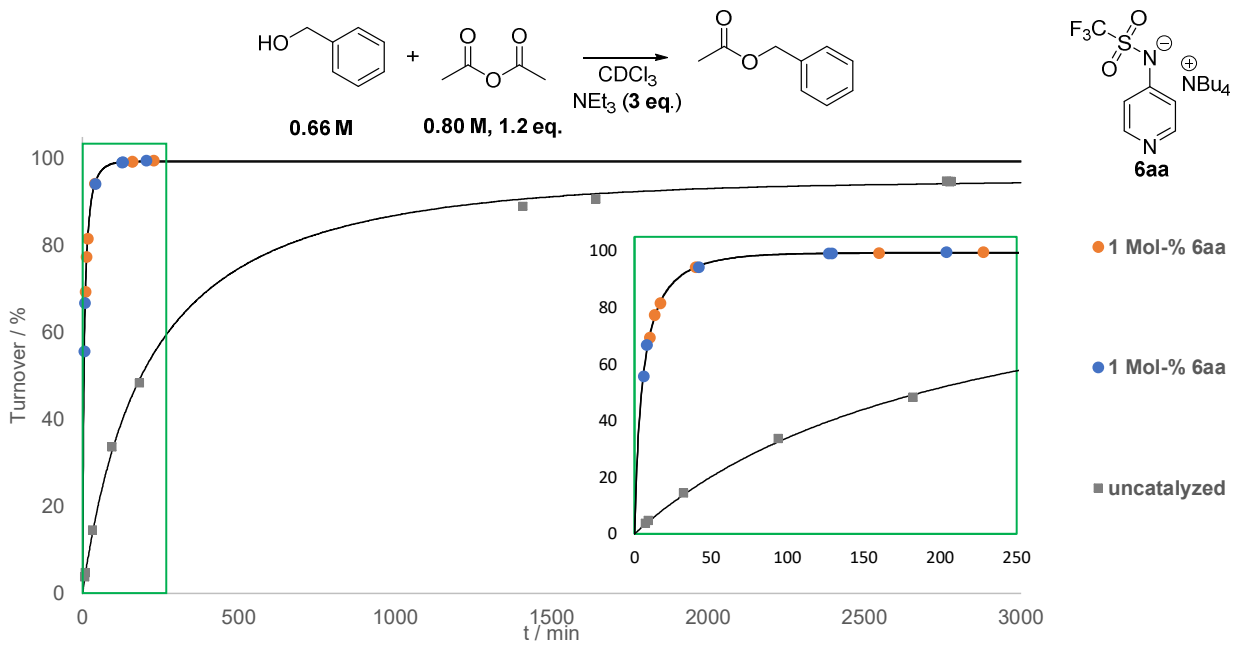

Figure S4: 100. *[Figure S100] Acylation of benzyl alcohol with acetic anhydride catalyzed by 1 mol-% ion pair catalyst* ***6aa*** *and uncatalyzed reaction at 23 °C.*

These results encouraged us to try a more challenging combination of alcohols and anhydrides and to compare our most active ion pair catalyst, **6cg** with common, neutral Lewis basic pyridine derivatives. As shown in **Figure S4: 101**, the reaction of a 1:1 mixture of 1-phenylethanol and pivalic anhydride was chosen because of a minimization of (uncatalyzed) background reaction and the general challenge of activating pivalic anhydride.

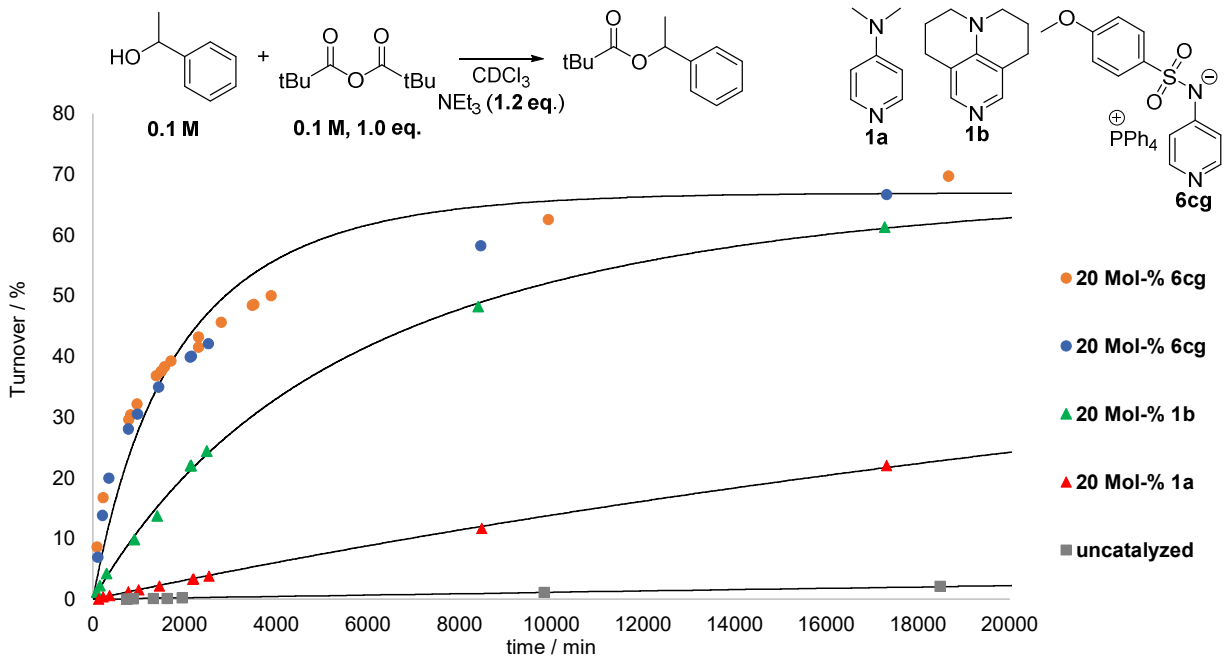

Figure S4: 101. *[Figure S101] Esterification of 1-phenylethanol, catalyzed by* ***6cg***, ***1b***, ***1a*** *(20 mol-% each compared to 1-phenylethanol), and uncatalyzed reaction at 23 °C.*

Again, turnover was determined by comparison of the integrals of the ^{1}H-NMR signals of the proton attached to the chiral carbon of both the ester and the benzyl alcohol in the same manner as described in the next section and in our previous study of esterification reactions.[2]

Due to the sluggishness of the reaction, it was not measured until completed in all cases and only observed for about two weeks. Still, a remarkable initial increase of reactivity is observed in the reactions catalyzed by **6cg** compared to DMAP **1a** and even TCAP **1b**. Unlike the neutral catalysts **1a** and **1b**, ion pair **6cg** is however unable to retain this performance under the investigated conditions. The turnover curve shows a distinct bend from about 20 % turnover on. We expect this to be caused by partial protonation of the catalyst's anion. This would also explain, why the shape of the simulated curve (done by COPASI, see below) gives a poor fit. However, the uncatalyzed reaction shows that the reaction would be expected to "flatline" if all catalyst was deactivated. Therefore, we think there is still some active catalyst in the mixtures even after one equivalent of acid was formed at 20 % turnover, which means that there is an equilibrium with the triethyl ammonium chloride that is not fully on the side of the protonated ion pair catalyst.

Due to the discussed issues with esterification reactions, we did not pursue this kind of chemistry any further and concentrated on addition reactions that do not increase the systems acidity with reaction progress, thus enabling us to benchmark the reactivity of the investigated ion pair catalysts more reliably.

Nevertheless, applications for using such ion pair catalysts for esterification reactions should not be completely ruled out in our opinion. First, the less basic trifluoromethane sulfonic amides appear to do well under classic esterification conditions. Secondly, if used to induce selectivity, usually there is no desire to convert all of the initially present alcohol, but ideally only the targeted isomer/functional group, etc. As we showed in **Figure S4: 101**, the investigated ion pair catalysts have the potential to give superior reactivity in the important first half life and remain highly modular which could potentially be used to impart selectivity.

Sample Preparation and Data Acquisition and Processing for the Esterification Reactions

Three different stock solutions were prepared under N_2 atmosphere:

- **SSF**: 3* the final concentration of the alcohol used and 3* the final concentration of NEt_3 (as given in **Table S4: 3**) and a recorded amount of internal standard Si_2Me_6 in $CDCl_3$
- **SSG**: 3* the final concentration of the appropriate anhydride in $CDCl_3$ (as given in **Table S4: 3**)
- **SSH**: 3* the final concentration of the corresponding catalyst in $CDCl_3$ (as given in **Table S4: 3**)

Samples were prepared by transferring 0.2 mL of SSF, 0.2 mL of SSH and 0.2 mL of SSG (total of 0.6 mL sample volume) into a dried, N_2-purged NMR tube. The sample was flame sealed under N_2 atmosphere. It was then stored in the bath of a thermostat set at 23 °C. The samples were only taken out of the thermostat for measuring ^{1}H NMR spectra.

Measured spectra were imported into MestReNova (Version 12.0.3) and superimposed. The following was done for the superimposed spectra in this order:

- Reference set (Si_2Me_6 set to 0.02 ppm)
- Automatic phase correction
- Automatic baseline correction (Whittaker Smoother)

For each reaction, the two signals highlighted in **Figure S4: 102** and **Figure S4: 103** were integrated. These signals represent the H-atoms attached to the α-carbons of the alcohol and the ester respectively:

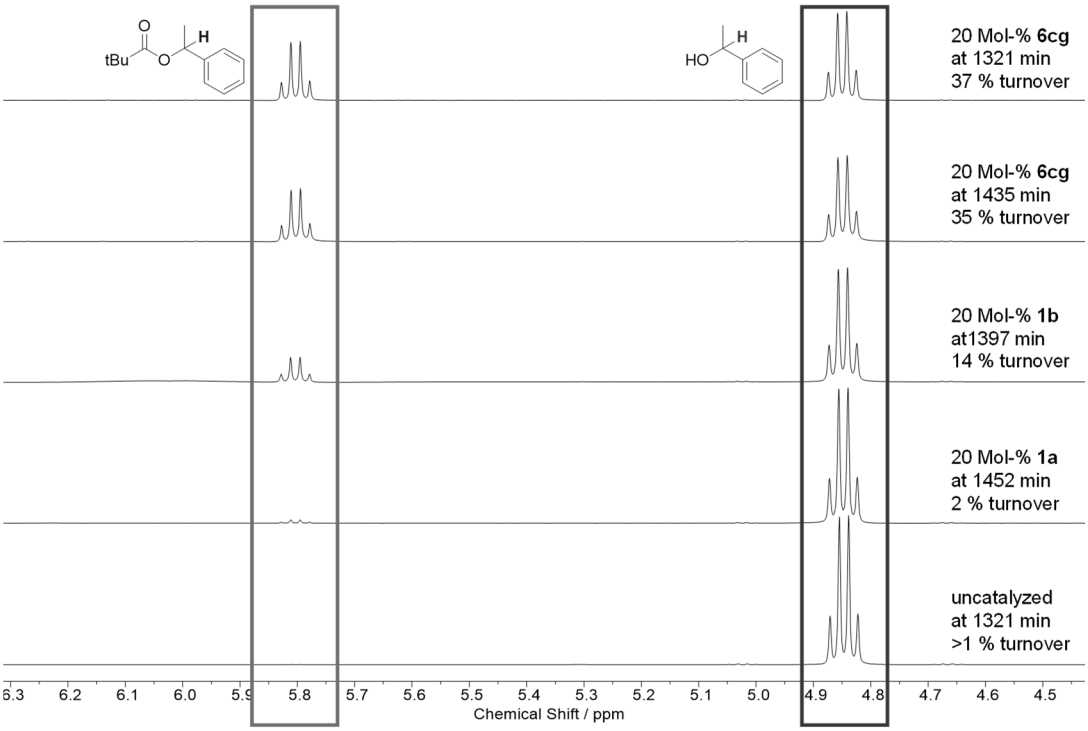

Figure S4: 102. *[Figure S102] Spectra of the esterification of 1-phenylethanol, catalyzed by different catalysts and uncatalyzed reaction, measured at similar reaction time.*

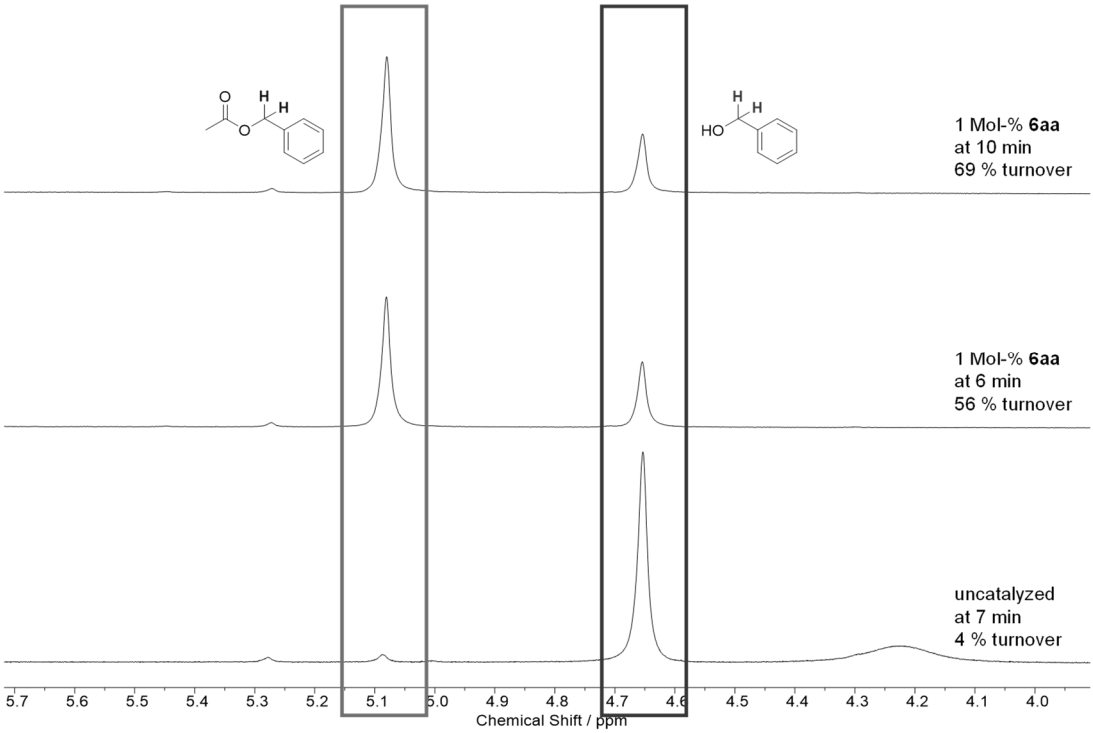

Figure S4: 103. *[Figure S103] Spectra of the esterification of benzyl alcohol, catalyzed by* ***6aa*** *and uncatalyzed reaction.*

The values of these integrals were used to calculate turnover according to Equation S4: 7:

$$T_{ester}\ /\ \% = \frac{\boldsymbol{Integral\ ester}}{\boldsymbol{Integral\ ester + Integral\ alcohol}} \times\ 100 \qquad \text{Eq. S4: 7}$$

The values obtained for turnover $\mathbf{T_{ester}}$ were used for calculating concentrations of the corresponding ester at the time *t* based on initial concentrations c_0 as shown by Equation S4: 8:

$$c_t\ [\text{ester}]\ /\ \text{mol L}^{-1} = \frac{c_0 alcohol \times (100 - \boldsymbol{T}_{ester(t)})}{100} \qquad \text{Eq. S4: 8}$$

Simulation of kinetic parameters was done using COPASI[3]. The obtained values for *t* and c_t[**ester**] were imported into the program and the *Parameter Estimation* (default settings) option was used for the simplified model shown in **Scheme S4: 5**.

$$\text{alcohol} + \text{anhydride} \underset{k_2}{\overset{k_1=k_{eff}}{\rightleftharpoons}} \text{ester}$$

Scheme S4: 5. *[Scheme S5] Simplified model used for fitting of the experimental data obtained for the esterification reations in COPASI.*

The fitting curves obtained from COPASI were used to emphasize catalytic performance in **Figure S4: 100** and **Figure S4: 101**.

Kinetic Data for the Esterification Reactions

Table S4: 3 gives the details for the performed esterification reactions while the curves fitted by COPASI are shown in **Figure S4: 104** – **Figure S4: 111**.

Table S4: 3. [Table S3] Details for the esterification benchmark reactions.

experiment	alcohol	anhydride	catalyst
esterification_01	0.66 mol L^{-1} benzyl alcohol	0.80 mol L^{-1} acetic anhydride	1 mol-% 6aa
esterification_02	0.66 mol L^{-1} benzyl alcohol	0.80 mol L^{-1} acetic anhydride	1 mol-% **6aa**
esterification_03	0.66 mol L^{-1} benzyl alcohol	0.80 mol L^{-1} acetic anhydride	none
esterification_04	0.1 mol L^{-1} 1-phenyl ethanol	0.1 mol L^{-1} pivolic anhydride	20 mol-% **6cg**
esterification_05	0.1 mol L^{-1} 1-phenyl ethanol	0.1 mol L^{-1} pivolic anhydride	20 mol-% **6cg**
esterification_06	0.1 mol L^{-1} 1-phenyl ethanol	0.1 mol L^{-1} pivolic anhydride	20 mol-% **1b**
esterification_07	0.1 mol L^{-1} 1-phenyl ethanol	0.1 mol L^{-1} pivolic anhydride	20 mol-% **1a**
esterification_08	0.1 mol L^{-1} 1-phenyl ethanol	0.1 mol L^{-1} pivolic anhydride	none

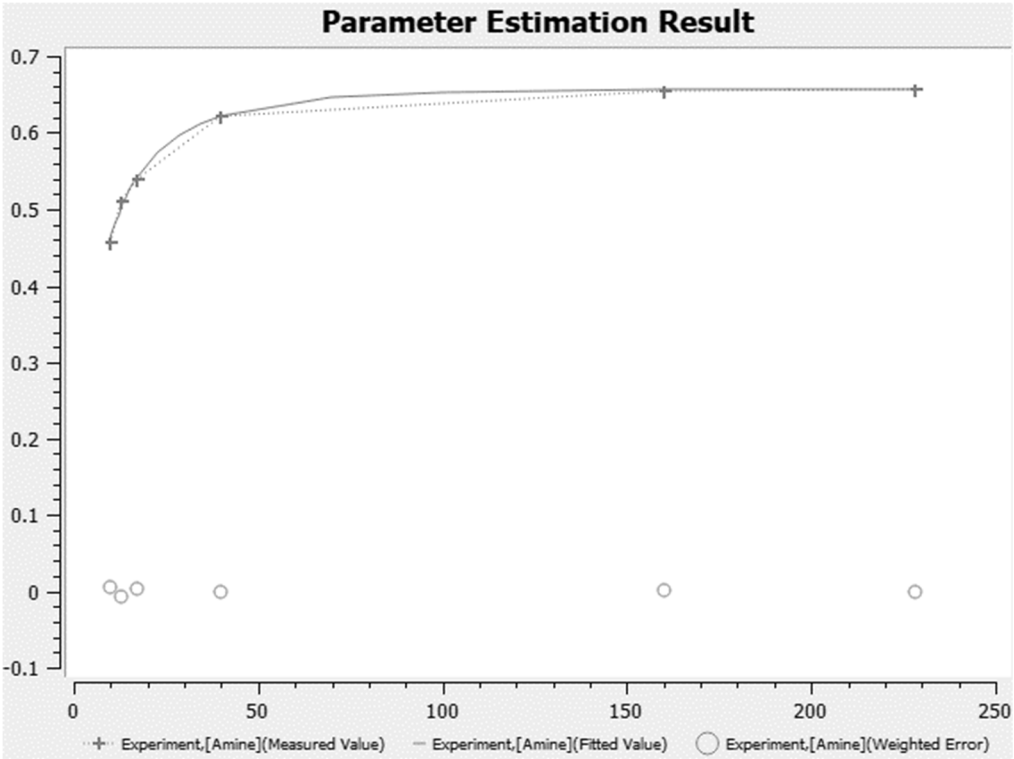

Figure S4: 104. *[Figure S104] Fitted turnover curve obtained as graphical output by COPASI for experiment esterification_01. Vertical axis gives the concentration of the product ester in mol L^{-1}, horizontal axis gives the time from 0 min to 250 min.*

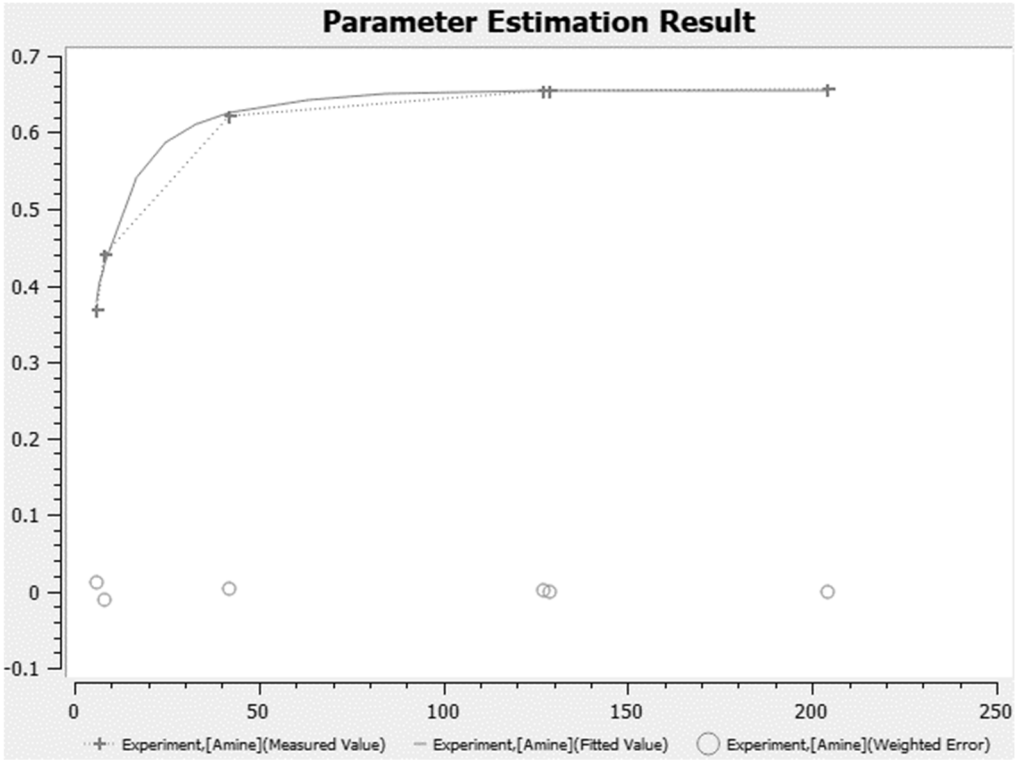

Figure S4: 105. *[Figure S105] Fitted turnover curve obtained as graphical output by COPASI for experiment esterification_02. Vertical axis gives the concentration of the product ester in mol L^{-1}, horizontal axis gives the time from 0 min to 250 min.*

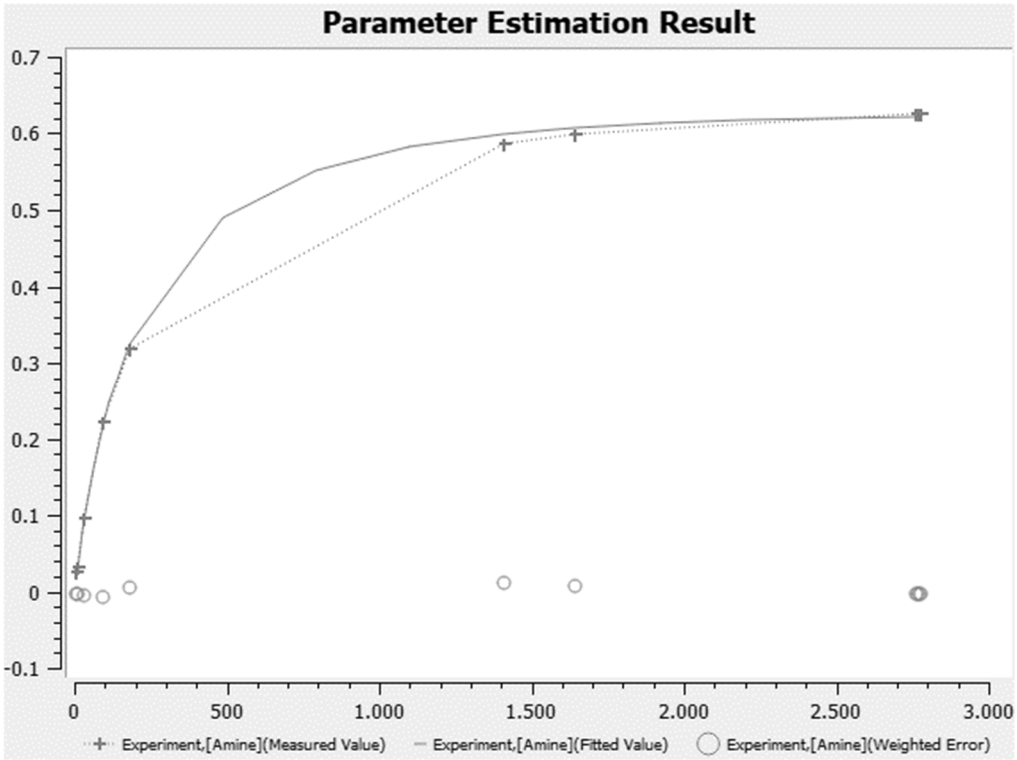

Figure S4: 106. *[Figure S106] Fitted turnover curve obtained as graphical output by COPASI for experiment esterification_03. Vertical axis gives the concentration of the product ester in mol L^{-1}, horizontal axis gives the time from 0 min to 3000 min.*

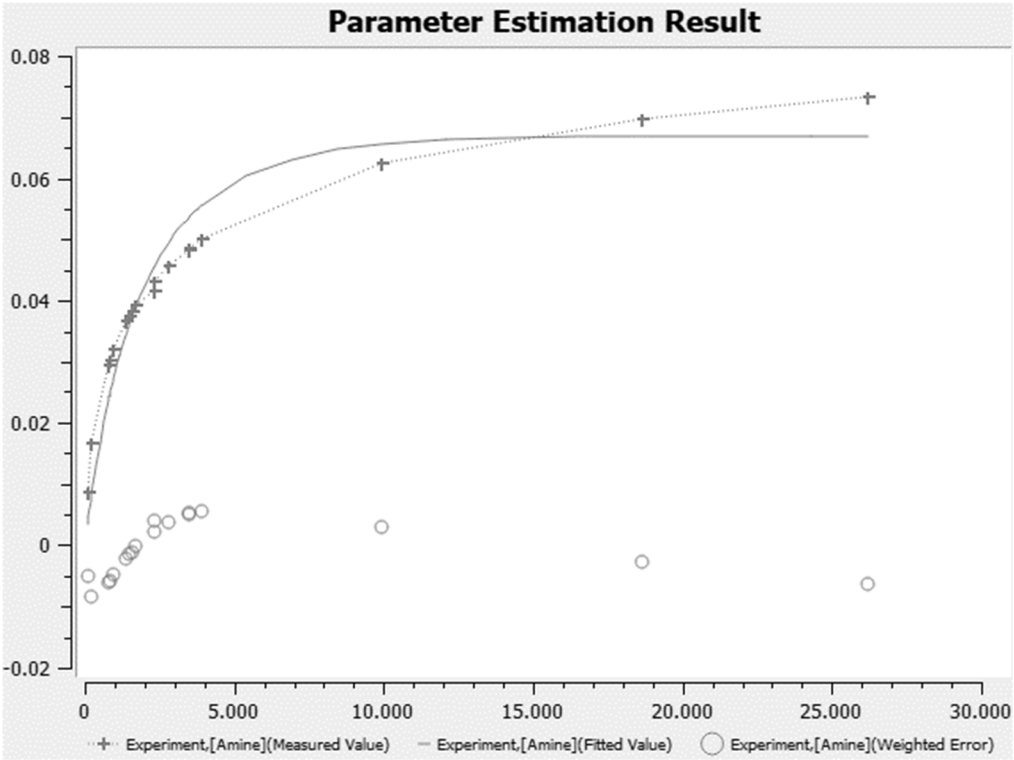

Figure S4: 107. *[Figure S107] Fitted turnover curve obtained as graphical output by COPASI for experiment esterification_04. Vertical axis gives the concentration of the product ester in mol L^{-1}, horizontal axis gives the time from 0 min to 30000 min.*

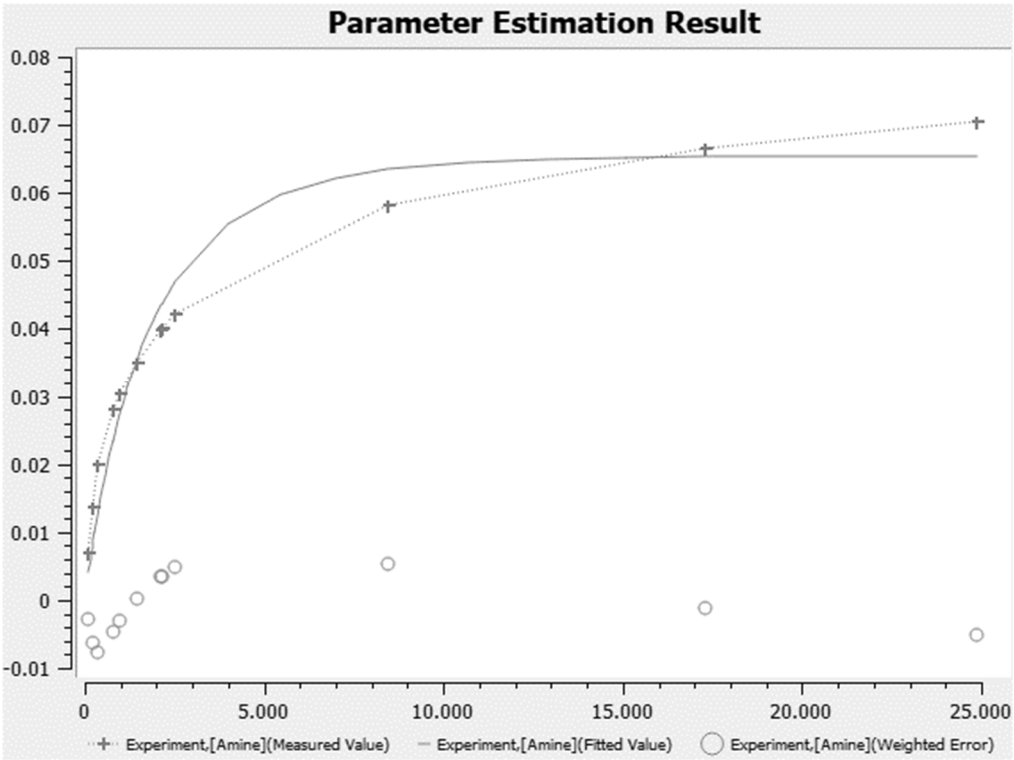

Figure S4: 108. *[Figure S108] Fitted turnover curve obtained as graphical output by COPASI for experiment esterification_05. Vertical axis gives the concentration of the product ester in mol L^{-1}, horizontal axis gives the time from 0 min to 25000 min.*

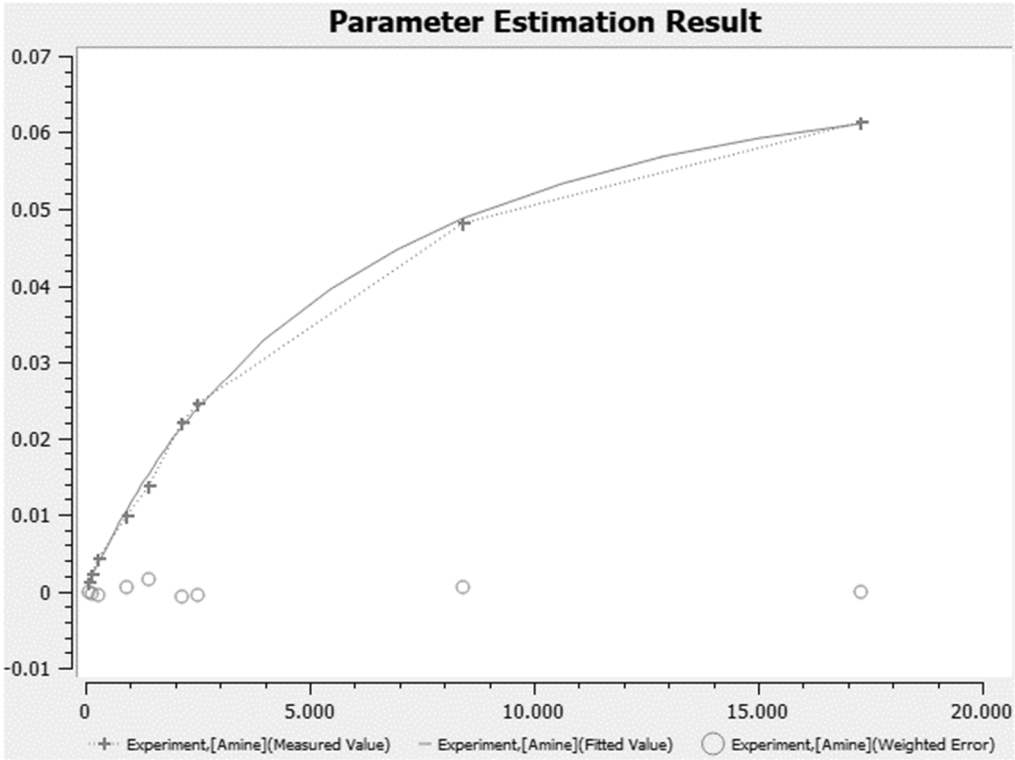

Figure S4: 109. *[Figure S109] Fitted turnover curve obtained as graphical output by COPASI for experiment esterification_06. Vertical axis gives the concentration of the product ester in mol L^{-1}, horizontal axis gives the time from 0 min to 20000 min.*

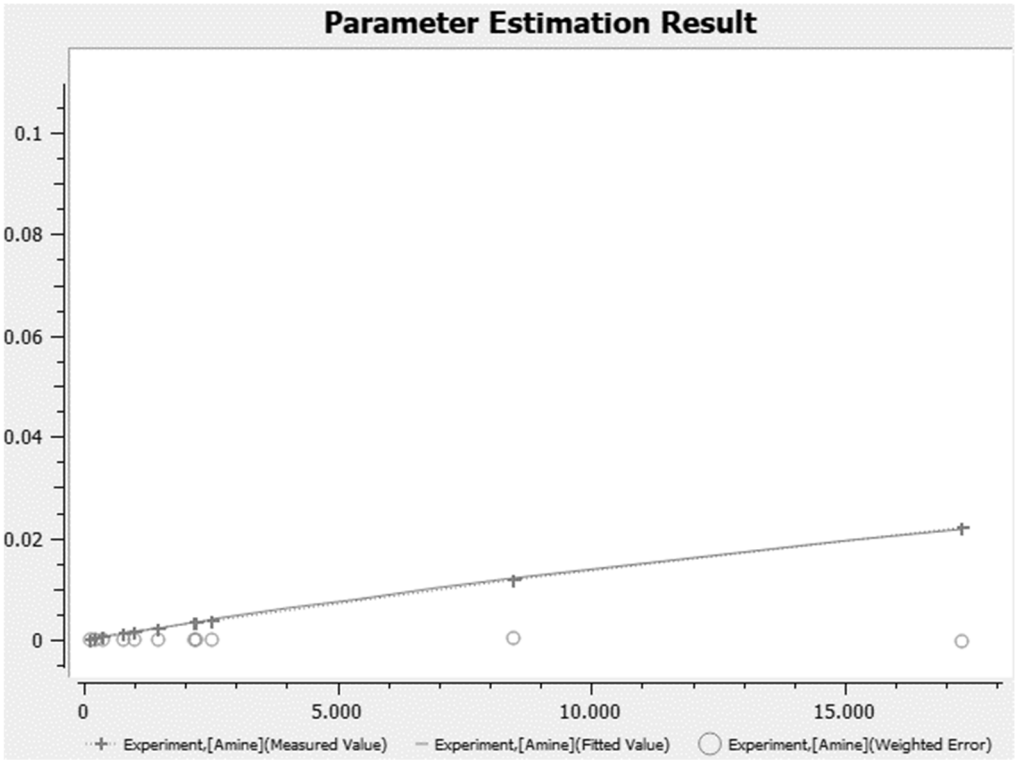

Figure S4: 110. *[Figure S110] Fitted turnover curve obtained as graphical output by COPASI for experiment esterification_07. Vertical axis gives the concentration of the product ester in mol L^{-1}, horizontal axis gives the time from 0 min to 20000 min.*

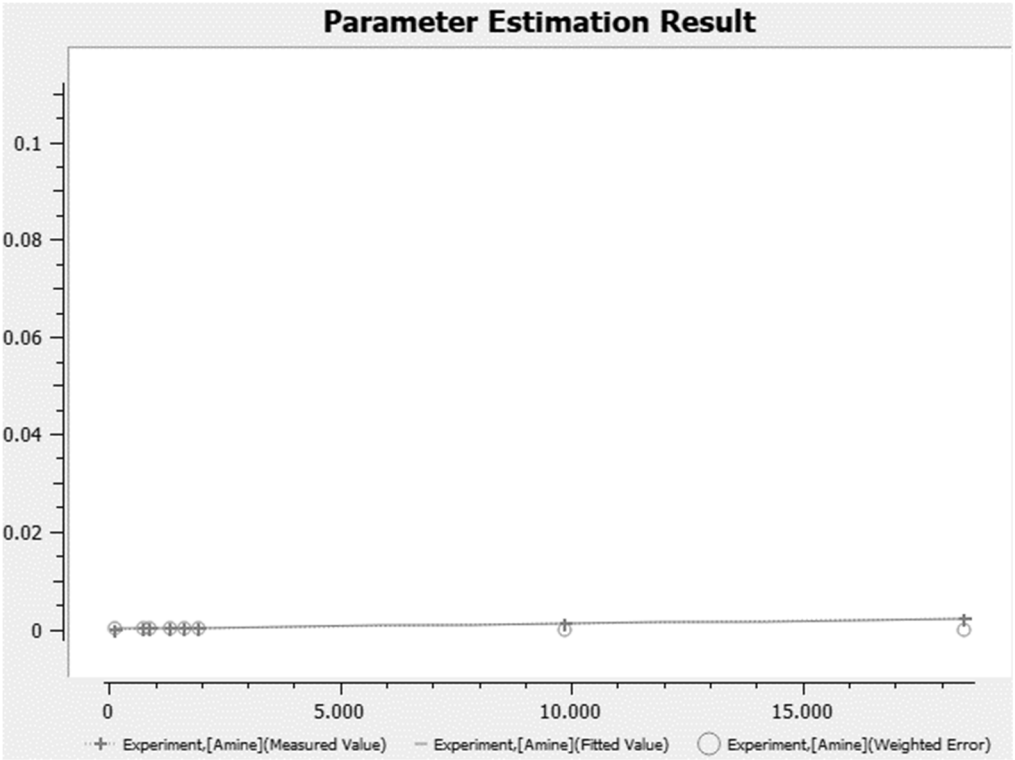

Figure S4: 111. *[Figure S111] Fitted turnover curve obtained as graphical output by COPASI for experiment esterification_08. Vertical axis gives the concentration of the product ester in mol L^{-1}, horizontal axis gives the time from 0 min to 19000 min.*

4.1.4 Deprotonation of More Acidic Cations in Ion Pair Catalysis

When performing the urethane benchmark reactions with catalysts containing the diethyl benzimidazolium cation (**6be**, **6ce**, **7e**) we observed some new, unexpected signals and decided to investigate 1:1 mixtures of the catalyst and isocyanate **17** in $CDCl_3$. **Figure S4: 112** and **Figure S4: 113** show spectra of these mixtures and spectra of the pure catalyst and isocyanate solutions.

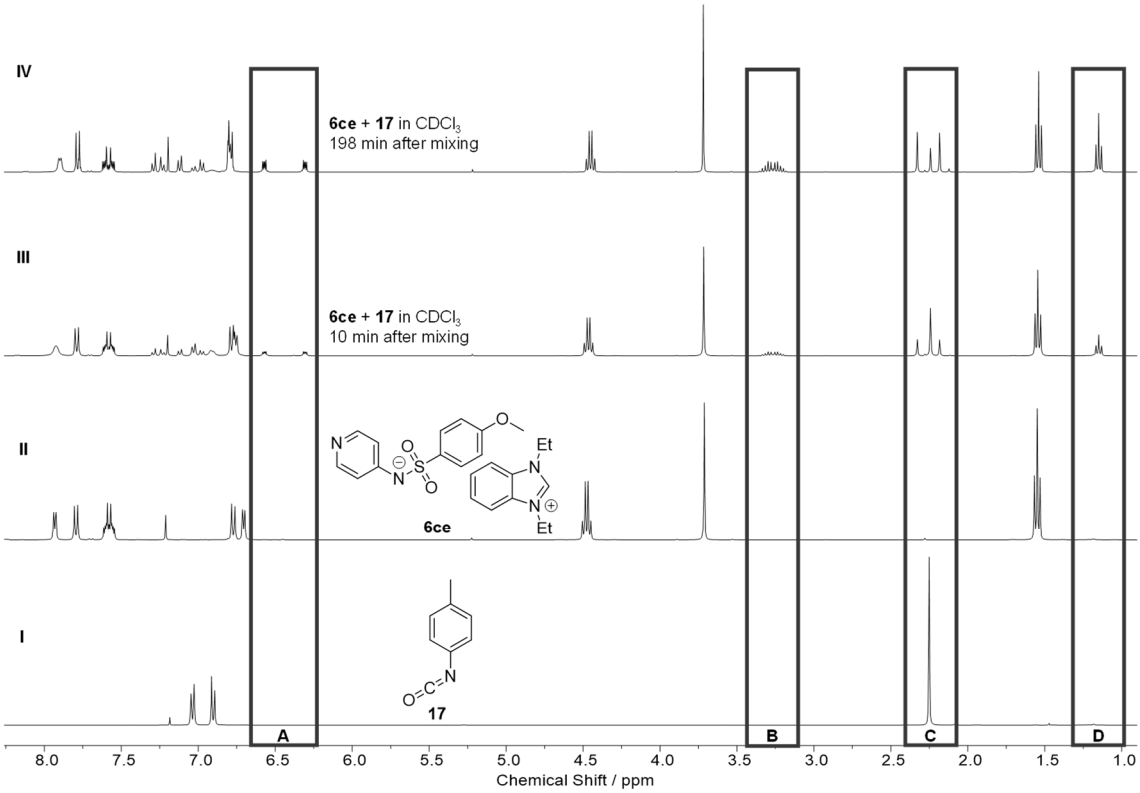

Figure S4: 112. *[Figure S112] Stacked ^{1}H NMR spectra of stock solution of isocyanate **17** (I), stock solution of catalyst **6ce** (II), and a 1:1 mixture (molar) of both stock solutions after different times of reaction (III, IV). All spectra are recorded in $CDCl_3$ at 400 MHz.*

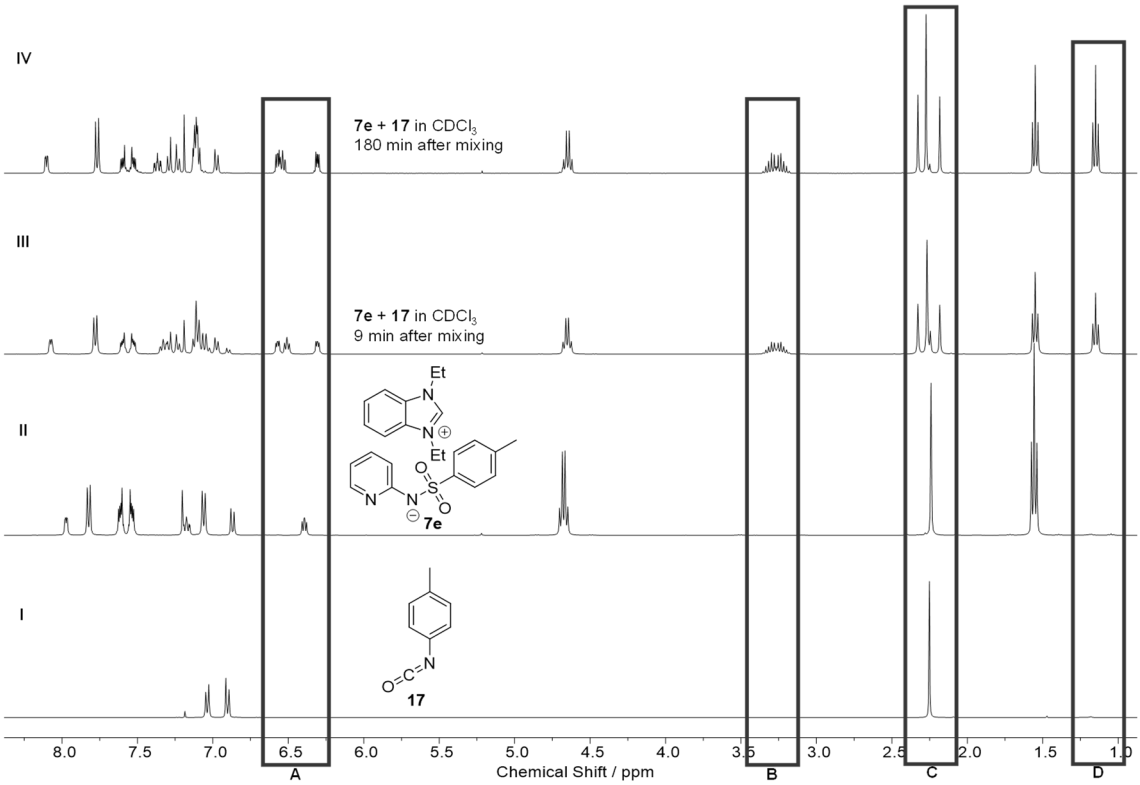

Figure S4: 113. *[Figure S113] Stacked ^{1}H NMR spectra of stock solution of isocyanate **17** (I), stock solution of catalyst **7e** (II), and a 1:1 mixture (molar) of both stock solutions after different times of reaction (III, IV). All spectra are recorded in $CDCl_3$ at 400 MHz.*

Both Figures show the same signals - although more pronounced - that we observed in the urethane benchmark reactions employing catalysts containing the benzimidazolium cation. More specifically, we observed a new set of multiplets (signals **A**), that by its distinct shape can be attributed to one of the aromatic protons of the benzimidazolium cation as shown in **Figure S4: 114**, although shifted by more than one ppm high-field. A very similar shift was reported by Lemal *et al.* for a comparable system: They found signals at 6.63 and 6.53 ppm for the corresponding *N*-heterocyclic carbene (NHC)-dimer of compound **26** in diglyme-d_{14} at room temperature. Upon heating to 110 °C, the signals shifted to 7.29 and 7.10 ppm and were attributed to the corresponding NHC.[6]

We decided to get an ESI-HR-MS of the reaction mixture and found the dominant signal in the positive spectrum to be of mass 308.17571 (**7e** + **17**) and 308.17572 (**6ce** + **17**) respectively.

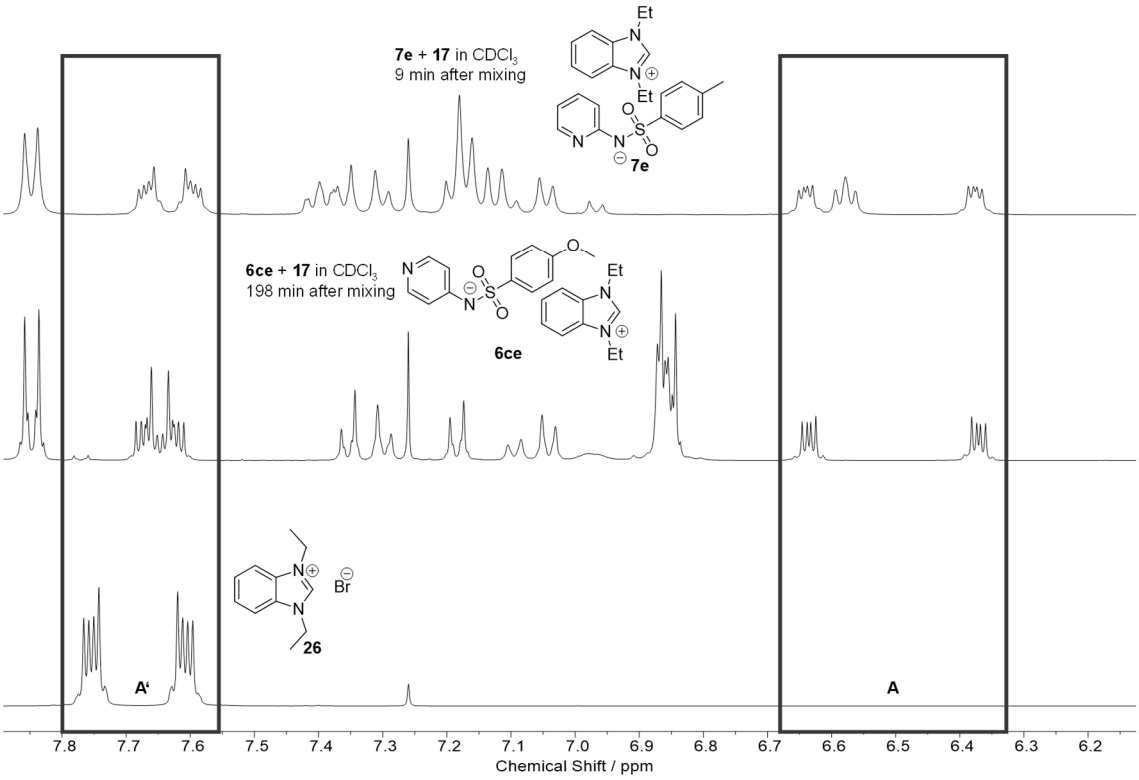

Figure S4: 114. *[Figure S114] Detailed view of the signals in area A and the area A', where the original signals of the corresponding aryl protons are found.*

These findings, together with the reported shifts for the NHC dimer referenced above allowed us to propose the structure given in **Scheme S4: 6** or an isomer of this structure. This is further supported by 2D NMR spectra directly linking one of the isocyanate *p*-methyl-signals in area **C** to the rest of the new signals via a single, well-separated ^{13}C signal (**Figure S4: 115**) and the integrals being in very good agreement as shown in **Figure S4: 116**.

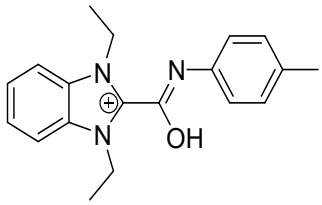

Exact Mass: 308.17574

Scheme S4: 6. *[Scheme S6] Structure proposed for the result of the positive ESI-HR-MS.*

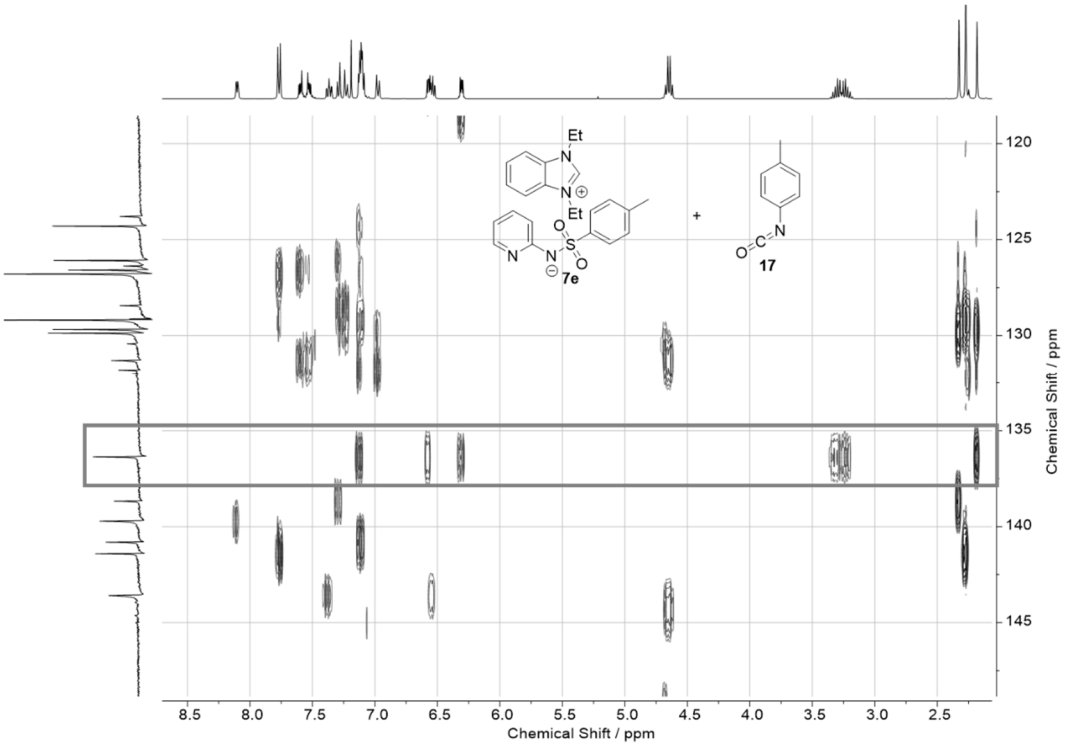

Figure S4: 115. *[Figure S115] ^{1}H-^{13}C HMBC NMR spectrum of a 1:1 mixture of **7e** and **17**. The ^{13}C signal interacting with both protons of the benzimidazole-unit and the isocyanate **17** is highlighted.*

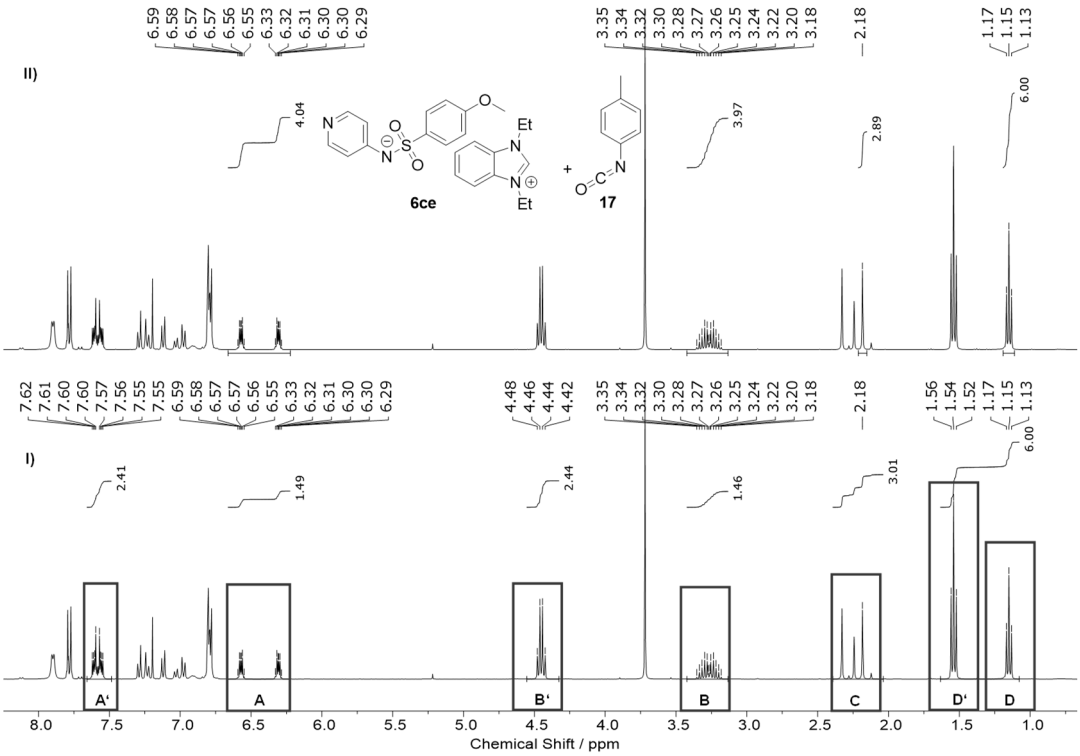

***Figure S4: 116**. [Figure S116] Identical ^{1}H NMR spectrum of a 1:1 mixture of **6ce** and **17**. Original signals and the new ones (**capital letter'** and **capital letter**) respectively are indicated in spectrum **I**).*

Spectra **I**) and **II**) are identical and differ only with respect to the integrated areas.

Spectrum **I**) gives separate integrals for **A'** and **A** adding up to four protons (aryl signals of benzimidazole-compounds) and **B'** and **B** adding up to four protons (CH_2-signals of benzimidazole-compounds). The integral area containing all different signals produced by the *p*-methyl signal of the isocyanate **C** adds up to three protons and **D'** and **D** are adding up to six protons representing the CH_3-groups of the benzimidazole-compounds.

Spectrum **II**), on the other hand gives only the well-separated integrals of the proposed NHC-isocyanate adduct species in the expected ratio of 4/4/3/6, confirming our assignment of the majorly formed compound.

In conclusion, these experiments showed why the attempted benchmark-reactions with ion pair catalysts containing benzimidazolium counter ions gave "wild" mixtures with low estimated turnovers, because the ion pairs acted as *in-situ* generators of the corresponding NHCs that reacted with the abundantly present isocyanate **17** to form adducts as detected by NMR and HR-MS. Furthermore, not identified products were generated as well. In case of the triphenylmethyl phosphonium and the benzyltriphenyl phosphonium cation, similar, although less pronounced effects are observed, although for low catalyst concentrations (3 mol-%), there is no effect detectable beyond the experimental error of the measurements itself.

4.1.5 Crystallographic Data

Table of selected anion-cation interactions observed by single-crystal X-ray diffraction

Values were obtained using the “Contacts”-function of Mercury 3.8 (Short Contacts, intermolecular, < sum of vdW radii (150 pm)) on unit cells. The given values represent the shortest distances found between the selected atoms for the unit cell and the surrounding “layer” of atoms.

Table S4: 4. [Table S4] Selected anion-cation interactions observed by single-crystal X-ray diffraction.

Entry	Catalyst	heteroatom(anion)→P/ N(cation)[a]	pyridine-N →cation[a]	amide-N →cation[a]	heteroatom(anion) →cation[a]
1	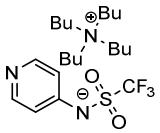 **6aa**	395.0 (O→N)	257.3 (α-H)	246.3 (α-H)	244.9 (O→β-H)
2	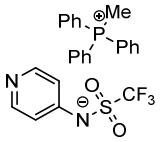 **6ac**	394.5 (pyridine-N→P)	248.6 (β-H)	249.4 (α-H)	245.0 (O→β-H)
3	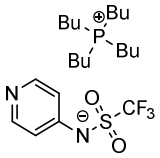 **6ad**	394.4 (O→P)	253.4 (α-H)	264.2 (α-H)	238.1 (O→α-H)
4	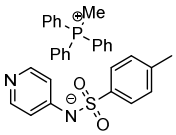 **6bc**	399.5 (O→P)	254.2 (α-H)	254.2 (α-H)	234.1 (O→α-H)
5	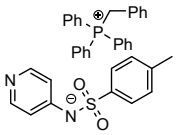 **6bf**	420.1 (O→P)	278.9 (δ-H)	291.0 (β-H)	230.8 (O→α-H)
6	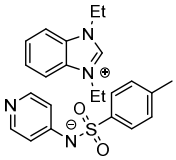 **6be**	366.8 (O→N)	270.2 (β-H)	268.0 (α-H)	213.3 (O→α-H)
7	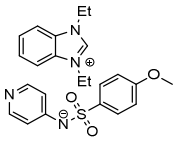 **6ce**	391.0 (SO_2-O→N)	244.7 (α-H)	255.9 (α-H)	222.0 (SO_2-O→ α-H)
8	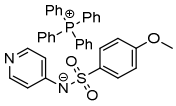 **6cg**	467.9 (Me-O→P)	285.7 (α-H)	267.6 (β-H)	241.4 (Me-O→α-H)

[a] in pm.

Table S4: 4 (continuation). [Table S4] Selected anion-cation interactions observed by single-crystal X-ray diffraction.

9	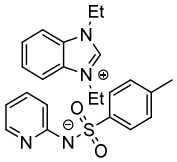 **7e**	388.4 (O→N)	243.6 (α-H)	217.6 (α-H)	217.6 (amide-N→α-H)
10	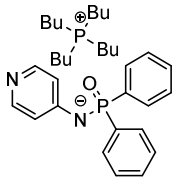 **10d**	368.9 (O→P)	247.9 (α-H)	286.2 (δ-H)	219.5 (O→α-H)
11	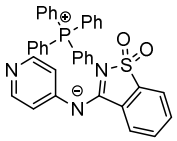 **15g**	506.6 (O→P)	251.8 (γ-H)	280.1 (β-H)	238.3 (O→γ-H)

[a] in pm.

As discussed in the main part of this publication, we found that in the solid state the cation is usually rather closer to the amide moiety as indicated by columns 3 and 7. The only true exception is the structurally different ion pair **7e**. In the case of our most active example **6cg**, the closest interactions originate from the methoxy group's oxygen still indicating that the cation is not coordinated by the pyridine part.

Tetrabutylammonium pyridin-4-yl((trifluoromethyl)sulfonyl)amide ***6aa***

Figure S4: 117 shows a single ion pair, **Figure S4: 118** gives the unit cell and crystallographic data for catalyst system **6aa** is given in **Table S4: 5**:

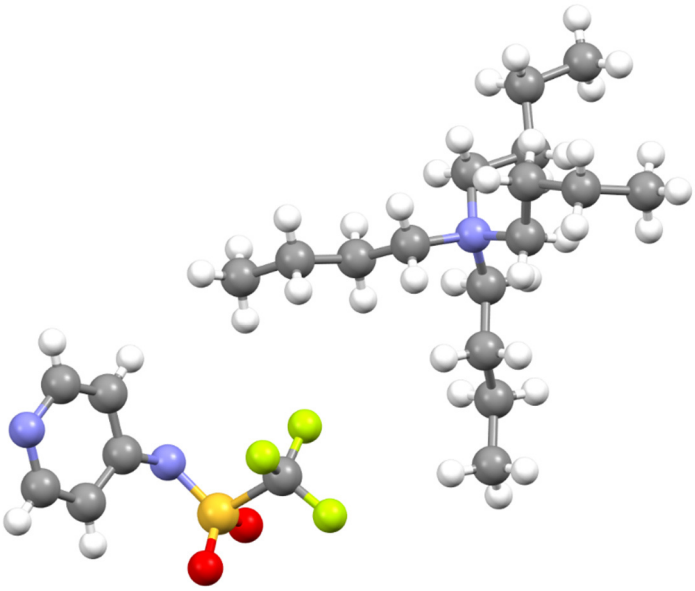

Figure S4: 117. *[Figure S117] Ion pair of catalyst* ***6aa****.*

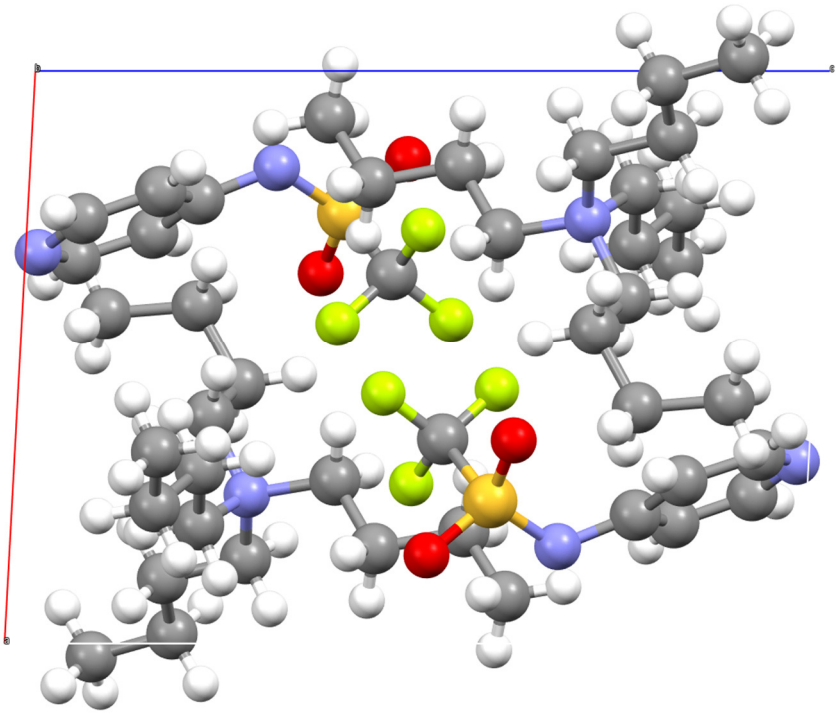

Figure S4: 118. *[Figure S118] Unit cell of catalyst* ***6aa*** *viewed along the b-axis.*

Table S4: 5. [Table S5] Crystallographic details for ion pair catalyst **6aa**.

net formula	$C_{22}H_{40}F_3N_3O_2S$
M_r/g mol^{-1}	467.63
crystal size/mm	0.100 × 0.080 × 0.050
T/K	100.(2)
radiation	MoKα
diffractometer	'Bruker D8 Venture TXS'
crystal system	triclinic
space group	'P -1'
a/Å	9.7164(18)
b/Å	10.1395(15)
c/Å	13.851(3)
α/°	71.337(5)
β/°	88.764(6)
γ/°	77.117(10)
V/Å^3	1258.5(4)
Z	2
calc. density/g cm^{-3}	1.234
μ/mm^{-1}	0.173
absorption correction	Multi-Scan
transmission factor range	0.9346–0.9705
refls. measured	24387
R_{int}	0.0406
mean σ(*I*)/*I*	0.0301
θ range	2.723–26.450
observed refls.	4504
x, y (weighting scheme)	0.0343, 0.6485
hydrogen refinement	constr
refls in refinement	5178
parameters	284
restraints	0
$R(F_{obs})$	0.0346
$R_w(F^2)$	0.0903
S	1.053
shift/error$_{max}$	0.001
max electron density/e Å^{-3}	0.361
min electron density/e Å^{-3}	−0.436

Methyltriphenylphosphonium pyridin-4-yl((trifluoromethyl)sulfonyl)amide ***6ac***

Figure S4: 119 shows a single ion pair, **Figure S4: 120** gives the unit cell and crystallographic data for catalyst system **6ac** is given in **Table S4: 6**:

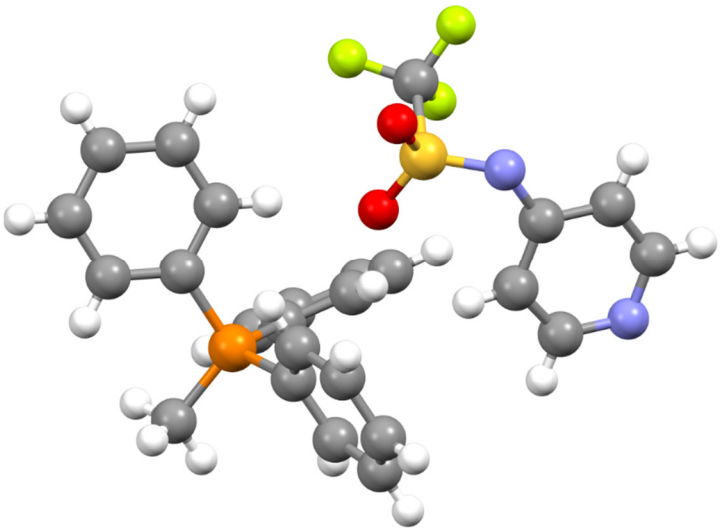

Figure S4: 119. *[Figure S119] Ion pair of catalyst* ***6ac****.*

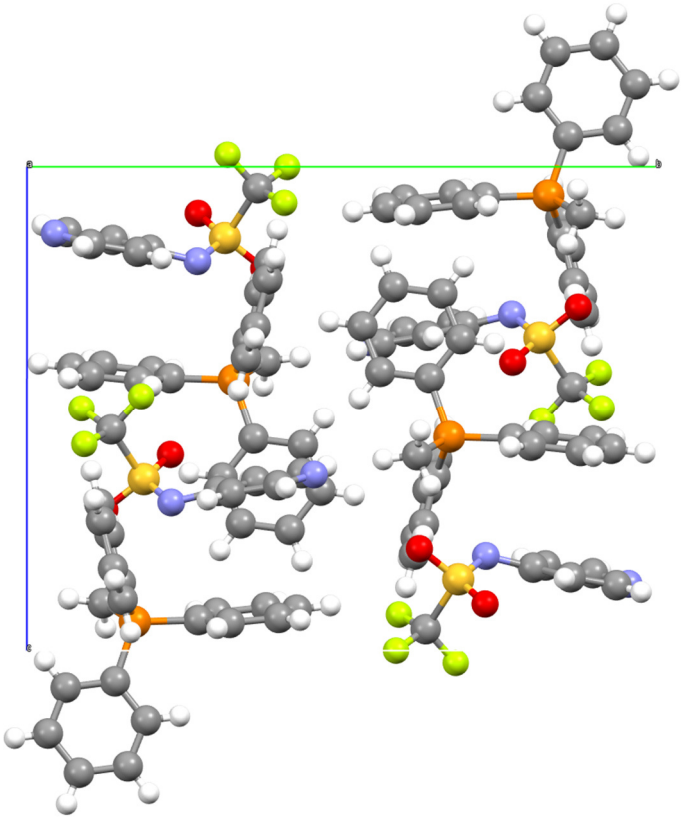

Figure S4: 120. *[Figure S120] Unit cell of catalyst* ***6ac*** *viewed along the a-axis.*

Table S4: 6. [Table S6]. Crystallographic details for ion pair catalyst **6ac**.

net formula	$C_{25}H_{22}F_3N_2O_2PS$
M_r/g mol^{-1}	502.47
crystal size/mm	0.100 × 0.090 × 0.060
T/K	100.(2)
radiation	MoKα
diffractometer	'Bruker D8 Venture TXS'
crystal system	monoclinic
space group	'P 1 21/n 1'
a/Å	10.2414(4)
b/Å	17.5228(6)
c/Å	14.1388(5)
α/°	90
β/°	107.3215(12)
γ/°	90
V/Å^3	2422.25(15)
Z	4
calc. density/g cm^{-3}	1.378
μ/mm^{-1}	0.248
absorption correction	Multi-Scan
transmission factor range	0.9303–0.9705
refls. measured	30328
R_{int}	0.0463
mean σ(*I*)/*I*	0.0395
θ range	3.137–30.508
observed refls.	6189
x, y (weighting scheme)	0.0365, 1.4492
hydrogen refinement	constr
refls in refinement	7370
parameters	308
restraints	0
$R(F_{obs})$	0.0371
$R_w(F^2)$	0.0993
S	1.048
shift/error$_{max}$	0.001
max electron density/e Å^{-3}	0.423
min electron density/e Å^{-3}	−0.468

Tetrabutylphosphonium pyridin-4-yl((trifluoromethyl)sulfonyl)amide ***6ad***

One of the butyl-chains of the phosphonium-cation is disordered. A split model was applied, the site occupation factor is ca. 1:1.

Figure S4: 121 shows a single ion pair, **Figure S4: 122** gives the unit cell and crystallographic data for catalyst system **6ad** is given in **Table S4: 7**:

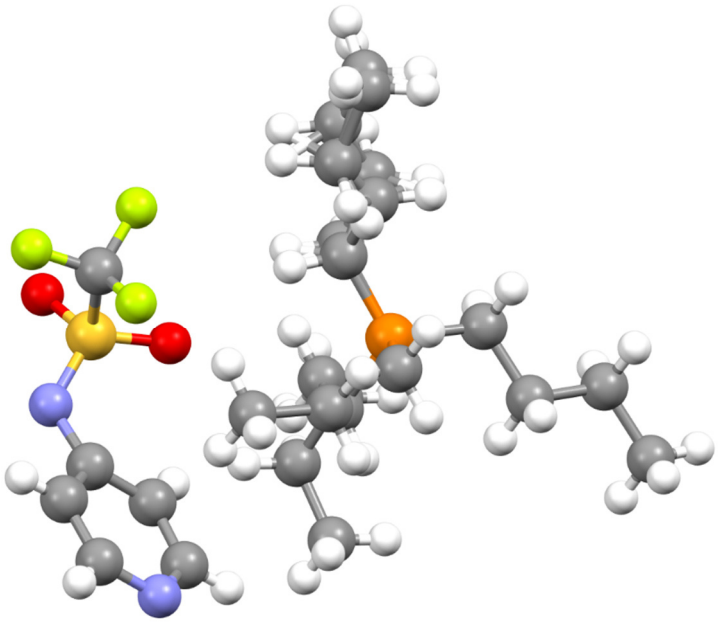

Figure S4: 121. *[Figure S121] Ion pair of catalyst* ***6ad****.*

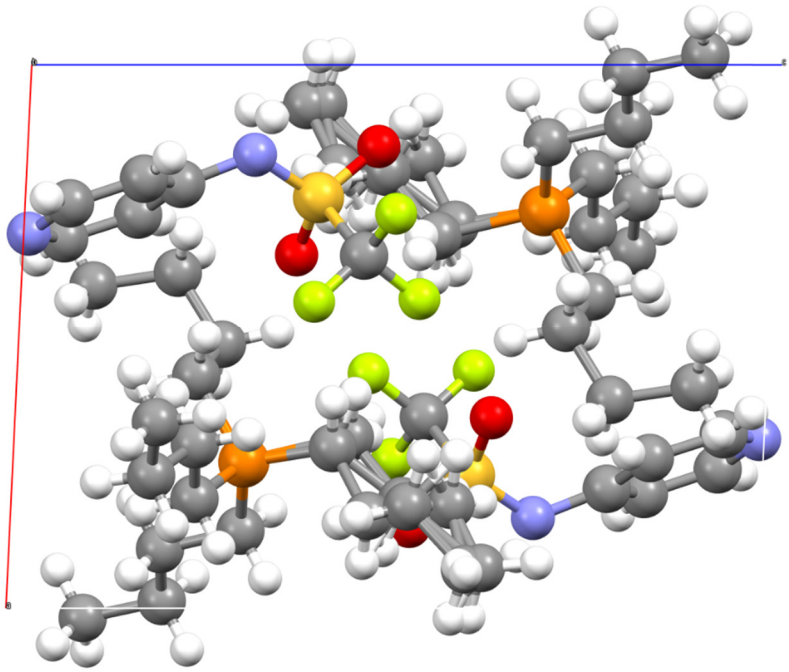

Figure S4: 122. *[Figure S122] Unit cell of catalyst* ***6ad*** *viewed along the b-axis.*

Table S4: 7. [Table S7] Crystallographic details for ion pair catalyst **6ad**.

net formula	$C_{22}H_{40}F_3N_2O_2PS$
M_r/g mol^{-1}	484.59
crystal size/mm	0.100 × 0.090 × 0.040
T/K	100.(2)
radiation	MoKα
diffractometer	'Bruker D8 Venture TXS'
crystal system	triclinic
space group	'P -1'
a/Å	9.8521(3)
b/Å	10.4233(4)
c/Å	13.8342(5)
α/°	72.0296(13)
β/°	88.1523(12)
γ/°	75.7263(12)
V/Å^3	1308.15(8)
Z	2
calc. density/g cm^{-3}	1.230
μ/mm^{-1}	0.226
absorption correction	Multi-Scan
transmission factor range	0.8946–0.9705
refls. measured	15218
R_{int}	0.0394
mean σ(*I*)/*I*	0.0573
θ range	3.167–28.279
observed refls.	4801
x, y (weighting scheme)	0.0395, 0.7033
hydrogen refinement	constr
refls in refinement	6472
parameters	322
restraints	0
$R(F_{obs})$	0.0473
$R_w(F^2)$	0.1164
S	1.032
shift/error$_{max}$	0.001
max electron density/e Å^{-3}	0.398
min electron density/e Å^{-3}	−0.368

One side chain disordered, split model applied, sof ratio ca. 1:1.

Methyltriphenylphosphonium pyridin-4-yl(tosyl)amide ***6bc***

Figure S4: 123 shows a single ion pair, **Figure S4: 124** gives the unit cell and crystallographic data for catalyst system **6bc** is given in **Table S4: 8**:

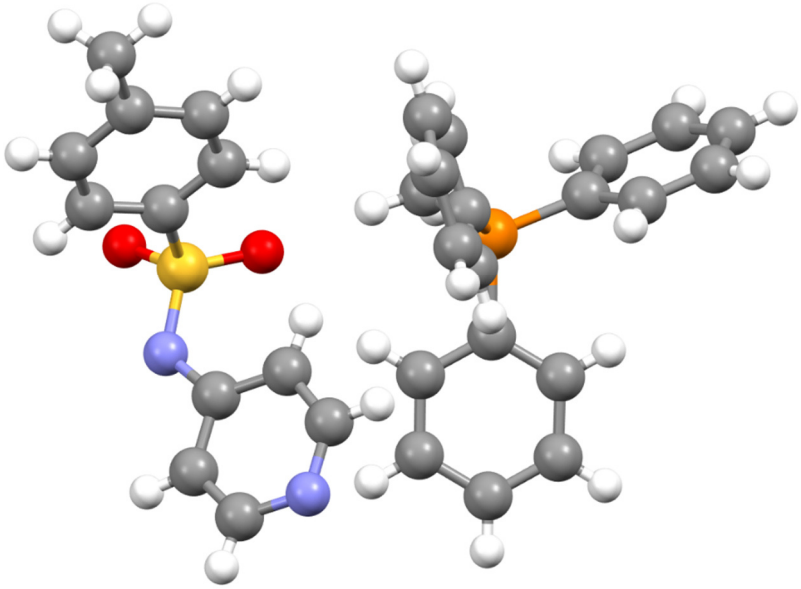

Figure S4: 123. *[Figure S123] Ion pair of catalyst* ***6bc****.*

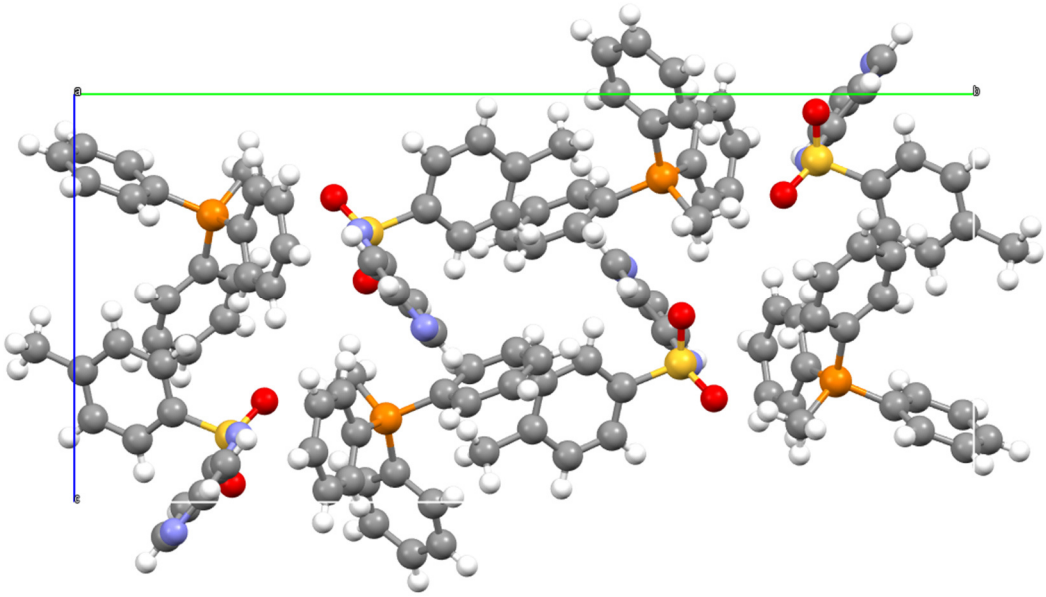

Figure S4: 124. *[Figure S124] Unit cell of catalyst* ***6bc*** *viewed along the a-axis.*

Table S4: 8. [Table S8] Crystallographic details for ion pair catalyst **6bc**.

net formula	$C_{31}H_{29}N_2O_2PS$
M_r/g mol^{-1}	524.59
crystal size/mm	0.100 × 0.090 × 0.050
T/K	100.(2)
radiation	MoKα
diffractometer	'Bruker D8 Venture TXS'
crystal system	monoclinic
space group	'P 1 21/n 1'
a/Å	9.6174(6)
b/Å	24.8400(18)
c/Å	11.3600(7)
α/°	90
β/°	97.197(3)
γ/°	90
V/Å^3	2692.5(3)
Z	4
calc. density/g cm^{-3}	1.294
μ/mm^{-1}	0.211
absorption correction	Multi-Scan
transmission factor range	0.9338–0.9705
refls. measured	43294
R_{int}	0.0378
mean σ(*I*)/*I*	0.0286
θ range	3.258–30.507
observed refls.	7198
x, y (weighting scheme)	0.0355, 1.8155
hydrogen refinement	constr
refls in refinement	8205
parameters	336
restraints	0
$R(F_{obs})$	0.0360
$R_w(F^2)$	0.0963
S	1.073
shift/error$_{max}$	0.001
max electron density/e Å^{-3}	0.447
min electron density/e Å^{-3}	−0.450

Benzyltriphenylphosphonium pyridin-4-yl(tosyl)amide ***6bf***

Figure S4: 125 shows a single ion pair, **Figure S4: 126** gives the unit cell and crystallographic data for catalyst system **6bf** is given in **Table S4: 9**:

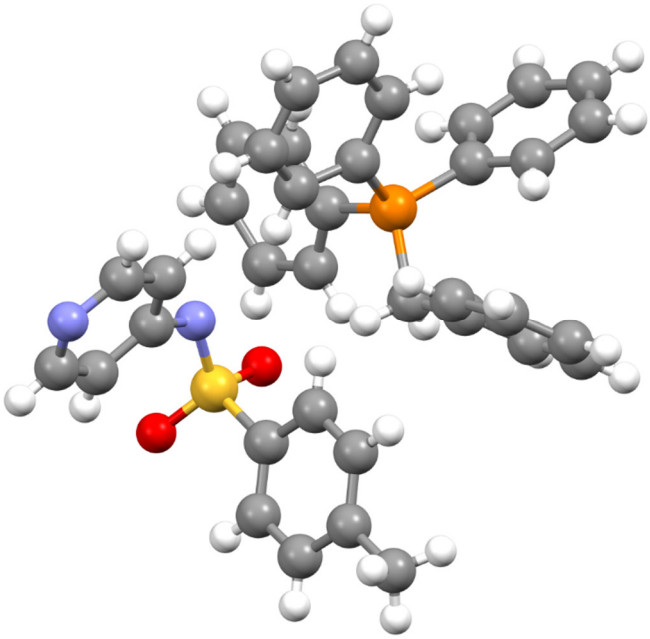

Figure S4: 125. *[Figure S125] Ion pair of catalyst* ***6bf****.*

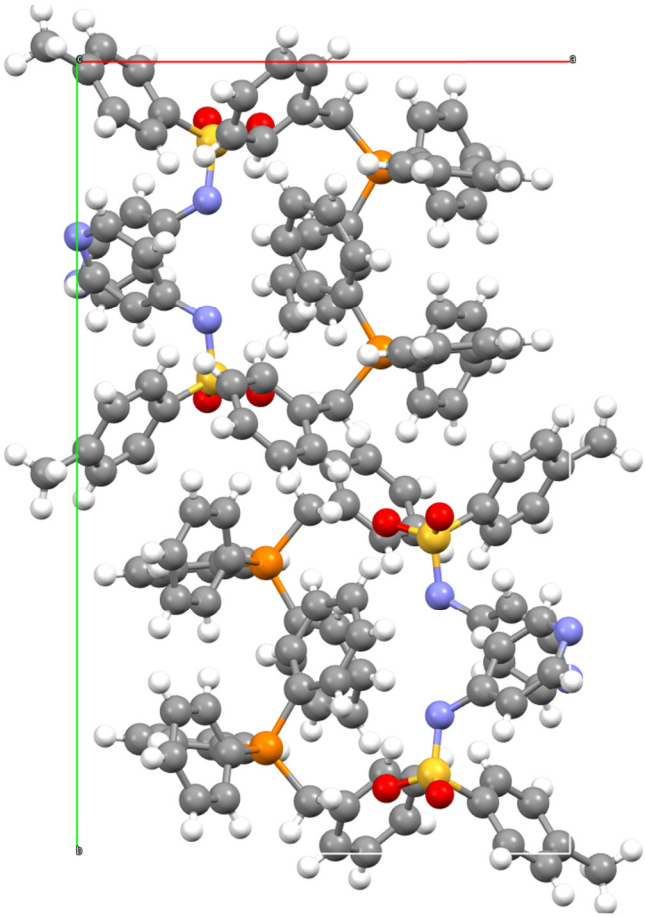

Figure S4: 126. *[Figure S126] Unit cell of catalyst* ***6bf*** *viewed along the c-axis.*

Table S4: 9. [Table S9] Crystallographic details for ion pair catalyst **6bf**.

net formula	$C_{37}H_{33}N_2O_2PS$
M_r/g mol^{-1}	600.68
crystal size/mm	0.060 × 0.050 × 0.040
T/K	296.(2)
radiation	MoKα
diffractometer	'Bruker D8Quest'
crystal system	monoclinic
space group	'P 1 21/c 1'
a/Å	13.7440(17)
b/Å	20.825(3)
c/Å	11.4009(18)
α/°	90
β/°	109.349(4)
γ/°	90
V/Å^3	3078.8(8)
Z	4
calc. density/g cm^{-3}	1.296
μ/mm^{-1}	0.194
absorption correction	Multi-Scan
transmission factor range	0.94–0.99
refls. measured	58691
R_{int}	0.0812
mean σ(*I*)/*I*	0.0397
θ range	3.142–26.372
observed refls.	5029
x, y (weighting scheme)	0.0525, 2.6093
hydrogen refinement	constr
refls in refinement	6275
parameters	389
restraints	3
$R(F_{obs})$	0.0628
$R_w(F^2)$	0.1453
S	1.080
shift/error$_{max}$	0.001
max electron density/e Å^{-3}	0.314
min electron density/e Å^{-3}	−0.316

DELU applied for C17-C18 and C18-C19.

1,3-Diethyl-benzimidazolium pyridin-4-yl(tosyl)amide ***6be***

Figure S4: 127 shows a single ion pair, **Figure S4: 128** gives the unit cell and crystallographic data for catalyst system **6be** is given in **Table S4: 10**:

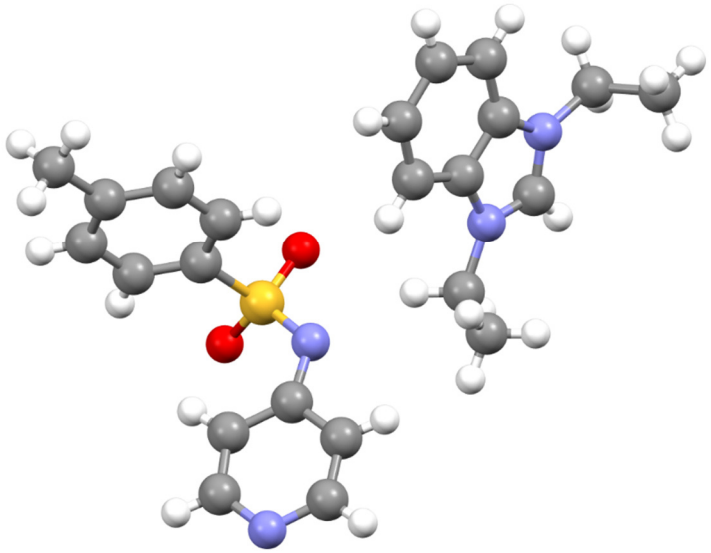

Figure S4: 127. *[Figure S127] Ion pair of catalyst* ***6be****.*

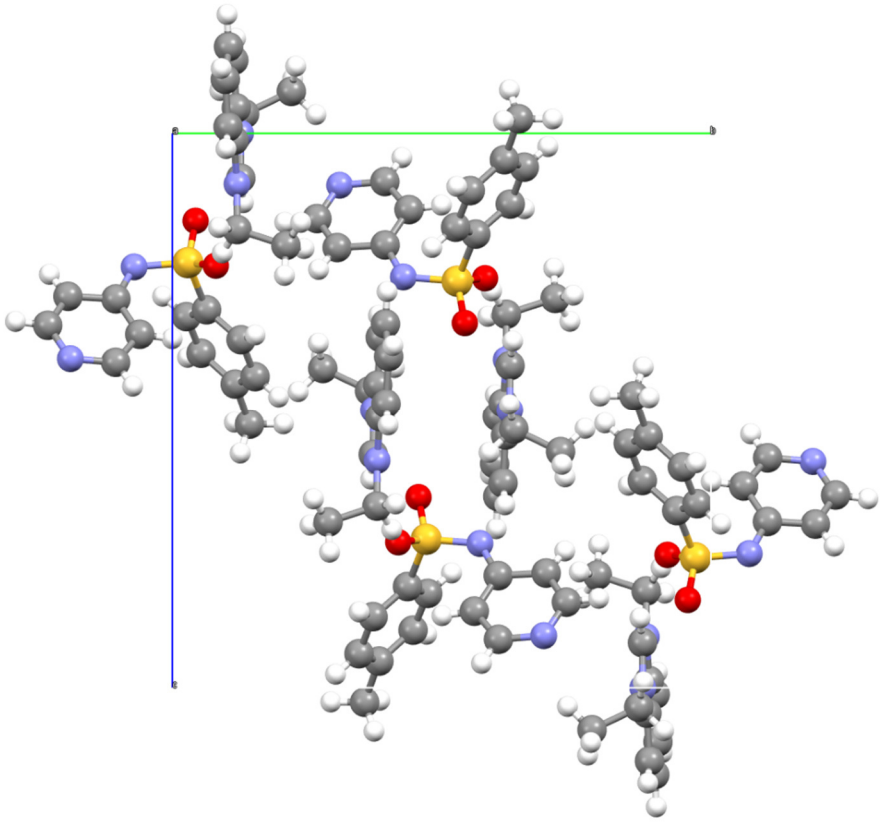

Figure S4: 128. *[Figure S128] Unit cell of catalyst* ***6be*** *viewed along the a-axis.*

Table S4: 10. [Table S10] Crystallographic details for ion pair catalyst **6be**.

net formula	$C_{23}H_{26}N_4O_2S$
M_r/g mol^{-1}	422.54
crystal size/mm	0.080 × 0.050 × 0.030
T/K	112.(2)
radiation	MoKα
diffractometer	'Bruker D8 Venture TXS'
crystal system	monoclinic
space group	'P 1 21/c 1'
a/Å	8.6461(8)
b/Å	15.4957(14)
c/Å	16.3096(13)
α/°	90
β/°	102.024(3)
γ/°	90
V/Å^3	2137.2(3)
Z	4
calc. density/g cm^{-3}	1.313
μ/mm^{-1}	0.179
absorption correction	Multi-Scan
transmission factor range	0.97–0.99
refls. measured	37309
R_{int}	0.0531
mean σ(*I*)/*I*	0.0314
θ range	2.872–27.097
observed refls.	3986
x, y (weighting scheme)	0.0381, 1.4408
hydrogen refinement	constr
refls in refinement	4709
parameters	274
restraints	0
$R(F_{obs})$	0.0376
$R_w(F^2)$	0.0993
S	1.034
shift/error$_{max}$	0.001
max electron density/e Å^{-3}	0.251
min electron density/e Å^{-3}	−0.440

Tetraphenylphosphonium ((4-methoxyphenyl)sulfonyl)(pyridin-4-yl)amide ***6cg***

Figure S4: 129 shows a single ion pair, **Figure S4: 130** gives the unit cell and crystallographic data for catalyst system **6cg** is given in **Table S4: 11**:

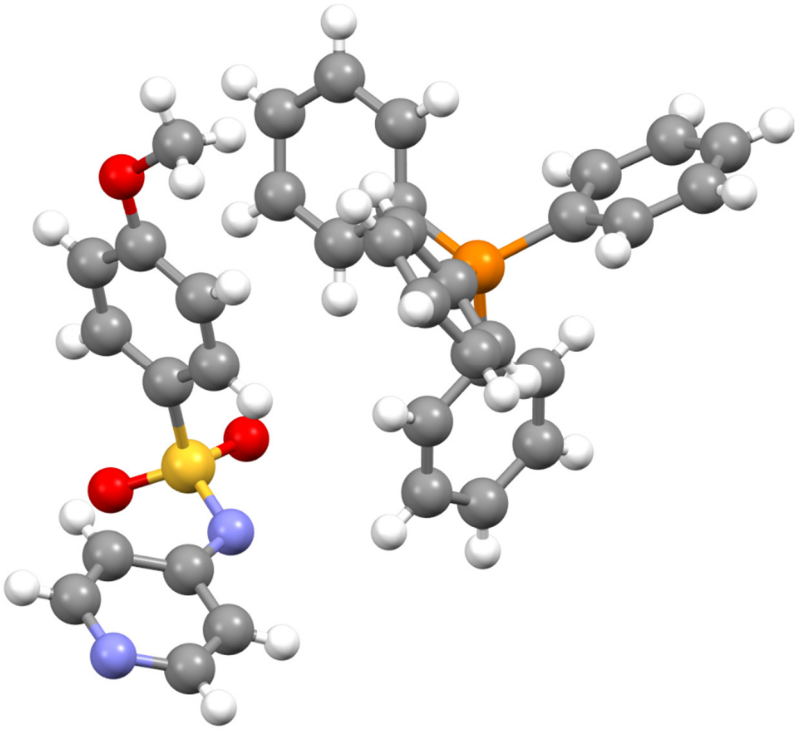

Figure S4: 129. *[Figure S129] Ion pair of catalyst* ***6cg****.*

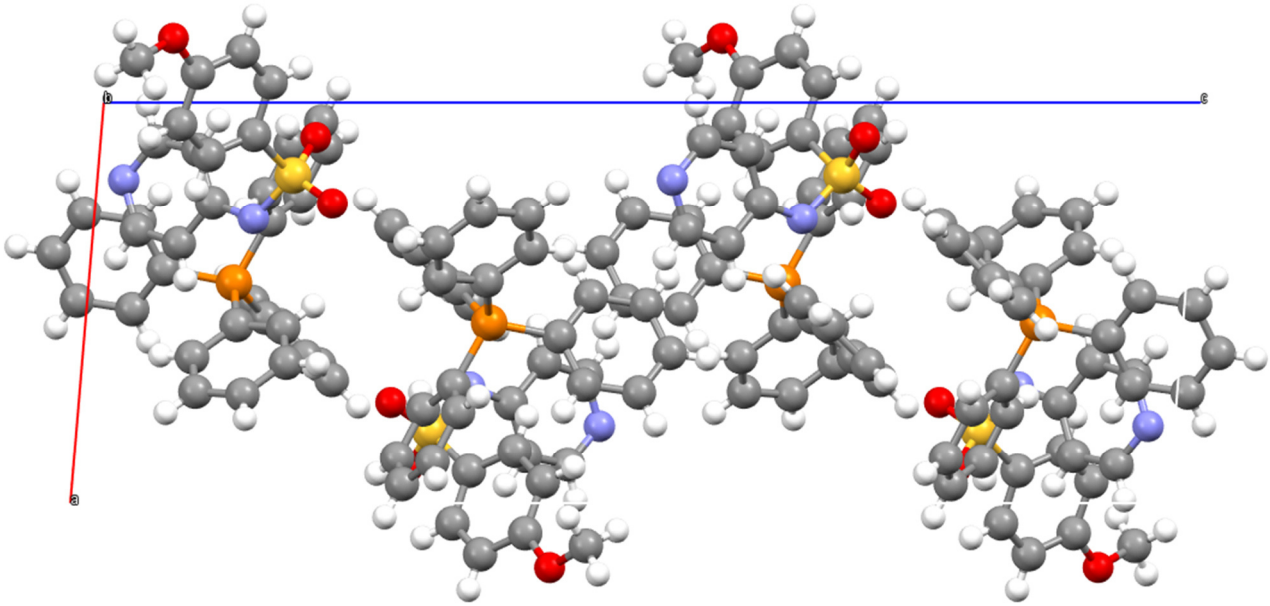

Figure S4: 130. *[Figure S130] Unit cell of catalyst* ***6cg*** *viewed along the b-axis.*

Table S4: 11. [Table S11] Crystallographic details for ion pair catalyst **6cg**.

net formula	$C_{36}H_{31}N_2O_3PS$
M_r/g mol^{-1}	602.66
crystal size/mm	0.090 × 0.070 × 0.050
T/K	298.(2)
radiation	MoKα
diffractometer	'Bruker D8 Venture TXS'
crystal system	monoclinic
space group	'P 1 21/c 1'
a/Å	9.8948(3)
b/Å	11.5408(3)
c/Å	26.9578(7)
α/°	90
β/°	94.7690(10)
γ/°	90
V/Å^3	3067.76(15)
Z	4
calc. density/g cm^{-3}	1.305
μ/mm^{-1}	0.197
absorption correction	Multi-Scan
transmission factor range	0.95–0.99
refls. measured	32004
R_{int}	0.0384
mean σ(*I*)/*I*	0.0319
θ range	2.867–27.103
observed refls.	5056
x, y (weighting scheme)	0.0440, 1.4908
hydrogen refinement	constr
refls in refinement	6770
parameters	389
restraints	0
$R(F_{obs})$	0.0436
$R_w(F^2)$	0.1165
S	1.030
shift/error$_{max}$	0.001
max electron density/e Å^{-3}	0.262
min electron density/e Å^{-3}	−0.309

1,3-Diethyl-benzimidazolium ((4-methoxyphenyl)sulfonyl)(pyridin-4-yl)amide ***6ce***

Figure S4: 131 shows a single ion pair, **Figure S4: 132** gives the unit cell and crystallographic data for catalyst system **6ce** is given in **Table S4: 12**:

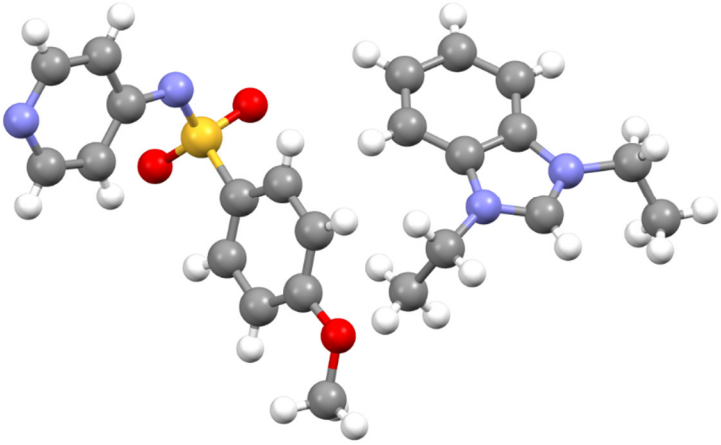

Figure S4: 131. *[Figure S131] Ion pair of catalyst* ***6ce****.*

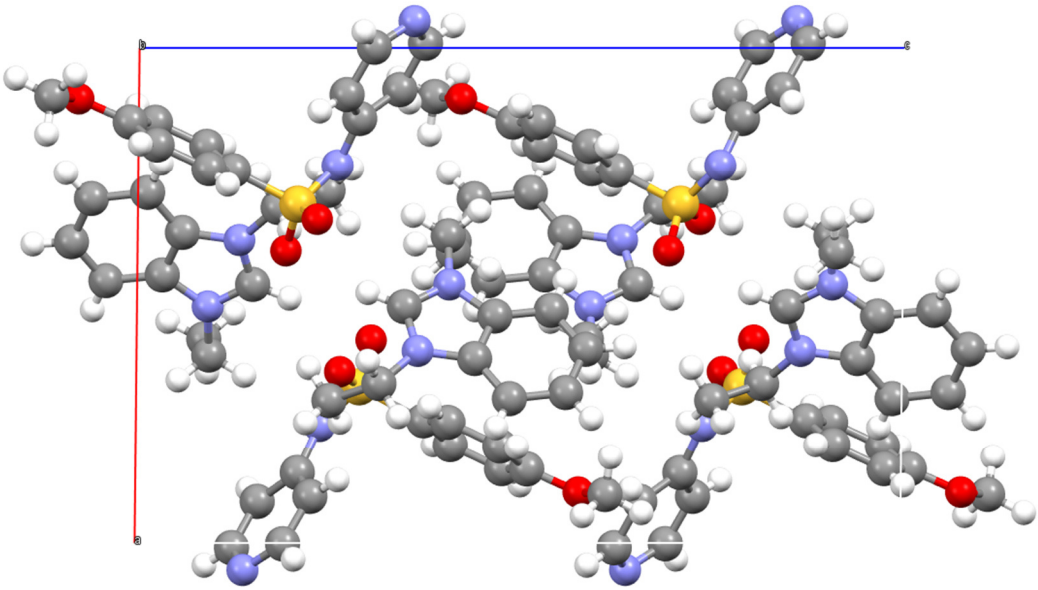

Figure S4: 132. *[Figure S132] Unit cell of catalyst* ***6ce*** *viewed along the b-axis.*

Table S4: 12. [Table S12] Crystallographic details for ion pair catalyst **6ce**.

net formula	$C_{23}H_{26}N_4O_3S$
M_r/g mol^{-1}	438.54
crystal size/mm	0.090 × 0.040 × 0.030
T/K	107.(2)
radiation	MoKα
diffractometer	'Bruker D8 Venture TXS'
crystal system	monoclinic
space group	'P 1 21/c 1'
a/Å	11.9827(9)
b/Å	9.6390(7)
c/Å	18.4664(15)
α/°	90
β/°	90.582(3)
γ/°	90
V/Å^3	2132.8(3)
Z	4
calc. density/g cm^{-3}	1.366
μ/mm^{-1}	0.185
absorption correction	Multi-Scan
transmission factor range	0.95–0.99
refls. measured	28433
R_{int}	0.0481
mean σ(*I*)/*I*	0.0322
θ range	2.934–26.372
observed refls.	3618
x, y (weighting scheme)	0.0382, 1.6219
hydrogen refinement	constr
refls in refinement	4342
parameters	283
restraints	1
$R(F_{obs})$	0.0402
$R_w(F^2)$	0.1050
S	1.050
shift/error$_{max}$	0.001
max electron density/e Å^{-3}	0.378
min electron density/e Å^{-3}	−0.408

1,3-Diethyl-benzimidazolium pyridin-2-yl(tosyl)amide ***7e***

Figure S4: 133 shows a single ion pair, **Figure S4: 134** gives the unit cell and crystallographic data for catalyst system **7e** is given in **Table S4: 13**:

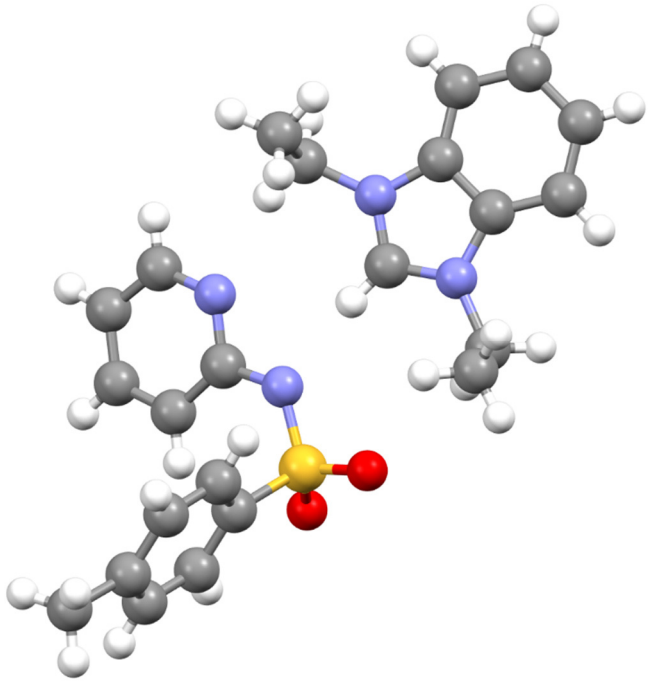

Figure S4: 133. *[Figure S133] Ion pair of catalyst* ***7e****.*

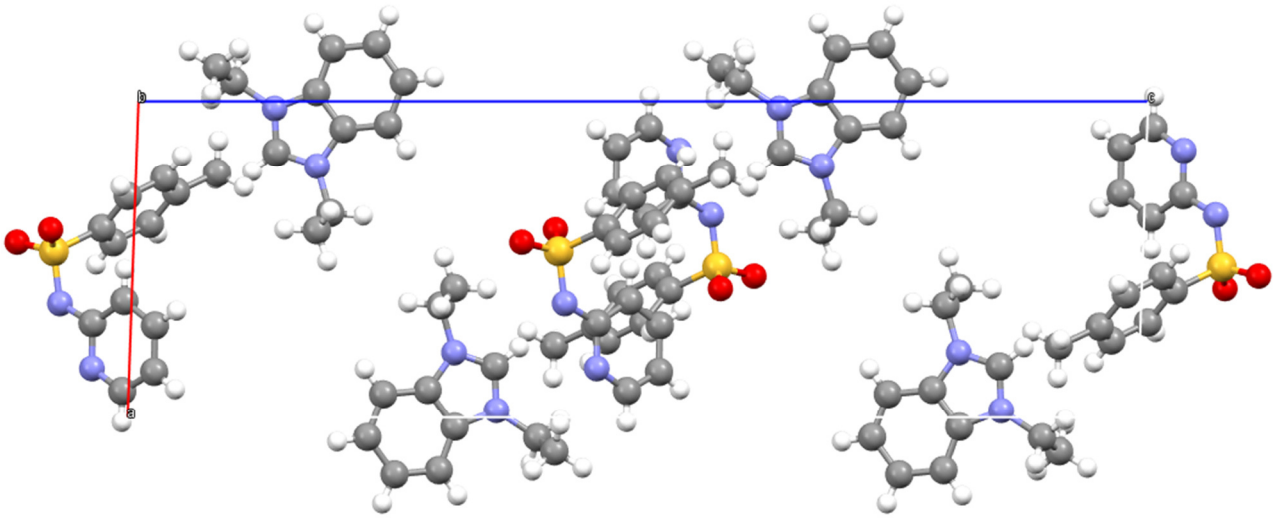

Figure S4: 134. *[Figure S134] Unit cell of catalyst* ***7e*** *viewed along the b-axis.*

Table S4: 13. [Table S13] Crystallographic details for ion pair catalyst **7e**.

net formula	$C_{23}H_{26}N_4O_2S$
M_r/g mol^{-1}	422.54
crystal size/mm	0.080 × 0.040 × 0.030
T/K	106.(2)
radiation	MoKα
diffractometer	'Bruker D8 Venture TXS'
crystal system	monoclinic
space group	'P 1 21/c 1'
a/Å	9.5001(3)
b/Å	14.8911(4)
c/Å	30.2630(9)
α/°	90
β/°	91.9590(10)
γ/°	90
V/Å^3	4278.7(2)
Z	8
calc. density/g cm^{-3}	1.312
μ/mm^{-1}	0.179
absorption correction	Multi-Scan
transmission factor range	0.94–0.99
refls. measured	63746
R_{int}	0.0532
mean σ(*I*)/*I*	0.0294
θ range	2.544–25.350
observed refls.	6407
x, y (weighting scheme)	0.0379, 2.4800
hydrogen refinement	constr
refls in refinement	7815
parameters	547
restraints	0
$R(F_{obs})$	0.0385
$R_w(F^2)$	0.0949
S	1.062
shift/error$_{max}$	0.001
max electron density/e Å^{-3}	0.285
min electron density/e Å^{-3}	−0.433

1,1,1-Trifluoro-N-(pyridin-4(1H)-ylidene)methanesulfonamide ***8a***

Recrystallization was done from H_2O.

Figure S4: 135 shows a single molecule, **Figure S4: 136** gives the unit cell and crystallographic data for sulfonamide **8a** is given in **Table S4: 14**:

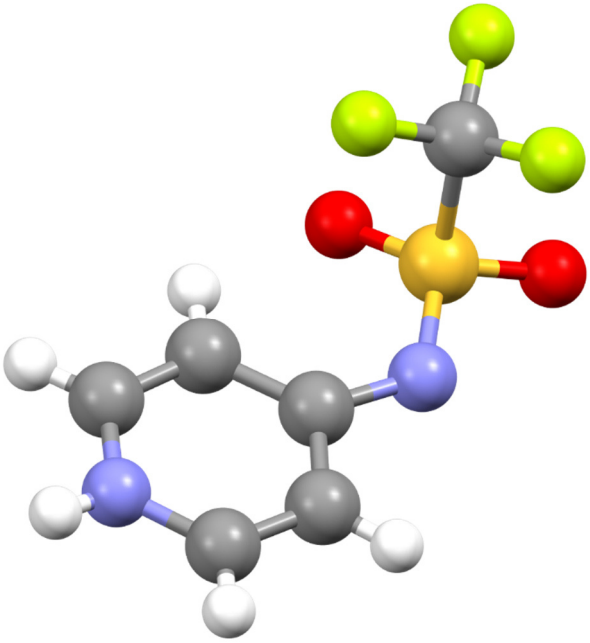

Figure S4: 135. *[Figure S135] Molecule of sulfonamide* ***8a****.*

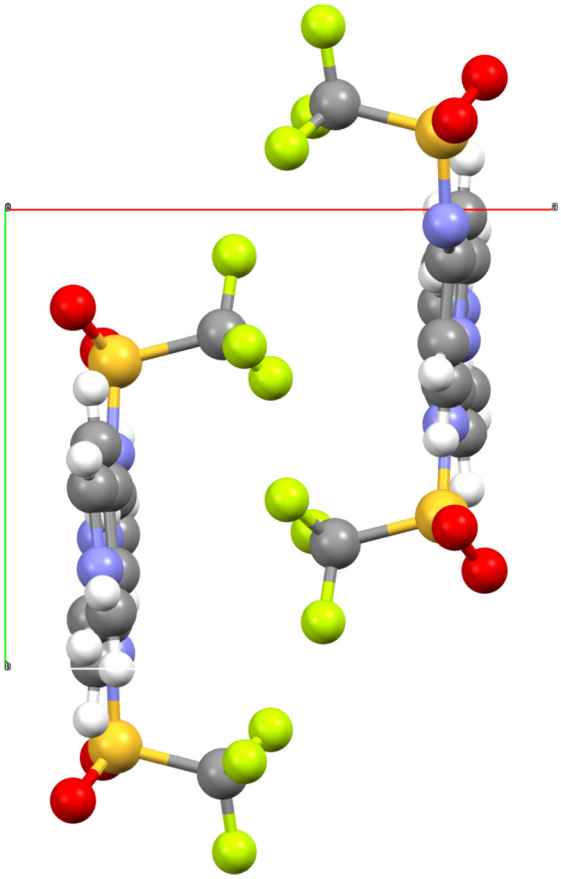

Figure S4: 136. *[Figure S136] Unit cell of sulfonamide* ***8a*** *viewed along the c-axis.*

Table S4: 14. [Table S14]. Crystallographic details for sulfonamide **8a**.

net formula	$C_6H_5F_3N_2O_2S$
M_r/g mol^{-1}	226.18
crystal size/mm	0.090 × 0.050 × 0.040
T/K	105.(2)
radiation	MoKα
diffractometer	'Bruker D8 Venture TXS'
crystal system	monoclinic
space group	'P 1 21/c 1'
a/Å	9.3732(7)
b/Å	7.5696(5)
c/Å	12.4533(8)
α/°	90
β/°	106.212(2)
γ/°	90
V/Å^3	848.44(10)
Z	4
calc. density/g cm^{-3}	1.771
μ/mm^{-1}	0.407
absorption correction	Multi-Scan
transmission factor range	0.94–0.98
refls. measured	17191
R_{int}	0.0431
mean σ(*I*)/*I*	0.0273
θ range	3.185–30.505
observed refls.	2260
x, y (weighting scheme)	0.0370, 0.5851
hydrogen refinement	H(C) constr, H(N) refall
refls in refinement	2573
parameters	131
restraints	0
$R(F_{obs})$	0.0326
$R_w(F^2)$	0.0892
S	1.070
shift/error$_{max}$	0.001
max electron density/e Å^{-3}	0.458
min electron density/e Å^{-3}	−0.383

4-Methyl-N-(pyridin-4(1H)-ylidene)benzenesulfonamide ***8b***

Recrystallization was done from DMSO.

Figure S4: 137 shows a single molecule, **Figure S4: 138** gives the unit cell and crystallographic data for sulfonamide **8b** is given in **Table S4: 15**:

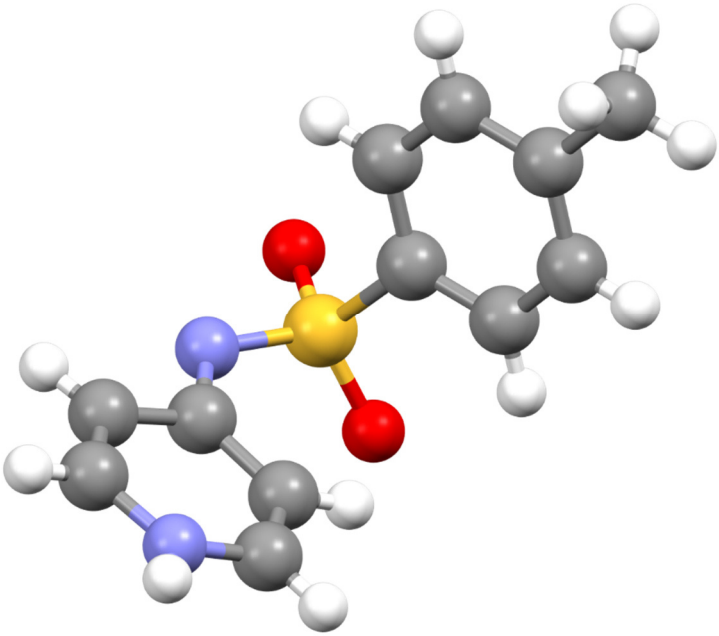

Figure S4: 137. *[Figure S137] Molecule of sulfonamide* ***8b****.*

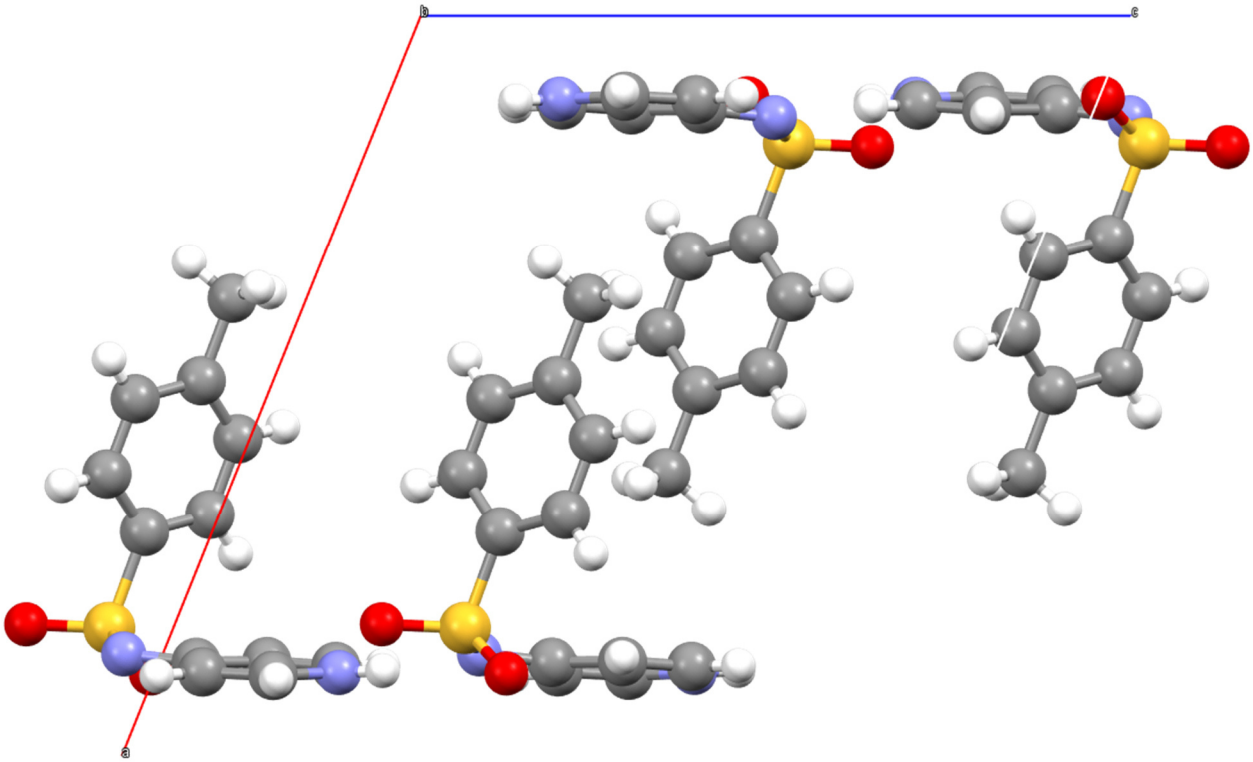

Figure S4: 138. *[Figure S138] Unit cell of sulfonamide* ***8b*** *viewed along the b-axis.*

Table S4: 15. [Table S15] Crystallographic details for sulfonamide **8b**.

net formula	$C_{12}H_{12}N_2O_2S$
M_r/g mol^{-1}	248.30
crystal size/mm	0.100 × 0.100 × 0.050
T/K	105.(2)
radiation	MoKα
diffractometer	'Bruker D8 Venture TXS'
crystal system	monoclinic
space group	'P 1 21/c 1'
a/Å	13.7763(6)
b/Å	7.4726(3)
c/Å	12.2799(6)
α/°	90
β/°	112.0110(10)
γ/°	90
V/Å^3	1172.01(9)
Z	4
calc. density/g cm^{-3}	1.407
μ/mm^{-1}	0.267
absorption correction	Multi-Scan
transmission factor range	0.86–0.99
refls. measured	17184
R_{int}	0.0440
mean σ(*I*)/*I*	0.0302
θ range	3.158–27.481
observed refls.	2170
x, y (weighting scheme)	0.0313, 1.7564
hydrogen refinement	H(C) constr, H(N) refall
refls in refinement	2675
parameters	159
restraints	0
$R(F_{obs})$	0.0455
$R_w(F^2)$	0.1168
S	1.102
shift/error$_{max}$	0.001
max electron density/e Å^{-3}	0.399
min electron density/e Å^{-3}	−0.520

4N-(1,4-dihydropyridin-4-yl)-4-methoxybenzenesulfonamide ***8c***

Recrystallization was done from a 1/2 mixture of pyridine/H_2O.

8c crystallized with one molecule of H_2O per sulfonamide, which coordinates at the amide-N.

Figure S4: 139 shows a single molecule, **Figure S4: 140** gives the unit cell and crystallographic data for sulfonamide **8c** is given in **Table S4: 16**:

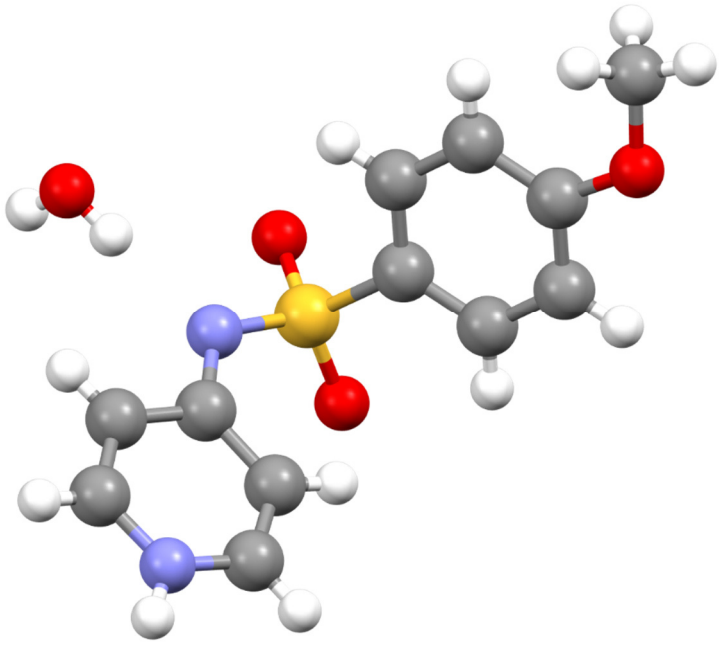

Figure S4: 139. *[Figure S139] Molecule of sulfonamide* ***8c****.*

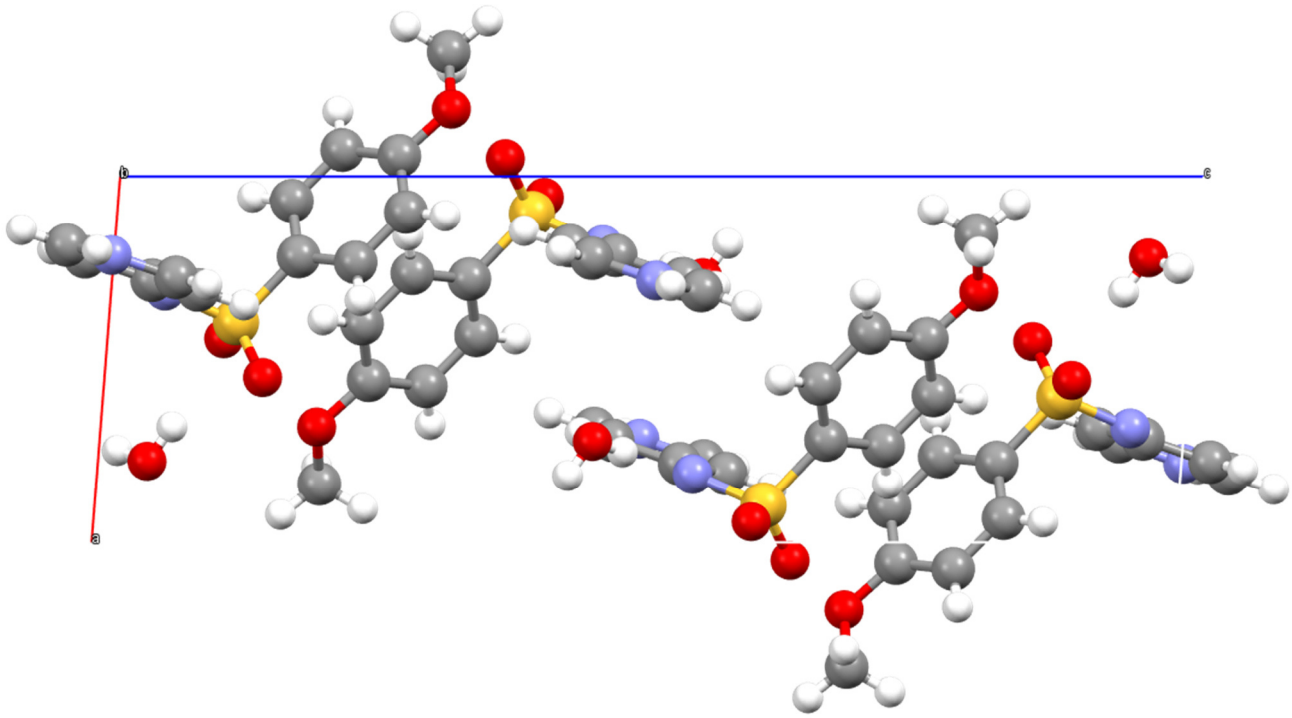

Figure S4: 140. *[Figure S140] Unit cell of sulfonamide* ***8c*** *viewed along the b-axis.*

Table S4: 16. [Table S16] Crystallographic details for sulfonamide **8c**.

net formula	$C_{12}H_{14}N_2O_4S$
M_r/g mol^{-1}	282.31
crystal size/mm	0.100 × 0.050 × 0.030
T/K	105.(2)
radiation	MoKα
diffractometer	'Bruker D8 Venture TXS'
crystal system	monoclinic
space group	'P 1 21/n 1'
a/Å	7.1584(4)
b/Å	8.4697(4)
c/Å	21.0760(11)
α/°	90
β/°	94.450(2)
γ/°	90
V/Å^3	1273.98(11)
Z	4
calc. density/g cm^{-3}	1.472
μ/mm^{-1}	0.266
absorption correction	Multi-Scan
transmission factor range	0.92–0.99
refls. measured	23725
R_{int}	0.0440
mean σ(*I*)/*I*	0.0319
θ range	2.942–30.497
observed refls.	3297
x, y (weighting scheme)	0.0388, 0.8028
hydrogen refinement	H(C) constr, H(N,O) refall
refls in refinement	3887
parameters	185
restraints	0
$R(F_{obs})$	0.0353
$R_w(F^2)$	0.0975
S	1.052
shift/error$_{max}$	0.001
max electron density/e Å^{-3}	0.402
min electron density/e Å^{-3}	−0.422

8c crystallized with one molecule of H_2O per sulfonamide, which coordinates at the amide-N.

Tetrabutylphosphonium (diphenylphosphoryl)(pyridin-4-yl)amide ***10d***

Disorder is addressed by a split-model. The unit cell contains two asymmetric units which in tun consist of three ion pairs.

Figure S4: 141 shows single ion pair, **Figure S4: 142** gives the unit cell and crystallographic data for catalyst system **10d** is given in **Table S4: 17**:

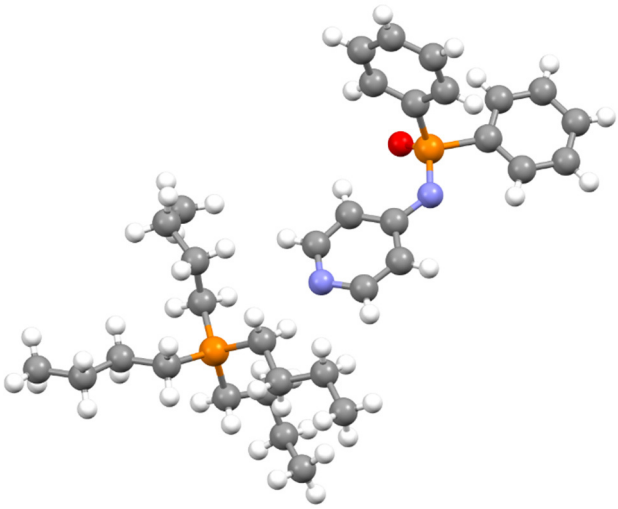

Figure S4: 141. *[Figure S141] Ion pair of catalyst* ***10d****.*

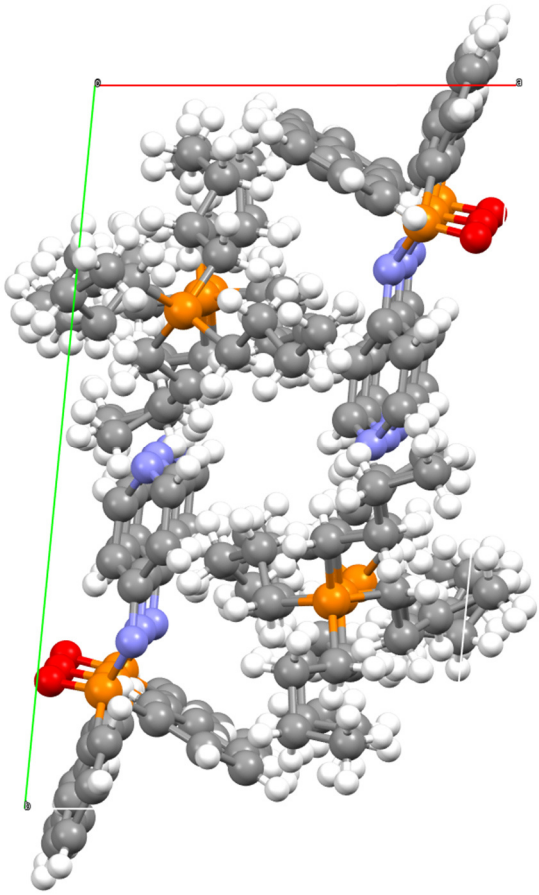

Figure S4: 142. *[Figure S142] Unit cell of catalyst* ***10d*** *viewed along the c-axis.*

Table S4: 17. [Table S17] Crystallographic details for ion pair catalyst 10d.

net formula	$C_{33}H_{50}N_2OP_2$
M_r/g mol^{-1}	552.69
crystal size/mm	0.436 × 0.191 × 0.138
T/K	143(2)
radiation	MoKα
diffractometer	'Oxford XCalibur'
crystal system	triclinic
space group	'P -1'
a/Å	10.0606(4)
b/Å	17.2822(5)
c/Å	28.0572(12)
α/°	97.836(3)
β/°	99.154(4)
γ/°	94.177(3)
V/Å^3	4748.9(3)
Z	6
calc. density/g cm^{-3}	1.160
μ/mm^{-1}	0.165
absorption correction	multi-scan
transmission factor range	0.98885–1.00000
refls. measured	25735
R_{int}	0.0466
mean σ(*I*)/*I*	0.1289
θ range	4.214–25.025
observed refls.	8233
x, y (weighting scheme)	0.0593, 0
hydrogen refinement	constr
refls in refinement	16587
parameters	1038
restraints	6
$R(F_{obs})$	0.0733
$R_w(F^2)$	0.1907
S	1.009
shift/error$_{max}$	0.001
max electron density/e Å^{-3}	0.596
min electron density/e Å^{-3}	−0.403

Disorder is addressed by a split-model. The unit cell contains two asymmetric units which in turn consist of three ion pairs.

*P,P-Diphenyl-N-(pyridin-4-yl)phosphonic amide **11***

Recrystallization was done from H_2O/EtOH.

11 crystallized with ½ molecule of H_2O per phosphonic amide molecule, which coordinates the amide-O of two molecules of **11** each.

Figure S4: 143 shows a single molecule, **Figure S4: 144** gives the unit cell and crystallographic data for phosphonic amide **11** is given in **Table S4: 18**:

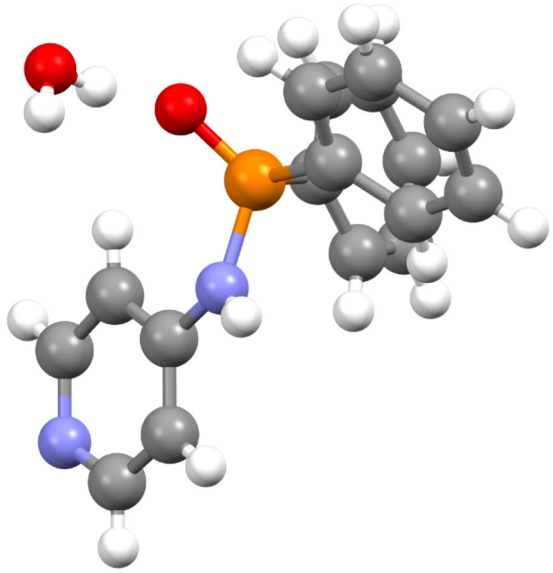

Figure S4: 143. *[Figure S143] Molecule of phosphonic amide **11**.*

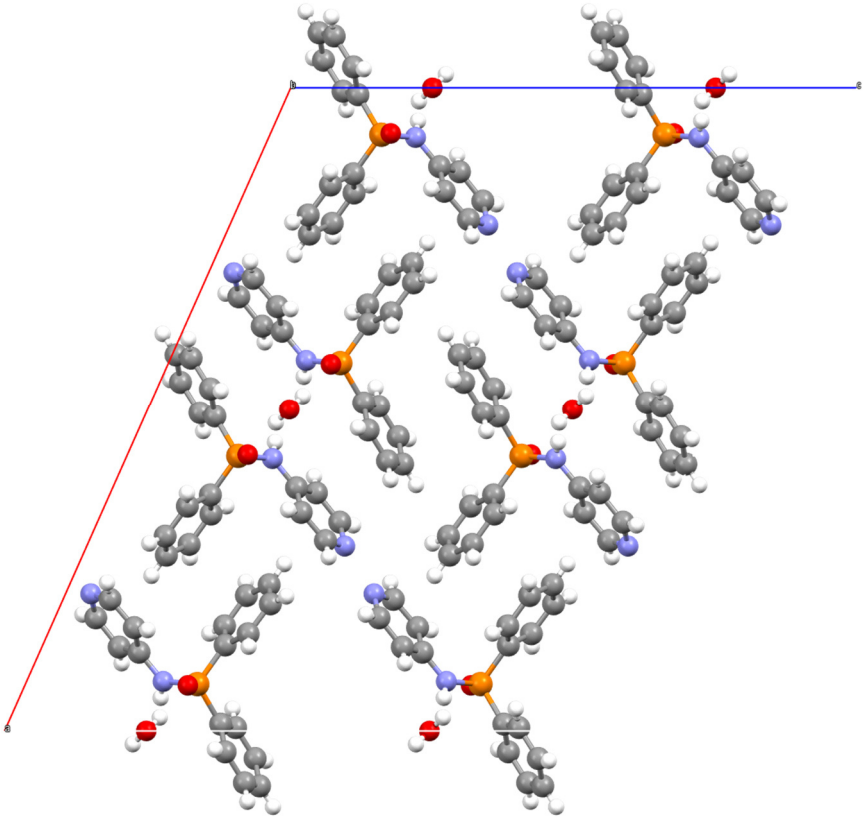

Figure S4: 144. *[Figure S144] Unit cell of phosphonic amide **11** viewed along the b-axis.*

Table S4: 18. [Table S18] Crystallographic details for phosphonic amide **11**.

net formula	$C_{34}H_{32}N_4O_3P_2$
M_r/g mol^{-1}	606.57
crystal size/mm	0.080 × 0.060 × 0.030
T/K	103.(2)
radiation	MoKα
diffractometer	'Bruker D8 Venture TXS'
crystal system	monoclinic
space group	'C 1 2/c 1'
a/Å	26.0481(8)
b/Å	6.0009(2)
c/Å	20.9637(7)
α/°	90
β/°	113.9890(10)
γ/°	90
V/Å^3	2993.83(17)
Z	4
calc. density/g cm^{-3}	1.346
μ/mm^{-1}	0.188
absorption correction	Multi-Scan
transmission factor range	0.97–0.99
refls. measured	25369
R_{int}	0.0426
mean σ(*I*)/*I*	0.0272
θ range	3.214–27.485
observed refls.	3097
x, y (weighting scheme)	0.0319, 3.9710
hydrogen refinement	H(C) constr, H(N,O) refall
refls in refinement	3426
parameters	203
restraints	0
$R(F_{obs})$	0.0321
$R_w(F^2)$	0.0850
S	1.057
shift/error$_{max}$	0.001
max electron density/e Å^{-3}	0.399
min electron density/e Å^{-3}	−0.369

11 crystallized with ½ molecule of H_2O per phosphonic amide molecule, which coordinates the amide-O of two molecules of **11** each.

3-(Pyridin-4-ylamino)benzo[d]isothiazole 1,1-dioxide ***14***

Recrystallization was done from DMSO.

Compound **14** crystallized with one molecule of DMSO per sulfonamide molecule, which coordinates at the H-atom of the secondary amine.

Figure S4: 145 shows a single molecule, **Figure S4: 146** gives the unit cell and crystallographic data for "extended" sulfonamide **14** is given in **Table S4: 19**:

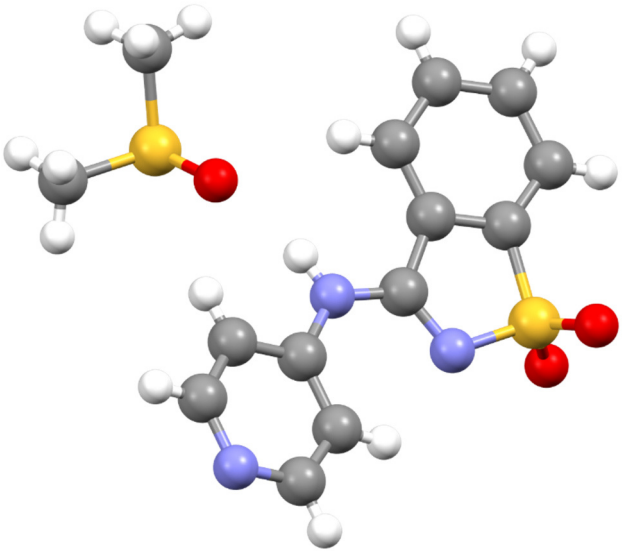

Figure S4: 145. *[Figure S145] Molecule of sulfonamide* ***14****.*

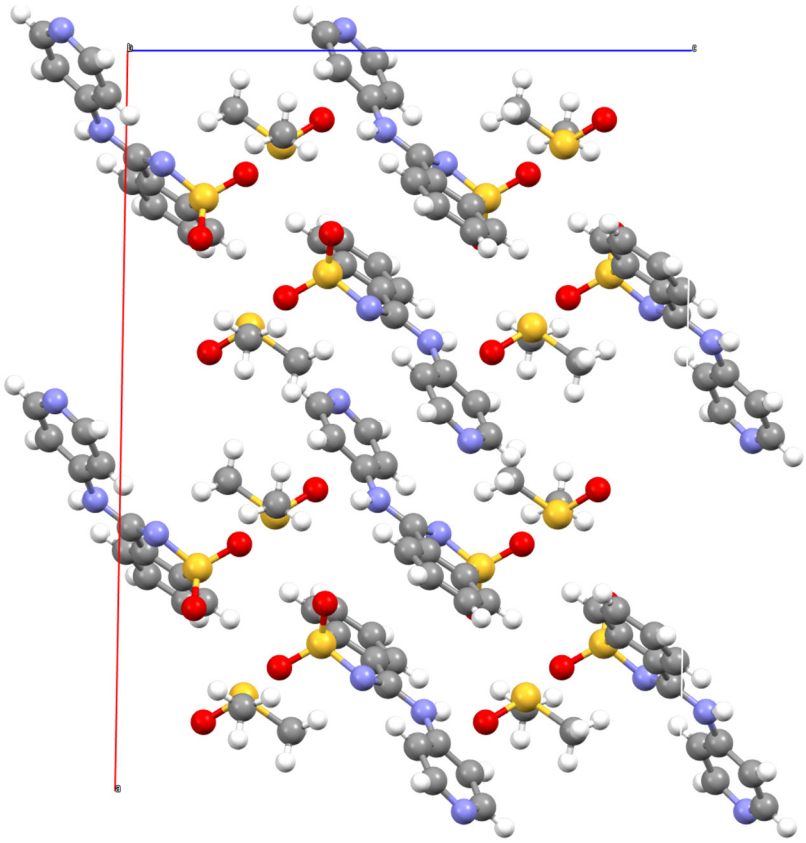

Figure S4: 146. *[Figure S146] Unit cell of sulfonamide* ***14*** *viewed along the b-axis.*

Table S4: 19. [Table S19] Crystallographic details for sulfonamide **14**.

net formula	$C_{14}H_{15}N_3O_3S_2$
M_r/g mol^{-1}	337.41
crystal size/mm	0.100 × 0.090 × 0.070
T/K	105.(2)
radiation	MoKα
diffractometer	'Bruker D8 Venture TXS'
crystal system	monoclinic
space group	'C 1 2/c 1'
a/Å	22.0954(14)
b/Å	8.0559(6)
c/Å	16.8525(11)
α/°	90
β/°	90.975(2)
γ/°	90
V/Å^3	2999.3(4)
Z	8
calc. density/g cm^{-3}	1.494
μ/mm^{-1}	0.371
absorption correction	Multi-Scan
transmission factor range	0.94–0.97
refls. measured	28539
R_{int}	0.0263
mean σ(*I*)/*I*	0.0191
θ range	3.016–30.503
observed refls.	4234
x, y (weighting scheme)	0.0346, 3.5011
hydrogen refinement	H(C) constr, H(N) refall
refls in refinement	4576
parameters	205
restraints	0
$R(F_{obs})$	0.0290
$R_w(F^2)$	0.0812
S	1.080
shift/error$_{max}$	0.001
max electron density/e Å^{-3}	0.406
min electron density/e Å^{-3}	−0.450

14 crystallized with one molecule of DMSO per sulfonamide molecule, which coordinates at the H-atom of the secondary amine.

Tetraphenylphosphonium (1,1-dioxidobenzo[d]isothiazol-3-yl)(pyridin-4-yl)amide ***15g***

Figure S4: 147 shows single ion pair, **Figure S4: 148** gives the unit cell and crystallographic data for catalyst system **15g** is given in **Table S4: 20**:

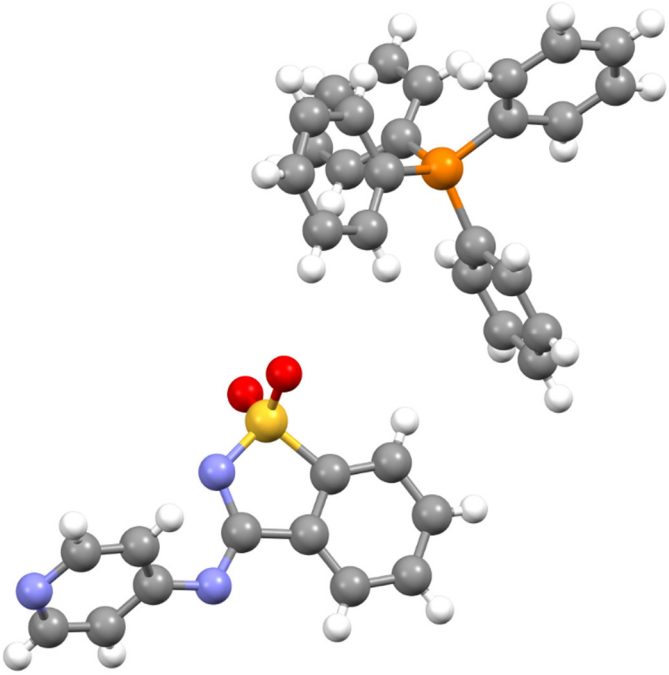

Figure S4: 147. *[Figure S147] Ion pair of catalyst* ***15g****.*

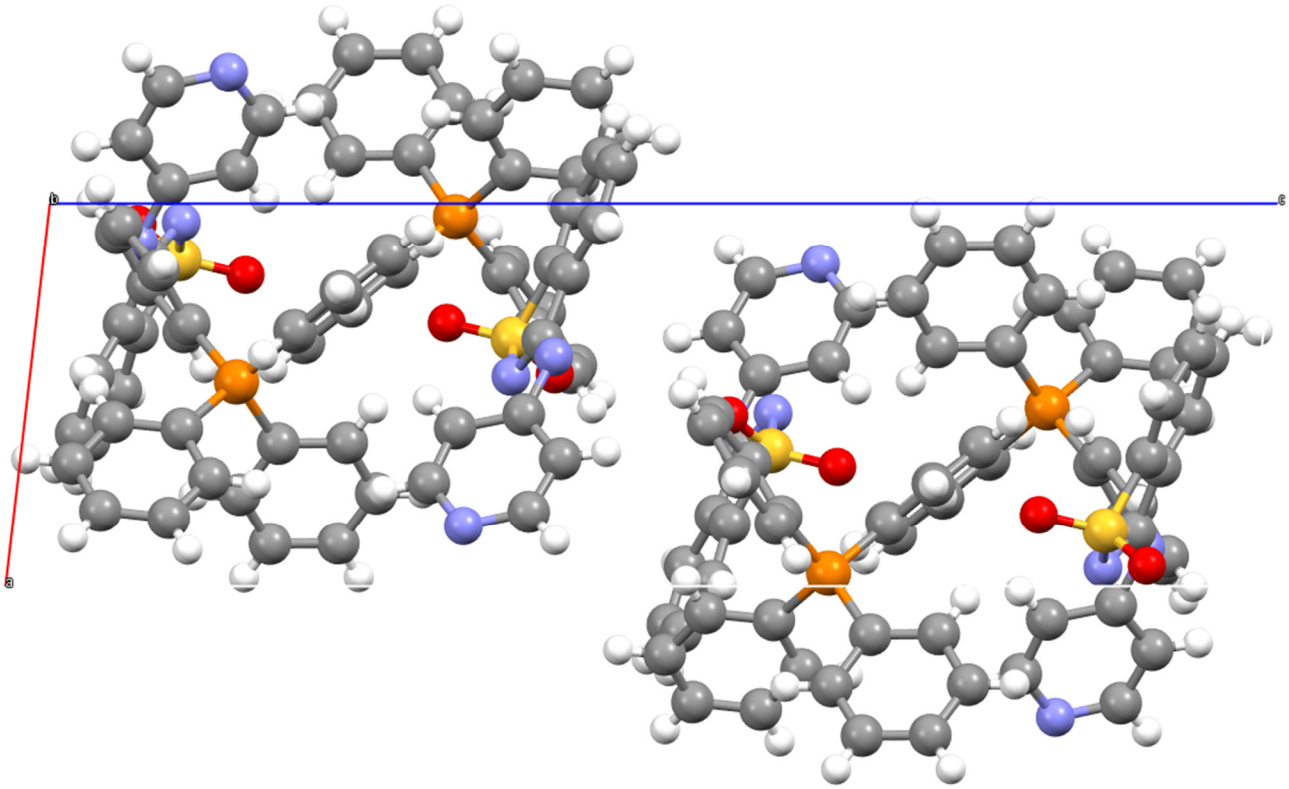

Figure S4: 148. *[Figure S148] Unit cell of catalyst* ***15g*** *viewed along the b-axis.*

Table S4: 20. [Table S20] Crystallographic details for ion pair catalyst **15g**.

net formula	$C_{33}H_{50}N_2OP_2$
M_r/g mol^{-1}	552.69
crystal size/mm	0.436 × 0.191 × 0.138
T/K	143(2)
radiation	MoKα
diffractometer	'Oxford XCalibur'
crystal system	triclinic
space group	'P -1'
a/Å	10.0606(4)
b/Å	17.2822(5)
c/Å	28.0572(12)
α/°	97.836(3)
β/°	99.154(4)
γ/°	94.177(3)
V/Å^3	4748.9(3)
Z	6
calc. density/g cm^{-3}	1.160
μ/mm^{-1}	0.165
absorption correction	multi-scan
transmission factor range	0.98885–1.00000
refls. measured	25735
R_{int}	0.0466
mean σ(*I*)/*I*	0.1289
θ range	4.214–25.025
observed refls.	8233
x, y (weighting scheme)	0.0593, 0
hydrogen refinement	constr
refls in refinement	16587
parameters	1038
restraints	6
$R(F_{obs})$	0.0733
$R_w(F^2)$	0.1907
S	1.009
shift/error$_{max}$	0.001
max electron density/e Å^{-3}	0.596
min electron density/e Å^{-3}	−0.403

Butyl p-tolylcarbamate ***16***

The unit cell contains four asymmetric units which in turn consist of four molecules each.

Figure S4: 149 shows a single molecule, **Figure S4: 150** gives the unit cell and crystallographic data for urethane **16** is given in **Table S4: 21**:

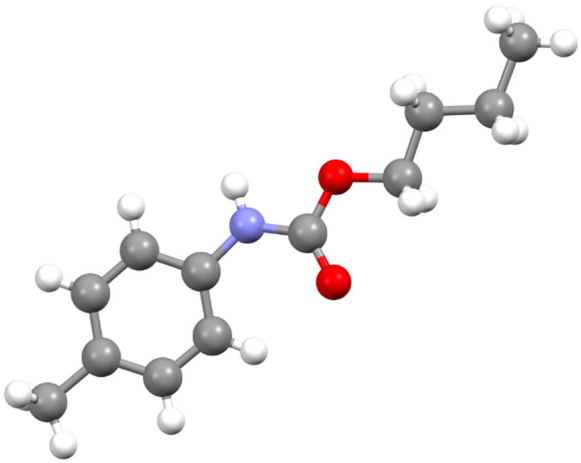

Figure S4: 149. *[Figure S149] Urethane* ***16****.*

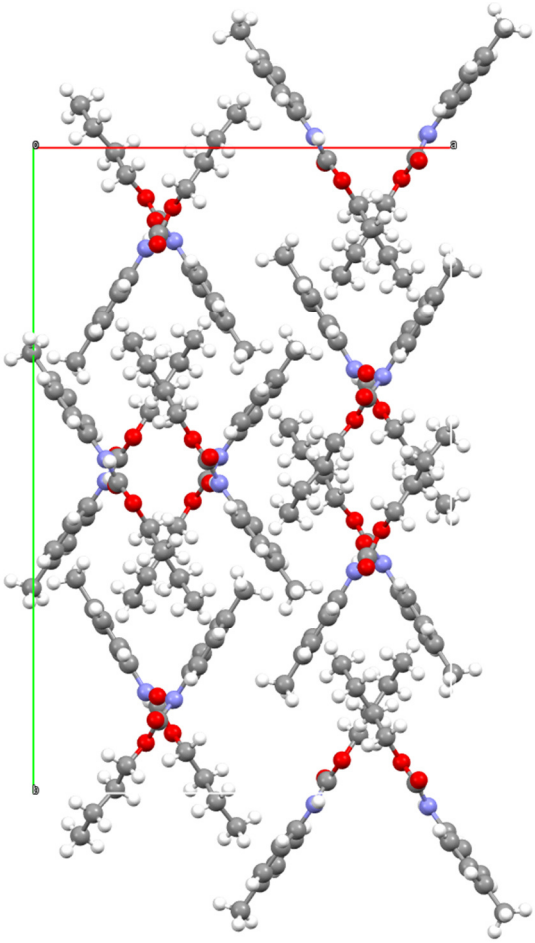

Figure S4: 150. *[Figure S150] Unit cell of urethane* ***16*** *viewed along the c-axis.*

Table S4: 21. [Table S21] Crystallographic details for urethane **16**.

net formula	$C_{12}H_{17}NO_2$
M_r/g mol^{-1}	207.26
crystal size/mm	0.100 × 0.030 × 0.030
T/K	153.(2)
radiation	MoKα
diffractometer	'Bruker D8 Venture TXS'
crystal system	monoclinic
space group	'C 1 c 1'
a/Å	18.1807(6)
b/Å	27.4981(7)
c/Å	9.6395(2)
α/°	90
β/°	102.0210(10)
γ/°	90
V/Å^3	4713.4(2)
Z	16
calc. density/g cm^{-3}	1.168
μ/mm^{-1}	0.079
absorption correction	Multi-Scan
transmission factor range	0.8905–0.9604
refls. measured	29658
R_{int}	0.0493
mean σ(*I*)/*I*	0.0728
θ range	3.145–30.508
observed refls.	10647
x, y (weighting scheme)	0.0640, 0.7848
hydrogen refinement	C-H: constr, N-H: refall
Flack parameter	0.5
refls in refinement	14193
parameters	565
restraints	2
$R(F_{obs})$	0.0572
$R_w(F^2)$	0.1410
S	1.019
shift/error$_{max}$	0.001
max electron density/e Å^{-3}	0.240
min electron density/e Å^{-3}	−0.198

4-Methyl-N-(pyridin-2-yl)benzenesulfonamide ***25***

Recrystallization was done from H_2O/EtOH.

Figure S4: 151 shows the dimer, **Figure S4: 152** gives the unit cell and crystallographic data for sulfonamide **25** is given in **Table S4: 22**:

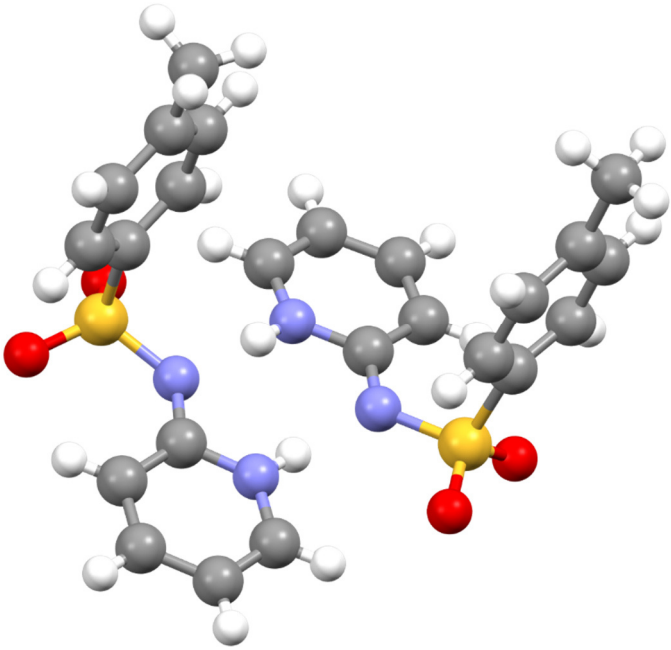

Figure S4: 151. *[Figure S151] Dimer of sulfonamide* ***25****.*

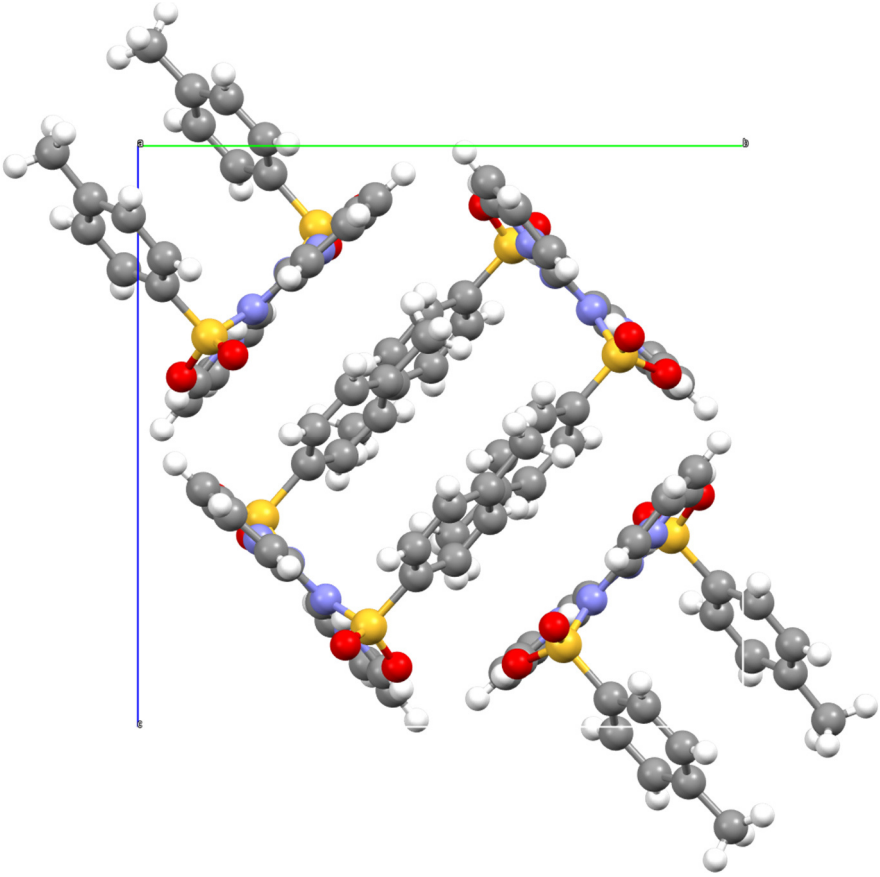

Figure S4: 152. *[Figure S152] Unit cell of sulfonamide* ***25*** *viewed along the a-axis.*

Table S4: 22. [Table S22] Crystallographic details for sulfonamide **25**.

net formula	$C_{12}H_{12}N_2O_2S$
M_r/g mol^{-1}	248.30
crystal size/mm	0.080 × 0.050 × 0.040
T/K	104.(2)
radiation	MoKα
diffractometer	'Bruker D8 Venture TXS'
crystal system	monoclinic
space group	'P 1 21/c 1'
a/Å	10.7237(4)
b/Å	14.8564(5)
c/Å	14.6583(5)
α/°	90
β/°	103.0200(10)
γ/°	90
V/Å^3	2275.26(14)
Z	8
calc. density/g cm^{-3}	1.450
μ/mm^{-1}	0.275
absorption correction	Multi-Scan
transmission factor range	0.95–0.99
refls. measured	35558
R_{int}	0.0533
mean σ(*I*)/*I*	0.0341
θ range	2.995–27.484
observed refls.	4271
x, y (weighting scheme)	0.0353, 1.6662
hydrogen refinement	H(C) constr, H(N) refall
refls in refinement	5190
parameters	317
restraints	0
$R(F_{obs})$	0.0361
$R_w(F^2)$	0.0967
S	1.073
shift/error$_{max}$	0.001
max electron density/e Å^{-3}	0.309
min electron density/e Å^{-3}	−0.461

4.1.6 Assigned NMR Spectra of Synthesized Compounds

Tetrabutylammonium pyridin-4-yl((trifluoromethyl)sulfonyl)amide ***6aa***

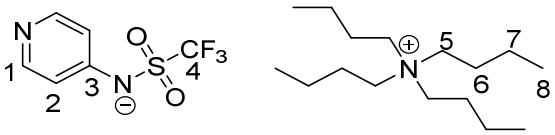

^{1}H NMR (400 MHz, $CDCl_3$) δ [ppm] = 8.14 (d, J = 6.3 Hz, 2H, H-1), 7.03 (d, J = 6.3 Hz, 2H, H-2), 3.20 – 3.04 (m, 8H, H-5), 1.54 (p, J = 8.1, 7.7 Hz, 8H, H-6), 1.35 (h, J = 7.3 Hz, 8H, H-7), 0.93 (t, J = 7.3 Hz, 12H, H-8).

^{13}C NMR (101 MHz, $CDCl_3$) δ [ppm] = 156.0 (C-3), 149.4 (C-1), 121.27 (q, J = 328.2 Hz, C-4), 118.1 (C-2), 58.76 (C-5), 23.91 (C-6), 19.66 (C-7), 13.60 (C-8).

^{19}F NMR (377 MHz, $CDCl_3$) δ [ppm] = −76.8.

a)

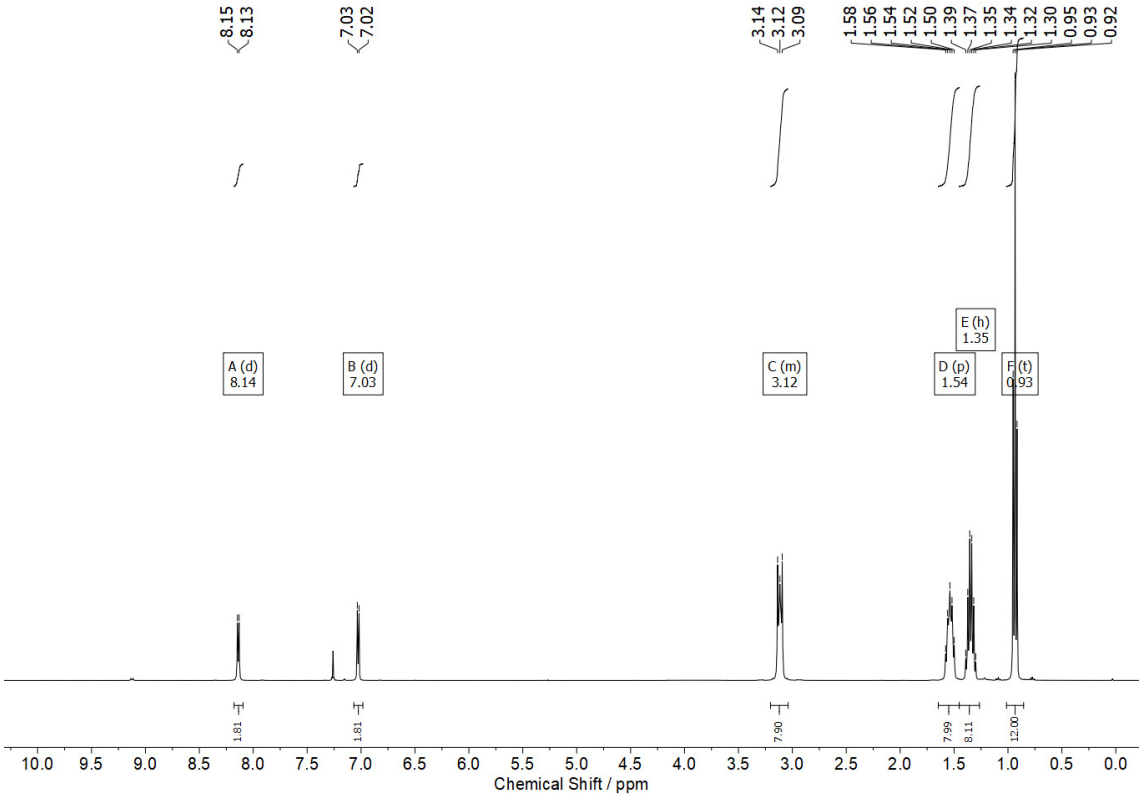

b)

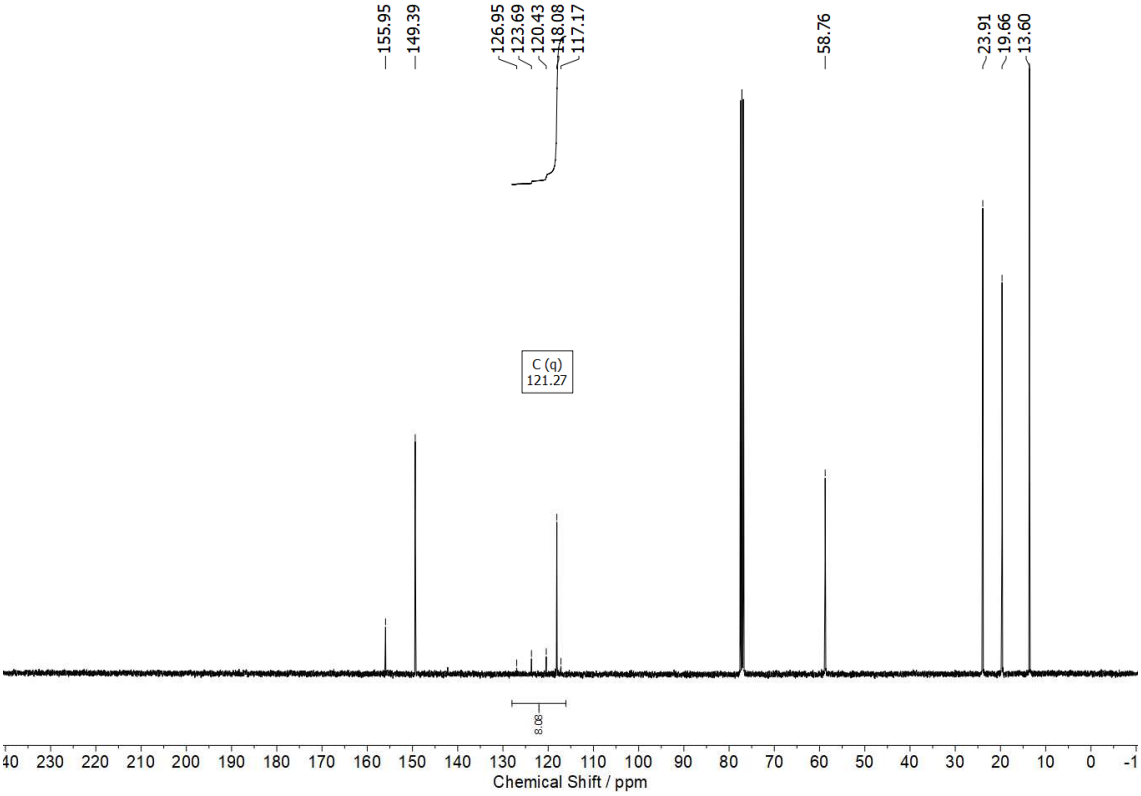

c)

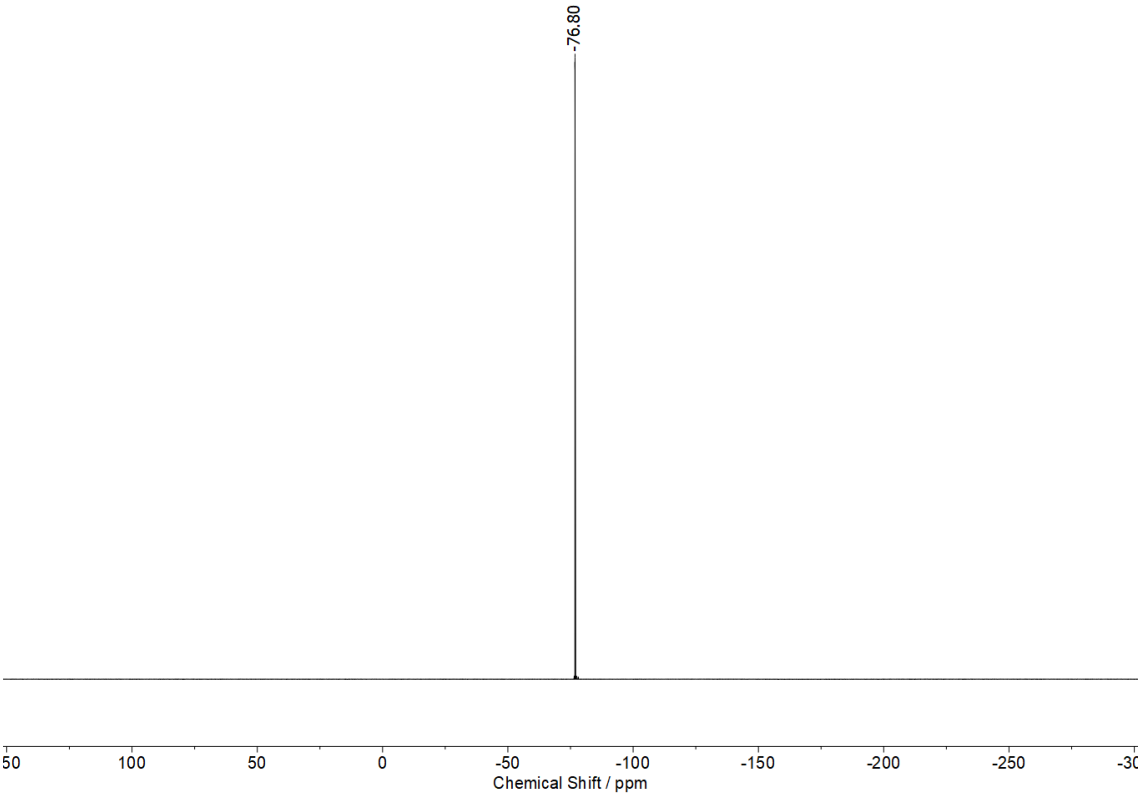

Figure S4: 153. *[Figure S153] NMR spectra of catalyst* ***6aa*** *($CDCl_3$, 400 MHz): a) ^1H NMR spectrum, b) ^{13}C NMR spectrum, c) ^{19}F NMR spectrum.*

Tetraoctylammonium pyridin-4-yl((trifluoromethyl)sulfonyl)amide ***6ab***

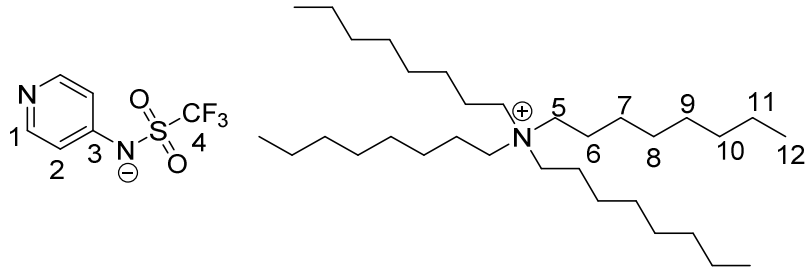

^{1}H NMR (400 MHz, $CDCl_3$) δ [ppm] = 8.15 (d, J = 6.2 Hz, 2H, H-1), 7.05 (d, J = 6.3 Hz, 2H, H-2), 3.33 – 2.97 (m, 8H, H-5), 1.72 – 1.50 (m, 8H, H-6), 1.50 – 1.10 (m, 40H, H-7/8/9/10/11), 0.85 (t, J = 6.8 Hz, 12H, H-12).

^{13}C NMR (101 MHz, $CDCl_3$) δ [ppm] = 155.8 (C-3), 149.6 (C-1), 122.3 (q, J = 328.2 Hz, C-4), 118.1 (C-2), 59.0 (C-5), 31.7 (C-7/8/9/10/11), 29.1 (C-7/8/9/10/11), 29.1 (C-7/8/9/10/11), 26.3 (C-7/8/9/10/11), 22.7 (C-7/8/9/10/11), 22.1 (C-6), 14.2 (C-12).

^{19}F NMR (377 MHz, $CDCl_3$) δ [ppm] = −76.8.

a)

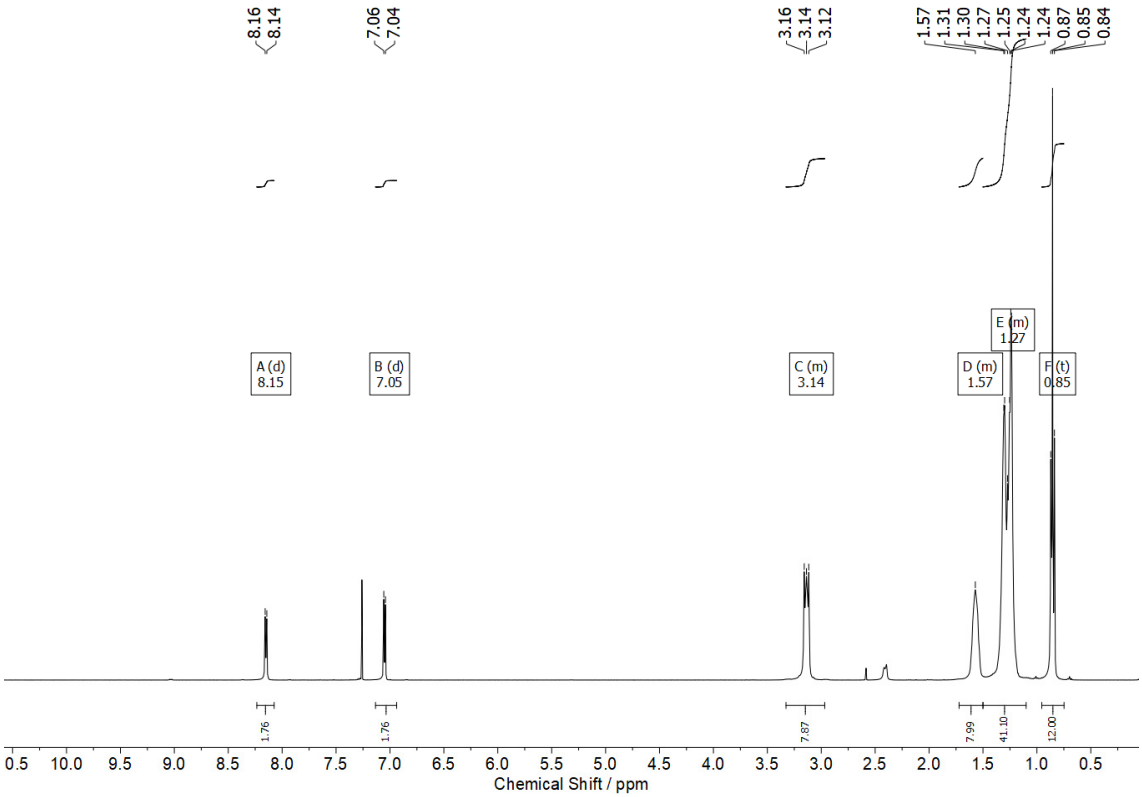

b)

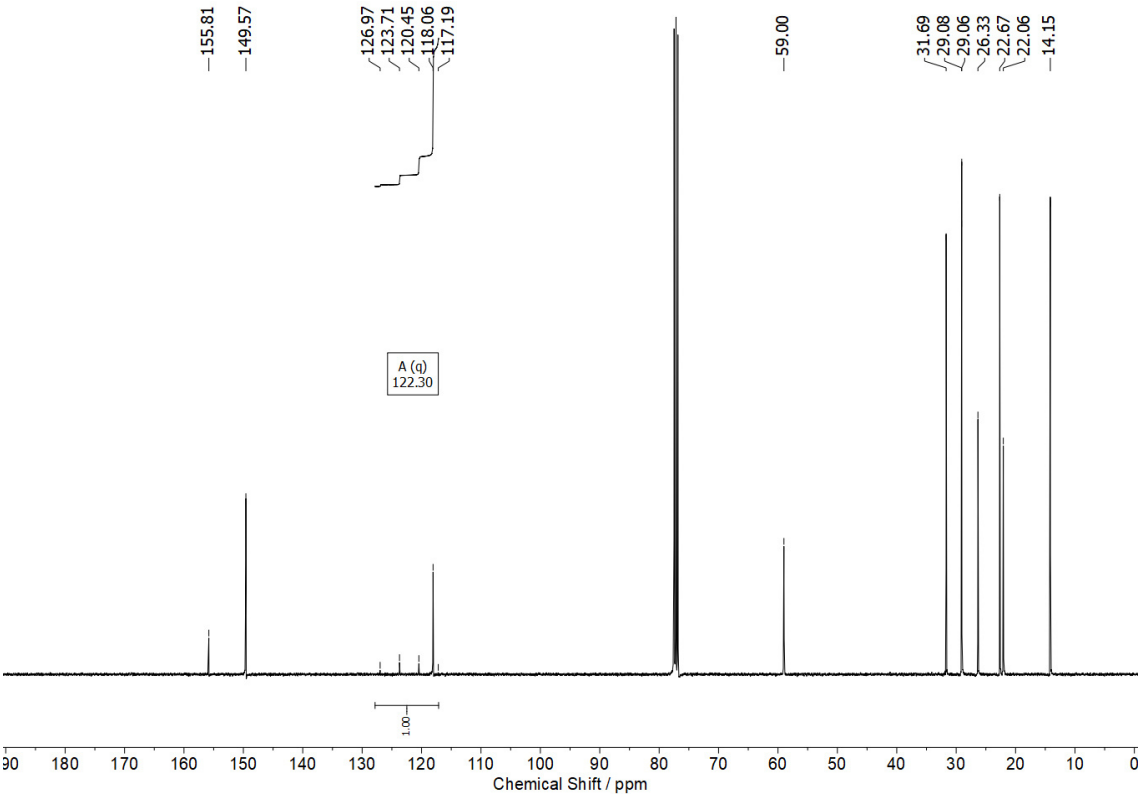

c)

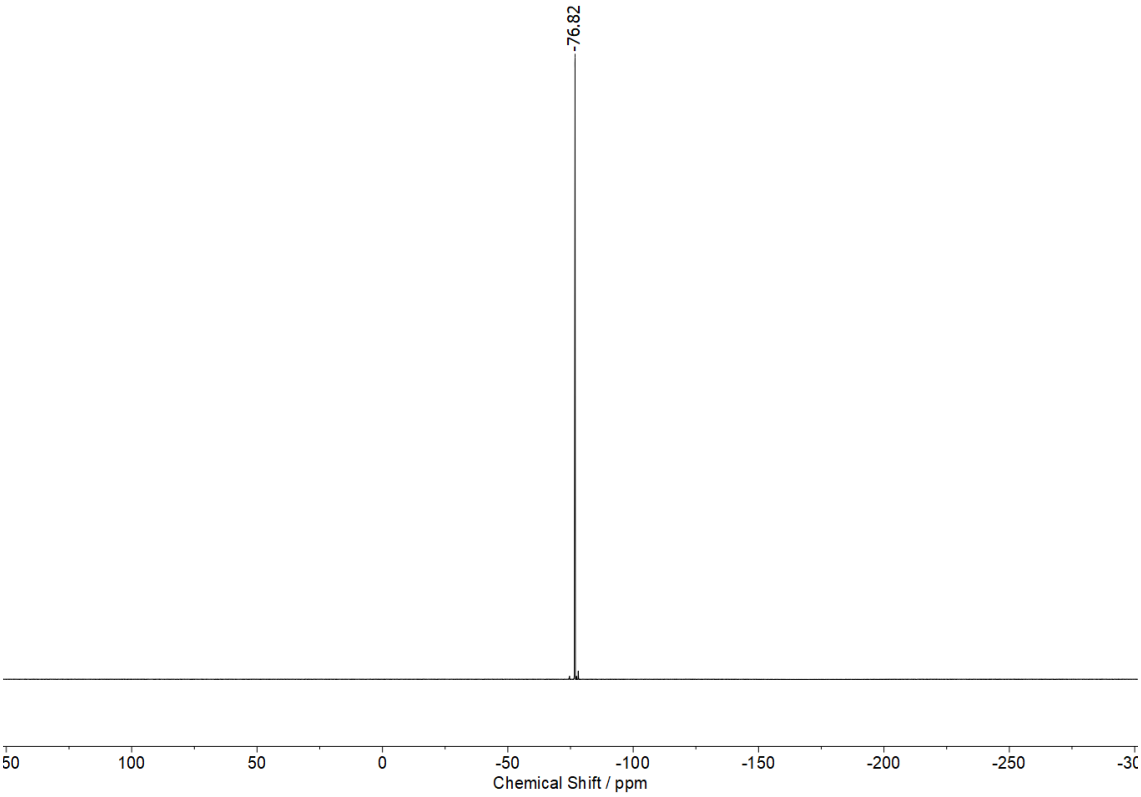

Figure S4: 154. *[Figure S154] NMR spectra of catalyst* ***6ab*** *($CDCl_3$, 400 MHz): a) ^1H NMR spectrum, b) ^{13}C NMR spectrum, c) ^{19}F NMR spectrum.*

Methyltriphenylphosphonium pyridin-4-yl((trifluoromethyl)sulfonyl)amide ***6ac***

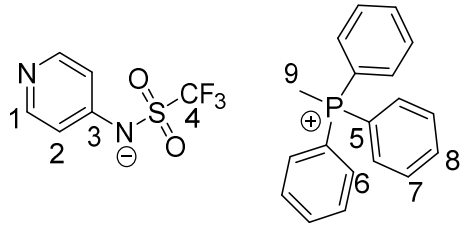

^{1}H NMR (400 MHz, $CDCl_3$) *δ* [ppm] = 8.05 (dd, *J* = 4.8, 1.5 Hz, 2H, H-1), 7.77 (tq, *J* = 7.0, 1.3 Hz, 3H, H-8), 7.63 (td, *J* = 7.9, 3.6 Hz, 6H, H-7), 7.60 – 7.52 (m, 6H, H-6), 6.94 (dd, *J* = 4.8, 1.5 Hz, 2H, H-2), 2.83 (d, *J* = 13.3 Hz, 3H, H-9).

^{13}C NMR (101 MHz, $CDCl_3$) *δ* [ppm] = 155.78 (C-3), 149.54 (C-1), 135.46 (d, *J* = 3.0 Hz, C-8), 133.04 (d, *J* = 10.7 Hz, C-6), 130.65 (d, *J* = 12.9 Hz, C-7), 122.06 (q, *J* = 328.2 Hz, C-4), 118.78 (d, *J* = 88.8 Hz, C-5), 118.04 (C-2), 9.66 (d, *J* = 58.4 Hz, C-9).

^{19}F NMR (377 MHz, $CDCl_3$) *δ* [ppm] = −76.8.

^{31}P NMR (162 MHz, $CDCl_3$) *δ* [ppm] = +21.2.

a)

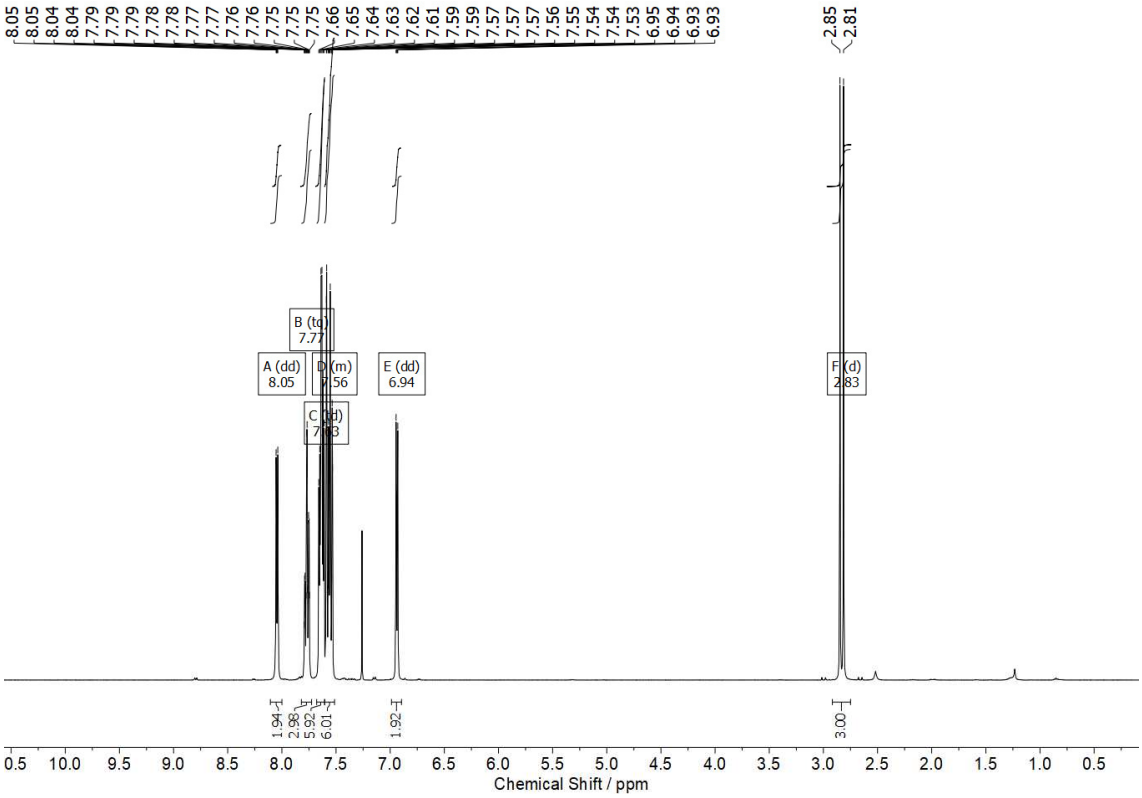

b)

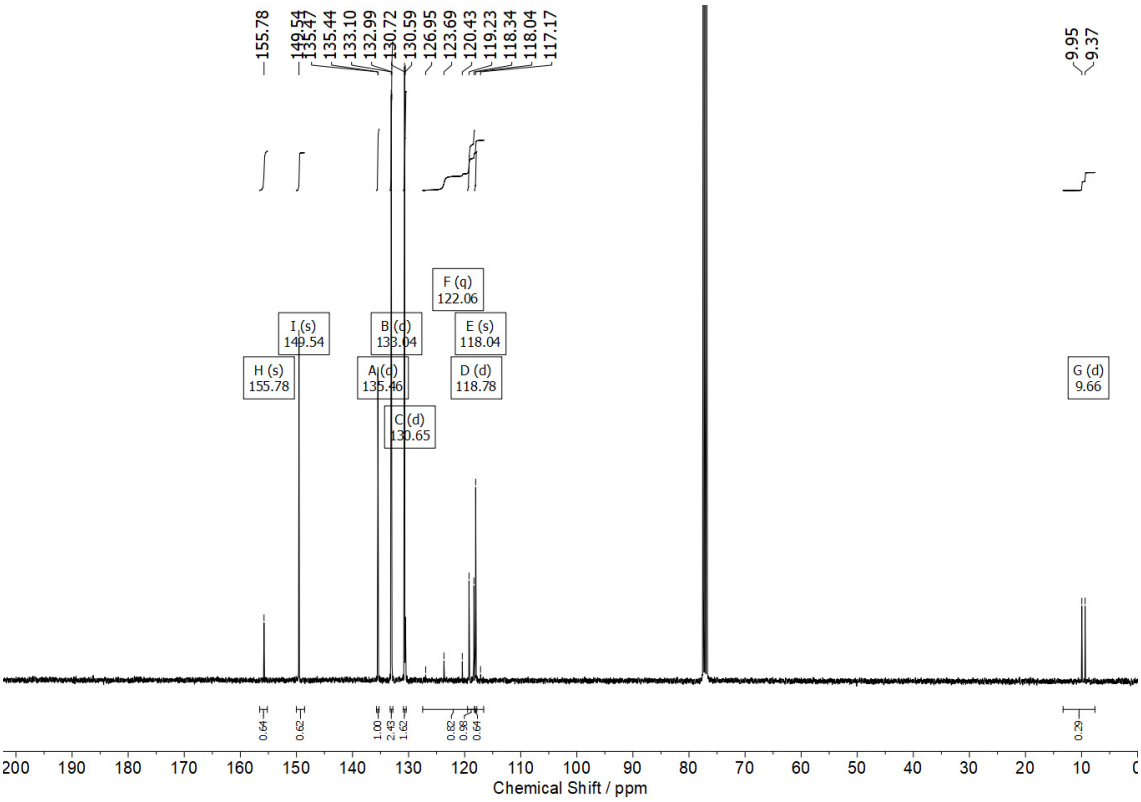
155.78
149.54
135.47
135.44
133.10
132.99
130.72
130.59
126.95
123.69
120.43
119.23
118.34
118.04
117.17
9.95
9.37
F (q)
122.06
I (s)
149.54
B (d)
133.04
E (s)
118.04
H (s)
155.78
A (d)
135.46
D (d)
118.78
C (d)
130.65
G (d)
9.66
0.64
0.62
1.00
2.43
1.62
0.82
0.98
0.64
0.29
200 190 180 170 160 150 140 130 120 110 100 90 80 70 60 50 40 30 20 10 0
Chemical Shift / ppm

c)

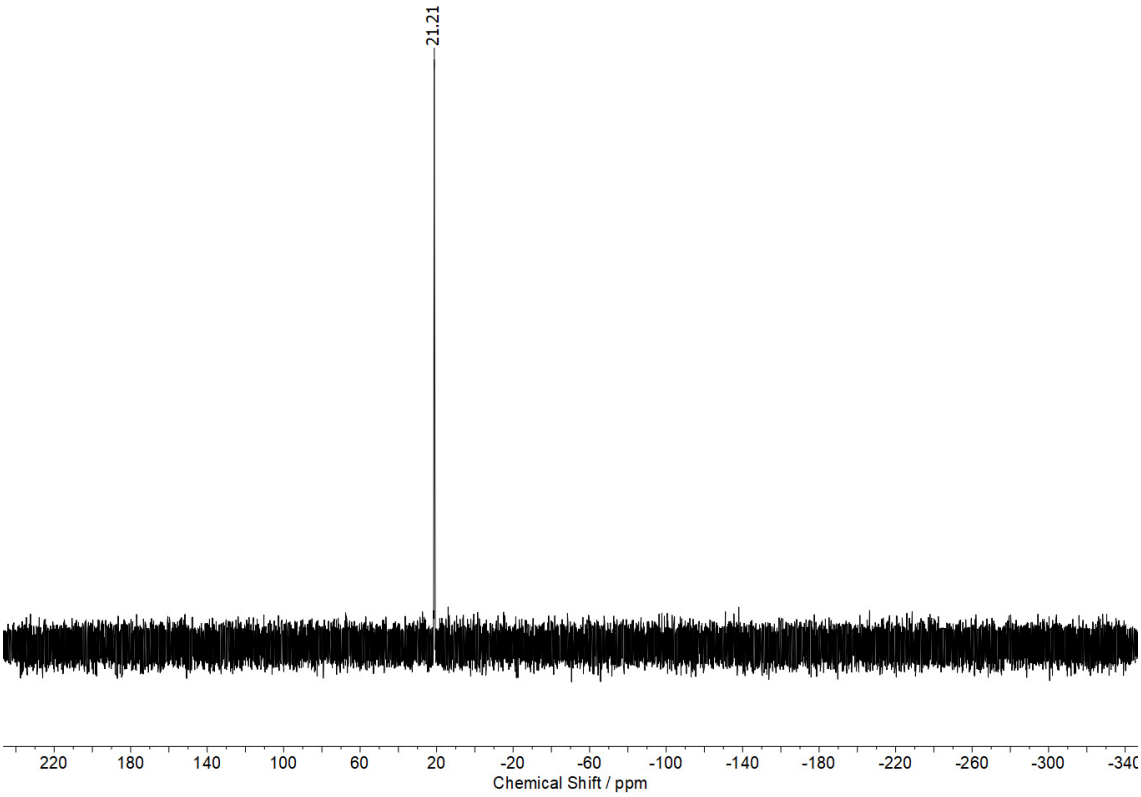
21.21
220 180 140 100 60 20 -20 -60 -100 -140 -180 -220 -260 -300 -340
Chemical Shift / ppm

d)

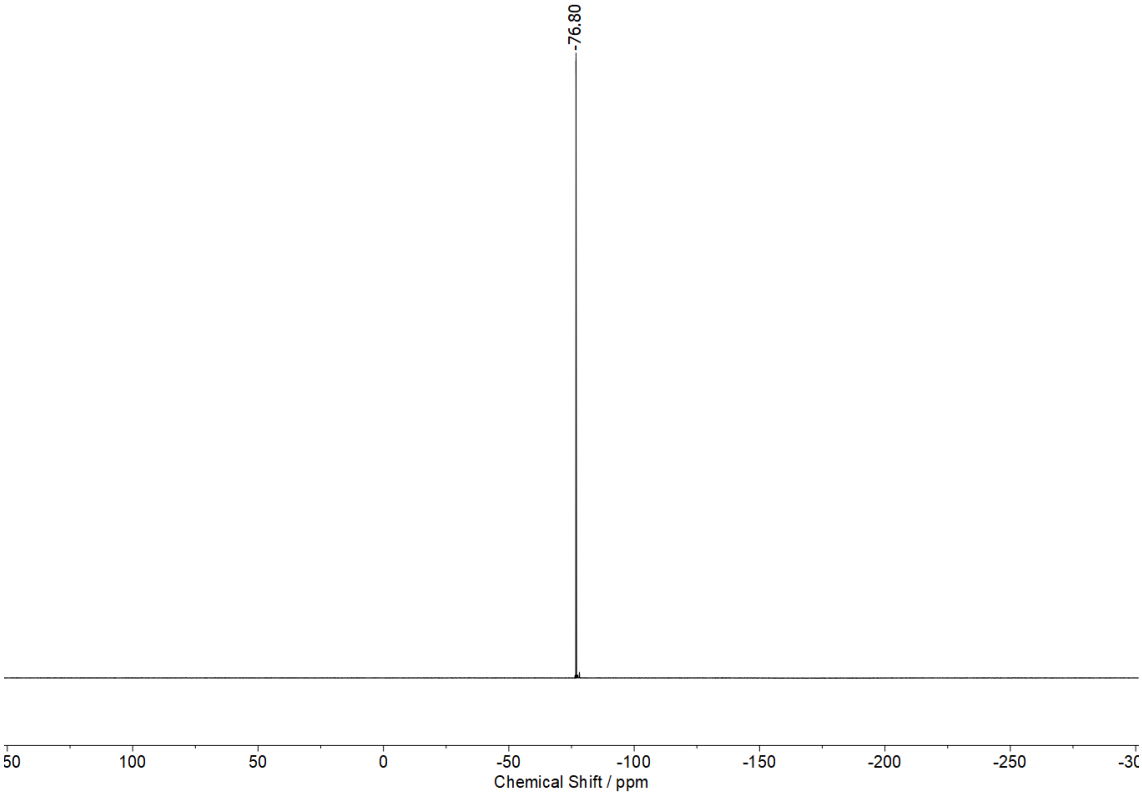

Figure S4: 155. *[Figure S155] NMR spectra of catalyst* ***6ac*** *($CDCl_3$, 400 MHz): a) ^{1}H NMR spectrum, b) ^{13}C NMR spectrum, c) ^{31}P NMR spectrum, d) ^{19}F NMR spectrum.*

Tetrabutylphosphonium pyridin-4-yl((trifluoromethyl)sulfonyl)amide ***6ad***

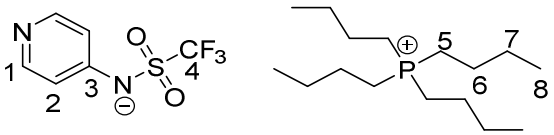

^{1}H NMR (400 MHz, $CDCl_3$) δ [ppm] = 8.16 (dd, J = 6.4, 3.2 Hz, 2H, H-1), 7.03 (dd, J = 6.3, 3.2 Hz, 2H, H-2), 2.27 – 2.02 (m, 8H, H-5), 1.57 – 1.34 (m, 16H, H-6/7), 0.92 (t, J = 6.9 Hz, 12H, H-8).

^{13}C NMR (101 MHz, $CDCl_3$) δ [ppm] = 155.67 (C-3), 149.67 (C-1), 122.08 (q, J = 328.3 Hz, C-4), 118.11 (C-2), 23.94 (d, J = 15.2 Hz, C-7), 23.66 (d, J = 4.8 Hz, C-6), 18.71 (d, J = 47.5 Hz, C-5), 13.40(C-8).

^{19}F NMR (377 MHz, $CDCl_3$) δ [ppm] = −76.8.

^{31}P NMR (162 MHz, $CDCl_3$) δ [ppm] = +33.2.

a)

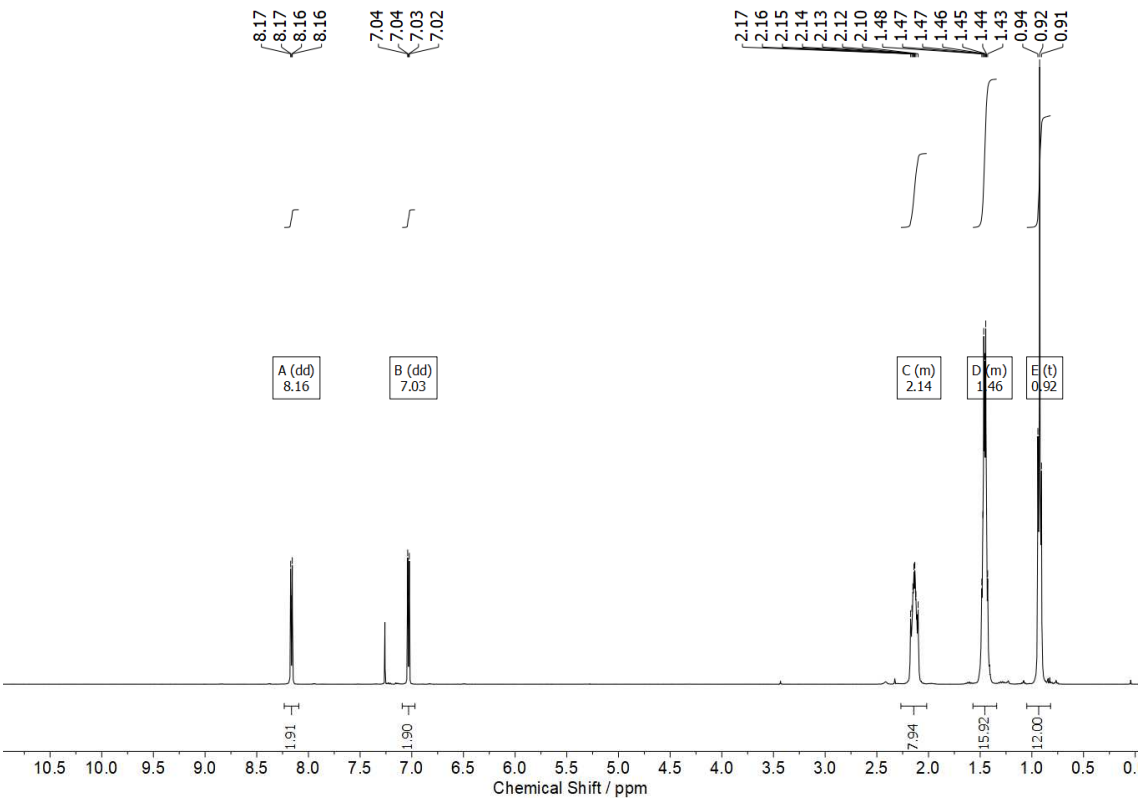
8.17
8.17
8.16
8.16
7.04
7.04
7.03
7.02
2.17
2.16
2.15
2.14
2.13
2.12
2.10
1.48
1.47
1.47
1.46
1.45
1.44
1.43
0.94
0.92
0.91
A (dd)
8.16
B (dd)
7.03
C (m)
2.14
D (m)
1.46
E (t)
0.92
1.91
1.90
7.94
15.92
12.00
10.5 10.0 9.5 9.0 8.5 8.0 7.5 7.0 6.5 6.0 5.5 5.0 4.5 4.0 3.5 3.0 2.5 2.0 1.5 1.0 0.5 0.
Chemical Shift / ppm

b)

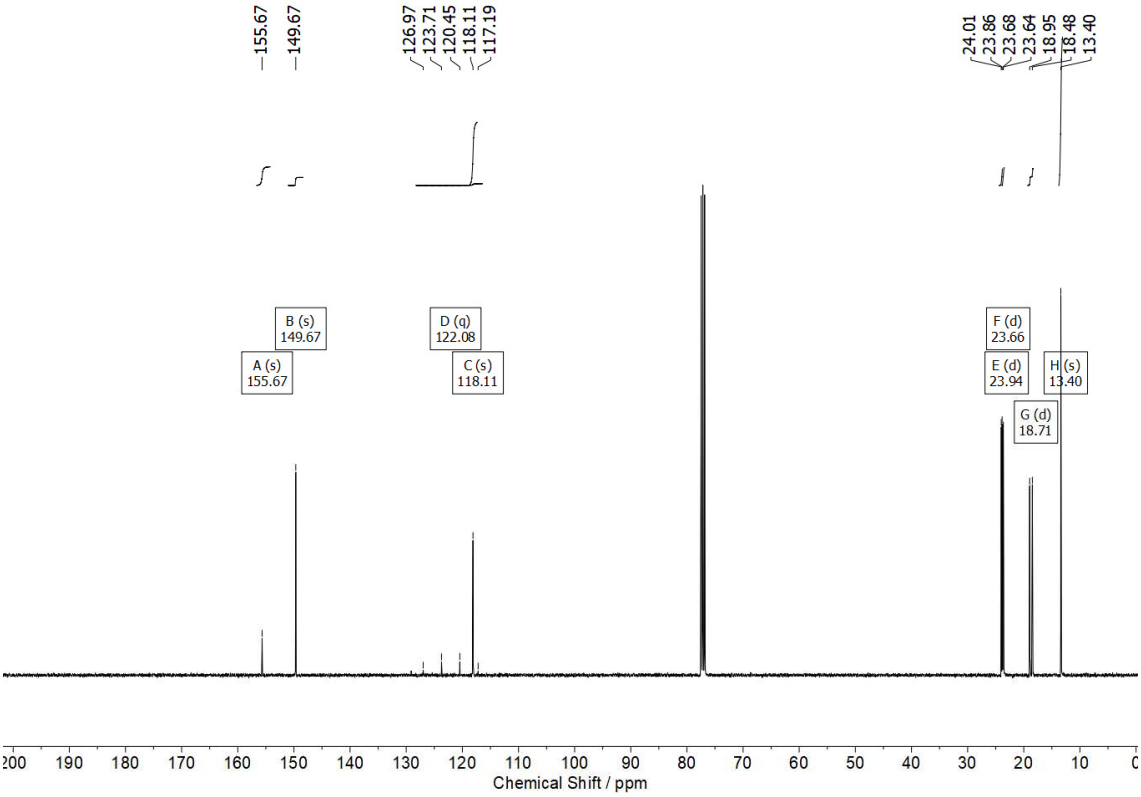
155.67
149.67
126.97
123.71
120.45
118.11
117.19
24.01
23.86
23.68
23.64
18.95
18.48
13.40
B (s)
149.67
A (s)
155.67
D (q)
122.08
C (s)
118.11
F (d)
23.66
E (d)
23.94
H (s)
13.40
G (d)
18.71
200 190 180 170 160 150 140 130 120 110 100 90 80 70 60 50 40 30 20 10 0
Chemical Shift / ppm

c)

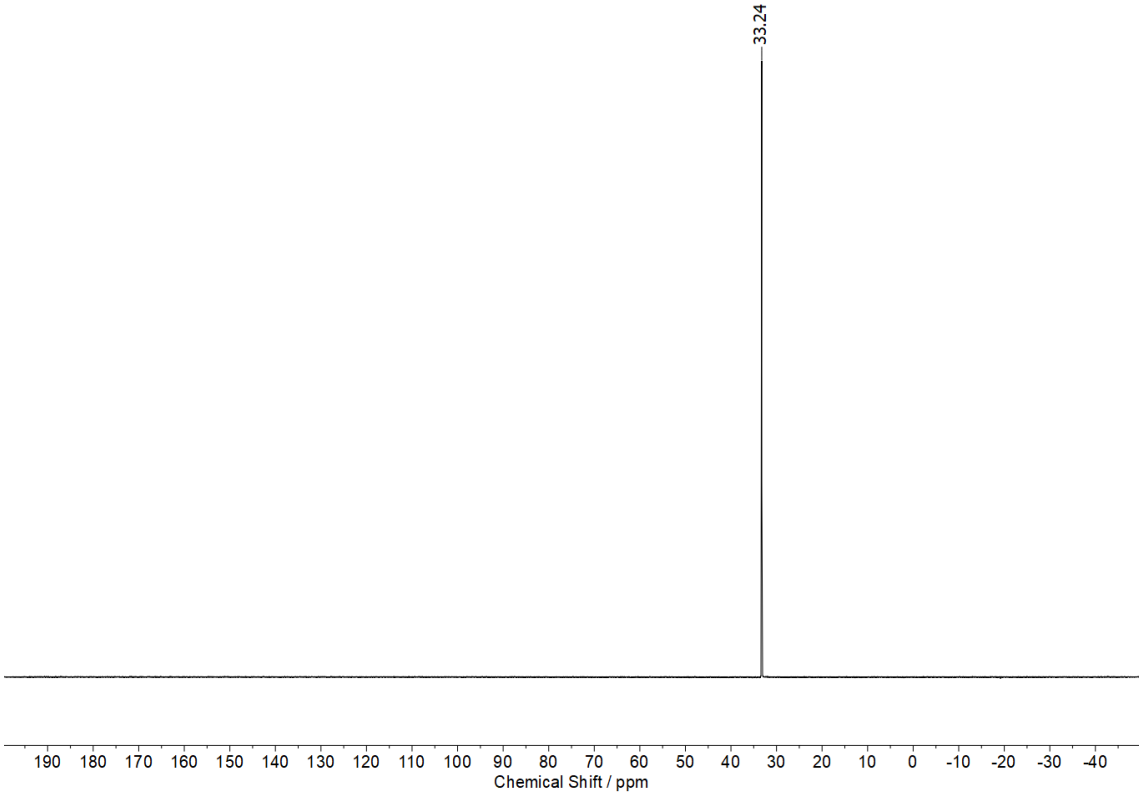

d)

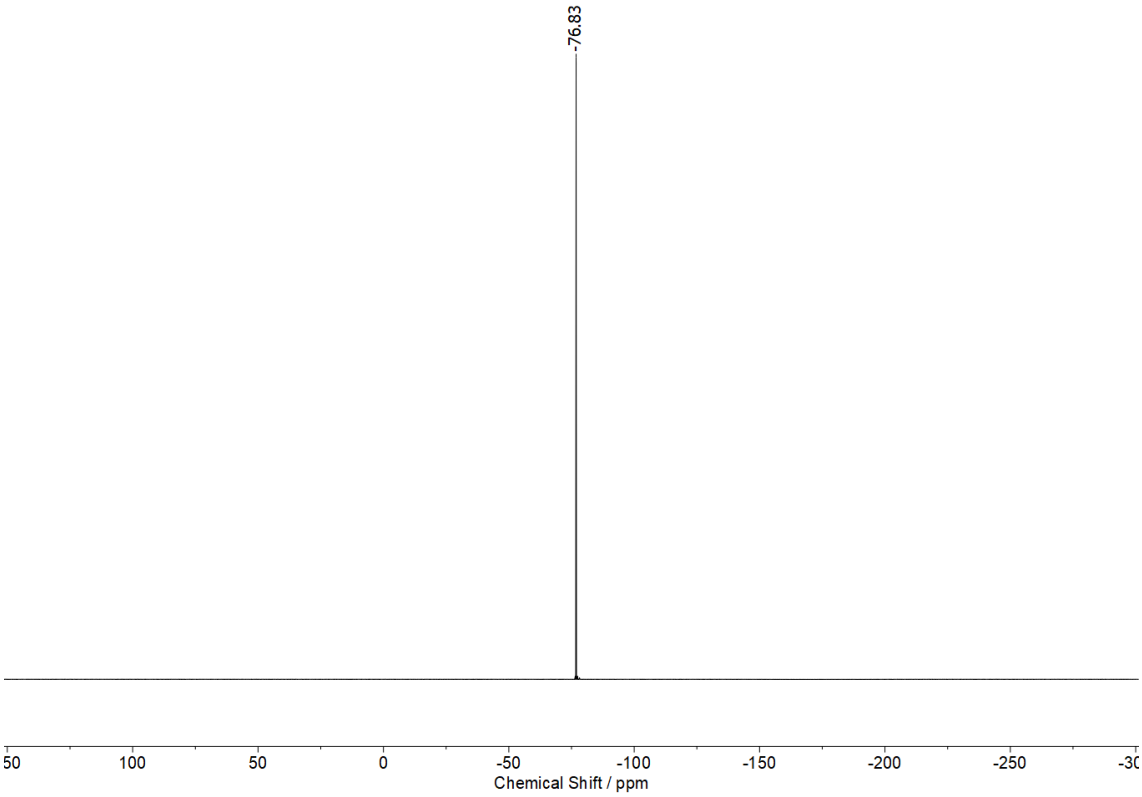

Figure S4: 156. *[Figure S156] NMR spectra of catalyst* ***6ad*** *($CDCl_3$, 400 MHz): a) ^{1}H NMR spectrum, b) ^{13}C NMR spectrum, c) $^{31}P\{^{1}H\}$ NMR spectrum, d) ^{19}F NMR spectrum.*

Methyltriphenylphosphonium pyridin-4-yl(tosyl)amide ***6bc***

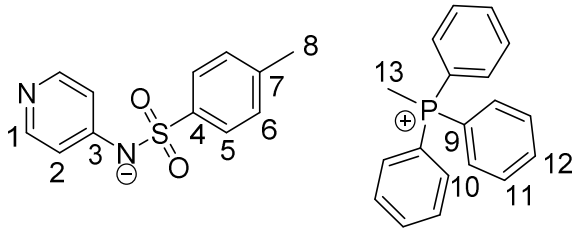

^{1}H NMR (400 MHz, $CDCl_3$) δ [ppm] = 7.87 (d, J = 6.1 Hz, 2H, H-1), 7.83 – 7.66 (m, 5H, H-5, H-12), 7.66 – 7.49 (m, 12H, H-10, H-11), 7.05 (d, J = 7.9 Hz, 2H, H-6), 6.71 (d, J = 6.2 Hz, 2H, H-2), 2.93 (d, J = 13.2 Hz, 3H, H-13), 2.26 (s, 3H, H-8).

^{13}C NMR (101 MHz, $CDCl_3$) δ [ppm] = 157.53 (C-3), 149.22 (C-1), 143.12 (C-4), 139.67 (C-7), 135.20 (d, J = 3.0 Hz, C-12), 133.14 (d, J = 10.7 Hz, C-10/11), 130.53 (d, J = 12.9 Hz, C-10/11), 128.76 (C-6), 126.78 (c-5), 119.06 (d, J = 88.6 Hz, C-9), 116.22 (C-2), 21.40 (C-8), 9.70 (d, J = 57.7 Hz, C-13).

^{31}P NMR (162 MHz, $CDCl_3$) δ [ppm] = +21.4.

a)

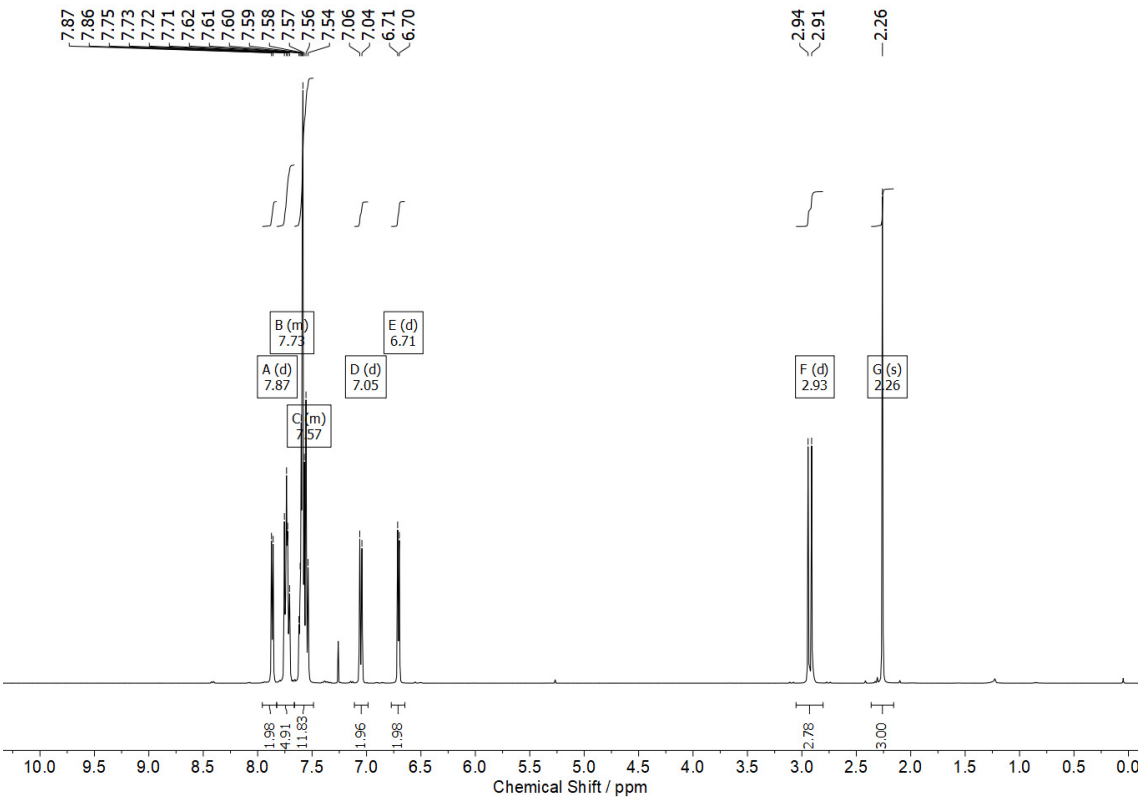

b)

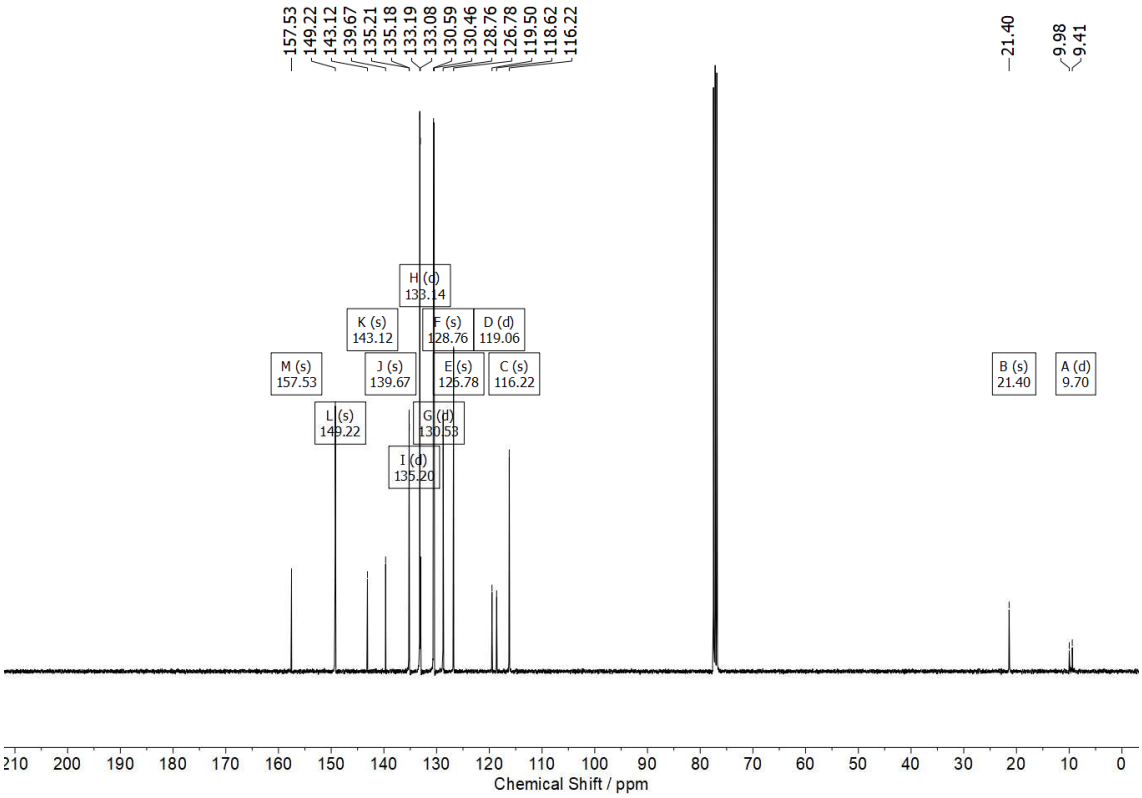

c)

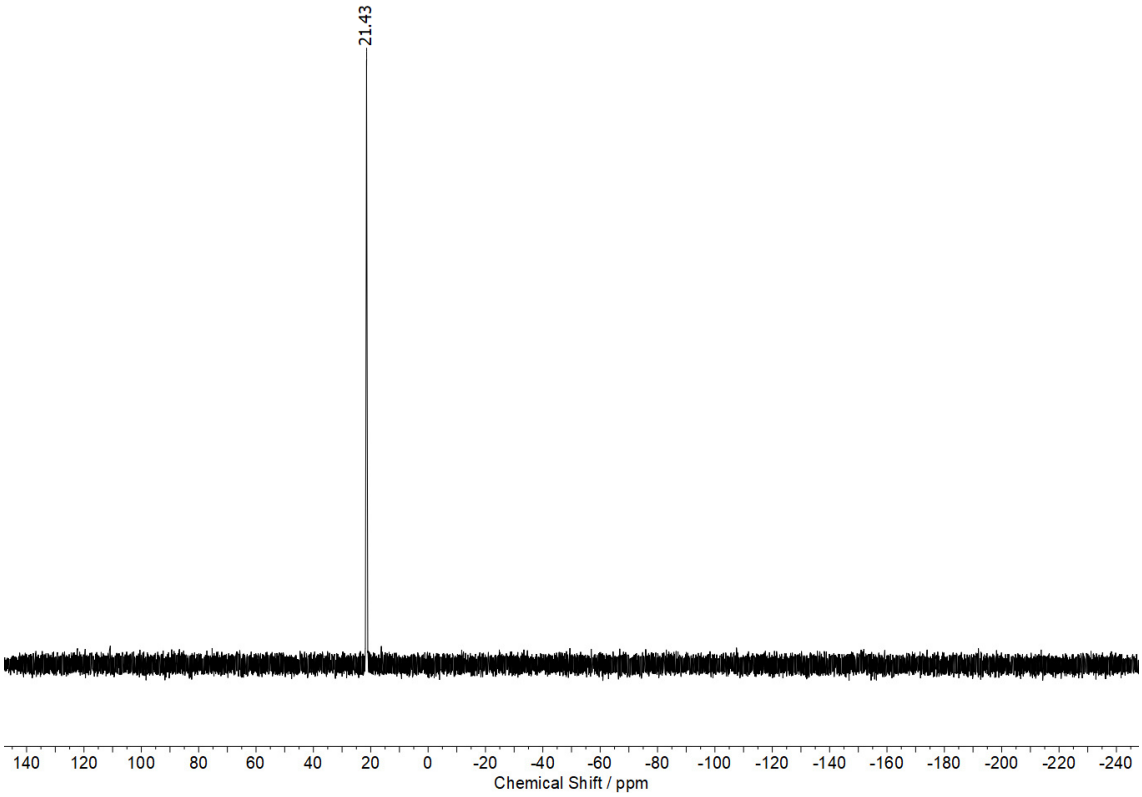

Figure S4: 157. *[Figure S157] NMR spectra of catalyst* **6bc** *($CDCl_3$, 400 MHz): a) ^{1}H NMR spectrum, b) ^{13}C NMR spectrum, c) $^{31}P\{^{1}H\}$ NMR spectrum.*

1,3-Diethyl-benzimidazolium pyridin-4-yl(tosyl)amide ***6be***

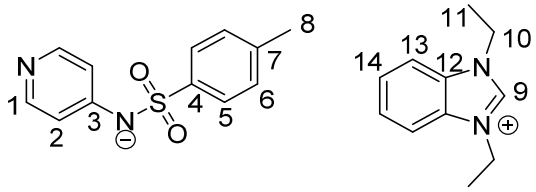

^{1}H NMR (400 MHz, $CDCl_3$) δ [ppm] = 10.49 (s, 1H, H-9), 7.95 (d, J = 6.3 Hz, 2H, H-1), 7.77 (d, J = 8.1 Hz, 2H, H-5), 7.69 – 7.51 (m, 4H, H-13, H-14), 7.10 (d, J = 8.0 Hz, 2H, H-6), 6.73 (d, J = 6.4 Hz, 2H, H-2), 4.49 (q, J = 7.3 Hz, 4H, H-10), 2.27 (s, 3H, H-8), 1.56 (t, J = 7.3 Hz, 6H- H-11).

^{13}C NMR (101 MHz, $CDCl_3$) δ [ppm] = 156.93 (C-3), 149.37 (C-1), 142.30 (C-4), 140.30 (C-7), 131.15 (C-12), 128.97 (C-6), 127.11 (C-13/14), 126.59 (C-5), 115.89 (C-2), 113.01 (C-13/14), 42.87 (C-10), 21.36(C-8), 14.76 (C-11).

a)

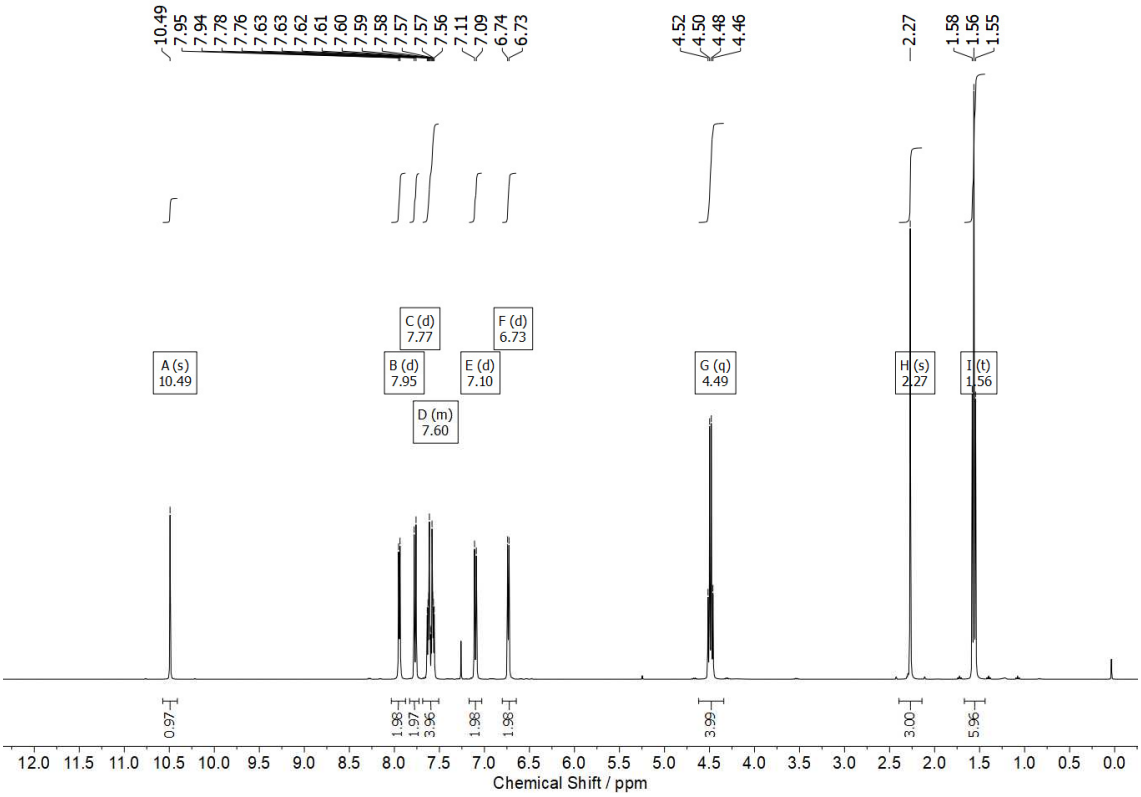

b)

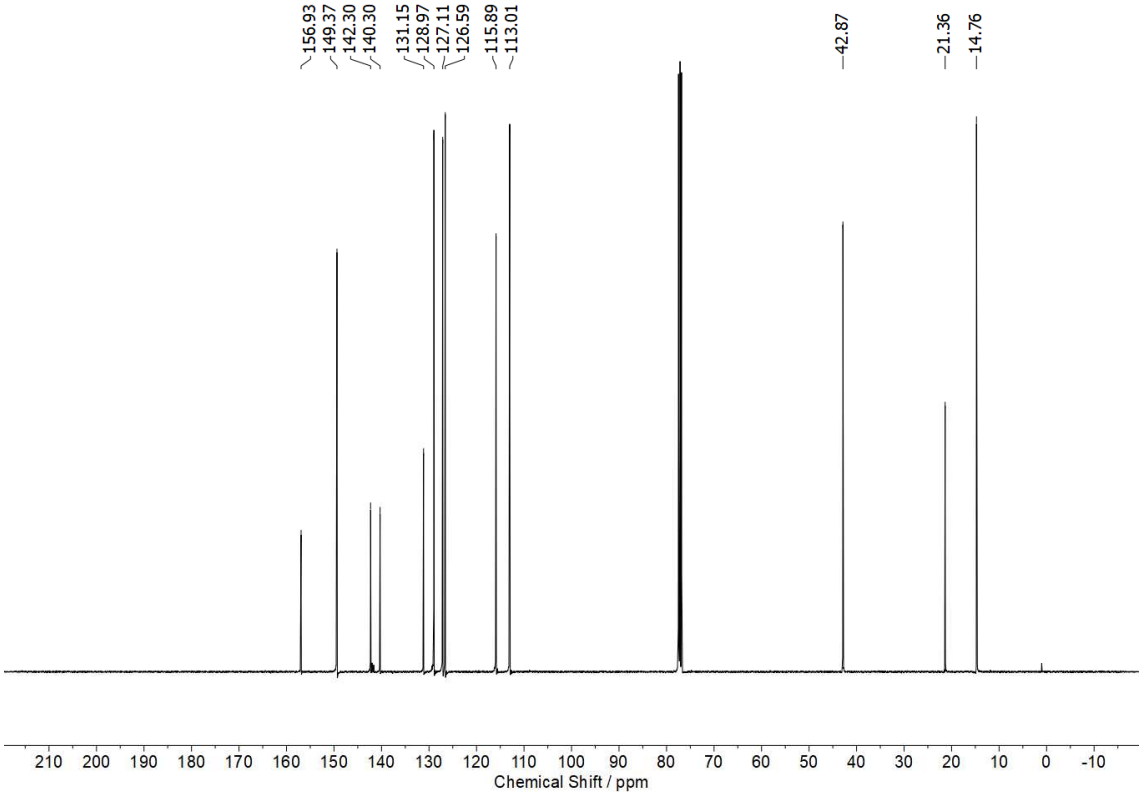

Figure S4: 158. *[Figure S158] NMR spectra of catalyst* ***6be*** *($CDCl_3$, 400 MHz): a) ^{1}H NMR spectrum, b) ^{13}C NMR spectrum.*

Benzyltriphenylphosphonium pyridin-4-yl(tosyl)amide ***6bf***

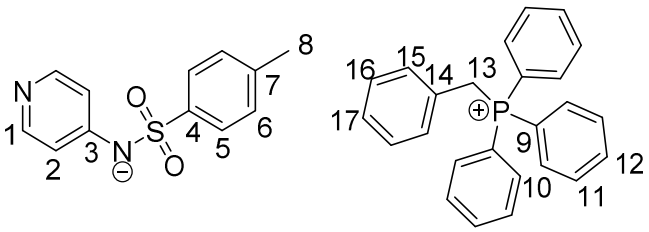

^{1}H NMR (400 MHz, $CDCl_3$) δ [ppm] = 7.84 (d, J = 6.4 Hz, 2H, H-1), 7.77 – 7.65 (m, 5H, H-5, H-12), 7.58 – 7.43 (m, 12H, H-10, H-11), 7.22 – 7.13 (m, 1H, H-17), 7.05 (t, J = 7.6 Hz, 2H, H-16), 7.01 (d, J = 8.0 Hz, 2H, H-6), 6.84 (d, J = 7.6 Hz, 2H, H-15), 6.73 (d, J = 6.4 Hz, 2H, H-2), 4.78 (d, J = 14.2 Hz, 2H, H-13), 2.23 (s, 3H, H-8).

^{13}C NMR (101 MHz, $CDCl_3$) δ [ppm] = 157.70 (C-3), 148.74 (C-1), 143.12 (C-4), 139.61 (C-7), 135.16 (d, J = 3.0 Hz, C-12), 134.10 (d, J = 9.7 Hz, C-10, C-11), 131.25 (d, J = 5.5 Hz, C-15), 130.26 (d, J = 12.6 Hz, C-10, C-11), 128.95 (d, J = 3.3 Hz, C-16), 128.68 (C-6), 128.59 (d, J = 3.8 Hz, C-17), 126.83 (d, J = 8.7 Hz, C-14), 126.76 (C-5), 117.43 (d, J = 85.8 Hz, C-9), 116.21 (C-2), 30.47 (d, J = 47.7 Hz, C-13), 21.35 (C-8).

^{31}P NMR{^{1}H} (162 MHz, $CDCl_3$) δ [ppm] = +22.7.

a)

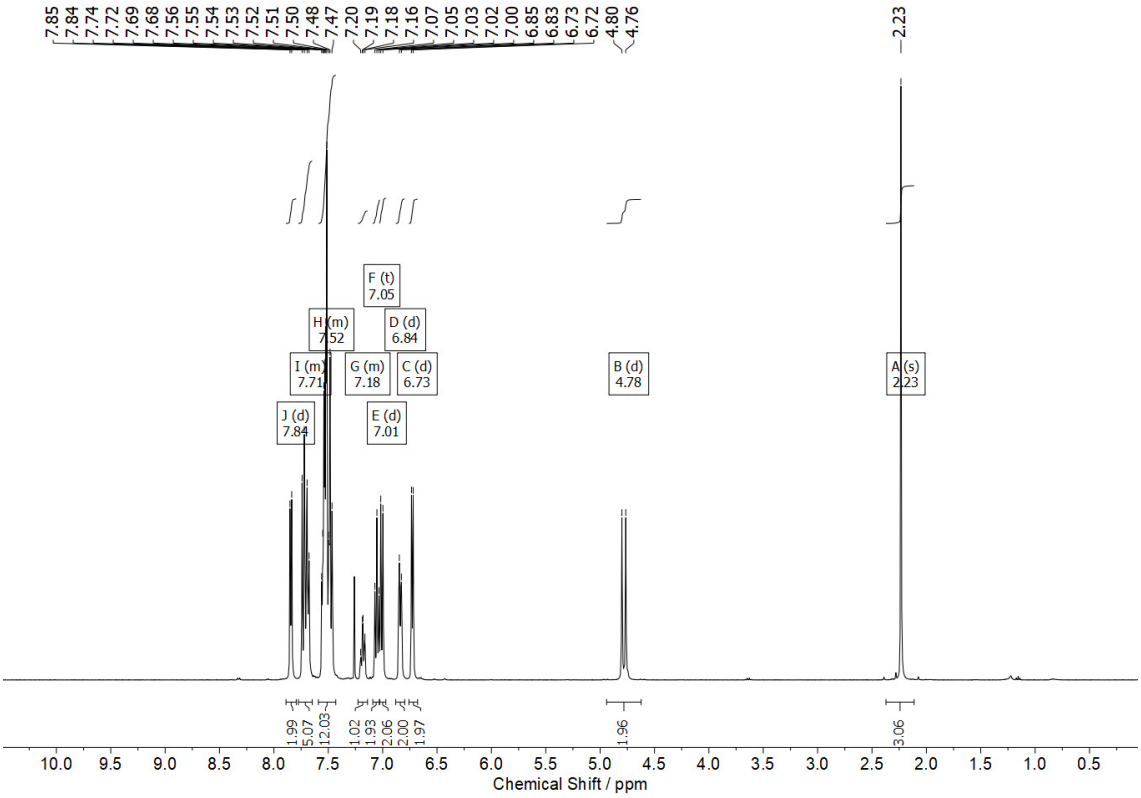
7.85
7.84
7.74
7.72
7.69
7.68
7.56
7.55
7.54
7.53
7.52
7.51
7.50
7.48
7.47
7.20
7.19
7.18
7.16
7.07
7.05
7.03
7.02
7.00
6.85
6.83
6.73
6.72
4.80
4.76
2.23
F (t) 7.05
H (m) 7.52
D (d) 6.84
I (m) 7.71
G (m) 7.18
C (d) 6.73
B (d) 4.78
A (s) 2.23
J (d) 7.84
E (d) 7.01
1.99
5.07
12.03
1.02
1.93
2.06
2.00
1.97
1.96
3.06
10.0 9.5 9.0 8.5 8.0 7.5 7.0 6.5 6.0 5.5 5.0 4.5 4.0 3.5 3.0 2.5 2.0 1.5 1.0 0.5
Chemical Shift / ppm

b)

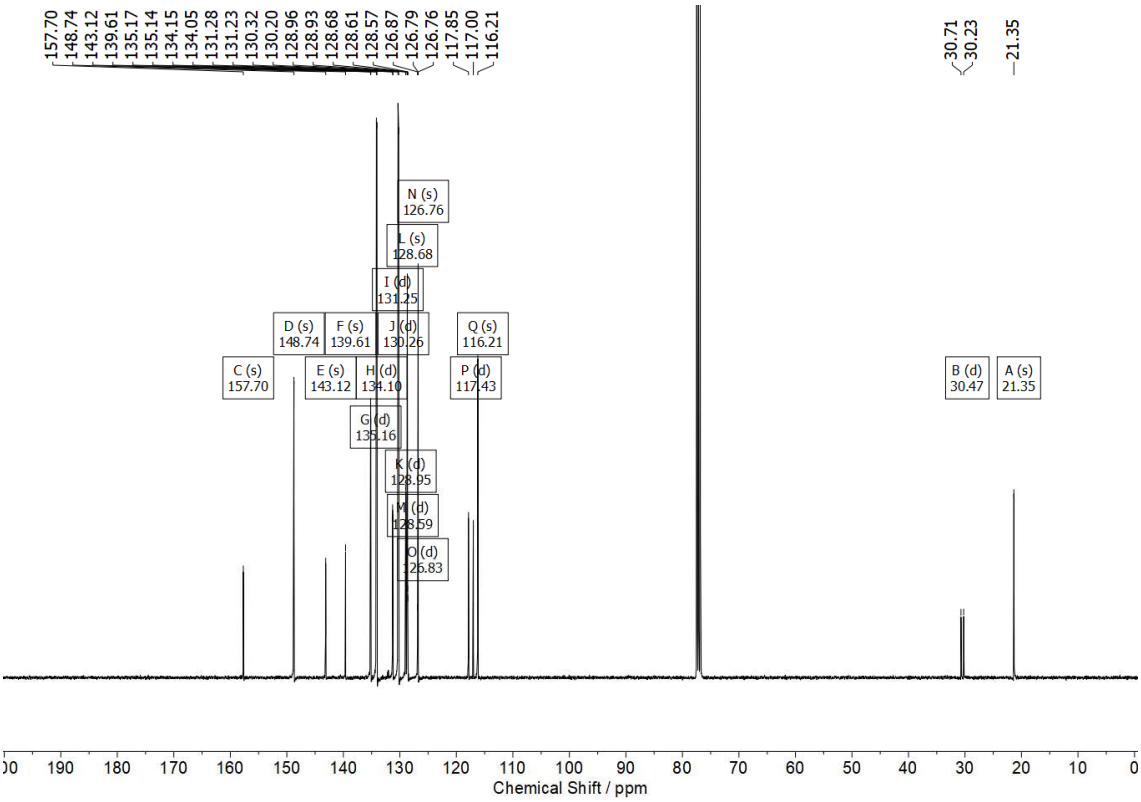
157.70
148.74
143.12
139.61
135.17
135.14
134.15
134.05
131.28
131.23
130.32
130.20
128.96
128.93
128.68
128.61
128.57
126.87
126.79
126.76
117.85
117.00
116.21
30.71
30.23
21.35
N (s) 126.76
L (s) 128.68
I (d) 131.25
D (s) 148.74
F (s) 139.61
J (d) 130.26
Q (s) 116.21
C (s) 157.70
E (s) 143.12
H (d) 134.10
P (d) 117.43
B (d) 30.47
A (s) 21.35
G (d) 135.16
K (d) 128.95
M (d) 128.59
O (d) 126.83
190 180 170 160 150 140 130 120 110 100 90 80 70 60 50 40 30 20 10 0
Chemical Shift / ppm

c)

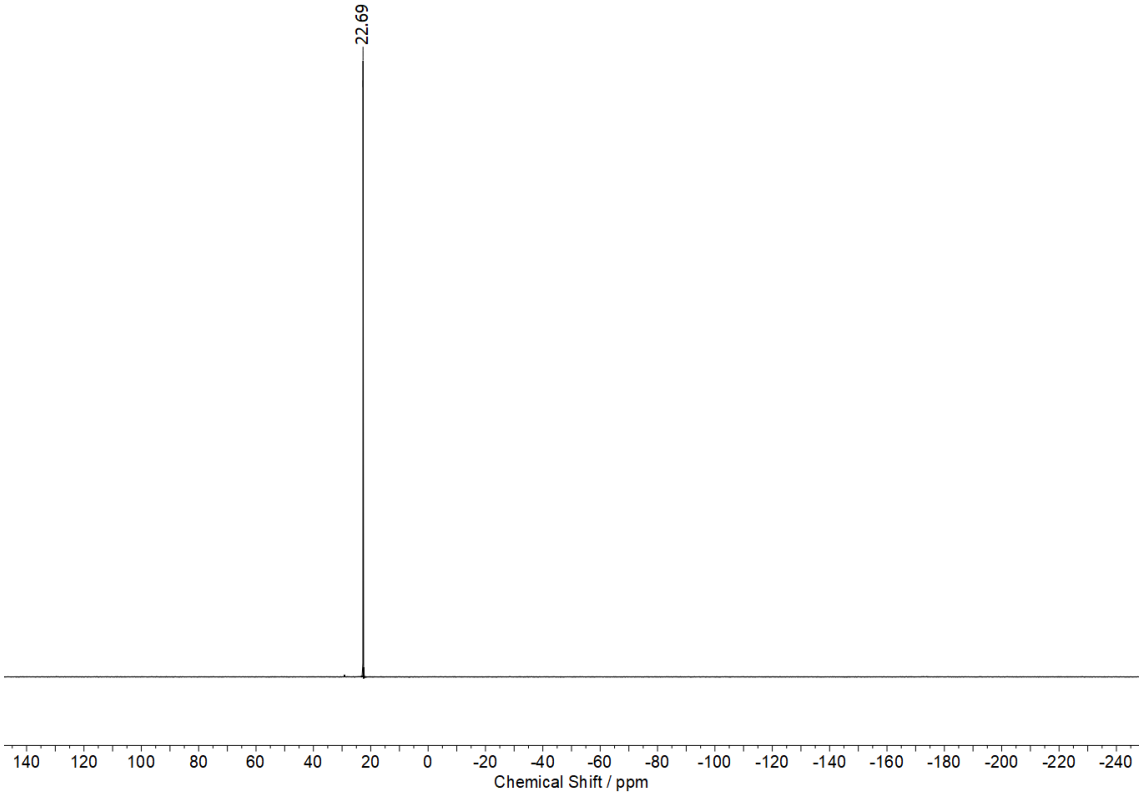

Figure S4: 159. *[Figure S159] NMR spectra of catalyst* ***6bf*** *($CDCl_3$, 400 MHz): a) ^1H NMR spectrum, b) ^{13}C NMR spectrum, c) $^{31}P\{^1H\}$ NMR spectrum.*

1,3-Diethyl-benzimidazolium ((4-methoxyphenyl)sulfonyl)(pyridin-4-yl)amide ***6ce***

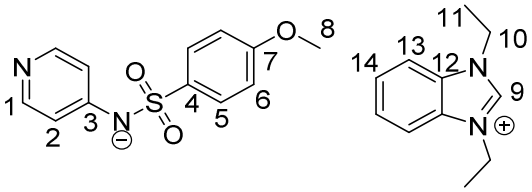

^{1}H NMR (400 MHz, $CDCl_3$) δ [ppm] = 10.53 (s, 1H, H-9), 7.97 (dd, J = 5.0, 1.4 Hz, 2H, H-1), 7.83 (dd, J = 8.8, 4.8 Hz, 2H, H-5), 7.70 – 7.55 (m, 4H, H-13, H-14), 6.81 (dd, J = 8.8, 4.9 Hz, 2H, H-6), 6.75 (dd, J = 4.9, 1.5 Hz, 2H, H-2), 4.51 (q, J = 7.3 Hz, 4H, H-10), 3.75 (s, 3H, H-8), 1.58 (t, J = 7.3 Hz, 6H, H-11).

^{13}C NMR (101 MHz, $CDCl_3$) δ [ppm] = 161.00 (C-7), 156.95 (C-3), 149.50 (C-1), 142.43 (C-9), 137.35 (C-4), 131.24 (C-12), 128.47 (C-5), 127.17(C-13/14), 115.92 (C-2), 113.56 (C-6), 113.05 (C-13/14), 55.42 (C-8), 42.96 (C-10), 14.85 (C-11).

a)

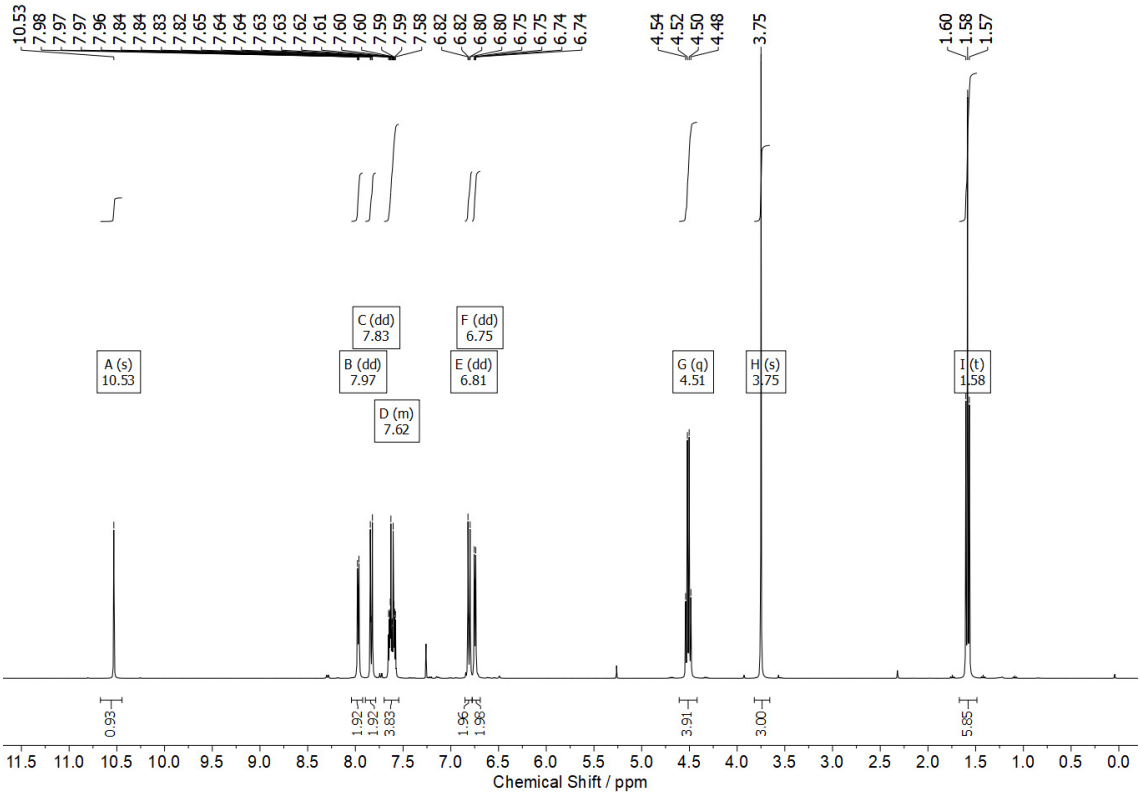

b)

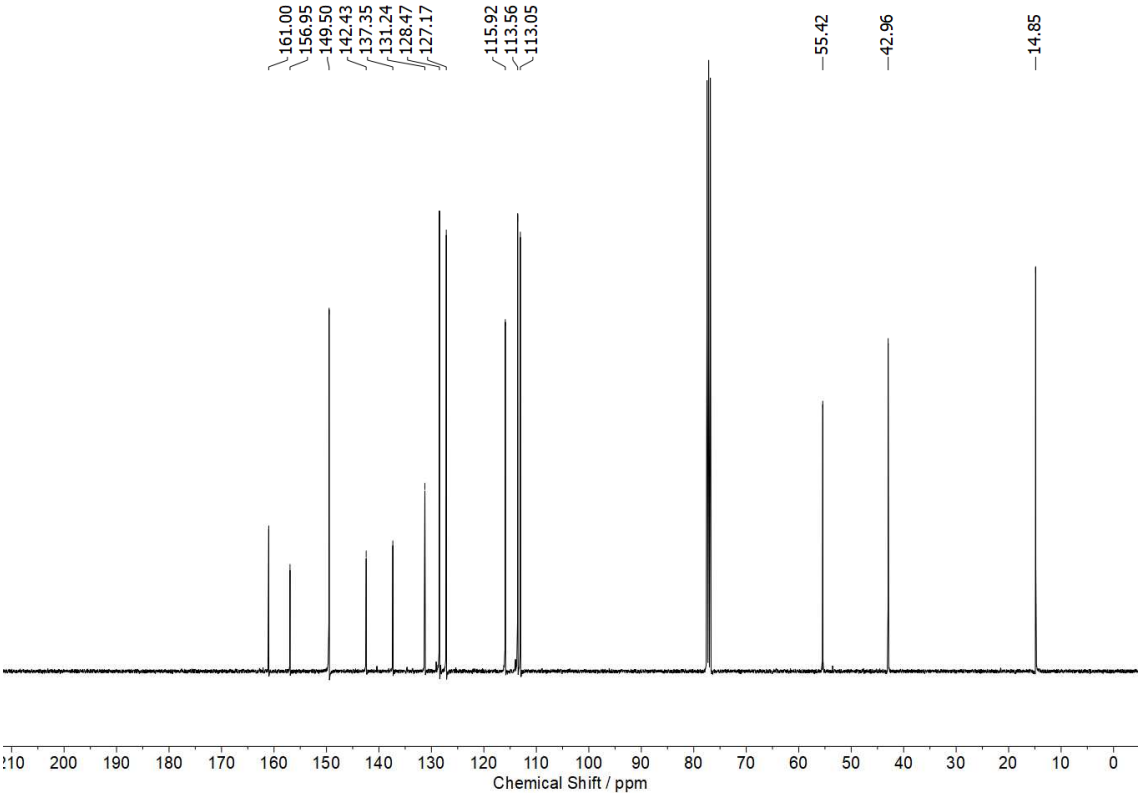

Figure S4: 160. *[Figure S160] NMR spectra of catalyst* **6ce** *($CDCl_3$, 400 MHz): a) ^1H NMR spectrum, b) ^{13}C NMR spectrum.*

Tetraphenylphosphonium ((4-methoxyphenyl)sulfonyl)(pyridin-4-yl)amide ***6cg***

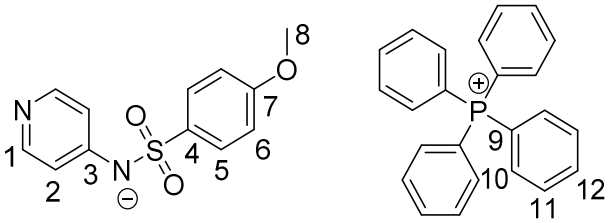

^{1}H NMR (400 MHz, $CDCl_3$) *δ* [ppm] = 7.88 – 7.75 (m, 8H, H-1, H-5, H-12), 7.70 (td, *J* = 7.8, 3.6 Hz, 8H, H-11), 7.53 (dd, *J* = 13.0, 7.5 Hz, 8H, H-10), 6.75 (d, *J* = 6.4 Hz, 2H, H-2), 6.72 (d, *J* = 8.8 Hz, 2H, H-6), 3.70 (s, 3H, H-8).

^{13}C NMR (101 MHz, $CDCl_3$) *δ* [ppm] = 160.37 (C-7), 157.76 (C-2), 148.86 (C-1), 138.77 (C-4), 135.85 (d, *J* = 3.0 Hz, C-12), 134.36 (d, *J* = 10.3 Hz, C-10), 130.83 (d, *J* = 12.9 Hz, C-11), 128.60 (C-5), 117.40 (d, *J* = 89.5 Hz, C-9), 116.20 (C-2), 113.11 (C-6), 55.32 (C-8).

^{31}P NMR (162 MHz, $CDCl_3$) *δ* [ppm] = +23.06.

a)

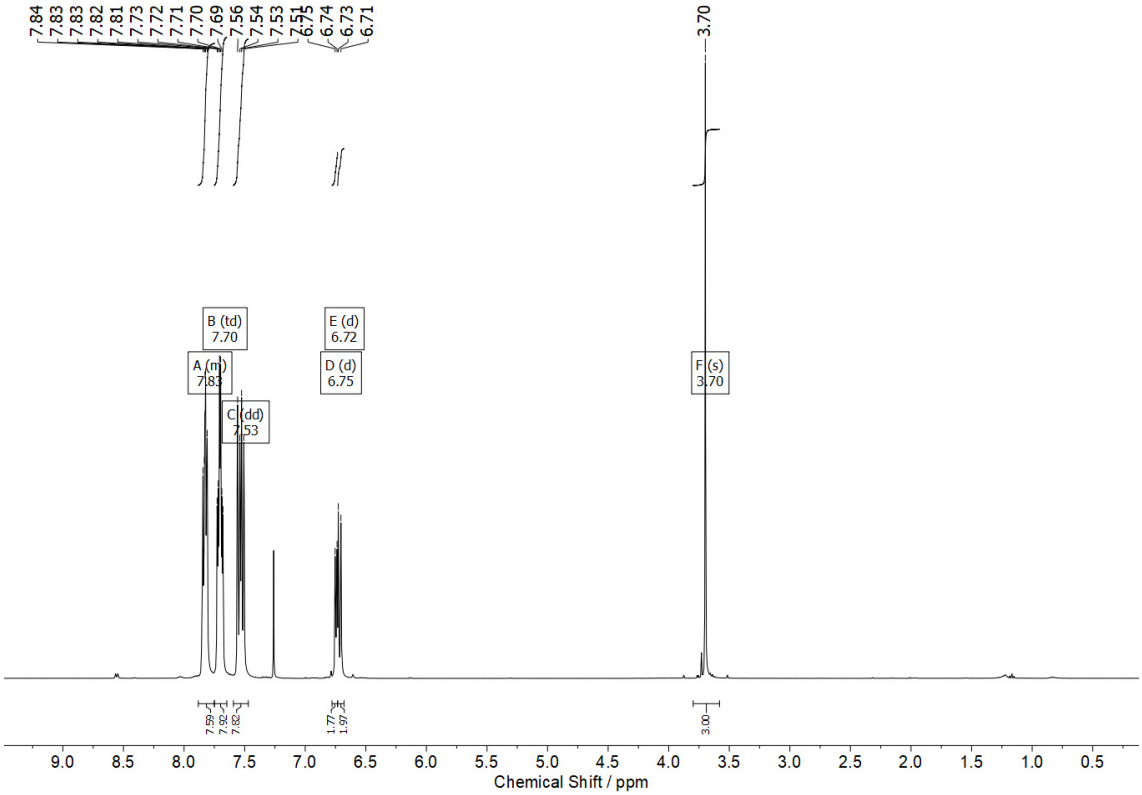

b)

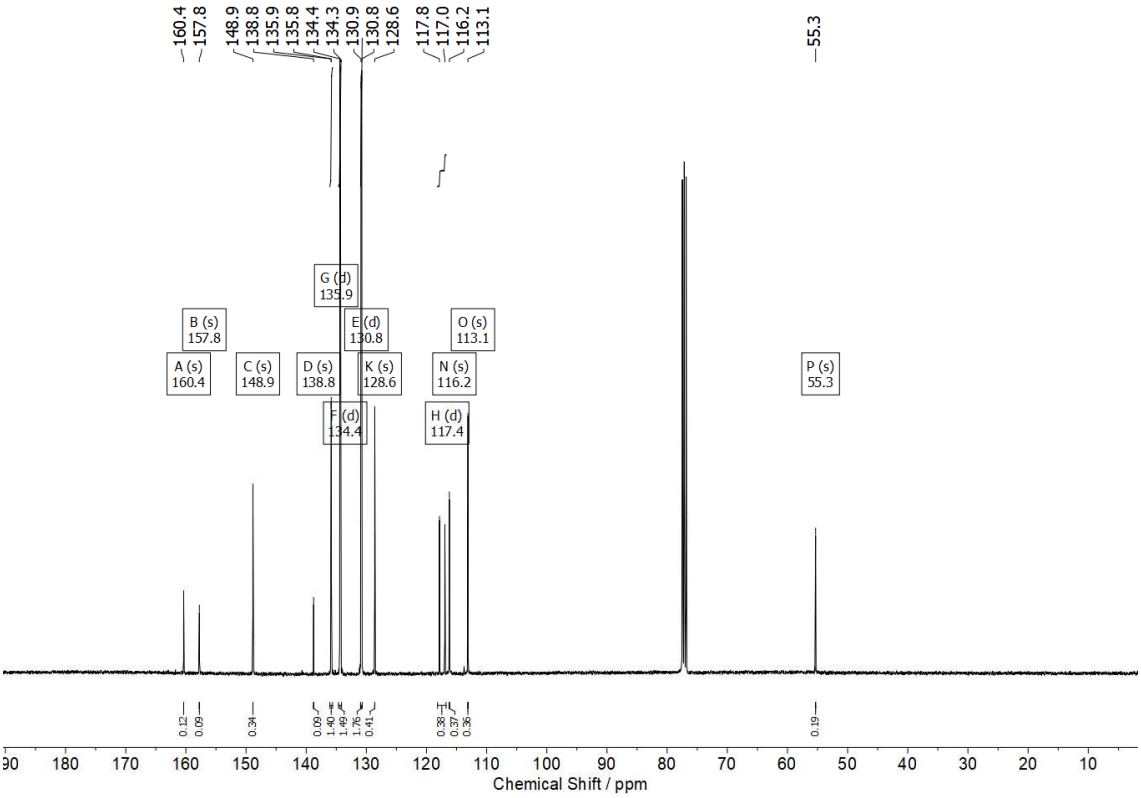

c)

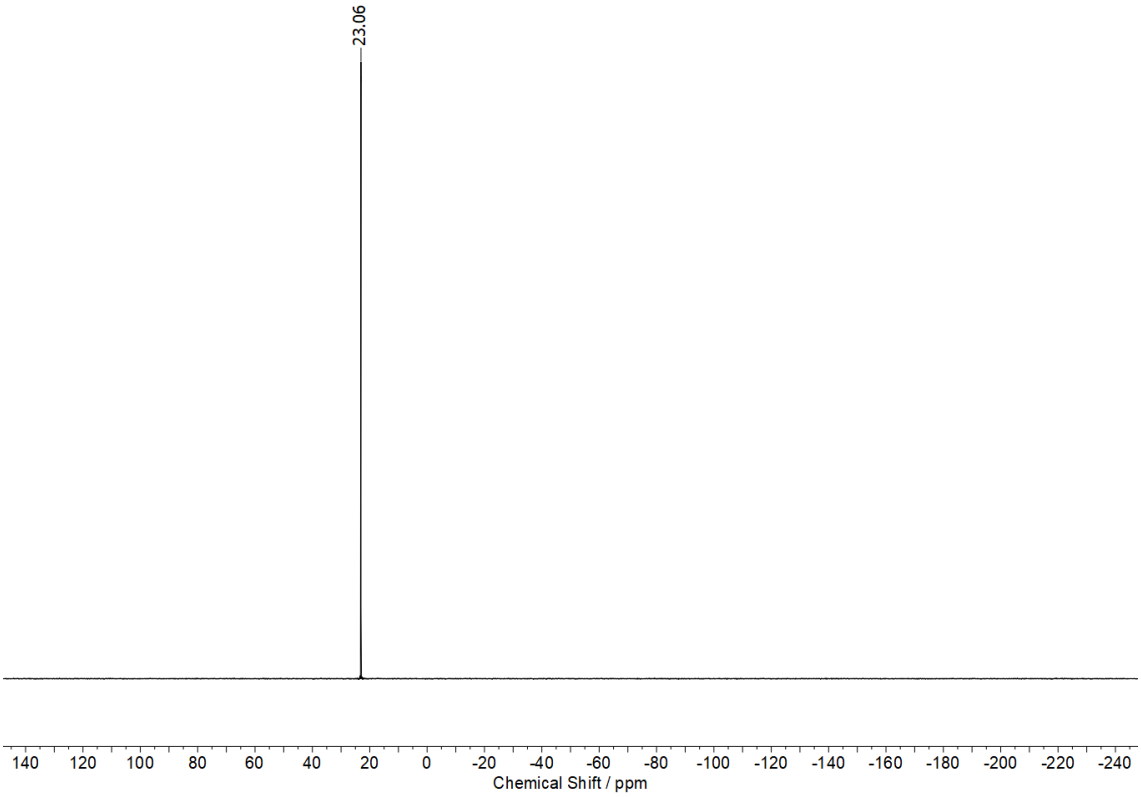

Figure S4: 161. *[Figure S161] NMR spectra of catalyst* ***6cg*** *($CDCl_3$, 400 MHz): a) ^{1}H NMR spectrum, b) ^{13}C* NMR spectrum, c) $^{31}P\{^1H\}$ NMR spectrum.

1,3-Diethyl-benzimidazolium pyridin-2-yl(tosyl)amide ***7e***

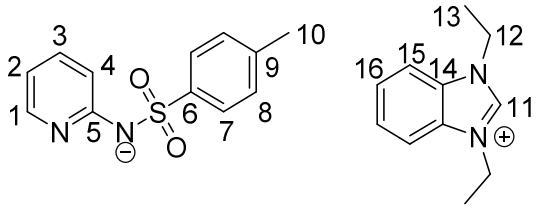

^{1}H NMR (400 MHz, $CDCl_3$) δ [ppm] = 11.85 (s, 1H, H-11), 8.02 (dd, J = 6.2, 1.3 Hz, 1H, H-1), 7.87 (d, J = 8.1 Hz, 2H, H-7), 7.74 – 7.50 (m, 4H, H-15, H-16), 7.22 (td, J = 8.7, 2.0 Hz, 1H, H-3), 7.10 (d, J = 8.0 Hz, 2H, H-8), 6.92 (d, J = 8.4 Hz, 1H, H-4), 6.44 (t, J = 6.0 Hz, 1H, H-2), 4.71 (q, J = 7.3 Hz, 4H, H-12), 2.28 (s, 3H, H-10), 1.59 (t, J = 7.3 Hz, 6H, H-13).

^{13}C NMR (101 MHz, $CDCl_3$) δ [ppm] = 161.78 (C-5), 147.95 (C-1), 144.72 (C-11), 143.27 (C-6), 139.77 (C-9), 136.70 (C-3), 131.32 (C-14), 128.77 (C-8), 126.80 (C-7), 126.69 (C-15/16), 114.26 (C-4), 112.97(C-2), 112.92 (C-15/16), 42.76 (C-12), 21.38 (C-10), 15.04 (C-13).

a)

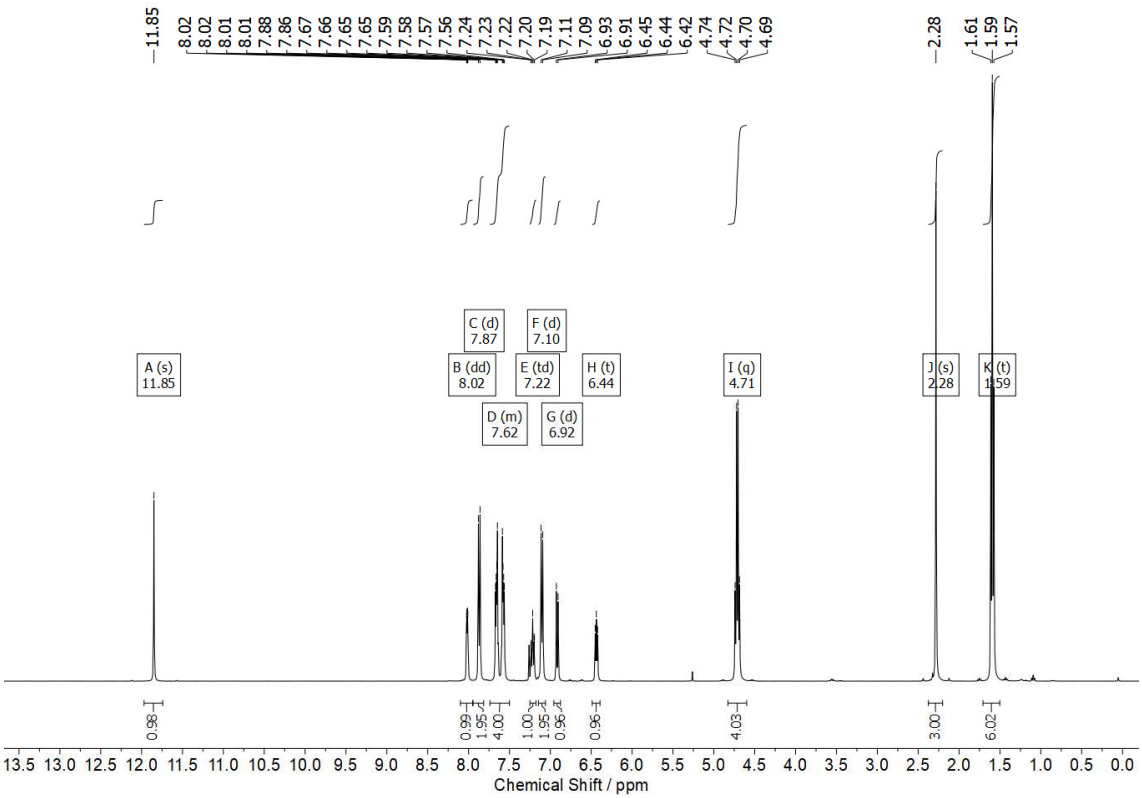

b)

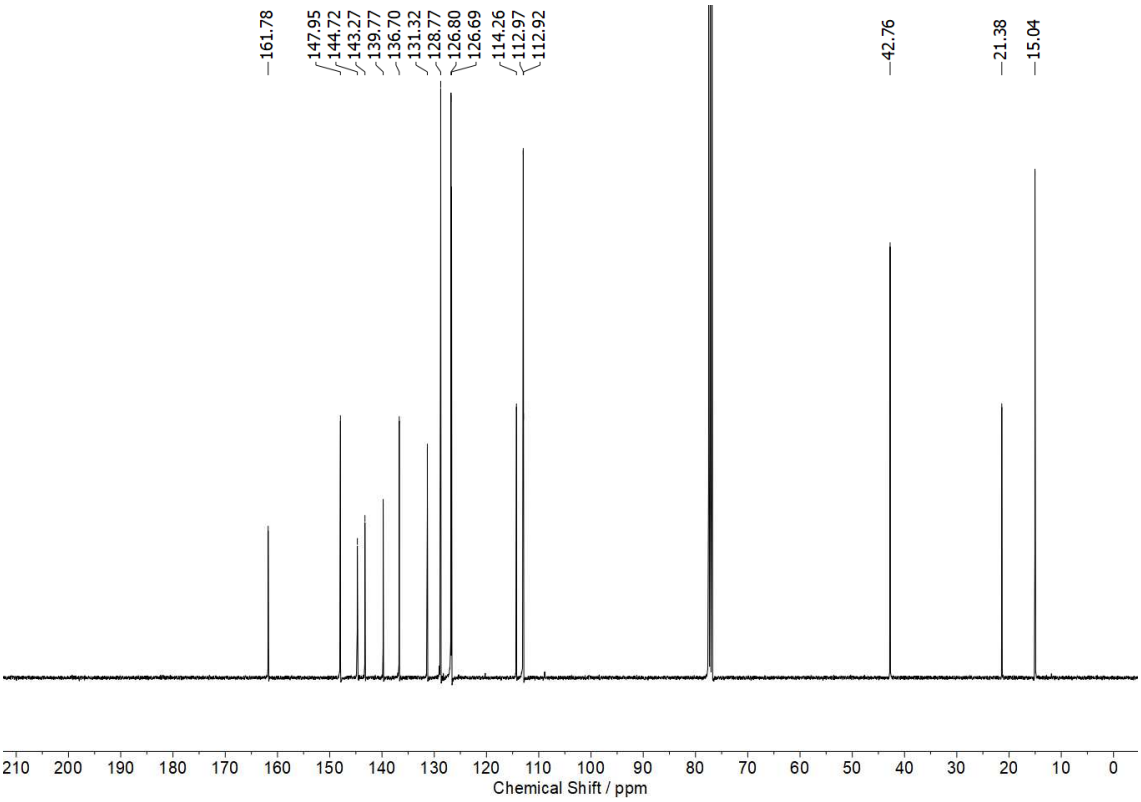

Figure S4: 162. *[Figure S162] NMR spectra of catalyst* ***7e*** *($CDCl_3$, 400 MHz): a) ^{1}H NMR spectrum, b) ^{13}C* NMR spectrum.

1,1,1-Trifluoro-N-(pyridin-4(1H)-ylidene)methanesulfonamide ***8a***

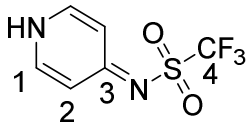

^{1}H NMR (400.22 MHz, DMSO-d_6): δ [ppm] = 13.63 (s, 1H, H-N), 8.28 (d, J = 7.4 Hz, 2H, H-1), 7.28 (d, J = 7.4 Hz, 2H, H-2).

^{13}C NMR (100.65 MHz, DMSO-d_6): δ [ppm] = 163.8 (C-3), 140.2 (C-1), 120.75 (q, J = 325.5 Hz, C-4), 116.99 (C-2).

^{19}F NMR (376.55 MHz, DMSO-d_6): δ [ppm] = −77.8.

a)

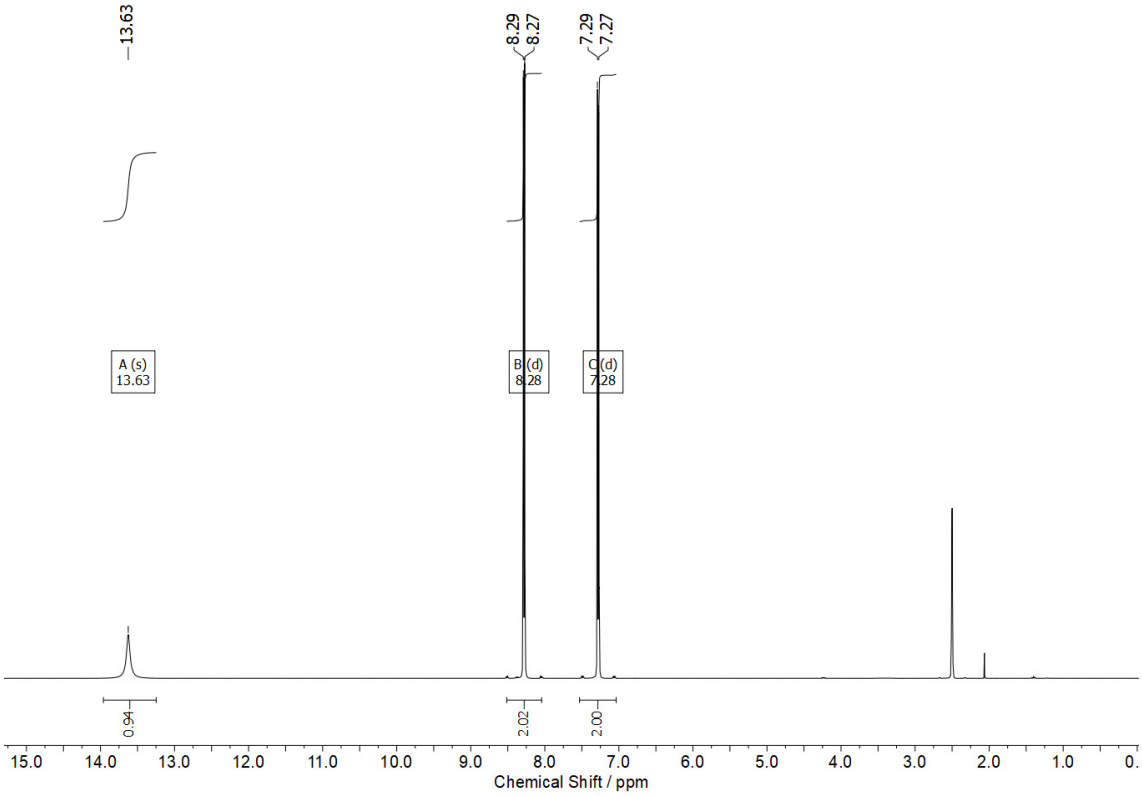
13.63
8.29
8.27
7.29
7.27
A (s)
13.63
B (d)
8.28
C (d)
7.28
0.94
2.02
2.00
15.0
14.0
13.0
12.0
11.0
10.0
9.0
8.0
7.0
6.0
5.0
4.0
3.0
2.0
1.0
0.
Chemical Shift / ppm

b)

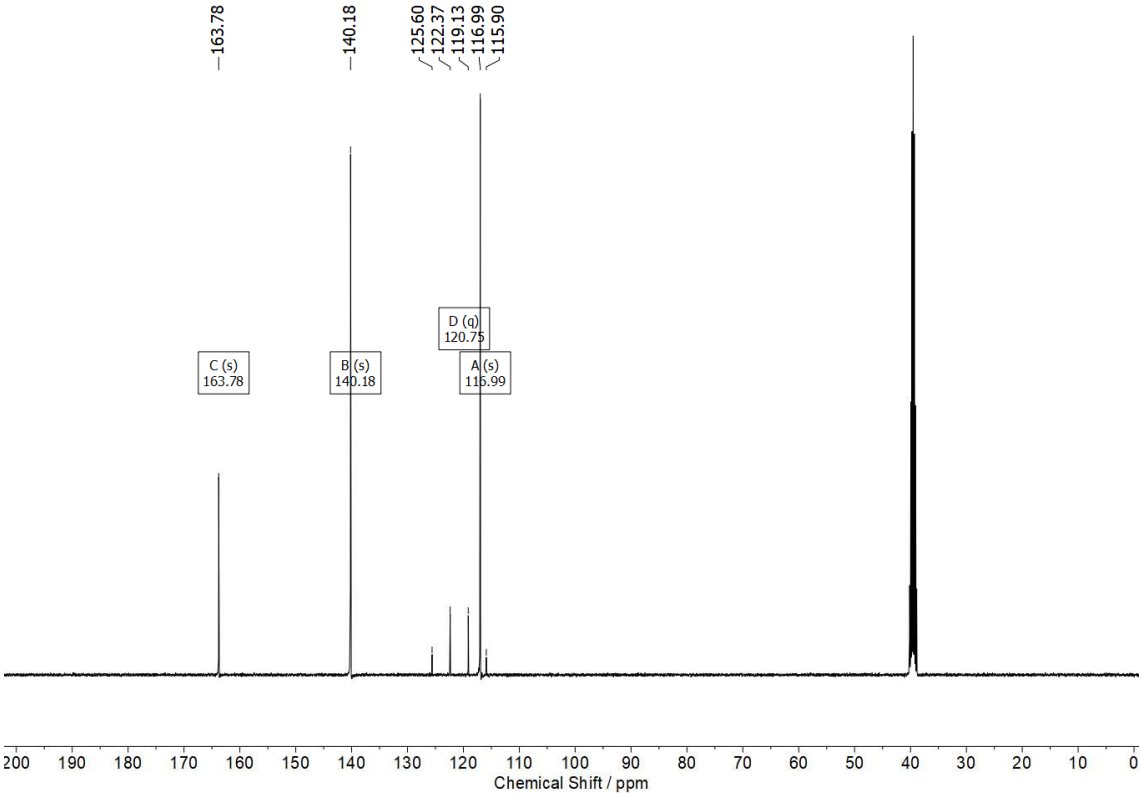
163.78
140.18
125.60
122.37
119.13
116.99
115.90
D (q)
120.75
C (s)
163.78
B (s)
140.18
A (s)
115.99
200
190
180
170
160
150
140
130
120
110
100
90
80
70
60
50
40
30
20
10
0
Chemical Shift / ppm

c)

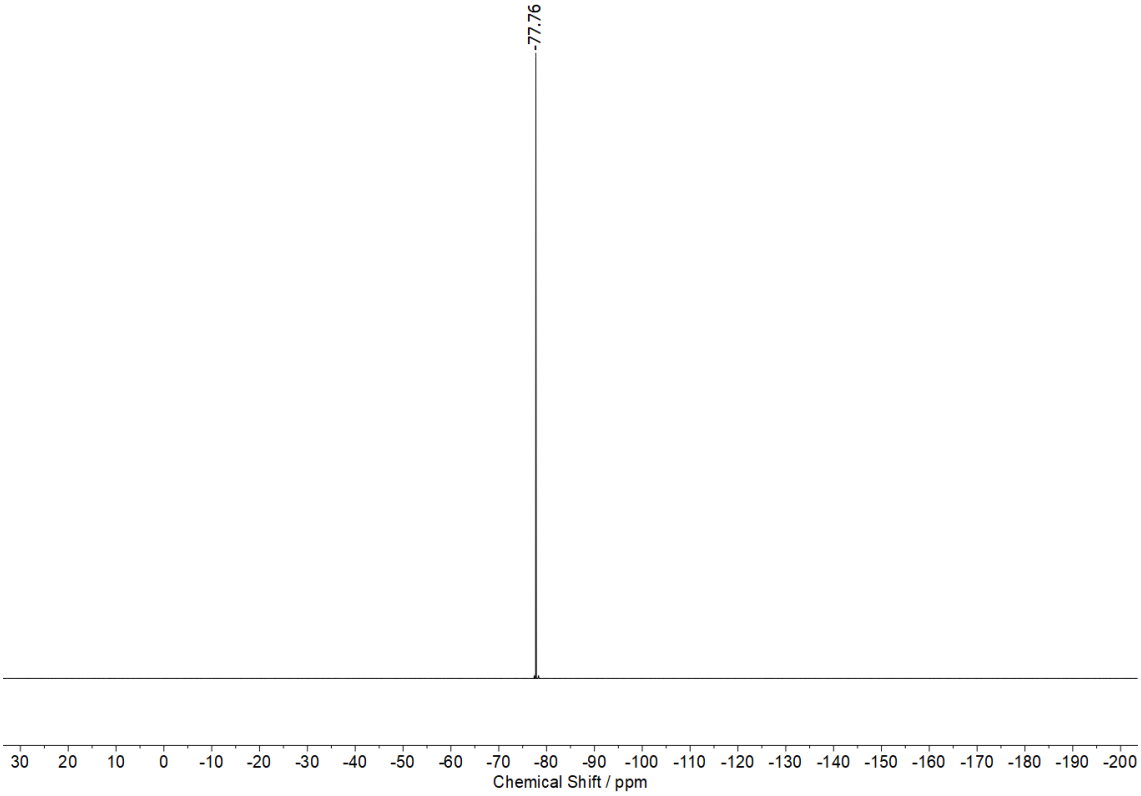

Figure S4: 163. *[Figure S163] NMR spectra of sulfonamide* ***8a*** *(DMSO-*d6*), 400 MHz): a)* ^{1}*H NMR spectrum, b)* ^{13}*C NMR spectrum, c)* ^{19}*F NMR spectrum.*

4-Methyl-N-(pyridin-4(1H)-ylidene)benzenesulfonamide ***8b***

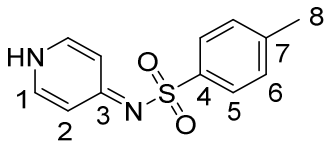

^{1}H NMR (400.22 MHz, DMSO-d_6): δ [ppm] = 12.25 (s, 1H, H-N), 8.01 (d, J = 5.9 Hz, 2H, H-1), 7.68 (d, J = 8.1 Hz, 2H, H-5), 7.30 (d, J = 7.9 Hz, 2H, H-6), 6.90 (d, J = 6.7 Hz, 2H, H-2), 2.33 (s, 3H, H-8).

^{13}C NMR (100.65 MHz, DMSO-d_6): δ [ppm] = 141.57 (C-1/C-3/C-4/C-7), 140.24 C-1/C-3/C-4/C-7), 129.27 (C-6), 126.23 (C-5), 114.27 (C-2), 20.94 (C-8). Due to the very low solubility of sulfonamide **8b**, not all expected carbon signals were resolved.

a)

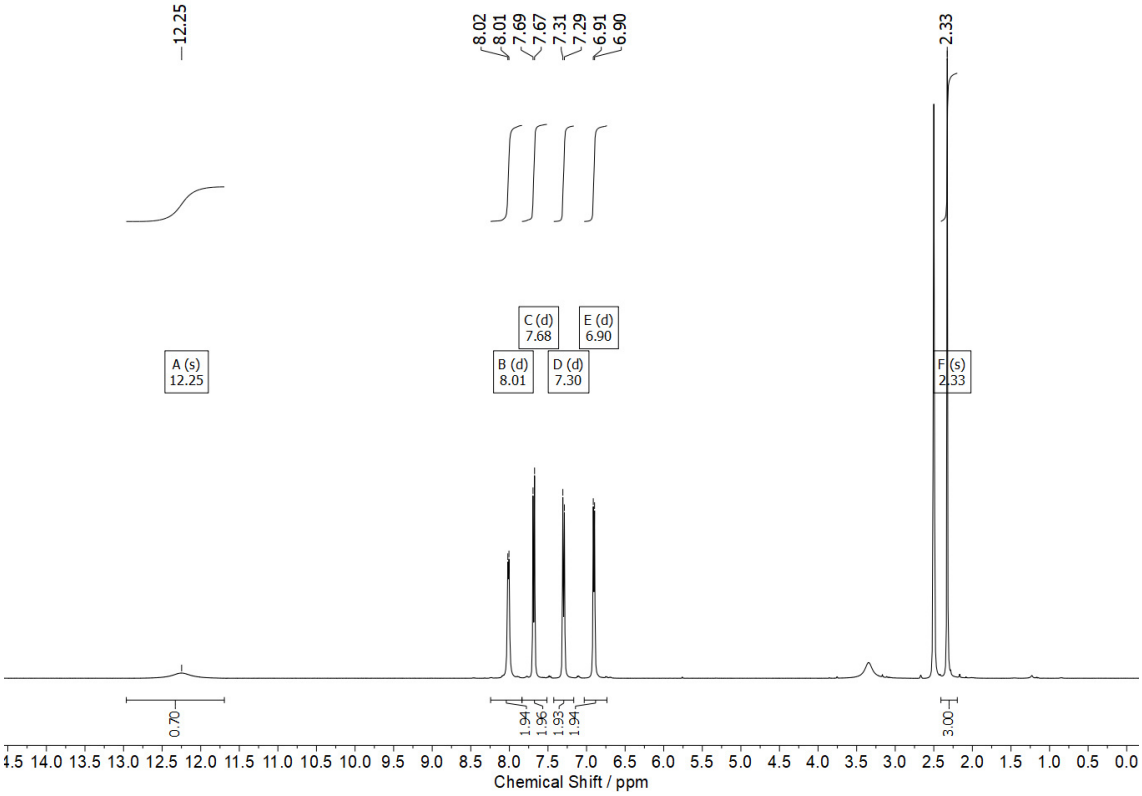

b)

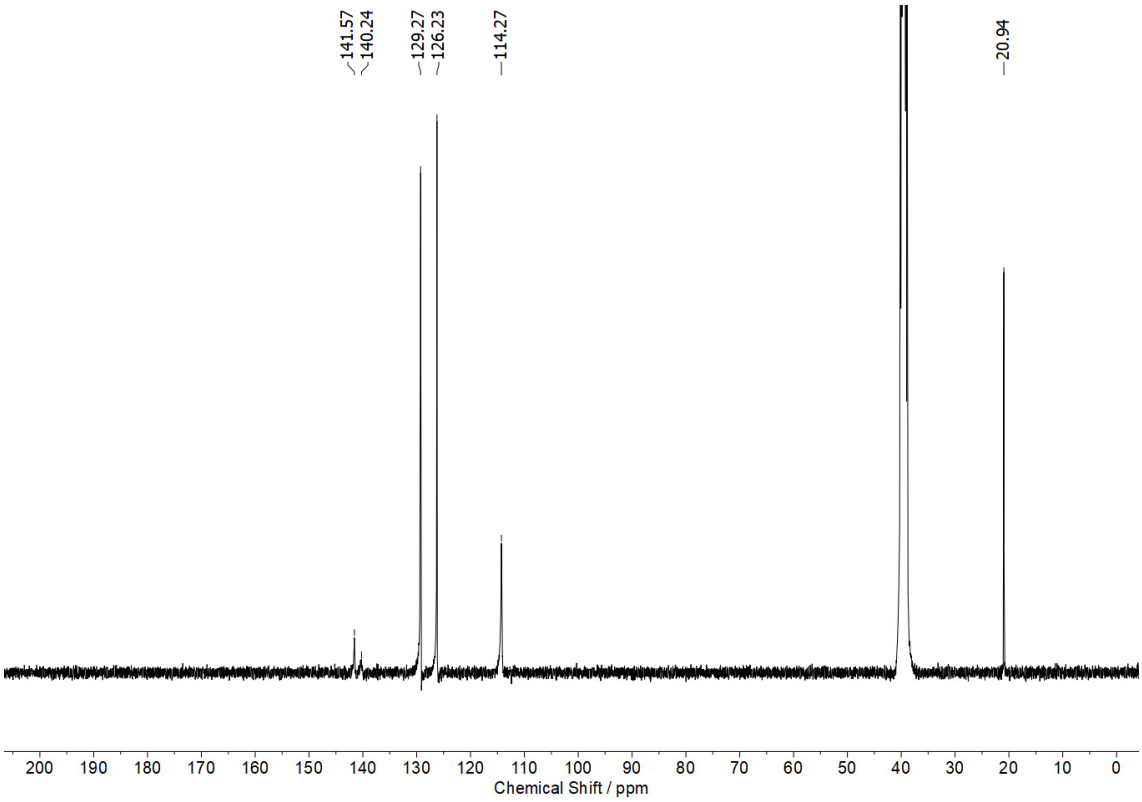

Figure S4: 164. *[Figure S164] NMR spectra of catalyst* ***8b*** *(DMSO-*d6*), 400 MHz): a) ^{1}H NMR spectrum, b) ^{13}C NMR spectrum.*

N-(1,4-dihydropyridin-4-yl)-4-methoxybenzenesulfonamide ***8c***

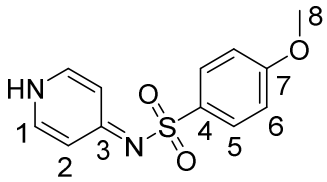

^{1}H NMR (400 MHz, DMSO-d_6) δ [ppm] = 12.12 (s, 1H, H-N), 8.04 (d, J = 6.2 Hz, 2H, H-1), 7.75 (d, J = 8.8 Hz, 2H, H-5), 7.02 (d, J = 8.8 Hz, 2H, H-6), 6.93 (d, J = 6.8 Hz, 2H, H-2), 3.78 (s, 3H, H-8).

^{13}C NMR (101 MHz, DMSO-d_6) δ [ppm] = 161.66 (C-7), 157.25 (C-3), 141.89 (C-1), 134.38 (C-4), 128.36 (C-5), 114.06 (C-6), 113.90 (C-2), 55.54 (C-8).

a)

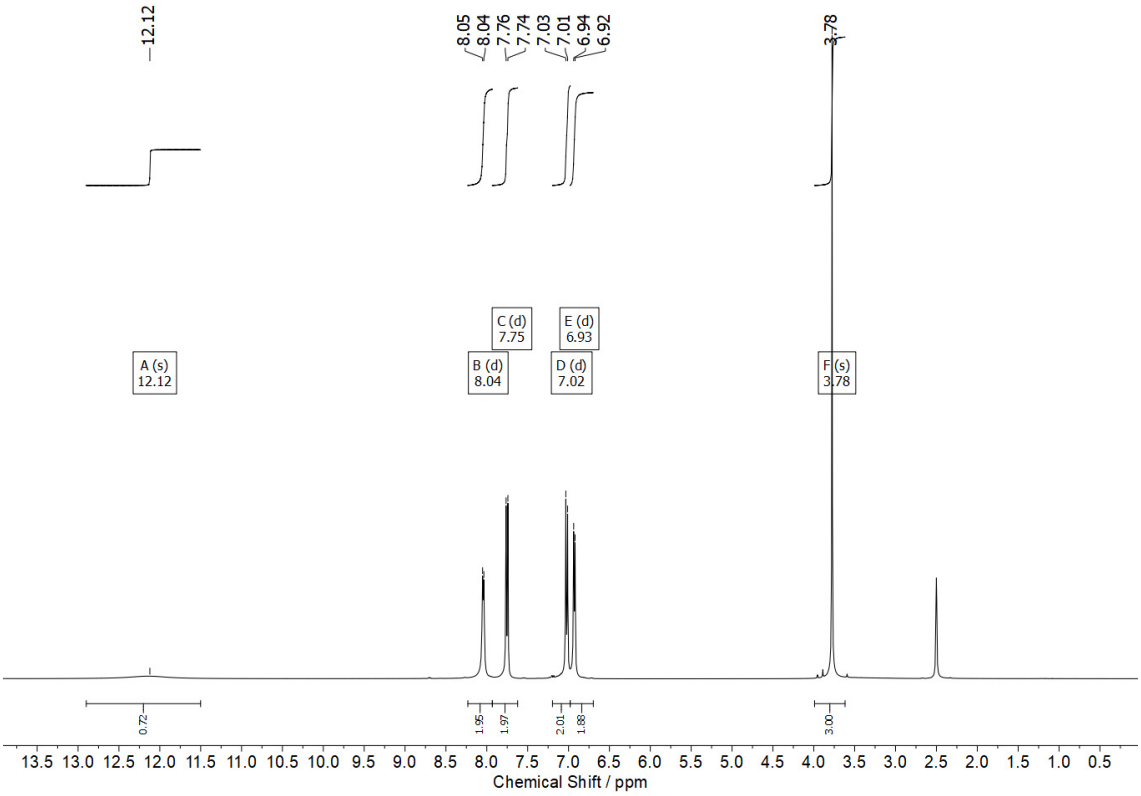

b)

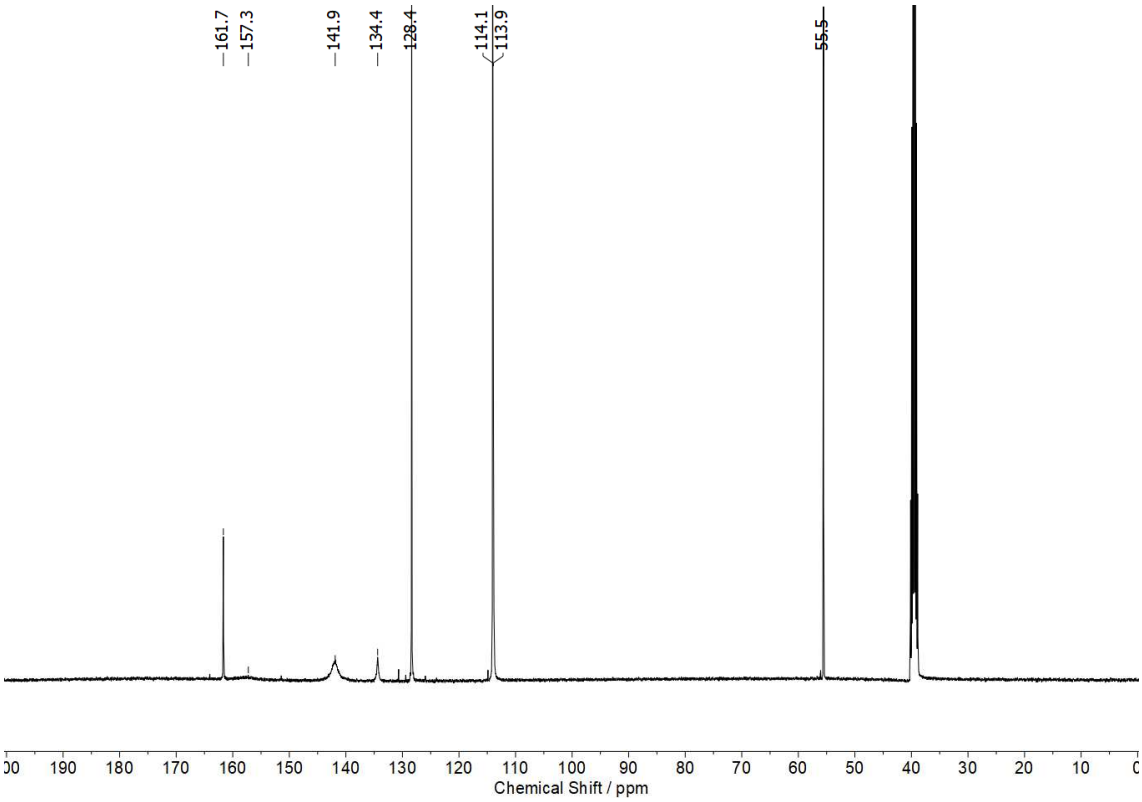

Figure S4: 165. *[Figure S165] NMR spectra of sulfonamide* ***8c*** *(DMSO-*d_6*, 400 MHz): a)* ^{1}*H NMR spectrum, b)* ^{13}*C NMR spectrum.*

Tetrabutylphosphonium (diphenylphosphoryl)(pyridin-4-yl)amide ***10d***

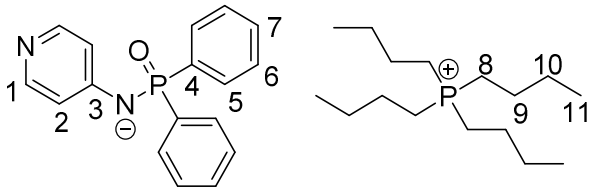

^{1}H NMR (400 MHz, toluene-d8) *δ* [ppm] = 8.42 – 8.22 (m, 4H, H-5), 8.12 (d, *J* = 5.3 Hz, 2H, H-1), 7.20 (td, *J* = 7.5, 2.2 Hz, 4H, H-6), 7.15 – 7.09 (m, 2H, H-7), 7.07 (d, *J* = 5.8 Hz, 2H, H-2), 2.22 – 1.92 (m, 8H, H-8), 1.30 (h, *J* = 7.2 Hz, 8H, H-10), 1.11 (dq, *J* = 15.6, 7.6 Hz, 8H, H-9), 0.88 (t, *J* = 7.3 Hz, 12H, H-11).

^{13}C NMR (101 MHz, toluene-d8) *δ* [ppm] = 163.18, 149.74 (d, *J* = 1.9 Hz, C-1), 142.65 (d, *J* = 122.0 Hz, C-4), 133.10 (d, *J* = 8.2 Hz, C-5), 129.40 (d, *J* = 2.4 Hz, C-7), 128.08 (d, *J* = 11.0 Hz, C-6), 119.40 (d, *J* = 21.1 Hz, C-2), 24.62 (d, *J* = 15.6 Hz, C-10), 24.36 (d, *J* = 4.7 Hz, C-9), 18.90 (d, *J* = 47.3 Hz, C-8), 14.17 (C-11).

^{31}P{^{1}H} NMR (162 MHz, toluene-d8) *δ* [ppm] = +32.16 (P^+), +10.86 (P=O).

a)

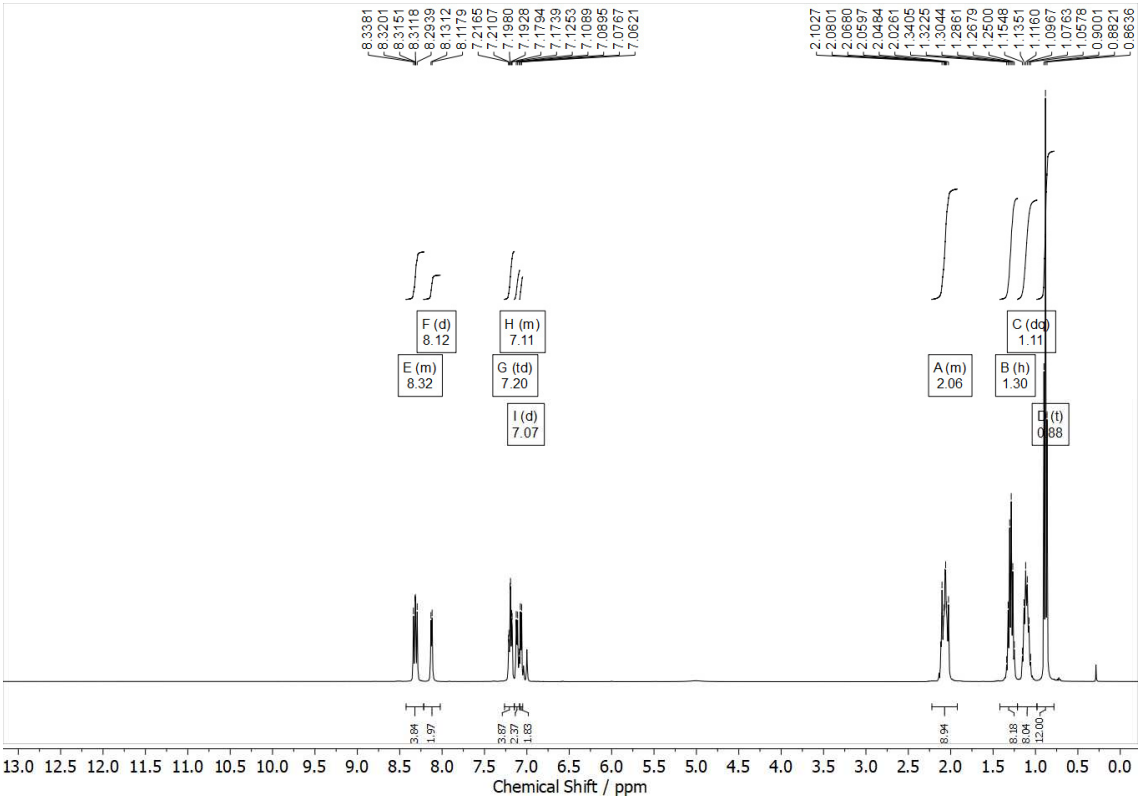
F (d)
8.12
E (m)
8.32
H (m)
7.11
G (td)
7.20
I (d)
7.07
A (m)
2.06
B (h)
1.30
C (dq)
1.11
D (t)
0.88
Chemical Shift / ppm

b)

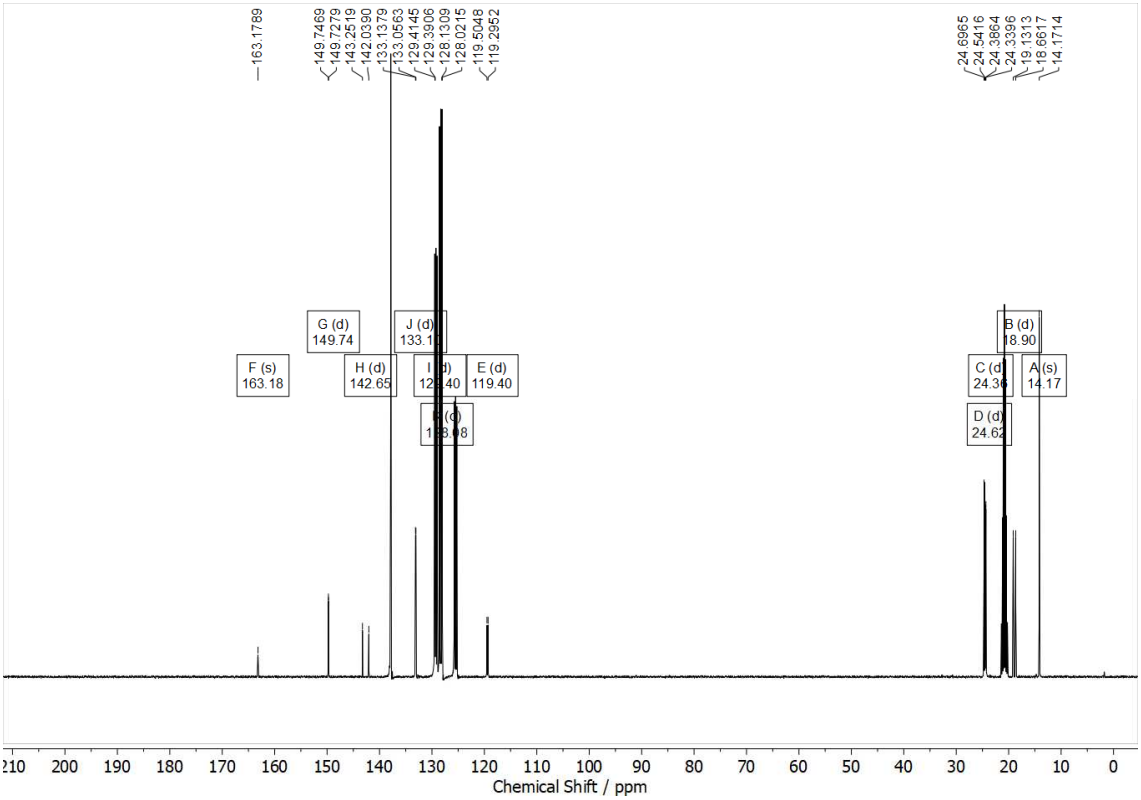
F (s)
163.18
G (d)
149.74
H (d)
142.65
E (d)
119.40
B (d)
18.90
A (s)
14.17
D (d)
24.62
Chemical Shift / ppm

c)

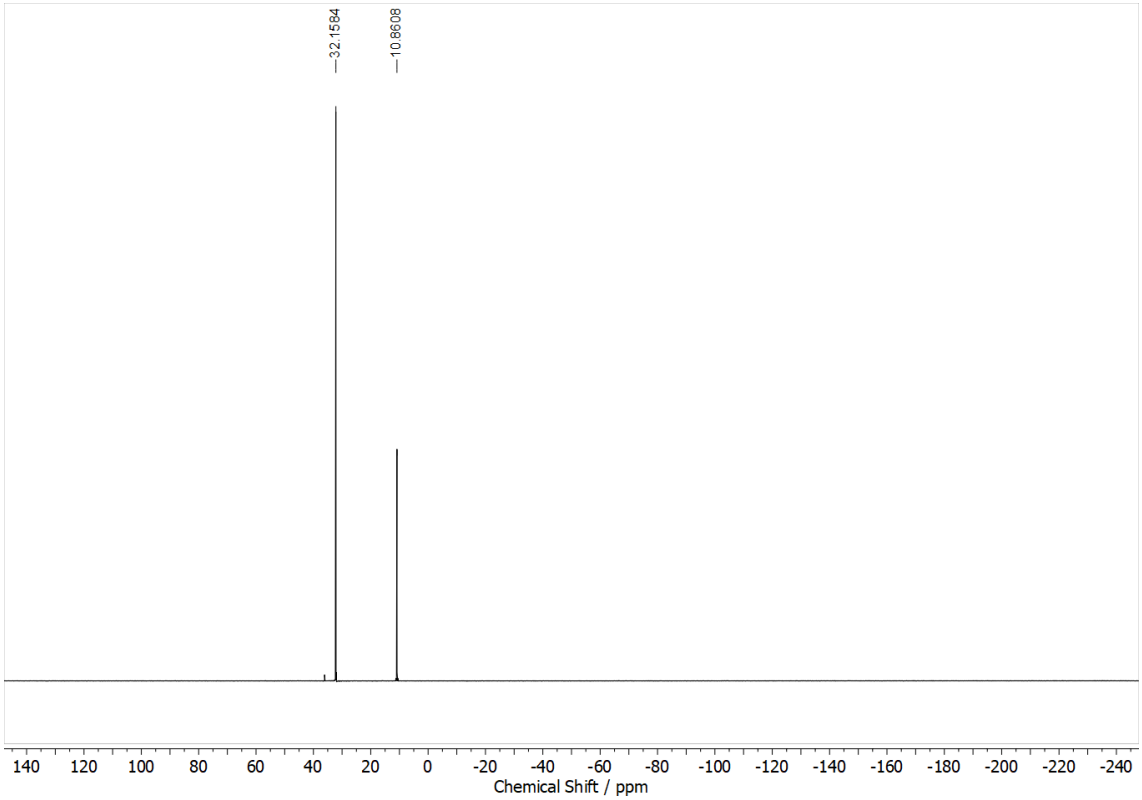

d)

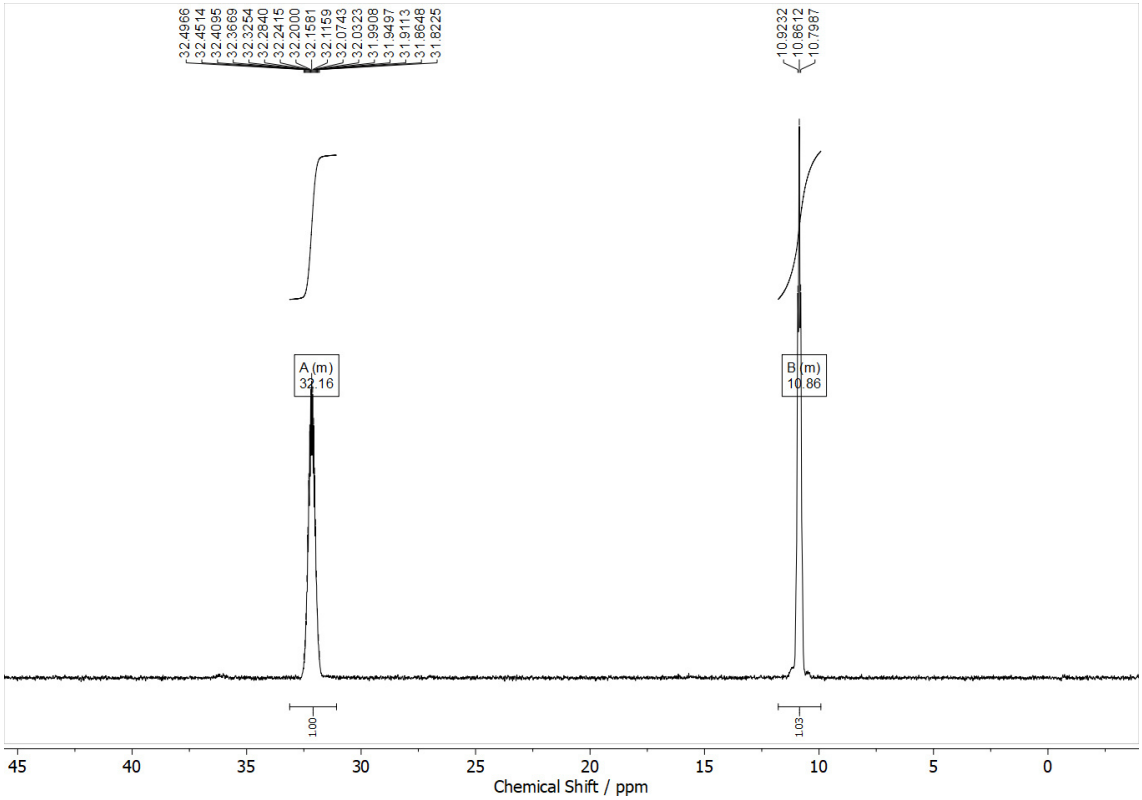

Figure S4: 166. *[Figure S166] NMR spectra of phosphonic amide catalyst* ***10d*** *$CDCl_3$, 400 MHz): a) ^1H NMR spectrum, b) ^{13}C NMR spectrum, c) $^{31}P\{^1H\}$ NMR spectrum. d) $^{31}P\{^1H\}$ NMR spectrum.*

P,P-Diphenyl-N-(pyridin-4-yl)phosphonic amide ***11***

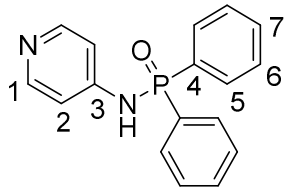

^{1}H NMR (400 MHz, $CDCl_3$) *δ* [ppm] = 8.15 (d, *J* = 6.0 Hz, 2H, H-1), 7.81 (dd, *J* = 12.6, 7.1 Hz, 4H, H-5), 7.54 (td, *J* = 7.5, 1.3 Hz, 2H, H-7), 7.44 (td, *J* = 7.5, 3.4 Hz, 4H, H-6), 6.85 (d, *J* = 6.2 Hz, 2H, H-2), 6.62 (s, 1H, H-N).

^{13}C NMR (101 MHz, $CDCl_3$) *δ* [ppm] = 150.28 (C-1), 148.44 (C-3), 132.80 (d, *J* = 2.8 Hz, C-7), 131.93 (d, *J* = 10.3 Hz, C-5), 131.01 (d, *J* = 128.9 Hz, C-4), 129.09 (d, *J* = 13.2 Hz, C-6), 113.08 (d, *J* = 6.8 Hz, C-2).

^{31}P{^{1}H} NMR (162 MHz, $CDCl_3$) *δ* [ppm] = +19.31.

a)

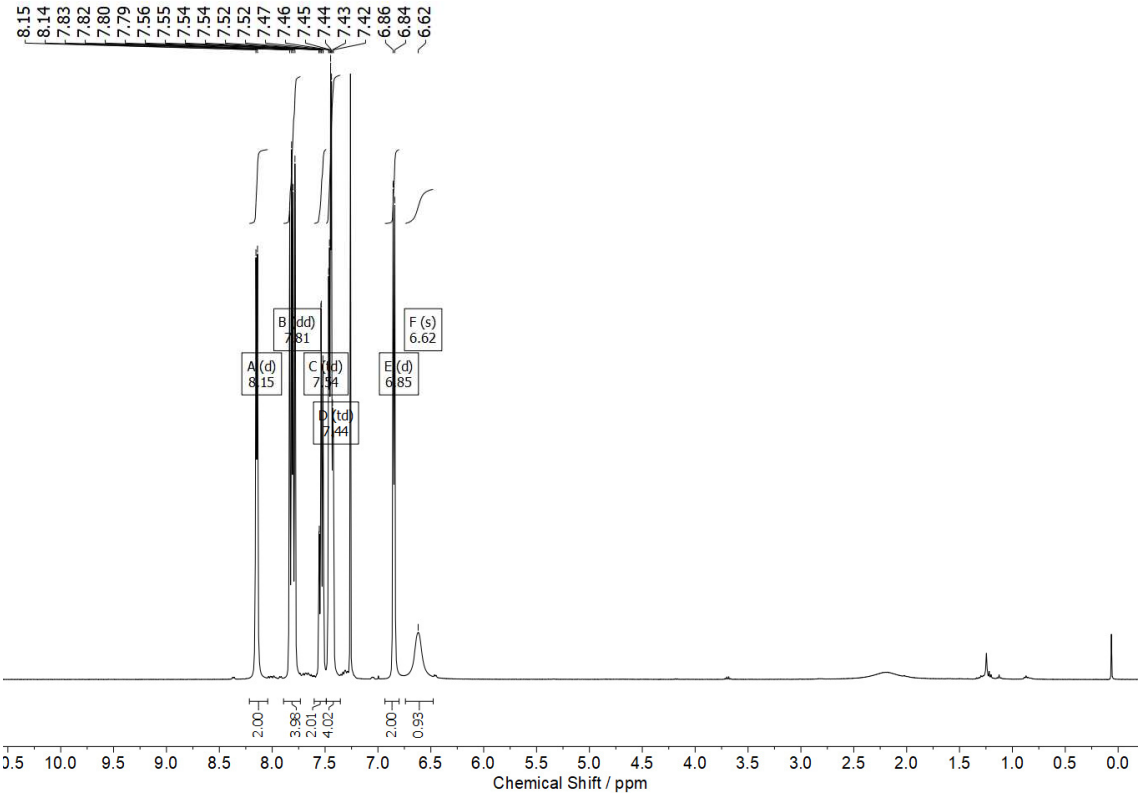

b)

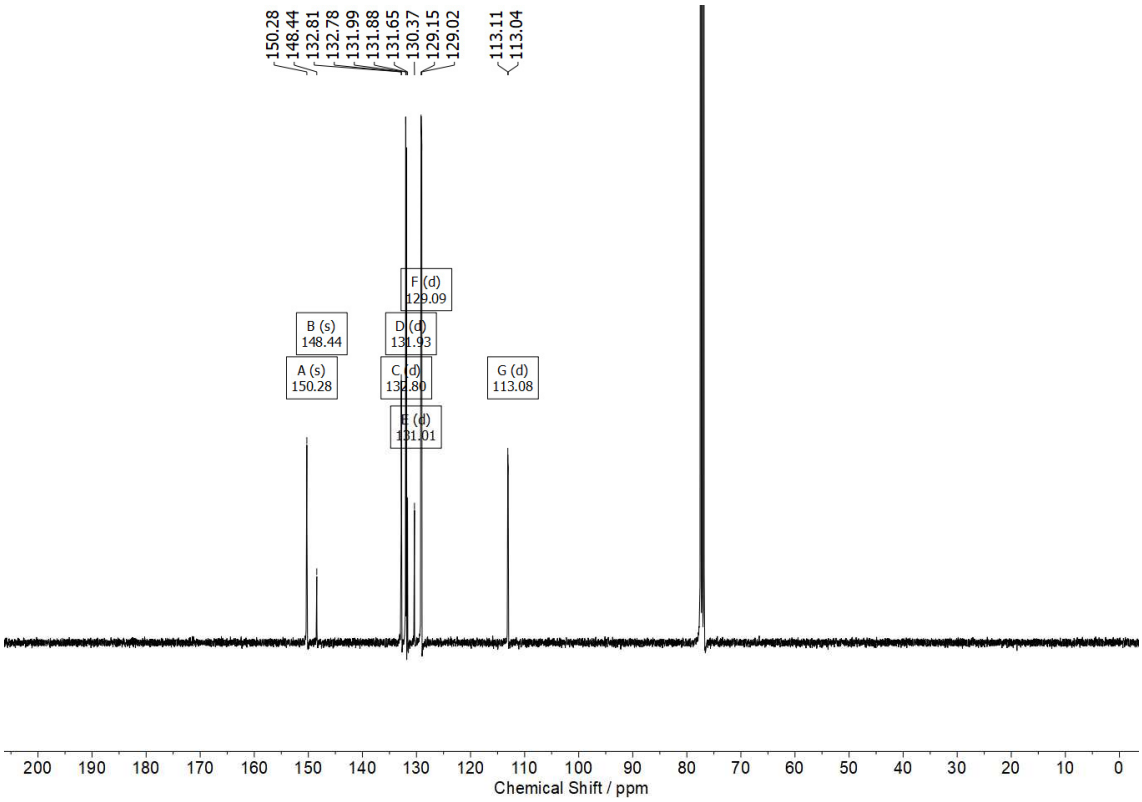

c)

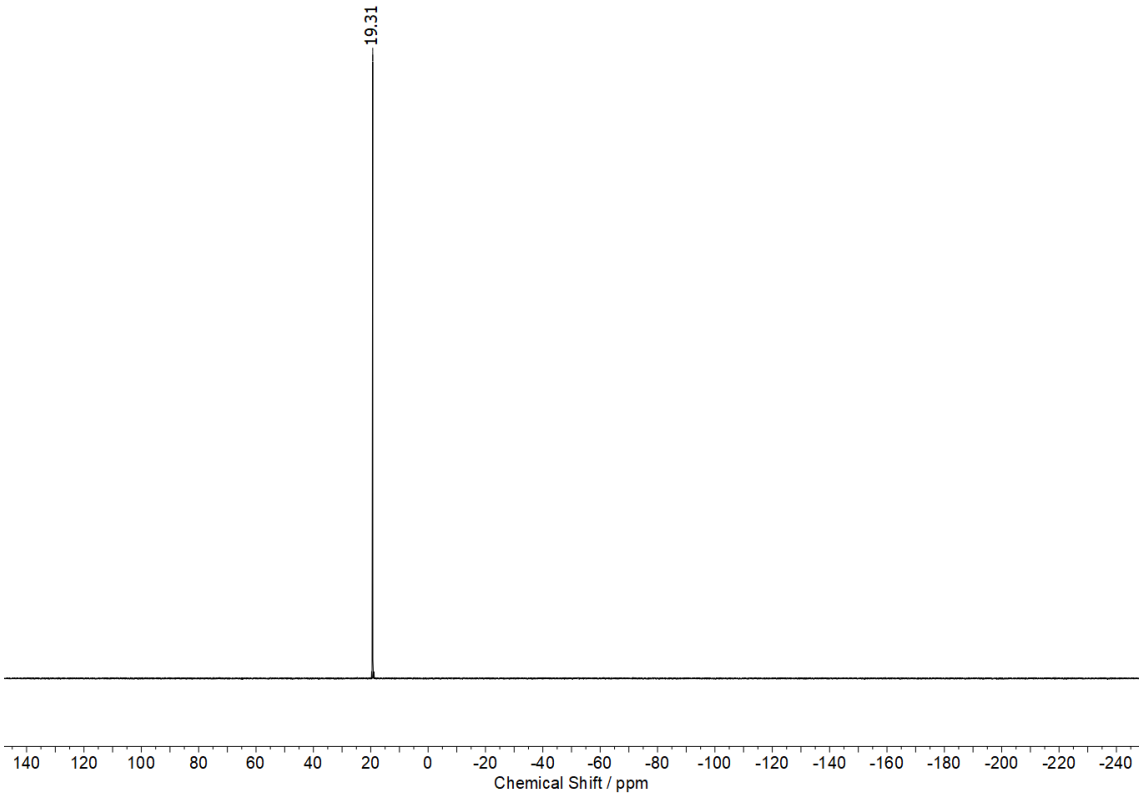

Figure S4: 167. *[Figure S167] NMR spectra of phosphonic amide* ***11*** *$CDCl_3$, 400 MHz): a) ^1H NMR spectrum, b) ^{13}C NMR spectrum, c) $^{31}P\{^1H\}$ NMR spectrum.*

3-Chlorobenzo[d]isothiazole 1,1-dioxide ***13***

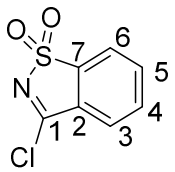

^{1}H NMR (400.22 MHz, $CDCl_3$): δ [ppm] = 7.96 – 7.90 (m, 1H, Ar-H), 7.90 – 7.80 (m, 3H, Ar-H).

^{13}C NMR (100.65 MHz, $CDCl_3$): δ [ppm] = 166.33 (C-1), 140.51 (C-2/7), 135.15 (C-3/4/5/6), 134.65 (C-3/4/5/6), 129.93 (C-2/7), 125.26 (C-3/4/5/6), 122.56 (C-3/4/5/6).

a)

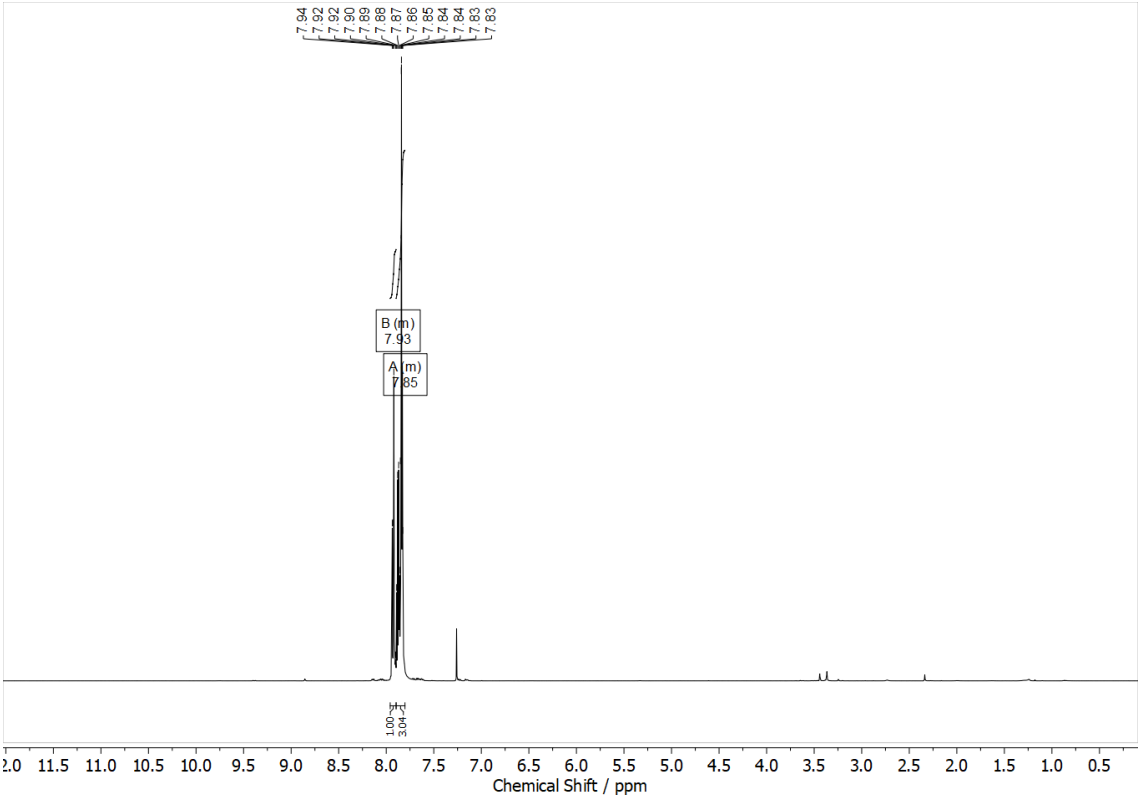

b)

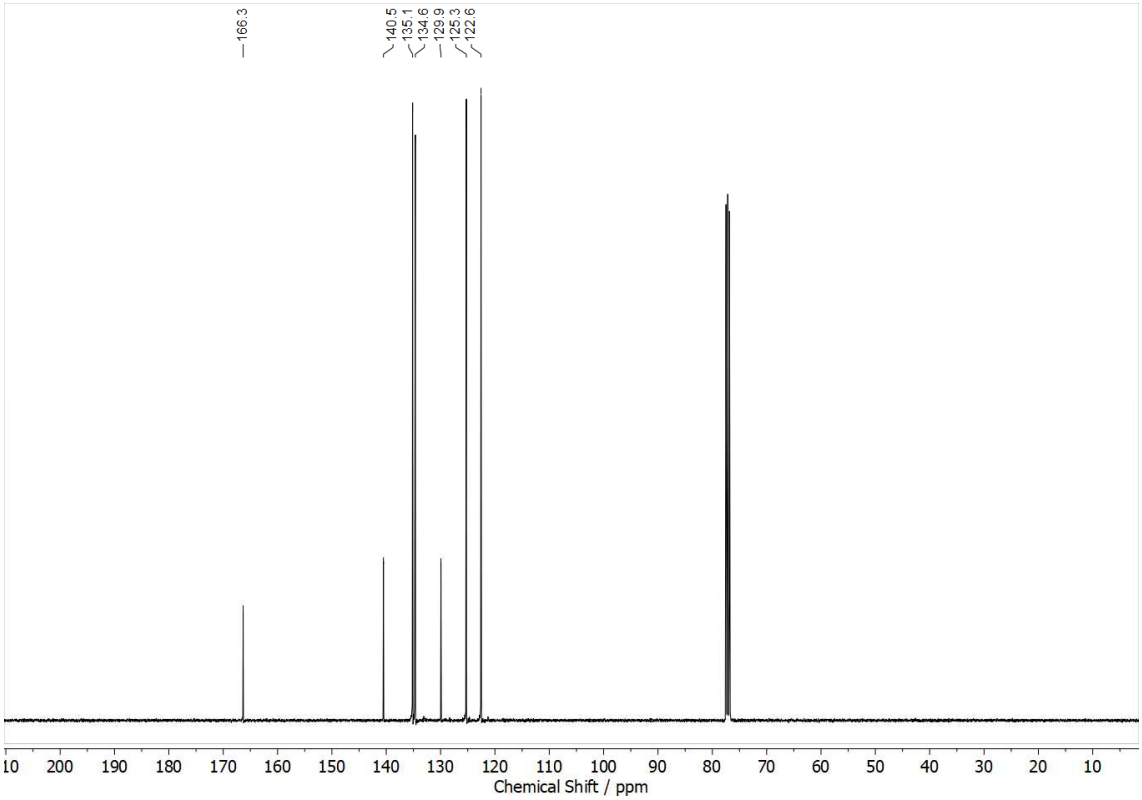

Figure S4: 168. *[Figure S168] NMR spectra of imidoyl chloride **13** ($CDCl_3$, 400 MHz): a) ^{1}H NMR spectrum, b) ^{13}C NMR spectrum.*

*3-(Pyridin-4-ylamino)benzo[d]isothiazole 1,1-dioxide **14***

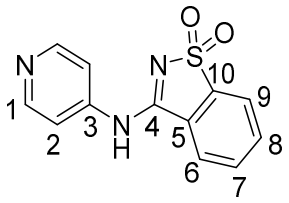

^{1}H NMR (400.22 MHz, DMSO-d_6): δ [ppm] = 11.14 (s, 1H, H-N), 8.62 (d, J = 5.7 Hz, 2H, H-1), 8.51 (d, J = 7.2 Hz, 1H, H-6), 8.12 (d, J = 6.7 Hz, 1H, H-9), 8.03 – 7.80 (m, 4H, H-2, H-7,H-8).

^{13}C NMR (100.65 MHz, DMSO-d_6): δ [ppm] = 157.64 (C-4), 150.51 (C-1), 144.98 (C-3), 140.40 (C-10), 134.08 (C-7/8), 133.63 (C-7/8), 128.22 (C-5), 124.06 (C-6), 121.76 (C-9), 115.67 (C-2).

a)

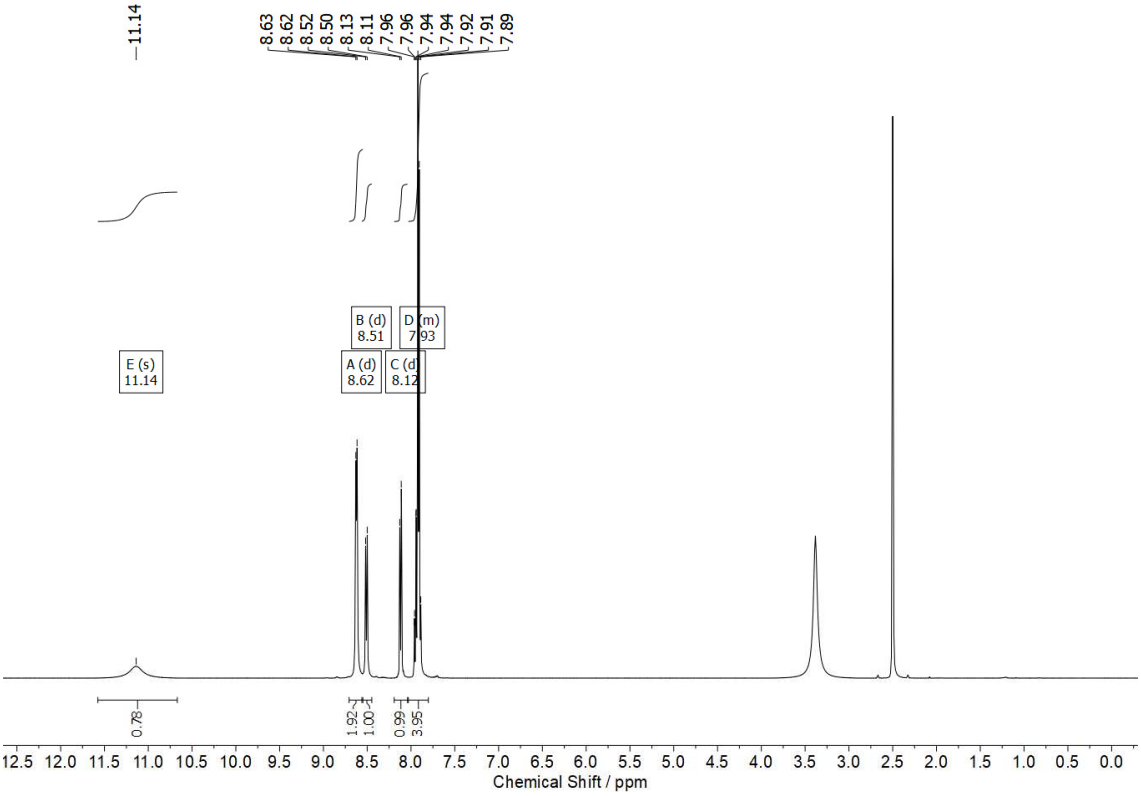

b)

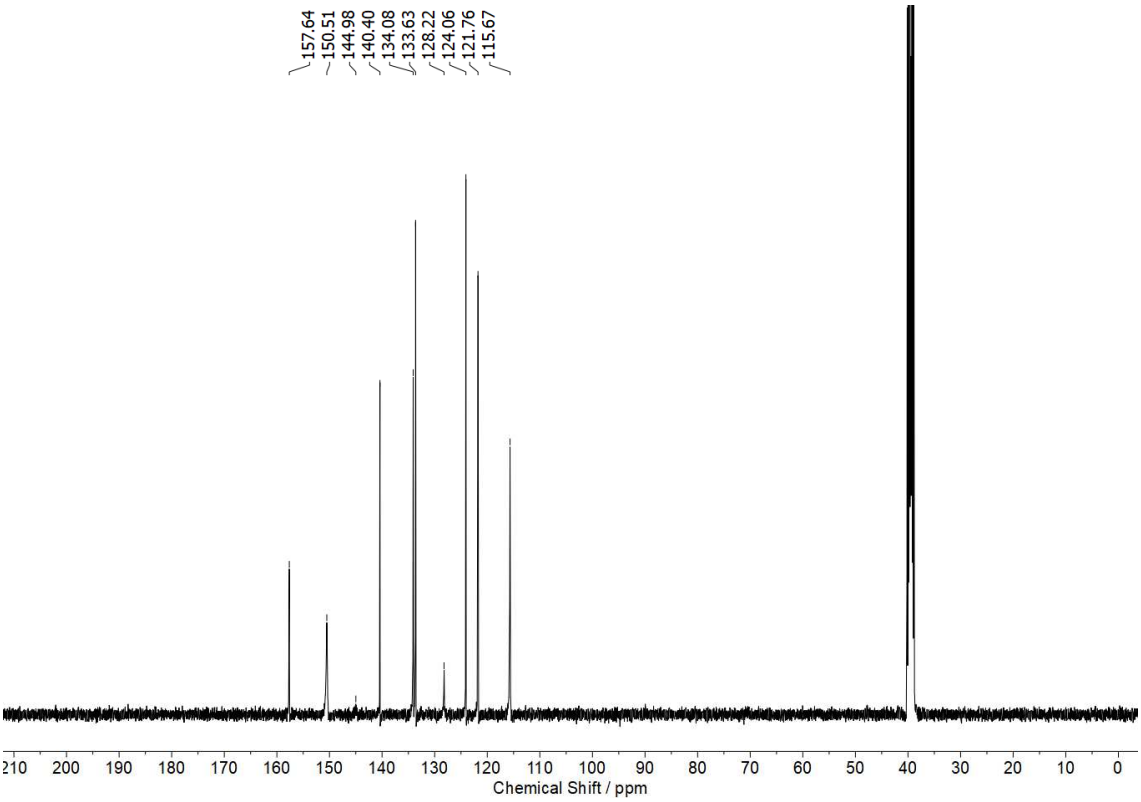

Figure S4: 169. *[Figure S169] NMR spectra of sulfonamide* ***14*** *(DMSO-*d_6*, 400 MHz): a)* ^{1}*H NMR spectrum, b)* ^{13}*C NMR spectrum.*

Tetraphenylphosphonium (1,1-dioxidobenzo[d]isothiazol-3-yl)(pyridin-4-yl)amide ***15g***

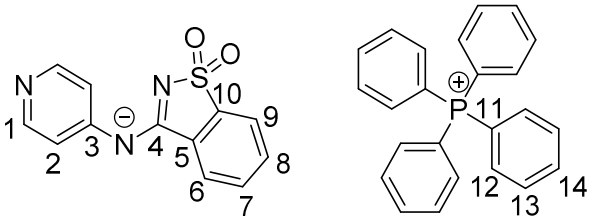

^{1}H NMR (400.22 MHz, $CDCl_3$): *δ* [ppm] = 8.17 (d, *J* = 5.9 Hz, 2H, H-1), 7.93 (dd, *J* = 6.0, 1.5 Hz, 1H, H-6), 7.85 – 7.76 (m, 4H, H-14), 7.74 – 7.61 (m, 9H, H-9, H-13), 7.51 (ddd, *J* = 13.0, 8.3, 1.1 Hz, 8H, H-12), 7.42 (ddd, *J* = 7.2, 5.3, 1.4 Hz, 2H, H-7,H-8), 7.38 (dd, *J* = 4.7, 1.5 Hz, 2H, H-2).

^{13}C NMR (100.65 MHz, $CDCl_3$): *δ* [ppm] = 158.90 (C-3), 158.13 (C-4), 149.43 (C-1), 142.55(C-5/10), 137.61 (C-5/10), 135.85 (d, *J* = 3.0 Hz (C-14)), 134.38 (d, *J* = 10.3 Hz, C-12), 130.96 (C-7/8), 130.80 (d, *J* = 12.9 Hz, C-13), 129.98 (C-7/8), 123.11 (C-6), 120.40 (C-2), 119.83 (C-9), 117.41 (d, *J* = 89.5 Hz, C-11).

^{31}P{^{1}H} NMR (162 MHz, $CDCl_3$) *δ* [ppm] = +22.06.

a)

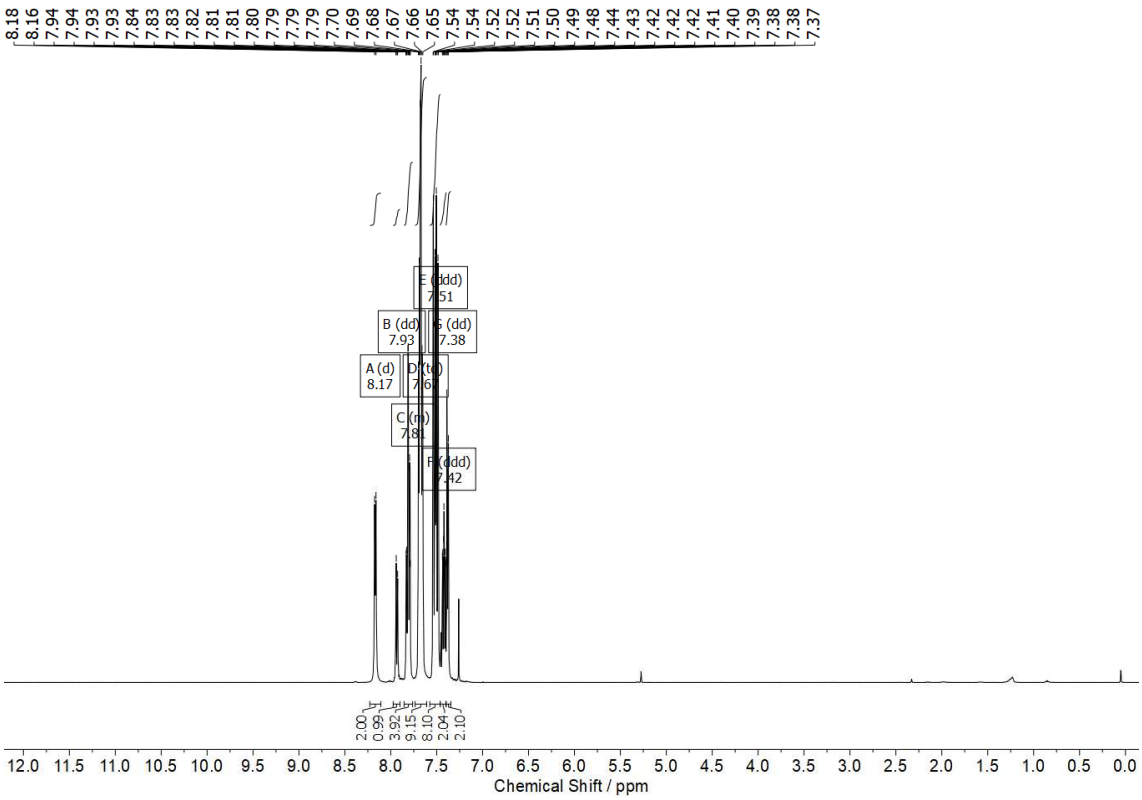

b)

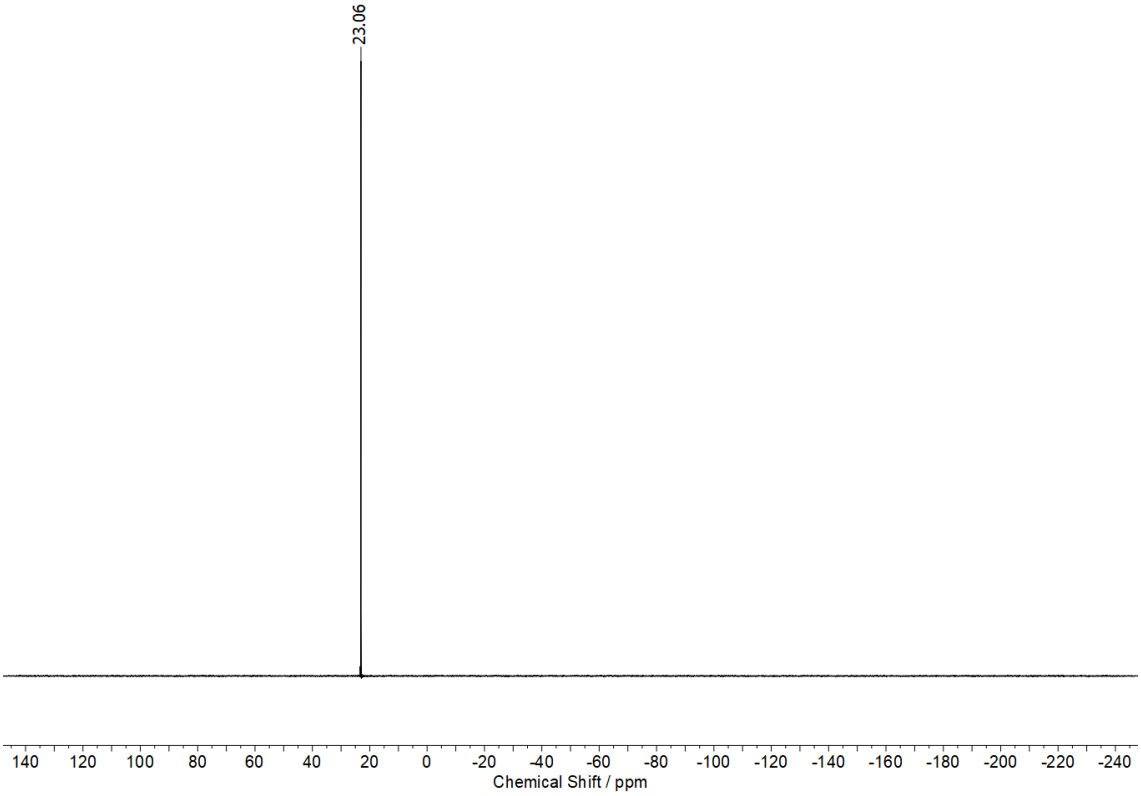

c)

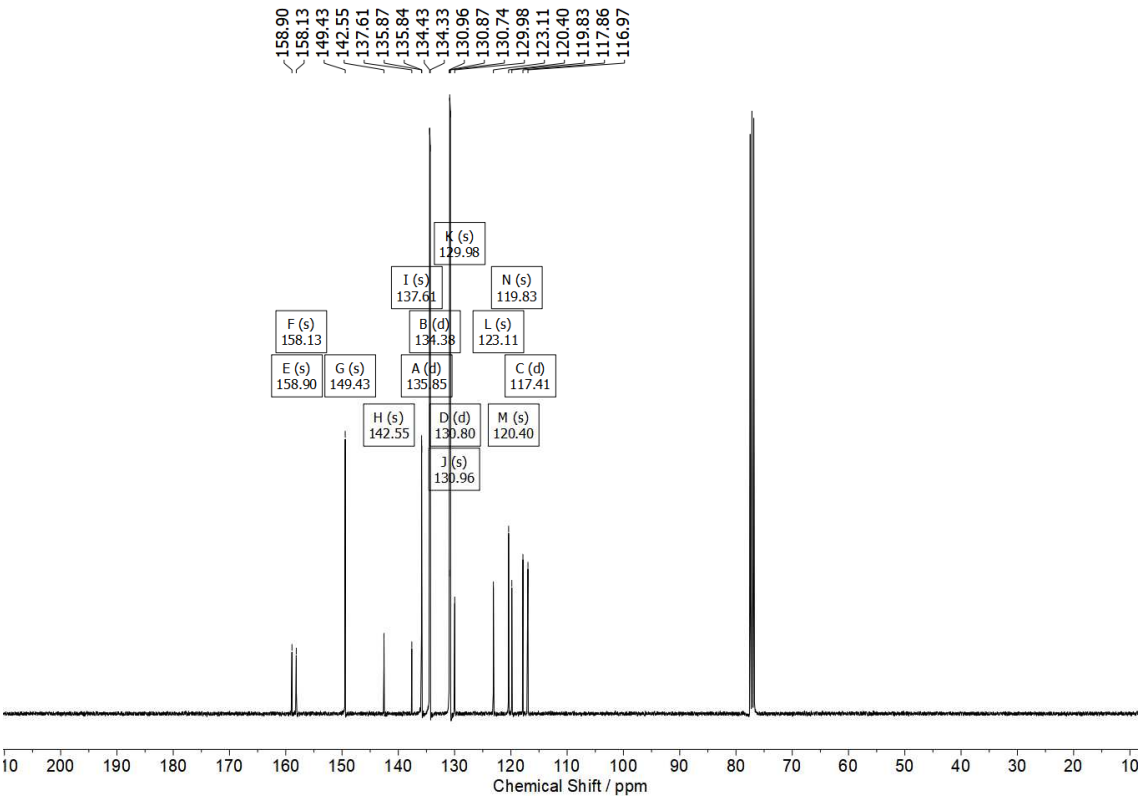

Figure S4: 170. *[Figure S168] NMR spectra of ion pair catalyst* ***15g*** *$CDCl_3$, 400 MHz): a) ^1H NMR spectrum, b) ^{13}C NMR spectrum, c) $^{31}P\{^1H\}$ NMR spectrum.*

Butyl p-tolylcarbamate ***16***

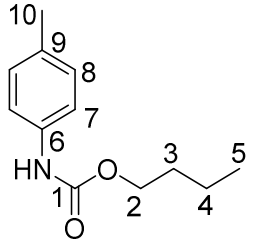

^{1}H NMR (600 MHz, $CDCl_3$) δ [ppm] = 7.33 – 7.21 (m, 2H, H-1), 7.10 (d, J = 8.4 Hz, 2H, H-8), 6.56 (s, 1H, H-N), 4.16 (t, J = 6.7 Hz, 2H, H-2), 2.30 (s, 3H, H-10), 1.65 (p, *J* = 6.7 Hz, 2H, H-9), 1.42 (h, *J* = 7.4 Hz, 2H, H-10), 0.95 (t, *J* = 7.4 Hz, 3H, H-11).

^{13}C NMR (151 MHz, $CDCl_3$) δ [ppm] = 154.0 (C-1), 135.5 (C-9), 133.0 (C-6), 129.7 (C-8), 118.9 (C-7), 65.2 (C-2), 31.1 (C-3), 20.9 (C-10), 19.2 (C-4), 13.9 (C-5).

a)

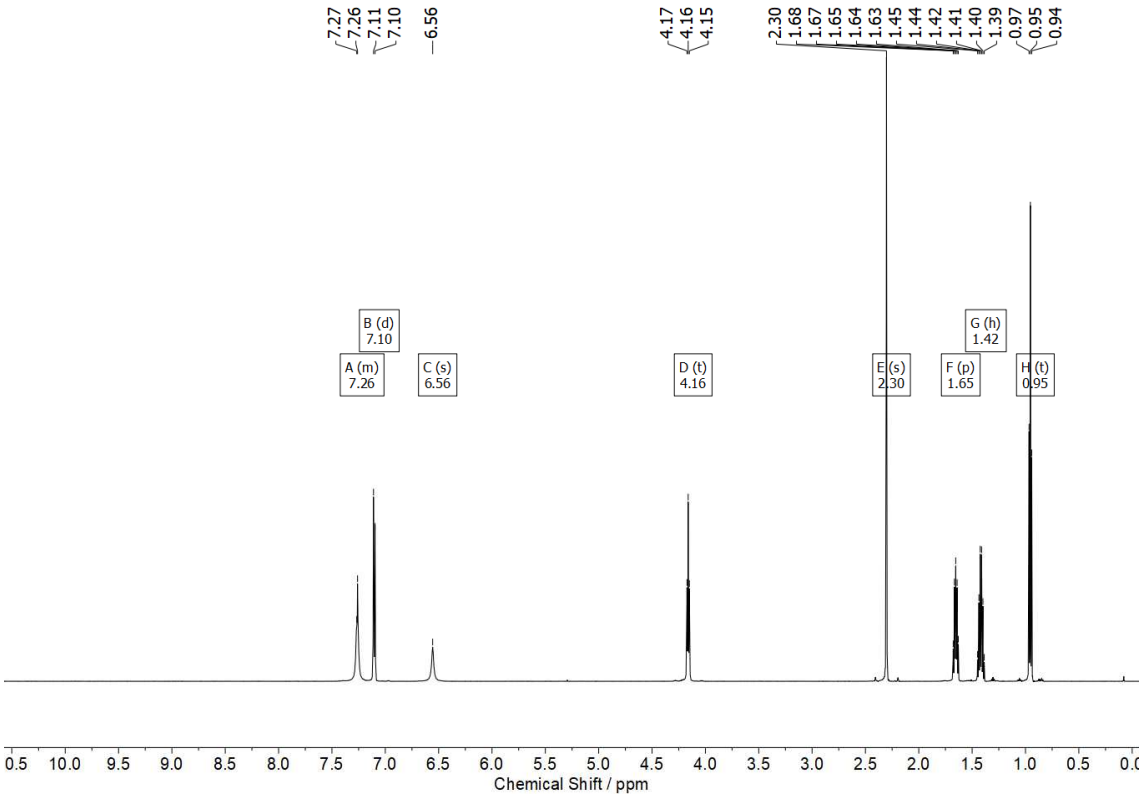

b)

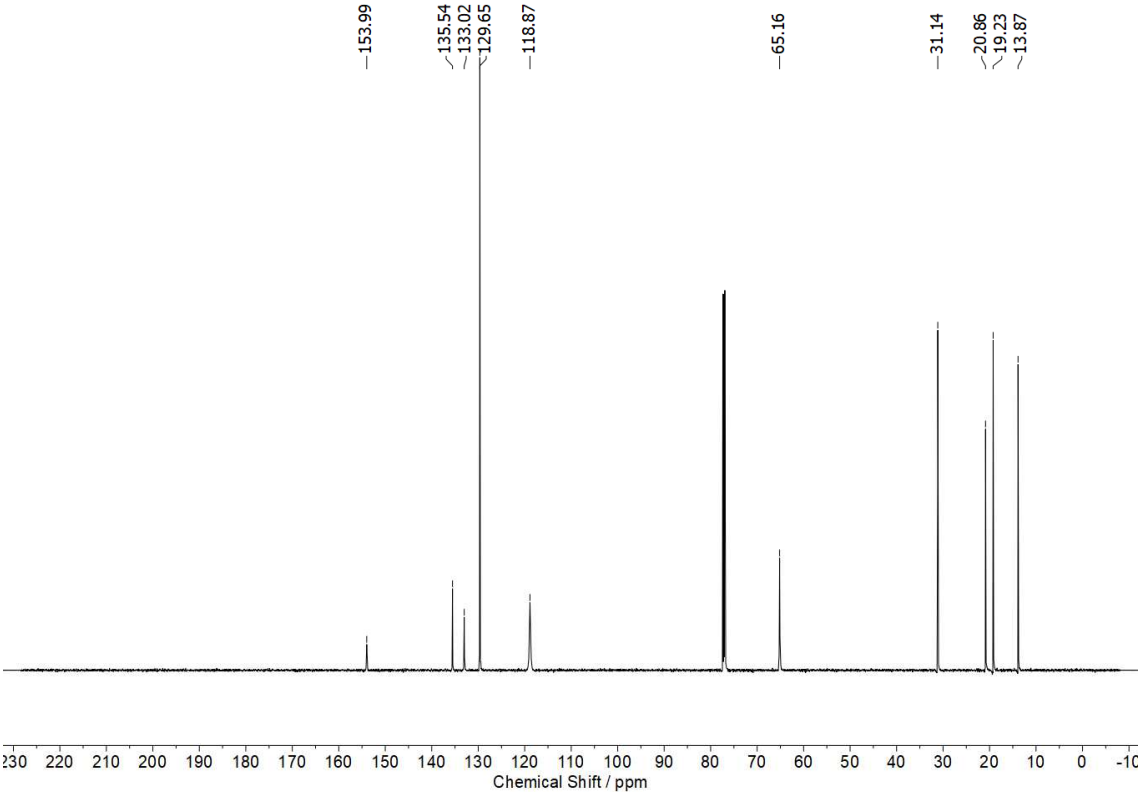

Figure S4: 171. *[Figure S171] NMR spectra of urethane **16** ($CDCl_3$, 600 MHz): a) ^1H NMR spectrum, b) ^{13}C NMR spectrum.*

*N-(4-chlorobenzylidene)-4-methylbenzenesulfonamide **19***

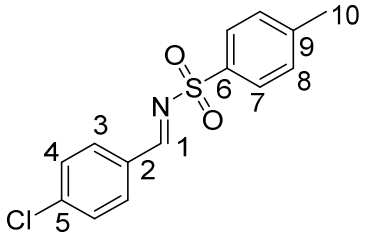

^{1}H NMR (400 MHz, $CDCl_3$) δ [ppm] = 8.98 (s, 1H, H-1), 7.97 – 7.78 (m, 4H, H-3, H-7), 7.45 (d, J = 8.5 Hz, 2H, H-4), 7.34 (d, J = 8.1 Hz, 2H, H-8), 2.43 (s, 3H, H-10).

^{13}C NMR (101 MHz, $CDCl_3$) δ [ppm] = 168.75 (C-1), 144.90 (C-6), 141.48 (C-5), 134.89 (C-9), 132.45 (C-3), 130.86 (C-2), 129.95 (C-8), 129.67 (C-4), 128.21 (C-7), 21.76 (C-10).

a)

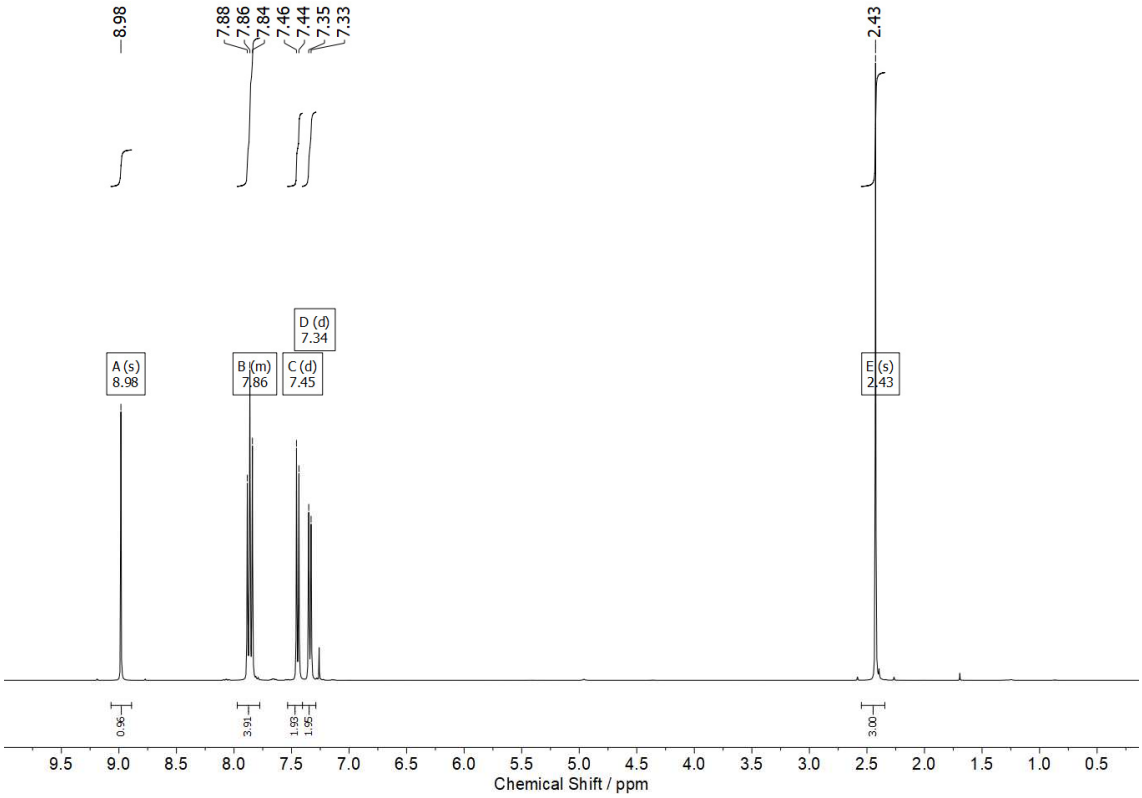

b)

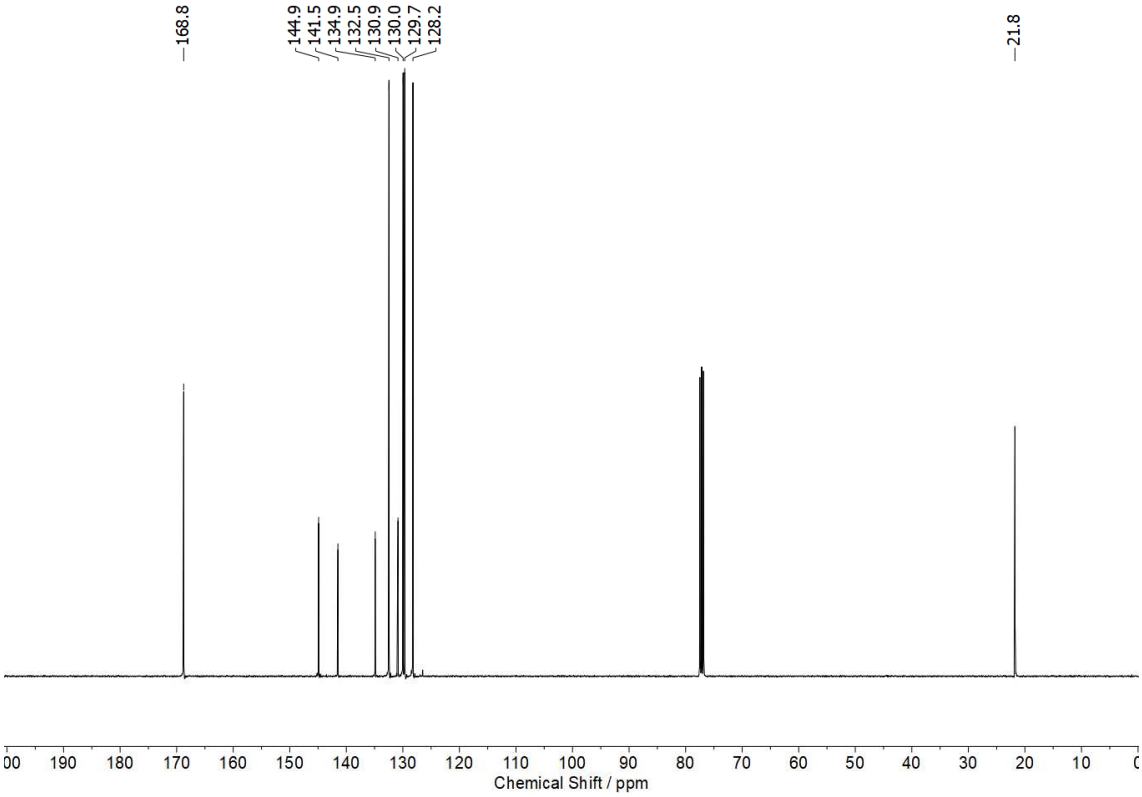

Figure S4: 172. *[Figure S172] NMR spectra of imine* ***19*** *($CDCl_3$, 400 MHz): a) ^1H NMR spectrum, b) ^{13}C* NMR spectrum.

N-((4-chlorophenyl)(6-oxocyclohex-1-en-1-yl)methyl)-4-methylbenzenesulfonamide ***21***

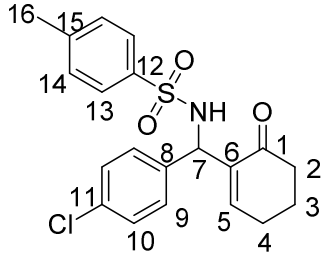

^{1}H NMR (400 MHz, $CDCl_3$) *δ* [ppm] = 7.61 (d, *J* = 8.3 Hz, 2H, H-13), 7.23 (d, *J* = 8.1 Hz, 2H, H-14), 7.18 (d, *J* = 8.6 Hz, 2H, H-10), 7.12 (d, *J* = 8.6 Hz, 2H, H-9), 6.79 (t, *J* = 4.1 Hz, 1H, H5), 6.00 (d, *J* = 9.6 Hz, 1H, H-N), 5.05 (d, *J* = 9.6 Hz, 1H, H-7), 2.41 (s, 3H, H-16), 2.38 – 2.01 (m, 4H, H-2, H-4), 1.94 – 1.58 (m, 2H, H-3).
^{13}C NMR (101 MHz, $CDCl_3$) *δ* [ppm] = 199.09 (C-1), 149.52 (C-5), 143.46 (C-12/C-15), 137.99 (C-11), 137.85 (C-12/C-15), 136.61 (C-6), 133.37 (C-8), 129.59 (C-14), 128.60 (C-10), 127.81 (C-9), 127.42 (C-13), 59.22 (C-7), 38.47 (C-2), 25.93 (C-4), 22.06 (C-3), 21.63 (C-16).

a)

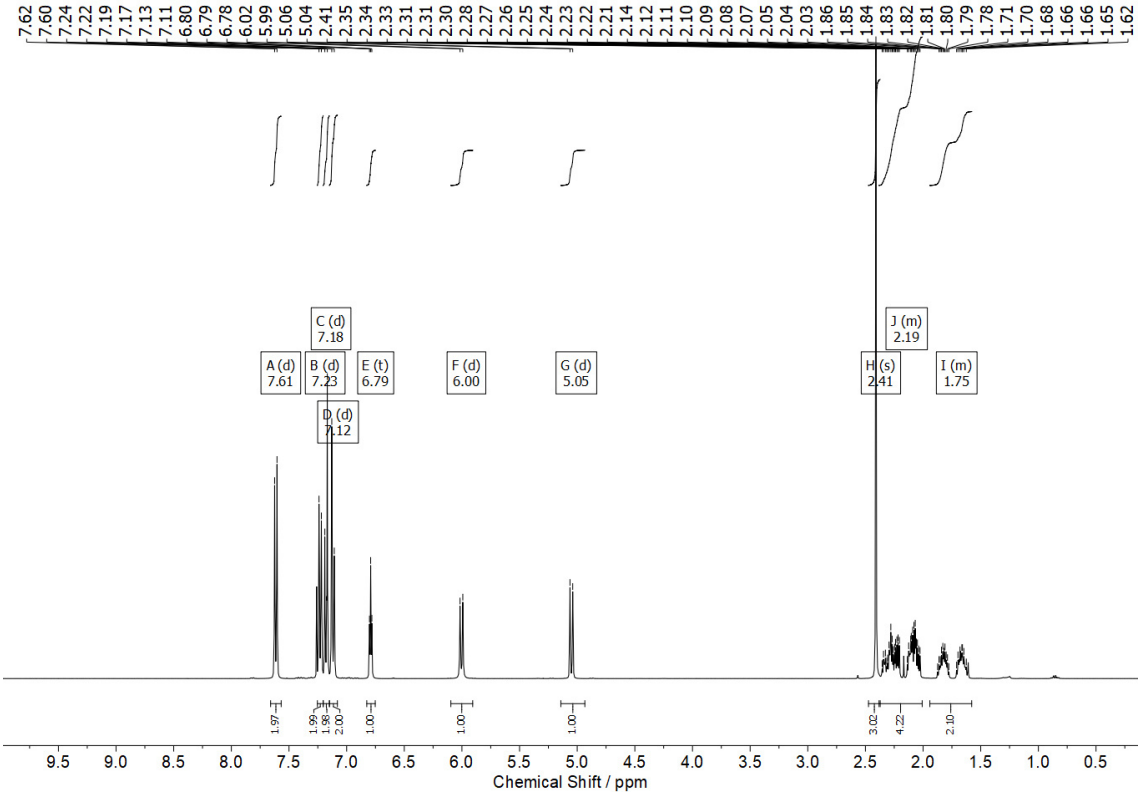

b)

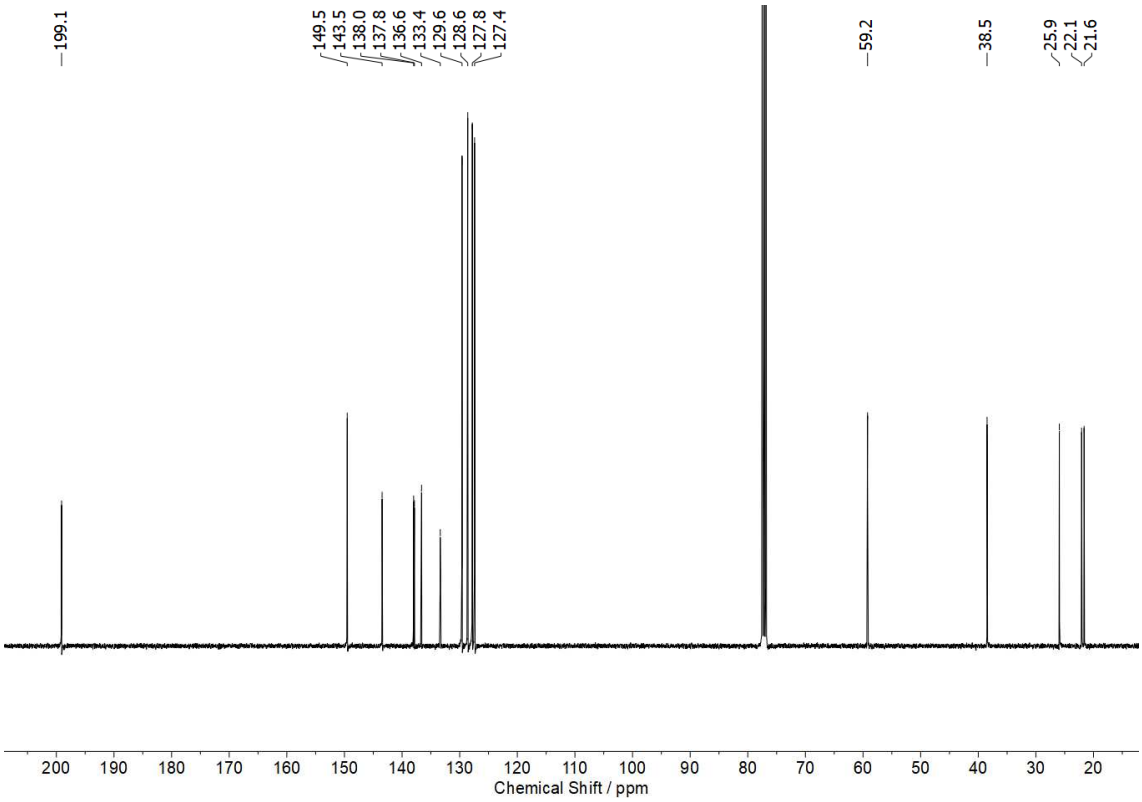

Figure S4: 173. *[Figure S173] NMR spectra of compound **21** ($CDCl_3$, 400 MHz): a) ^1H NMR spectrum, b) ^{13}C NMR spectrum.*

*Tetrabutylammonium bis((trifluoromethyl)sulfonyl)amide **24***

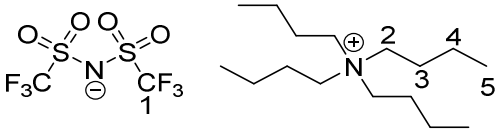

^{1}H NMR (400 MHz, $CDCl_3$) δ [ppm] = 3.27 – 3.04 (m, 8H, H-2), 1.58 (p, J = 8.1, 7.7 Hz, 8H, H-3), 1.39 (h, J = 7.3 Hz, 8H, H-4), 0.97 (t, J = 7.3 Hz, 12H, H-5).

^{13}C NMR (101 MHz, $CDCl_3$) δ [ppm] = 120.03 (q, J = 321.6 Hz, C-1), 58.68 (C-2), 23.86 (C-3), 19.59 (C-4), 13.53 (C-5).

^{19}F NMR (377 MHz, $CDCl_3$) δ [ppm] = −78.82.

a)

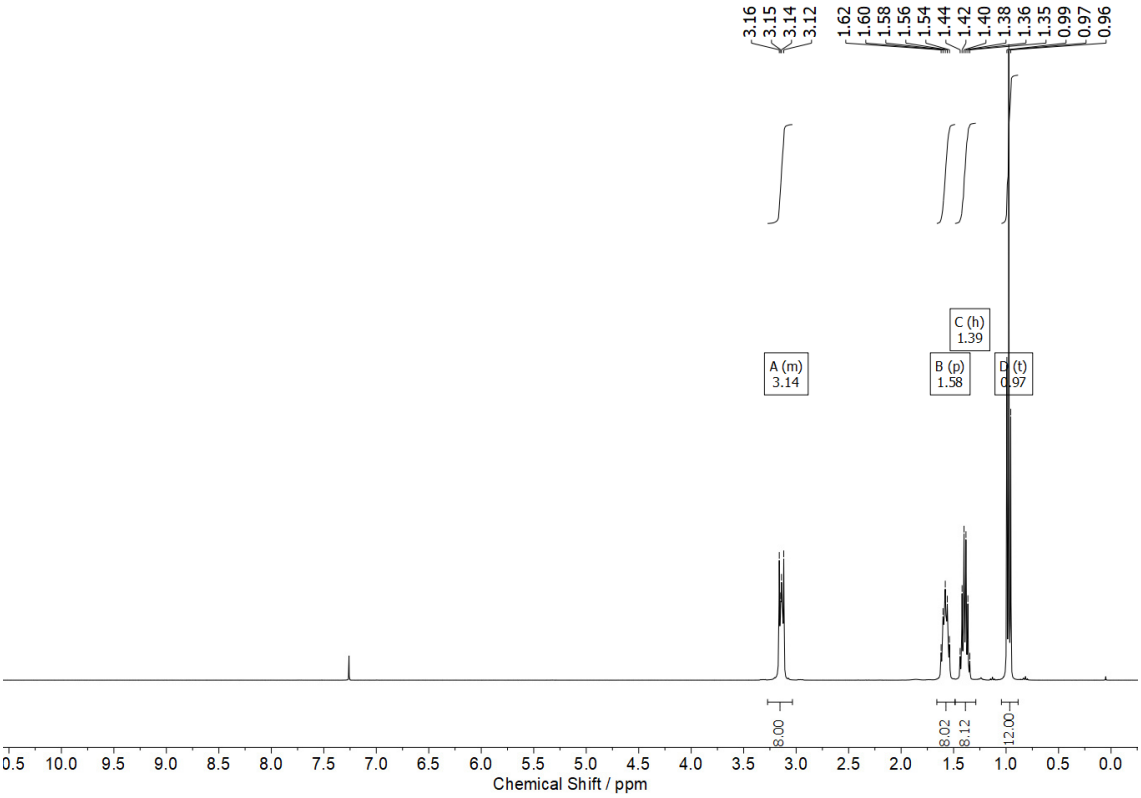
3.16
3.15
3.14
3.12
1.62
1.60
1.58
1.56
1.54
1.44
1.42
1.40
1.38
1.36
1.35
0.99
0.97
0.96
A (m)
3.14
B (p)
1.58
C (h)
1.39
D (t)
0.97
8.00
8.02
8.12
12.00
Chemical Shift / ppm

b)

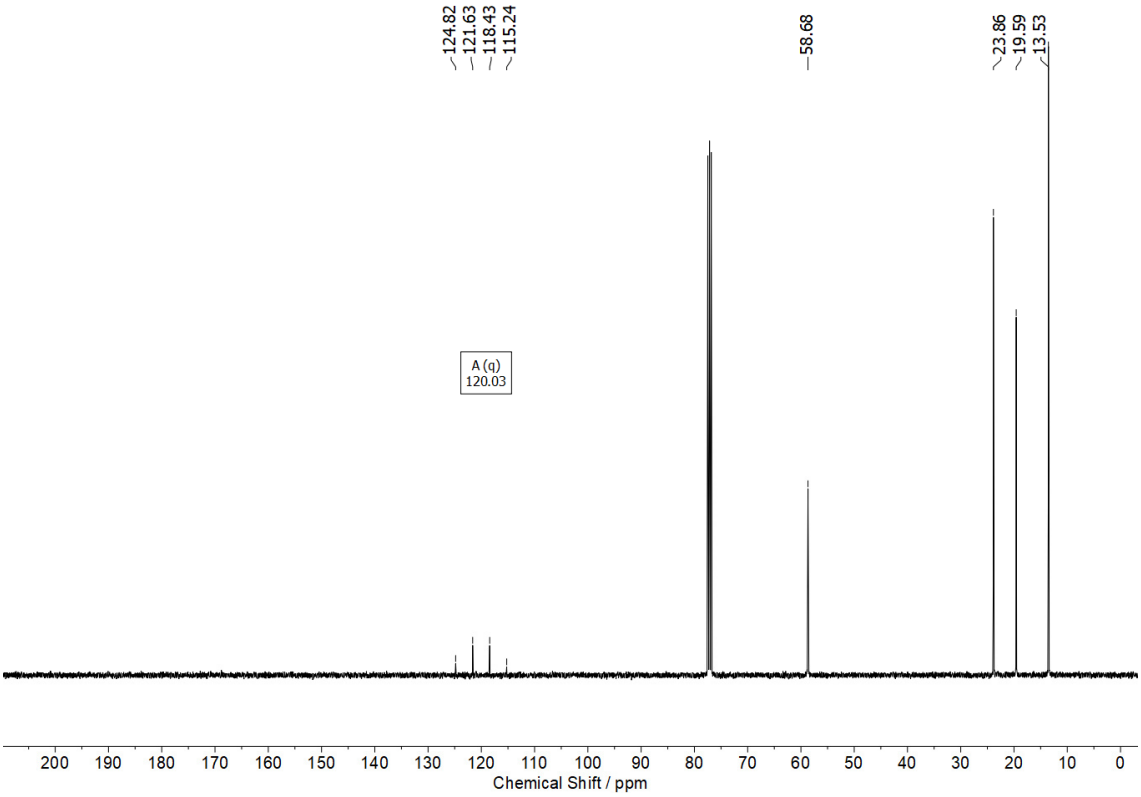
124.82
121.63
118.43
115.24
58.68
23.86
19.59
13.53
A (q)
120.03
Chemical Shift / ppm

c)

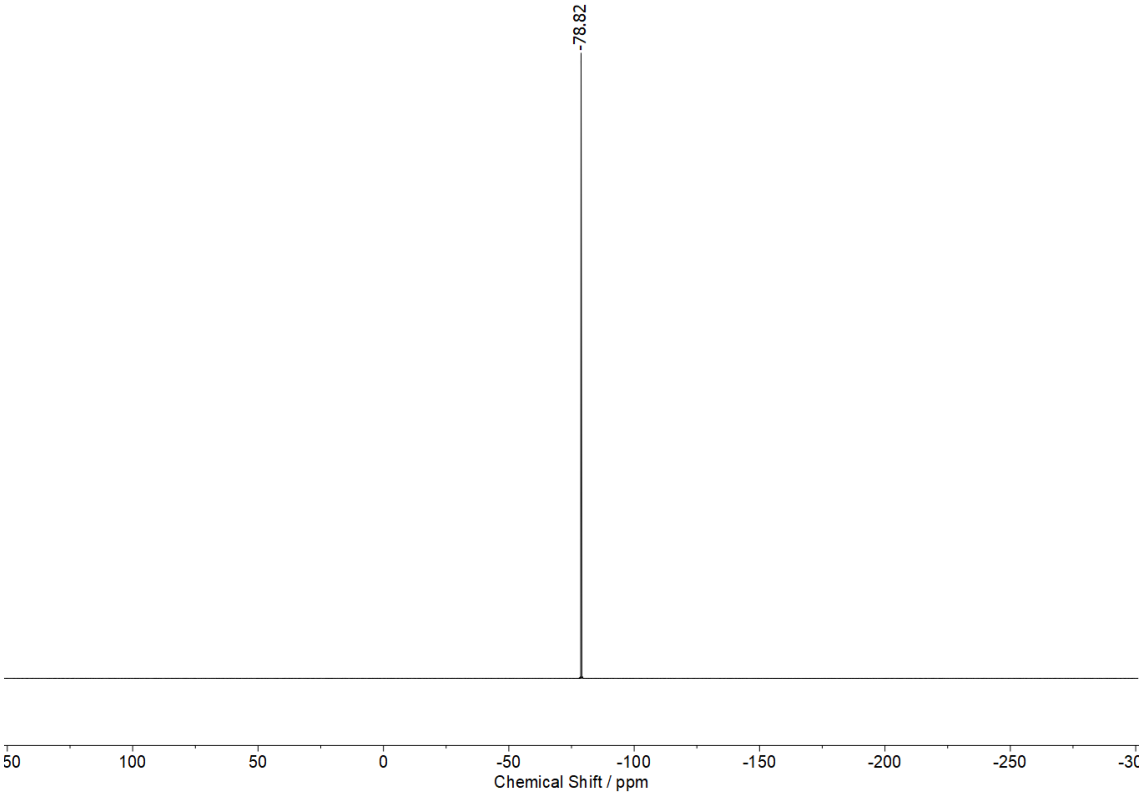

Figure S4: 174. *[Figure S174] NMR spectra of compound* ***24*** *($CDCl_3$, 400 MHz): a) ^{1}H NMR spectrum, b) ^{13}C NMR spectrum, c) ^{19}F NMR spectrum.*

4-Methyl-N-(pyridin-2-yl)benzenesulfonamide ***25***

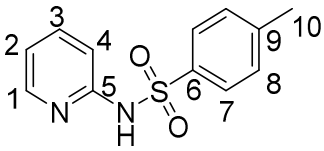

^{1}H NMR (400.22 MHz, DMSO-d_6): δ [ppm] = 11.90 (s, 1H, H-N), 8.01 (d, J = 4.6 Hz, 1H, H-1), 7.76 (d, J = 8.2 Hz, 2H), 7.73 – 7.64 (m, 1H, H-3), 7.33 (d, J = 8.1 Hz, 2H), 7.13 (d, J = 8.6 Hz, 1H, H-4), 6.92 – 6.77 (m, 1H, H-2), 2.33 (s, 3H, H-10).

^{13}C NMR (100.65 MHz, DMSO-d_6): δ [ppm] = 153.07 (C-5), 143.74 (C-1), 142.50 (C-9), 140.24 (C-3), 138.95 (C-6), 129.43 (C-8), 126.66 (C-7), 115.78 (C-4), 113.56 (C-2), 20.97 (C-10).

a)

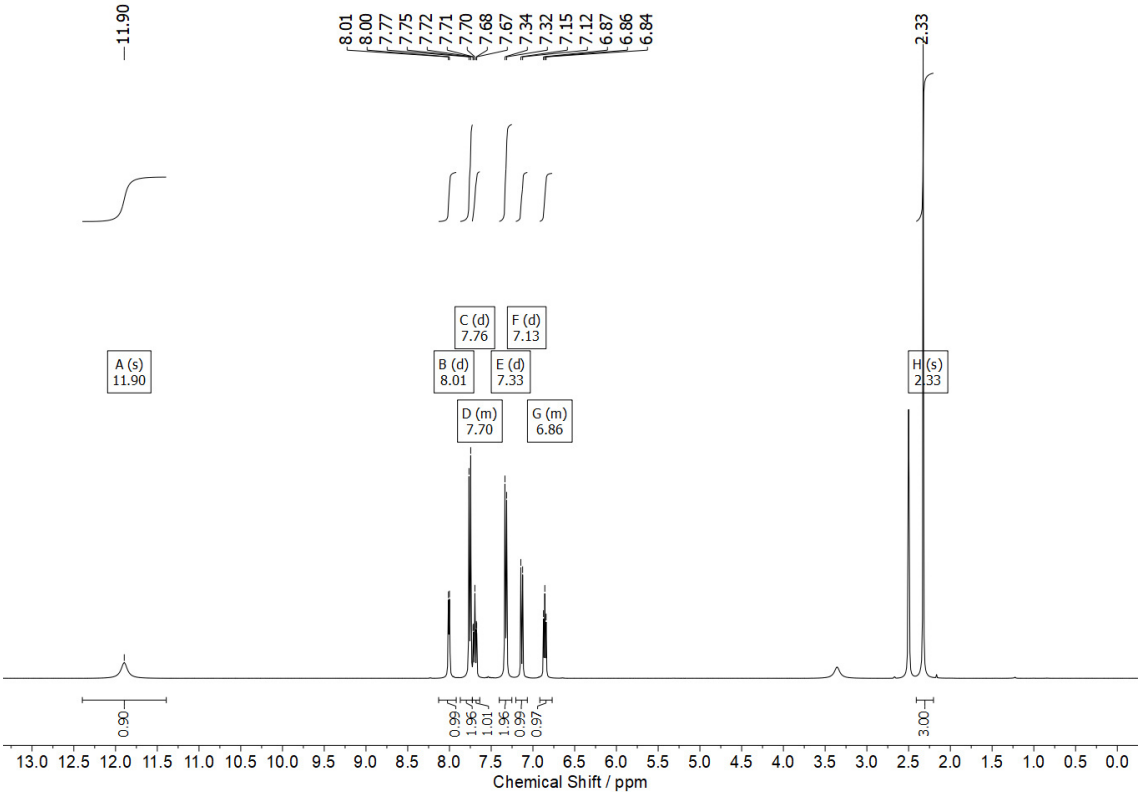

b)

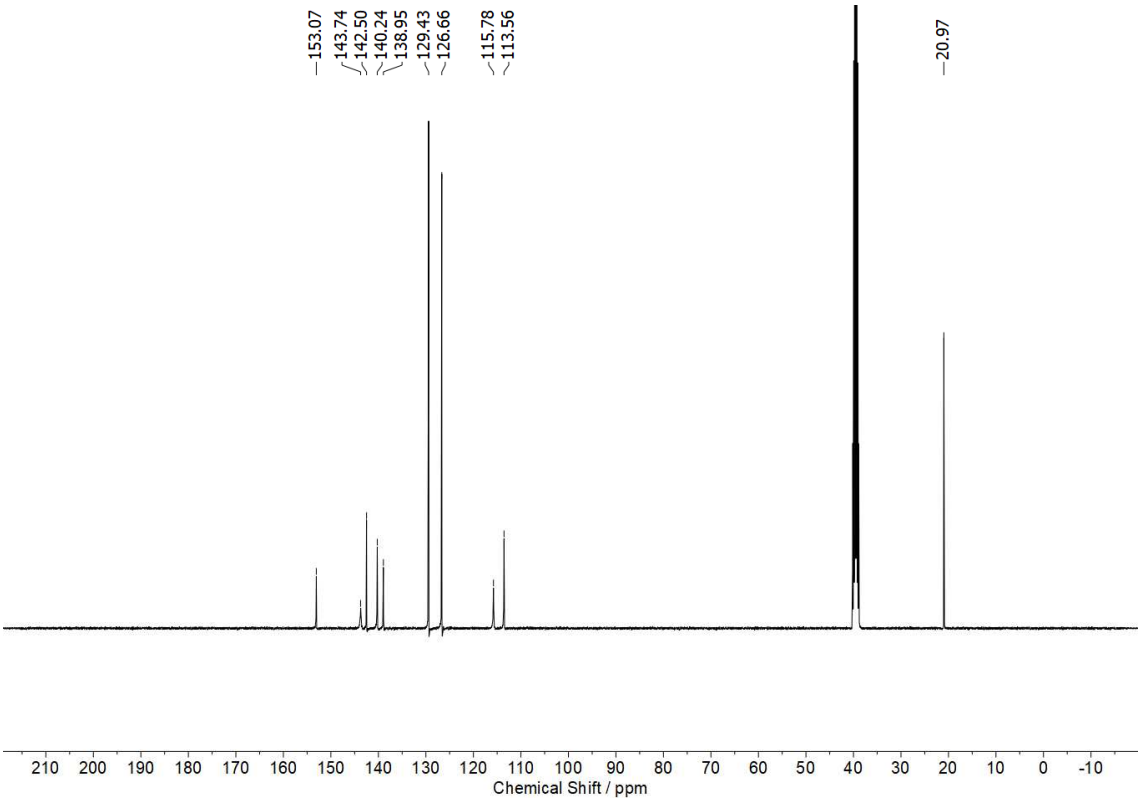

Figure S4: 175. *[Figure S175] NMR spectra of sulfonamide* ***25*** *(DMSO-*d_6*, 400 MHz): a)* ^{1}*H NMR spectrum, b)* ^{13}*C NMR spectrum.*

1,3-Diethyl-benzimidazolium bromide ***26***

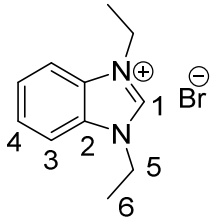

^{1}H NMR (400 MHz, $CDCl_3$) *δ* [ppm] = 11.25 (s, 1H, H-1), 7.90 – 7.69 (m, 2H, H-3/H-4), 7.69 – 7.50 (m, 2H, H3/H-4), 4.65 (q, *J* = 7.3 Hz, 4H, H-5), 1.67 (t, *J* = 7.3 Hz, 6H, H-6).

^{13}C NMR (101 MHz, $CDCl_3$) *δ* [ppm] = 141.75 (C-1), 131.10 (C-2), 127.23 (C-3/C-4), 113.16 (C-3/C-4), 42.90 (C-5), 14.91 (C-6).

a)

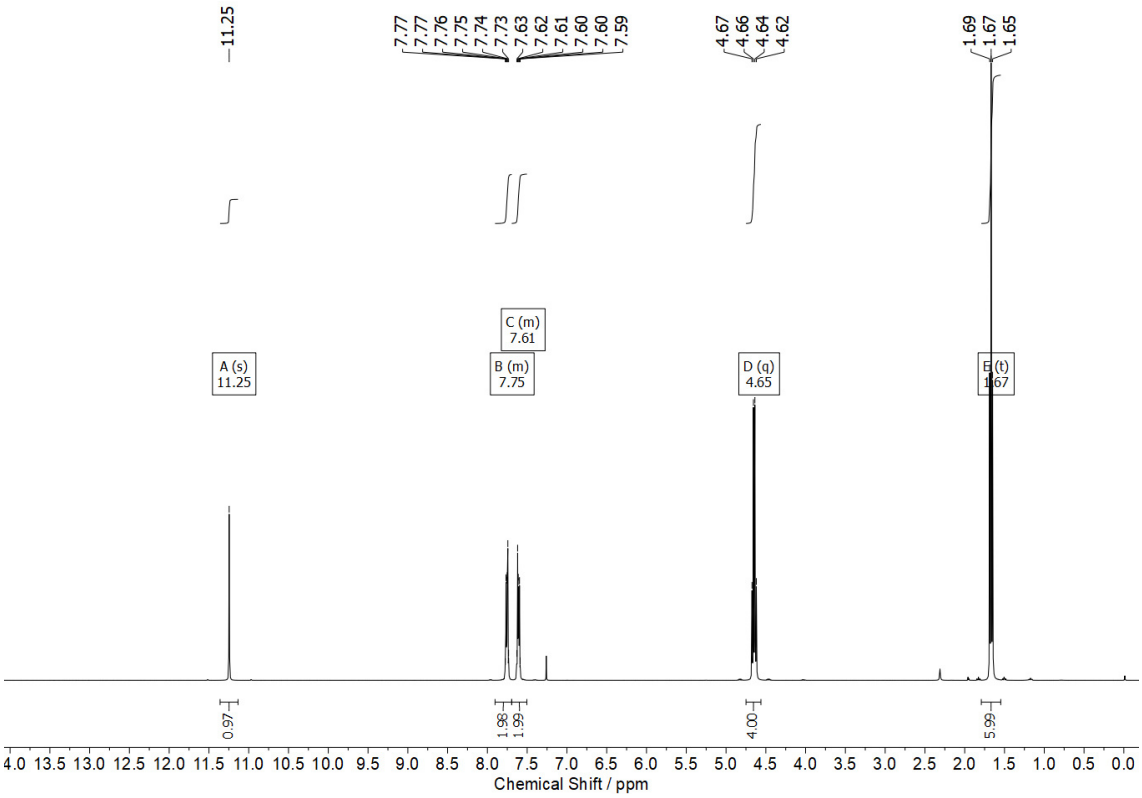

b)

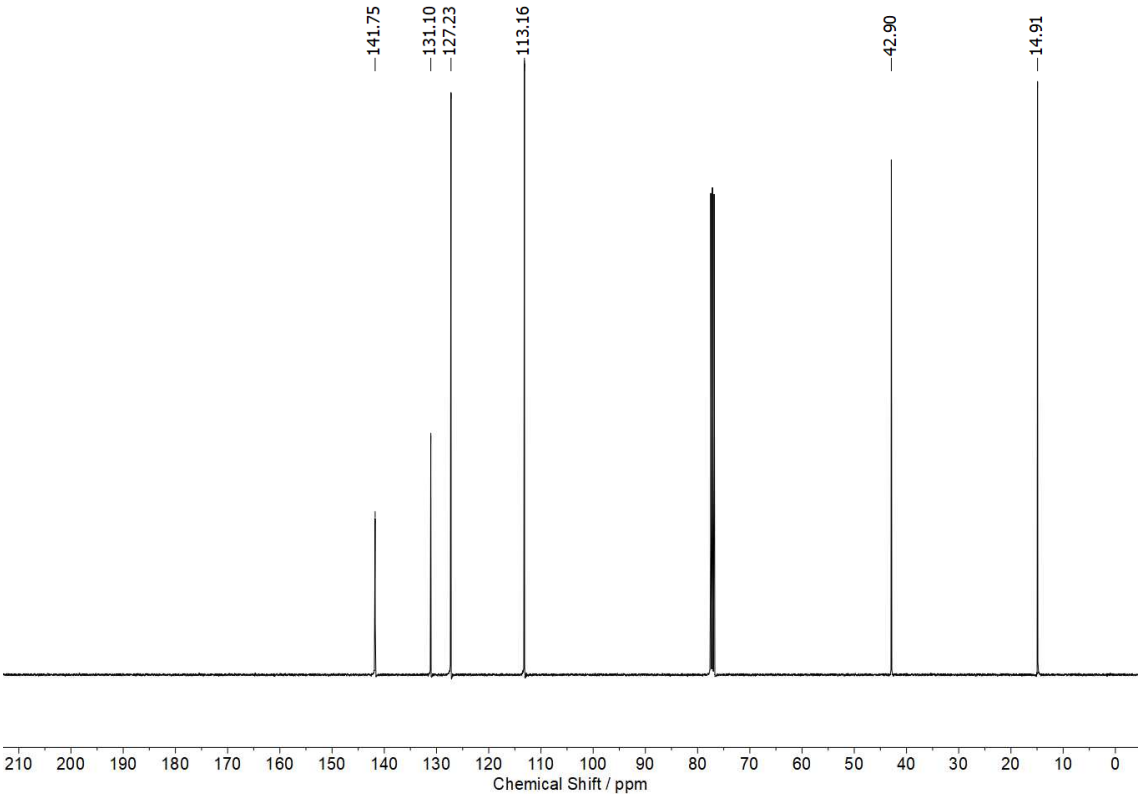

Figure S4: 176. *[Figure S176] NMR spectra of benzimidazolium bromide* ***26*** *($CDCl_3$, 400 MHz): a) ^1H NMR spectrum, b) ^{13}C NMR spectrum.*

Computational Part

4.1.7 General Computational Methods

Recent studies investigating silylation reactions mediated by Lewis Base organocatalysts showed that reliable results that take dispersive interactions into account are obtained at the DLPNO-CCSD(T)/def2-TZVPP//SMD($CHCl_3$)/B3LYP-D3/6-31+G(d) level of theory (abbreviated as CC in the following) and therefore we used it for the calculation of ΔMCA and ΔPIA values in this study.[7] Initial coordinates for monomolecular systems were generated by applying the OPLS_2005 force field implemented in MacroModel (Schrödinger program package).[8] Optimizations were done differently for monomolecular systems and ion pairs. In the first case, optimization at the SMD($CHCl_3$)/B3LYP-D3/6-31+G(d) level of theory was followed by calculation of thermal corrections at 298.15 K without scaling using the rigid rotor/harmonic oscillator model at the same level.

For ion pair systems, 150 sets of starting coordinates were randomized using the stochastic kick procedure developed by Saunders and further adapted by Sakic.[9] 50 sets of coordinates were generated starting from the pairing of the best, second best and third best conformers each of cation and anion optimized beforehand. Pre-optimization was done at the SMD($CHCl_3$)/B3LYP-D3/6-31+G(d) (abbreviated as DFT in the following) level of theory using the scf=(conver=6) and int=(SG1Grid) options. For this pre-optimization, jobs were submitted (and if not terminated normally) resubmitted in a randomized fashion until at least 100 structures had been terminated normally. Out of these, a minimum of 30 (the energetically most favored ones) conformers were selected and optimized at the SMD($CHCl_3$)/B3LYP-D3/6-31+G(d) level of theory followed by calculation of thermal corrections at 298.15 K without scaling using the rigid rotor/harmonic oscillator model at the same level.

All values reported at the SMD($CHCl_3$)/B3LYP-D3/6-31+G(d) level of theory were done with Gaussian 09, Revision D.01.[10]

Single point energies were calculated at the DLPNO-CCSD(T)/def2-TZVPP level of theory with ORCA Version 4.0.0.2 using the fully optimized DFT geometries.[11] Thermal corrections previously obtained at the SMD($CHCl_3$)/B3LYP-D3/6-31+G(d) level were added to generate the final single point values.

All ΔMCA and ΔPIA values given in this study are the best DFT or coupled cluster conformers generated as described above.

To represent tetraalkyl ammonium and tetraalkyl phosphonium cations (as present in catalyst systems (**6aa**, **6ab**, **6ad**, and **10d**), without having to face the huge conformational space that comes with it, we calculated the corresponding tetraethyl phosphonium-containing catalyst systems (**6ah** and **10h**) as shown in **Table S4: 23**.

Table of Calculated Compounds

Table S4: 23 gives the identifier as well as the structure of the compounds calculated for this study.

Table S4: 23. [Table S23] Compounds calculated for this study.

Entry	Identifier	Compound
1	**1a**	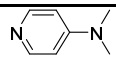
2	**1a-Me**	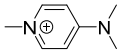
3	**1a-PhNCO**	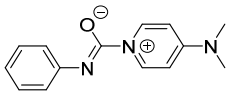
4	**1b**	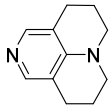
5	**1b-Me**	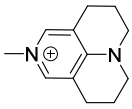
6	**1b-PhNCO**	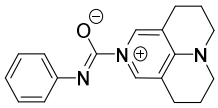
7	**1c**	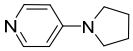
8	**1c-Me**	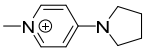
9	**1c-PhNCO**	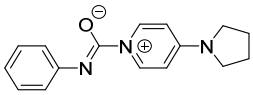
10	**1d**	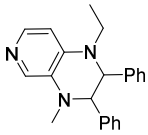
11	**1d-Me**	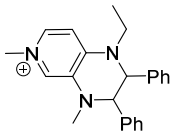
12	**1d-PhNCO**	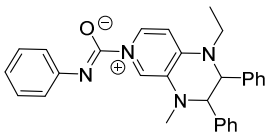
13	**1e**	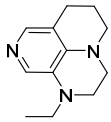
14	**1e-Me**	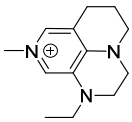
15	**1e-PhNCO**	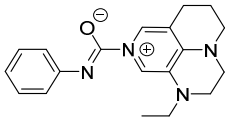

Table S4: 23 (continuation). [Table S23] Compounds calculated for this study.

16	**1f**	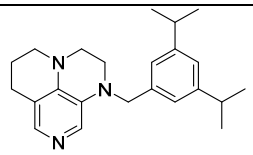
17	**1f-Me**	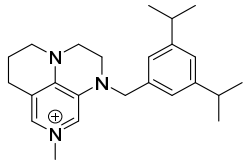
18	**1f-PhNCO**	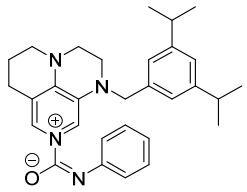
19	**1g**	
20	**1g-Me**	
21	**1g-PhNCO**	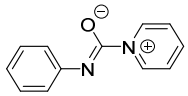
22	**6a**	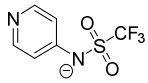
23	**6a-Me**	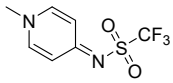
24	**6a-Me2**	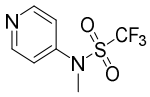
25	**6a-PhNCO**	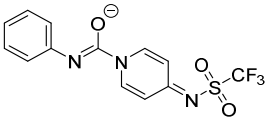
26	**6a-PhNCO2**	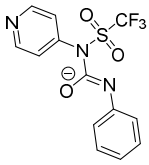
27	**6ac**	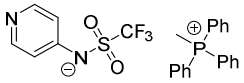
28	**6ac-Me**	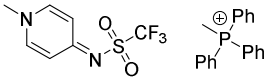
29	**6ac-PhNCO**	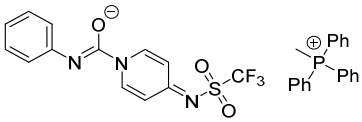
30	**6ah**	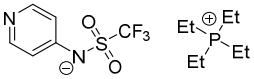

Table S4: 23 (continuation). [Table S23] Compounds calculated for this study.

31	**6ah-Me**	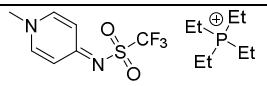
32	**6ah-Me2**	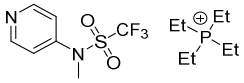
33	**6ah-PhNCO**	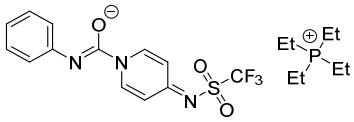
34	**6ah-PhNCO2**	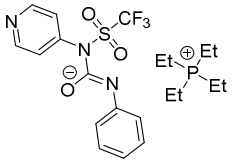
35	**6b**	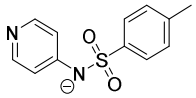
36	**6b-Me**	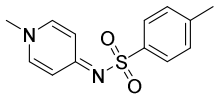
37	**6b-Me2**	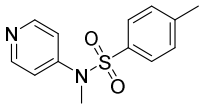
38	**6b-PhNCO**	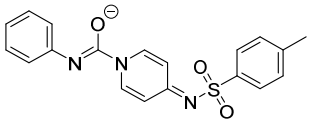
39	**6b-PhNCO2**	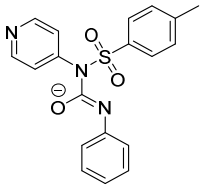
40	**6bc**	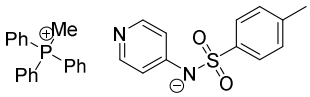
41	**6bc-Me**	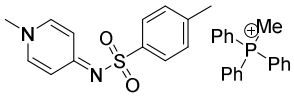
42	**6bc-Me2**	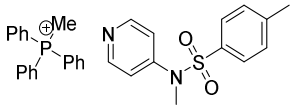
43	**6bc-PhNCO**	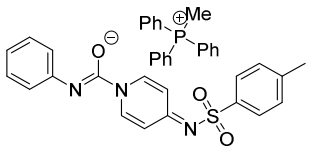

Table S4: 23 (continuation). [Table S23] Compounds calculated for this study.

44	**6bc-PhNCO2**	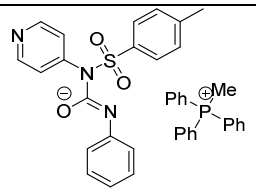
45	**6c**	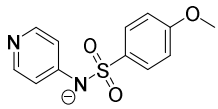
46	**6c-Me**	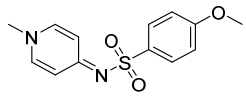
47	**6c-Me2**	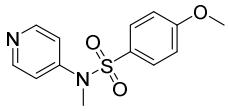
48	**6c-PhNCO**	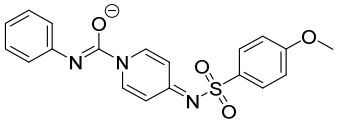
49	**6c-PhNCO2**	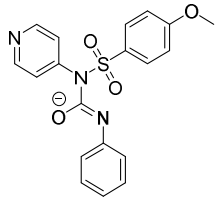
50	**6cg**	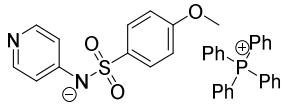
51	**6cg-Me**	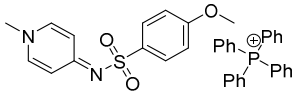
52	**6cg-Me2**	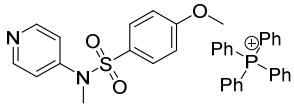
53	**6cg-PhNCO**	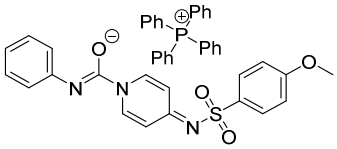
54	**6cg-PhNCO2**	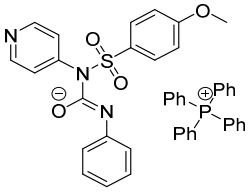
55	**8a**	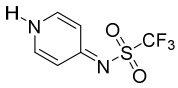

Table S4: 23 (continuation). [Table S23] Compounds calculated for this study.

56	**10**	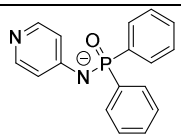
57	**10-Me**	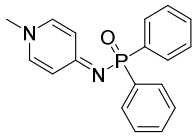
58	**10-Me2**	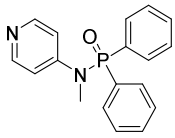
59	**10-PhNCO**	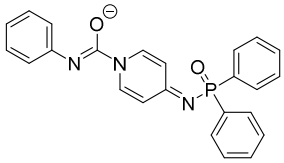
60	**10-PhNCO2**	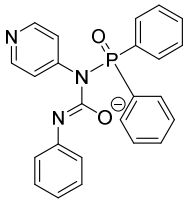
61	**10h**	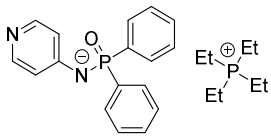
62	**10h-Me**	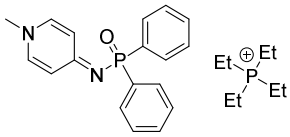
63	**10h-PhNCO**	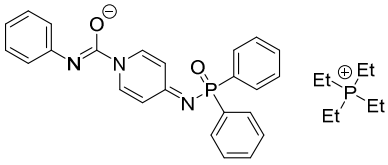
64	**11**	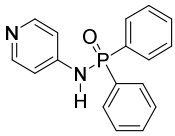
65	**14**	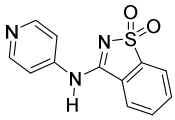
66	**15**	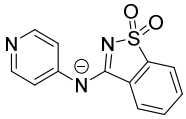
67	**15-Me**	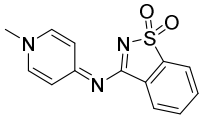

Table S4: 23 (continuation). [Table S23] Compounds calculated for this study.

68	**15-Me2**	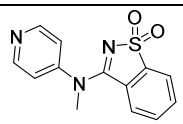
69	**15-PhNCO**	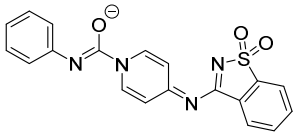
70	**15-PhNCO2**	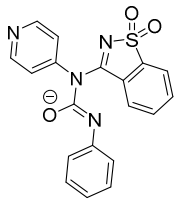
72	**15g**	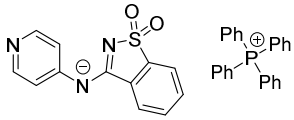
73	**15g-Me**	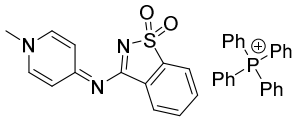
74	**15g-Me2**	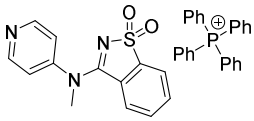
75	**15g-PhNCO**	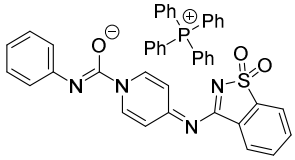
76	**15g-PhNCO2**	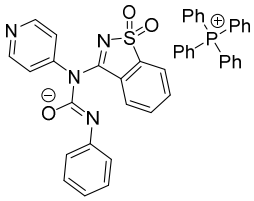
77	**22**	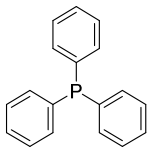
78	**22-Me**	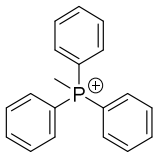
79	**22-PhNCO**	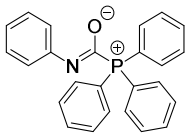
80	**23**	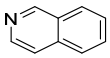

Table S4: 23 (continuation). [Table S23] Compounds calculated for this study.

81	**23-Me**	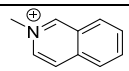
82	**23-PhNCO**	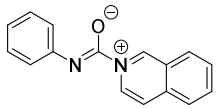

4.1.8 Calculated Phenyl Isocyanate Affinities (ΔPIAs) and Methyl Cation Affinities (ΔMCAs)

Table S4: 24 gives the values calculated for ΔPIA and ΔMCA for the neutral catalysts, ion pair catalysts, and anion catalysts.

Table S4: 24. [Table S24] Phenyl Isocyanate Affinities (ΔPIAs) and Methyl Cation Affinities (ΔMCAs).

Entry	Catalyst	Lewis basic atom[a]	ΔH298K SMD(CHCl3)/B3LYP-D3/ 6-31+G(d)		ΔH298K DLPNO-CCSD(T)/def2-TZVPP// SMD(CHCl3)/B3LYP-D3/6-31+G(d)	
			ΔMCA[b]	ΔPIA[b]	ΔMCA[b]	ΔPIA[b]
1	**1a**	N1	-37.0	-25.7	-35.2	-24.8
2	**1c**	N1	-40.9	-27.2	-38.4	-26.3
3	**1b**	N1	-48.8	-32.5	-43.9	-29.9
4	**1d**	N1	-45.7	-30.6	-39.0	-27.7
5	**1e**	N1	-52.2	-34.2	-46.3	-32.2
6	**1f**	N1	-54.7	-39.3	-47.8	-37.2
7	**22**	N1	-45.2	+8.2	-53.7	+8.8
8	**23**	N1	-7.1	-1.7	-2.3	-0.5
9	**6ac**	N1	-43.2	-38.1	-38.4	-38.3
10	**6ah**	N1	-40.5	-30.9	-37.9	-31.8
11	**6ah**	N2	-0.8	+10.7	-12.2	+3.9
12	**6bc**	N1	-64.8	-56.7	-63.0	-58.1
13	**6bc**	N2	-57.9	-28.5	-64.0	-34.7
14	**6cg**	N1	-65.6	-61.2	-62.7	-61.7
15	**6cg**	N2	-61.2	-24.4	-67.8	-31.4
16	**15g**	N1	-47.0	-45.7	-43.0	-42.1
17	**15g**	N2	-32.0	-11.9	-42.8	-27.9
18	**10h**	N1	-72.2	-53.1	-68.0	-53.3
19	**6a**	N1	-81.7	-33.9	-84.7	-36.4
20	**6a**	N2	-48.3	+21.0	-65.2	+14.0
21	**6b**	N1	-99.9	-46.8	-102.8	-47.6
22	**6b**	N2	-97.9	-9.5	-109.3	-16.9
23	**6c**	N1	-100.1	-46.9	-103.5	-47.7
24	**6c**	N2	-99.8	-10.1	-111.2	-17.5
25	**15**	N1	-85.5	-34.0	-86.5	-34.3
26	**15**	N2	-57.7	+3.4	-78.2	-14.5
27	**10**	N1	-115.3	-56.0	-116.6	-55.4
28	**10**	N2	-120.5	-42.3	-133.1	-52.6

[a] N1 = pyridine-N; N2 = amide-N. [b] in kJ mol^{-1}.

4.1.9 Effect of Exclusion of Cations for Computed Affinity Values

Entries 1 - 18 of **Table S4: 24** have already been shown and discussed in the main part of this publication. The results summarized in Entries 19 – 28 of **Table S4: 24** were briefly discussed. They give the affinity values determined from calculations of the anion-isocyanate and anion-methyl cation adducts only. **Figure S4: 177** is a plot of the DFT-derived affinities of the ion pair catalyst adduct to isocyanate and methyl cation (Entries 9, 10,12, 14, 16, 18 of **Table S4: 24**) vs. those of the corresponding "naked" anion-adduct (Entries 19, 21, 23, 25, 27 of **Table S4: 24**), which shows the effect of including the counter-cation in the calculation. The reference in this case is the symmetrical distribution of the monomolecular systems (unlabeled in the Figure), that do naturally only give one value.

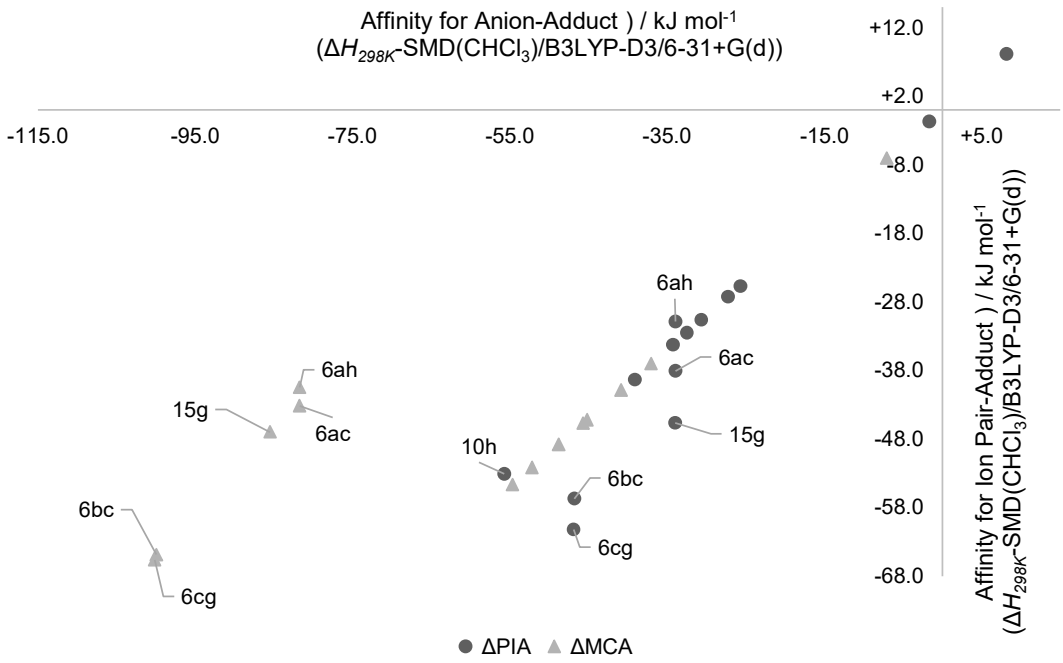

Figure S4: 177. *[Figure S177] DFT ion pair-adduct affinities vs. anion-adduct affinities for the pyridine-N (in kJ mol⁻¹). Neutral catalysts have been included to show the monomolecular case.*

Although the inclusion of the counter-cation is computationally quite expensive (because of the theoretically limitless conformational space, but also the increasing size of the system), there is some obvious benefit. In the case of the ΔPIA values, the ionic catalyst systems noticeably disagree with the symmetrical plot of the neutral organocatalysts. For most of the examples shown here, the exclusion of the cation destabilized the adduct, as was shown in Scheme 3 of the main manuscript of this publication for the case of **6cg**. A similar (although less pronounced) observation is made for catalyst systems **6ac**, **15g**, and **6bc**. Only the systems **6ah**, and **10h** are slightly stabilized by omission of the cation for reasons that we did not jet manage to discern. The obvious thing to point out though, is that those two are both containing tetraethyl phosphonium counter ions. It seems not impossible, that the added stabilization in the other cases could be attributed to aromatic interactions like π-π stacking.

The effect of the absence of the counter ion in the case of the ΔMCA values is much more pronounced. We propose this to be caused by the quenching of the charged character of the anionic "warhead" under formation of a neutral molecule.

Furthermore, the anion-adduct affinities show irregularities with regard to the experimental results: **6bc** and **6cg**, that gave quite different values in our experimental study are similar for both ΔMCA and ΔPIA. Also, the ΔPIA-values calculated for anion-adducts for **6aa**, **6ac** and **15g**, are similar which is not at all observed in the experiment (**Table S4: 24**, Entries 19, 25). This brings us to **Figure S4: 178**, which shows the effect of inclusion or exclusion of the cation onto the correlation with experimentally determined values. In all cases the pyridine-nitrogen atom is the one considered for calculation of the affinities:

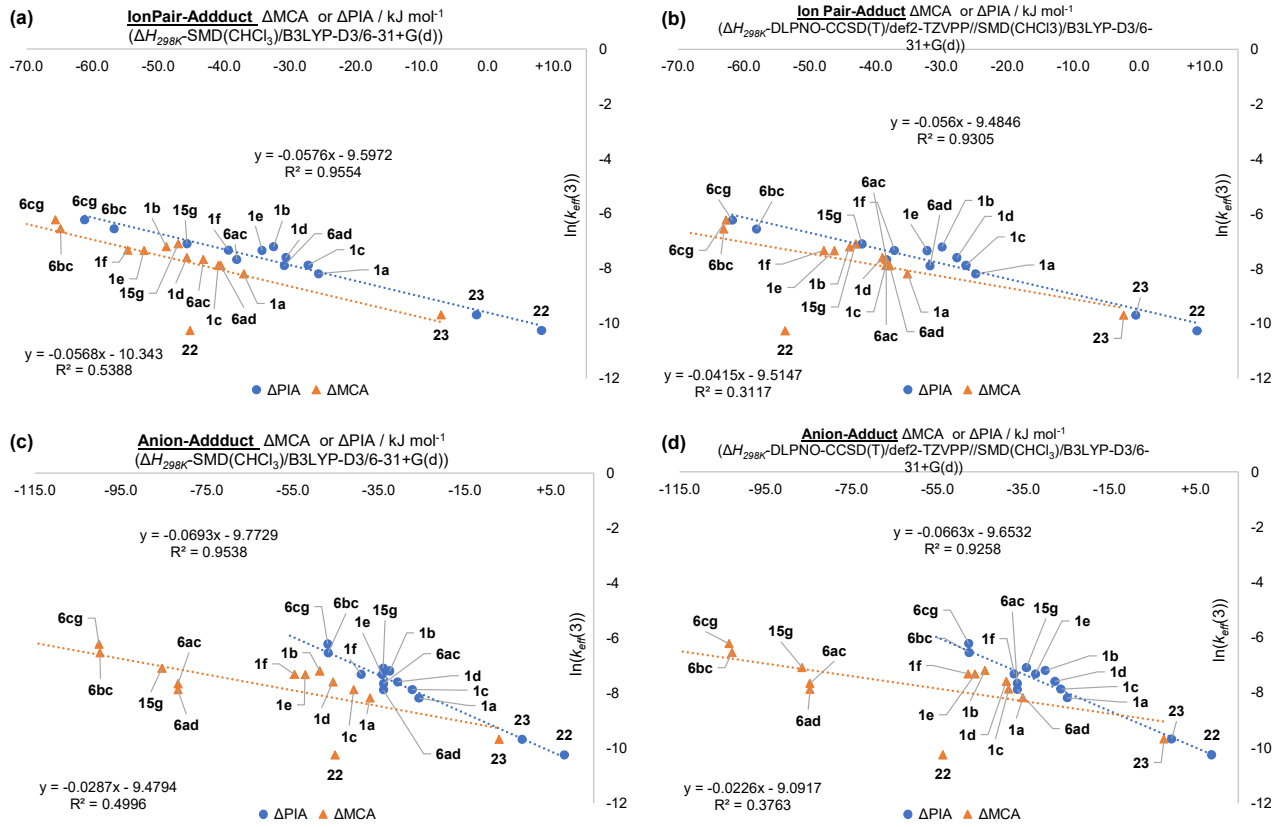

Figure S4: 178. *[Figure S178] Plots of experimentally determined ln(k_{eff}(3))-values of the urethane benchmark reaction vs. calculated ΔMCA and ΔPIA values (all for pyridine-N). (a) vs. DTF-values (already shown in the main body of this publication) and (b) vs. CC-values. (c) is a plot vs. the DFT-derived values when the cation is excluded and (d) gives correlation vs. the affinities obtained at CC level of theory.*

We observe that the quality of the correlation does not change when plotting either the ion-pair affinity or the anion affinity values against the experimentally derived values. However, the slope of the fit changes when omitting the cation in the calculations, which indicates some fundamental change to the correlation.

The same trend observed in **Figure S4: 177** is evident again: The ΔPIA values show very good correlation with the experimentally derived values independent of the method. Most noticeable is the shift of **15g**, which in the experiment tested far more reactive than the neutral catalysts and now is amongst them (**Table S4: 24**, Entries 16, 25).

The correlation for the ΔMCA values is quite poor independent of inclusion of the cations due to the values determined for the triphenylphosphine **22** as discussed in the main part of this publication. However, the affinity values for the anion-methyl cation “adduct” are increased massively to overestimate our experimental data much in the same way as triphenylphosphine **22**. For the ionic catalysts, we think this is due to the change of the system charge from minus one to zero as mentioned above.

In total, the effects discussed above show, that the inclusion of the cation into the calculation of affinities (and likely also mechanistic studies) is a step that should be considered to get a more reliably representation of the catalyst systems. Since we observe a huge effect of adducts that change their charge, this is probably also of importance for esterification or silylation reactions catalyzed by ion pair pyridinyl systems because of the leaving-group induced change in charge.

While ΔPIA values calculated from anion-adducts appear to be usable for ranking of reactivity amongst such ionic systems to some extent, they fail to represent experimental findings when comparison with neutral organocatalysts is desired.

4.1.10 Affinity Values of Pyridine-N vs. Amide-N

The results for the affinity values – and in extension therefore Lewis basicities – of the competing nitrogen atoms have already been discussed in the main body of this publication. **Figure S4: 179** shows the effect mentioned there in a graph giving a plot of the affinities obtained for the pyridine-N (N1) vs. those of the amide-N (N2) (all calculated at DFT level of theory). The values for the neutral catalysts do all represent the pyridine-N (or P-atom in the case of **22**) and have been included to show the symmetrical plot for identical values (labeling was omitted for these cases to improve clarity).

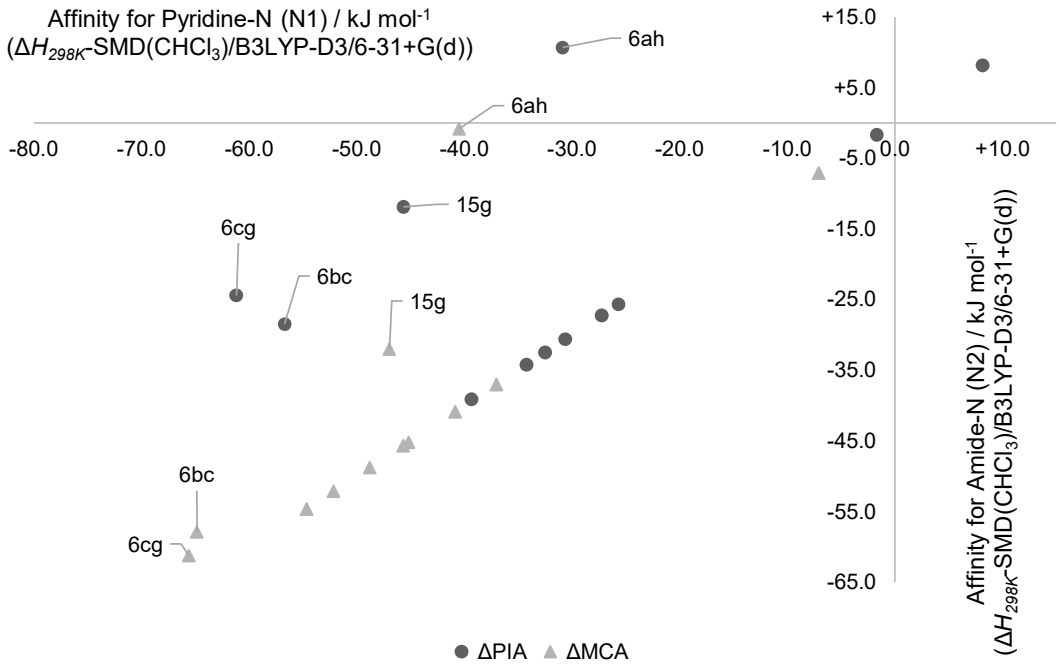

Figure S4: 179. *[Figure S179] Plot of affinity values for the pyridine-N vs. those for the amide-N obtained at the DFT level of theory.*

This graph shows nicely the observed trend of all the pyridine-N affinity values being at generally more negative values than the ones generated for amide-N adducts. The only two cases where this is less pronounced are the ΔMCA values of **6bc** and **6cg**. The ΔPIA values on the other hand show a clear preference for catalytic activation by the pyridine-N for all investigated systems, hinting at the pyridine-N being responsible for the observed catalytic activity.

Figure S4: 180 shows affinity values calculated for pyridine-N and amide-N plotted against experimentally determined $k_{eff}(3)$ values for the urethane benchmark reaction.

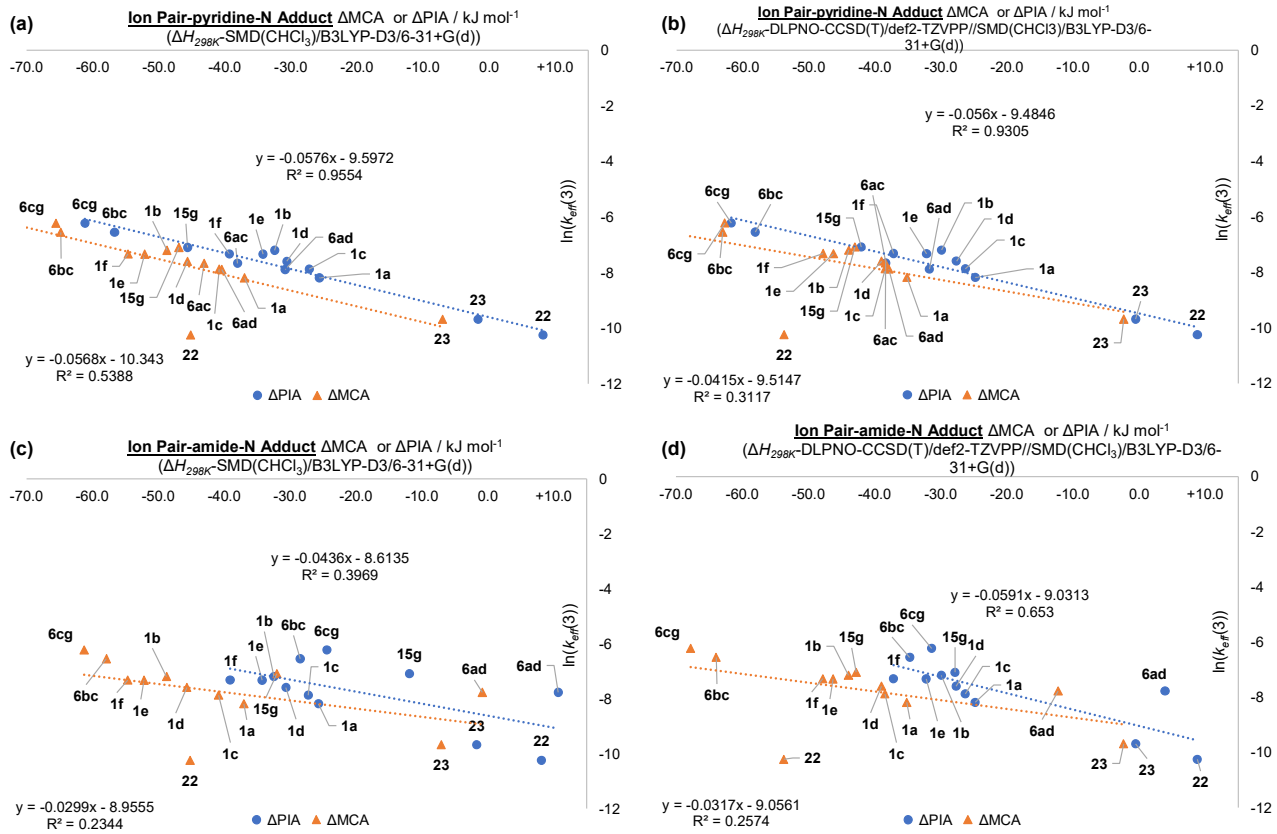

Figure S4: 180. *[Figure S180] Plots of experimentally determined ln(k_{eff}(3))-values of the urethane benchmark reaction vs. calculated ΔMCA and ΔPIA values. (a) and (b) give plots of pyridine-N affinities of DFT and CC methods respectively. (c) and (d) gives plots of amide-N affinities of DFT and CC methods respectively.*

Independent of the computational method used, we found that the amide-N derived affinities correlate much poorer with the experimentally determined values. Additionally, the ΔPIA values calculated for the amide-N adducts of all ion pair catalysts are similar or lower than those for the more active organocatalysts, which is contradicted by our experimental observations.

These results combined with the ones discussed above and in the main body of this publication lead us to firmly believe, that the pyridine-N atom is the catalytically active center in the investigated ion pair Lewis base organocatalysts.

References

[1] C. Six, F. Richter in *Isocyanates, Organic, Ullman's Encyclopedia of Industrial Chemistry*, Wiley-VCH, **2003**; F. Richter, *Nachr. Chem.* **2007**, *55*, 380 – 384; J. Helberg, Y. OE, H. Zipse, *Chem. Eur. J.* **2018**, *24*, 14387-14391.

[2] J. Helberg, M. Marin-Luna, H. Zipse, *Synthesis* **2017**, *49*, 3460-3470; R. Tandon, T. Unzner, T. A. Nigst, N. De Rycke, P. Mayer, B. Wendt, O. R. P. David, H. Zipse, *Chem. Eur. J.* **2013**, *19*, 6435-6442; P. Patschinski, C. Zhang, H. Zipse *J. Org. Chem.* **2014**, *79*, 8348-8357.

[3] S. Hoops, S. Sahle, R. Gauges, C. Lee, J. Pahle, N. Simus, M. Singhal, L. Xu, P. Mendes, U. Kummer, *Bioinformatics*, **2006**, *22*, 3067 – 3074.

[4] M. Shi, Y.-M. Xu, G.-L. Zhao, X.-F. Wu, Eur. *J. Org. Chem.* **2002**, 3666 - 3679; L. He, T.-Y. Jian, S. Ye *J. Org. Chem.* **2007**, *72*, 7466 – 7468; C. Lindner, R. Tandon, Y. Liu, B. Maryasin, H. Zipse, *Org. Biomol. Chem.* **2012**, *10*, 3210 – 3218.

[5] C. B. Fischer, S. Xu, H. Zipse, *Chem. Eur. J.* **2006**, *12*, 5779 – 5784.

[6] Y. Liu, P. E. Lindner, D. M. Lemal, *J. Am. Chem. Soc.***1999**,*121*,10626 – 10627.

[7] M. Marin-Luna, P. Patschinski, H. Zipse, *Chem. Eur. J.* **2018**, *24*, 15052 – 15058; M. Marin-Luna, B. Pölloth, F. Zott, H. Zipse, *Chem. Sci.* **2018**, *9*, 6509 – 6515; A. D. Becke, *J. Chem. Phys.* **1993**, *98*, 5648 – 5652; A. V. Marenich, C. J. Cramer,D. G. Trular, J. Phys. Chem. B 2009, 113, 6378–6396; S. Grimme, J. Antony, S. Ehrlich, H. Krieg, *J. Chem. Phys.* **2010**, *132*, 154104 – 154119; C. Riplinger and F. Neese, *J. Chem. Phys.*, **2013**, *138*, 034106; C. Riplinger, B. Sandhoefer, A. Hansen, F. Neese, *J. Chem. Phys.*, **2013**, *139*, 134101; F. Weigend, R. Ahlrichs, *Phys. Chem. Chem. Phys.* **2005**, *7*, 3297 – 3305; A. Hellweg, C. Hattig, S. Hofener, W. Klopper, *Theor. Chem. Acc.* **2007**, *117*, 587.

[8] MacroModel, Schrödinger, LLC, New York, NY, **2018**.

[9] M. Saunders, *J. Comput. Chem.* **2004**, *25*, 621; V.Vrček, O. Kronja M. Saunders, *J. Chem. Theory Comput.* **2007**, *3*, 1223; D. Sakic, M. Hanzevacki, D. M. Smith, V. Vrcek, *Org. Biomol. Chem.* **2015**, *13*, 11740 – 11752.

[10] Gaussian 09, Revision D.01, M. J. Frisch, G. W. Trucks, H. B. Schlegel, G. E. Scuseria, M. A. Robb, J. R. Cheeseman, G. Scalmani, V. Barone, B. Mennucci, G. A. Petersson, H. Nakatsuji, M. Caricato, X. Li, H. P. Hratchian, A. F. Izmaylov, J. Bloino, G. Zheng, J. L. Sonnenberg, M. Hada, M. Ehara, K. Toyota, R. Fukuda, J. Hasegawa, M. Ishida, T. Nakajima, Y. Honda, O. Kitao, H. Nakai, T. Vreven, J. A. Montgomery, Jr., J. E. Peralta, F. Ogliaro, M. Bearpark, J. J. Heyd, E. Brothers, K. N. Kudin, V. N. Staroverov, T. Keith, R. Kobayashi, J. Normand, K. Raghavachari, A. Rendell, J. C. Burant, S. S. Iyengar, J. Tomasi, M. Cossi, N. Rega, J. M. Millam, M. Klene, J. E. Knox, J. B. Cross, V. Bakken, C. Adamo, J. Jaramillo, R. Gomperts, R. E. Stratmann, O. Yazyev, A. J. Austin, R. Cammi, C. Pomelli, J. W. Ochterski, R. L. Martin, K. Morokuma, V. G. Zakrzewski, G. A. Voth, P. Salvador, J. J. Dannenberg, S. Dapprich, A. D. Daniels, O. Farkas, J. B. Foresman, J. V. Ortiz, J. Cioslowski, and D. J. Fox, Gaussian, Inc., Wallingford CT, **2013**.

[11] F. Neese, *WIREs Comput Mol Sci.* **2012**, *2*, 73 – 78; F. Neese, *WIREs Comput Mol Sci.* **2018**, *8*, 1 – 6.

Thermochemical Data

Table S4: 25. Table of Thermochemical Data (sorted by ΔH_{298K}(CC).

Nr.	H_{298K}(DFT)/Hartree	ΔH_{298K}(DFT)/kJ mol^{-1}	E_{298K}(DFT)/Hartree	H_{298K}(CC)/Hartree	ΔH_{298K}(CC)/kJ mol^{-1}	E_{298K}(CC)/Hartree
1a-001	-382.127410	0.00	-382.299549	-381.416284	0.00	-381.573299
1a-Me-002	-421.853065	+0.39	-422.069489	-421.064066	+0.60	-421.207869
1a-Me-001	-421.853214	0.00	-422.069542	-421.064295	0.00	-421.207977
1a-PhNCO-002	-781.783639	+26.23	-782.070340	-780.357903	+22.39	-780.603868
1a-PhNCO-001	-781.793628	0.00	-782.080726	-780.366432	0.00	-780.617834
Nr.	H_{298K}(DFT)/Hartree	ΔH_{298K}(DFT)/kJ mol^{-1}	E_{298K}(DFT)/Hartree	H_{298K}(CC)/Hartree	ΔH_{298K}(CC)/kJ mol^{-1}	E_{298K}(CC)/Hartree
1b-Me-002	-576.662400	0.00	-576.953434	-575.575527	+0.06	-575.794312
1b-Me-001	-576.662368	+0.08	-576.953475	-575.575549	0.00	-575.794400
1b-PhNCO-007	-936.591252	+25.41	-936.953034	-934.868003	+21.74	-935.185036
1b-PhNCO-006	-936.591294	+25.30	-936.953227	-934.868007	+21.73	-935.185197
1b-PhNCO-005	-936.591687	+24.27	-936.953564	-934.868396	+20.71	-935.185109
1b-PhNCO-004	-936.591863	+23.81	-936.953737	-934.868463	+20.53	-935.185360
1b-PhNCO-003	-936.600394	+1.41	-936.962542	-934.875935	+0.91	-935.198100
1b-PhNCO-002	-936.600529	+1.05	-936.962650	-934.875959	+0.85	-935.198217
1b-PhNCO-001	-936.600930	0.00	-936.963097	-934.876283	0.00	-935.198263
1b-002	-536.931667	+1.20	-537.178614	-535.923029	+3.05	-536.150546
1b-001	-536.932123	0.00	-537.179099	-535.924189	0.00	-536.151986
Nr.	H_{298K}(DFT)/Hartree	ΔH_{298K}(DFT)/kJ mol^{-1}	E_{298K}(DFT)/Hartree	H_{298K}(CC)/Hartree	ΔH_{298K}(CC)/kJ mol^{-1}	E_{298K}(CC)/Hartree
1c-Me-002	-499.253370	+0.13	-499.506871	-498.315476	+0.26	-498.495956
1c-Me-001	-499.253421	0.00	-499.506908	-498.315576	0.00	-498.496031
1c-PhNCO-003	-859.183086	+25.94	-859.507427	-857.608438	+22.55	-857.889460
1c-PhNCO-002	-859.183157	+25.76	-859.507379	-857.608527	+22.32	-857.889434
1c-PhNCO-001	-859.192967	0.00	-859.517639	-857.617027	0.00	-857.903369

Table S4: 25 (continuation). Table of Thermochemical Data (sorted by Δ*H298K*(CC).

1c-001	-459.526159	0.00	-459.735742	-458.666309	0.00	-458.858005
Nr.	H_{298K}(DFT)/Hartree	ΔH_{298K}(DFT)/kJ mol^{-1}	E_{298K}(DFT)/Hartree	H_{298K}(CC)/Hartree	ΔH_{298K}(CC)/kJ mol^{-1}	E_{298K}(CC)/Hartree
1d-005	-1016.125648	+4.51	-1016.554274	-1014.201302	+5.06	-1014.600809
1d-004	-1016.125019	+6.16	-1016.553668	-1014.201511	+4.51	-1014.600943
1d-003	-1016.126551	+2.13	-1016.555089	-1014.202468	+2.00	-1014.601808
1d-002	-1016.126904	+1.21	-1016.555471	-1014.202765	+1.22	-1014.602219
1d-001	-1016.127364	0.00	-1016.555451	-1014.203229	0.00	-1014.601766
1d-Me-005	-1055.853323	+8.25	-1056.326501	-1053.849974	+7.14	-1054.245677
1d-Me-004	-1055.85437	+5.50	-1056.327149	-1053.850126	+6.74	-1054.245476
1d-Me-003	-1055.855214	+3.29	-1056.327676	-1053.851306	+3.64	-1054.246181
1d-Me-002	-1055.856026	+1.16	-1056.328853	-1053.852273	+1.10	-1054.247612
1d-Me-001	-1055.856466	0.00	-1056.329413	-1053.852693	0.00	-1054.247636
1d-PhNCO-010	-1415.786517	+23.49	-1416.329657	-1413.147077	+19.41	-1413.637972
1d-PhNCO-009	-1415.787146	+21.84	-1416.330065	-1413.147676	+17.83	-1413.637591
1d-PhNCO-008	-1415.787546	+20.79	-1416.330724	-1413.148044	+16.87	-1413.639136
1d-PhNCO-007	-1415.792653	+7.38	-1416.336146	-1413.151298	+8.32	-1413.646588
1d-PhNCO-006	-1415.792519	+7.73	-1416.336124	-1413.152278	+5.75	-1413.647644
1d-PhNCO-005	-1415.793509	+5.13	-1416.336925	-1413.152555	+5.02	-1413.64777
1d-PhNCO-004	-1415.793762	+4.47	-1416.337187	-1413.15322	+3.28	-1413.648411
1d-PhNCO-003	-1415.795038	+1.12	-1416.338624	-1413.154199	+0.71	-1413.648894
1d-PhNCO-002	-1415.795269	+0.51	-1416.338522	-1413.154291	+0.46	-1413.64934
1d-PhNCO-001	-1415.795464	0.00	-1416.339007	-1413.154468	0.00	-1413.649226
Nr.	H_{298K}(DFT)/Hartree	ΔH_{298K}(DFT)/kJ mol^{-1}	E_{298K}(DFT)/Hartree	H_{298K}(CC)/Hartree	ΔH_{298K}(CC)/kJ mol^{-1}	E_{298K}(CC)/Hartree
1e-Me-007	-671.2727	+18.29	-671.611402	-670.021437	+13.84	-670.287096
1e-Me-006	-671.273142	+17.13	-671.611849	-670.021931	+12.54	-670.287498
1e-Me-005	-671.277554	+5.55	-671.616679	-670.02508	+4.27	-670.292271
1e-Me-004	-671.277963	+4.47	-671.6171	-670.025122	+4.16	-670.292244
1e-Me-003	-671.278402	+3.32	-671.617172	-670.025359	+3.54	-670.292173
1e-Me-002	-671.279517	+0.39	-671.6185	-670.026524	+0.48	-670.293492
1e-Me-001	-671.279667	0.00	-671.61837	-670.026708	0.00	-670.293452
1e-PhNCO-010	-1031.209124	+22.19	-1031.61899	-1029.320349	+18.58	-1029.68517
1e-PhNCO-009	-1031.215706	+4.91	-1031.62569	-1029.325641	+4.68	-1029.694067
1e-PhNCO-008	-1031.215716	+4.89	-1031.625631	-1029.325856	+4.12	-1029.693945
1e-PhNCO-007	-1031.216193	+3.63	-1031.626016	-1029.326033	+3.65	-1029.694451
1e-PhNCO-006	-1031.216098	+3.88	-1031.6259	-1029.326169	+3.30	-1029.694292
1e-PhNCO-005	-1031.216157	+3.73	-1031.626007	-1029.326206	+3.20	-1029.694405
1e-PhNCO-004	-1031.216996	+1.53	-1031.627058	-1029.326796	+1.65	-1029.695031
1e-PhNCO-003	-1031.217184	+1.03	-1031.627124	-1029.327007	+1.10	-1029.695433
1e-PhNCO-002	-1031.21745	+0.33	-1031.627294	-1029.327221	+0.54	-1029.695309
1e-PhNCO-001	-1031.217577	0.00	-1031.627363	-1029.327425	0.00	-1029.695875
1e-007	-631.543106	+13.12	-631.837765	-630.371031	+9.01	-630.644395
1e-006	-631.545096	+7.89	-631.839524	-630.371564	+7.61	-630.644775
1e-005	-631.545553	+6.69	-631.84017	-630.371948	+6.60	-630.644833
1e-004	-631.54586	+5.89	-631.840704	-630.372563	+4.98	-630.64556
1e-003	-631.546628	+3.87	-631.841622	-630.372596	+4.90	-630.64567
1e-002	-631.54669	+3.71	-631.841432	-630.372932	+4.01	-630.646164
1e-001	-631.548102	0.00	-631.842769	-630.374461	0.00	-630.647647

Table S4: 25 (continuation). Table of Thermochemical Data (sorted by Δ*H298K*(CC).

Nr.	H_{298K}(DFT)/Hartree	ΔH_{298K}(DFT)/kJ mol^{-1}	E_{298K}(DFT)/Hartree	H_{298K}(CC)/Hartree	ΔH_{298K}(CC)/kJ mol^{-1}	E_{298K}(CC)/Hartree
1f-Me-010	-1098.717845	+10.62	-1099.290885	-1096.628310	+6.84	-1097.122947
1f-Me-009	-1098.720261	+4.28	-1099.293218	-1096.628516	+6.30	-1097.122812
1f-Me-008	-1098.720281	+4.23	-1099.292731	-1096.629058	+4.88	-1097.122943
1f-Me-007	-1098.721347	+1.43	-1099.294122	-1096.629522	+3.66	-1097.123473
1f-Me-006	-1098.721042	+2.23	-1099.293951	-1096.629741	+3.08	-1097.124282
1f-Me-005	-1098.721162	+1.91	-1099.294524	-1096.629797	+2.94	-1097.124155
1f-Me-004	-1098.721317	+1.51	-1099.294315	-1096.629972	+2.48	-1097.124575
1f-Me-003	-1098.721378	+1.35	-1099.293913	-1096.630126	+2.07	-1097.124339
1f-Me-002	-1098.721771	+0.32	-1099.294162	-1096.630657	+0.68	-1097.124773
1f-Me-001	-1098.721891	0.00	-1099.294368	-1096.630916	0.00	-1097.125234
1f-PhNCO-010	-1458.657423	+8.84	-1459.301352	-1455.928450	+11.75	-1456.523161
1f-PhNCO-009	-1458.657320	+9.11	-1459.301428	-1455.928638	+11.26	-1456.523543
1f-PhNCO-008	-1458.657854	+7.71	-1459.302058	-1455.928994	+10.33	-1456.525546
1f-PhNCO-007	-1458.657535	+8.55	-1459.301659	-1455.929023	+10.25	-1456.523949
1f-PhNCO-006	-1458.657519	+8.59	-1459.301573	-1455.929025	+10.24	-1456.524791
1f-PhNCO-005	-1458.657607	+8.36	-1459.301821	-1455.929247	+9.66	-1456.524327
1f-PhNCO-004	-1458.659430	+3.57	-1459.303131	-1455.931235	+4.44	-1456.526208
1f-PhNCO-003	-1458.660641	+0.39	-1459.304122	-1455.932866	+0.16	-1456.527753
1f-PhNCO-002	-1458.660790	0.00	-1459.304522	-1455.932890	+0.10	-1456.527707
1f-PhNCO-001	-1458.660587	+0.53	-1459.304329	-1455.932927	0.00	-1456.527623
1f-010	-1058.988385	+2.59	-1059.517138	-1056.976337	+4.56	-1057.473995
1f-009	-1058.988394	+2.57	-1059.517118	-1056.976429	+4.31	-1057.473913
1f-008	-1058.988296	+2.83	-1059.516814	-1056.976468	+4.21	-1057.473766
1f-007	-1058.988635	+1.94	-1059.517342	-1056.976718	+3.55	-1057.474317
1f-006	-1058.988654	+1.89	-1059.517156	-1056.976786	+3.38	-1057.474245
1f-005	-1058.988676	+1.83	-1059.517155	-1056.977033	+2.73	-1057.474401
1f-004	-1058.989049	+0.85	-1059.517983	-1056.977203	+2.28	-1057.475176
1f-003	-1058.989270	+0.27	-1059.518161	-1056.977213	+2.26	-1057.475072
1f-002	-1058.989247	+0.33	-1059.518051	-1056.977767	+0.80	-1057.477963
1f-001	-1058.989373	0.00	-1059.518314	-1056.978072	0.00	-1057.478355
Nr.	H_{298K}(DFT)/Hartree	ΔH_{298K}(DFT)/kJ mol^{-1}	E_{298K}(DFT)/Hartree	H_{298K}(CC)/Hartree	ΔH_{298K}(CC)/kJ mol^{-1}	E_{298K}(CC)/Hartree
1g-Me-001	-287.928064	0.00	-288.066040	-287.383966	0.00	-287.442793
1g-PhNCO-002	-647.863222	+25.14	-648.071509	-646.682029	+21.05	-646.856923
1g-PhNCO-001	-647.872796	0.00	-648.081694	-646.690046	0.00	-646.870350
1g-001	-248.216362	0.00	-248.310532	-247.749343	0.00	-247.833295
Nr.	H_{298K}(DFT)/Hartree	ΔH_{298K}(DFT)/kJ mol^{-1}	E_{298K}(DFT)/Hartree	H_{298K}(CC)/Hartree	ΔH_{298K}(CC)/kJ mol^{-1}	E_{298K}(CC)/Hartree
6ac-010	-2264.557977	+2.74	-2265.012947	-2261.122278	+6.29	-2261.525030
6ac-009	-2264.557995	+2.69	-2265.012963	-2261.122338	+6.13	-2261.524859
6ac-008	-2264.557683	+3.51	-2265.013038	-2261.122353	+6.09	-2261.527948
6ac-007	-2264.557831	+3.12	-2265.013228	-2261.122377	+6.03	-2261.527961
6ac-006	-2264.558002	+2.67	-2265.012737	-2261.123026	+4.32	-2261.526280
6ac-005	-2264.557779	+3.26	-2265.012816	-2261.123110	+4.10	-2261.527003
6ac-004	-2264.558565	+1.19	-2265.013752	-2261.123201	+3.86	-2261.528809
6ac-003	-2264.559020	0.00	-2265.013824	-2261.124159	+1.35	-2261.529197
6ac-002	-2264.558915	+0.28	-2265.013895	-2261.124459	+0.56	-2261.531886
6ac-001	-2264.558997	+0.06	-2265.013733	-2261.124672	0.00	-2261.532301

Table S4: 25 (continuation). Table of Thermochemical Data (sorted by Δ*H298K*(CC).

Nr.	H_{298K}(DFT)/Hartree	ΔH_{298K}(DFT)/kJ mol^{-1}	E_{298K}(DFT)/Hartree	H_{298K}(CC)/Hartree	ΔH_{298K}(CC)/kJ mol^{-1}	E_{298K}(CC)/Hartree
6a-002	-1188.707899	+6.91	-1188.827589	-1187.152309	+8.52	-1187.212049
6a-001	-1188.710531	0.00	-1188.830358	-1187.155553	0.00	-1187.215384
Nr.	H_{298K}(DFT)/Hartree	ΔH_{298K}(DFT)/kJ mol^{-1}	E_{298K}(DFT)/Hartree	H_{298K}(CC)/Hartree	ΔH_{298K}(CC)/kJ mol^{-1}	E_{298K}(CC)/Hartree
6ac-Me-010	-2304.285732	+3.74	-2304.784658	-2300.772483	+3.79	-2301.182997
6ac-Me-009	-2304.285840	+3.46	-2304.784726	-2300.772714	+3.18	-2301.186838
6ac-Me-008	-2304.286729	+1.12	-2304.785737	-2300.773318	+1.59	-2301.183694
6ac-Me-007	-2304.286420	+1.93	-2304.785387	-2300.773326	+1.57	-2301.186969
6ac-Me-006	-2304.286520	+1.67	-2304.785745	-2300.773335	+1.55	-2301.184530
6ac-Me-005	-2304.286665	+1.29	-2304.785774	-2300.773362	+1.48	-2301.185010
6ac-Me-004	-2304.286546	+1.60	-2304.785311	-2300.773427	+1.31	-2301.186806
6ac-Me-003	-2304.286404	+1.98	-2304.785077	-2300.773504	+1.11	-2301.184341
6ac-Me-002	-2304.286430	+1.91	-2304.785074	-2300.773911	+0.04	-2301.188391
6ac-Me-001	-2304.287157	0.00	-2304.786019	-2300.773925	0.00	-2301.185721
6ac-PhNCO-010	-2664.228592	+3.58	-2664.798532	-2660.078291	+4.41	-2660.591607
6ac-PhNCO-009	-2664.228531	+3.74	-2664.798710	-2660.078336	+4.29	-2660.588076
6ac-PhNCO-008	-2664.229014	+2.48	-2664.798967	-2660.078380	+4.18	-2660.585576
6ac-PhNCO-007	-2664.228727	+3.23	-2664.799036	-2660.078380	+4.18	-2660.587442
6ac-PhNCO-006	-2664.229117	+2.21	-2664.799422	-2660.078486	+3.90	-2660.588508
6ac-PhNCO-005	-2664.229566	+1.03	-2664.799284	-2660.078786	+3.11	-2660.587006
6ac-PhNCO-004	-2664.229314	+1.69	-2664.799504	-2660.078974	+2.62	-2660.588446
6ac-PhNCO-003	-2664.229355	+1.58	-2664.799304	-2660.079015	+2.51	-2660.587967
6ac-PhNCO-002	-2664.228622	+3.51	-2664.798741	-2660.079053	+2.41	-2660.589797
6ac-PhNCO-001	-2664.229957	0.00	-2664.800153	-2660.079971	0.00	-2660.589197
Nr.	H_{298K}(DFT)/Hartree	ΔH_{298K}(DFT)/kJ mol^{-1}	E_{298K}(DFT)/Hartree	H_{298K}(CC)/Hartree	ΔH_{298K}(CC)/kJ mol^{-1}	E_{298K}(CC)/Hartree
6ah-010	-1846.623055	+3.65	-1847.028738	-1844.002933	+2.40	-1844.363476
6ah-009	-1846.623270	+3.09	-1847.029013	-1844.002955	+2.35	-1844.364486
6ah-008	-1846.623772	+1.77	-1847.029762	-1844.002967	+2.32	-1844.367014
6ah-007	-1846.623319	+2.96	-1847.029098	-1844.003067	+2.05	-1844.365298
6ah-006	-1846.623755	+1.82	-1847.029626	-1844.003140	+1.86	-1844.364601
6ah-005	-1846.623277	+3.07	-1847.029064	-1844.003146	+1.85	-1844.365472
6ah-004	-1846.623239	+3.17	-1847.028954	-1844.003187	+1.74	-1844.361991
6ah-003	-1846.623396	+2.76	-1847.028962	-1844.003342	+1.33	-1844.363811
6ah-002	-1846.623463	+2.58	-1847.028989	-1844.003578	+0.71	-1844.364833
6ah-001	-1846.624447	0.00	-1847.030103	-1844.003849	0.00	-1844.367460
6ah-Me2-010	-1886.335106	+3.56	-1886.784532	-1883.641515	+4.25	-1884.011731
6ah-Me2-009	-1886.335711	+1.97	-1886.785168	-1883.641654	+3.88	-1884.013500
6ah-Me2-008	-1886.335715	+1.96	-1886.785125	-1883.641706	+3.74	-1884.013473
6ah-Me2-007	-1886.335029	+3.76	-1886.784697	-1883.641714	+3.72	-1884.011986
6ah-Me2-006	-1886.334831	+4.28	-1886.784502	-1883.641753	+3.62	-1884.011748
6ah-Me2-005	-1886.335826	+1.67	-1886.784969	-1883.641775	+3.56	-1884.013682
6ah-Me2-004	-1886.335112	+3.54	-1886.784345	-1883.642032	+2.89	-1884.011620
6ah-Me2-003	-1886.335528	+2.45	-1886.784573	-1883.642253	+2.31	-1884.012076
6ah-Me2-002	-1886.335624	+2.20	-1886.784498	-1883.642681	+1.18	-1884.011947
6ah-Me2-001	-1886.336461	0.00	-1886.785935	-1883.643132	0.00	-1884.014248
6ah-Me-010	-1886.350844	+1.90	-1886.800483	-1883.652440	+1.20	-1884.019444
6ah-Me-009	-1886.351115	+1.19	-1886.800678	-1883.652466	+1.13	-1884.021553

Table S4: 25 (continuation). Table of Thermochemical Data (sorted by Δ*H298K*(CC).

6ah-Me-008	-1886.351519	+0.13	-1886.800859	-1883.652609	+0.76	-1884.020259
6ah-Me-007	-1886.351484	+0.22	-1886.800756	-1883.652610	+0.75	-1884.020175
6ah-Me-006	-1886.351270	+0.78	-1886.800537	-1883.652636	+0.69	-1884.019966
6ah-Me-005	-1886.351387	+0.47	-1886.800615	-1883.652712	+0.49	-1884.020929
6ah-Me-004	-1886.351567	0.00	-1886.800826	-1883.652720	+0.46	-1884.020504
6ah-Me-003	-1886.351510	+0.15	-1886.800847	-1883.652843	+0.14	-1884.021548
6ah-Me-002	-1886.351544	+0.06	-1886.800839	-1883.652893	+0.01	-1884.021202
6ah-Me-001	-1886.351472	+0.25	-1886.800870	-1883.652897	0.00	-1884.021205
6ah-PhNCO2-010	-2246.274112	+7.09	-2246.794198	-2242.941030	+5.31	-2243.408351
6ah-PhNCO2-009	-2246.274750	+5.41	-2246.795196	-2242.941044	+5.27	-2243.412959
6ah-PhNCO2-008	-2246.274431	+6.25	-2246.794425	-2242.941229	+4.79	-2243.411660
6ah-PhNCO2-007	-2246.275449	+3.58	-2246.795316	-2242.941277	+4.66	-2243.410564
6ah-PhNCO2-006	-2246.275955	+2.25	-2246.796331	-2242.941475	+4.14	-2243.414420
6ah-PhNCO2-005	-2246.274555	+5.93	-2246.794299	-2242.941506	+4.06	-2243.412517
6ah-PhNCO2-004	-2246.274928	+4.95	-2246.795236	-2242.941602	+3.81	-2243.413247
6ah-PhNCO2-003	-2246.276812	0.00	-2246.797100	-2242.942768	+0.75	-2243.417327
6ah-PhNCO2-002	-2246.276164	+1.70	-2246.796606	-2242.942792	+0.68	-2243.418863
6ah-PhNCO2-001	-2246.276751	+0.16	-2246.796816	-2242.943052	0.00	-2243.417962
6ah-PhNCO-010	-2246.291456	+3.11	-2246.812395	-2242.955701	+2.48	-2243.419572
6ah-PhNCO-009	-2246.291077	+4.10	-2246.811680	-2242.955719	+2.44	-2243.418997
6ah-PhNCO-008	-2246.291117	+4.00	-2246.811848	-2242.955786	+2.26	-2243.419149
6ah-PhNCO-007	-2246.291720	+2.42	-2246.812374	-2242.955940	+1.86	-2243.420427
6ah-PhNCO-006	-2246.292640	0.00	-2246.813677	-2242.955972	+1.77	-2243.423831
6ah-PhNCO-005	-2246.292009	+1.66	-2246.812627	-2242.956058	+1.55	-2243.419323
6ah-PhNCO-004	-2246.292016	+1.64	-2246.812490	-2242.956083	+1.48	-2243.421038
6ah-PhNCO-003	-2246.292054	+1.54	-2246.812568	-2242.956086	+1.47	-2243.420989
6ah-PhNCO-002	-2246.291832	+2.12	-2246.812438	-2242.956355	+0.77	-2243.419413
6ah-PhNCO-001	-2246.292145	+1.30	-2246.812853	-2242.956647	0.00	-2243.421062
Nr.	H_{298K}(DFT)/Hartree	ΔH_{298K}(DFT)/kJ mol^{-1}	E_{298K}(DFT)/Hartree	H_{298K}(CC)/Hartree	ΔH_{298K}(CC)/kJ mol^{-1}	E_{298K}(CC)/Hartree
6a-Me2-002	-1228.439305	+3.45	-1228.602584	-1226.813734	+3.37	-1226.962686
6a-Me2-001	-1228.440619	0.00	-1228.603784	-1226.815017	0.00	-1226.964188
6a-Me-001	-1228.453362	0.00	-1228.616700	-1226.822428	0.00	-1226.956484
6a-PhNCO2-004	-1588.348686	+26.95	-1588.582178	-1586.082124	+23.13	-1586.248265
6a-PhNCO2-003	-1588.358949	0.00	-1588.593173	-1586.090619	+0.83	-1586.260225
6a-PhNCO2-002	-1588.355809	+8.24	-1588.589548	-1586.090692	+0.64	-1586.258426
6a-PhNCO2-001	-1588.357859	+2.86	-1588.591873	-1586.090935	0.00	-1586.259767
6a-PhNCO-010	-1588.369070	+28.41	-1588.603106			
6a-PhNCO-009	-1588.370158	+25.55	-1588.604452			
6a-PhNCO-008	-1588.370242	+25.33	-1588.604491			
6a-PhNCO-007	-1588.370269	+25.26	-1588.604584			
6a-PhNCO-006	-1588.370343	+25.06	-1588.604634	-1586.101420	+22.87	-1586.269587
6a-PhNCO-005	-1588.378436	+3.81	-1588.612952	-1586.107847	+6.00	-1586.282446
6a-PhNCO-004	-1588.378390	+3.94	-1588.612939	-1586.107864	+5.95	-1586.282534
6a-PhNCO-003	-1588.378508	+3.63	-1588.613056	-1586.108188	+5.10	-1586.282580
6a-PhNCO-002	-1588.379889	0.00	-1588.614515	-1586.110109	+0.06	-1586.284253
6a-PhNCO-001	-1588.379837	+0.14	-1588.614343	-1586.110132	0.00	-1586.284137

Table S4: 25 (continuation). Table of Thermochemical Data (sorted by Δ*H298K*(CC).

Nr.	H_{298K}(DFT)/Hartree	ΔH_{298K}(DFT)/kJ mol^{-1}	E_{298K}(DFT)/Hartree	H_{298K}(CC)/Hartree	ΔH_{298K}(CC)/kJ mol^{-1}	E_{298K}(CC)/Hartree
6bc-Me2-010	-2237.531620	+8.92	-2238.137564	-2233.878982	+9.77	-2234.400670
6bc-Me2-009	-2237.531824	+8.39	-2238.137737	-2233.879084	+9.50	-2234.398976
6bc-Me2-008	-2237.531262	+9.86	-2238.137623	-2233.879188	+9.23	-2234.398157
6bc-Me2-007	-2237.532009	+7.90	-2238.137852	-2233.879625	+8.08	-2234.397708
6bc-Me2-006	-2237.531860	+8.29	-2238.137828	-2233.879626	+8.08	-2234.397353
6bc-Me2-005	-2237.532068	+7.75	-2238.138244	-2233.879794	+7.64	-2234.398717
6bc-Me2-004	-2237.532087	+7.70	-2238.137872	-2233.879982	+7.14	-2234.397630
6bc-Me2-003	-2237.531941	+8.08	-2238.137853	-2233.880660	+5.36	-2234.398387
6bc-Me2-002	-2237.534993	+0.07	-2238.140952	-2233.882549	+0.40	-2234.403825
6bc-Me2-001	-2237.535018	0.00	-2238.140970	-2233.882703	0.00	-2234.403916
6bc-Me-010	-2237.536384	+3.39	-2238.141945	-2233.879527	+7.42	-2234.393995
6bc-Me-009	-2237.536726	+2.49	-2238.142672	-2233.879613	+7.20	-2234.390022
6bc-Me-008	-2237.536547	+2.96	-2238.142315	-2233.879827	+6.63	-2234.396891
6bc-Me-007	-2237.536745	+2.44	-2238.142602	-2233.879861	+6.55	-2234.390129
6bc-Me-006	-2237.536716	+2.52	-2238.142447	-2233.880206	+5.64	-2234.397280
6bc-Me-005	-2237.536931	+1.95	-2238.143018	-2233.880540	+4.76	-2234.397161
6bc-Me-004	-2237.536882	+2.08	-2238.143142	-2233.880704	+4.33	-2234.397543
6bc-Me-003	-2237.537454	+0.58	-2238.143235	-2233.881546	+2.12	-2234.394192
6bc-Me-002	-2237.537662	+0.03	-2238.143210	-2233.882328	+0.07	-2234.398077
6bc-Me-001	-2237.537675	0.00	-2238.143271	-2233.882354	0.00	-2234.398132
6bc-PhNCO2-010	-2597.464247	+11.32	-2598.141405	-2593.173785	+10.10	-2593.785219
6bc-PhNCO2-009	-2597.464428	+10.84	-2598.141355	-2593.173885	+9.84	-2593.785202
6bc-PhNCO2-008	-2597.464599	+10.39	-2598.141636	-2593.174150	+9.14	-2593.785340
6bc-PhNCO2-007	-2597.465292	+8.57	-2598.142695	-2593.174461	+8.33	-2593.784867
6bc-PhNCO2-006	-2597.464355	+11.03	-2598.141150	-2593.175054	+6.77	-2593.782144
6bc-PhNCO2-005	-2597.464182	+11.49	-2598.141471	-2593.175087	+6.68	-2593.781393
6bc-PhNCO2-004	-2597.464690	+10.15	-2598.141603	-2593.175562	+5.43	-2593.786850
6bc-PhNCO2-003	-2597.468370	+0.49	-2598.144913	-2593.177386	+0.65	-2593.790269
6bc-PhNCO2-002	-2597.468557	0.00	-2598.144986	-2593.177455	+0.46	-2593.790524
6bc-PhNCO2-001	-2597.468487	+0.18	-2598.144961	-2593.177632	0.00	-2593.790599
6bc-PhNCO-010	-2597.476584	+7.13	-2598.154390	-2593.184349	+5.77	-2593.786838
6bc-PhNCO-009	-2597.476491	+7.38	-2598.153922	-2593.184546	+5.25	-2593.792159
6bc-PhNCO-008	-2597.477241	+5.41	-2598.154598	-2593.184673	+4.92	-2593.787500
6bc-PhNCO-007	-2597.477754	+4.06	-2598.155000	-2593.184750	+4.72	-2593.789499
6bc-PhNCO-006	-2597.477157	+5.63	-2598.154393	-2593.184789	+4.61	-2593.791187
6bc-PhNCO-005	-2597.477195	+5.53	-2598.154458	-2593.184804	+4.57	-2593.788638
6bc-PhNCO-004	-2597.477284	+5.30	-2598.154616	-2593.184858	+4.43	-2593.787537
6bc-PhNCO-003	-2597.477263	+5.35	-2598.154531	-2593.184883	+4.37	-2593.786854
6bc-PhNCO-002	-2597.477190	+5.54	-2598.154589	-2593.184917	+4.28	-2593.786779
6bc-PhNCO-001	-2597.479301	0.00	-2598.156824	-2593.186546	0.00	-2593.790060
6bc-010	-2197.800044	+3.23	-2198.361947	-2194.220872	+7.48	-2194.722723
6bc-009	-2197.801274	0.00	-2198.363182	-2194.221148	+6.76	-2194.720399
6bc-008	-2197.800646	+1.65	-2198.363254	-2194.221326	+6.29	-2194.720246
6bc-007	-2197.800471	+2.11	-2198.362530	-2194.221541	+5.72	-2194.720531
6bc-006	-2197.800551	+1.90	-2198.362541	-2194.221570	+5.65	-2194.719717
6bc-005	-2197.800640	+1.66	-2198.362649	-2194.221731	+5.22	-2194.721602

Table S4: 25 (continuation). Table of Thermochemical Data (sorted by Δ*H298K*(CC).

6bc-004	-2197.799930	+3.53	-2198.361951	-2194.222651	+2.81	-2194.722926
6bc-003	-2197.800641	+1.66	-2198.362519	-2194.222726	+2.61	-2194.723242
6bc-002	-2197.801097	+0.46	-2198.363536	-2194.222996	+1.90	-2194.719771
6bc-001	-2197.801258	+0.04	-2198.363480	-2194.223721	0.00	-2194.730857
Nr.	H_{298K}(DFT)/Hartree	ΔH_{298K}(DFT)/kJ mol^{-1}	E_{298K}(DFT)/Hartree	H_{298K}(CC)/Hartree	ΔH_{298K}(CC)/kJ mol^{-1}	E_{298K}(CC)/Hartree
6b-Me2-003	-1161.695475	+10.14	-1161.965524	-1159.924792	+12.56	-1160.170543
6b-Me2-002	-1161.699337	0.00	-1161.969786	-1159.929551	+0.06	-1160.176041
6b-Me2-001	-1161.699311	+0.07	-1161.969760	-1159.929575	0.00	-1160.176083
6b-Me-003	-1161.700049	+0.16	-1161.970467	-1159.925395	+4.42	-1160.160618
6b-Me-002	-1161.700056	+0.14	-1161.970433	-1159.925433	+4.32	-1160.160625
6b-Me-001	-1161.700109	0.00	-1161.970457	-1159.927079	0.00	-1160.159289
6b-PhNCO2-006	-1521.603386	+18.44	-1521.944168			
6b-PhNCO2-005	-1521.604275	+16.11	-1521.945245	-1519.194842	+14.70	-1519.455527
6b-PhNCO2-004	-1521.604404	+15.77	-1521.945246	-1519.195366	+13.32	-1519.453916
6b-PhNCO2-003	-1521.607866	+6.68	-1521.949030	-1519.199344	+2.88	-1519.461704
6b-PhNCO2-002	-1521.610411	0.00	-1521.951600	-1519.199910	+1.39	-1519.463732
6b-PhNCO2-001	-1521.610334	+0.20	-1521.951407	-1519.200441	0.00	-1519.464158
6b-PhNCO-010	-1521.614784	+25.77	-1521.956282			
6b-PhNCO-009	-1521.615006	+25.19	-1521.956359			
6b-PhNCO-008	-1521.615046	+25.09	-1521.956380			
6b-PhNCO-007	-1521.615121	+24.89	-1521.956727			
6b-PhNCO-006	-1521.617107	+19.68	-1521.958558	-1519.205486	+17.51	-1519.467576
6b-PhNCO-005	-1521.623102	+3.94	-1521.964938	-1519.208918	+8.50	-1519.477063
6b-PhNCO-004	-1521.623205	+3.67	-1521.964960	-1519.209015	+8.24	-1519.477055
6b-PhNCO-003	-1521.624542	+0.15	-1521.966188	-1519.211930	+0.59	-1519.479265
6b-PhNCO-002	-1521.624572	+0.08	-1521.966175	-1519.211970	+0.48	-1519.479328
6b-PhNCO-001	-1521.624601	0.00	-1521.966338	-1519.212154	0.00	-1519.479488
6b-002	-1121.948210	+5.62	-1122.174923	-1120.249087	+11.09	-1120.401708
6b-001	-1121.950352	0.00	-1122.177274	-1120.253312	0.00	-1120.406034
Nr.	H_{298K}(DFT)/Hartree	ΔH_{298K}(DFT)/kJ mol^{-1}	E_{298K}(DFT)/Hartree	H_{298K}(CC)/Hartree	ΔH_{298K}(CC)/kJ mol^{-1}	E_{298K}(CC)/Hartree
6cg-Me2-010	-2504.434062	+3.38	-2505.102931	-2500.309238	+4.55	-2500.891996
6cg-Me2-009	-2504.433870	+3.88	-2505.102134	-2500.309518	+3.81	-2500.889366
6cg-Me2-008	-2504.433665	+4.42	-2505.102136	-2500.309525	+3.80	-2500.889417
6cg-Me2-007	-2504.434291	+2.78	-2505.102887	-2500.309693	+3.36	-2500.891825
6cg-Me2-006	-2504.435348	0.00	-2505.103967	-2500.309726	+3.27	-2500.892800
6cg-Me2-005	-2504.434507	+2.21	-2505.102774	-2500.309733	+3.25	-2500.891625
6cg-Me2-004	-2504.433680	+4.38	-2505.102320	-2500.309752	+3.20	-2500.890209
6cg-Me2-003	-2504.435206	+0.37	-2505.104005	-2500.309781	+3.12	-2500.892815
6cg-Me2-002	-2504.434671	+1.78	-2505.103542	-2500.310638	+0.87	-2500.891178
6cg-Me2-001	-2504.435012	+0.88	-2505.103661	-2500.310971	0.00	-2500.891321
6cg-Me-010	-2504.436414	+1.56	-2505.105631	-2500.306659	+6.23	-2500.879546
6cg-Me-009	-2504.436787	+0.59	-2505.105689	-2500.306705	+6.11	-2500.879713
6cg-Me-008	-2504.437010	0.00	-2505.105323	-2500.307011	+5.31	-2500.881710
6cg-Me-007	-2504.435262	+4.59	-2505.104197	-2500.307369	+4.37	-2500.882757
6cg-Me-006	-2504.435476	+4.03	-2505.104209	-2500.307685	+3.54	-2500.883084
6cg-Me-005	-2504.435630	+3.62	-2505.104710	-2500.307948	+2.85	-2500.873535
6cg-Me-004	-2504.436141	+2.28	-2505.104509	-2500.308369	+1.74	-2500.882663

Table S4: 25 (continuation). Table of Thermochemical Data (sorted by Δ*H298K*(CC).

6cg-Me-003	-2504.435850	+3.05	-2505.104762	-2500.308584	+1.18	-2500.873236
6cg-Me-002	-2504.436243	+2.01	-2505.104986	-2500.308597	+1.14	-2500.882114
6cg-Me-001	-2504.435971	+2.73	-2505.105275	-2500.309033	0.00	-2500.877225
6cg-010	-2464.698590	+4.54	-2465.323401	-2460.648144	+6.24	-2461.211209
6cg-009	-2464.699267	+2.76	-2465.324142	-2460.648196	+6.10	-2461.205062
6cg-008	-2464.698904	+3.72	-2465.323500	-2460.648323	+5.77	-2461.208642
6cg-007	-2464.698602	+4.51	-2465.323151	-2460.648492	+5.32	-2461.212032
6cg-006	-2464.699018	+3.42	-2465.323716	-2460.648527	+5.23	-2461.207068
6cg-005	-2464.699043	+3.35	-2465.323649	-2460.648692	+4.80	-2461.207238
6cg-004	-2464.699133	+3.12	-2465.323761	-2460.648701	+4.78	-2461.209375
6cg-003	-2464.698966	+3.55	-2465.324040	-2460.649512	+2.65	-2461.206798
6cg-002	-2464.700214	+0.28	-2465.325314	-2460.650518	+0.01	-2461.206242
6cg-001	-2464.700320	0.00	-2465.325436	-2460.650520	0.00	-2461.205993
6cg-PhNCO2-010	-2864.363561	+6.54	-2865.102905	-2859.598953	+11.07	-2860.274943
6cg-PhNCO2-009	-2864.362770	+8.62	-2865.102527	-2859.599259	+10.26	-2860.263361
6cg-PhNCO2-008	-2864.362721	+8.75	-2865.102029	-2859.599269	+10.24	-2860.272700
6cg-PhNCO2-007	-2864.363086	+7.79	-2865.102664	-2859.599534	+9.54	-2860.262741
6cg-PhNCO2-006	-2864.362274	+9.92	-2865.101252	-2859.600069	+8.14	-2860.264075
6cg-PhNCO2-005	-2864.363600	+6.44	-2865.102784	-2859.600586	+6.78	-2860.264279
6cg-PhNCO2-004	-2864.362955	+8.13	-2865.101451	-2859.600703	+6.47	-2860.270722
6cg-PhNCO2-003	-2864.362227	+10.05	-2865.101696	-2859.601081	+5.48	-2860.264493
6cg-PhNCO2-002	-2864.363990	+5.42	-2865.103645	-2859.602546	+1.63	-2860.268759
6cg-PhNCO2-001	-2864.366053	0.00	-2865.105728	-2859.603168	0.00	-2860.269136
6cg-PhNCO-010	-2864.377722	+6.13	-2865.117593	-2859.611086	+9.59	-2860.280331
6cg-PhNCO-009	-2864.377082	+7.81	-2865.116909	-2859.611319	+8.98	-2860.281042
6cg-PhNCO-008	-2864.377175	+7.56	-2865.116924	-2859.611762	+7.82	-2860.281226
6cg-PhNCO-007	-2864.377268	+7.32	-2865.117056	-2859.612614	+5.58	-2860.276212
6cg-PhNCO-006	-2864.378784	+3.34	-2865.118861	-2859.613304	+3.77	-2860.278836
6cg-PhNCO-005	-2864.380055	0.00	-2865.120685	-2859.613990	+1.97	-2860.278112
6cg-PhNCO-004	-2864.380028	+0.07	-2865.120133	-2859.613998	+1.95	-2860.277209
6cg-PhNCO-003	-2864.379959	+0.25	-2865.120062	-2859.614028	+1.87	-2860.277233
6cg-PhNCO-002	-2864.379668	+1.02	-2865.119881	-2859.614390	+0.92	-2860.274752
6cg-PhNCO-001	-2864.379681	+0.98	-2865.119504	-2859.614739	0.00	-2860.277311
Nr.	H_{298K}(DFT)/Hartree	ΔH_{298K}(DFT)/kJ mol^{-1}	E_{298K}(DFT)/Hartree	H_{298K}(CC)/Hartree	ΔH_{298K}(CC)/kJ mol^{-1}	E_{298K}(CC)/Hartree
6c-Me2-004	-1236.900657	+10.60	-1237.176659	-1235.033197	+12.23	-1235.284493
6c-Me2-003	-1236.901039	+9.60	-1237.176928	-1235.033366	+11.79	-1235.284723
6c-Me2-002	-1236.904689	+0.01	-1237.180899	-1235.037852	+0.01	-1235.289634
6c-Me2-001	-1236.904694	0.00	-1237.181015	-1235.037855	0.00	-1235.289938
6c-Me-004	-1236.904780	+0.10	-1237.181211	-1235.033172	+4.62	-1235.274012
6c-Me-003	-1236.904755	+0.17	-1237.181260	-1235.034360	+1.50	-1235.272363
6c-Me-002	-1236.904787	+0.08	-1237.181174	-1235.034929	0.00	-1235.272560
6c-Me-001	-1236.904819	0.00	-1237.181224	-1235.034930	0.00	-1235.272536
6c-003	-1197.152648	+6.12	-1197.385457	-1195.356524	+11.46	-1195.514467
6c-002	-1197.154557	+1.11	-1197.387538	-1195.360264	+1.64	-1195.518226
6c-001	-1197.154978	0.00	-1197.387692	-1195.360890	0.00	-1195.518706
6c-PhNCO2-010	-1596.808343	+18.17	-1597.155178			
6c-PhNCO2-009	-1596.808389	+18.05	-1597.155188			

Table S4: 25 (continuation). Table of Thermochemical Data (sorted by Δ*H298K*(CC).

6c-PhNCO2-008	-1596.809359	+15.50	-1597.156310	-1594.301989	+16.46	-1594.565569
6c-PhNCO2-007	-1596.809045	+16.33	-1597.156085	-1594.302685	+14.63	-1594.568502
6c-PhNCO2-006	-1596.809632	+14.79	-1597.156386	-1594.303097	+13.55	-1594.568920
6c-PhNCO2-005	-1596.812581	+7.04	-1597.159881	-1594.306847	+3.70	-1594.574707
6c-PhNCO2-004	-1596.812910	+6.18	-1597.160069	-1594.307264	+2.61	-1594.575080
6c-PhNCO2-003	-1596.815264	0.00	-1597.162533	-1594.307795	+1.22	-1594.577544
6c-PhNCO2-002	-1596.815033	+0.61	-1597.162321	-1594.308145	+0.30	-1594.577089
6c-PhNCO2-001	-1596.815236	+0.07	-1597.162553	-1594.308258	0.00	-1594.577475
6c-PhNCO-010	-1596.822184	+18.61	-1597.169736			
6c-PhNCO-009	-1596.822350	+18.17	-1597.170017			
6c-PhNCO-008	-1596.827827	+3.79	-1597.175633	-1594.316610	+8.27	-1594.589905
6c-PhNCO-007	-1596.827851	+3.73	-1597.175510	-1594.316724	+7.97	-1594.589867
6c-PhNCO-006	-1596.828915	+0.94	-1597.176818	-1594.319229	+1.40	-1594.591833
6c-PhNCO-005	-1596.828924	+0.91	-1597.176642	-1594.319316	+1.17	-1594.591695
6c-PhNCO-004	-1596.829122	+0.39	-1597.176932	-1594.319456	+0.80	-1594.592327
6c-PhNCO-003	-1596.829053	+0.57	-1597.176805	-1594.319517	+0.64	-1594.592047
6c-PhNCO-002	-1596.829033	+0.63	-1597.176843	-1594.319571	+0.50	-1594.592230
6c-PhNCO-001	-1596.829272	0.00	-1597.176951	-1594.319761	0.00	-1594.592363
Nr.	H_{298K}(DFT)/Hartree	ΔH_{298K}(DFT)/kJ mol^{-1}	E_{298K}(DFT)/Hartree	H_{298K}(CC)/Hartree	ΔH_{298K}(CC)/kJ mol^{-1}	E_{298K}(CC)/Hartree
8a-005	-1189.159822	+22.18	-1189.293242	-1187.614175	+9.01	-1187.733044
8a-004	-1189.159903	+21.97	-1189.293216	-1187.614344	+8.56	-1187.733053
8a-003	-1189.160022	+21.66	-1189.293312	-1187.614621	+7.84	-1187.733587
8a-002	-1189.167846	+1.11	-1189.301506	-1187.617563	+0.11	-1187.722982
8a-001	-1189.168270	0.00	-1189.302174	-1187.617606	0.00	-1187.722020
Nr.	H_{298K}(DFT)/Hartree	ΔH_{298K}(DFT)/kJ mol^{-1}	E_{298K}(DFT)/Hartree	H_{298K}(CC)/Hartree	ΔH_{298K}(CC)/kJ mol^{-1}	E_{298K}(CC)/Hartree
10h-Me-010	-1879.932767	+3.04	-1880.551904	-1876.799559	+2.32	-1877.332792
10h-Me-009	-1879.932952	+2.55	-1880.551570	-1876.799635	+2.12	-1877.333466
10h-Me-008	-1879.932296	+4.28	-1880.550984	-1876.799637	+2.11	-1877.333855
10h-Me-007	-1879.932906	+2.68	-1880.551116	-1876.799754	+1.81	-1877.331089
10h-Me-006	-1879.933218	+1.86	-1880.551977	-1876.799896	+1.43	-1877.332677
10h-Me-005	-1879.933733	+0.50	-1880.552829	-1876.800181	+0.69	-1877.334166
10h-Me-004	-1879.933191	+1.93	-1880.551700	-1876.800241	+0.53	-1877.332837
10h-Me-003	-1879.933824	+0.27	-1880.552786	-1876.800340	+0.27	-1877.334450
10h-Me-002	-1879.933925	0.00	-1880.552832	-1876.800417	+0.07	-1877.334526
10h-Me-001	-1879.933350	+1.51	-1880.552313	-1876.800442	0.00	-1877.334254
10h-PhNCO-010	-2239.869020	+6.18	-2240.558770	-2236.097149	+9.95	-2236.718122
10h-PhNCO-009	-2239.869239	+5.60	-2240.559924	-2236.097163	+9.91	-2236.723991
10h-PhNCO-008	-2239.869124	+5.90	-2240.558823	-2236.097427	+9.22	-2236.719444
10h-PhNCO-007	-2239.869339	+5.34	-2240.558858	-2236.097601	+8.76	-2236.719455
10h-PhNCO-006	-2239.868947	+6.37	-2240.559031	-2236.098053	+7.57	-2236.723896
10h-PhNCO-005	-2239.869489	+4.94	-2240.560273	-2236.098928	+5.27	-2236.724603
10h-PhNCO-004	-2239.870572	+2.10	-2240.560437	-2236.099060	+4.93	-2236.730061
10h-PhNCO-003	-2239.869623	+4.59	-2240.559938	-2236.099392	+4.06	-2236.726203
10h-PhNCO-002	-2239.869059	+6.07	-2240.559313	-2236.099658	+3.36	-2236.724545
10h-PhNCO-001	-2239.871372	0.00	-2240.561421	-2236.100937	0.00	-2236.727281
10h-010	-1840.192728	+5.21	-1840.767934	-1837.138177	+4.57	-1837.660110
10h-009	-1840.193193	+3.99	-1840.768166	-1837.138399	+3.99	-1837.661443

Table S4: 25 (continuation). Table of Thermochemical Data (sorted by Δ*H298K*(CC).

10h-008	-1840.193224	+3.91	-1840.768189	-1837.138605	+3.45	-1837.661737
10h-007	-1840.193657	+2.78	-1840.768833	-1837.138877	+2.73	-1837.661656
10h-006	-1840.193837	+2.30	-1840.768990	-1837.138914	+2.64	-1837.661544
10h-005	-1840.193989	+1.90	-1840.768912	-1837.139152	+2.01	-1837.661763
10h-004	-1840.193616	+2.88	-1840.768906	-1837.139205	+1.87	-1837.664243
10h-003	-1840.194215	+1.31	-1840.768876	-1837.139338	+1.52	-1837.660513
10h-002	-1840.194543	+0.45	-1840.769386	-1837.139842	+0.20	-1837.662204
10h-001	-1840.194714	0.00	-1840.769421	-1837.139918	0.00	-1837.663197
Nr.	H_{298K}(DFT)/Hartree	ΔH_{298K}(DFT)/kJ mol^{-1}	E_{298K}(DFT)/Hartree	H_{298K}(CC)/Hartree	ΔH_{298K}(CC)/kJ mol^{-1}	E_{298K}(CC)/Hartree
10-Me2-004	-1222.029868	+4.00	-1222.362562	-1219.968062	+8.67	-1220.269215
10-Me2-003	-1222.030102	+3.39	-1222.362973	-1219.968967	+6.30	-1220.271118
10-Me2-002	-1222.029867	+4.01	-1222.362573	-1219.969643	+4.52	-1220.270540
10-Me2-001	-1222.031393	0.00	-1222.364044	-1219.971366	0.00	-1220.273934
10-Me-003	-1222.029131	+0.81	-1222.361626	-1219.964723	+0.96	-1220.259742
10-Me-002	-1222.029376	+0.17	-1222.361759	-1219.965023	+0.17	-1220.259963
10-Me-001	-1222.029439	0.00	-1222.361727	-1219.965088	0.00	-1220.259723
10-PhNCO2-009	-1581.939963	+16.81	-1582.343515			
10-PhNCO2-008	-1581.940273	+15.99	-1582.344005			
10-PhNCO2-007	-1581.940404	+15.65	-1582.344020			
10-PhNCO2-006	-1581.941408	+13.01	-1582.345198	-1579.241687	+13.42	-1579.564215
10-PhNCO2-005	-1581.943125	+8.50	-1582.347175	-1579.243399	+8.92	-1579.566577
10-PhNCO2-004	-1581.943105	+8.56	-1582.347163	-1579.243414	+8.88	-1579.566634
10-PhNCO2-003	-1581.944659	+4.48	-1582.348154	-1579.245524	+3.34	-1579.564640
10-PhNCO2-002	-1581.946364	0.00	-1582.350175	-1579.246582	+0.57	-1579.572014
10-PhNCO2-001	-1581.946310	+0.14	-1582.350137	-1579.246798	0.00	-1579.571959
10-PhNCO-010	-1581.942537	+23.71	-1582.346174			
10-PhNCO-009	-1581.943051	+22.36	-1582.346740			
10-PhNCO-008	-1581.943073	+22.30	-1582.346640	-1579.240611	+18.98	-1579.561761
10-PhNCO-007	-1581.946645	+12.92	-1582.350518	-1579.242579	+13.81	-1579.566499
10-PhNCO-006	-1581.946731	+12.69	-1582.350627	-1579.242674	+13.56	-1579.566570
10-PhNCO-005	-1581.951449	+0.31	-1582.355471	-1579.247455	+1.01	-1579.574785
10-PhNCO-004	-1581.951409	+0.41	-1582.355329	-1579.247515	+0.85	-1579.574670
10-PhNCO-003	-1581.951435	+0.34	-1582.355359	-1579.247643	+0.51	-1579.574778
10-PhNCO-002	-1581.951437	+0.34	-1582.355401	-1579.247824	+0.04	-1579.574742
10-PhNCO-001	-1581.951566	0.00	-1582.355376	-1579.247839	0.00	-1579.574568
10-002	-1182.273833	0.00	-1182.562834	-1180.286039	+0.03	-1180.499782
10-001	-1182.273806	+0.07	-1182.562746	-1180.286051	0.00	-1180.499646
Nr.	H_{298K}(DFT)/Hartree	ΔH_{298K}(DFT)/kJ mol^{-1}	E_{298K}(DFT)/Hartree	H_{298K}(CC)/Hartree	ΔH_{298K}(CC)/kJ mol^{-1}	E_{298K}(CC)/Hartree
11-004	-1182.738869	+47.64	-1183.041973	-1180.754574	+54.02	-1181.014846
11-003	-1182.745220	+30.97	-1183.048135	-1180.760959	+37.26	-1181.026740
11-002	-1182.753586	+9.00	-1183.056661	-1180.770657	+11.80	-1181.042220
11-001	-1182.757014	0.00	-1183.059680	-1180.775150	0.00	-1181.046302
Nr.	H_{298K}(DFT)/Hartree	ΔH_{298K}(DFT)/kJ mol^{-1}	E_{298K}(DFT)/Hartree	H_{298K}(CC)/Hartree	ΔH_{298K}(CC)/kJ mol^{-1}	E_{298K}(CC)/Hartree
14-005	-1175.376657	+37.56	-1175.588973	-1173.604534	+45.69	-1173.773945
14-004	-1175.375986	+39.32	-1175.587831	-1173.607772	+37.19	-1173.791691
14-003	-1175.385480	+14.40	-1175.598500	-1173.610772	+29.32	-1173.782332
14-002	-1175.382951	+21.04	-1175.595685	-1173.613902	+21.10	-1173.794445
14-001	-1175.390964	0.00	-1175.603813	-1173.621938	0.00	-1173.800258

Table S4: 25 (continuation). Table of Thermochemical Data (sorted by Δ*H298K*(CC).

Nr.	H_{298K}(DFT)/Hartree	ΔH_{298K}(DFT)/kJ mol^{-1}	E_{298K}(DFT)/Hartree	H_{298K}(CC)/Hartree	ΔH_{298K}(CC)/kJ mol^{-1}	E_{298K}(CC)/Hartree
15g-Me2-010	-2482.193218	+10.64	-2482.828102	-2478.088324	+8.38	-2478.626061
15g-Me2-009	-2482.193328	+10.35	-2482.827911	-2478.088479	+7.97	-2478.625684
15g-Me2-008	-2482.193814	+9.08	-2482.828341	-2478.088502	+7.91	-2478.630232
15g-Me2-007	-2482.193510	+9.87	-2482.828392	-2478.088577	+7.71	-2478.626812
15g-Me2-006	-2482.194381	+7.59	-2482.829210	-2478.088632	+7.57	-2478.628778
15g-Me2-005	-2482.193982	+8.64	-2482.828509	-2478.088845	+7.01	-2478.626482
15g-Me2-004	-2482.194637	+6.92	-2482.829349	-2478.089146	+6.22	-2478.628190
15g-Me2-003	-2482.194037	+8.49	-2482.828644	-2478.089679	+4.82	-2478.628039
15g-Me2-002	-2482.194662	+6.85	-2482.829474	-2478.090792	+1.90	-2478.626891
15g-Me2-001	-2482.197271	0.00	-2482.832034	-2478.091514	0.00	-2478.632736
15g-Me-010	-2482.200448	+6.61	-2482.834441	-2478.088319	+8.62	-2478.627853
15g-Me-009	-2482.200668	+6.03	-2482.835598	-2478.088452	+8.27	-2478.623334
15g-Me-008	-2482.199598	+8.84	-2482.833955	-2478.088483	+8.19	-2478.624872
15g-Me-007	-2482.199511	+9.07	-2482.833911	-2478.088484	+8.19	-2478.624865
15g-Me-006	-2482.201305	+4.36	-2482.835877	-2478.089716	+4.95	-2478.623471
15g-Me-005	-2482.200767	+5.77	-2482.835384	-2478.090016	+4.17	-2478.624875
15g-Me-004	-2482.199672	+8.65	-2482.834439	-2478.090145	+3.83	-2478.618649
15g-Me-003	-2482.201298	+4.38	-2482.835916	-2478.090343	+3.31	-2478.624872
15g-Me-002	-2482.201731	+3.24	-2482.836278	-2478.091197	+1.07	-2478.625218
15g-Me-001	-2482.202966	0.00	-2482.837558	-2478.091603	0.00	-2478.625475
15g-PhNCO2-010	-2842.130905	+9.01	-2842.836908	-2837.388399	+9.21	-2838.027616
15g-PhNCO2-009	-2842.131163	+8.34	-2842.837065	-2837.388655	+8.54	-2838.028500
15g-PhNCO2-008	-2842.131461	+7.55	-2842.836710	-2837.388976	+7.69	-2838.027079
15g-PhNCO2-007	-2842.131376	+7.78	-2842.836710	-2837.389124	+7.30	-2838.027537
15g-PhNCO2-006	-2842.132384	+5.13	-2842.838270	-2837.389476	+6.38	-2838.028020
15g-PhNCO2-005	-2842.132033	+6.05	-2842.838094	-2837.389508	+6.30	-2838.027140
15g-PhNCO2-004	-2842.132423	+5.03	-2842.838245	-2837.389571	+6.13	-2838.027999
15g-PhNCO2-003	-2842.134338	0.00	-2842.840059	-2837.389717	+5.75	-2838.024982
15g-PhNCO2-002	-2842.134072	+0.70	-2842.839893	-2837.389754	+5.65	-2838.027854
15g-PhNCO2-001	-2842.134092	+0.65	-2842.839578	-2837.391906	0.00	-2838.029333
15g-PhNCO-010	-2842.144133	+8.05	-2842.849875	-2837.394588	+7.17	-2838.031605
15g-PhNCO-009	-2842.144340	+7.50	-2842.849722	-2837.394841	+6.51	-2838.032374
15g-PhNCO-008	-2842.144382	+7.39	-2842.850238	-2837.395218	+5.52	-2838.030619
15g-PhNCO-007	-2842.144548	+6.96	-2842.849917	-2837.395326	+5.24	-2838.031567
15g-PhNCO-006	-2842.145432	+4.64	-2842.851177	-2837.395711	+4.22	-2838.034539
15g-PhNCO-005	-2842.145077	+5.57	-2842.850640	-2837.395921	+3.67	-2838.034148
15g-PhNCO-004	-2842.145739	+3.83	-2842.851365	-2837.396406	+2.40	-2838.036621
15g-PhNCO-003	-2842.145642	+4.09	-2842.851319	-2837.396895	+1.12	-2838.035066
15g-PhNCO-002	-2842.147040	+0.41	-2842.852595	-2837.397131	+0.50	-2838.035548
15g-PhNCO-001	-2842.147198	0.00	-2842.852904	-2837.397320	0.00	-2838.035695
15g-010	-2442.470444	+7.70	-2443.061271	-2438.436775	+10.02	-2438.964503
15g-009	-2442.470568	+7.37	-2443.061216	-2438.436967	+9.52	-2438.964379
15g-008	-2442.470032	+8.78	-2443.060797	-2438.438221	+6.23	-2438.965605
15g-007	-2442.471497	+4.93	-2443.062254	-2438.438414	+5.72	-2438.967012
15g-006	-2442.471516	+4.88	-2443.062098	-2438.438560	+5.34	-2438.965147
15g-005	-2442.470485	+7.59	-2443.061286	-2438.438596	+5.24	-2438.962376

Table S4: 25 (continuation). Table of Thermochemical Data (sorted by Δ*H298K*(CC).

15g-004	-2442.471516	+4.88	-2443.061933	-2438.438686	+5.00	-2438.964781
15g-003	-2442.472064	+3.44	-2443.062598	-2438.439042	+4.07	-2438.964730
15g-002	-2442.471411	+5.16	-2443.062155	-2438.439447	+3.01	-2438.964696
15g-001	-2442.473375	0.00	-2443.064301	-2438.440592	0.00	-2438.968677
Nr.	H_{298K}(DFT)/Hartree	ΔH_{298K}(DFT)/kJ mol^{-1}	E_{298K}(DFT)/Hartree	H_{298K}(CC)/Hartree	ΔH_{298K}(CC)/kJ mol^{-1}	E_{298K}(CC)/Hartree
15-Me2-001	-1214.659964	0.00	-1214.902365	-1212.812682	0.00	-1213.020212
15-Me-002	-1214.660753	+25.73	-1214.902927	-1212.807894	+20.89	-1213.006719
15-Me-001	-1214.670553	0.00	-1214.912884	-1212.815851	0.00	-1213.016854
15-PhNCO2-005	-1574.574119	+19.18	-1574.887096	-1572.087610	+18.11	-1572.318155
15-PhNCO2-004	-1574.574700	+17.65	-1574.887631	-1572.088231	+16.48	-1572.319265
15-PhNCO2-003	-1574.577749	+9.65	-1574.891149	-1572.092927	+4.15	-1572.328809
15-PhNCO2-002	-1574.579225	+5.77	-1574.892680	-1572.094046	+1.21	-1572.330245
15-PhNCO2-001	-1574.581424	0.00	-1574.894792	-1572.094508	0.00	-1572.333003
15-PhNCO-007	-1574.577502	+47.69	-1574.890640			
15-PhNCO-006	-1574.577582	+47.48	-1574.890567			
15-PhNCO-005	-1574.578226	+45.79	-1574.891483	-1572.085926	+42.31	-1572.318806
15-PhNCO-004	-1574.579396	+42.72	-1574.892548	-1572.086900	+39.75	-1572.320613
15-PhNCO-003	-1574.586121	+25.06	-1574.899370	-1572.093594	+22.18	-1572.328377
15-PhNCO-002	-1574.587243	+22.12	-1574.900549	-1572.093860	+21.48	-1572.332481
15-PhNCO-001	-1574.595667	0.00	-1574.909289	-1572.102041	0.00	-1572.342492
15-002	-1174.916634	+25.36	-1175.115188	-1173.139543	+22.93	-1173.264526
15-001	-1174.926292	0.00	-1175.125207	-1173.148275	0.00	-1173.276290
Nr.	H_{298K}(DFT)/Hartree	ΔH_{298K}(DFT)/kJ mol^{-1}	E_{298K}(DFT)/Hartree	H_{298K}(CC)/Hartree	ΔH_{298K}(CC)/kJ mol^{-1}	E_{298K}(CC)/Hartree
22-Me-001	-1075.816070	0.00	-1076.149411	-1073.934962	0.00	-1074.192507
22-002	-1036.087156	+0.01	-1036.377953	-1034.279856	+0.04	-1034.548855
22-001	-1036.087159	0.00	-1036.377950	-1034.279872	0.00	-1034.548874
22-PhNCO-002	-1435.733666	+17.90	-1436.138498	-1433.210924	+16.54	-1433.577970
22-PhNCO-001	-1435.740483	0.00	-1436.145378	-1433.217222	0.00	-1433.583981
Nr.	H_{298K}(DFT)/Hartree	ΔH_{298K}(DFT)/kJ mol^{-1}	E_{298K}(DFT)/Hartree	H_{298K}(CC)/Hartree	ΔH_{298K}(CC)/kJ mol^{-1}	E_{298K}(CC)/Hartree
23-001	-401.825524	0.00	-401.969205	-401.056657	0.00	-401.185707
23-Me-001	-441.539916	0.00	-441.727628	-440.692172	0.00	-440.803142
23-PhNCO-003	-801.473861	+22.94	-801.731823	-799.990234	+19.23	-800.210840
23-PhNCO-002	-801.473416	+24.10	-801.731281	-799.990311	+19.02	-800.210499
23-PhNCO-001	-801.482597	0.00	-801.740914	-799.997557	0.00	-800.223110